UCRL-TR-202708

"PIERO CALDIROLA" INTERNATIONAL CENTRE FOR THE PROMOTION OF SCIENCE
AND INTERNATIONAL SCHOOL OF PLASMA PHYSICS

INTERNATIONAL CONFERENCE ON

ULTRASHORT HIGH-ENERGY RADIATION AND MATTER

VILLA MONASTERO, VARENNA, ITALY *October 7 -10, 2003*

ORGANISED BY
- çPiero Caldirolaé International Centre for the Promotion of Science and International School of Plasma Physics, Milano, Italy
- University of Milano Bicocca, Milano, Italy

PURPOSE
The workshop is intended as a forum to discuss the latest experimental, theoretical and computational results related to the interaction of high energy radiation with matter. High energy is intended to mean soft x-ray and beyond, but important new results from visible systems will be incorporated. The workshop will be interdisciplinary amongst scientists from many fields, including: plasma physics; x-ray physics and optics; solid state physics and material science; biology ; quantum optics.
Topics will include, among other subjects:
understanding damage thresholds for x-ray interactions with matter
developing ~ 5 keV x-ray sources to investigate damage,
developing ~ 100 keV Thomsom sources for material studies,
developing short pulse (100 fs and less) x-ray diagnostics,
developing novel X-ray optics
developing models for the response of biological samples to ultra intense, sub ps x-rays high-energy radiation

DIRECTORS
A.Wootton, Lawrence Livermore National Laboratory, USA
D.Batani, University of Milano Bicocca, Italy

SCIENTIFIC COMMITTEE
Rene Bakker, Sincrotrone Trieste, Italy
Dimitri Batani, University of M ilano Bicocca, Italy
Michel Belakhovsky, CEA-Grenoble, France
Thomas Brabec, University of Ottawa ,Canada
Todd Ditmire, University of Texas, USA
Ernst Fill MPQ, Garching, Germany
Antonio Giulietti, CNR, Pisa, Italy
Janos Hajdu, Biomedical Center, Uppsala, Sweden
Dieter Hoffmann, GSI Darmstadt, Germany
Charles Joachain, Universiteê Libre de Bruxelles, Belgium
Cristina Lenardi, University of Milano, Italy
Maurizio Lontano, IFP, CNR, Milano, Italy
Victor Malka, LOA - ENSTA Palaiseau, France
Sergio Martellucci, University of Roma çTor Vergataé, Italy
Juergen Meyer-ter-Vehn, MPQ, Garching, Germany
David Meyerhoffer, University of Rochester, USA
Alan Michette, Kingês College, London, UK
Kazutaka Nakamura, Tokyo Institute of Technology, Japan
Piergiorgio Nicolosi, University of Padova, Italy
Luigi Palumbo, University of Roma "La Sapienza"
Francesco Pegoraro, University of Pisa, Italy
Armando Reale, University of LêAquila, Italy
Marcus Roth, GSI Darmstadt, Germany
Antoine Rousse, LOA - ENSTA Palaiseau, France
Wolfang Sandner, Max-Born-Institut, Berlin, Germany
Elio Sindoni, University of M ilano Bicocca and ISPP, Italy
Thomas Tschentscher, Hasylab, DESY, Hamburg, Germany
Alan Wootton, Lawrence Livermore National Laboratory, USA

LOCAL ORGANISING COMMITTEE
D. Batani, University of M ilano Bicocca, Italy
T. Desai, University of M ilano Bicocca, Italy
M.Milani, University of Milano Bicocca, Italy
M. Lontano, IFP, CNR, Milano, Italy
D. Pifferetti, ISSP, Italy
E. Sindoni, University of M ilano Bicocca and ISPP, Italy

SPONSORED BY:
çPiero Caldirolaé International Centre for the Promotion of Science

Disclaimer
This document was prepared as an account of work sponsored by an agency of the United States Government. Neither the United States Government nor the University of California nor any of their employees, makes any warranty, express or implied, or assumes any legal liability or responsibility for the accuracy, completeness, or usefulness of any information, apparatus, product, or process disclosed, or represents that its use would not infringe privately owned rights. Reference herein to any specific commercial product, process, or service by trade name, trademark, manufacturer, or otherwise, does not necessarily constitute or imply its endorsement, recommendation, or favoring by the United States Government or the University of California. The views and opinions of authors expressed herein do not necessarily state or reflect those of the United States Government or the University of California, and shall not be used for advertising or product endorsement purposes.

This work was performed under the auspices of the U.S. Department of Energy by University of California, Lawrence Livermore National Laboratory under Contract W-7405-Eng-48

"FEMTO" Programme of the European Science Foundation (ESF).

APPLICATIONS:
Application and hotel reservation forms can be obtained from the Organizing Secretariat at the following address:
Mrs. Donatella Pifferetti, Via Nazionale, 85, 23821 Abbadia Lariana (LC), Italy , e-mail: isplasma@tin.it, Fax +39-0341-732490
They can also be downloaded from the conference web site (www.ispp.it). Information on hotel categories and prices are also available at the web site.

CONTRIBUTED PAPERS
Contributed papers for the workshop will be selected on the basis of a one page abstract. No particular form is required. These abstracts should be sent to: D. Batani, Fax +39-02 64482585, e-mail batani@mib.infn.it

REGISTRATION FEE
A registration fee of _ 360 should be paid **in Varenna at the registration desk.**
Alternatively, the same fee can be paid by bank transfer to: Banca Popolare di Lecco, Division of the Deutsche Bank, Via IV November, 23829 Varenna (LC), Italy, account n. c/c 9500/E, ABI 03104, CAB 51830, SWIFT DEUTITM1029, in favour of International School of Plasma Physics, indicating clearly the participants'names. All bank expenses are at participants' charge.
The fee covers admission to the Workshop and social events.

FURTHER INFORMATION CAN BE OBTAINED FROM
D. Batani, University of M ilano Bicocca
Fax +39-02-64482585 email batani@mib.infn.it

LIST OF INVITED TALKS:
RICHARD R. FREEMAN, University of California Davies
"The use of ultra-high intensity, short pulse lasers in fusion energy development"

LEONIDA GIZZI, CNR, Pisa
"Recent results in laser-plasma X-ray sources"

FRED HARTEMANN, Lawrence Livermore National Laboratory
"Basic concepts in advanced X-ray sources"

ALAN MICHETTE, King's College, London
"Recent developments in laser-plasma sources and optics for x-ray microscopy and microprobing"

PAOLO VILLORESI, University of Padova
"Toward the single-cycle regime in the generation of high-order laser harmonics"

MICHELE BERTOLO, Elettra,.Trieste
"Synchrotron radiation: properties and related analysis techniques"

MATT ZEPF, Queen's University Belfast "gamma ray beam production and probing in laser matter interaction"

JACEK KRZYWINSKI, Warsaw University
"Results from the TTF phase 1 on FEL beam induced damage of optical elements"

RENE BAKKER, Sincrotrone Trieste, Italy
"Development of VUV and X-ray FELs"

RICHARD LONDON, Lawrence Livermore National Laboratory
"The physics of photon- materials interactions"

JÜRGEN MEYER-TER-VEHN, MPQ Garching
"Plasma physics with X-rays"

KLAUS EIDMANN, MPQ Garching
"Isochoric heating of matter by intense X-ray pulses"

ANTONIO RITUCCI, University of L'Aquila
"Table top X ray laser systems"

BRIGITTE CROS, LPGP, University of Orsay
"Soft X-ray laser driven by a guided ultra-short laser pulse"

MARCO BELLINI, Istituto Nazionale Ottica Applicata, Firenze
"Generation and applications of XUV harmonics"

MARKUS ROTH, TU-Darmstadt, Germany
"X-Ray and particle diagnostics for warm dense matter research"

KAZUTAKA G. NAKAMURA, Tokyo Institute of Technology
"Picosecond time-resolved X-ray diffraction from laser-shocked semiconductors"

JOHN COSTELLO, Dublin City University
"Photoabsorption and Photoionization Imaging and Spectroscopy with Laser Plasma Light Sources"

ROUSSE ANTOINE, LOA, Ensta, Palaiseau
"Novel laser-produced plasma ultrafast x-ray sources and their applications"

KATSUNOBU NISHIHARA, Institute of Laser Engineering, Osaka
"Laser-Produced-Plasma for EUV Light Source for Lithography"

LUCIA MANCINI, Elettra, Trieste, Italy
"X-ray imaging applications of third generation synchrotron sources in material science".

ANDRE' EGBERT, Laser Zentrum Hannover
"High-repetition rate electron-based ultrashort hard-x-ray source and first applications"

ELKE PLÖNJES, Hasylab / Desy, Hamburg, Germany
"Layout and photon beam diagnostics at the VUV FEL user facility at DESY"

MERDJI HAMED, Service des Photons Atomes et Molecules, CEA, France
"Manipulating intense XUV coherent light"

THOMAS TSCHENTSCHER, Hasylab / Desy
"Short Wavelength FEL facilities and experiments"

ANATOLY FAENOV, Nat.Res.Inst. Phys. Measurements, Moscow
"Hot electron influence on the radiation properties of matter under interaction by short laser pulses"

JÜRGEN STEIN, MPQ, Garching, Germany
"Hot electron diagnostics using X-rays and Cerenkov radiation"

YUJI FUKUDA, Advanced Photon Research Center, JAERI
"Generation of energetic ions and x rays from clusters irradiated by ultrafast, high-intensity laser pulses

ANDREI SAVELEV, Lomonosov Moscow State University
"Efficient hard X-ray source using femtosecond plasma at solid and liquid targets"

ERNST FILL, MPQ, Garching, Germany
"Photopumping of XUV lasers by XFEL radiation"

LUIGI PALUMBO, Universita' Roma "La Sapienza"
"The SPARC/X projects at LNF"

EDMOND TURCU, Rutherford Appleton Laboratory, UK
"Soft X-ray laser plasma sources and applications"

CHARLES JOACHAIN, Universite' Libre de Bruxelles
"Interaction of Ultra-Intense Laser Pulses with Relativistic Ions

Contents

List of Participants 6

Oral Presentations

Conference on Ultra-short High Energy Radiation and Matter 17
D. Batani/A. Wootton

Development of VUV and X-ray FELs 26
Rene Bakker

Generation and Applications of XUV Harmonics 62
Marco Bellini

Synchrotron Radiation: Properties and related Analysis Techniques 89
Michele Bertolo

Photoabsorption Spectroscopy & Imaging with Laser-Plasma X-VUV Continua 121
John Costello

Soft X-ray Laser Driven by a Guided Ultra-short Laser Pulse 188
Brigitte Cros

High-repitition Rate Electron-based Ultrashort Hard-x-ray Source and First Applications 208
Andre Egbert

Isochoric Heating of Matter by Ultrashort Laser Pulses 233
Klaus Eidmann

Hot Electron Influence on the Radiation Properties of Matter Under Interaction by Short Laser Pulses 255
Anatoly Faenov

Photopumping of XUV Lasers by XFEL-radiation 279
Ernst Fill

The Use of Ultra-high Intensity Short Pulse Lasers in Fusion Energy Development 299
Richard Freeman

Generation of Energetic Ions and X-rays from Clusters Irradiated by Ultrafast, High-intensity Laser Pulses 351
Yuji Fukuda

Recent Results in Laser-plasma X-ray Sources 370
Leonida Gizzi

Basic Concepts in Advanced X-ray Sources 426
Fred Hartemann

Interaction of Ultra-Intense Laser Pulses with Relativistic Ions 466
Charles Joachain

Interaction of Ultra-short VUV Pulses with Solids 485
Jaeck Krzywinski

The Physics of X-ray Material Interactions 533
Richard London

X-ray Imaging Applications of 3rd Generation Synchrotron Sources in Material Science 569
Lucia Mancini

Contents

Oral Presentations

Manipulating Intense XUV Coherent Light 608
Hamed Merdji

Dense Plasma Physics with DESY XFEL and TTF2 631
J. Meyer-ter-Vehn

Developments in Laser-Plasma Sources & Optics for X-ray Microscopy and Microprobing 652
Alan Michette

Picosecond Time-resolved X-ray Diffraction from Laser-shocked Semiconductors 676
Kazutaka Nakamura

Laser-produced-plasma for EUV Light Source for Lithography 696
Katsunobu Nishihara

The SPARC/X Projects 713
Luigi Palumbo

Layout and Photon Beam Diagnostics for the VUV-FEL User Facility at DESY 757
Elke Plonjes

Tabletop Soft X-ray Laser Systems: Characterization and Applications 776
Antonio Ritucci

X-ray and Particle Diagnostics for Warm Dense Matter Research 796
Markus Roth

Ultrafast X-rays: Production with Laser-produced Plasma and Applications 817
Antoine Rousse

Efficient Hard X-ray Source Using Femtosecond Plasma at Solid and Liquid Targets 887
Andrei Savelev

Hot Electron Diagnostics Using X-rays and Cerenkov Radiation 888
Jurgen Stein

Short-wavelength Free-electron Lasers Facilities and Experiments 900
Thomas Tschentscher

Soft X-ray Laser-plasma Sources and Applications 933
I.C.Edmond Turcu

Toward the Single-cycle Regime in the Generation of Higher-order Harmonics and Multiphoton Ionization 960
Paolo Villoresi

Gamma Ray Beam Production and Probing 1002
Matthew Zepf

Contents

Poster Presentations

Carbon Single Layers for Total Reflectance and Their Combination in Carbon/Carbon Multilayers 1024
Reiner Dietsch

Influence of Optical Thickness and Hot Electrons on Rydberg Spectra of Ne- and F-like Copper Ions 1025
A. Faenov

X-ray Spectral Diagnostics for Satellite Lines of H-like Mg Ions Measured by High Resolution Spectrometer 1046
T. Kato

Flatness Study of X-UV Beamsplitters for Michelson Interferometry 1067
Anne-Sphie Morlens

Spectrally Tunable X-ray imaging and Backlighting Schemes Based on the Spherically Bent Crystals 1068
T. Pikuz

X-ray Microscopy of Caenorhabditis Elegans Nematode Using a Laser Plasma Pulsed X-ray Source 1082
G. Poletti

A 46.9 nm Tabletop Soft X-ray Laser: Characterization and Applications 1083
A. Ritucci

Simulations of the Phonon-Bragg Switch in GaAs 1084
J. Sheppard

Introduction to New Light Source I & the Simulation of a Thomson 1085
Scattering X-ray Source
B. Xia

International conference on
ULTRASHORT HIGH-ENERGY RADIATION AND MATTER

Villa Monastero, Varenna, Italy
October 7 – 10, 2003

LIST OF PARTICIPANTS

Bakker René
Sincrotrone Trieste S.C.p.A.
Strada Statale, 14
Km. 163,5 in AREA Science Park
34012 BASOVIZZA TRIESTE
Italy
Tel. +39 040 375 8551
Fax +39 040 375 8029
rene.bakker@elettra.trieste.it

Batani Dimitri
Dipartimento di Fisica "G. Occhialini"
Università degli Studi di Milano Bicocca and INFM
Piazza della Scienza, 3
20126 MILANO
Italy
Tel. +39 02 6448 2313
Fax +39 02 6448 2585
batani@mib.it

Bellini Marco
INOA – Istituto Nazionale di Ottica Applicata
Largo E. Fermi, 6
50125 FIRENZE
Italy
Tel. +39 055 4572493
Fax +39 055 4572451
bellini@ino.it

Bertolo Michele
Sincrotrone Trieste S.C.p.A.
Strada Statale, 14
Km. 163,5 in AREA Science Park
34012 BASOVIZZA TRIESTE
Italy
Tel. +39 040 375 8021
Fax +39 040 375 8565
bertolo@elettra.trieste.it

Boscolo Ilario
Università degli Studi di Milano
Dipartimento di Fisica
Via Celoria, 16
20133 MILANO
Italy
Tel. +39-02 5031 7658
ilario.boscolo@mi.infn.it

Canova Federico
Università di Milano – Bicocca
Piazza della Scienza, 3
20126 MILANO
Italy
Tel. +39-02 6448 2208
canova@mib.infn.it

Costello John
Dublin City University
and National Centre for Plasma Sci. & Technology
Collins Avenue, Glasnevin
DUBLIN 9
Ireland

Tel. +353 1 7005304
Fax +353-1 7005384
john.costello@dcu.ie

Cros Brigitte
LPGP
Bat. 210, Université Paris XI
91405 ORSAY
France

Tel. +33 1 69 15 81 77
Fax +33 1 69 15 78 44
Brigitte.cros@lpgp.u-psud.fr

Desai Tara
Dipartimento di Fisica “G. Occhialini”
Università degli Studi di Milano Bicocca and INFM
Piazza della Scienza, 3
20126 MILANO
Italy

Tel. +39 02 6448 2329
Fax +39 02 6446 2367
TARA.DESAI@MIB.INFN.IT

Dietsch Reiner
AXO DRESDEN GmbH
Siegfried-Rädel-Str. 31
01809 HEIDENAU
Germany

Tel. +49 (0) 351 2583 249
Fax +49 (0) 351 2583 314
reiner.dietsch@axo-dresden.de

Egbert André
Laser Zentrum Hannover e V.
Hollerithallee 8
30419 HANNOVER
Germany

Tel. +49 511 2788 218
Fax +49 511 2788 100
AE@LZH.DE

Eidmann Klaus
Max Planck Institut Für Quantenoptik
Hans Kopfermann Str. 1
85748 GARCHING
Germany

Tel. +49 89 3290 5244
Fax +49 89 3290 5200
eidman@mpq.mpg.de

Faenov Anatoly
Multicharged Ions Spectra Data Center of VNIIFTRI
MISDC of VNIIFTRI
Moscow Region, 141570
Russia

Tel. +7-095 535 9135
Fax +7-095 535 9343
faenov@yahoo.com

Fill Ernst
Max Planck Institut Für Quantenoptik
Hans Kopfermann Str. 1
85748 GARCHING
Germany

Tel. +49 89 3290 5725
Fax +49 89 3290 5200
ernst.fill@mpq.mpg.de

Francucci Massimo
Università di Roma “TOR VERGATA”
Dipartimento STFE
Via del Politecnico 1
00133 ROMA
Italy

Tel. +39-06 72597246 or 72597211
Fax +39-06 72597145
francucci@ing.uniroma2.it

Freeman Richard
Ohio State University
EU III, 425 Stillman, 1947 College Rd.
COLUMBUS OHIO 43206
USA

Tel. +1-614 292 8908

Freeman@mps.OHIO-STATE.EDU

Fukuda Yuji
Advanced Photon Research Center (APRC)
Japan Atomic Energy Research Institute
8-1 Umemidai, Kizu-cho, Souraku-gun
KYOTO 619-0215
Japan

Tel. +81 774 71 3334
Fax +81 774 71 3338
fukuda@apr.jaeri.go.jp

Gizzi Leonida Antonio
ILIL-IPCF, Consiglio Nazionale delle Ricerche
Via G. Moruzzi 1
56124 PISA
Italy

Tel. +39-050 315 2257
Fax +39 050 315 2230
la.gizzi@ipcf.cnr.it

Goldstein William
Lawrence Livermore National Laboratory
7000 East Avenue,
LIVERMORE, CA 94550
USA

Tel. +1-925 422 2515
Fax +1-925 523 9307
goldstein3@llnl.gov

Grimoldi Elisa
Dipartimento di Fisica “G. Occhialini”
Università degli Studi di Milano Bicocca
Piazza della Scienza, 3
20126 MILANO
Italy

Tel. +39-0331 604233
elgrimo@tin.it

Hartemann Fred
Lawrence Livermore National Laboratory
7000 East Avenue,
LIVERMORE, CA 94550
USA

Tel. +1-925 423 3398
Fax +1-925 423 2463
HARTEMANN1@LLNL.GOV

Hoffmann Dieter H.H.
GSI Darmstadt
Planckstr. 1
64291 DARMSTADT
Germany

Tel. +49-6159 71 2664
Fax +49-6151 71 2888
d.hoffmann@gsi.de

Joachain Charles
Physique Théorique
Université Libre de Bruxelles
Campus Plaine CP 227
Bd. du Triomphe
1050 BRUXELLES
Belgium
Tel. +32 2 650 55 78
Fax +32 2 650 50 98
cjoacha@ulb.ac.be

Kato Takako
Data and Planning Center
National Institute for Fusion Science
Oroshi-cho, Toki
GIFU, 509-5292
Japan
Tel. +81-572 58 2259
Fax +81-572 58 2628
takako@nifs.ac.jp

Klisnick Annie
CNRS-LIXAM
Université Paris-Sud
Bat. 350
91405 ORSAY
France
Tel. +33-1 69 15 76 17
Fax +33-1 69 15 58 11
annie.klisnick@lixam.u-psud.fr

Krzywinski Jacek
Institute of Physics of the Polish Academy of Sciences
Al. Lotnikow 32/46
02-668 WARSAW
Poland
Tel. +48-22 843 66 0229 71
Fax +48-22 843 09 26
jacek.krzywinski@desy.de

Labate Luca
Intense Laser Irradiation Laboratori
IPCF (CNR)
Via Moruzzi 1
56124 PISA
Italy
Tel. +39-050 315 2255
Fax +39-050 315 2230
luca@ipcf.cnr.it

Lebo Ivan
Technical University – MIREA
Prospect Vernadskogo 78
MOSCOW
Russia
Tel. +7-095 132 68 47
Fax +7 095 434 8665 & 095-132 11 96
lebo@sci.lebedev.ru
lebo@mirea.ru

Lenardi Cristina
Università degli Studi di Milano
Via Trentacoste 2 (??)
20134 MILANO
Italy
Tel. +39-02 503 15796
Fax +39-02 503 15775
Cristina.lenardi@unimi.it

Lobkaeva Eugenia
Russian Federal Nuclear Center
RFNC-VNIIEF
37M Pr. Mira,
SAROV
Nizhni Novgorod Region, 607190
Russia
Tel. +7-83130 6 9610
Fax +7-83130 3 6300
lep@bfrc.vniief.ru

London Richard
Lawrence Livermore National Laboratory
L-30, Lawrence Livermore National Laboratory
LIVERMORE, CA 94550
USA
Tel. +1-925 423 2021
Fax +1-925 423 9969
rlondon@llnl.gov

Lontano Maurizio
Istituto di Fisica del Plasma "Piero Caldirola"
Consiglio Nazionale delle Ricerche
EURATOM-ENEA-CNR Association
Via Roberto Cozzi, 53
20125 Milano
Italy
Tel. +39-02-66 173 260
Fax +39-02-66 173 239
lontano@ifp.mi.cnr.it

Lucchini Gianni
Dipartimento di Fisica “G. Occhialini”
Università degli Studi di Milano Bicocca
Piazza della Scienza, 3
20126 MILANO
Italy
Tel. +39 02 64482219
Fax
gianni.lucchini@mib.infn.it

Manclossi Mauro
Laboratoire d’Optique Appliquée (LOA)
Chemin de la Humière
91761 PALAISEAU
France
Tel. +33-1 69 31 99 91
mauro.manclossi@ensta.fr

Mancini Lucia
Sincrotrone Trieste S.C.p.A.
Strada Statale, 14
Km. 163,5 in AREA Science Park
34012 BASOVIZZA TRIESTE
Italy
Tel. +39 040 375 8248
Fax +39 040 375 8776
lucia.mancini@elettra.trieste.it

Marconi Joska
Dipartimento di Fisica “G. Occhialini”
Università degli Studi di Milano Bicocca
Piazza della Scienza, 3
20126 MILANO
Italy
Tel. +39-039 9908140
Fax
pulsardinevefrattale@libero.it

Merdji Hamed
CEA/SPAM
Centre d’Etudes de Saclay, Bat. 522
91191 GIF SUR IVETTE
France
Tel. +33-1 69 08 51 63
Fax +33-1 69 08 12 13
merdji@drecam.cea.fr

Meyer-ter-Vehn Jürgen
Max Planck Institut Für Quantenoptik
Hans Kopfermann Str. 1
85748 GARCHING
Germany
Tel. +49 89 3290 5137
Fax +49 89 3290 5200
meyer-ter-vehn@mpq.mpg.de

Michette Alan
King's College London
Department of Physics
Strand
LONDON, WC2R 2LS
UK

Tel. +44-20 7848 2811
Fax +44-20 7848 2420
alan.michette@kcl.ac.uk

Morlens Anne-Sophie
LIXAM
Chemin de la Hunière
91761 PALAISEAU
France

Tel. +33-1 69 31 98 31
Fax +33-1 69 31 98 98
anneso_morlens@yahoo.it

Nakamura Kazutaka
Materials and Structures Laboratory,
Tokyo Institute of Technology
4259 Nagatsuta, Yokohama,
KANAGAWA 226-8503
Japan

Tel. +81-45 924 5397
Fax +81-45 924 5360
nakamura@msl.titech.ac.jp

Nicolosi Piergiorgio
INFM – Dipartimento di Ingegneria dell'Informazione
Università di Padova
Via Gradenigo, 6/A
35131 PADOVA
Italia

Tel. +39-049 8277 674
Fax +39-049 8277 699
nicolosi@dei.unipd.it

Nishihara Katsunobu
Osaka University
Institute of Laser Engineering
2-6, Yamada-oka, Suita
OSAKA 565-0871
Japan

Tel. +81-6-6879 8725
Fax +81-6 6877 8799
nishihara@ile.osaka-u.ac.jp

Orsini Francesco
Università di Milano
Via Trentacoste, 2
20134 MILANO
Italy

Tel. +39-02-50315797
Fax +39-02 50315775
francesco.orsini@unimi.it

Palumbo Luigi
Università di Roma "LA SAPIENZA"
Dipartimento di Energetica
Via A. Scarpa, 14
00161 ROMA
Italy

Tel. +39-06 4976 6533
Fax +39-06 4424 0183
luigi.palumbo@uniroma1.it

Passoni Matteo
Politecnico di Milano
Dipartimento di Ingegneria Nucleare
Via Ponzio 34/3
20133 MILANO
Italy

Tel. +39-02 2399 6330
Fax +39-022399 6309
matteo.passoni@polimi.it

Patalano Giovanbattista
Piazza Leonardo da Vinci
Politecnico di Milano
20133 MILANO
Italy

Tel. +39-0349 3550602
giovanbattista_patalano@yahoo.com

Pikuz Tatiana
Multicharged Ions Spectra Data Center of VNIIFTRI
MISDC of VNIIFTRI
Moscow Region, 141570
Russia

Tel. +7-095 535 9135
Fax +7-095 535 9343
tapikuz@yahoo.com

Plönjes Elke
DESY
Notkestr. 85
22589 HAMBURG
Germany

Tel. +49-40 8998 2602
Fax +49-40 8998 4475
elke.ploenjes@desy.de

Poletti Giulio
Università di Milano
Via Trentacoste, 2
20134 MILANO
Italy

Tel. +39-02-50315778
Fax +39-02-50315776
giulio.poletti@unimi.it

Redmer Ronald
University of Rostock
Department of Physics
18051 ROSTOCK
Germany

Tel. +49-381 498 6910
Fax +49-381 498 6942
Ronald.redmer@physik.uni-rostock.de

Ritucci Antonio
Dipartimento di Fisica
Università dell'Aquila
Via Vetoio
67010 COPPITO L'AQUILA
Italy

Tel. +39-0862 433094
Fax +39-0862 433033
antonio.ritucci@aquila.infn.it

Rossetti Stefano
Università degli Studi di Milano Bicocca
Piazza della Scienza, 3
20126 MILANO
Italy

dott.ross@tin.it

Roth Markus
Technische Universität Darmstadt
Schlossgartenstr. 9
64289 DARMSTADT
Germany

Tel. +49-6151 165417
Fax +49-6151 164321
markus.roth@physik.tu-darmstadt.de

Rousse Antoine
LOA
Chemin de la Humière
91761 PALAISEAU
France

Tel. +33-1-69 31 99 01
Fax +33 1-69 31 99 96
antoine.rousse@ensta.fr

Savel'ev Andrei
International Laser Center M.V. Lomonosov
Moscow State University
Vorobyevy gory
MOSCOW
Russia

Tel. +7-095 9394148
Fax +7-095 9393113
savelev@femto.phys.msu.ru

Serafini Luca
INFN – Milano
Via Celoria, 16
20133 MILANO
Italy

Tel. +39-0250317673
Fax +39-02-50317487
luca.serafini@mi.infn.it

Sheppard Jonathan
Department of Physics
University of Oxford
Clarendon Laboratory
Parks Road
OXFORD, OX1 3PU
UK

Tel. +44-1865 272301
Fax +44-1865 282296
j.sheppard1@physics.ox.ac.uk

Sindoni Elio
Università degli Studi di Milano Bicocca and
International School of Plasma Physics
Piazza della Scienza, 3
20126 MILANO
Italy

Tel. +39 02 6448 2746
Fax +39 02 6448 2794
elio.sindoni@unimib.it

Sobierajski Ryszard
Warsaw University of Technology
Institute of Physics
ul. Koszykowa 75
00-662 WARSAW
Poland

Tel. +48-602 478677

sobieraj@if.pw.edu.pl

Springer Paul
Lawrence Livermore National Laboratory
7000 East Avenue, L-051
LIVERMORE, CA 94550
USA

Tel. +1-925 423 9221
Fax +1-925 422 5411
springer6@LLNL.gov

Stein Jürgen
Max Planck Institut Für Quantenoptik
Hans Kopfermann Str. 1
85748 GARCHING
Germany

Tel. +49 89 3290 5246
Fax +49 89 3290 5200
Juergen.Stein @mpq.mpg.de

Strati Federico
Università degli Studi di Milano – Bicocca
Piazza della Scienza, 3
20126 MILANO
Italy

Tel. +39-02 64482208
strati@mib.infn.it

Thiele Robert
University of Rostock
Department of Physics
18051 ROSTOCK
Germany

Tel. +49-381 498 6776
Fax +49-381 498 6942
Robert.thiele@stud.uni-rostock.de

Troussel Philippe
CEA Company
Centre d'Ile de France
BP 12
91680 BRUYERES-LE CHATEL
France

Tel. +33-01 69 26 57 79
Fax +33-01 69 26 70 97
troussel@cea.fr

Tschentscher Thomas
HASYLAB/DESY
NotkestrASSE 85
22589 HAMBURG
Germany

Tel. +49-40 8998 3904
Fax +49-40 8998 4475
thomas.tschentscher@desy.de

Turcu I.C. Edmond
Central Laser Facility,
Rutherford Appleton Laboratory,
Chilton, Didcot, Oxfordshire OX11 0QX,
United Kingdom

Tel. +44-1235-445603
Fax
i.c.e.turcu@rl.ac.uk

Valueva Julia
Russian Federal Nuclear Center
RFNC-VNIIEF
37M Pr. Mira,
SAROV
Nizhni Novgorod Region, 607190
Russia

Tel. +7-83130 3 9304
Fax +7-83130 3 6300
vjv@bfrc.vniief.ru

Veres Gabor
KFKI Research Institute for Particle and Nuclear Physics
POB 49
1525 BUDAPEST
Hungary

Tel. +36-1 392 2222
Fax +36-1 392 2598
veres@rmki.kfki.hu

Villoresi Paolo
INFM – Università degli Studi di Padova
Via Gradenigo, 6/A
35131 PADOVA
Italia

Tel. +39-49 827 7644
Fax +39-49 827 7699
paolo.villoresi@unipd.it

Wootton Alan
Lawrence Livermore National Laboratory
7000 Eat Avenue
LIVERMORE, CA 94550
USA

Tel. +1-925 422 6533
Fax +1-925 523 9307
woottonl@llnl.gov

Xia Bing
Department of Engineering Physics
Tsinghua University
BEIJING 100084
P.R. China

Tel. +86-10 6277 5070

xiabing@tsinghua.org.cn

Zepf Matthew
Queen's University Belfast
School of Mathematics and Physics
University Road
BELFAST BT 71NN
UK

Tel. +44-28 90 273123
Fax +44-28 90 273 110
m.zepf@qub.ac.uk

ORAL PRESENTATIONS

Conference on
Ultra-short High Energy Radiation and Matter

October 7 through 10, 2003 Villa Monastero

Dimitri Batani and Alan Wootton

This Conference is sponsored by:

the “Piero Caldirola” International School of Plasma Physics, Milano, Italy

the “FEMTO” Programme of the European Science Foundation (ESF)

Please remember to wear your badge always:

you need it to enter Villa Monastero

you need it at the restaurants for discounted prices

TIME SCHEDULE

	MONDAY 6 OCTOBER	TUESDAY 7 OCTOBER	WEDNESDAY 8 OCTOBER	THURSDAY 9 OCTOBER	FRIDAY 10 OCTOBER	SATURDAY 11 OCTOBER
8.45	ARRIVALS	WOOTTON OPENING				DEPARTURES
9.00		HARTEMANN	LONDON	8.55 RITUCCI 9.15 FILL	TURCU	
9.35		BERTOLO	MEYER-TER-VEHN	TSCHENTSCHER	ROUSSE	
10.10		CROS	ZEPF	ROTH	KRZYWINSKI	
10.30 – 11.00		COFFEE BREAK				
11.00		JOACHAIN	FREEMAN	MANCINI	NAKAMURA	
11.20			EIDMANN	EGBERT	PLÖNJES	
11.40		MICHETTE	FUKUDA	SAVELEV	MERDJI	
12.00 – 15.30		LUNCH				
15.30 – 16.50		POSTER SESSION		15.00 TRAVEL TO PIONA ABBEY and VALTELLINA, WINE CAVES, AND 19.00 SOCIAL DINNER	POSTER SESSION	
16.00 – 16.20		COFFEE BREAK			COFFEE BREAK	
16.50		BELLINI	GIZZI		COSTELLO	
17.25		BAKKER	KLISNICK		17.25 - 19.00: ROUND TABLE & CONCLUSIONS	
18.00		NISHIHARA	PALUMBO			
18.20		VILLORESI				
18.40-19.00		STEIN	FAENOV			
21.30		WELCOME PARTY	CONCERT			

PLENARY TALKS (35 MINS) INVITED TALKS (20 MINS)

CHAIRMEN

Tuesday 7 Oct.,	Morning:	Wootton,
	Afternoon:	Lenardi,
Wednesday 8 Oct.,	Morning:	Lontano,
	Afternoon:	Turcu,
Thursday 9 Oct.,	Morning:	Nicolosi,
Friday, 10 Oct.,	Morning:	Faenov,
	Afternoon:	Milani

Afternoon-chairs should also take care of poster sessions.

The role of the chairmen is to promote questions and discussione, to take notes for the final round table, to observe the time table strictly

Contributions (oral and poster) to the Conferente on "ULTRASHORT HIGH-ENERGY RADIATION AND MATTER" will be published in a special issue of

Laser and Particle Beams

CAMBRIDGE | Instructions for Contributors

D.Hoffman, Editor in Chief

Conference, manuscript should ONLY be sent to the guest editors (A.Wootton and D.Batani) at the email address: batani@mib.infn.it.

They will be submitted to normal review procedure

(reviewers will be selected from conference attendees)

The background to the conference is the availability of short pulse, high brightness x-ray sources

High brightness, sub ps sources of x-rays are coming on line. This drives photon - material interaction research:

- requirements for designing experiments and diagnostics
- basic science possibilities

Examples of specific current interest:

- using visible photons as surrogates for x-rays to understand damage processes
- using existing sub ps x-ray lasers to investigate damage threshold
- developing ~ 5 keV x-ray sources to investigate damage
- developing ~ 100 keV Thomson sources for material studies
- developing short pulse (100 fs and less) x-ray diagnostics
- developing novel X-ray optics
- developing models for the response of bio-samples to ultra intense, sub ps x-rays

Relevant R&D is undertaken in many fields of science

Relevant R&D is performed in multiple fields, in multiple countries. E.g. damage-relevant papers appear in journals of biophysics, plasmas, material science, optics.

Therefore to learn what is happening in the field of ‘Ultra-short High Energy Radiation and Matter’ we intend a conference that is interdisciplinary, introducing researchers who might otherwise not have the opportunity to meet.

We do not intend or want a conference just on plasma physics, or x-ray optics, etc. To assist this interdisciplinary nature the day-to-day organization is not by topic, but is on purpose mixed.

The topics are not rigid, but to guide discussions

1. X-ray sources
    - 1.1 X-ray source development, general
    - 1.2 Incoherent X-ray sources from laser-plasmas
    - 1.3 Harmonics
    - 1.4 Synchrotrons
    - 1.5 FEL's
    - 1.6 Capillary
    - 1.7 X-ray lasers from laser-plasmas
2. X-ray Optics Diagnostics and X-ray diagnostics
3. Photon Material Interactions
4. Plasma Physics
5. Bio Medical applications
6. Material and other applications

Discussions are intended to:

- summarize exciting developments,
- note cross disciplinary R&D,
- answer specific questions that arise,

Development of VUV and X-ray FELs

development of

4th generation light-sources

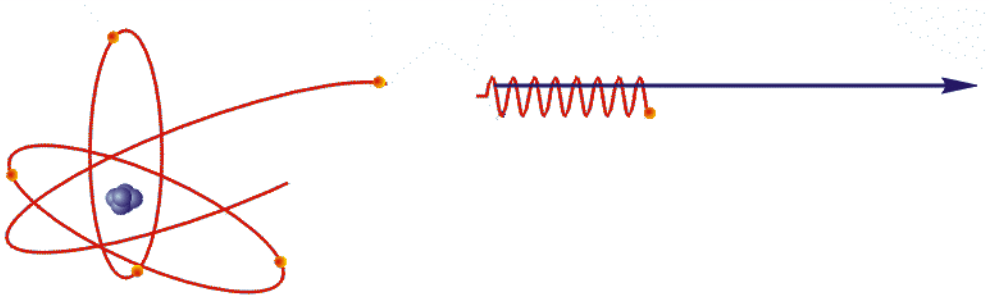

René Bakker
Sincrotrone Trieste S.C.p.A. di interesse nazionale
Strada Statale 14 - km 163,5 in AREA Science Park
34012 Basovizza, Trieste ITALY

tel: +39 (0)40 375 8551
fax: +39 (0)40 375 8029
email: rene.bakker@elettra.trieste.it

http://www.elettra.trieste.it/projects/lightsrc/linac-fel/

Outline

- Introduction
  - (to the Free-Electron Laser or FEL)
- Going to shorter wavelengths
- Projects for the future:
  - 4th generation FEL light-sources
- What to expect

Lasers & Free-Electron Lasers

lasers: **bounded electrons**

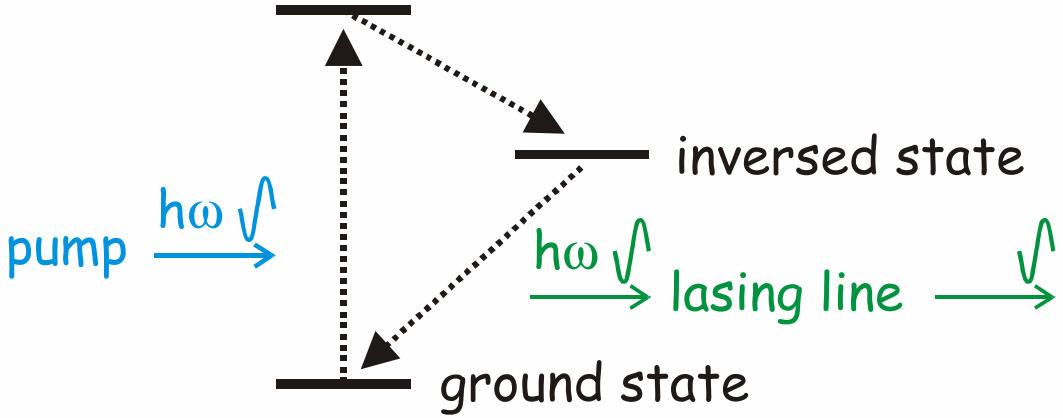

the transition-properties and hence, the radiated wavelengths are determined by energy states in the active material and not by the electron properties

free electron lasers: **non-bounded electrons**

but……
the electrons are forced to radiate , i.e., by producing dipole radiation

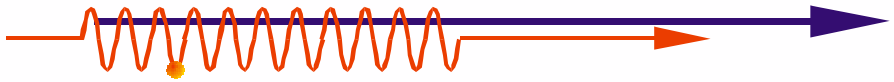

wavelength determined by the electron properties → external forces

Undulator Radiation

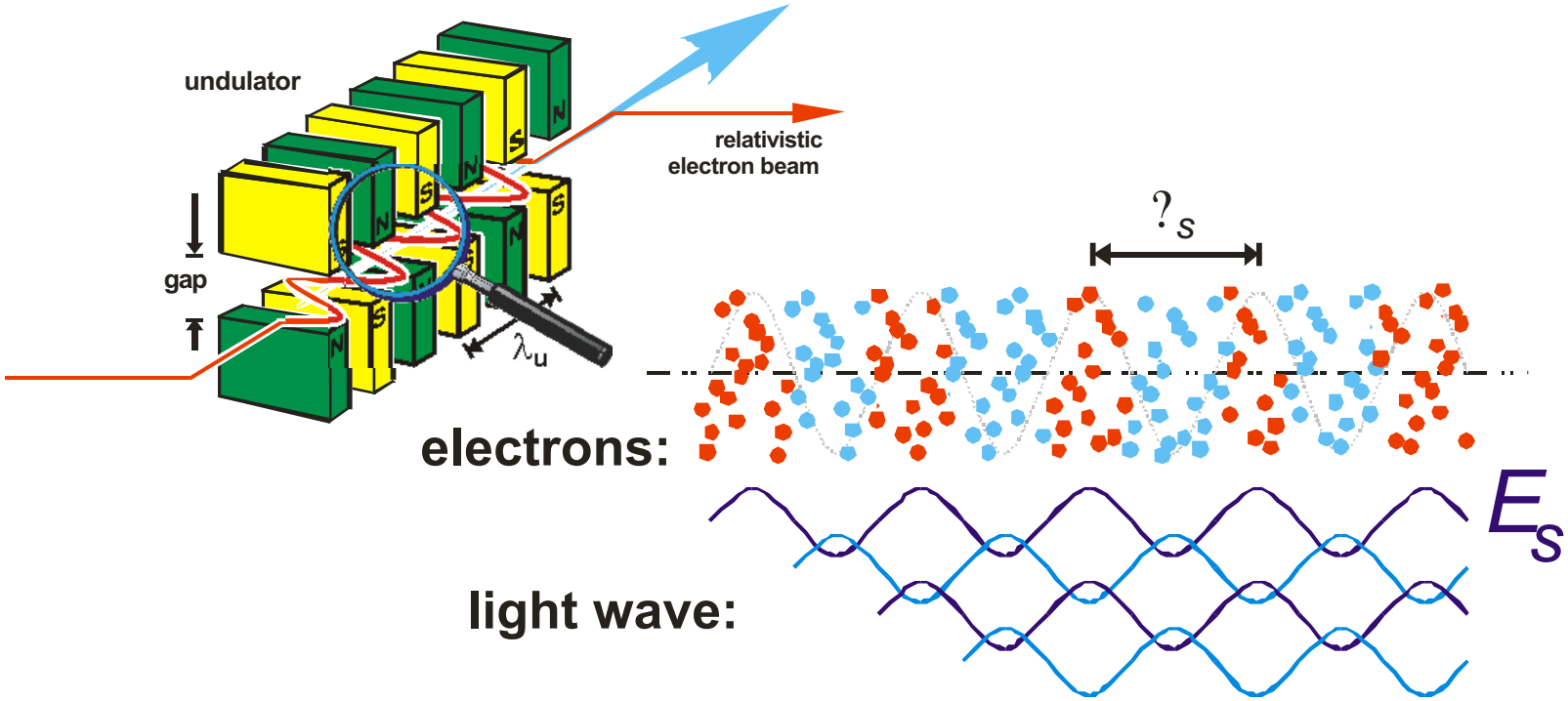

Radiated Power :

$P \propto n_e$ (number of electrons)

destructive interference

$\longrightarrow$ **shotnoise radiation**

FEL Radiation (coherent)

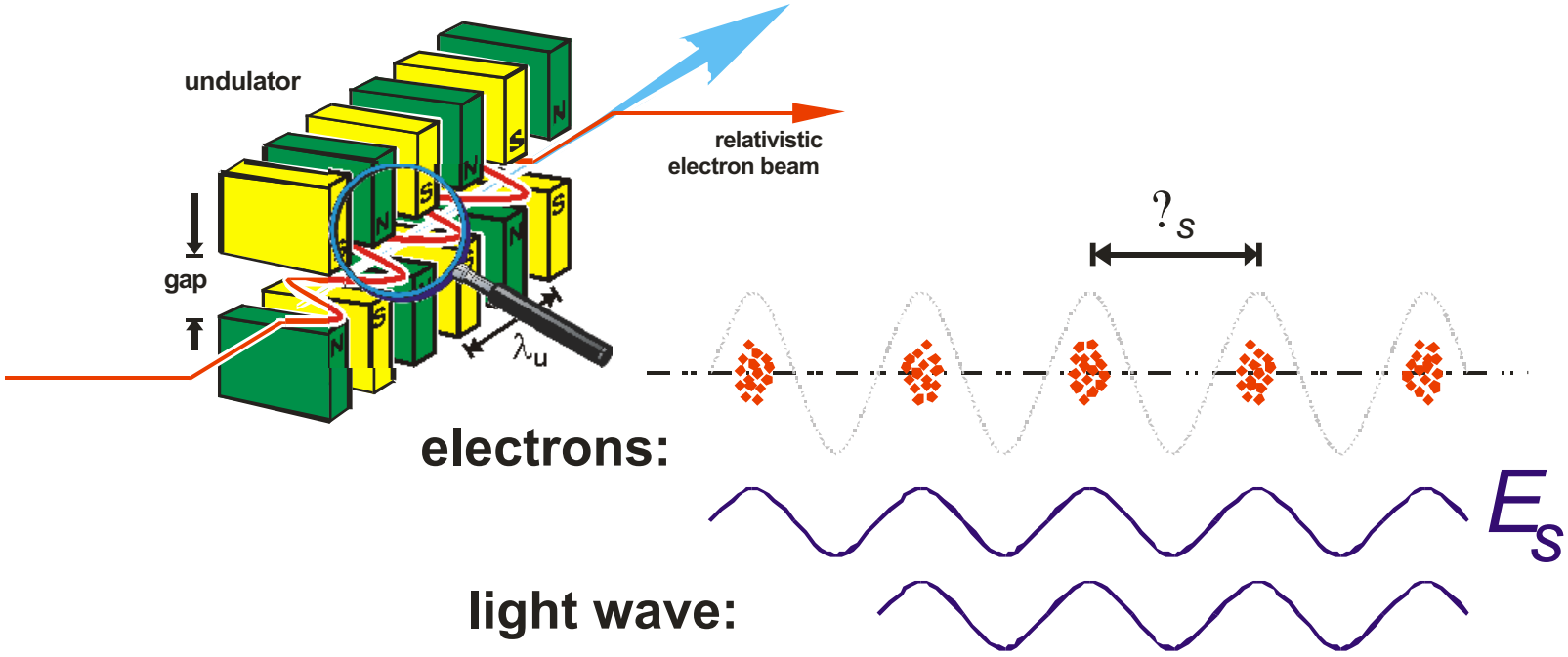

Radiated Power :

$$P \propto n_e^2 \quad \text{number of electrons} \quad n_e \sim 10^6 - 10^9$$

constructive interference

$\longrightarrow$ **enhanced emission**

Classical FEL Scheme

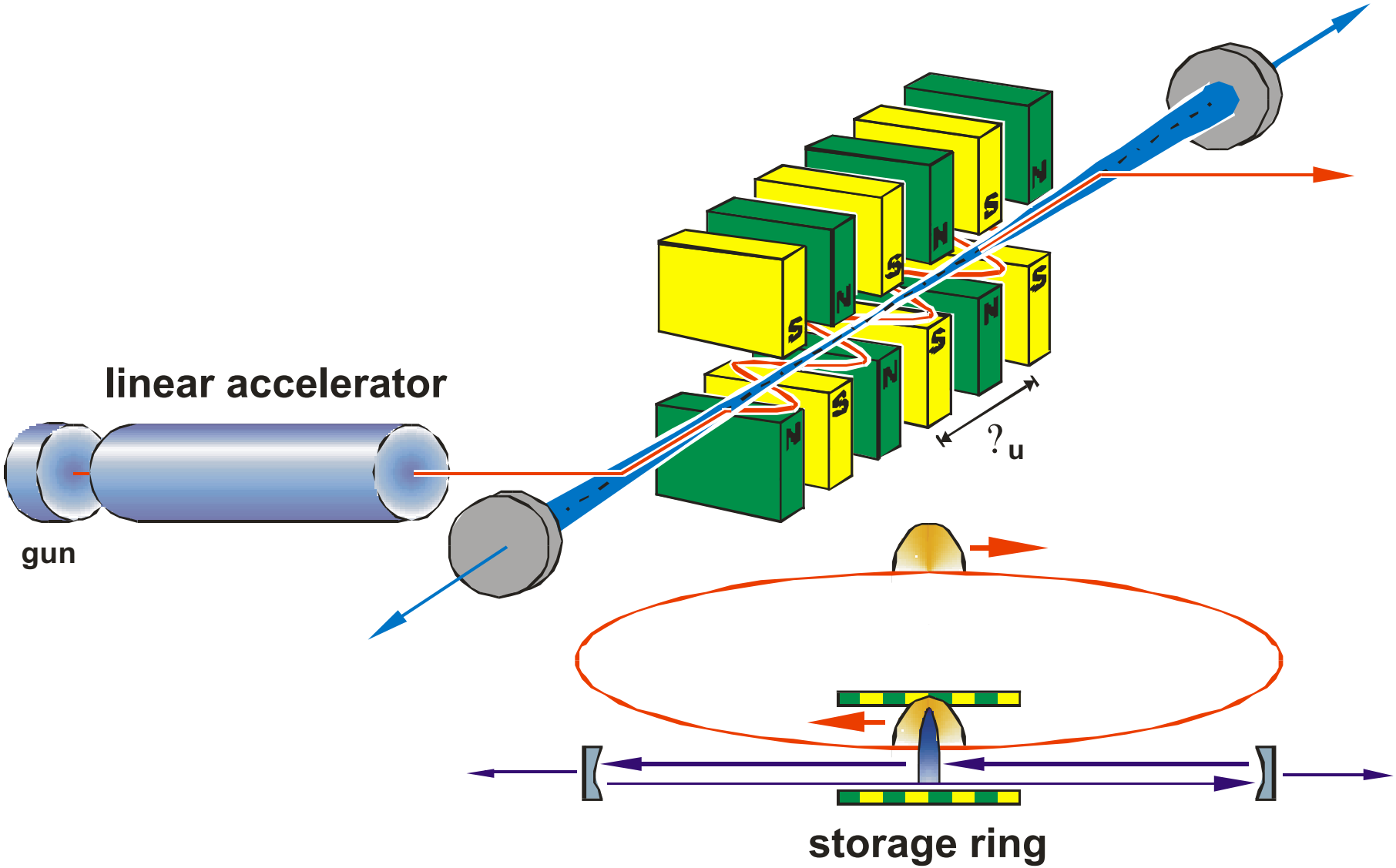

Advantages

- Works for any wavelength
  - mm-waves → 80 nm → 0.85 Å → 0.1 Å → ……?
- Continuously tunable wavelength (fast)
- High power / Brilliance:
  - kW to 100 GW of peak power with short pulses (fs)
  - up to 2 kW of time-averaged output power demonstrated
- Full coherent radiation (transverse and longitudinal)
  - i.e., $\Delta\lambda/\lambda$ = 0.1 (transform limited) → 10^{-8}
- Flexible output (polarization, pulse-length, …..)

Drawbacks

- Expensive:
  - IR: 10 M€ → UV: 40 M€ → XUV: 100 M€ → X-Ray: 650 M€
- Radiation hazard
- Complex technology
  - High demands on the electron beam quality
  - High demands on the electron beam stability
  - Optics
- For X-ray FEL:
  - non-demonstrated
  - technology

N.B. Technological challenges increase towards shorter wavelengths!

FEL facilities worldwide

4th generation development

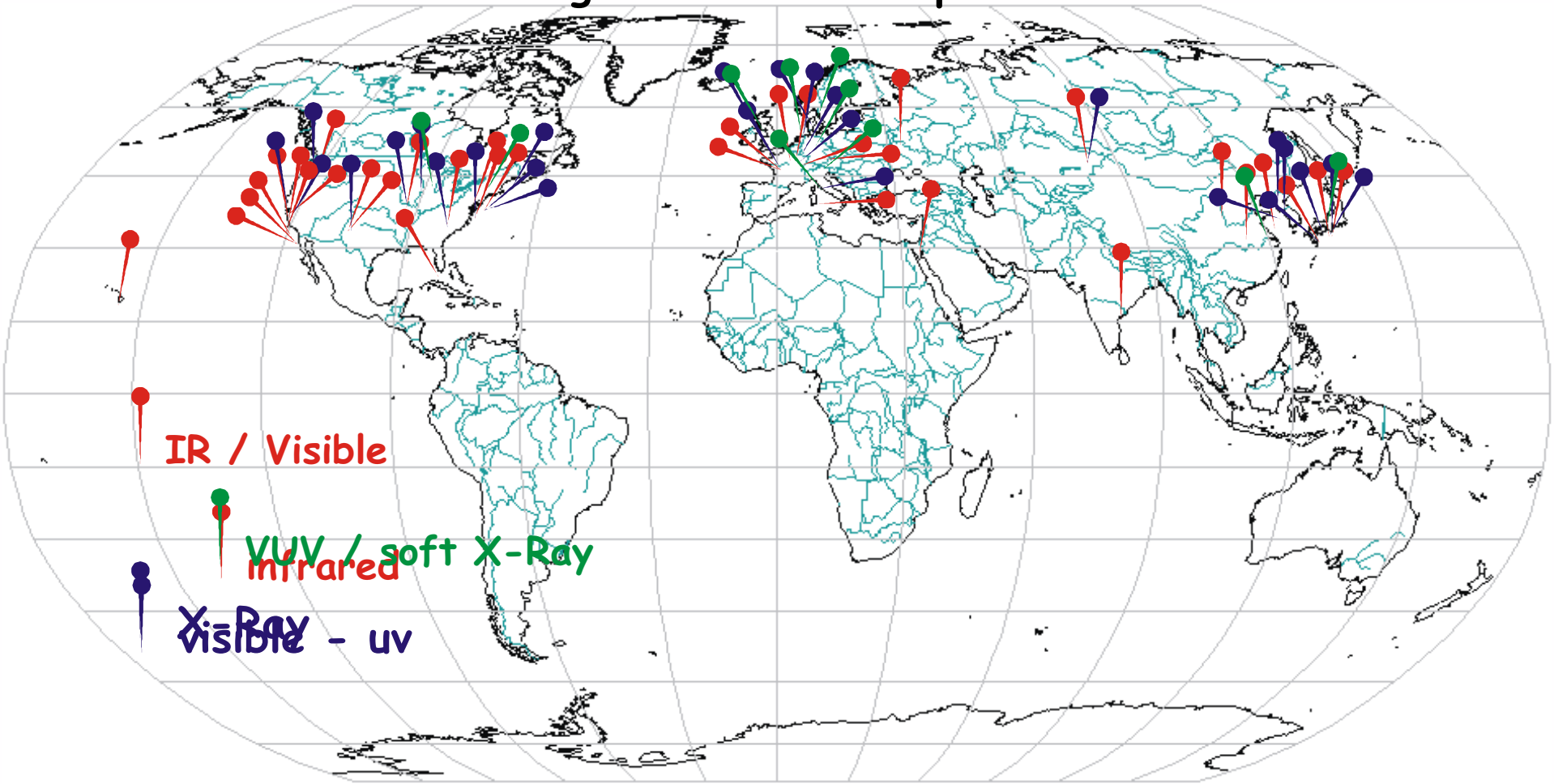

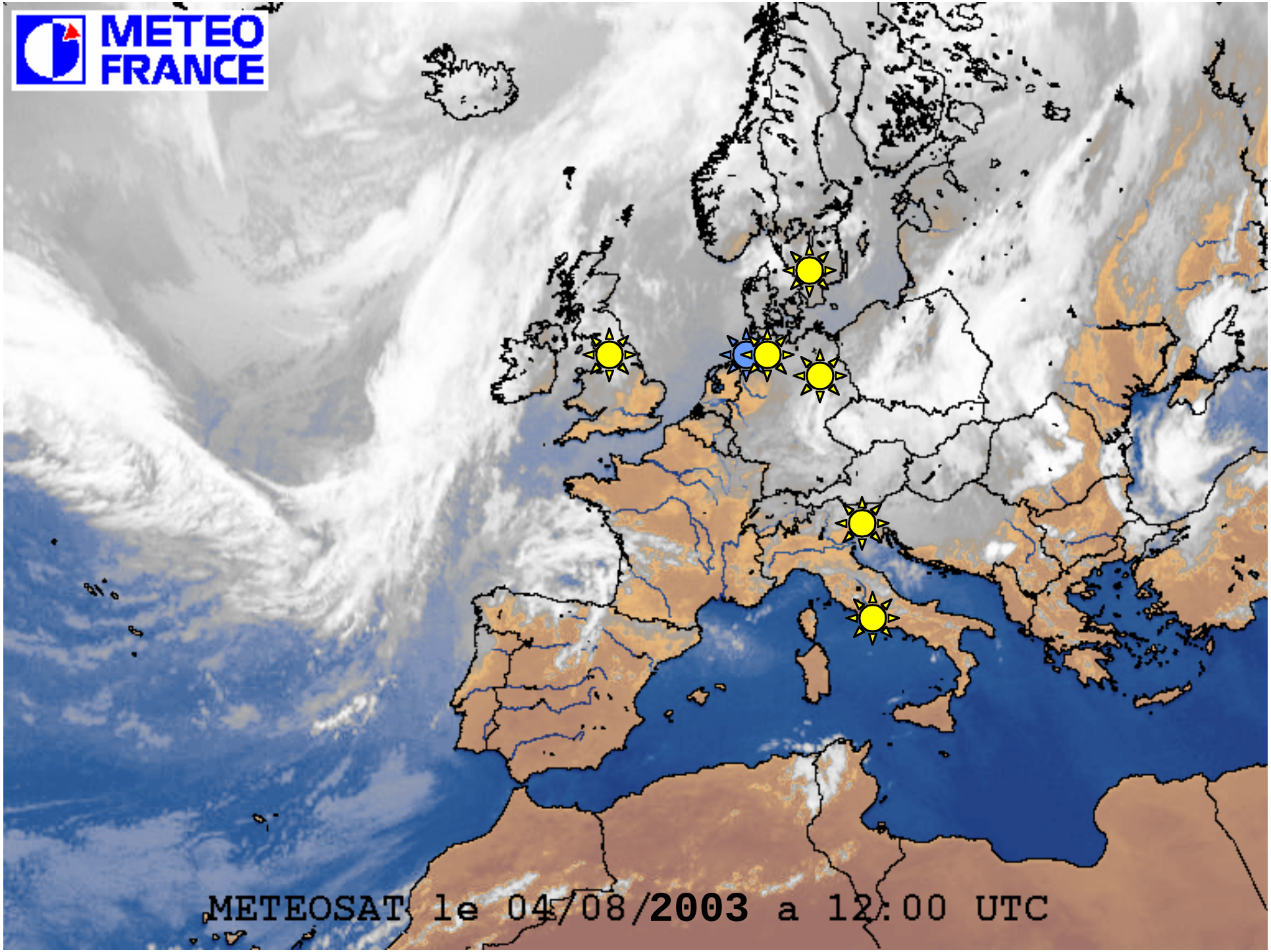
METEO FRANCE
METEOSAT le 04/08/2003 a 12:00 UTC

Performance Overview

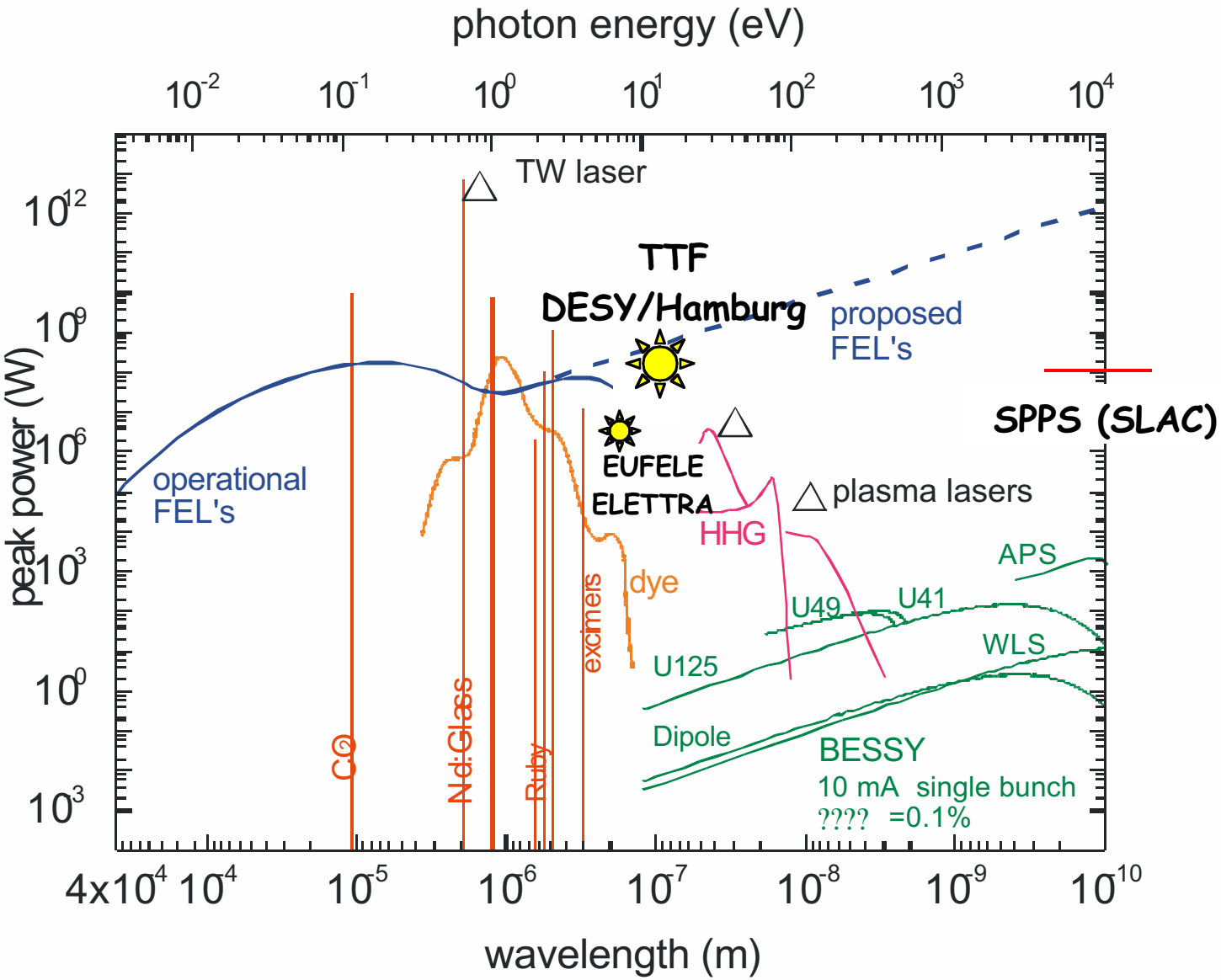

The Elettra Storage Ring FEL

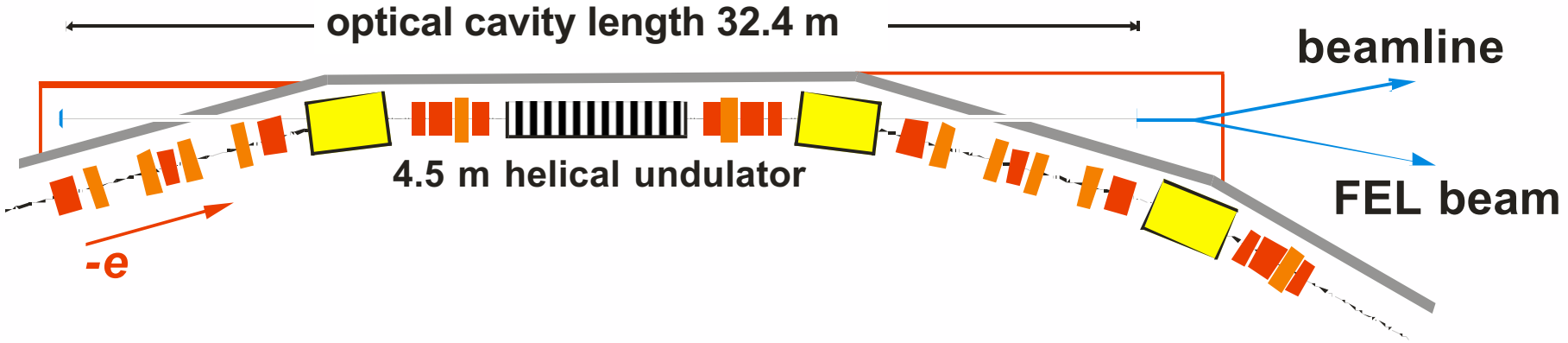

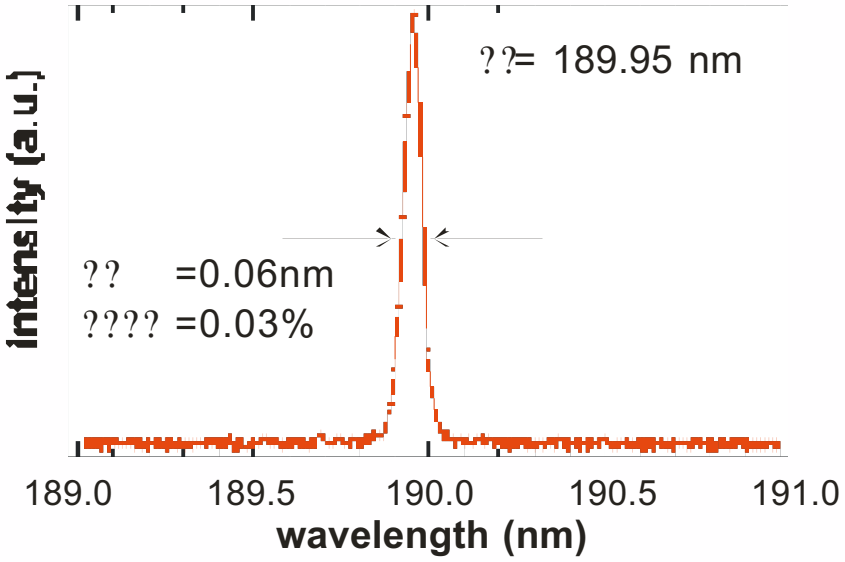

Storage ring operation*	1.0	GeV
Tunability range	350 – 190	nm
	3.5 – 6.5	eV
Average power	? 1	W
Pulse length (FWHM)	~ 5	ps
Peak power	? 40	kW
Pulse energy	? 0.2	mJ
Photon flux**	? 10^{18}	photons/s
Polarization	circular (linear may also be possible)	
Repetition rate	4.6	MHz
Synchronization with synchrotron radiation	1:1	

*4-bunch operation, **within the laser bandwidth

FEL → SASE FEL

Classical FEL Scheme

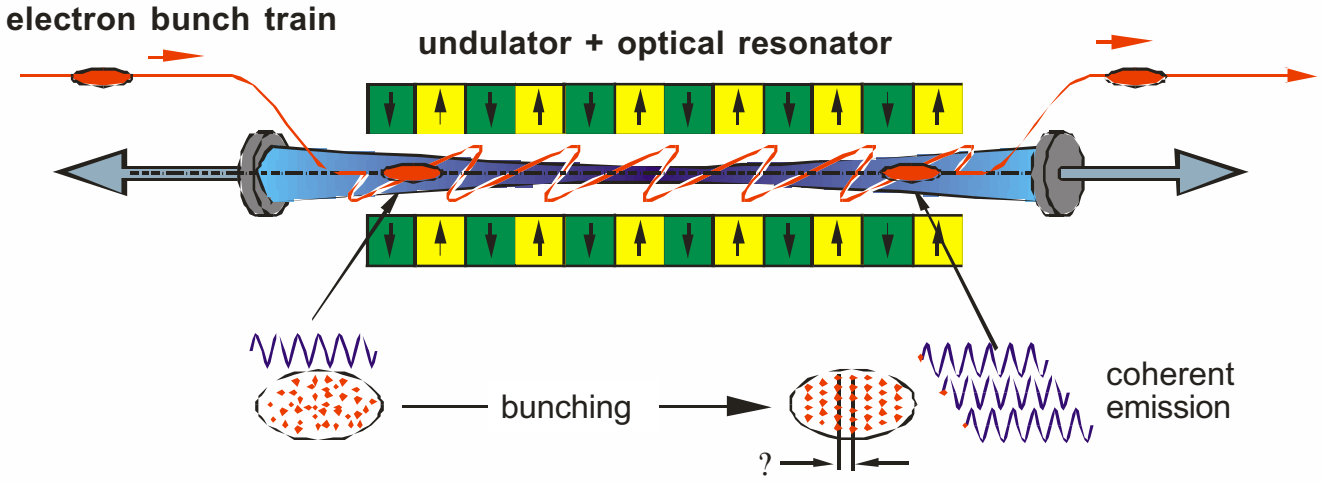

SASE FEL Scheme

(Self Amplified Spontaneous Emission)

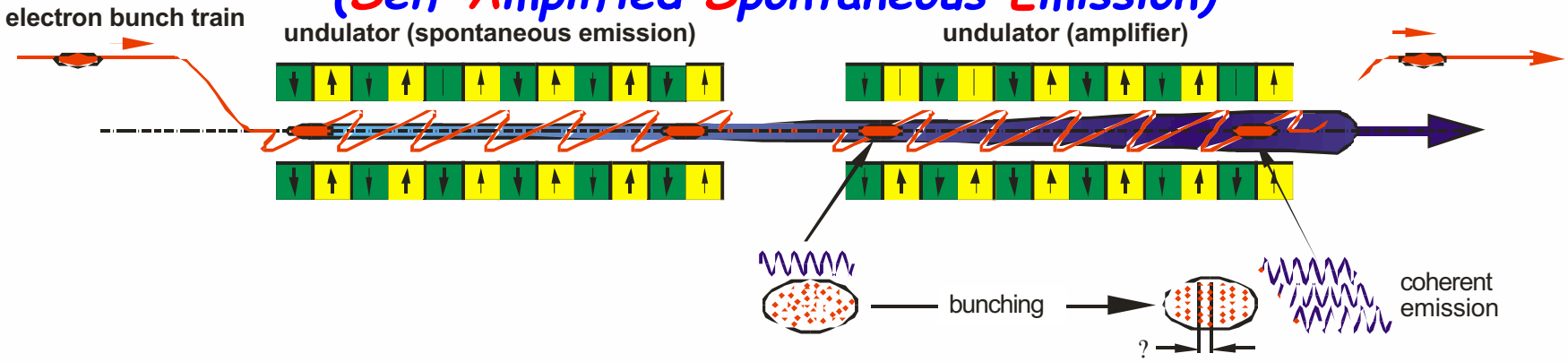

The SASE FEL Scheme

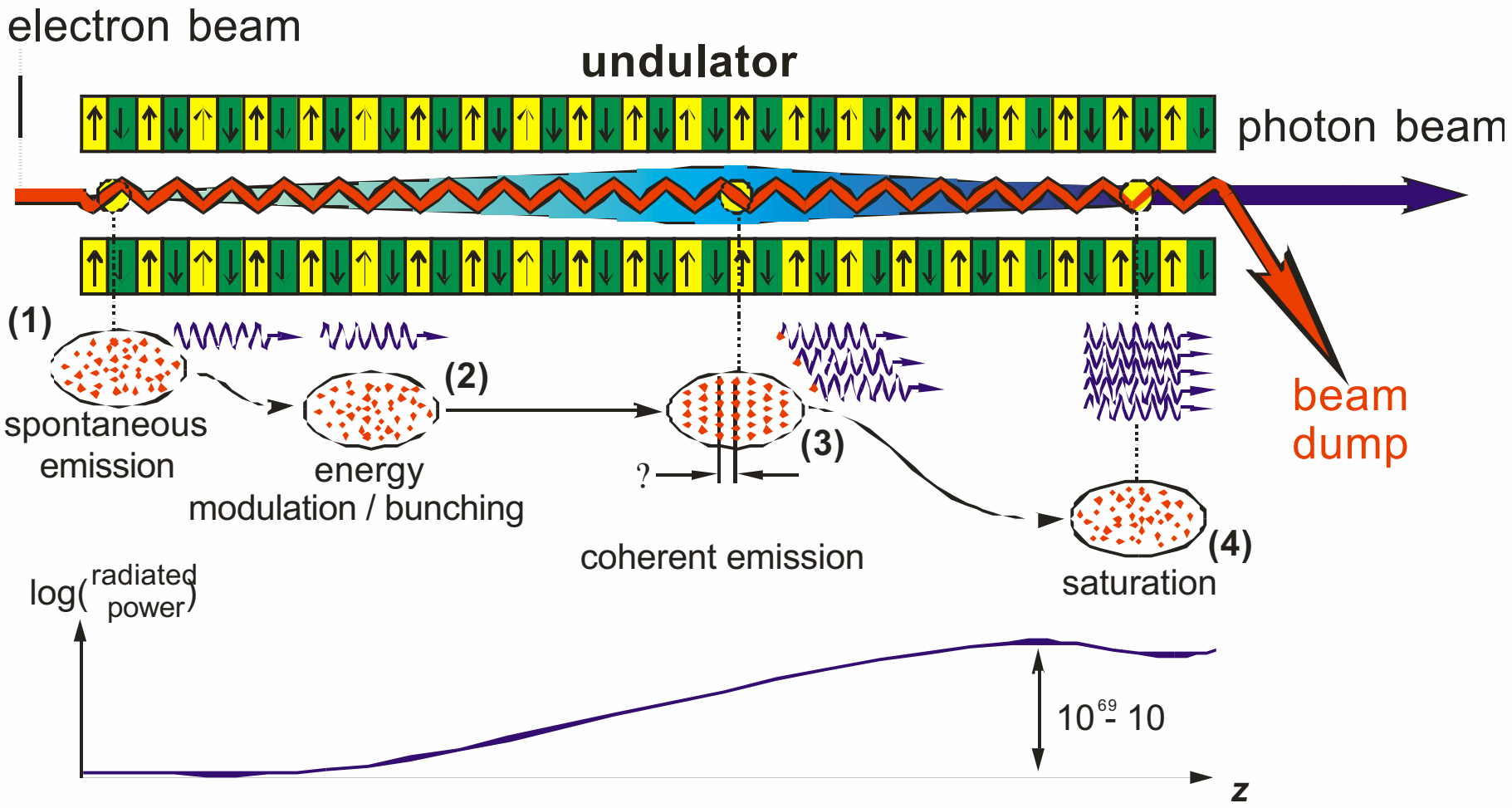

History of SASE

1980	First proposal	
1996	First experimental observation	
	UCLA:	λ = 16 μm
Dec. 1999	APS:	lasing at λ = 523 nm
Feb. 2000	DESY:	lasing at λ = 80 nm
Sep. 2000	APS:	saturation at λ = 523 nm
Feb. 2001	VISA/BNL:	saturation at λ = 800 nm
Apr. 2001	APS:	saturation at λ = 385 and λ = 265 nm
Sep. 2001	DESY:	saturation at λ = 100 nm
Oct. 2001	First user experiments @ DESY-TTF	

Development steps towards VUV and X-ray FELs

SASE FEL Facilities

Funded, under construction, or operational

!	4GLS (Daresbury)	(UK)	λ > 12 nm	(0.1 keV)
!	LEUTL / APS*	(US)	λ > 120 nm	
!	SPARC#	(I)	λ = 500 nm	
!	SCSS* (SPring8)	(J)	λ > 3 nm	(0.4 keV)
!	TTF (DESY)	(US)	λ > 1.5 Å	(8 keV)
!	TTF (DESY)*	(D)	λ > 6 nm	(0.2 keV)
!	VISA (BNL)#	(US)	λ = 800 nm	

Pl

TESLA (DESY)

MIT (US)

BESSY (D)

!		(D)	λ > 0.85 Å	(14 keV)
!	MIT (US)		λ > 3 Å	(4 keV)
!	BESSY (D), ELETTRA (I), SPARX (I), ….			(~ 1 keV)

FEL development

* Hybrid between FEL development & user facility

SPARC

elettra

Sorgente Pulsata e Amplificata di Radiazione Coerente

ENEA INFN elettra Synchrotron Light Laboratory

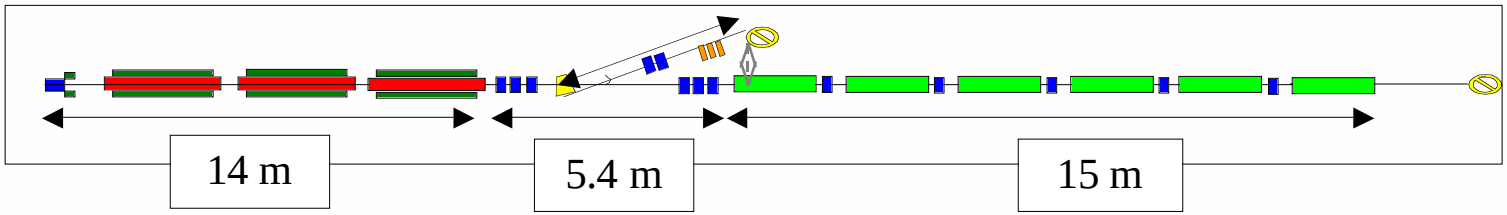

Beam parameters

155 MeV - 1.1 nC - 10 ps

Peak current 110 A / 100 A (50% bunch)

Energy spread 0.6 10^{-3} - Emitt. 1 mm mrad (slice)

Undulator Parameters

Period length 2.8 cm – 78 p./section – 6 sections

K 2.14 – Nominal wavelength 500 nm

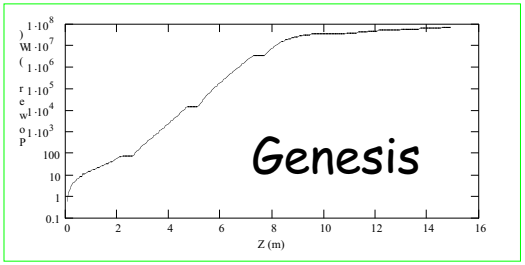

Two main issues:

- The generation of ultra-high peak brightness electron beams
- Experimental study of SASE-FEL process with generation of higher harmonics.

Courtesy Luca Giannessi (ENEA)

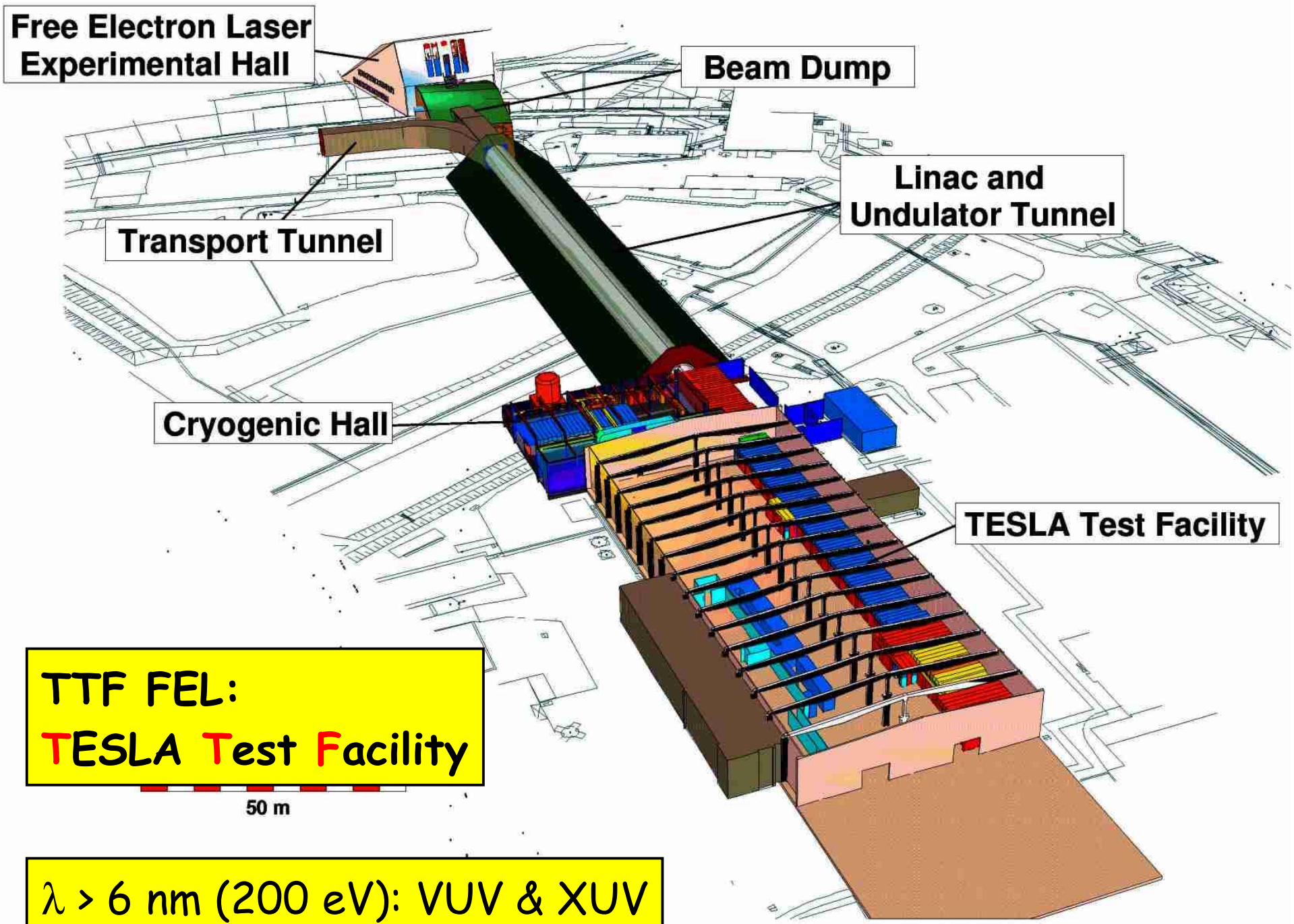

TTF FEL:
TESLA Test Facility

λ > 6 nm (200 eV): VUV & XUV

Some basic TTF2 milestones

- Now — Commissioning
- July 2004 — First beam through undulator
- Oct. 2004 — First Lasing @ ca. 30 nm
- Dec. 2004 — FEL Saturation @ ca. 30 nm
- Jan. 2005 — First period for FEL pilot users

FERMI@ELETTRA (1.2 nm)

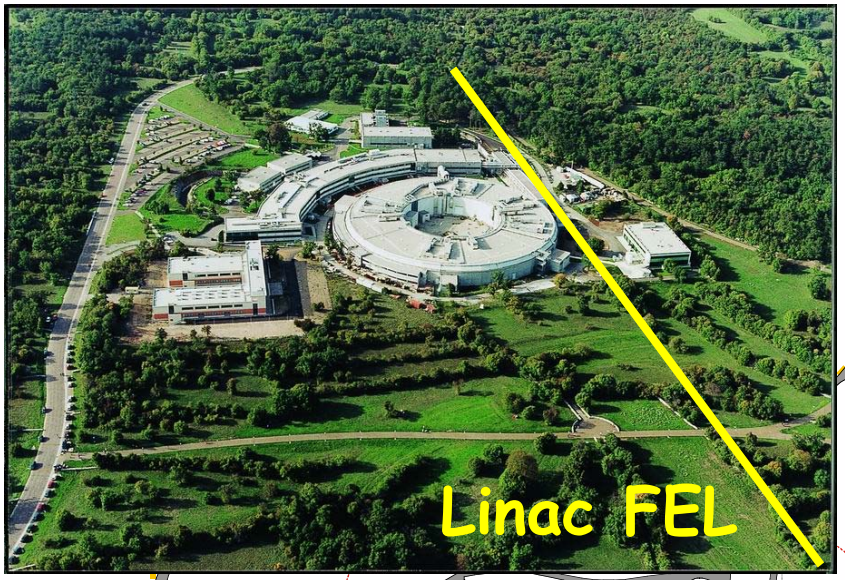

TESLA X-ray FEL

elettra

λ > 0.85 Å (14 keV): X-rays

linear collider

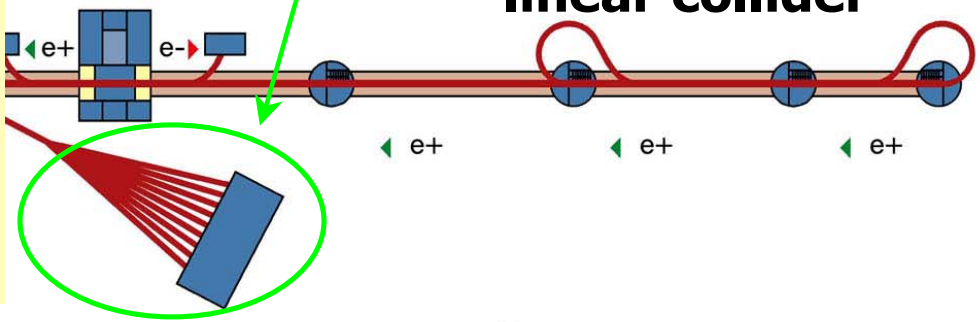

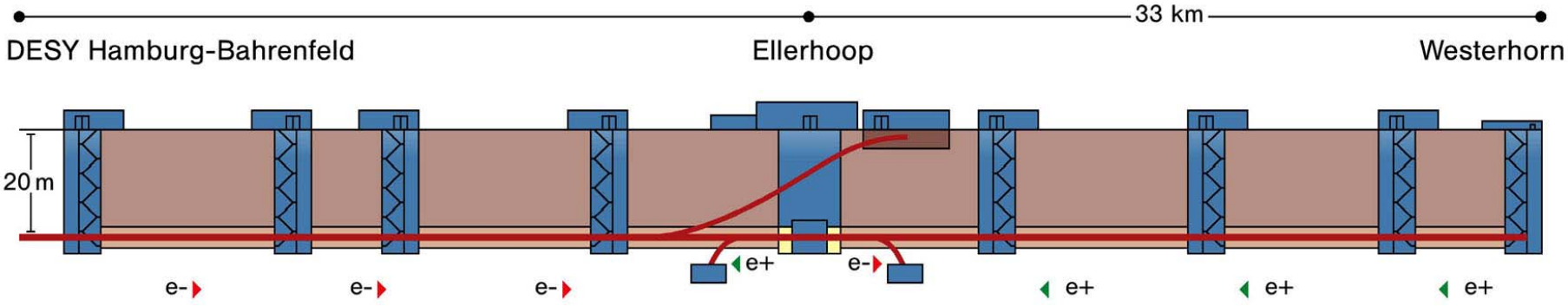

Side view

René Bakker

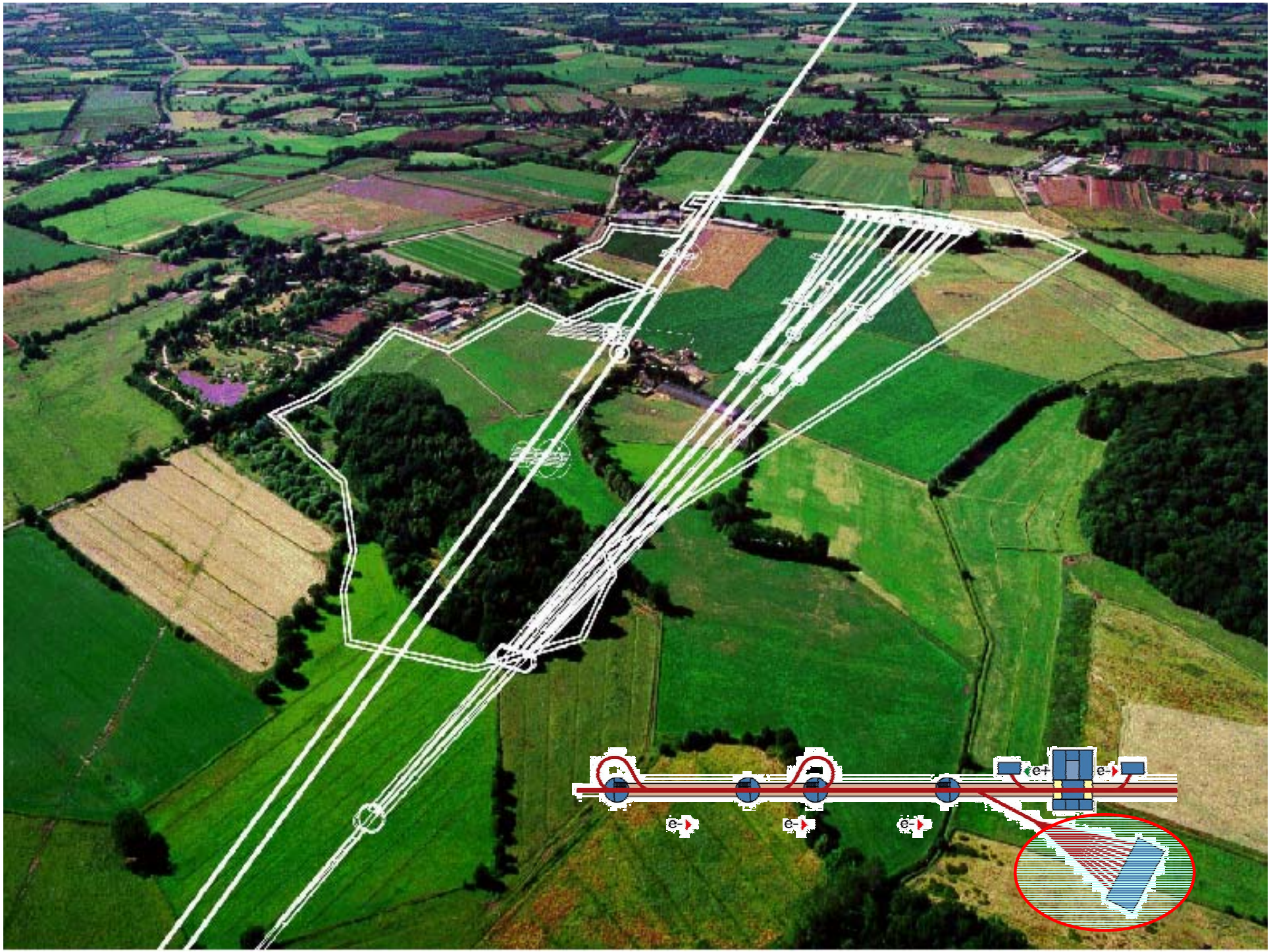
e-
e-
e-
e+
e+

The SASE FEL Scheme

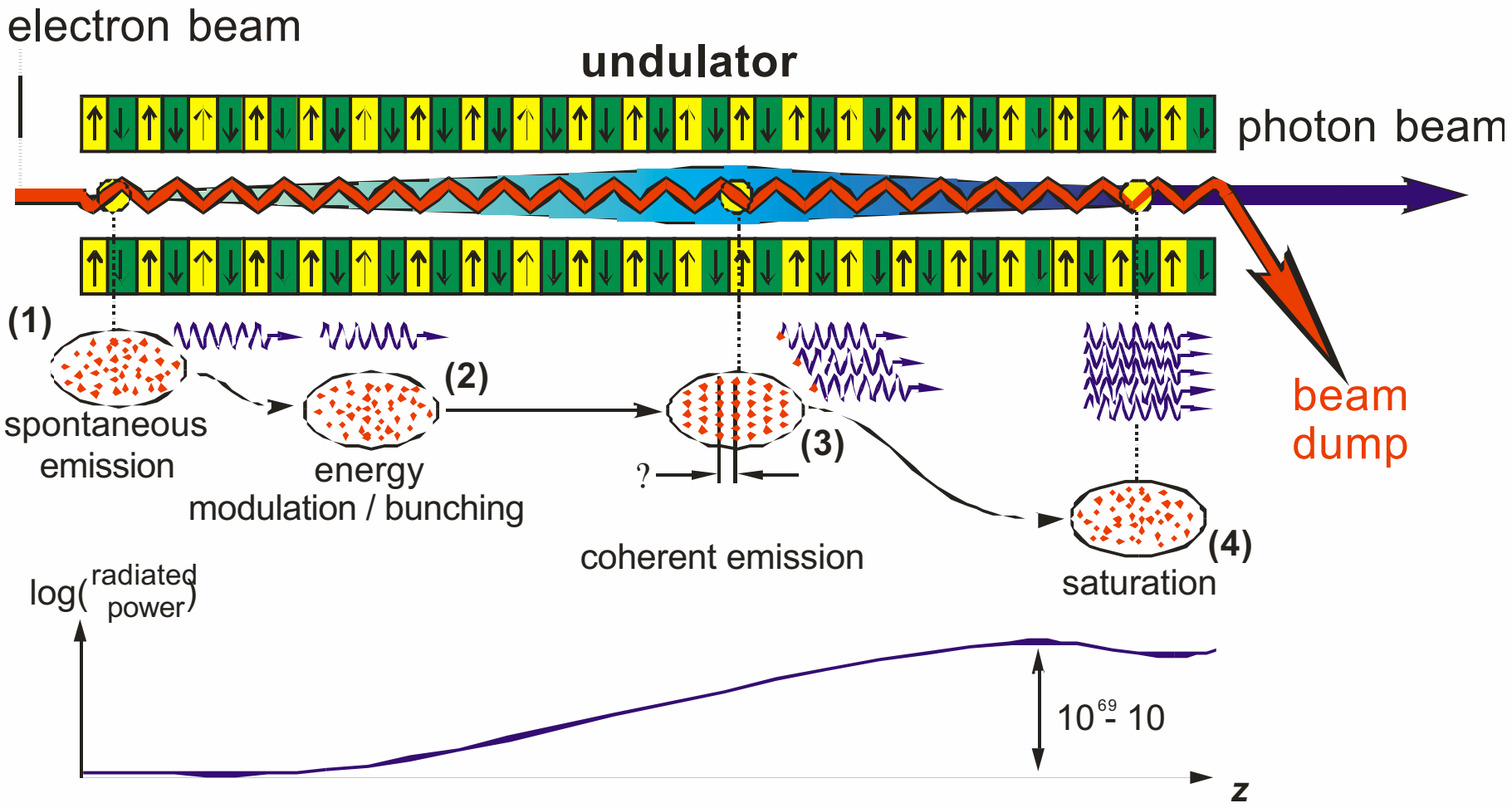

Overall Spectrum

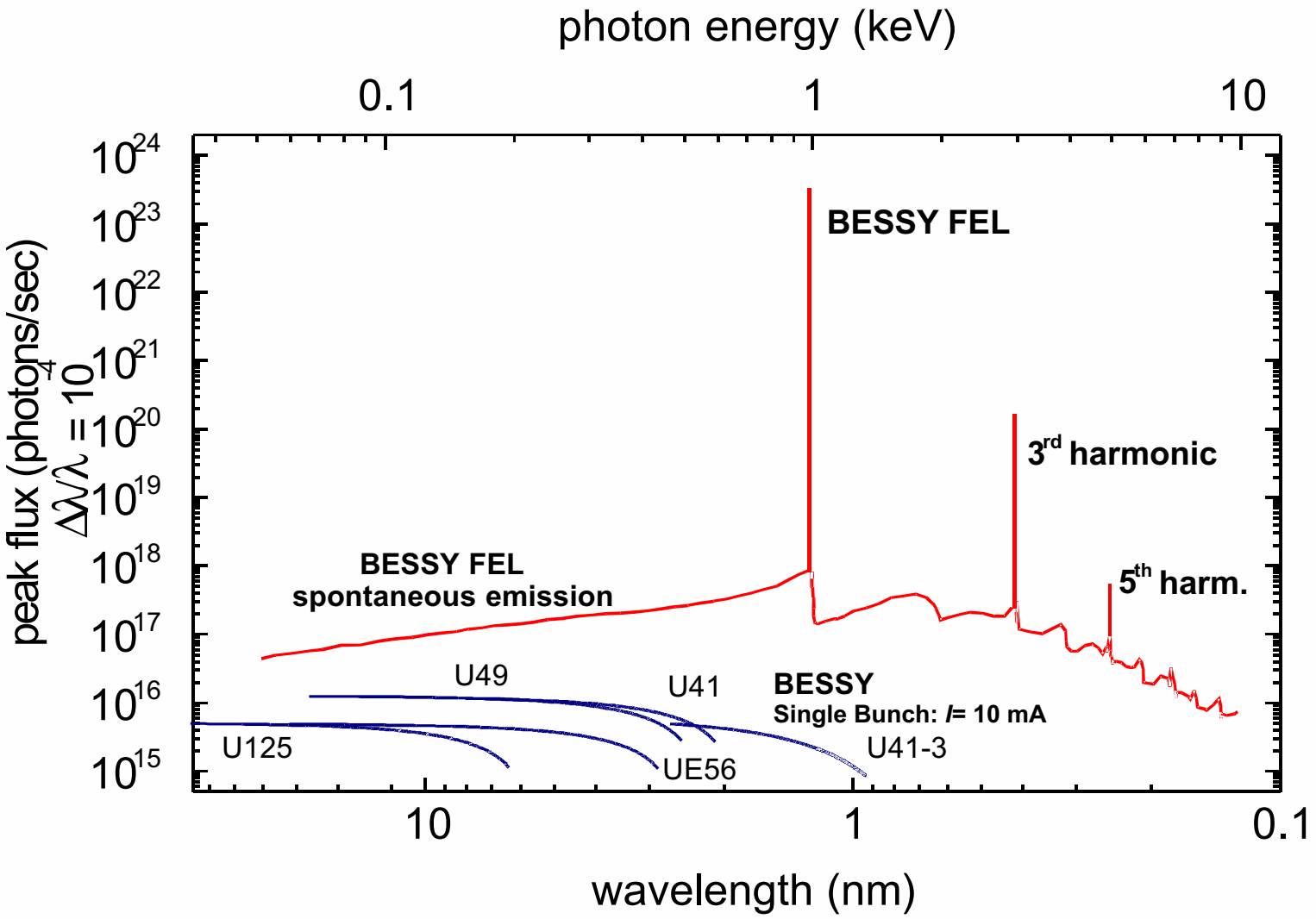

Short Bunch Generation in the SLAC Linac

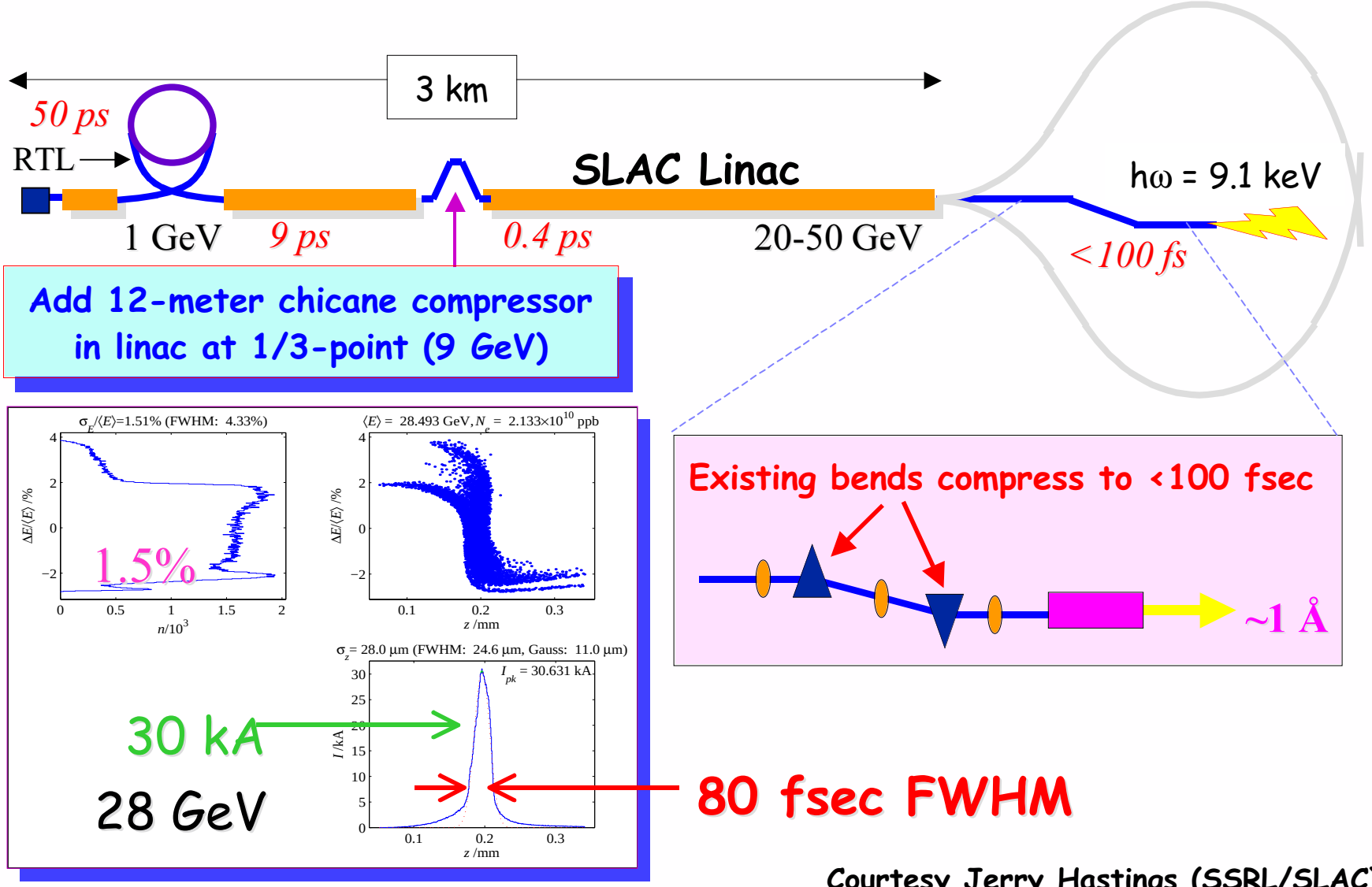

Courtesy Jerry Hastings (SSRL/SLAC)

TTF1: Observed Results

Energy of the μ–pulse along the undulator

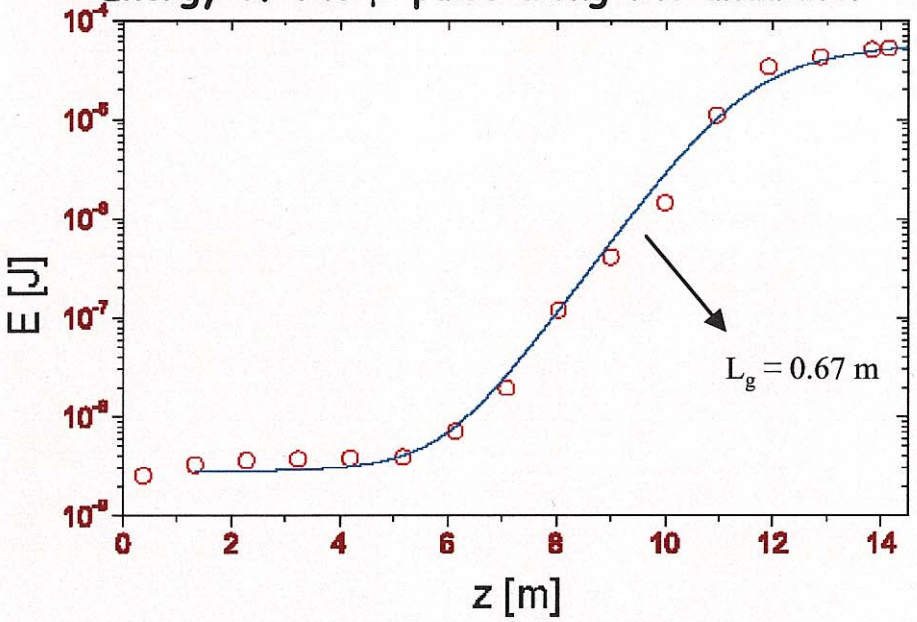

Energy fluctuation along the undulator

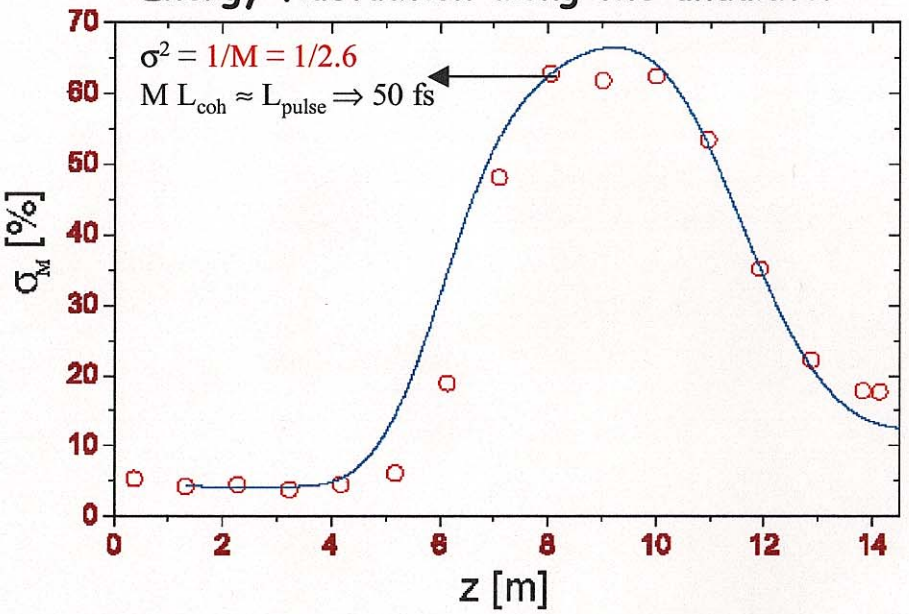

Average energy in the radiation pulse versus undulator length

Fluctuations of energy in the radiation pulse versus undulator length

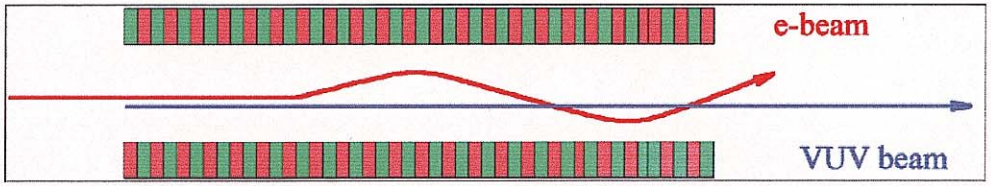

Correctors in the undulator were used to control the length of the interaction between electron beam and radiation

TESLA

Courtesy Bart Faatz (DESY)

Output properties

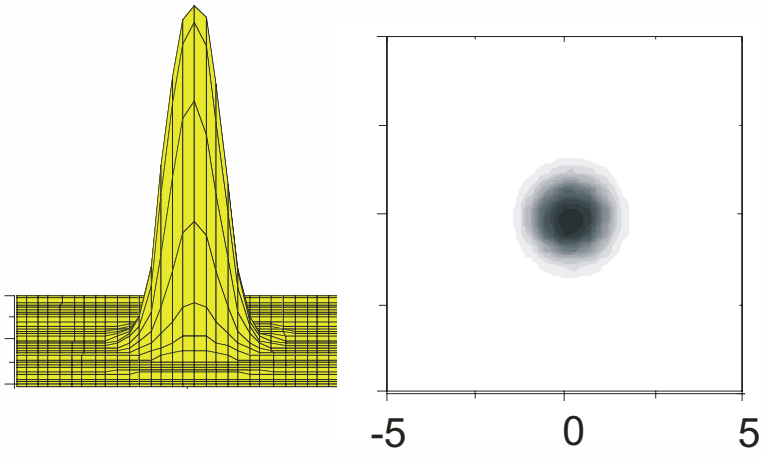

Transverse:

diffraction limited TEM_{00} mode

Longitudinal:

spikes

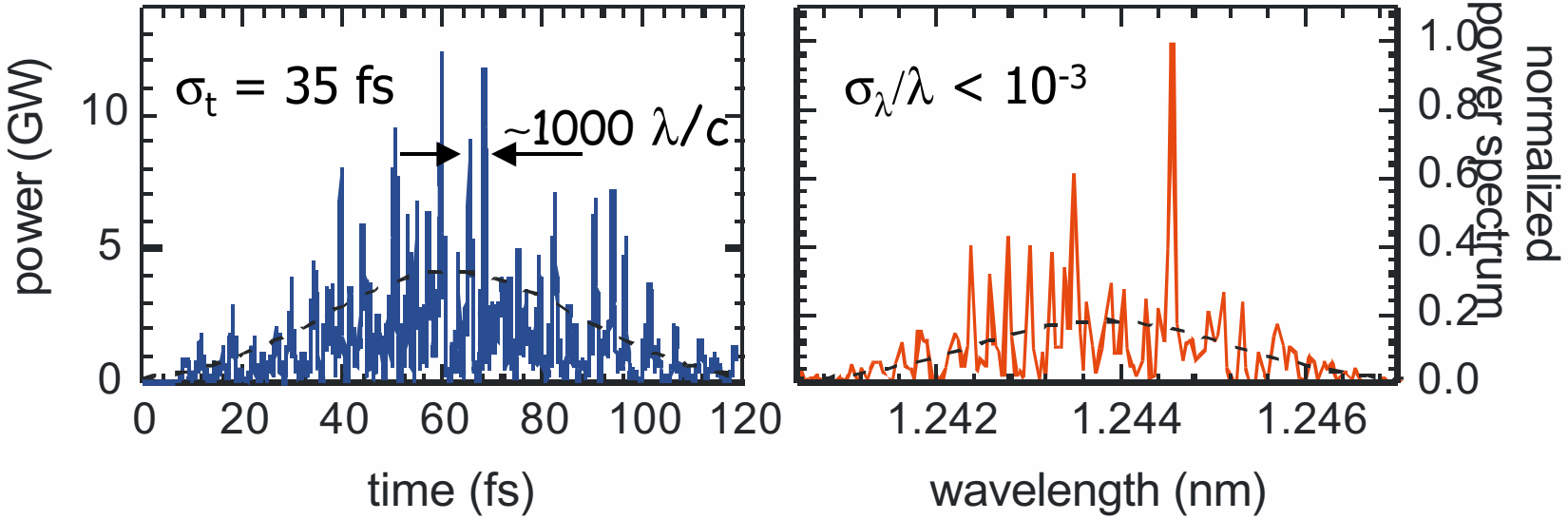

TTF1: Spectrum

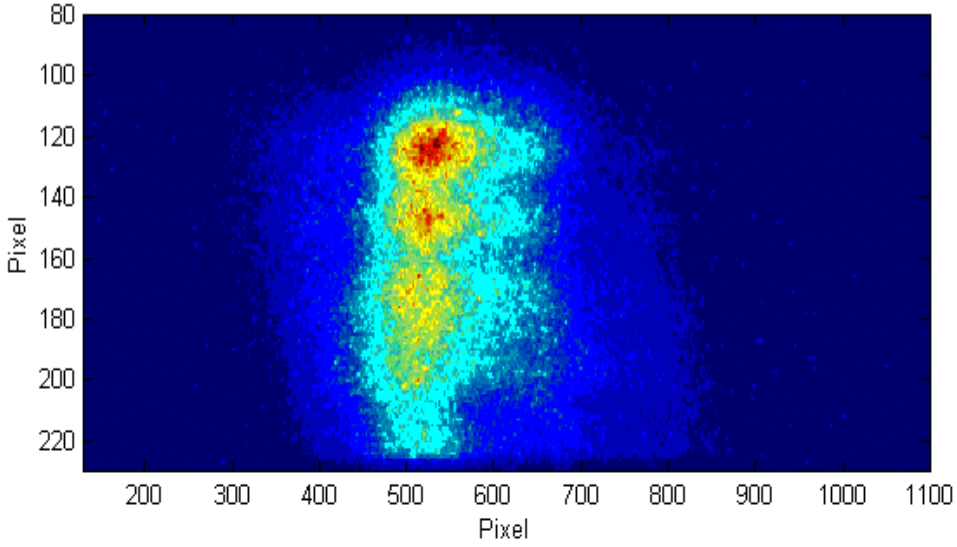

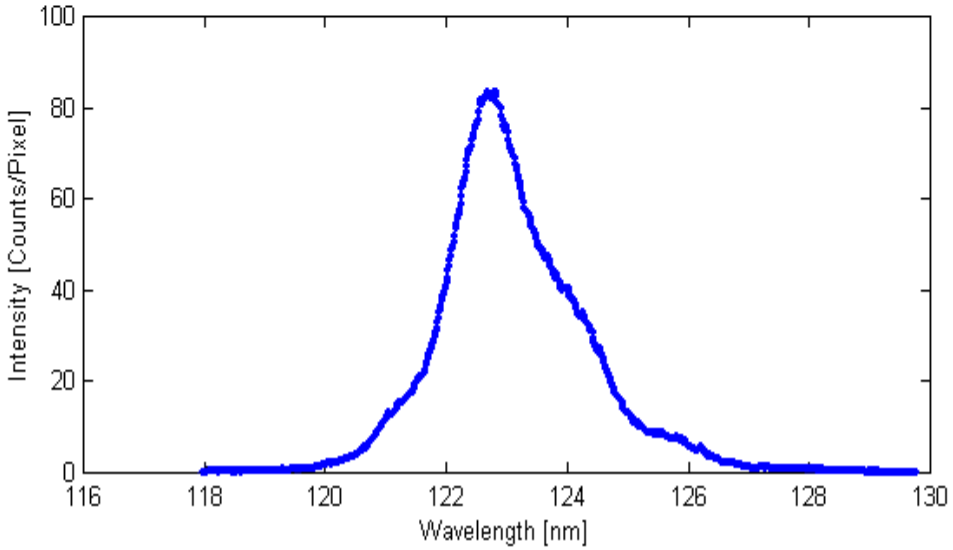

Between 2 and 3 spikes

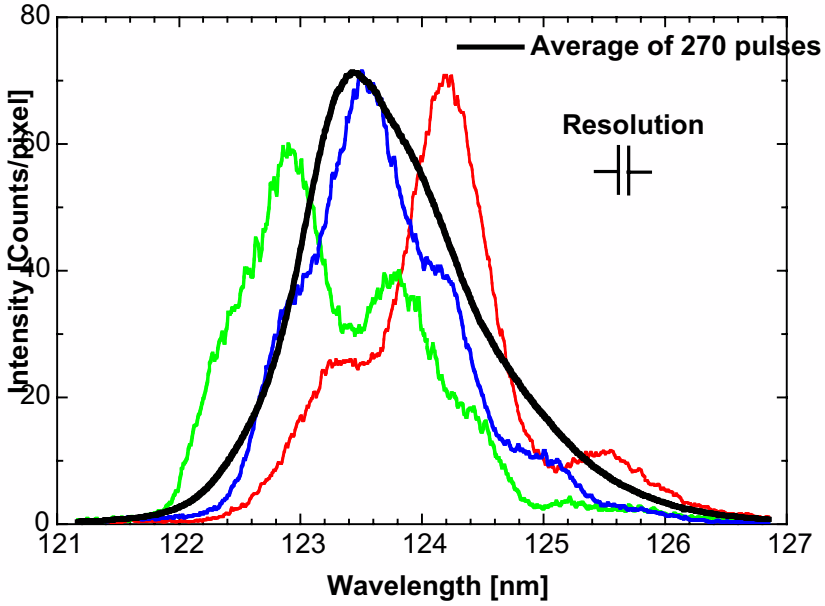

Courtesy Bart Faatz (DESY)

TTF1: Exp. vs Simulation

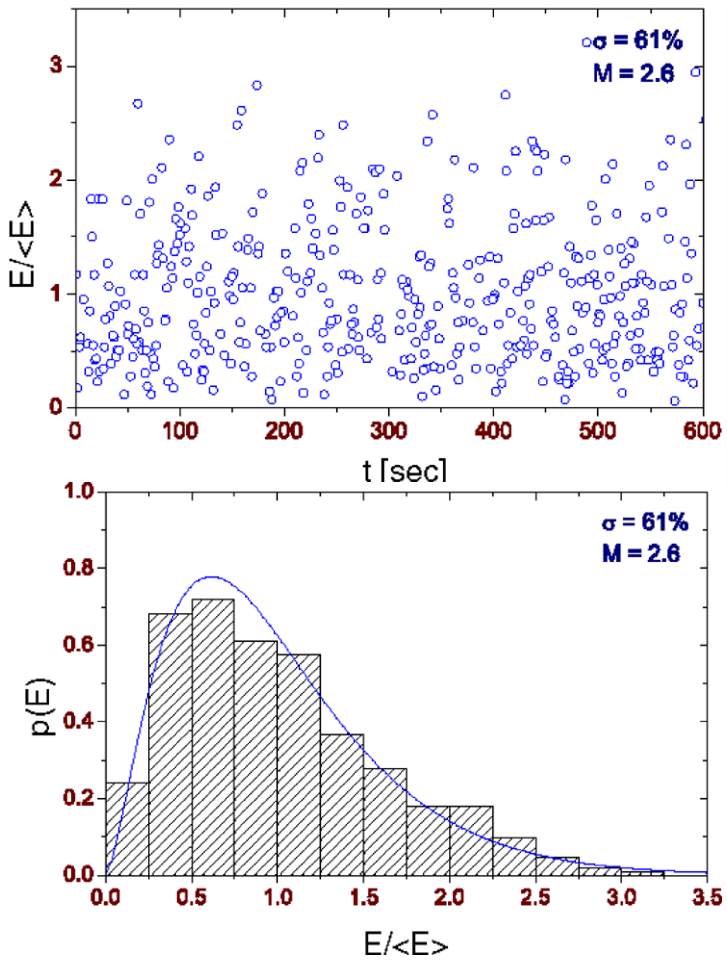

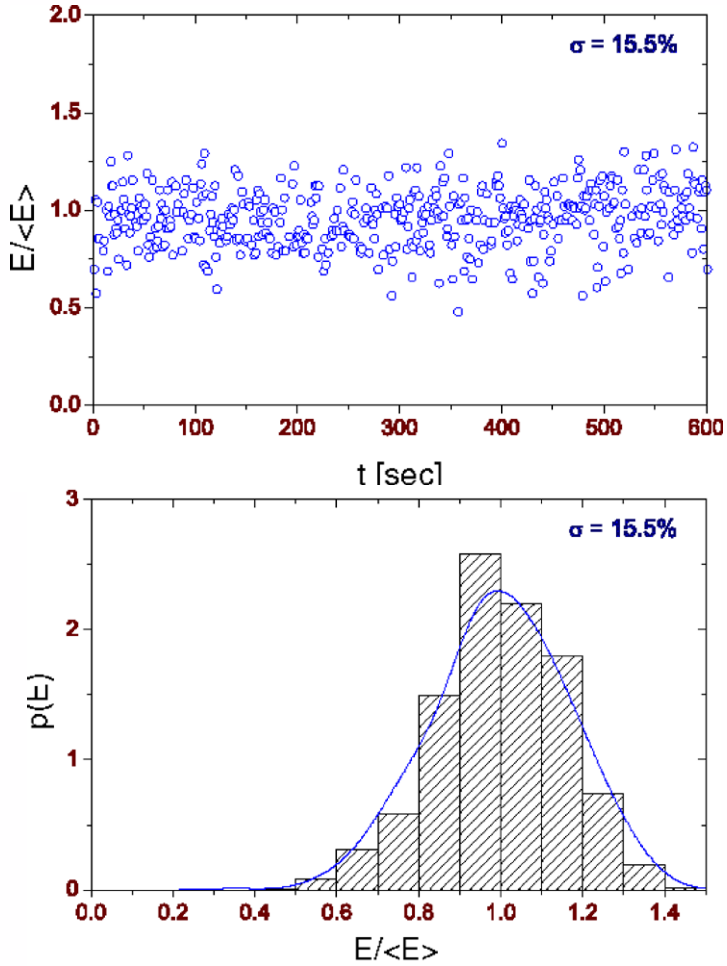

Signal from the radiation detector (top figures) and corresponding probability distributions (bottom figures) for linear (left) and saturation (right) regime. Solid curves represent simulation results with code FAST.

Courtesy Bart Faatz (DESY)

Tuning of the pulse-length

TESLA

Modes:
M ≅ 2 - 3

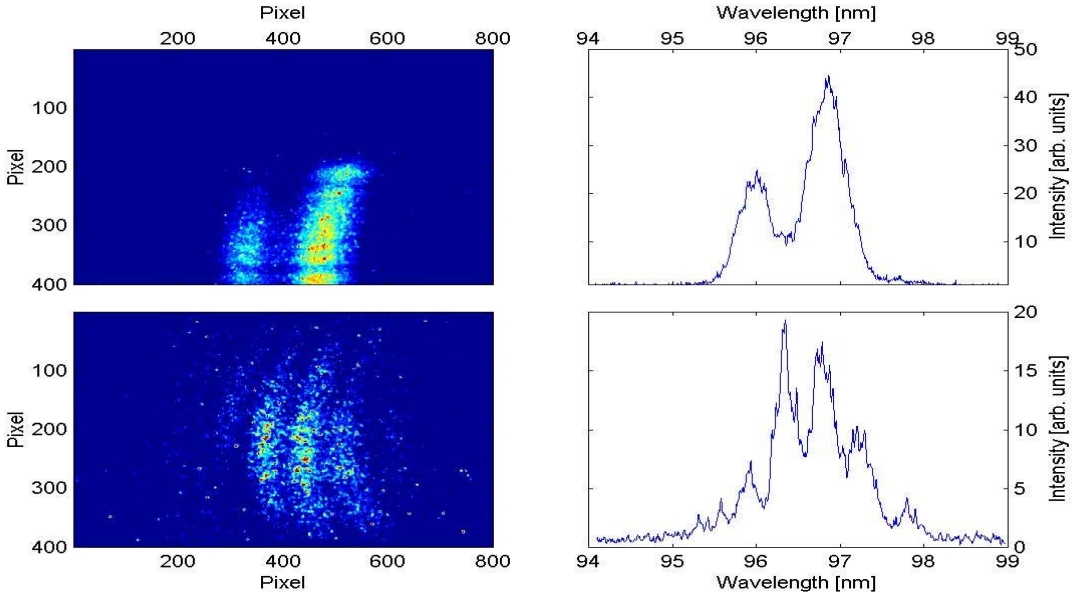

Modes:
M ≅ 7 - 10

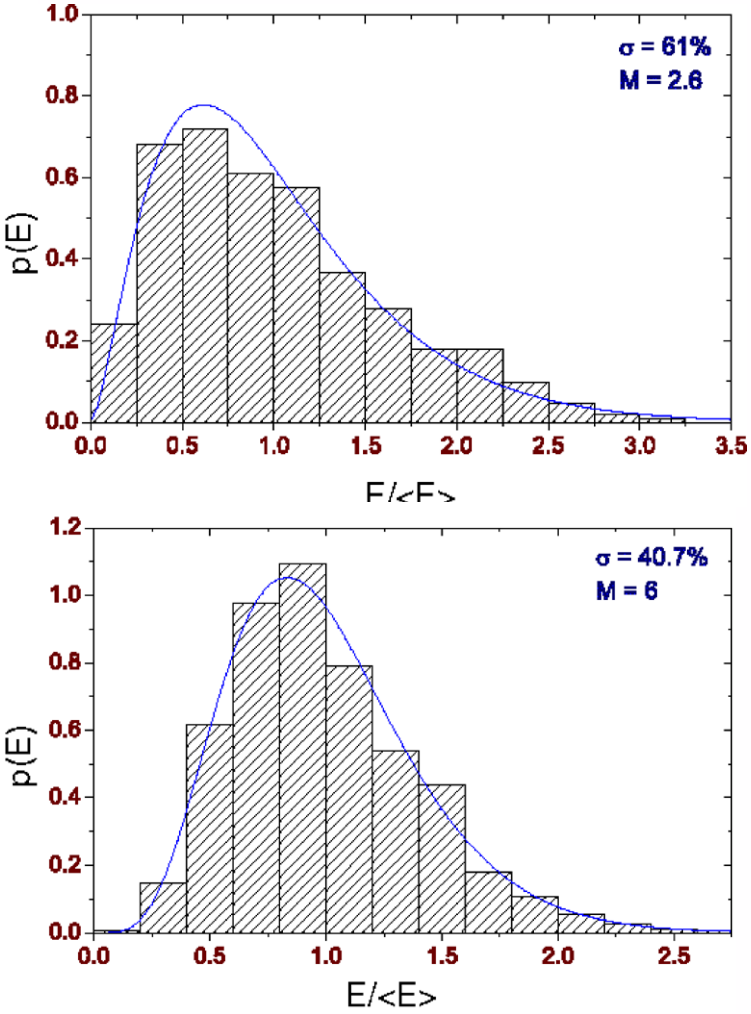

Left figures – spectral measurement. Bottom figures – probability distributions of the radiation energy in the linear regime. Solid curves represent gamma distribution.

Courtesy Bart Faatz (DESY)

Pulse Slicing

For the LCLS: Pulse-length reduction down to 3 fs

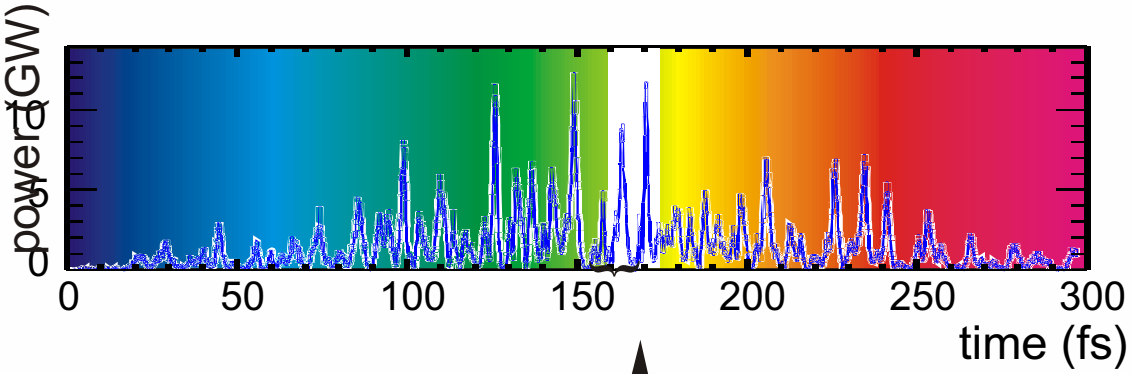

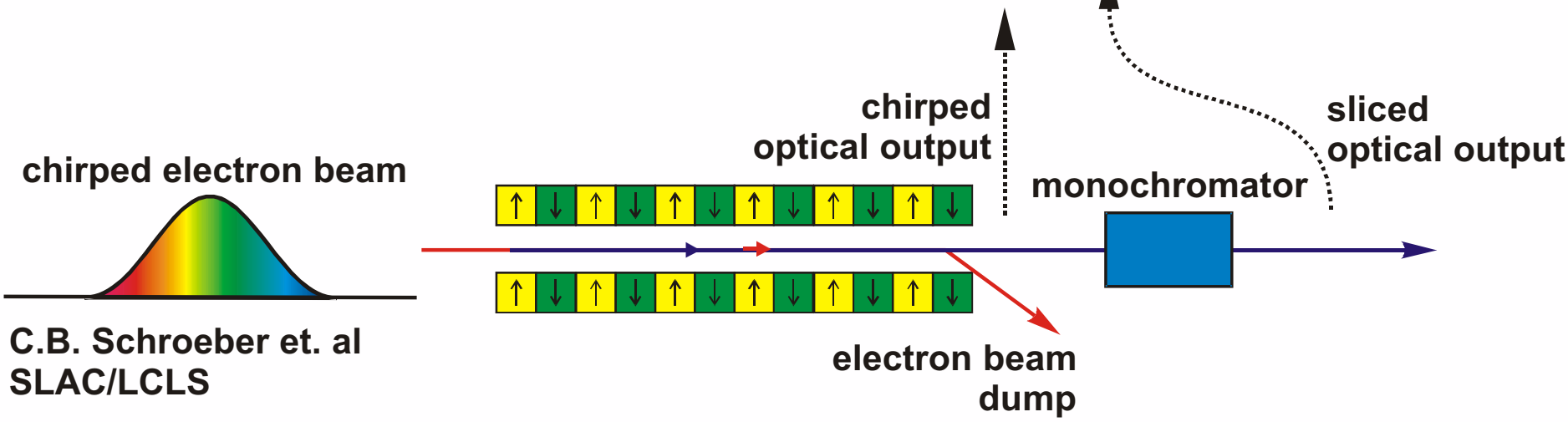

C.B. Schroeber et. al
SLAC/LCLS

Seeding: 2-stage FEL

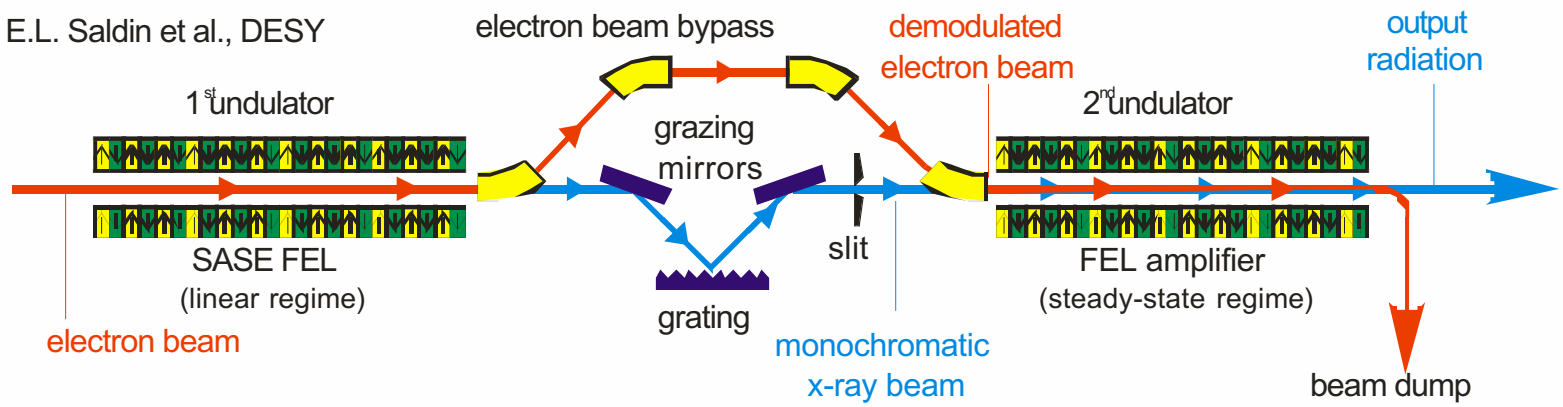

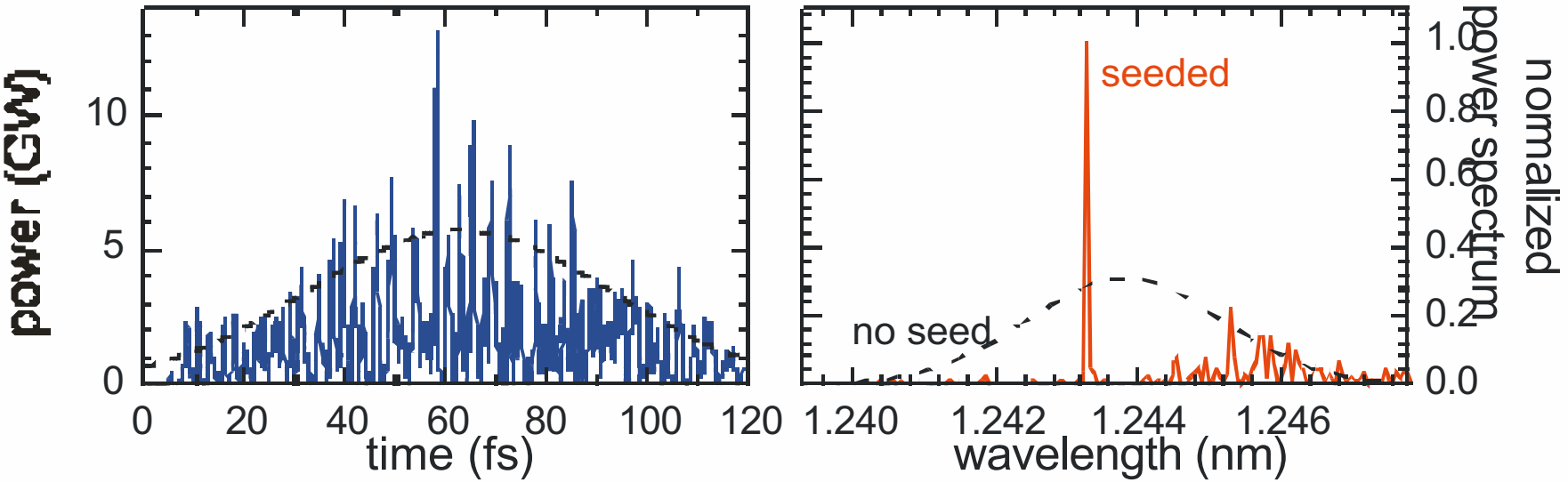

Seeding: HGHG

High Gain Harmonics Generation

→ an FEL is an excellent harmonics generator

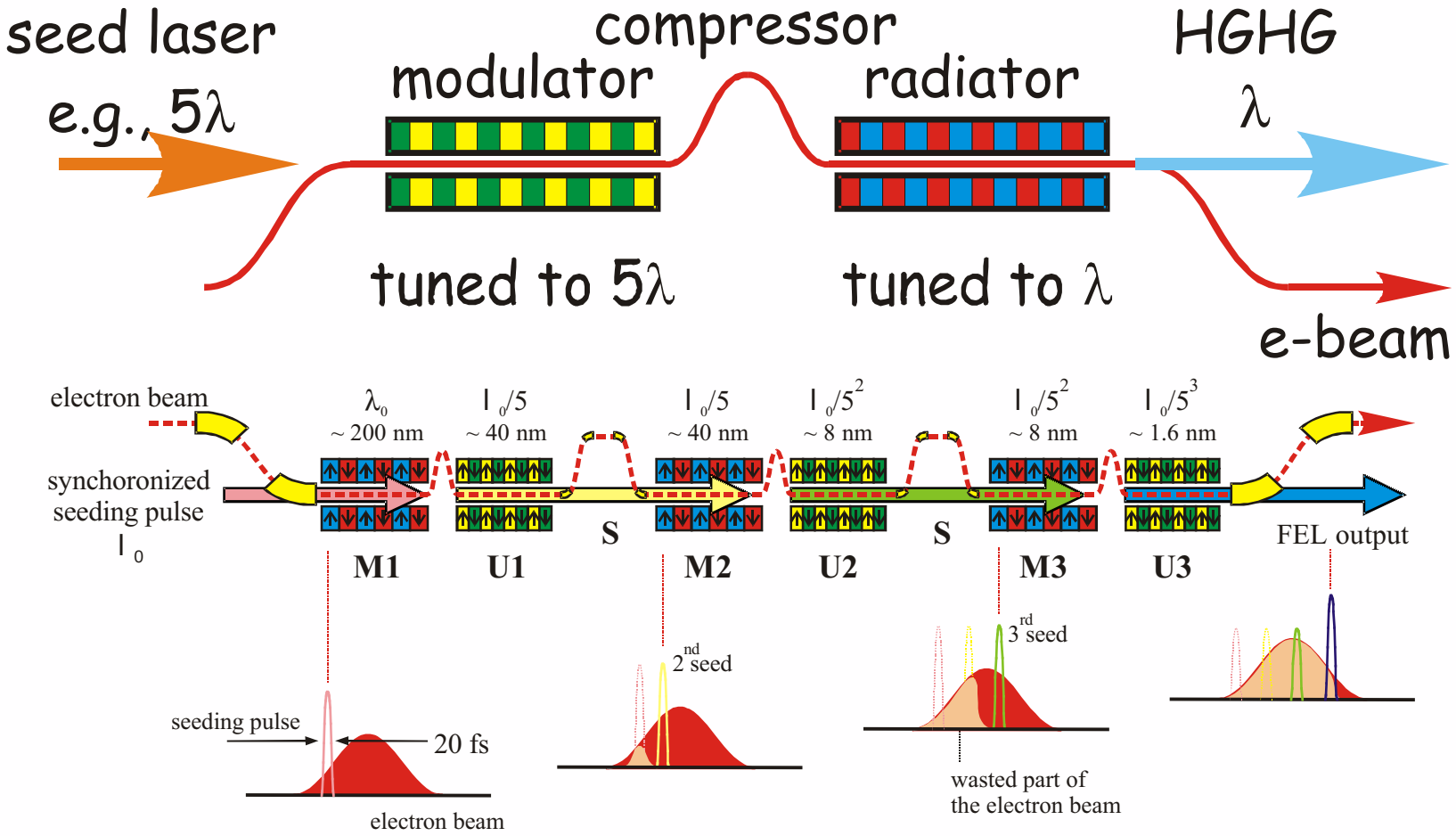

Spectrum of HGHG and SASE at 266 nm under the same electron beam condition

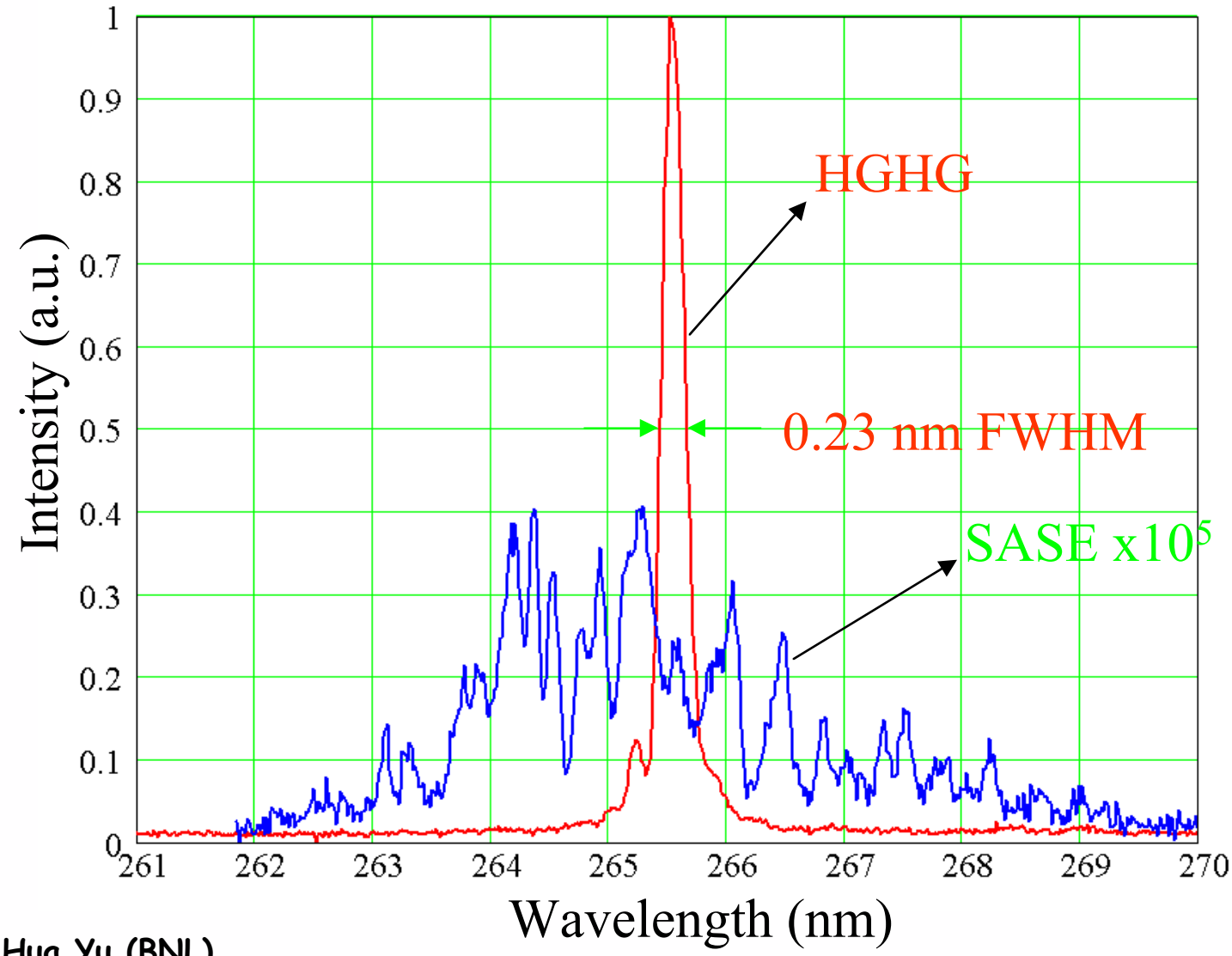

Courtesy Li Hua Yu (BNL)

Shot to Shot Intensity Fluctuation

Shows High Stability of HGHG output

SASE

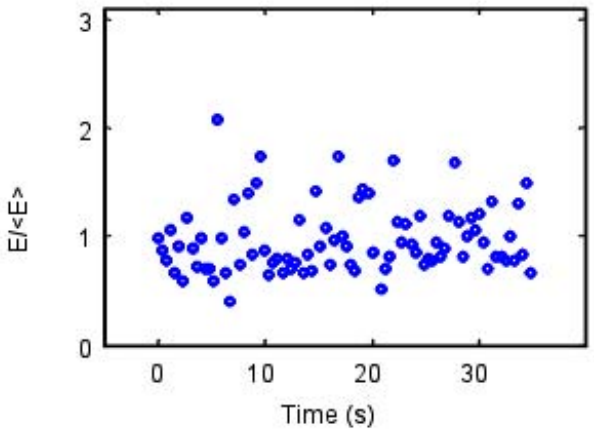

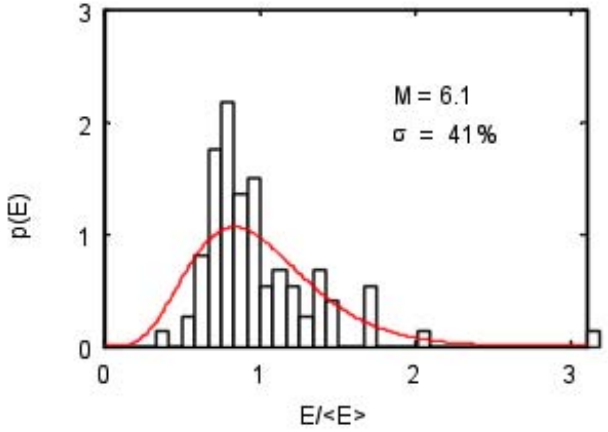

HGHG

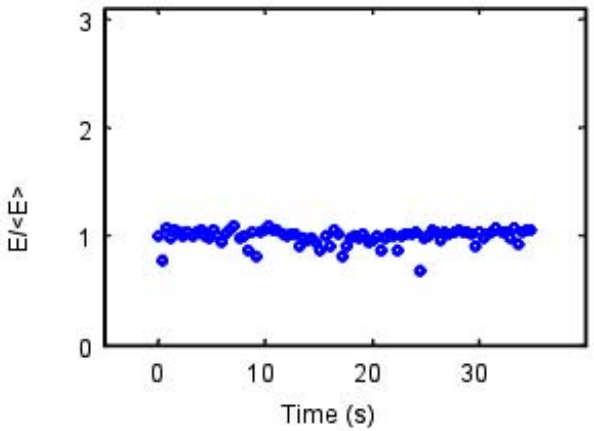

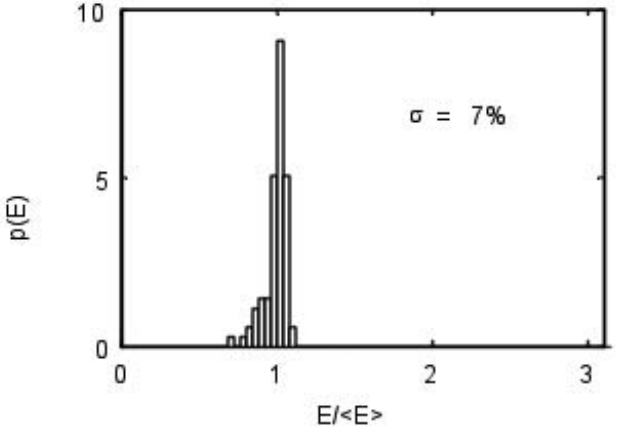

Courtesy Li Hua Yu (BNL)

Perspective

A promising source that still needs development

- High peak-power:
  - 10 to 100 GW or 10^{13} to 10^{14} photons/pulse
- Short pulses
  - 200 fs (VUV) - 50 fs (X-ray)
  - later possibly down to 20 fs or even 5 fs
- Full transverse coherence
- Large longitudinal coherence

  $\forall\ \Delta\lambda/\lambda < 10^{-3}$, later down to 10^{-4} or 10^{-5} (seeded)
- Flexible timing/polarization

Related topics:

- Synchronization with fs-lasers
- Seeding options
- Increase of the average power

Generation and applications of XUV harmonics

Marco Bellini
(bellini@ino.it)

Istituto Nazionale di Ottica Applicata
(INOA)

European Laboratory for Non Linear Spectroscopy (LENS)

Largo E. Fermi, 6
Firenze
ITALY

Harmonic generation

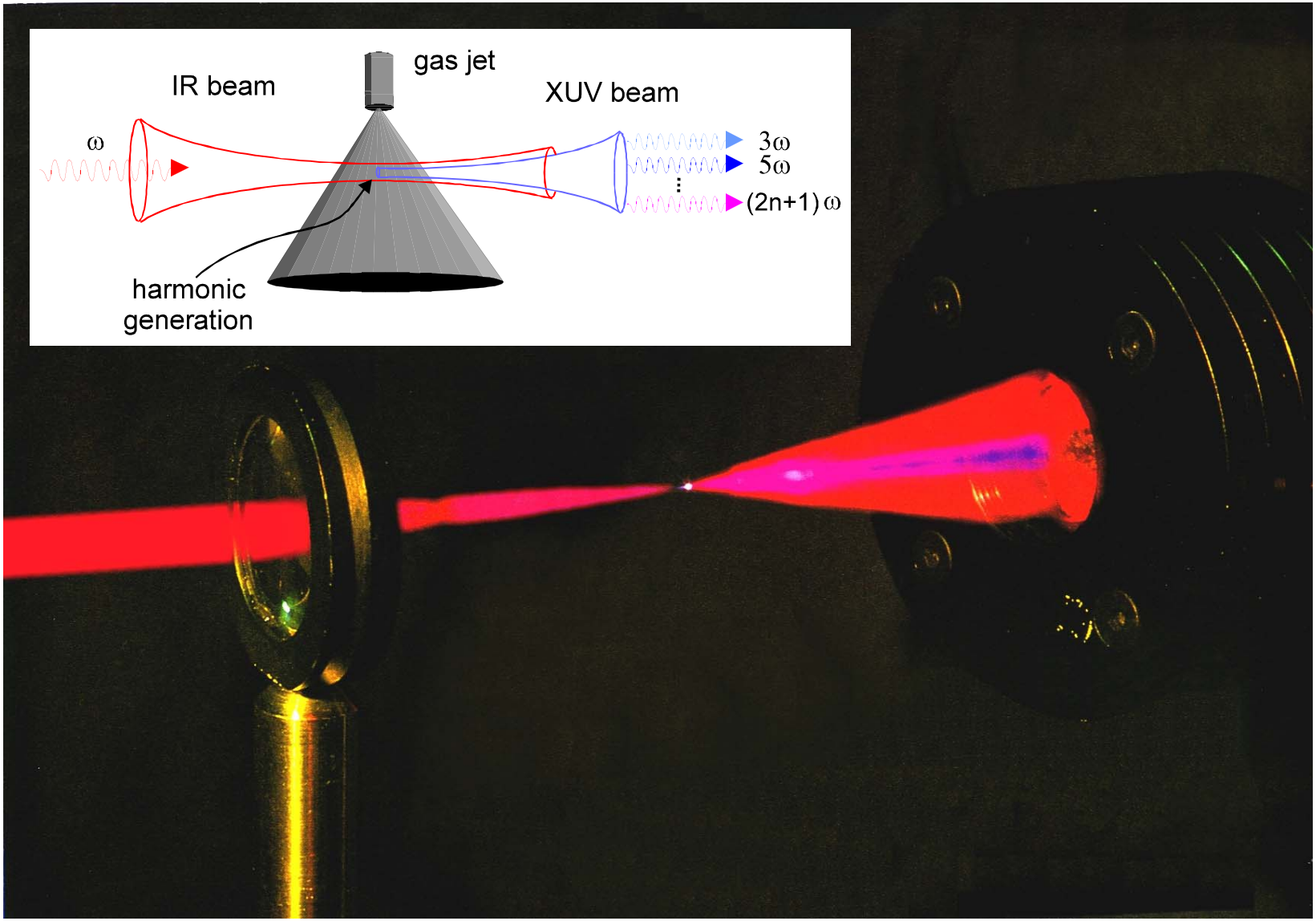

Harmonic spectra

I) Exponential decrease for the first orders

II) Extended "Plateau" with costant intensity

III) Fast decrease at the end of the "plateau"

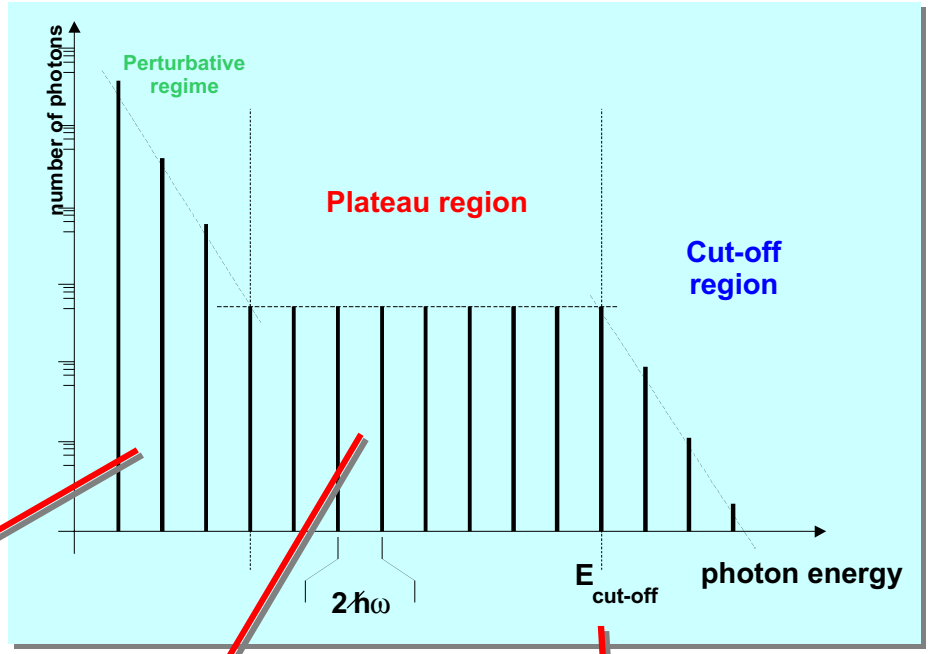

$I_q \approx I^q$

As predicted by lowest order perturbation theory

Plateau

Stable intensity over many orders

$E_{cut\text{-}off}$

End of the region of good efficiency

Physical mechanism I

Semi-classical model

P. B. Corkum, *Phys. Rev. Lett.*, **71** ,1994 (1993)

I) Tunnel ionization

II) Oscillations in the laser field

III) Recombination with the ion

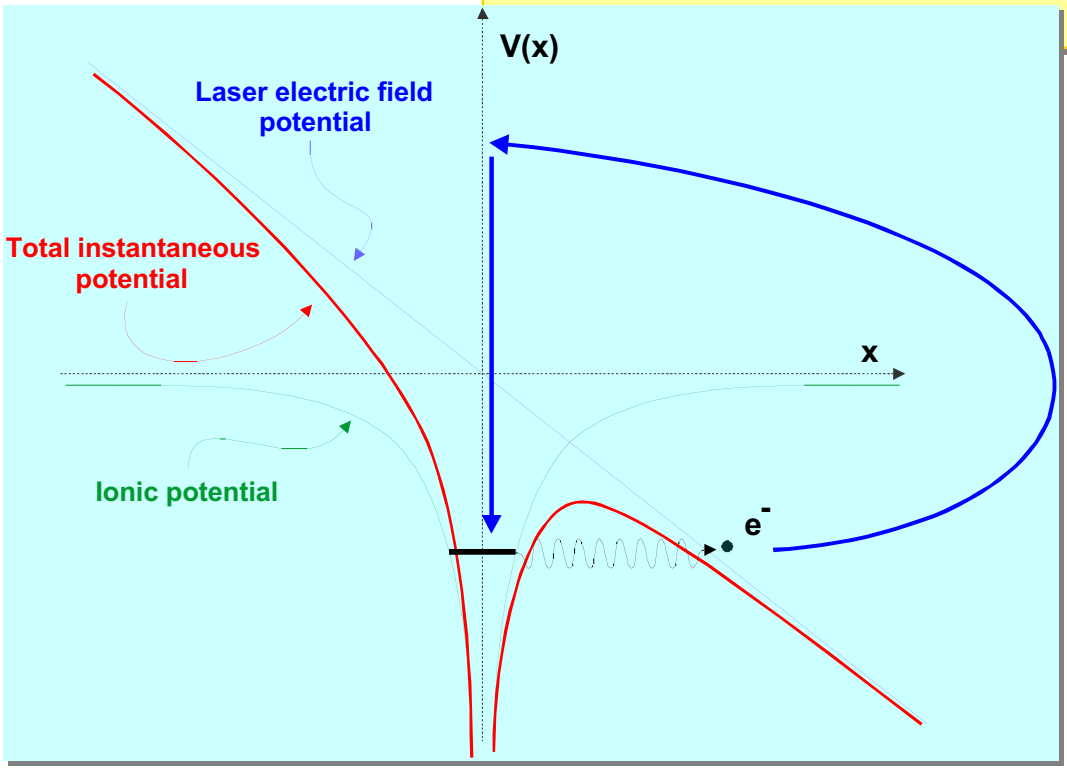

Classical motion of an electron in a laser field I

Force on the electron: $F = e\left(E_L + \mathrm{v} \times B_L\right)$ but $\begin{cases} |B_L| = \dfrac{|E_L|}{c} \\ \mathrm{v} << c \end{cases}$ $\Rightarrow$ $F \approx eE_L$

$E_L(t) = E_0 \sin(\omega_L t + \varphi)$

Field is switched on at t=0

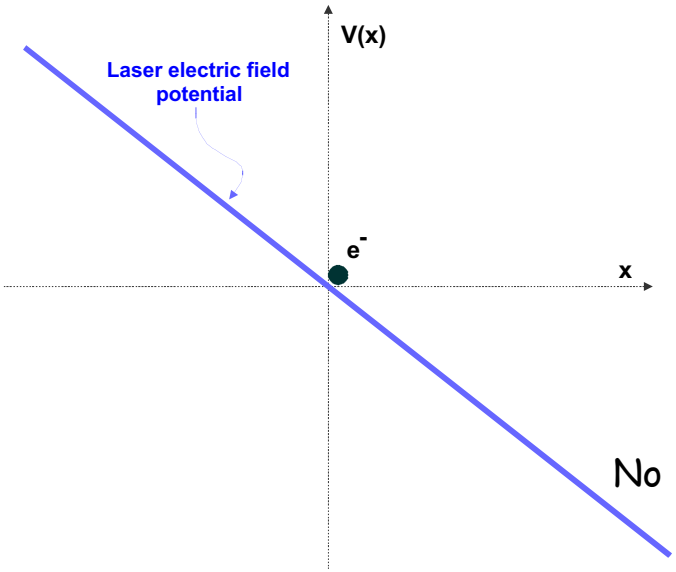

1-Dimensional motion:

(linear laser polarization along x)

$F = m\ddot{x}$ $\quad \ddot{x} = \dfrac{eE_0}{m}\sin(\omega_L t + \varphi)$

$\Downarrow \quad (e = m = 1)$

No initial velocity v(0)=0

$$\mathrm{v}(t) = -\frac{E_0}{\omega_L}\cos(\omega_L t + \varphi) + \frac{E_0}{\omega_L}\cos(\varphi)$$

$$\mathrm{x}(t) = -\frac{E_0}{\omega_L^2}\left(\sin(\omega_L t + \varphi) - \sin(\varphi)\right) + \frac{E_0}{\omega_L}\cos(\varphi)t$$

Start in the origin x(0)~0

Classical motion of an electron in a laser field II

$$x(t) = -\frac{E_0}{\omega_L^2}\left(\sin(\omega_L t + \varphi) - \sin(\varphi)\right) + \frac{E_0}{\omega_L}\cos(\varphi)t$$

Some electrons come back and recombine with the ion

Ionization energy
+
Residual kinetic energy
———————
Harmonic photon energy

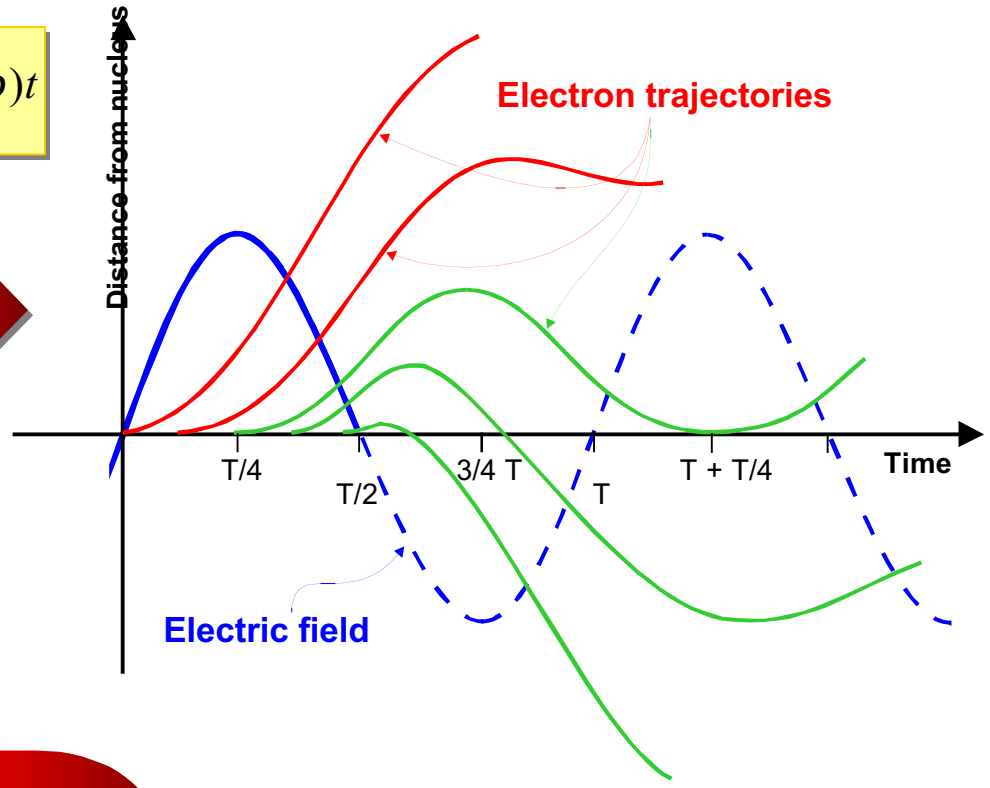

$$v(t) = -\frac{E_0}{\omega_L}\cos(\omega_L t + \varphi) + \frac{E_0}{\omega_L}\cos(\varphi)$$

Oscillation

Linear drift

Averaged kinetic oscillation energy $\langle v^2/2 \rangle$:

Ponderomotive Energy U_P

$$\left\langle E_{kin}^{osc} \right\rangle = \frac{E_0^2}{2\omega_L^2}\left\langle \cos^2(\omega_L t + \varphi) \right\rangle = \frac{E_0^2}{4\omega_L^2} = U_P$$

Linear vs. circular polarization

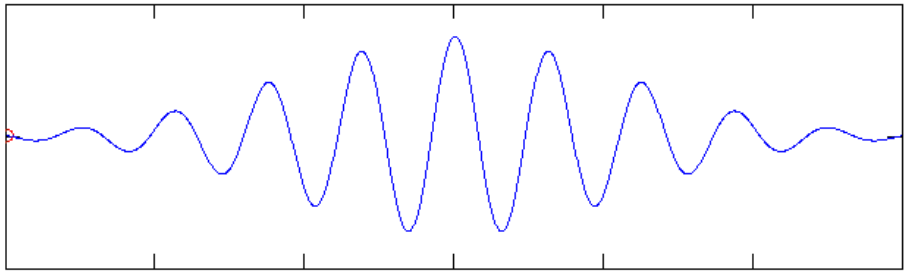

Linear polarization

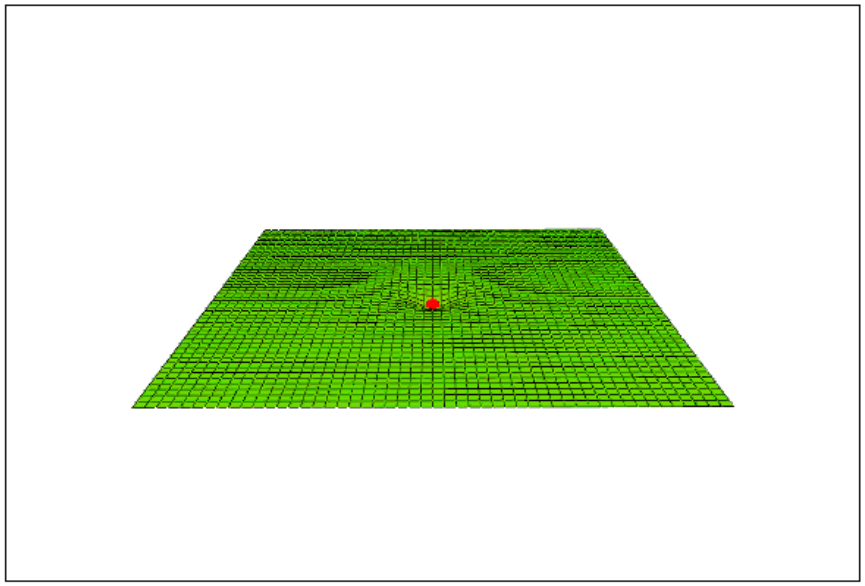

Circular polarization

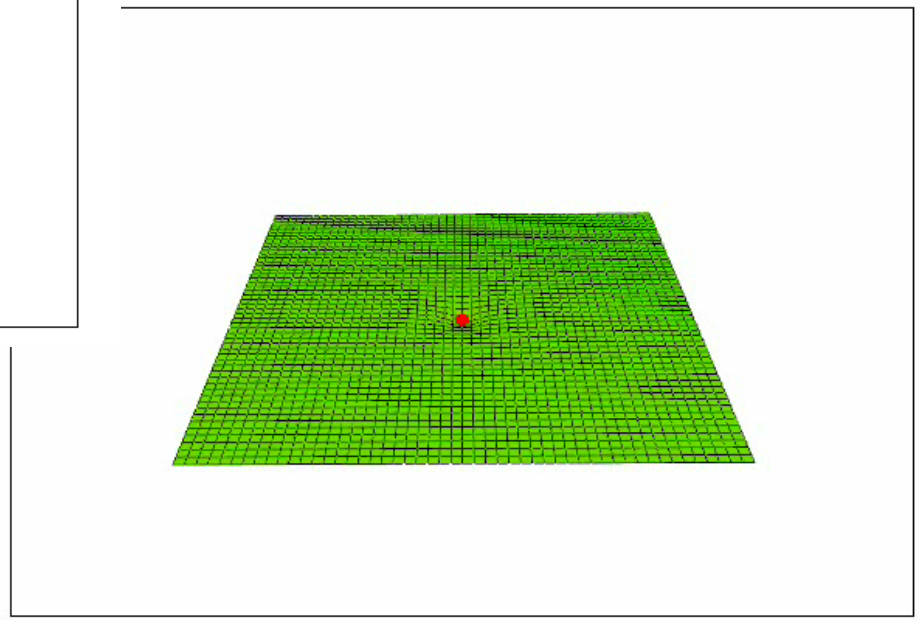

Calculation of the cut-off energy

Find the conditions for maximum kinetic energy at the time of recombination t_r

I) Find t_r by imposing $x(t_r)=0$

II) Plot final kinetic energy=$v(t_r)^2/2$ vs. the time of "birth" of the electron

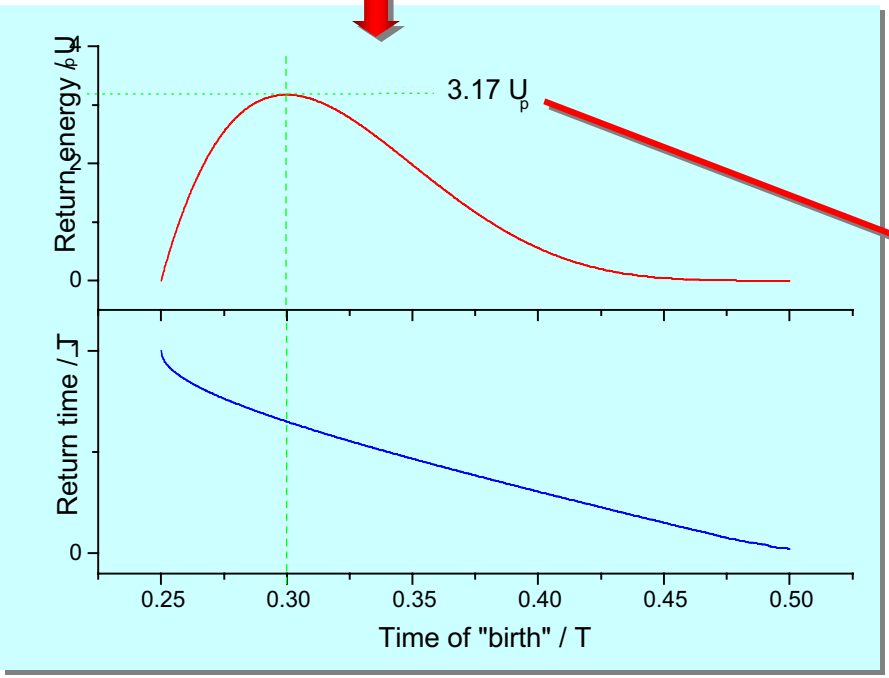

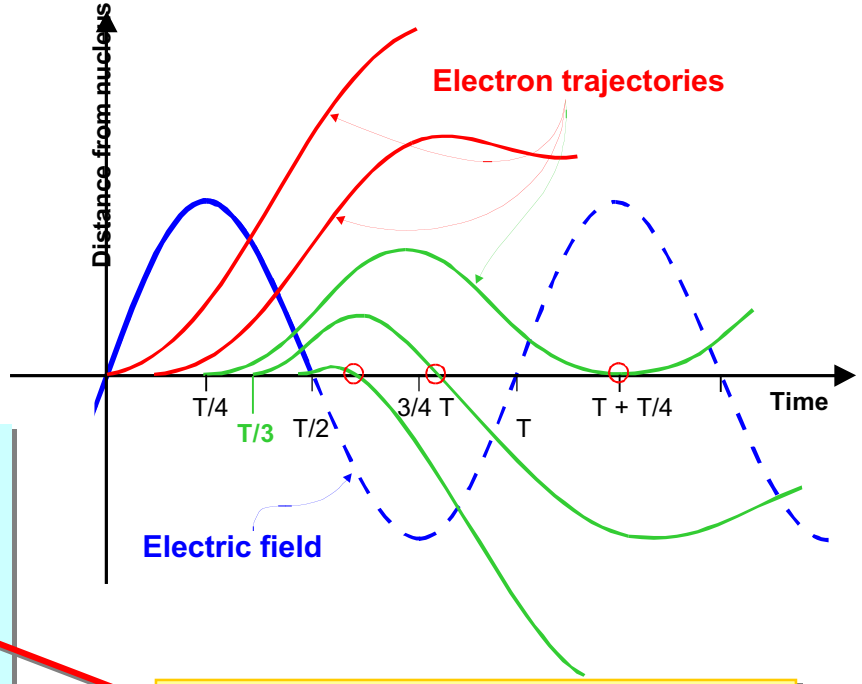

$$E_{cut\text{-}off} \approx I_p + 3U_p$$

I_p Ionization potential of the gas

$U_p \propto I\lambda^2$ Ponderomotive energy

Very high orders can be generated (XUV and soft X-rays)

Extending the cut-off

$$E_{cut\text{-}off} \approx I_p + 3U_p$$

I_p Ionization potential of the gas

$U_p \propto I\lambda^2$ Ponderomotive energy

Increase I_p

Use longer wavelengths

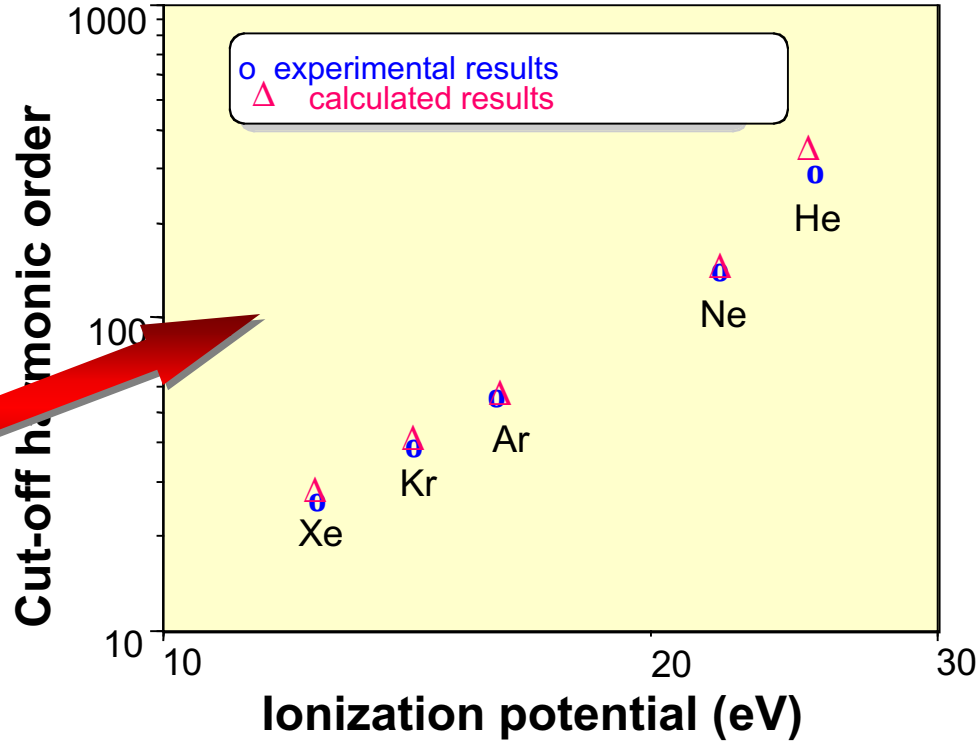

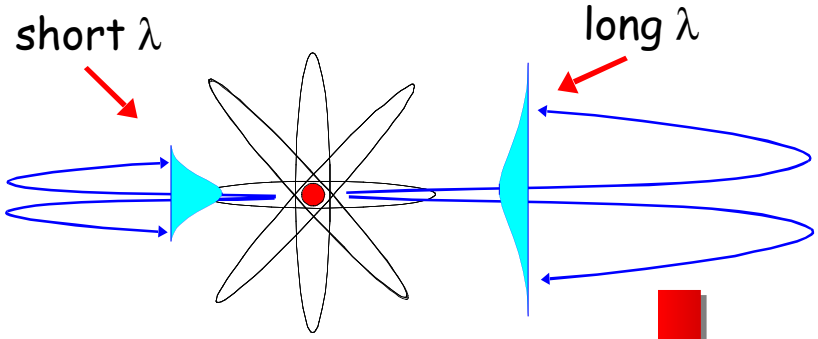

Use higher intensities

May increase $E_{cut\text{-}off}$ but lowers conversion efficiency

Neutral depletion

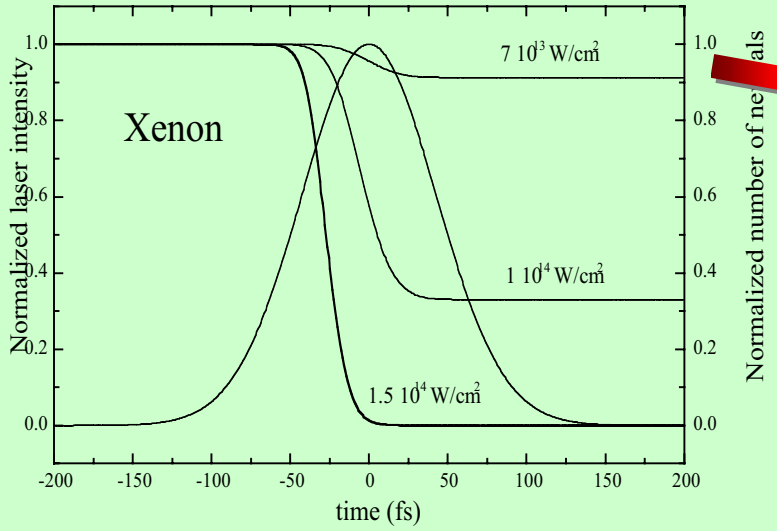

All the atoms can be completely ionized before the peak of the pulse

No neutral atoms left for harmonic generation

argon

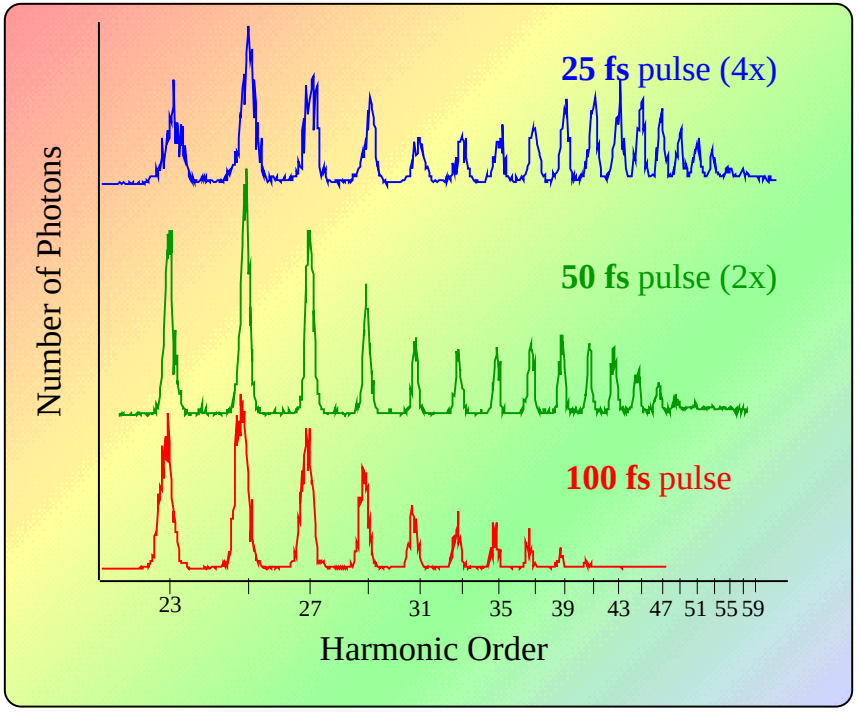

$W(I)$ Ionization rate

τ_p Pulse duration

$W(I_s)\tau_p \sim 1$

I_s

Saturation intensity

I_s increases with shorter pulses and hardly-ionized atoms

PRL 76,752 (1996)
PRL 77,1743 (1996)
PRL 78,1251 (1997)

Typical experimental setup

Harmonics are easy to produce

(if compared to synchrotron sources)

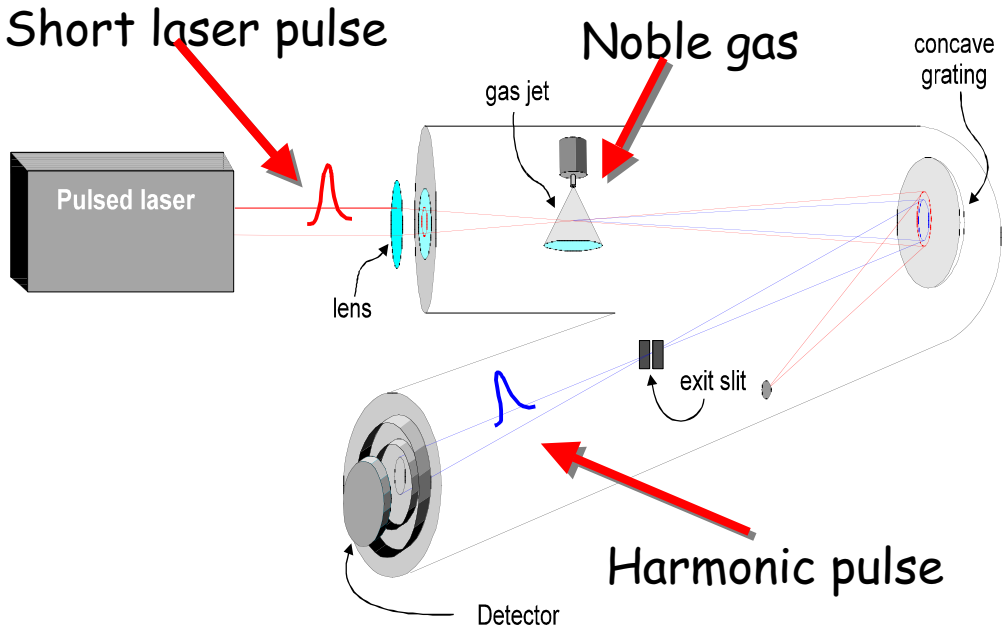

Heavy noble gases have higher polarizabilities

More efficient production of low orders

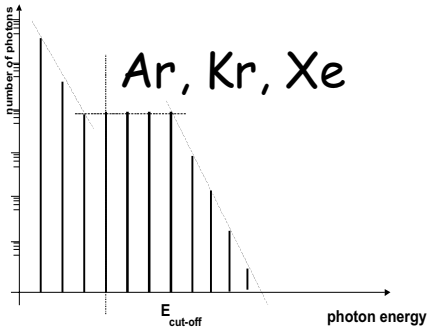

Light noble gases can stand higher intensities before full ionization

Highest orders

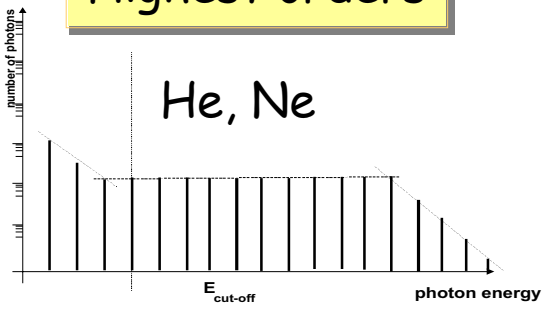

The VUV, XUV, and soft x-ray regions

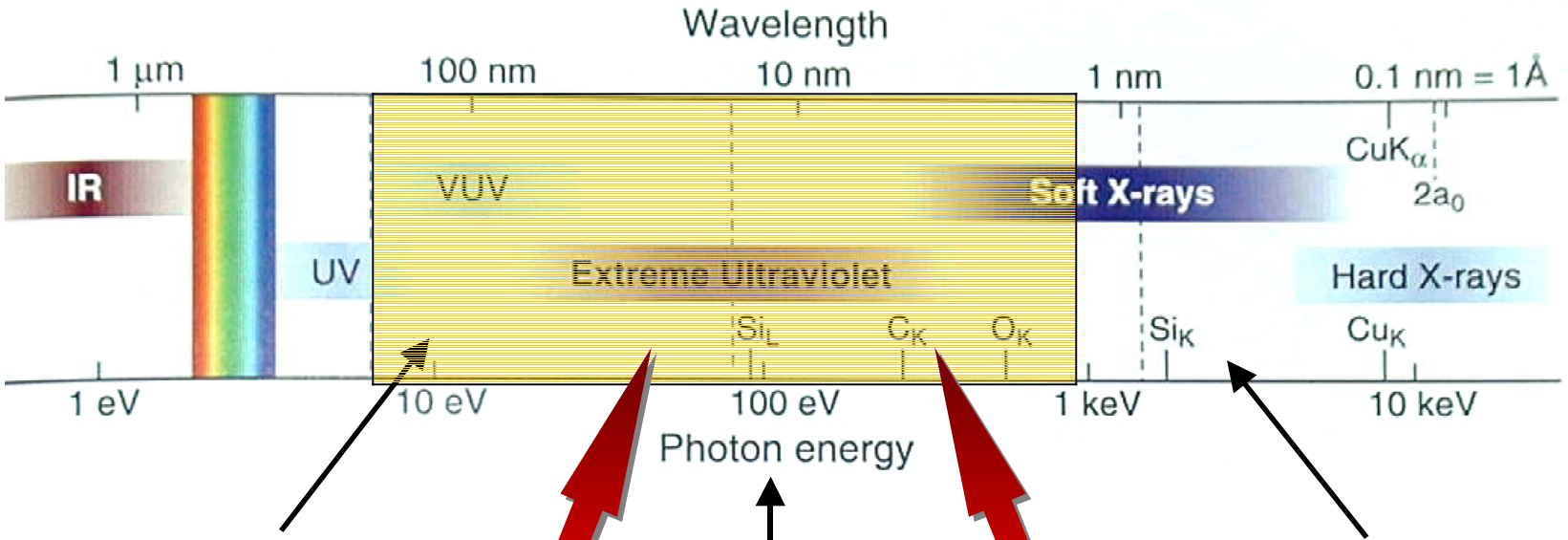

Vacuum-ultraviolet (VUV)
180 nm > λ > 50 nm
Absorbed by <<1 mm of air
Ionizing to many materials

Extreme-ultraviolet (XUV)
50 nm > λ > 5 nm
Ionizing radiation to *all* materials

Soft x-rays
5 nm > λ > 0.5 nm
Strongly interacts with *core electrons* in materials

High-order laser harmonics

Generation of extreme wavelengths

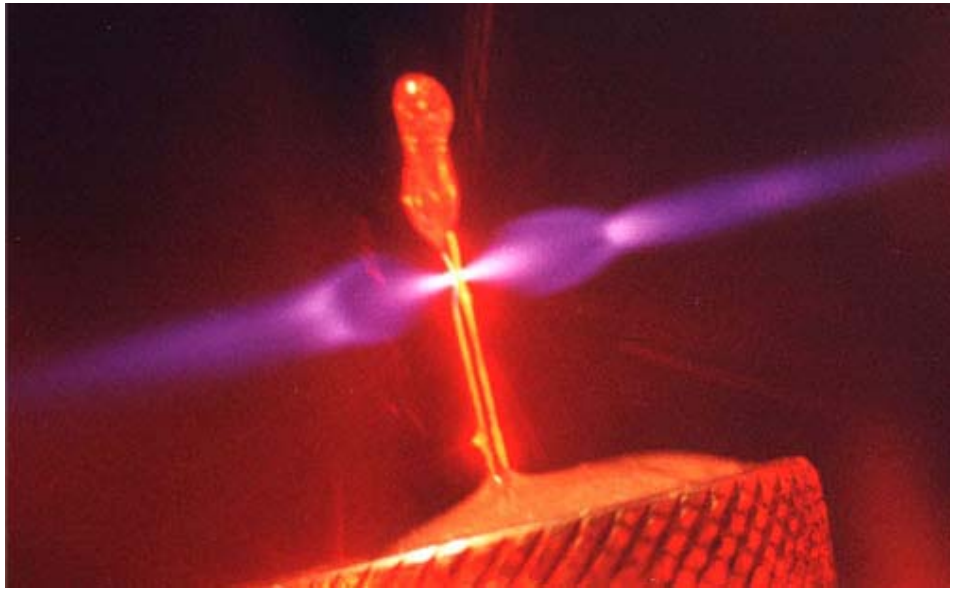

Current world record:

< 3 nm (> 250th order !!)

from 5 fs laser pulses in He

Z. Chang et al, *PRL* 79, 2967 (1997)

C. Spielmann et al., *Science* 278, 661 (1997)

"water window"
(biological applications)

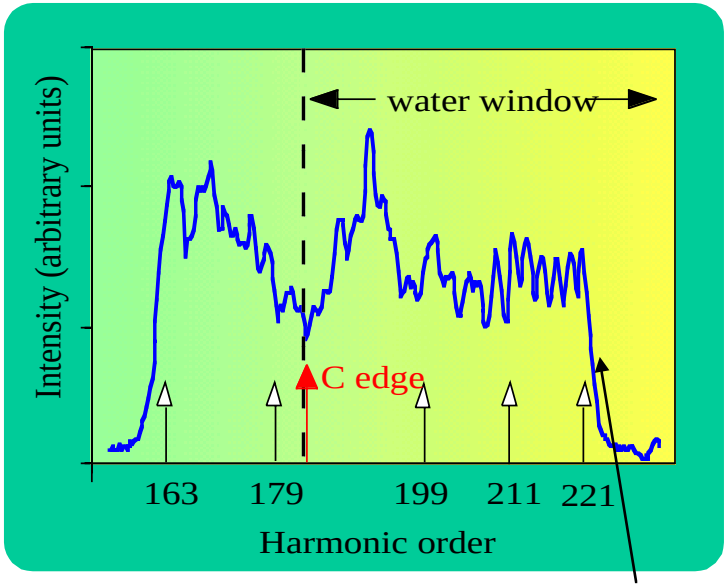

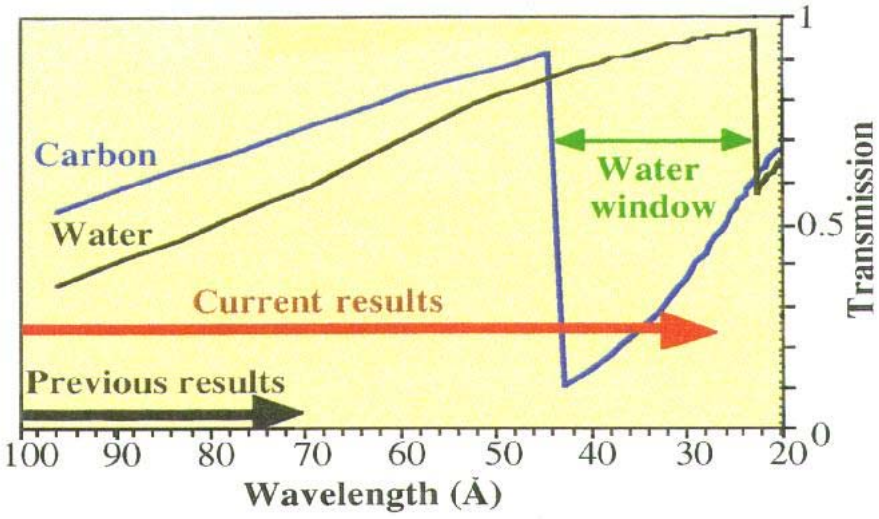

Why only odd harmonic orders ?

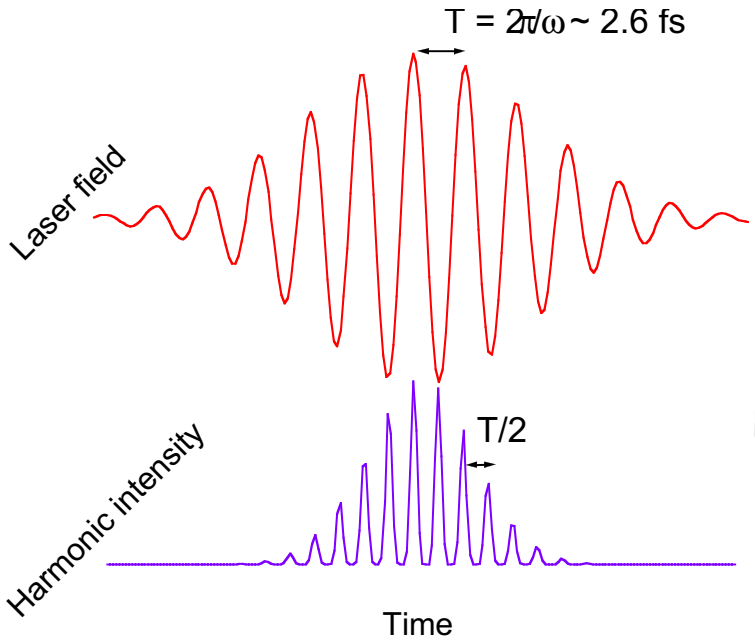

Train of harmonic pulses generated every half optical period

Fourier transform

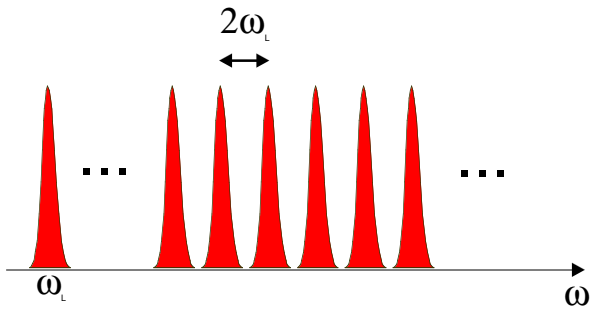

Photon view

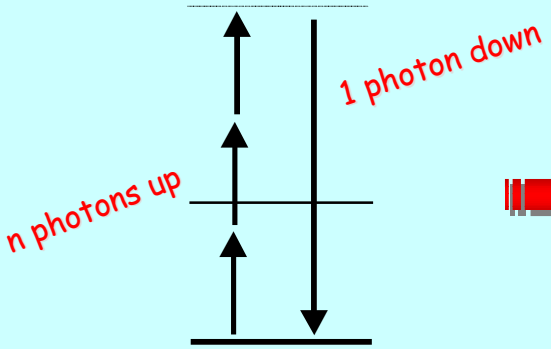

n+1 must be even to conserve parity

n must be odd

Increasing the efficiency (Phase-Matching)

Minimize the phase drift between the induced polarization and the emitted field

$\Delta k \rightarrow 0$ ⇒ $L_{coherence} \rightarrow \infty$

Neutral gas dispersion → $\Delta\varphi_{ND} = \frac{2\pi q z}{\lambda}\left(n(q\omega) - n(\omega)\right)$

Free-electron dispersion → $\Delta\varphi_{el} \approx \frac{z\omega_P^2}{2cq\omega}\left(q^2 - 1\right)$

Geometrical dephasing → $\Delta\varphi_G = (1-q)\tan^{-1}\left(\frac{2z}{b}\right)$

Induced dipole phase → $\Delta\varphi_D = -\sum_j \alpha_j I(z,t)$

The phase accumulated in the electron trajectory determines the harmonic phase

$$\varphi = \frac{2\pi}{h}\int_{t_{ion}}^{t_{ret}}\left(\frac{p^2}{2m} + I_P\right)dt \approx \frac{2\pi}{h}U_P\tau$$

$$\varphi \propto \tau I$$

Total phase mismatch

$$\Delta\varphi = \Delta\varphi_{ND} + \Delta\varphi_{el} + \Delta\varphi_G + \Delta\varphi_D$$

Has to be kept constant in the medium length

Defocusing by free electrons

$$n(z,P) = \sqrt{1 - \frac{N_e(z,P)}{N_c}}$$

Refractive index
of the ionized medium

The ionized gas behaves as a divergent lens

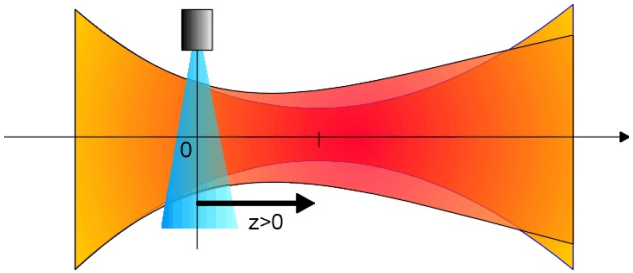

Particular geometries may enhance
the conversion efficiency

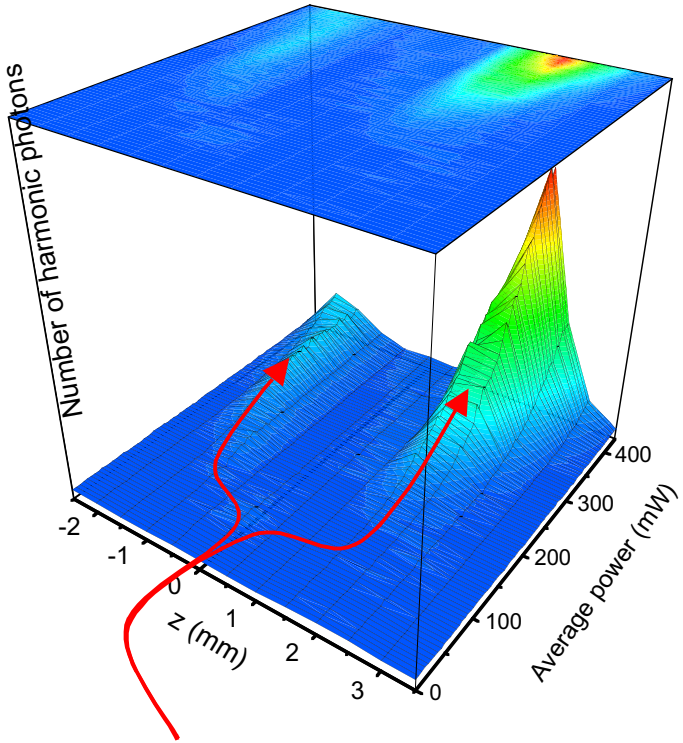

Reduced divergence for
z>0

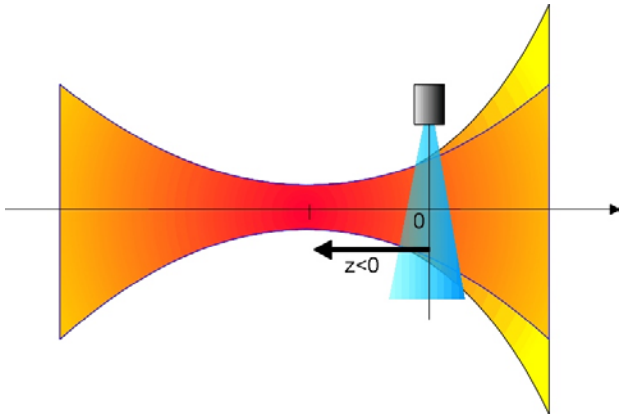

Increased divergence for
z<0

Test of the phase lock with spatially separated sources

Michelson interferometer

+

Young's double slit

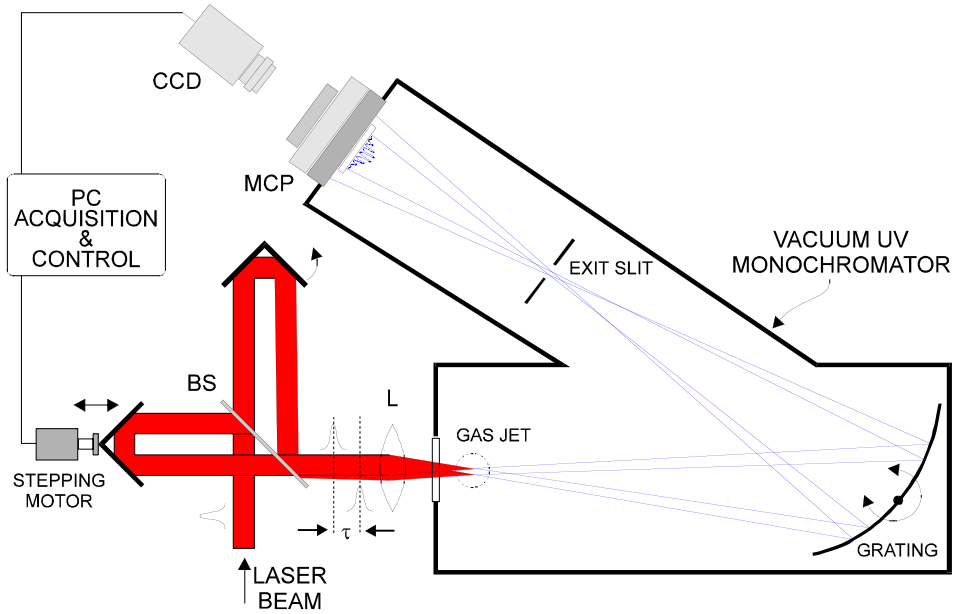

Coherent process ?

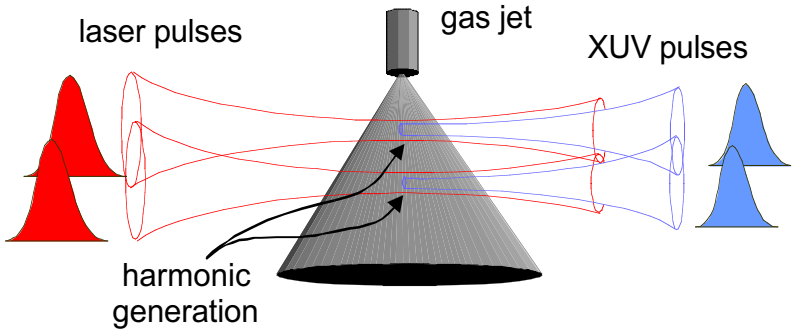

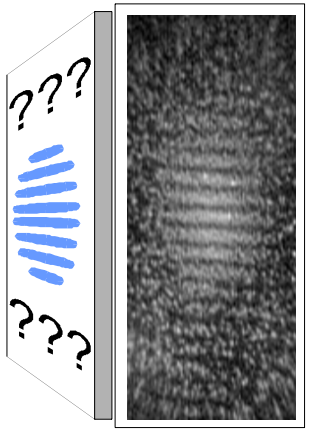

- Harmonics are locked in phase
- Good temporal coherence
- Info about the fundamental physical processes
- XUV interferometry is possible

R. Zerne et al., *Phys. Rev. Lett.*, **79**, 1006 (1997)

XUV interferometry with harmonics

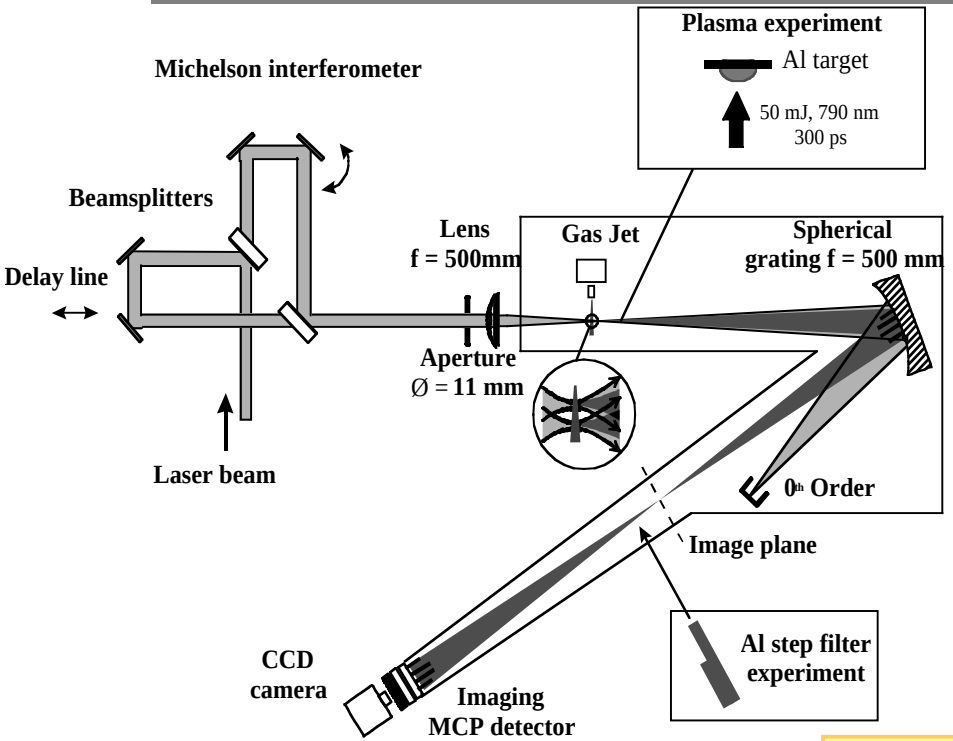

Measuring refraction indexes in the XUV

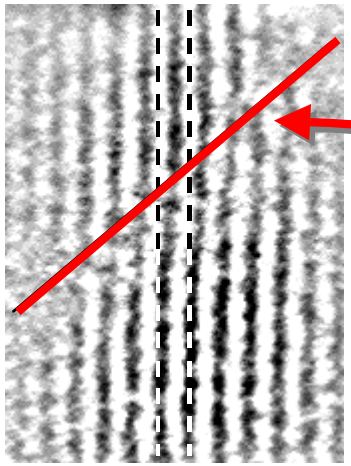

13th harmonic
(λ~60 nm)

Aluminium
step (~70 nm) filter

Measuring densities of laser-produced plasmas

- 11th harmonic (λ~73 nm)
- 1.2 ns delay between pump and XUV probe
- High temporal resolution
- Electron densities up to 10^{20} el/cm^3

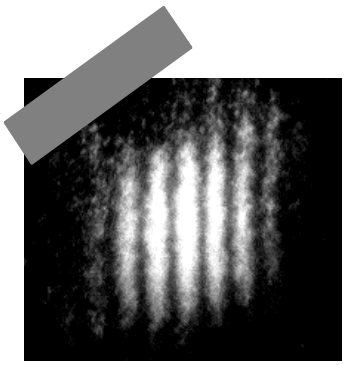

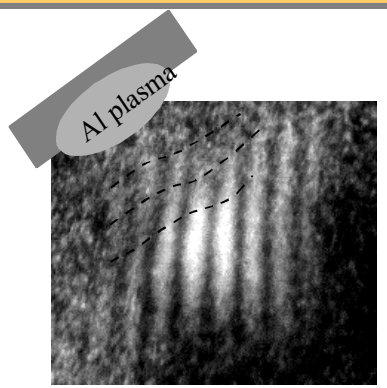

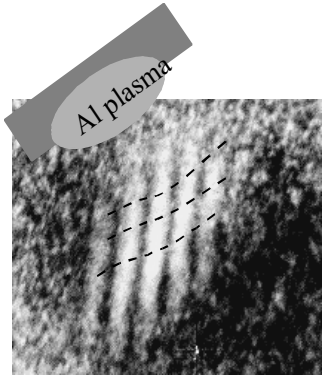

D. Descamps et al., *Opt. Lett.*, **25**, 135 (2000)

Temporal coherence and physical insight

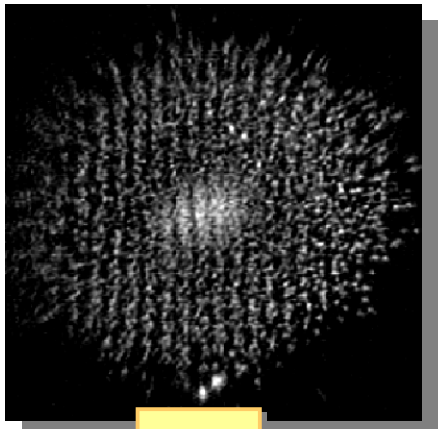

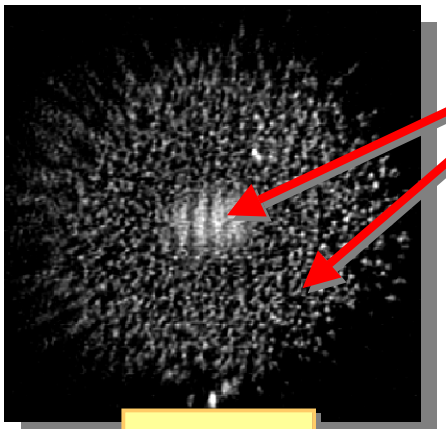

Two regions with different properties

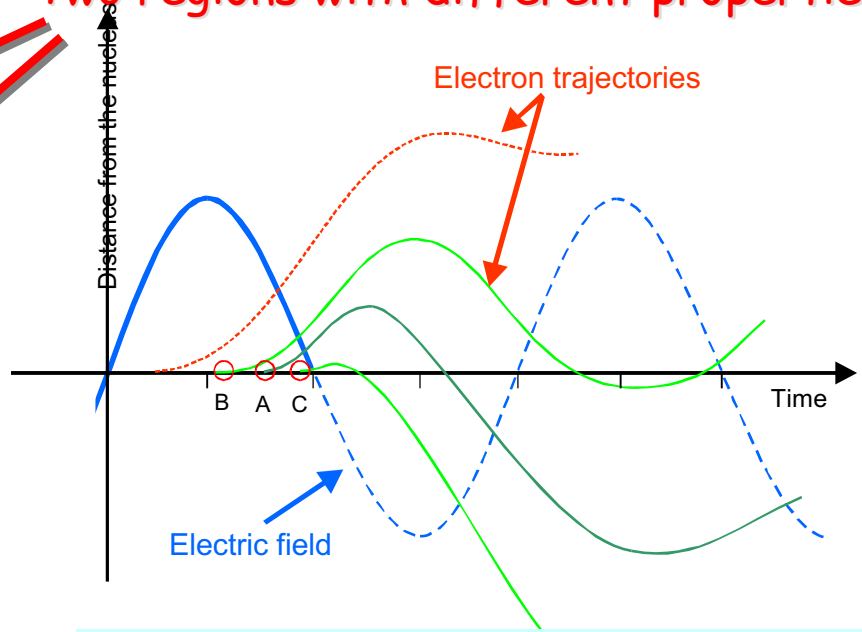

Nonlinear "dipole" phase of harmonics

$$\phi_{ind}(r,t) \propto \tau_{return}\, I_{laser}(r,t)$$

defocusing chirp

Electrons that spend a longer time in the continuum produce harmonics which are more phase-modulated

Short "flights" ⇒ good coherence

Long "flights" ⇒ poor coherence

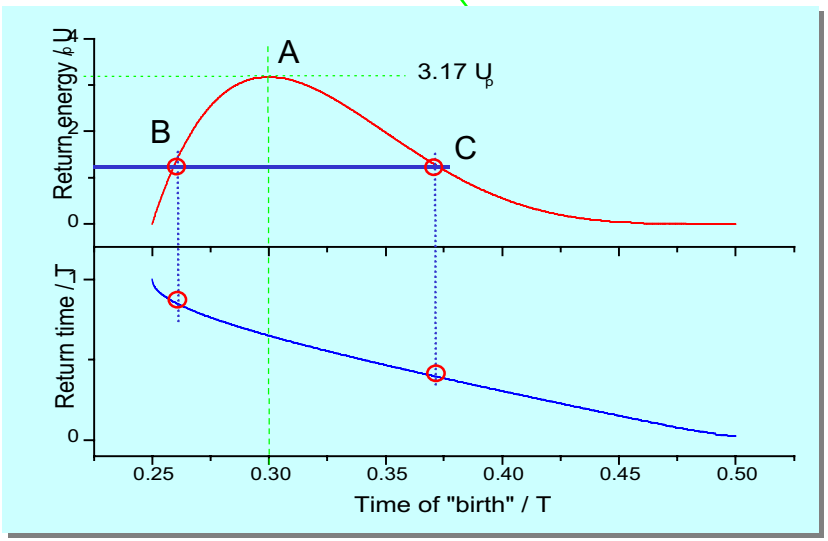

M. Bellini et al., *Phys. Rev. Lett.*, **81**, 297 (1998)
C. Lyngå et al., *Phys. Rev. A*, **60**, 4823 (1999)

Atomic, molecular and surface spectroscopy

Exploit the high temporal resolution in the XUV

Pump-probe experiments:

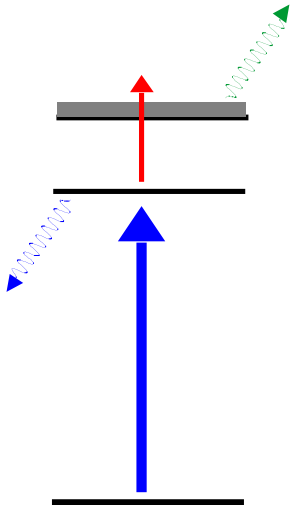

Lifetimes of highly excited levels

Photoionization cross sections

Relaxation of conduction electrons

Measurement of harmonic pulse durations

XUV-IR cross-correlation

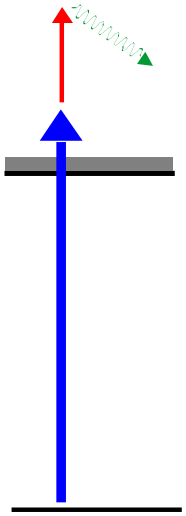

XUV auto-correlation

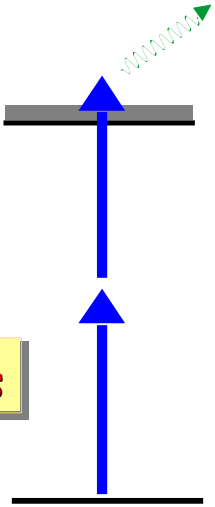

Nonlinear optics with harmonics

High resolution with harmonics

A single ultrashort pulse has a very broad spectrum

Pairs of phase-locked pulses reach a resolution given by the inverse of the time delay

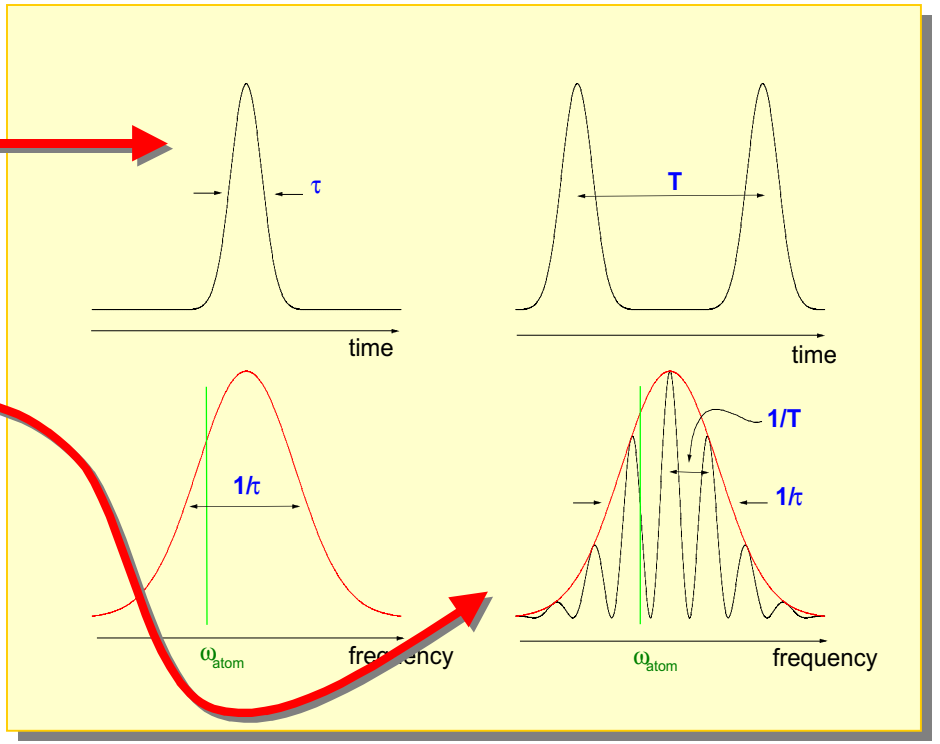

Do it with harmonics …

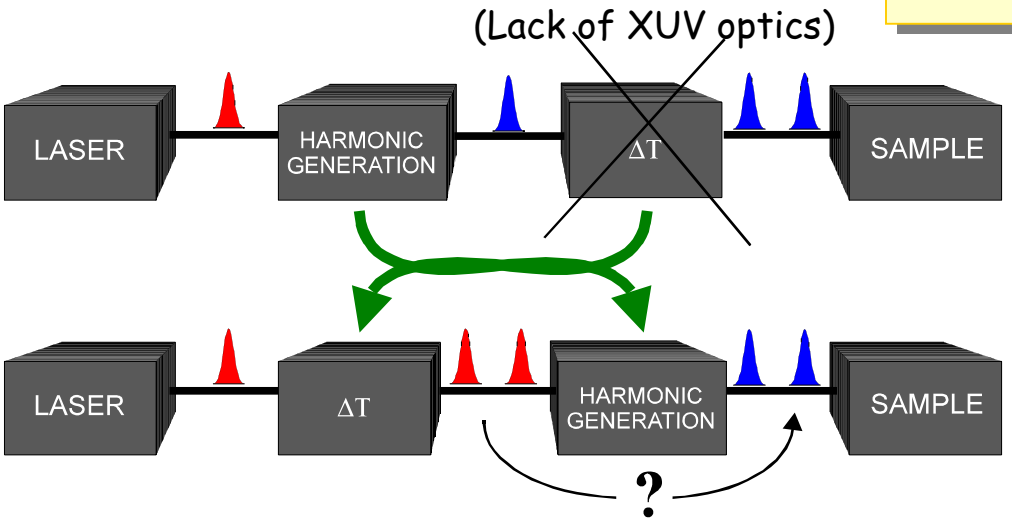

Is the phase lock preserved in the generation process ?

High spectral resolution

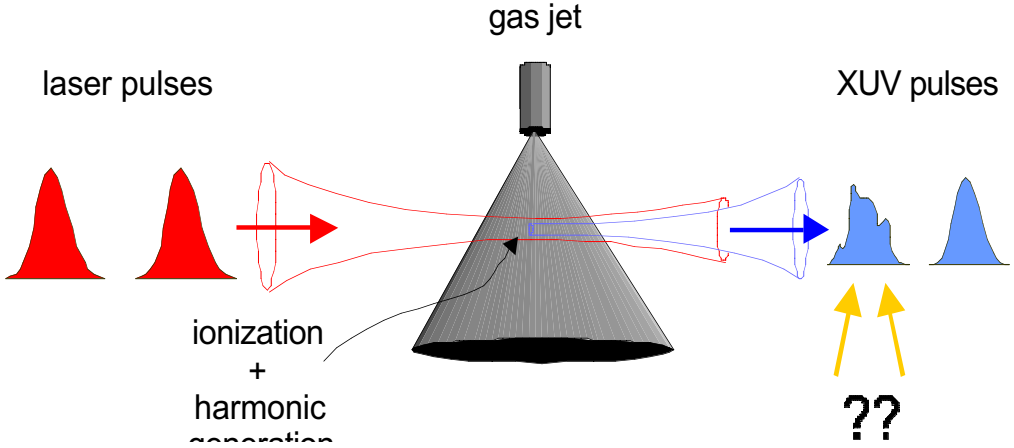

What is the effect of the gas ionization induced by the first pulse on the second one?

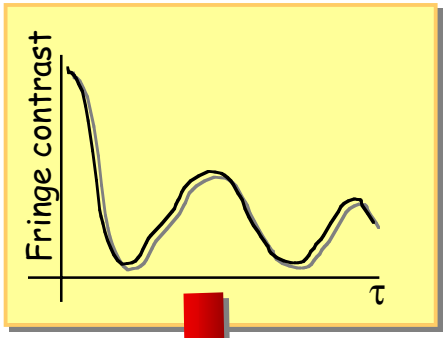

Fourier transform

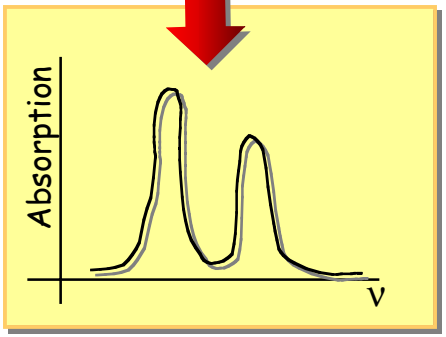

Scan the delay τ and observe fringes in the excitation

The achievable resolution is only limited by the maximum delay

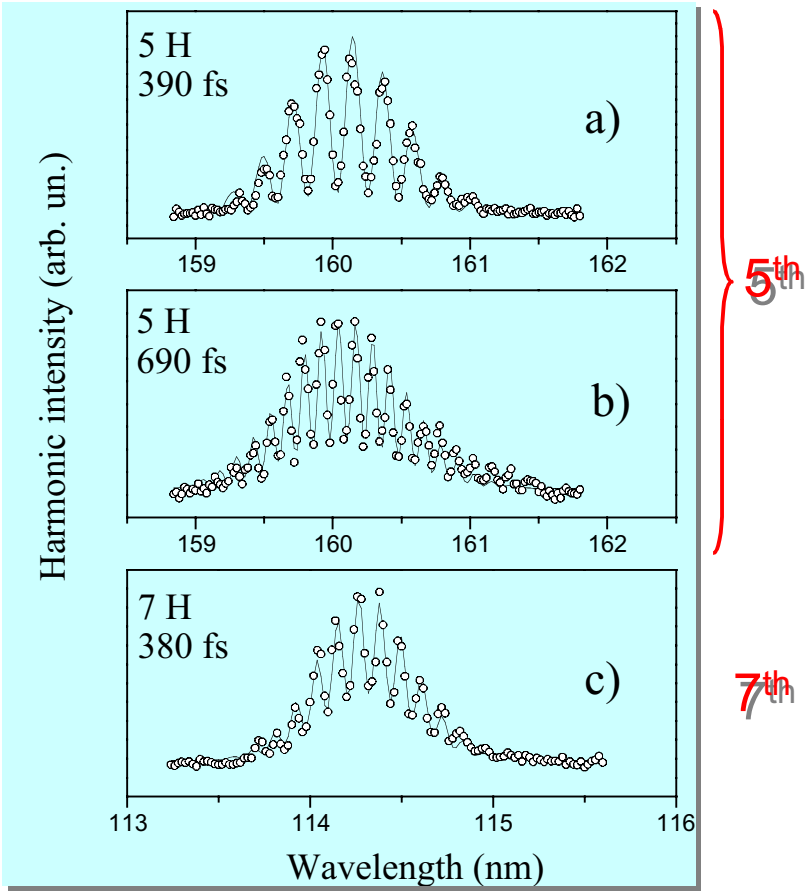

M. Bellini et al., *Opt. Lett.*, **26**, 1010 (2001)

XUV Ramsey-type spectroscopy

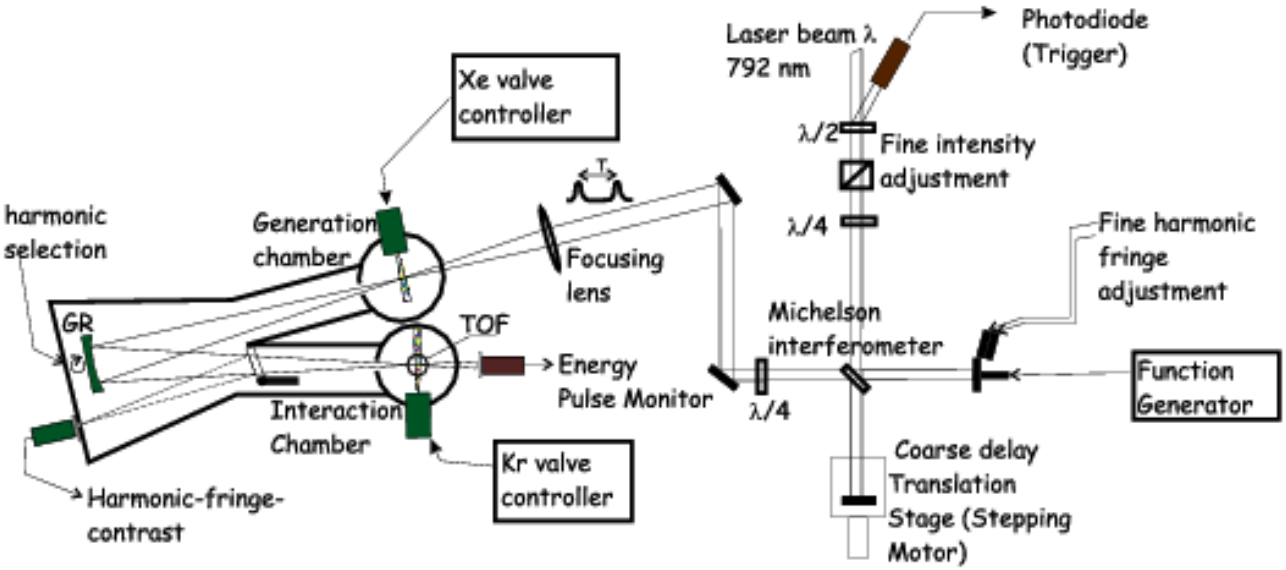

Excitation of two Kr autoionizing states

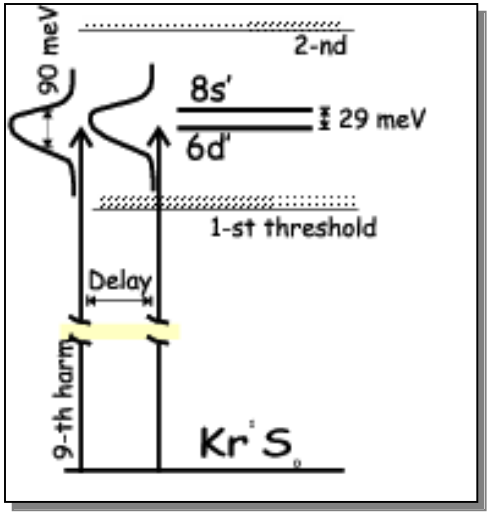

Two phase-locked and time-delayed 9th-harmonic pulses (88 nm)

Experimental observation of quantum interferences in the ionization signal

S. Cavalieri et al., *Phys. Rev. Lett.*, **89**, 133002 (2002)

290 attosecond fringe period !

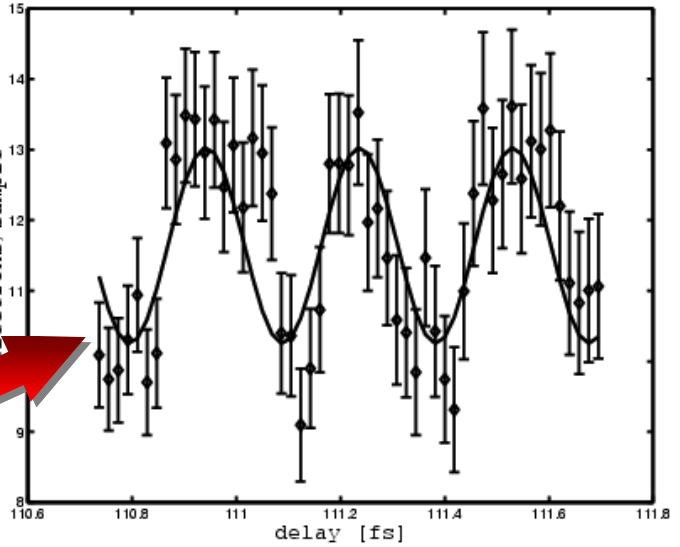

Attosecond (10^{-18}!!!) pulses

Ultrahigh temporal resolution for direct observation of extremely fast events
(electronic wavepacket motion)

Temporal point of view

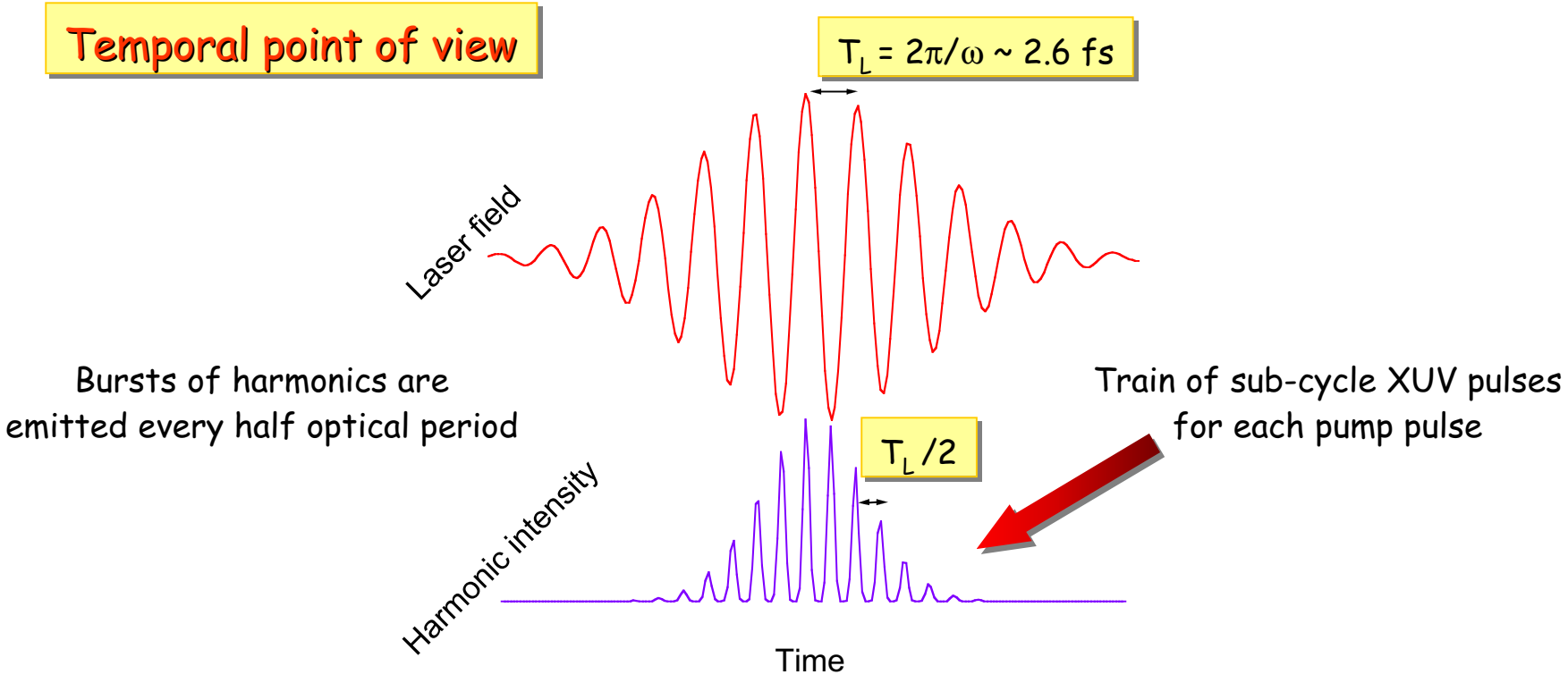

With few-cycle pump pulses one can obtain a single attosecond pulse

Attosecond pulses: absolute phase

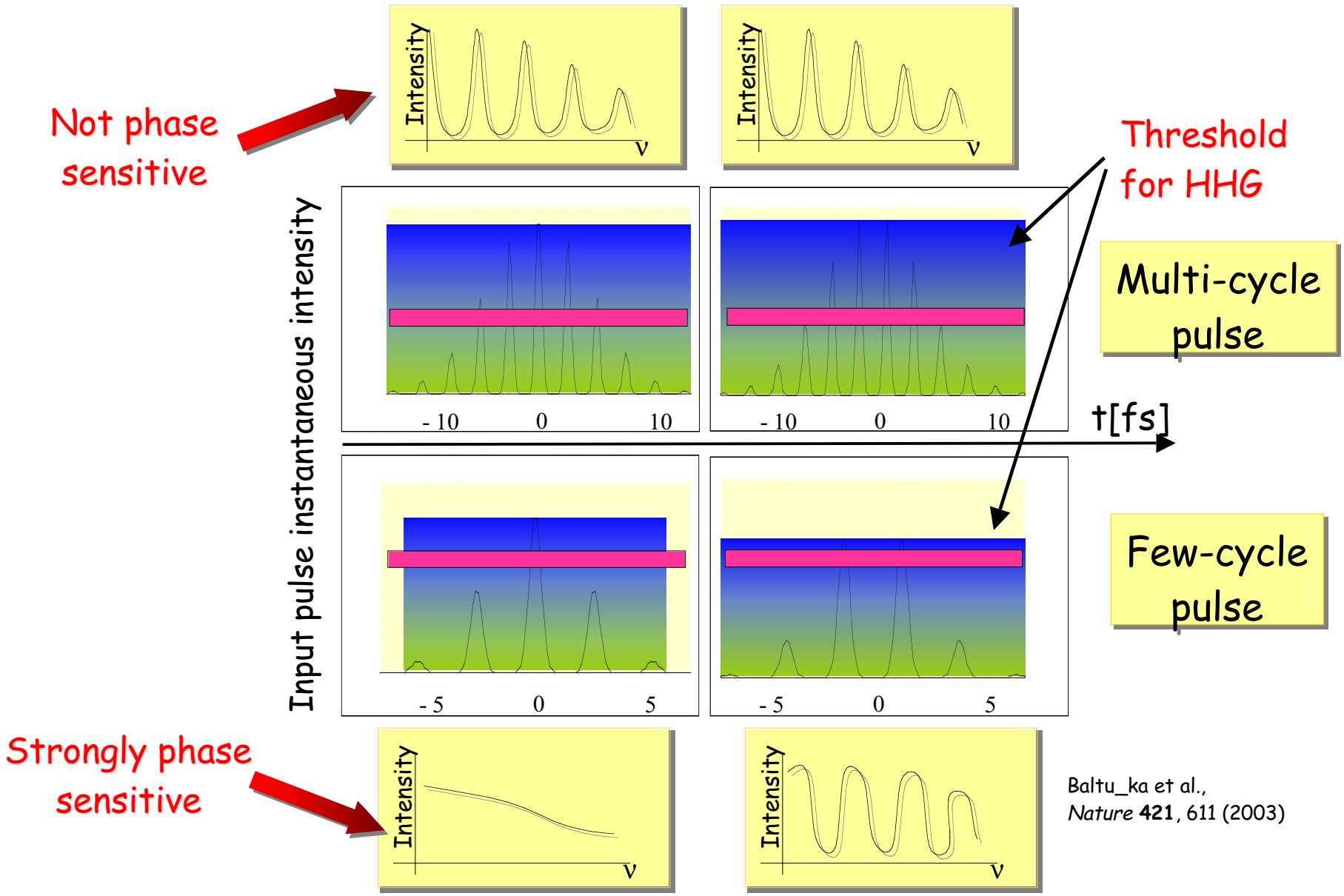

Baltu_ka et al.,
Nature **421**, 611 (2003)

Conclusions

Microscopic physical processes are well understood

Ultrashort and temporally coherent

High conversion efficiency possible

High-order harmonics are a convenient source of coherent radiation in the XUV and soft X-rays

Brightness comparable to synchrotron light but much more compact and with higher temporal resolution

- Spectroscopy in the XUV
- Biological applications
- XUV interferometry
- Attosecond pulses

Credits

C. Corsi [2]
A. Tortora [1,2]
S. Cavalieri [3]
R. Eramo
L. Pampaloni [3]
M. Materazzi [1]

A. L'Huillier, etc.	*Lund University*
T. W. Hänsch,	*MPQ – Garching*
P. Salières, etc.	*CEA - Saclay*

[1] *Istituto Nazionale di Ottica Applicata, INOA*
[2] *European Laboratory for Nonlinear Spectroscopy, LENS*
[3] *Department of Physics, University of Firenze*

Synchrotron radiation: properties and related analysis techniques

Michele Bertolo - Sincrotrone Trieste
bertolo@elettra.trieste.it

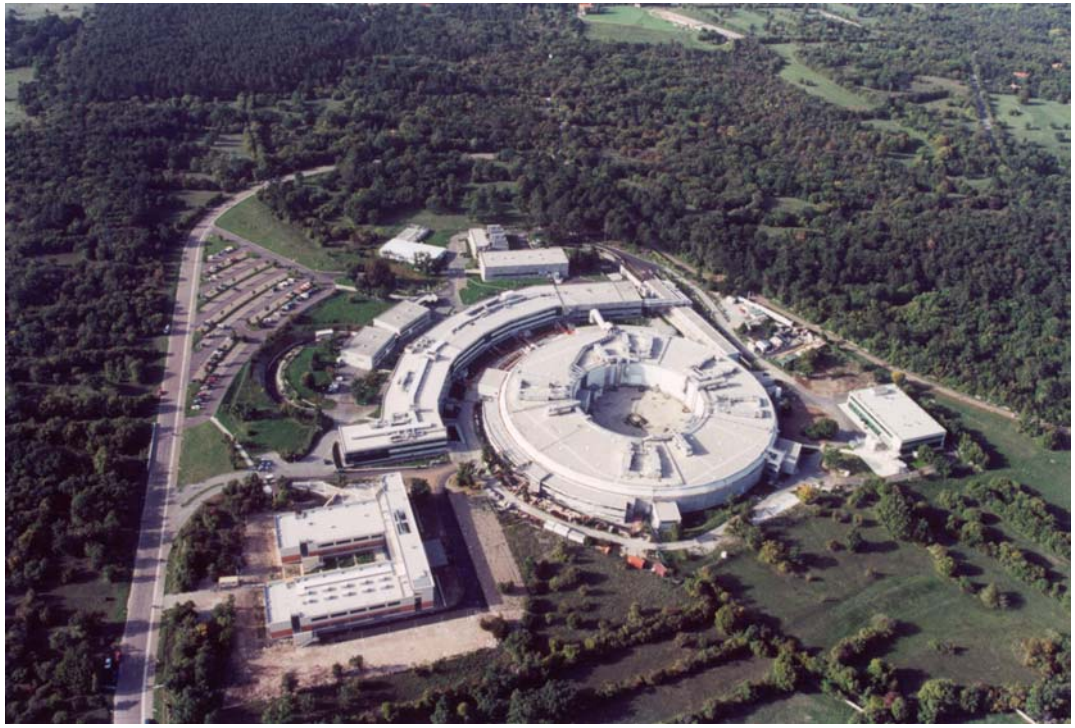

http://www.elettra.trieste.it

Varenna, 7th October 2003

- Properties of synchrotron radiation

- Analysis techniques
  - photoemission and photoabsorption
  - microscopy
  - x-ray diffraction
  - radiology

- Micro- and nanofabrication

Radiation from Electrons in a Synchrotron

F. R. ELDER, A. M. GUREWITSCH, R. V. LANGMUIR,
AND H. C. POLLOCK
Research Laboratory, General Electric Company,
Schenectady, New York
May 7, 1947

HIGH energy electrons which are subjected to large accelerations normal to their velocity should radiate electromagnetic energy.[1–4] The radiation from electrons in a betatron or synchrotron should be emitted in a narrow cone tangent to the electron orbit, and its spectrum should extend into the visible region. This radiation has now been observed visually in the General Electric 70-Mev synchrotron.[5] This machine has an electron orbit radius of 29.3 cm and a peak magnetic field of 8100 gausses. The radiation is seen as a small spot of brilliant white light by an observer looking into the vacuum tube tangent to the orbit and toward the approaching electrons. The light is quite bright when the x-ray output of the machine at 70 Mev is 50 roentgens per minute at one meter from the target and can still be observed in daylight at outputs as low as 0.1 roentgen.

The synchrotron x-ray beam is obtained by turning off the r-f accelerating resonator and permitting subsequent changes in the field of the magnet to change the electron orbit radius so as to contract or expand the beam to suitable targets. If the electrons are contracted to a target at successively higher energies, the intensity of the light radiation is observed to increase rapidly with electron energy.

Phys. Rev.
71 (1947) 829

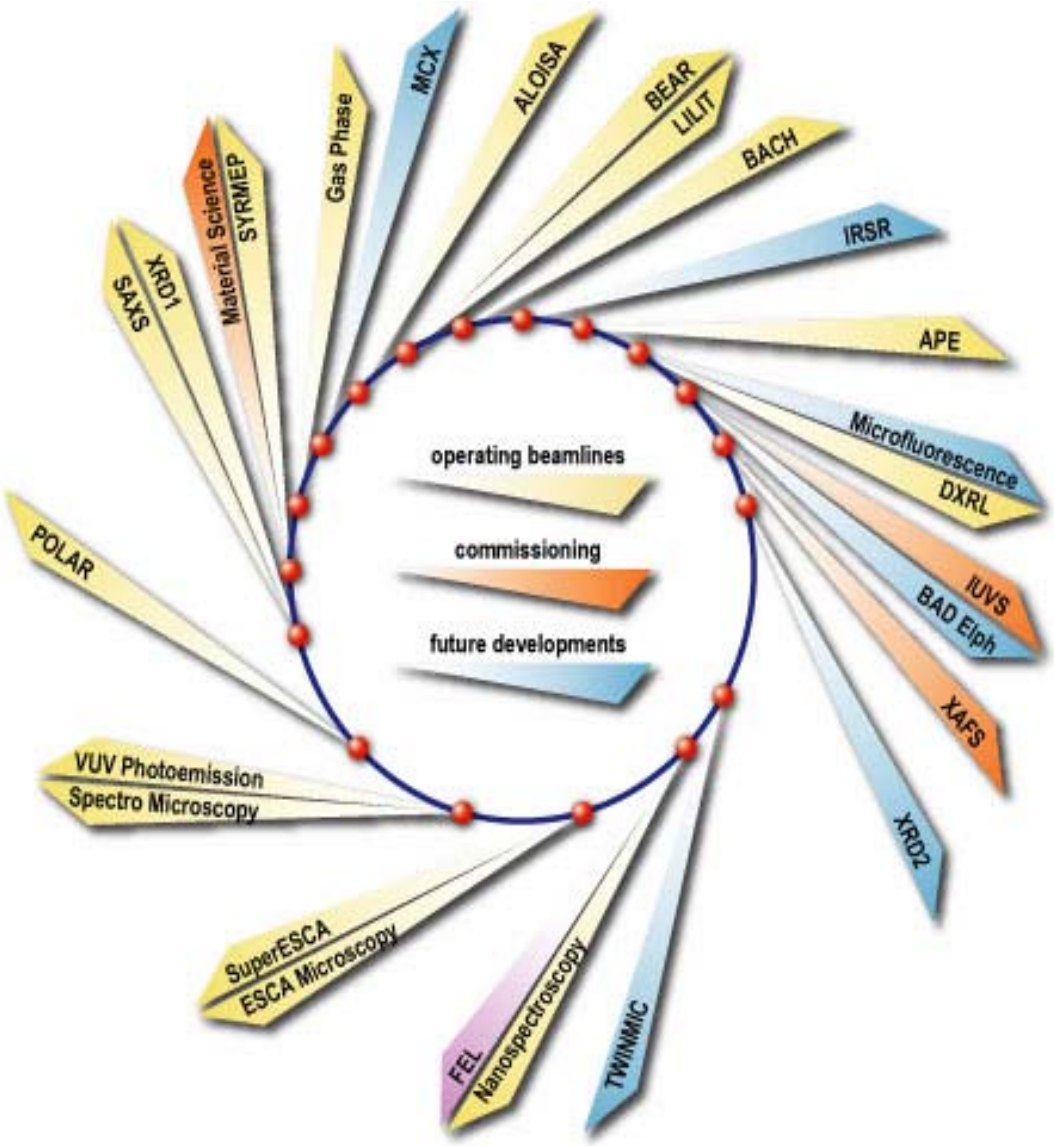

ELETTRA

circumference = 259.2 m
beam energy = 2.0/2.4 GeV

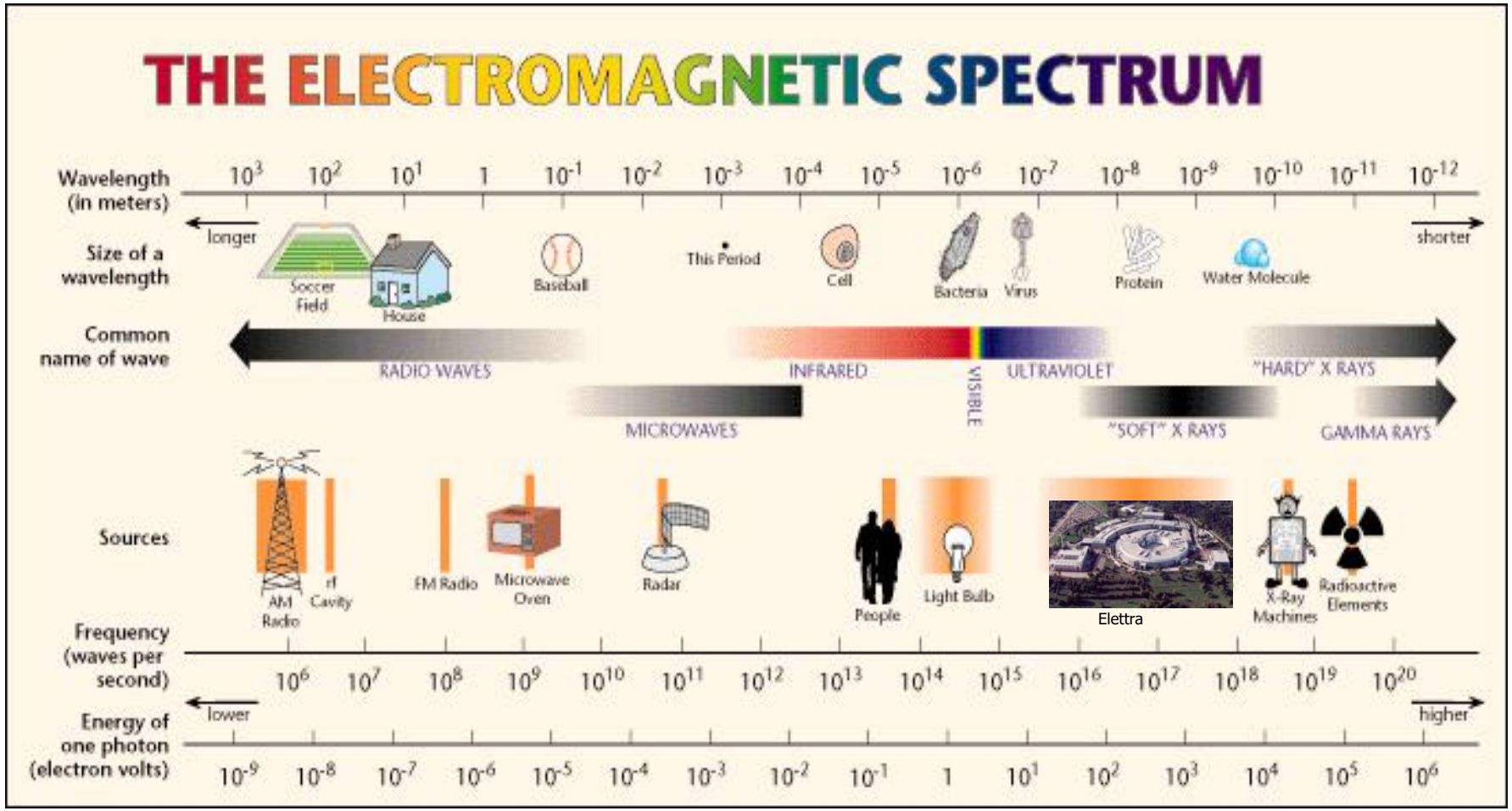
THE ELECTROMAGNETIC SPECTRUM
Wavelength (in meters)
longer
shorter
Size of a wavelength
Soccer Field
House
Baseball
This Period
Cell
Bacteria
Virus
Protein
Water Molecule
Common name of wave
RADIO WAVES
INFRARED
VISIBLE
ULTRAVIOLET
"HARD" X RAYS
MICROWAVES
"SOFT" X RAYS
GAMMA RAYS
Sources
AM Radio
rf Cavity
FM Radio
Microwave Oven
Radar
People
Light Bulb
Elettra
X-Ray Machines
Radioactive Elements
Frequency (waves per second)
lower
higher
Energy of one photon (electron volts)

Properties of synchrotron radiation

- emission in a small solid angle

- continuous spectrum from the infrared to the hard x-rays

- high brightness

- high degree of polarization

- pulsed time structure

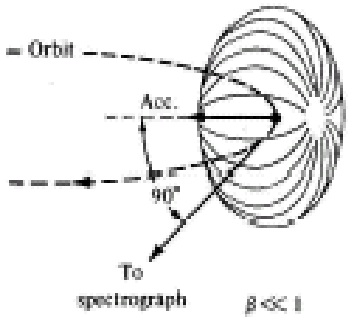

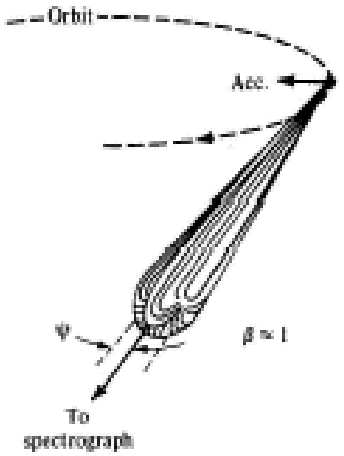

Classical case:

$dP/d\Omega \propto \sin^2\vartheta$

Relativistic case:

$\beta = v/c \qquad \gamma = \frac{1}{\sqrt{1-\beta^2}}$

$\psi \sim 1/\gamma$

case of ELETTRA
energy of the electrons: 2 GeV
$\gamma \sim 4000$
$\psi \sim 250$ μrad

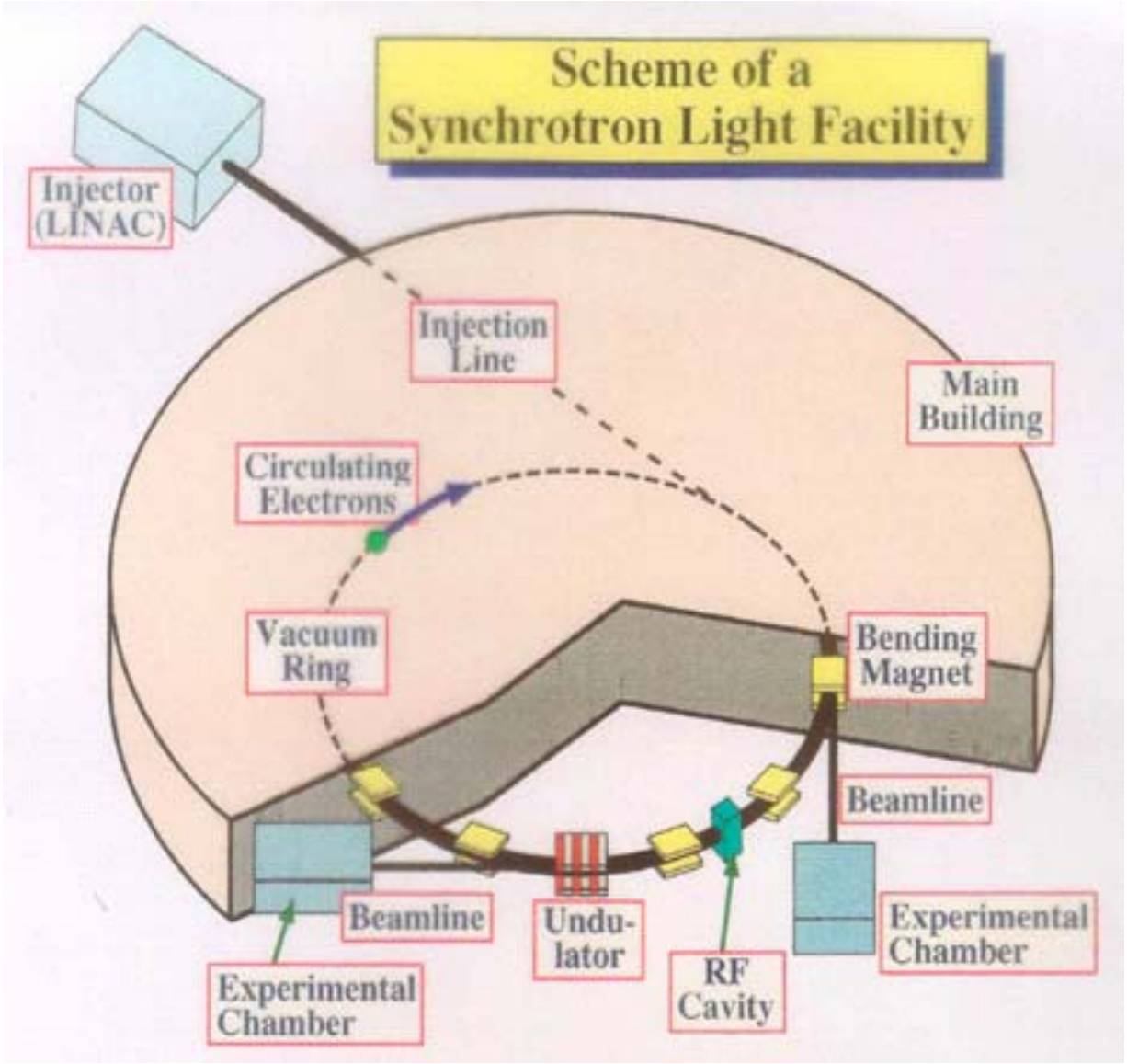
Scheme of a
Synchrotron Light Facility
Injector
(LINAC)
Injection
Line
Main
Building
Circulating
Electrons
Vacuum
Ring
Bending
Magnet
Beamline
Beamline
Undu-
lator
RF
Cavity
Experimental
Chamber
Experimental
Chamber

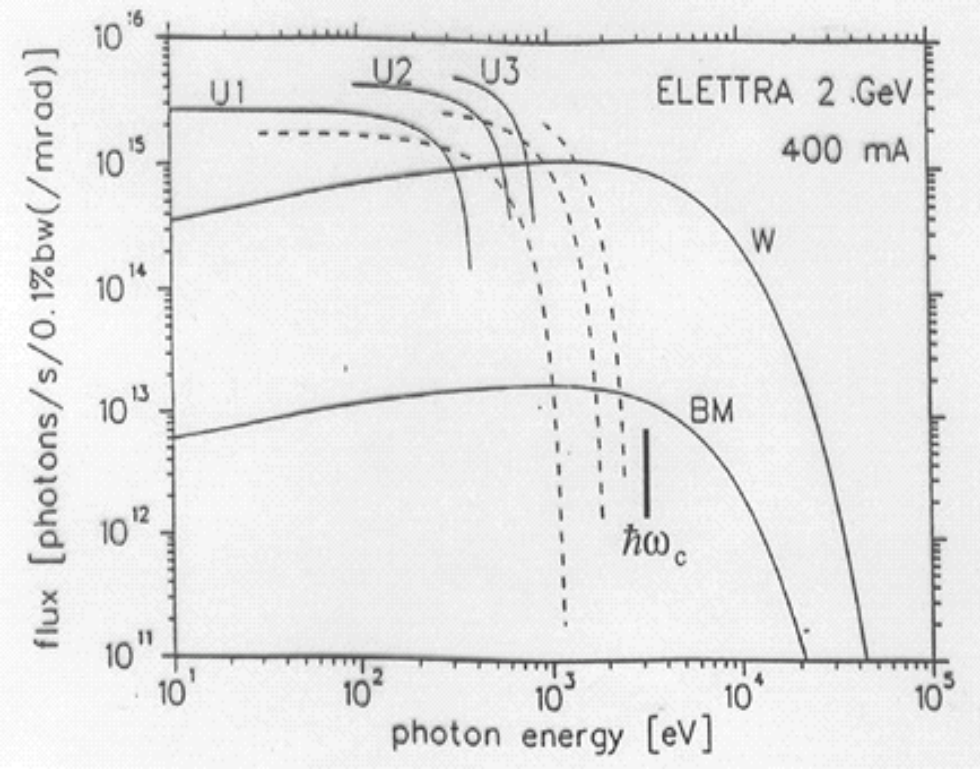

BM = bending magnet
W/U = wiggler/undulator

bending magnet

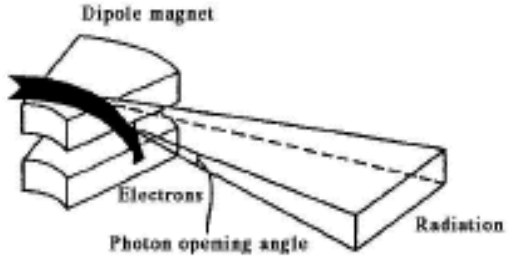

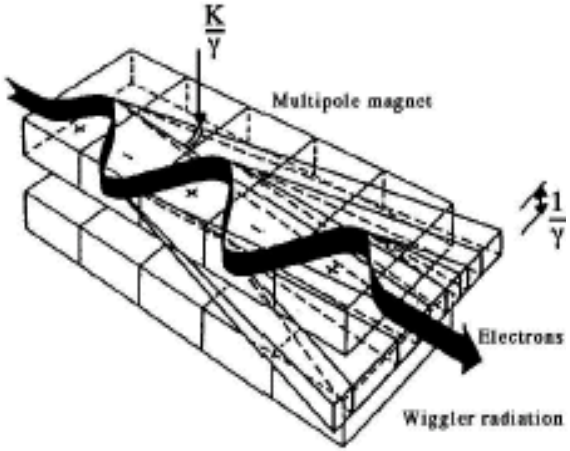

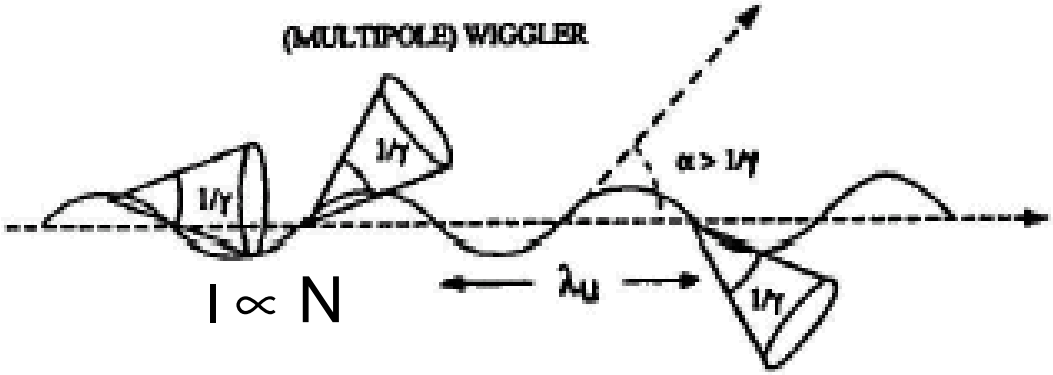

$I \propto N$

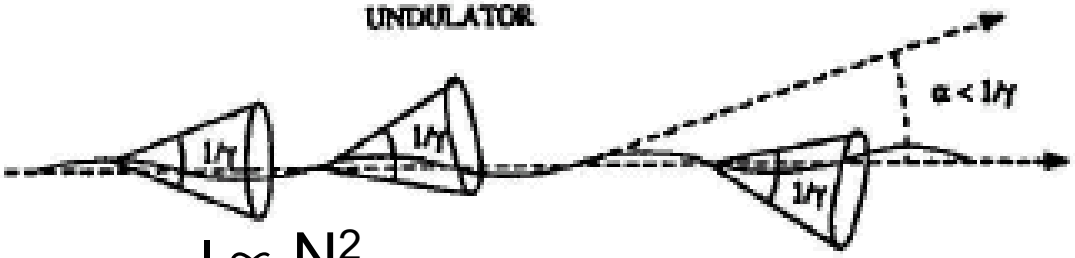

$I \propto N^2$

Definition of brightness (or brilliance)

$$\text{brightness} = \frac{\text{photons}}{t} \frac{1}{\sigma_x \sigma_y \sigma'_x \sigma'_y \text{BW}}$$

$\sigma_x\sigma_Y$ = area from which synchrotron radiation is emitted
$\sigma'_x\sigma'_Y$ = solid angle into which synchrotron radiation is emitted
BW (bandwidth) = $\Delta E/E$, typically BW = 0.1 %

units = photons/s$\times$mm$^2\times$mrad$^2\times$0.1%BW

(normalized to a given ring current I, typically 100 mA)

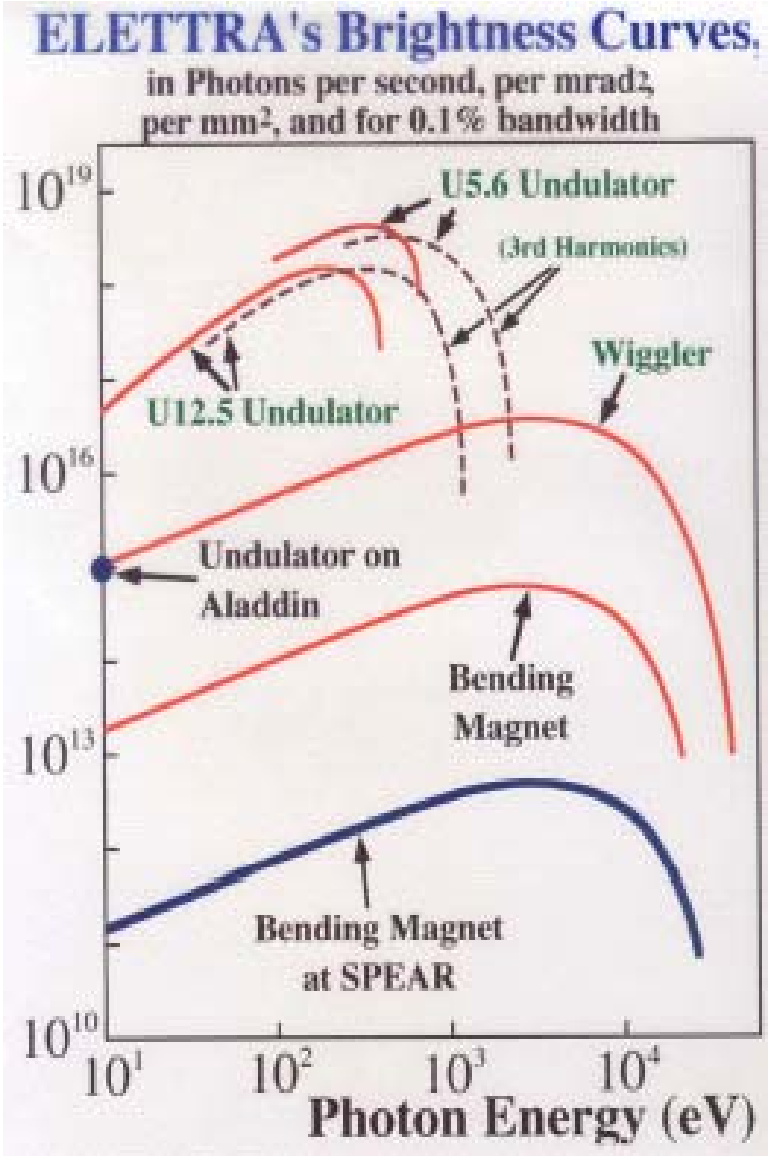
ELETTRA's Brightness Curves.
in Photons per second, per mrad2,
per mm2, and for 0.1% bandwidth
10^19
10^16
10^13
10^10
U5.6 Undulator
(3rd Harmonics)
Wiggler
U12.5 Undulator
Undulator on
Aladdin
Bending
Magnet
Bending Magnet
at SPEAR
10^1
10^2
10^3
10^4
Photon Energy (eV)

Pulsed structure and polarization

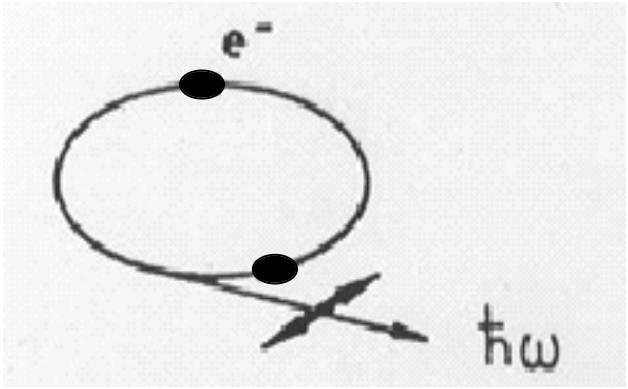

N. of bunches: 1-432

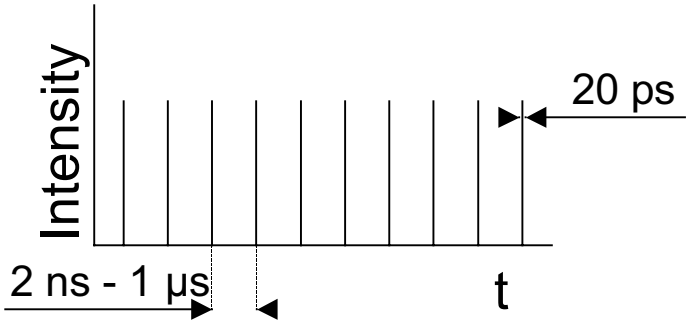

Polarization

typically:
linear in the orbit plane

at particular geometries or with special devices:
elliptical (right or left)

- Properties of synchrotron radiation

- Analysis techniques
  - photoemission and photoabsorpt
  - microscopy
  - x-ray diffraction
  - radiology

- Micro- and nanofabrication

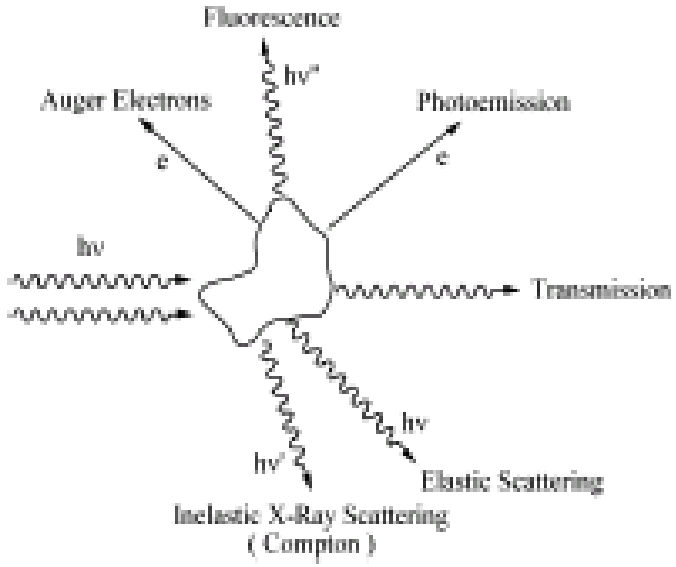

Photoemission spectroscopy
or ESCA (Electron Spectroscopy for Chemical Analysis

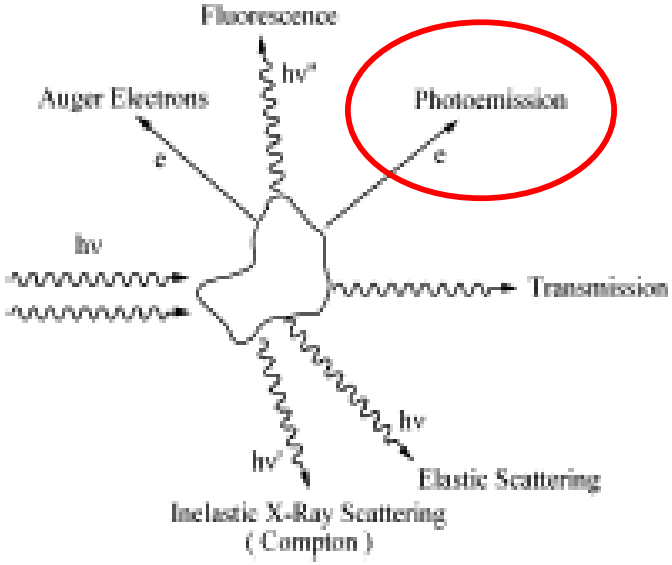

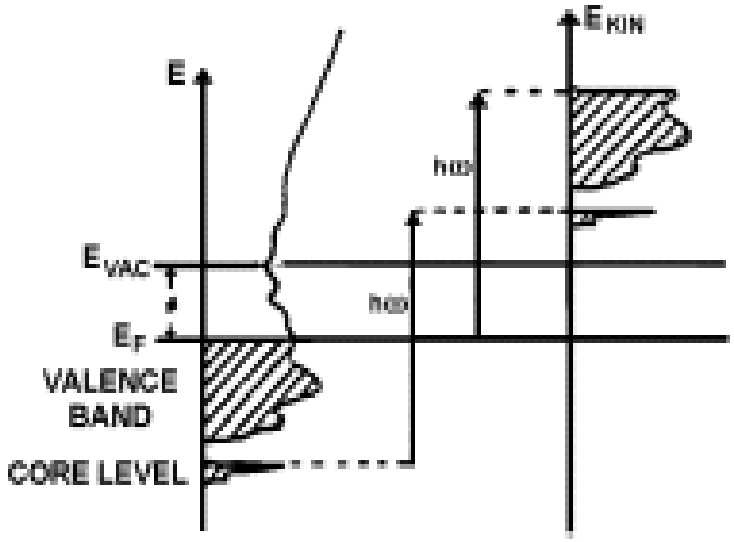

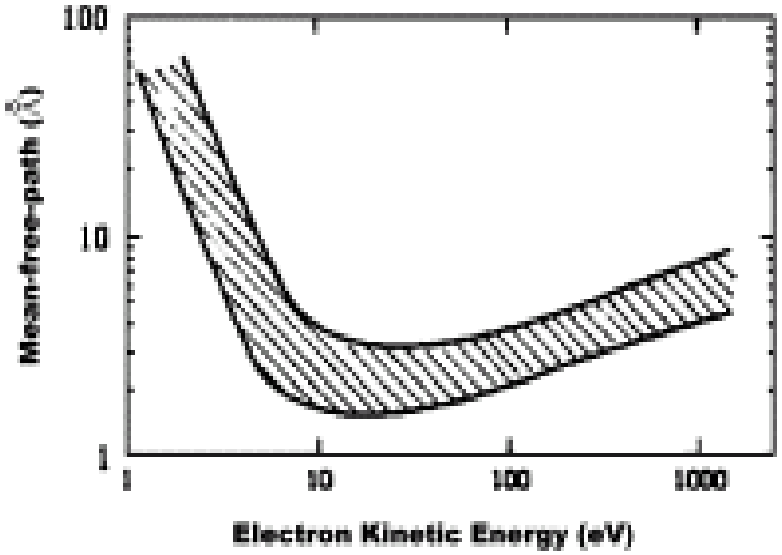

Surface sensitive

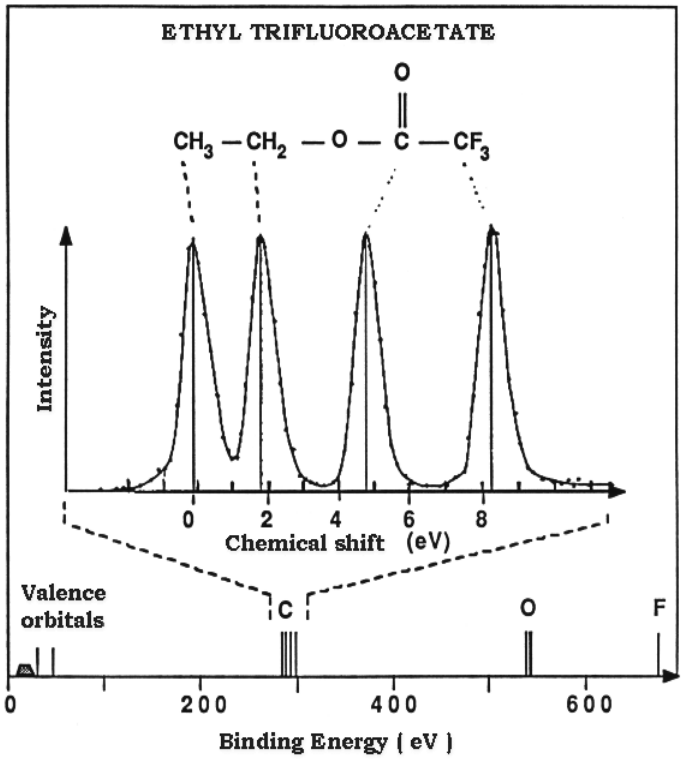

The binding energy of the core level indicates the chemical element

The *exact* binding energy gives an information on the chemical environment of a given element

Adsorption and dissociation of NO on the Rh(110) surface

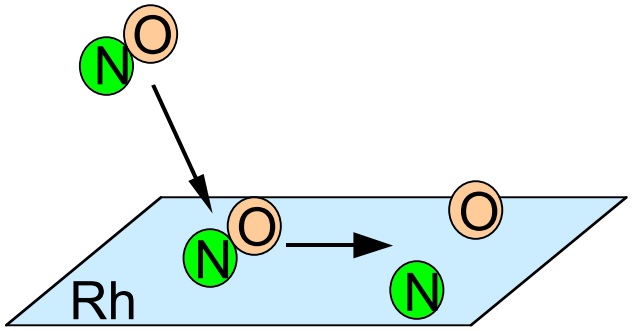

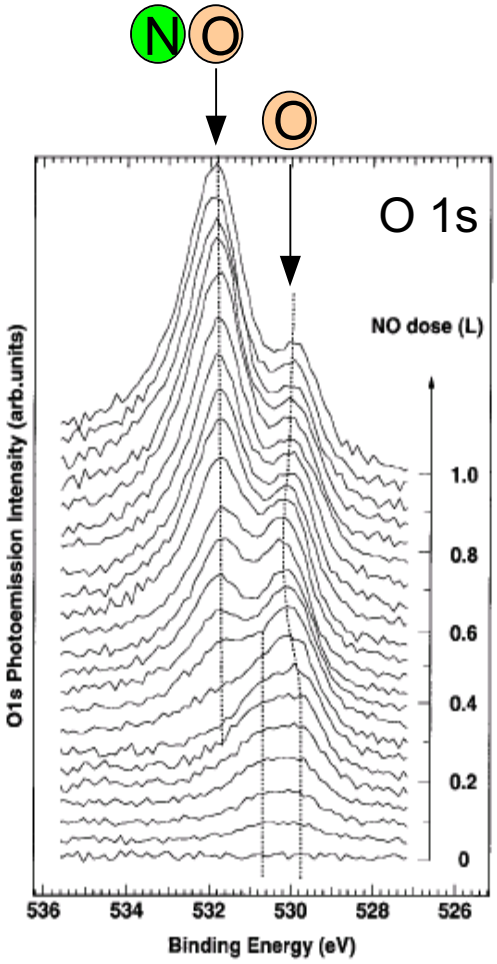

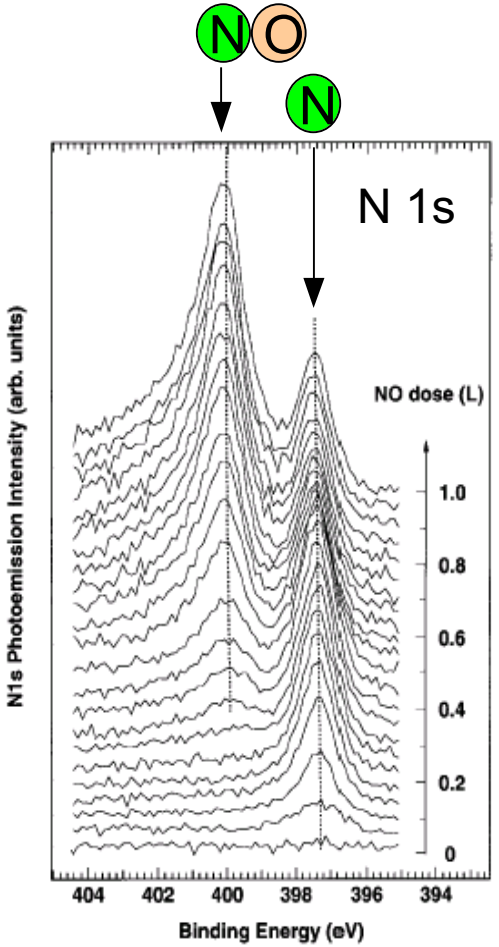

Varenna, 7th October 2003

Fotoabsorption

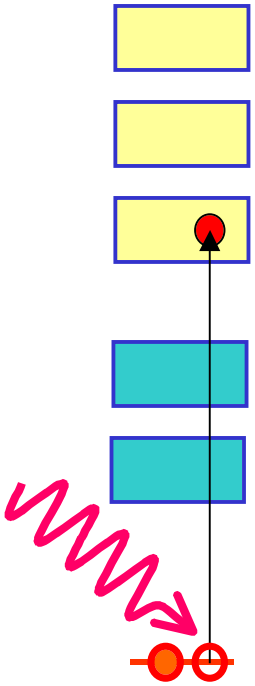

- Presence of specific bonds in a given molecule (e.g., C-C, C=C, C≡ C and C-H bonds in hydrocarbons)
- Determination of the lengths of these intra-molecular bonds
- Determination of the orientation of molecules (or functional groups thereof) adsorbed on a surface
- Determination of the orbitals involved in the chemisorption bond of a molecule on a surface

- Analysis techniques
  - photoemission and photoabsorption
  - microscopy
  - x-ray diffraction
  - radiology

$$\text{brightness} = \frac{\text{photons}}{t} \frac{1}{\sigma_x \sigma_y \sigma'_x \sigma'_y BW}$$

$\sigma_x\sigma_Y$ = area from which synchrotron radiation is emitted
$\sigma'_x\sigma'_Y$ = solid angle into which synchrotron radiation is emitted

$$S\Delta D = \text{constant} = S'\Delta D'$$

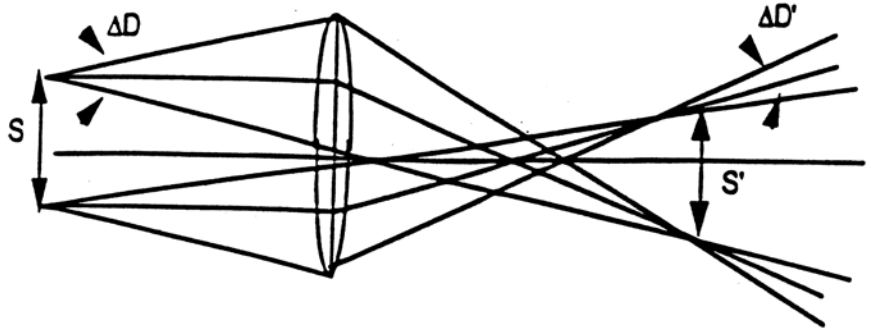

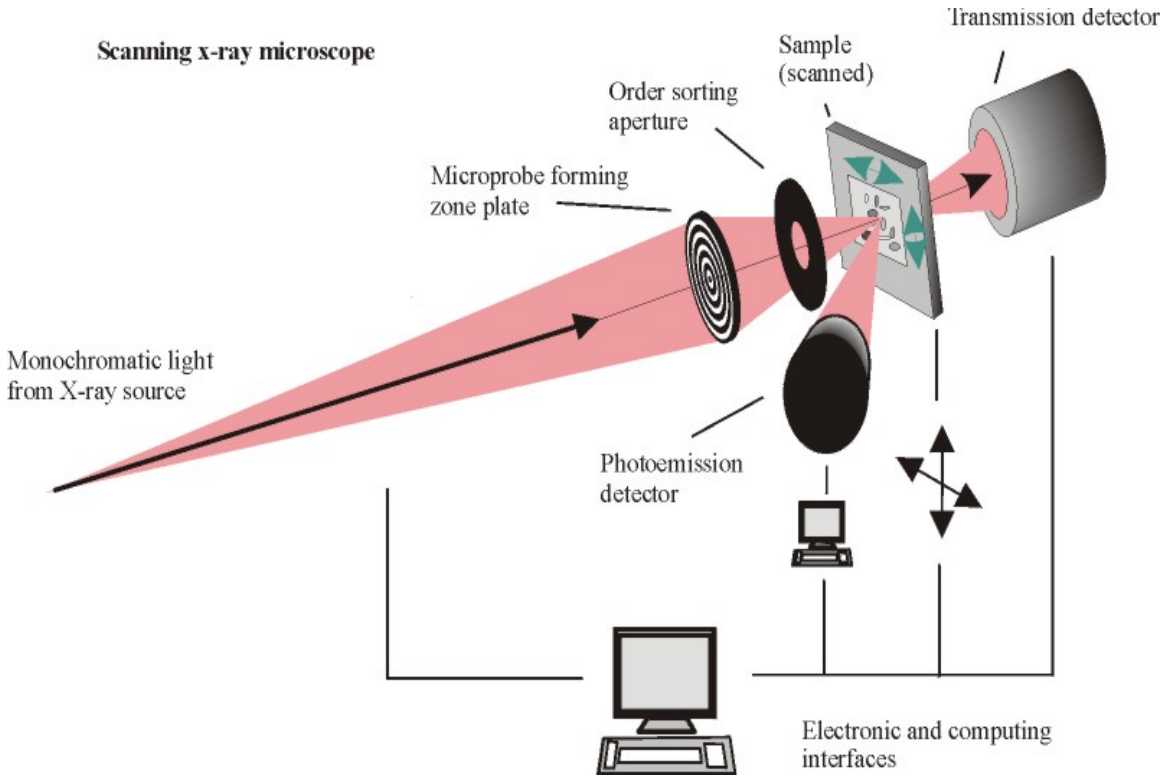
Scanning x-ray microscope
Transmission detector
Sample
(scanned)
Order sorting
aperture
Microprobe forming
zone plate
Monochromatic light
from X-ray source
Photoemission
detector
Electronic and computing
interfaces

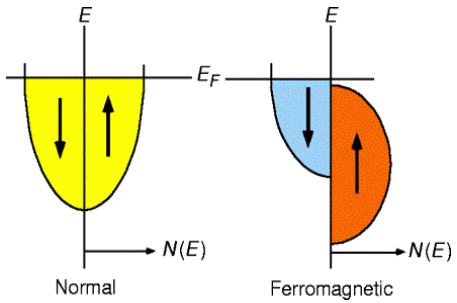

Magnetic Technologies in Computers

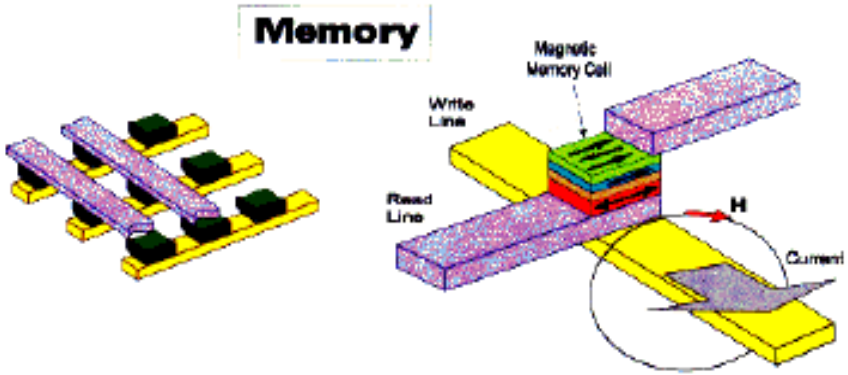

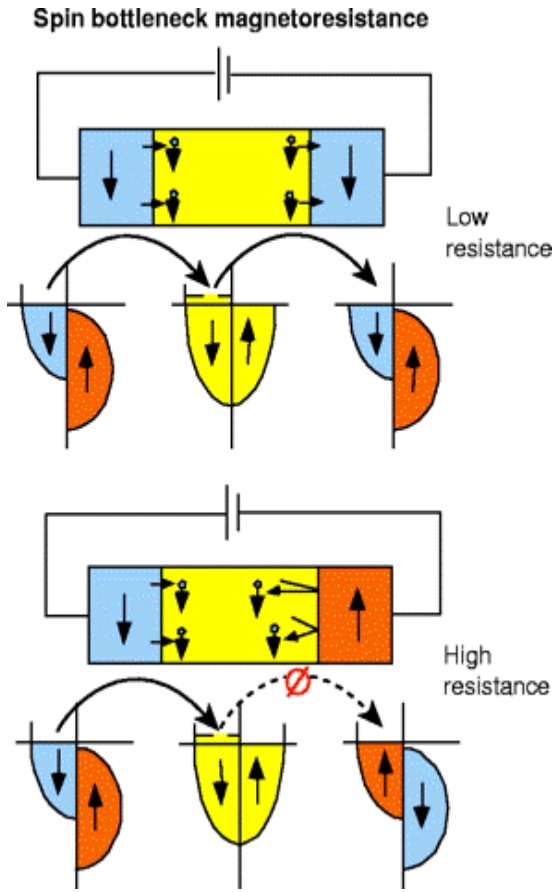

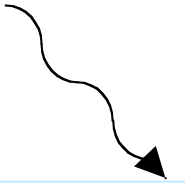

1.2 nm Co (ferromagnetic)

40 nm $LaFeO_3$ (antiferromagnetic)

substrate

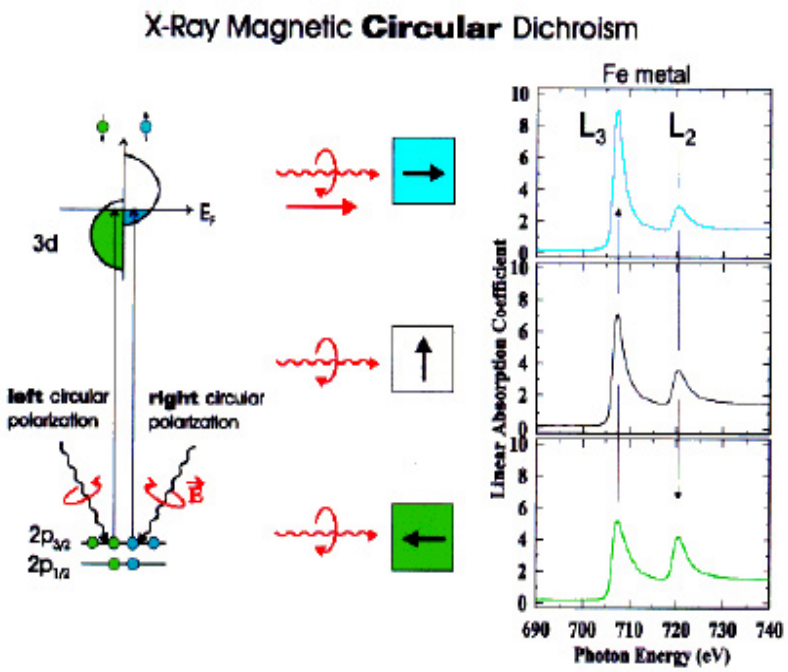

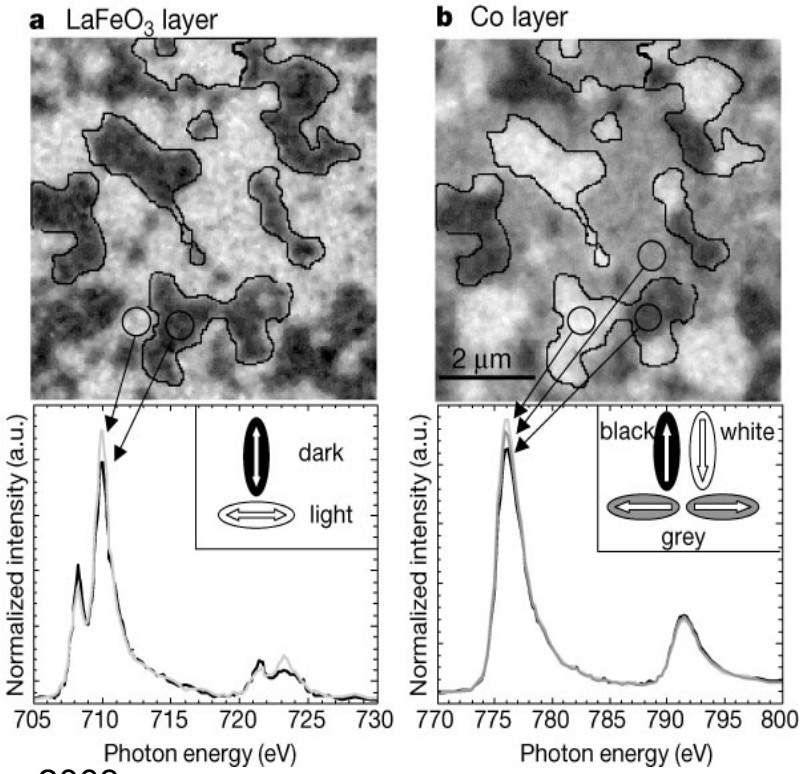

- Analysis techniques
  - photoemission and photoabsorpt
  - microscopy
  - x-ray diffraction
  - radiology

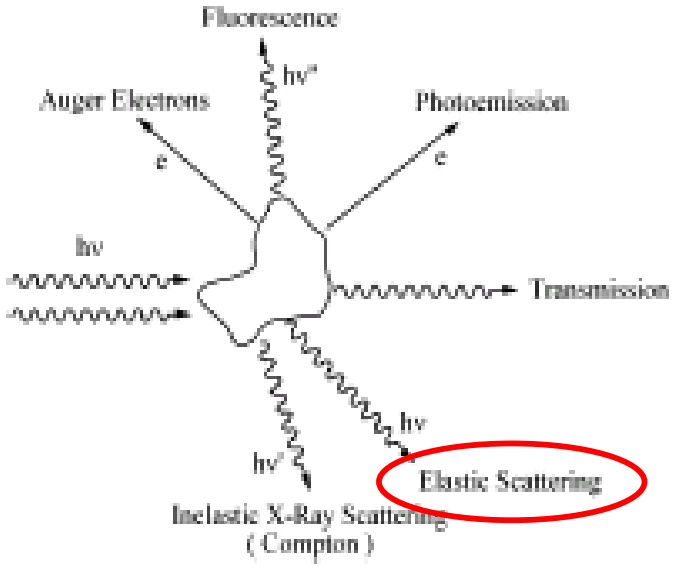

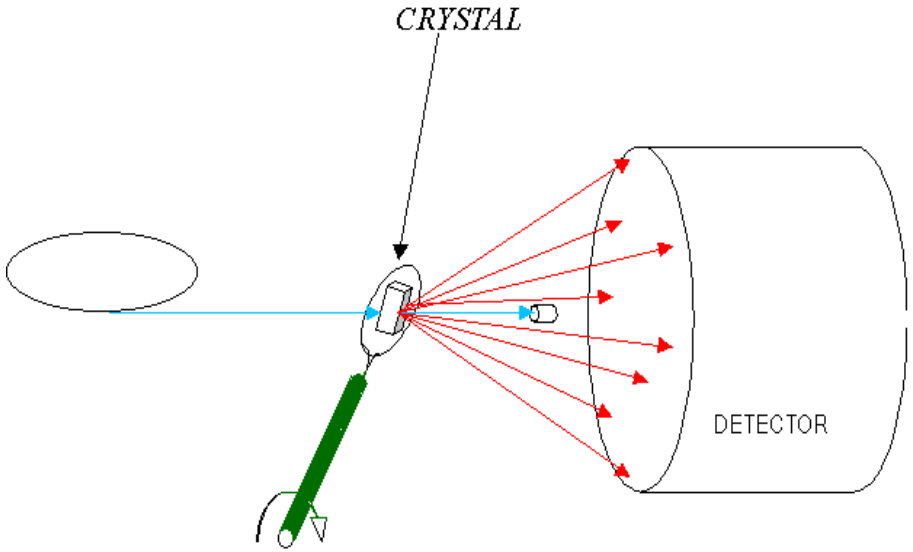

interatomic distances in the matter: d ~ 2-3 Å
wavelength λ ~ 1 Å

energy (eV) ~ 12.400/ λ(Å)

λ = 1 Å $\Rightarrow$ energy = 12.400 eV (hard x-rays)

Determination of molecular structures

Human serum
Vitamin D binding protein

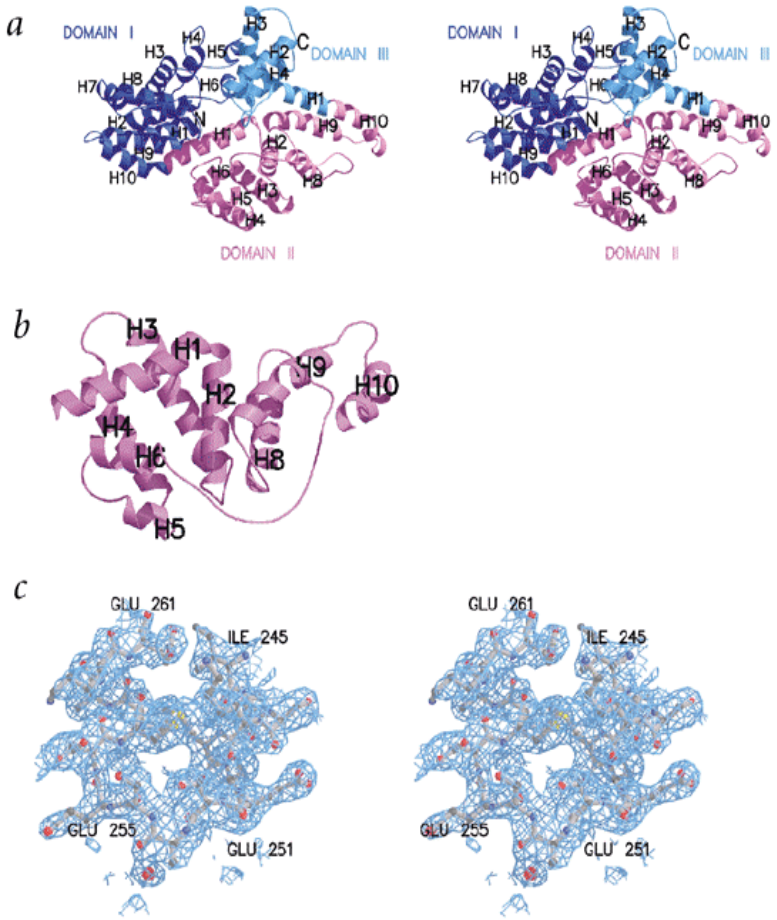

Varenna, 7th October 2003

Coronavirus Main Proteinase ($3CL^{pro}$) Structure: Basis for Design of Anti-SARS Drugs

Kanchan Anand,[1,2]† John Ziebuhr,[3]† Parvesh Wadhwani,[4] Jeroen R. Mesters,[1,2] Rolf Hilgenfeld[1,2]*

A novel coronavirus has been identified as the causative agent of severe acute respiratory syndrome (SARS). The viral main proteinase (M^{pro}, also called $3CL^{pro}$), which controls the activities of the coronavirus replication complex, is an attractive target for therapy. We determined crystal structures for human coronavirus (strain 229E) M^{pro} and for an inhibitor complex of porcine coronavirus [transmissible gastroenteritis virus (TGEV)] M^{pro}, and we constructed a homology model for SARS coronavirus (SARS-CoV) M^{pro}. The structures reveal a remarkable degree of conservation of the substrate-binding sites, which is further supported by recombinant SARS-CoV M^{pro}-mediated cleavage of a TGEV M^{pro} substrate. Molecular modeling suggests that available rhinovirus $3C^{pro}$ inhibitors may be modified to make them useful for treating SARS.

Varenna, 7th October 2003

- Analysis techniques
  - photoemission and photoabsorption
  - microscopy
  - x-ray diffraction
  - radiology

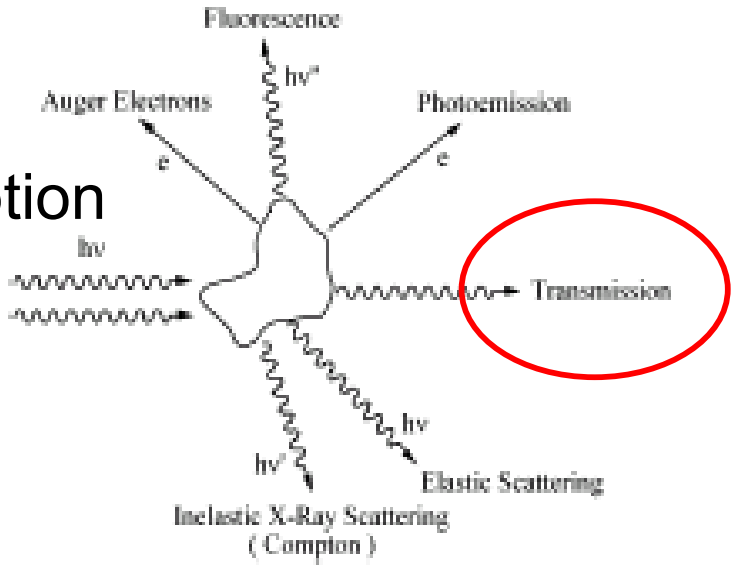

Goal of modern radiology:
Improvement of radiographic methods for the detection of low contrast and small size details delivering low dose

Radiology with synchrotron radiation:
- Choice of optimum wavelength
- Novel imaging techniques based on phase effects
  (Phase Contrast and Diffraction Enhanced Imaging)

Conventional radiology

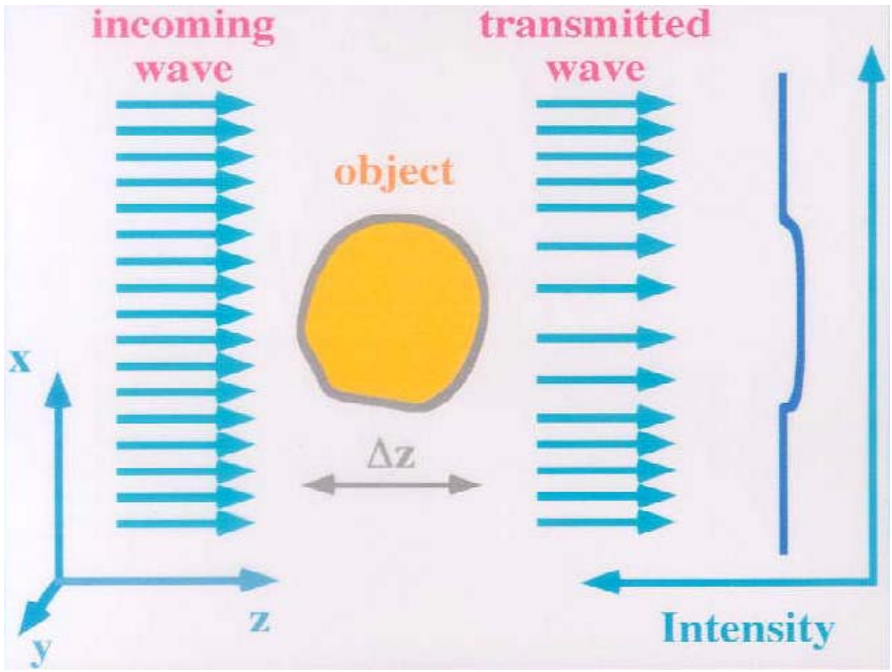

Phase Contrast Imaging

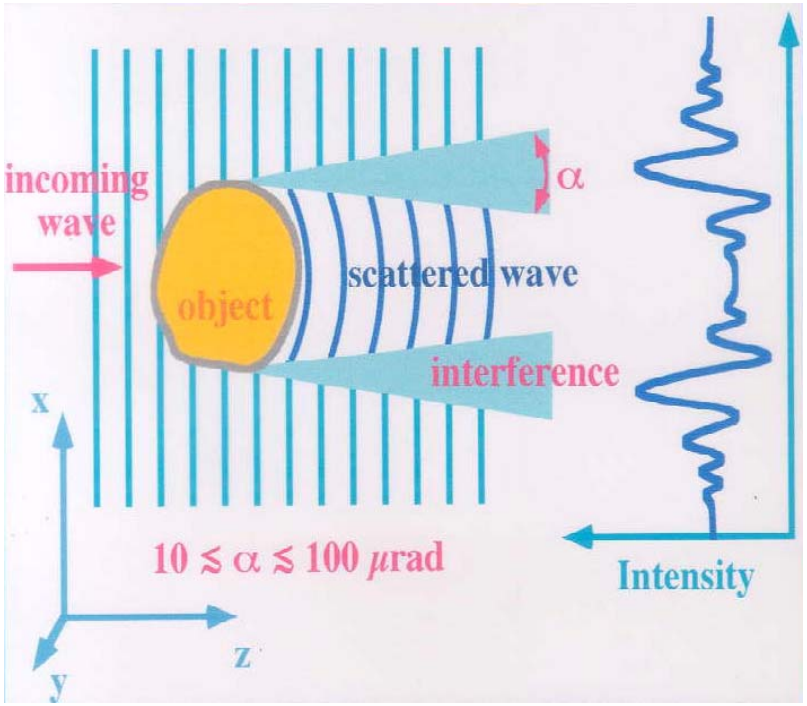

Mammary tissue + quartz spheres (100 μm diameter)

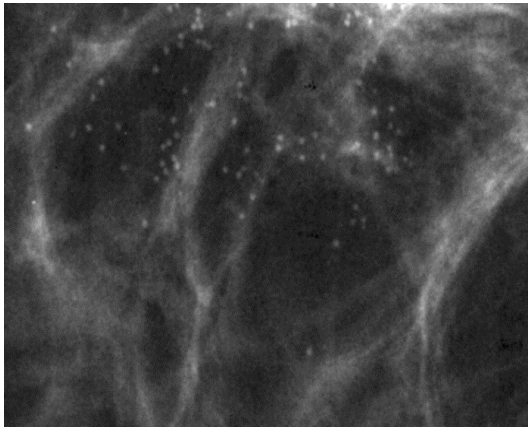

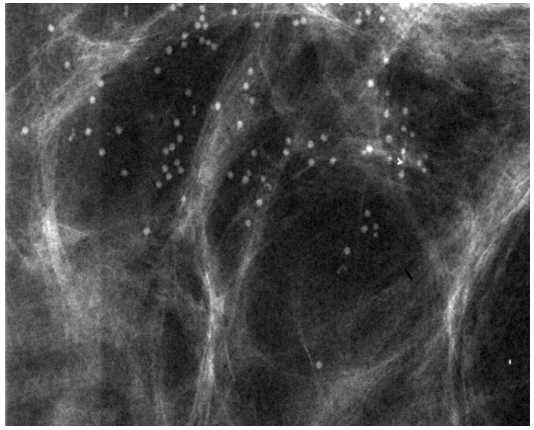

Nylon fibers

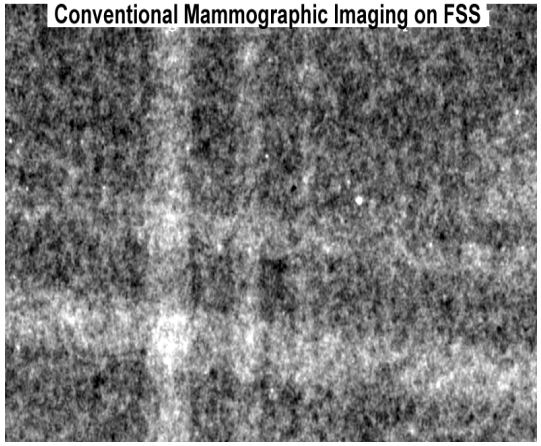

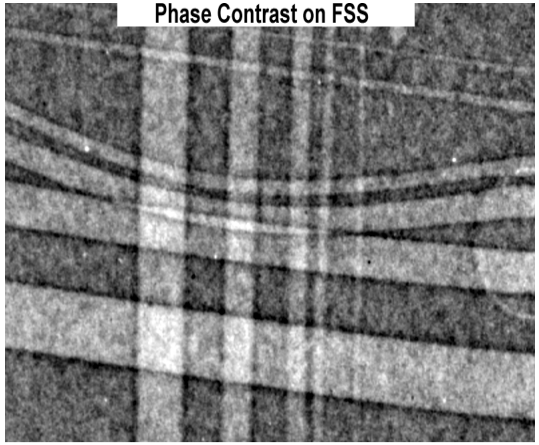

Conventional radiology

Phase Contrast Imaging

Mouse lung

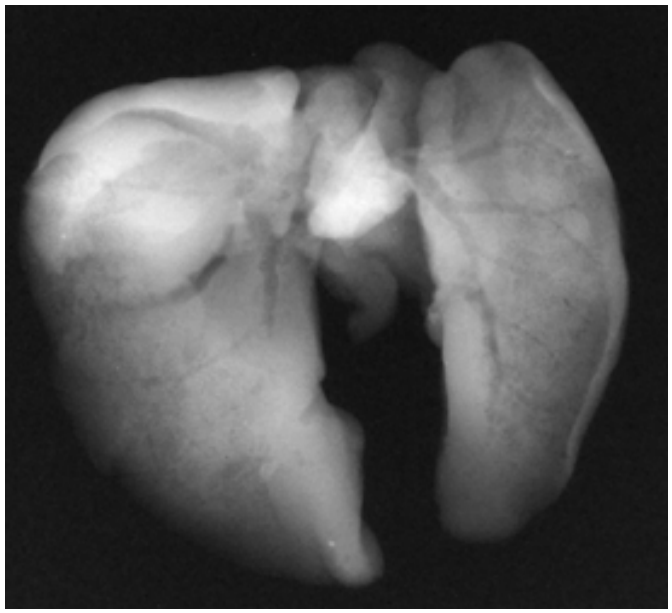

Conventional radiology

Diffraction Enhanced Imaging

- Properties of synchrotron radiation

- Analysis techniques
  - photoemission and photoabsorption
  - microscopy
  - x-ray diffraction
  - radiology

- Micro- and nanofabrication

Micro- and nanofabrication by x-ray lithography

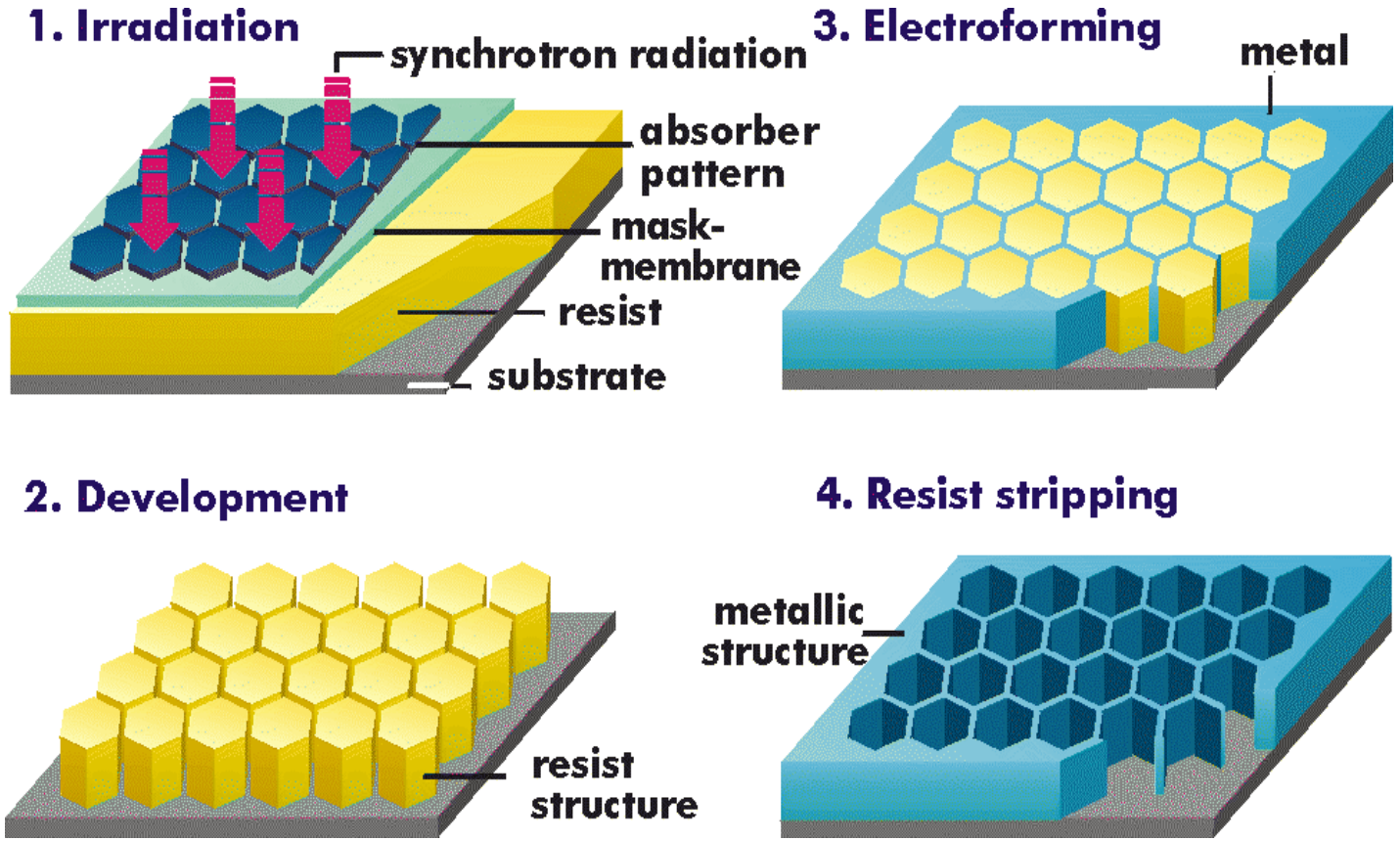

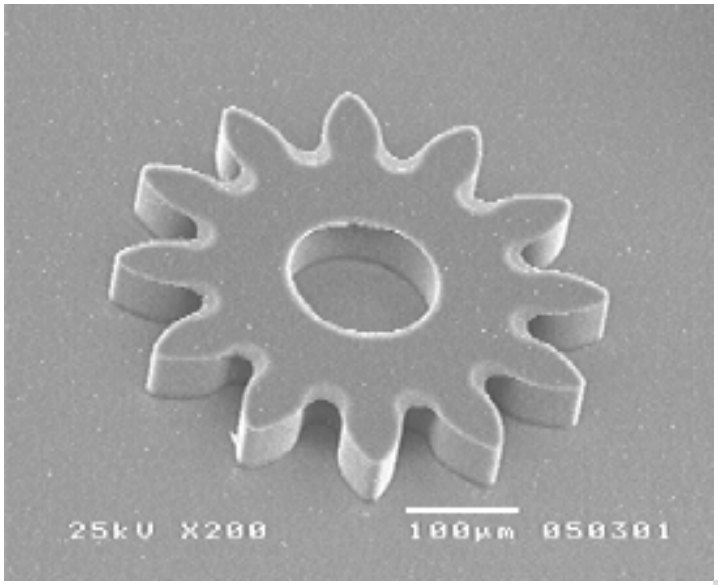

microgear

microturbine

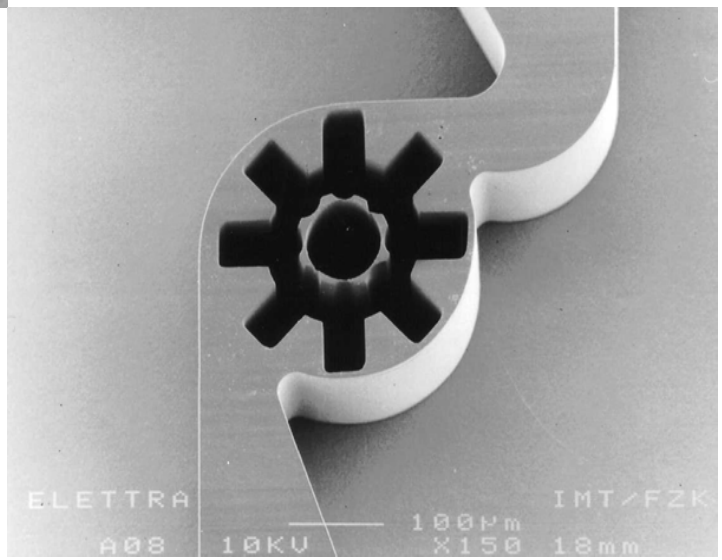

Photoabsorption Spectroscopy & Imaging with *Laser-Plasma* X-VUV Continua

(Atomic Photoionization with LPP)

John T. Costello

National Centre for Plasma Science & Technology (NCPST)
and School of Physical Sciences, Dublin City University

www.physics.dcu.ie/~jtc & john.costello@dcu.ie

Ultrashort High Energy Radiation & Matter, Varenna, Oct. 10 - 2003

Outline of Talk

Part I - Laser Plasma *'Line-Free'* Continuum Sources

- Origin, Brief History & Update

Part II - Dual Laser Plasma Experiments - Some Case Studies

- X-VUV Photoabsorption Spectroscopy
- VUV (Monochromatic) Photoabsorption Imaging

  Into the X-ray: Point Projection Absorption Spectroscopy

Part III - Next Steps Atomic Photoionization

- Photoionization of Atoms in Intense Laser Fields - 'Pump Probe' Experiments with X-VUV FELs

Collaborators and Contributors

Picosecond Continuum Sources
RAL - Edmund Turcu & Waseem Shaikh
QUB - Ciaran Lewis, Richard O'Rourke and A MacPhee
DCU - *Oonagh Meighan* and Cormac McGuinness

VUV Photoabsorption Imaging Facility - VPIF
Padua - Piergiorgio Nicolosi and Luca Poletto
DCU - John Hirsch, Kevin Kavanagh, Amit Neogi & Eugene Kennedy

Table Top -Point Projection Absorption Spectroscopy
QUB - Ciaran Lewis
DCU - Adrian Murphy

DESY 'Pump Probe' EU-RTD Project
Hasylab- Josef Feldhaus, Elke Ploenjes, Kai Tiedke et al.
Orsay- Michael Meyer & Patrick O'Keefe,
Lund- Jorgen Larsson et al.
MBI- Ingo Will et al.
DCU- Eugene Kennedy & John Hirsch
Padua- P Nicolosi

NCPST - CLPR

The CLPR node comprises 6 laboratories focussed on PLD (2) & photoabsorption spectroscopy/ imaging (4)

Staff: **John T. Costello, Eugene T. Kennedy, Jean-Paul Mosnier and Paul van Kampen**

PDs: **John Hirsch , Deirdre Kilbane +** ***2 Vacancies***

PGs: **Kevin Kavanangh, Adrian Murphy +** ***1 Vacancy*** **(JC), Jonathan Mullen (PVK), Alan McKiernan, Mark Stapleton & Rick O'Hare (JPM), Eoin O'Leary & Pat Yeates (ETK)**

MCFs: **Jaoine Burghexta (Navarra) and Nely Paravanova (Sofia)**

Part I -
Laser Plasma Continua

Laser Plasma Source Parameter Range

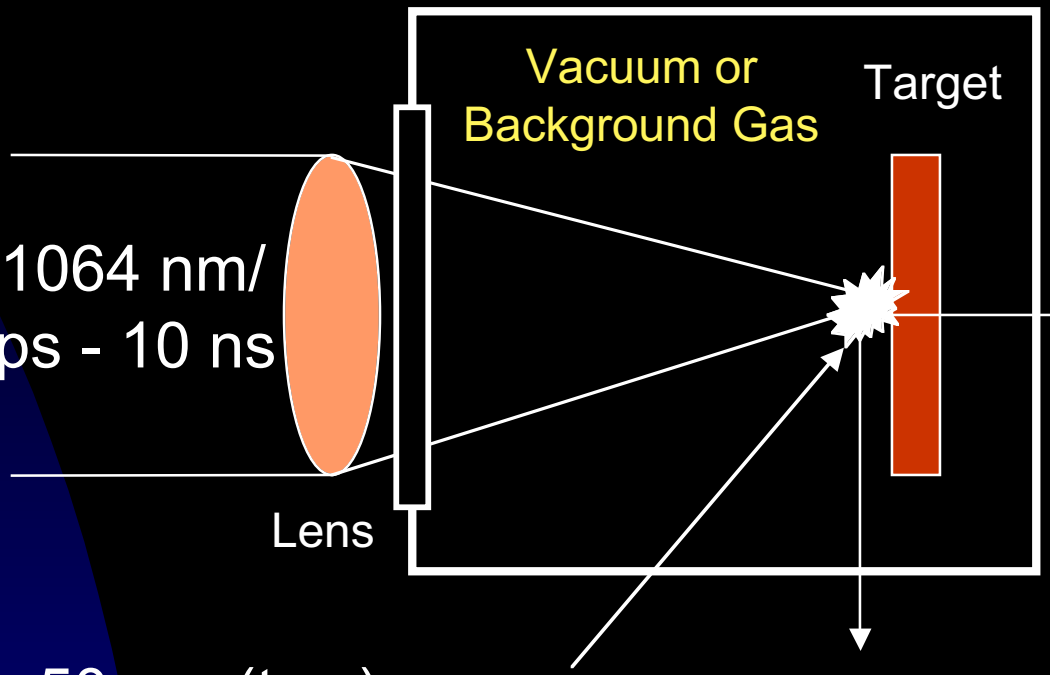

Laser Pulse 1064 nm/
0.01 - 1 J/ 5ps - 10 ns

Plasma
Assisted
Chemistry

Spot Size = 50 μm (typ.)

Φ: 10^{11} - 10^{14} W.cm^{-2}

T_e : 10 - 1000 eV

N_e: 10^{21} cm^{-3}

$V_{expansion} \geq 10^6$ cm.s^{-1}

Emitted -
Atoms,
Ions,
Electrons,
Clusters,
IR - X-ray Radiation

Laser Produced ‘Rare Earth’ Continua -
Physical Origin, History & Update

Laser Plasma *Rare Earth* XUV Continua

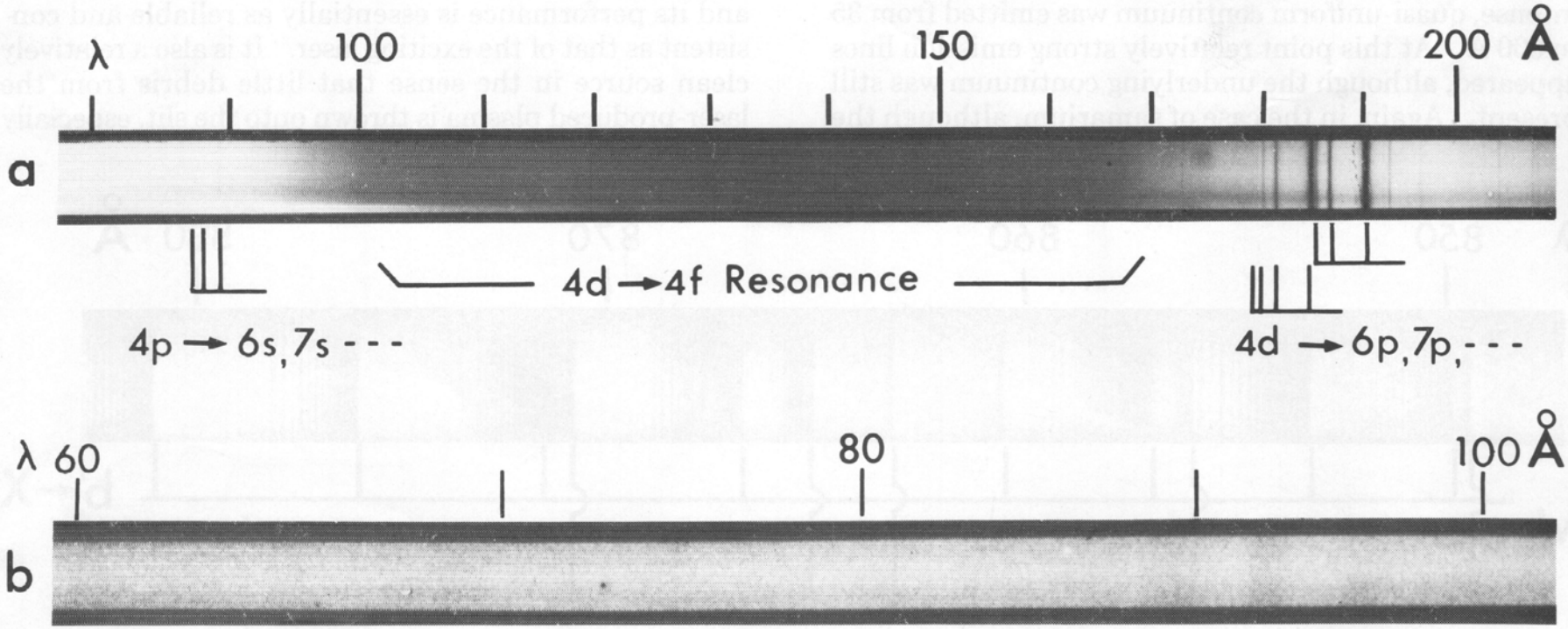

Fig. 1. (a) Absorption spectrum of xenon from 80 to 200 Å. The xenon pressure in the spectrograph was 0.05 Torr, and the number of laser pulses used was 30. For details of the xenon spectrum in this region see Madden and Codling.[5] The unmarked weak lines near 200 Å are due to 0 V. Oxygen present in the target gives rise to some emission lines as well. (b) The ytterbium continuum from 60 to 100 Å. The number of laser shots was 20. As in (a), the spectrum was obtained on a Kodak SC5 plate.

P K Carroll et al., Opt.Lett **2**, 72 (1978)

What is the Origin of the Continuum ?

Continua emitted from laser produced rare-earth (and neighbouring elements) plasmas are predominantly free-bound in origin and overlaid by Unresolved Transition Arrays (UTA) containing many millions of lines which share the available oscillator strength.

Brief History/ Highlights of Laser Plasma Rare-Earth' Continua -1990

1. First report of line free continua - P K Carroll et al., Opt.Lett **2**, 72 (1978)
2. First full study/ applications - P K Carroll et al., Appl.Opt. **19**, 1454 (1980)
3. VUV Radiometric Transfer Standard - G O'Sullivan et al., Opt.Lett **7**, 31 (1982)
4. Absolute Calibration with Synchrotron - J Fischer et al, Appl.Opt. **23**, 4252 (1984)
5. Photoelectron Spectroscopy - Ch. Heckenkamp et al., J.Phys.D **14**, L203 (1981)
6. First Study for XUV lithography - D J Nagel et al., Appl.Opt. **19**, 1454 (1980)
7. XUV Reflectometer - S Nakayama et al., Physica Scripta **41**, 754 (1990)
8. First Industrial Application - DuPont - Insulator Band Structure
   VUV Reflectance Spectroscopy - R H French, Physica.Scripta **41**, 404 (1990) - System subsequently made available commercially from ARC

For a review of the early years including applications in photoabsorption spectroscopy see :

1. J T Costello et al., Physica Scripta **T34**, 77 (1991)
2. P Nicolosi et al., J.Phys.IV **1**, 89 (1991)

Recent Developments in LP Continua I

→psec LPLS (RAL/QUB/DCU)

O Meighan et al., Appl.Phys.Lett **70**, 1497 (1997)

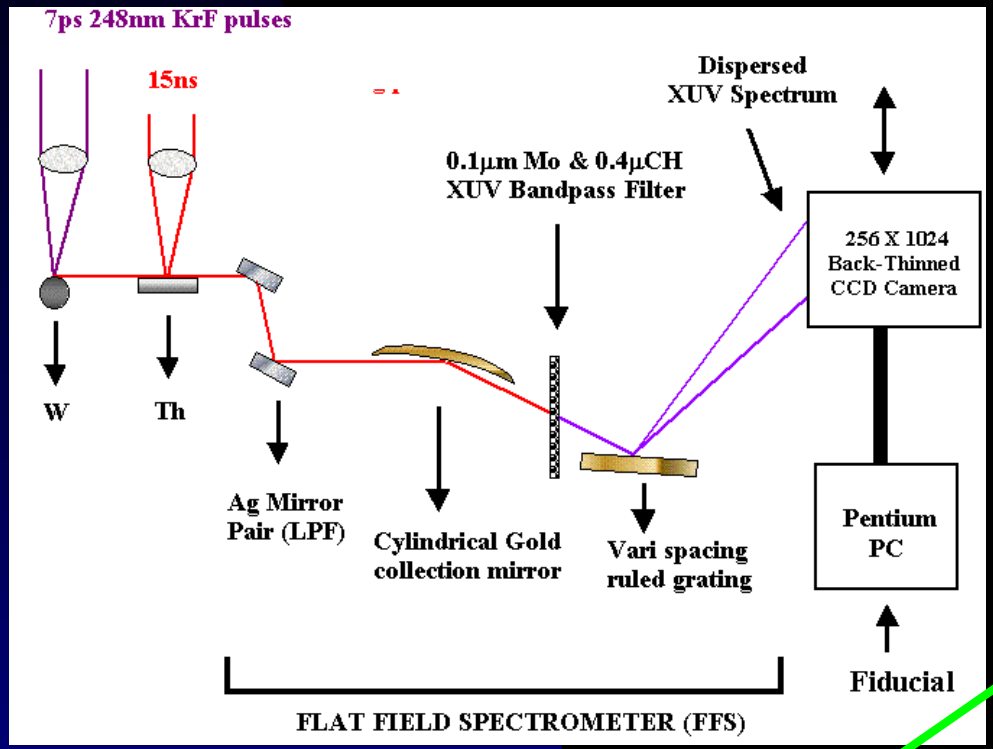

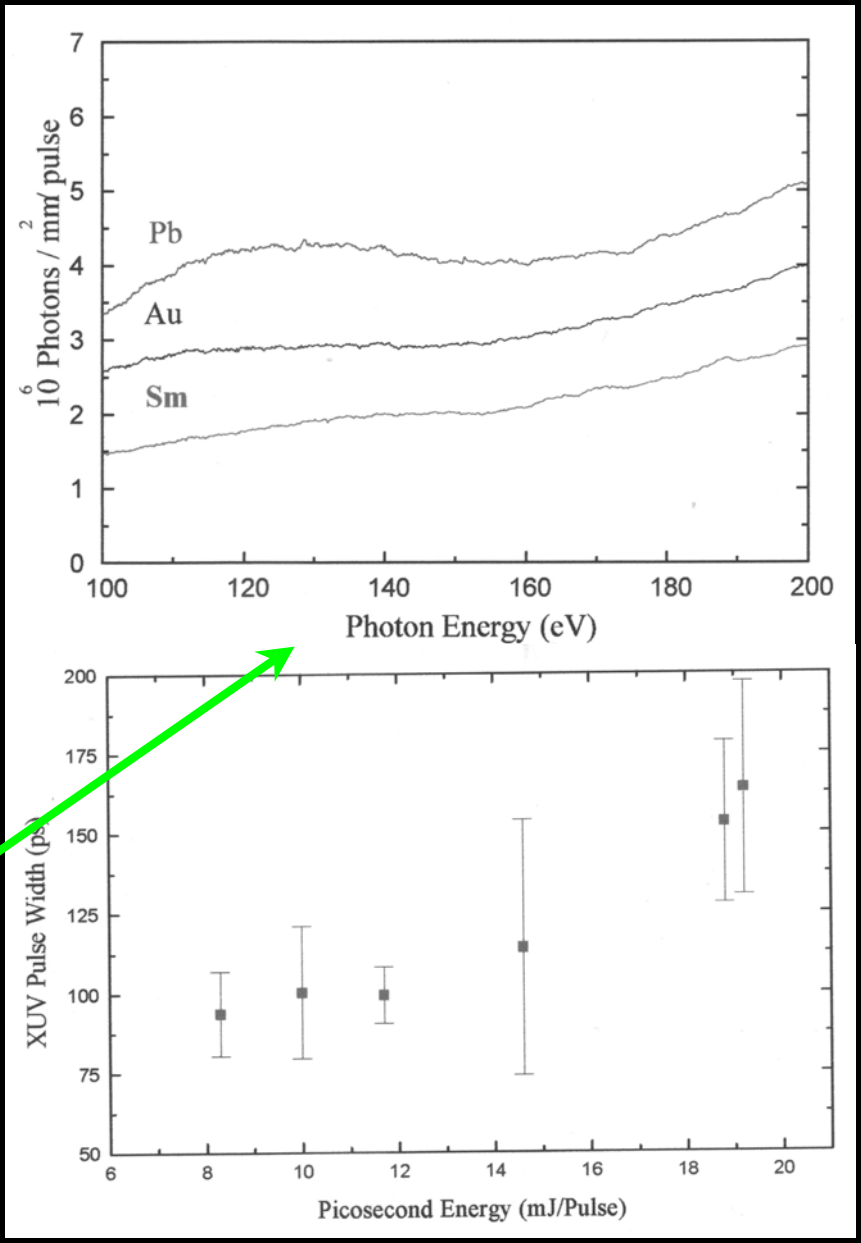

O Meighan et al., J.Phys.B:AMOP **33**, 1159 (2000)

*See also, M H Sher et al., Opt.Lett **18**, 646 (1993)*

Recent Developments in LP Continua -II

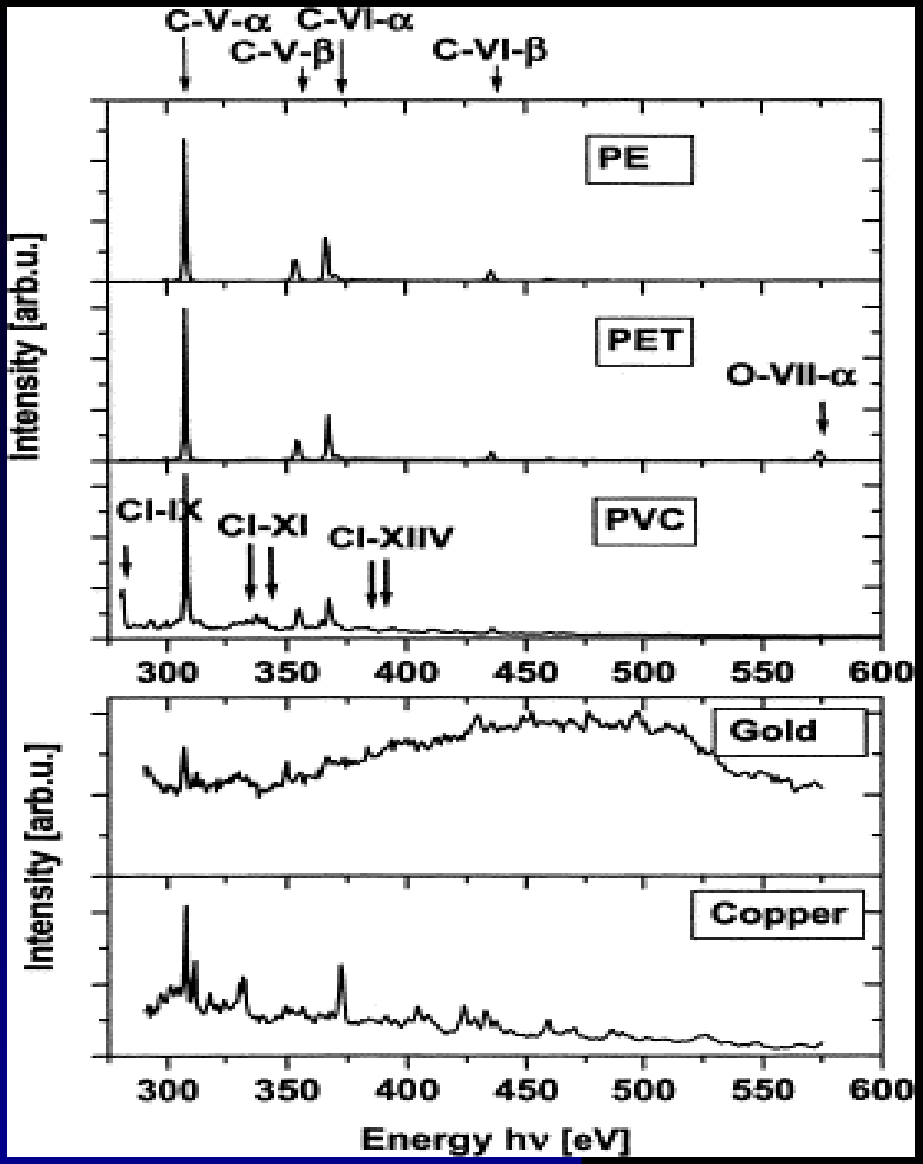

MBI Source - 2 trains per second/
25 - 400 Micro-Pulses per train

Laser: 15 mJ - 0.5 mJ per micropulse
& 25 ps pulse duration

XUV Pulse Duration -
(44 ps - Cu and 73 ps - PET)

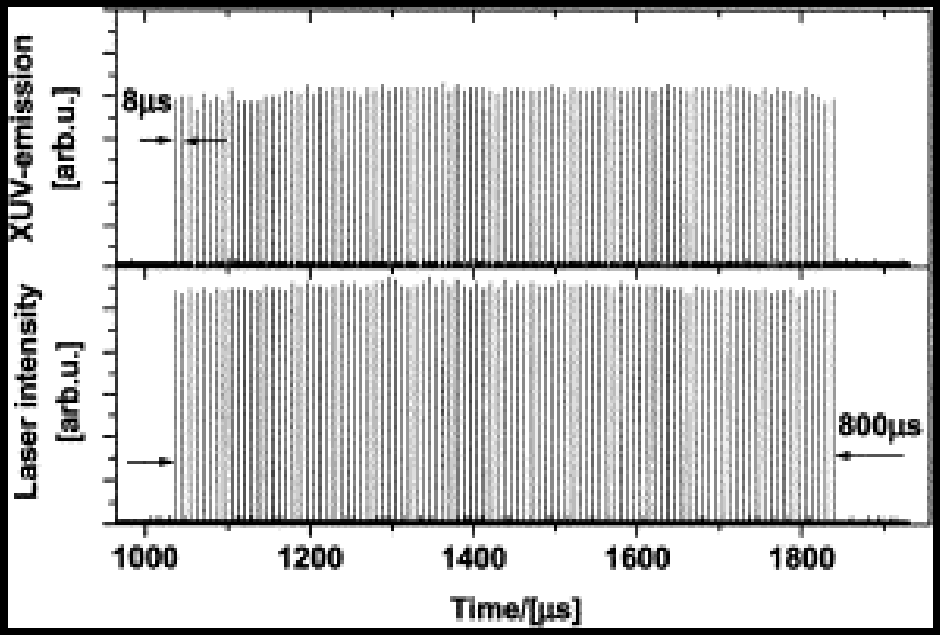

M Beck et al., Opt. Comm. **190,** pp317-326 (2001)

10^{11} Ph./1%/sr/train !!

Recent Developments in LP Continua -III

Photoionization Mass Spectrometry - Osnabruck

R Flesch et al., Rev.Sci.Instrum **71**, 1319 (2000)

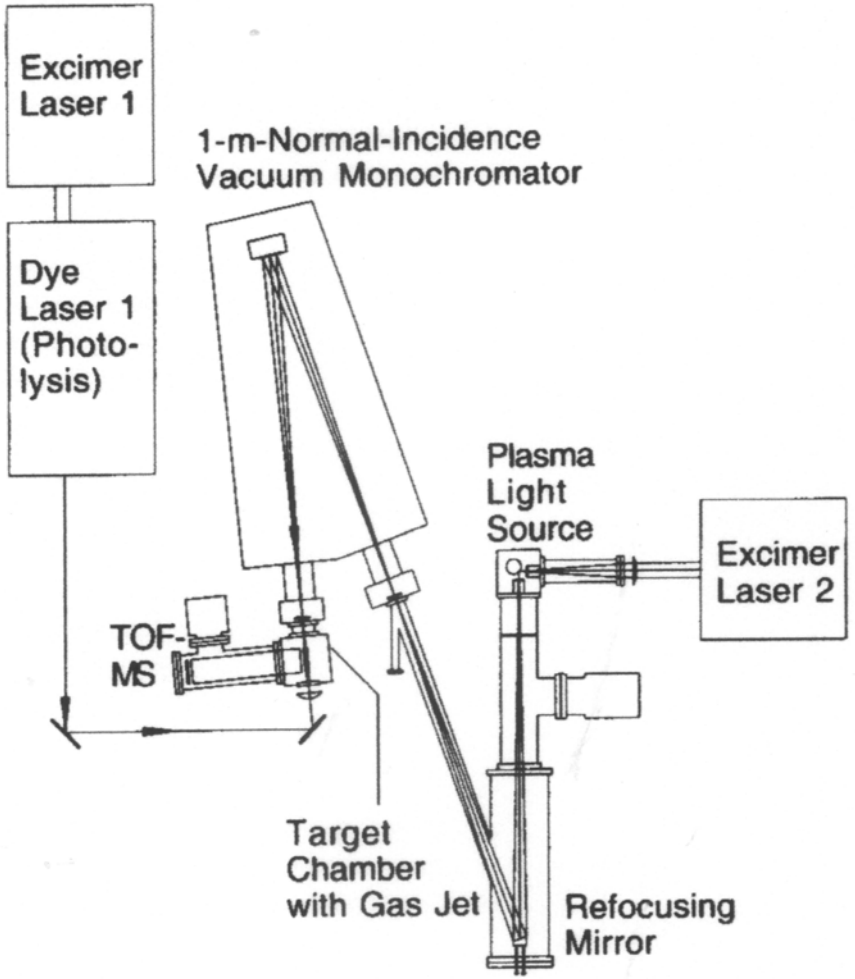

FIG. 1. Schematic diagram of the experimental setup.

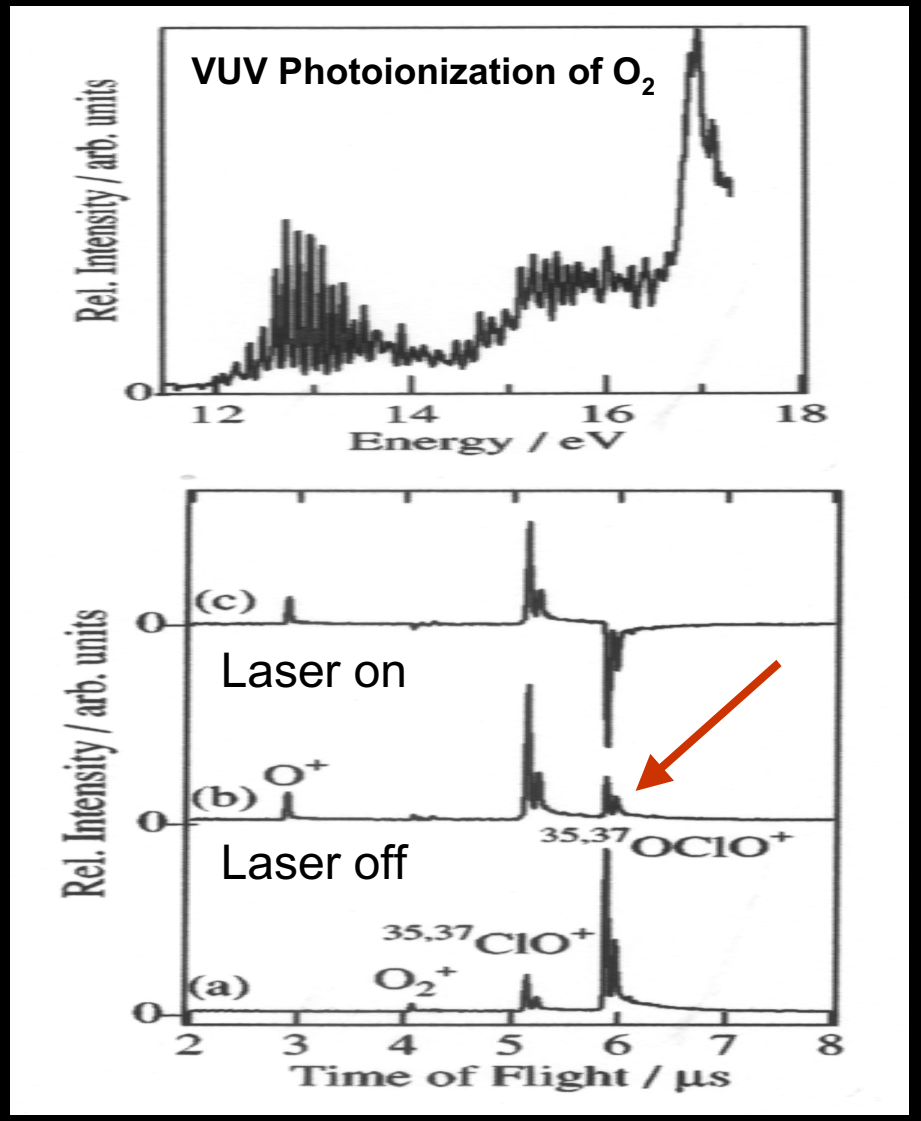

Summary - LP Continuum Light Sources

1. Table-top continuum light source now well established
2. Covers Deep-UV to soft X-ray spectral range
3. Pulse duration can be < 100 ps !
4. Continuum flux ~ 10^{14} photons/pulse/sr/nm (0.8J/10ns)
5. Low cost laboratory source - **needs greater awareness**
6. *Next step* -
   Working on (100 ps) + (6ns) Pre-plasma source -
   we already see a flux gain of up to X4 with Cu-
   A Murphy et al., Proc SPIE, **4876**, 1202 (2003)

Problem of plasma debris for work in clean environments -
proposals to solve, Michette, O'Sullivan, Attwood,…

Part II - Dual Laser Plasma Photoabsorption Experiments -

*****Ionic Photoionization*****

Why do X-VUV ionic photoionization?

Why Photoabsorption ?

- Access to ground/ metastable state (Dark) species
- Electric dipole excitation yields tractable spectra

Why specifically at VUV/XUV photon energies ?

- Photoionization continua
- Inner-shell/ multi-electron excitations

Data relevant to-

- Astrophysical spectra and models
- Laboratory plasma modelling & *diagnostics*
- Fundamental many-body theory
- X-ray laser schemes
- ICF

Photoionization of Atomic Ions

Not a lot known so far -

Nice review by John West in:

J.Phys.B:AMOP **34**, R45 (2001)

Covers DLP Experiments &
Merged Synchrotron + Ion Beams

Selected DLP Case Studies

1. Silicon ions - Tsukuba
2. Carbon ions - Padua

DLP Studies on Si - (FOM) & Tsukuba - I

Motivation - Optical properties of deposited Si nanoparticles

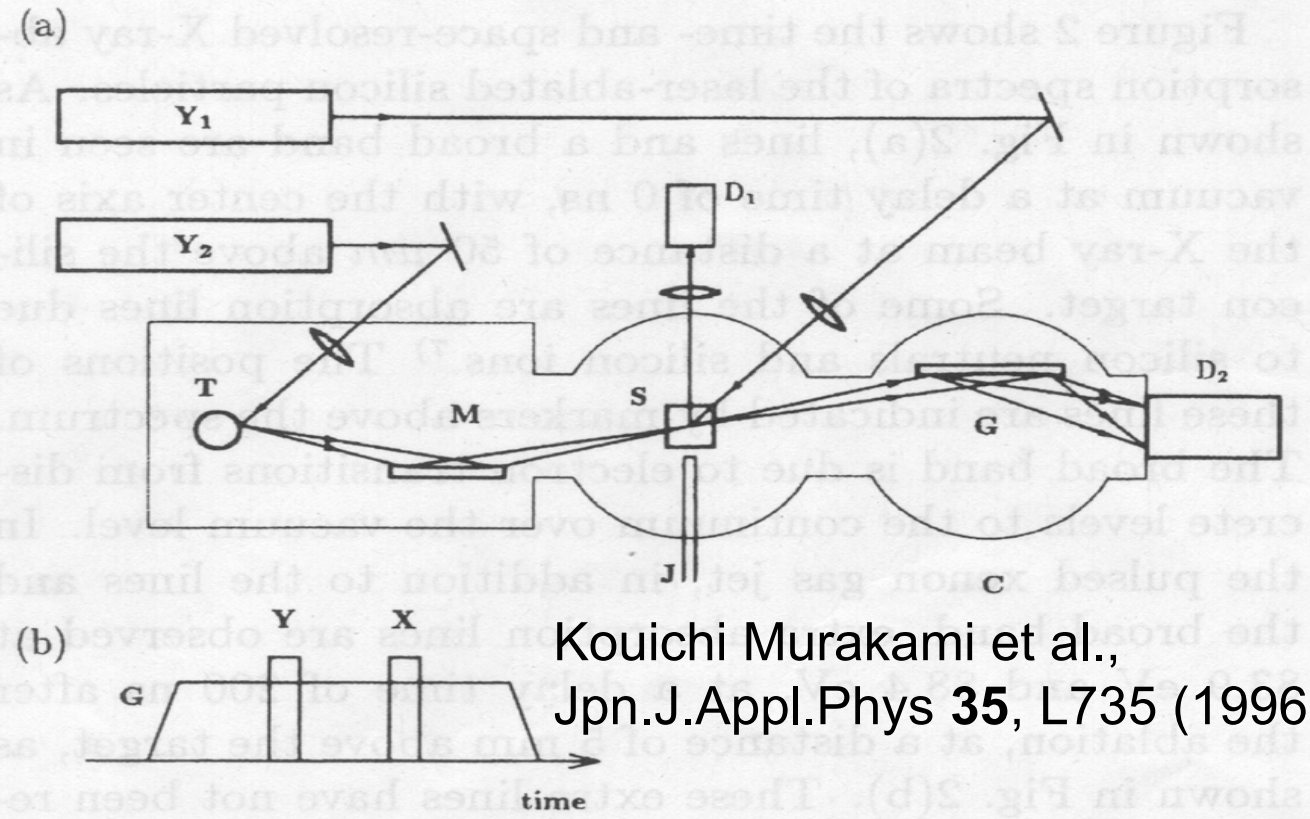

Kouichi Murakami et al.,
Jpn.J.Appl.Phys **35**, L735 (1996)

Fig. 1. (a) A schematic diagram of the experimental setup for time- and space- resolved soft X-ray absorption spectroscpy. (b) Time sequence of a pulsed gas jet (G), YAG laser light pulse for the laser ablation (Y) and the X-ray light pulse for absorption measurement (X).

DLP Studies on Si - (FOM) & Tsukuba - II

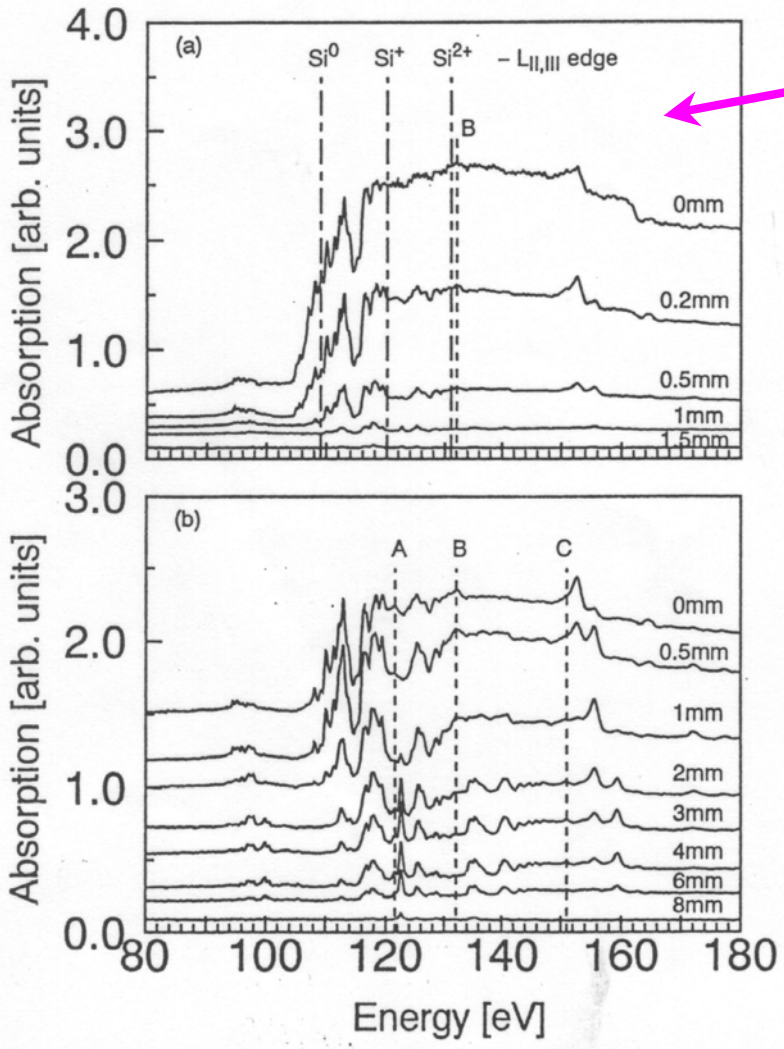

Fig. 6. X-ray absorption spectra at an energy density of 20 J/cm^2 and a delay time of 40 ns (a), and at 20 J/cm^2 and a delay time of 120 ns (b).

Murakami et al.,
Jpn.J.Appl.Phys **33**, 2586 (1994)

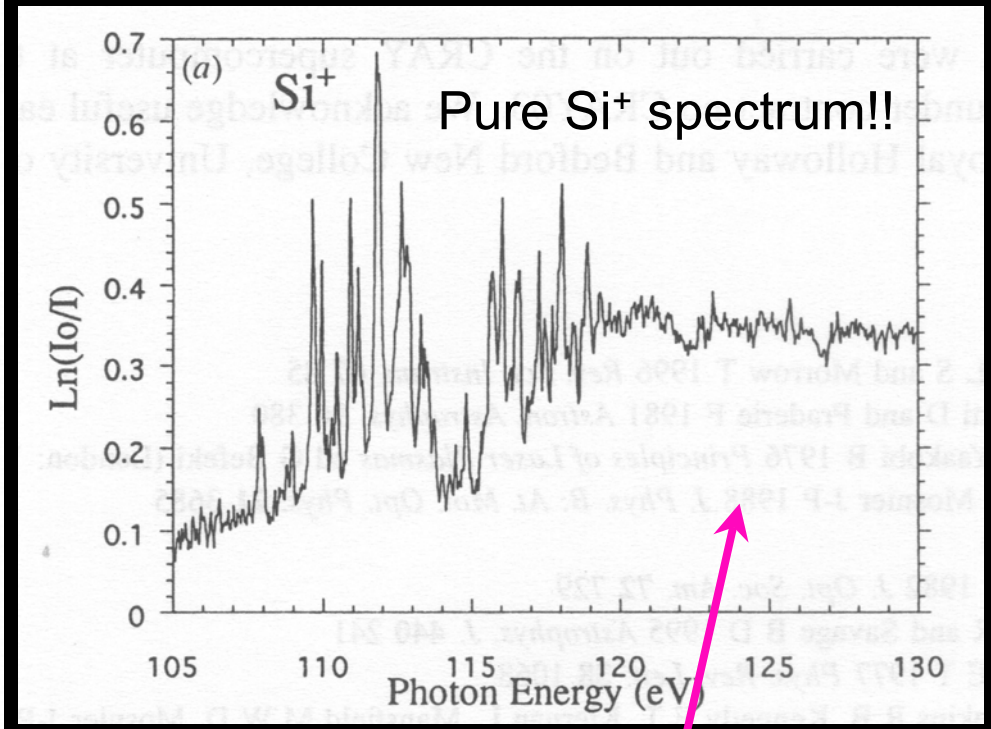

J. T. Costello et al.,
J.Phys.B:AMOP **31**, 677 (1998)

Summary - Tsukuba

Work centres on determining conditions under which clusters .vs. atoms/ atomic ions are formed with a view to optimising nanocluster formation and enhancing their optical properties, (lifetime, efficiency, wavelength, ..)

XUV permits them to access more highly charged ions in their PLD plumes

The Tsukuba group now combine XUV-DLP with PLD / Photo-Luminescence Spectroscopy - potential for 'Closed Loop Control' here

DLP Studies on C Ions (Padua)- I
VUV Photoabsorption - *Absolute Cross-sections* !

Motivation: Ions of astrophys. interest, tests of databases (Opacity, etc.)

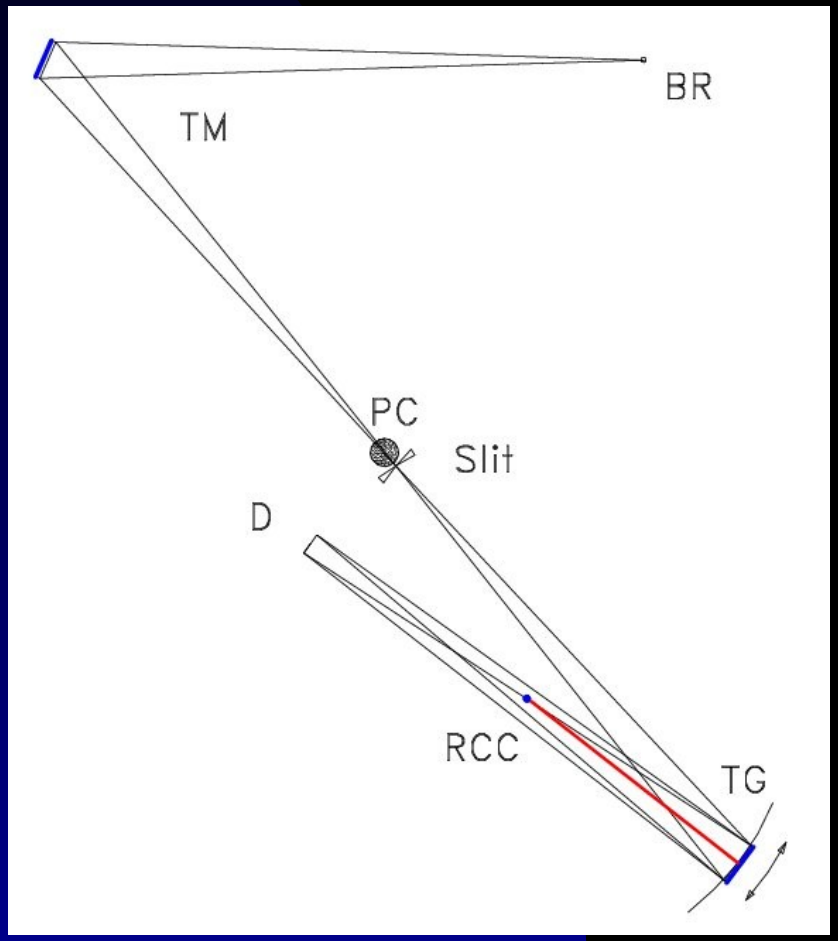

Normal Incidence DLP Setup

P Recanatini, P Nicolosi & P Villoresi,
Phys. Rev. A **64**, Art. No. 012509 (2001)

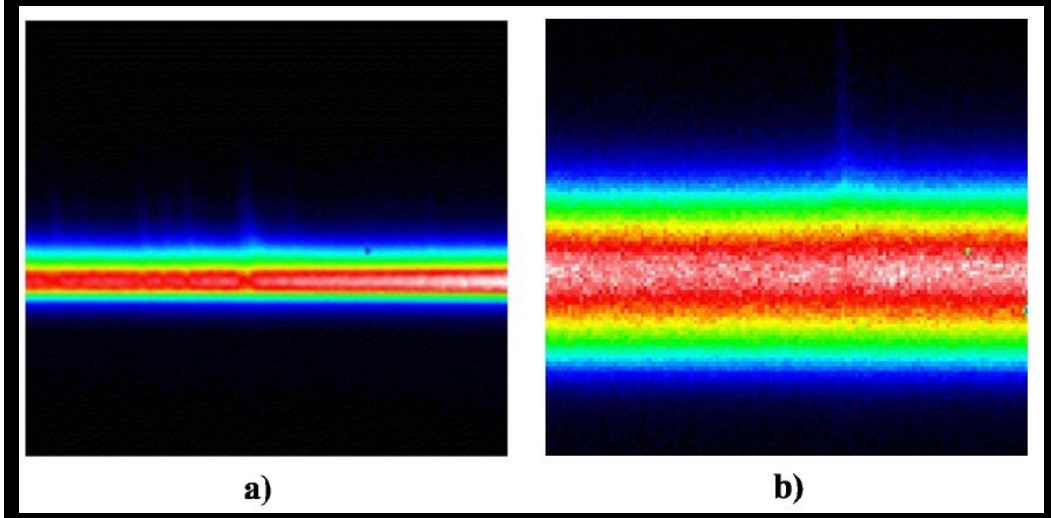

Spaced resolved emission from a W plasma
in the VUV around (a) 49 nm and (b) 69 nm

DLP Studies on Ions (Padua) - II, C^+

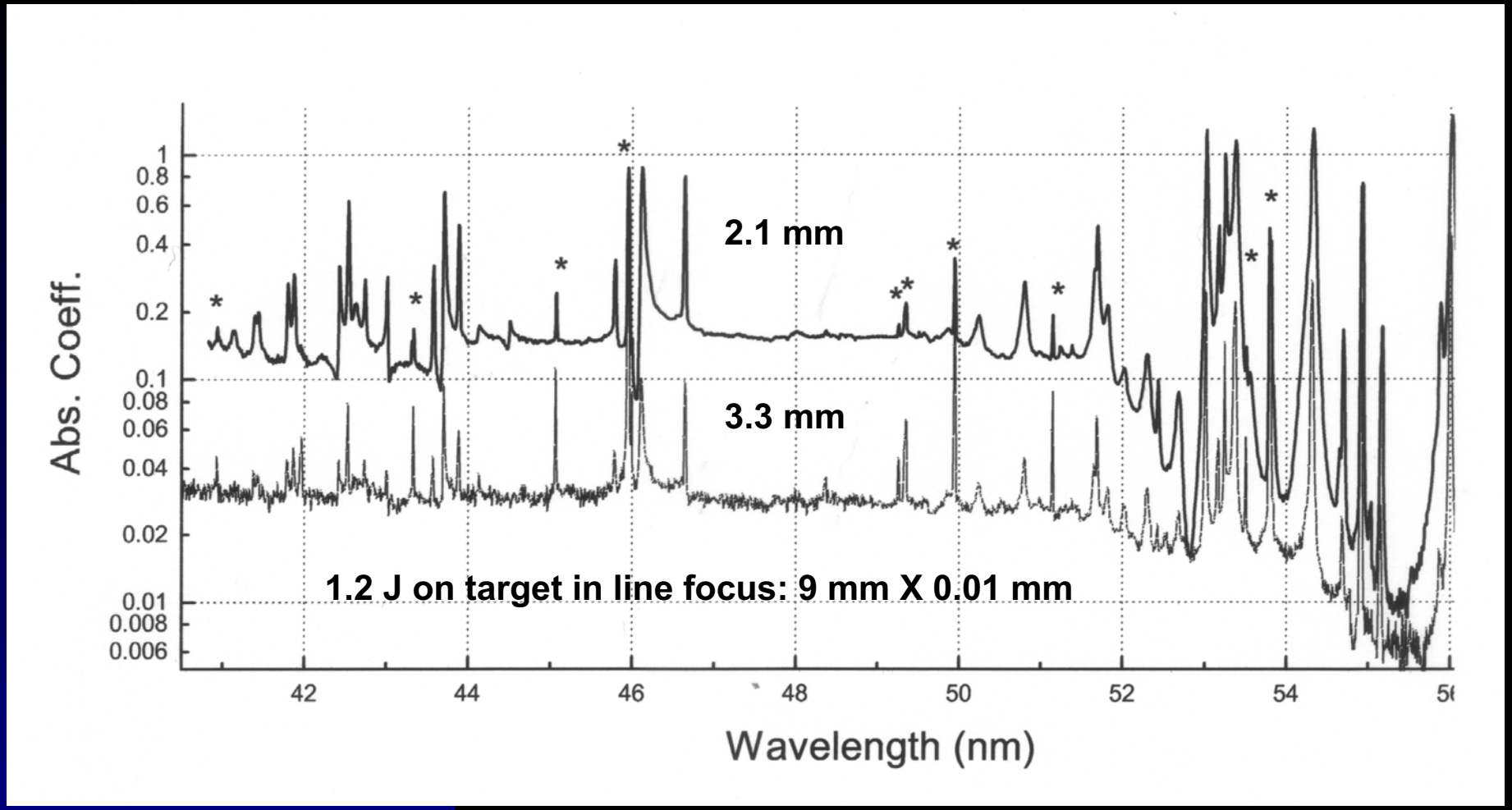

Absorption spectra of C+ taken at an inter-plasma delay of 58 ns and at 2.1 and 3.3 mm above the carbon target surface

DLP Studies on C Ions (Padua) - III
K-shell absorption along the C-isonuclear sequence

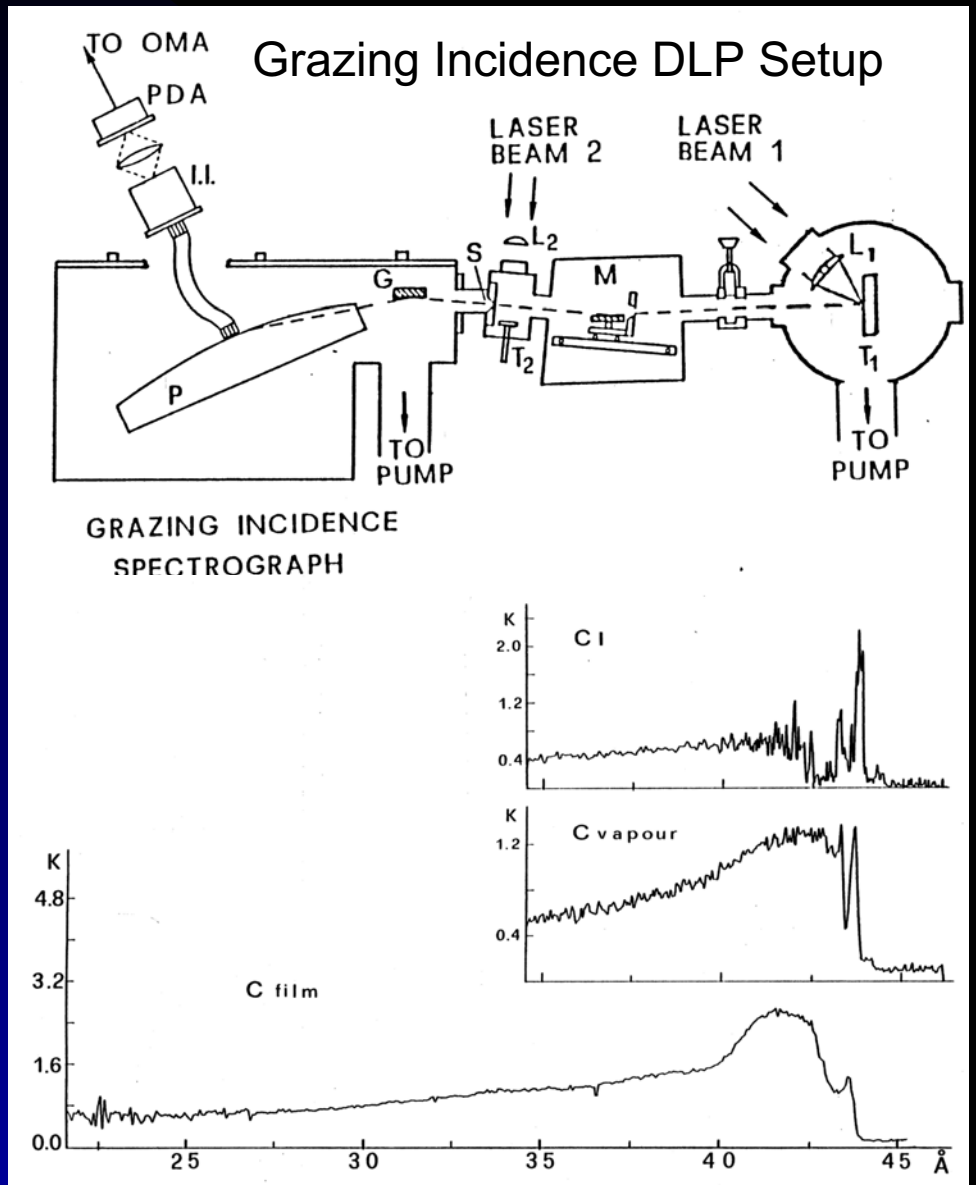

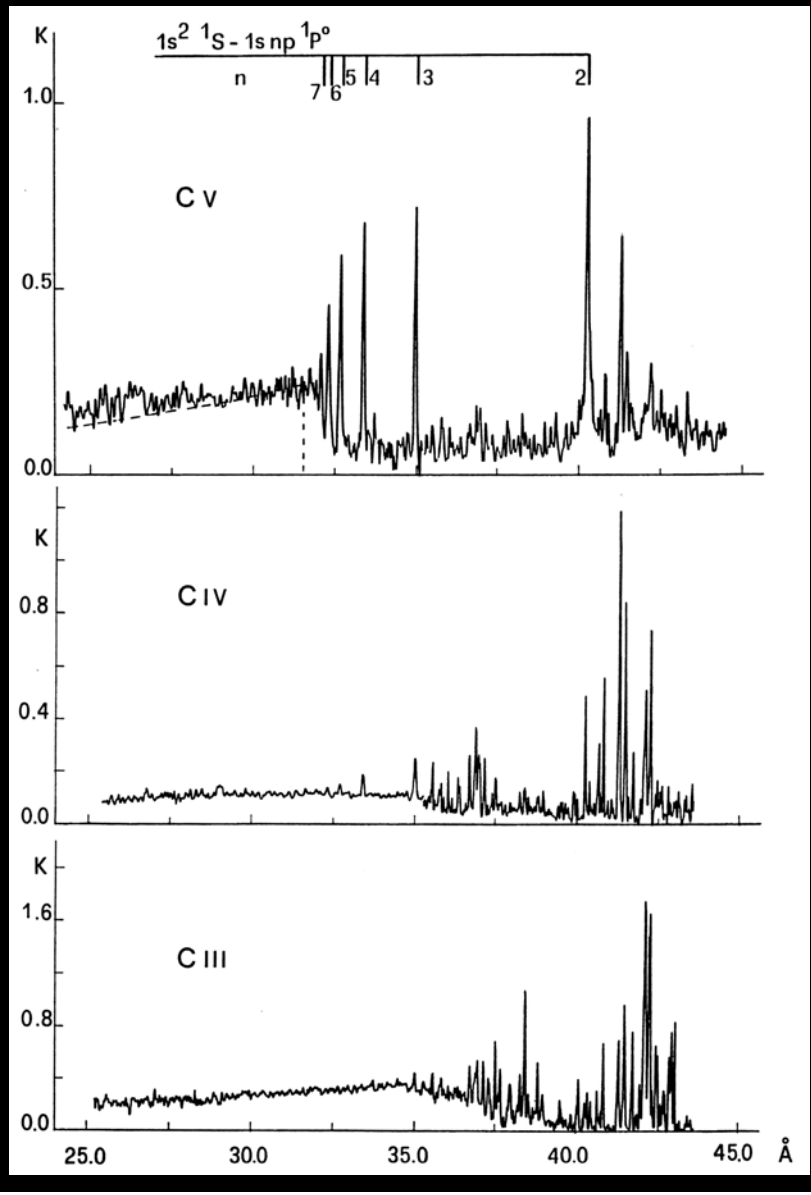

Summary - Padua

Work centres low-Z ions of astrophysical interest

All isonuclear sequences of Be, B and C measured.

Designed and built DLP systems to work from VUV to Soft X-ray (Carbon K)

Have determined absolute photoabsorption cross sections using DLP

Dublin

Have published ca. 60 papers on DLP photoabsorption experiments on selected atoms and ions from all rows of the periodic table.

Motivation - almost always exploration of some 'quirk' of the photoionization process in a many electron atom !

But no time to discuss them now !!!!!

Because I want to talk about.....

VUV Photoabsorption Absorption Imaging

VUV Photoabsorption Imaging

Collaboration between DCU & Univ. Padua

Key paper:

J Hirsch, E Kennedy, J T Costello, L Poletto & P Nicolosi

Rev.Sci. Instrum. **74**, 2992 (2003)

Principle tested at RAL-CLF in
a QUB/RAL/DCU expt. 1999

VUV Photoabsorption Imaging Principle

John Hirsch et al, J.Appl.Phys. **88**, 4953 (2000)

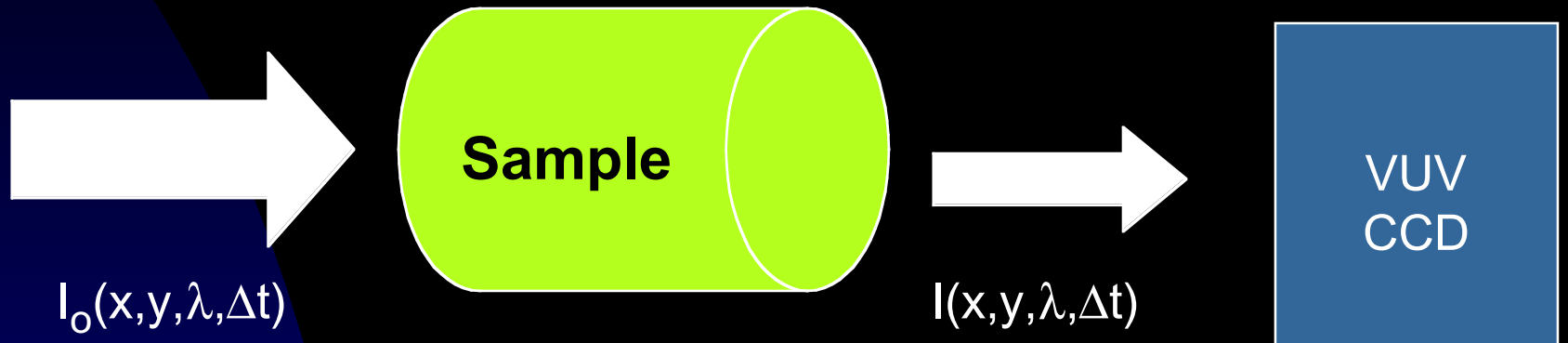

$$I = I_0 e^{-\sigma \int n(l)dl}$$

Pass a *collimated* VUV beam through the plasma sample and measure the spatial distribution of the absorption.

Motivations

1. Direct imaging of light emitted by a plasma using gated array detectors (e.g., ICCD) provides information on excited species only

2. Probing plasma plumes using tuneable lasers provides information on non-emitting species but is limited to wavelengths > 200 nm or so

Why a pulsed, tuneable and collimated beam ?

- **Pulsed**

Automatic time resolution:

the VUV pulse duration ~ laser pulse duration (~1-30 ns)

- **Tuneable**

Can access all resonance lines of all atoms & moderately charged ions with resonances between 30 nm and 100 nm (present system)

- **Collimated**

Can place the sample and CCD anywhere along the beam

Advantages of using a VUV beam

1. VUV light can probe the higher (electron) density regimes not accessible in visible absorption experiments

2. The refraction of the VUV beam in a plasma is reduced compared to visible light with deviation angles scaling as λ^2

3. The images analysis is not complicated by interference patterns since the VUVcontiuum source has a small coherence length (μms)

4. VUV light can be used to photoionize atoms and ions - this process simplifies greatly the equation of radiative transfer (no bound states).

5. Fluorescence to electron emission branching ratio for many inner shell transitions can be 10^{-4} or even smaller => almost all photons are converted to electrons

VUV Photoabsorption Imaging Facility-

'V-P-I-F'

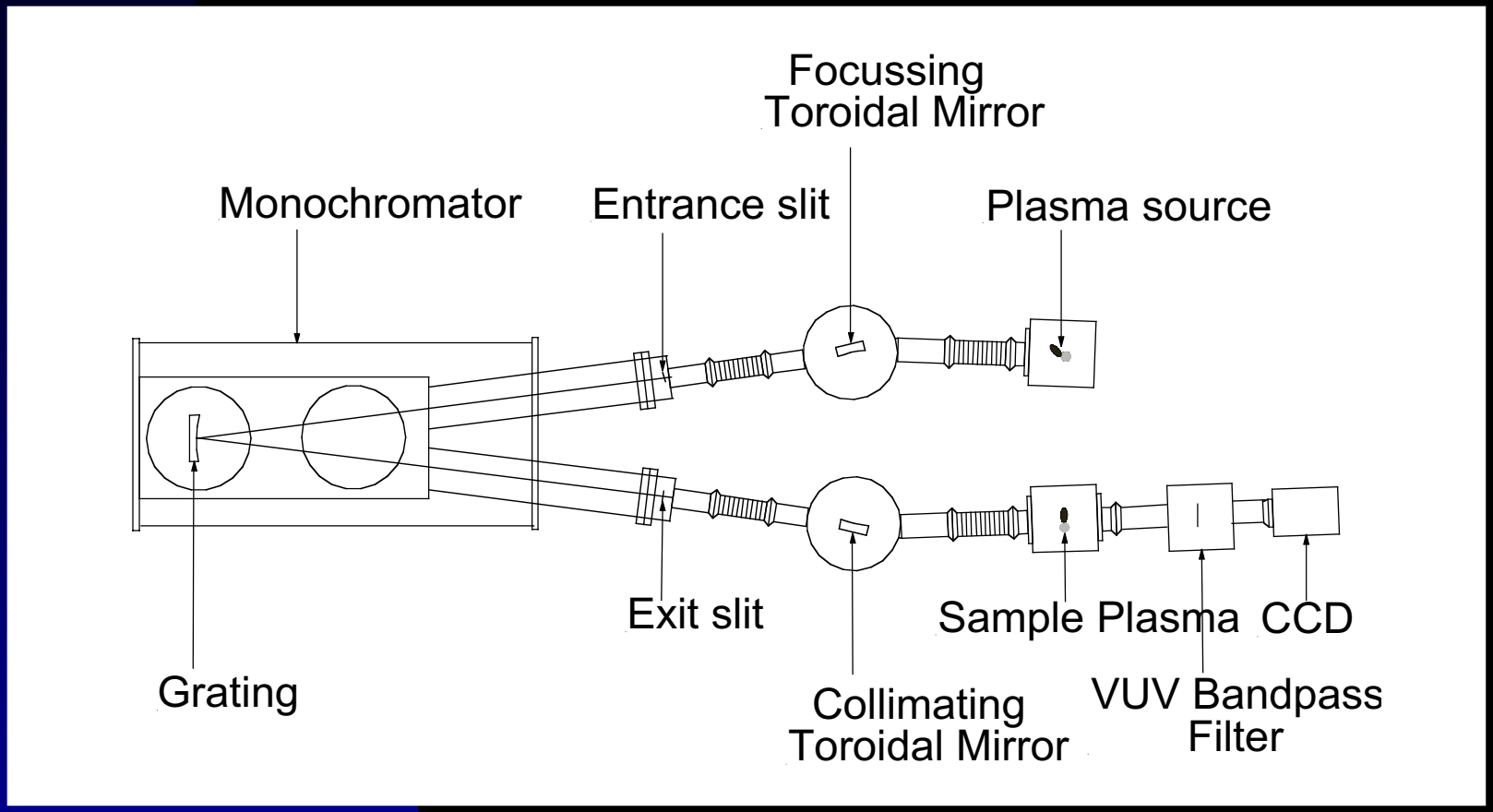

VPIF - The obligatory picture !

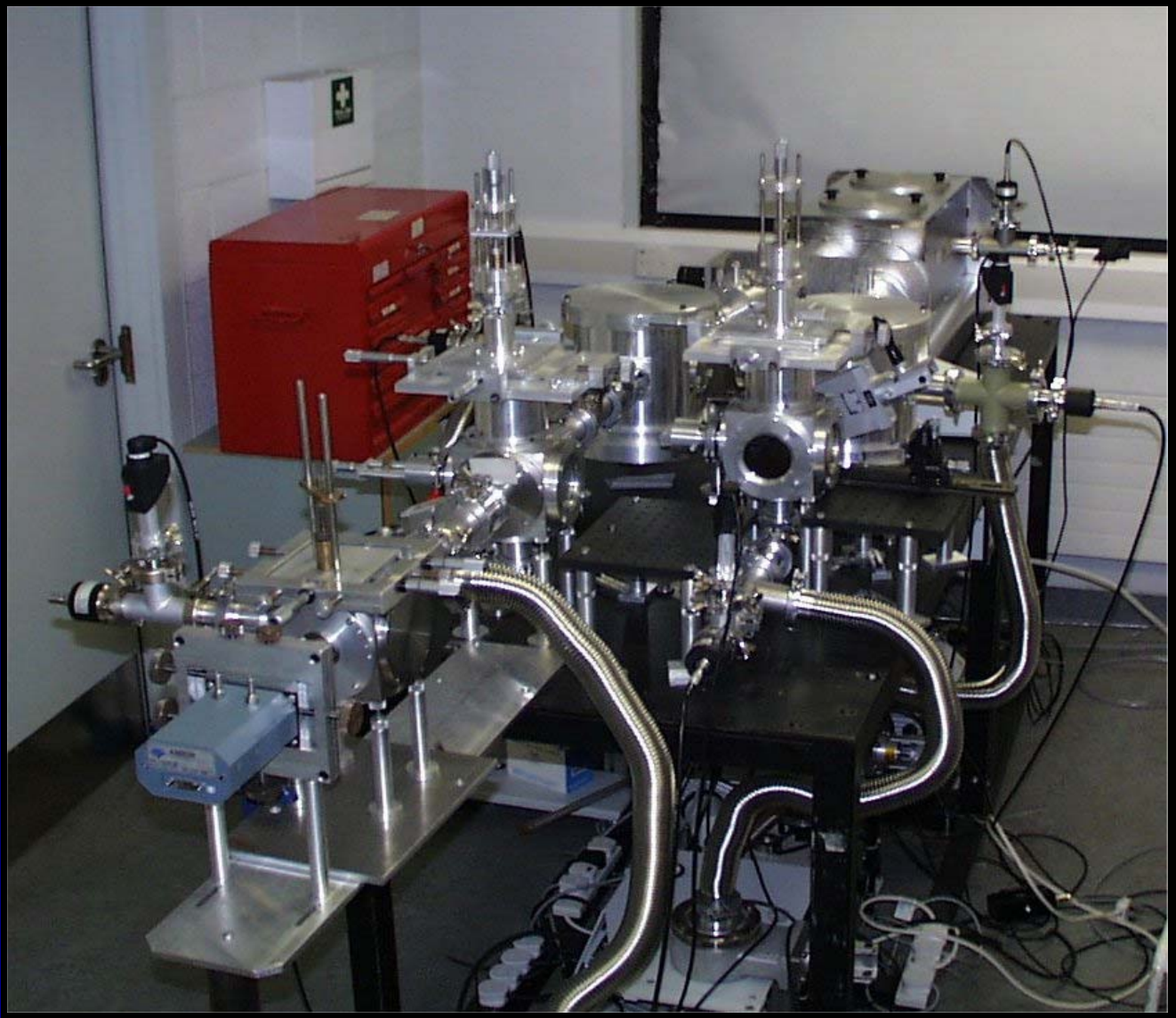

VPIF Specifications

Time resolution:	~10 ns (200 ps with new EKSPLA)
Inter-plasma delay range:	0 - 10 μsec
Delay time jitter:	± 1ns
Monochromator:	Acton™ VM510 (f/12, f=1.0 m)
VUV photon energy range:	10 - 35 eV
VUV bandwidth:	0.025 eV @25 eV (50μm/50μm slits)
	~0.05 nm @ 50 nm
Detector:	Andor™ BN-CCD,
	1024 x 2048/13 μm x 13 μm pixels
Spatial resolution:	~120 μm (H) x 150 μm (V)

What do we extract from I and Io images ?

Absorbance: $$A = \log_{10}\left(\frac{\int I_0(x,y,t,\lambda)d\lambda}{\int I(x,y,t,\lambda)d\lambda}\right)$$

Equivalent Width: $$W_\lambda = \Delta\lambda\left(\frac{\int [I_0 - I]d\lambda}{\int I_0 d\lambda}\right)$$

$$W_\lambda = \int [1 - e^{-\sigma(\lambda)NL}]\mathrm{d}\lambda$$

Some Preliminary Results:

Time resolved W_λ maps of Ca plume species

Tune system to 3 unique resonances

Ca: $3p^6 4s^2\ (^1S) - 3p^5 4s^2 3d\ (^1P)$

Ca^+: $3p^6 4s\ (^2S) - 3p^5 4s^2 3d\ (^2P)$

Ca^{2+}: $3p^6\ (^1S) - 3p^5 3d\ (^1P)$

Maps of equivalent width of atomic calcium using the 3p-3d resonance at 39.48 nm (31.4 eV) - 200 mJ on line focus 3mm x 0.015 mm

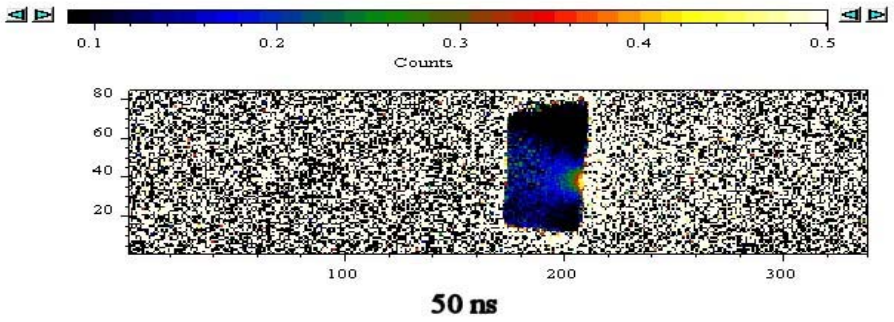

50 ns

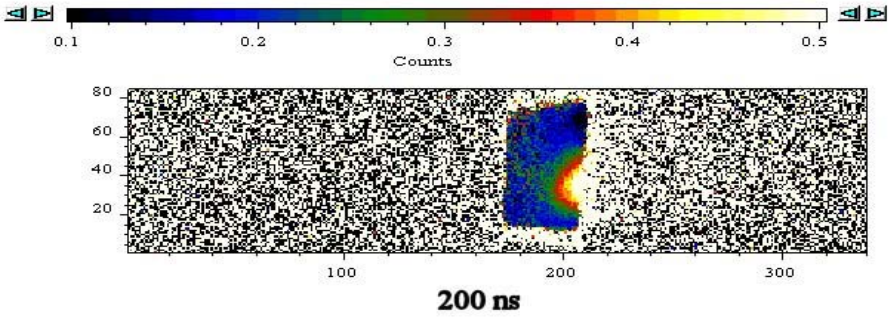

200 ns

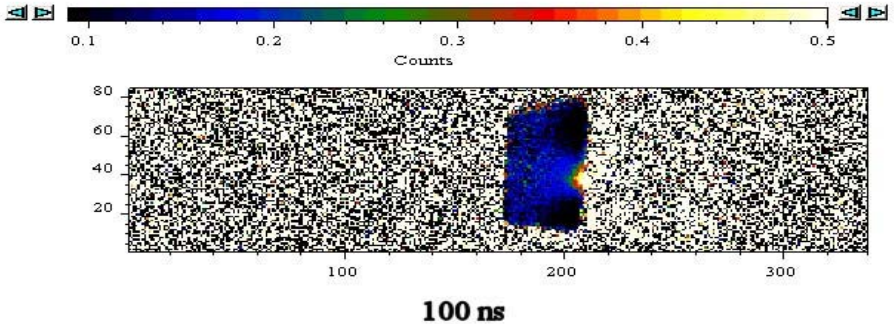

100 ns

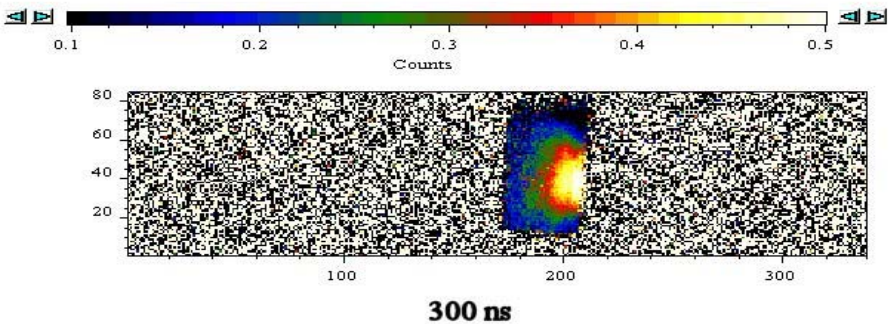

300 ns

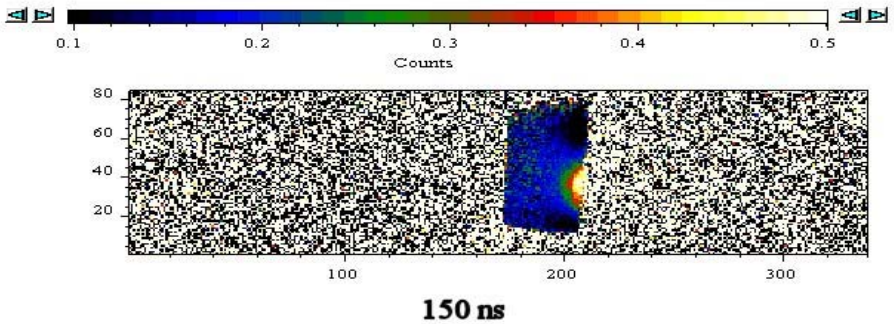

150 ns

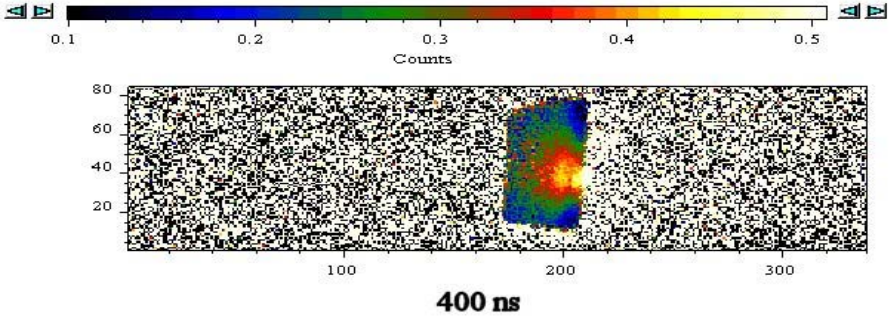

400 ns

Maps of equivalent width of Ca^{+} using the 3p-3d resonance at 31.4 eV - (200 mJ/15ns on line focus 5 mm x 0.015 mm)

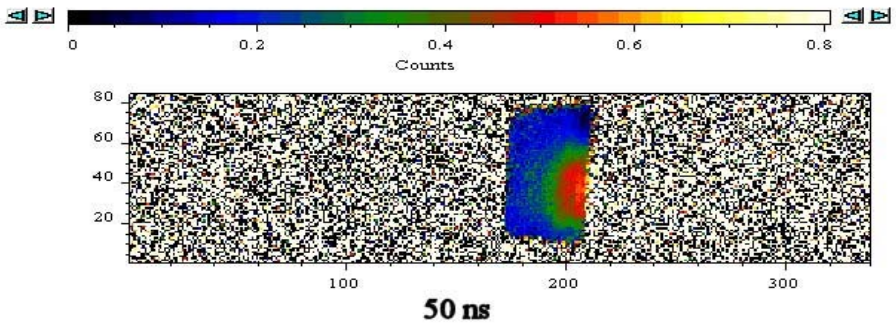

50 ns

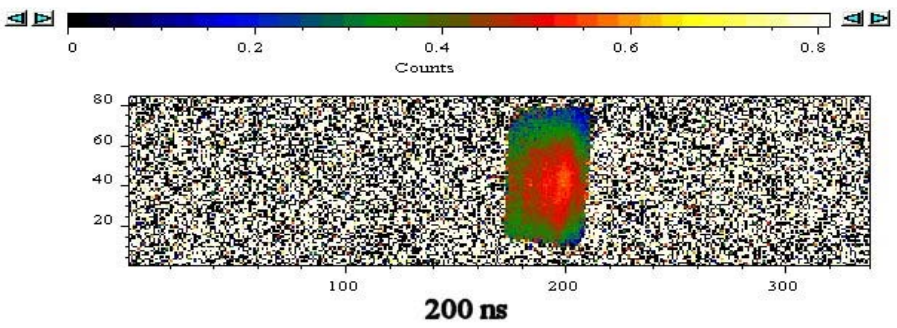

200 ns

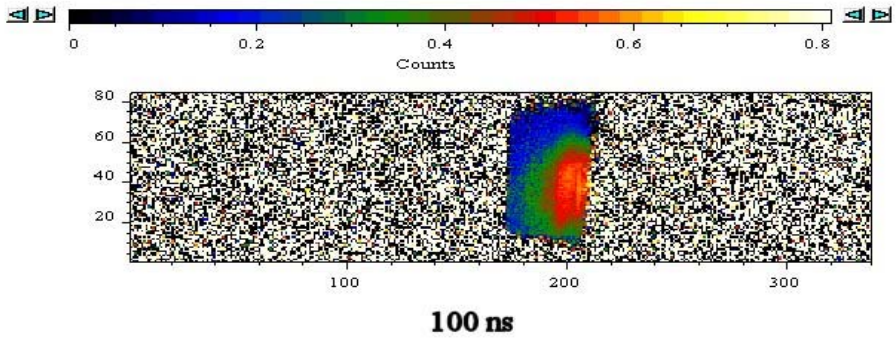

100 ns

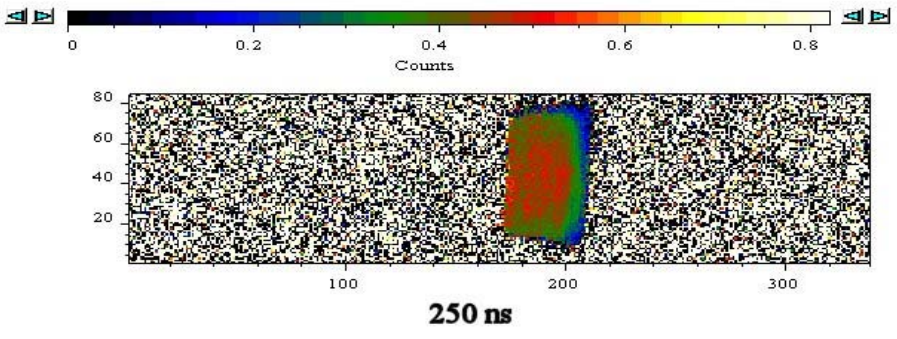

250 ns

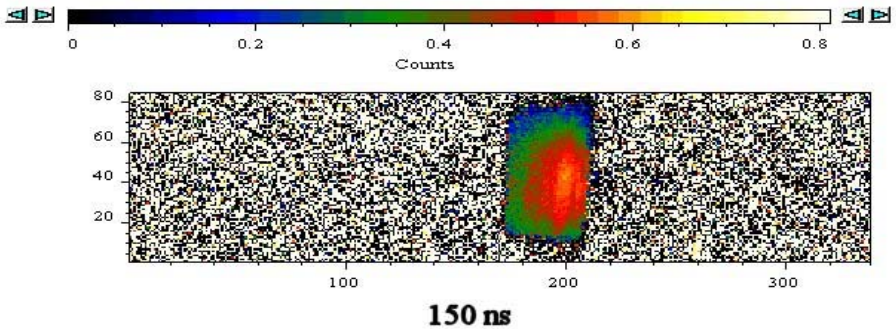

150 ns

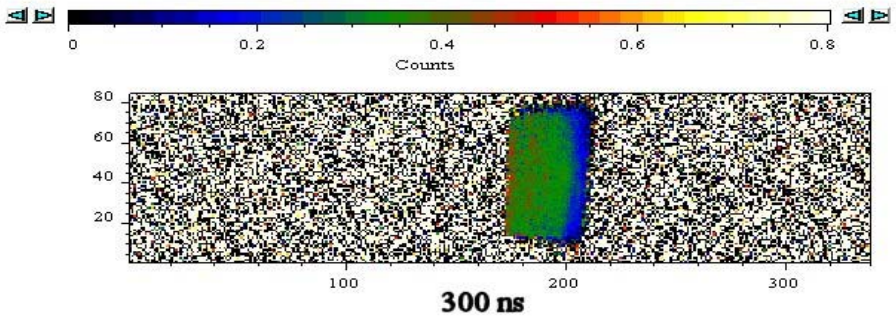

300 ns

Maps of equivalent width of Ca^{2+} using the 3p-3d resonance at 34.7 eV - 200 mJ/15ns on line focus 5mm x 0.015 mm

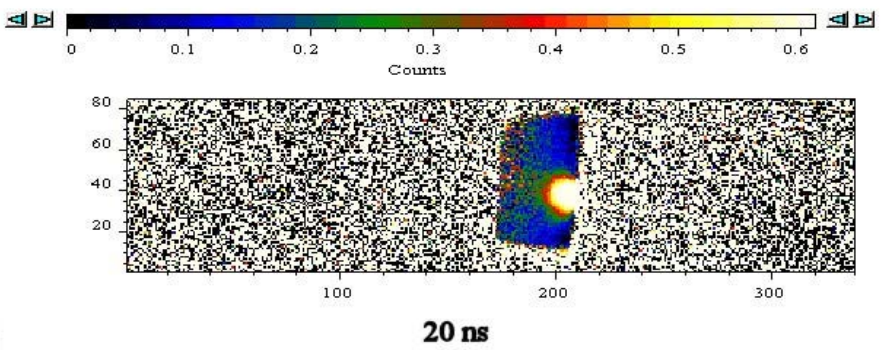

20 ns

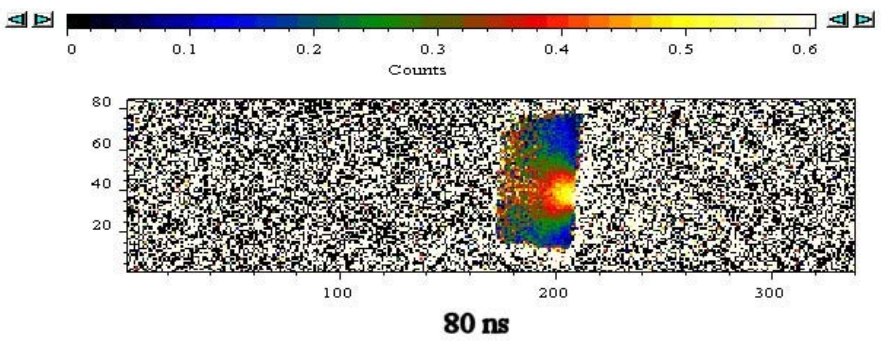

80 ns

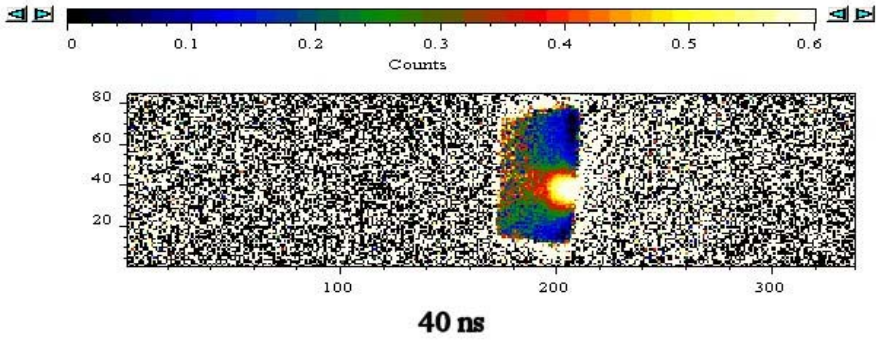

40 ns

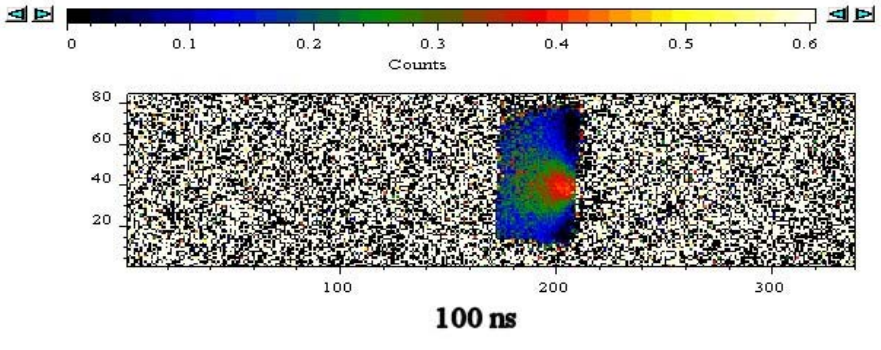

100 ns

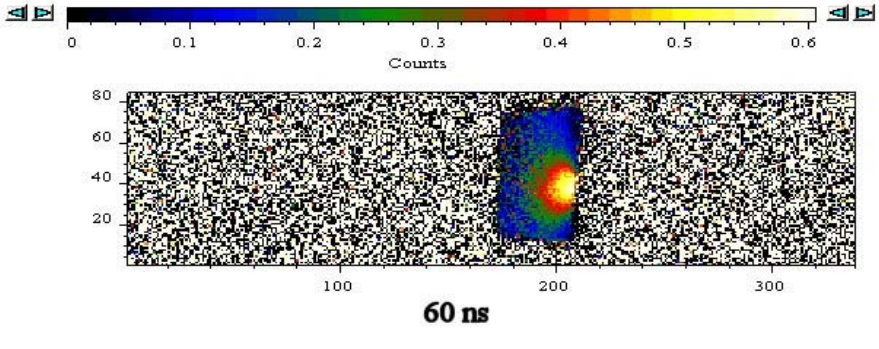

60 ns

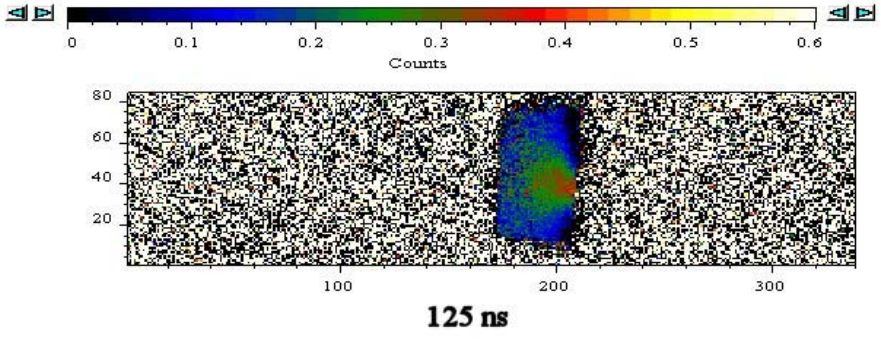

125 ns

Expansion of singly ionized calcium plume component using the 3p-3d resonance at 37.34 nm (33.2 eV)

7 frames: 5 ns, 20 ns, 35 ns, 50 ns, 75 ns, 100 ns &125 ns

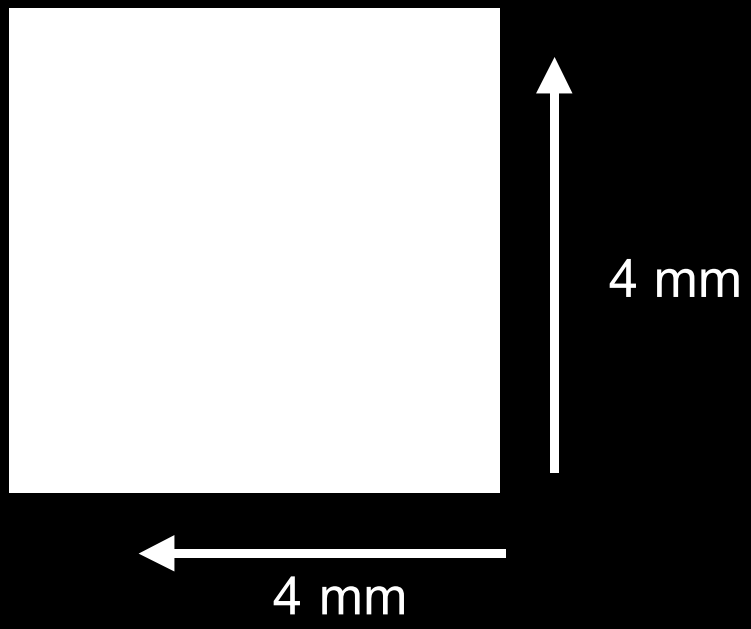

Plume Expansion Profile of Singly Charged Ions

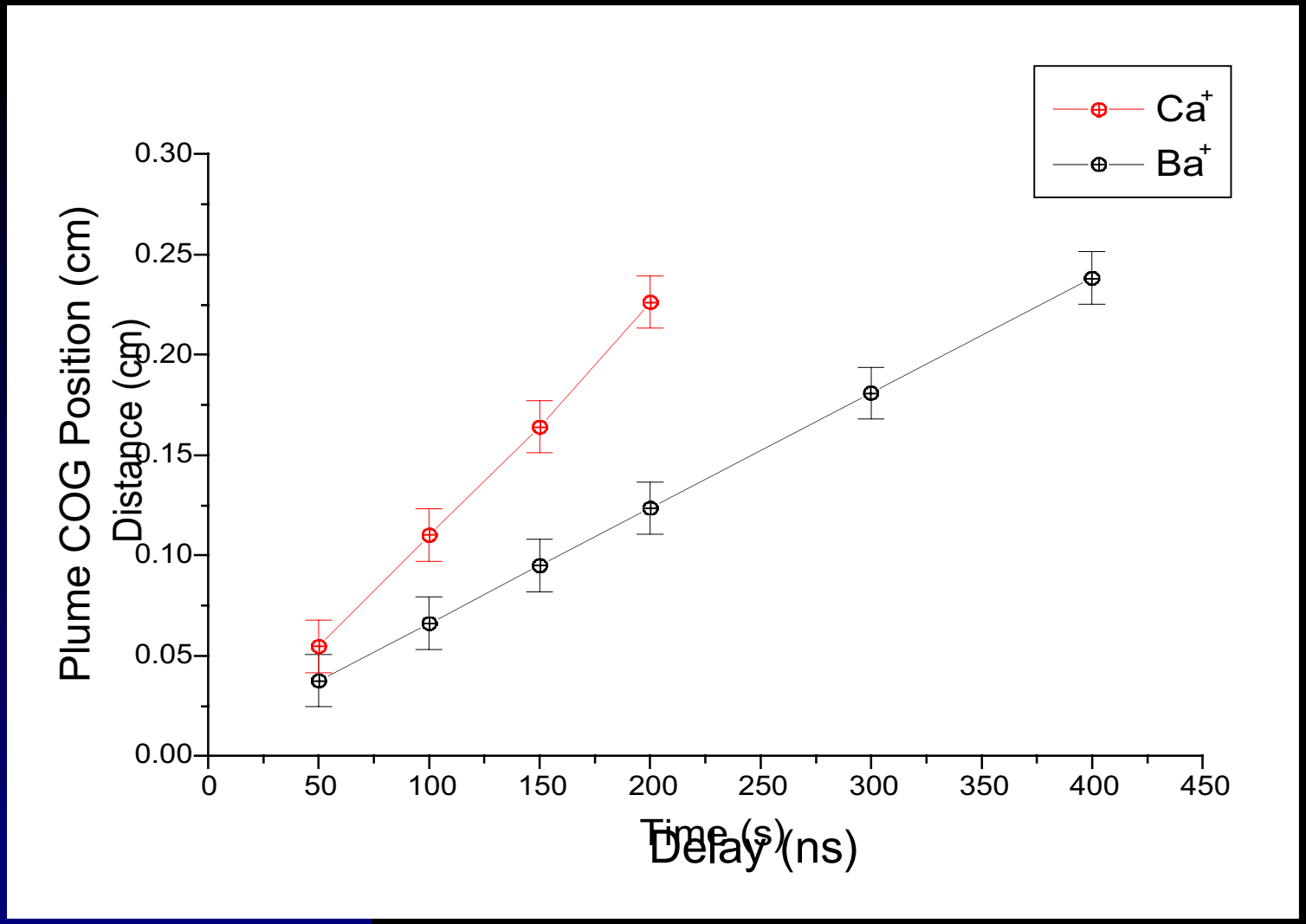

Ca^+ plasma plume velocity
experiment: 1.1×10^6 cms^{-1}
simulation: 9×10^5 cms^{-1}

Ba^+ plasma plume velocity
experiment: 5.7×10^5 cms^{-1}
simulation: 5.4×10^5 cms^{-1}

You can also extracts maps of column density, e.g., *Singly Ionized Barium*

Since we measure ***resonant photoionization***, e.g.,

$Ba^{+}(5p^{6}6s\ ^{2}S)+h\upsilon \rightarrow Ba^{+*}(5p^{5}6s6d\ ^{2}P) \rightarrow Ba^{2+}(5p^{6}\ ^{1}S)+e^{-}$

$h\upsilon$ = 26.54 eV (46.7 nm) and

the **ABSOLUTE** VUV photoionization cross-section

for Ba^{+} has been measured:

Lyon et al., J.Phys.B **19**, 4137 (1986)

We should be able to extract *maps of column density* -

$$'NL' = \int n(l)dl$$

Maps of equivalent width of Ba^{+} using the 5p-6d resonance at 26.55 eV (46.7 nm)

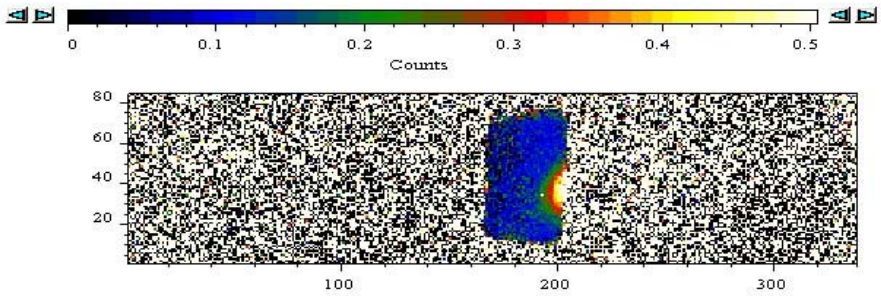

100 ns

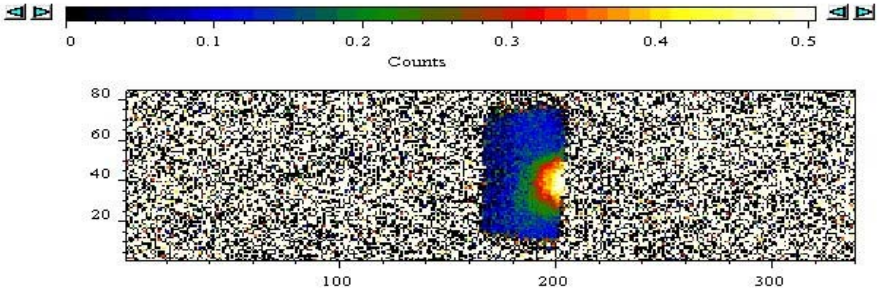

200 ns

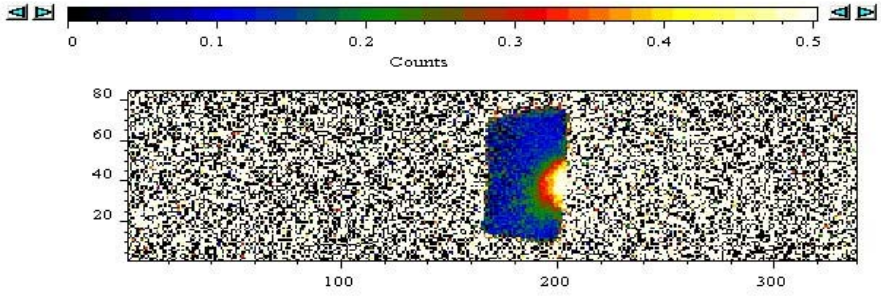

150 ns

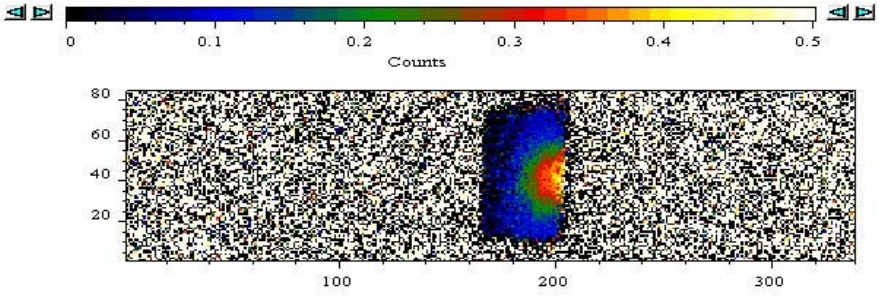

300 ns

Convert from W_E to NL

Compute W_E for a range of NL and fit a function f(NL) to a plot of NL .vs. W_E

Apply pixel by pixel

$$W_E = \int [1 - e^{-\sigma(\lambda)NL}] d\lambda$$

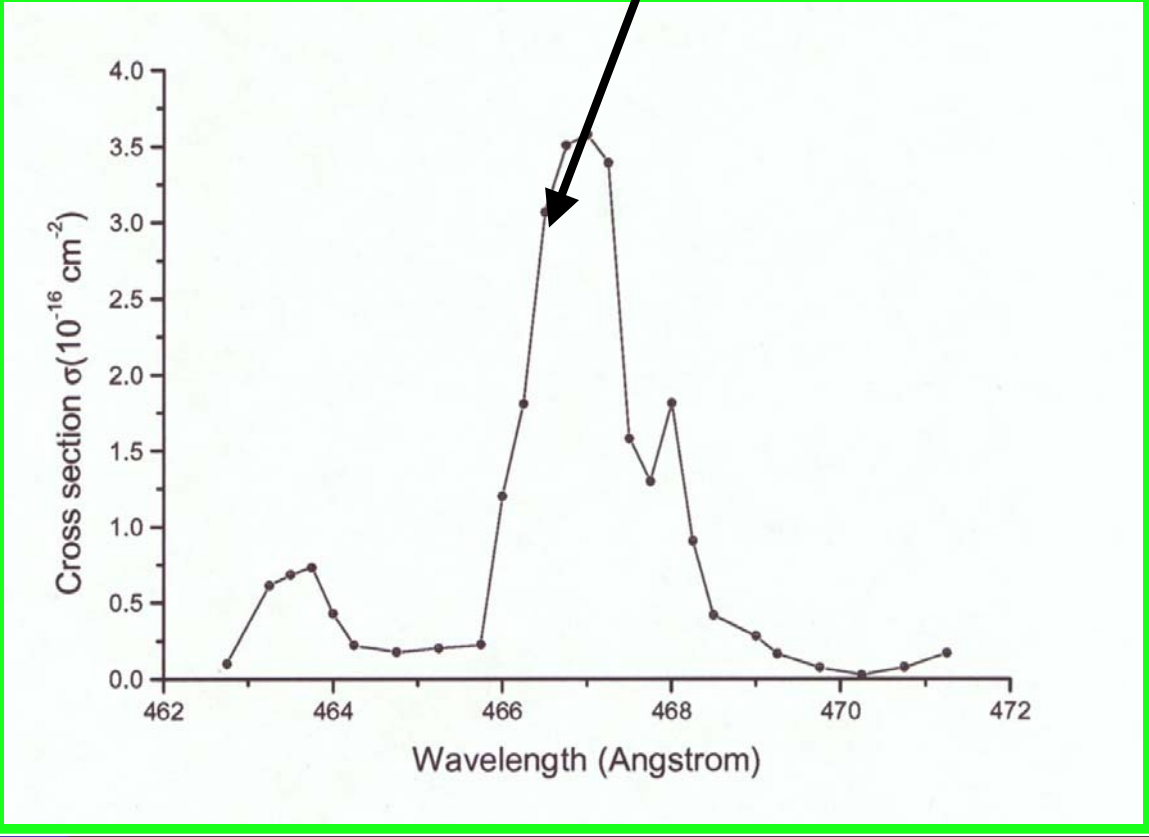

Result - Column Density [NL] Maps

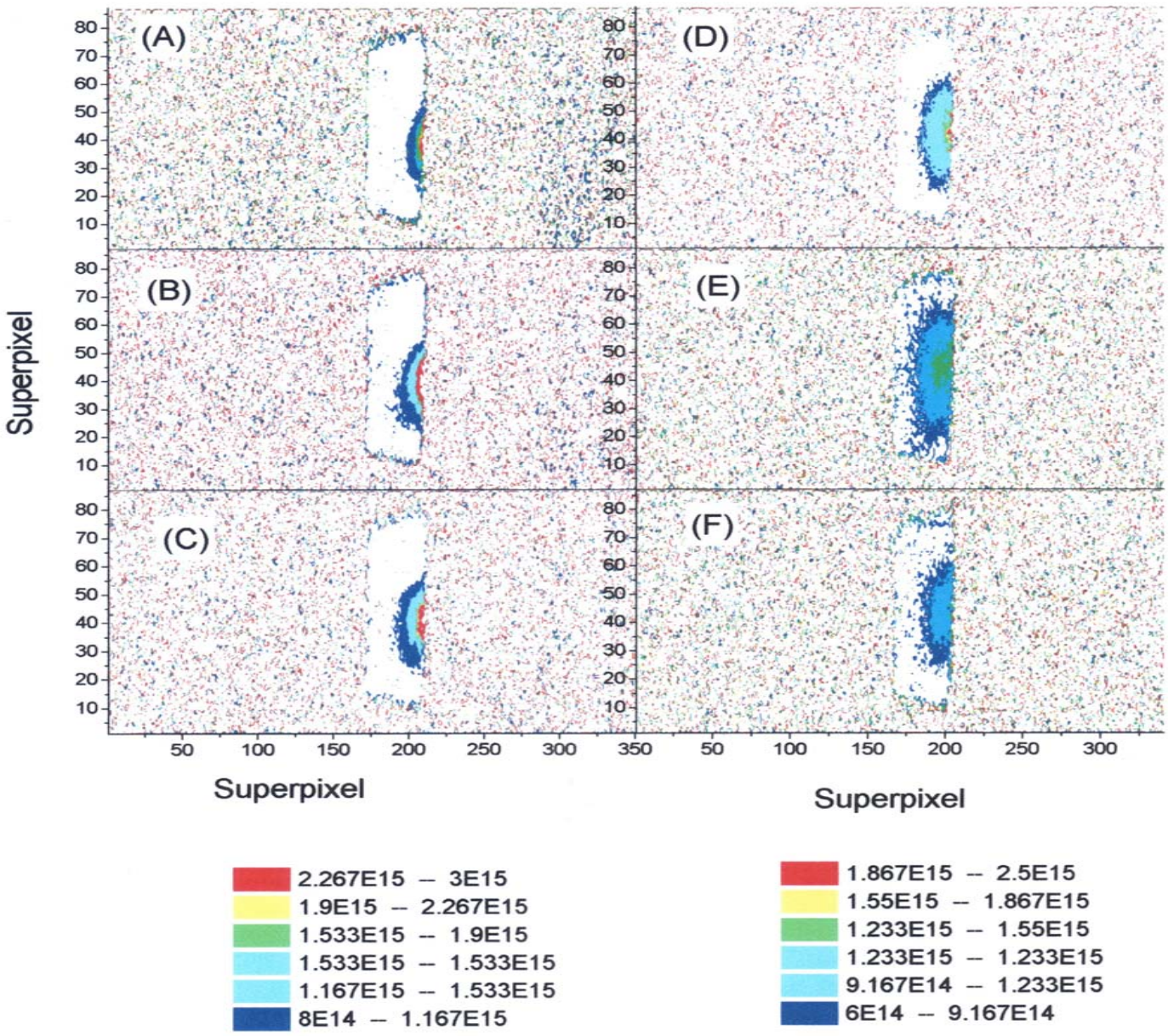

(A) 100 ns
(B) 150 ns
(C) 200 ns
(D) 300 ns
(E) 400 ns
(F) 500 ns

VPIF - Summary

VPIF - Provides pulsed, collimated and tuneable VUV beam for probing dynamic and static samples

Spectral (1000) & spatial (<100 μm) resolution and divergence (< 0.2 mrad) all in excellent agreement with ray tracing results

Extracted time and space resolved maps of column density for various time delays

Measured plume velocity profiles compare quite well with simple simulations based on adibatic expansion

Current & Future Applications

Space Resolved Thin Film VUV Transmission and Reflectance Spectroscopy - PVK

‘Colliding-Plasma’ Plume Imaging

Combining ICCD Imaging/Spectroscopy & P/Imag

Non-Resonant Photoionization Imaging

VUV Projection Imaging ?

Photoion Spectroscopy of Ion Beams ?

Into the X-ray range-Table-Top Point Projection Absorption Spectroscopy

'TT-PPAS'

Collaboration with C Lewis (et al.) PLIP Div., QUB

PPAS - well established diagnostic

H Merdji et al., Phys. Rev. E **57**, 1042 (1998)
T Shelkovenko et al., Rev. Sci. Instrum **72**, 667 (2001)
M Fajardo et al., Phys. Rev. Lett **86**, 1231 (2001)

J Balmer et al., Phys. Rev. A **40**, 330 (1989)

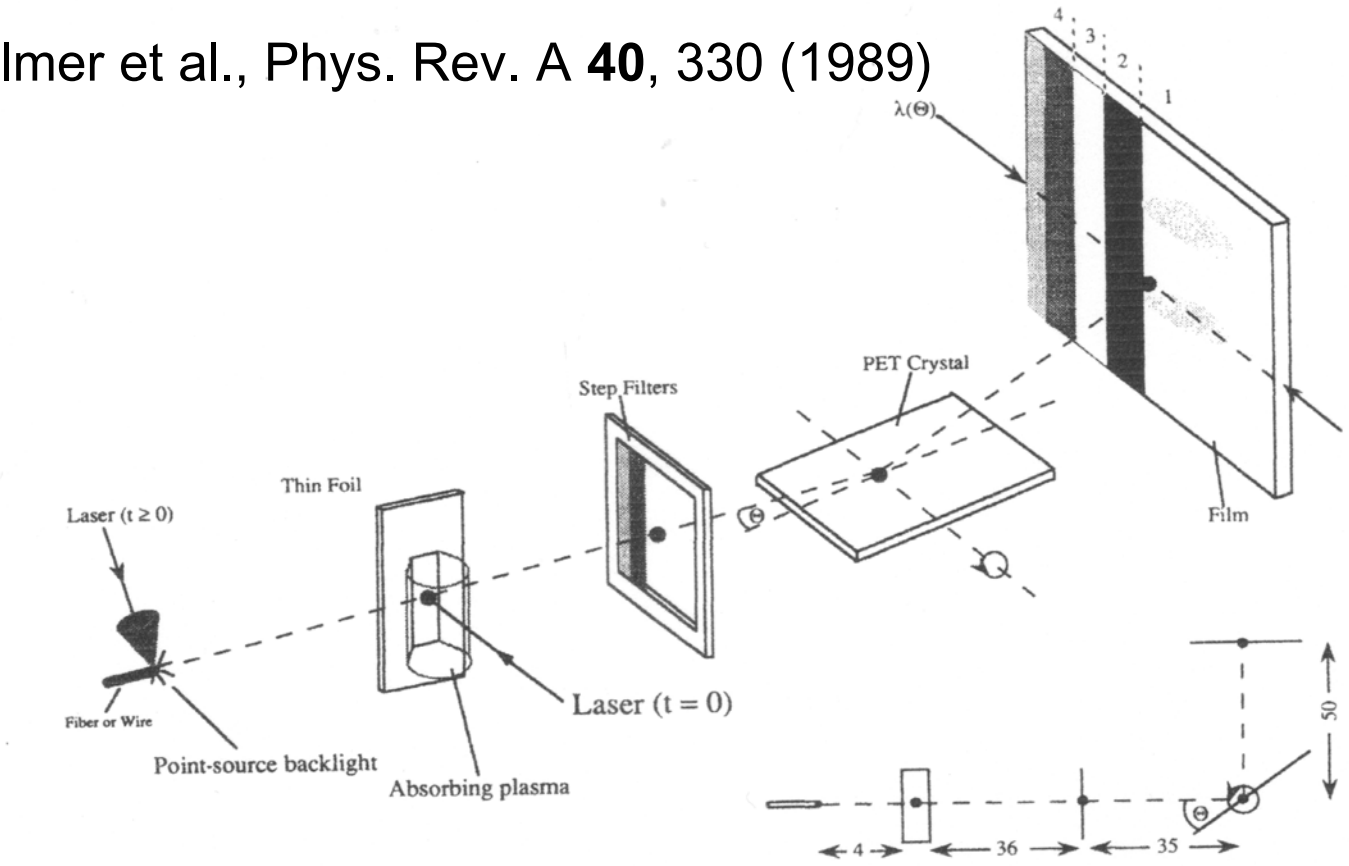

FIG. 1. Experimental setup and typical scale dimensions shown in millimeters. The regions imaged onto the film plane are discussed in the text.

X-ray Spectrometer System at DCU

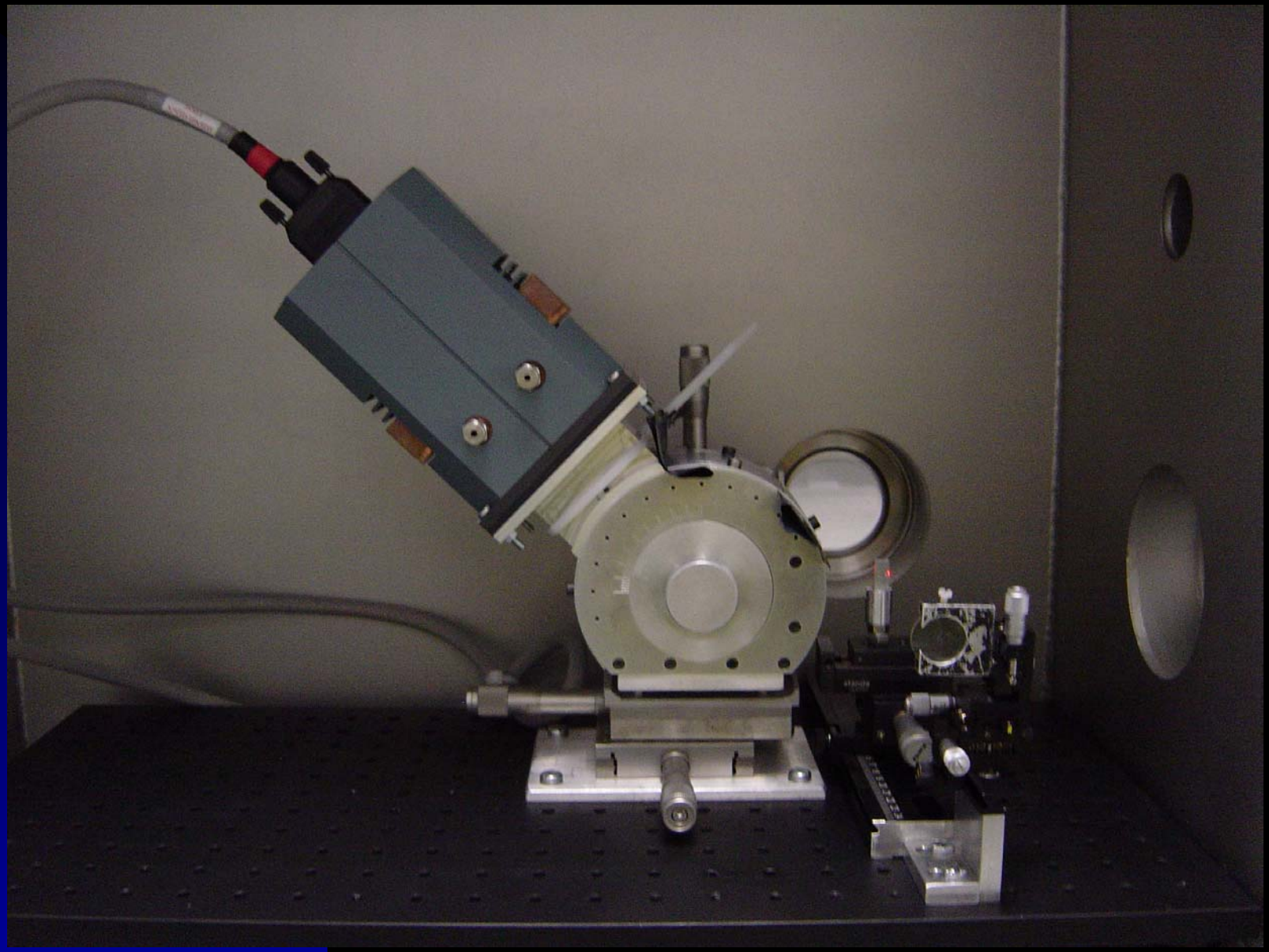

Source Laser: EKSPLA 312P, 500 mJ in 170 ps
Spot size: < 50 μm (from edge trace)
Irradiance: ~10^{14} W.cm^{-2}
T_e: >1 keV (medium Z)

'Sample Plasma Laser': Spectron 858G, 2J/15 ns.

First emission spectra - end of last week - no optimisation

Cu

10.653 A

10.599 A

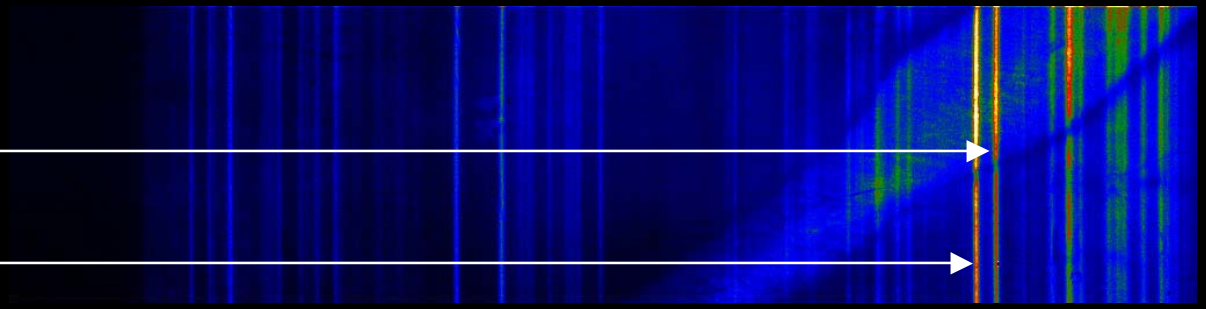

Sm

(single shot)

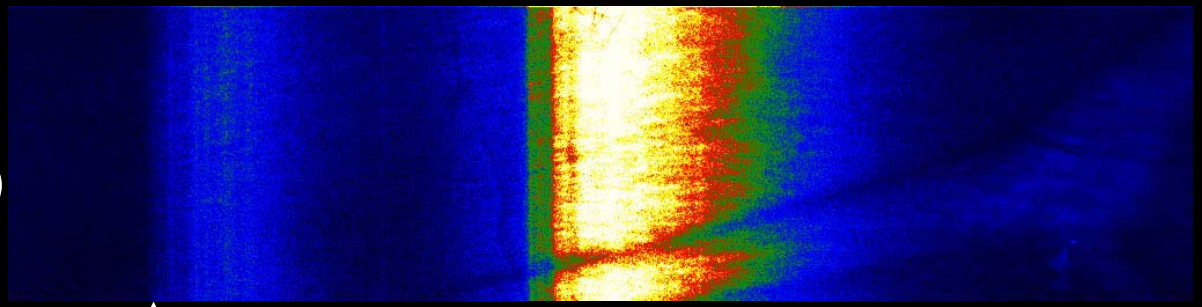

Al K-edge

400 grid image
single shot Sm

(~65 μm C-C)

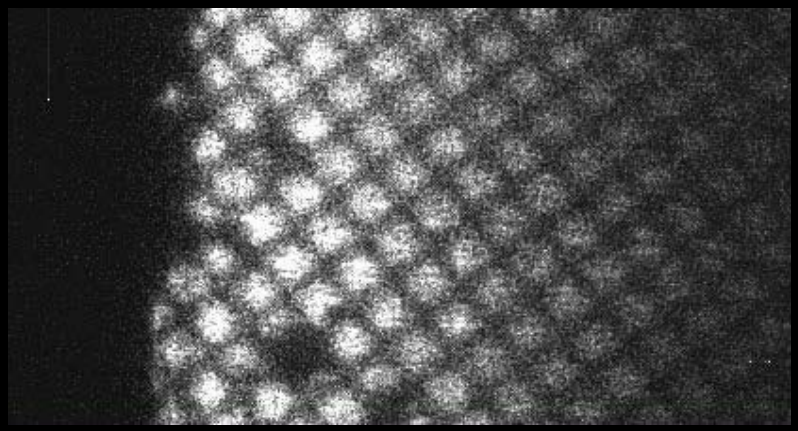

Part III - Next steps in fundamental photoionization studies ?

Atoms and Molecules in Laser Fields

1. Attosecond pulse generation/ HHG
2. **Photoionization of *'state prepared'* species**
   (a) Weak Optical + Weak X-VUV
   (b) Intense Optical + Weak (Intense) X-VUV
3. Atoms, Molecules, Cluster & Ions in Intense Fields

   (Multiple-Photon and Optical Field-Ionization)

Pump-probe experiments in the gas phase (project: II-02-037-FEL)

M. Meyer, LU.R.E., Orsay, France

→ **IIA- characterization of fs - FEL pulses**

- cross correlation experiments (Ar, Xe, He)

→ **IIB - application of fs - FEL pulses**

- interference in molecular dissociation (H_2)
- coupling of autoionization states (Xe, He)

Participating groups:

L.U.R.E., Orsay, France
M. Meyer, L. Nahon, P. O'Keeffe

Lund Laser Center / MAX-Lab, Lund, Sweden
J. Larsson, A. L'Huillier, S. Sorenson

Max-Born Institut, Berlin, Germany
I. Will, H. Redlin

HASYLAB, Hamburg, Germany
J. Feldhaus, E. Ploenjes, K. Tiedke

Dublin City University, Dublin, Ireland
J. Costello & E. Kennedy

X-VUV FELs + Femtosecond OPAs- The Ultimate Photoionization Expt ?

Tuneable: *TTF1: 80 - 110 nm*
Ultrafast: *100 fs pulse duration*
High PRF: *1 - 10 bunch trains/sec with up to 11315pulses/bunch*
Energy: Up to 1 mJ/bunch
Intense: 100 μJ (single pulse) /100 fs /1 μm => 10^{17} W.cm^{-2}

- *Moving to XUV (TTF2: 2005) and X-ray (2011):*

Project Title: *'Pump-Probe' with DESY-VUV-FEL (EU-RTD)*
Aim: ***FEL + OPA synchronisation with sub ps jitter***
Key Ref: **http://tesla.desy.de/new_pages/TDR_CD/start.html**
Personnel: **DESY, MBI, CLPR-DCU, LURE, LLC, BESSY**

Femtosecond X-VUV + IR

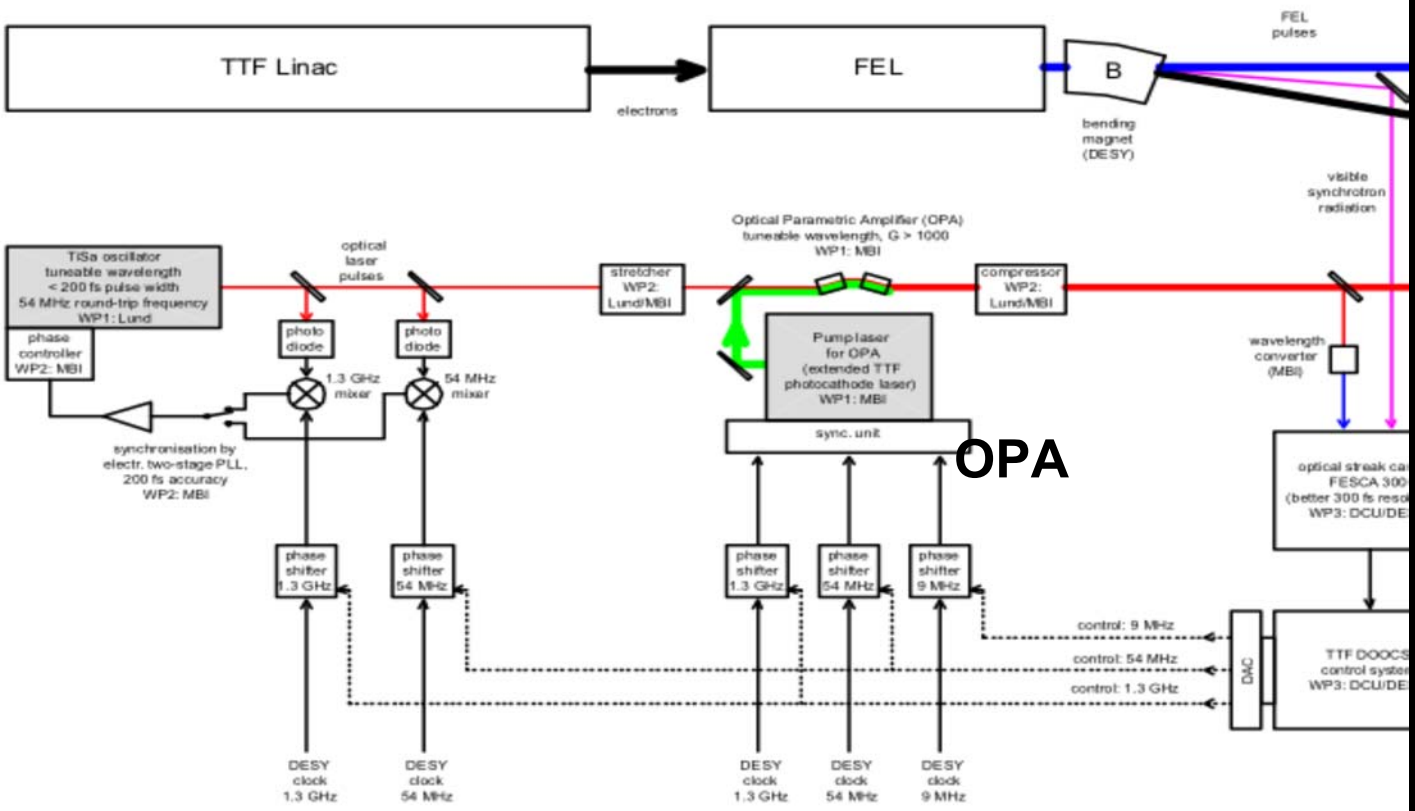

Synchronisation scheme (7/15/01)
- provides stable phase lock
- a bending magnet generates optical pulses from the electron bunches
- an optical streak camera provides absolute calibration
- allows for programmed phase scans

Requirements:
- jitter between electron bunches and FEL pulses should be much smaller than 200 fs
- short-term jitter between electron bunches and RF should be much smaller than 200 fs

Two subsets of experiments

II-A.

Direct photoionization in a non-resonant laser field

II-B

Resonant photoionization in a resonant laser field

Lets look at II-A - ‘Direct photoionization in a non-resonant laser field’ first*

*Slides provided by Patrick O’Keefe and Michael Meyer, LURE, ORSAY !

Ponderomotive streaking of the ionization potential as a method for measuring pulse durations in the XUV domain with fs resolution

E.S. Toma, H.G. Muller, P.M. Paul, P. Berger, M. Cheret, P. Agostini, C. LeBlanc, G. Mullot, G. Cheriaux

Phys. Rev. A 62, Art. No. 061801 (2000)

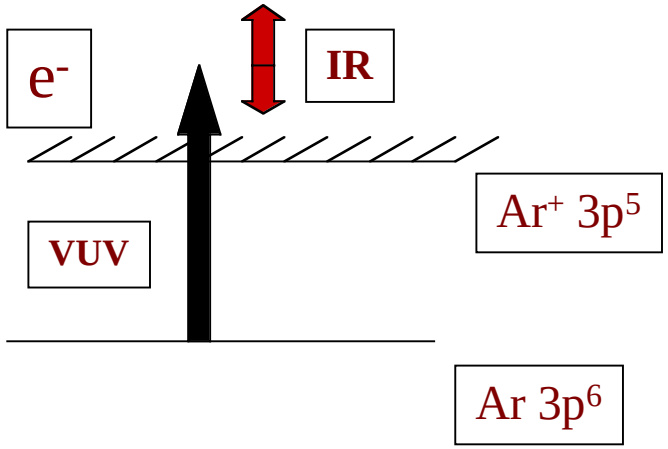

presence of IR:

- shift of IP
- broadening of PES peaks
- sidebands

Test-experiments at LLC: M. Meyer, P. O'Keefe (LURE), A. L'Huillier (LLC)

fs-laser system: Ti:Saph. 800 nm, 50 fs, 1 kHz

VUV --> HHG, $\Delta T \approx$ 30 fs, 1 kHz,

IR --> up to 0.5 mJ --> 1-10 TW/cm^2

PES: magnetic bottle spectrometer

- high angular acceptance
- high energy resolution for $E_{kin} < 10$ eV

Cross correlation experiments using high order harmonics

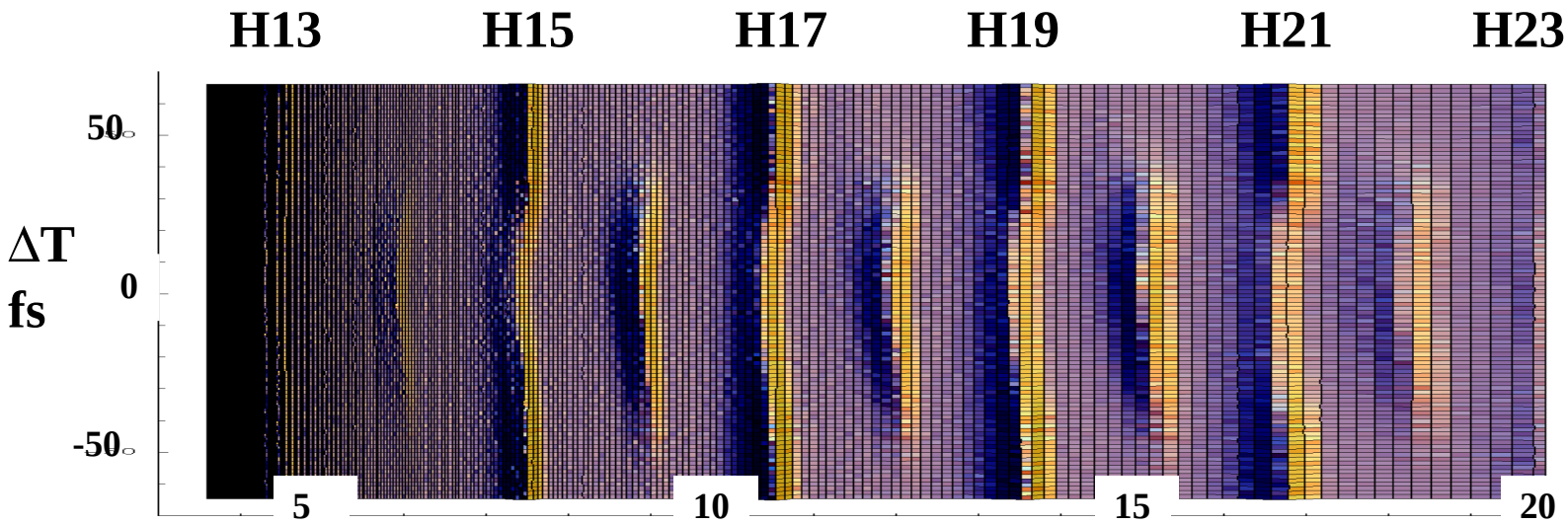

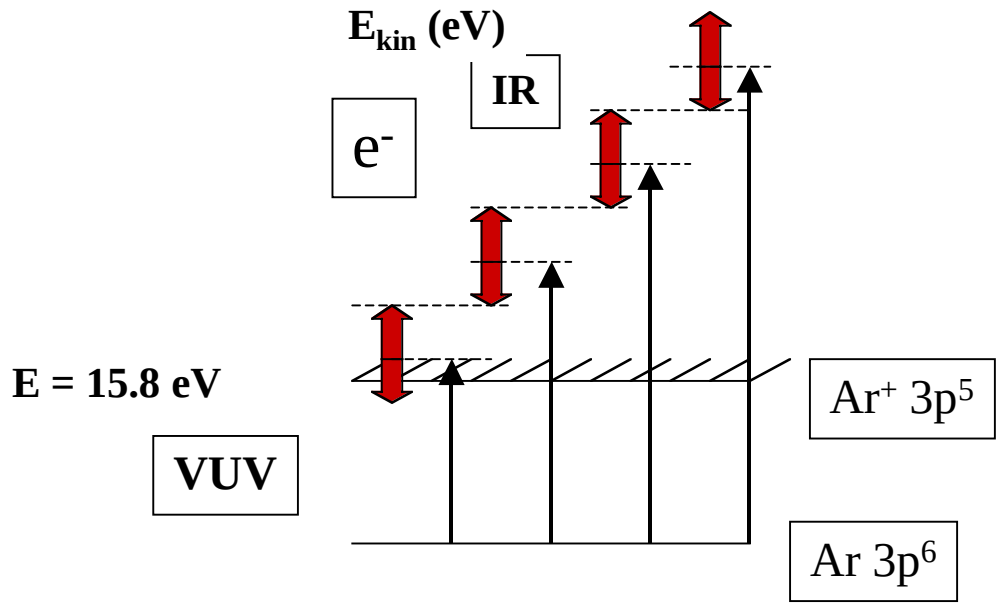

Generation (HHG)
λ(laser) = 800nm
H11 = 17 eV
H13 = 20 eV
H15 = 23 eV
:
:

But far more interesting would be:

Type IIB-Experiments

Resonant photoionization in an intense/resonant fields

=>Study intensity controlled autoionization !!

Proposed experiment at the FEL

Exp.: **Two-photon double-resonant excitation**
FEL : hν = 65.1 eV (tunable) Laser : λ = 750 - 800 nm (tunable)

Coupling of He Doubly Excited States

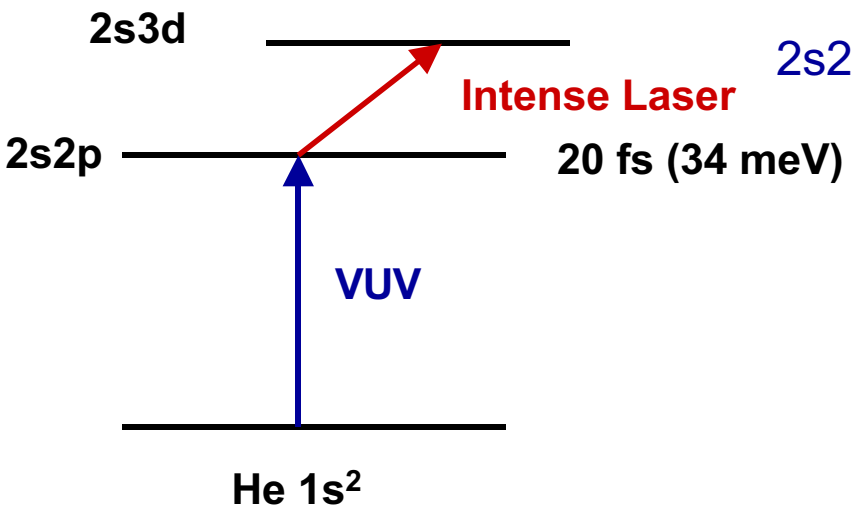

2s2p ^{1}P – 2s3d ^{1}D

A. I. Magunov, I. Rotter and S. I. Strakhova
J. Phys. B32, 1489 (1999)
H. Bachau, Lambropoulos and Shakeshaft
PRA 34, 4785 (1986)

H. Bachau, Lambropoulos and Shakeshaft, PRA **34**, 4785 (1986)

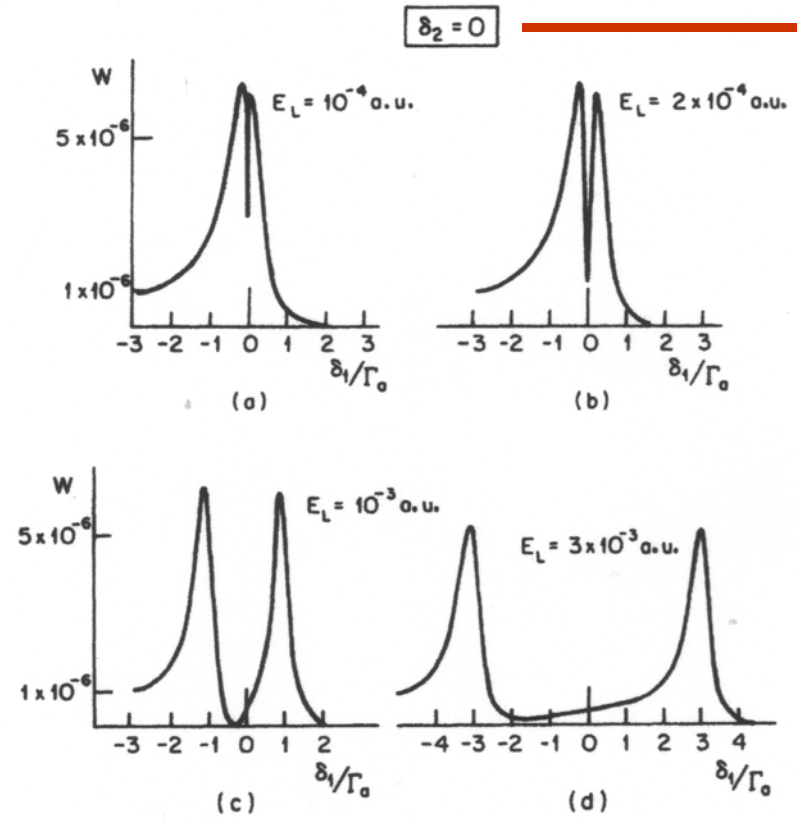

FIG. 2. The line shape of total ionization as a function of $\delta_1=\hbar\omega_1-(E_D-E_g)$ in units of Γ_a the autoionization width of the state ^1P. The strong laser is tuned exactly on resonance with the transition $^1P\rightarrow{}^1D$ which implies $\delta_2=0$. W is the total ionization probability which, owing to the weakness of the first source (synchrotron), is proportional to its intensity I_s and the time T, i.e., $W\sim I_sT$. For the calculations, we have taken $T=10^6$ a.u. and $I_s=1.4\times10^5$ W/cm^2. E_L is the field strength of the laser in atomic units. Note that 1 a.u. of E_L corresponds to 1.4×10^{17} W/cm^2.

Laser on Resonance ($\delta_2 = 0$)
& scan the XUV photon energy

$$1s^2(^1S) + h\nu_{XUV} - \{2s2p\ (^1P) + (\text{intense})h\nu_{Laser} <=> 2s3d\ (^1D)\}$$

Conclusions

Single VUV - X-ray photon photoionization (and concomitant correlation) in atoms and ions is now well understood

Photoionization of atoms (much less so ions) in intense IR/VIS laser fields is now well established also (MPI .vs. OFI)

What's left ? - Coupling of the above two !!

Atoms in intense VUV/XUV (high frequency) fields - first result Nature 2002

Single- (and later multi-) photon photoionization of atoms in resonant and intense laser fields

♣Go raibh maith agaibh

Thank you for your attention

www.ncpst.ie

www.physics.dcu.ie/~jtc

Soft X-ray laser driven by a guided ultra-short laser pulse

Brigitte Cros

Laboratoire de Physique des Gaz et des Plasmas

CNRS-Université Paris XI, France

Interaction et Transport de Faisceaux Intenses dans les Plasmas

G. Matthieussent, G. Maynard: LPGP,

A. Butler, A. J. Gonsalves, C. M. McKenna, D. J. Spence, S. M. Hooker: U. Oxford,

S. Sebban, T. Mocek, I. Bettaibi: LOA, NE Andreev: IHED

Outline

- Soft X-ray laser in the OFI collisional scheme
  - Characteristics
  - Limitations
- Prospects for improving performances
  - Demonstration in plasma wave guide
  - Guiding of laser pulses in capillary tubes

Interest of OFI collisional schemes

- Simple operation: a single short pulse, pump laser and a gaz target
  - Longitudinal pumping
  - Ion stage produced by OFI and controlled by laser intensity
  - Electron energy distribution controlled by laser polarization
- Reduce the size of soft X-ray laser systems
- Increase repetition rates
- Achieve shorter wavelength laser systems

Example: the Xe IX laser system

B. E. Lemoff *et al. Opt. Lett.* **19** 569 (1994).

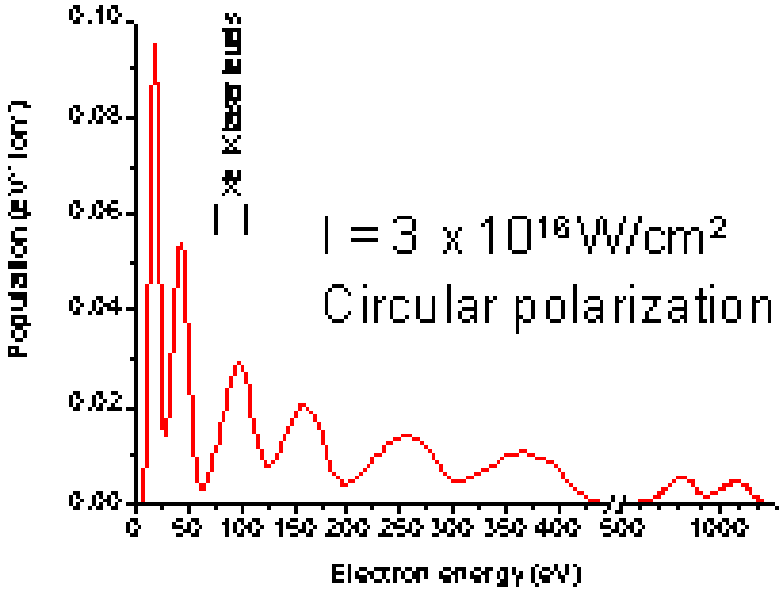

Pd-like xenon

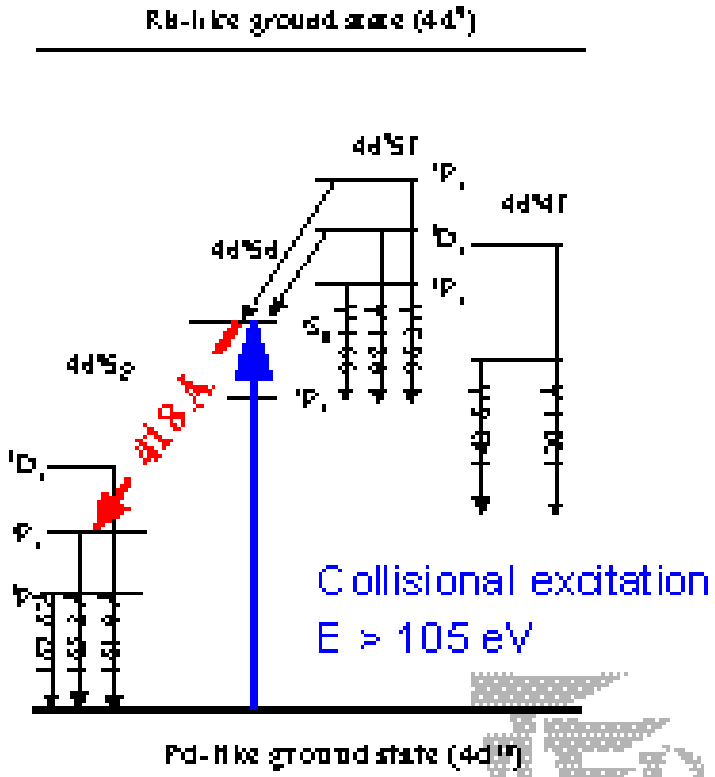

Laser transition: $4d^9\,5d\ ^1S_0 \longrightarrow 4d^9\,5p\ ^1P_1$ transition at 41.81 nm

Saturated gain achieved in a gas cell

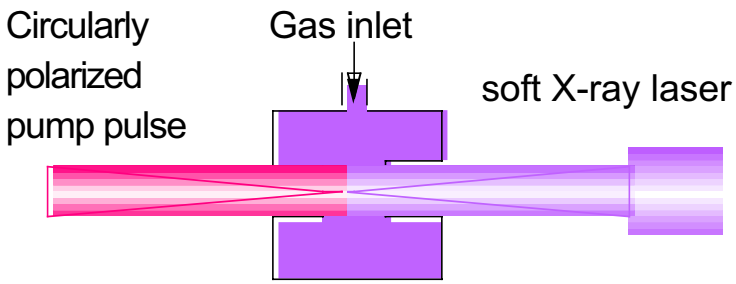

Sebban *et al. Phys. Rev. Lett.* **86** 3004 (2001)

G= 67 cm^{-1}

Isat=2◊10^{7} W.cm^{-2}

G.L=15

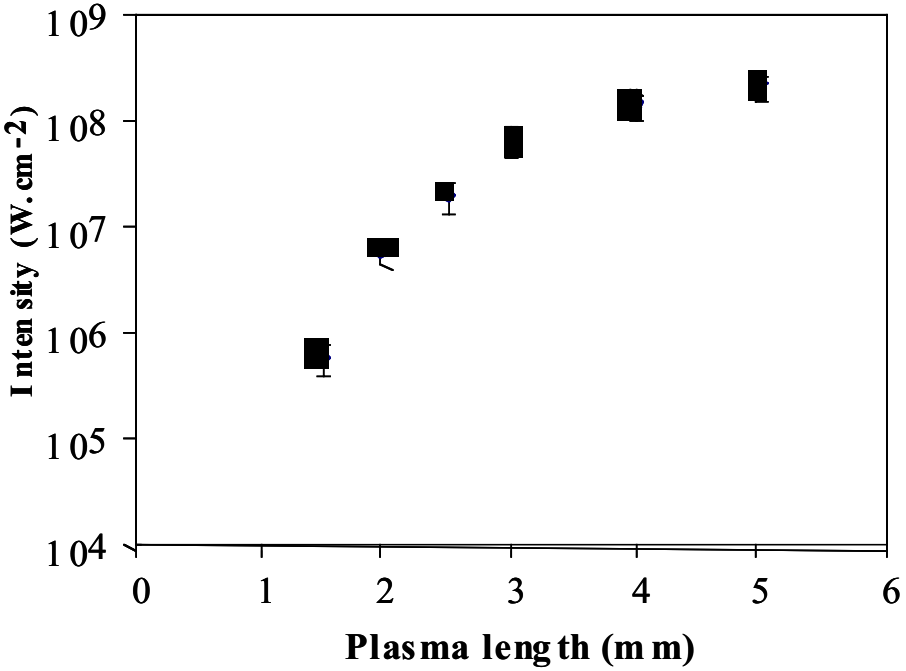

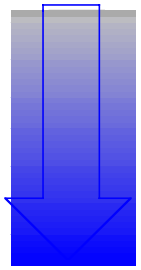

Saturation

How to improve performance?

- Increase density or length
- Solve propagation problems

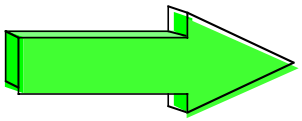

Some form of laser guiding is necessary

Optical guiding to overcome diffraction

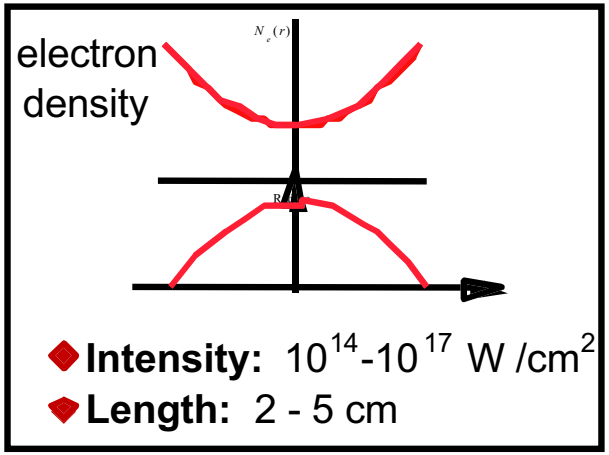

- **Intensity:** 10^{14}-10^{17} W /cm^2
- **Length:** 2 - 5 cm

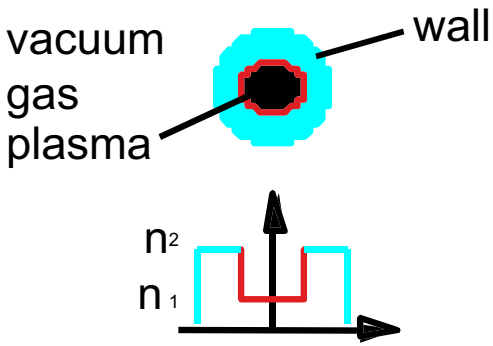

- **Intensity:** a few 10^{17} W / cm^2
- **Length:** 1 cm - 12 cm

Plasma channels

- Parabolic density profile
- Supports matched guiding for a beam waist
- Provided there is no further ionization by the propagating pulse

Capillary waveguides

- eigen mode structure

Capillary tube as a wave guide:

Principle

Incident beam

I_0

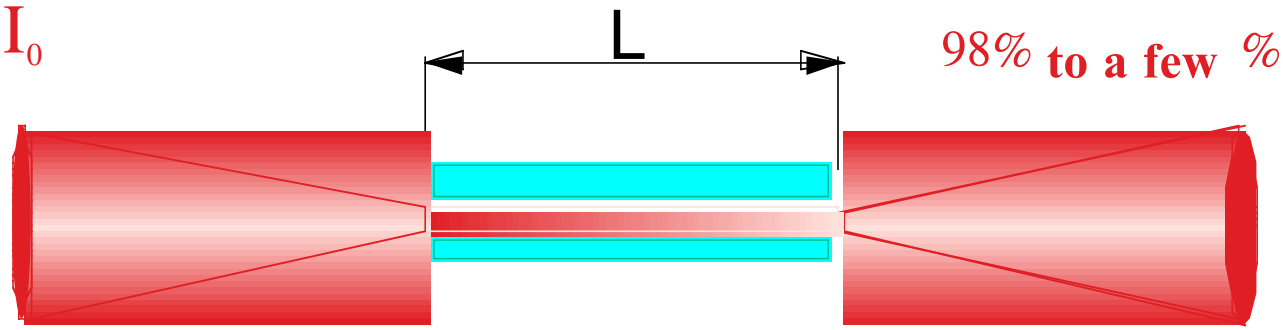

Transmited beam

98% to a few % I_0

Inner radius a

typically from 10µm to 100µm

L : 1 to 10 cm

Gas filled capillary tube set-up

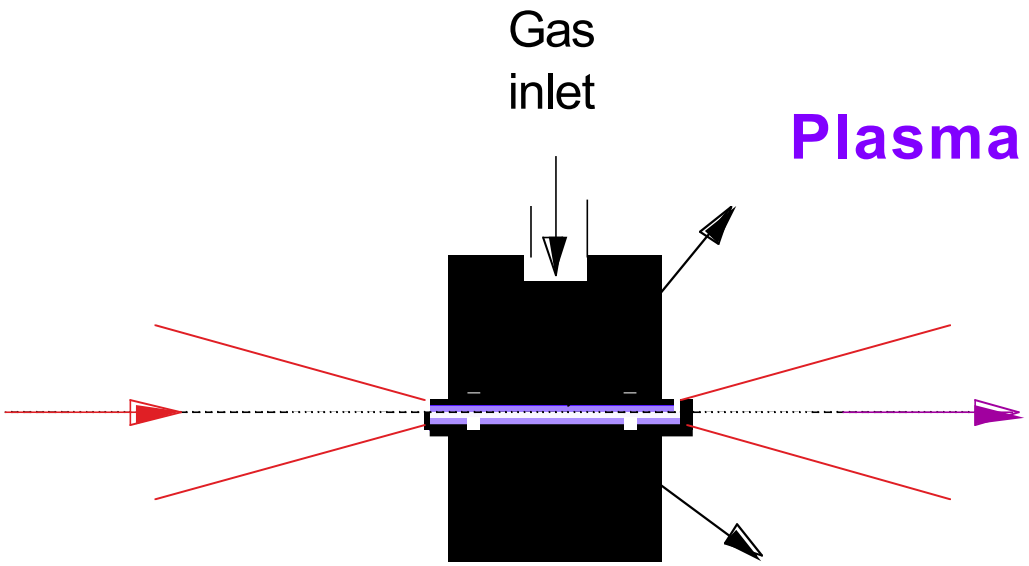

Up to 150 mJ coupled to the tube
35 fs, 0.8 µm
circularly polarized

LOA: Salle jaune Ti:Saph laser

Energy output in Xenon filled tube

Focal spot in vacuum

Apertured beam (4 cm)

#03310hz24

750 mJ in the focal plane

150 mJ inside the tube

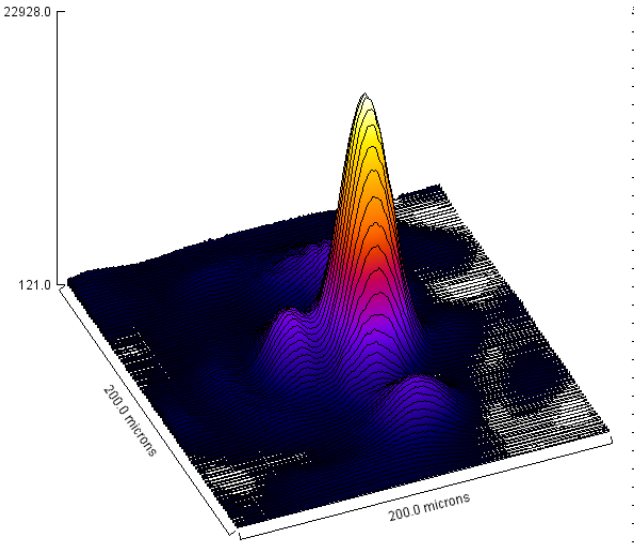

Tube ouput #032celsj3710hz24

L = 2 cm, 20 mbar Xenon

Output energy 60 mJ (T = 0.4)

$I_{out} \sim 8 \times 10^{16}$ W/cm^2

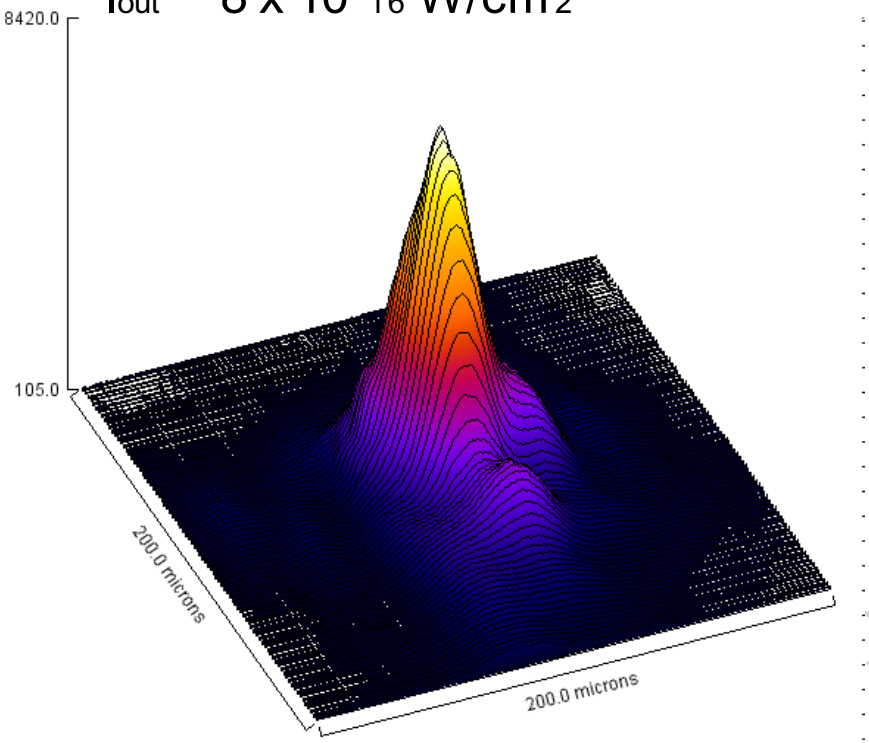

Transmission in gas filled tubes

Transmission for Xenon filled tubes and for different input energies: $0.6 \times 10^{16} < I < 3 \times 10^{17}$ W/cm^2

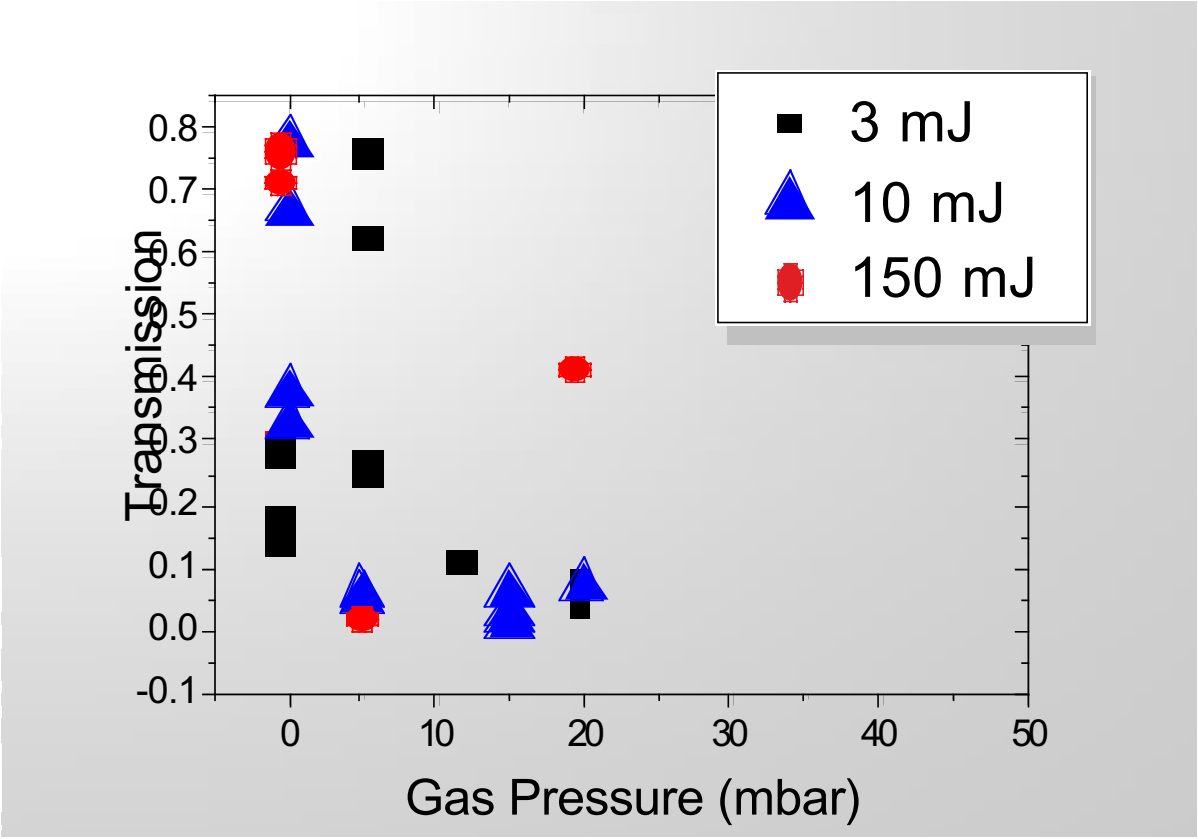

OFI ionization of Xenon

Simulations by N. Andreev

Gas cell:

L = 4 mm

200 mJ, 40 fs

4.7 10 $_{17}$ W/cm $_{2}$

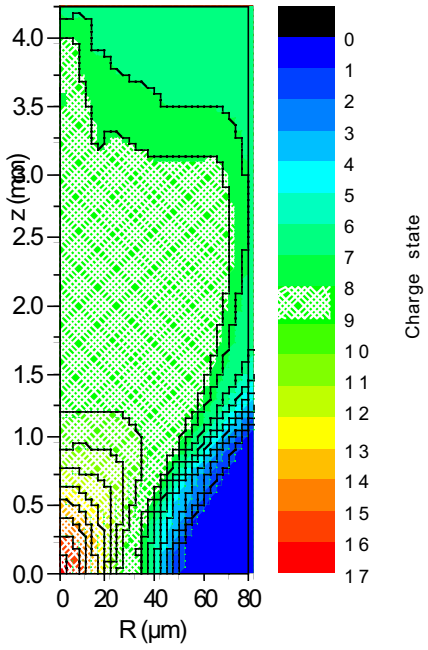

Capillary tube: L = 22 mm

200 mJ, 40 fs

4.7 10 $_{17}$ W/cm $_{2}$

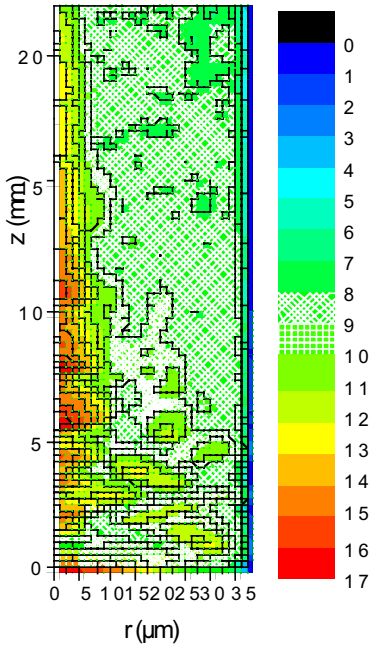

20 mJ, 40 fs

4.7 10 $_{16}$ W/cm $_{2}$

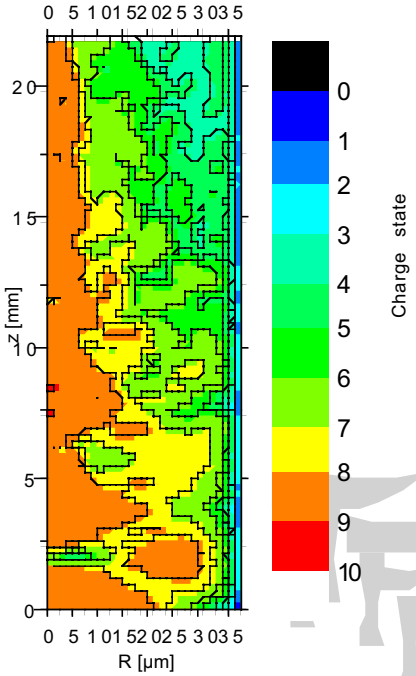

Summary for capillary tubes

- Shot to shot transmission exhibits strong fluctuations
  - improve focal spot quality and tube alignment
  - pointing stability
- simulation needed to predict the optimum parameters for lasing
  - laser energy
  - gas pressure
  - tube length

Set-up for the capillary discharge

LOA Salle Jaune

Ti:Saph laser

0.8 µm
35 fs
200 mJ
Circular
polarization

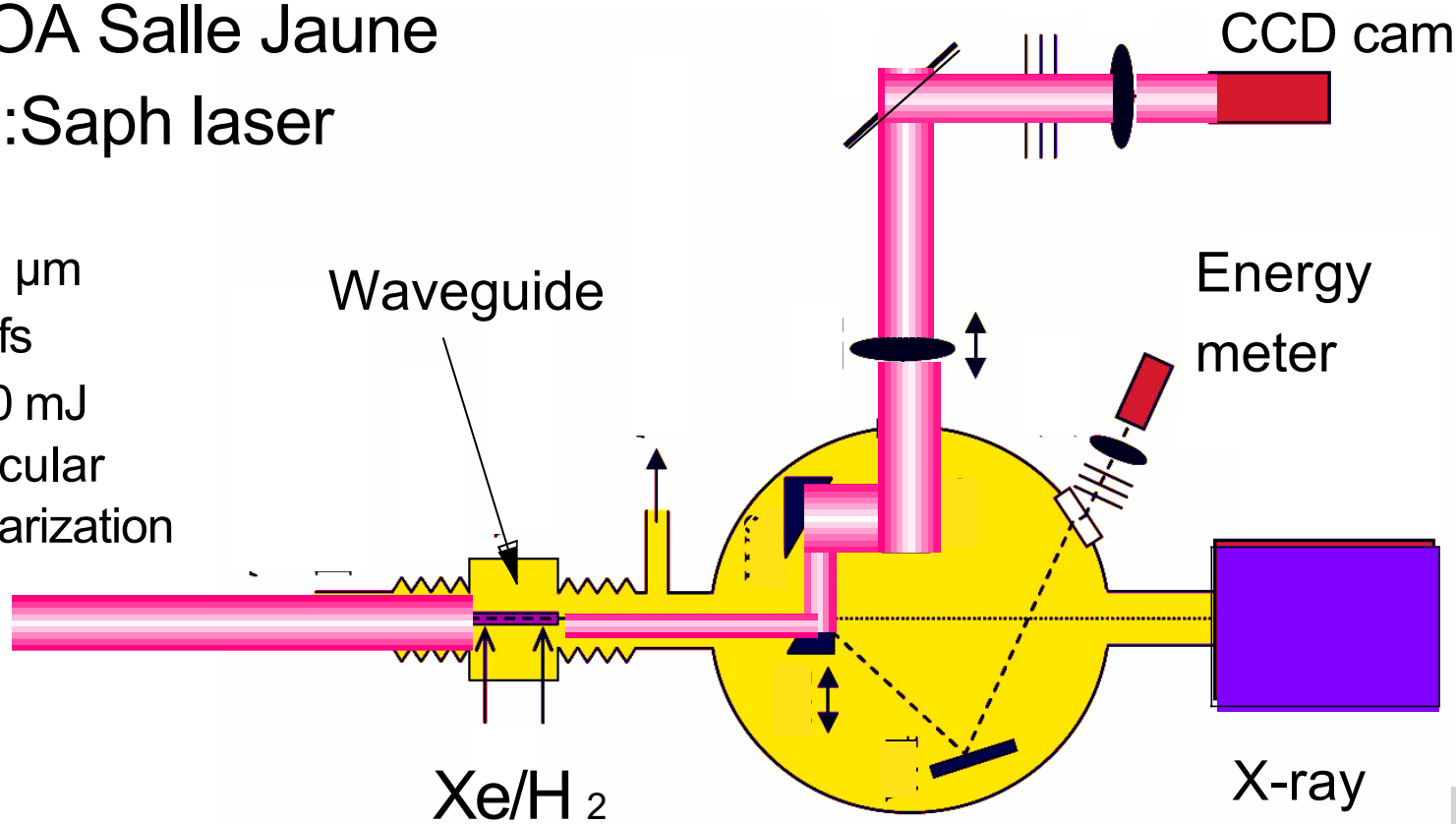

Characteristics of the discharge

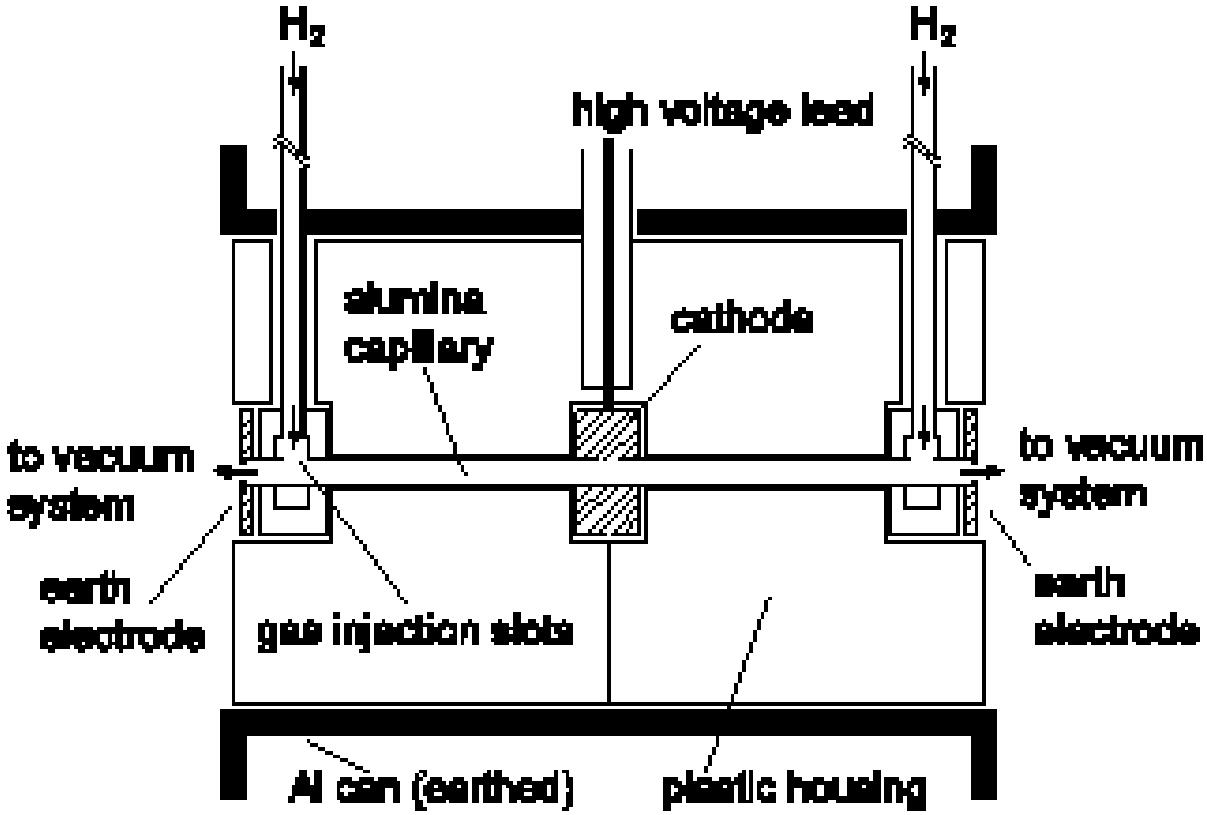

- Alumina capillary:
  diameter 300 µm
  Length 30 mm
- Pulsed gas flow ~ 2s
- Charging capacitor ~7nF charged to 20-30 kV
- Discharge current is approximately sinusoidal with quater period of ~190 ns. Peak current ~550 A per arm.

Parabolic plasma density profiles

D. J. Spence & S. M. Hooker *Phys. Rev. E* **63** 015401 (2000)

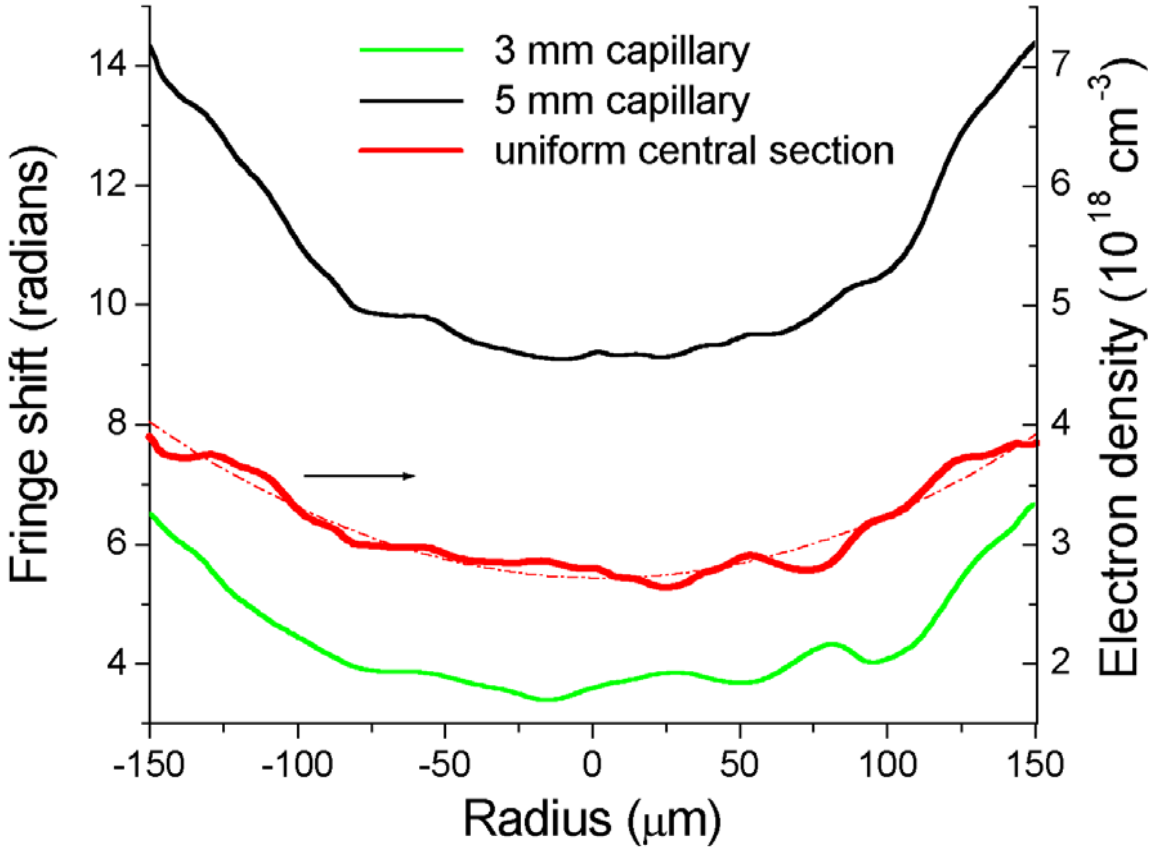

- Hydrogen pressure 63 mbar
- Central section has parabolic electron density profile corresponding to a matched spot size of 37 μm

Strong lasing at 41.8 nm in Xe^{8+}

Signal is 4 times larger for the capillary discharge

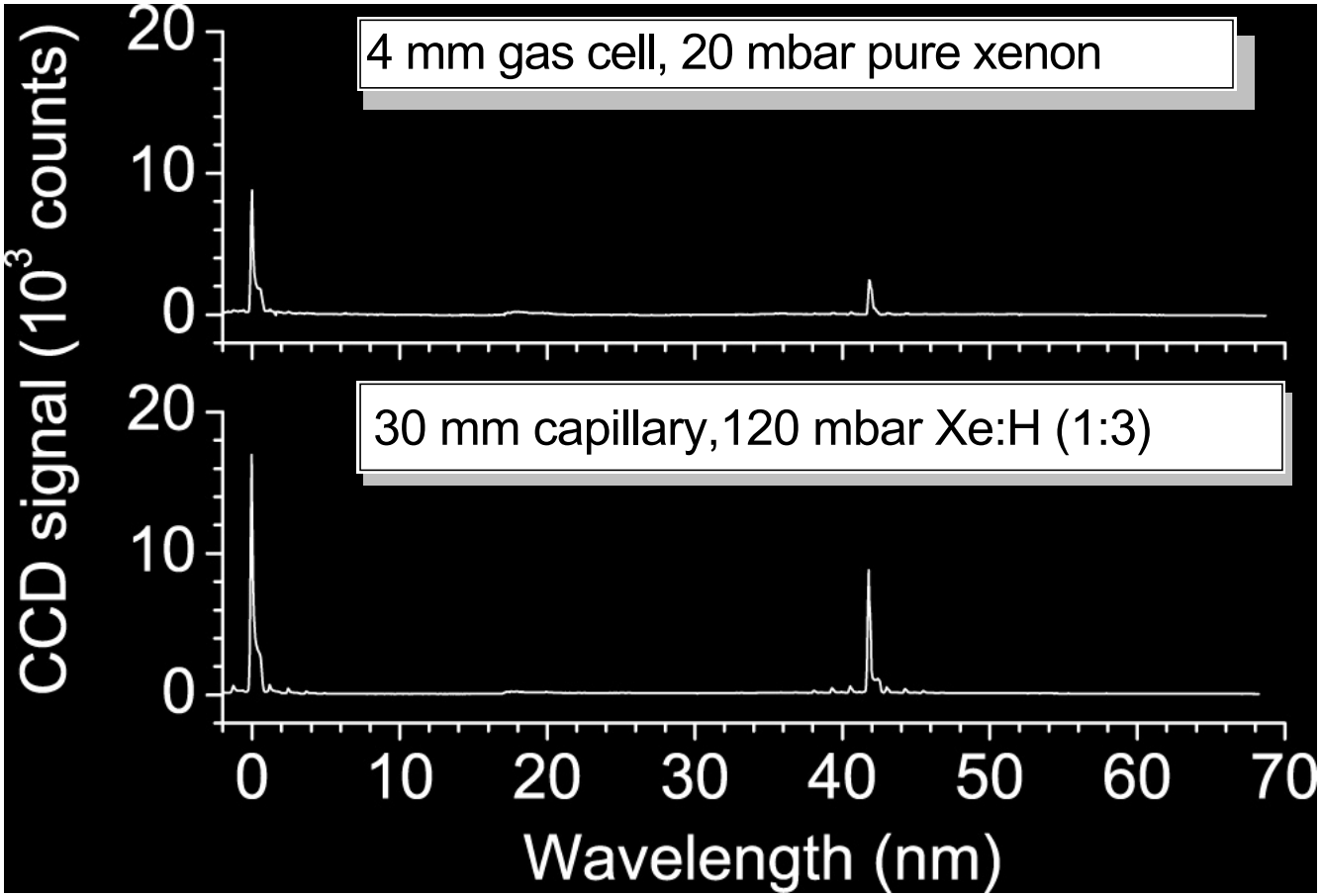

Lasing sensitive to guiding conditions

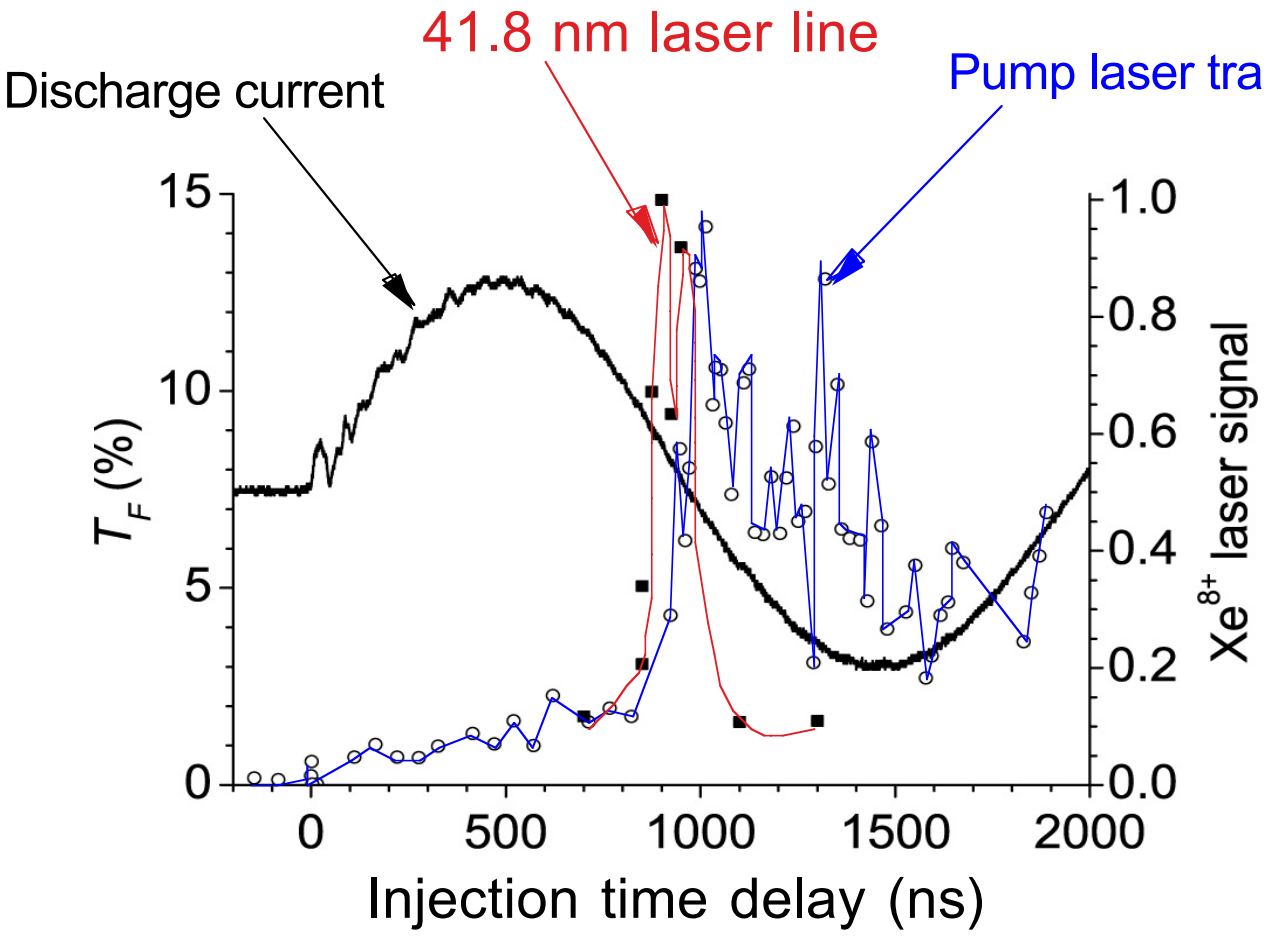

- 30 mm capillary
- Gas mixture
  1:3 Xe:H
  Pressure 120 mbar
- Input intensity
  2.5×10^{17} W/cm^2

Xenon ionization stage

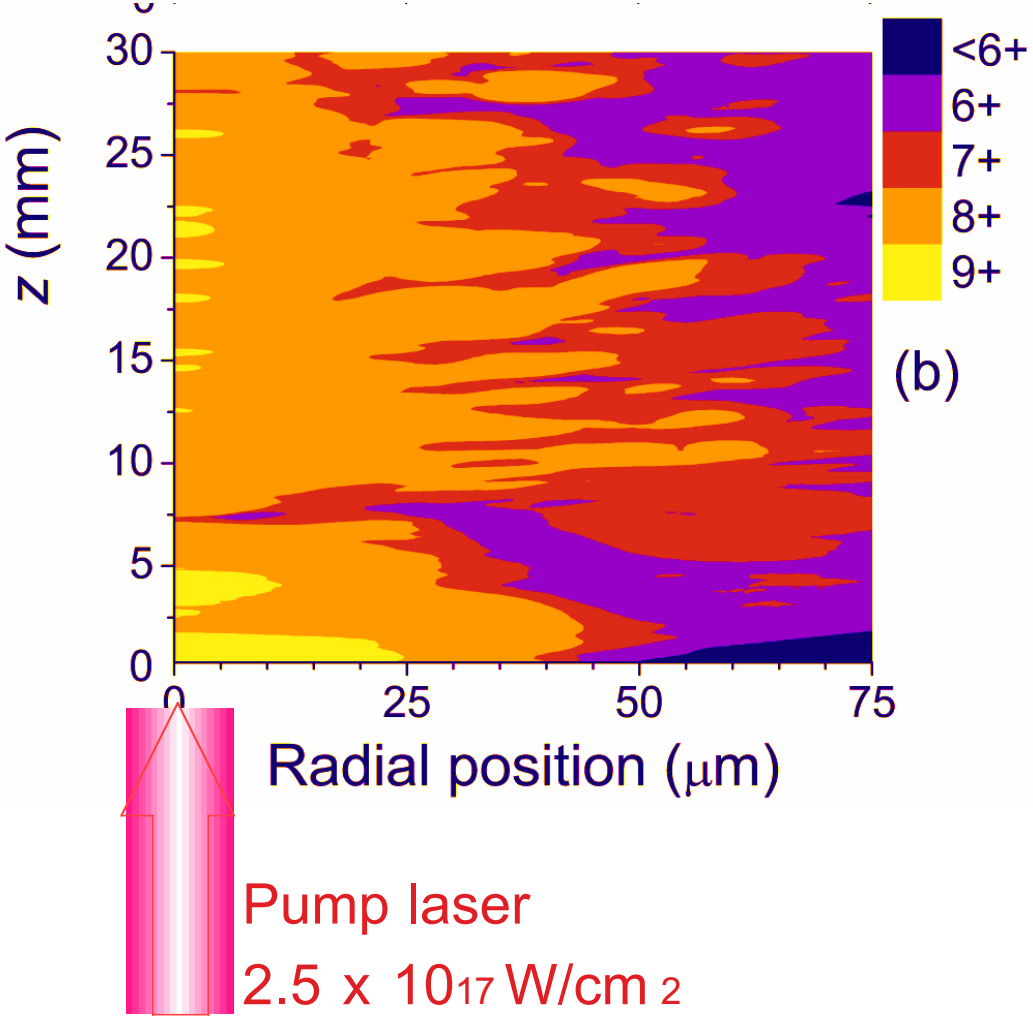

- Simulation result
- 30 mm capillary
- Gas mixture
  1:3 Xe:H
  Pressure 120 mbar
- Xe assumed to be pre-ionised to 5+ by the discharge

Summary

- First demonstration of collisionaly excited OFI laser driven within a waveguide: Increase in gain length achieved
- More work needed for capillary tube guiding:
  - Achieve transmission reproducibility: improve focal spot quality, pointing stability
  - Simulation needed to predict the optimum parameters for lasing : laser energy, gas pressure, tube length
- Increased energy extraction and reduced beam divergence are the goals of future experiments

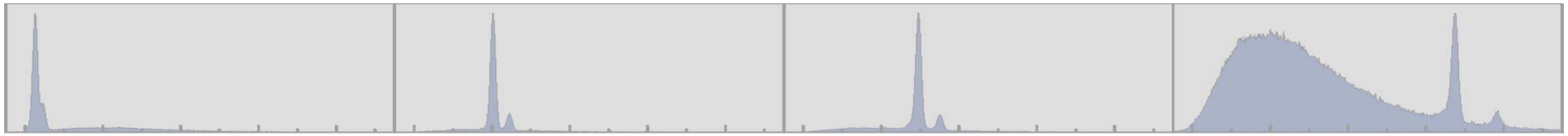

International Conference on Ultrashort High-Energy Radiation and Matter
Villa Monastero, Varenna, Italy, 7-10 October 2003

High-repetition rate electron-based ultrashort hard-x-ray source and first applications

André Egbert and Boris N. Chichkov

Laser Zentrum Hannover e.V.

Hollerithallee 8, D-30419 Hannover, Germany

Phone: +49-511-2788-218, fax: +49-511-2788-100, e-mail: ae@lzh.de

Outline

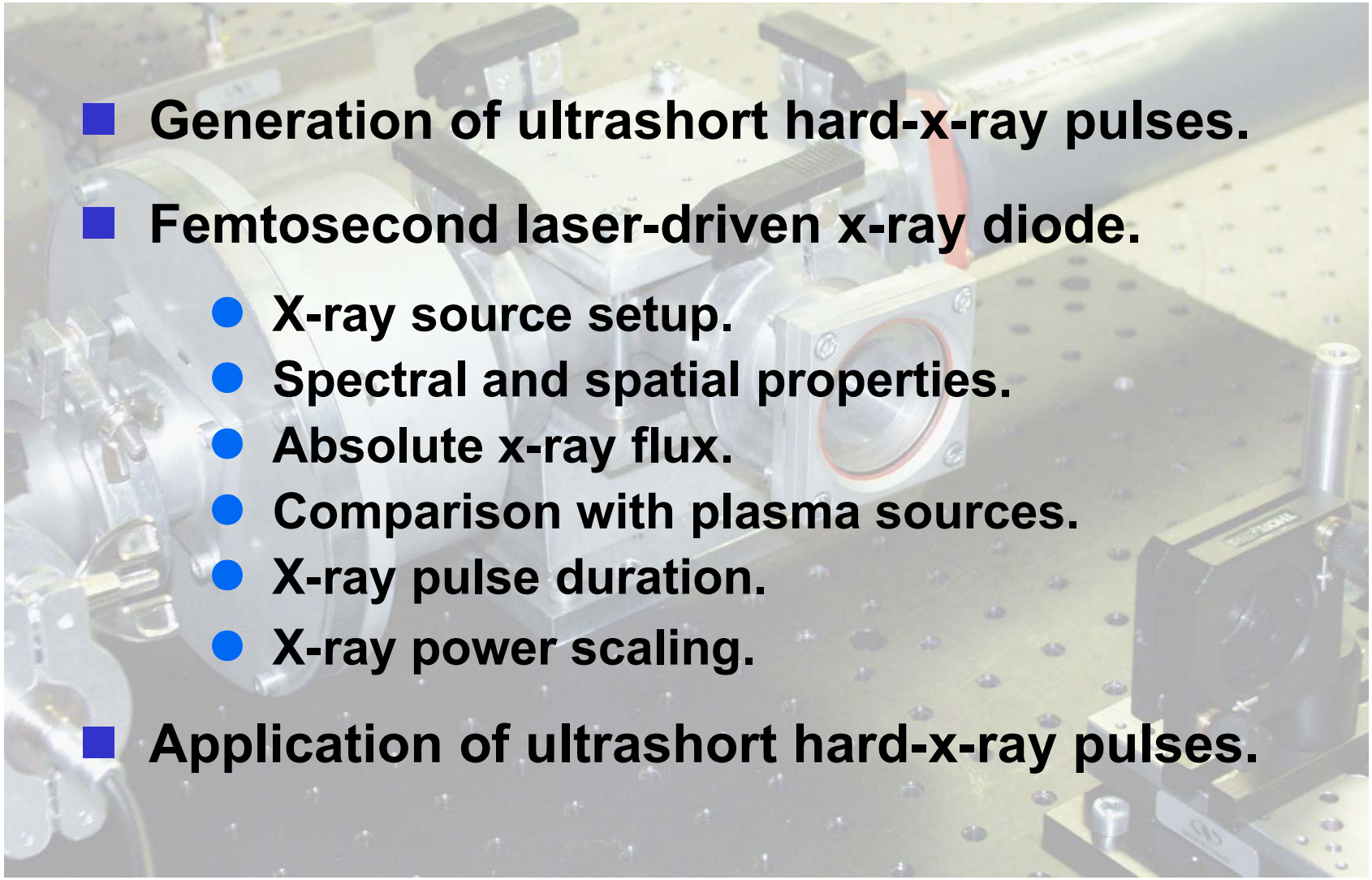

- Generation of ultrashort hard-x-ray pulses.
- Femtosecond laser-driven x-ray diode.
  - X-ray source setup.
  - Spectral and spatial properties.
  - Absolute x-ray flux.
  - Comparison with plasma sources.
  - X-ray pulse duration.
  - X-ray power scaling.
- Application of ultrashort hard-x-ray pulses.

Ultrashort hard-x-ray pulses

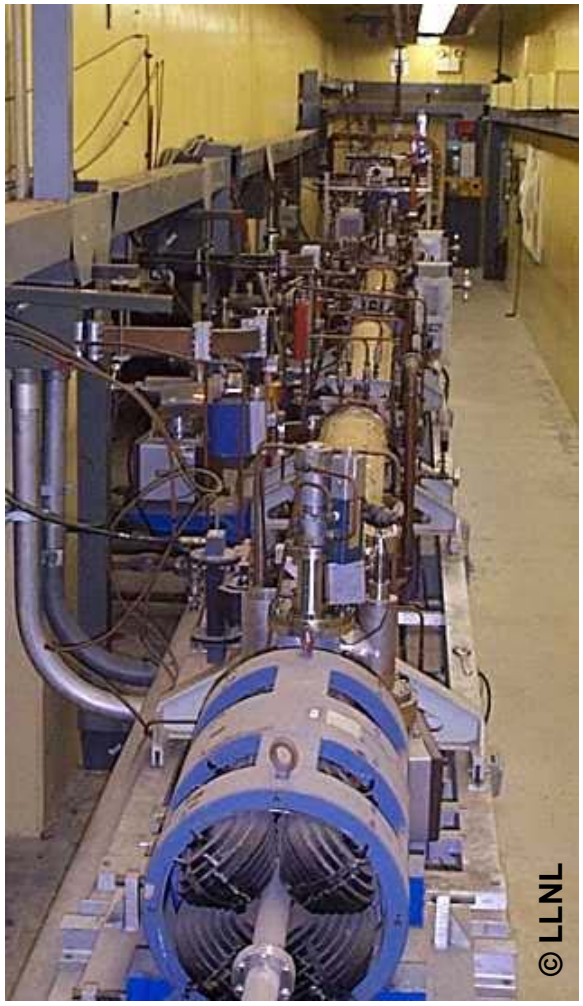

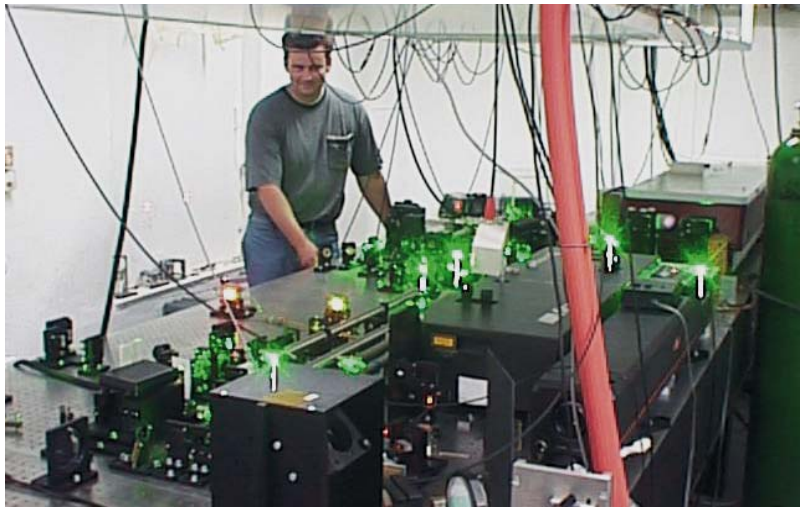

- Synchrotron-based x-ray sources
- Thomson scattering sources
- Terawatt fs laser-plasma x-ray sources
- **Short-pulse laser-driven x-ray diodes**

Femtosecond laser-driven x-ray diode

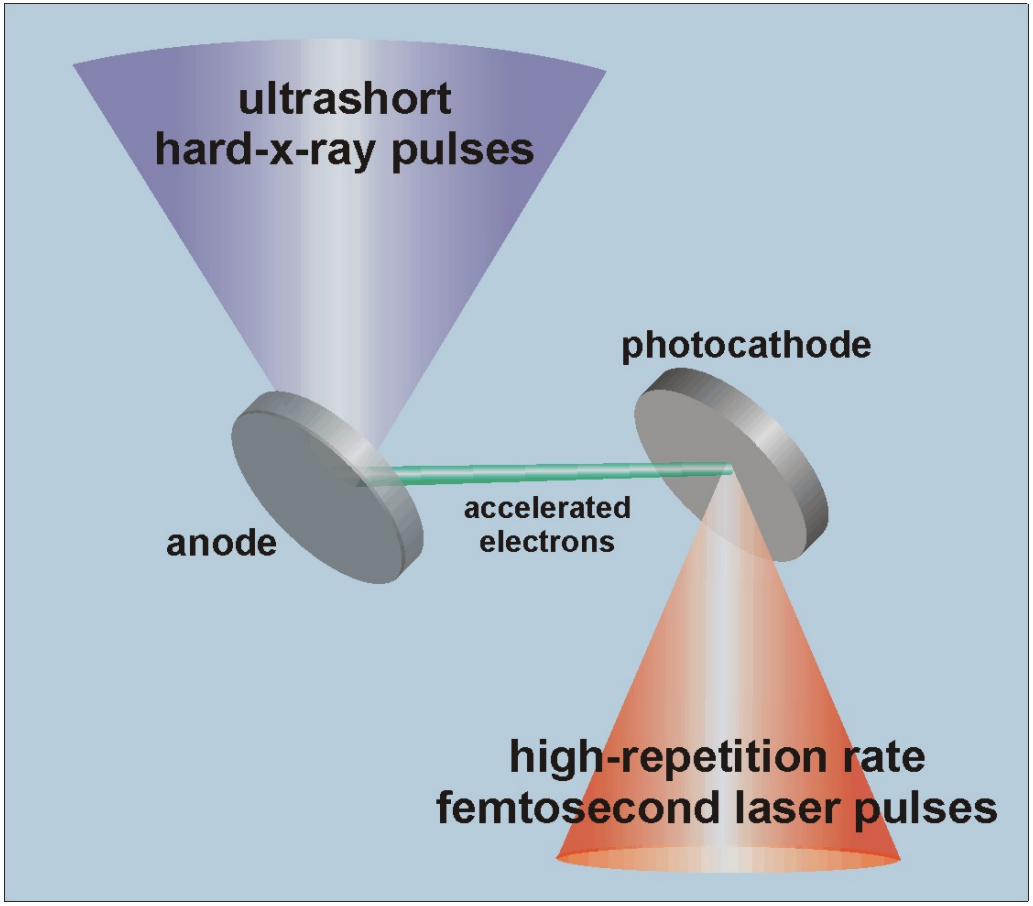

Advantages of this source:

- very compact setup
- stable, long-term operation
- debris-free
- power gain from HV field
- low-intensity laser pulses
- high-repetition rate
- high average x-ray power

Europhys. Lett. 56, 228 (2001); Opt. Eng. 41, 2658 (2002); Appl. Phys. Lett. 81, 2328 (2002)

Previous work

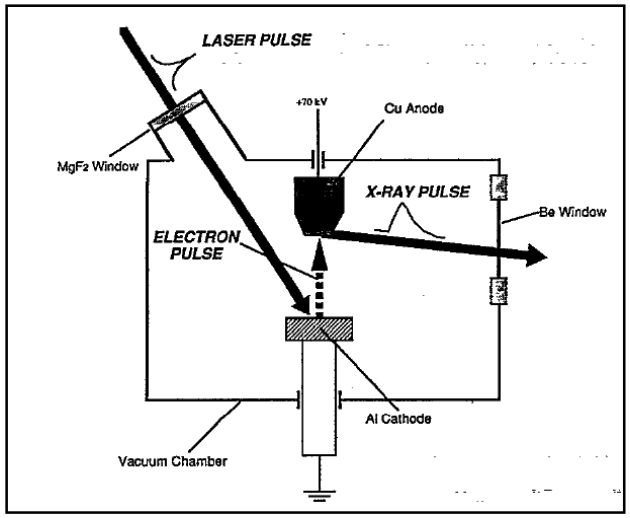

Rentzepis et al., J. Chem. Phys. 104, 10001 (1996)

- laser system: 1.8 ps, 193 nm, 500 µJ, 300 Hz
- x-ray spot size: 3 mm
- x-ray output: 10^7 photons/pulse, 3×10^9/s (Cu anode)
- ν x-ray pulse duration: <10 ps

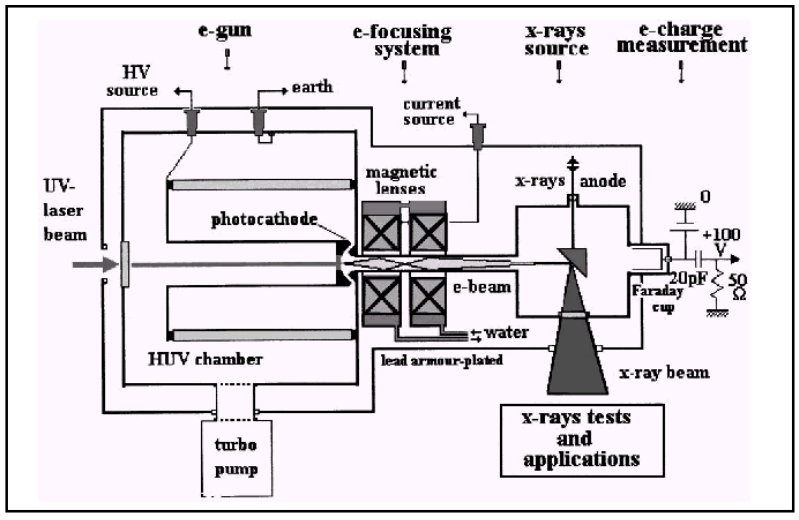

Girardeau-Montaut et al., NIM A 452, 361 (2000)

- laser system: 16 ps, 213 nm, 70 µJ, 10 Hz
- x-ray spot size: 250 µm
- x-ray output: 10^7 photons/pulse, 10^8/s (Tl anode)
- ν x-ray pulse duration: 200 ps

X-ray source setup

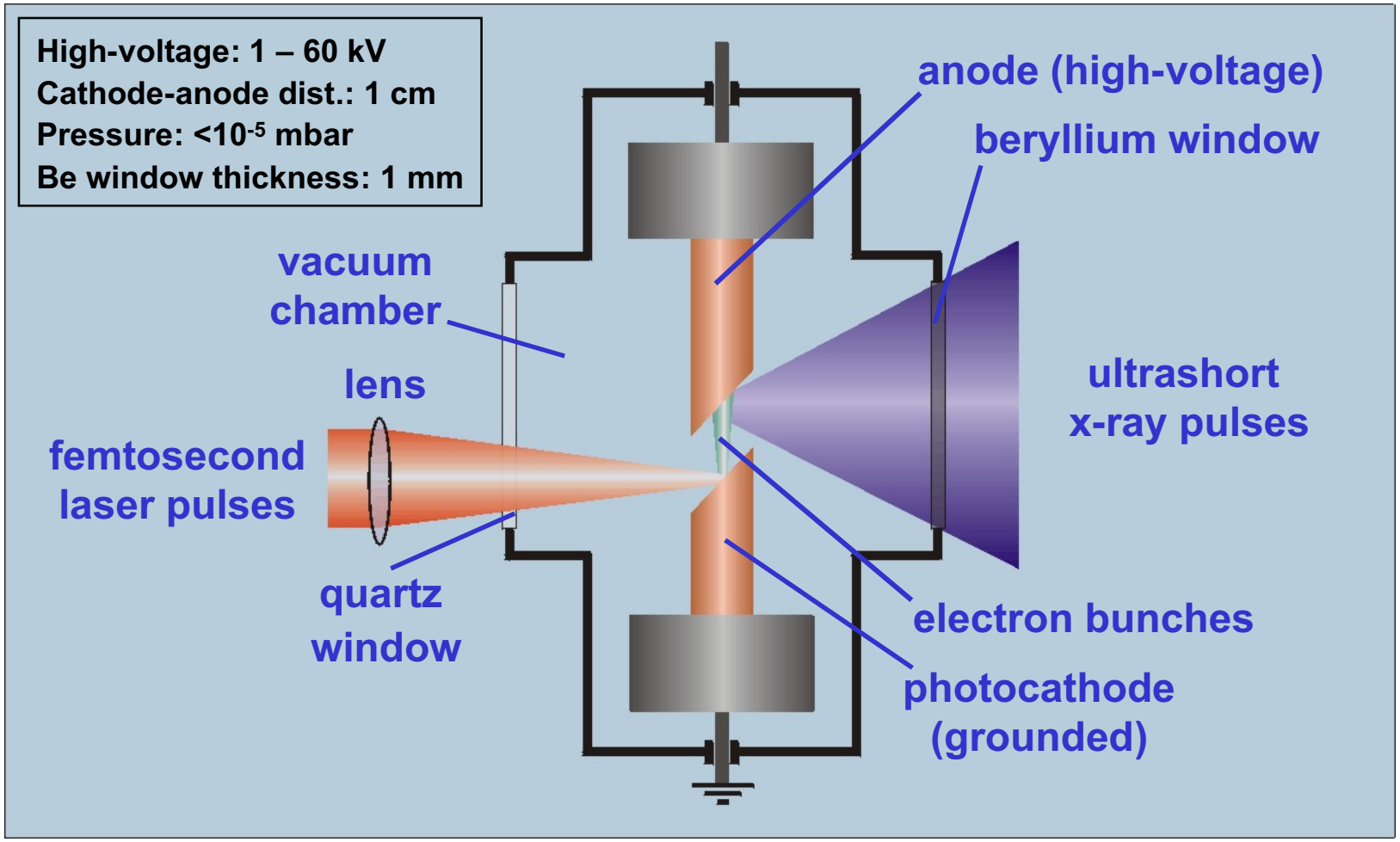

Femtosecond laser-driven x-ray diode

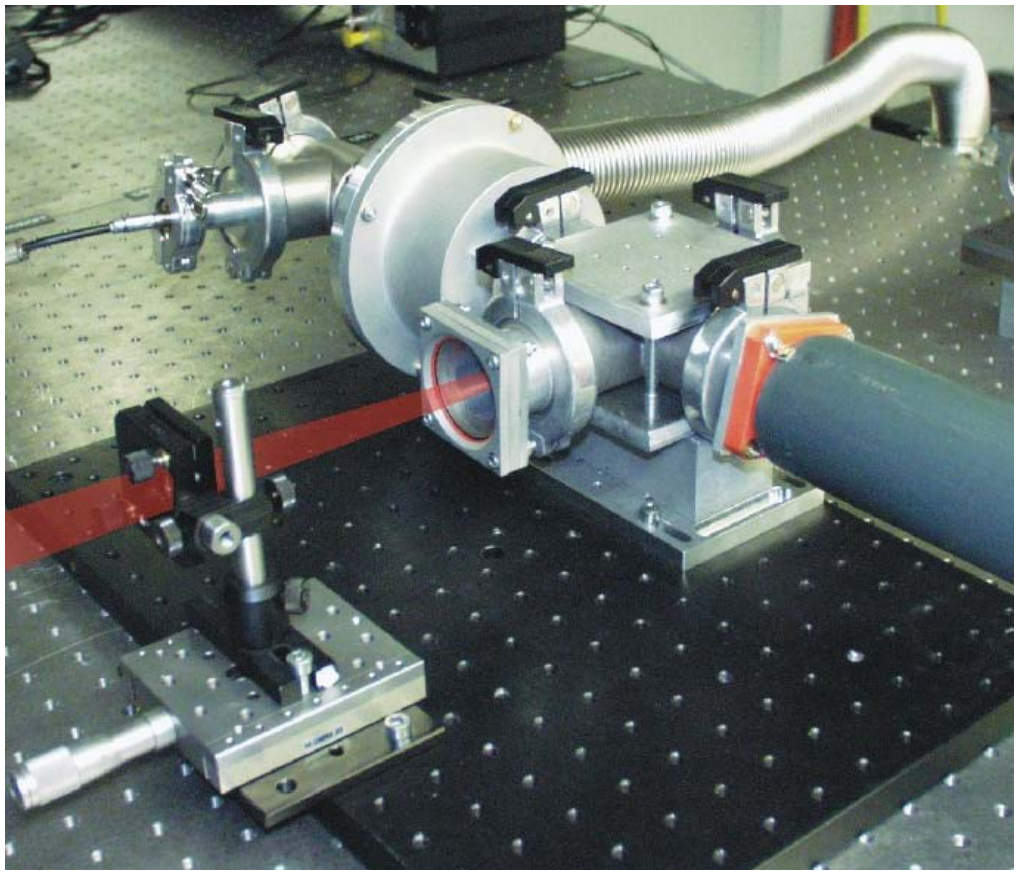

RegA 9000 (Coherent Inc.)

- laser wavelength: 780 nm
- pulse energy: 4 µJ
- pulse duration: 160 fs
- repetition rate: 250 kHz

Photocathode quantum efficiency

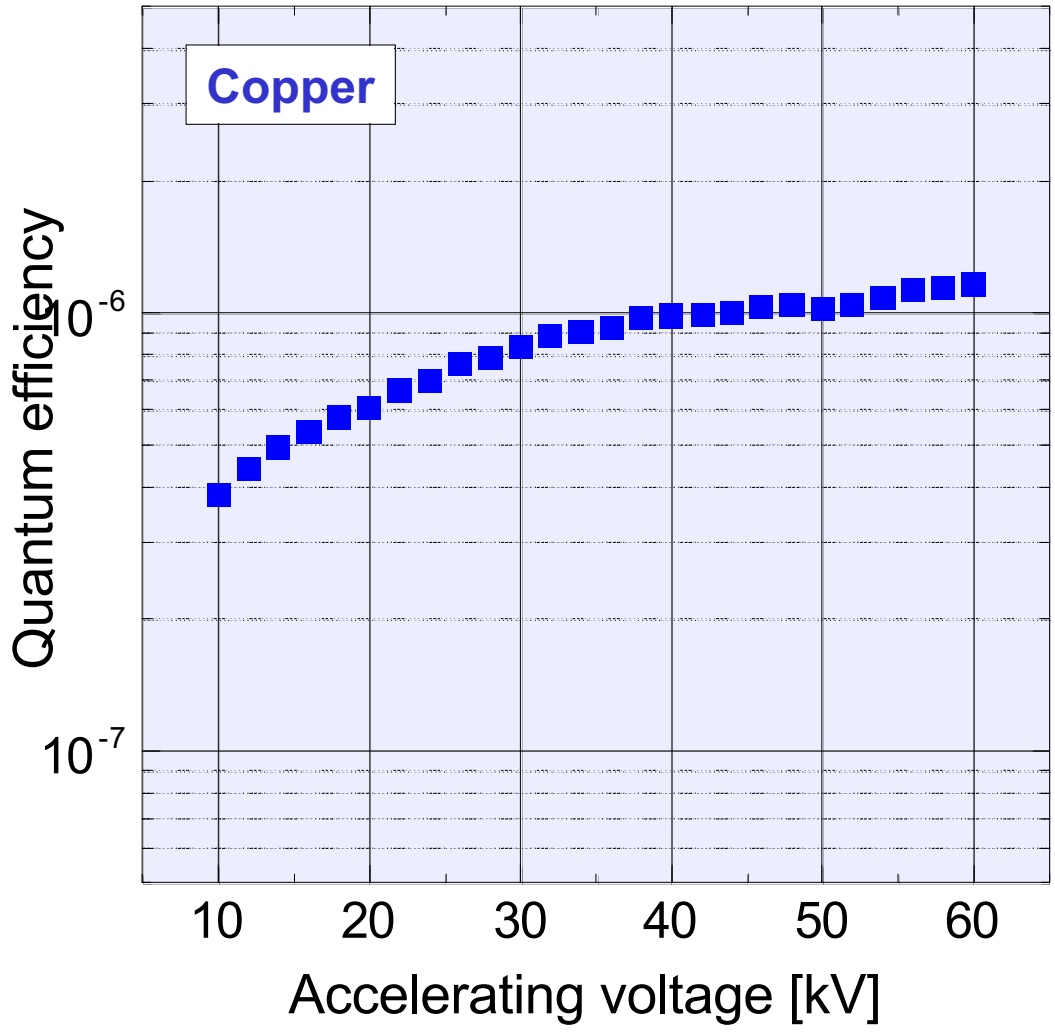

Laser parameters

- Wavelength: 780 nm
- Pulse energy: 2.5 µJ
- Pulse duration: 160 fs
- Repetition rate: 250 kHz

Cathode performance (60 kV)

- Quantum efficiency: **1.2×10^{-6}**
- Pulse charge: **1.8 pC/pulse**
- Electron current: **450 nA**

Hard-x-ray spectra

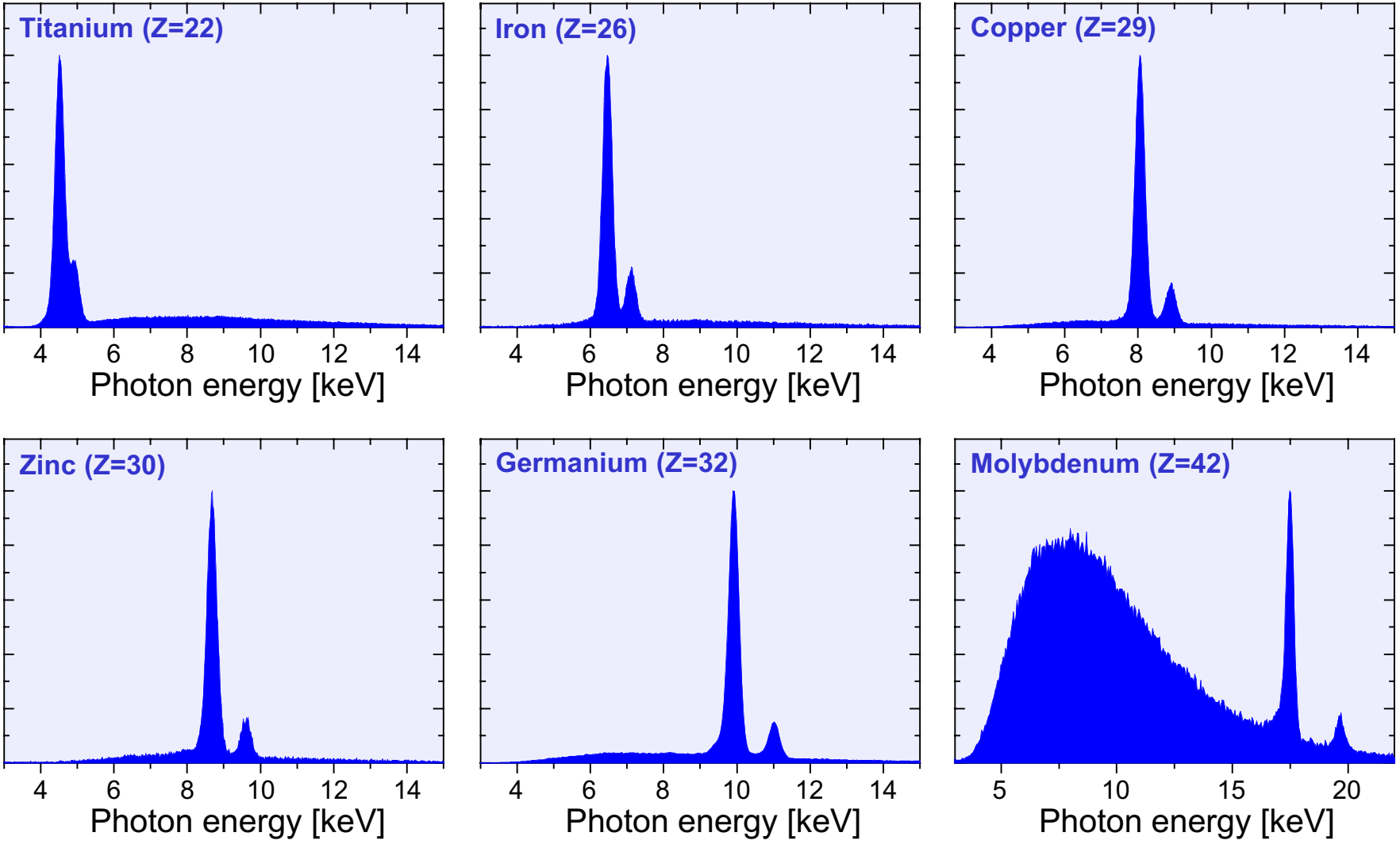

detector: AMPTEK XR-100CR, accel. voltage: 30 kV

Copper anode conversion efficiency

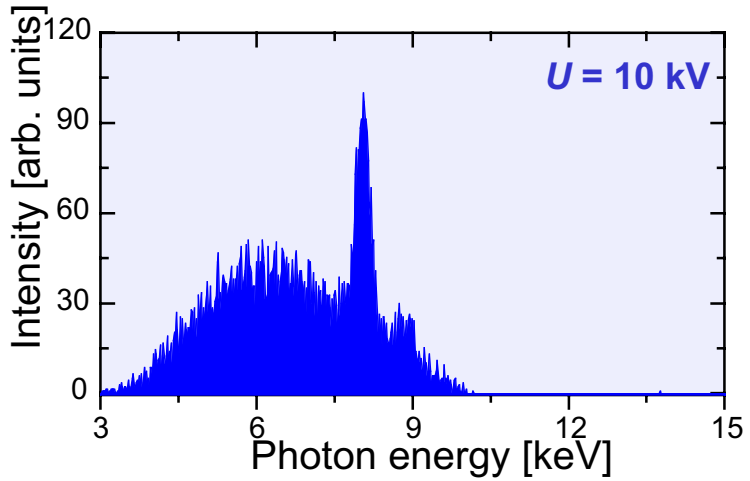

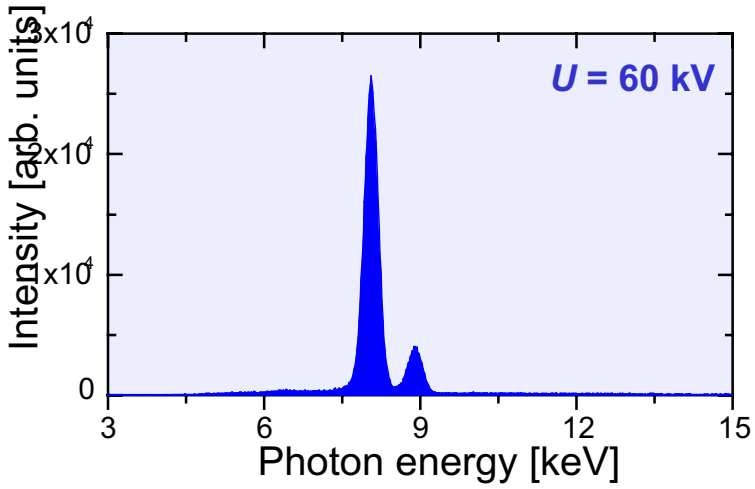

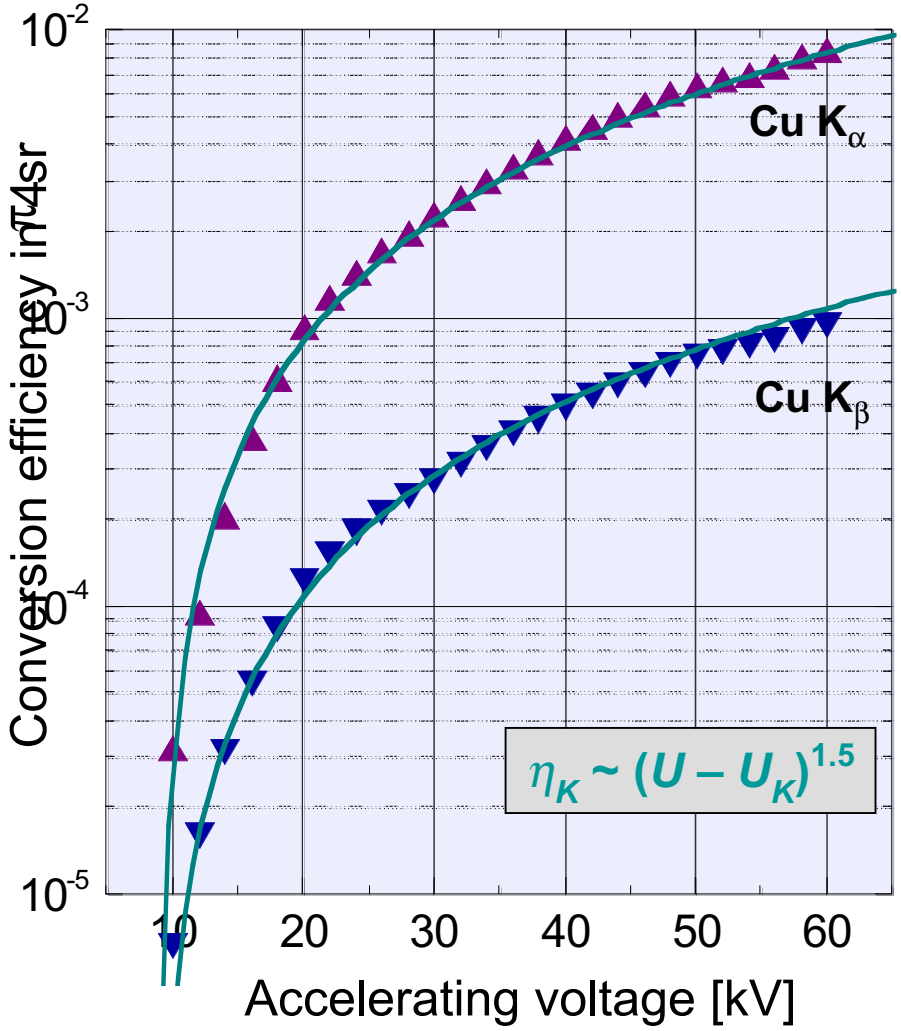

Copper K_α x-ray flux

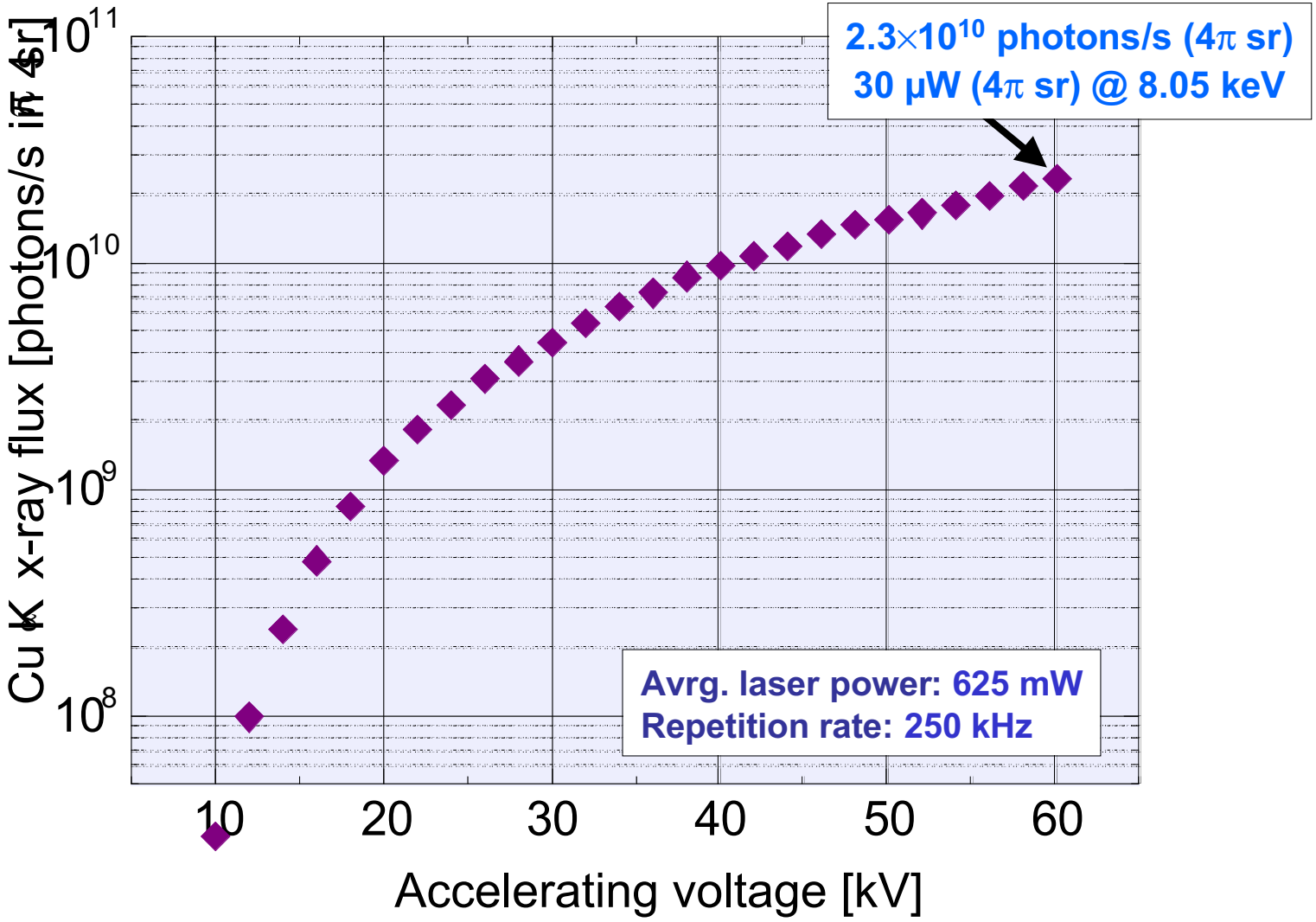

Comparison with plasma x-ray sources

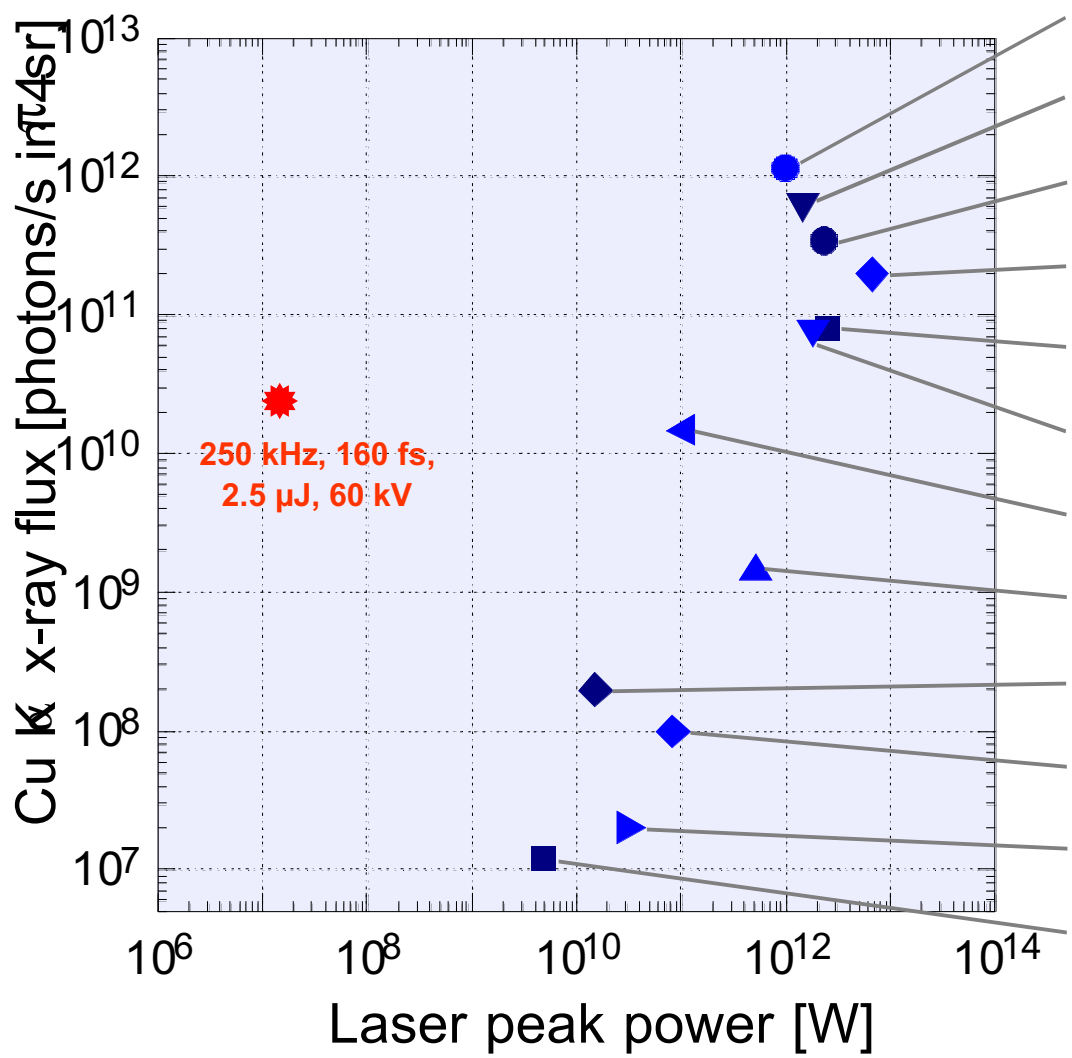

Eder et al., Appl. Phys. B **70**, 211 (2000)
10 Hz, 200 fs, 200 mJ, copper slab

Yoshida et al., Appl. Phys. Lett. **73**, 2393 (1998)
10 Hz, 42 fs, 60 mJ, copper disc

Fill et al., Rev. Sci. Instr. **73**, 2190 (2002)
10 Hz, 130 fs, 300 mJ, copper tape

Chen et al., Proc. SPIE **5030**, 923 (2003)
10 Hz, 70 fs, 460 mJ, copper disc

Guo et al., Rev. Sci. Instr. **72**, 41 (2001)
20 Hz, 30 fs, 75 mJ, copper wire

Cheng et al., Appl. Opt. **41**, 5148 (2002)
50 Hz, 24 fs, 43 mJ, copper wire

Lee et al., Proc. SPIE. **4978**, 77 (2003)
2 kHz, 40 fs, 4.2 mJ, copper wire

Fujimoto et al., Jpn. J. Appl. Phys. **38**, 6754 (1999)
10 Hz, 42 fs, 21 mJ, copper disc

Stiel et al., to be published
1 kHz, 25 fs, 0.37 mJ, copper cylinder

Jiang et al., Opt. Lett. **27**, 963 (2002)
2 kHz, 40 fs, 3.2 mJ, copper wire

Hagedorn et al., Appl. Phys. B **77**, 49 (2003)
1 kHz, 30 fs, 0.9 mJ, copper disc

Tompkins et al., Rev. Sci. Instr. **69**, 3113 (1998)
1 kHz, 100 fs, 0.5 mJ, copper nitrate solution

X-ray source size

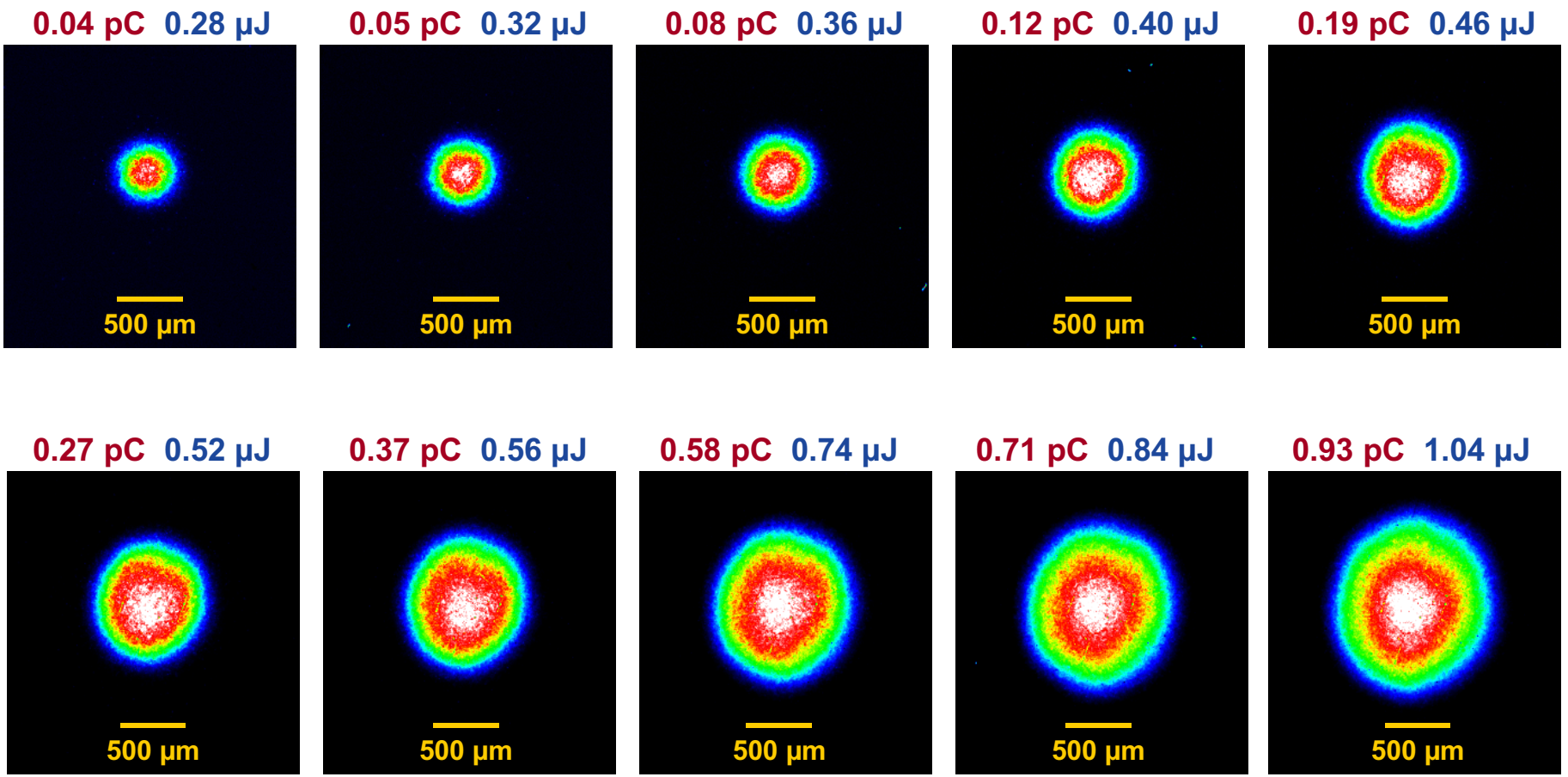

accelerating voltage: 50 kV, pinhole diameter: 150 µm, magnification: 2.5×

laser wavelength: 780 nm, pulse duration: 160 fs, repetition rate: 250 kHz

Variation of electron pulse charge

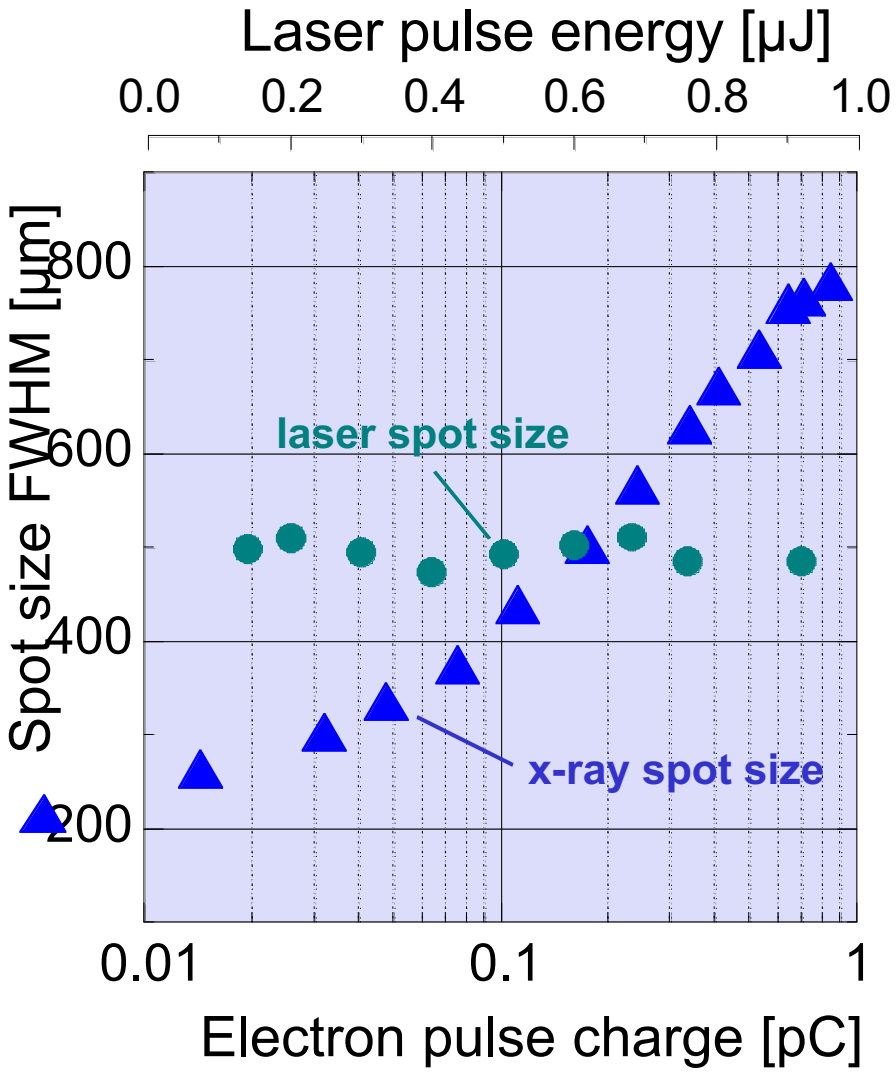

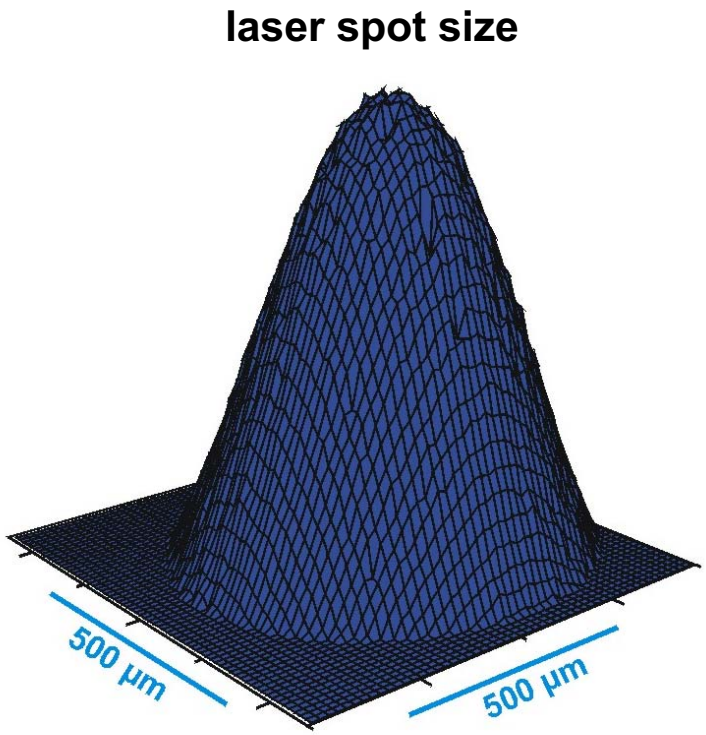

pulse energy: 0.5 µJ

Modeling of electron pulse duration

ASTRA (A Space Charge Tracking Algorithm) by K. Flöttmann, DESY Hamburg

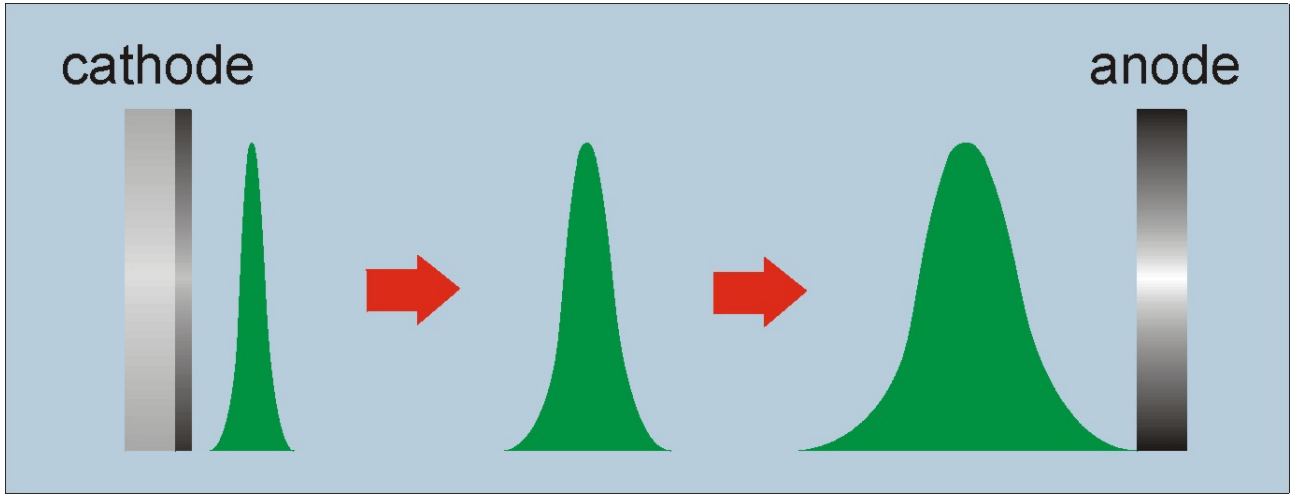

www.desy.de/~mpyflo/

Parameters:

- cathode – anode distance d
- initial electron pulse duration τ_0
- initial electron spot size A_0
- electron energy distribution ΔE
- electron pulse charge Q
- accelerating voltage U

Electron pulse broadening

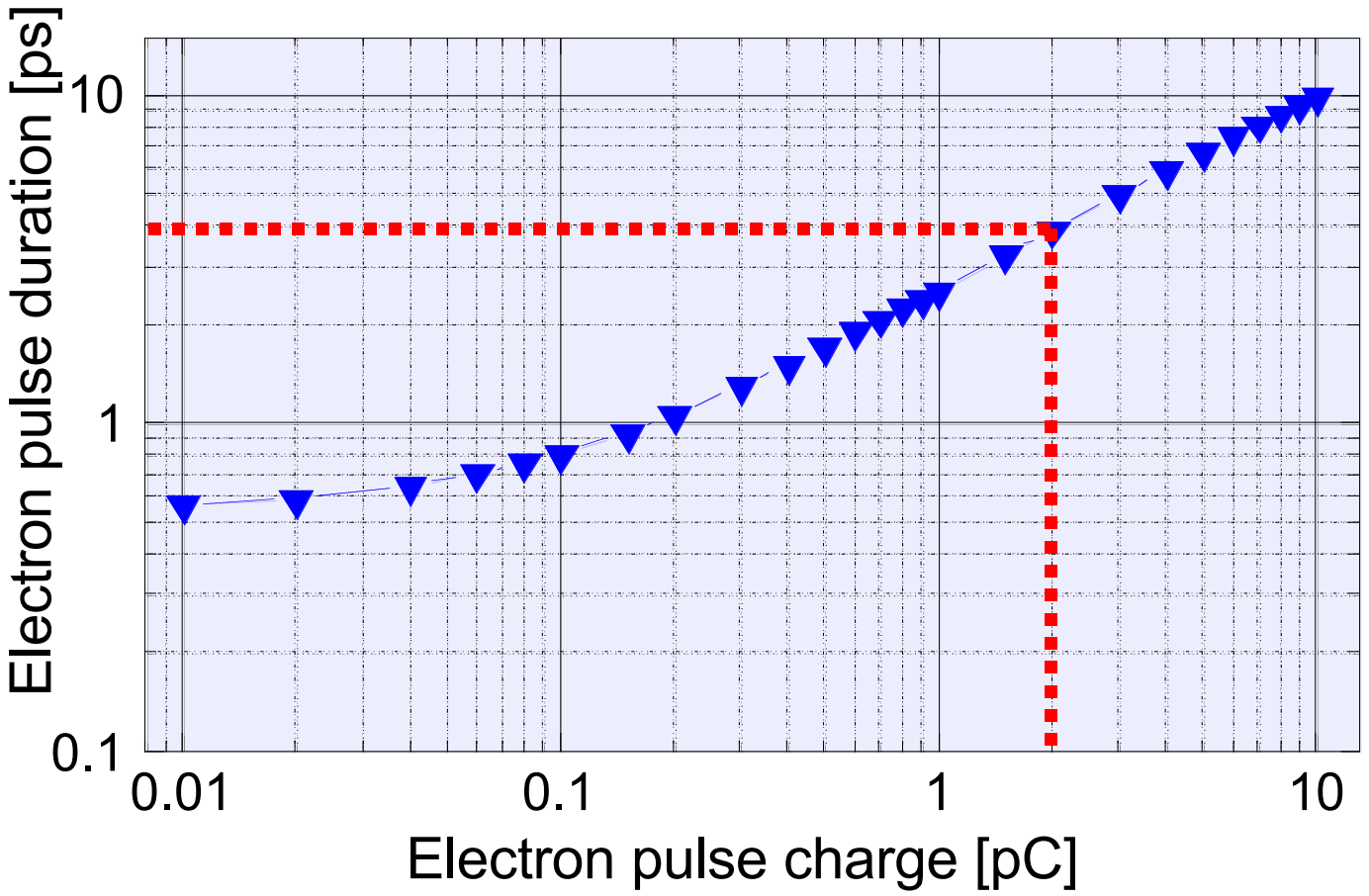

Parameters: τ_0 = 100 fs, U = 50 kV, d = 1 cm, ΔE = 1 eV, A_0 = 10^{-3} cm^2.

Ultrafast x-ray streak camera

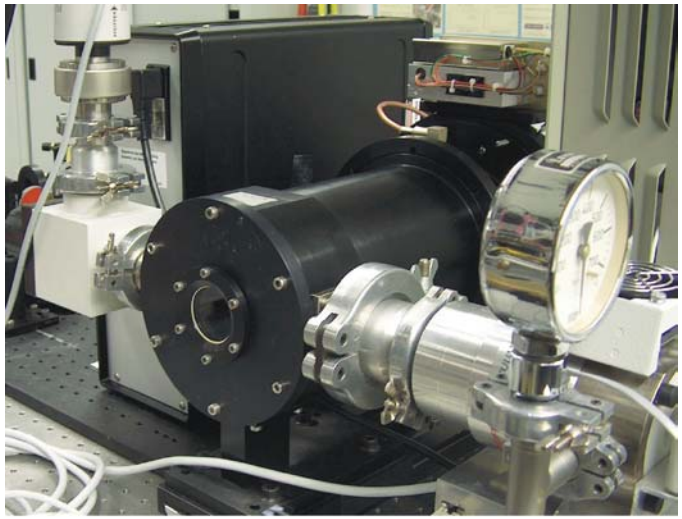

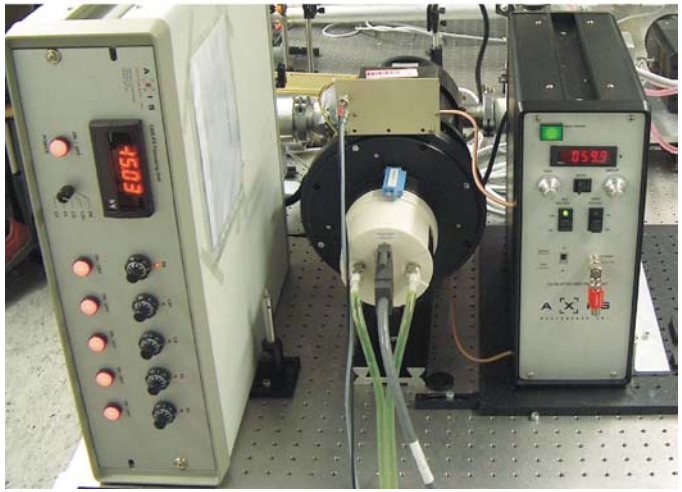

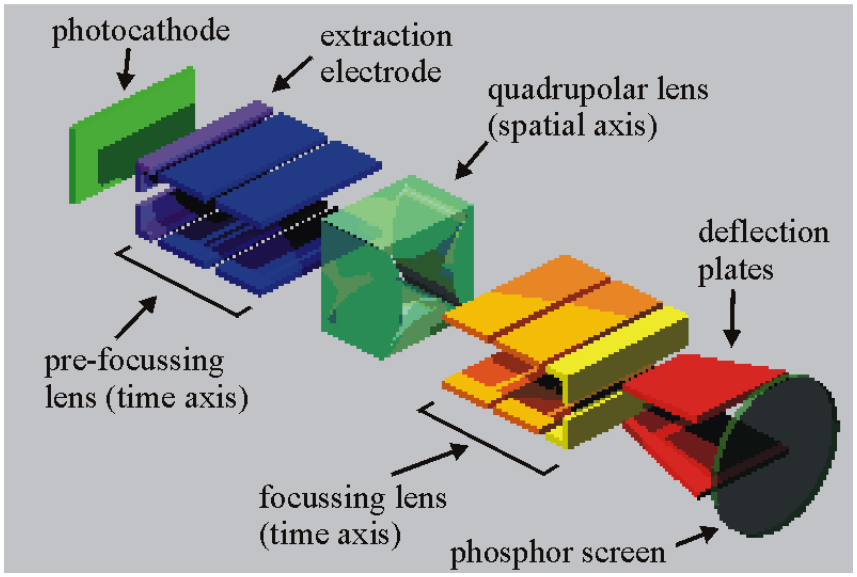

- Measurement of x-ray pulse duration with ultrafast x-ray streak camera.
- Accumulation regime based on photoconductive (semiconductor) switches.
- Temporal resolution of ~1 ps achieveable.

X-ray power scaling

Cu cathode

fs laser → 10^{-6} → electrons

Cu anode

electrons → 10^{-2} → K_α x-rays

high-QE cathode

fs laser → 10^{-2} → electrons

Cu anode

electrons → 10^{-2} → K_α x-rays

Laser Focus World **36**, 77 (Oktober 2000)

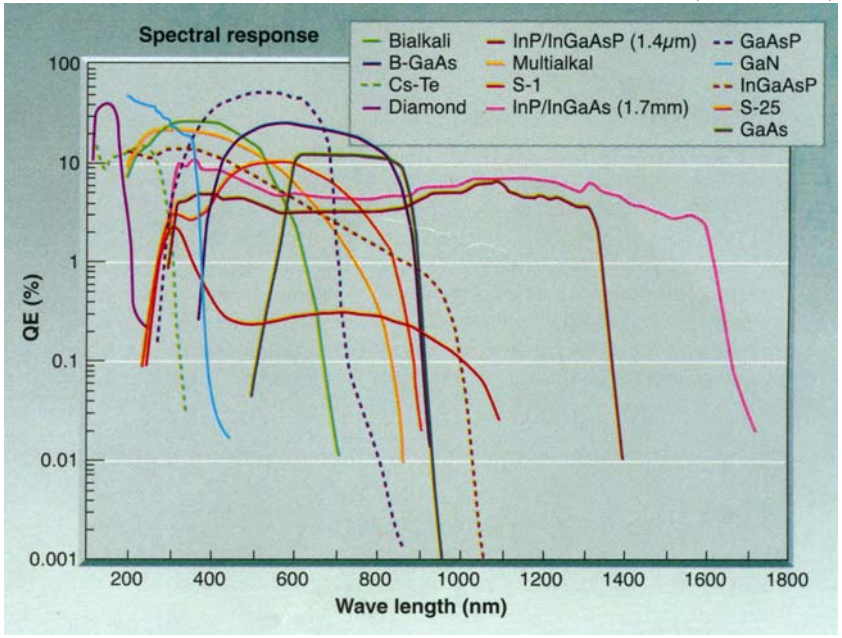

photomultiplier tube

High-efficiency photocathodes

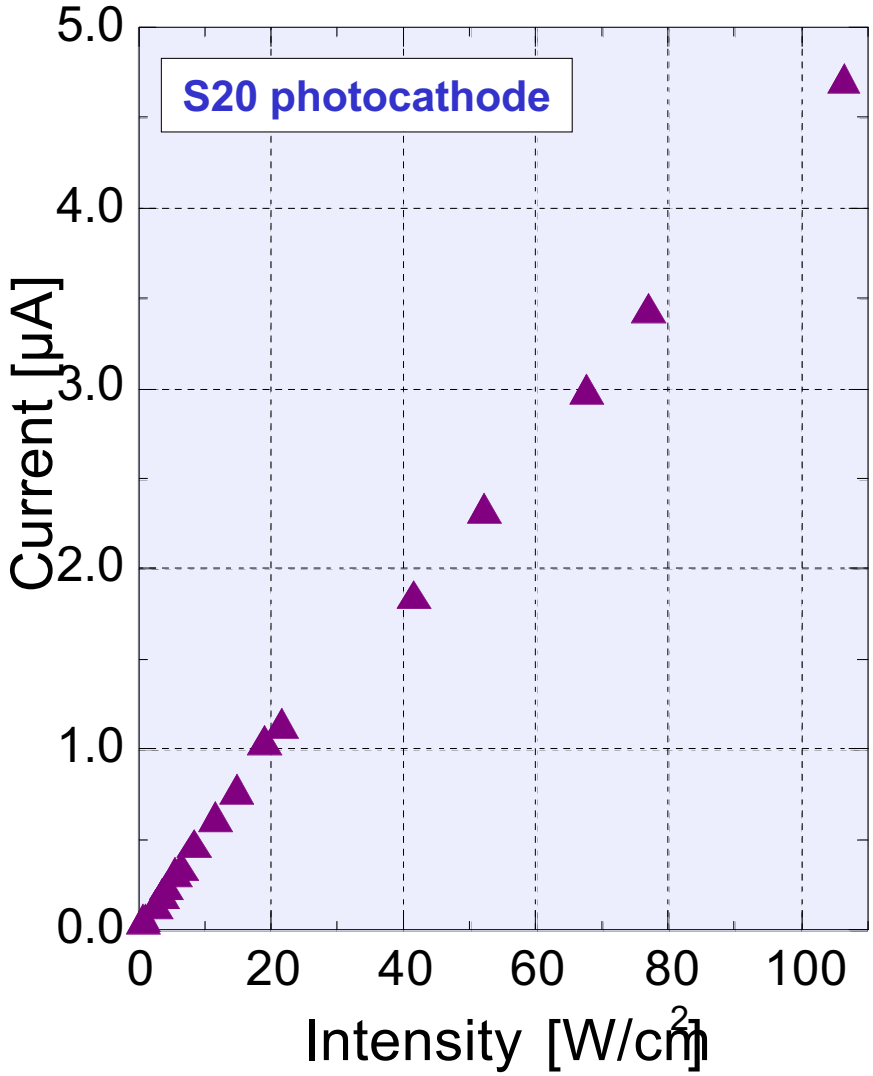

Laser parameters:

- Wavelength: 780 nm
- Pulse energy: 1 ... 10 pJ
- Pulse duration: 120 fs
- Spot diameter: 1 cm
- Repetition rate: 82 MHz

Photocathode performance:

- Quantum efficiency: 10^{-2}
- Pulse charge: **0.06 pC/pulse**
- Electron current: **4.7 µA**

Corresponds to Cu K_α x-ray flux of 2.4×10^{11} photons/s (4π sr)

Advanced x-ray diode design

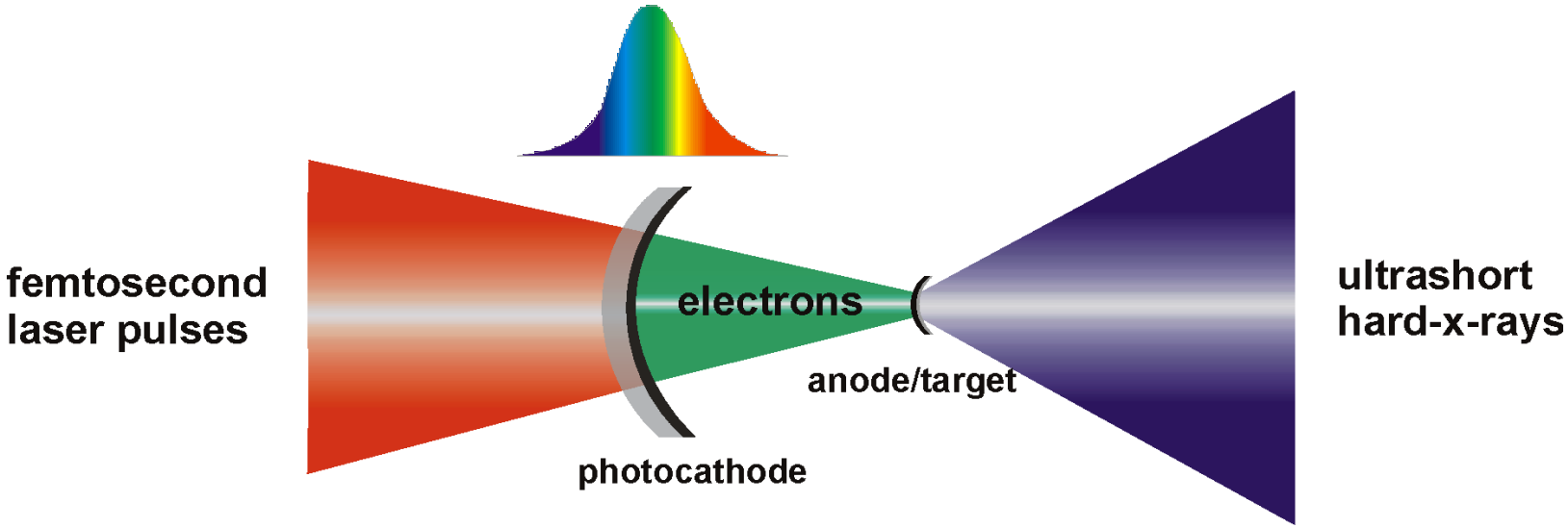

- High-efficiency photocathode, high-repetition rate fs laser system.
- Curved photocathode/anode configuration.
- Reduction of space-charge effects due to large electron spot.
- Optimization of x-ray pulse duration by pulse shaping techniques.

Time-gated medical x-ray imaging

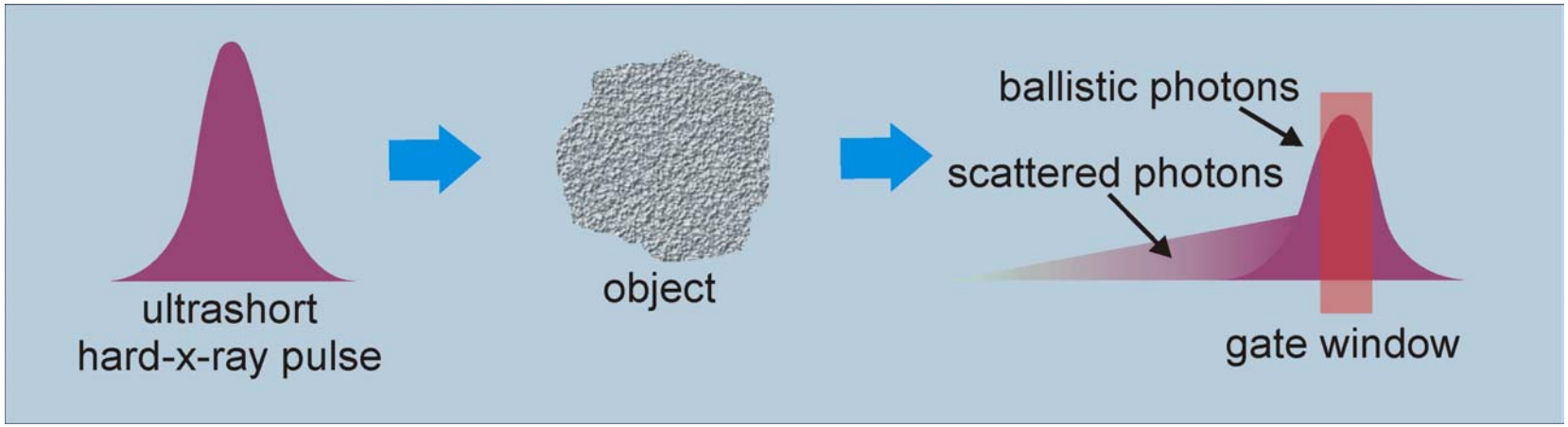

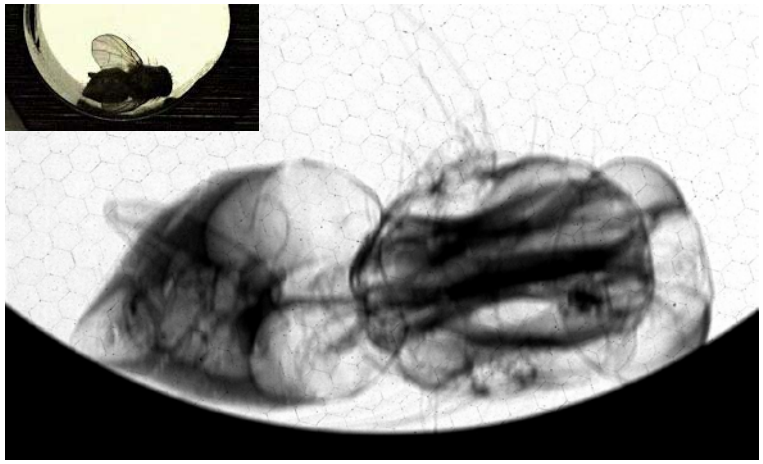

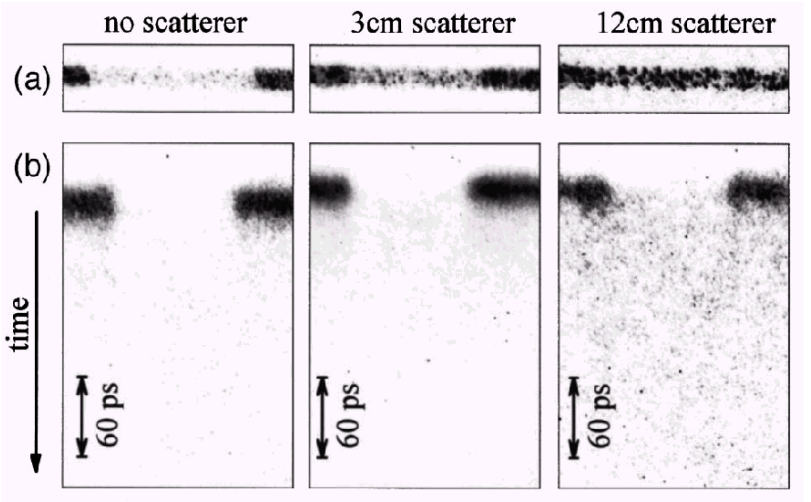

M. Grätz et al., Med. Phys. 26, 438 (1999)

Time-gated 2D x-ray detectors

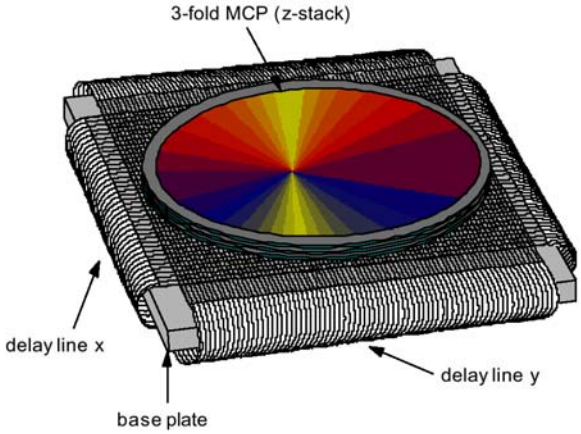

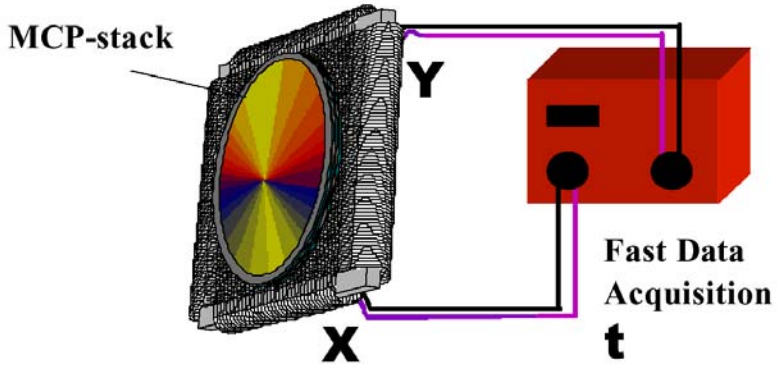

Current technical data

- time resolution: **125 ps**
- spatial resolution: **50 µm**
- max. count rate: **1 MHz**

Under development

- time resolution: **60 ps**
- spatial resolution: **25 µm**
- max. count rate: **4 MHz**

SURFACE CONCEPT

www.surface-concept.de

Summary

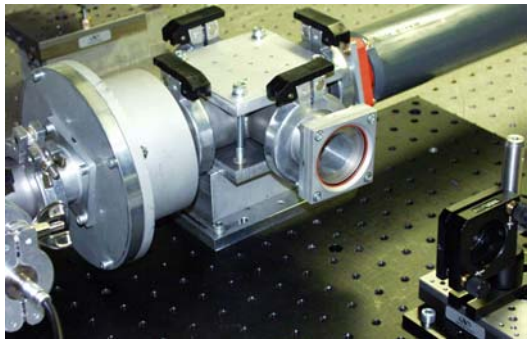

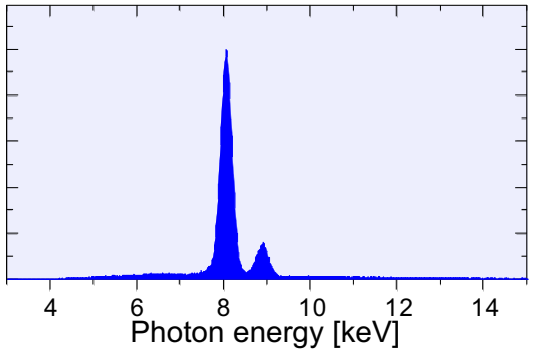

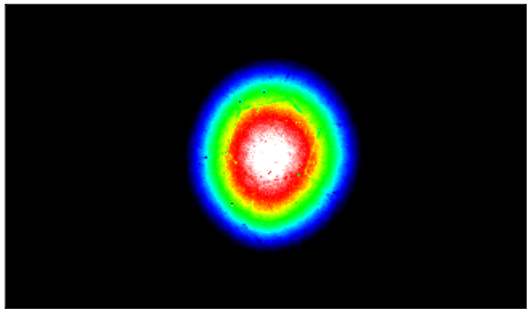

- A compact, high-repetition rate femtosecond laser-driven hard-x-ray diode has been set up and investigated.
- The source has been characterized in terms of x-ray spectra, source size, and absolute x-ray yield.
- Copper K_α fluxes of 2×10^{10} photons/s in 4π sr have been obtained and a comparison with plasma x-ray sources has been performed.
- Possibilities for x-ray power scaling using high-efficiency photocathodes have been studied.
- Application: time-gated medical x-ray imaging.

Acknowledgement

Deutsche Forschungsgemeinschaft (SPP1134)

phoenix|x-ray Systems + Services GmbH
S. Becker, E. Neuser, H. Appelt

Max-Planck Institut für Quantenoptik, Garching
K. Eidmann, E. Fill

Electron Tubes Ltd.
A. Cormack, R. McAlpine

Deutsches Elektronen-Synchrotron Hamburg
K. Flöttmann

Compact electron-based ultrashort hard-x-ray source

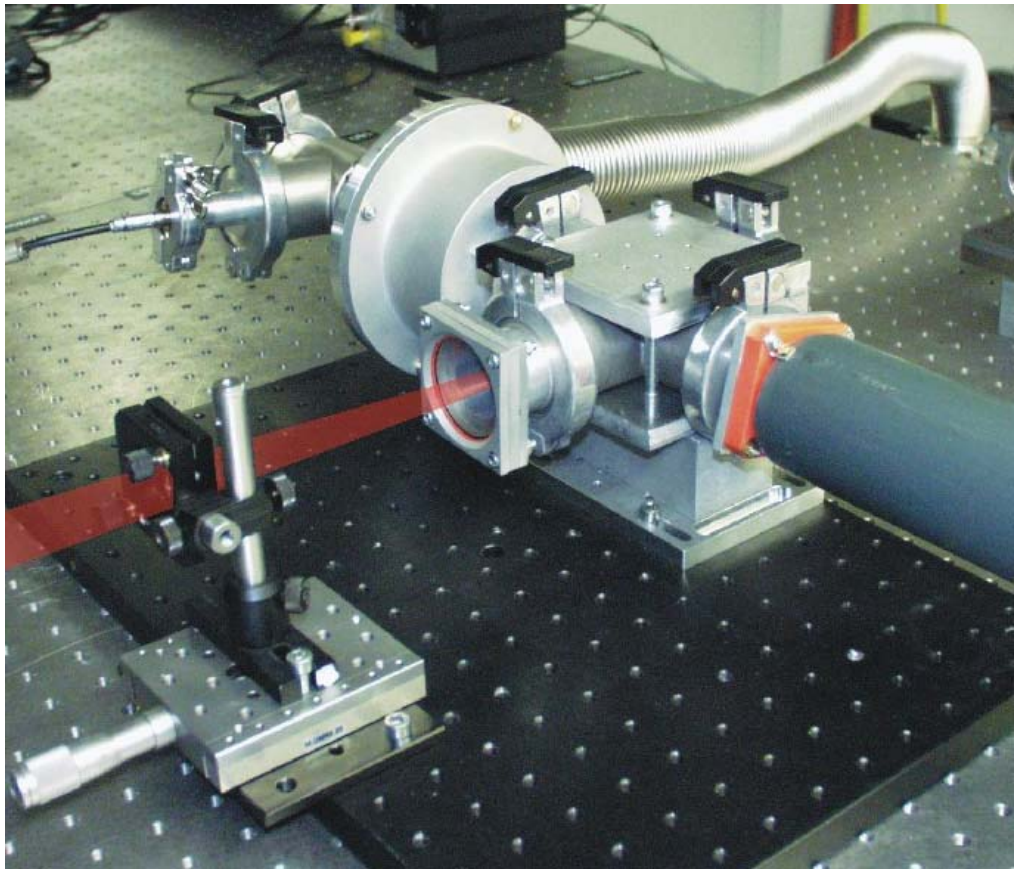

Please contact ae@lzh.de for further information.

INTERNATIONAL CONFERENCE ON
ULTRASHORT HIGH-ENERGY RADIATION AND MATTER
25-27 NOVEMBER 2001, BORDEAUX

Isochoric heating of matter by ultrashort laser pulses

K. Eidmann, U. Andiel, F. Pisani, K. Witte, J. Meyer-ter-Vehn
Max Planck Institut für Quantenoptik, Garching, Germany
R.C. Mancini, P. Hakel
Dep. of Physics, University of Nevada, Reno, USA
G.C. Junkel-Vives, J. Abdallah
Los Alamos National Laboratory, Los Alamos, NM, USA
I. Uschmann, E. Förster
Friedrich Schiller Universität, Jena, Deutschland
A. Pukhov
Universität Düsseldorf, Deutschland

outline

- principle and motivation of isochoric heating
- x-ray spectroscopy of isochorically heated Al

  (K-shell spectra, comparison with theory, dense plasma line shift, time resolved spectra)
- electron transport in plasma
- conclusions

isochoric heating is possible when the pulse duration (τ) is shorter than the expansion time

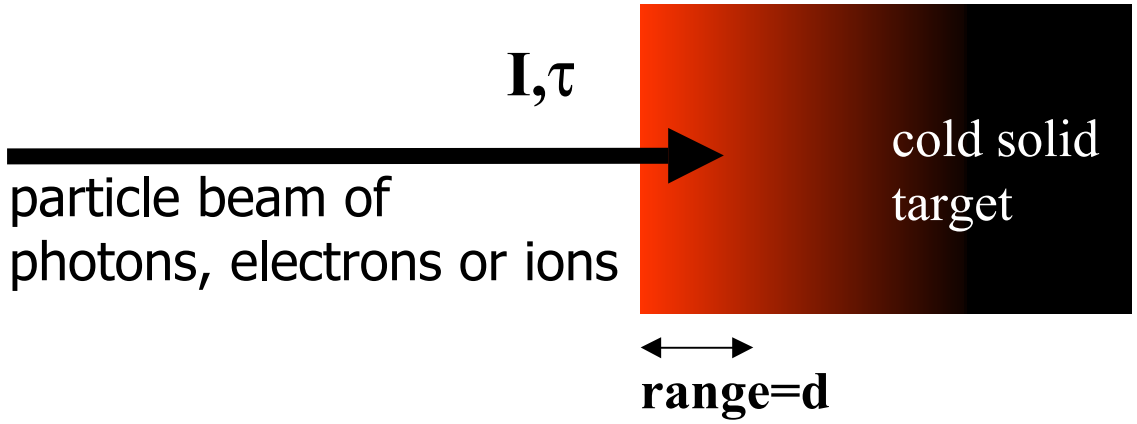

expansion time: $\tau \leq \tau_{exp} = d/s \qquad \left(s = \sqrt{ZkT/m_i} \right)$

example: kT=1keV; d=1μm ⟶ τ_{exp}=4 ps

→ **with ultrashort pulses of sub-ps duration isochoric heating at solid density is possible**

Such dense plasmas are important for eos and opacity studies, interaction of intense beams with matter, astrophysics, planetary plasmas, ICF, ...

principle of isochoric heating with electrons generated by ultrashort laser pulses

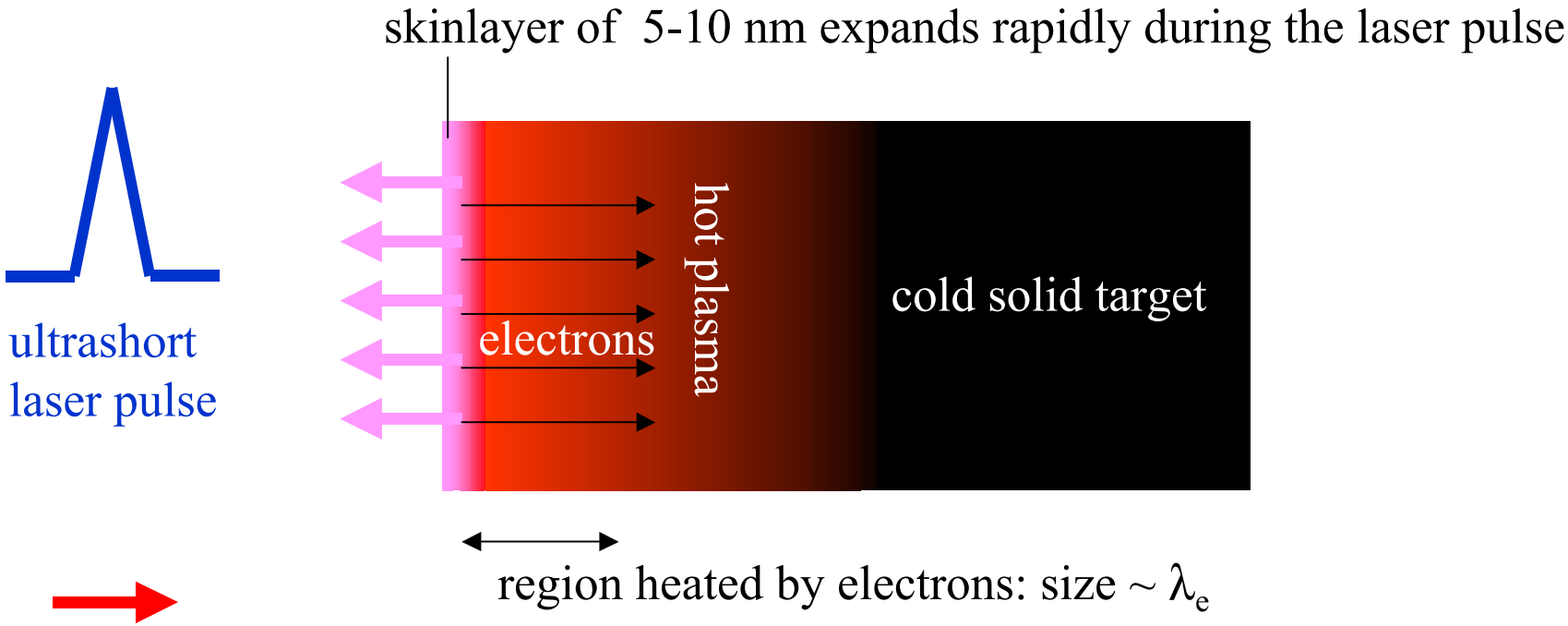

- **generation of hot plasma at solid state density**
- **electron transport in plasma is a key issue (fast ignitor relevance!)***

* typical ionization time is 20fs ⇒ for longer pulses the electrons interact with plasma!

which temperatures are achievable by isochoric heating?

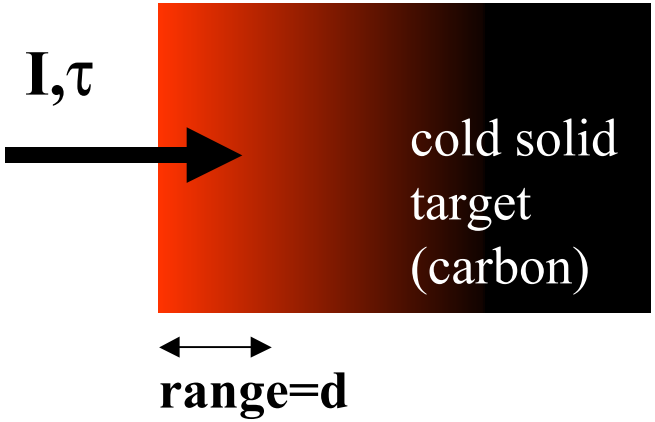

$$\text{internal energy} = \frac{I\tau}{\rho d}$$

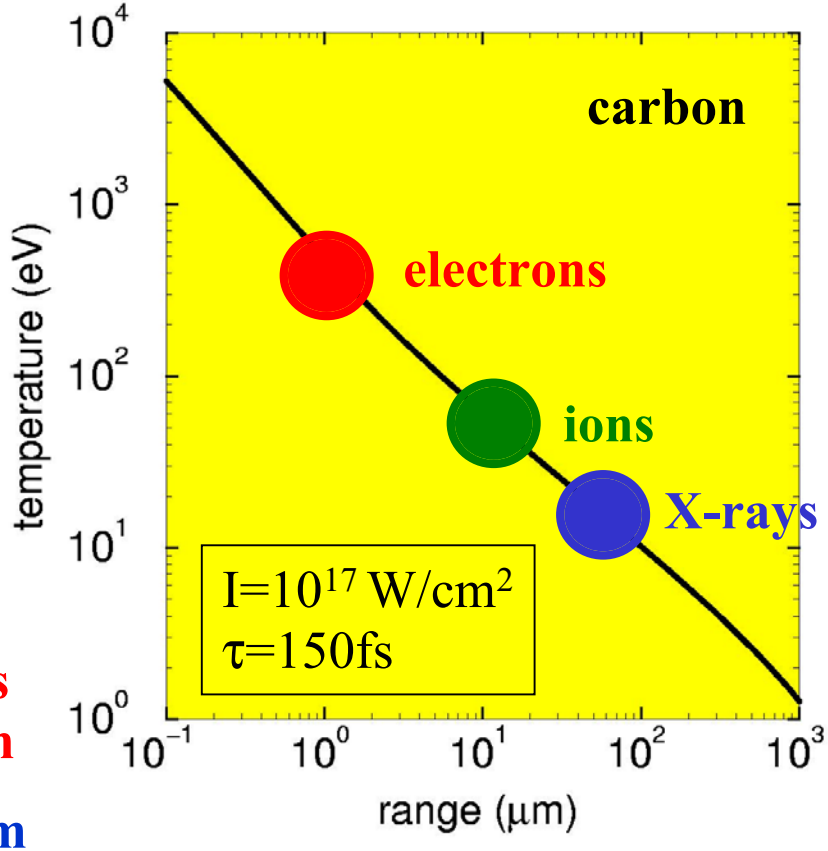

electrons generated by intense laser pulses (MPQ experiment, kT_{hot}=20keV): d=1 μm

X-rays (FEL, hν=3keV): d=50 μm

ions (1MeV protons in carbon): d=10 μm
(Patel et al., PRL 91, 125004-1 (2003))

experimental setup

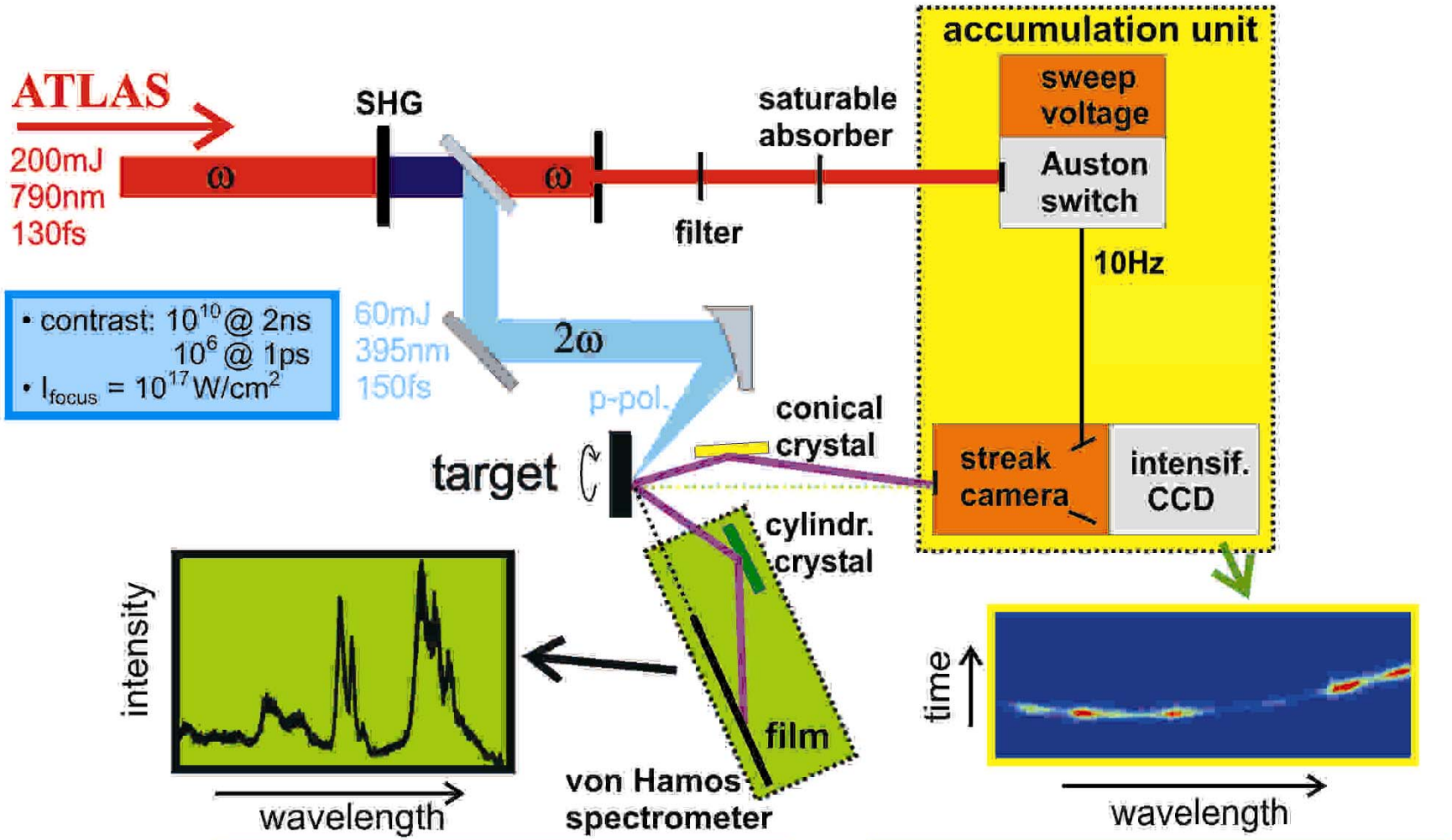

spectra at low and high density differ strongly (massive Al target)

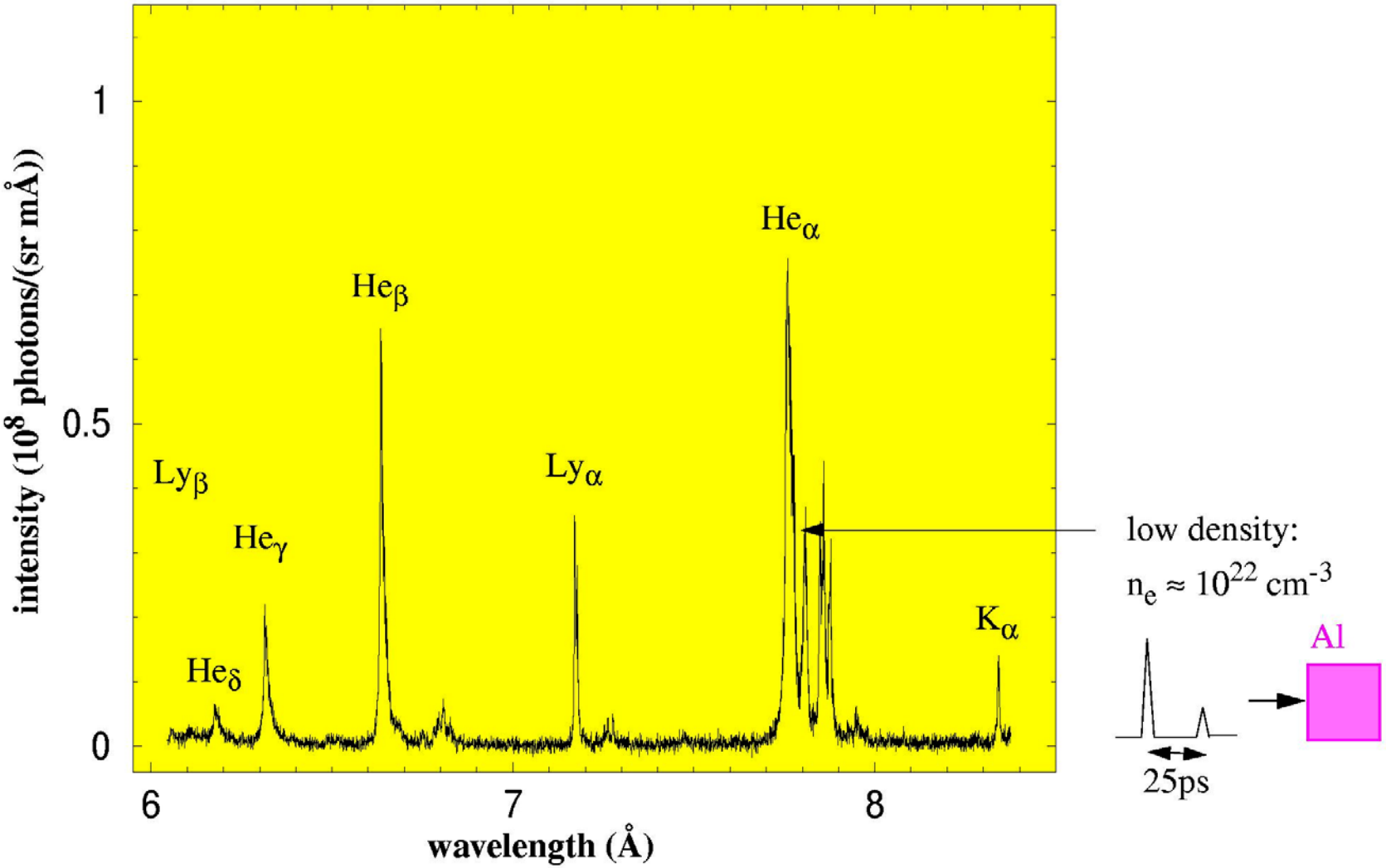

Saemann et al., PRL, 82, 4843 (1999), K. Eidmann, AIP Proceedings, vol.547, 238 (2000)

spectra at low and high density differ strongly (massive Al target)

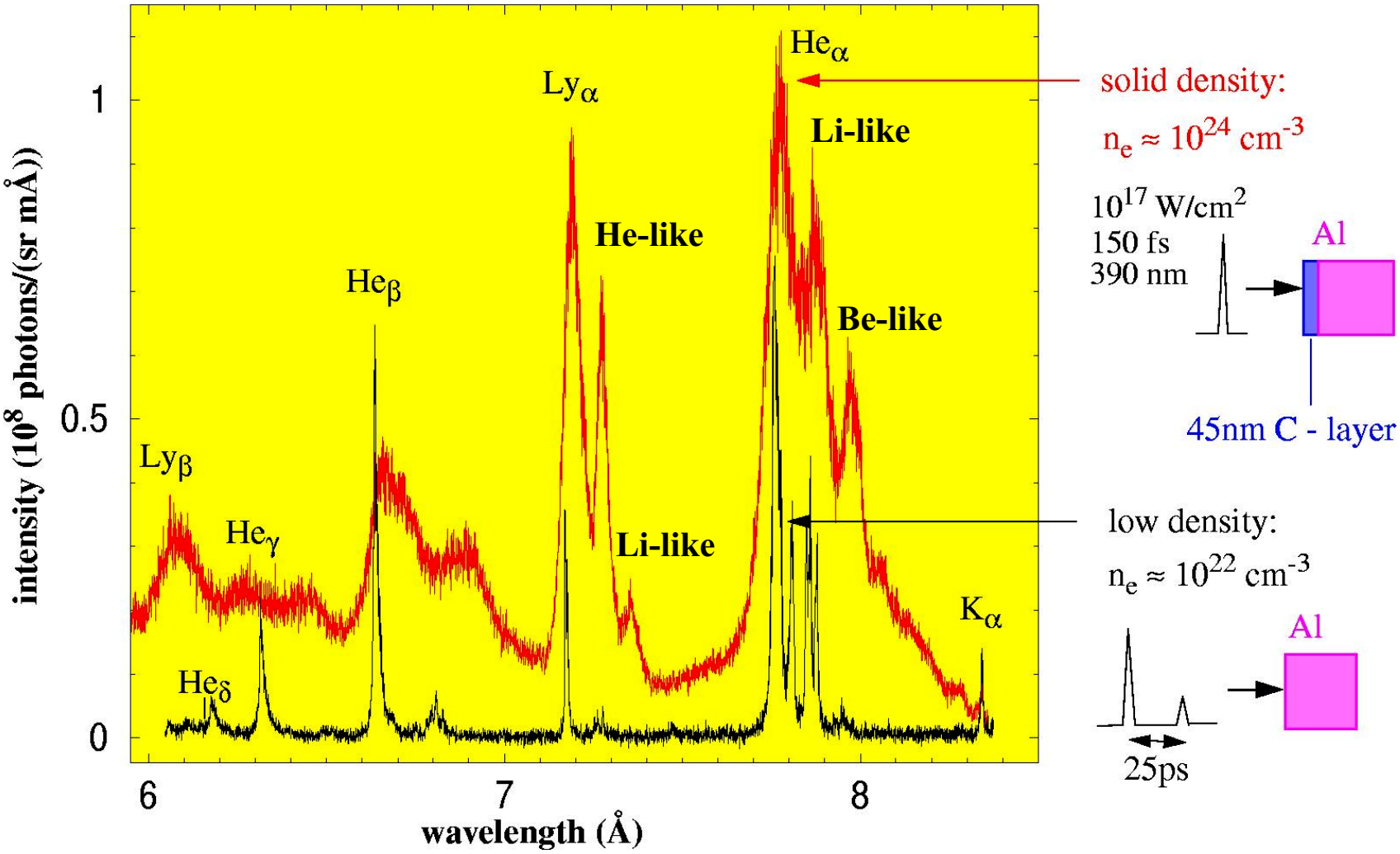

Saemann et al., PRL, 82, 4843 (1999), K. Eidmann, AIP Proceedings, vol.547, 238 (2000)

spectra from 25 nm Al sample layers buried at different depths in carbon

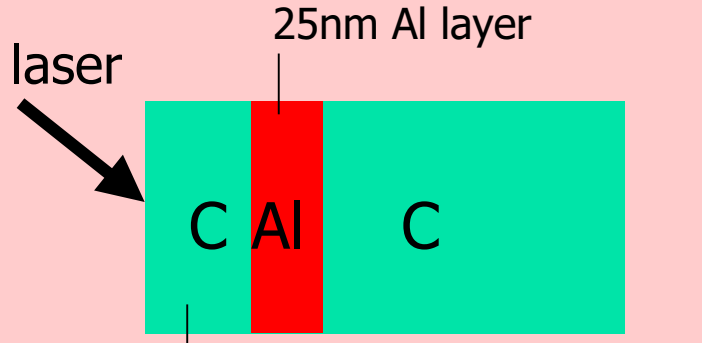

advantages:

- **well defined thickness**
- **negligible axial gradients**

we find:

- **line intensity independent of layer depth**
- **line ratio Ly-β/He-β gives T_e=450eV for all depths**
- **line width and shift grows with depth**
- **carbon recombination continuum (T_e=250eV)**

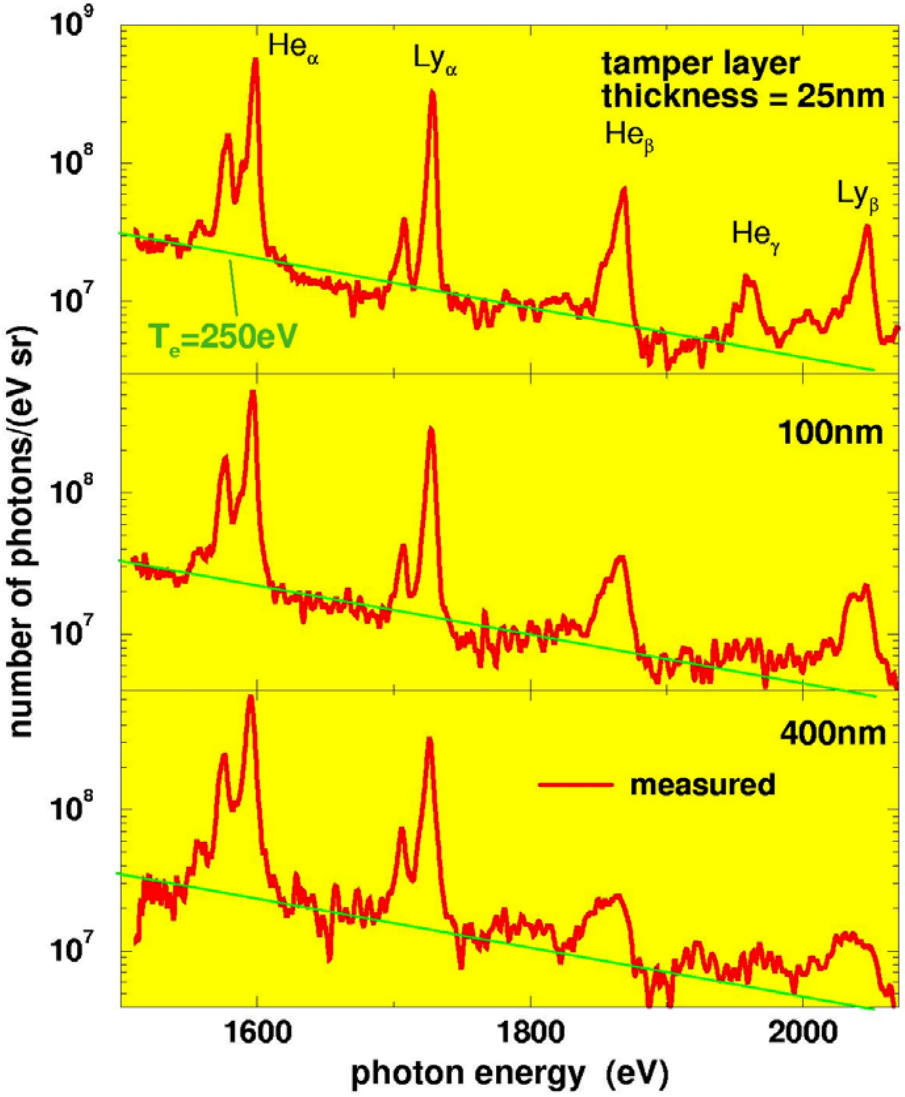

time-depedent modelling by postprocessing

1) time history of temperature and density from a hydrodynamic code (MULTI)

2) populations of all involved levels by solving rate equations (CRAK)
   - > energy levels, radiative ionization and exitation (CATS)
   - > collisional excitation (ACE)
   - > ionization and autoionization (GIPPER)

3) calculation of the spectra
   - > static ion broadening (APEX)
   - > multi-electron broadening (MERL)
   - > high order satellite emission up to B-like Al
   - > dense plasma line shifts (DPLS) for resonance lines and satellites based on the quantum theory of Junkel et al. (PRE 62, 5584 (2000))
   - > opacity effects are included by solving the radiation transport equation

hot plasma at solid density

hydrogen-like Al at $n_e \approx 7 \times 10^{23} cm^{-3}$

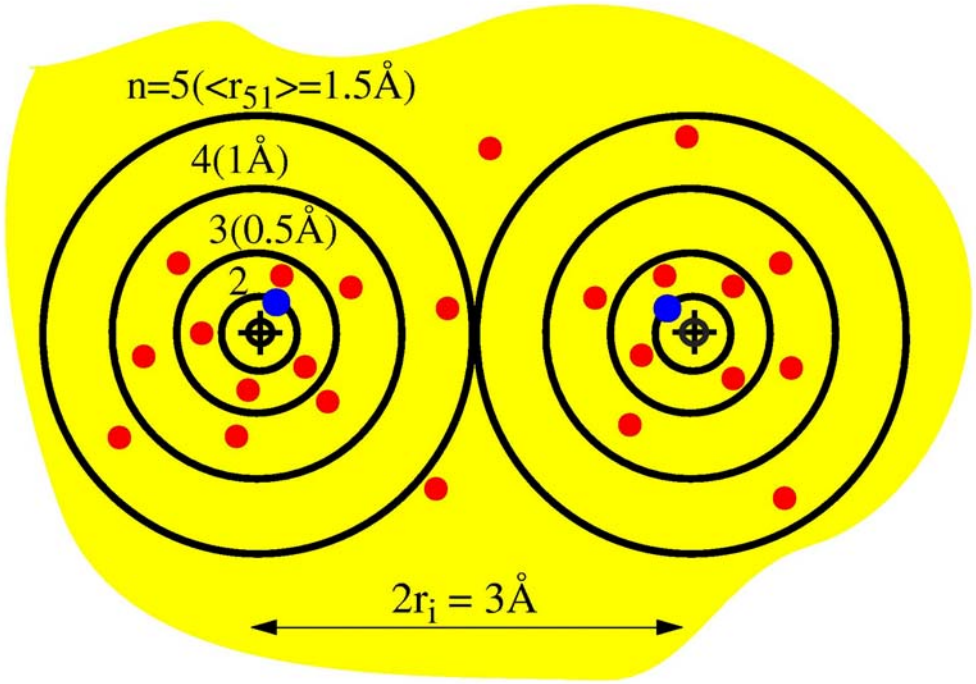

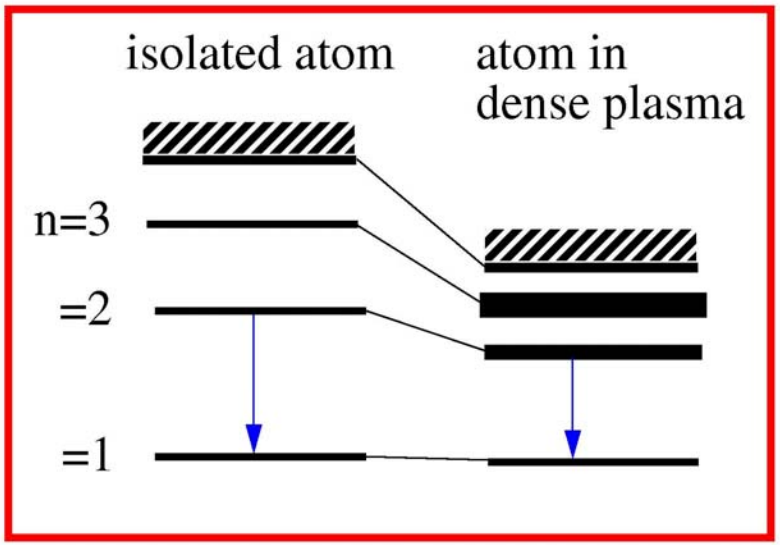

strong line broadening and shift of emitted x-rays

for T_e=500eV:
plasma pressure p≈0.5Gbar,
$E_{coul} \approx 4E_{therm}$ (strongly coupled)

measured spectra from Al sample layers agree well with calculation

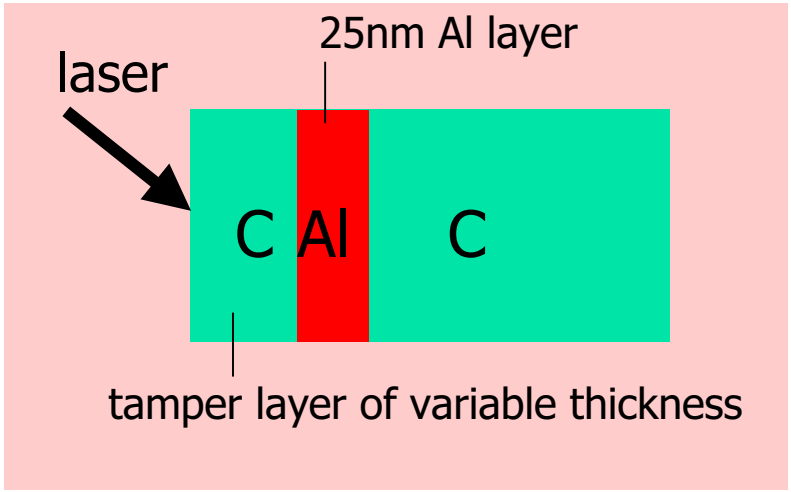

good agreement for

- **line ratios**
- **line shapes**
- **line shifts**

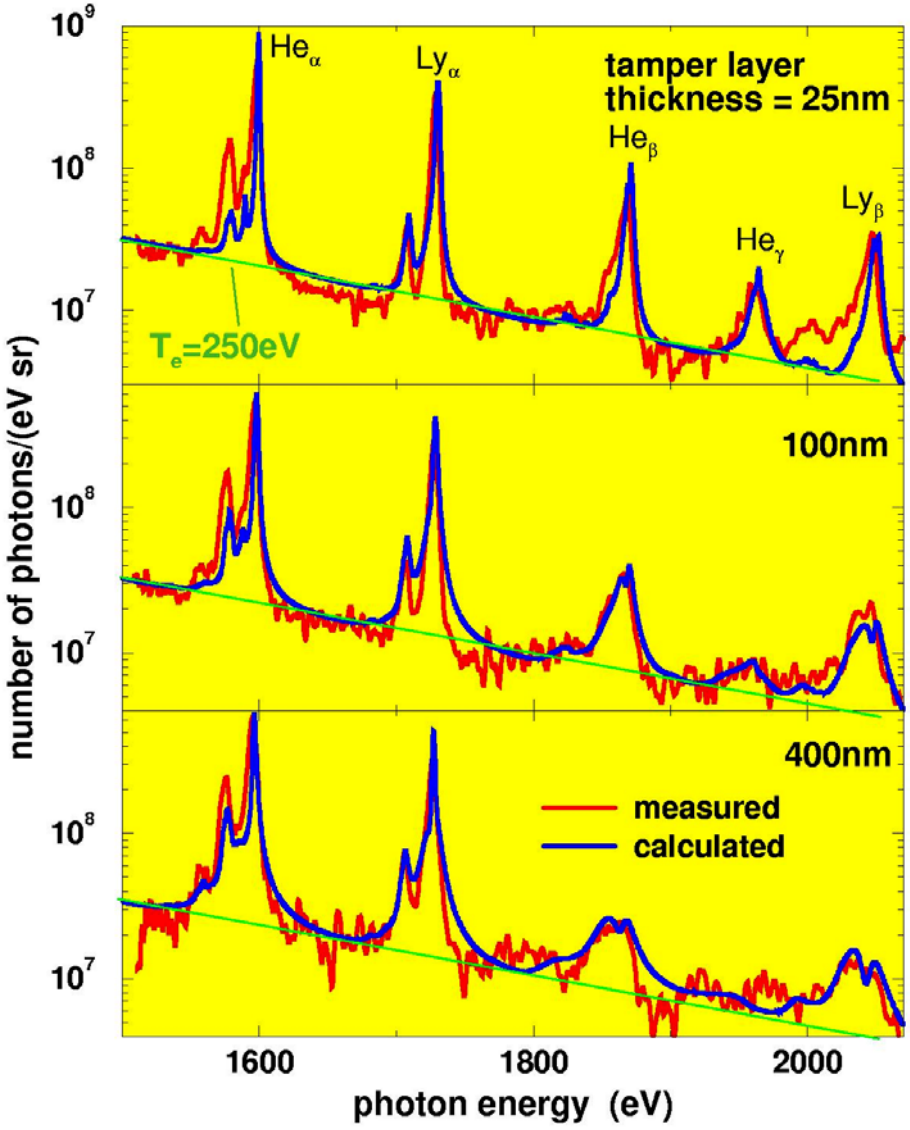

line emission from Al tracer layers buried in carbon shows an increasing redshift with depth

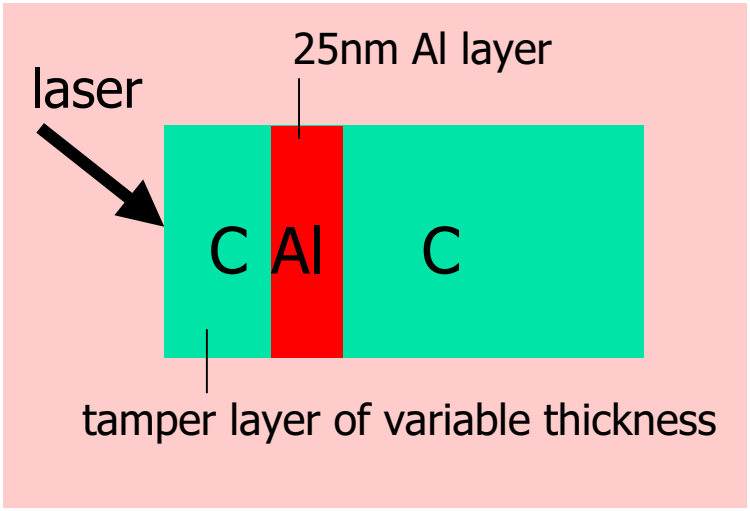

wavelength calibration with an accuracy of ±0.3eV was achieved by superimposing the Si K-α line on the Al spectrum

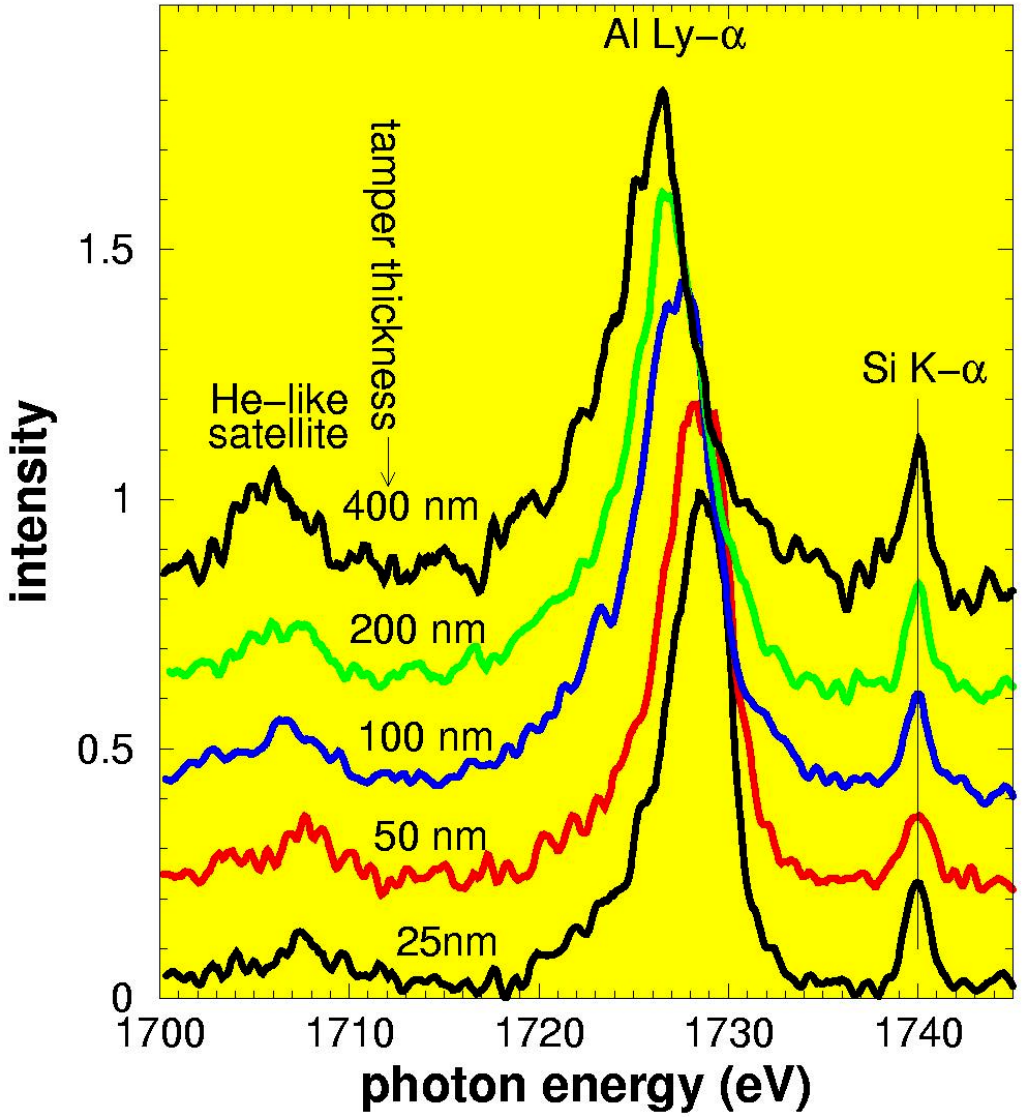

measured and calculated line shifts

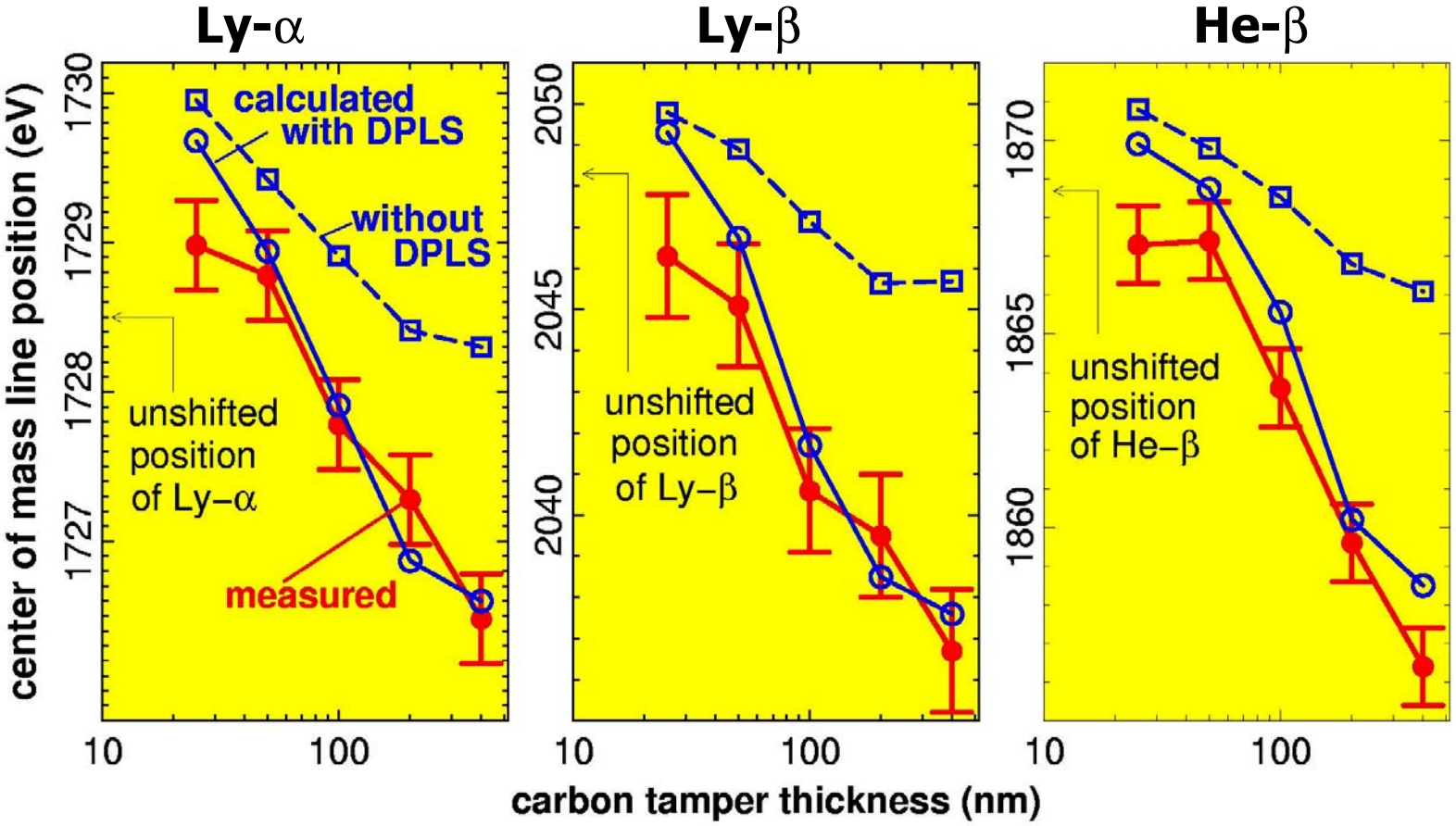

- **merging with satellites is not sufficient to explain the measured shift**
- **consideration of the dense plasma line shift (DPLS) reproduces the measured shift**

U. Andiel et al., EPL, 60 861(2002), Eidmann et al., JQSRT, 81 133 (2003)

measured and calculated line durations are typically a few picoseconds

time-resolved emission of the Ly-α and He-α lines:

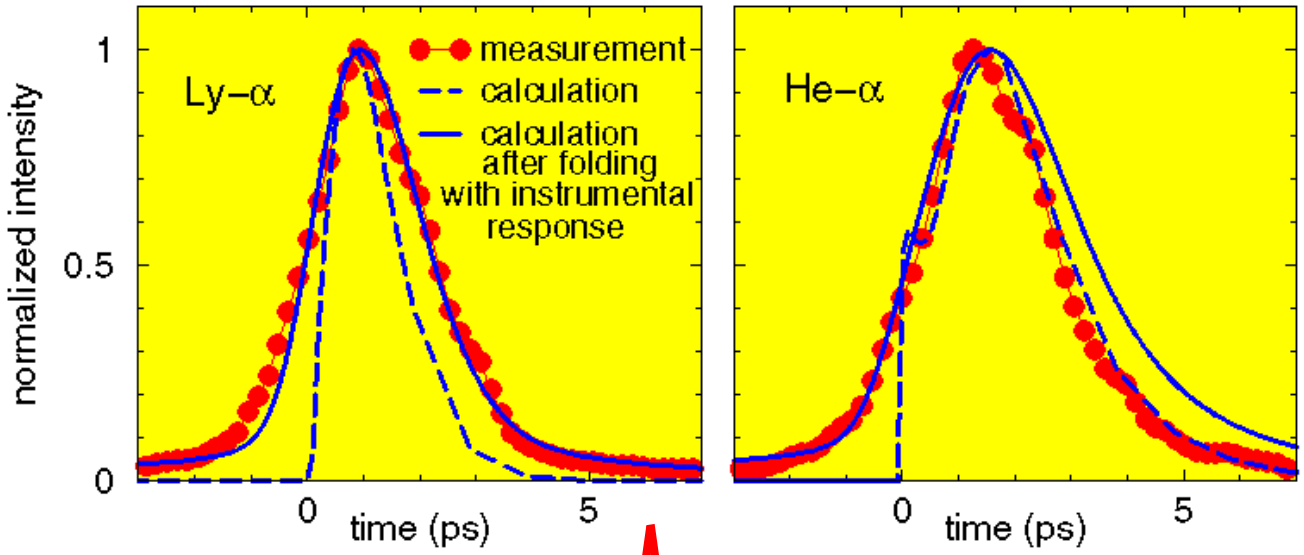

150 fs laser-pulse

time-history of density and temperature:

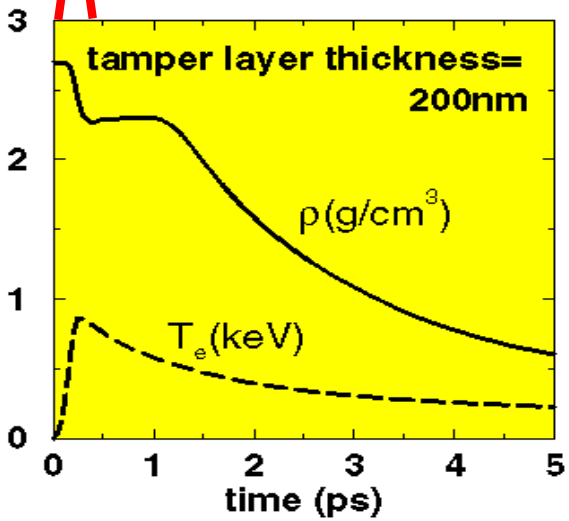

up to a tamper-layer depth of 400 nm temperature is independent of depth

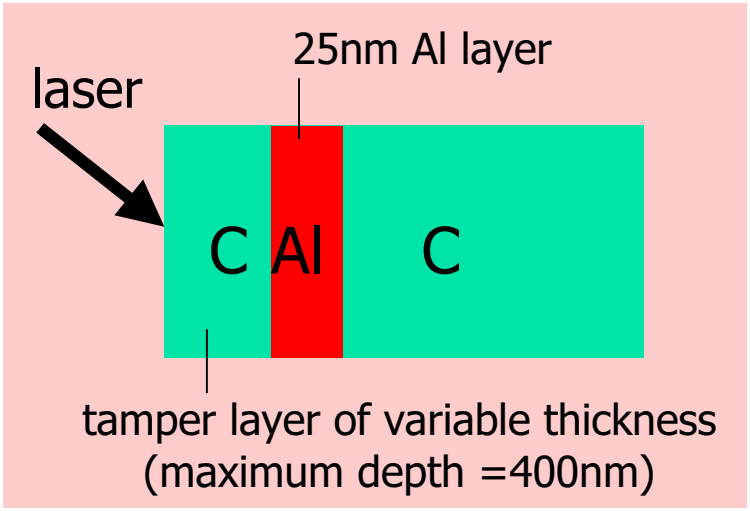

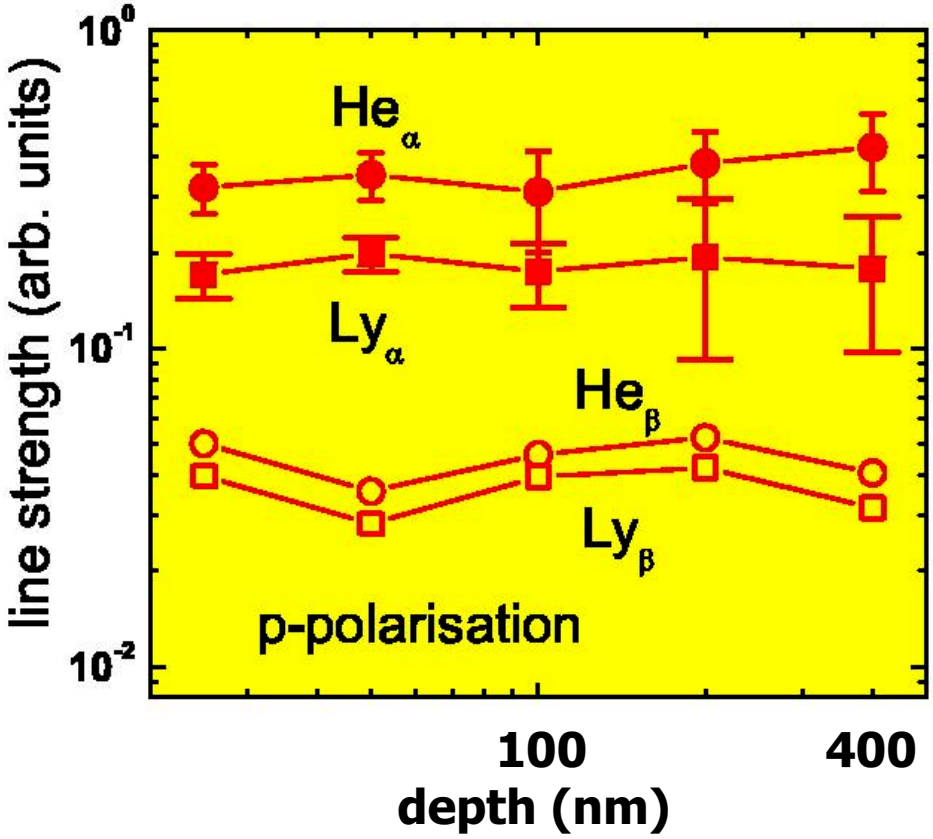

→ **Ratio of Ly-ß/He-ß gives kT ≈ 500eV for all depths ≤ 400nm**

thickness of the heated depth was measuered with a diamond tamper layer

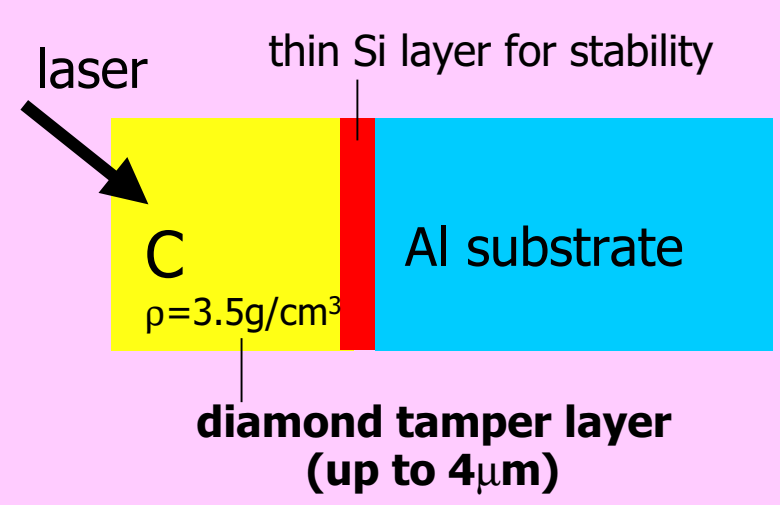

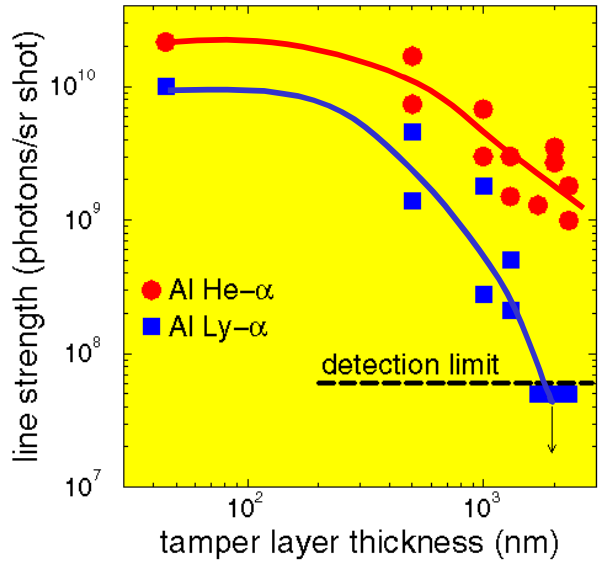

- the Al is heated through a diamond depth of ≈1.5μm up to ≈300eV
- for the measured $T_{e,hot}$=20 keV the range in diamond is 2.7μm

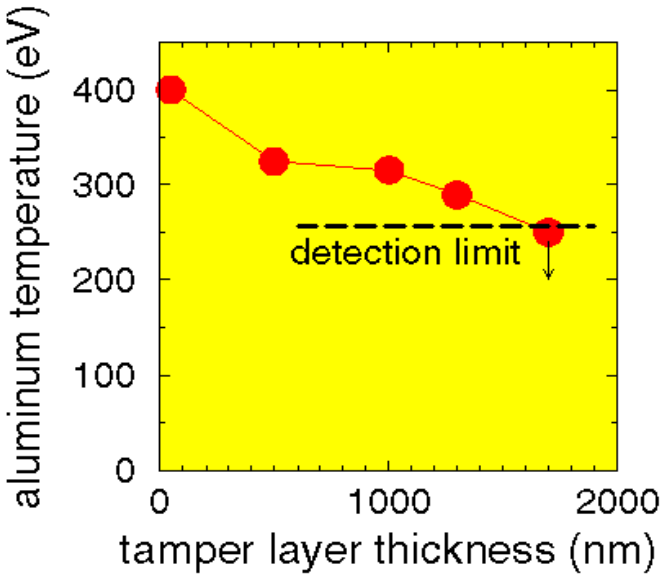

scaling of isochoric heating

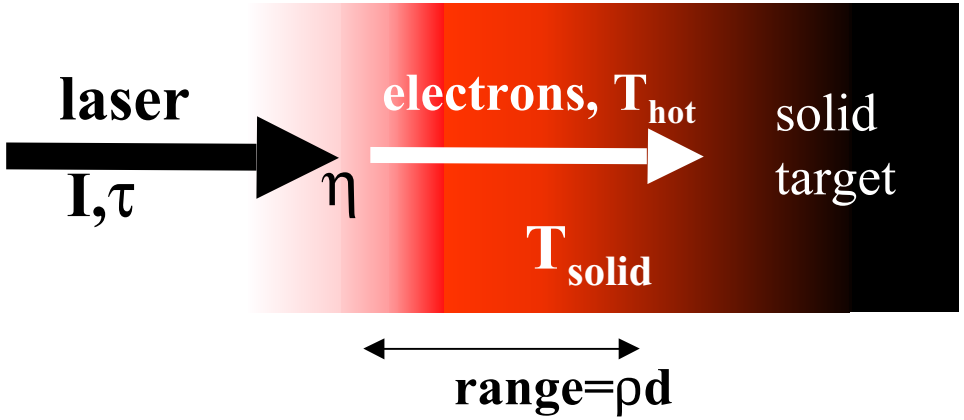

range = $\rho d \approx \rho\lambda_e \propto T_{hot}^2$

assume $T_{hot} \propto (I\cdot\lambda^2)^{1/2}$ $\Rightarrow$ **range = $\rho d \propto I\lambda^2$**

internal energy = $\eta\cdot I\cdot\tau/\rho d$

$\eta(I,\tau,$preplasma ...$)$ = coupling efficiency

$T_{solid} \propto$ internal energy $\propto \eta\cdot\tau/\lambda^2$ (independent of I !)

($T_{hot} \propto (I\cdot\lambda^2)^{1/3} \Rightarrow T_{solid} \propto (I\cdot\lambda^2)^{1/3}\cdot\eta\cdot\tau/\lambda^2$)

lateral instability effects?

Electric current into the target:

$$j_{electric} = e \cdot n_{cr} \cdot v_{hot} = 6.7 \cdot 10^{12}\ A/cm^2$$

$$(v_{hot} \approx 10^{10}\ cm/s \ \ (for\ T = 20\ keV))$$

$$I_{electric} = r^2 \cdot \pi \cdot j_{electric} = 1.3 \cdot 10^7\ A$$

$$I_{Alven} = 17 \cdot kA \cdot \beta \cdot \gamma\,,\ \beta = 0.3,\ \gamma = 1 \qquad I_{Alven} = 5.1\ kA$$

→ $I_{electric} = 2500\ I_{Alven}$!

Anomalous diffusion of hot electrons in solids

Collisional 3D VLPL simulation

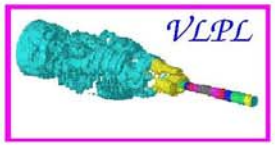

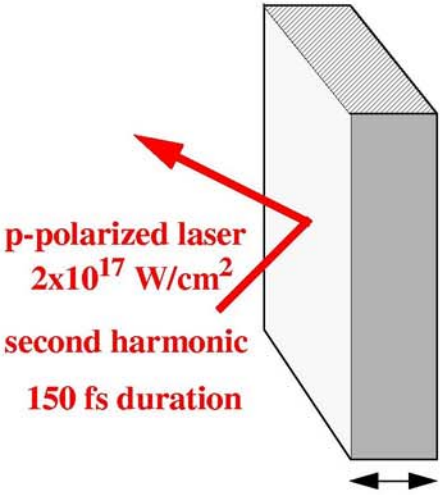

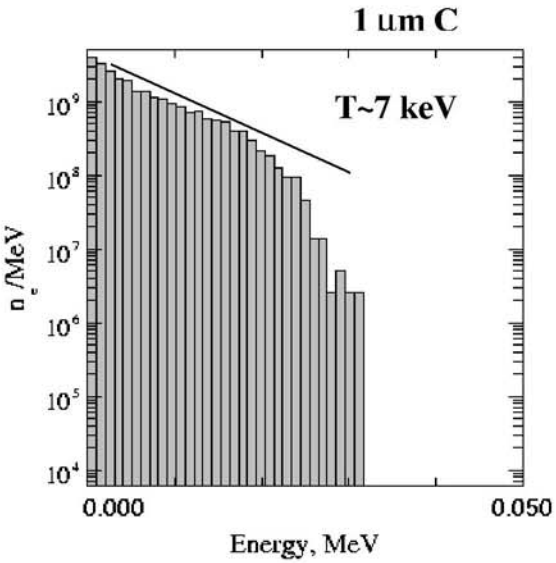

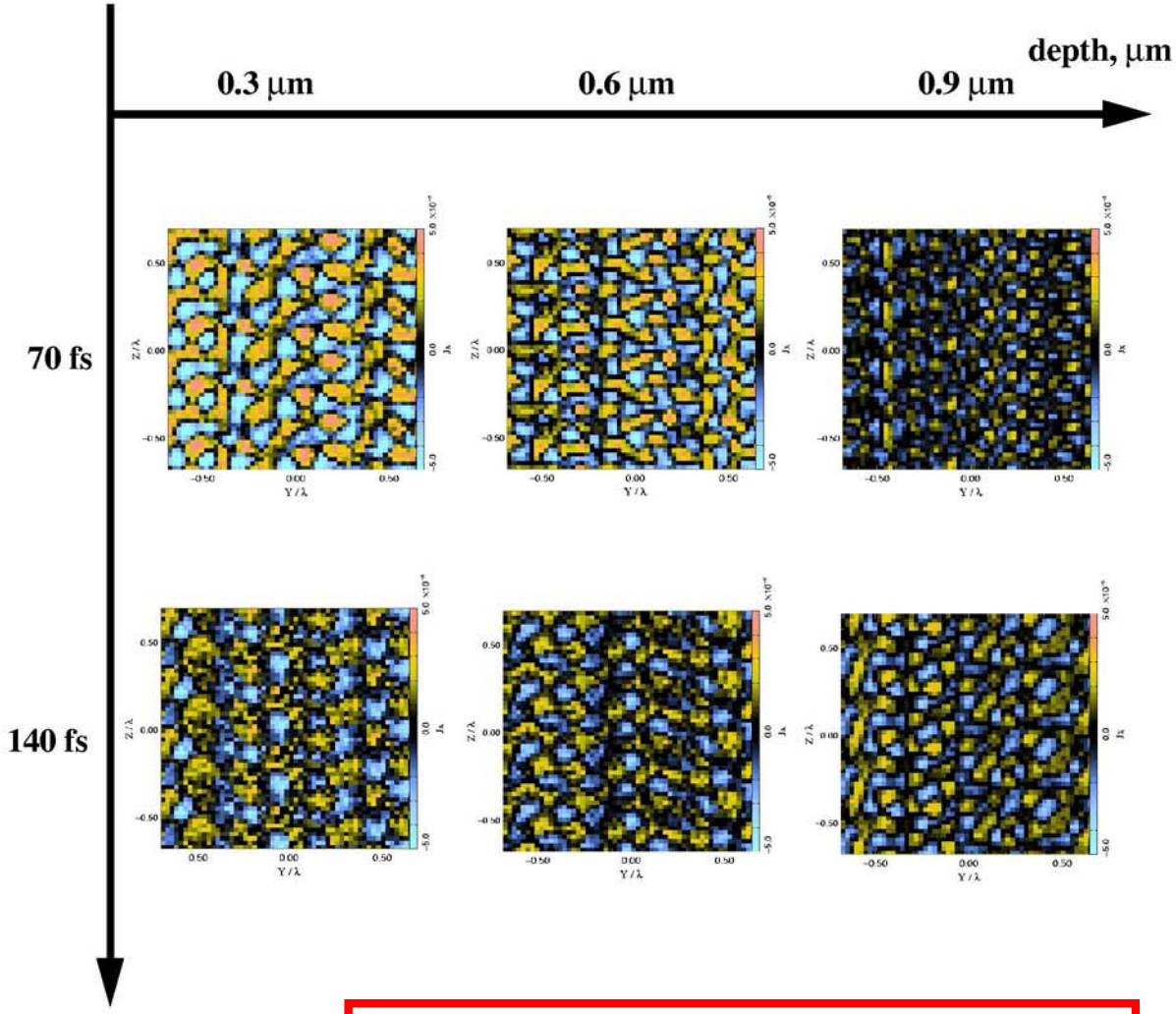

lateral modulation of j_x with a wavelength of about 50-100nm

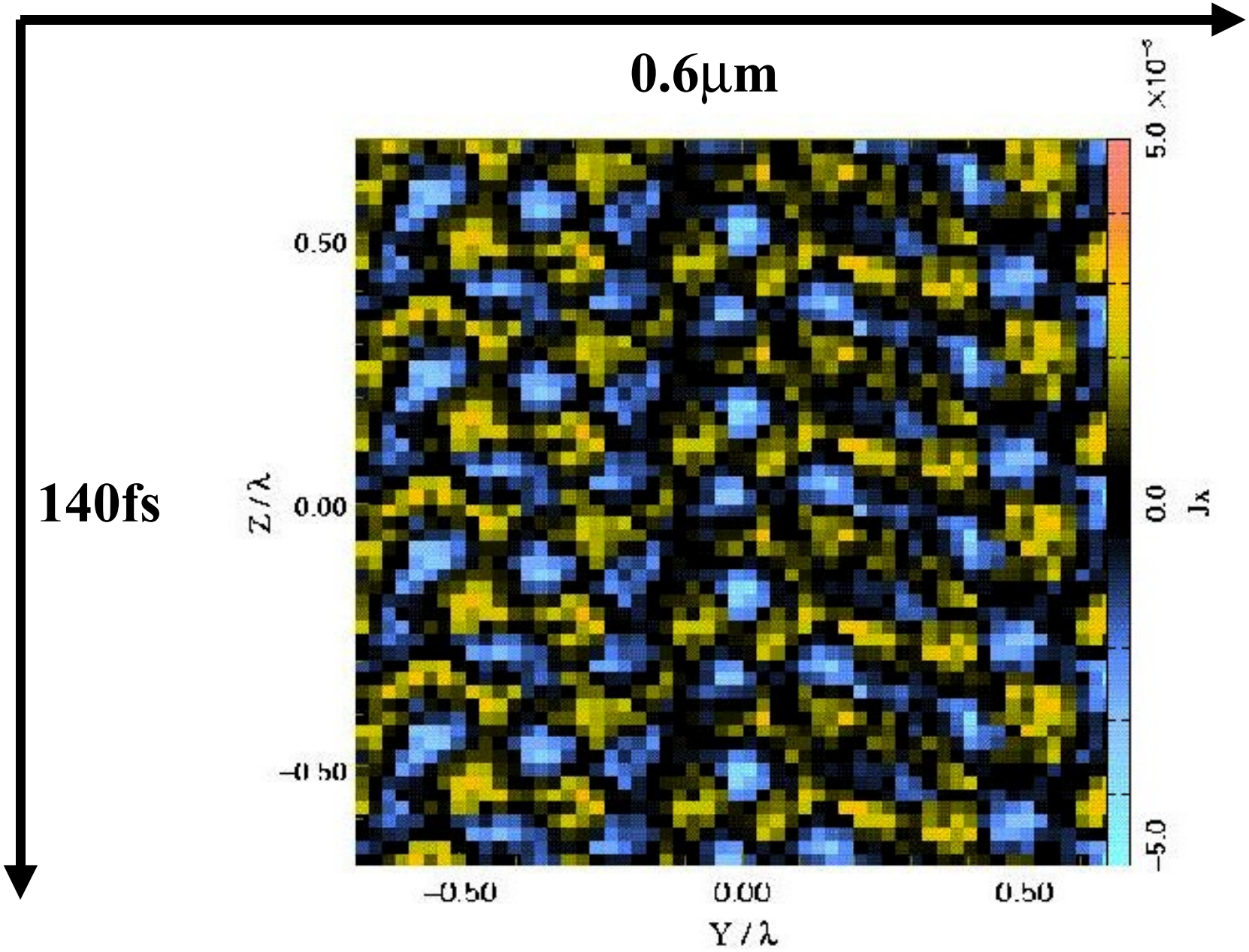
0.6μm
140fs
5.0 ×10⁻⁵
0.0
Jx
−5.0
0.50
0.00
−0.50
Z / λ
−0.50
0.00
0.50
Y / λ

summary

- isochoric heating (up to T=500eV) of solid Al with electrons generated by ultrashort laser pulses has been demonstrated
- Al-K-shell spectroscopy at near solid density

  (dense plasma lineshift was measured by using the sample layer technique)
- the target is heated up to a depth of about 1.5µm

  (demonstrated with diamond covered Al substrates)
- the electron transport is important

  fully collision dominated?

  lateral instabilities?

  fast ignitor relevance (the hot electrons interact with plasma!)

International Conference on
ULTRASHORT HIGH-ENERGY RADIATION AND MATTER
Villa Monastero, Varenna, Italy October 7 -10, 2003

Hot electron influence on the radiation properties of matter under interaction by short laser pulses

A.Ya. Faenov

Multicharged Ions Spectra Data Center

of National Institute for Physical-Technical and Radio-Technical Measurements,

Moscow, 141570, Russia

Collaborators

J. Abdallah, Jr., G. Csanak
Theoretical Division, T_4, Los Alamos National Laboratory, P.O. Box 1663, Los Alamos, NM 87545, USA
K. B. Fournier
Lawrence Livermore National Laboratory, P.O. Box 808, L_41, Livermore, CA 94550, USA
F.B.Rosmej
GSI-Darmstadt, Plasmaphysik,Planckstrasse 1, D-64291 Darmstadt, Germany
S. B. Hansen, A. S. Shlyaptseva
Physics Department, University of Nevada, Reno, NV 89557,USA
M. Francucci, S. Martellucci, G. Petrocelli
INFM _ Dipartimento di Scienze e Tecnologie Fisiche ed Energetiche, Universit‘a di Roma Tor Vergata, Via di Tor Vergata, 00133 Roma, Italy
F. Flora, S. Bollanti, P. Di Lazzaro, D. Murra
ENEA, Dipartimento Innovazione, Settore Fisica Applicata, 00044 Frascati, Roma, Italy
A.Reale, L. Reale, G Tomassetti, A. Ritucci
Dipartimento di Fisica e INFM, INFN g.c. LNGS, Universit‘a dell'Aquila, 67010 L'Aquila, Italy
T. Auguste, S. Dobosz, S. Hulin, P. Monot, P. D'Oliveira
Commissariat ‘a l'Energie Atomique, Centre d'Etudes de Saclay, DRECAM, Service de Photons Atomes et Mol’ecules, Bat. 522, 91191 Gif_Sur_Yvette, France
Y. Fukuda, Y. Akahane, M. Aoyama, N. Inoue, H. Ueda, K. Yamakawa
Advanced Photon Research Center, Japan Atomic Energy Research Institute, 8-1 Umemidai, Kizu-cho, Souraku-gun, Kyoto 619-0215, Japan
V.S. Belyaev, V.I Vinogradov, A.S. Kurilov, A.I, A.P. Matafonov
Central Research Institute of Machine Building, Korolev, Moscow region, 141070, Russia
I.Yu. Skobelev, A.I. Magunov, T. A. Pikuz
Multicharged Ions Spectra Data Center of VNIIFTRI, Moscow, 141570, Russia

Topics

I. Hot electron influence to formation of X-ray spectra (general features)

II. Spectra of solid targets irradiated by ns and fs laser pulses.

1) K-Spectra

2) L-spectra

III. Spectra of cluster targets irradiated by ns and fs laser pulses.

1) K-Spectra

2) L-Spectra

IV. Conclusions

Excitation of resonance and dielectronic lines in plasma

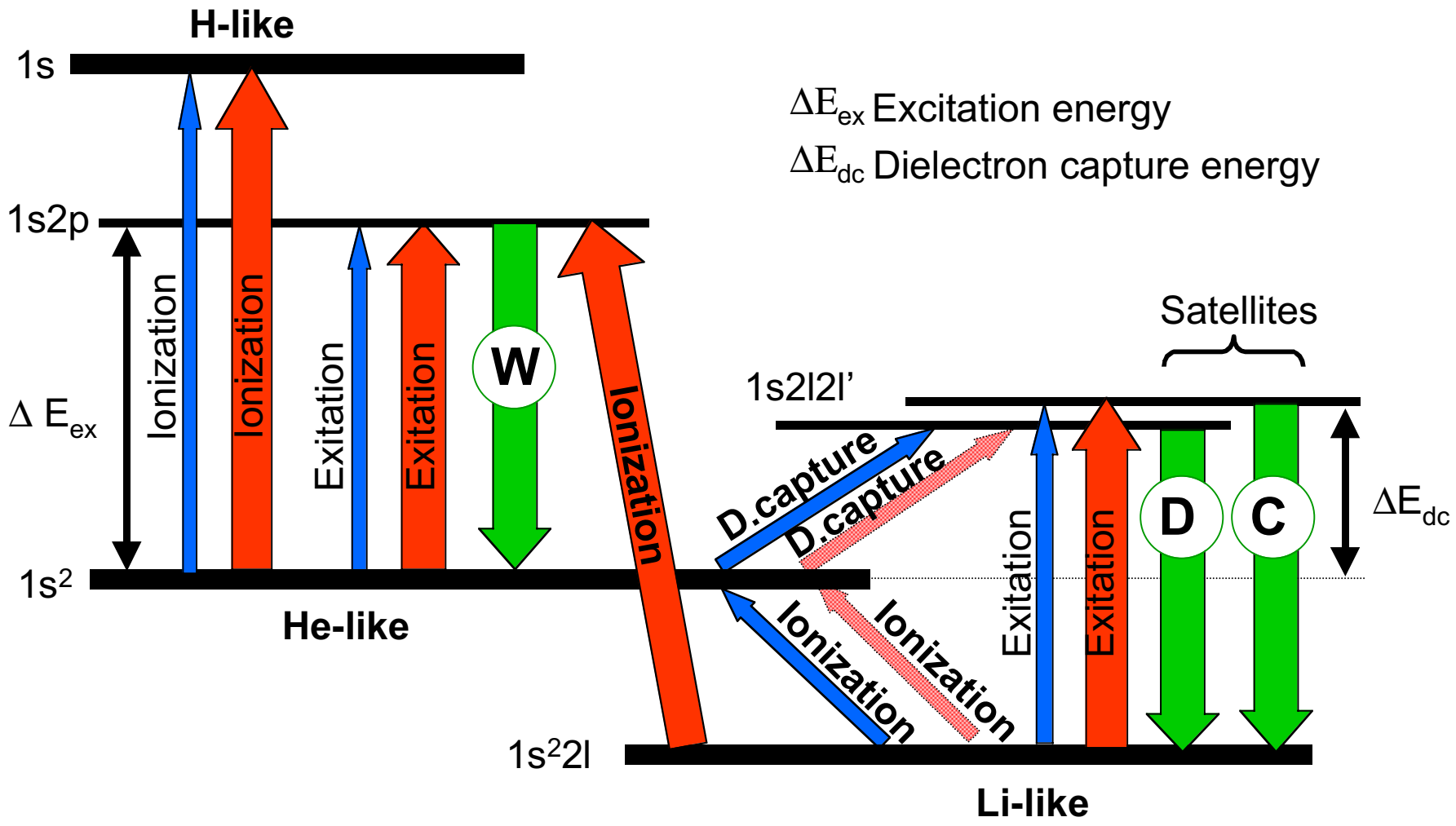

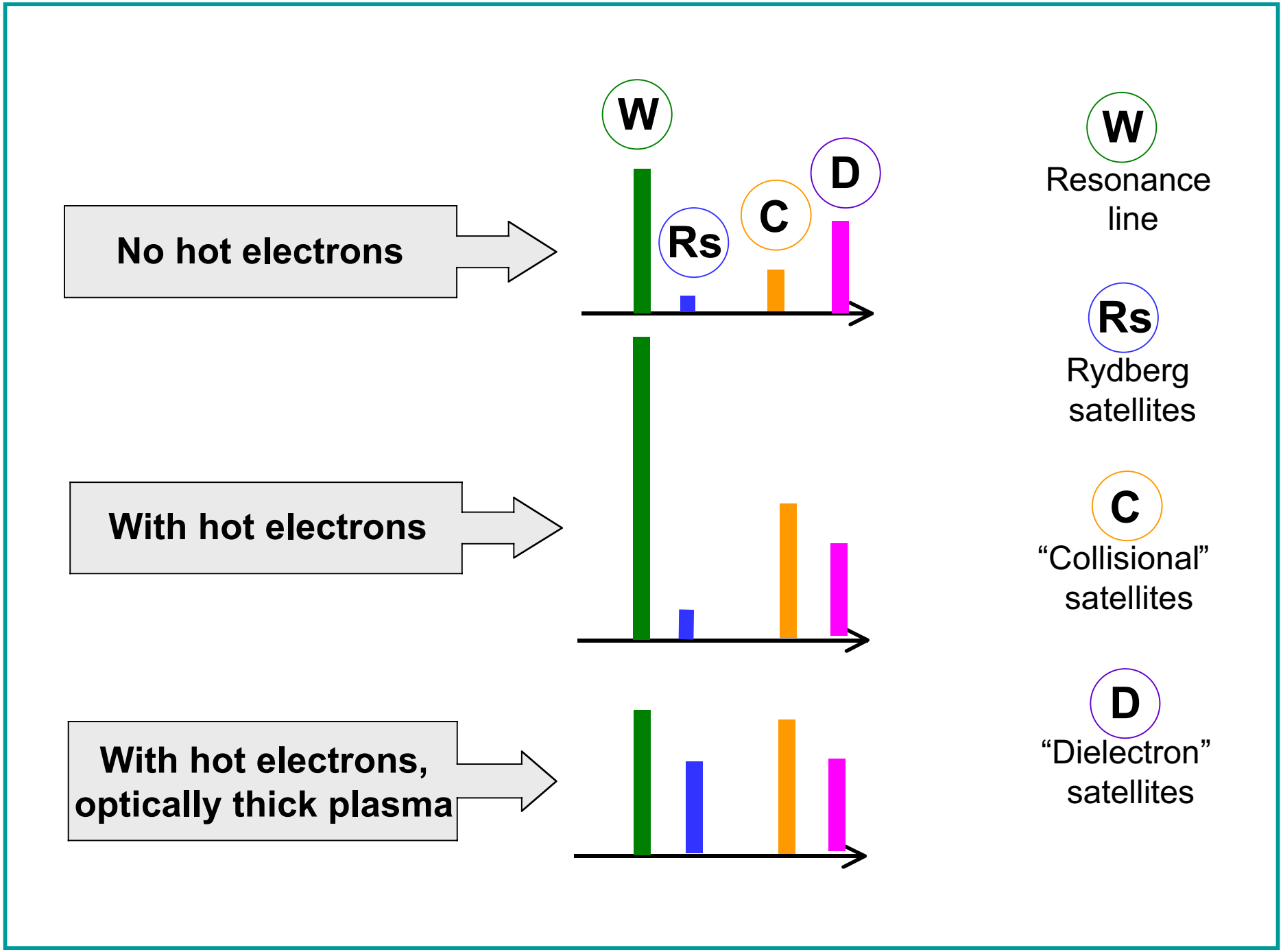
No hot electrons
With hot electrons
With hot electrons, optically thick plasma
W
Rs
C
D
W
Resonance line
Rs
Rydberg satellites
C
“Collisional” satellites
D
“Dielectron” satellites

Hot electron influence to Mg satellite spectrum: simulations

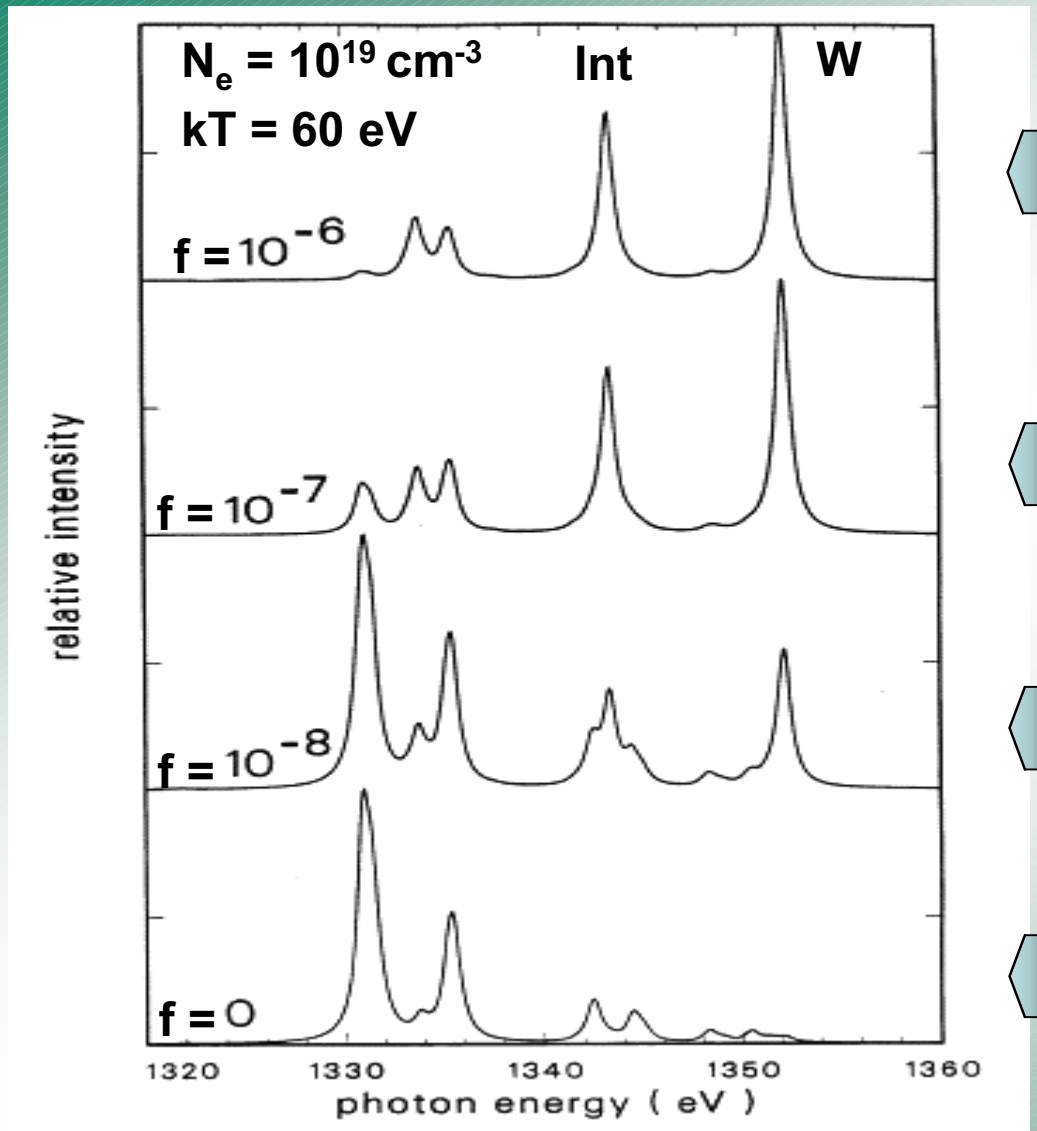

- ***j k l*** is barely noticeable
- The high density signature of ***j k l, a – d, q r*** is attained
- Significant effect by exitating both the ***Int and W*** lines
- ***j k l*** satellite lines of Li-like Mg is dominant

J.Abdallah Jr. *et al,* JQSRT, **62**, (1999) 1-11

Mg spectrum: Influence of electron density N_e or hot electron fraction could be recognized (simulations)

kT = 200 eV **$N_e = 5 \cdot 10^{21}$ kT = 200 eV**

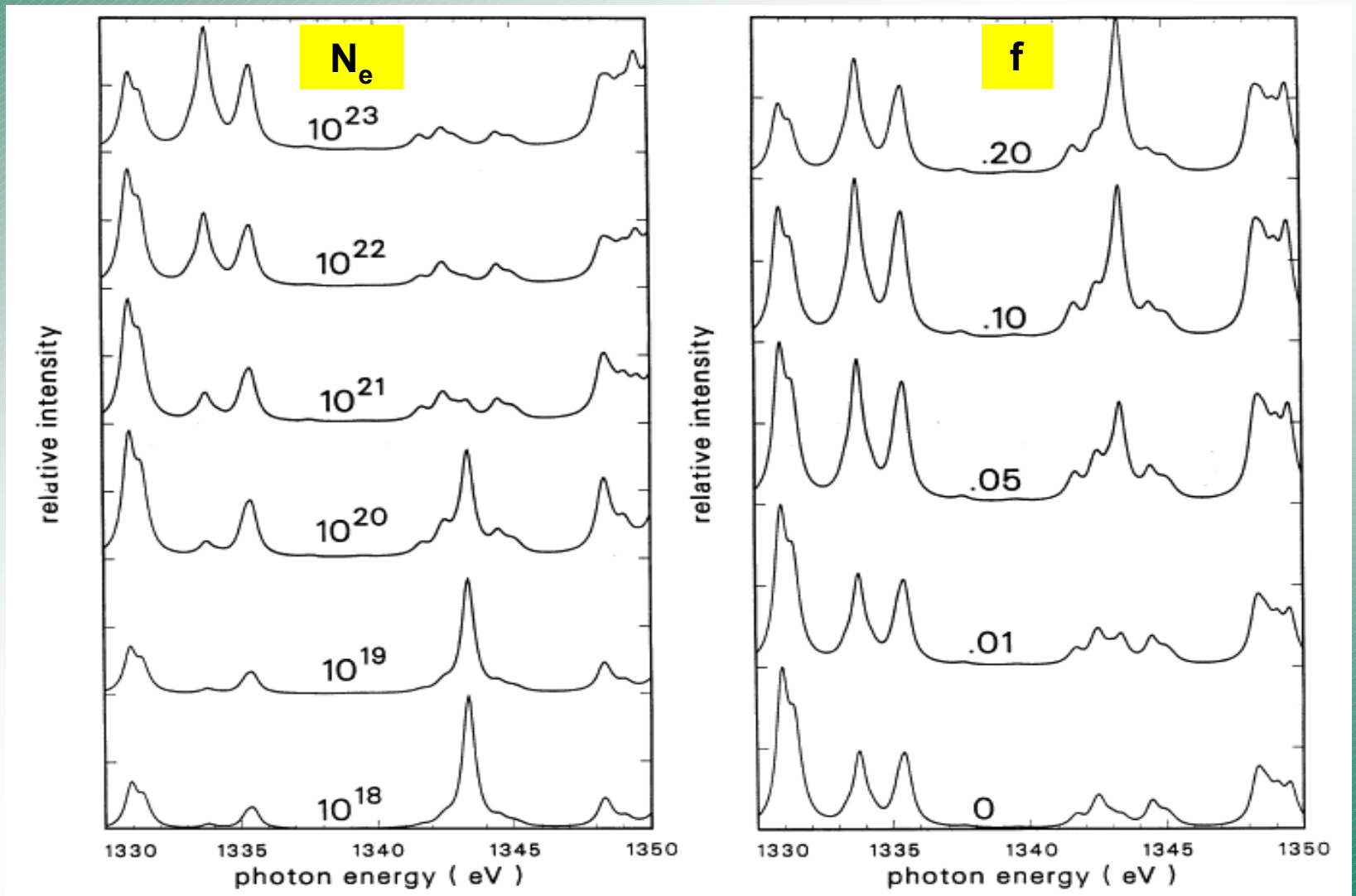

J.Abdallah Jr. *et al,* JQSRT, **62**, (1999) 1-11

Trident Nd:YAG laser

Mg target

τ = 1 ns

P = 10^{16} W/cm^2

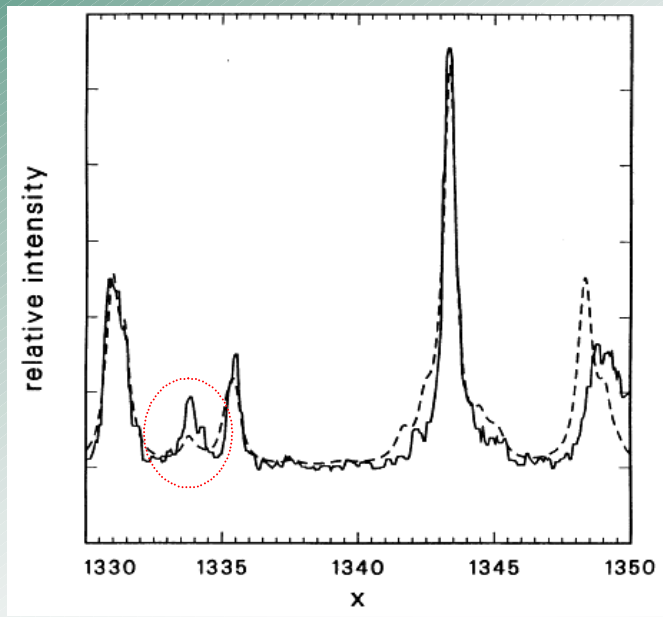

$N_e = 1.5 \cdot 10^{20}$

kT = 400 eV

f= 0.00

τ = 600 fs

P = 10^{19} W/cm^2

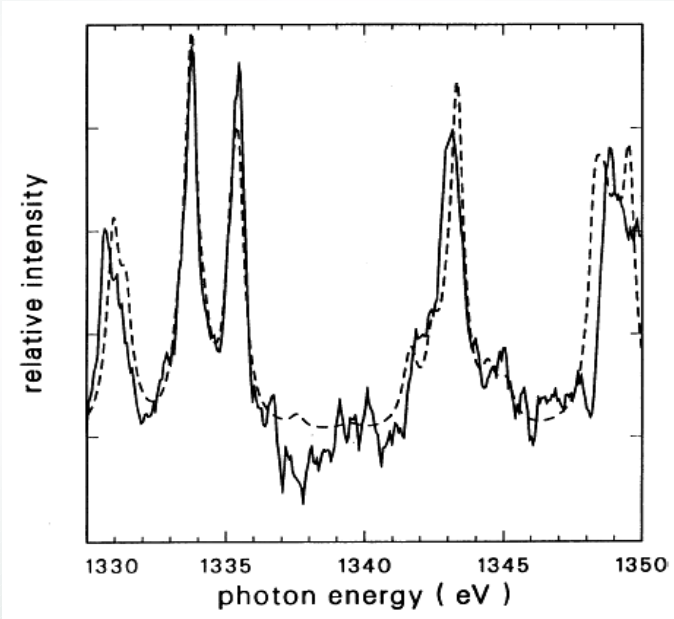

$N_e = 5 \cdot 10^{21}$

kT = 180 eV

f = 0.1

——— Experiment

..... Simulation

J.Abdallah Jr. *et al,* JQSRT, **62**, (1999) 1-11

He- like Ar: experimental spectra

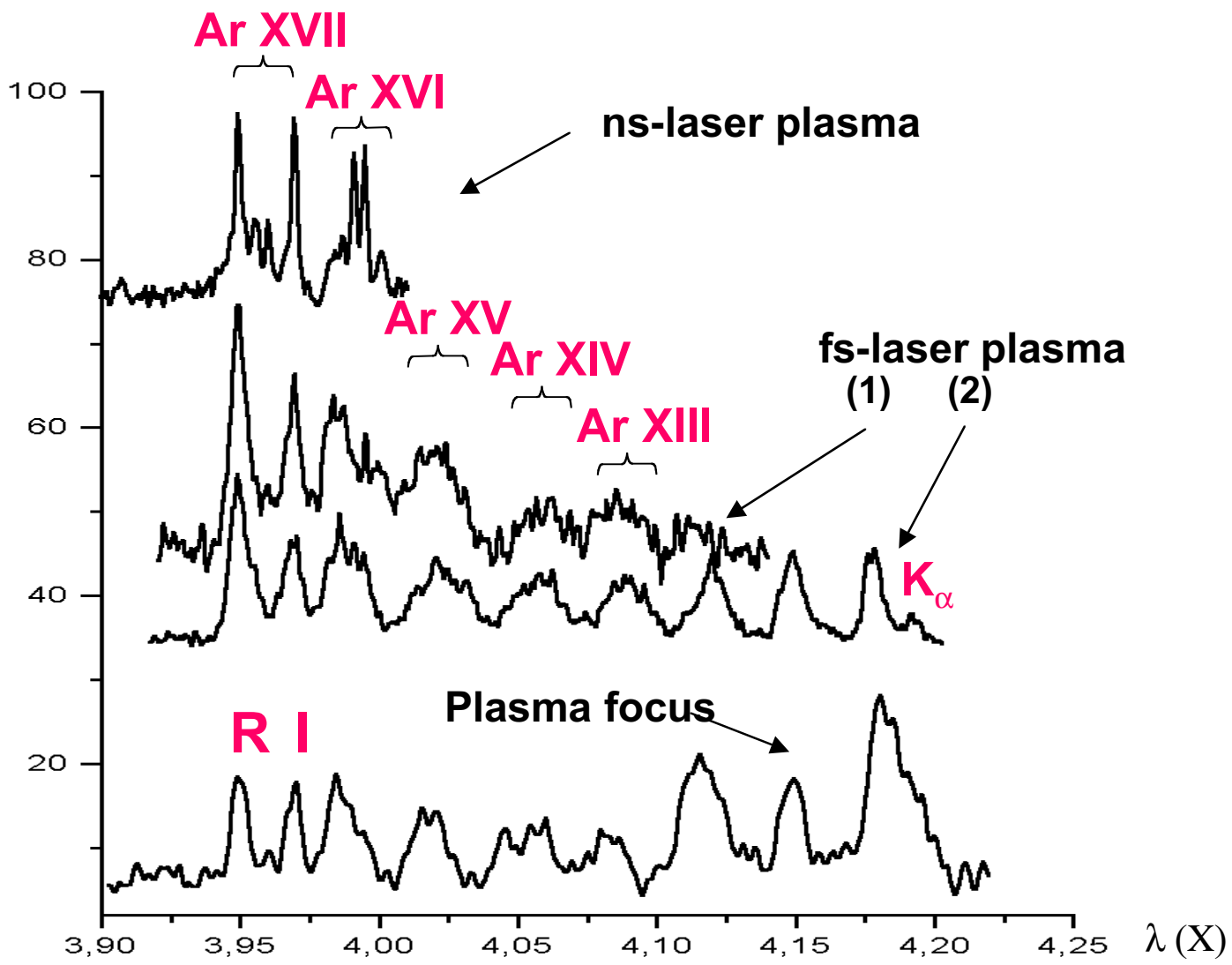

Spectra near He_α and He_β of Ar: hot electron and electron density influence

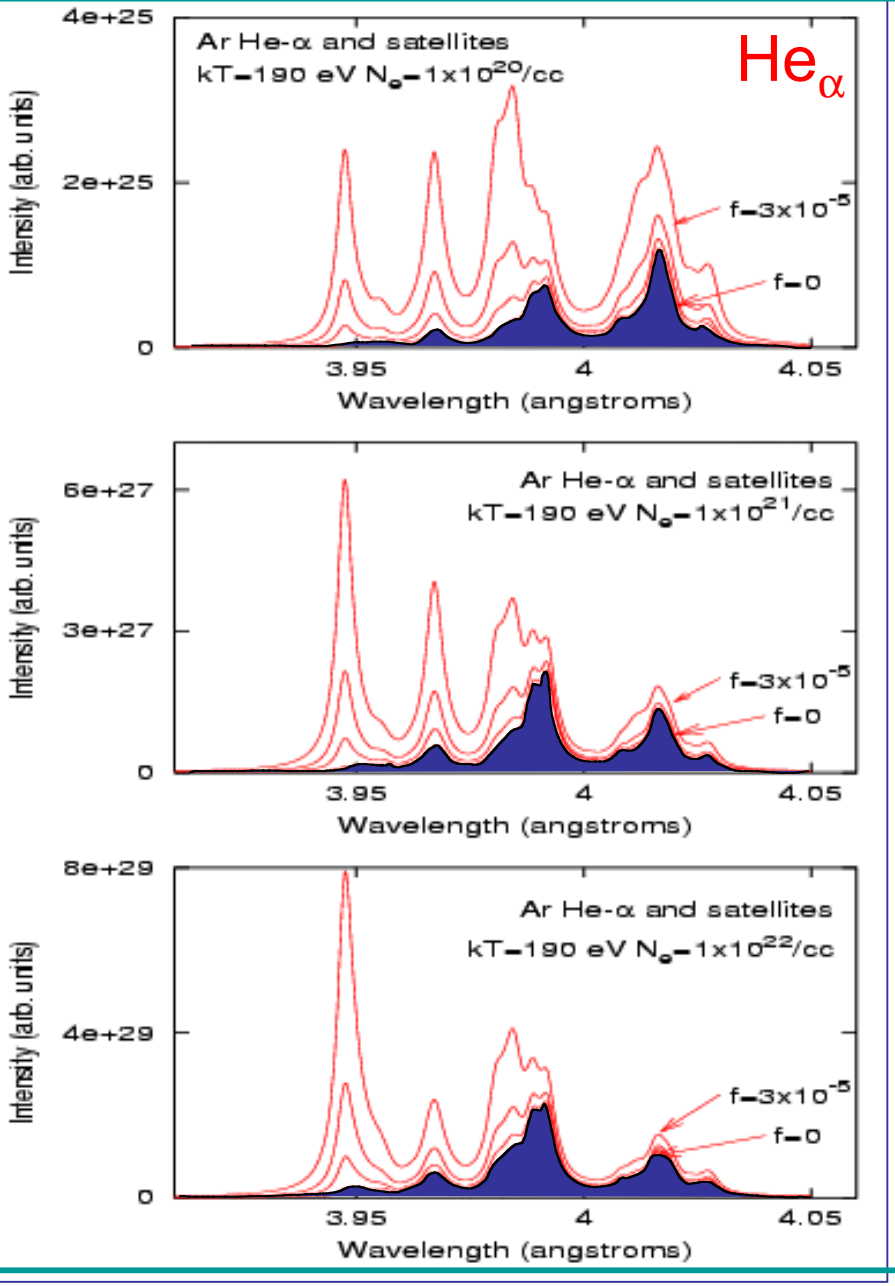

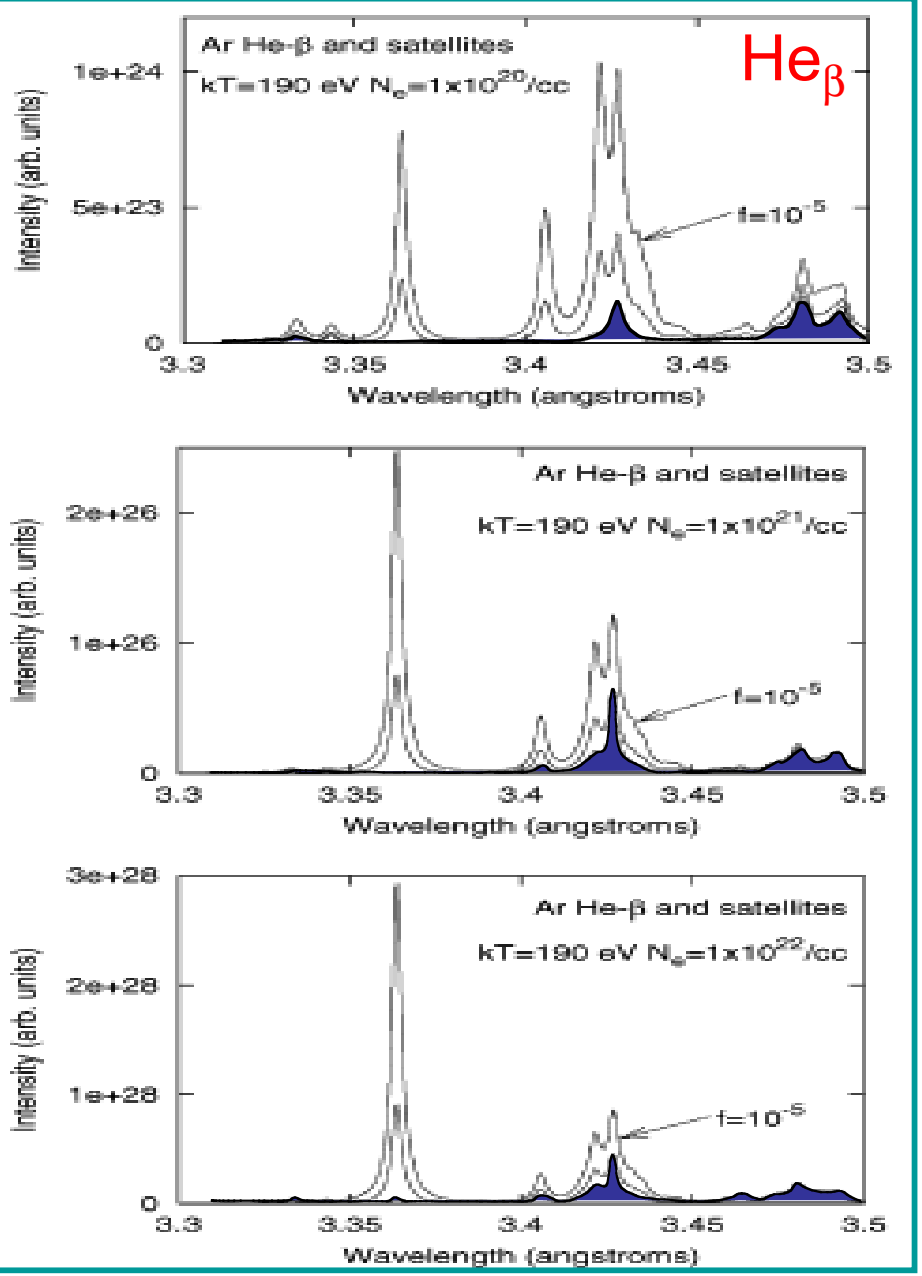

G. C. Junkel-Vives *et al,* JQSRT,**71**, (2001) 417-430

Spectra near Ly_α of Ar: hot electron and bulk electron temperature influence (N_e just above critical density)

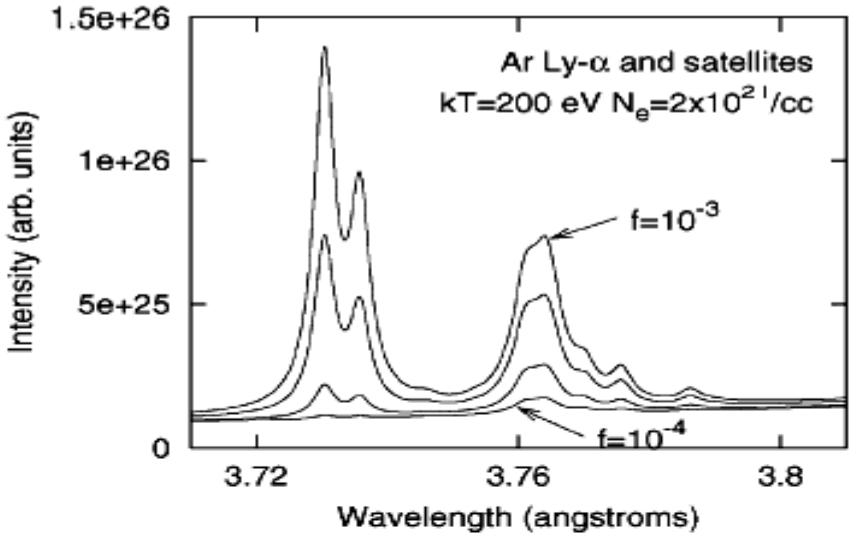

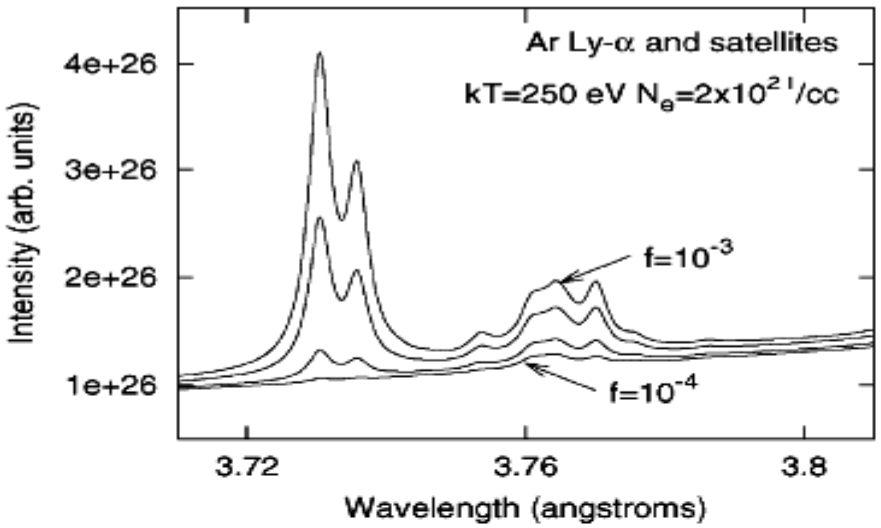

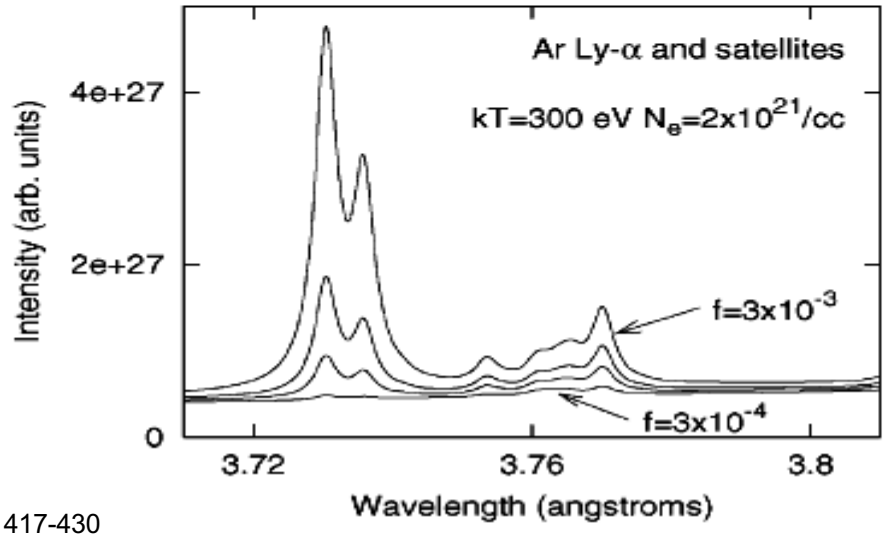

G. C. Junkel-Vives *et al,* JQSRT,**71**, (2001) 417-430

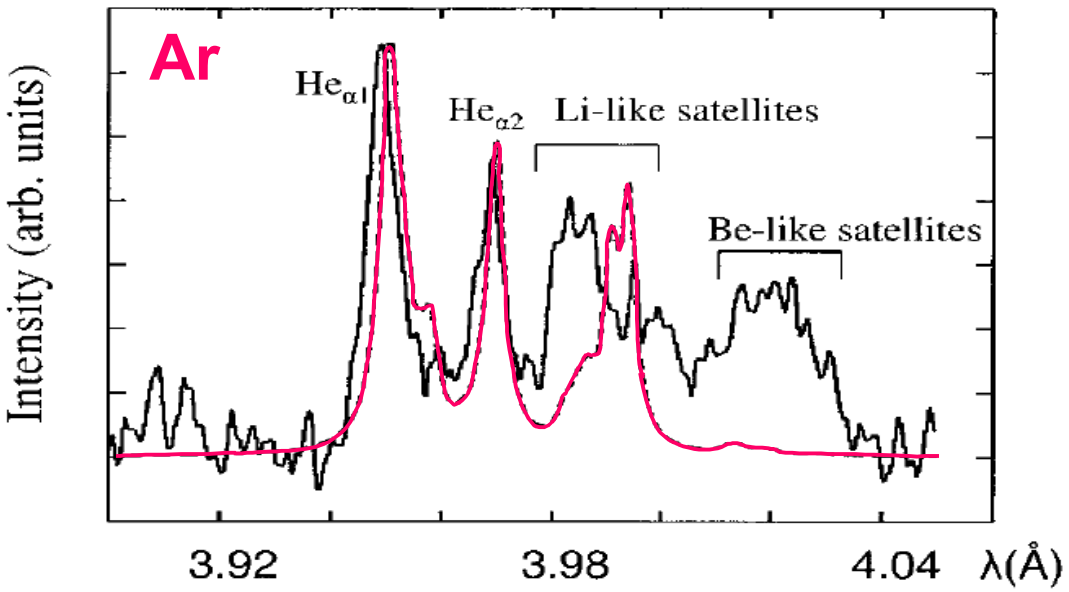

One-temperature (f = 0) steady-state fs laser-produced plasma
T_e =550 eV, N_e = 10^{21} cm^{-3}

Experiment
Simulation

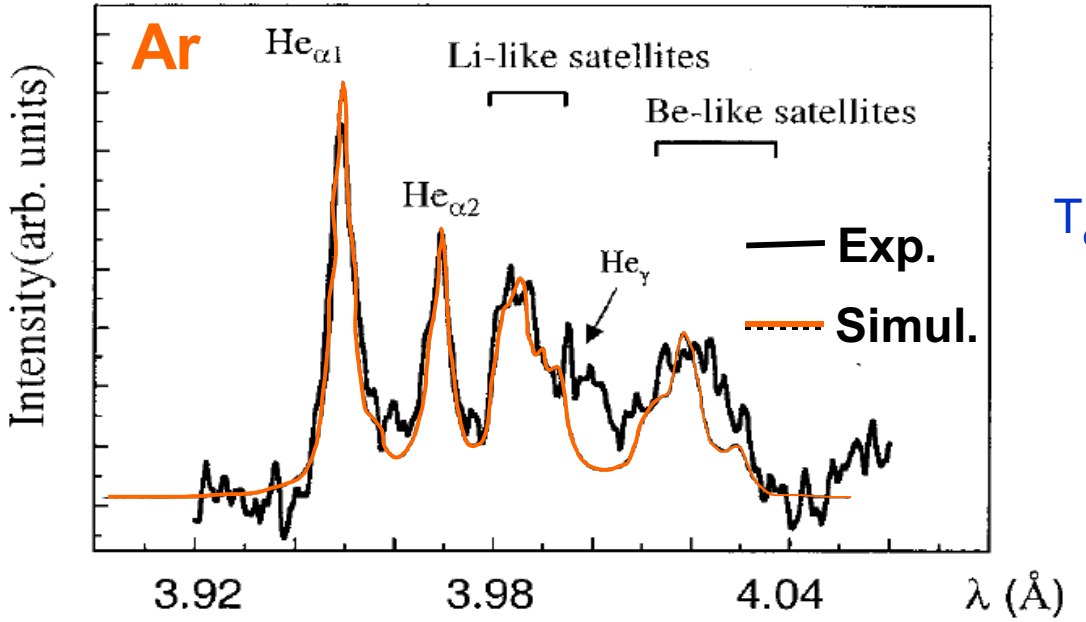

Two components plasma:

cold plasma –
T_e =190 eV, N_e = $1.5 \cdot 10^{20}$ cm^{-3}
f = 0
hot plasma –
T_e =400 eV, N_e = $2 \cdot 10^{21}$ cm-3
f = 10^{-2}

J. Abdallah *et al,* PRA, **63**, 032706

Conical nozzle (Bordeaux University, France): Experimental data and theory

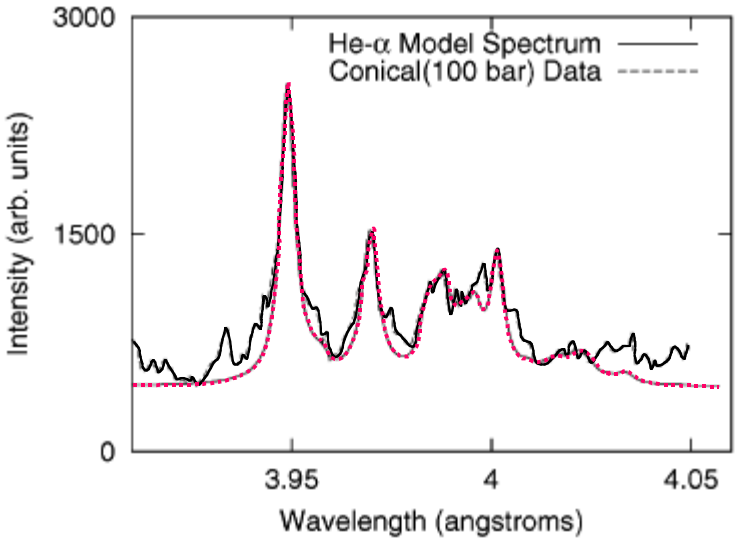

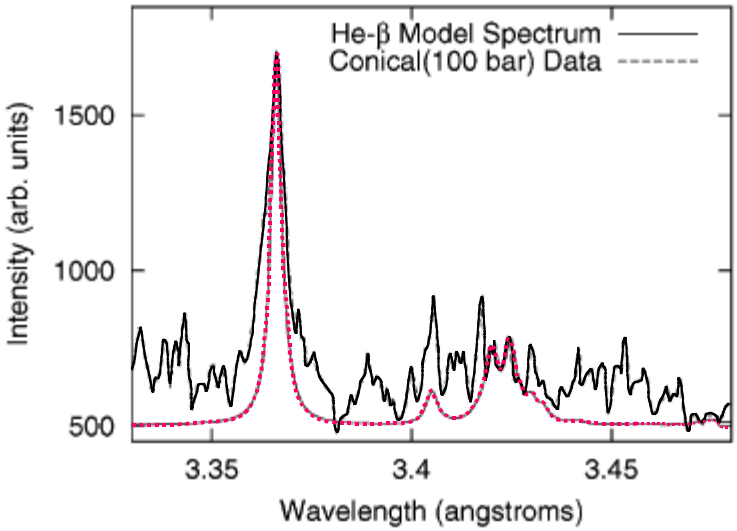

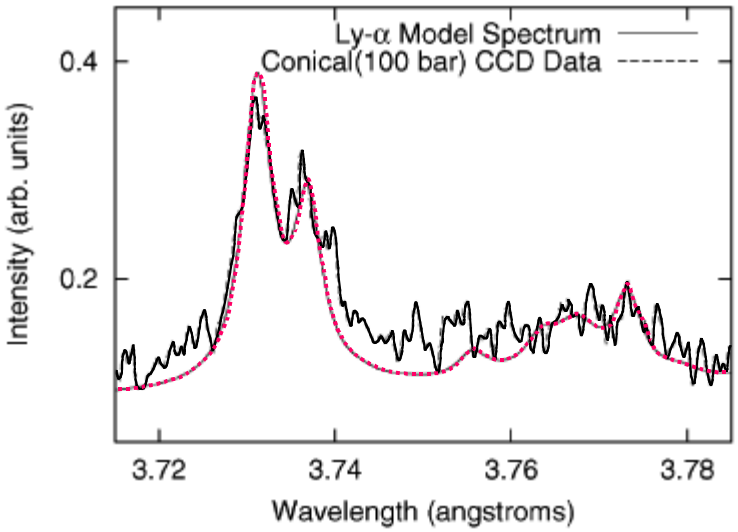

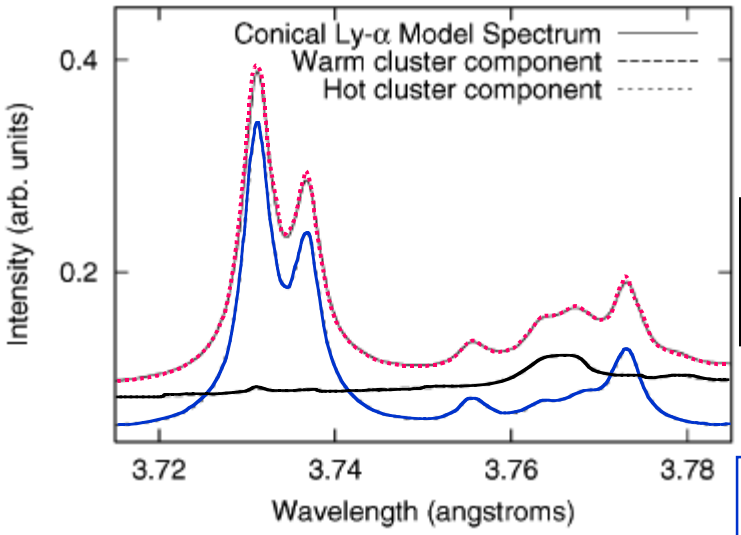

$N_e = 1.5 \cdot 10^{21}$ cm^{-3}
T_e = 195 eV
$f = 8 \cdot 10^{-5}$

$N_e = 2 \cdot 10^{21}$ cm^{-3}
T_e = 400 eV
f = 0.01

G. C. Junkel-Vives *et al,* JQSRT,**71**, (2001) 417-430

4-2 Kr spectrum: kinetics model

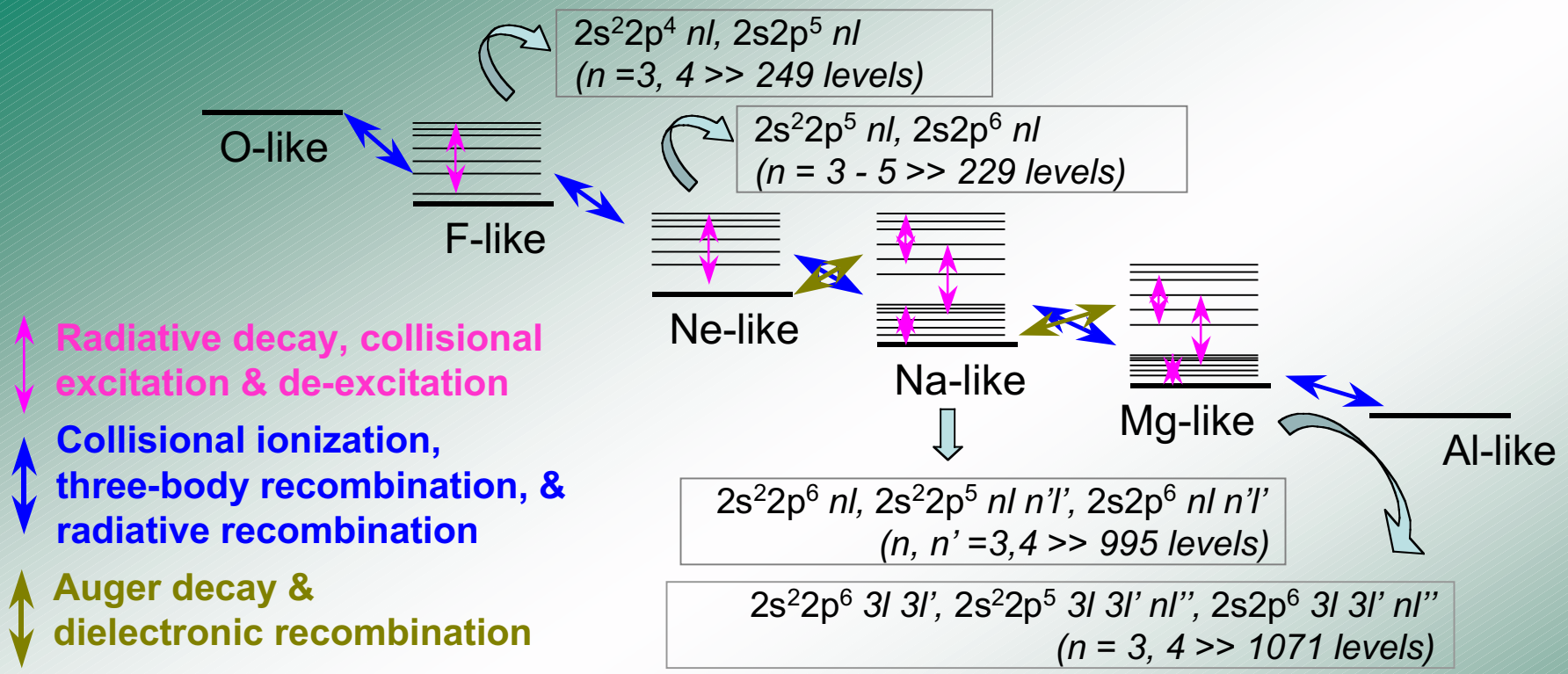

Ion	Levels	Configurations	Autoion. Conf.
F	249	$2s^2\,2p^5$, $2s2p^6$, $2s^2\,2p^4nl$, $2s\,2p^5\,nl$; $n=3,\ 4$	
Ne	157	$2s^2\,2p^6$, $2s^2\,2p^5\,nl$, $2s\,2p^6\,nl$; $n=3-5$	
Na	995	$2s^2\,2p^6\,nl$; $n=3,\ 4$	$2s^2\,2p^4\,n\,ln'l'$, $2s\,2p^5\,n\,l\,n'l'$; $n,n'=3,\ 4$
Mg	914	$2s^2\,2p^6\,nl\,nl'$; $n=3$	$2s^2\,2p^5\,3l\,3l'nl''$, $2s^2\,2p^6\,3l\,3l'nl''$; $n=3,\ 4$

S. B. Hansen *et al,* PRE **66**, 046412 (2002)

$N_e = 2 \cdot 10^{21}$ cm^{-3}

No hot electrons

No opacity

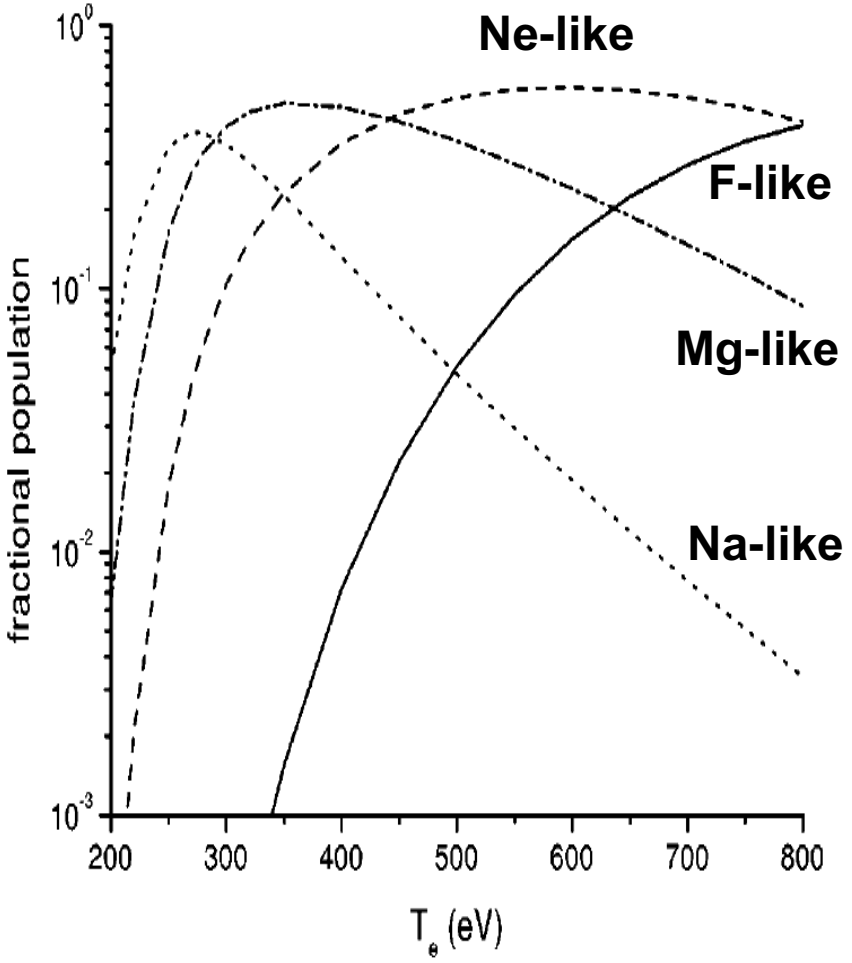

$N_e = 2 \cdot 10^{21}$ cm^{-3}

T_e = 200 eV

No opacity

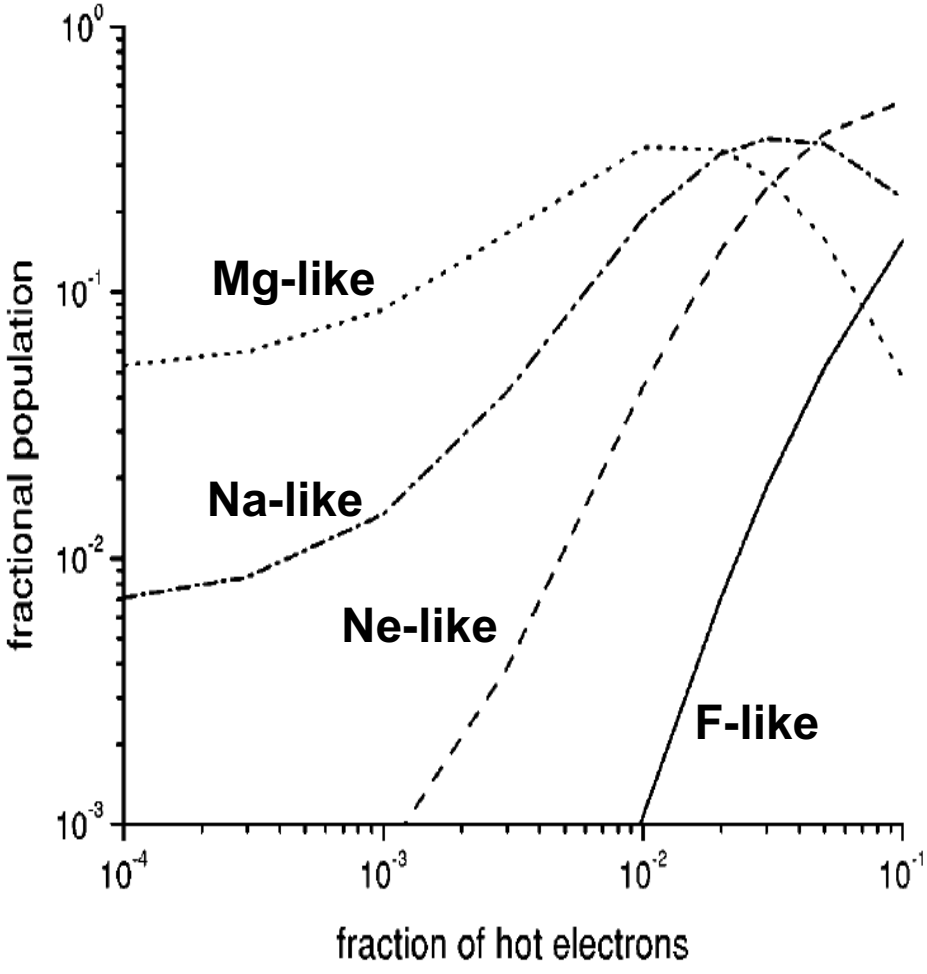

S. B. Hansen *et al,* PRE **66**, 046412 (2002)

4-2 Kr experimental spectra

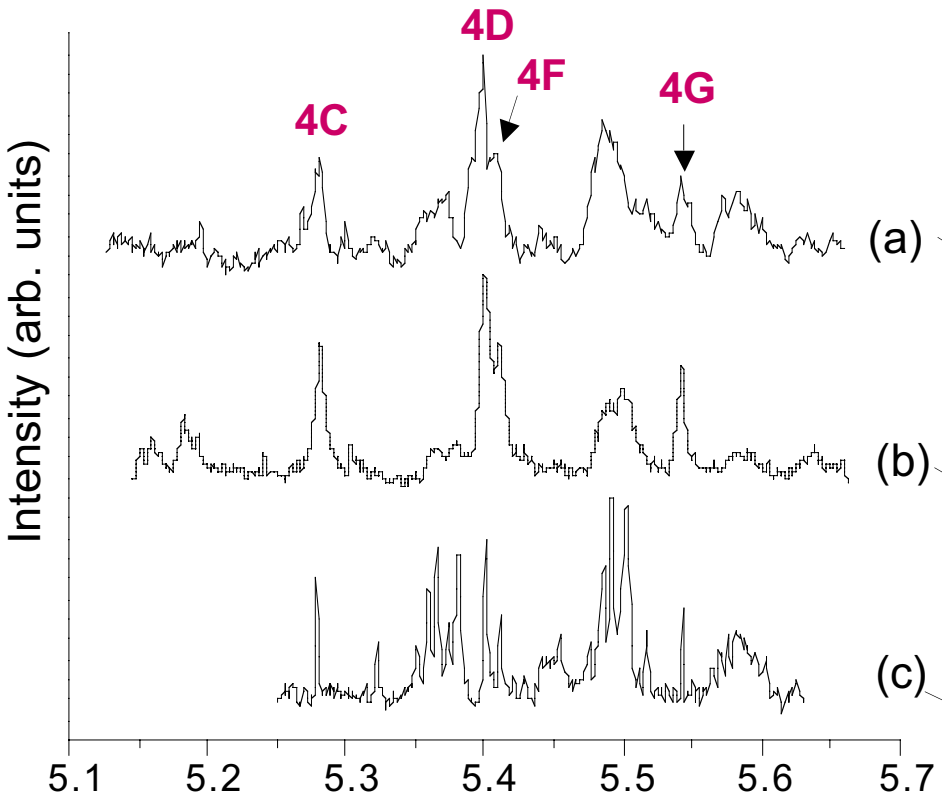

fs laser **(Laval nozzle)**
(Bordeaux University, France)

fs laser (conical nozzle)
(Saclay, France)

ns laser (gas puff)

[V. M. Dyakin *et al,* Quantum Electron. **27** 691 (1997)]

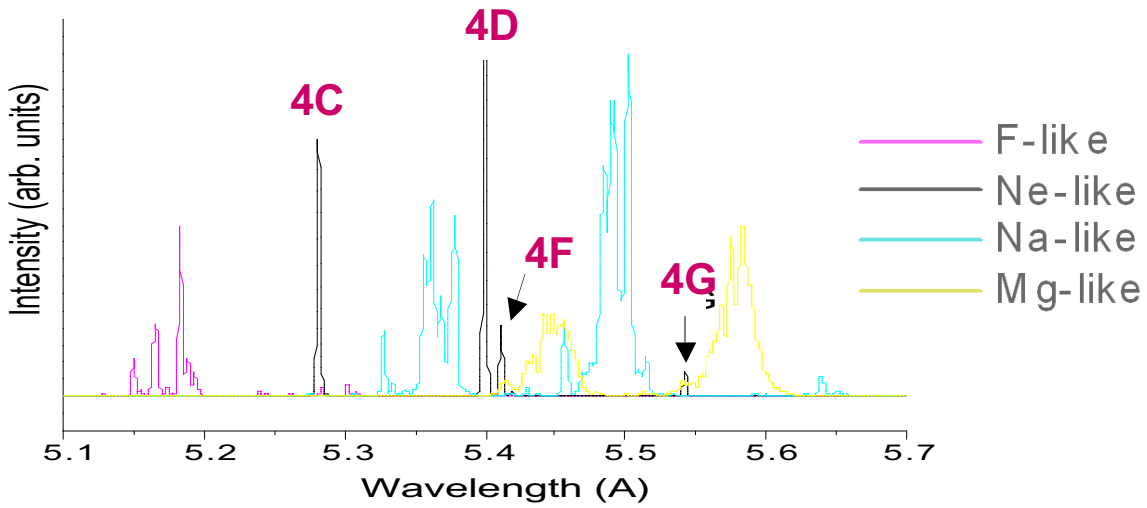

S. B. Hansen *et al,* PRE **66**, 046412 (2002)

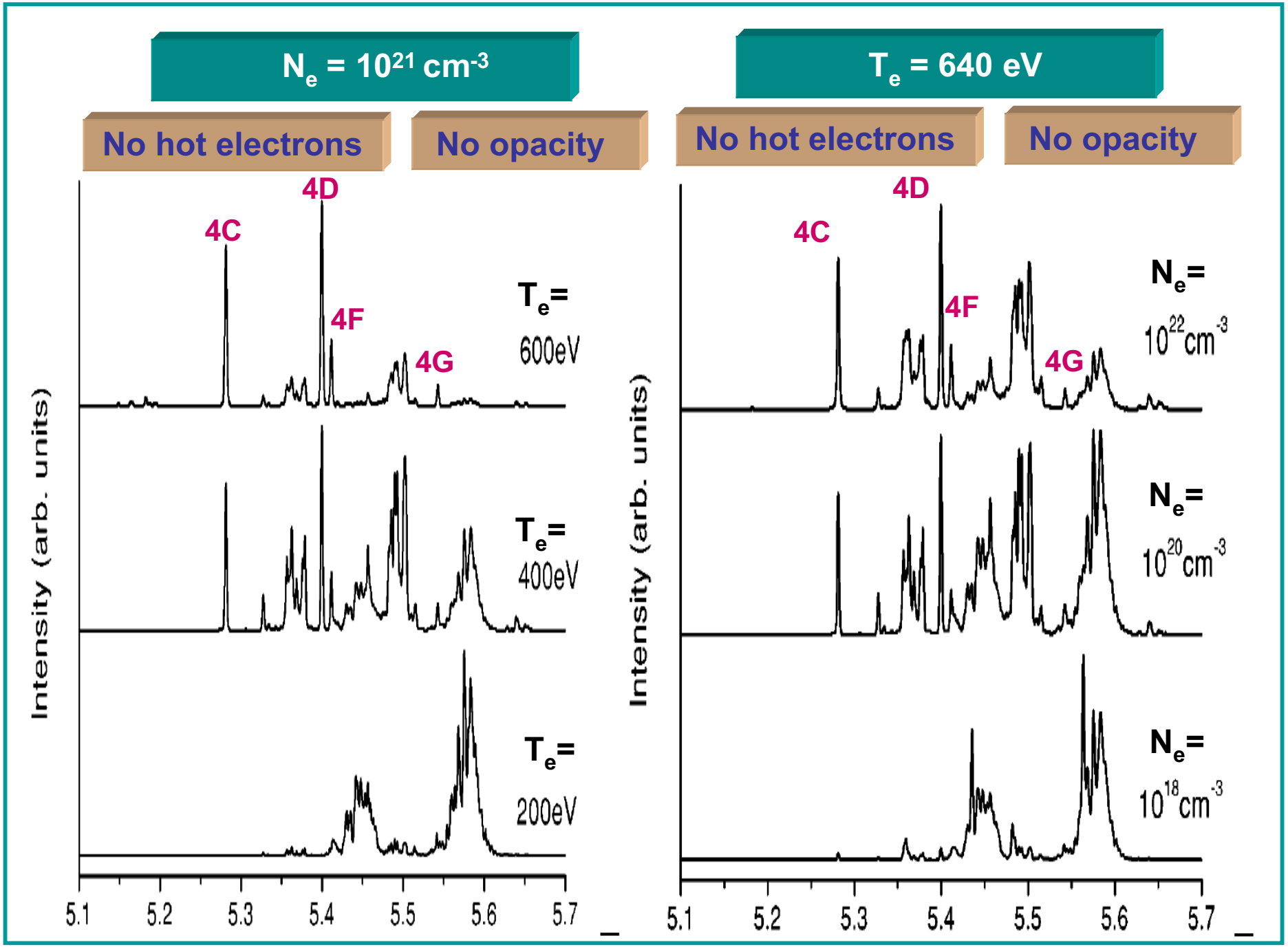

S. B. Hansen *et al,* PRE **66**, 046412 (2002)

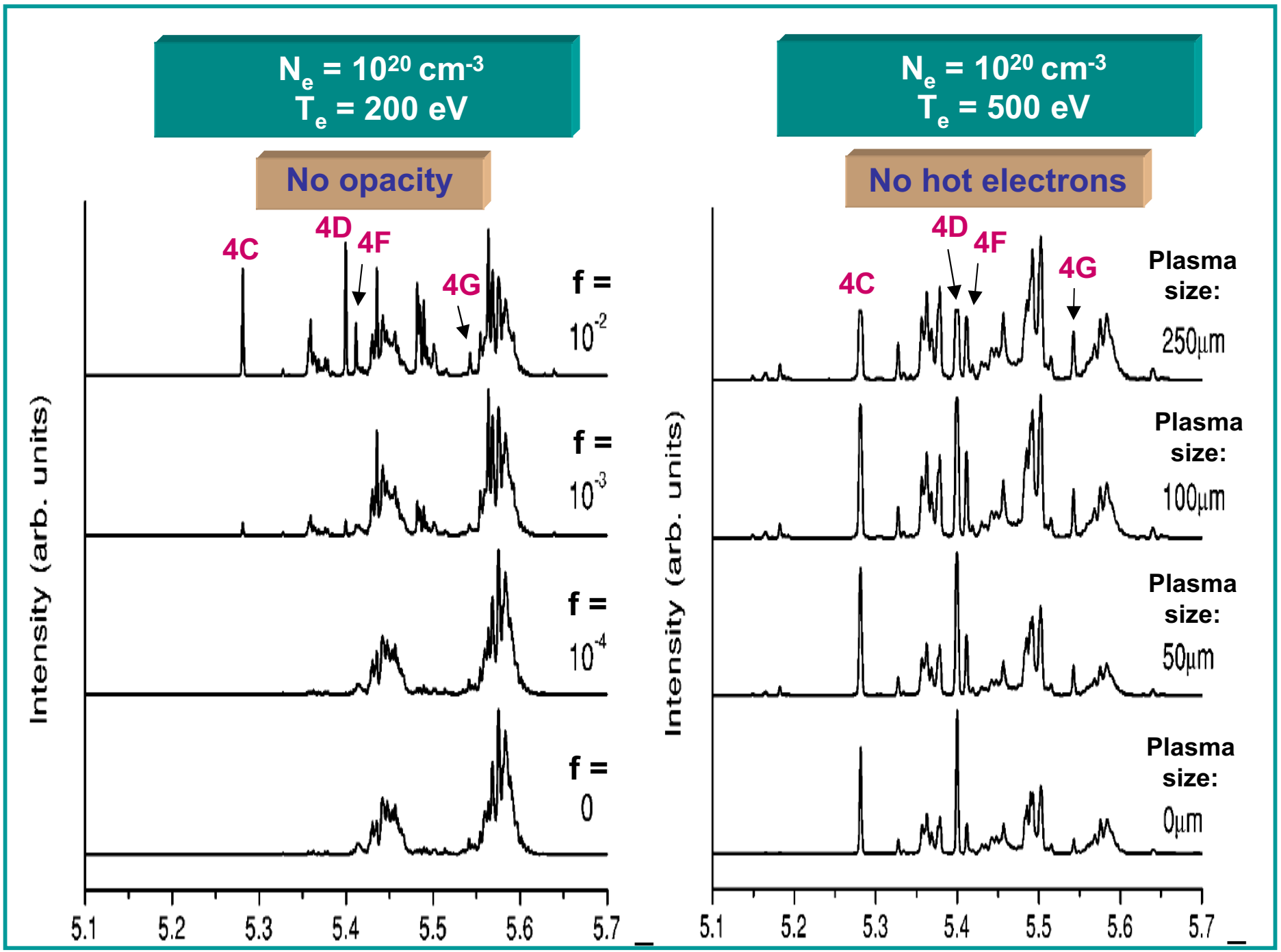

S. B. Hansen *et al,* PRE **66**, 046412 (2002)

fs laser (conical nozzle)
(Saclay, France)

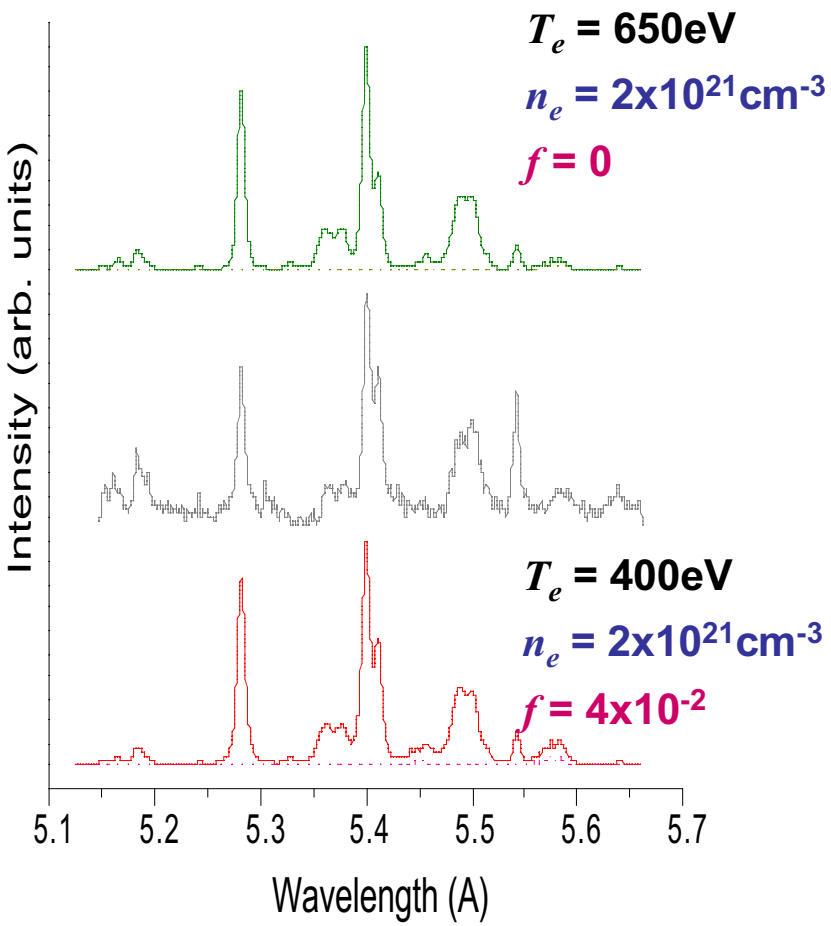

fs laser (Laval nozzle)
(Bordeaux University, France)

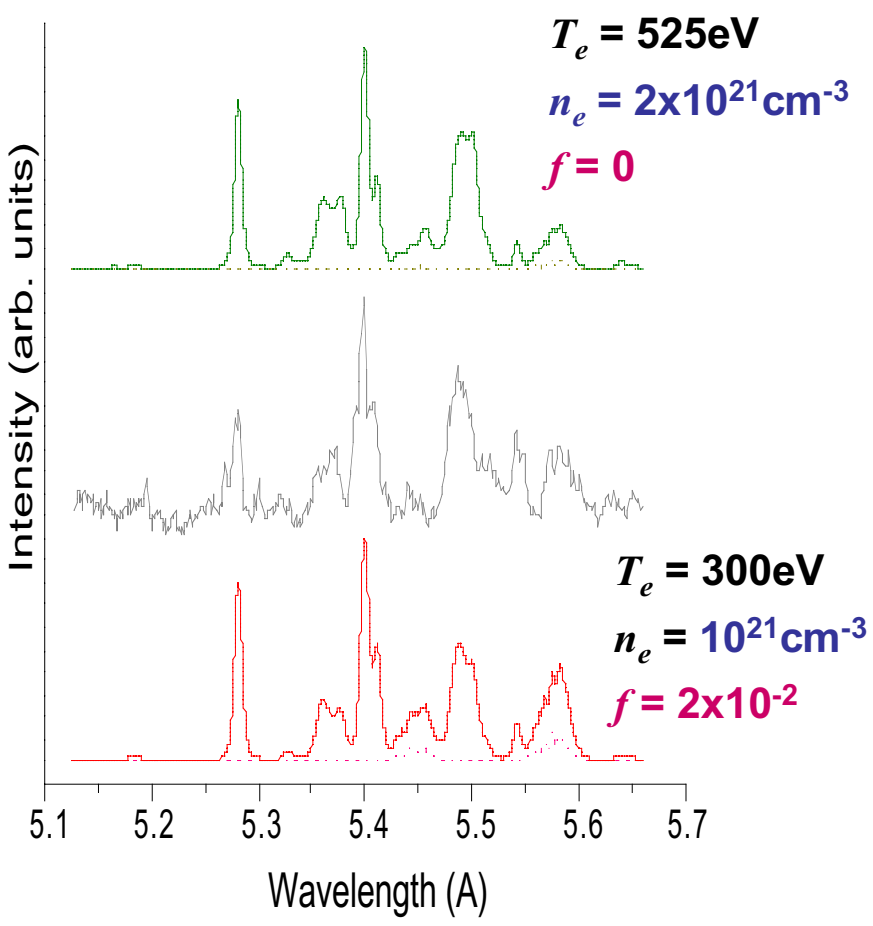

S. B. Hansen *et al,* PRE **66**, 046412 (2002)

CR spectrum for each ion considered in LPP simulations, structure data for n ≤ 9 included

T_e=250 eV, N_e=10^{21} cm^{-3}, L=50 μm

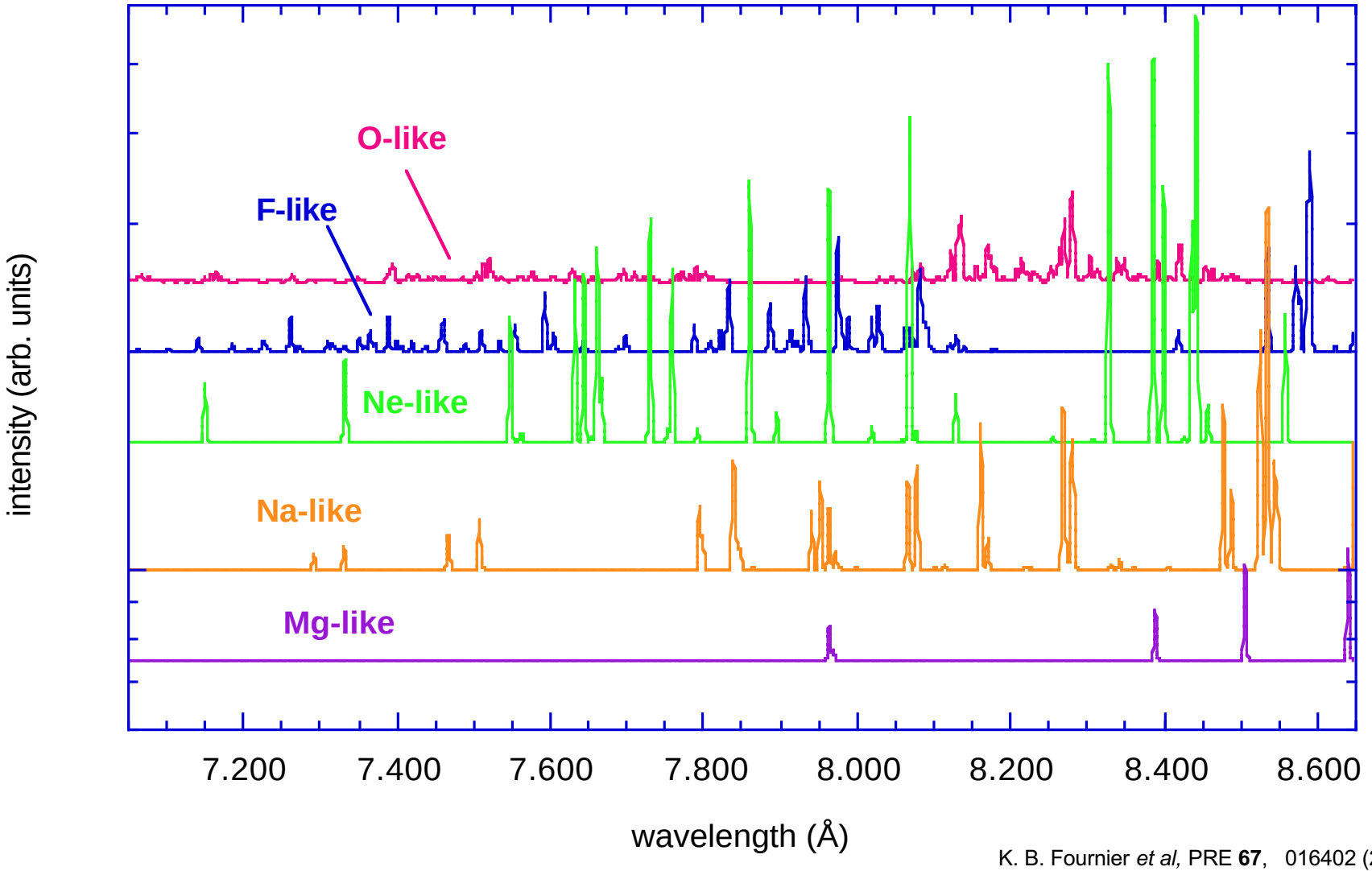

K. B. Fournier *et al,* PRE **67**, 016402 (2003)

Dependence of CR model on hot electron fraction, escape factors are not included

T_e=200 eV, $N_e=10^{21}$ cm^{-3} , T_{hot} = 5 keV

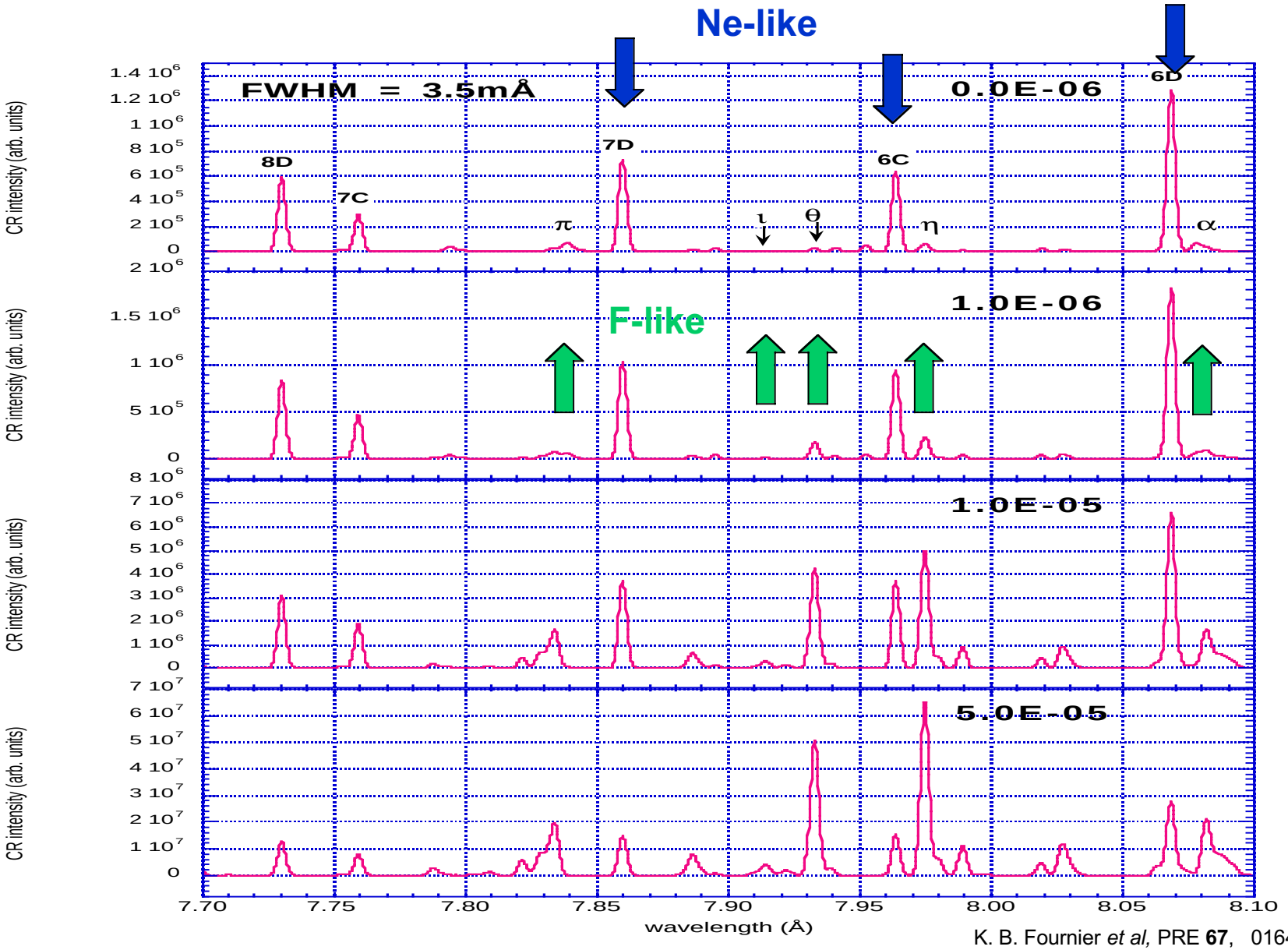

K. B. Fournier *et al,* PRE **67**, 016402 (2003)

Nd:glass laser ("Neodym" - Russia): E = 1 J, τ = 1 ps, I = 2 · 10^{16} W/cm^2

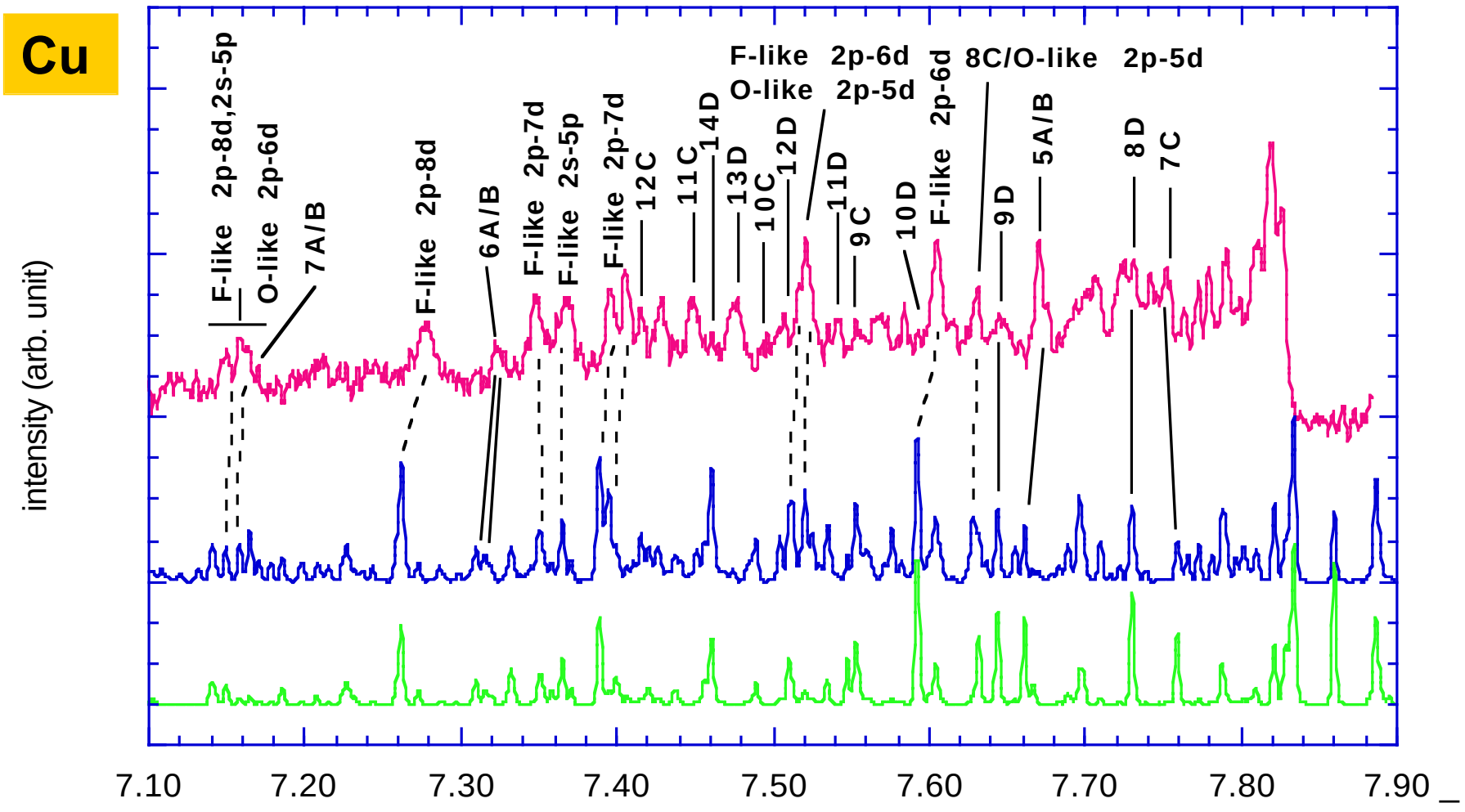

T_e = 300eV, N_e=10^{22} cm^{-3}, f_{hot} = 10^{-5}, L=30μm

T_e = 300eV, N_e=10^{21} cm^{-3}, f_{hot} = 10^{-5}, L=50μm

K. B. Fournier *et al,* PRE **67**, 016402 (2003)

Ti:Sa (60fs) Laser: Experimental data compared to CR model with T_{bulk} = 200eV, Ne=10^{22} cm^{-3}, f_{hot} = 5×10^{-5}

Cu

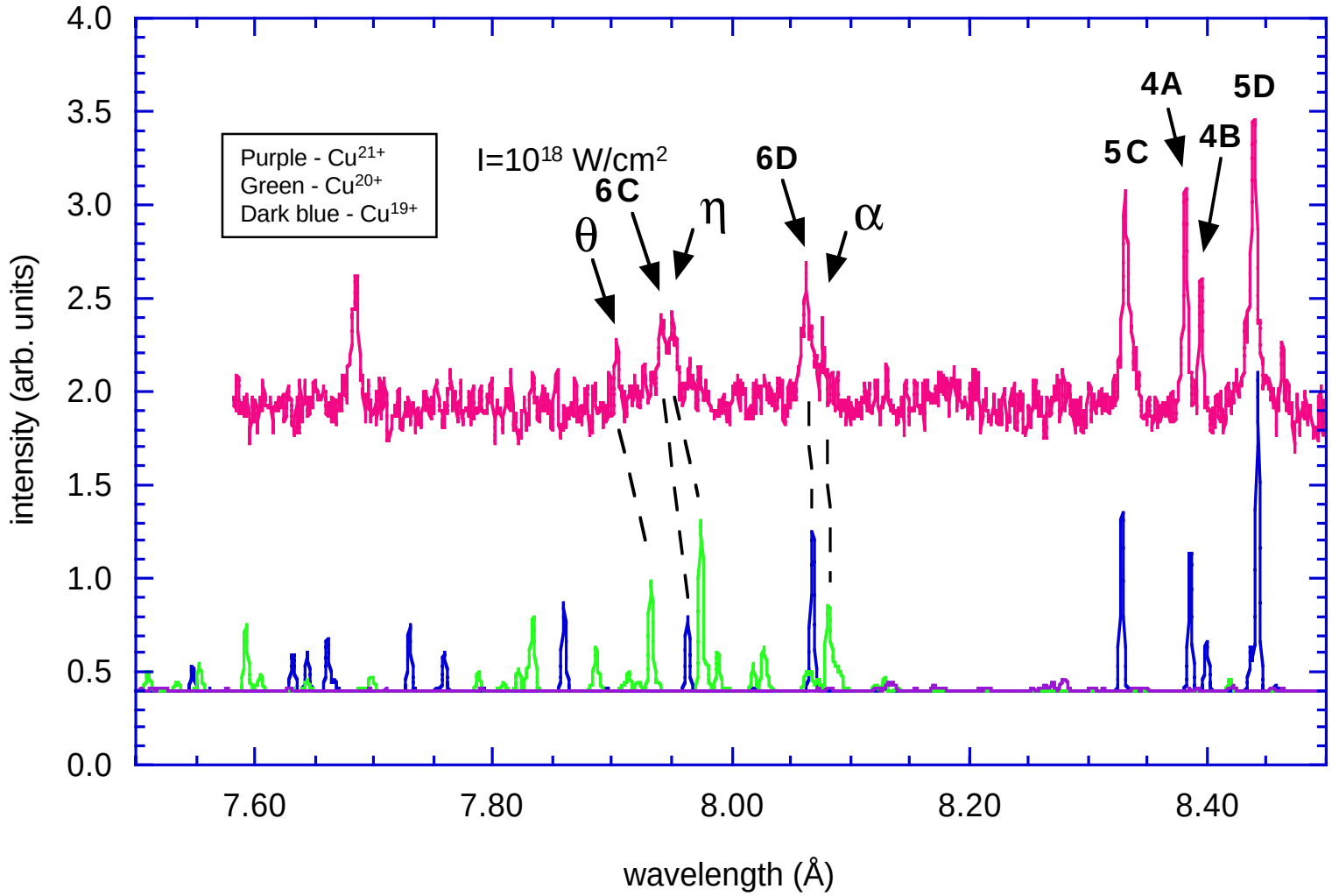

Hot electrons are necessary to reproduce observed relative intensities

K. B. Fournier *et al,* PRE **67**, 016402 (2003)

Conclusions

- X-Ray emission of pico- and femtosecond laser-produced plasma can be described only when hot electrons are taken into account

- Hot electrons:
  - increase sharply intensities of “collisional” satellites due to enhancing of inner-shell electron excitation,
  - increase intensities of resonance lines due to enhancing of both outer-shell electron excitation and inner-shell electron ionization
  - increase plasma ionization state

- Comparison of highly-resolved X-Ray measurements with detailed plasma kinetic calculations allows:
  - to determine fraction of hot electrons,
  - to identify new satellite transitions
  - to measure plasma ionization state, plasma electron temperature and density

Photopumping of XUV lasers by XFEL-radiation

Ke Lan[1], Ernst Fill and Jürgen Meyer-ter-Vehn

Max-Planck-Institut für Quantenoptik, Garching

[1]on leave from the Institute of Applied Physics and Computational Mathematics, P.O. Box 8009-12 Beijing, China

- Motivation
- Photopumping of X-ray lasers
- Results for He I and He II
- Outlook

Photopumped X-ray lasers – three ways for their realization

- ***Innershell XRL***
- *Photo-resonant pumping*
- **Photo-ionization pumping**

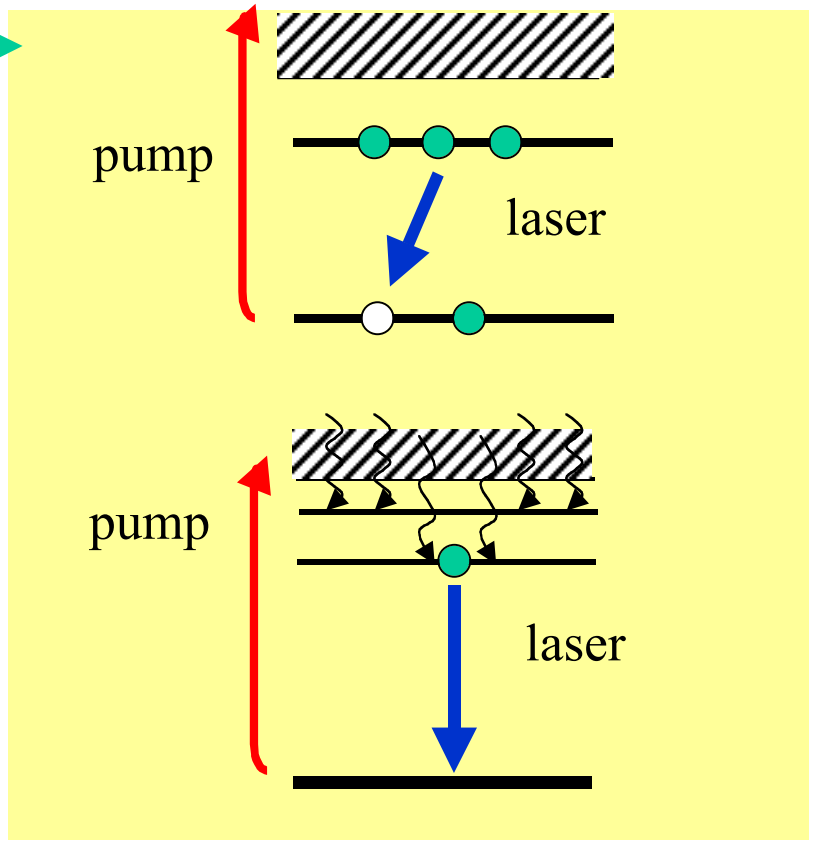

Bunkin et al., Sov. J. Quantum Electron. 11 (1981) 971.

Goodwin & Fill, J. Appl. Phys. 64, (1988) 1005.

Soft X-Ray Lasers and Applications
Session: Hard X-Rays

Free-Electron Laser at the TESLA Test Facility at DESY: towards a tunable, short-pulsed soft X-Ray source

Christopher Gerth, Deutsches Elektronen-Synchrotron DESY

- **FEL at TTF Phase I (1999 - 2002)**
  VUV: 180 - 80 nm
  Proof-of-Principle
  First Results
- **FEL at TTF Phase II (2004)**
  Soft X-rays: 60 - 6 nm
  User facility
- **TESLA with an integrated hard X-Ray User Facility**
  Hard X-rays: 25 nm - 0.1 nm
  Proposal pending, 2010?

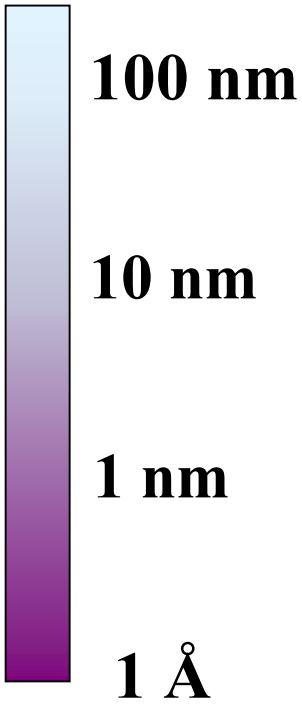

TTF phase II XFEL will emit radiation with the following parameters

- Continuously tunable (20 eV < hν < 200 eV)
- Bandwidth ≈ 1 eV
- 10^{13} – 10^{14} photons/pulse
- Few μm focus diameter
- Pulse duration 100 fs
- Rep. rate: 10^4 pulses 100 ns apart @ 5Hz
  bunch length ≈1 ms

See Ch. Gerth, „*Free-Electron Laser at the TESLA Test Facility at DESY*“, SPIE 4505 (2001) 131

We consider two lasers in helium:

- He I laser at $\lambda = 58.4$ nm

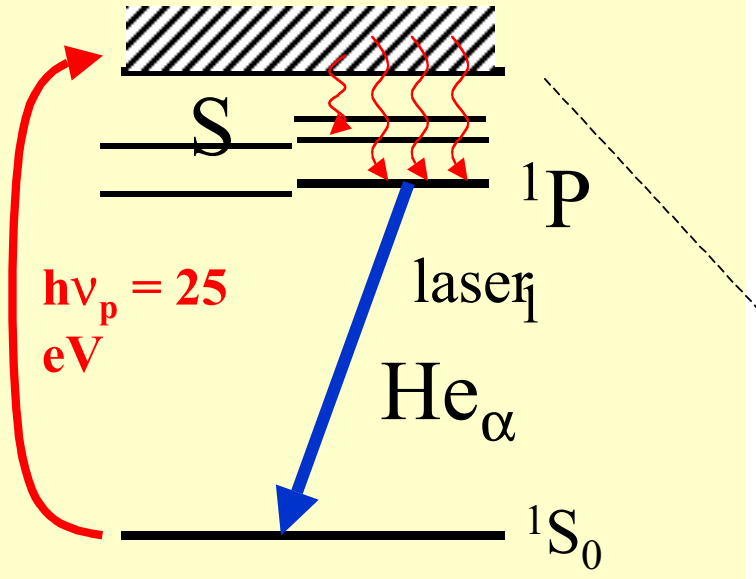

- He II laser at $\lambda = 30.4$ nm

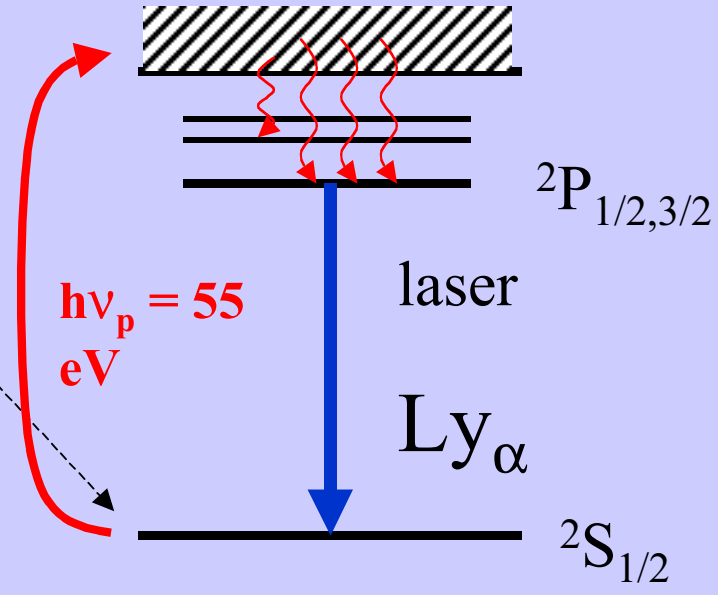

Simulations are carried out with the following parameters

- $I_p(t) = I_0 \sin^2(\pi t/2\tau)$, $0 \le \tau \le 2\tau$; 0 otherwise

  τ = 100 fs; $h\nu_p$ = 25 eV (He I) ; 55 eV (He II); 68 eV (Li II)
- $\partial T_e/\partial t = W_{coll} + W_{rad} + W_p$; $T_{e,0} = 2/3\ (h\nu_p - U_i)$

  $\partial N_i/\partial t = R_{coll} + R_{rad} + R_p$
- $\Delta\nu_{laser} = \Delta\nu_{stark}$ (Griem, *Spectral Line Broadening*...)

Range of intensities and densities:

$3\text{x}10^{13} < I_0 < 10^{16}$ W/cm^2;

$5\text{x}10^{18} < N_0 < 10^{21}$/cm^3

He I laser needs only 10^{14} W/cm^2

Electron temperature vs. time

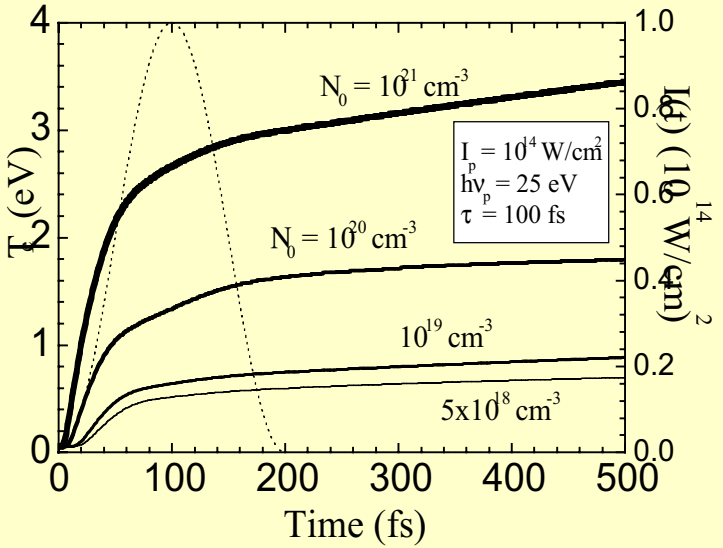

Heating mechanisms, mainly three-body recombination, increase T_e over ist initial value

Gain coefficient vs. time

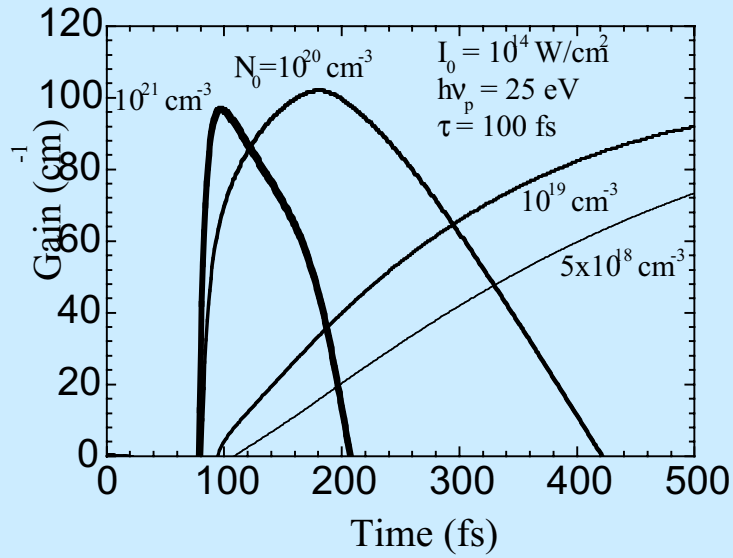

Gain duration decreases with increasing gas density

Time evolution of He I gain for different I_0

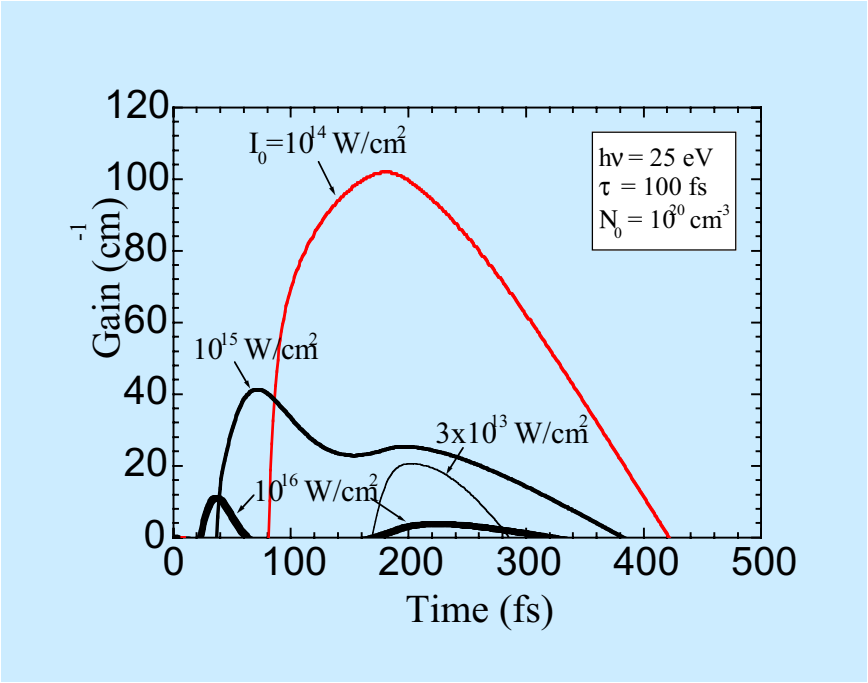

An optimum pump intensity around 10^{14} W/cm^2 generates 100 cm^{-1} of gain. At lower intensity not enough atoms are ionized; at higher intensity heating and ionization from upper laser level decrease gain

He II laser requires 10^{15} W/cm^2

Electron temperature vs. time

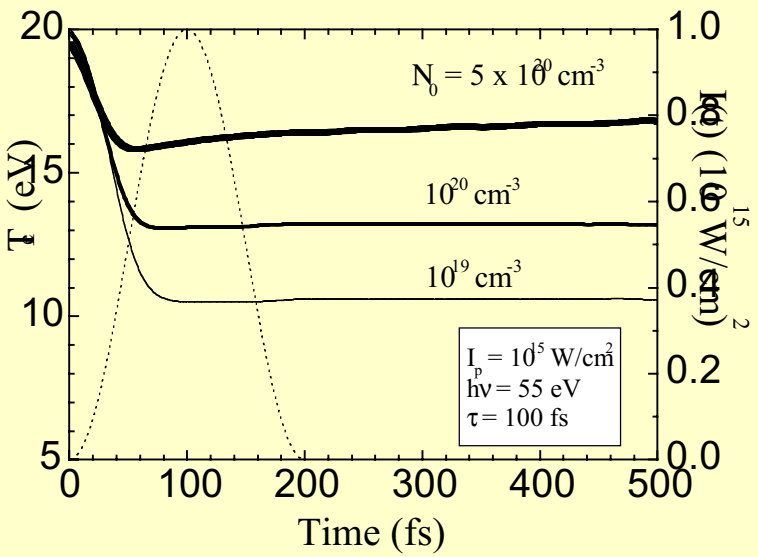

Gain coefficient vs. time

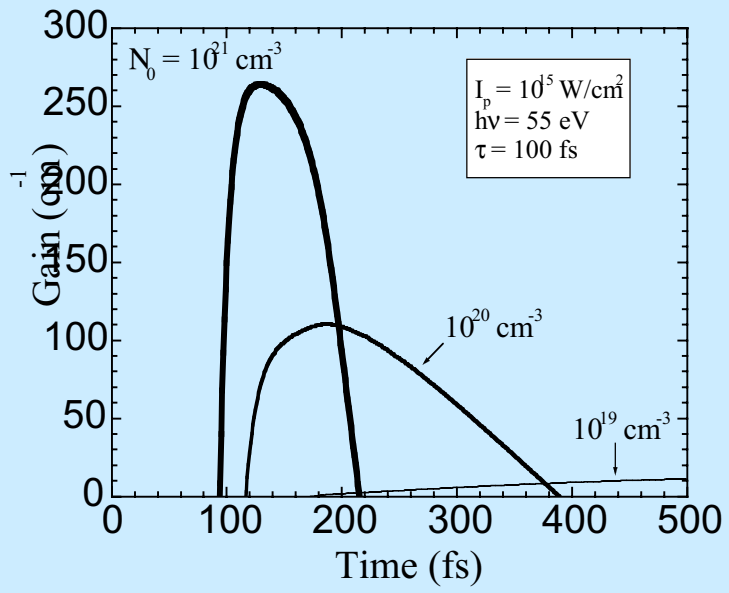

Electron temperature starts at 20 eV due to excess energy of pump photons. Second ionization reduces temperature. Gain is comparable to He I gain, however note tenfold pump intensity.

Gain of He II laser vs. Pump intensity

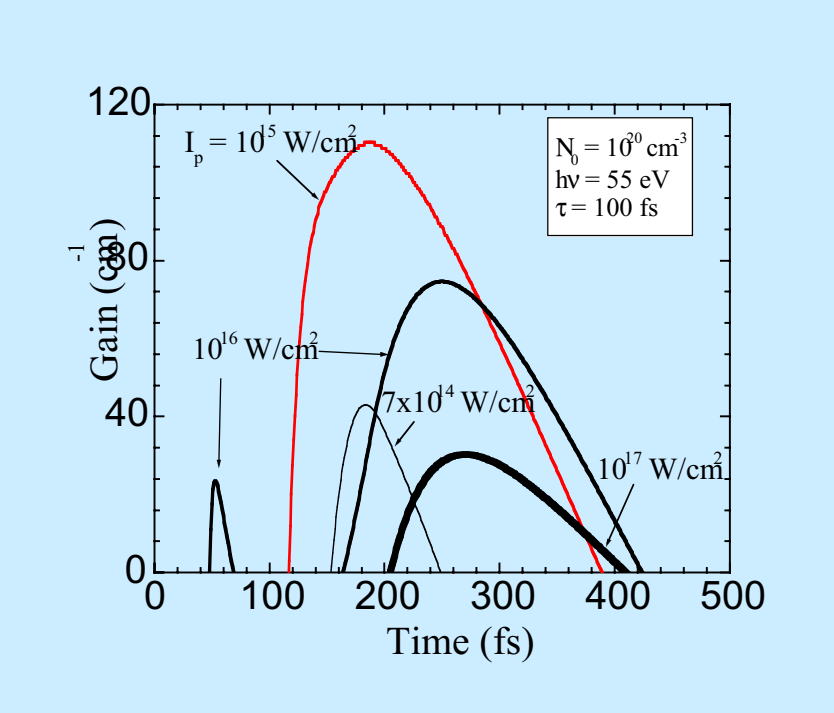

Again, there is an optimum pump intensity; too high an intensity increases the electron temperature and ionizes from the upper laser level

Critical issues for achieving a high gain length product

- **Absorption of pump pulse in medium**

  Small signal absorption would allow only short propagation distance.

  However absorption is strongly saturated.

- Deflection of X-ray beam due to electron density gradient

- Velocity matching of X-ray pulse propagation to gain propagation ($v_g < c$)

Depletion of He I ground state leads to saturation of the absorption

- Absorption coefficient of He I

  $\alpha = \sigma N_0 \approx 70\ cm^{-1}$ @ 25 eV, $10^{19}\ cm^{-3}$

- Ground state depletion rate

  $R_g = -\sigma I / h\nu \rightarrow R_g = -1.8 \times 10^{14}\ s^{-1}$ @ $10^{14}\ W/cm^2$

$\Rightarrow$ Pump pulse can propagate....

$$\mathrm{He}-\alpha \text{ in He},\ N_0 = 10^{19}\ \mathrm{cm}^{-3},\ I_p = 10^{14}\ \mathrm{W/cm}^2,\ \tau = 100\ \mathrm{fs},\ h\nu = 25\ \mathrm{eV}$$

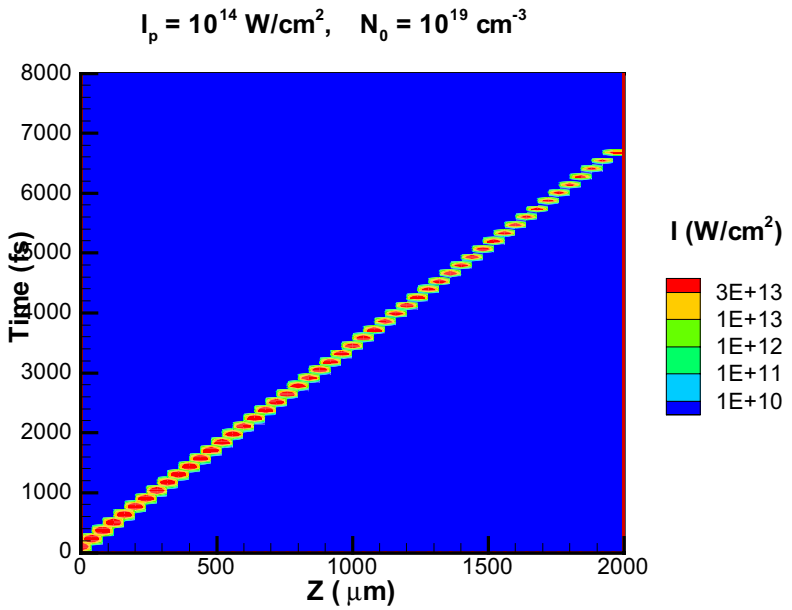

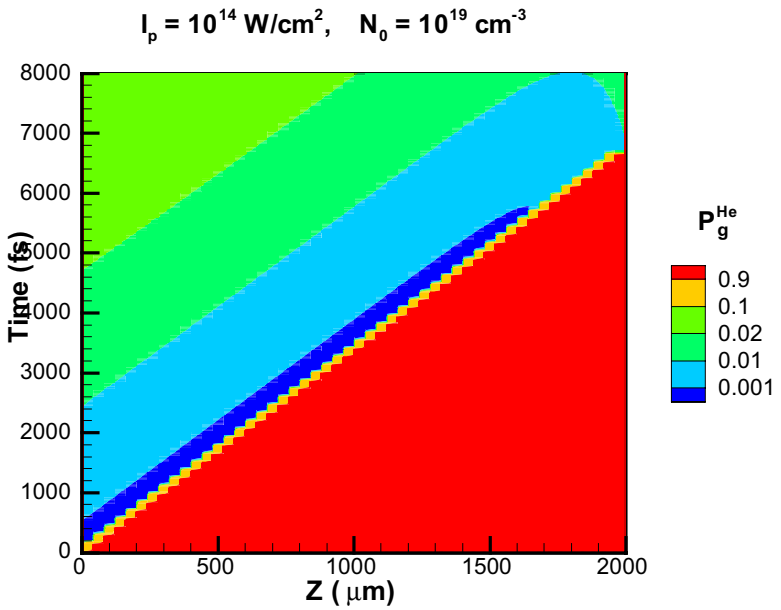

$$\mathrm{He}-\alpha \text{ in He},\ N_0 = 10^{19}\ \mathrm{cm}^{-3},\ I_p = 10^{14}\ \mathrm{W/cm}^2,\ \tau = 100\ \mathrm{fs},\ h\nu = 25\ \mathrm{eV}$$

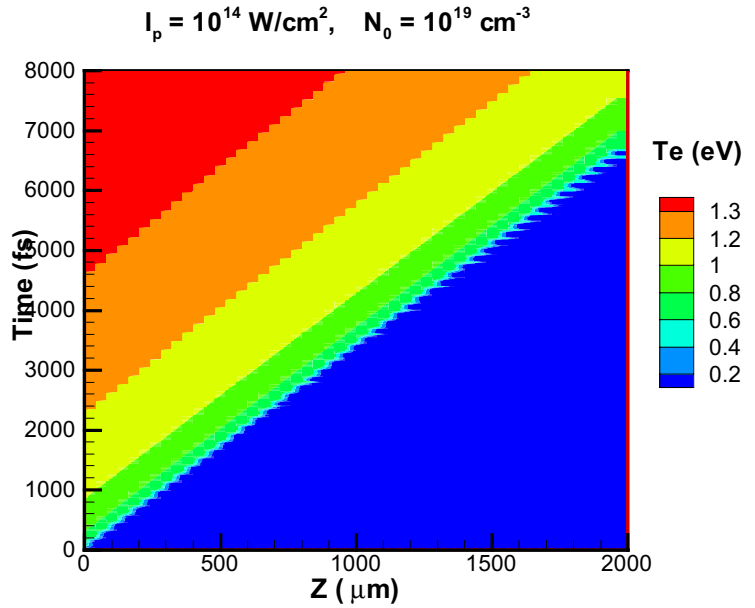

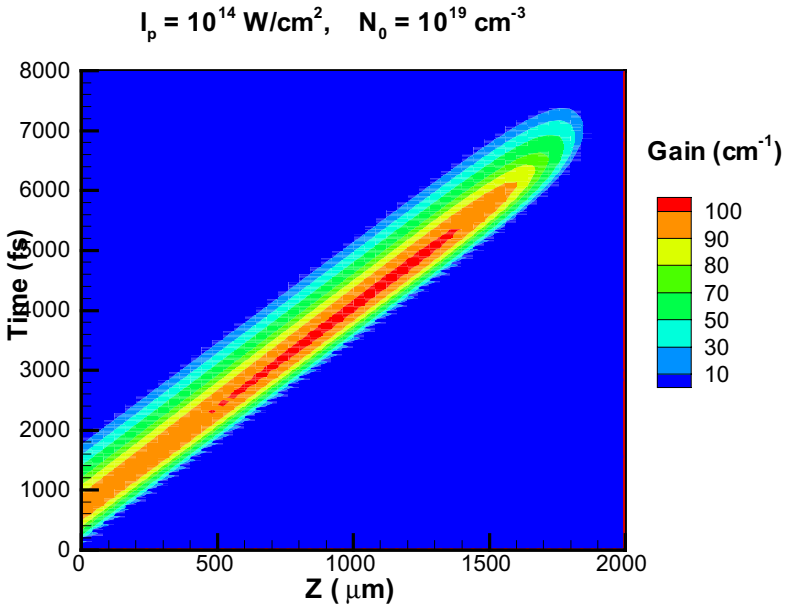

$$\mathrm{He}-\alpha \text{ in He},\ N_0 = 10^{20}\ \mathrm{cm}^{-3},\ I_p = 10^{14}\ \mathrm{W/cm}^2,\ \tau = 100\ \mathrm{fs},\ h\nu = 25\ \mathrm{eV}$$

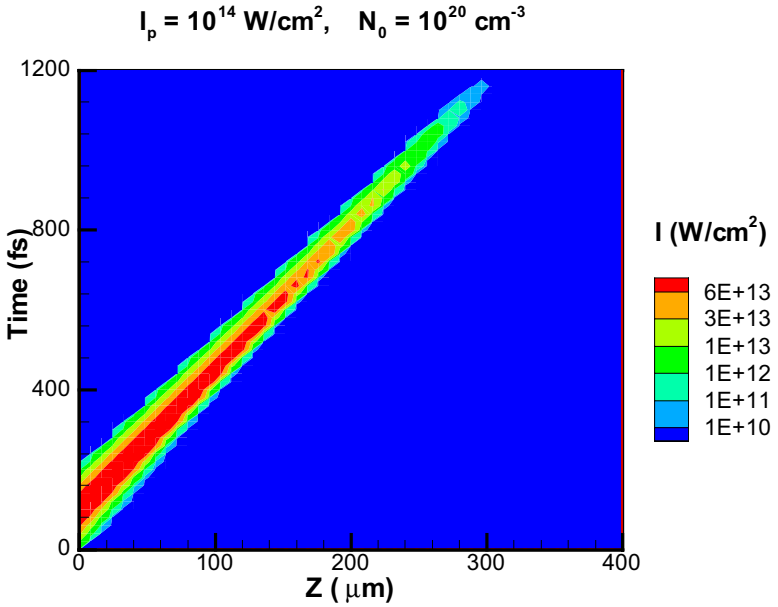

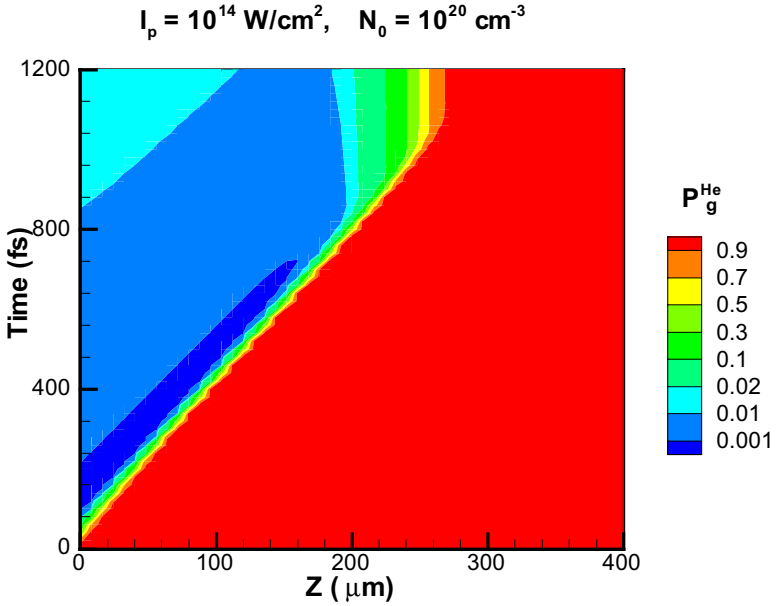

$$\mathrm{He}-\alpha \text{ in He},\ N_0 = 10^{20}\ \mathrm{cm}^{-3}, I_p = 10^{14}\ \mathrm{W/cm}^2,\ \tau = 100\ \mathrm{fs},\ h\nu = 25\ \mathrm{eV}$$

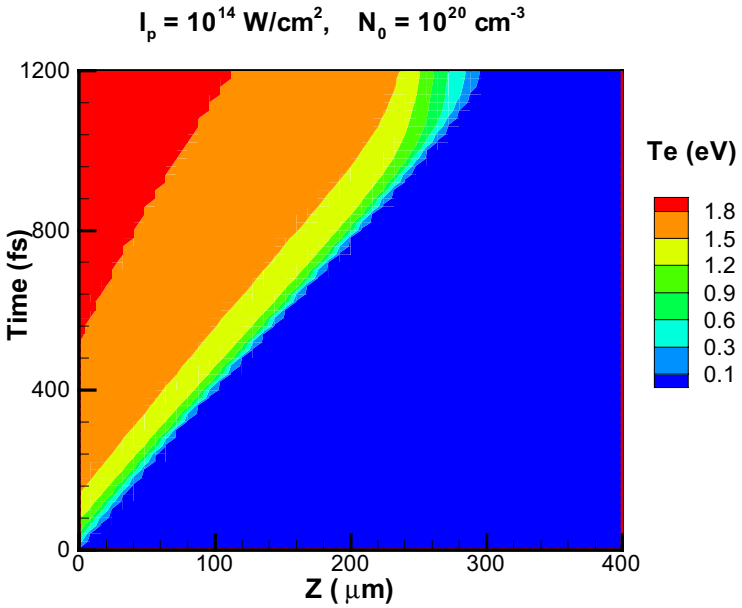

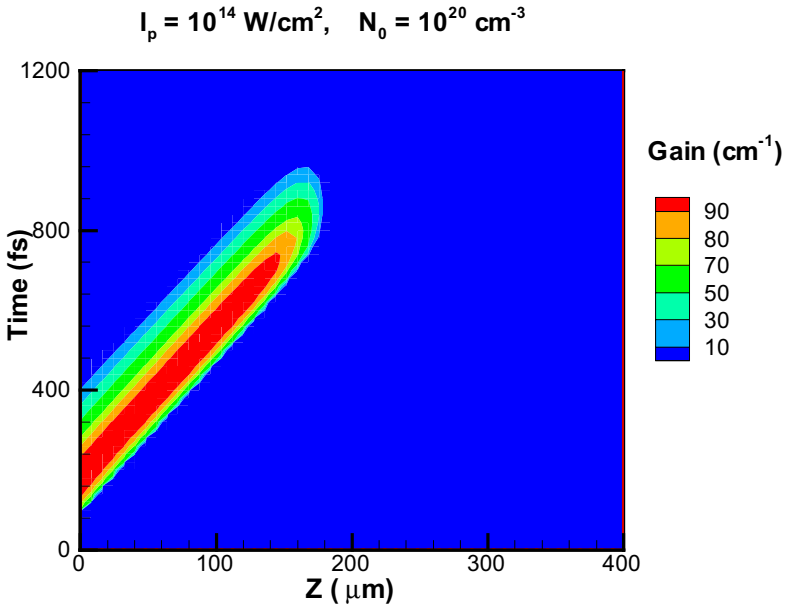

$$\mathrm{He}-\alpha \text{ in He},\ N_0 = 10^{19}\ \mathrm{cm}^{-3},\ I_p = 10^{16}\ \mathrm{W/cm}^2,\ \tau = 100\ \mathrm{fs},\ h\nu = 25\ \mathrm{eV}$$

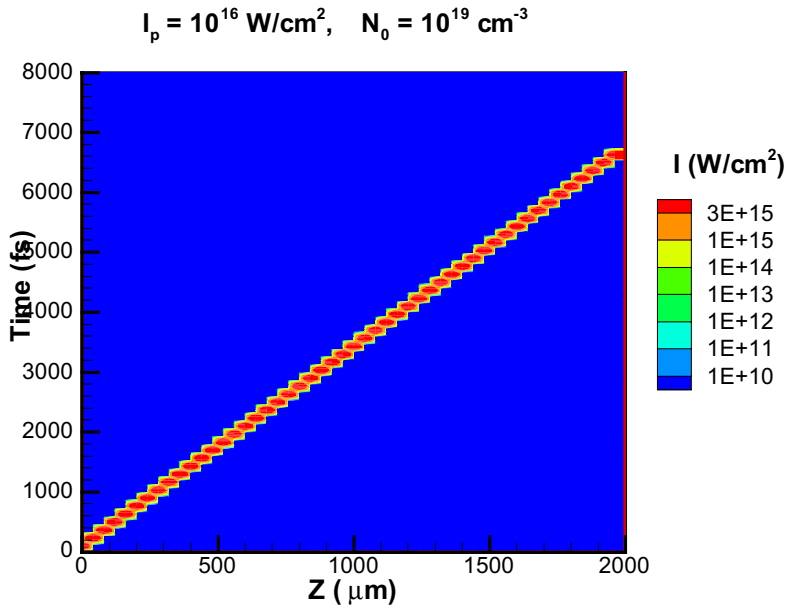

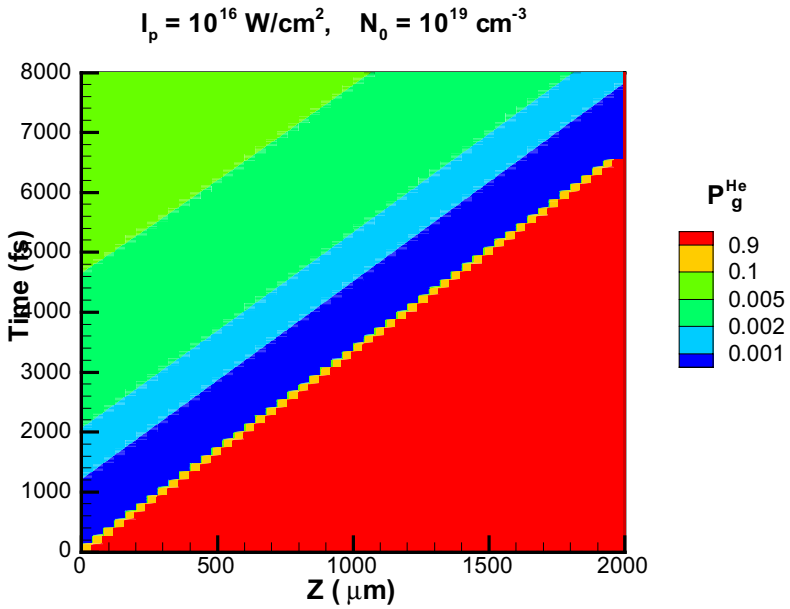

$$\mathrm{He}-\alpha \text{ in He},\ N_0 = 10^{19}\ \mathrm{cm}^{-3},\ I_p = 10^{16}\ \mathrm{W/cm}^2,\ \tau = 100\ \mathrm{fs},\ h\nu = 25\ \mathrm{eV}$$

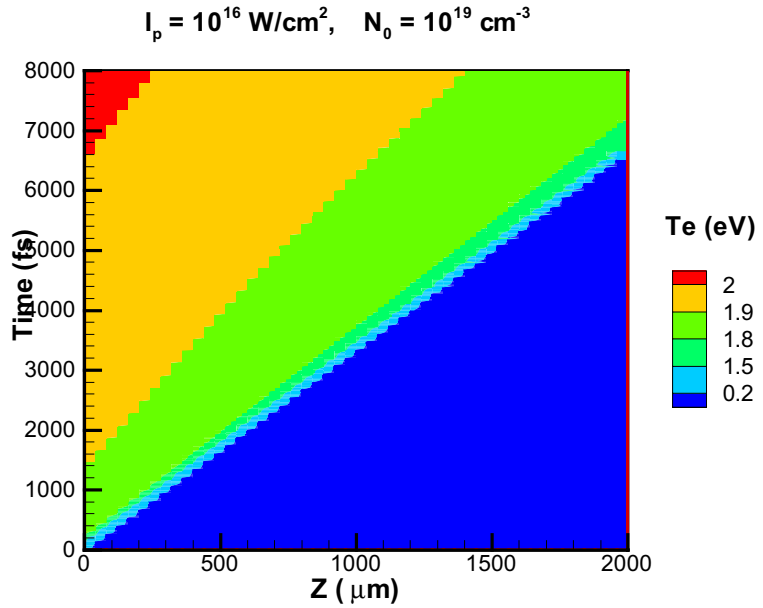

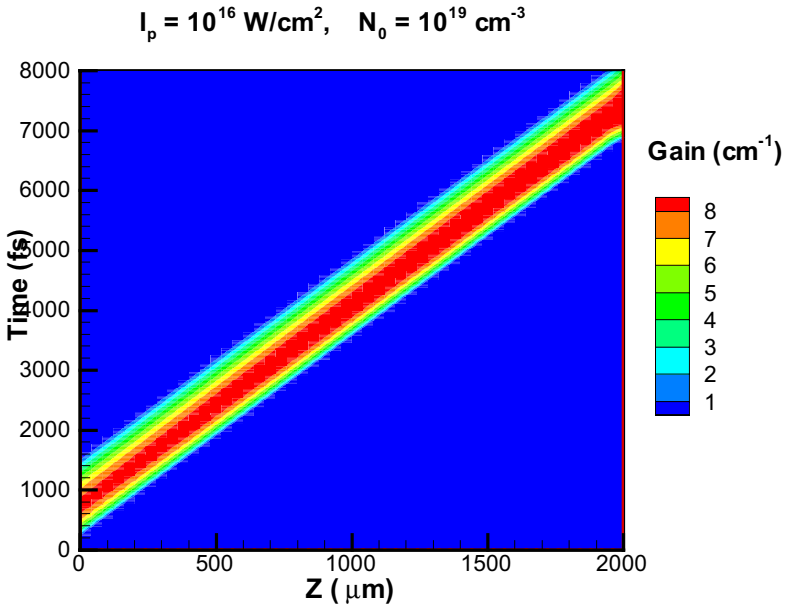

Innershell ionization of Li results in high gain at 19.9 nm

- Single 2s electron → no Auger effect
- Rapid 2s → 2p transfer required
- Gain duration is limited by ionization from upper level
- Experimentally quite challenging: low vapour pressure of Li requires high temperature (1270^{0}C for 10^{19} cm^{-3})

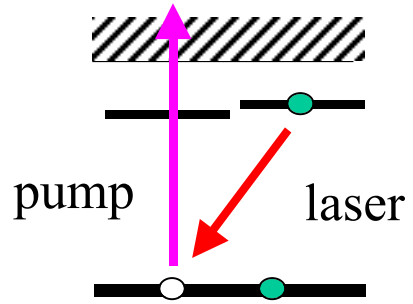

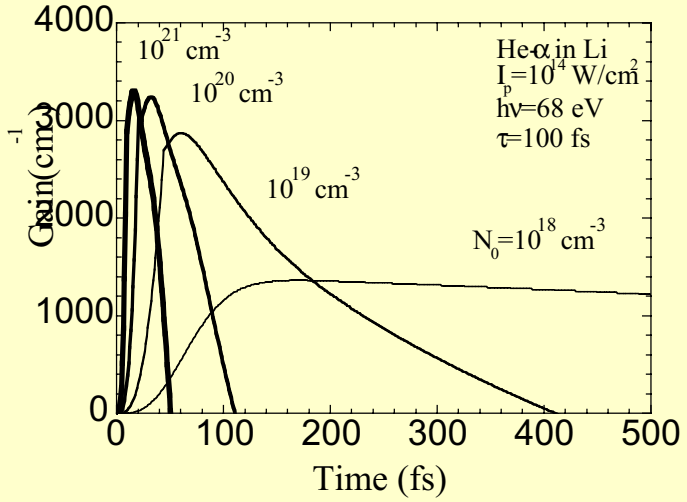

Conclusions and outlook

- Photopumping of soft XRL´s seems feasible
  (He I, $\lambda = 58.4$ nm; He II, $\lambda = 30.4$ nm; Li II, $\lambda = 19.9$ nm)
- Photoionization-recombination and innershel ionization schemes investigated
- High gain generated by radiation with parameters accessible by TESLA XFEL
- Absorption of pump pulse no problem due to saturation (He I @10^{19} cm^{-3} → gain length product ≥ 15)
- Will a truly photopumped XRL finally be realized?

<THE OHIO STATE UNIVERITY>

THE USE OF ULTRA-HIGH INTENSITY SHORT PULSE LASERS IN FUSION ENERGY DEVELOPMENT

INTERNATIONAL CONFERENCE OF ULTRASHORT HIGH-ENERGY RADIATION AND MATTER
VARENNA, ITALY

R.R. Freeman
The Ohio State University
C. Anderson, J. Hill, J. King,R. Snavely
University of California, Davis
R. Stephens, T. Cowan
General Atomics
M. Key, A. Mackinnon, S. Hatchett, M. Tabak
University of California, LLNL

Essential Collaborators across the world

GENERAL ATOMICS

Y. Aglitskiy[1], F. Amiranoff[2], D. Batani[4], S.D. Baton[2] ,T. Hall[5], M. Koenig[2], K.L. Lancaster[6], E. Martinolli[4], P. Norreys[6], E. Perelli-Cippo[4], M. Rabec Le Gloahec[3], C. Rousseaux[3], J.J. Santos[2], F. Scianitti[4]

- *Science Applications International Corporation, McLean, VA 22102 USA*
- *Laboratoire pour l'Utilisation des Lasers Intenses, UMR 7605, CNRS-CEA-Universite' Paris VI-Ecole Polytechnique, 91128 Palaiseau, France*
- *Commissariat a l'energie Atomique, 91680 Bruyeres-le-Chatel, France*
- *Dipartimento di Fisica "G. Ochialini", Universita' degli Studi di Milano-Bicocca and INFM, Piazza della Scienza 3, 20126 Milan, Italy*
- *Department of Physics, University of Essex, Colchester CO4 SSQ, United Kingdom*
- *Rutherford Appleton Laboratory, Chilton, Oxon, OX11OQX, United Kingdom*

GENERAL ATOMICS

FUSION *NOT* FISSION

Bombs

Power Plants

$^{235}U + n \rightarrow$ fission products + 2 n (5MeV)

Bad stuff

$^{3}H + ^{2}H \rightarrow He + n$ (17.6 MeV)

Stars

Bombs

The difference between FI and conventional ICF is simple at the conceptual level

Conventional ICF

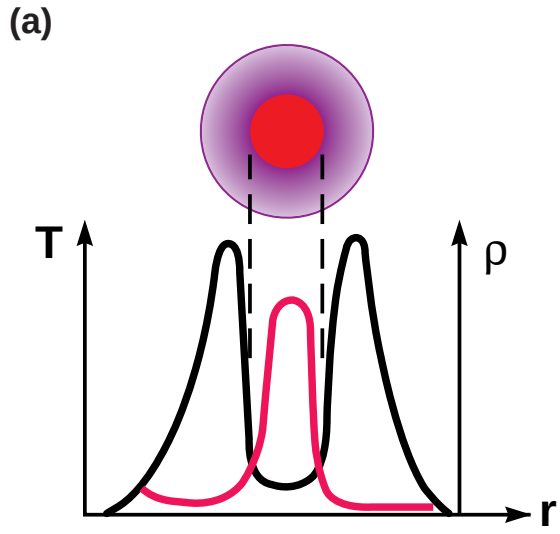

Low-density central spot ignites a high-density cold shell

$\rho T_{hot} \approx \rho T_{cold}$ (isobaric)

Fast Ignitor

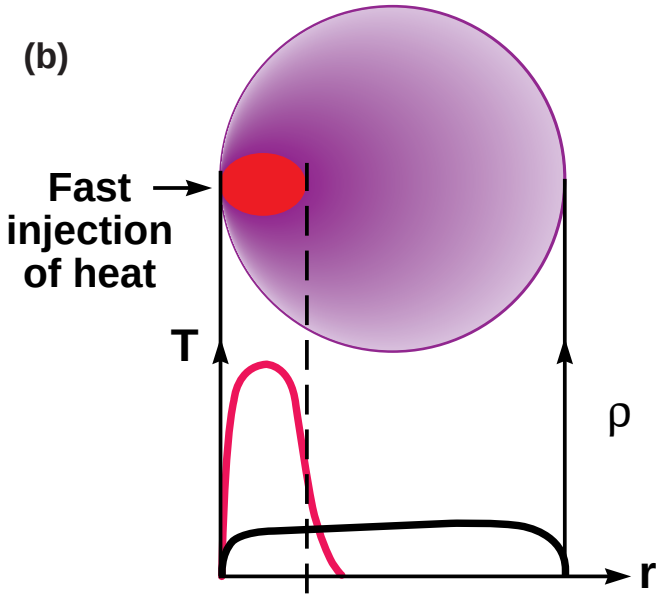

Fast-heated side spot ignites high-density fuel ball

$\rho_{hot} \approx \rho_{cold}$ (isochoric)

50-00-0397-0426Bbp01

Context: The *Fast Igniter* concept

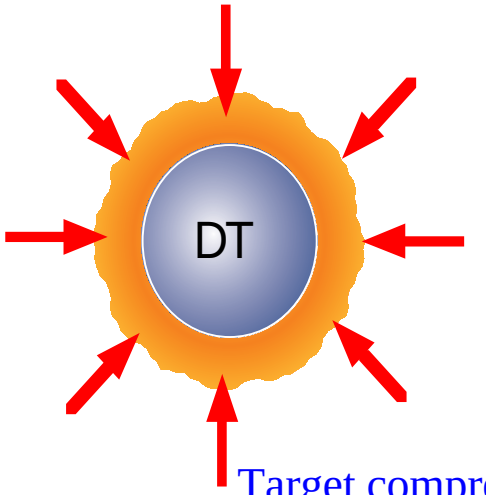

Target compression

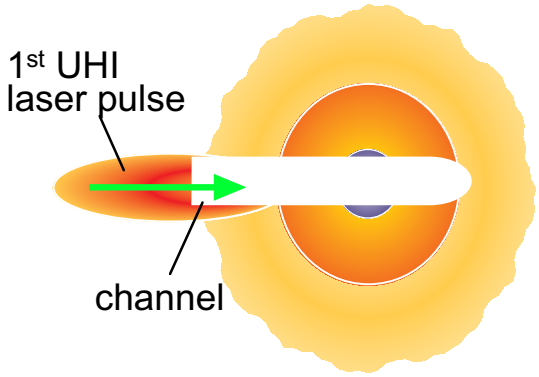

Under-dense channel hollowing

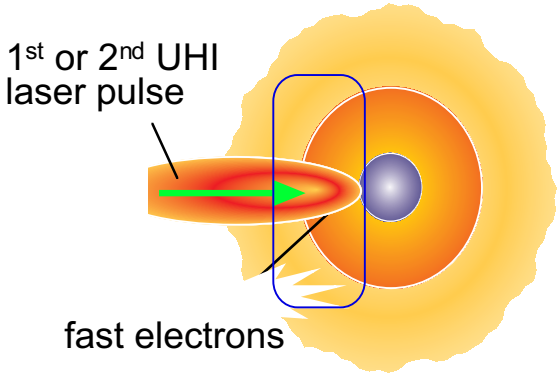

Fast electrons
generation
and transport

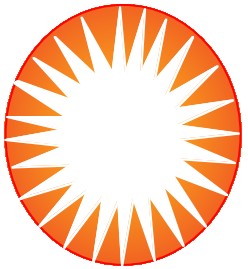

Target ignition

The physics of electron transport in dense plasma is complex - but central to many applications

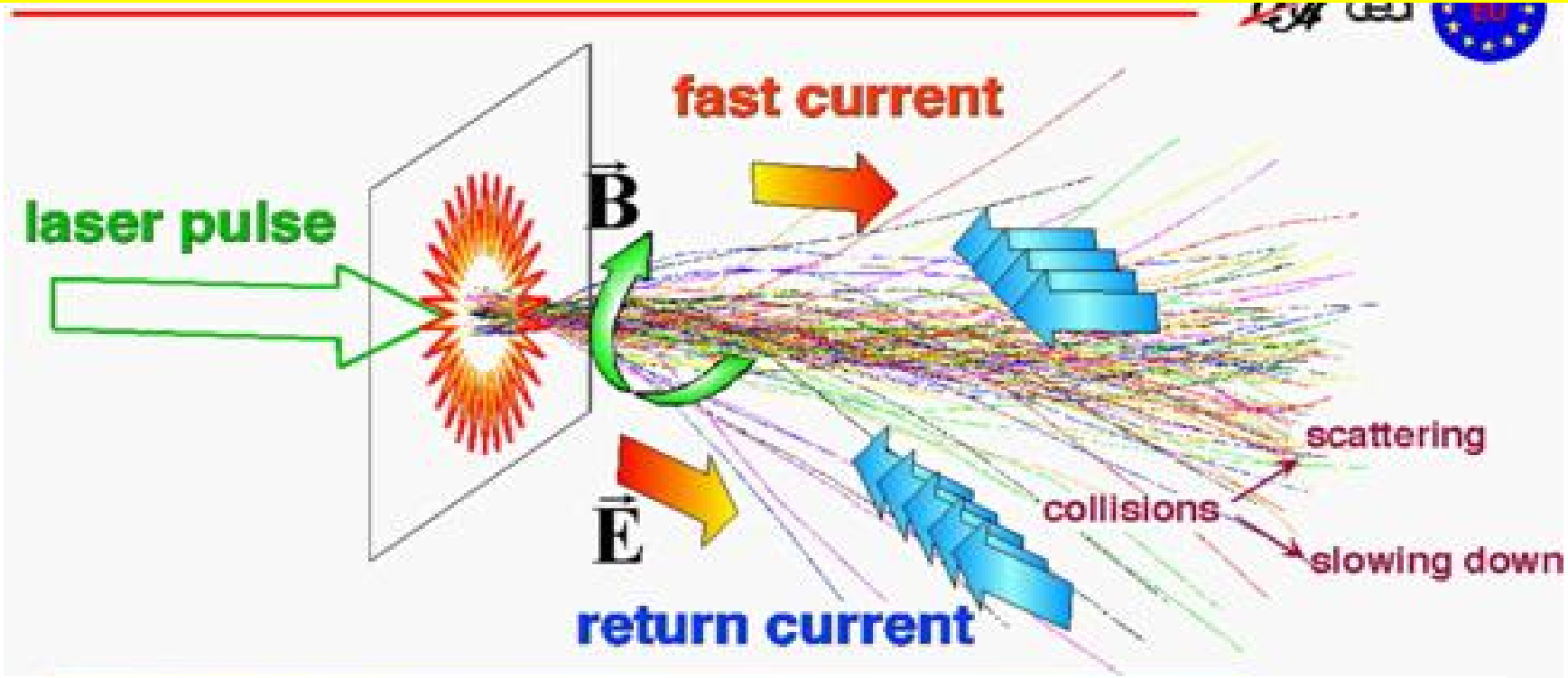

- Relativistic current cancelled by cold return current
- Net current < Alfven limit (17$\beta\gamma$ kA)
- Strong magnetic guiding , resistive E field and Weibel instability

LASER GENERATED ELECTRONS AT CRITICAL SURFACE MUST MIGRATE IN A COLLIMATED FASHION TO THE DENSE INTERIOR OF THE TARGET WITHOUT SPREADING

GENERAL ATOMICS

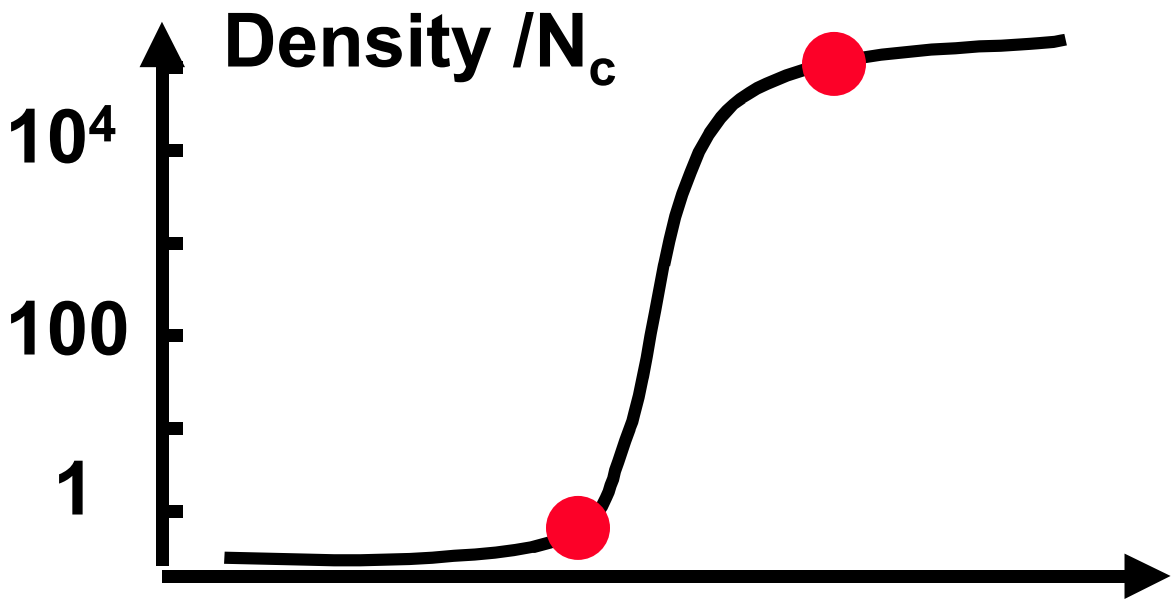

Anomalous
Energy loss ?

Shaping/collimating beam?

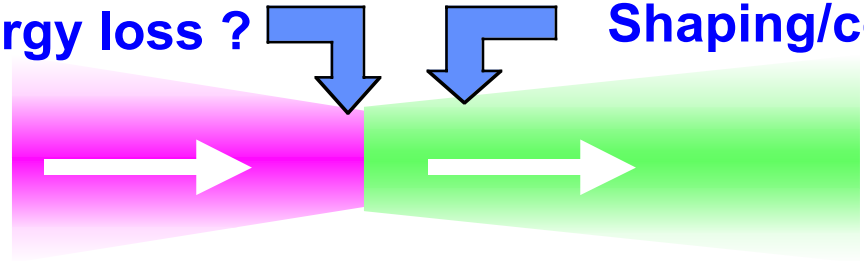

Laser Electrons

CHARGE TRANSPORT CODES SUGGEST THAT THE FI CONCEPT SHOULD WORK JUST FINE

GENERAL ATOMICS

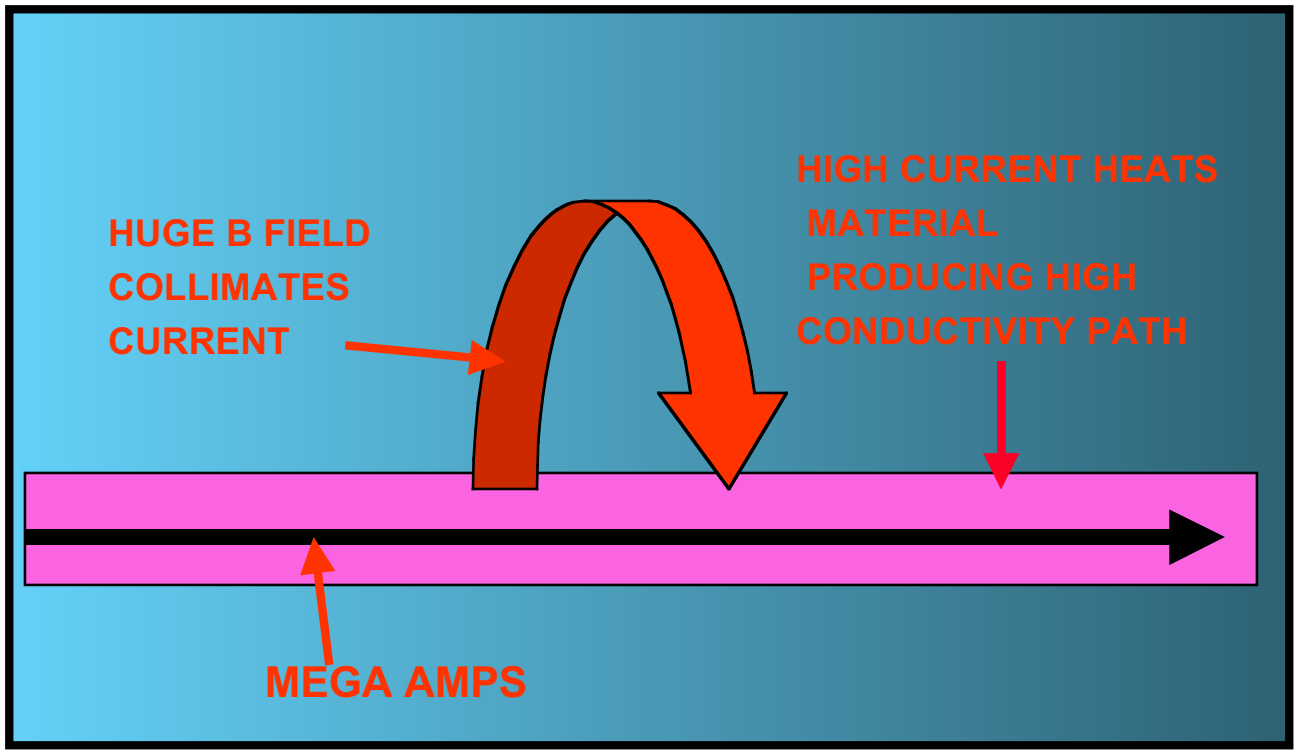

INCREASING DENISTY

NOTE: These codes always assume the current is already inside the material

Typical Kα 2-D image

GENERAL ATOMICS

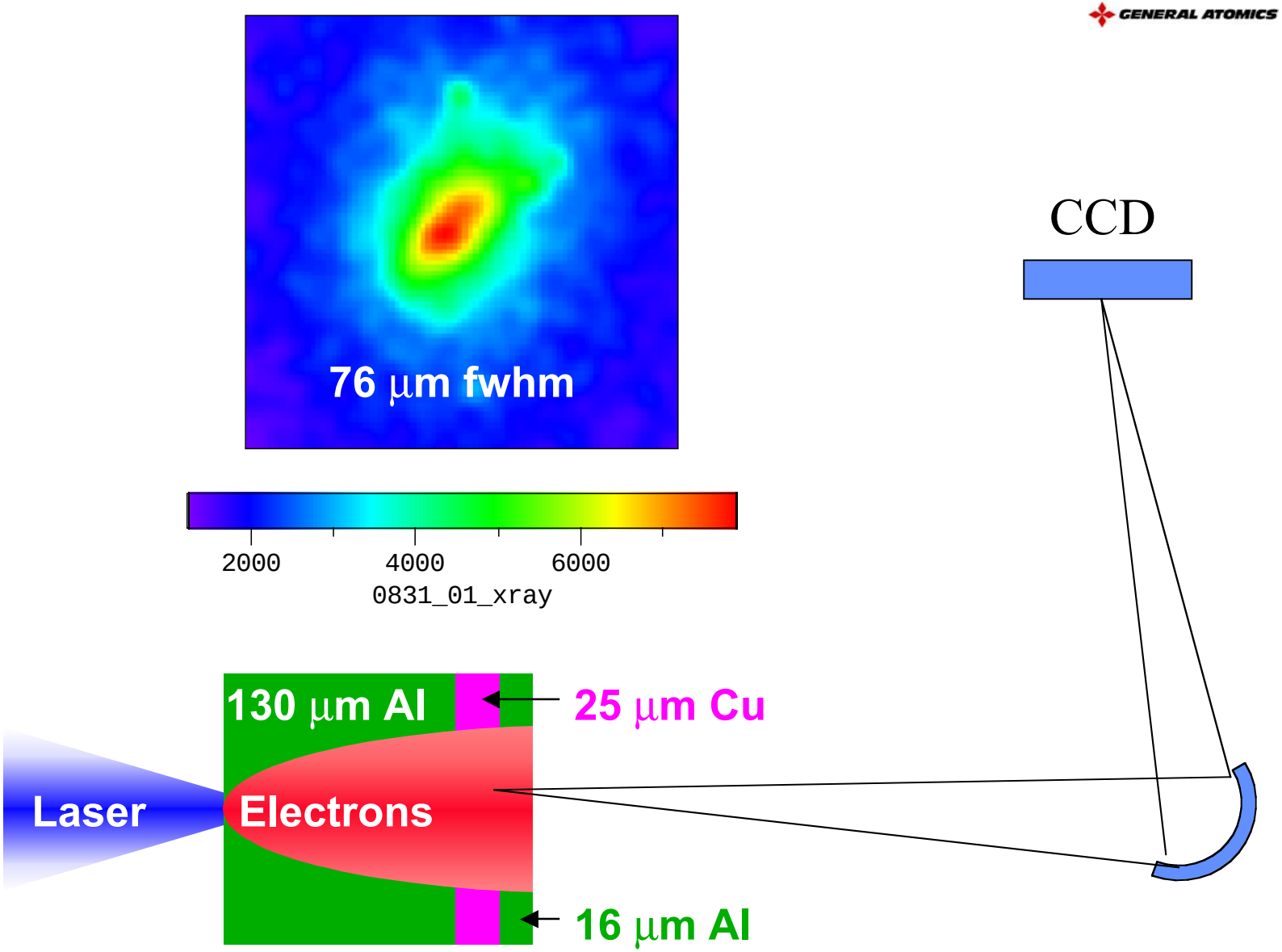

Our results were surprising and revealed essential non-understandings

GENERAL ATOMICS

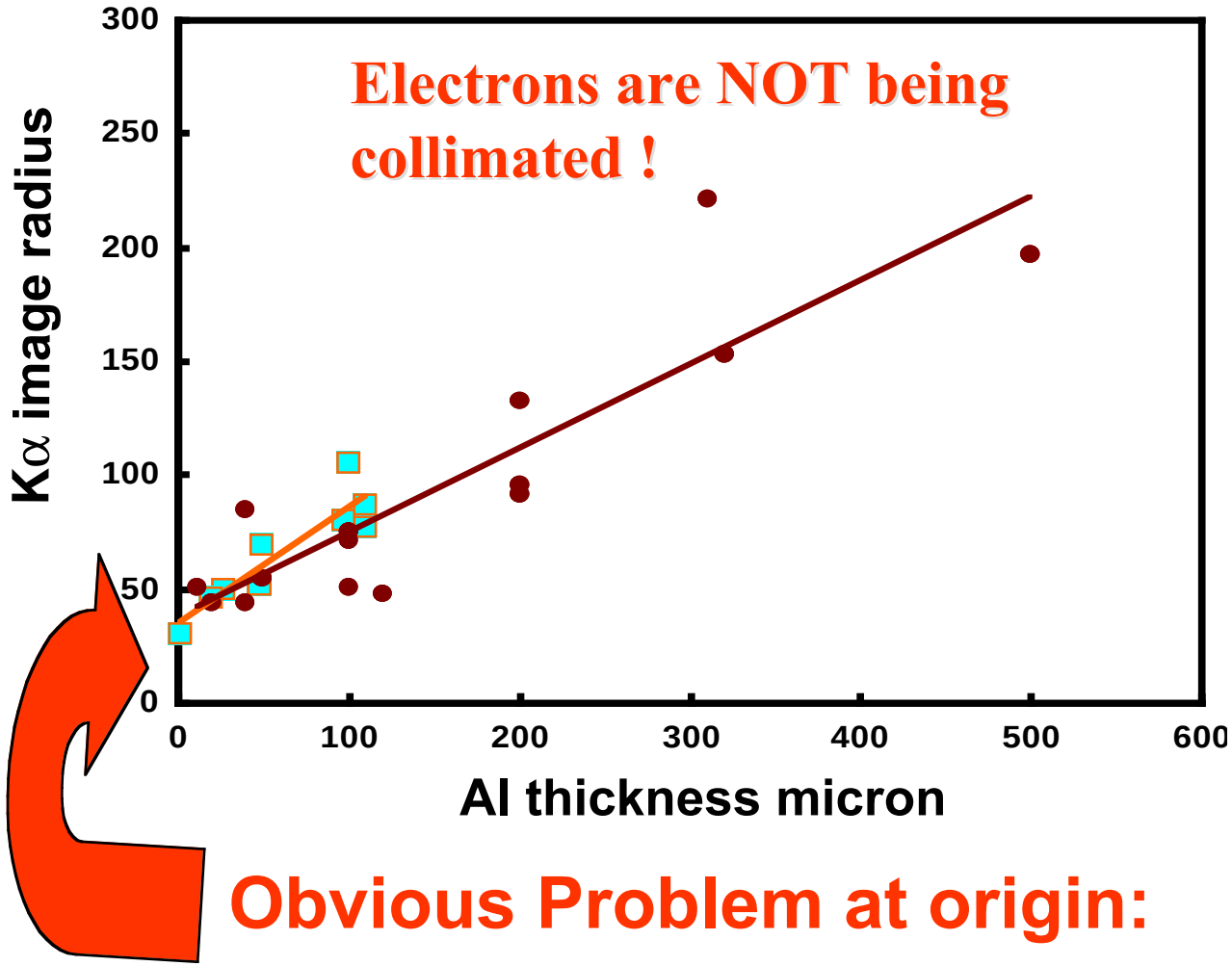

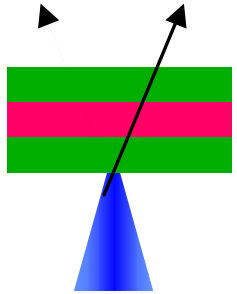

Obvious Problem at origin:

Laser radius: <10 _

Collimation of electron transport from laser to ignition hot spot sets efficiency ε

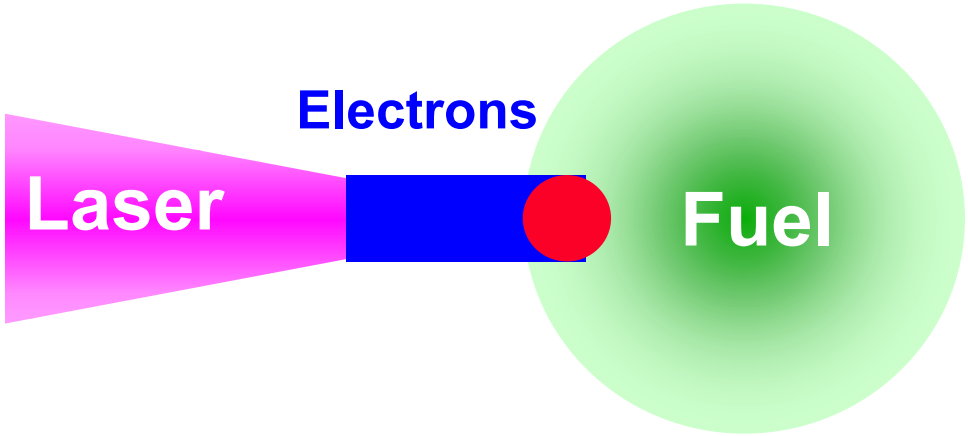

- Ignition energy and laser intensity scale as $\varepsilon^{-1} = (\phi_b/\phi_s)^2$

- Ideal collimated
- Divergent

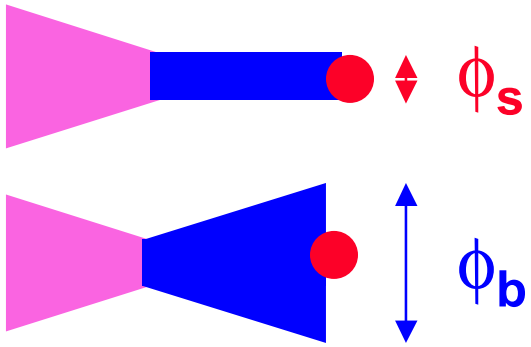

Application of "side view" techniques to monitor electrons within material

GENERAL ATOMICS

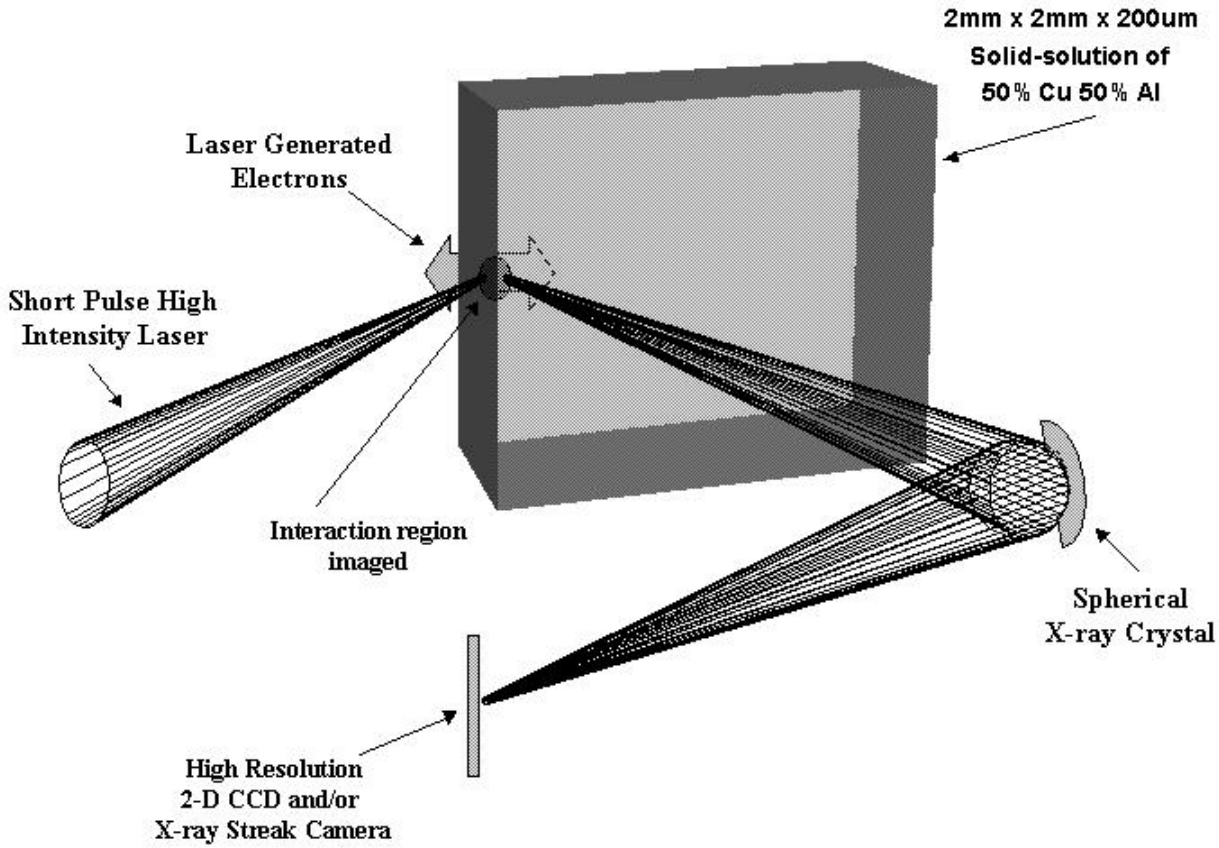

Side view confirms that electrons are NOT collimated

AL ATOMICS

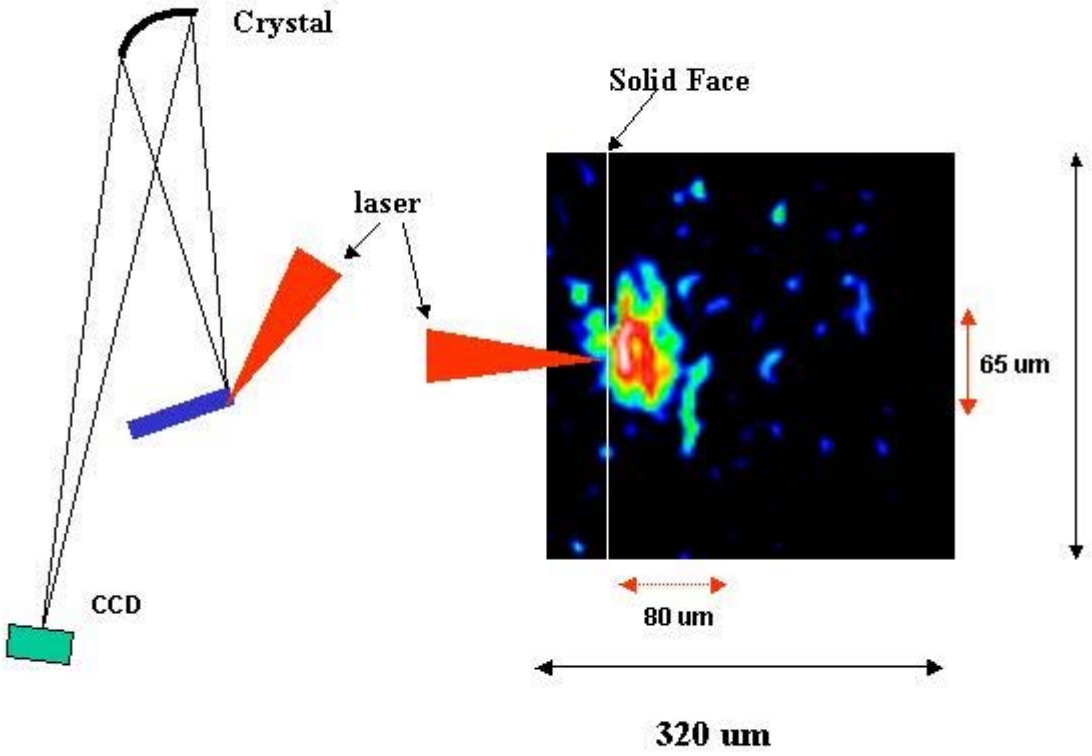

Essentially, real Laser/matter interactions exist in a messy environment

GENERAL ATOMICS

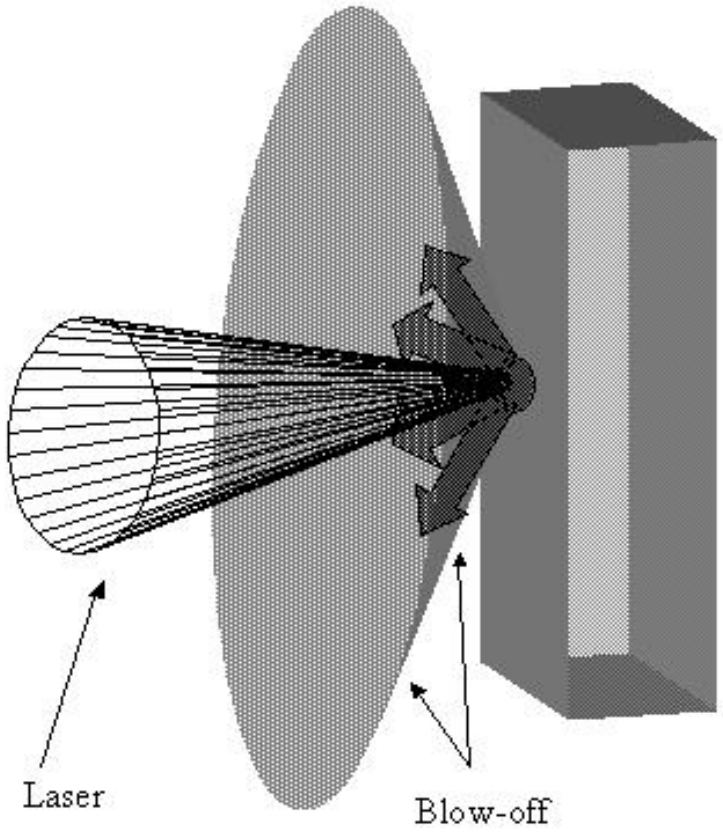

Real Laser/solid material interfaces are dominated by complex physics

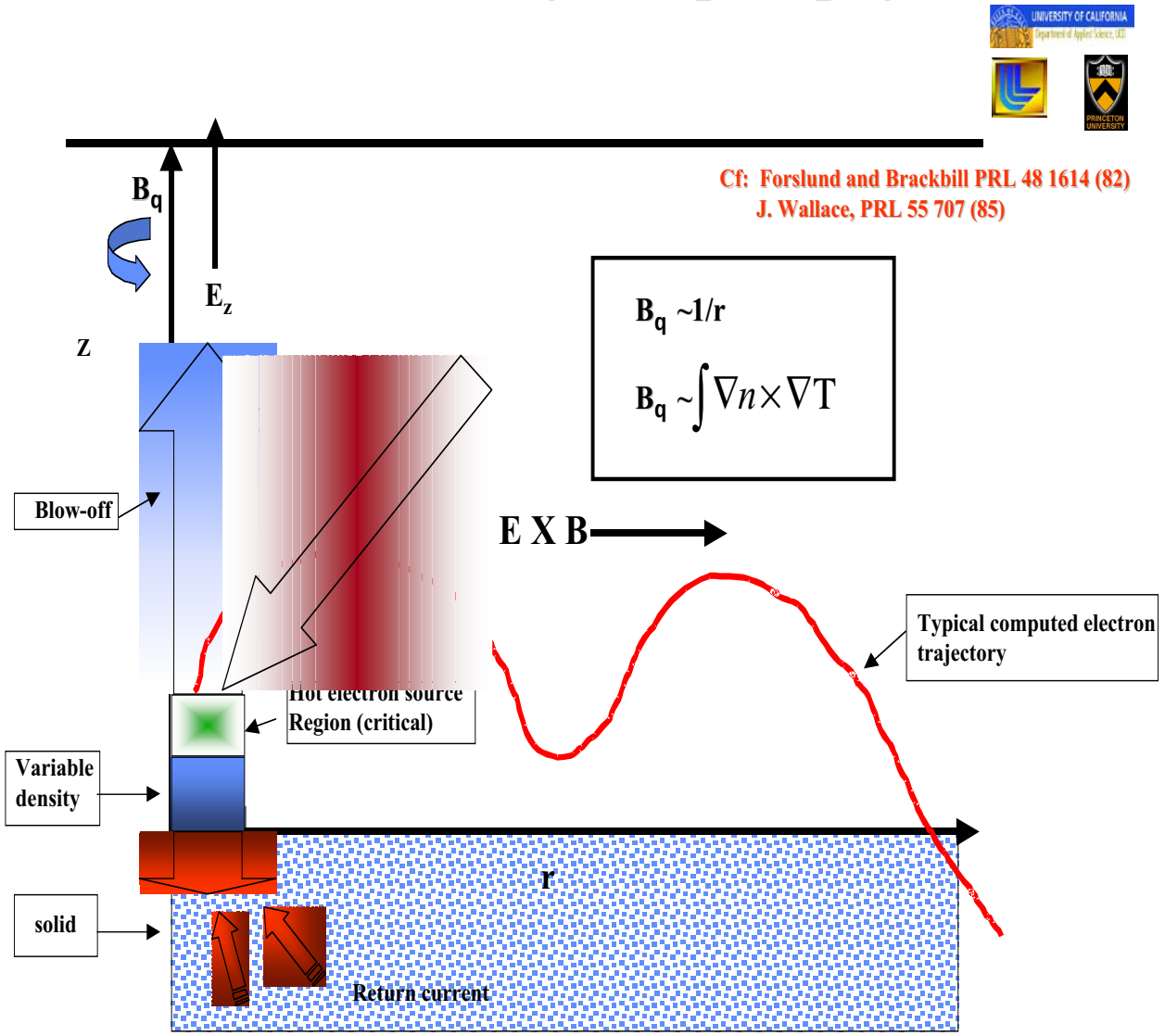

23

We are developing a new tool to help understand the ionization mechanism: time resolved proton radiography

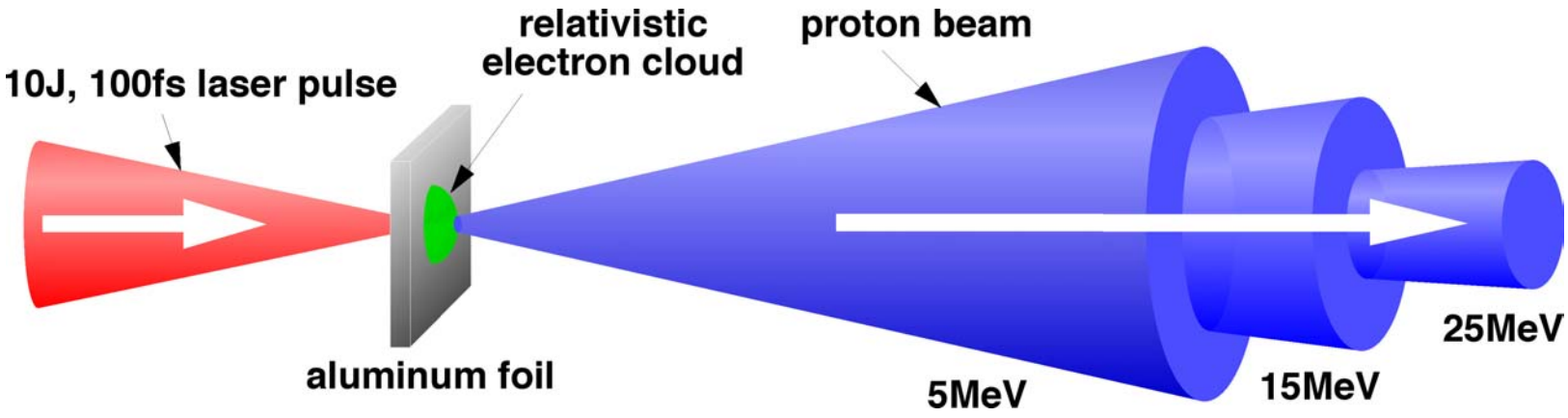

Highly collimated (1-20°)
High flux (few % laser energy)
Energetic (upto 25MeV)
Temporally short (few ps)

Example of proton radiography's sensitivity to E & B Fields: Perfect complement to x-ray radiography

GENERAL ATOMICS

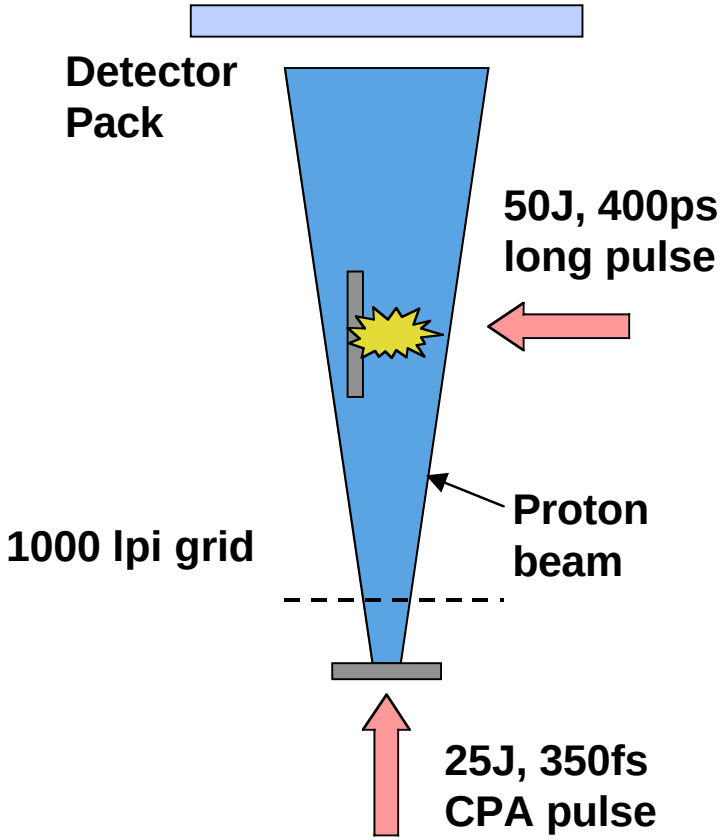

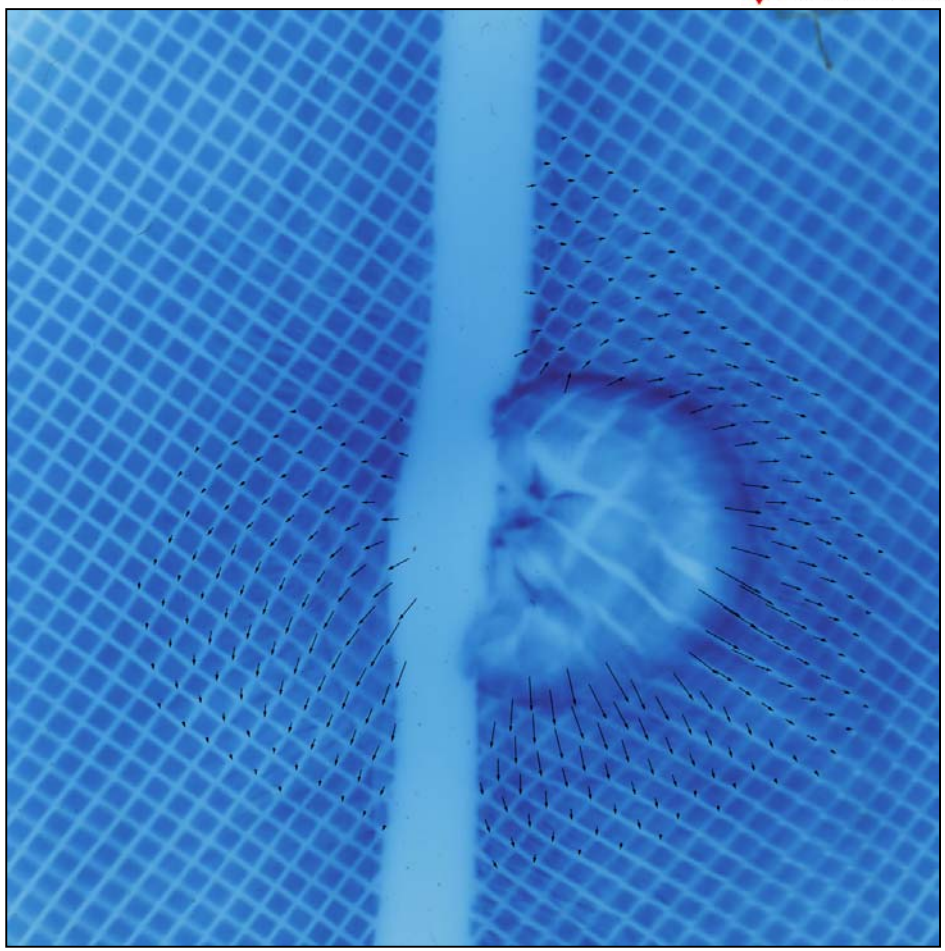

Experiment at Laboratoire pour l'Utilisation des Lasers Intenses, France

PK Patel *et al.*

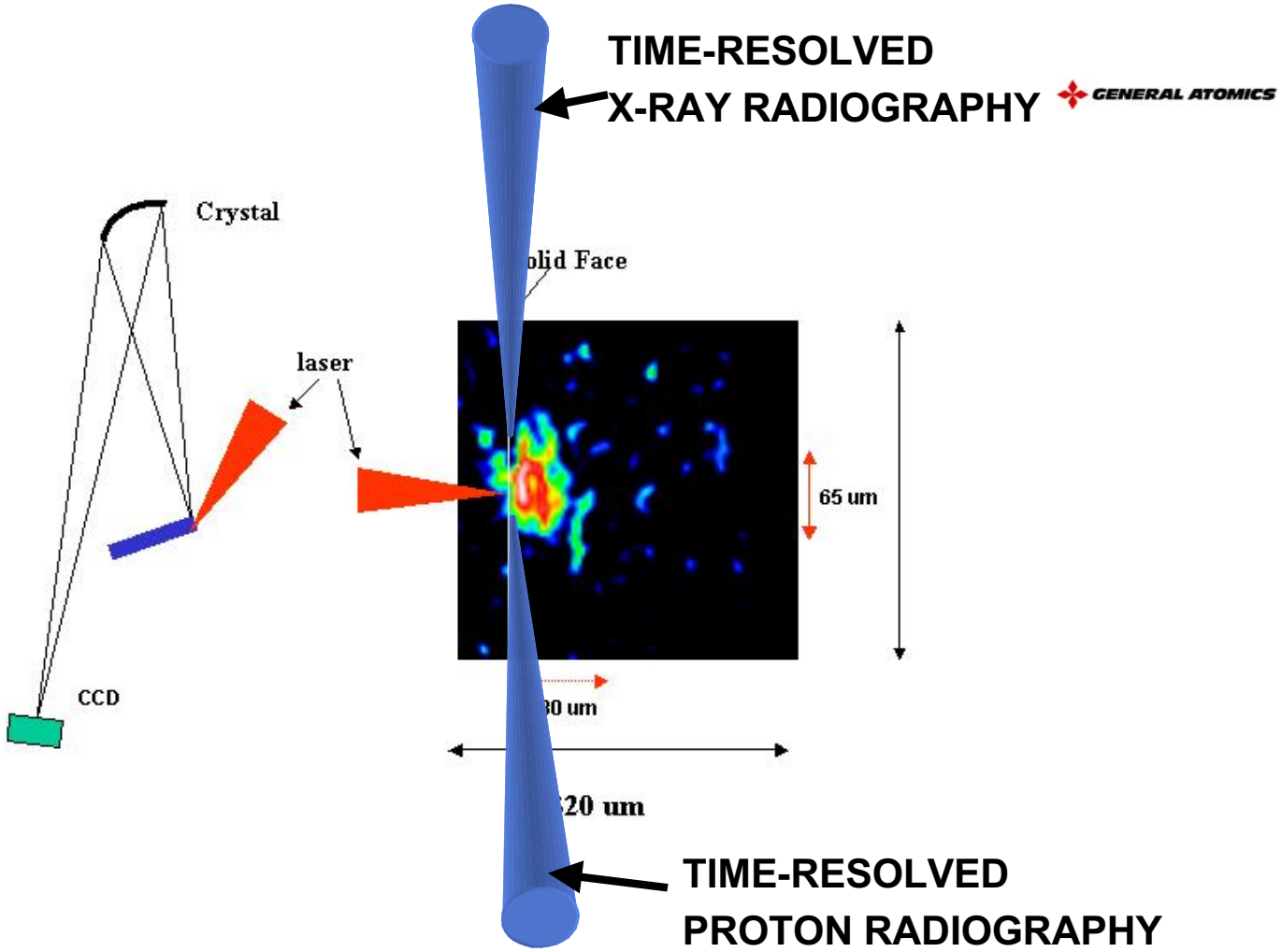

Next generation of transport experiment will use time-resolved X-ray and Proton radiography with-time resolved Kα imaging

Cone inserted into targets may be the only method of injecting electrons into the dense core

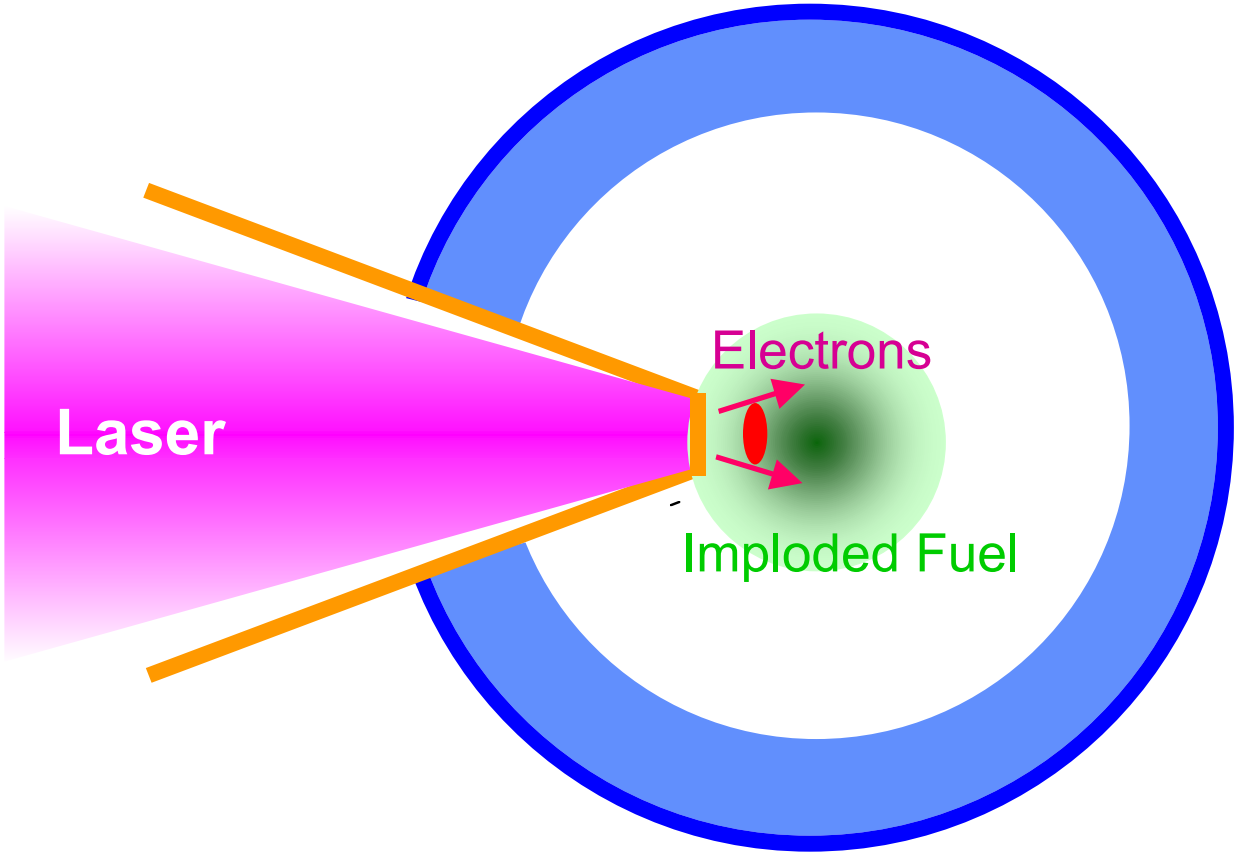

Summary US Roadmap for IFE by Fast Ignition

GENERAL ATOMICS

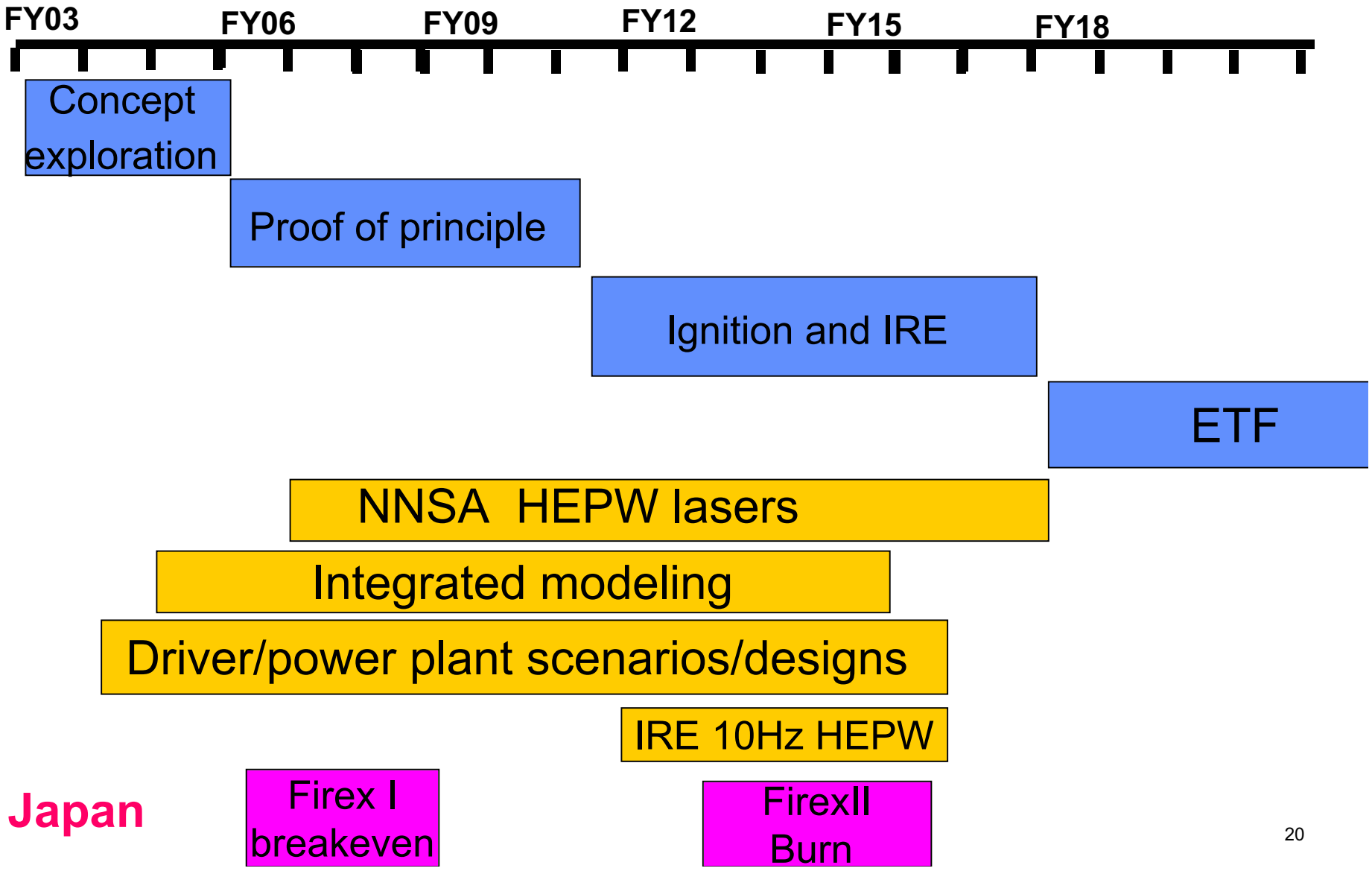

- **Relativistic quiver energy of a free electron is**

$(\gamma\text{-}1)\, m_e c^2$ where $\gamma=(1+I\lambda^2/1.4\times10^{18}\mathrm{Wcm}^{-2})^{1/2}$

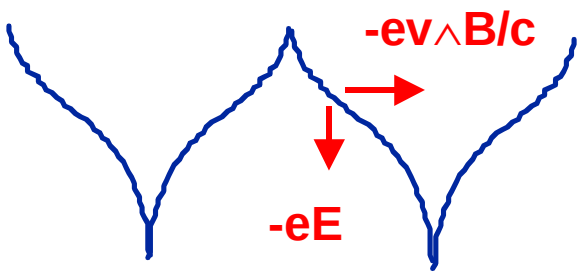

Trajectory has forward motion due to magnetic force in plane polarized beam

- **At 10^{21} Wcm^{-2} quiver energy is 10 MeV scaling as $I^{1/2}$**
- **Electric field is 100 kV/nm or 180 a.u. - scaling as $I^{1/2}$**

field ionizes bound electrons with up to 4 keV binding energy

GENERAL ATOMICS

- Relativistic quiver energy E_Q of a free electron is

  $(\gamma\text{-}1)\ m_e c^2$ where $\gamma=(1+I\lambda^2/1.4\times10^{18}\mathrm{Wcm}^{-2})^{1/2}$

- Relativistic mass increase causes self focusing
- Relativistic electron current produces G gauss mag. fields
- Subcritical density acceleration - electrons to >> E_Q
- Critical density absorption - electrons at E_Q
- Light pressure (300Gbar at 10^{21} $\mathrm{Wcm}^{-2)}$ drives critical density ions to >1 MeV/nucleon
- Electron current (100MA , 10MeV at 1PW) is 300x Alfven limit and initiates Weibel instability

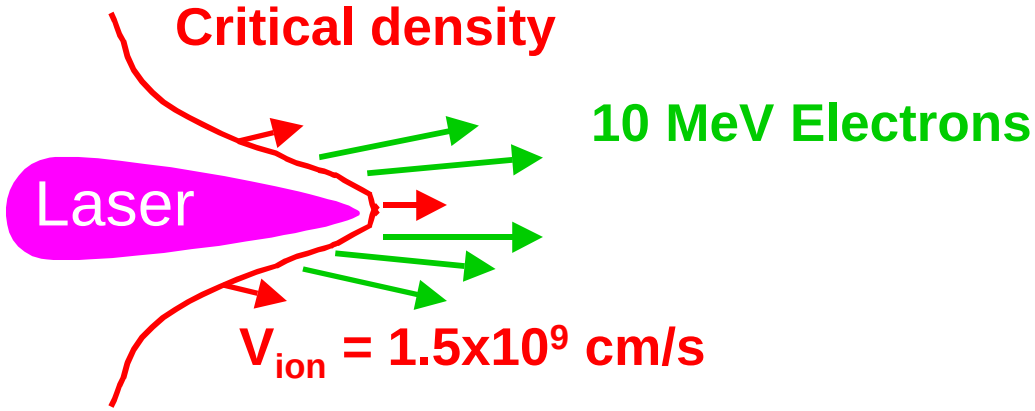

Highly unstable !

- **Light pressure at 10^{21} Wcm^{-2} = 300 Gbar - scaling as I**
  drives protons at > critical density to 1MeV energy

- **Absorption at critical density creates intense relativistic electron source of energy similar to the quiver energy**
  e.g electron current for 1 PW power at 10 MeV is
  100 MA from a 10 micron spot = 300x Alfven limit

Hole boring through 10x overdense plasma
3D Particle-In-Cell Simulations

GENERAL ATOMICS

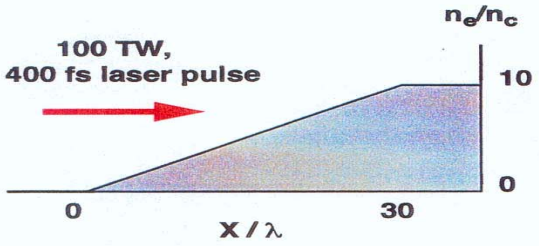

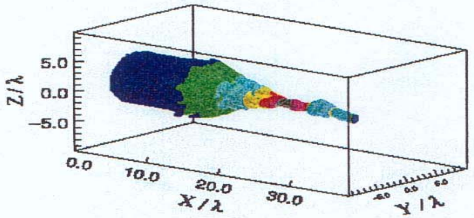

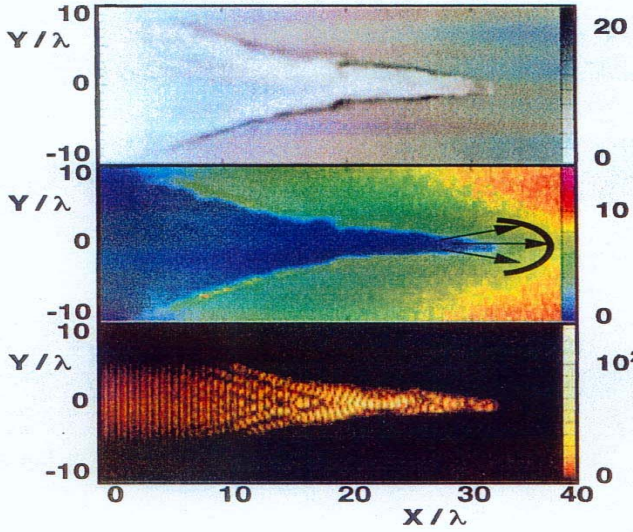

The super-channel *is stably formed* at far overcritical densities

Fast electrons generated in the channel modify refraction index already *in front of laser beam*

Incident intensity of 5×10^{19} W/cm^2 is amplfied up to 10^{21} W/cm^2 *in the super-channel*

The petawatt laser uses chirped pulse amplification in one beam line of the 10 beam Nova Laser

GENERAL ATOMICS

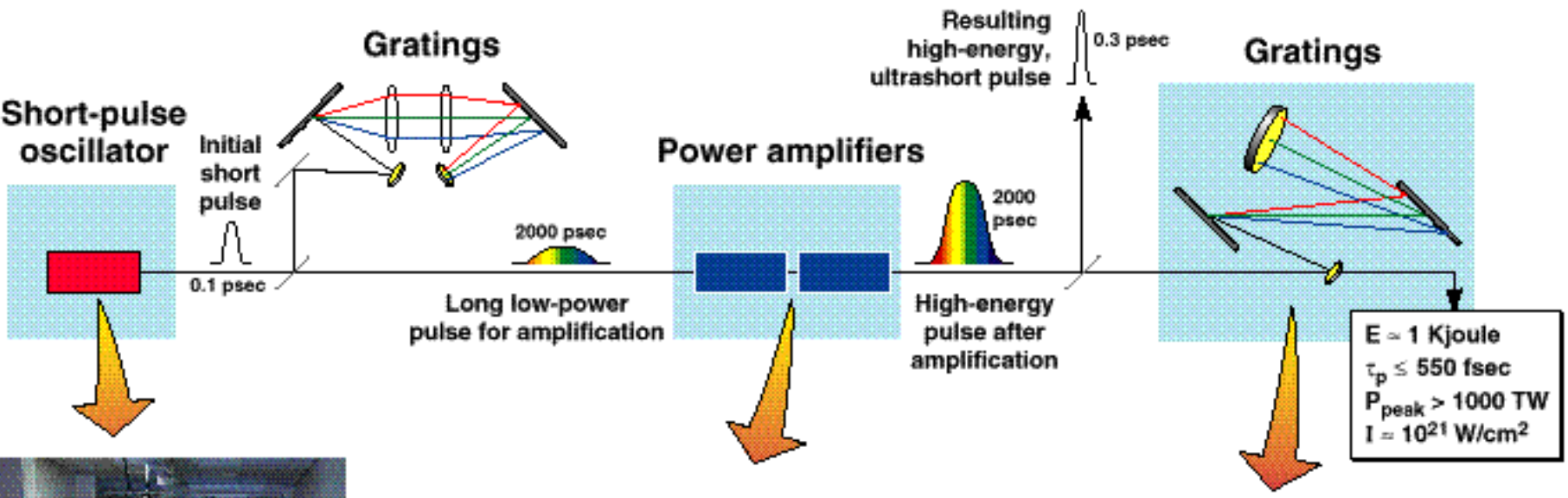

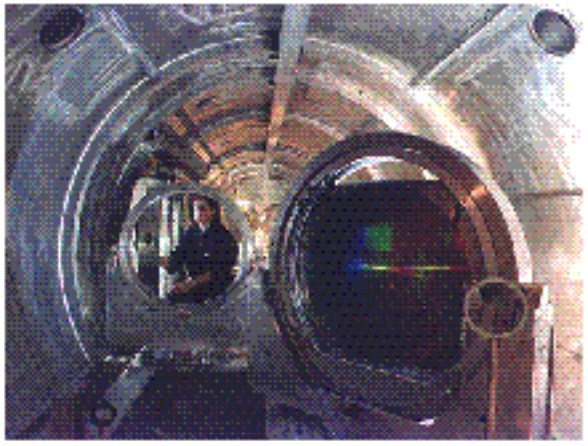

New high resolution imaging of Cu and Ti Kα and 80 nm XUV Planckian emission

GENERAL ATOMICS

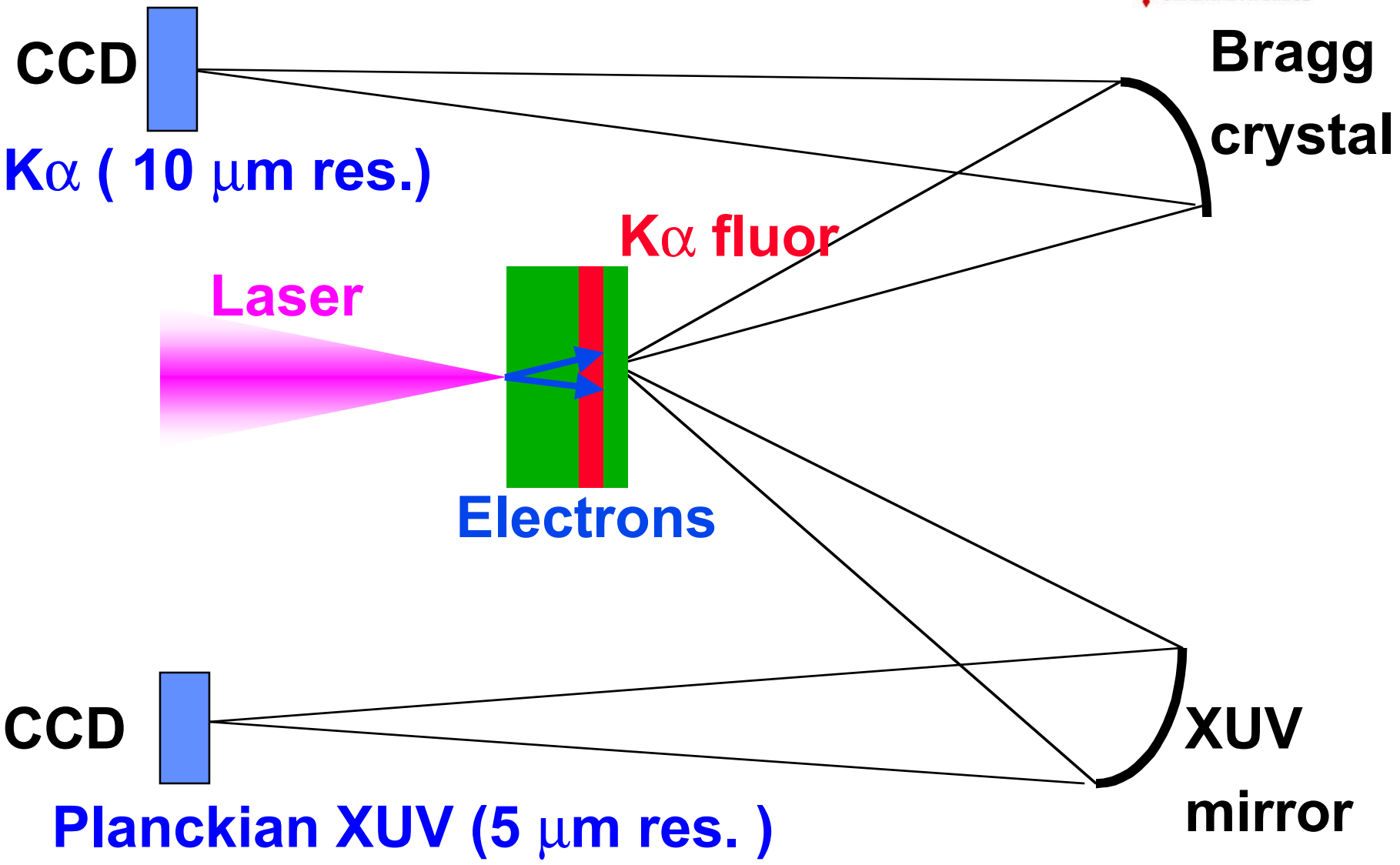

Best case Kα (electron flux) and XUV (heating) patterns are similar (RAL)

GENERAL ATOMICS

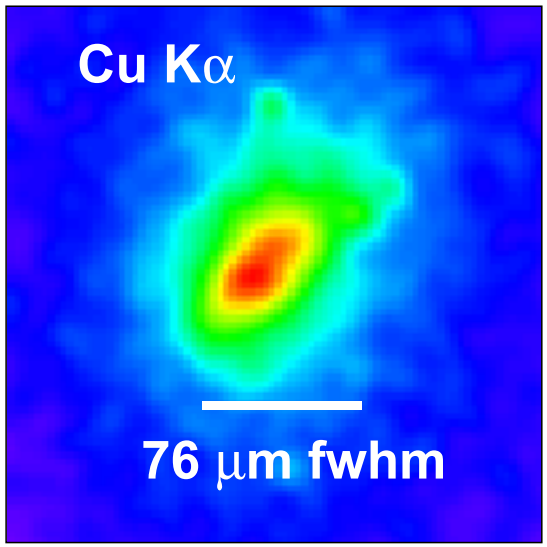

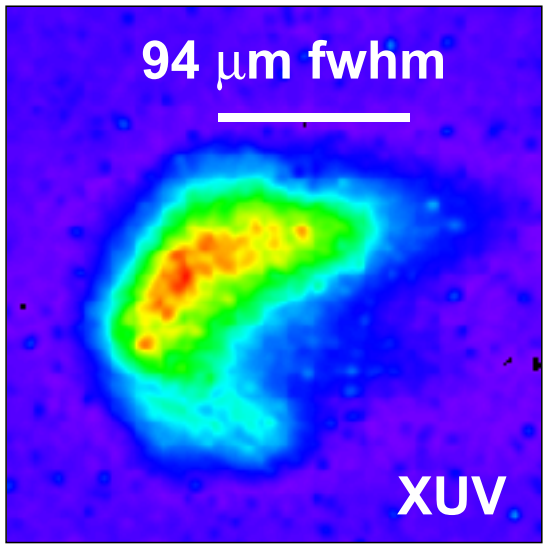

But fwhm >> laser focal spot

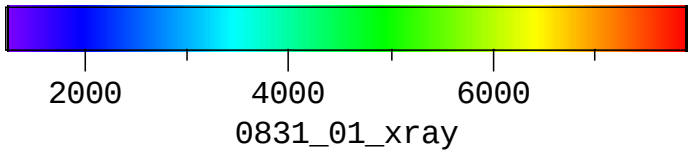

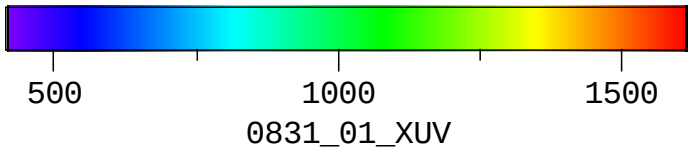

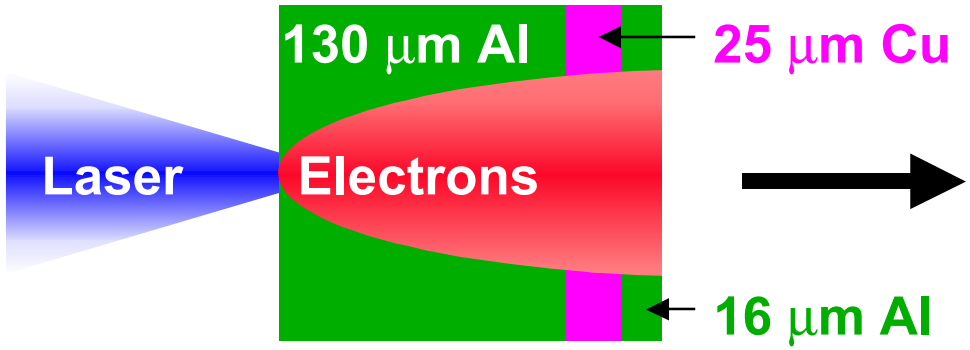

Images of 8keV Cu Kα and 18 nm Planck XUV RAL laser

LULI and RAL Kα data show similar cone angle and minimum radius via Al layer

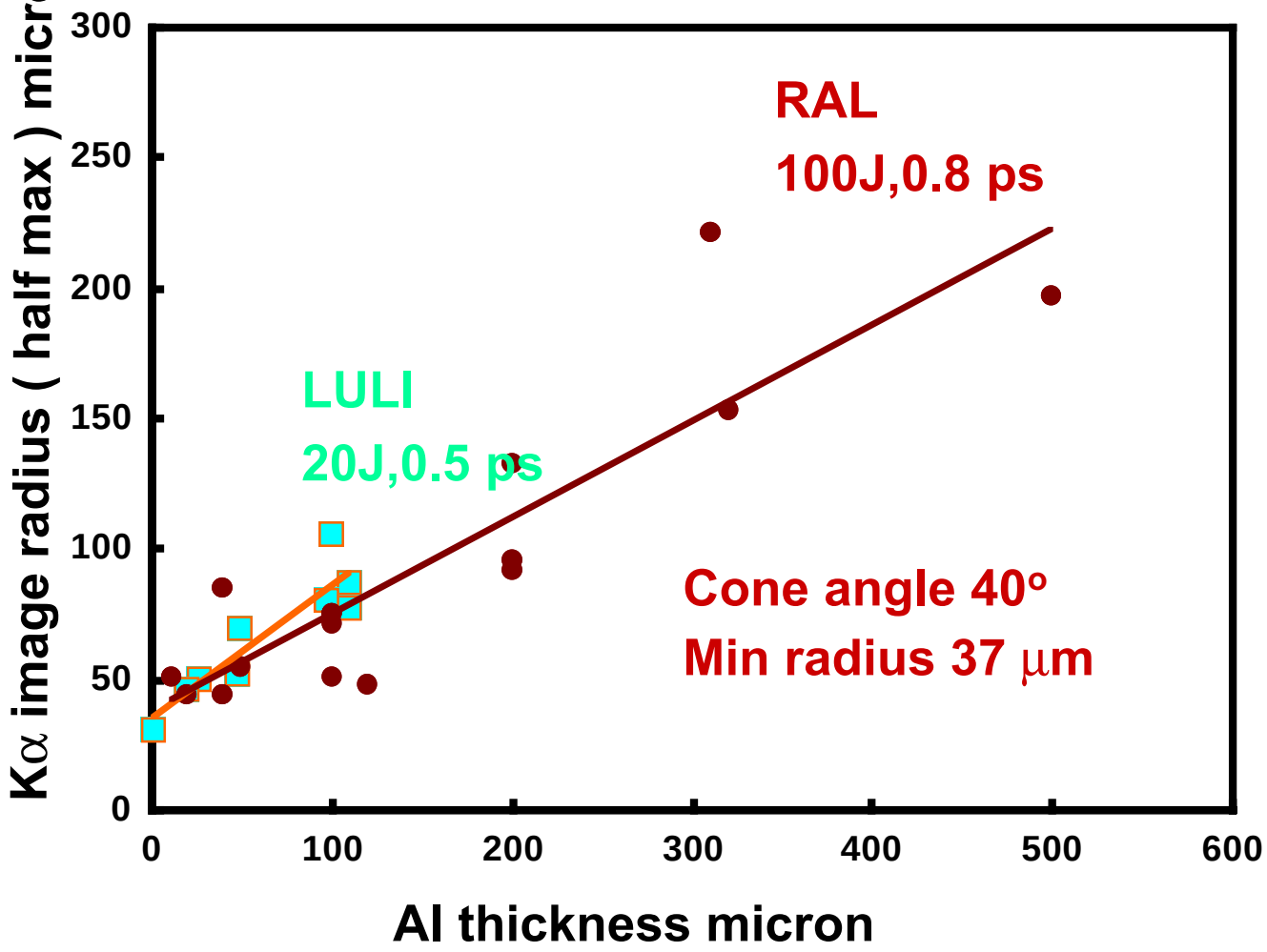

GENERAL ATOMICS

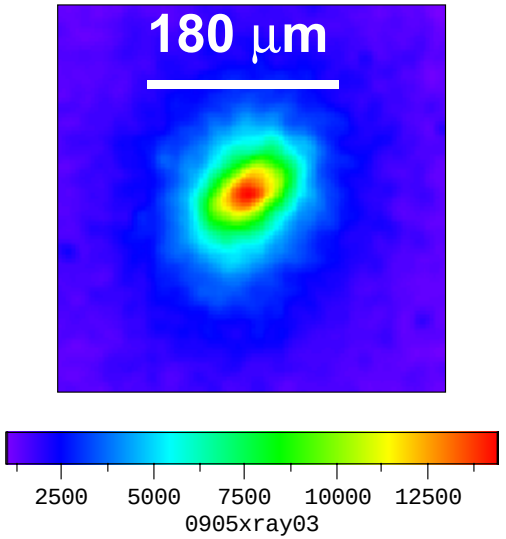

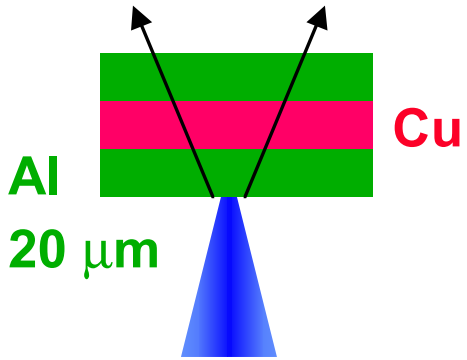

Electron transport in CH target shows beam break up with 80° divergence (RAL)

GENERAL ATOMICS

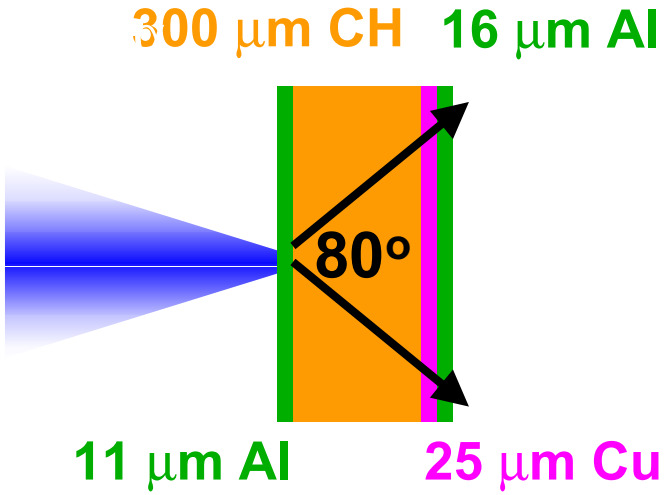

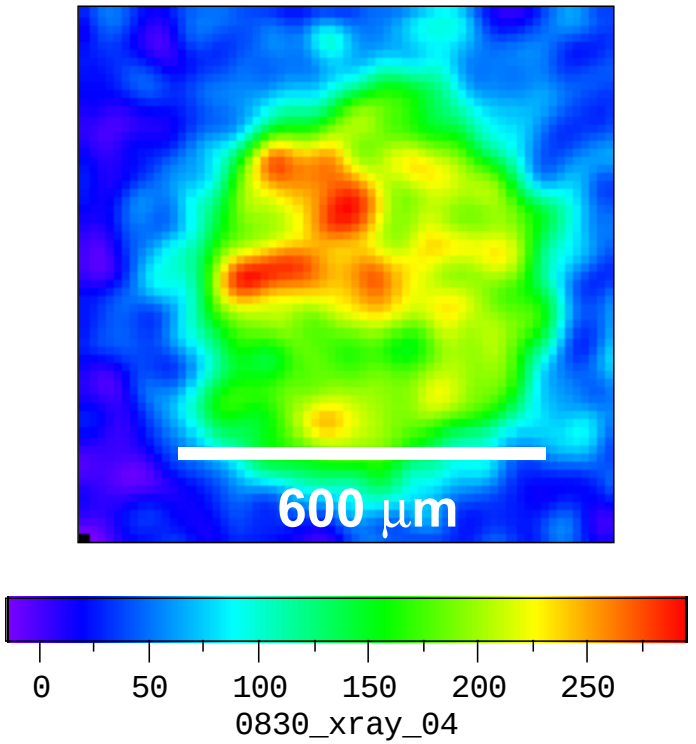

Image of 8 keV Cu Kα

Due to CH being initially an insulator?

LLNL PETWATT
"HEATING" RINGS
(CF KOCH THIS WORKSHOP)

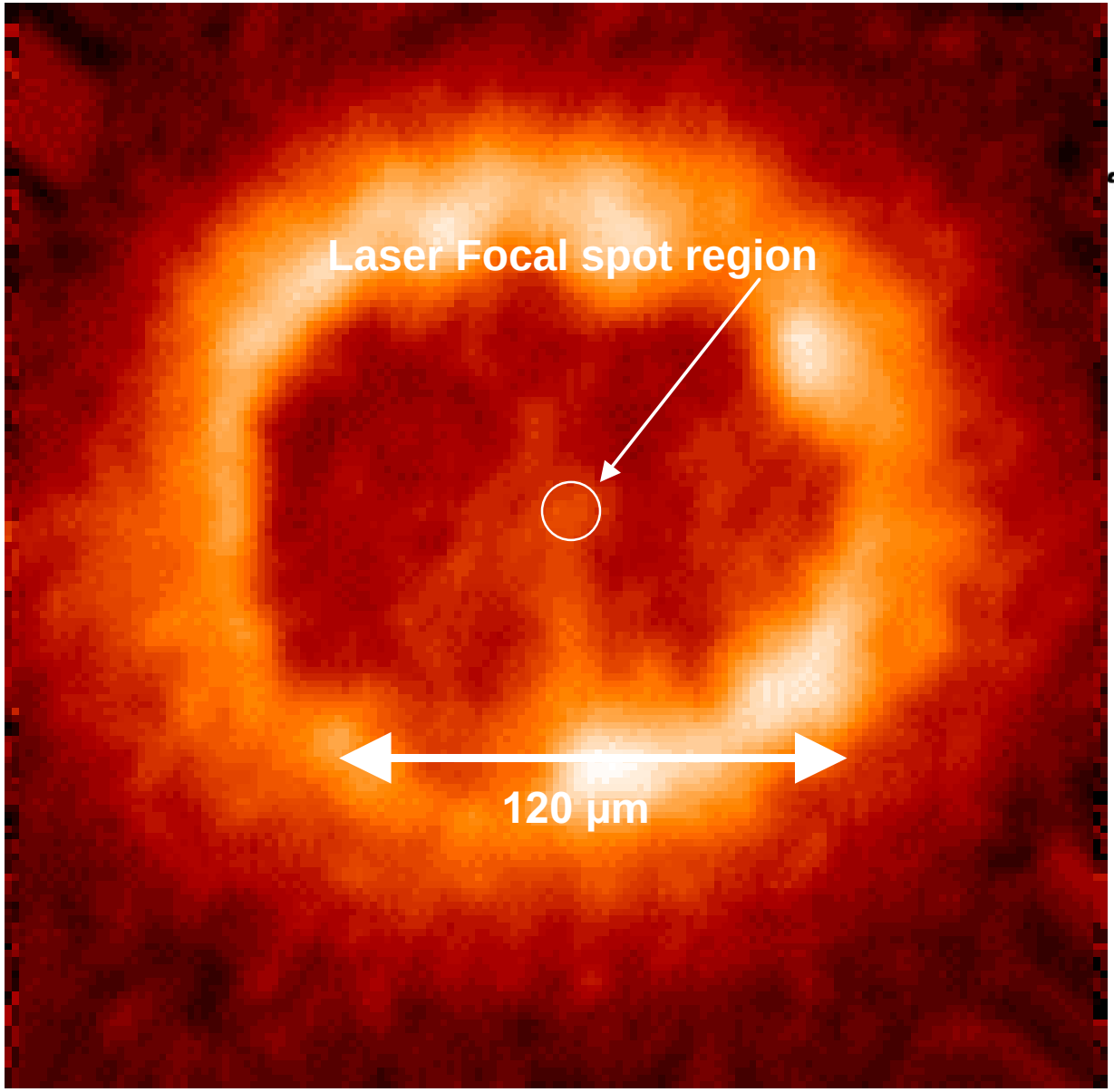

The Primary Diagnostic is a Radiochromic Film Cone:
Tantalum Filtered-Excellent Dynamic Range ~10^4

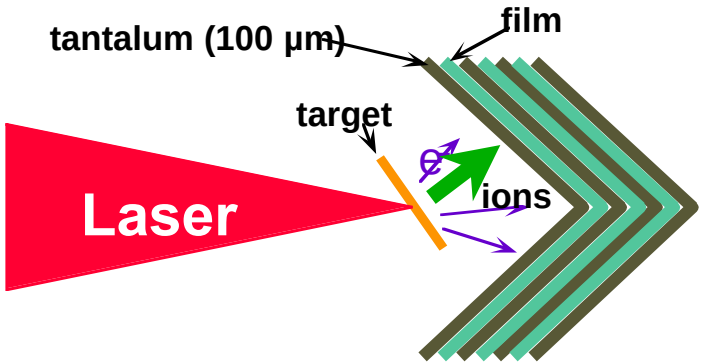

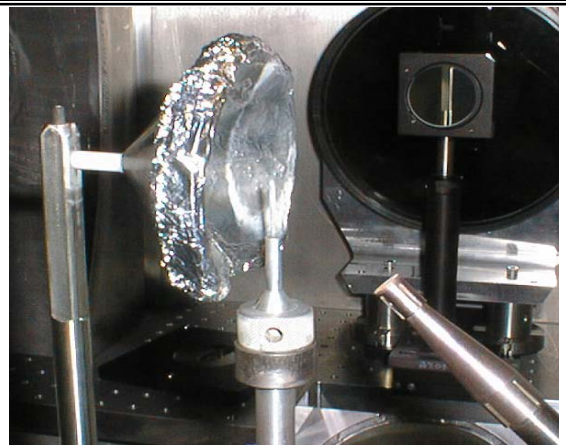

Pre-Shot Setup

Spectral Response

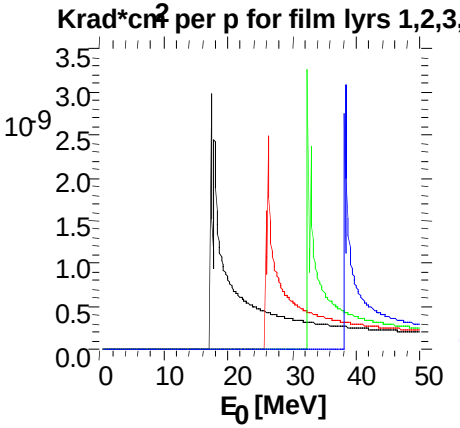

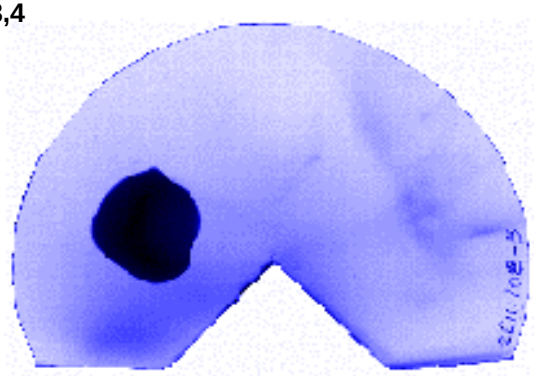

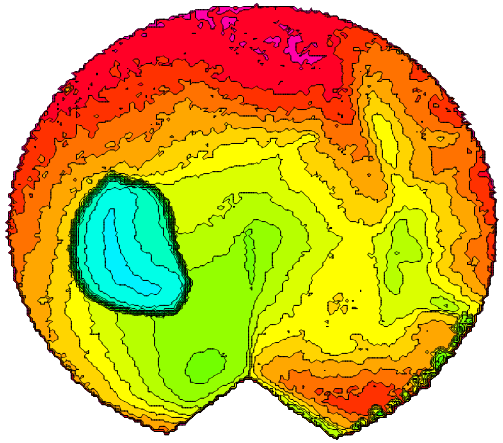

False Color Helps With Low and High Energy Deposition Visualization

rasnavely_apsdpp99

Schematic 1-D model

GENERAL ATOMICS

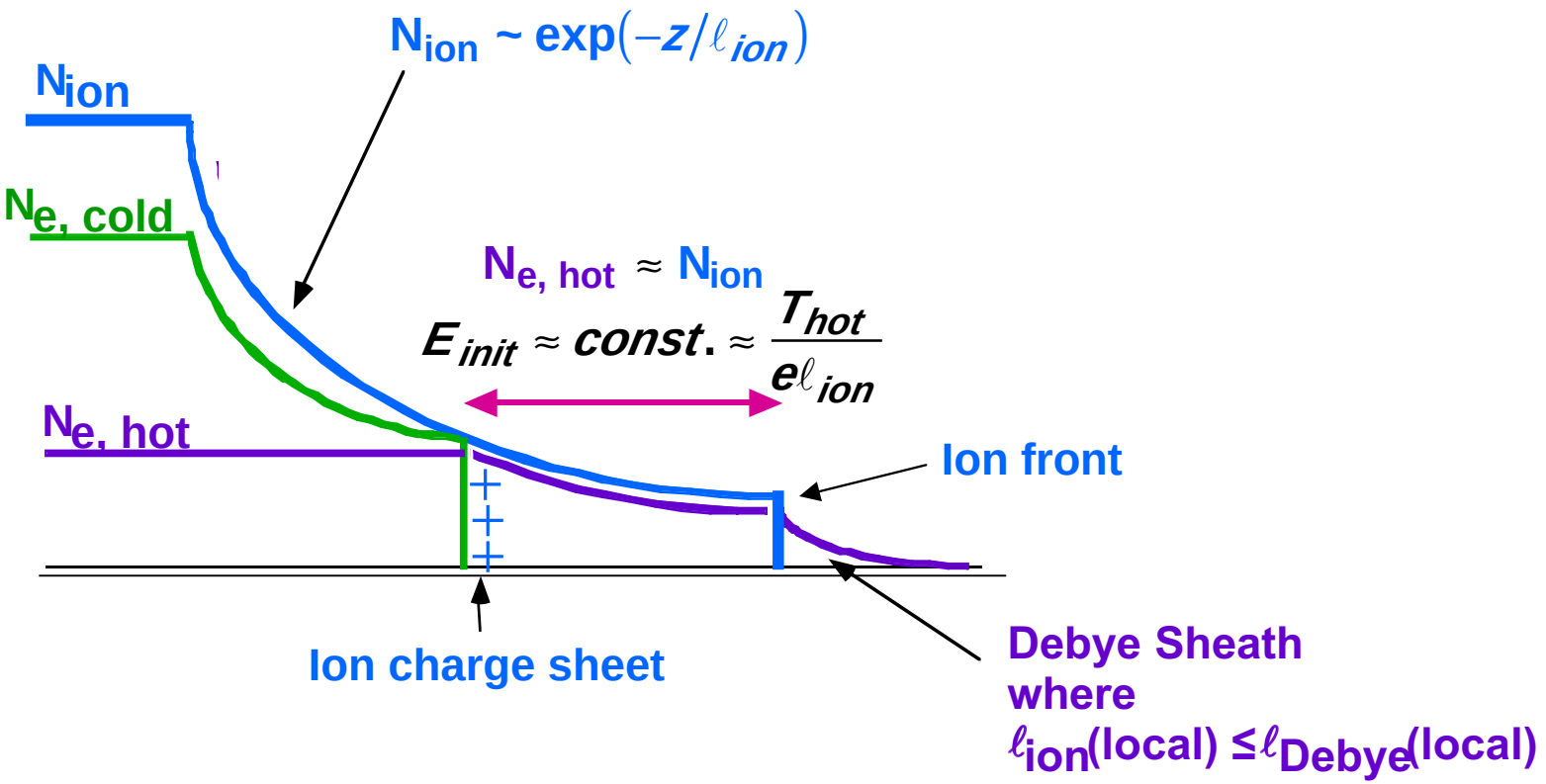

Ion acceleration continues until hots are energetically depleted — by dE/dx or by accelerating ions — in a few ps.

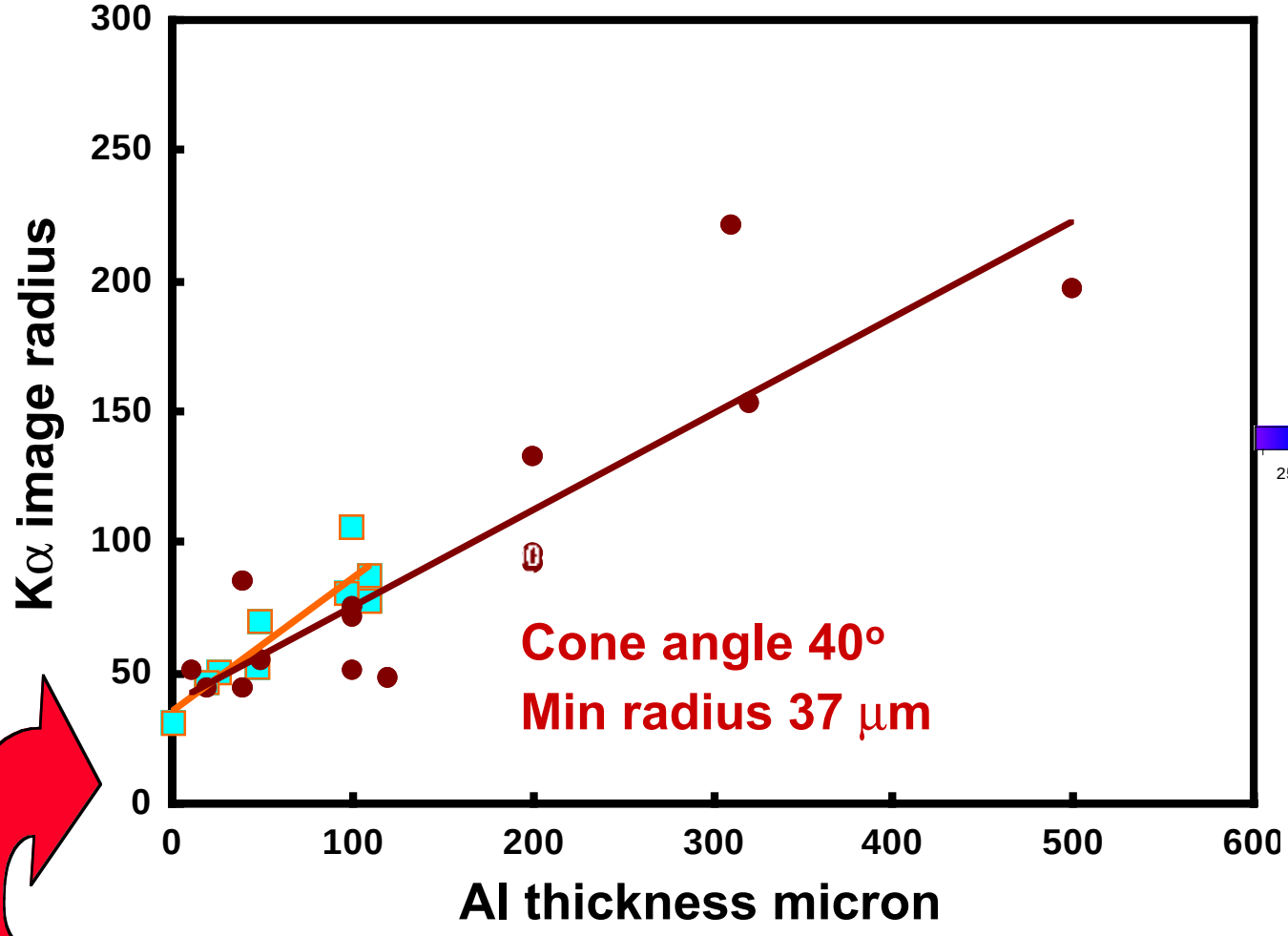

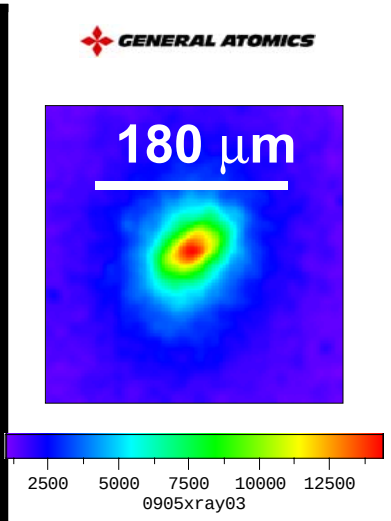

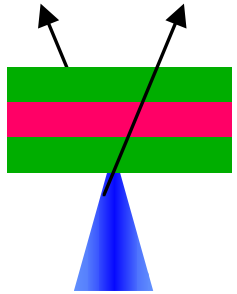

Obvious Problem: Laser radius: <10 _

Ever-present prepulse creates plasma on front (laser side) of target, measured by interferometry.

Time = To-80ps

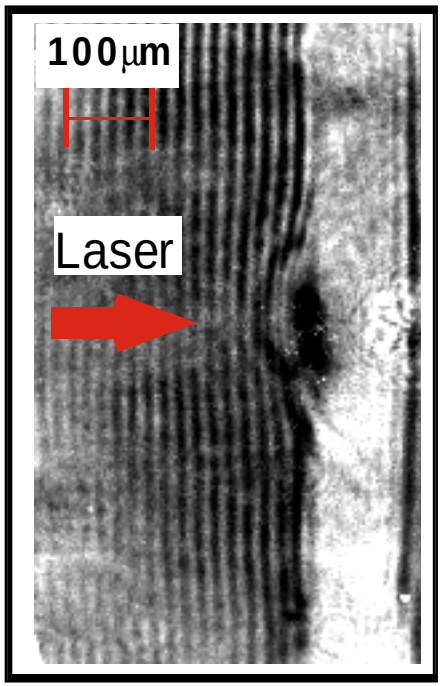

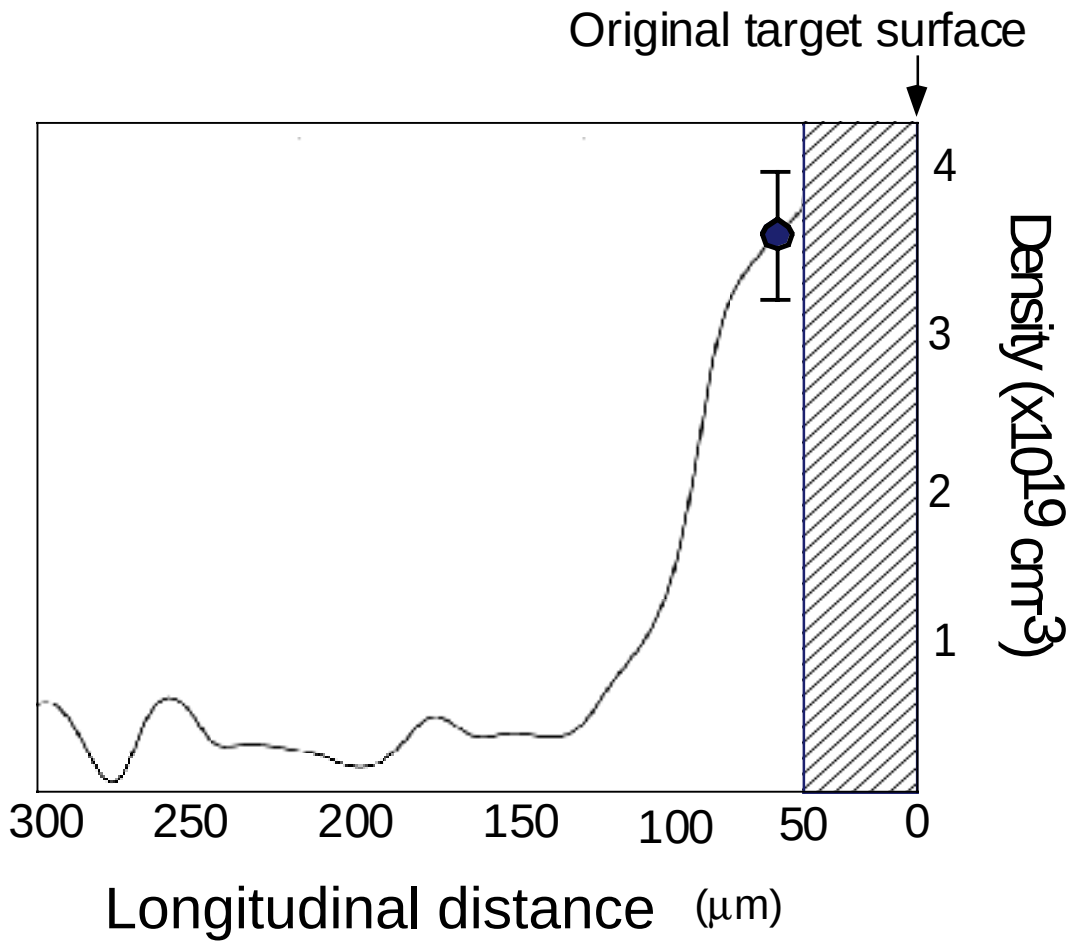

Target : 50μm CH

#29022311; E ~ 600J

τ_p = 5ps; I ~ 5x10^{19} Wcm^{-2}

GENERAL ATOMICS

Cf: Forslund and Brackbill PRL 48 1614 (82)
J. Wallace, PRL 55 707 (85)

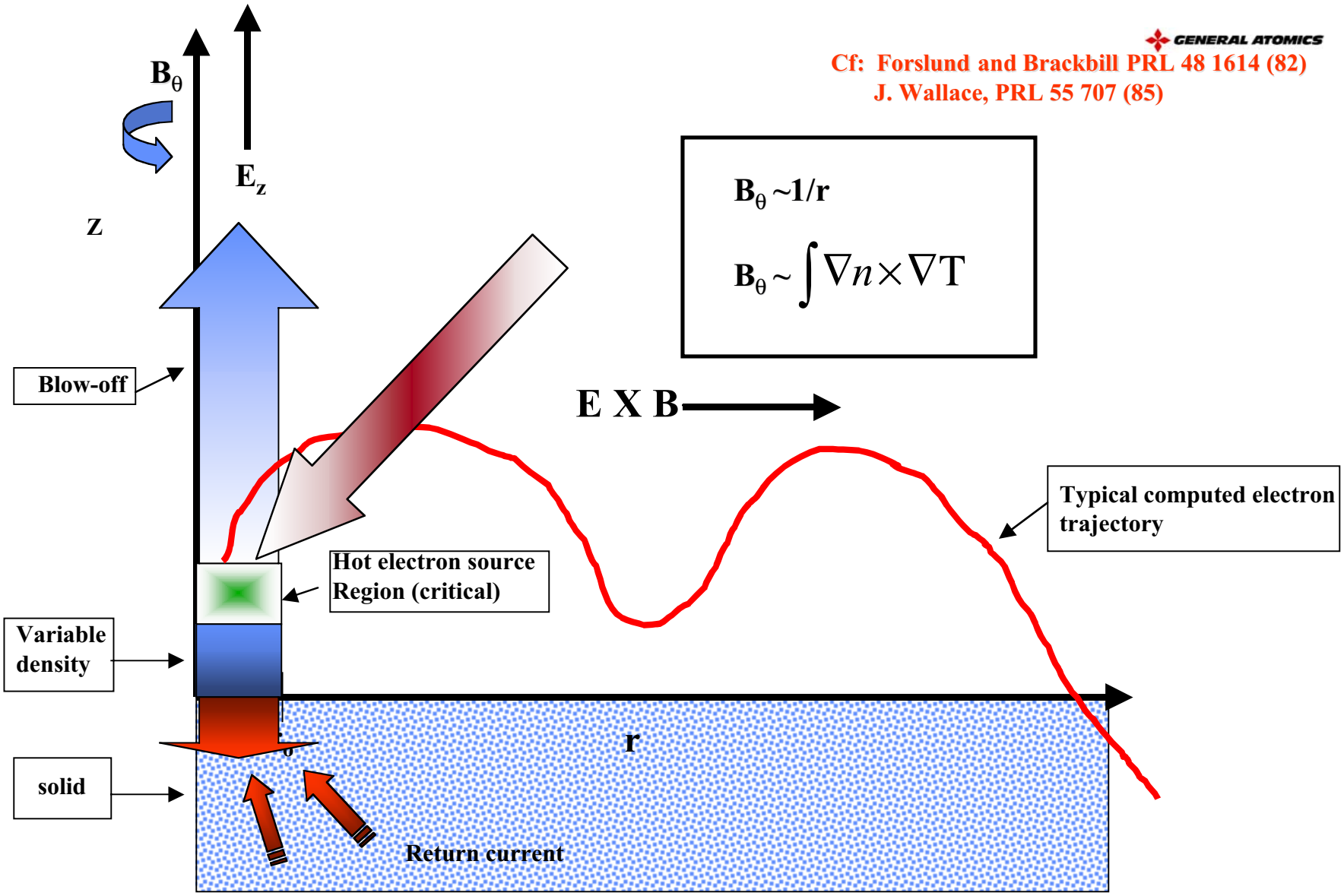

Modeling is now done with "Ideal" Laser Pulses

GENERAL ATOMICS

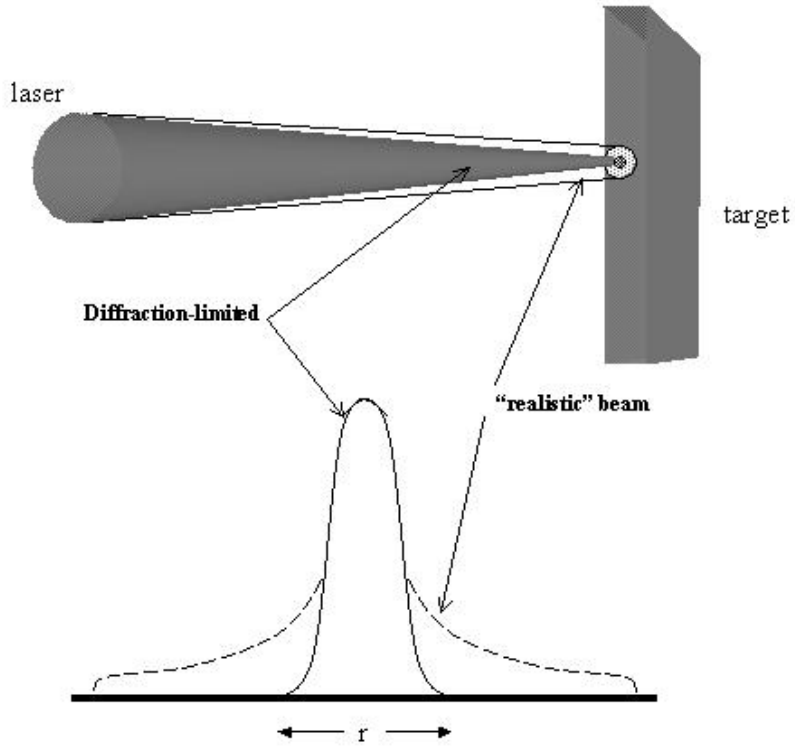

UNIVERSITY OF CALIFORNIA
Department of Applied Science, UCD

General Atomics

Modeling is now done with "Ideal" Laser Pulses

GENERAL ATOMICS

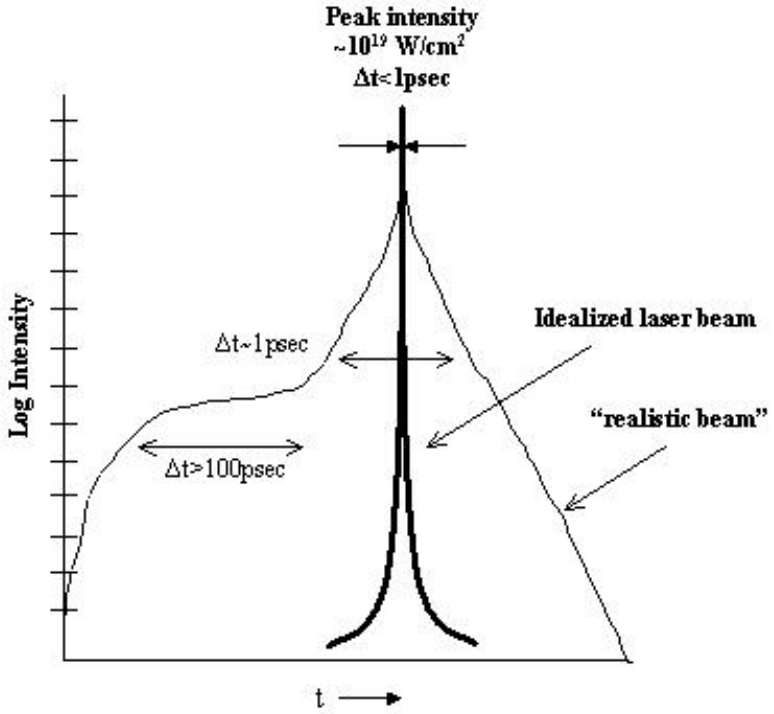

UNIVERSITY OF CALIFORNIA
Department of Applied Science, UCD

General Atomics

A “REAL” interaction environment

GENERAL ATOMICS

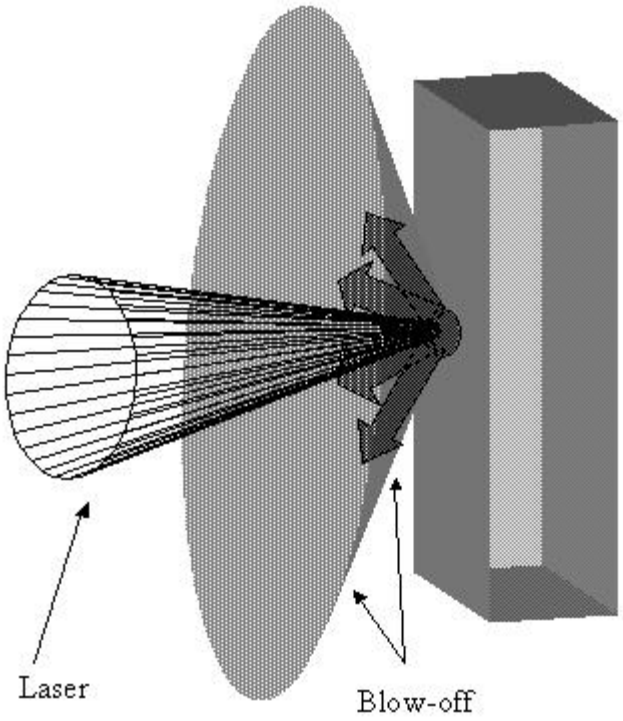

UNIVERSITY OF CALIFORNIA
Department of Applied Science, UCD

General Atomics

Refluxing electrons dominate the target

GENERAL ATOMICS

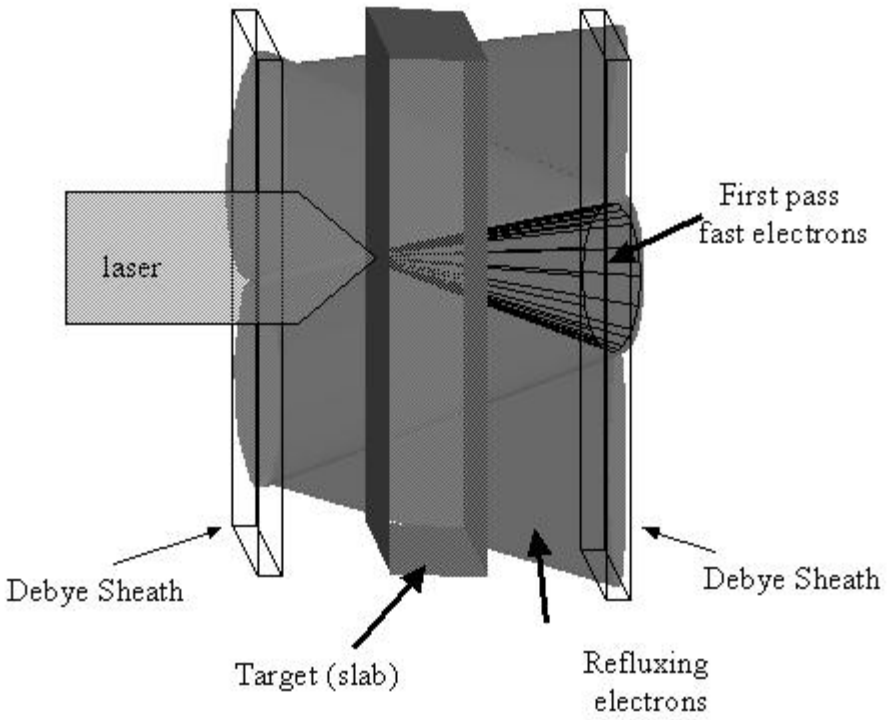

UNIVERSITY OF CALIFORNIA
Department of Applied Science, UCD

General Atomics

New Techniques

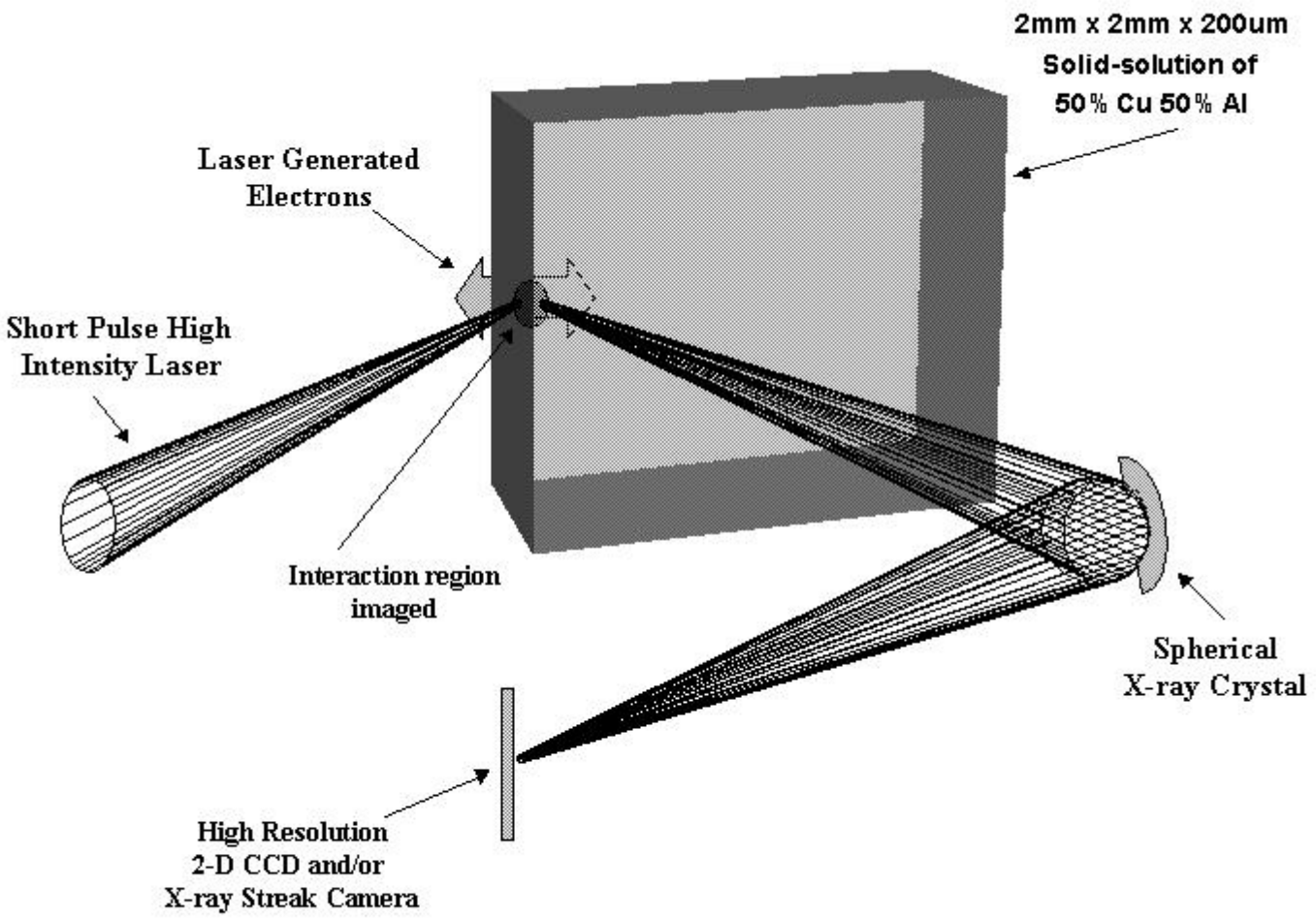

UNIVERSITY OF CALIFORNIA
Department of Applied Science, UCD

General Atomics

First results of side-imaging of currents

AL ATOMICS

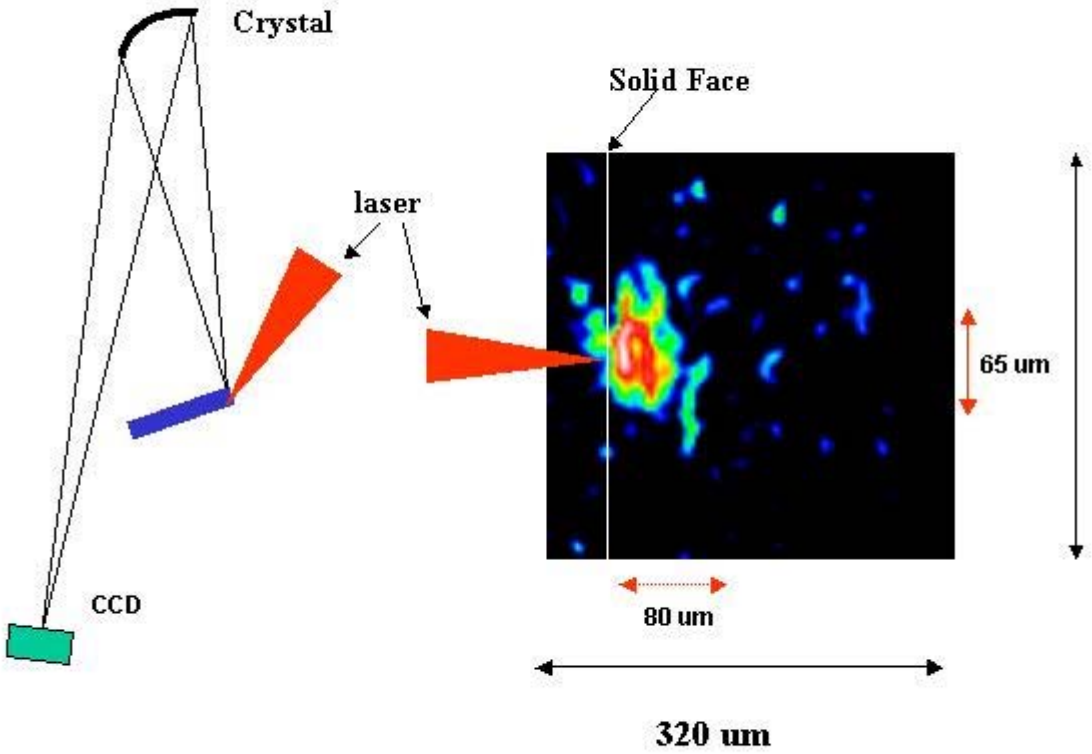

UNIVERSITY OF CALIFORNIA
Department of Applied Science, UCD

General Atomics

Grooved targets are used to measure proton emitting surface area

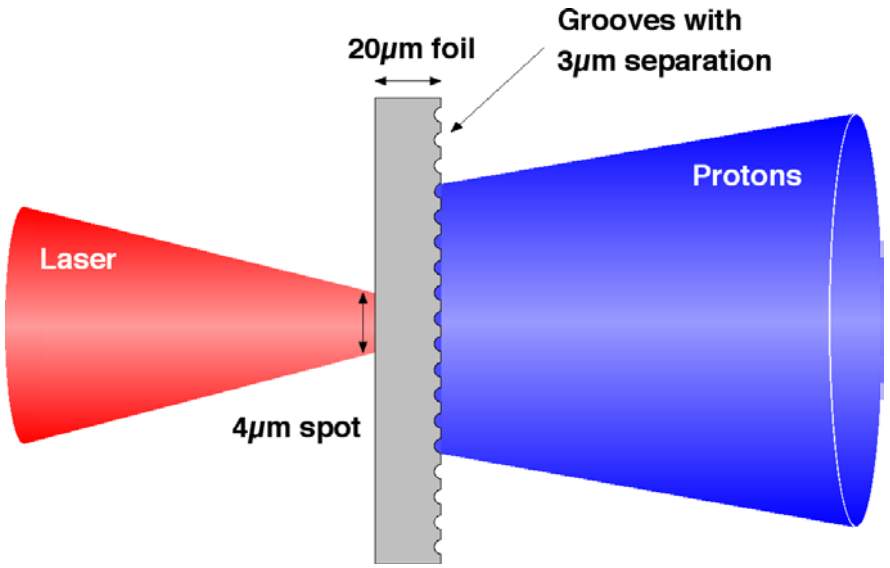

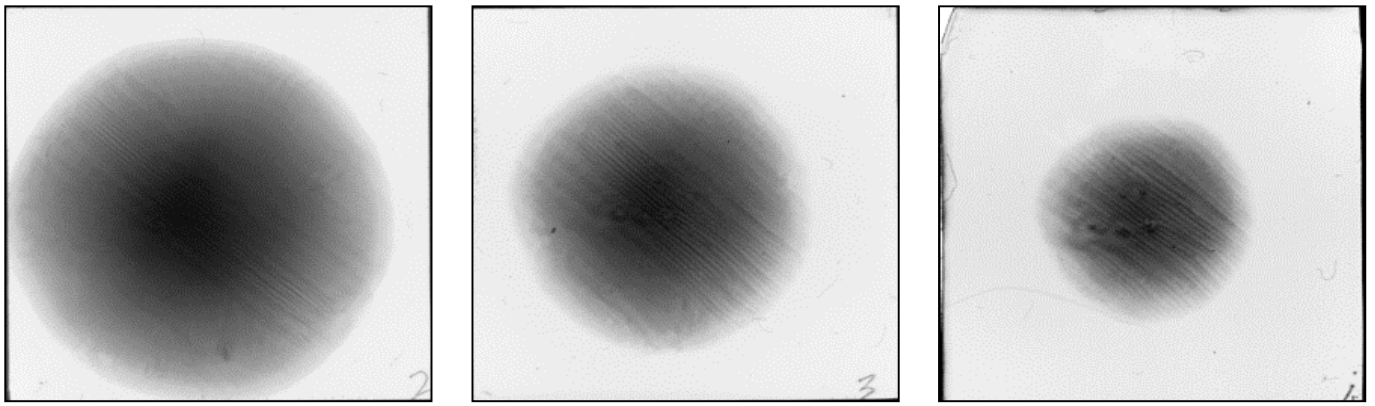

245um 190um 140um

Implies an extremely low beam emittance or transverse spread

We can produce a well-characterised intense proton beam using the 10J, 100fs JanUSP laser

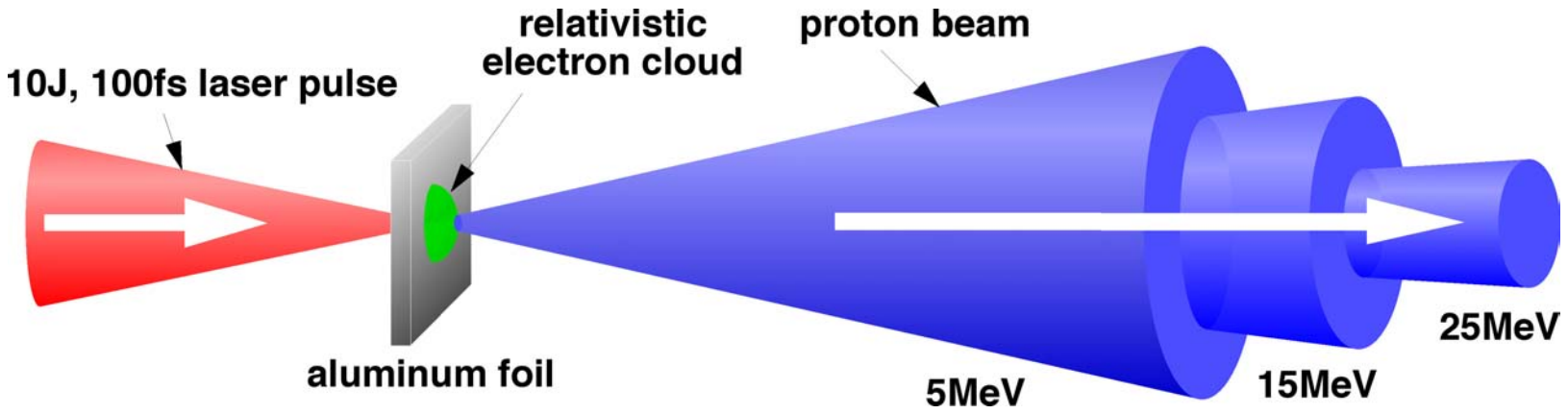

Highly collimated (1-20°)
High flux (few % laser energy)
Energetic (upto 25MeV)
Temporally short (few ps)

P K Patel *et al*

We can even see *sub-micron* spatial features in the proton radiographs

GENERAL ATOMICS

Optical image of 12.5μm diameter wires

Proton image in 6MeV energy protons

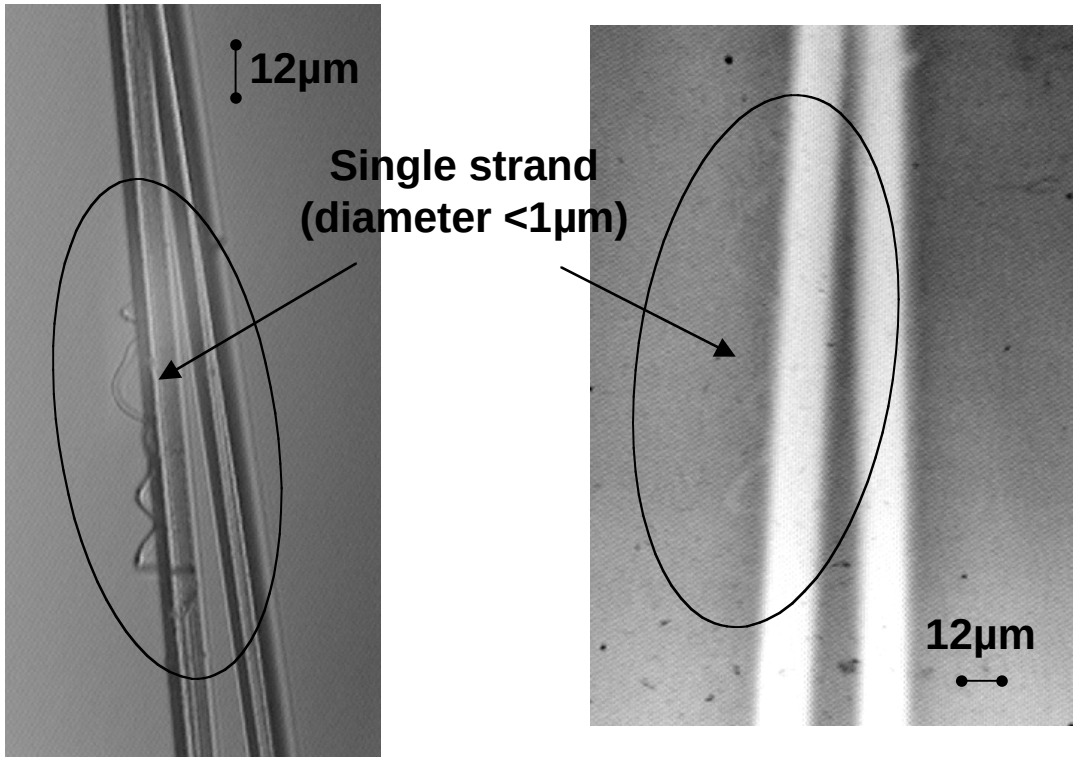

Proton probing potentially offers 2-D micron spatial resolution combined with picosecond temporal resolution

P K Patel *et al*

We developed a Monte-Carlo proton transport code to analyse radiography data

GENERAL ATOMICS

Proton transport through a wire

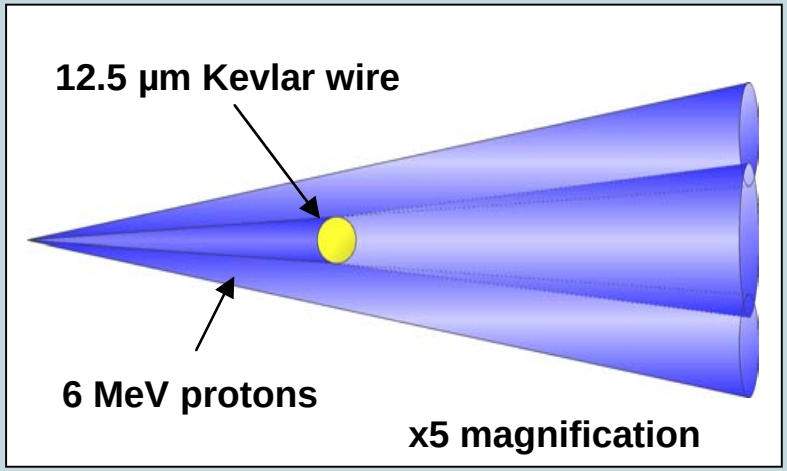

Code includes source size, multiple scattering, and detector response

Calculated lineout across wire

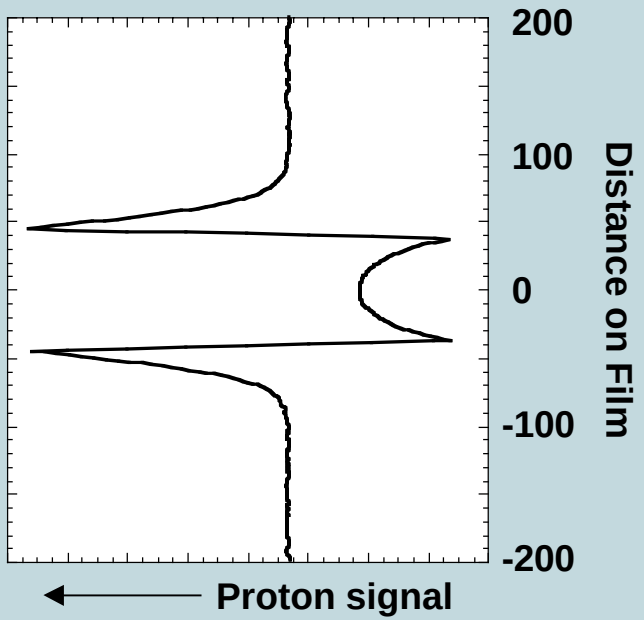

Code reproduces 'limb-darkening' observed in experimental data

Multiple scattering actually enhances the image contrasting, explaining our ability to radiograph extremely small objects

We have radiographed thick opaque foils imprinted with 1μm sinusoidal ripples

GENERAL ATOMICS

Probing an Opaque Rippled Foil

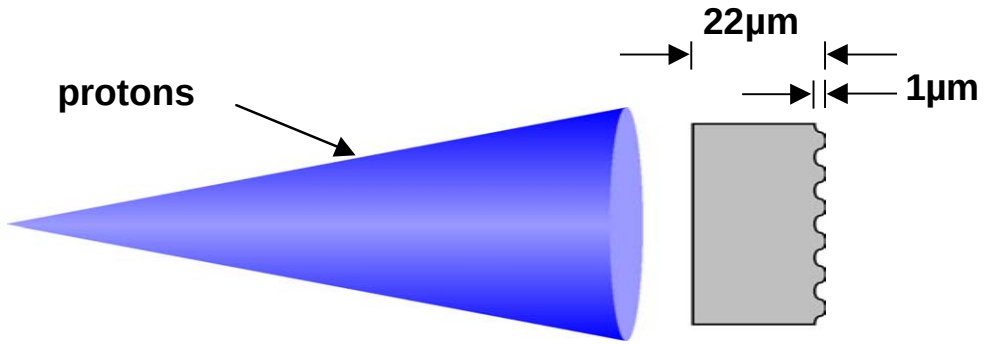

Proton Radiograph

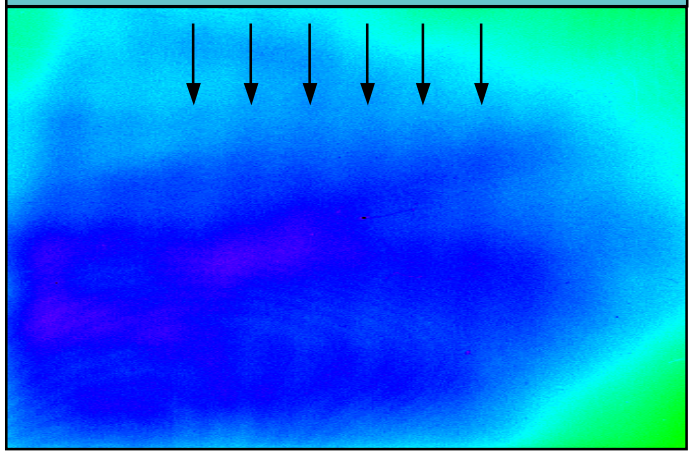

Lineout across Image

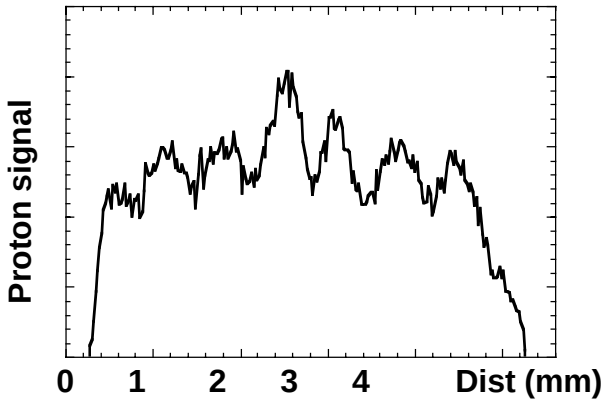

Protons can distinguish better than 4% variations in thickness or density of large samples (NB of *any* material)

Time-resolved proton radiography of a direct drive imploding shell

GENERAL ATOMICS

6 x 50J, 1ns beams in symmetric direct drive implosion geometry

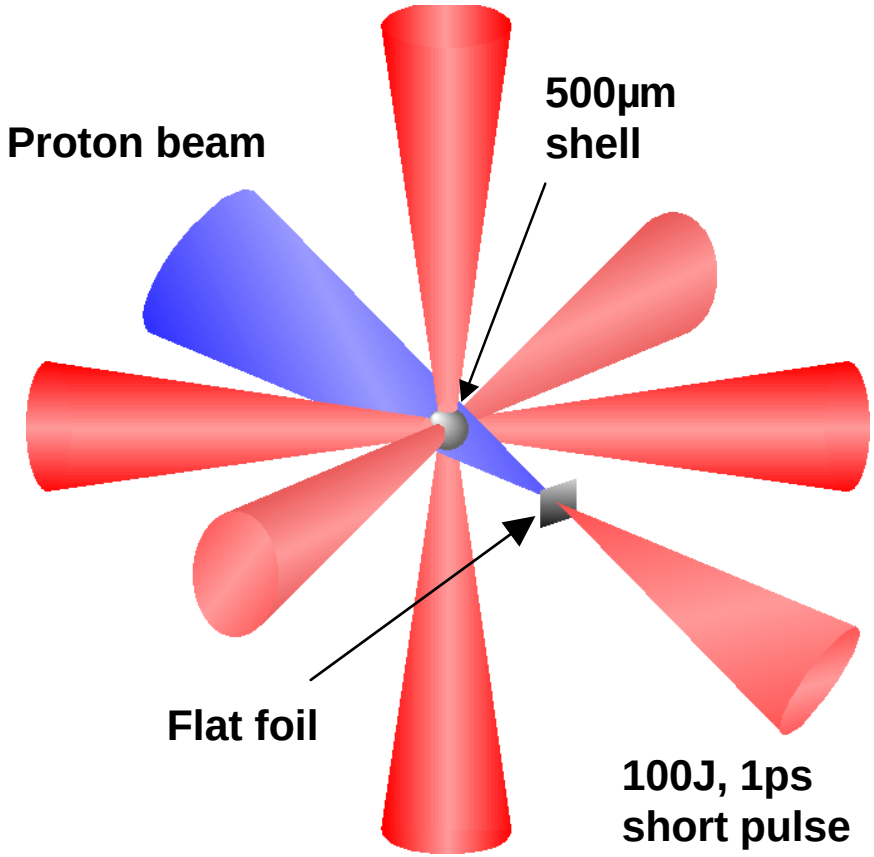

500μm diameter CH shells 3 or 7μm wall thickness

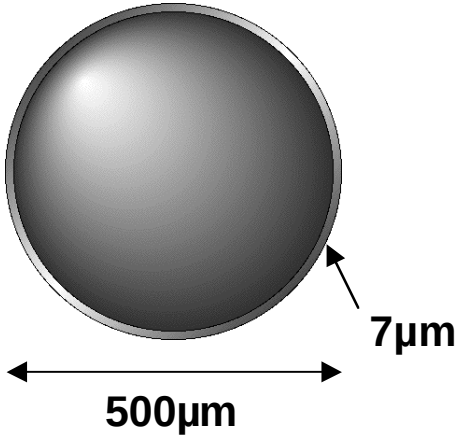

Experiment at the Rutherford Appleton Laboratory, United Kingdom

We obtained the first proton radiographs of a collapsing shell

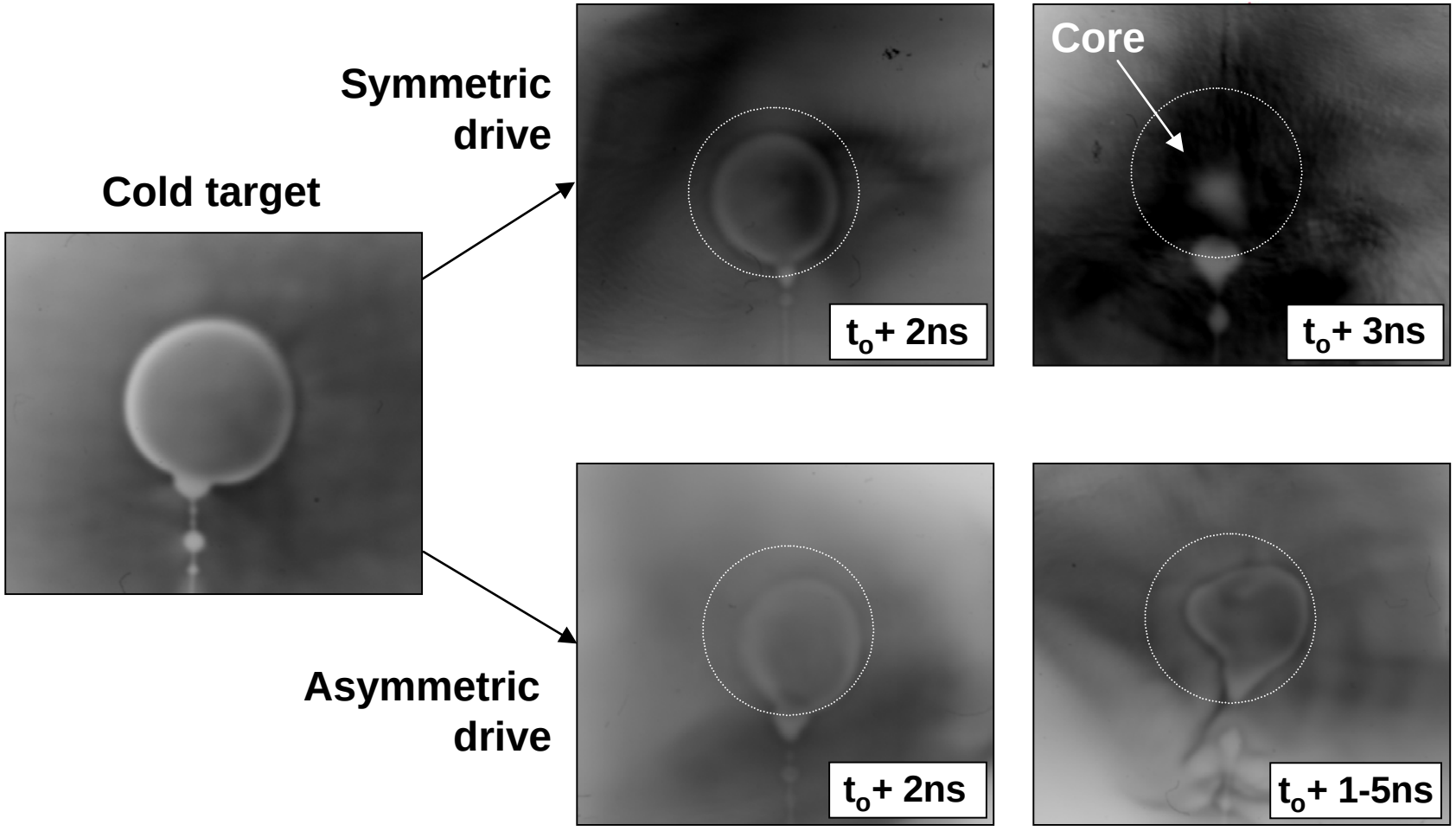

Proton radiographs provide information on compression symmetry and peak density with high spatial and temporal resolution

PK Patel *et al.*

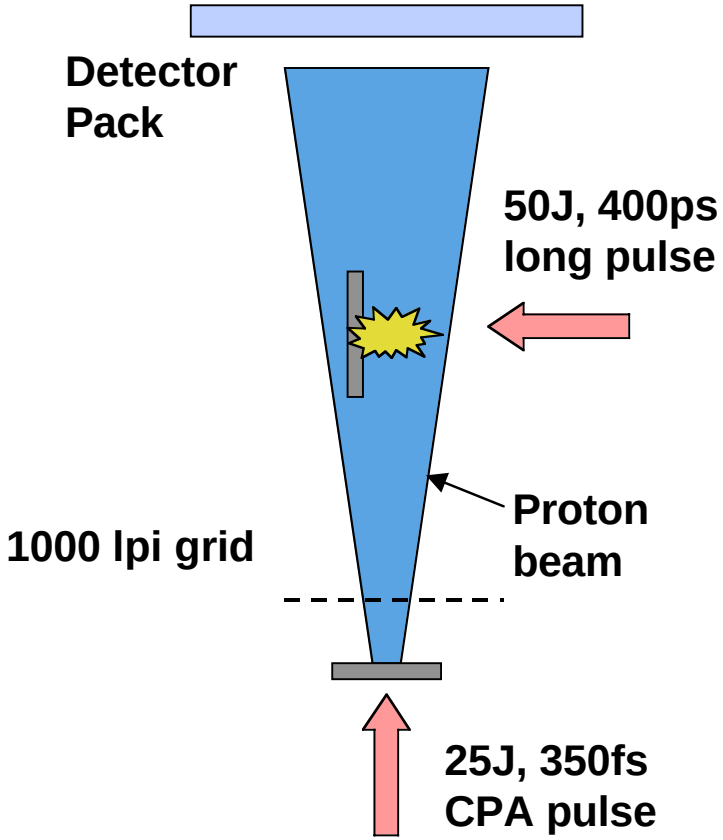

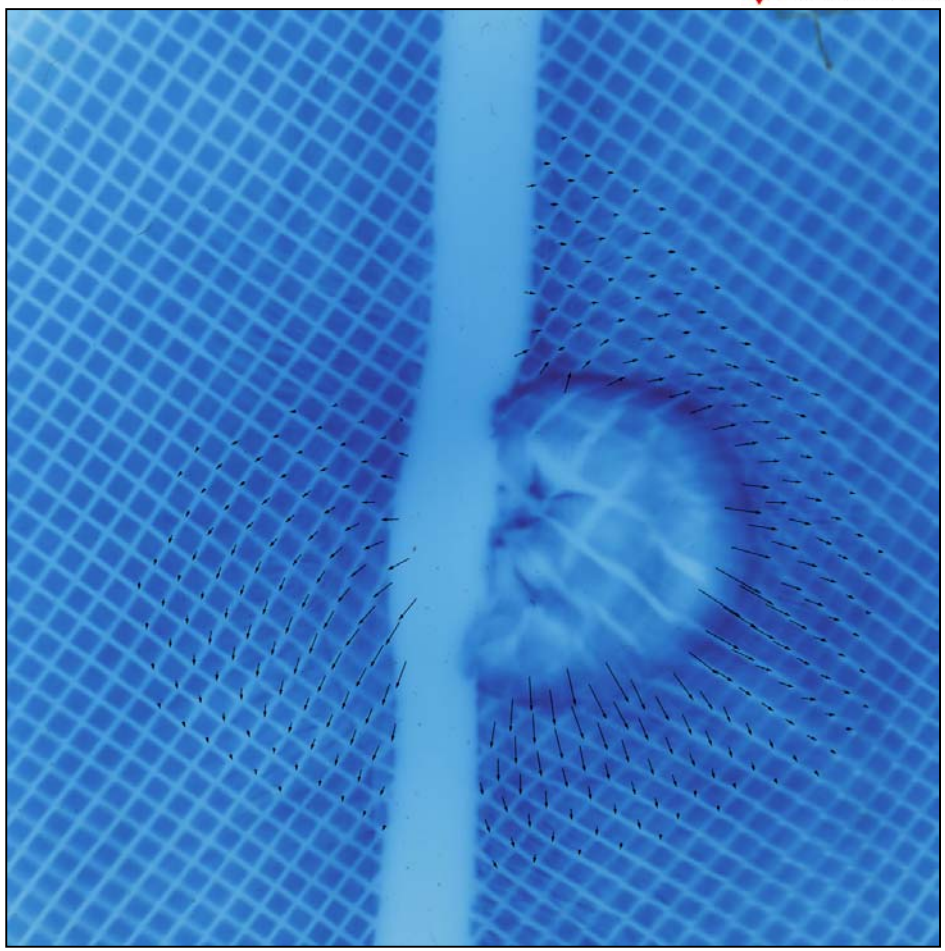

Experiment at Laboratoire pour l'Utilisation des Lasers Intenses, France

PK Patel *et al.*

First results of side-imaging of currents

AL ATOMICS

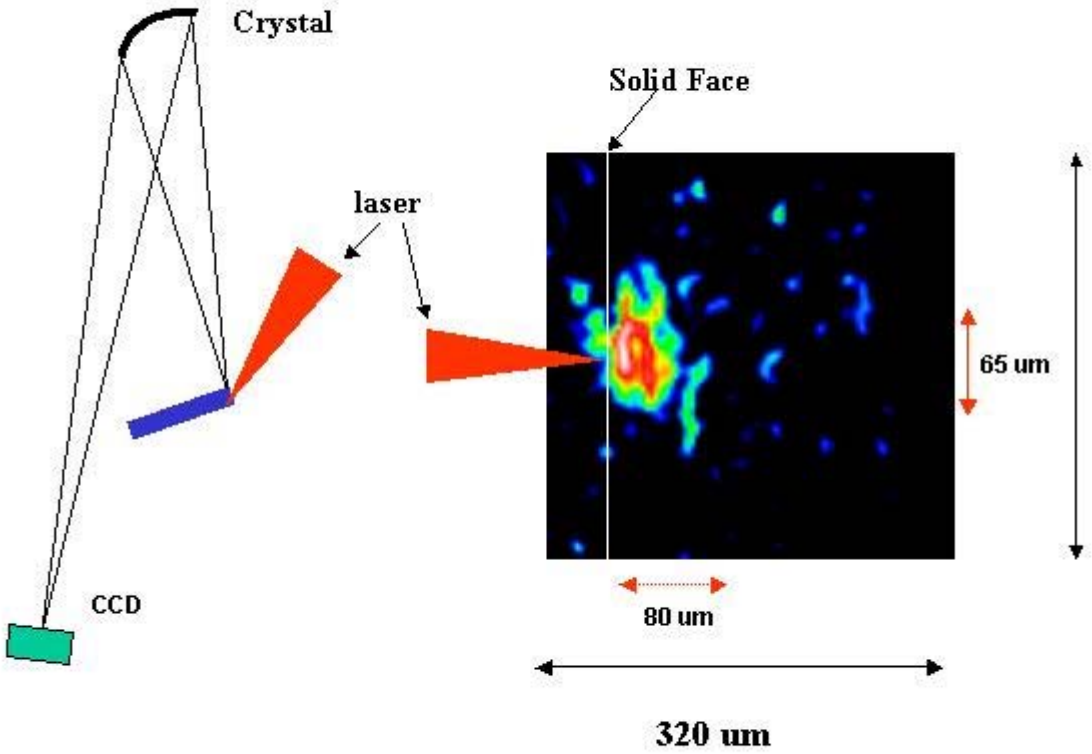

UNIVERSITY OF CALIFORNIA
Department of Applied Science, UCD

General Atomics

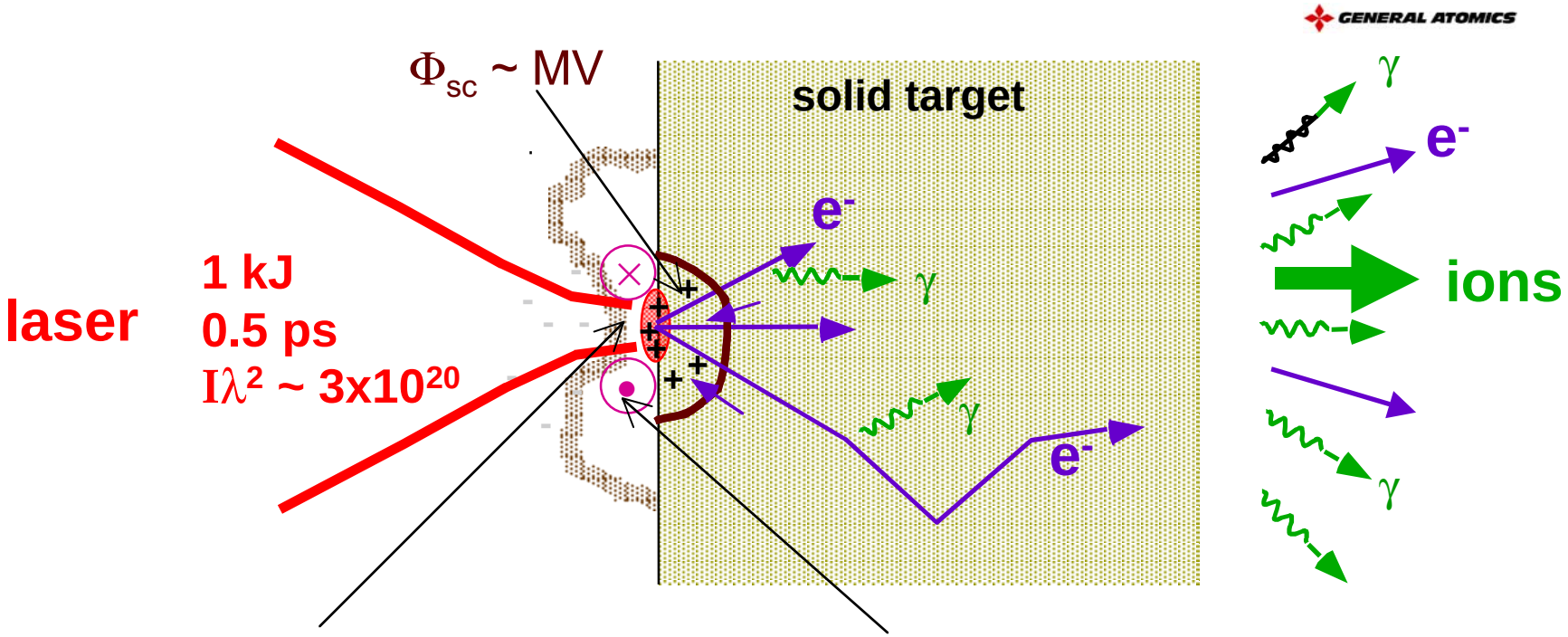

- **Cycle-averaged oscillation energy:** B > 10 MG

$$E_{avg} = mc^2[1+ a_o^2/2]^{1/2} \text{ > 5 MeV}$$

$$\sim U_{ponderomotive}$$

Fast ignition presents challenges in science and technology - cone target electron ignition is most advanced

GENERAL ATOMICS

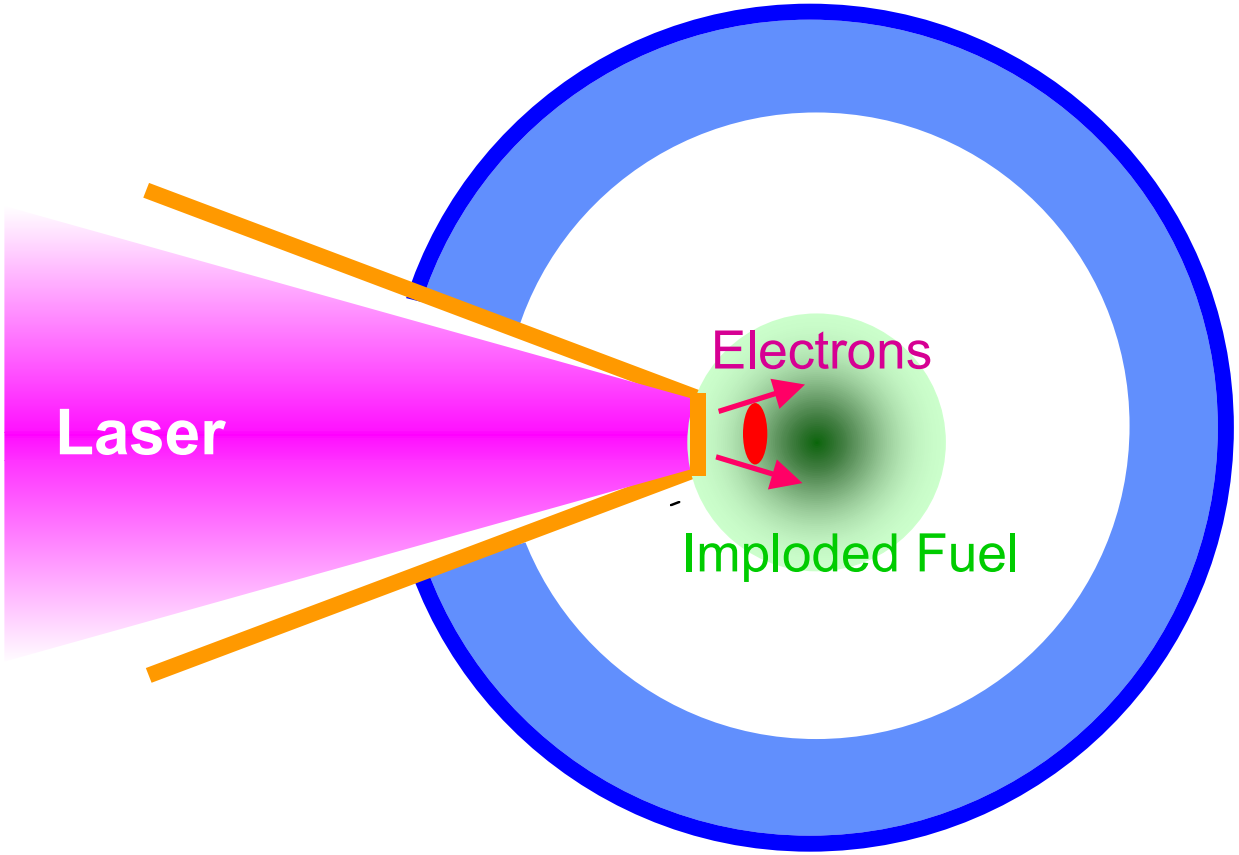

Generation of energetic ions and x rays from clusters irradiated by ultrafast, high-intensity laser pulses

Y. Fukuda[1], Y. Akahane[1], M. Aoyama[1], N. Inoue[1], H. Ueda[1], Y. Kishimoto[2], T. Masaki[2], K. Yamakawa[1], A. Ya. Faenov[3], A. I. Magunov[3], T. A. Pikuz[3], I. Yu. Skobelev[3], J. Abdallah, Jr.[4], G. Csanak [4], A. S. Boldarev[5], V. A. Gasilov[5]

[1]*Advanced Photon Research Center, JAERI, Japan*
[2]*Naka Fusion Research Eatblishment, JAERI, Japan*
[3]*Multicharged Ions Spectra Data Center of VNIIFTRI, Russia*
[4]*Theoretical Division, Los Alamos National Laboratory, USA*
[5]*Institute of Mathematical Modeling, Russian Academy of Sciences, Russia*

The International Conference on
Ultrashort High-Energy Radiation and Matter,

Villa Monastero, Varenna, Italy October 7-10, 2003

Collaborators

Program Leader: Koichi Yamakawa

Advanced Photon Research Center, JAERI, Japan

1. Cluster generation, x-ray measurements, laser operation and control:

Yuji Fukuda, Yutaka Akahane, Makoto Aoyama, Norihiro Inoue, Hideki Ueda

Advanced Photon Research Center, JAERI, Japan

Anatoly Ya. Faenov, Tatiana A. Pikuz, Alexandr I. Magunov, Igor Yu. Skobelev

Multicharged Ions Spectra Data Center of VNIIFTRI, Russia

2. Time-dependent Boltzmann-kinetic model:

Joseph Abdallah,Jr., George Csanak

Theoretical Division, Los Alamos National Laboratory, USA

3. 2D-hydrodinamic calculation for the special nozzle:

Alexei S. Boldarev, Vldaimir A. Gasilov

Institute of Mathematical Modeling, Russian Academy of Sciences, Russia

4. 3D-PIC code simulation:

Yasuaki Kishimoto, Tomohiro Masaki

Naka Fusion Research Eatblishment, JAERI, Japan

Energetic Particle Generation via Intense Laser-Cluster Interaction

ÅClusters absorb most of the incident laser energy

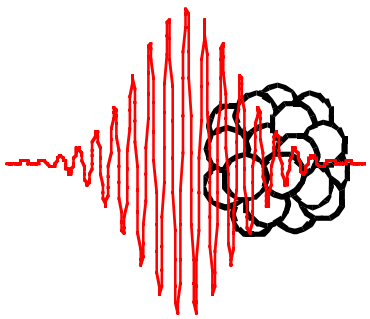

Cluster heating

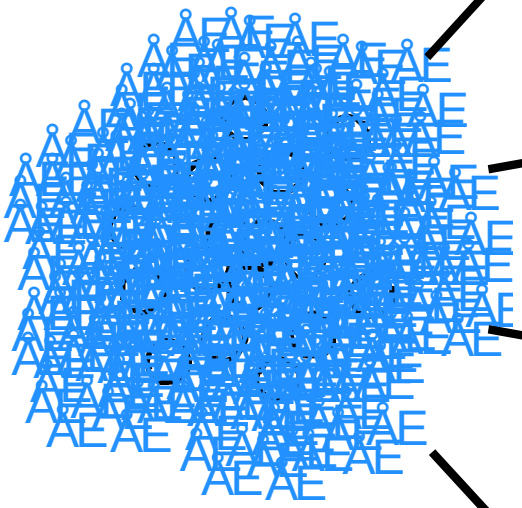

Cluster explosion

- Energetic electrons (a few keV)
- Energetic multiply charged ions (> 1 MeV)
- *Bright X-rays (0.1-10 keV)*
- Neutrons by D-D fusion

T. Ditmire et al., *Nature* **386**, 54 (1997).

J. Posthumus, *Molecules and Clusters in Intense Laser Fields* (Cambridge Univ. Press,Cambridge, 2001).

Research Purpose

- **Purpose of our research:**
  - *To better understand a fundamental aspect of the laser-cluster interaction via x-ray emission properties.*
    - X-ray emission spectra could reflect *the temporal dynamics of the cluster-plasma creation*.
  - To develop ultrafast intense (debris free) x-ray sources.

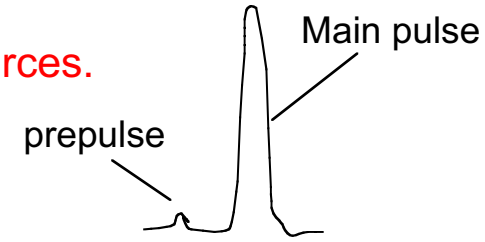

- **Technical difficulties:**
  - *Destruction of clusters by a laser prepulse*.
    - The destruction of clusters dramatically decrease x-ray emissions.
  - *X-ray spectroscopy with high resolution*.
    - The detailed examination of the temporal dynamics requires high resolution spectra.

In this study…

- **To increase x-ray emissions, we have tried…**
  - to increase a laser peak intensity above *10^{19} W/cm^2* with *30 fs* laser pulse,
  - to decrease *a prepulse intensity* using Pockels cell switches,
  - to increase *a cluster size* using a specially designed conical nozzle.

- **These approaches contribute to…**
  - decreasing a preplasma creation,
  - a direct interaction between high-density clusters and main fs-pulses,
  - increasing x-ray emissions.

- **High resolution x-ray spectra were measured using a combination of…**
  - a spherically bent, mica crystal spectrometer,
  - a high resolution x-ray CCD camera.

- **To explore the temporal dynamics of cluster-plasma creation…**
  - the calculation based on *a time-dependent Boltzmann-kinetic model* has been carried out.

JAERI 100 TW, 20 fs, 10 Hz Ti:sapphire Laser System

K. Yamakawa et al., *Opt. Lett.* **23**, 1468 (1998).
M. Aoyama et al., *Opt. Lett.* **28**, 1594 (2003).

Schematic Diagram of Experimental Setup

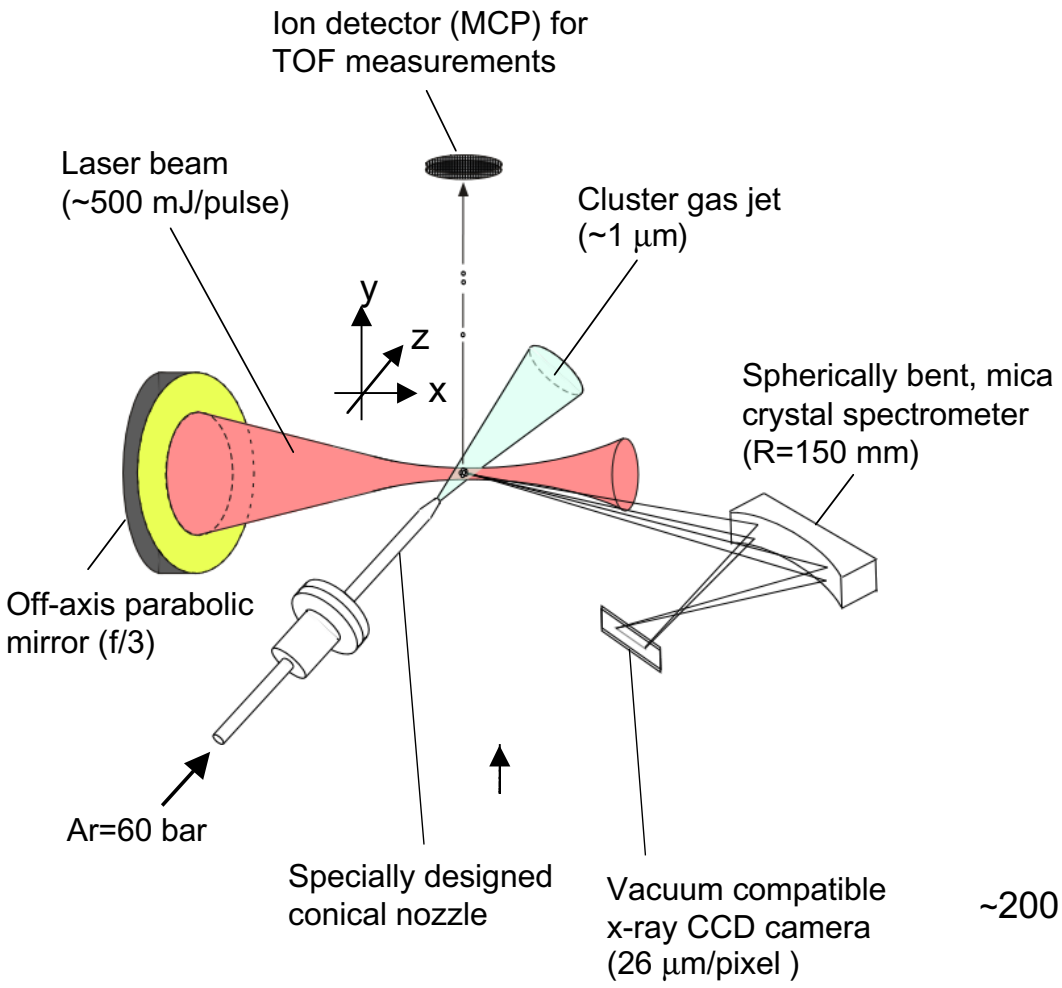

Laser spot image

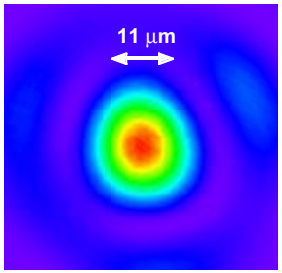

ÅSpot size: 11 μm at $1/e^2$
ÅPeak intensity: up tp $3x10^{19}$ W/cm^2

X-ray CCD image

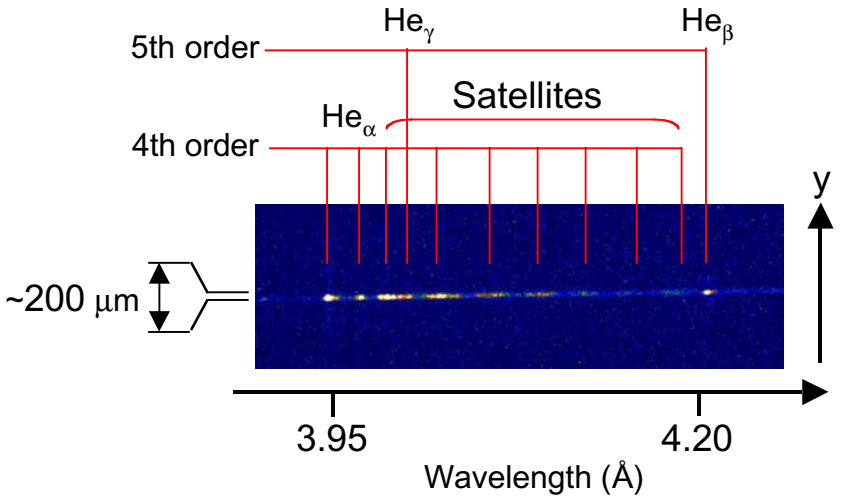

Specially Designed Conical Nozzle

A. S. Boldarev, V. A. Gasilov, (2003)

2D-hydrodinamic calculations for Ar jet at different gas pressures

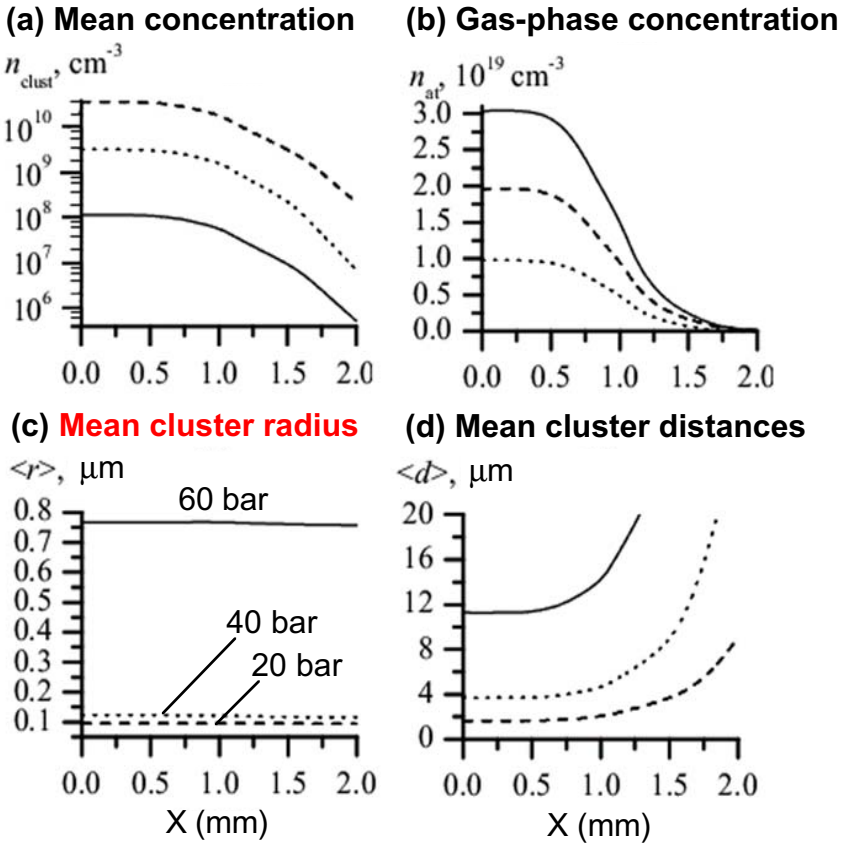

Dimensions

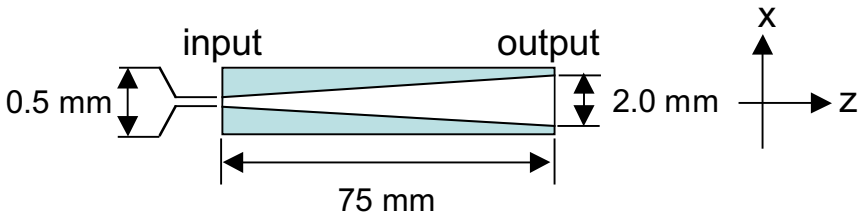

- Ar=20~40 bar:
  - Mean cluster diameter: ~200 nm
- *Ar=60 bar:*
  - *Mean cluster diameter: ~1.5 μm*
- **Note that…**
  - A rapid increase in cluster size as a function of gas pressure.
  - *No additional cooling*.

X-ray Emissions from Micron-Sized Ar Clusters

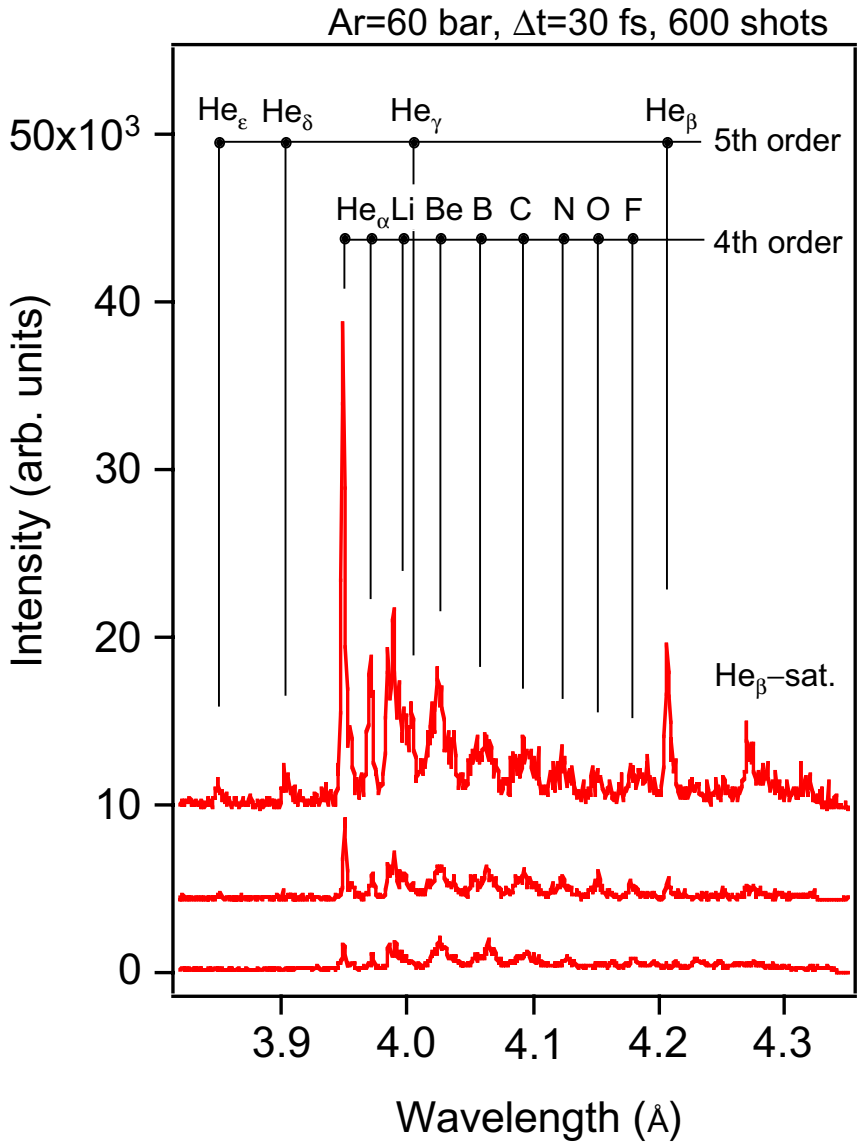

- **Upper trace:**
  - *I= 1.3x10^{19} W/cm^2, C= 5x10^{-6}*
- **Middle trace:**
  - *I*= 2.5x10^{18} W/cm^2, *C*= 4x10^{-4}
- **Lower trace:**
  - I= 2.5x10^{18} W/cm^2, *C= 2x10^{-2}*
  - Line yield of He-like ion falls down.
- **Photon numbers of He$_{\alpha 1}$ line in all solid angle 4π:**
  - *N= 2x10^8 photons/shot/pixel*
- **Total power of He$_{\alpha 1}$ line:**
  - *P= ~100 kW*
- **Conversion efficiency for He$_{\alpha 1}$ line:**
  - η = ~1x10^{-8}

Cluster Size Dependence of X-ray spectra

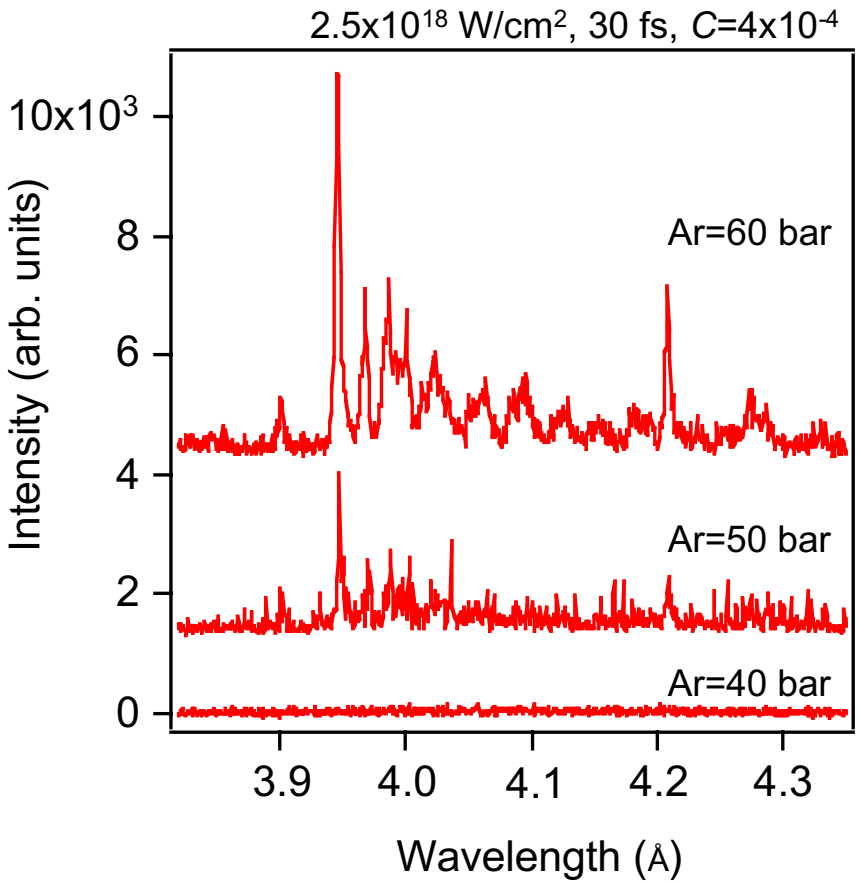

- At Ar=40 bar,
  - no signal was observed.
- According to the calculation…
  - *Ar=60 bar, cluster size= ~1.5 μm*
  - *Ar=40 bar, cluster size= ~200 nm*
- At Ar=40 bar,
  - *clusters are completely destroyed before the arrival of the main pulse*.
- This result demonstrates…
  - the role of big clusters,
  - the validity of nozzle designing.

Time Dependent Boltzmann-Kinetic Model

J. Abdallah,Jr. and G. Csanak et al., submitted to Phys. Rev. A (2003)

The atomic kinetics and Boltzmann equation were solved simultaneously.

- **Boltzmann Equation**

$$\frac{df_i}{dt} = S_i(\mathbf{f},\mathbf{N}),\ i = 1,2,\cdots,100$$

$f_i = f(E_i,t)$: electron energy distribution function (EEDF) of bin *i*

$S_i(\mathbf{f},\mathbf{N})$: a function which include elastic and inelastic e-e collisions

- **EEDF** changes by *e-e* collisions as a function of time

- **Rate Equation for Atomic Kinetics**

$$\frac{dN_j}{dt} = R_j(\mathbf{f},\mathbf{N}),\ j = 1,2,\cdots,3000$$

N_j : population density of level j

$R_j(\mathbf{f},\mathbf{N})$: a function which include all population altering processes

- **Population density** changes by radiation, excitation, ionization as a function of time

The level populations are collected as a function of time, and are used to calculate time integrated line emission spectra.

Temporal Evolution of EEDF

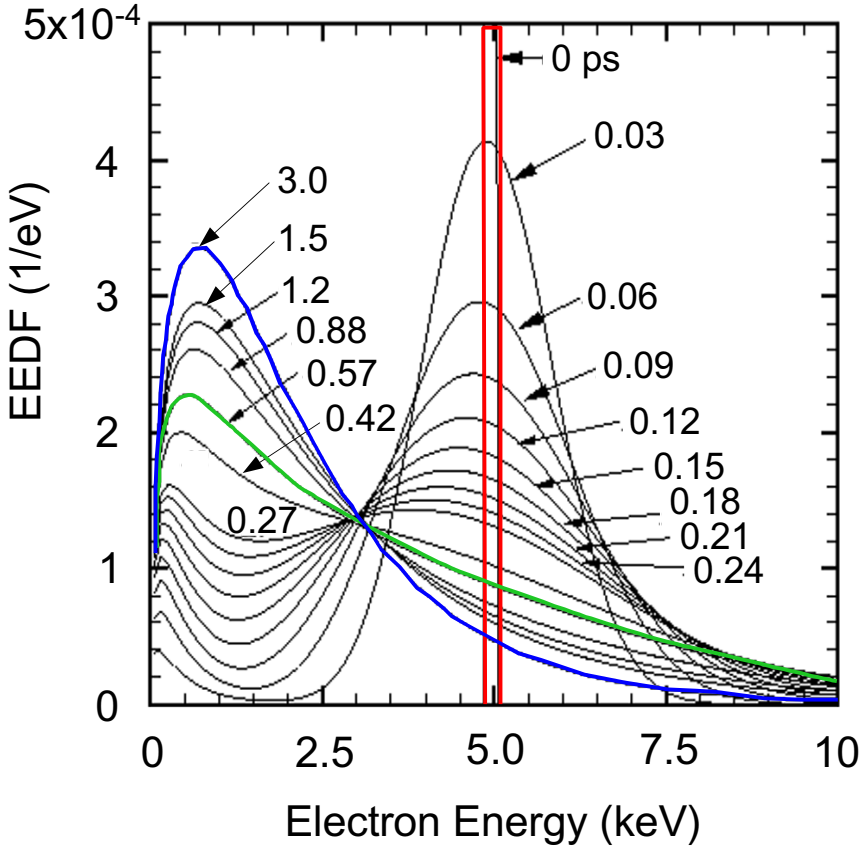

- At 0 ps,
  the EEDF is set spiked at 5 keV,
  which represents *nonequilibrium plasma*.
- The EEDF broadens very quickly due to
  electron-electron collisions.
- As time increases,
  the low energy component gets larger,
  and the 5 keV component gets smaller.
- By ~0.5 ps,
  there is no noticeable bump at 5 keV,
  and the EEDF approaches Maxwellian.
- At 3 ps,
  electrons are *thermalized*,
  and the EEDF is completely *Maxwellian*.

Temporal Evolution of Ion Fractions

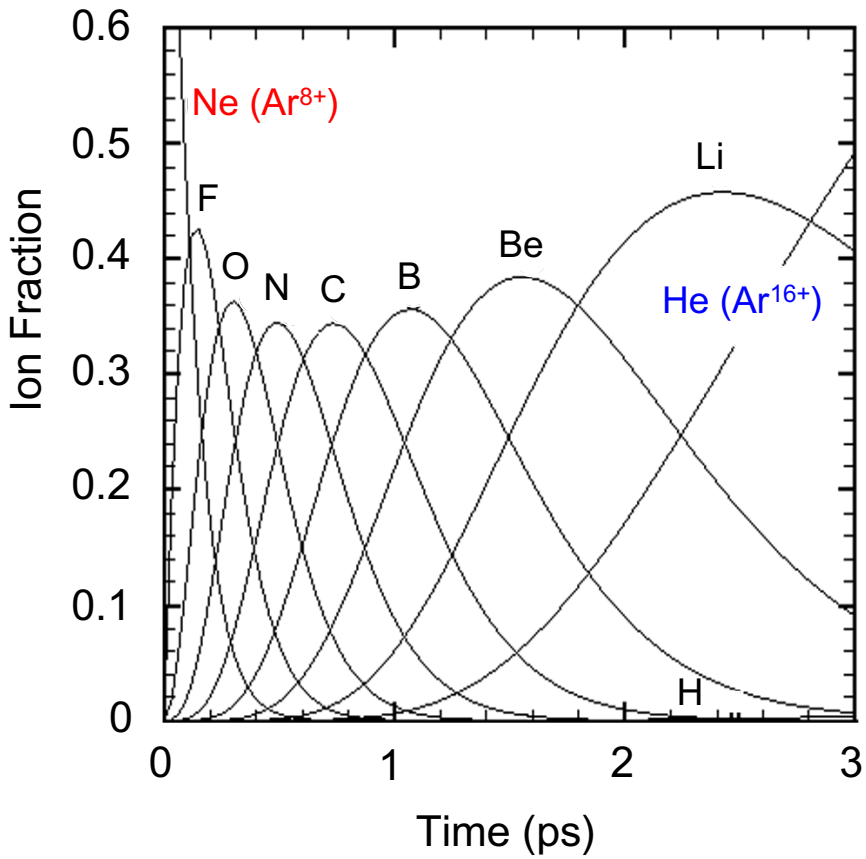

- Initially,
  all the ions were assumed to be in the ground-state of *Ne-like (Ar^{8+}) ion*, which could be produced by laser prepulse.

- As time increases,
  the ion composition is shifted to higher charges due to *collisional ionization*.

- After *~1 ps*,
  the population of *He-like (Ar^{16+}) ion* increases.

- After ~3 ps,
  the *expansion and cooling* of the cluster prevent further ionization.

Temporal Evolution of Time-Integrated Ar K-shell Spectra

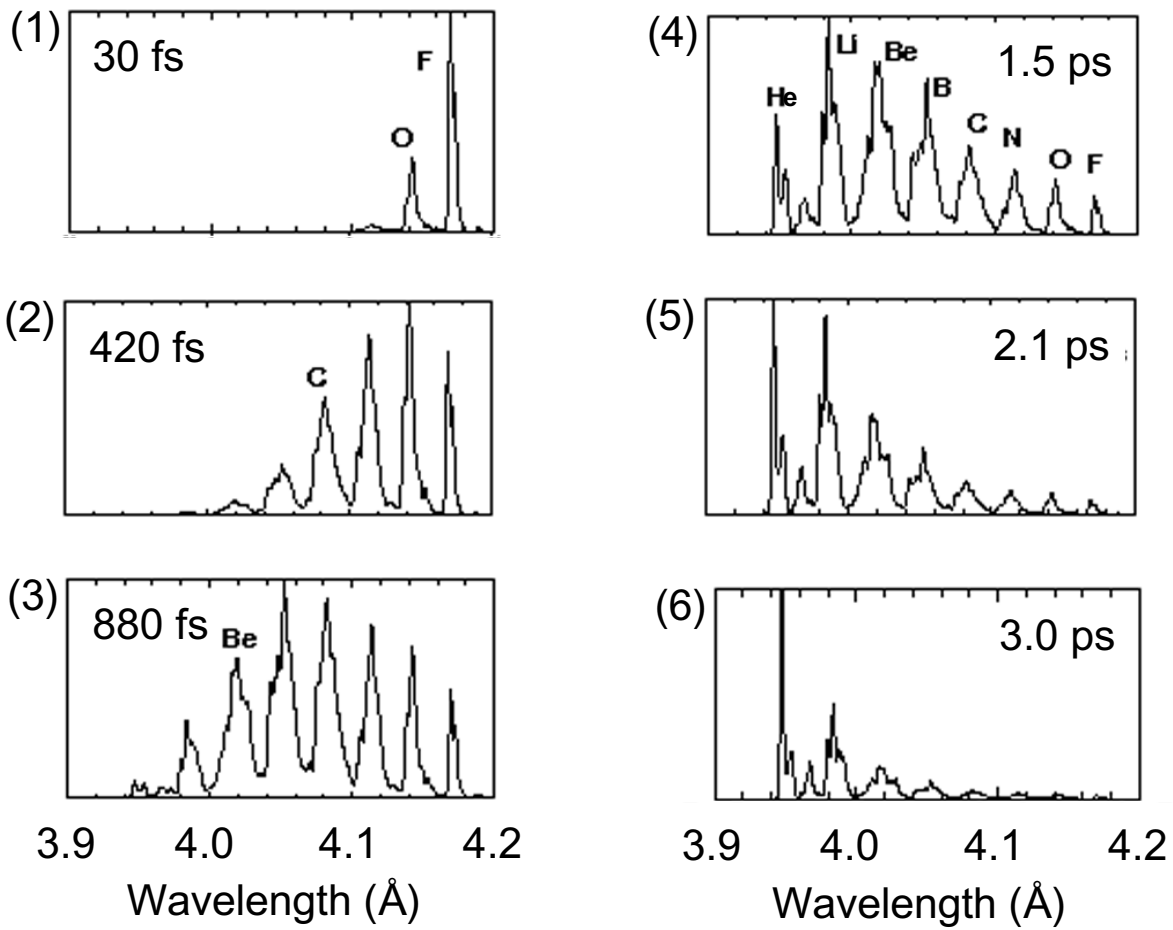

- (1)~(2):
  At early times, emissions from *F-like (Ar^{9+}) to C-like (Ar^{12+}) ions* are observed.
- (3)~(4):
  By ~1.5 ps, emissions from *all the ion charge states* are observed.
- (4)~(6):
  From ~1.5 ps, *enhancement of He-like (Ar^{16+}) emission* with respect to the satellites.

Comparison of Calculated Spectra and Experiment

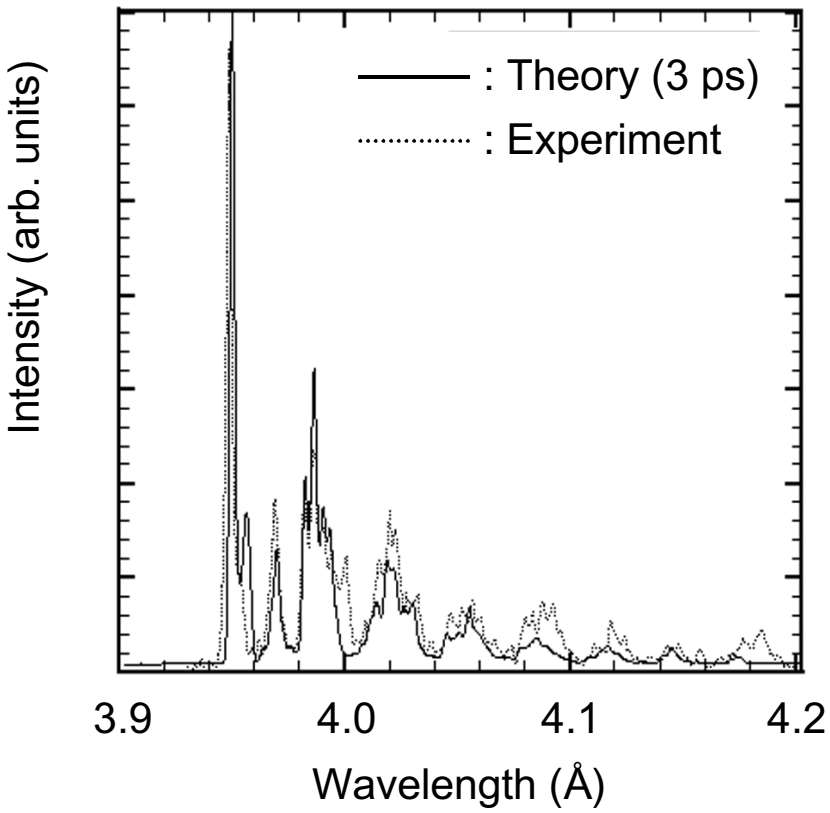

- The agreement between the calculation and the experiment is quite good.
- Note that…
  - the previous *static model could not predict* the features of the observed spectra.

L-shell Emissions from Micron-Sized Kr Clusters

• Average cluster size: ~1 μm

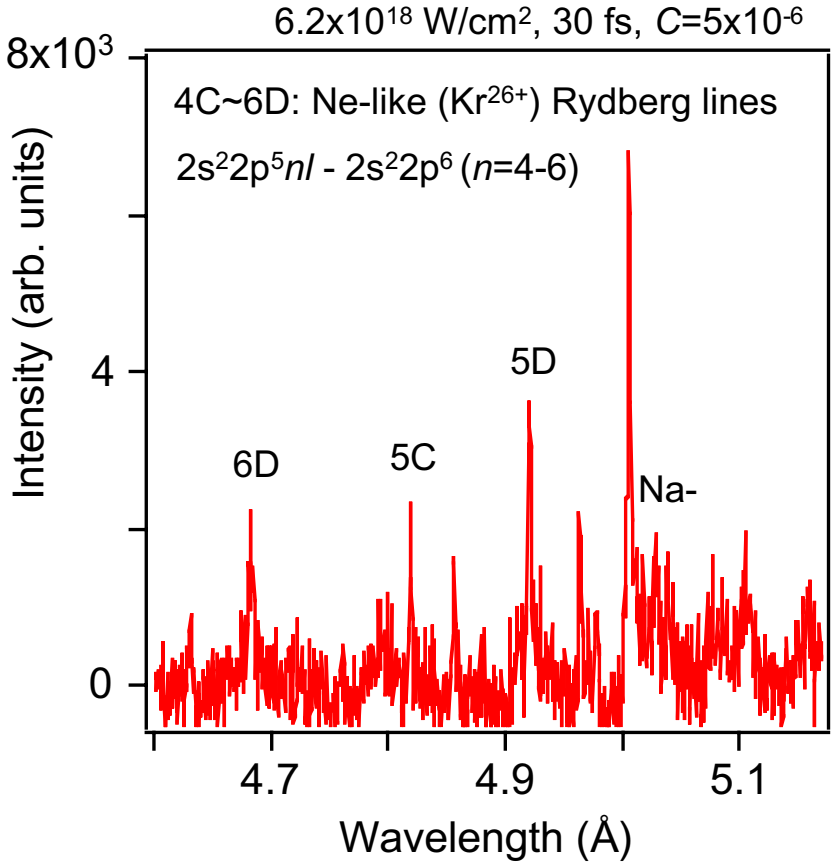

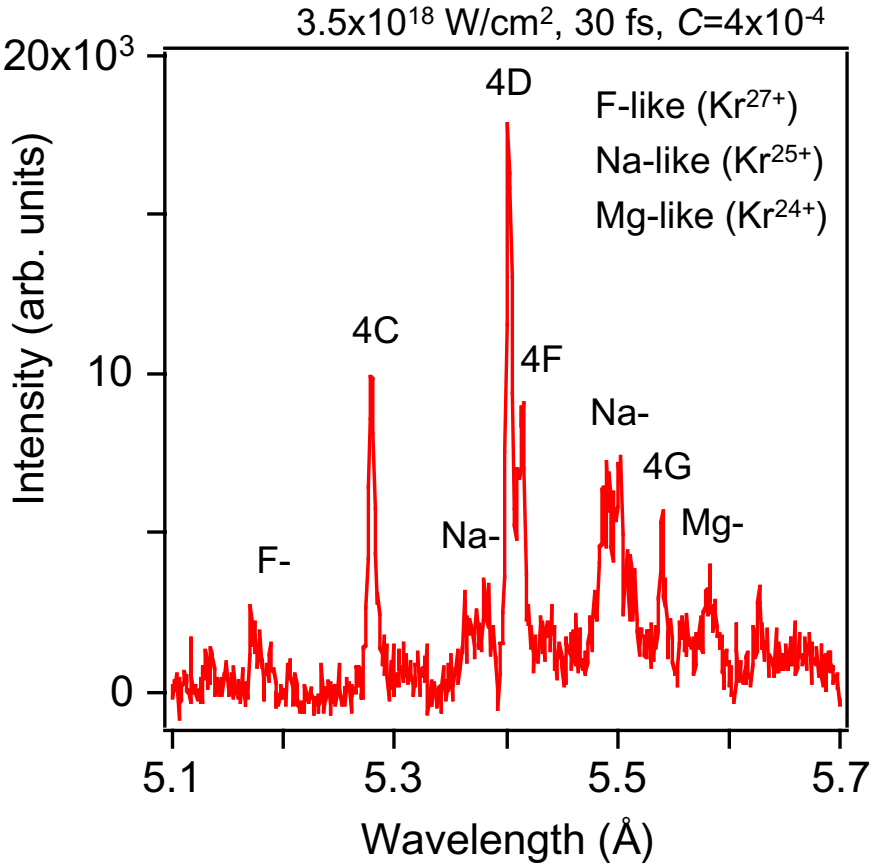

L-shell Emissions from Xe Clusters

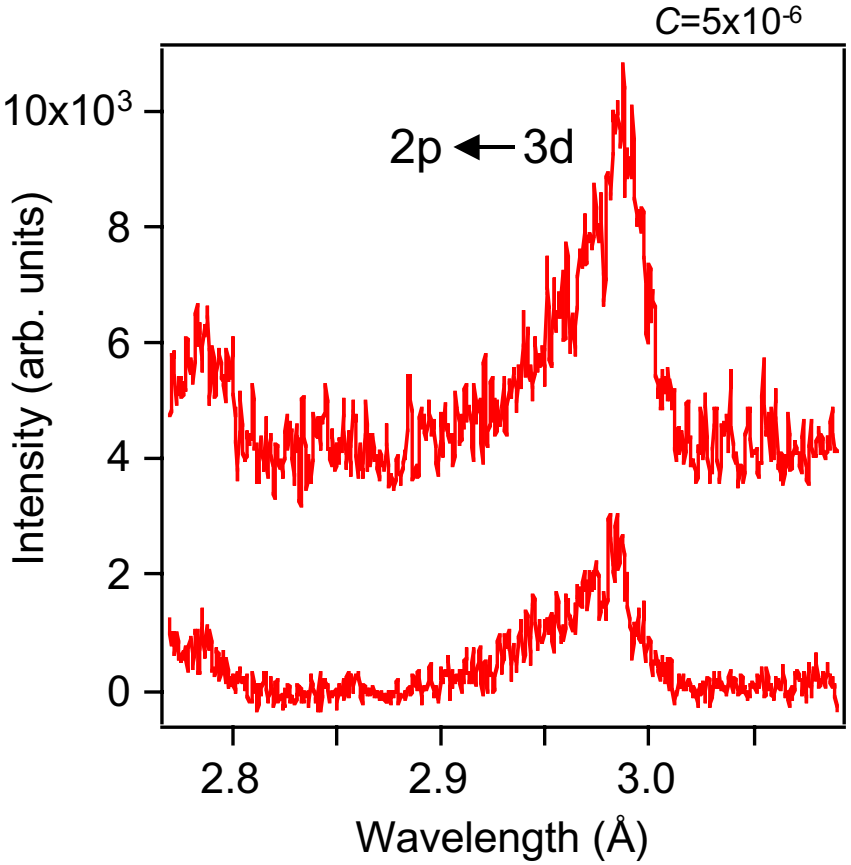

- Average cluster size: ~600 nm
- **Upper trace:**
  - I=1.6x10^{19} W/cm^2, 30 fs
- **Lower trace:**
  - I=4.0x10^{17} W/cm^2, 500 fs

Summary

- High resolution K-shell x-ray spectra were measured for micron-sized Ar clusters with laser intensities above *10^{19} W/cm^2* and *30-fs* pulses.

- To make these measurements possible,
  - *a special nozzle* was designed.
  - *a laser prepulse intensity* was decreased.

- The novel calculation with *the time-dependent EEDF and corresponding level population* gave a good agreement with the experiments.

- **It is suggested that the role of fs-laser pulse is**
  - **the *prompt generation of nonequilibrium plasma***
  - ***with high energy (~5 keV) free electrons***
  - ***before the cluster explosion*.**

Ion Energy Spectrum from Massive Ar Clusters

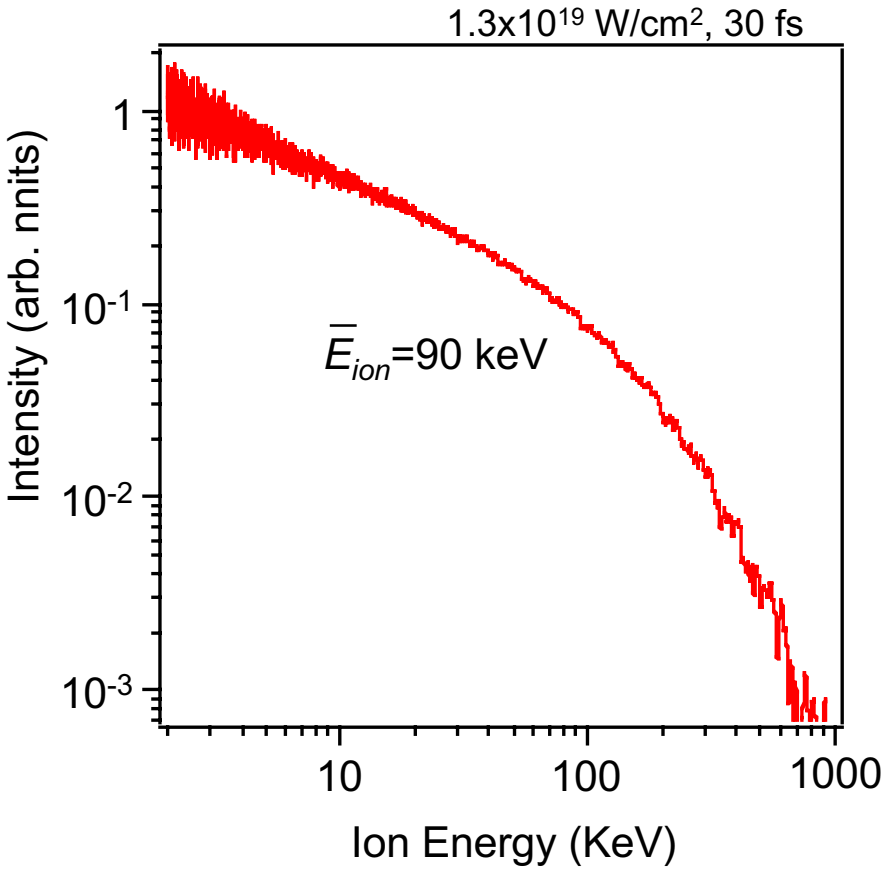

- Maximum Ion energy: ~800 keV
- Mean Ion energy: ~90 keV

Recent results in laser-plasma X-ray sources

Leonida A. Gizzi
Intense Laser Irradiation Lab.
IPCF-CNR, Pisa, Italy

The Intense Laser Irradiation Laboratory

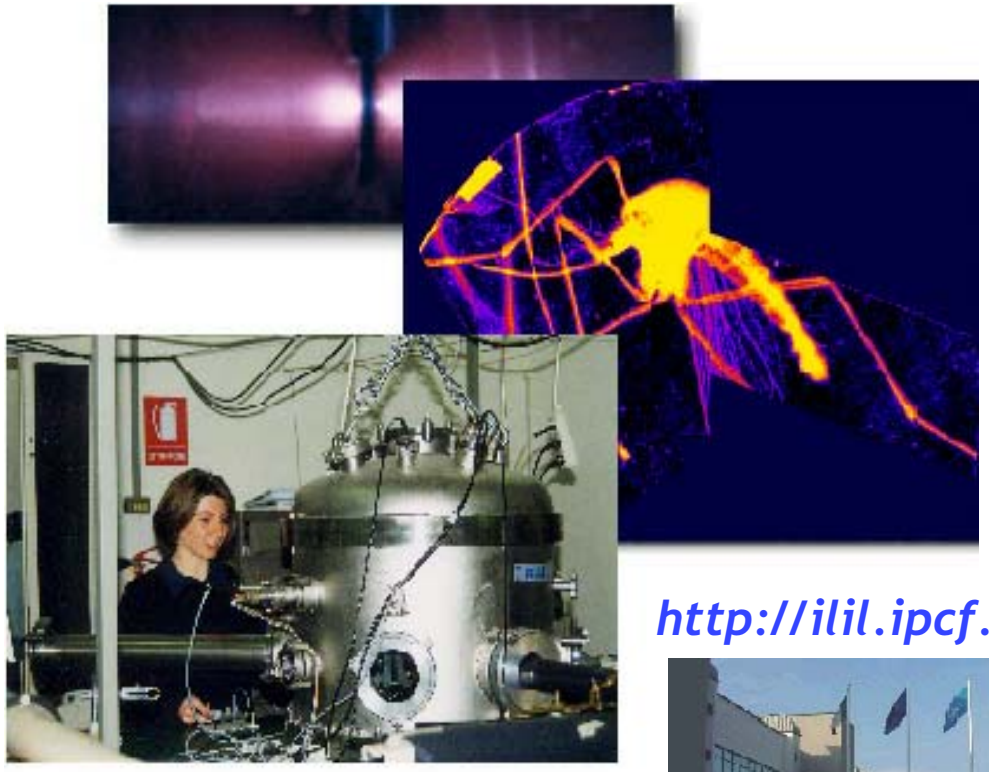

The ILIL staff

Antonio Giulietti

Danilo Giulietti

Leonida A. Gizzi

Paolo Tomassini

Walter Baldeschi

Antonella Rossi

Postdoc fellow

Stephane Laville

EU Network XPOSE fellow

Ph.D students

Marco Galimberti

Luca Labate

Flavio Zamponi

Graduated fellows

Alessio Misuri

Paola Squillacioti

Carlo A. Cecchetti

Petra Koester

Gabriele Palladino

http://ilil.ipcf.cnr.it @

CNR Campus, Pisa, Italy

Outline

1. BASIC X-RAY EMISSION PROCESSES
2. PLASMA CHARACTERISATION AND MODELLING
3. LASER-PLASMA X-RAY SOURCES
4. APPLICATIONS OF LP X-RAY SOURCES
5. PERSPECTIVES

BASIC X-RAY EMISSION PROCESSES

CONSIGLIO NAZIONALE DELLE RICERCHE
Istituto per i Processi Chimico-Fisici

X-rays From Intense Lasers

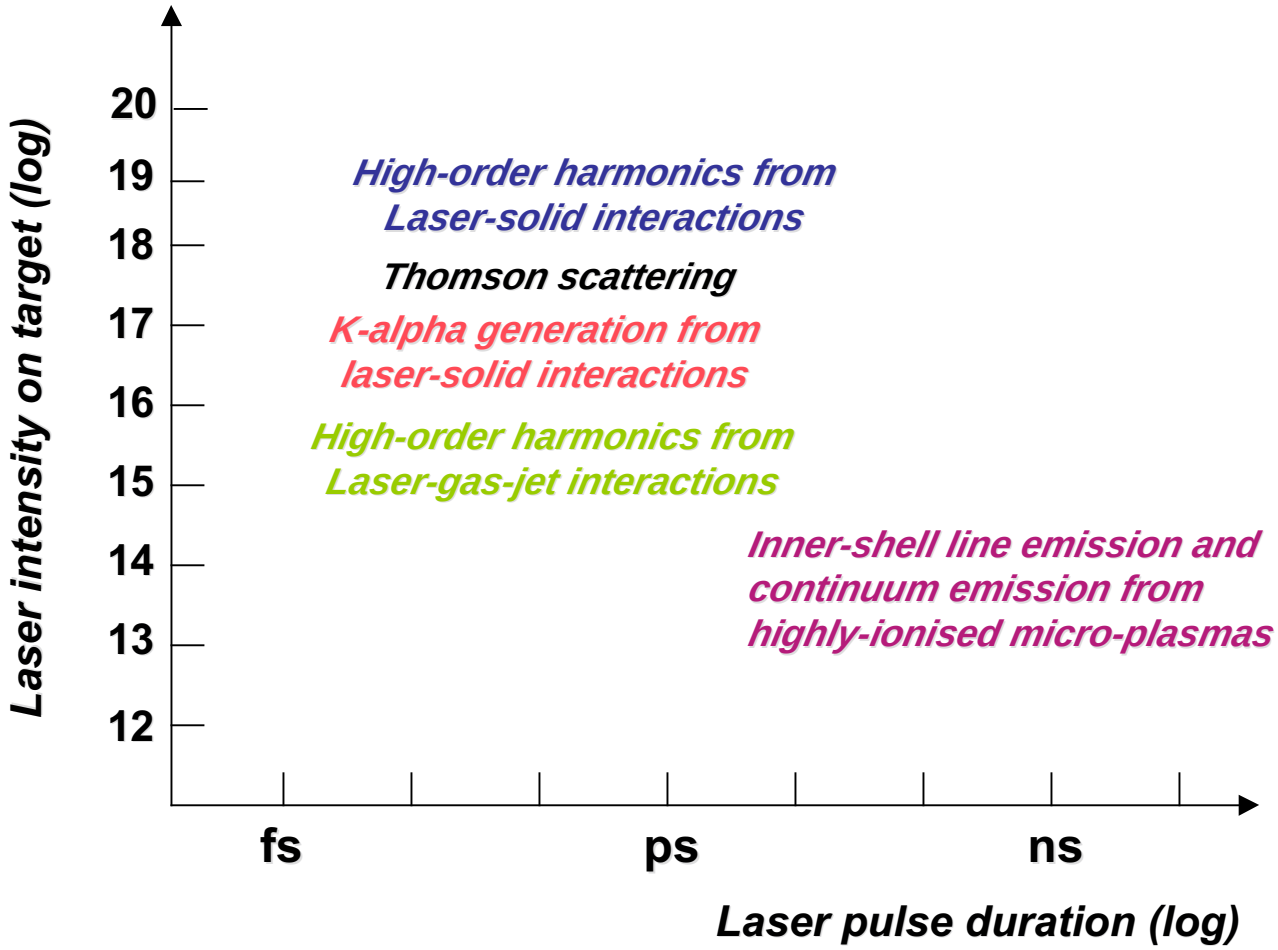

Basic Properties

Laser-plasma X-rays consist of characteristic line-emission and continuum emission from bremsstrahlung and recombination

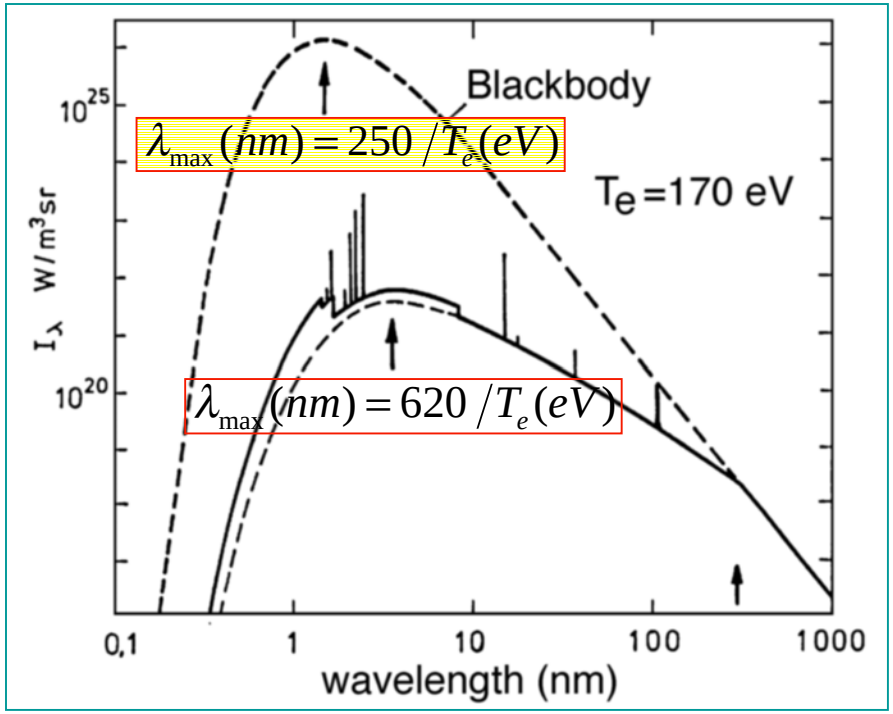

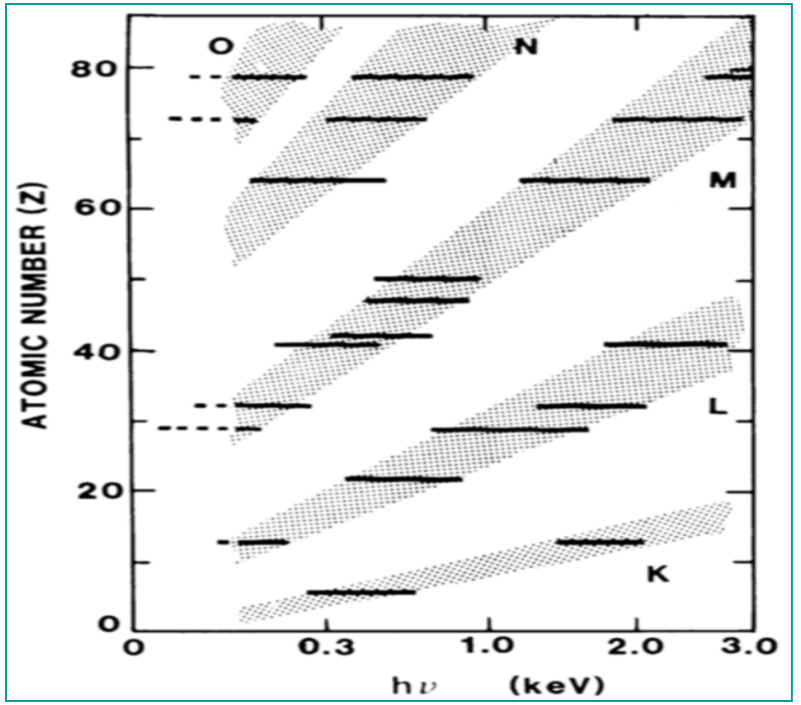

Characteristic emission wavelength depends on the atomic number

K.M. Gilbert et al., J. Appl. Phys.**51**, 1449 (1980)

Laser Plasmas

Typical parameters

LASER PARAMETERS

Pulselength: ns down to ps
Intensity on target: up to 10^{15} W/cm^2

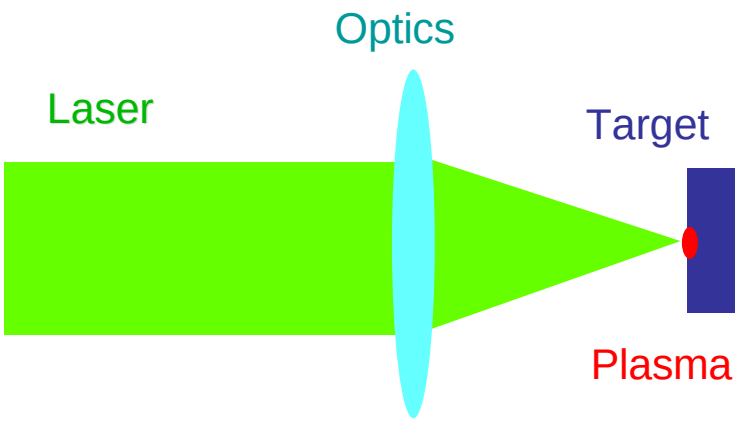

PLASMA TRANSVERSE SIZE	10 µm to ≈ 1 mm
EXPANSION VELOCITY	≈ 10^6 - 10^7 cm/s
ELECTRON TEMPERATURE	100 eV to ≈1000 eV
ELECTRON DENSITY	up to 10^{23} cm^{-3}
ION TEMPERATURE	≤ T_e
ION DENSITY	≈ N_e

Basic Hydrodynamics

X-ray emission from laser-solid interactions occurs in a narrow layer at the critical density

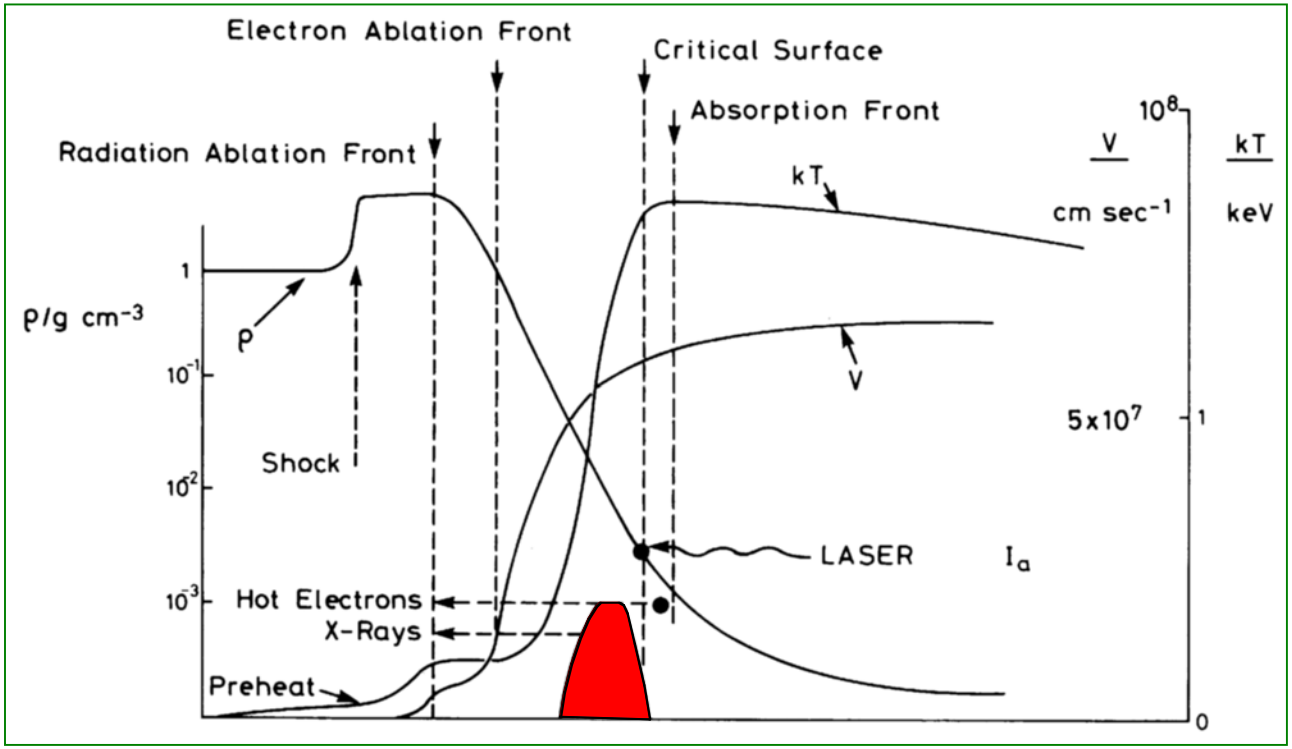

X-ray spectroscopy in the 0.1-2 nm range

Bragg diffraction from known singlecrystals (Si, TlAP, KDP, ADP etc.) is used to obtain point-source spectra

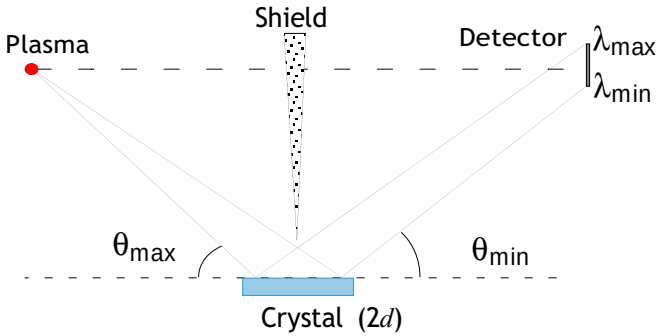

$$n\lambda = 2d\sin\theta$$

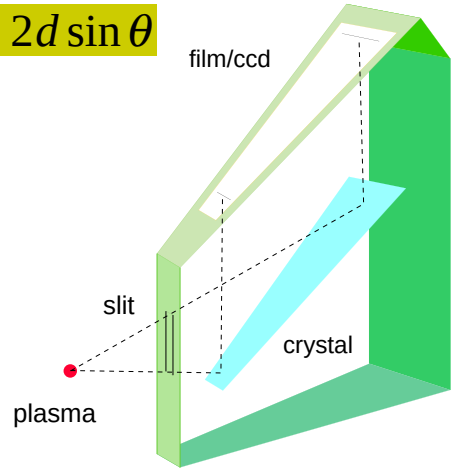

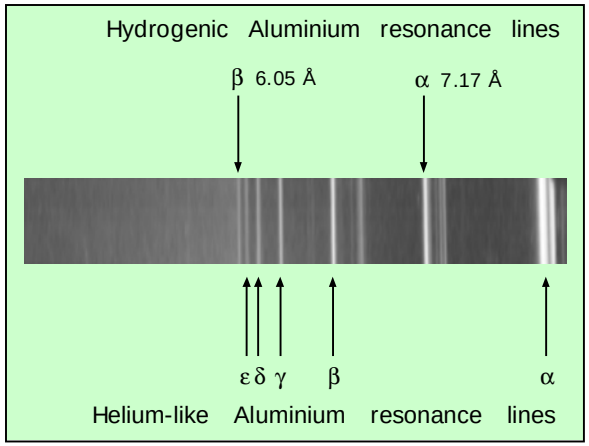

K-shell emission from a plasma produced by 3 ns laser irradiation of solid Al, obtained with a TlAP flat crystal.

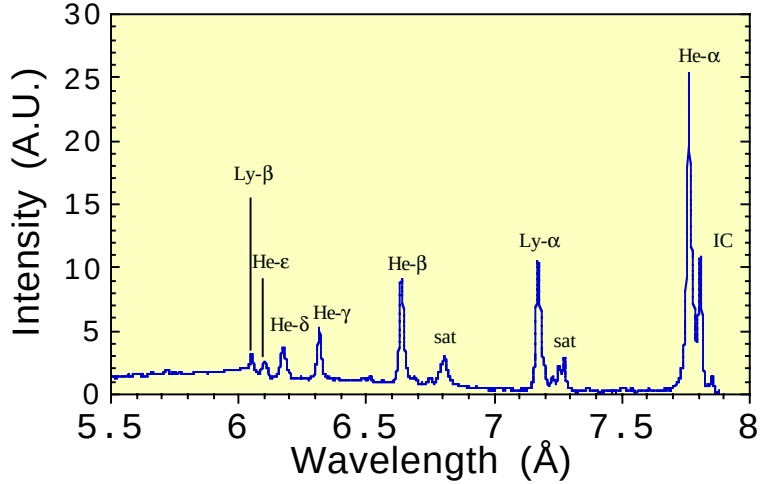

High dynamic range X-ray spectroscopy

X-ray Charge Coupled Devices enable single shot detection of spectra

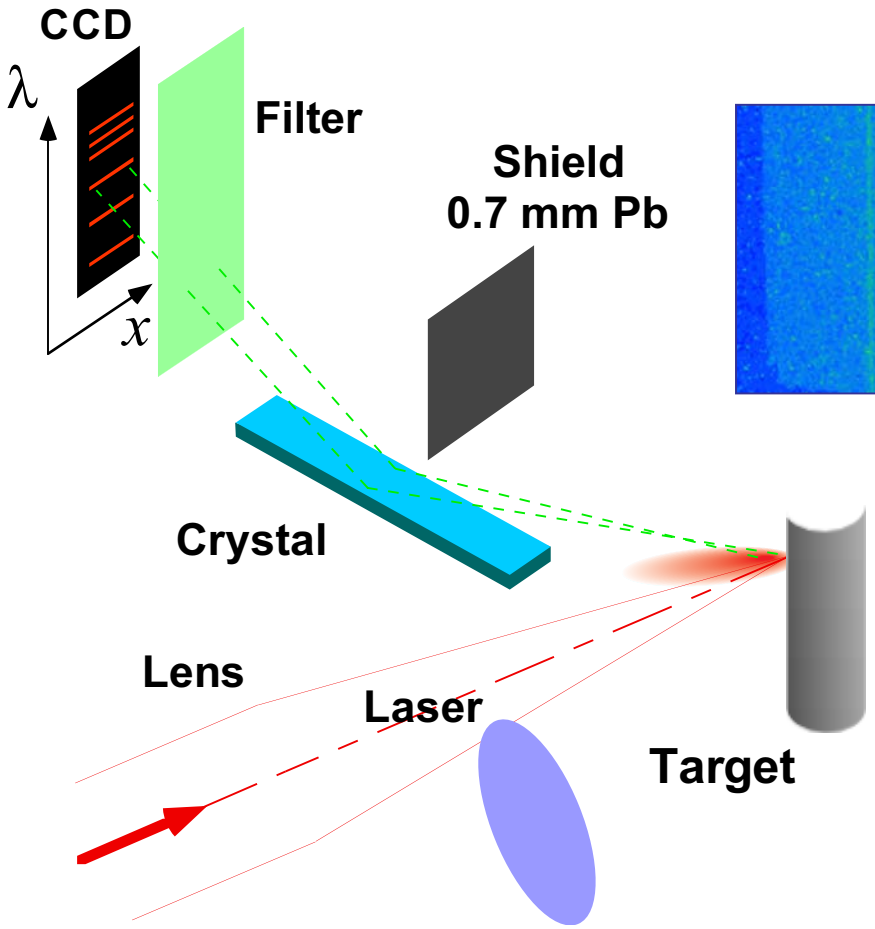

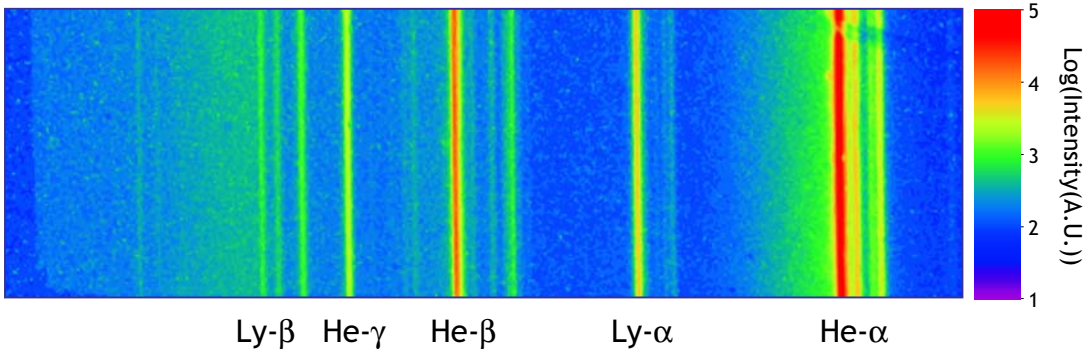

High dynamic range CCDs can produce spectra with S/N > 1000

High dynamic range X-ray spectroscopy

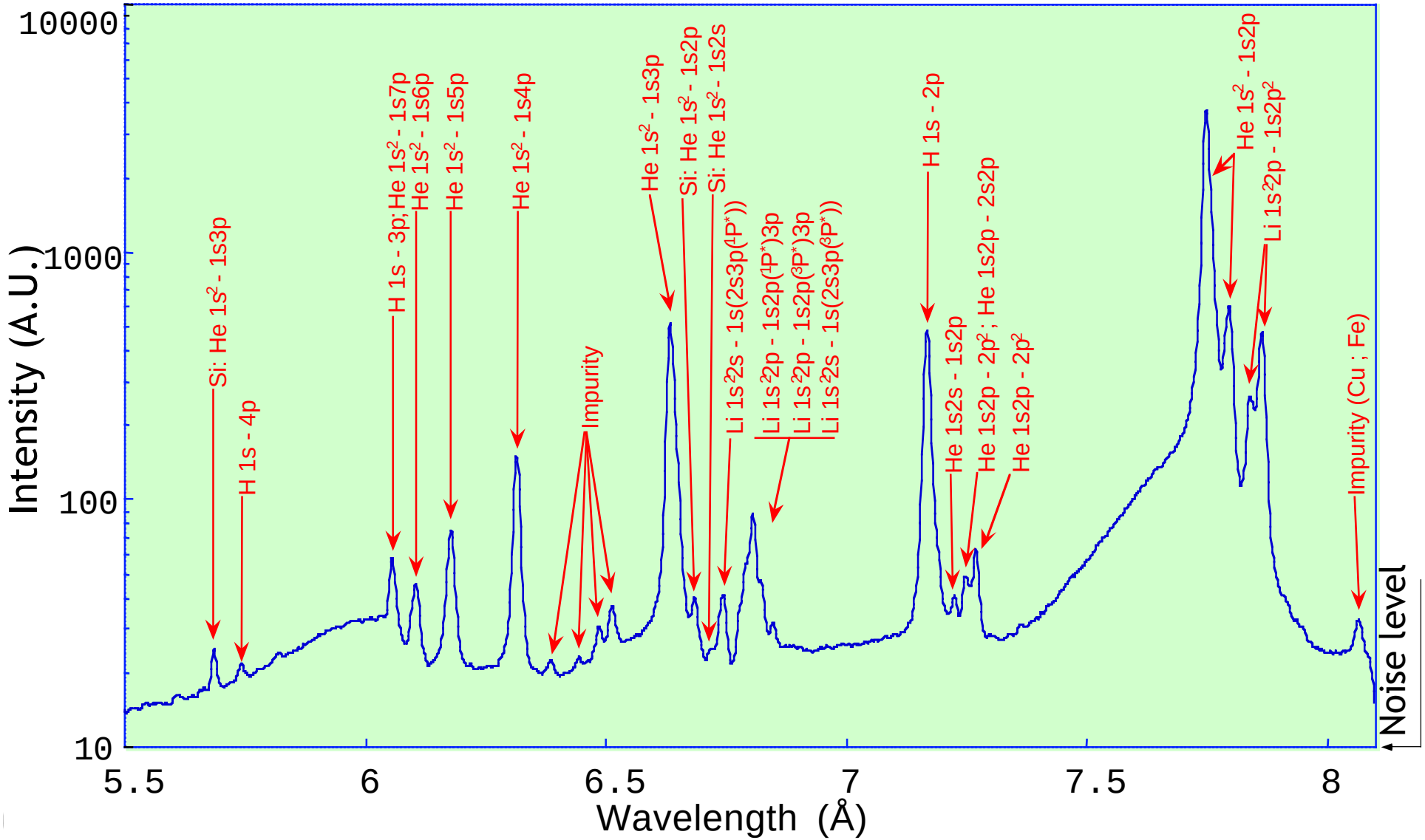

Spectroscopy with Spatial Resolution

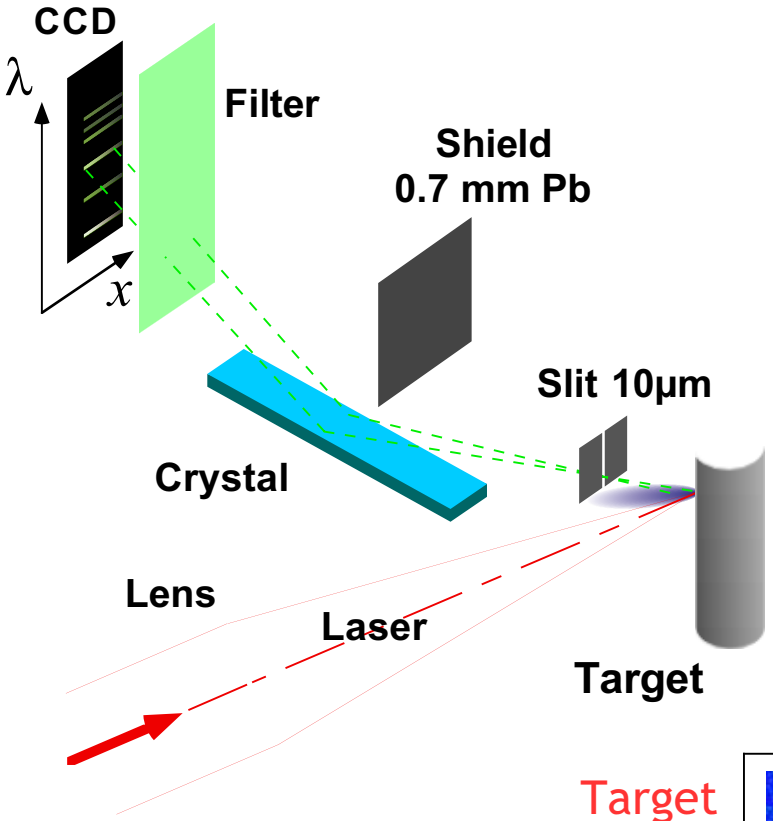

The use of a micrometer-wide slit, oriented along the spectral dispersion axis, allows the spatial distribution of X-ray emission to be resolved along one axis with a spatial resolution given by the equivalent pin-hole camera configuration

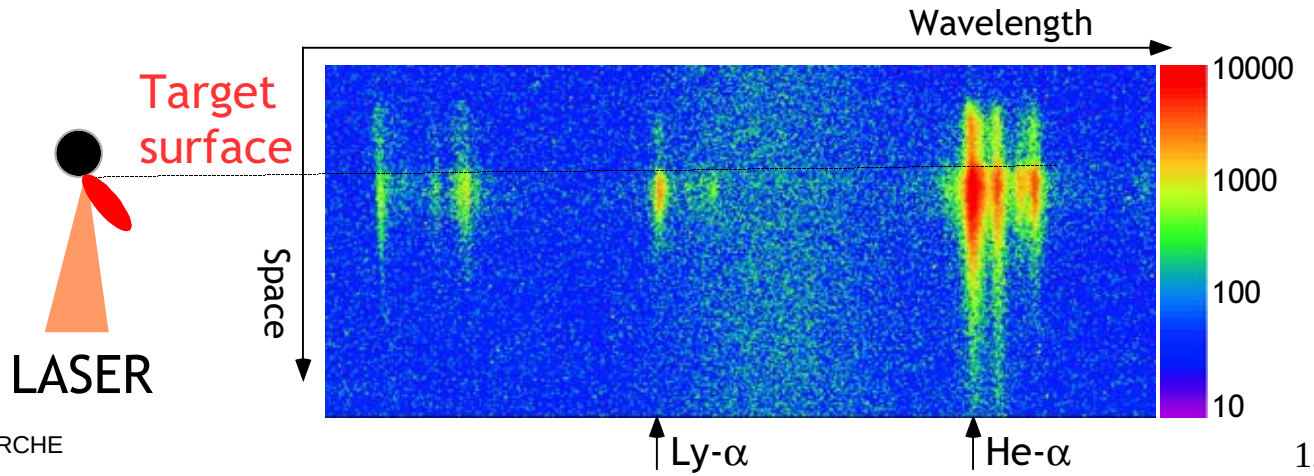

Spectroscopy with temporal resolution

An X-ray streak-camera equipped with a crystal spectrometer enables temporal analysis of X-ray emission with picosecond resolution

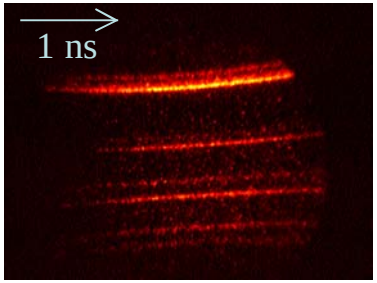

ALLUMINIUM

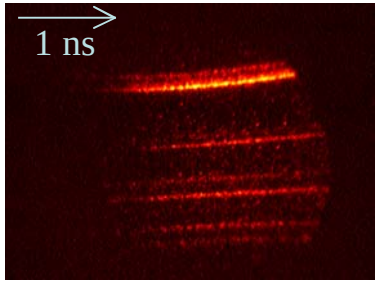

ALLUMINIUM

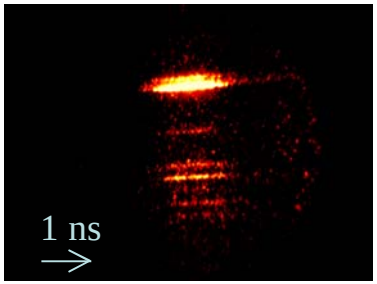

SILICON

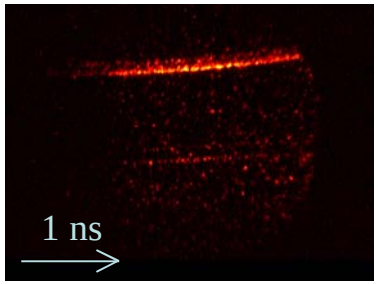

SILICON

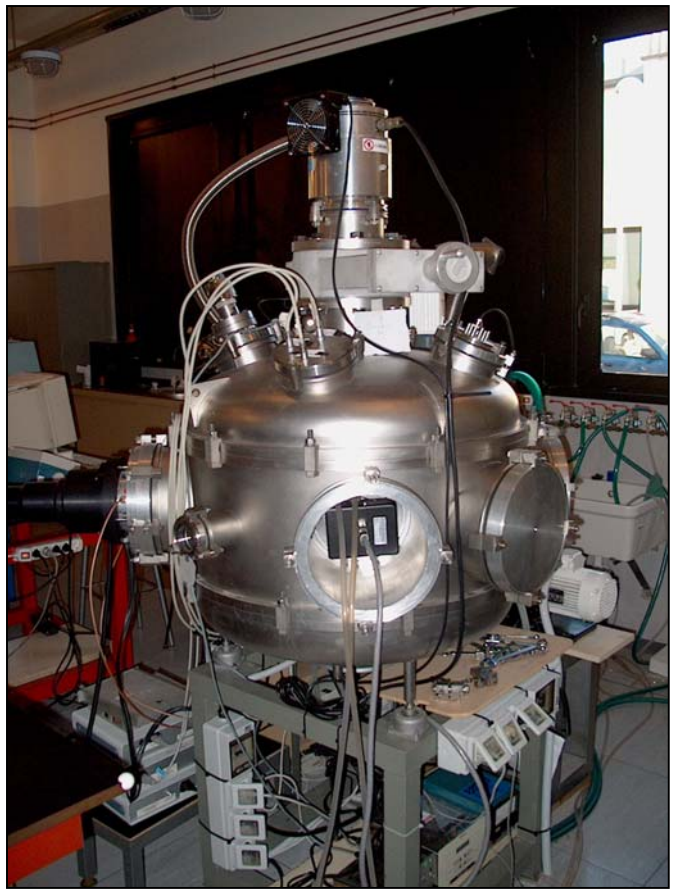

PLASMA CHARACTERISATION AND MODELLING

CONSIGLIO NAZIONALE DELLE RICERCHE
Istituto per i Processi Chimico-Fisici

Characterisation of Laser-Plasmas

Experimental data:

X-ray spectroscopy
Line intensity ratios are measured as a function of space and time

+

Interferometry
Plasma electron density in the regions of interest ic obtained from refractive index measurements

HYDRODYNAMIC SIMULATIONS

A comparison between experimental data and predictions of numerical simulations yields plasma physical conditions in the region and at the time of interest

EQUILIBRIUM MODEL

Numerical Codes

Hydrodynamic properties of plasmas (electron density and temperature, expansion velocity etc.) can be modelled using Lagrangian or Eulerian numerical codes

Examples of Hydrodynamic Codes
Medusa[1] 1-D
Pollux[2] 2-D

Examples of Atomic Physics
RATION/FLY[3]

Similarly, a description of X-ray emission properties of laser-plasmas can be obtained from numerical codes that account for a collisional-radiative equilibrium

[1] Christiansen *et al., Comput.Phys.Commun.* ***7***, 271 (1974)
[2] Pert G.J., *J. Comput. Phys.* ***43***, 111 (1981)
[3] Lee *et al.., J. Quant. Spectrosc. Radiat. Transfer* ***32***, 91 (1984)

Test cases for kinetic codes

The understanding of radiative properties of non-LTE plasmas requires an accurate prediction of atomic level populations

A wide range of non-LTE kinetic codes have been developed independently over the years. A systematic comparison of these codes, based upon a set of test-cases, has been promoted) to investigate primarily ionization of inner shells for given plasma conditions in either steady-state or time-dependent regime:*

Element	Case	Total number	Grid	Number in temperature and density arrays
Carbon	C–SS	18	Te: 5, 10, 20, 40, 60, 80	6
			Ne: 10^{16}, 10^{20}, 10^{22}	3
Aluminum	Al–SS	18	Te: 50, 100, 200, 400, 600, 800	6
			Ne: 10^{20}, 10^{22}, 10^{23}	3
Argon	Ar–SS	16	Te: 675, 900, 1500, 2200	4
			Ne: 10^{12}, 3×10^{14}, 10^{18}, 10^{21}	4
Germanium	Ge–SS	27	Te: 150, 200, 250, 300, 350, 400, 450, 500, 600	9
			Ne: 10^{17}, 10^{20}, 3×10^{22}	3
Gold	Au–SS	6	Te: 800, 1200, 1600, 2000, 2400, 2800	6
			Ne: 10^{20}	1

Case	Initial condition	Time increment	Start	Stop	Case description
TD–C	Fully stripped	0.2690 (log)	0.1 ps	0.1 ns	Recombination laser
TD–Al	LTE	0.2174 (log)	5.0 ps	1.5 ns	Exploding foil
TD–Ar	LTE	20.0 ps (linear)	20.0 ps	2.0 ns	ICF implosion core

*) R.W. Lee et al., JQSRT, *58*, 737 (1997)

Codes comparison

Time dependent recombination of Carbon starting from the fully stripped state Z*=6:

Curves spread depends upon the number of principal quantum number (PQN) levels included in the calculation.

Average ionization of Aluminium as a function of the electron temperature for an electron density of 10^{21} cm^{-3}.

Large spread (except eround the He-like Al stage) of average ionization and fractional ionization

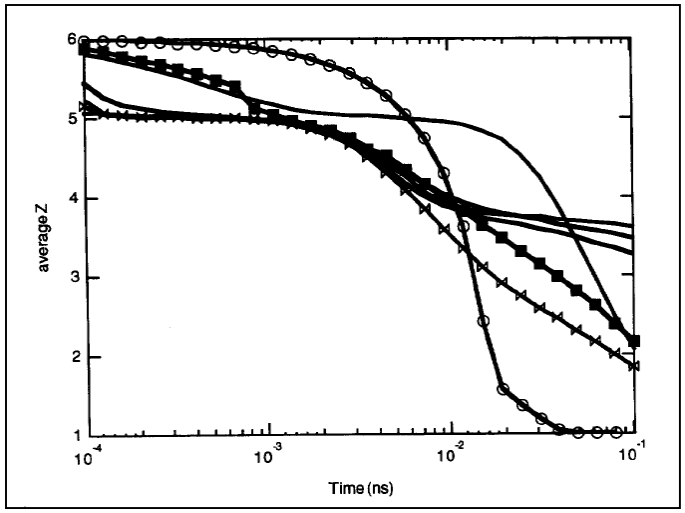

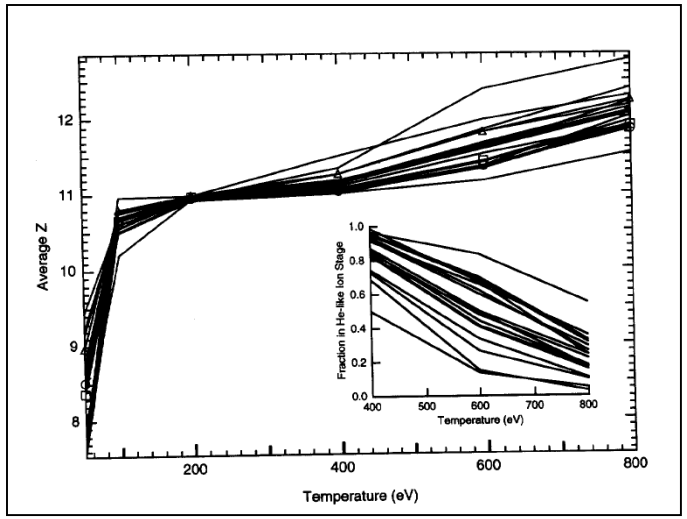

Comparison of results for relatively simple cases show substantial discrepancies between different codes. The completeness of level description (many PQN) is a key issue in order to obtain a consistent description of the ionization history across codes.

Codes benchmarking

•The validity test of kinetic codes requires plasma production under well controlled conditions.

•Several irradiation schemes are used to produce suitable test-plasmas including disk/solid target, exploding thin foil, microdot on thin substrate etc…

Disk/solid

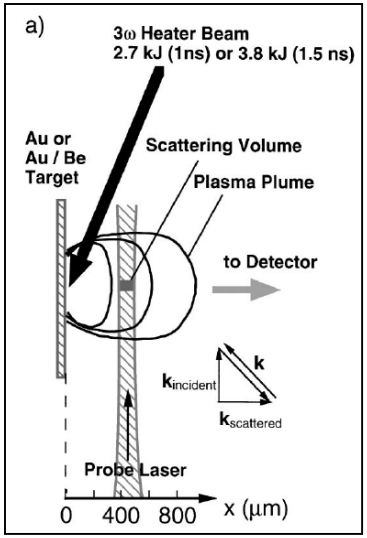

from S.H.Glenzer et al. JQSRT, **63**, 253 (2000).

Exploding Foil

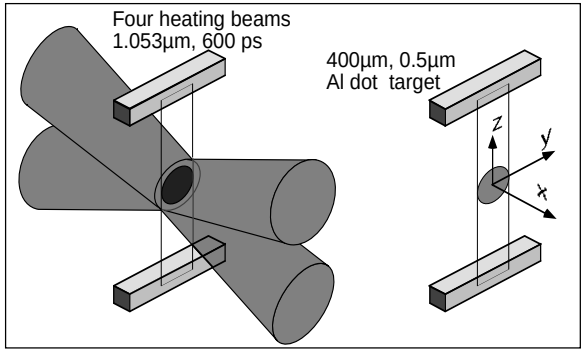

from L.A.Gizzi et al. PRE, **49**, 5628 (1994)

Microdot

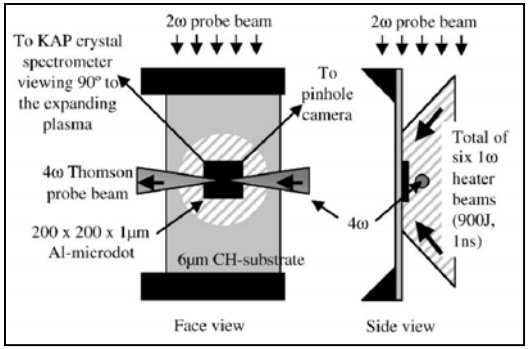

from D.M. Chambers et al. PRE, **66**, 026410 (2002).

Where possible, independent plasma characterisation is carried out using X-ray imaging (PHC), Thomson scattering, optical interferometry and with the aid of hydrodynamic simulations.

Transient ionization in ns laser-plasmas

Ionization from a charge state *Z to a charge state Z+1*

$$\tau_{Z\to Z+1} = N_{Z+1}/\left|dN_{Z+1}/dt\right|$$

$$\frac{dN_{Z+1}}{dt} = n_e\left[(S_c^Z + S_R^Z)N_Z - (\alpha_{3B}^{Z+1} + \alpha_{RR}^{Z+1})N_{Z+1}\right]$$

Here n_e is the plasma electron density, N_Z is the population of the charge state Z, S_c^Z and S_R^Z are the rates of collisional and photo- ionization from the charge state Z respectively while α_{3b}^{Z+1} and α_{RR}^{Z+1} are the rates of three-body and radiative recombination from the charge state $Z+1$.

Calculations show that relaxation time from He-like to H-like Al is comparable to the rise-time of nanosecond pulses

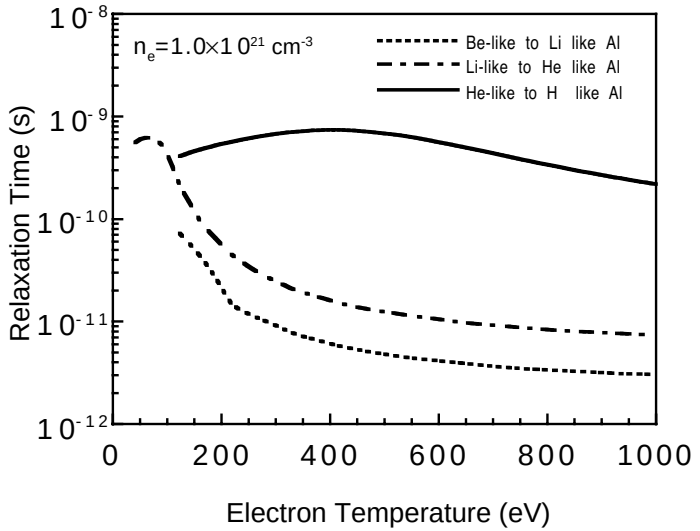

Experimental technique

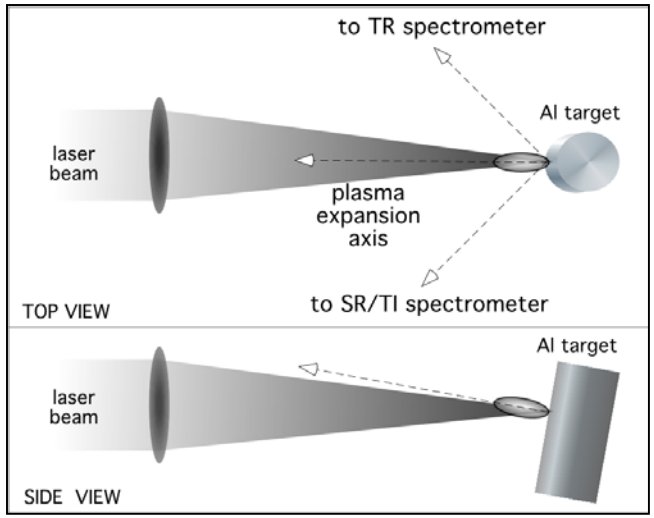

- ***Tight-focus irradiation of solid target using single longitudinal and transverse mode Nd:YLF laser pulse;***
- ***Comparison of streak-camera X-ray spectra with CCD spectra for relative intensity calibration.***

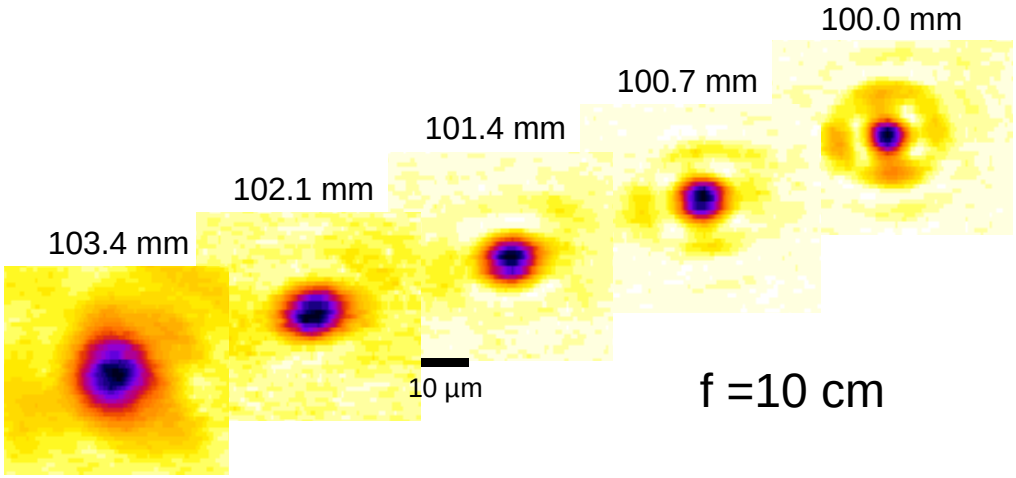

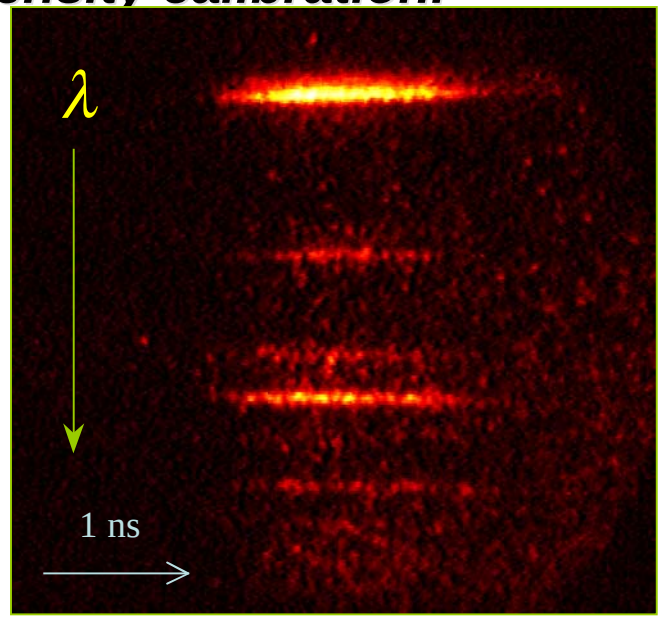

Raw data at low sweep speed

Cross-calibration of spectra

Corrected and calibrated spectrum of early-stage X-ray emission at higher temporal resolution

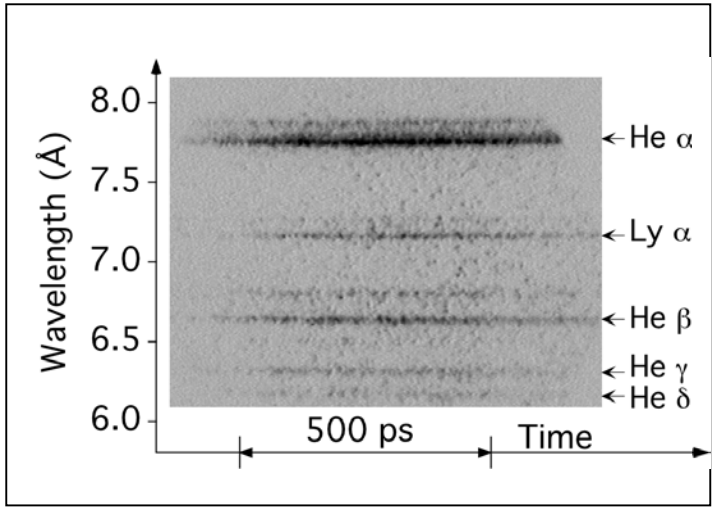

Cross-calibration

Simultaneous time integrated spectrum is taken along an equivalent line of sight

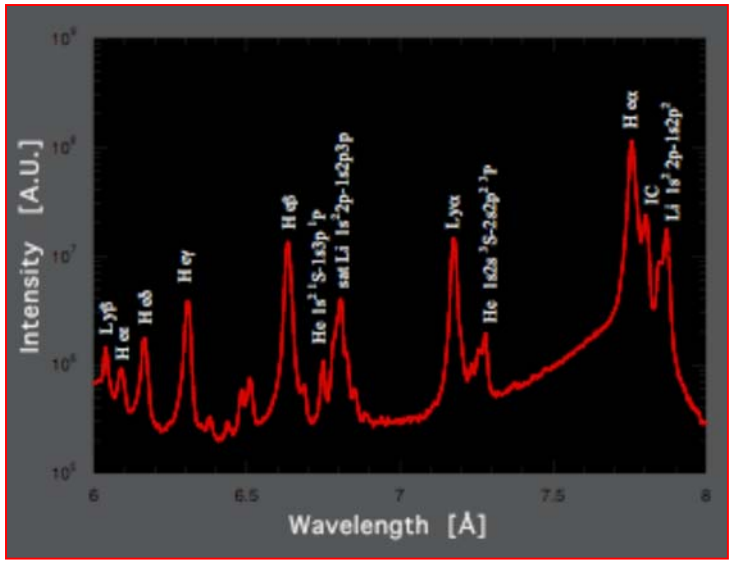

Hydrodynamic modelling

Map of the electron temperature of the plasma produced by laser irradiation of a solid Al target at the peak of a 3ns gaussian laser pulse as predicted by POLLUX

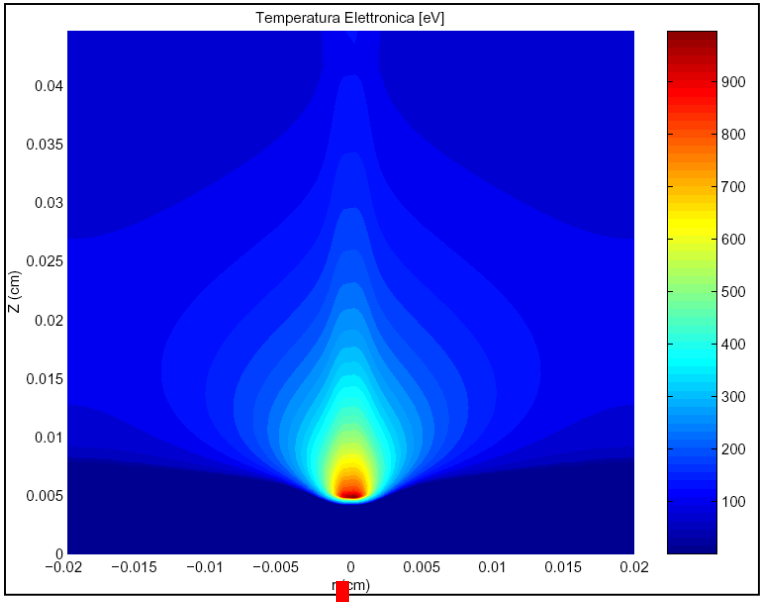

Intensity on target:
1E14 W/cm^2
Pulse duration:
3 ns gaussian
Laser focal spot:
8µm
Target:
50 µm thick Al

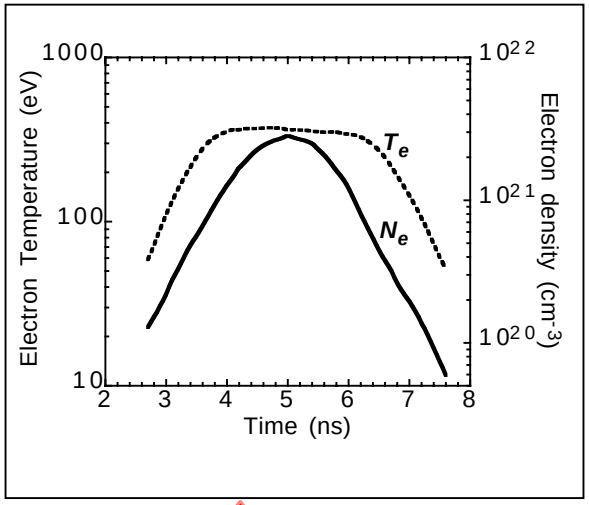

X-ray emissivity is calculated from electron density and temperature maps given by POLLUX using the code FLY

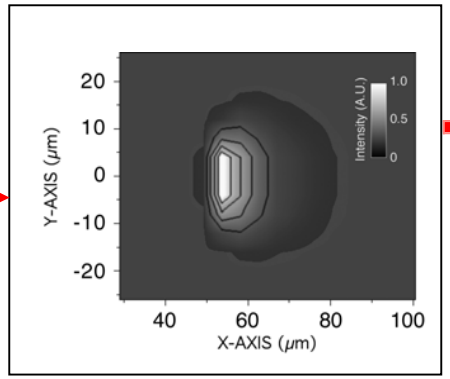

Laser

Narrow X-ray emitting region with well-defined density and temperature conditions.

Hydrodynamics and X-ray emission

X-ray emission at 1.6 keV (He-like Al $1s^2$-1s2p) from a plasma produced by laser irradiation of an Al target

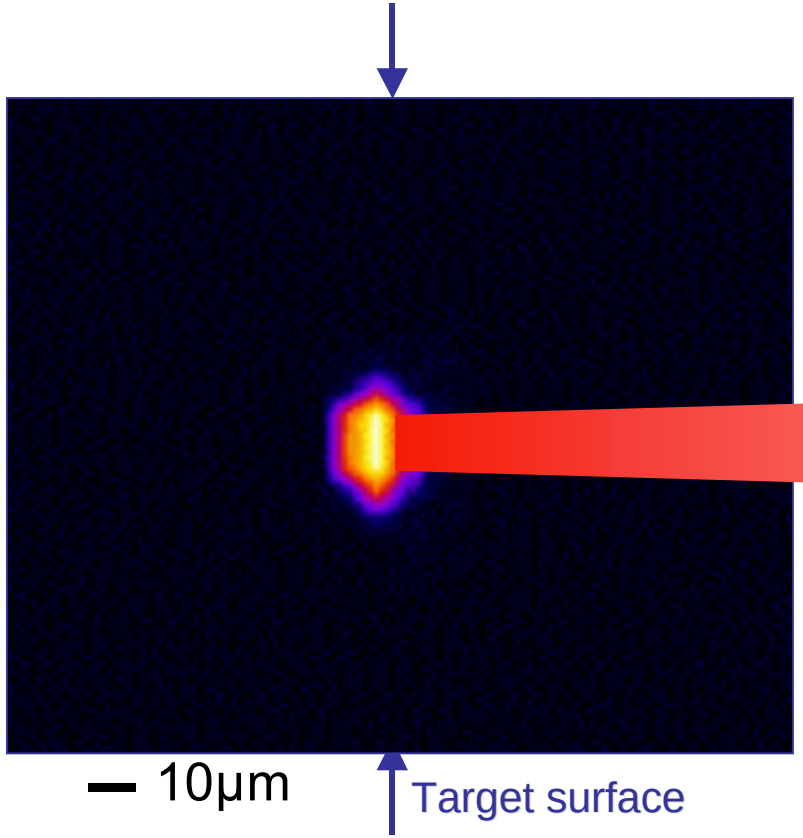

Total simulation time: 2 ns
Frame every 200 ps

Laser pulse, 3ns FWHM

Electron density and temperature maps obtained from hydrocode (POLLUX) are post-processed using time-dependent X-ray emission code (FLY)

Evidence of transient ionisation

Temporal evolution of Lyα to Heβ intensity ratio:
Experiment vs. *ss/td* modelling

3ns FWHM pulse is peaked at 4.5 ns

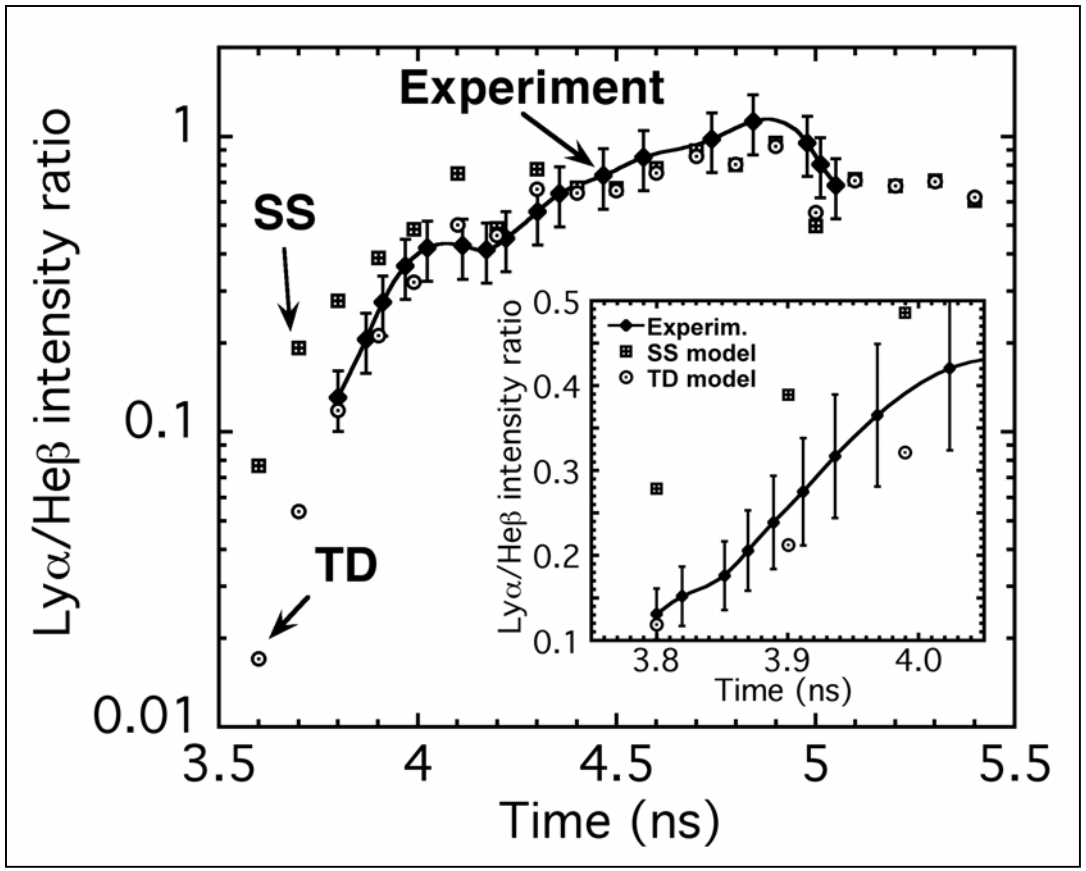

Early during the emission, time dependent and steady-state model show different results. Later on, both models give identical ratio. Early stage experimental ratio agrees well with *td* calculations.

L.A.Gizzi et al., Letter on Phys. Plasmas, in press (2003).

Radiative cooling in ps laser plasmas

A high contrast 12 ps laser pulse is focused onto a solid target of Fluorine salts (LiF through SrF_2)

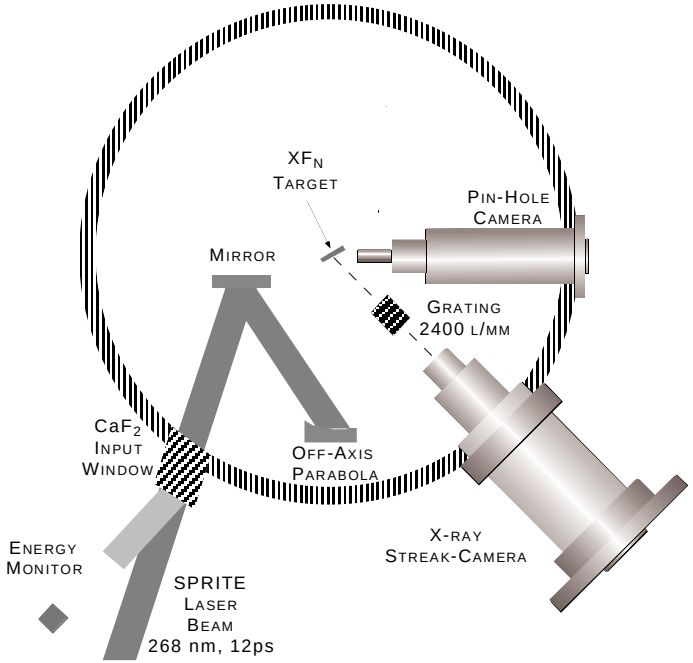

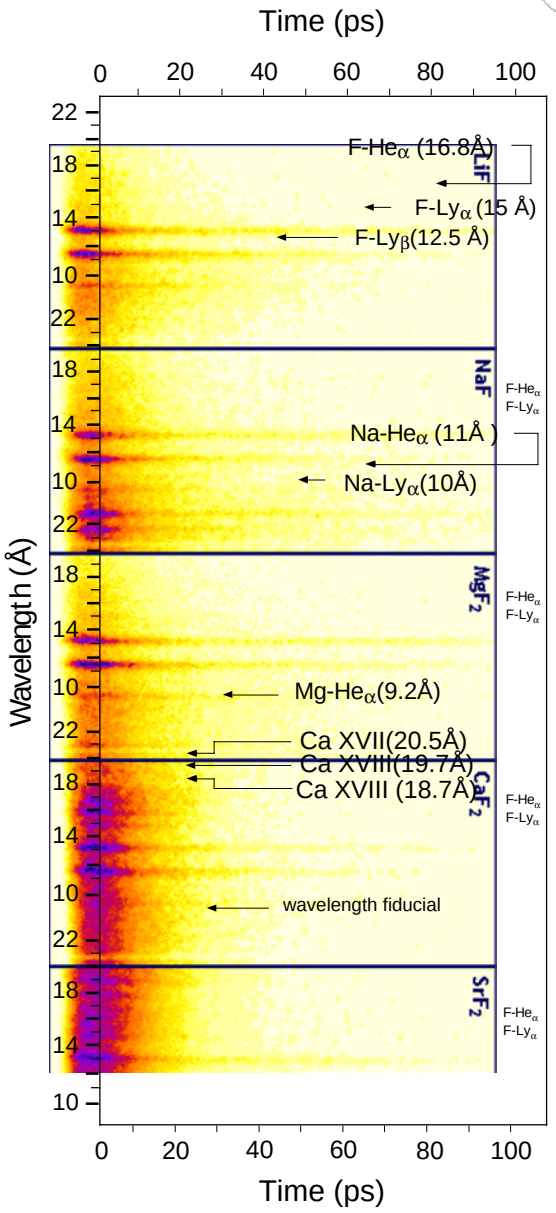

Modelling of picosecond X-ray emission using MEDUSA and RATION

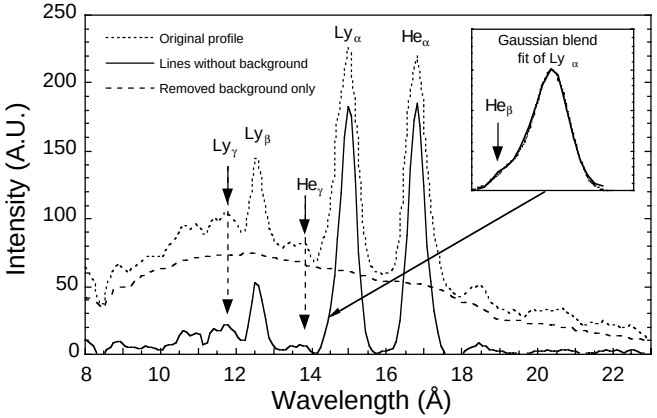

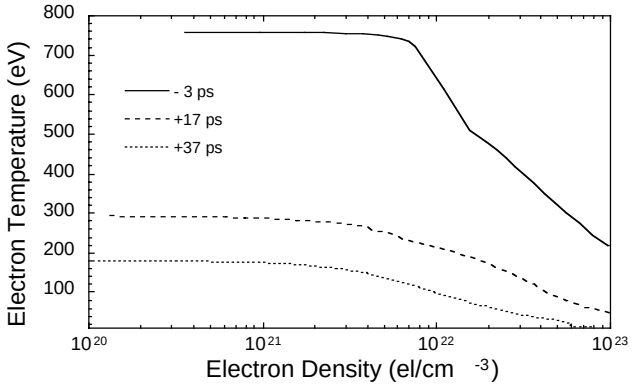

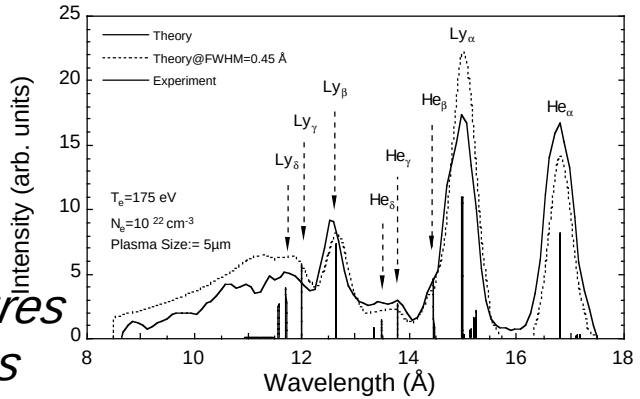

1D modelling provides satisfactory description of time-integrated K-shell spectra of Fluorine.

Line intensity ratios and electron temperatures at the peak of the emission for the five types of target.

Target	LiF	NaF	MgF_2	CaF_2	SrF_2
Ly_α/He_α (±10%)	0.94	1.10	1.05	0.97	0.84
Temperature (eV)	186–194	192–216	191–203	187–197	183–187

Temperature history vs. atomic number

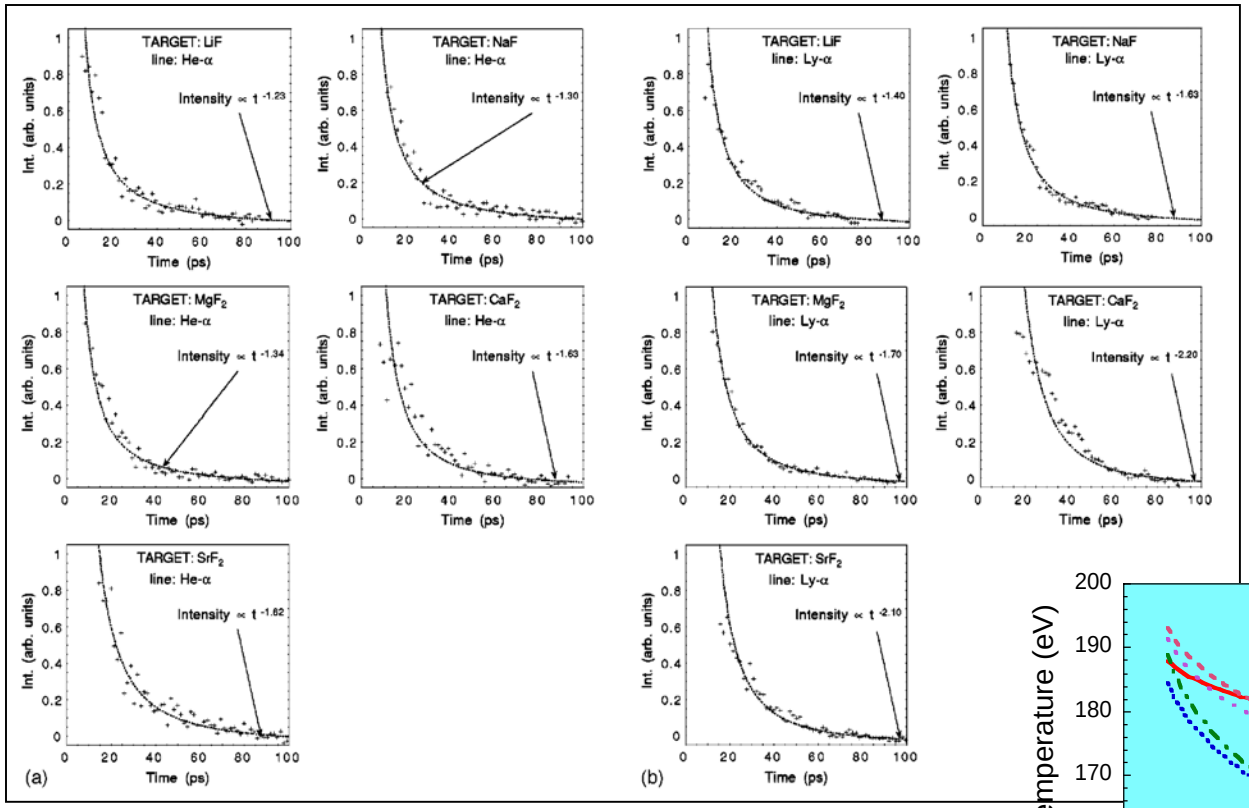

Electron temperature as obtained from H-like to He-like intensity ratio exhibits a faster decay for higher-Z targets as a result of stronger radiation cooling

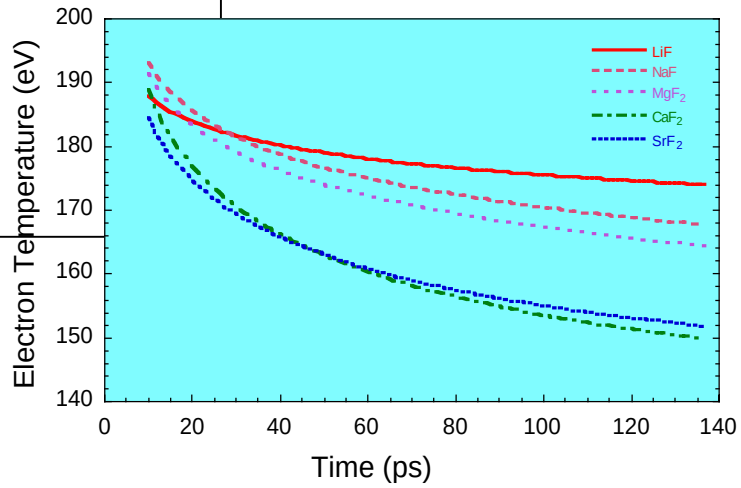

L.A.Gizzi et al., Phys. Rev. E, ***52***, 2721 (2000).

LASER-PLASMA X-RAY SOURCES

CONSIGLIO NAZIONALE DELLE RICERCHE
Istituto per i Processi Chimico-Fisici

Source Size

15 μm laser spot on Cu target at 6E12 W/cm^2

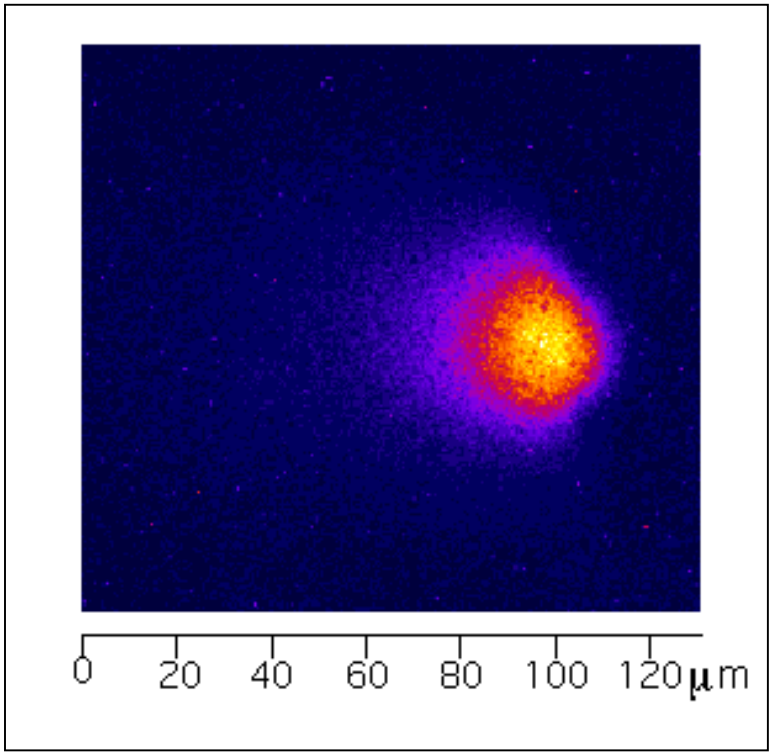

View: 45° from laser axis

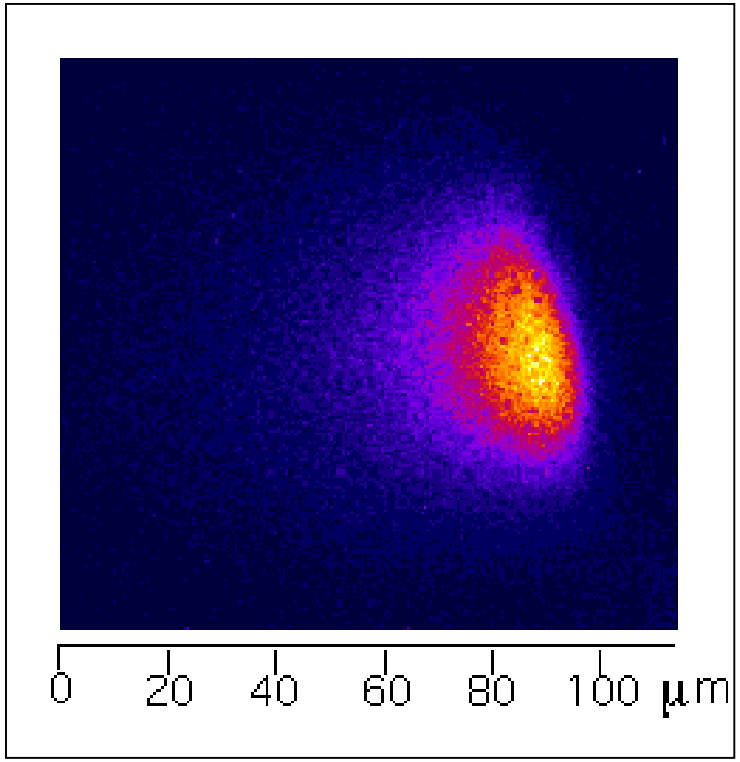

View:75° from laser axis

≈25 μm FWHM source size

X-ray μ-Imaging of the Plasma: Pin-hole Camera Arrays

An estimate of the size of the X-ray emitting region is typically obtained using a pin-hole camera

The use of pin-hole arrays with different filters allows the effective source size in different X-ray spectral regions to be evaluated

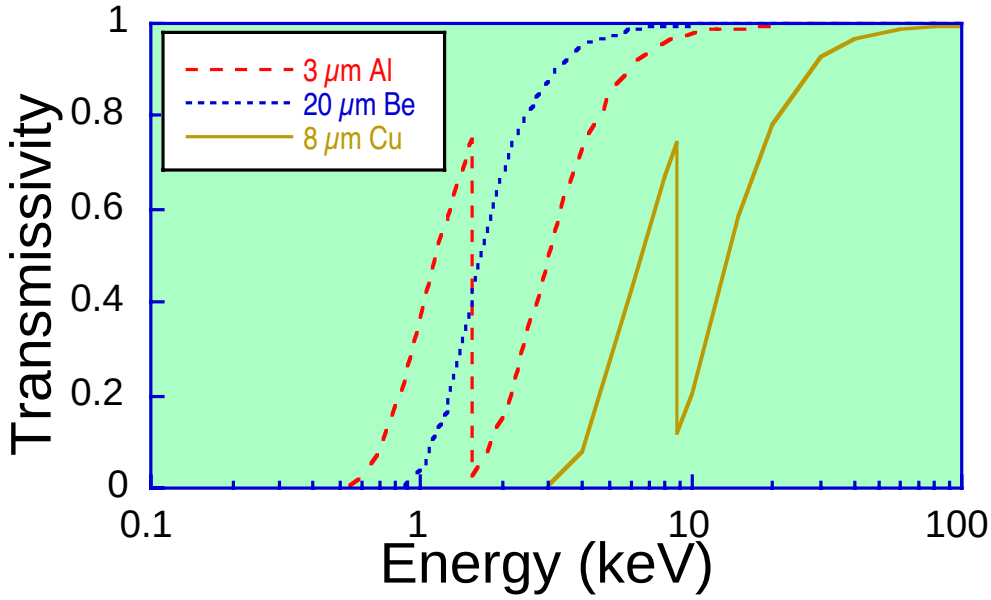

Optimum pin-hole diamater

$$d_{ph} = \sqrt{2.44\lambda\, q/(1+M)}$$

Space resolution

$$\Delta x_{plasma} = d_{ph}(1+1/M)$$

q = pin-hole-image distance

Effective Source Size

Plasma produced by a picosecond laser pulse focused onto a solid Al target at an intensity of 10^{16} W/cm² in a 25μm FWHM focal spot.

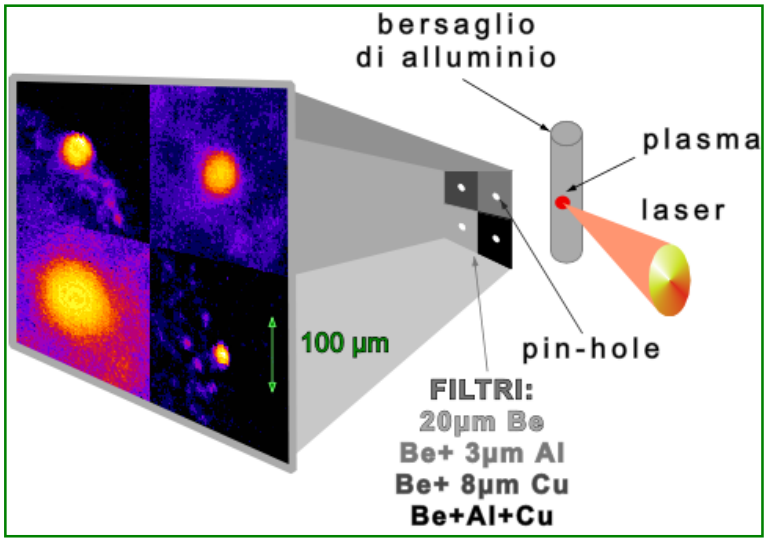

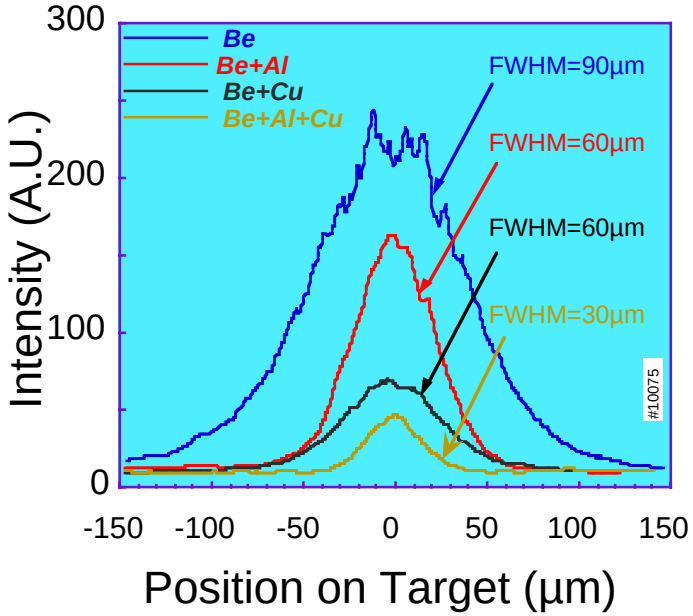

Measurements with pin-hole arrays show that the effective size of the X-ray emitting region becomes smaller at higher photon energy range.

Accessible photon energies for small laser systems

Up to Z=22-23, He-a K-shell emission lines can be obtained using small 10 Hz Nd lasers.

At higher Z, emission originate from L and M shells

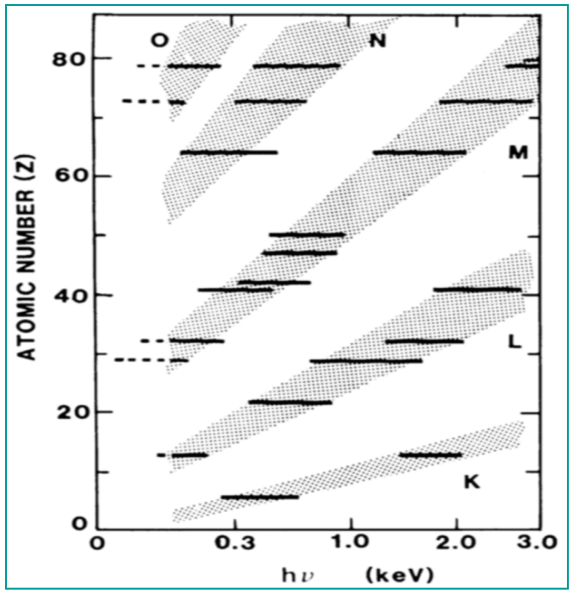

	Hydrogen-like		Helium-like	
Element	**2*p*1/2**	**2*p*3/2**	**2*p* 3P1**	**2*p* 1P1 (eV)**
13 Al	**1727.7**	**1729.0**	**1588.3**	**1598.4**
14 Si	**2004.3**	**2006.1**	**1853.9**	**1865.1**
15 P	2301.7	2304.0	2140.3	2152.6
16 S	2619.7	2622.7	2447.3	2460.8
17 Cl	**2958.5**	**2962.4**	**2775.1**	**2789.8**
18 Ar	3318	3323	3124	3140
19 K	3699	3705	3493	3511
20 Ca	**4100**	**4108**	**3883**	**3903**
21 Sc	4523	4532	4295	4316
22 Ti	**4966**	**4977**	**4727**	**4750**
23 V	5431	5444	5180	5205
24 Cr	5917	5932	5655	5682
25 Mn	6424	6442	6151	6181
26 Fe	6952	6973	6668	6701
27 Co	7502	7526	7206	7242
28 Ni	8073	8102	7766	7806
29 Cu	8666	8699	8347	8392
30 Zn	9281	9318	8950	8999
31 Ga	9917	9960	9575	9628

“Tunability” of laser-plasma sources

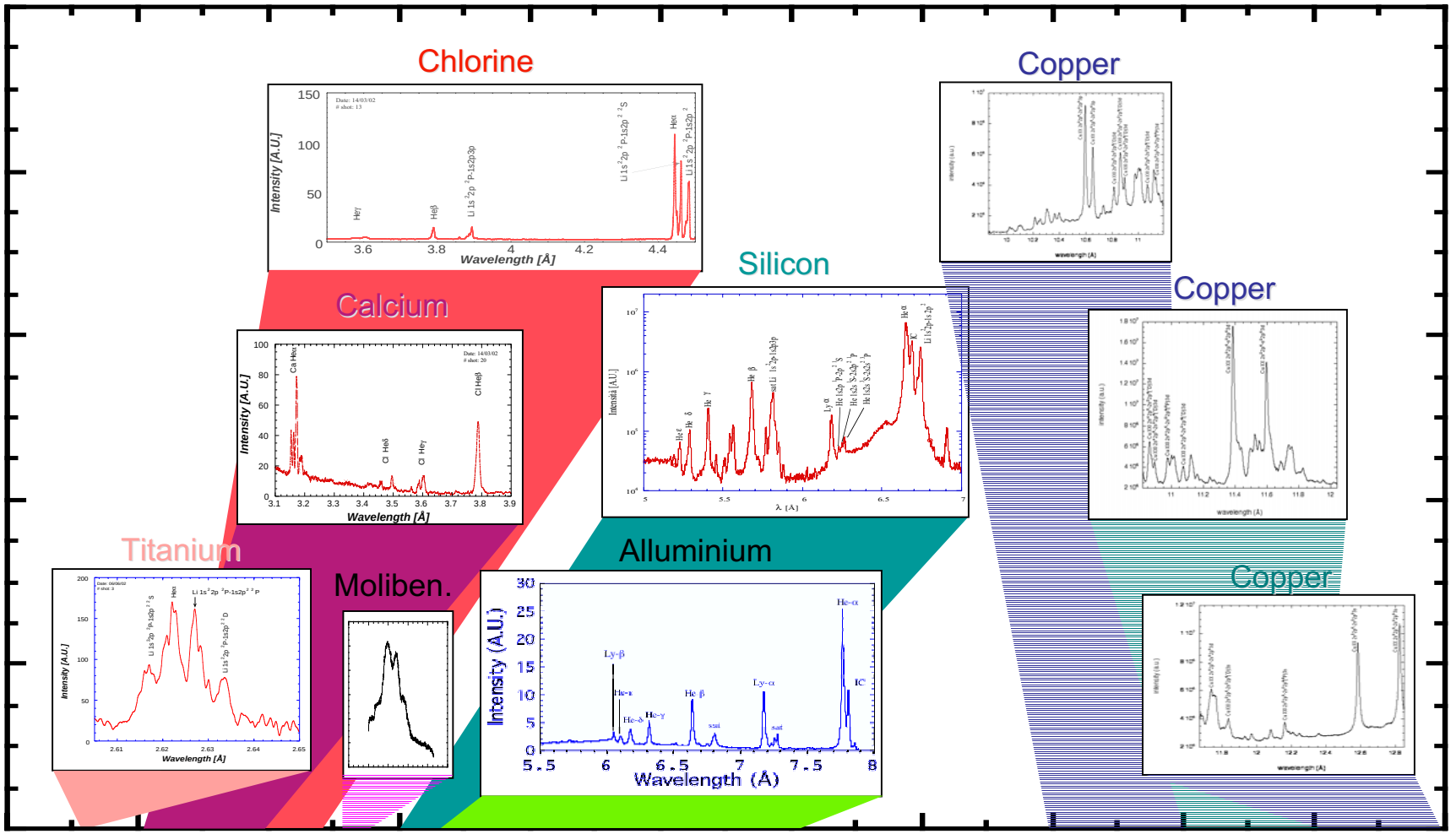

APPLICATIONS OF LP X-RAY SOURCES

CONSIGLIO NAZIONALE DELLE RICERCHE
Istituto per i Processi Chimico-Fisici

X-RAY MONOCROMATOR FOR CCD CALIBRATION

Bragg diffraction from a crystal is used to select narrow band soft X-ray radiation for CCD detector calibration in the single photon regime

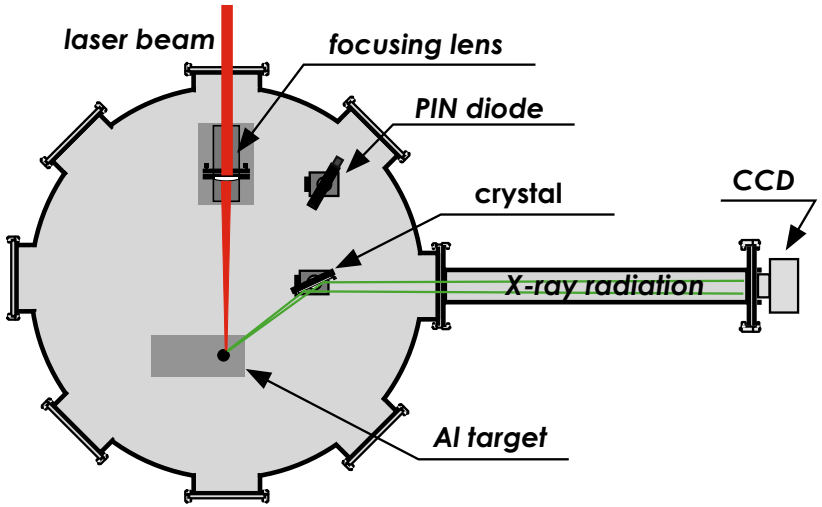

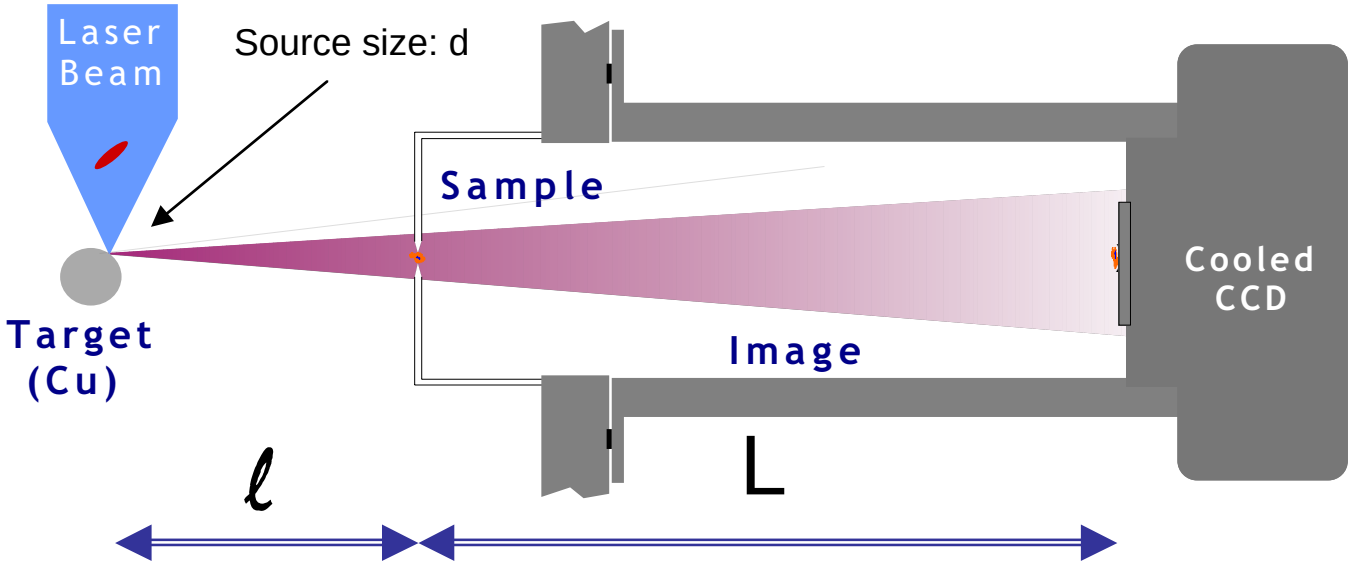
Laser
Beam
Source size: d
Sample
Target
(Cu)
Image
Cooled
CCD
ℓ
L

Characterisation using a zone-plate

A Fresnel zone-plate with known geometrical properties is used as a sample to determine magnification and resolution properties of the imaging system

X-ray image of a zone-plate: M=4.7

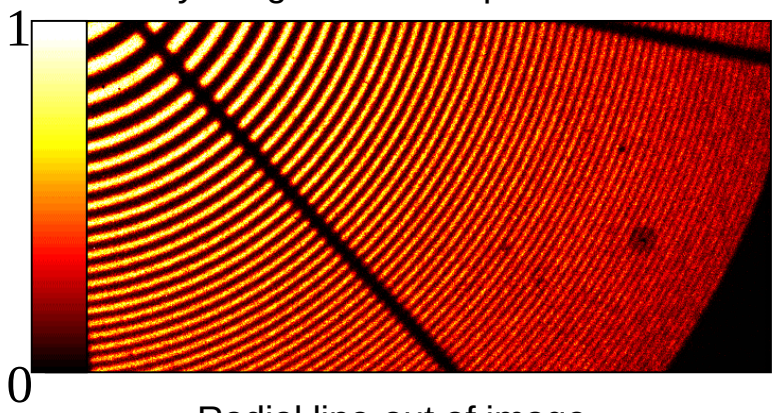

Radial line-out of image

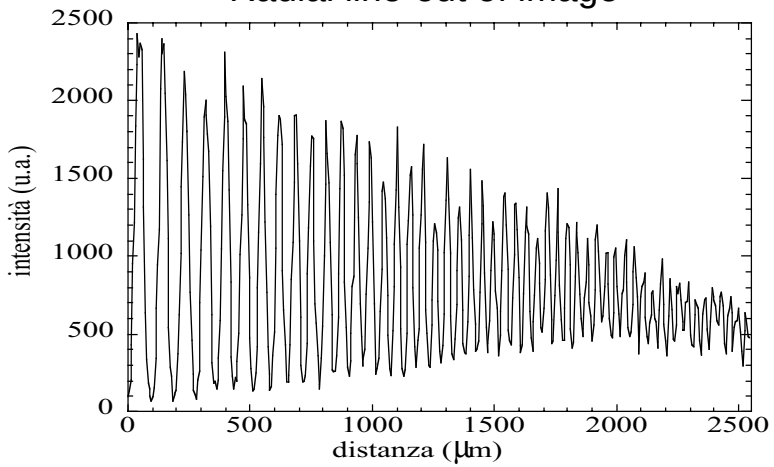

Resolution definitions using a step-function

Source Profile: $f(x) = Ae^{-\frac{(x-x_O)^2}{2\sigma^2}}$

Sample Profile: $g(x) = \vartheta(x - s_O)$

⇒ ***Image profile:***

$$I(x) = a\, erf\left(\frac{x - x'_o}{\sqrt{2}(M-1)\sigma}\right) + d$$

Space resolution condition: $\Delta x = 2\sigma$

A 26 µm (FWHM) source size (PLX@ILIL) *yelds a resolution of approx. 20µm at the object plane*

μ-radiography of biological tissues

X-RAY μ-RADIOGRAPHY OF A MOSQUITO

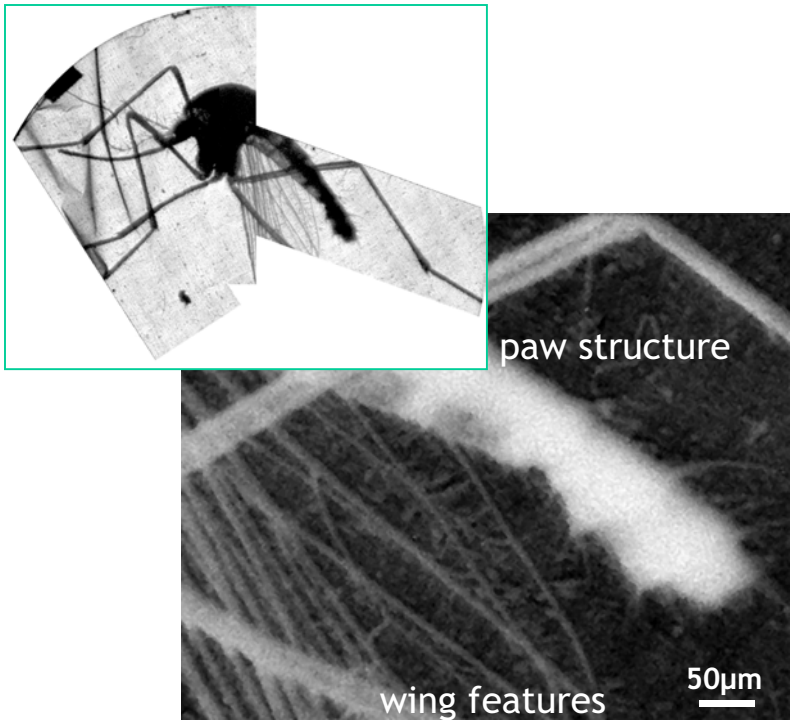

X RAY μ-RADIOGRAPHY OF MICE HEART SLICES

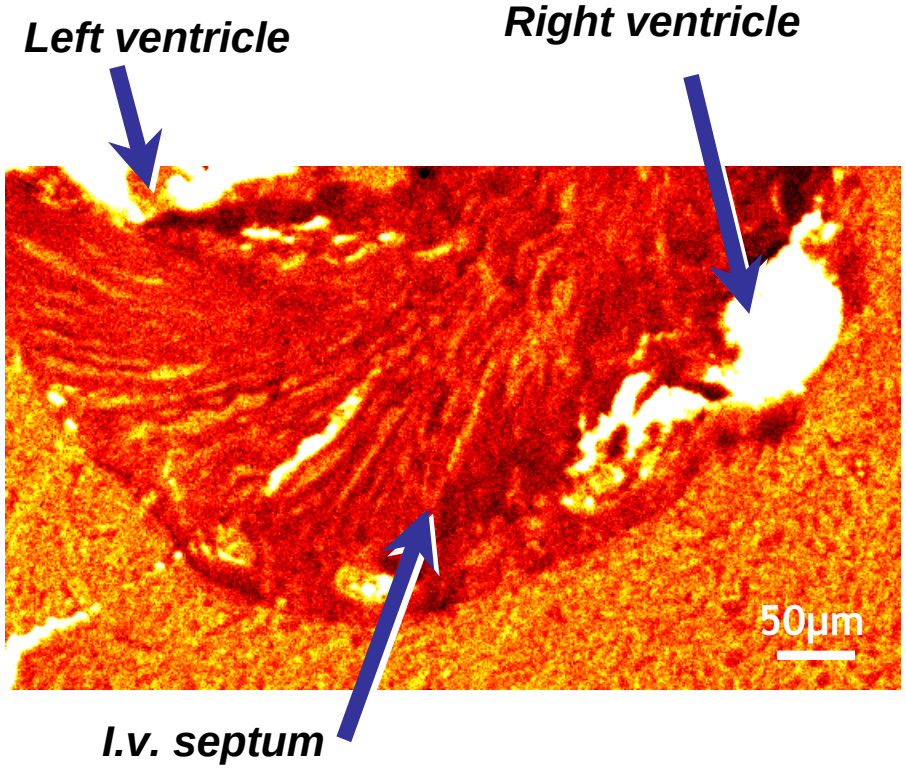

In collaboration with G.Sambuceti et al,
Istituto di Fisiologia Clinica, CNR, Pisa (Italy)

Contact Microscopy

•In the limit of M=1 (no magnification), the spatial resolution of the imaging system depends only upon the detector resolution.

•The sample is placed directly in contact with an X-ray sensitive layer (e.g. a PMMA photo resist) and exposed to X-rays

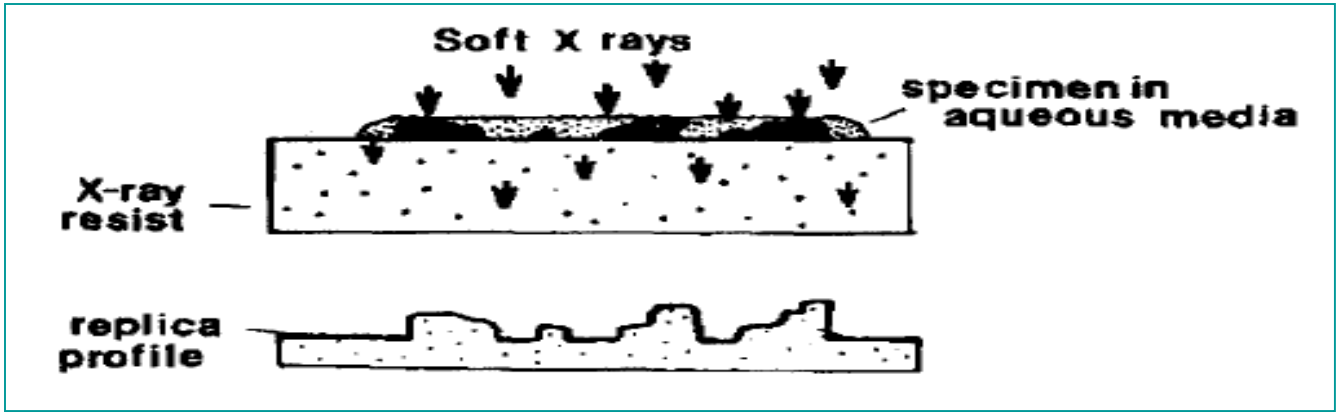

•The photo-resist is then processed and read with an Atomic Force Microscope (AFM)

Recent results) on SXCM of multicellular organisms*

Experiments performed using the PALS Asterix Iodine laser system in Prague (1.314 μm, ~ 400 ps, 600J, ~ 10^{14} – 10^{16} W/cm^2)

Three types of planar solid targets were used viz. Teflon (CF_2) (K-shell centered at 0.9 keV), molybdenum (Mo) and gold (Au) to produce X-rays.

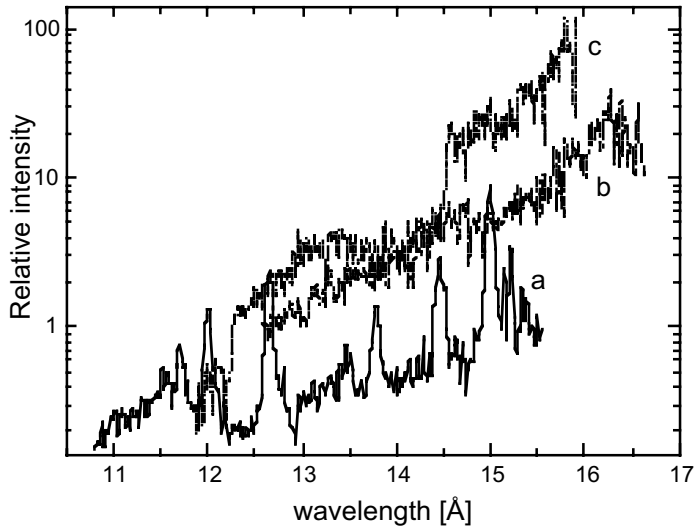

X-ray intensity versus X-ray wavelength for a) Teflon, b) gold and c) molybdenum. Laser intensity on the target surface was 5x10^{14}, 2.6x10^{14}, 2.75x10^{14} W/cm^2 respectively. Al filter thickness was 5 μm for Teflon and 14 μm for Au and Mo.

***) X-ray microscopy and imaging of Caenorhabditis elegans nematode using a laser plasma pulsed x-ray source**, G. Poletti, F.Orsini, J.Ullschmied, J.Skala, B.Kralikova, M.Pfeifer, C.Kadlec, T.Mocek, A.Präg, F.Cotelli, C.Lora Lamia, D.Batani, A.Bernardinello, T.Desai, A.Zullini, *submitted, J. Appl. Phys* (2003)

Specimen for SXCM *)

Schematic drawing of *Caenorhabditis elegans*

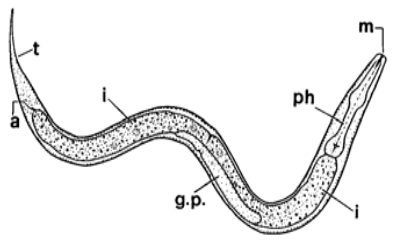

The roundworm *Caenorhabditis elegans* is a small, free living soil nematode.The simple body plan, convenience of manipulation, and short life cycle of *Caenorhabditis elegans* make it one of the most widely used model system.

In the sample holders, a droplet of water containing the biological specimens was sandwiched between a silicon nitride window and a photo resist (PMMA-Polymethilmetacrylate) with the minimum level of fluid (water).

)** ***X-ray microscopy and imaging of Caenorhabditis elegans nematode using a laser plasma pulsed x-ray source, G. Poletti, F.Orsini, J.Ullschmied, J.Skala, B.Kralikova, M.Pfeifer, C.Kadlec, T.Mocek, A.Präg, F.Cotelli, C.Lora Lamia, D.Batani, A.Bernardinello, T.Desai, A.Zullini, *submitted, J. Appl. Phys* (2003)

SXCM of a Caenorhabditis elegans nematode)*

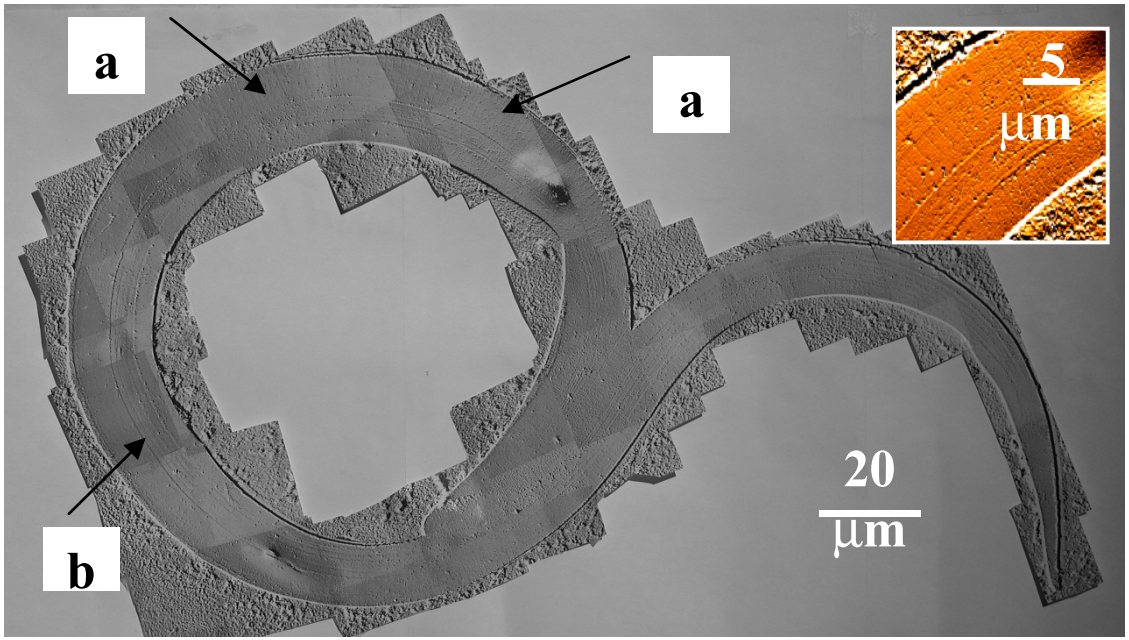

Reconstruction of a *Caenorhabditis elegans* nematode SXCM imprint on a PMMA photon resist, obtained combining 72 AFM error signal images. Each single AFM image has a scan area of 20x20 μm^2. The nematode length is 500 μm approximately. (a) Cuticle annuli; (b) tri-ridged lateral field. In the insert a single AFM error signal image is showed.

)** ***X-ray microscopy and imaging of Caenorhabditis elegans nematode using a laser plasma pulsed x-ray source, G. Poletti, F.Orsini, J.Ullschmied, J.Skala, B.Kralikova, M.Pfeifer, C.Kadlec, T.Mocek, A.Präg, F.Cotelli, C.Lora Lamia, D.Batani, A.Bernardinello, T.Desai, A.Zullini, *submitted, J. Appl. Phys* (2003)

Future steps …

o water layer thickness;

o X-ray beam intensity;

o device geometry;

o photo resist chemical development;

o wavelength control (monochromatisation) of X-ray beam

o scaling to a table-top, “handy” system.

Monochromatic imaging with curved crystals

Differential Absorption Imaging

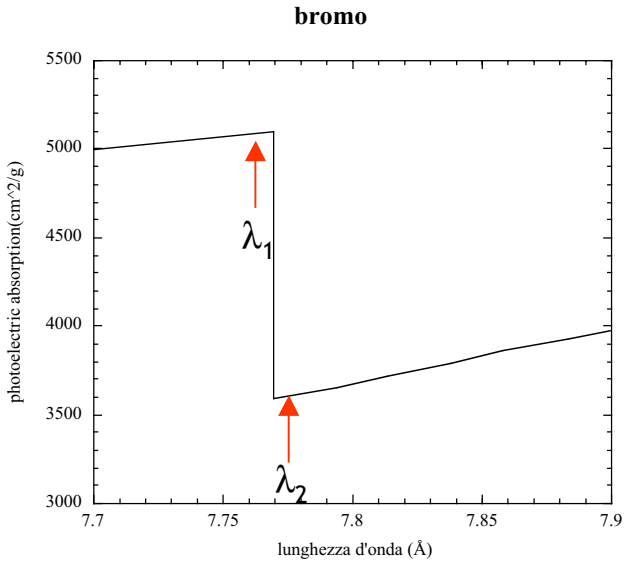

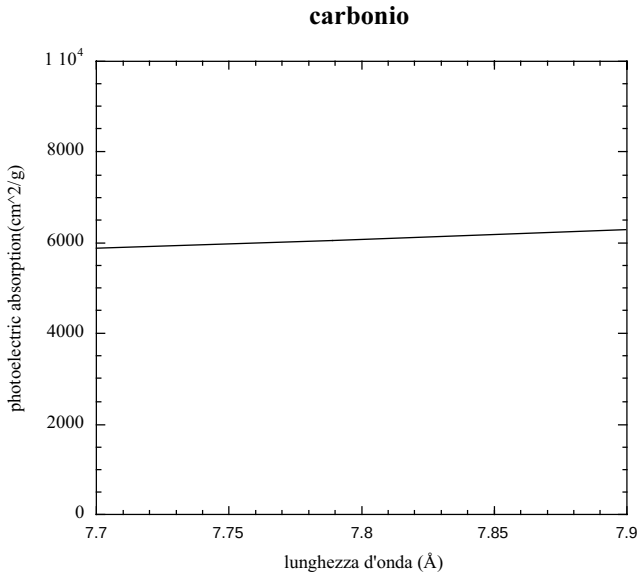

Difference in optical depth:

$$\Delta t(x,y) = \ln\left(\frac{I_1(x,y)}{I_{01}(x,y)}\right) - \ln\left(\frac{I_2(x,y)}{I_{02}(x,y)}\right) = \sum_i \Delta\mu_i \int_{campione} \rho_i(x,y,z)\, dz$$

$$\Delta\sigma = \sqrt{\left(\frac{\Delta(\Delta\mu)}{\Delta\mu^2}\ln I\right)^2 + \left(\frac{\Delta I}{I\,\Delta\mu}\right)^2}$$

$\Delta I/I = 10^{-4}$

$\Delta\mu = (1506 \pm 10)\text{cm}^2/\text{g}$

Detection Limit: $\Delta\sigma = 1.3\times10^{-7}\text{g/cm}^2$

See C. Tillman et al., J. Opt. Soc. Am, ***13***, 209 (1996)

Monochromatic imaging with LP using spherically bent crystals

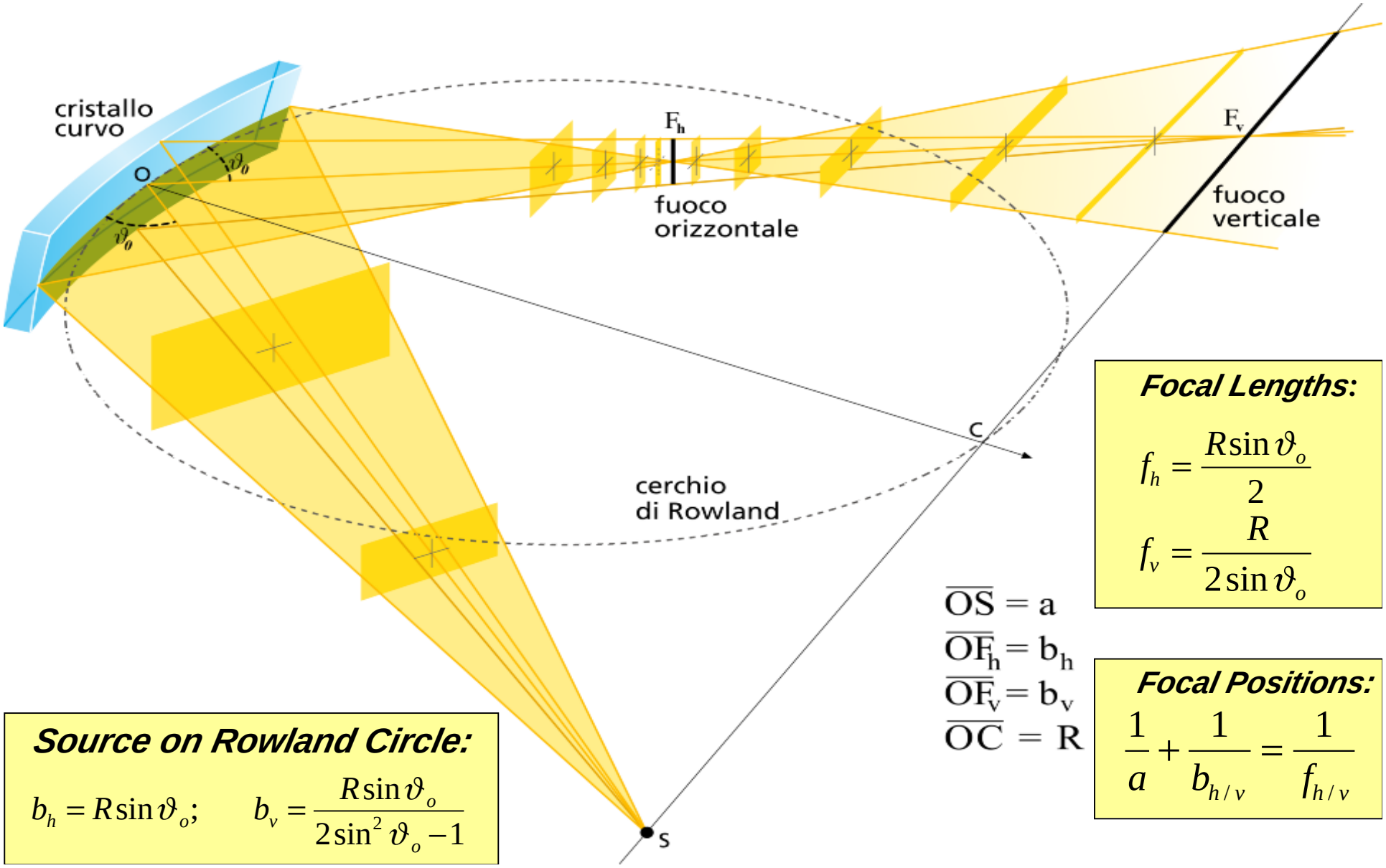

Source on Rowland Circle:

$$b_h = R\sin\vartheta_o; \qquad b_v = \frac{R\sin\vartheta_o}{2\sin^2\vartheta_o - 1}$$

$\overline{OS} = a$

$\overline{OF_h} = b_h$

$\overline{OF_v} = b_v$

$\overline{OC} = R$

Focal Lengths:

$$f_h = \frac{R\sin\vartheta_o}{2}$$

$$f_v = \frac{R}{2\sin\vartheta_o}$$

Focal Positions:

$$\frac{1}{a} + \frac{1}{b_{h/v}} = \frac{1}{f_{h/v}}$$

Reflected Wavelengths

Horizontal plane ***Vertical plane***

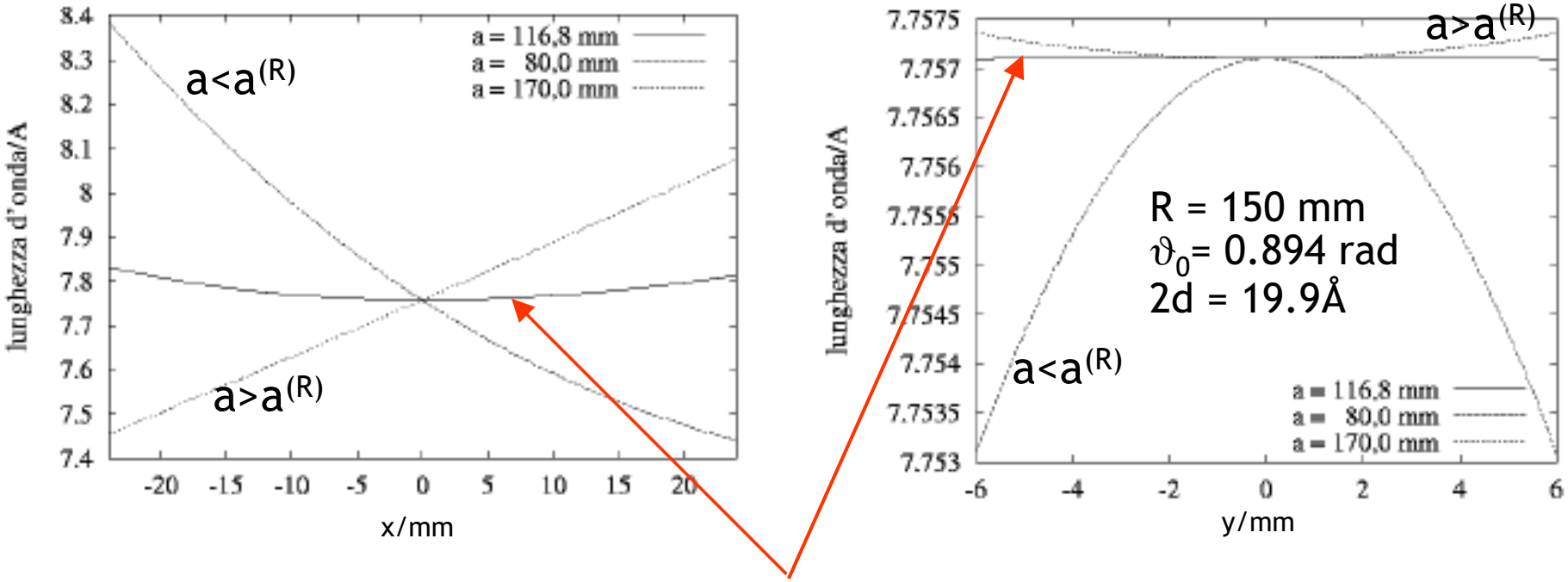

Source on Rowland Circle: $a = a^{(R)}$

When the source is on the Rowland Circle, the reflected spectral range is minimum: the crystal behaves as a monochromator.

XCIM - X-ray Crystal Imaging Microscope *)

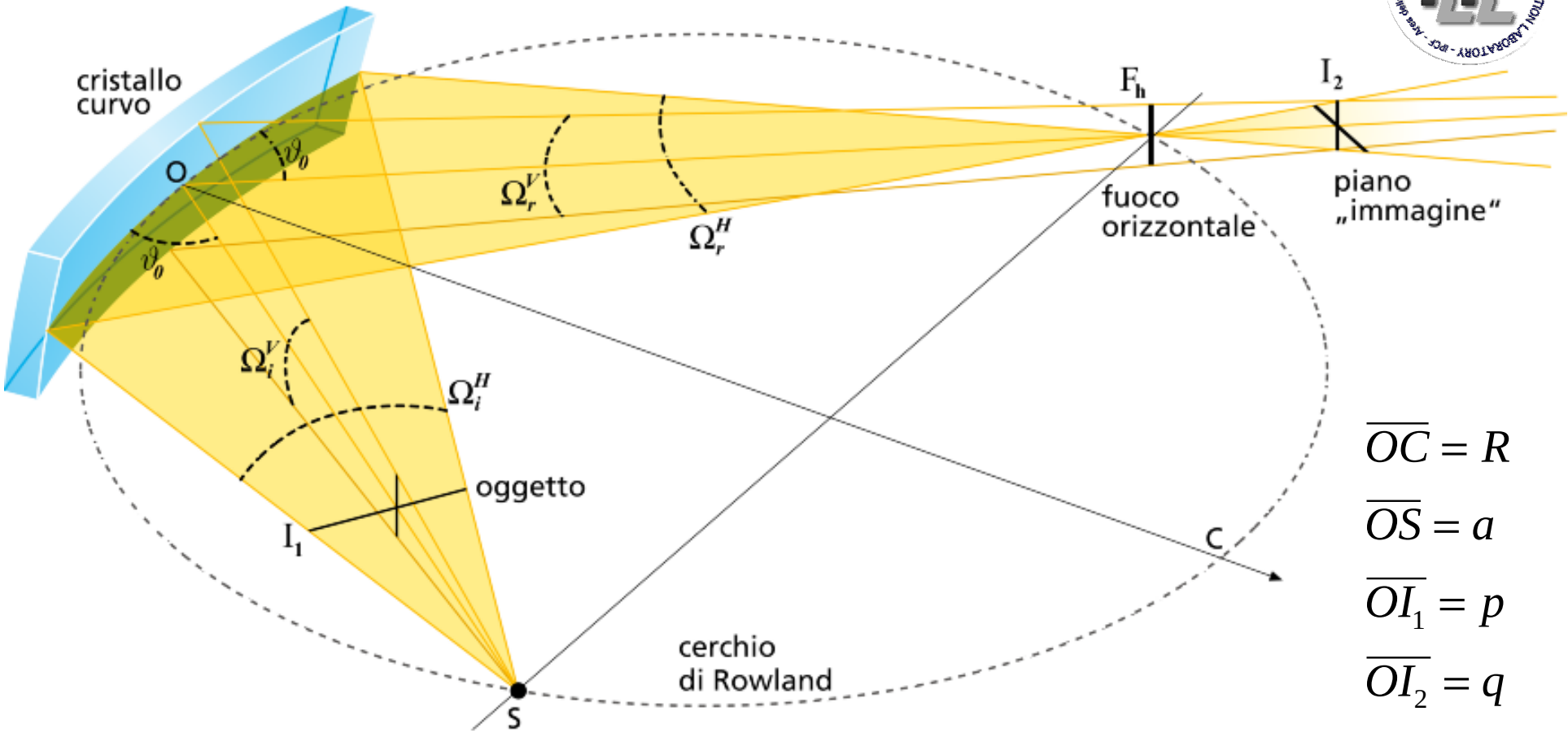

$$\overline{OC} = R$$

$$\overline{OS} = a$$

$$\overline{OI_1} = p$$

$$\overline{OI_2} = q$$

"Image plane" at a distance q from the crystal given by the condition of equal vertican and horizontal magnification :

$$\frac{\Omega_h^r(q-b_h)}{\Omega_h^i(a-p)} = M_h = M_v = \frac{\Omega_v^r(b_v-q)}{\Omega_v^i(a-p)}$$

Focusing condition:

$$\Omega_h^r\, b_h = \Omega_h^i\, a$$

$$\Omega_v^r\, b_v = \Omega_v^i\, a$$

$\Rightarrow$

Source on Rowland circle:

$$q = \frac{R}{\sin\vartheta_o}$$

$$M = \cot^2\vartheta_o \frac{1}{1-p/a}$$

*)Pikuz *et al.*, Laser and Particle Beams,19:285, 2001
Sanchez del Rio *et al.*, Review of Scientific Instr., 72:3291, 2001

Ray-tracing simulations of X-ray μ-radiography#)

- XCIM (X-ray Crystal Imaging Microscope*) scheme allows monochromatic radiography of thin objects with μm resolution to be obtained
- XCIM scheme is based upon the use of a spherically bent crystal

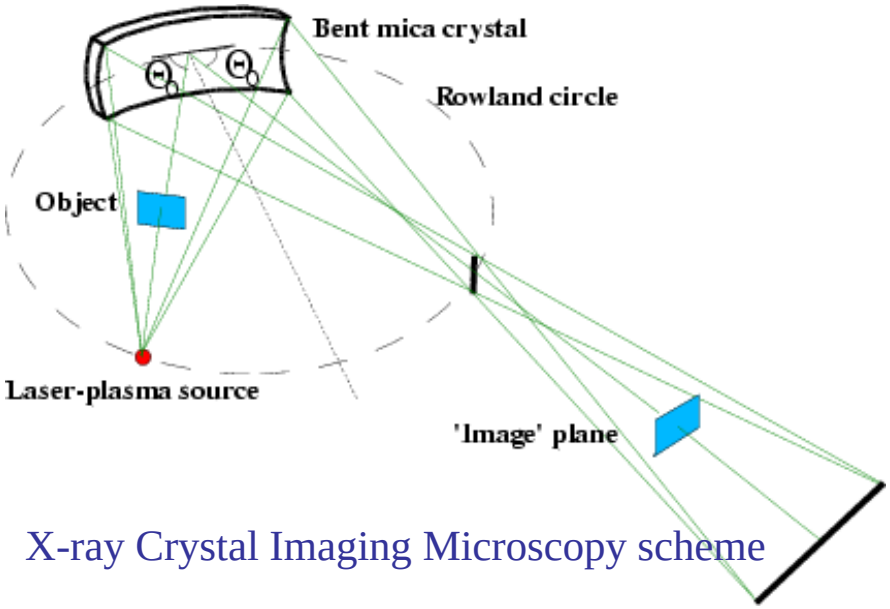

X-ray Crystal Imaging Microscopy scheme

*) T.A. Pikuz et al., *Laser Part. Beams* 19,285 (2001); M. Sanchez del Rio et al., *Rev. Sci. Instrum*. 72, 3291 (2001)

- **Ray-tracing simulations of the system with the ORTO ray-tracing code**):**
  - **C++, fully object-oriented code**
  - **arbitrary shapes and sizes of the source can be considered**
  - **different forms of the crystal rocking curves can be taken into account**
  - **typical running times: 5min for $5x10^6$ sampled rays (Linux based P4)**

#) L.Labate et al., *Ray-tracing simulation of an X-ray optics based upon a bent crystal for differential absorption applications*, IPCF Internal Report N. 1/072003 (prot.307/2003), Pisa.

Ray-tracing simulations: horizontal focus

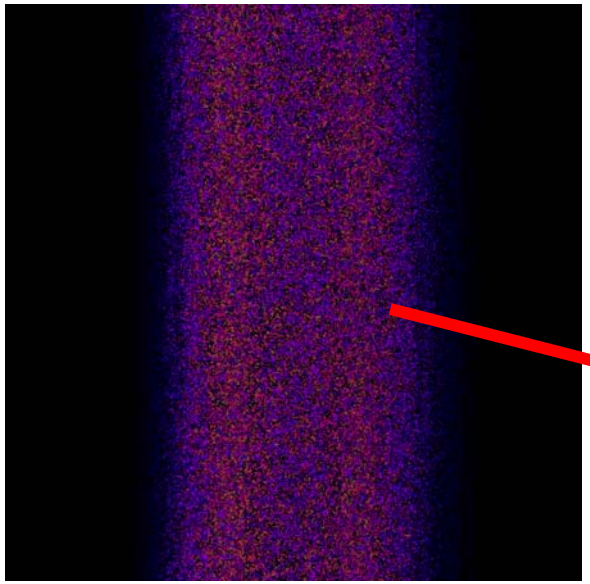

Spherical aberration and astigmatism: intensity distribution around the horizontal focus (without objects)

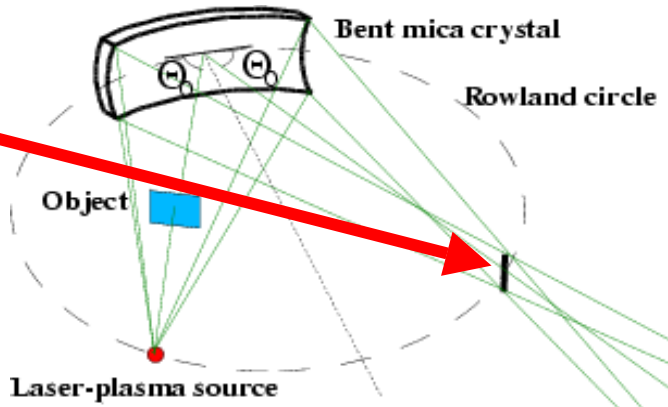

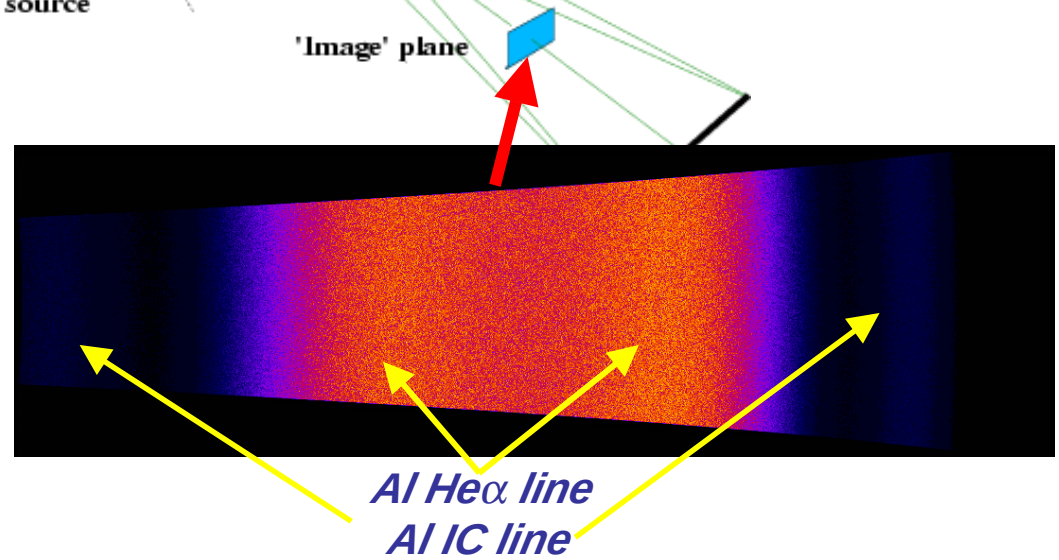

X-ray intensity distribution at the image point using an Al plasma source and the crystal set to focus near the Heα line (no objects)

#) L.Labate et al., IPCF-CNR Internal Report N. 1/072003.

Ray-tracing simulations: imaging a test object

Ray-tracing of the XCIM scheme with Fresnel zone plate as a test object

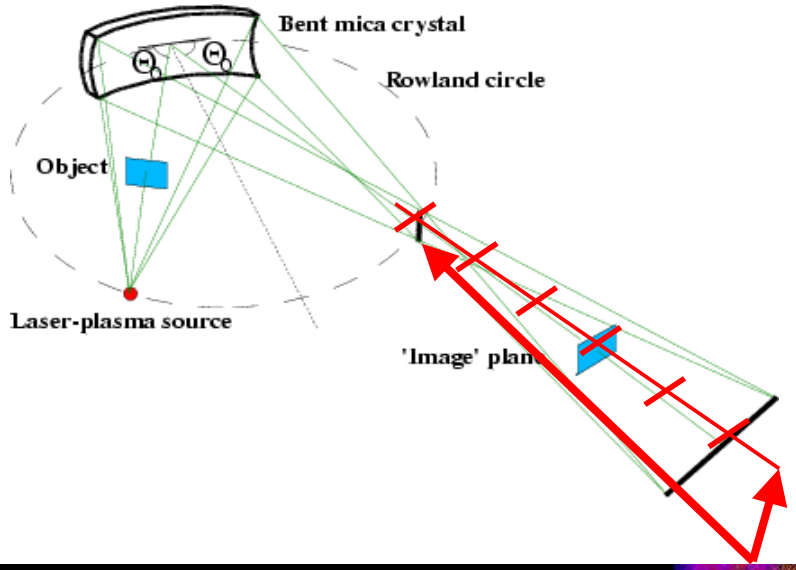

X-ray pattern at different distances from the crystal to detector

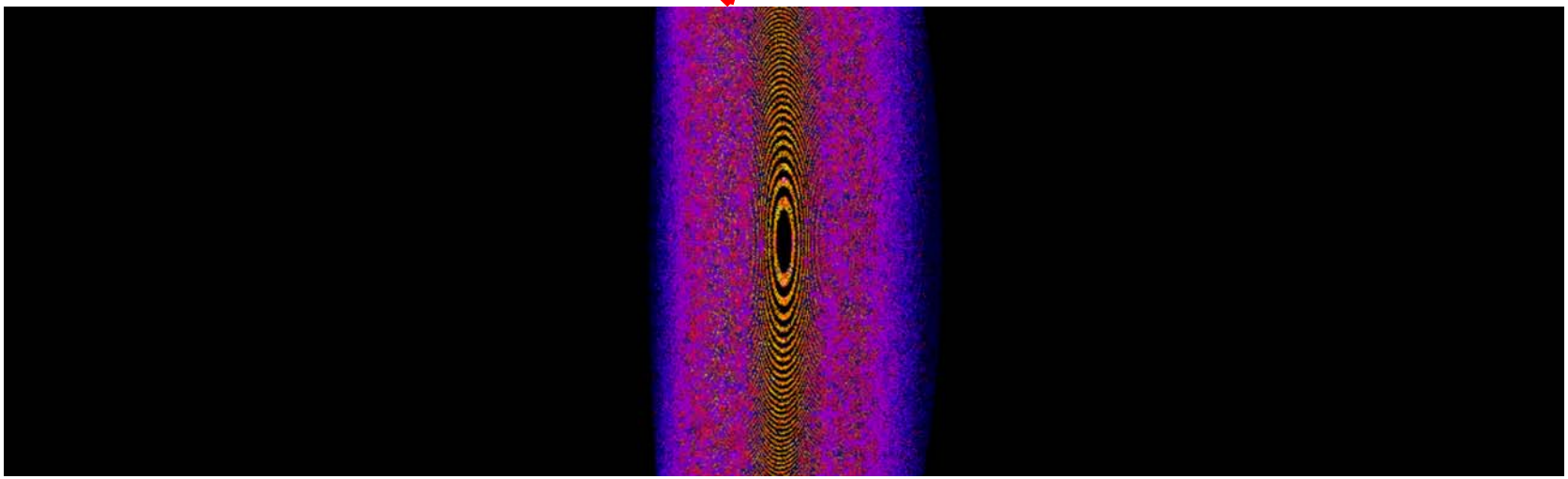

Monochromatic X-ray Beam from LP X-rays

Central wavelength on crystal:

a) λ_0=7.742 Å

b) λ_0=7.748 Å

c) λ_0=7.750 Å

Target: Al, Intensity on target: 2E13W/cm²

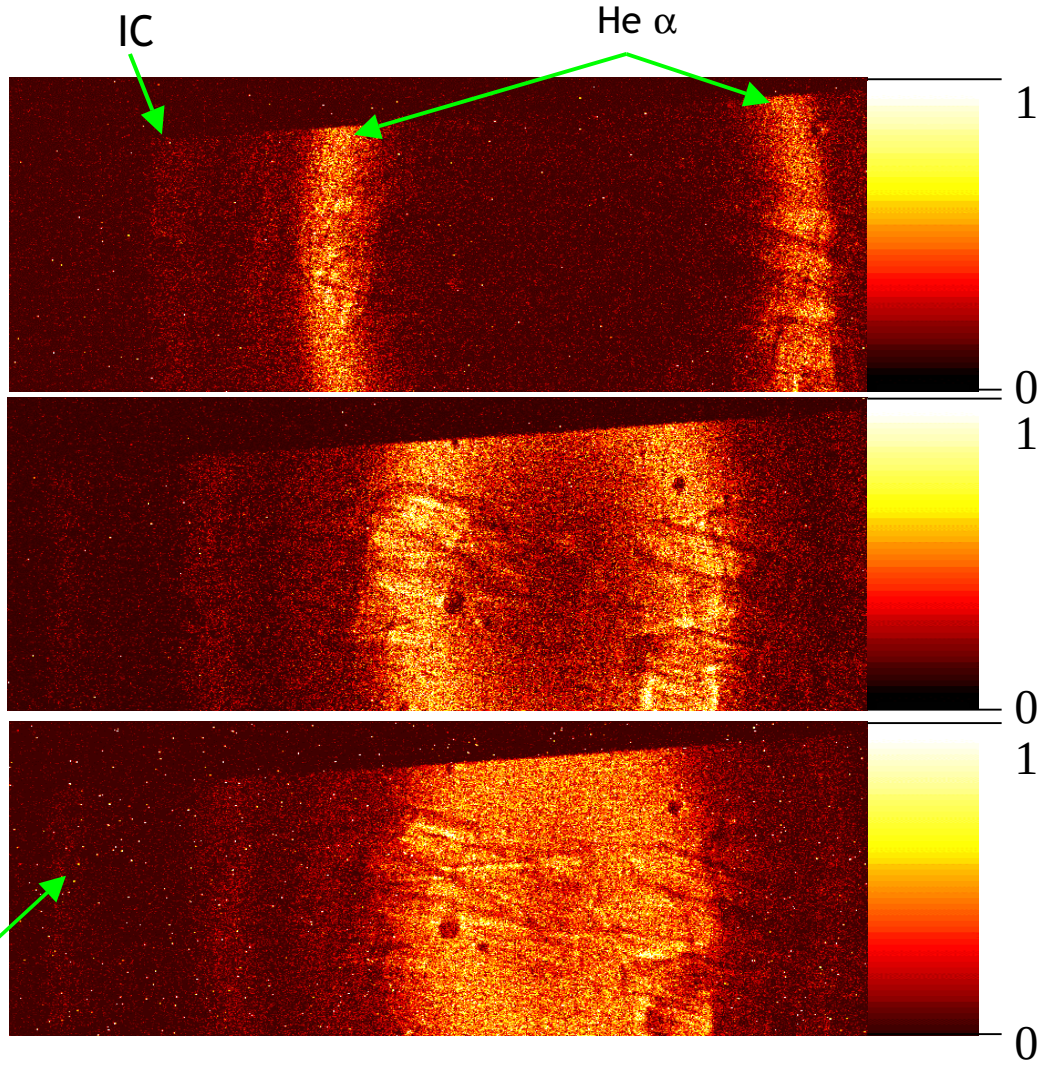

Lithium-like

M. Galimberti et al., *Towards differential micro-imaging using a laser-plasma soft X-ray source*XPOSE Annual Meeting, Cargese (France), July 2003

Spatial resolution of XCIM

XCIM scheme:

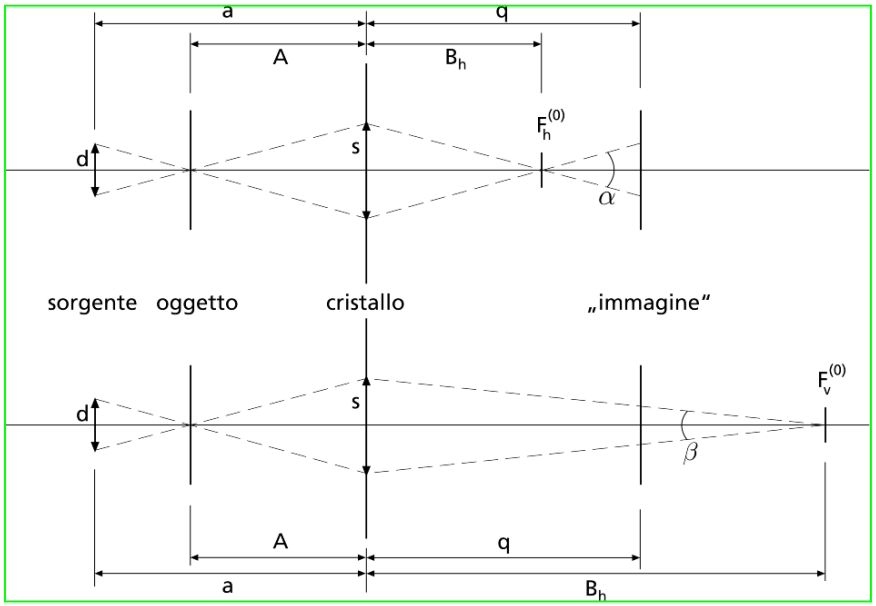

$$\Delta x_h = \frac{A(q - B_h)}{B_h(a - A)M} d$$

$$\Delta x_v = \frac{A(B_v - q)}{B_v(a - A)M} d$$

Source on Rowland circle

$$\Rightarrow \quad \Delta x_h = \frac{\left(M + 1 - \frac{2}{\sin^2 \vartheta_o}\right)}{M} d$$

$$\Delta x_v = \frac{(M+1)}{M} d$$

Projection imaging scheme:

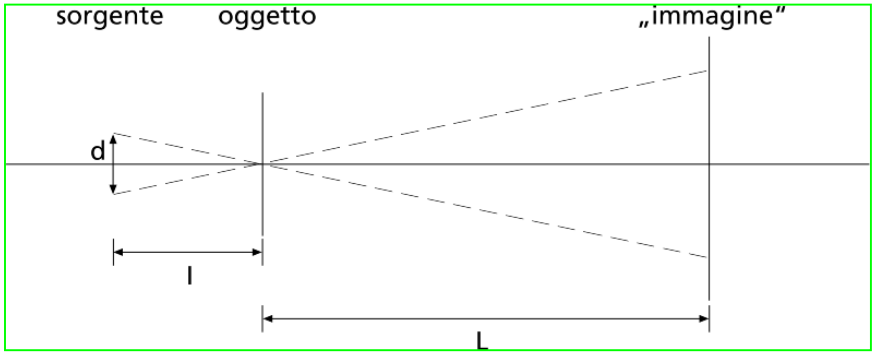

$$\Rightarrow \quad \Delta x = \frac{(M-1)\, d}{M}$$

Unlike direct (optics-free projection μ-imaging), the intrinsic resolution of XCIM is limited by the X-ray source size

Test image with XCIM configuration

Image of a Frenel Zone plate with a <u>monochromatic beam</u> at 1.6 keV (Al He-α line)

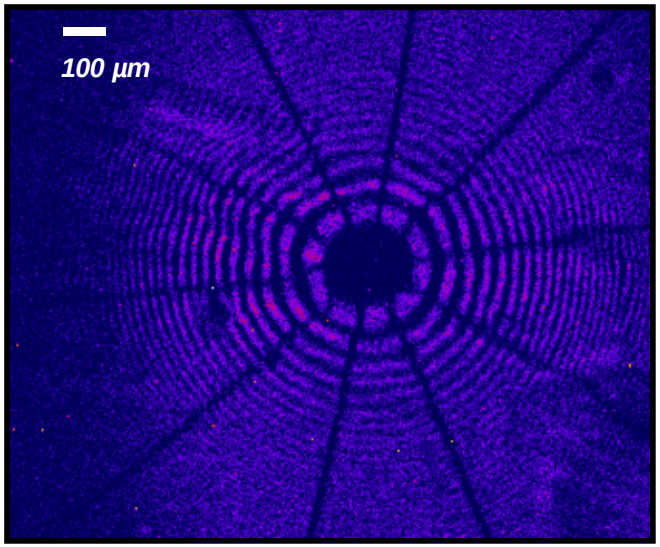

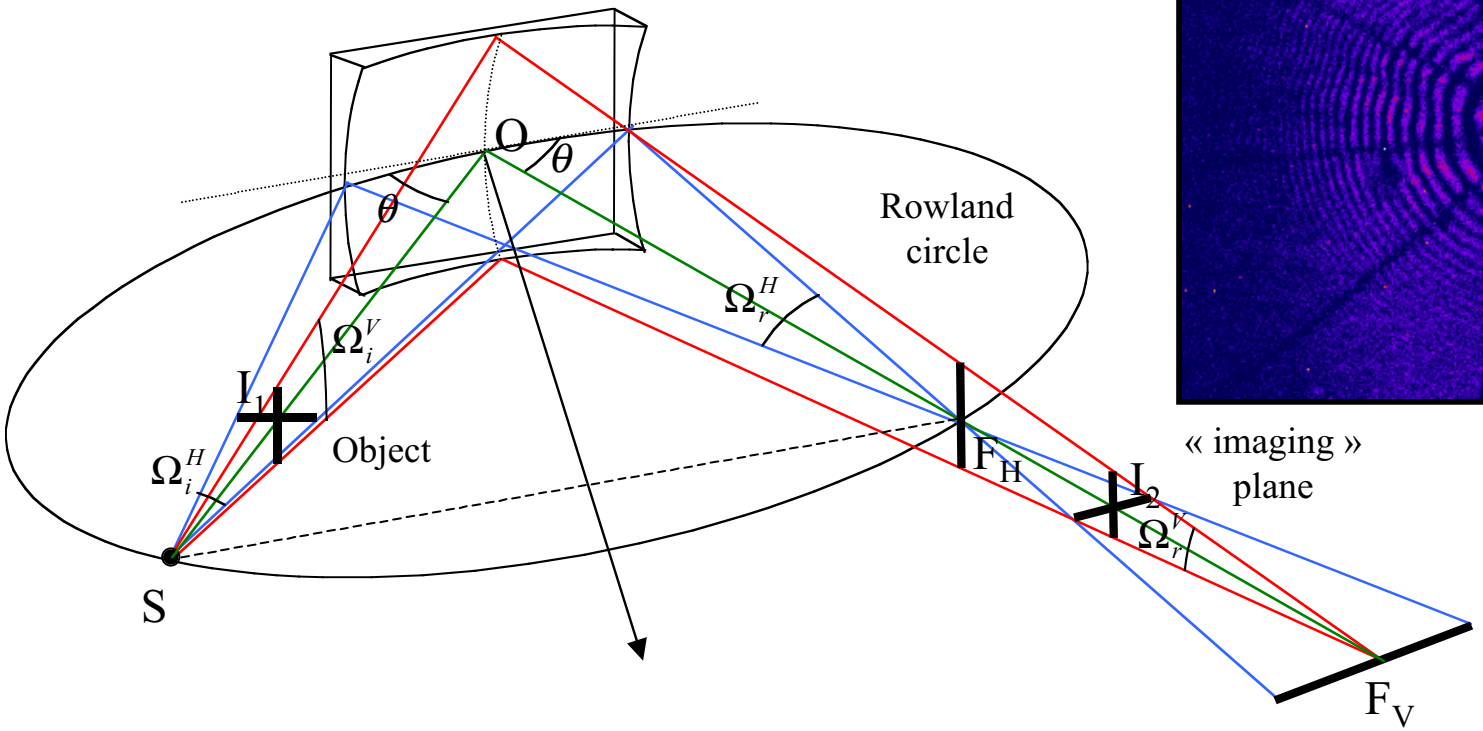

Image resolution:

$$\Delta x_h = 16.8 \pm 2.3 \mu m; \quad \Delta x_v = 52.3 \pm 9.1 \mu m$$

Activity in progress

A joint project on short and ultra-short LP X-ray sources for applications (including microscopy) between:

- **ILIL@Istituto per i Processi Chimico-Fisici IPCF - CNR**
- **Istituto per lo Studio dei Materiali Nanostrutturati - CNR (G. Cappuccio)**
- **Dipartimento di Fisica G. Occhialini – Università di Milano-Bicocca (D. Batani)**

Objectives:

- **Monochromatisation, collimation and focusing of soft X-rays using crystals and policapillary optics;**
- **Monochromatic projection for processing-free μ-imaging and differential absorption imaging;**
- **High resolution microscopy in the water-window.**

Basic Concepts in Advanced X-Ray Sources

*F.V. Hartemann, LLNL, Physics & Advanced Technologies**

1. **Overview**
2. **Compton Scattering**
3. **PLEIADES**
4. **Experimental Results**
5. **Material Physics Applications**
6. **Nonlinear Compton Scattering**

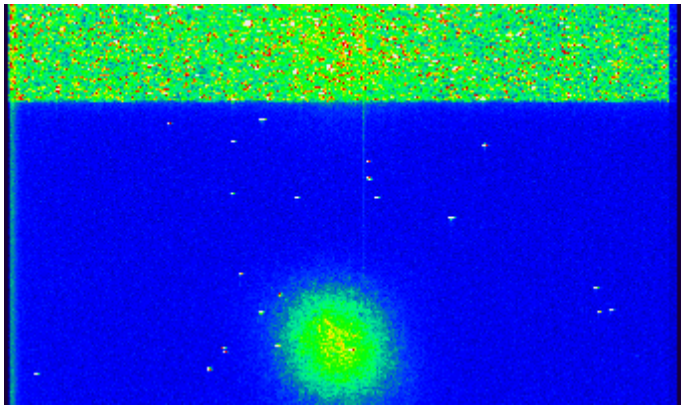

In collaboration with: S.G. Anderson, C.P.J. Barty, W.J. Brown, J.K. Crane, R.R. Cross, D.N. Fittinghoff, D.J. Gibson, J. Kuba, G.P. Le Sage, J. Rosenzweig, A.M. Tremaine, E. Hartouni, A. Wootton, and P.T. Springer

Picosecond X-Ray Sources Overview

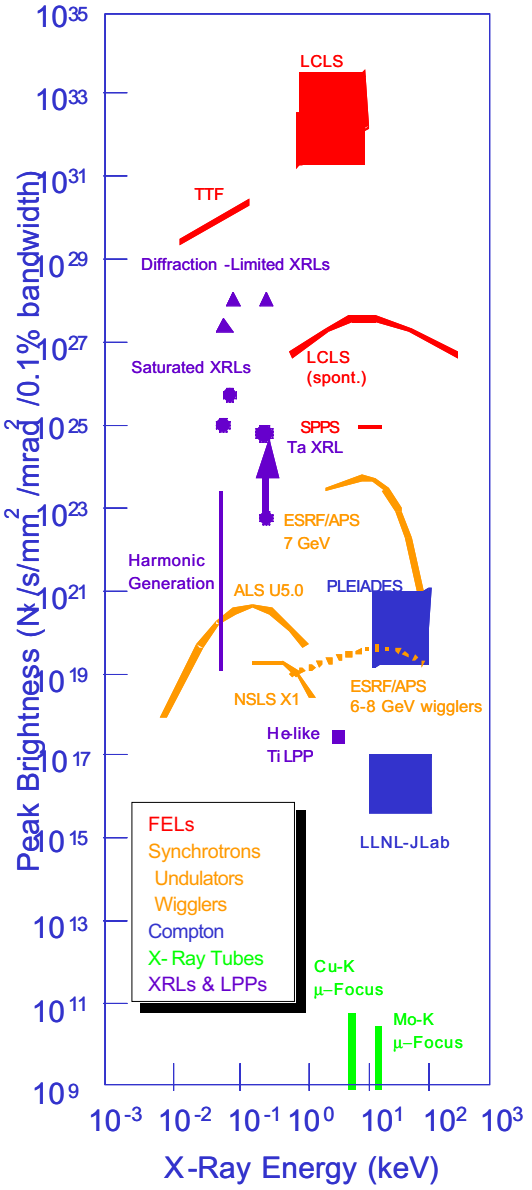

X-Ray FELs

Synchrotrons

X-Ray Lasers

Laser-Plasma Sources

Compton Scattering

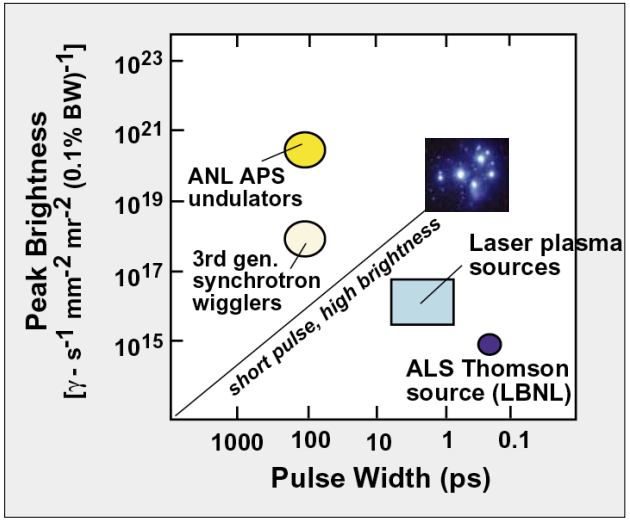

Compton Scattering X-Ray Source

Physics & Advanced Technologies

High-Brightness RF Gun

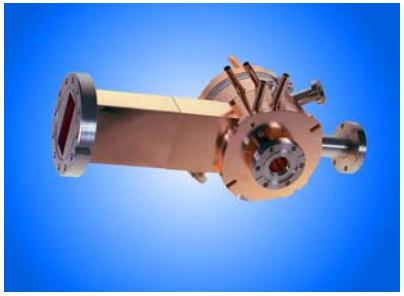

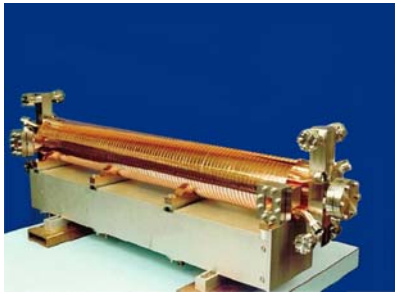

TW-Class CPA Laser

High-Gradient Linac

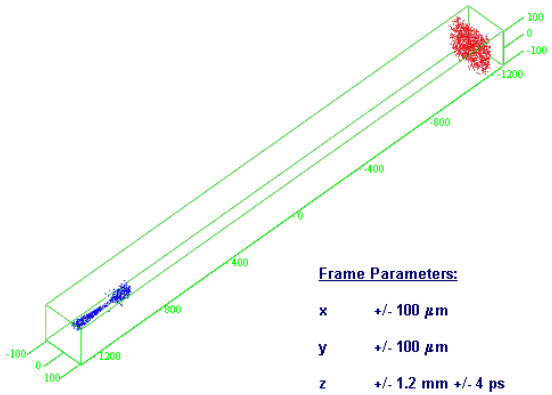

Animation/Simulation by Fred V. Hartemann & Winthrop J. Brown

$TIME_{FRAME}$ = −4 ps

(Z,X,Y),(Z1,X1,Y1)

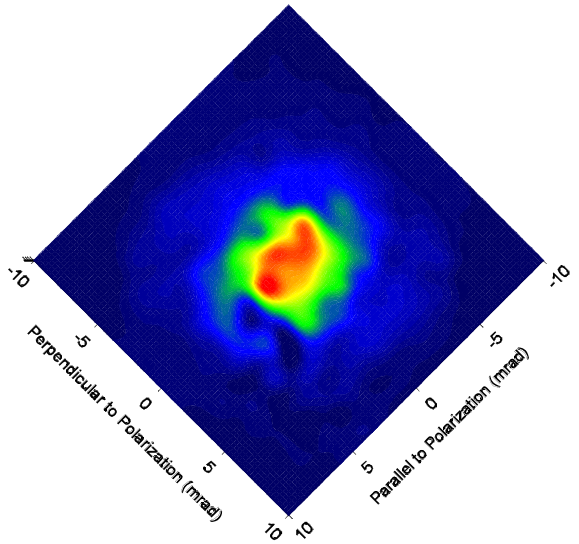

Compton Scattering

Monochromatic, tunable x-rays can be produced by Compton scattering

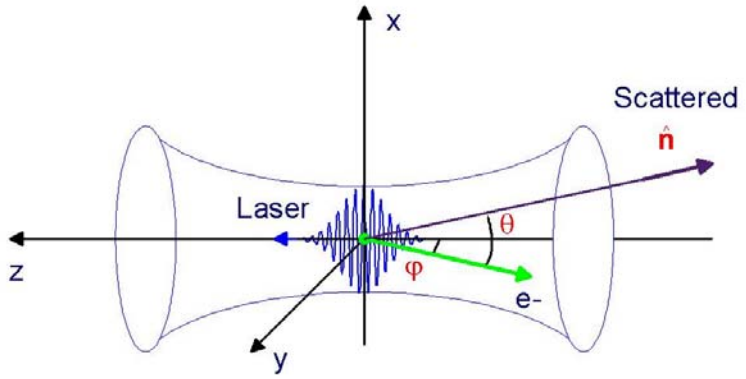

φ Incidence angle

θ Scattering angle

γ Initial electron energy

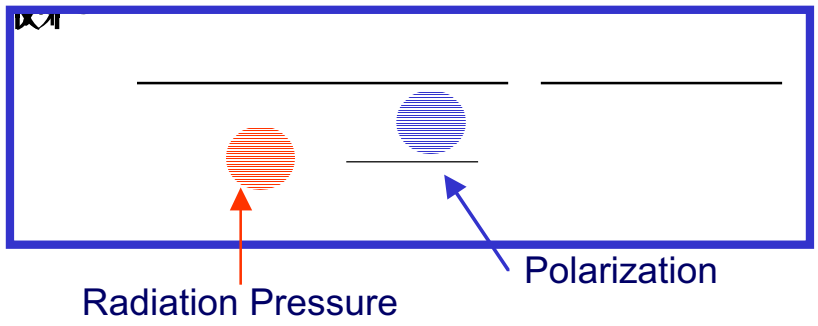

ω_0 Laser frequency

A_0 Normalized vector potential (measured in units of m_0c/e)

σ Polarization state

No recoil

For head-on collisions ($\varphi = \pi$), in the linear ($A_0 << 1$), ultra-relativistic (U.R.) regime, the frequency of photons scattered on-axis ($\theta = 0$) is approximately $\omega_x \sim 4\gamma^2\omega_0$. For Ti:$Al_2O_3$, $h\nu_0 = 1.55$ eV: for $\gamma = 50$, $h\nu_x = 15.5$ keV.

Brightness

Why Ultra-Short Laser Pulses?

The Compton Scattering Cross-Section σ is Small

Laser Photon Density:

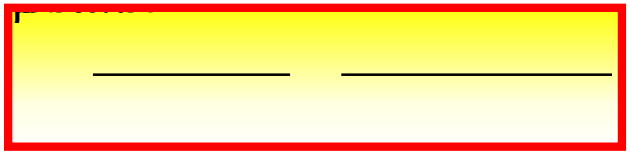

Interaction Volume:

$$V = \sigma\, z_0 = \sigma \frac{\pi w_0^2}{\lambda_0}$$

Interaction Probability:

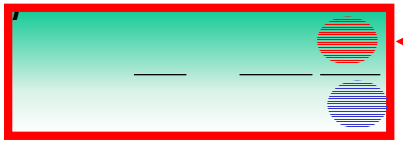

Laser Pulse Energy

Laser Pulse Duration

Why Low Emittance and Diffraction-Limited Laser?

X-Ray Brightness Scales as 1/ [Spot Size]^4

➡ **Short Rayleigh Range, Short Pulse**

LLNL's 3D Compton Scattering Code

Physics & Advanced Technologies

Step 1: PARMELA-SUPERFISH Design

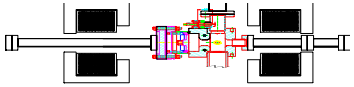

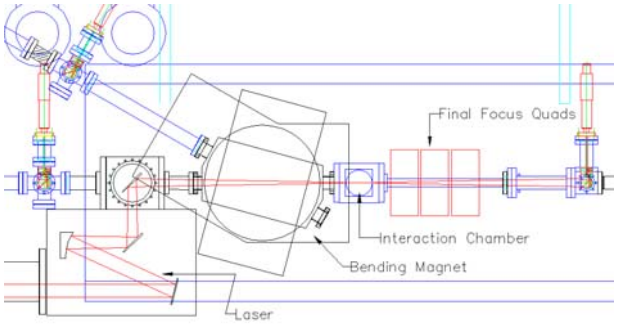

Step 2: Phase Space

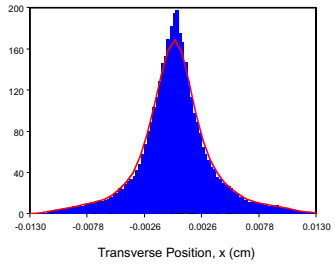

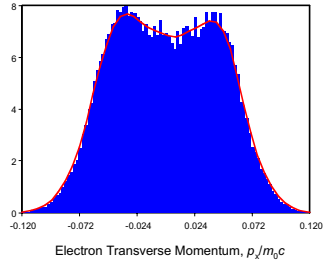

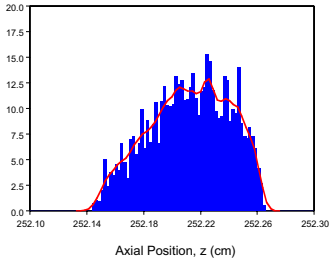

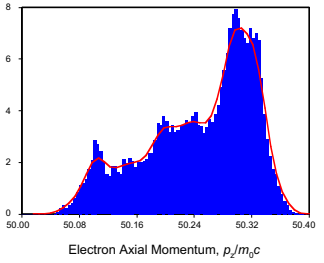

Step 3: 3D X-Ray Simulations

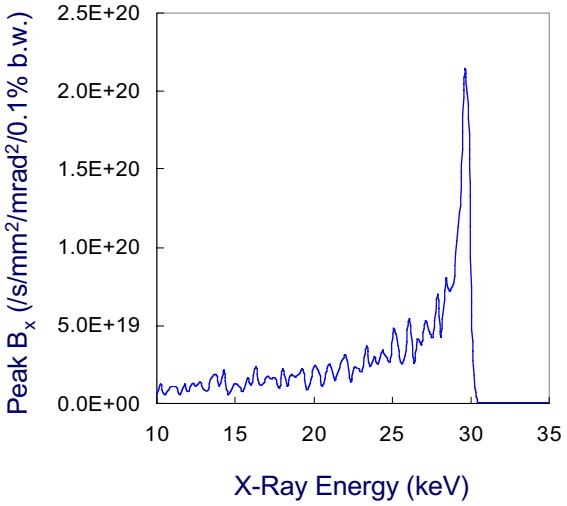

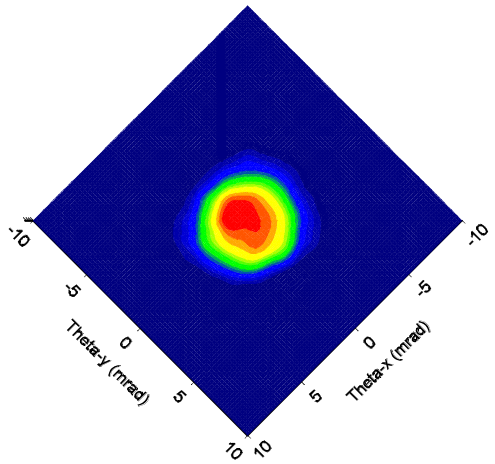

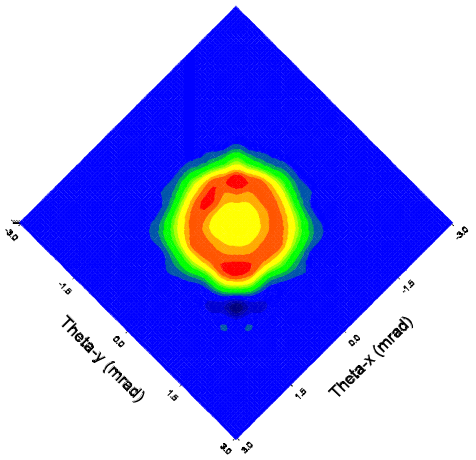

3D Time-Domain Code

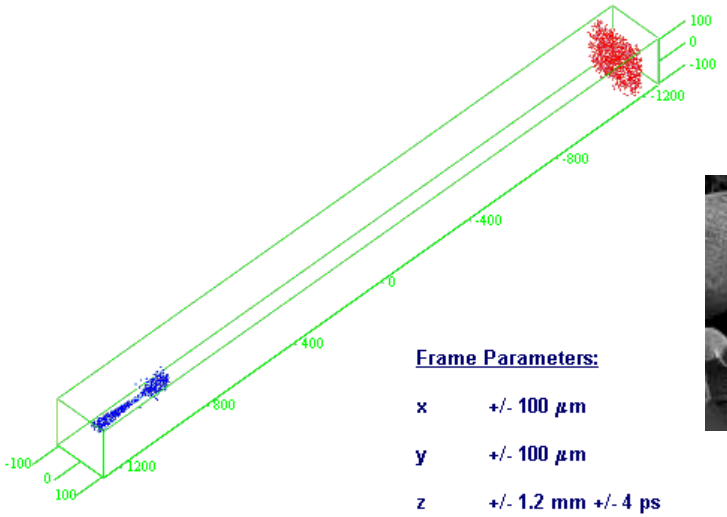

Frame Parameters:

x	+/- 100 μm
y	+/- 100 μm
z	+/- 1.2 mm +/- 4 ps

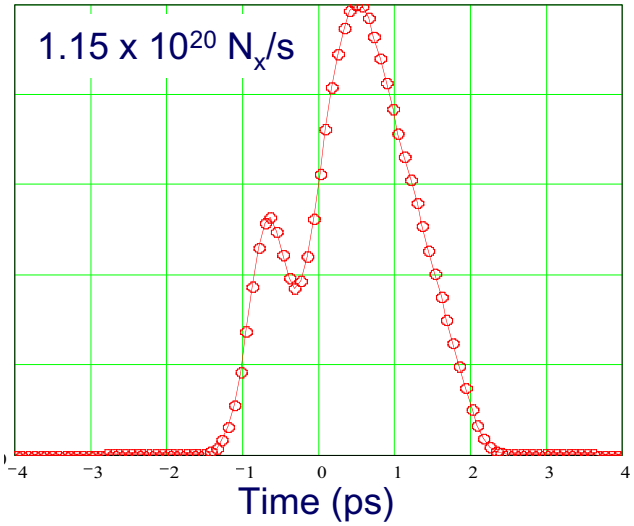

Animation/Simulation by Fred V. Hartemann & Winthrop J. Brown

$TIME_{FRAME} = -4$ ps

(Z,X,Y),(Z1,X1,Y1)

180°, No Delay

$nframe := 50 \qquad t := zmin + (zmax - zmin)\cdot\frac{FRAME}{nframe} \qquad t\cdot\frac{z0}{c}\cdot 10^{12} = -3.78 \quad ps$

$X_{i,j} := G(x_j,0,z_i,t)\cdot H(x_j,0,z_i,t) + if(x_j < 0.99\cdot xmin,1,0) \qquad \Sigma_{i,j} := G(x_j,0,z_i,t) + H(x_j,0,z_i,t) + if(x_j < 0.99\cdot xmin,2,0)\cdot 0$

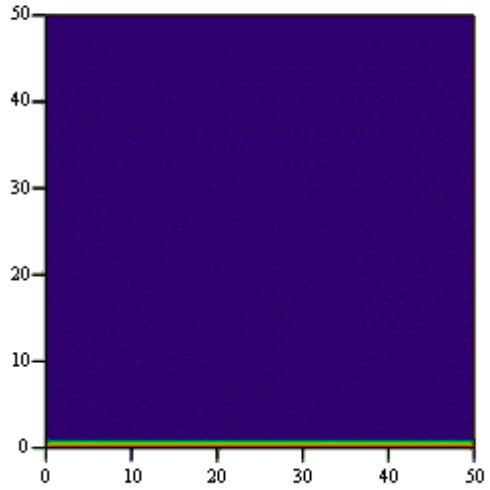

X

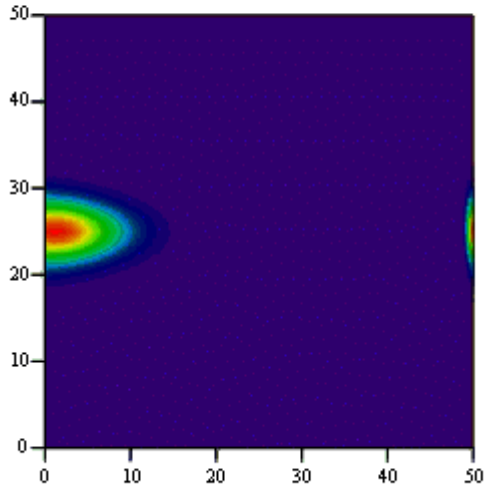

Σ

180°, 5 ps Delay

Physics & Advanced Technologies

$nframe := 50$ $\quad t := zmin + (zmax - zmin)\cdot\frac{FRAME}{nframe}$ $\quad t\cdot\frac{z0}{c}\cdot 10^{12} = -3.78$ ps

$X_{i,j} := G(x_j, 0, z_i, t)\cdot H(x_j, 0, z_i, t) + if(x_j < 0.99\cdot xmin, 1, 0)$ $\quad \Sigma_{i,j} := G(x_j, 0, z_i, t) + H(x_j, 0, z_i, t) + if(x_j < 0.99\cdot xmin, 2, 0)\cdot 0$

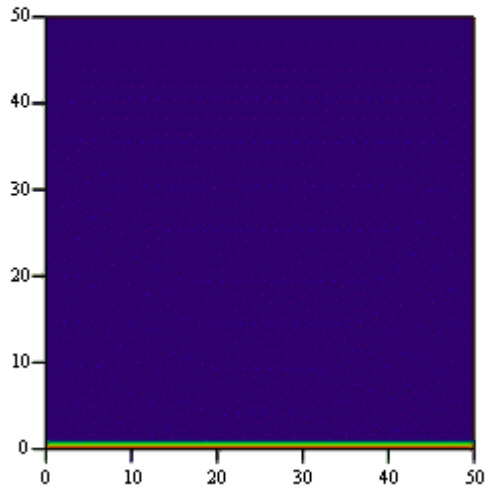

X

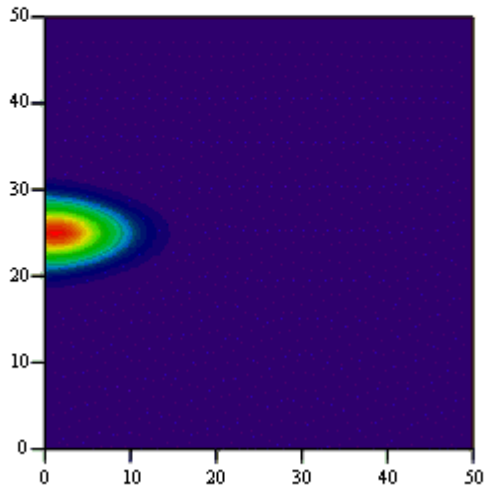

Σ

90°, No Delay

$nframe := 50 \qquad t := zmin + (zmax - zmin)\cdot\frac{FRAME}{nframe} \qquad t\cdot\frac{z0}{c}\cdot 10^{12} = -3.78 \quad ps$

$X_{i,j} := G(x_j,0,z_i,t)\cdot H(x_j,0,z_i,t) + if(x_j < 0.99\cdot xmin,1,0)$

$\Sigma_{i,j} := G(x_j,0,z_i,t) + H(x_j,0,z_i,t) + if(x_j < 0.99\cdot xmin,2,0)\cdot 0$

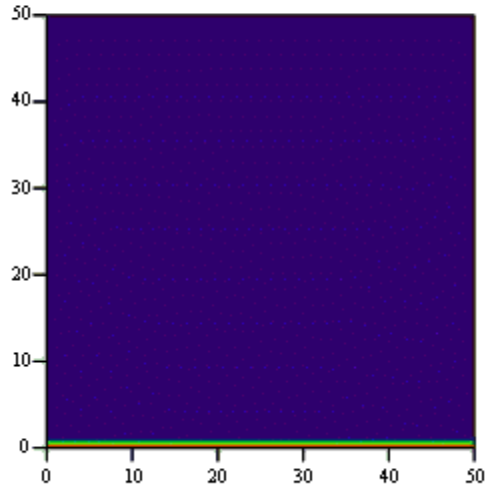

X

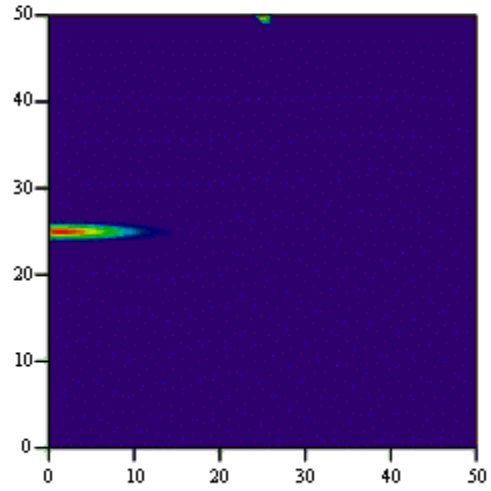

Σ

Timing Jitter & Interaction Geometry

Physics & Advanced Technologies

180° Lorentzian fit (7.5 ps HWHM)

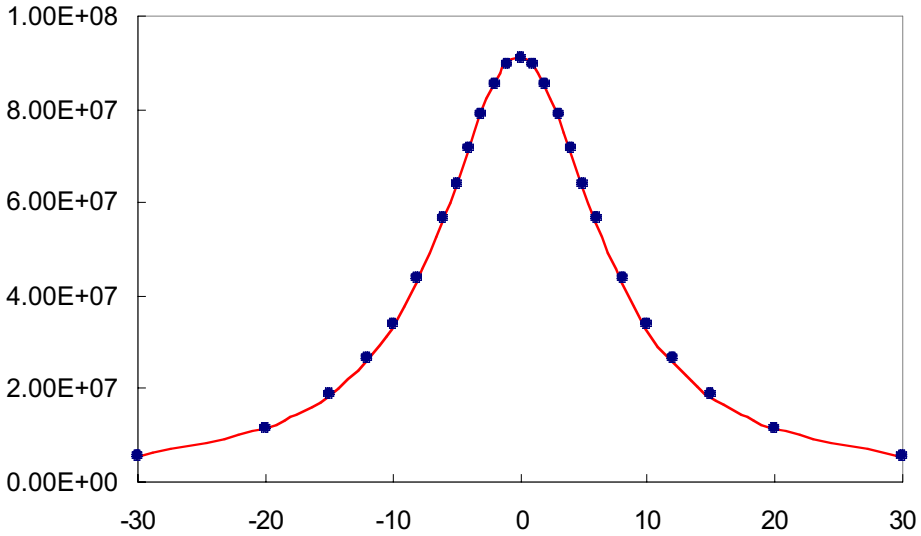

Laser Pulse Duration	50 fs (FWHM)
Focal Spot Size	20 μm (FWHM)
Laser Pulse Energy	100 mJ
Electron Bunch Duration	2 ps (FWHM)
Electron Bunch Charge	1 nC
Bunch Focal Spot Size	20 μm (FWHM)
Normalized Emittance	5 π-mm.mrad

90° Gaussian fit (1.0 ps HWHM)

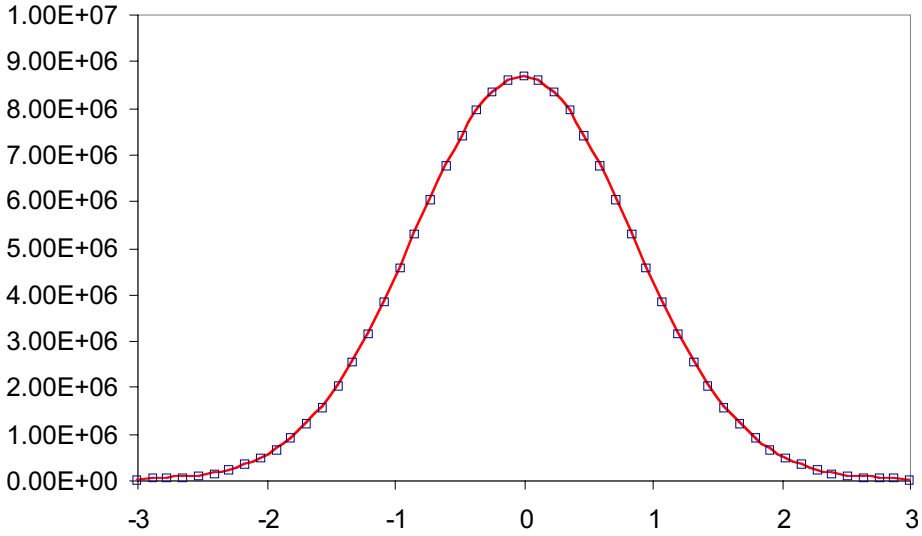

172° Gaussian fit (1.2 ps HWHM)

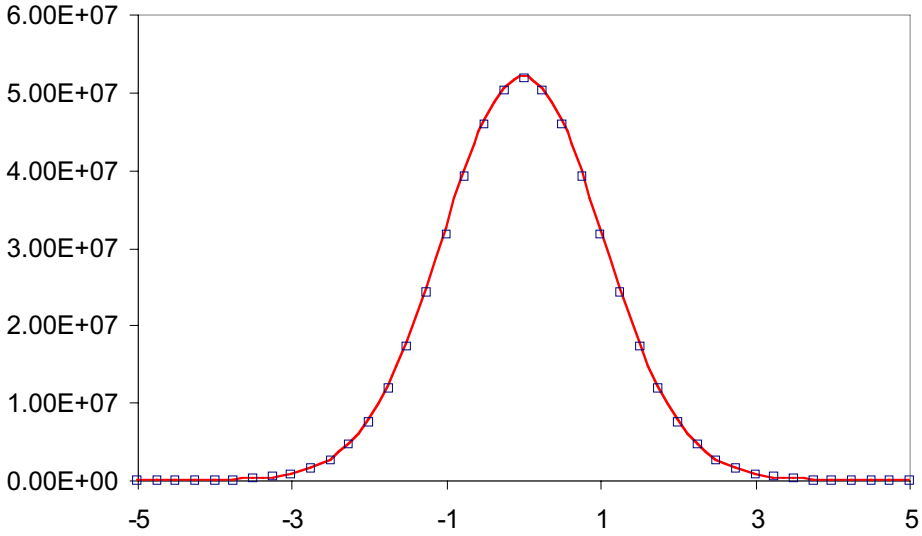

Picosecond Laser-Electron InterAction for the Dynamic Evaluation of Structures

- Laser: fs - ps, J
- Electron beam: fs – ps, nC, 10's of MeVs
- Spot size: μm

- Peak brightness: > 10^{20} photons/s/mrad^2/mm^2/0.1% bw
- X-ray pulse: subpicosecond

- Picosecond radiography
- Femtosecond diffraction
- NIF backlighter
- Stockpile stewardship
- Warm dense matter

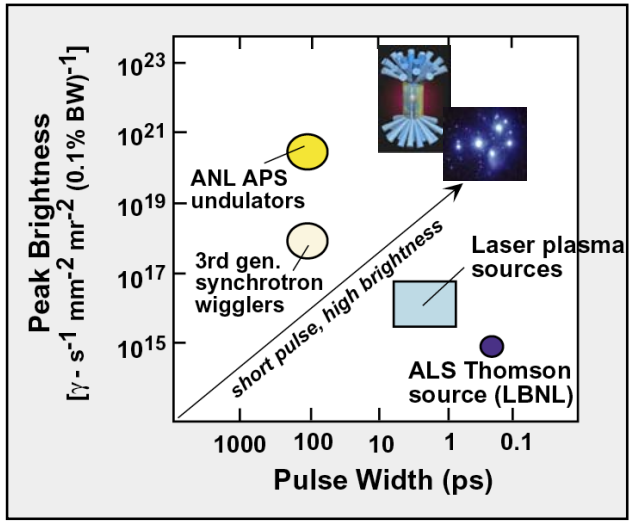

PLEIADES Overview

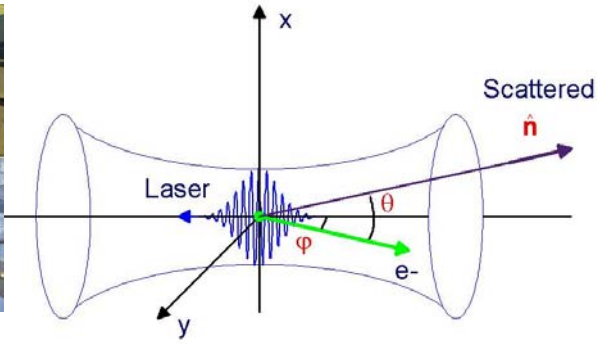

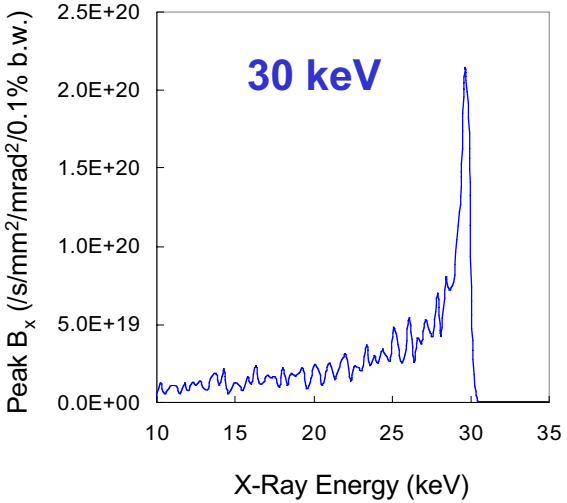

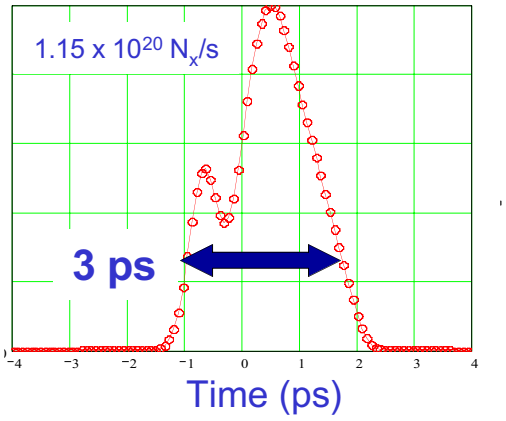

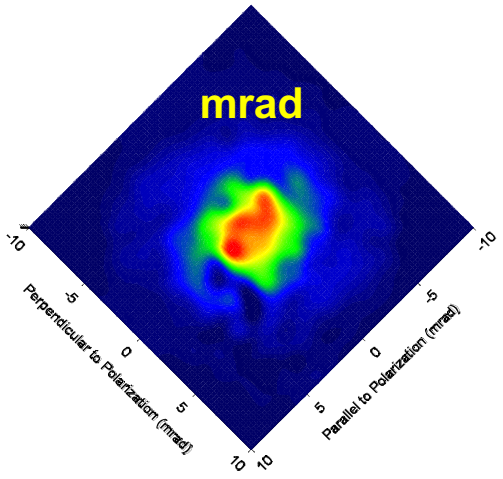

FALCON/OPAL

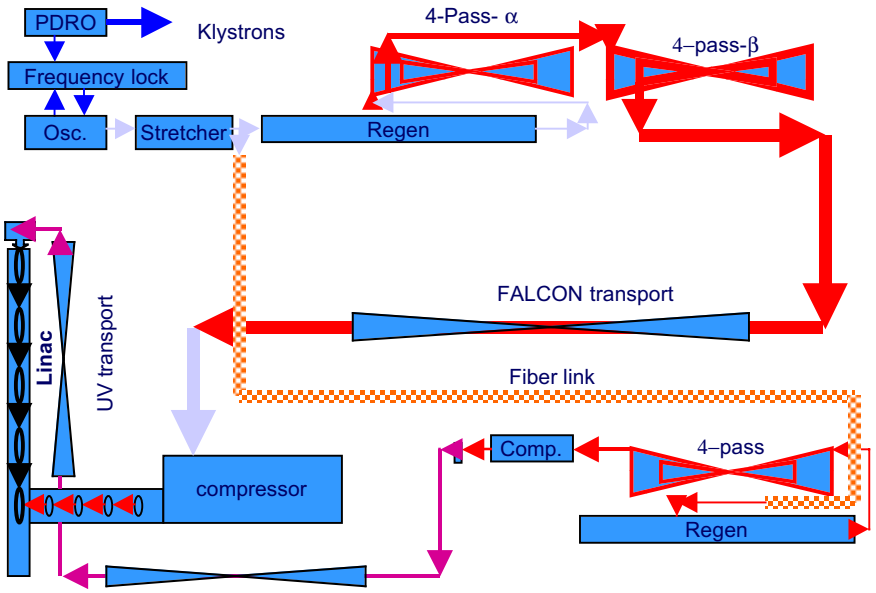

Ti:Al_2O_3 OPCPA Hybrid

800 nm

500 mJ (compressed)

50 fs FTL

20 μm FWHM (M^2 ~ 1.5)

10 Hz

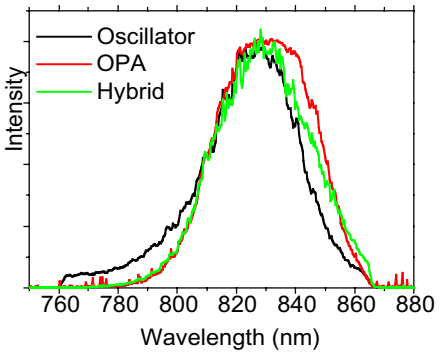

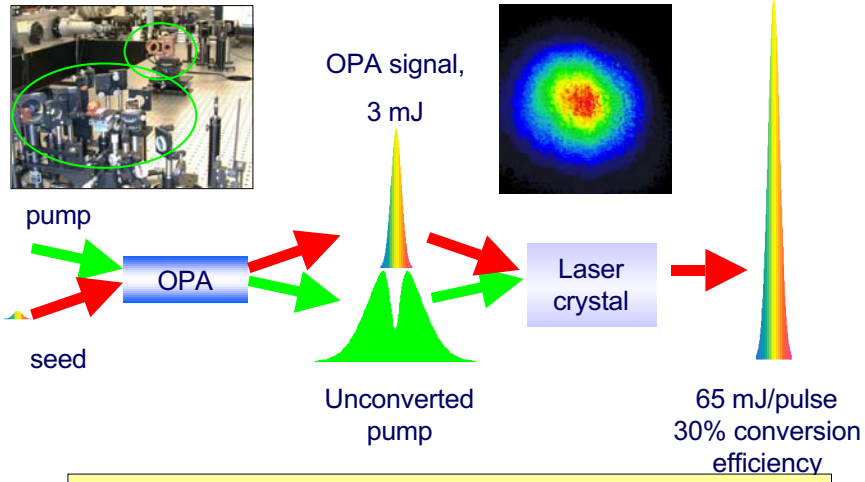

Inherent 10^8 extinction in the prepulse will improve fidelity in pump-probe experiments

FALCON Pulse Characteristics

Physics & Advanced Technologies

Pulse Duration

GRENOUILLE Traces

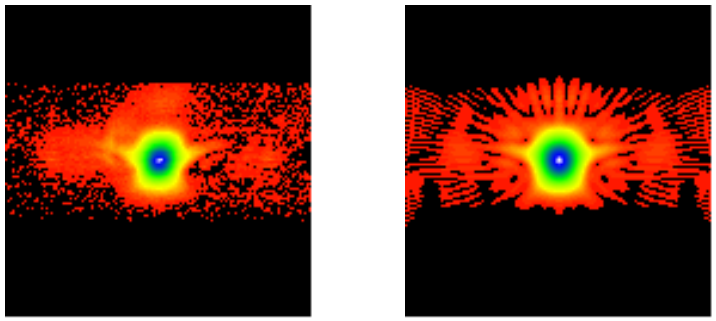

Measured | Retrieved

$\Delta t = 54$ fs

$1/e^2$ Radius at focus: 36 μm

$M^2 = 1.4$

Compressed energy: 180 mJ

Photoinjector UV Laser

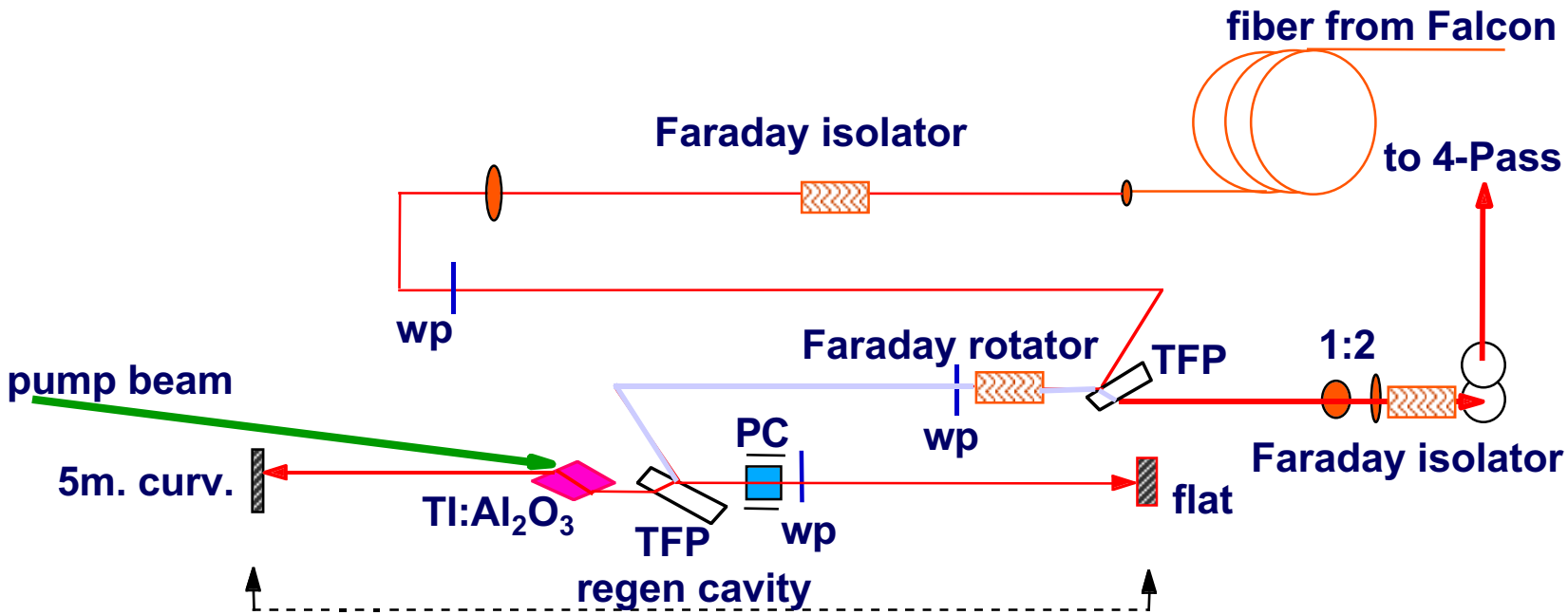

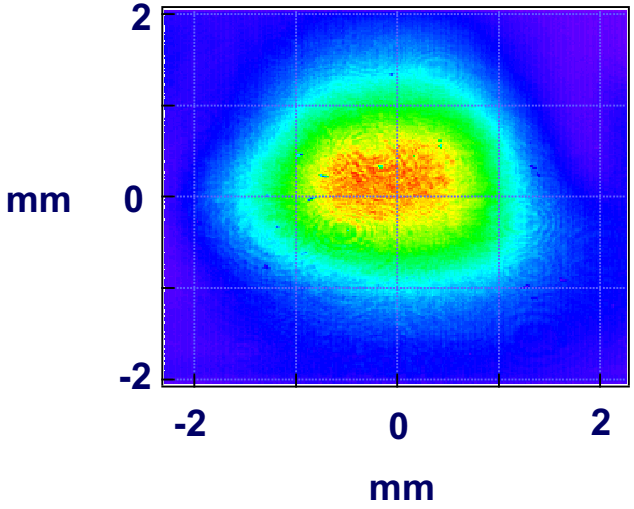

- 10 X 20 Brewster crystal (vertical orientation-S)
- Pump energy: 290-310 mJ
- Pump fluence: 4-5 J/cm^2
- Input energy: 60 pJ
- Output energy: 90-100 mJ

Electron Beam Diagnostics

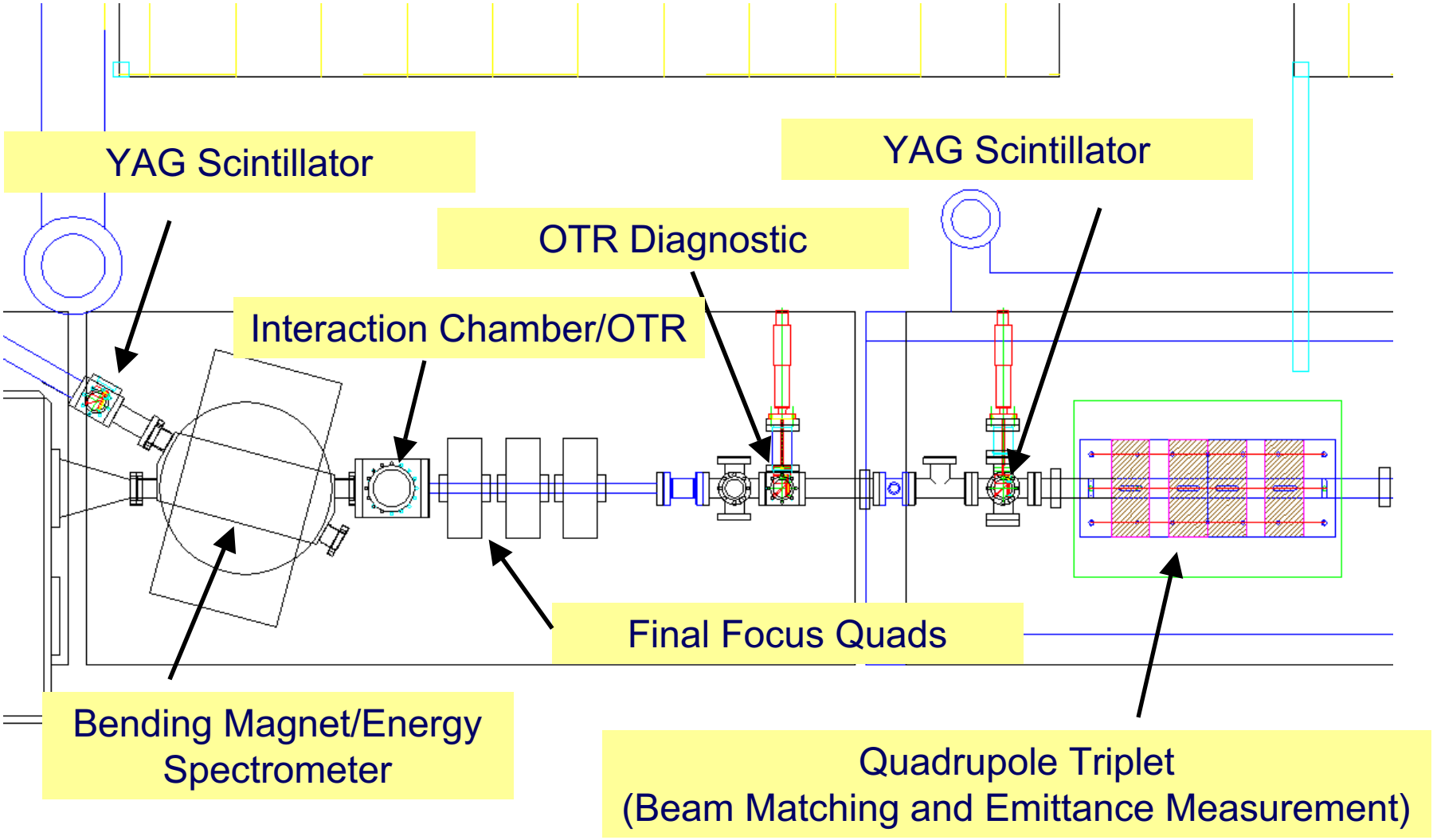

Emittance Measurements

Emittance

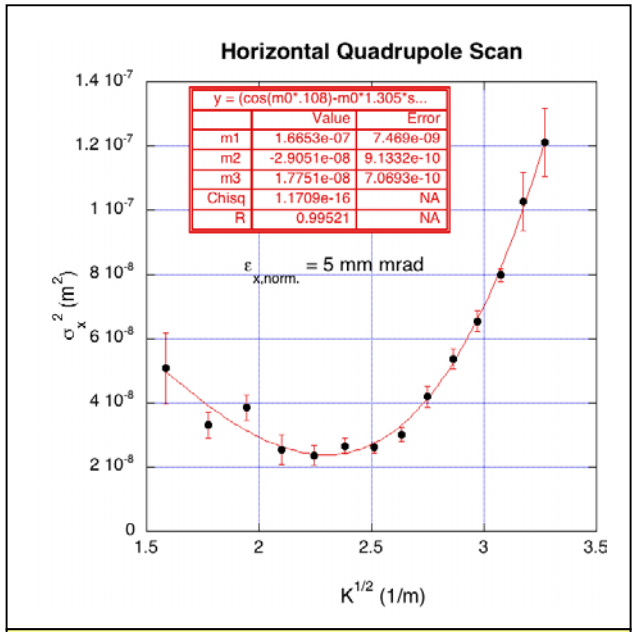

ε_x = 5 mm mrad

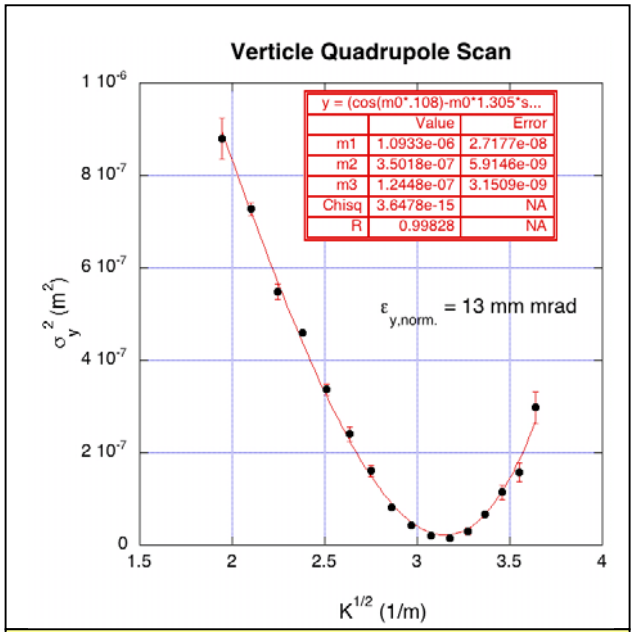

ε_Y = 13 mm mrad

Bunch Charge

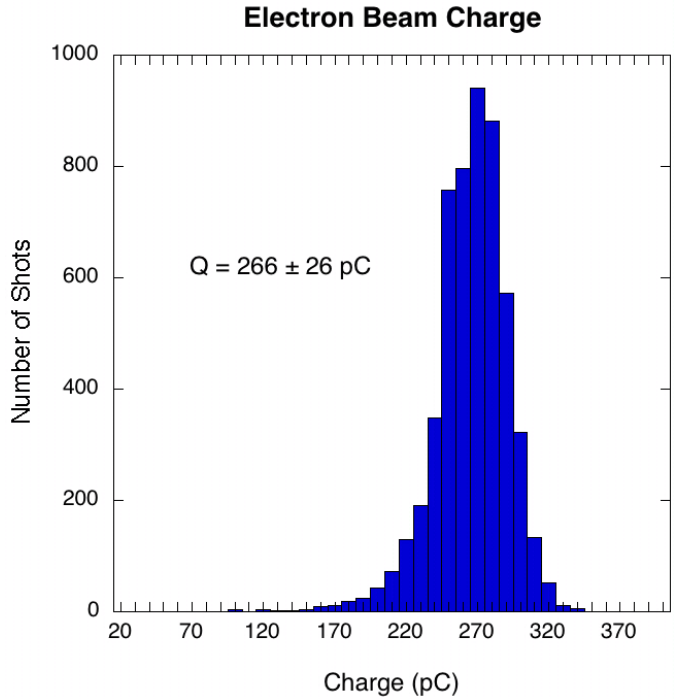

<q> = 266 pC

Electron Beam Measurements

Physics & Advanced Technologies

Energy Spectrometer

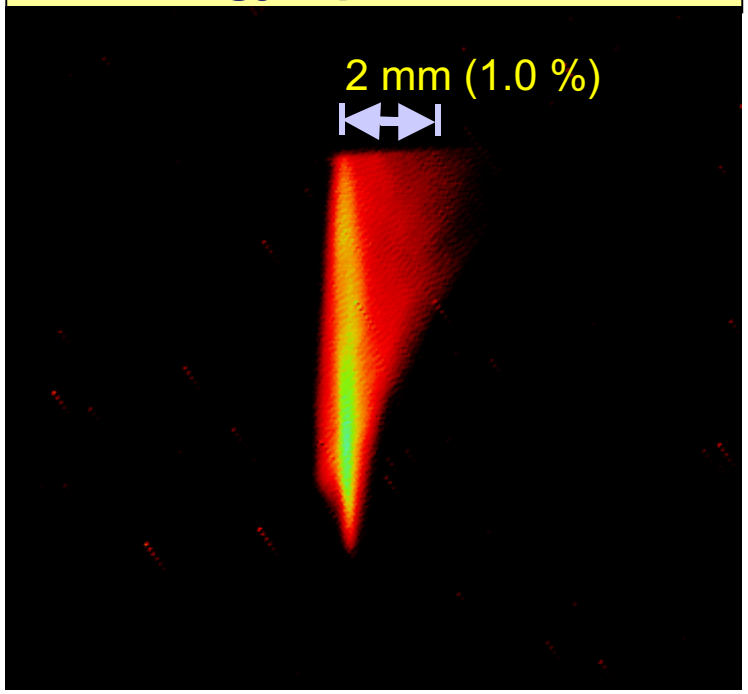

$E = 59.2$ MeV

$\sigma_E = 0.2$ %

Beam Spot At Interaction

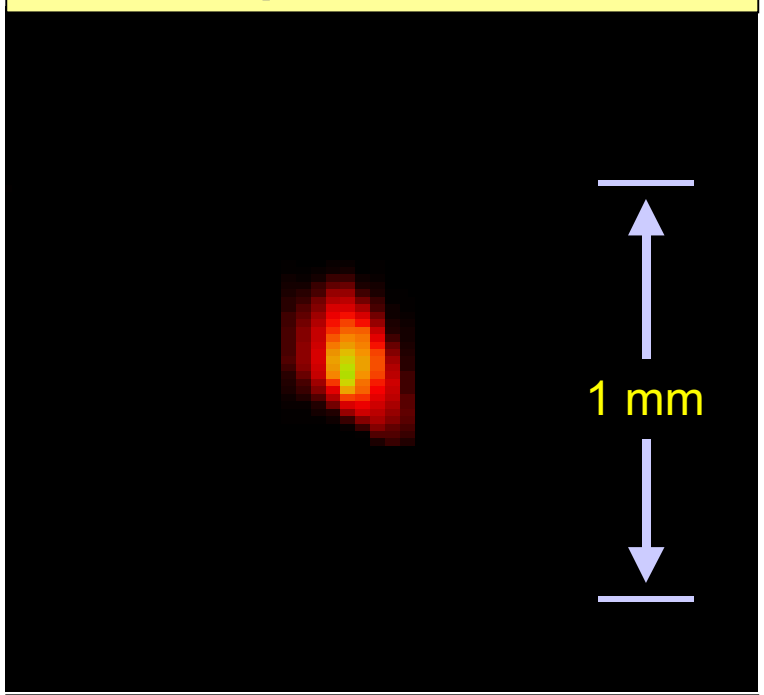

$\sigma_x = 79$ μm

$\sigma_y = 56$ μm

180° Geometry Implemented

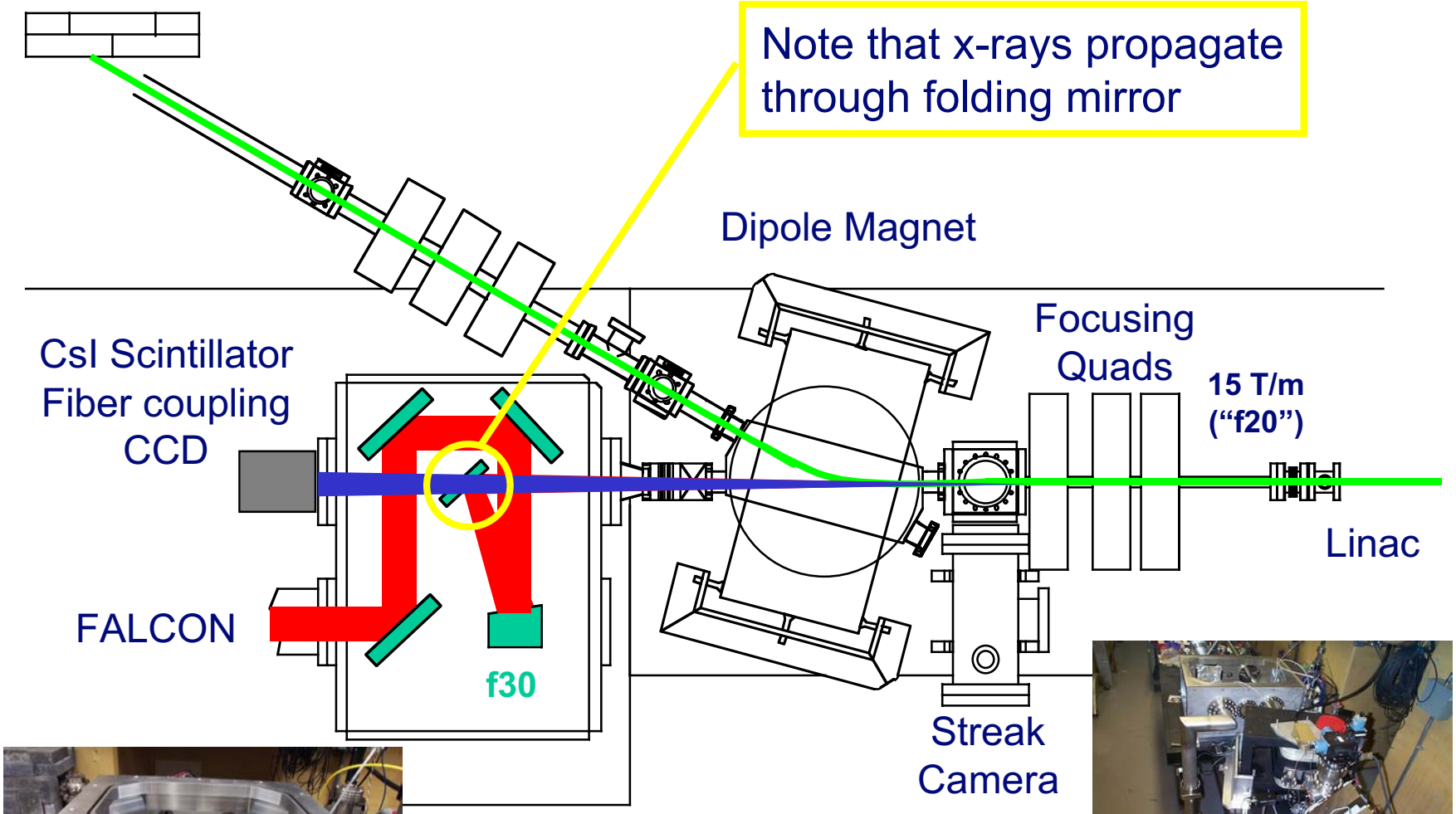

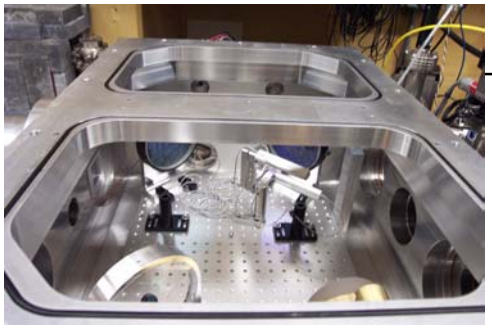

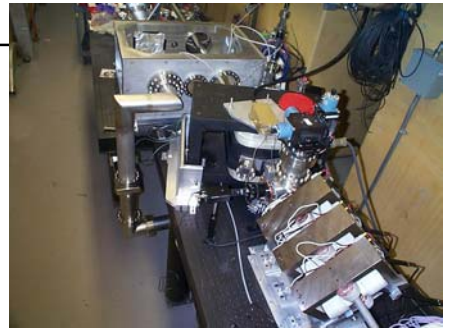

Jitter & Synchronization

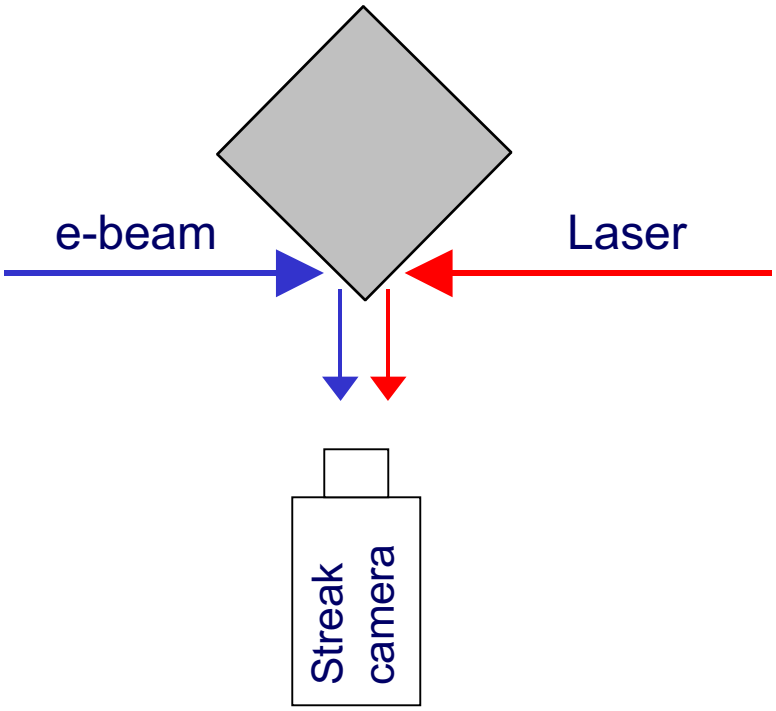

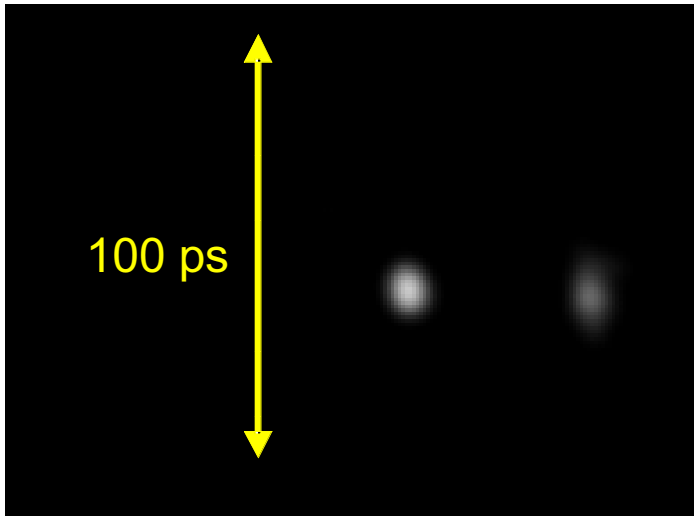

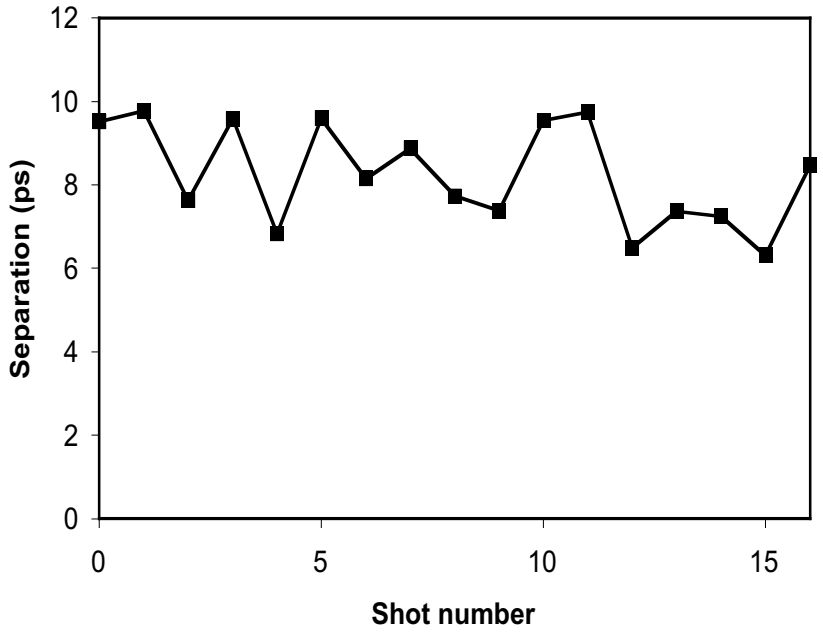

RMS timing jitter = 1.3 ps

PLEIADES 1st Light

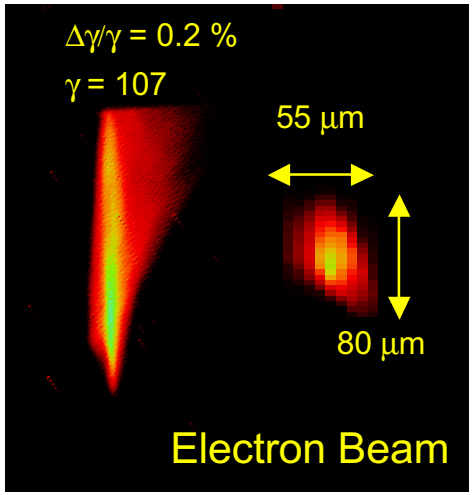

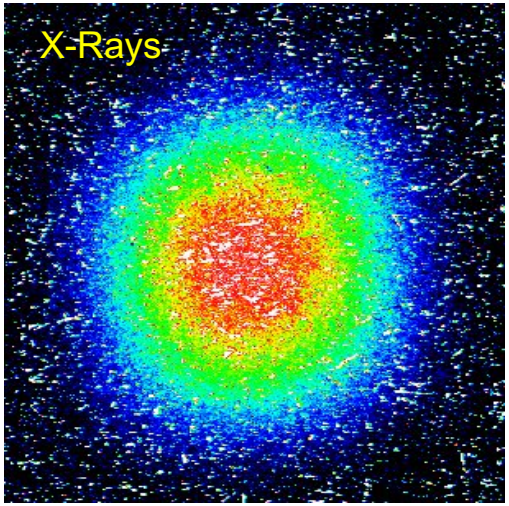

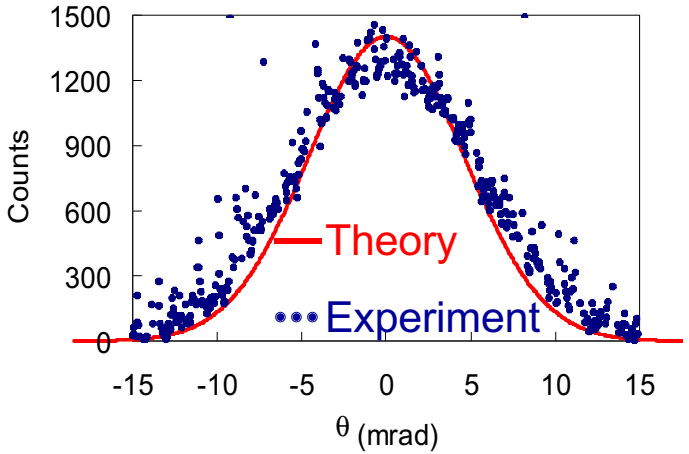

200 ms X-Ray CCD Capture

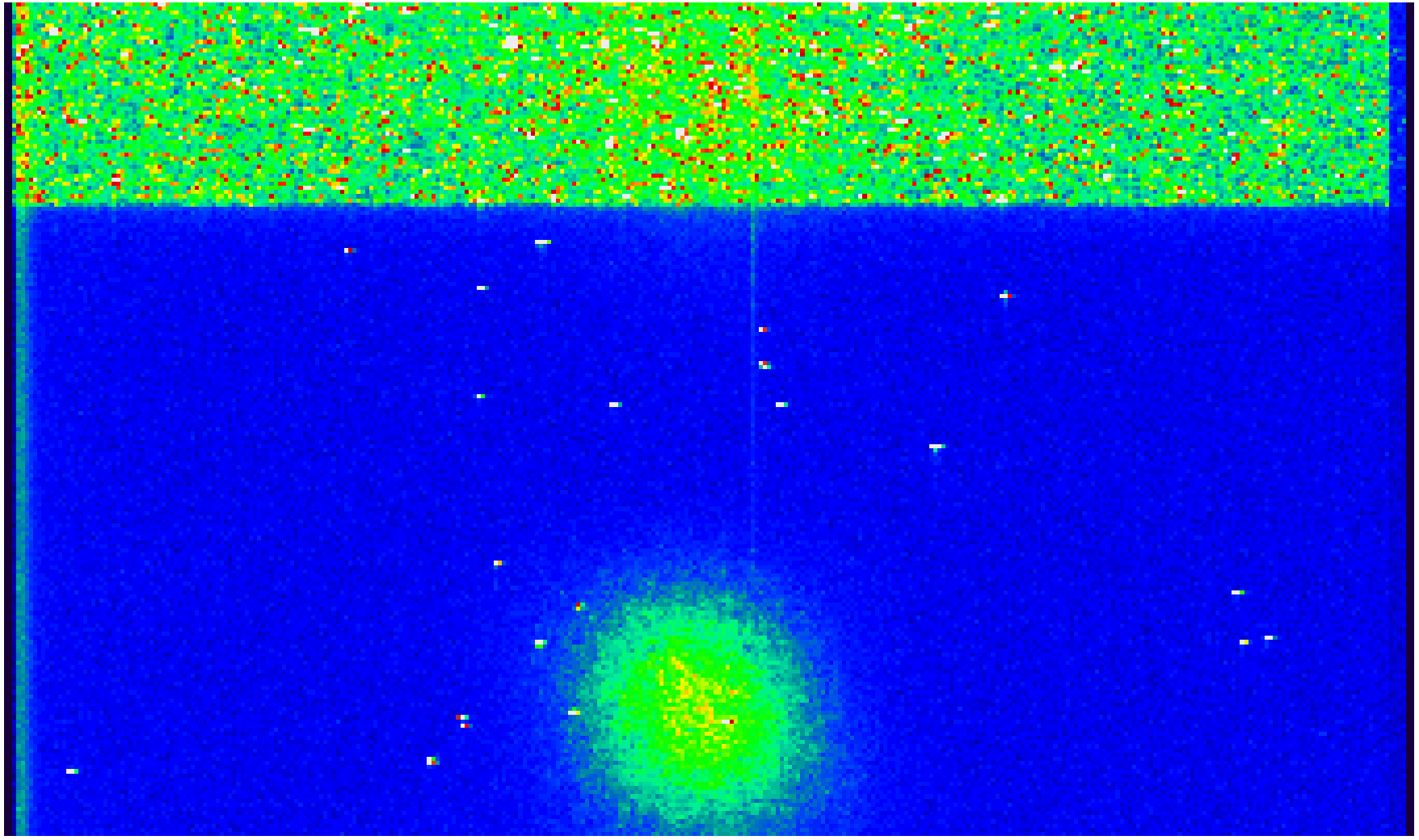

Linear Theory vs. Experiment

- Fused Silica flat (800 nm fold mirror) attenuates x-rays according to their energies (higher att. at low energy)
- Angular correlation between scattering angle & energy results in narrowing of the angular distribution:
- X-Ray energy distribution is given by:

- X-Ray energy distribution is given by:

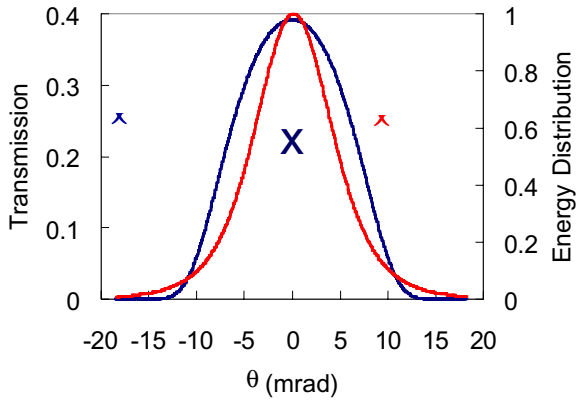

=

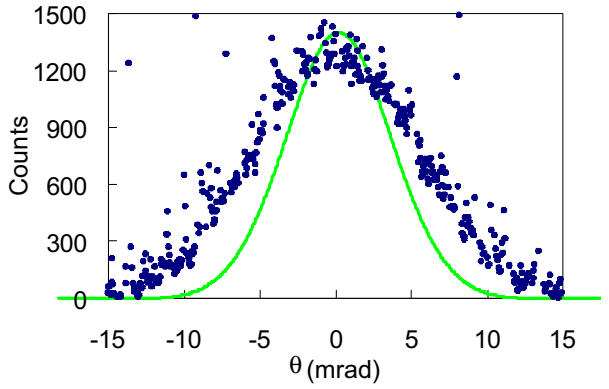

Linear Theory vs. Experiment

- However, emittance and 3D focusing broaden angular distribution:

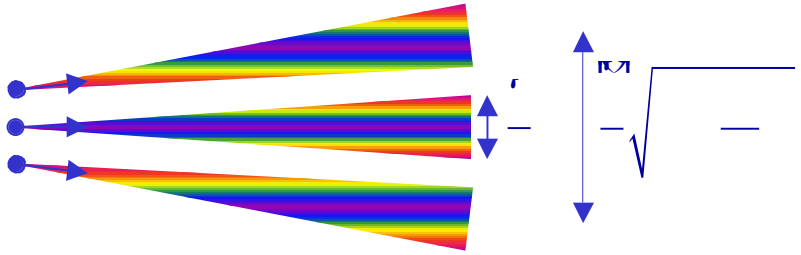

- All these effects must be accounted for to match data

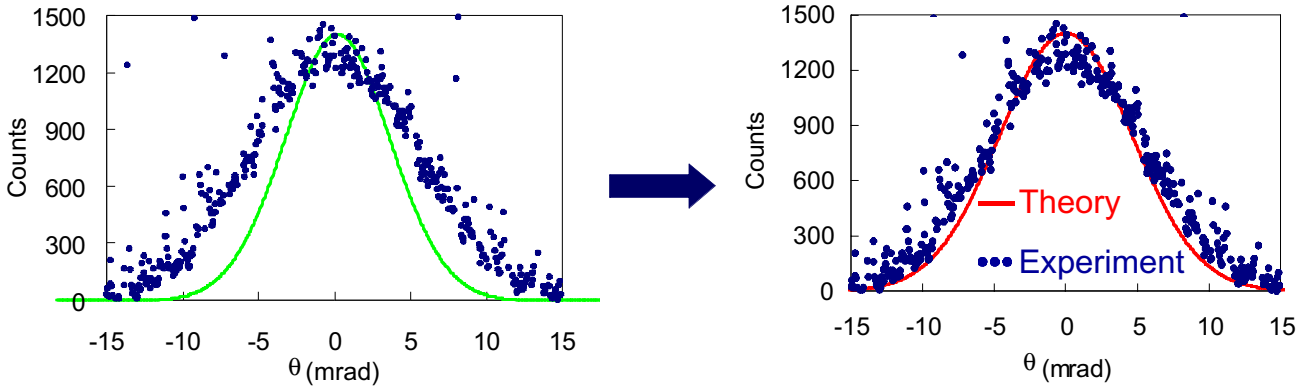

X-Ray Dose per Shot

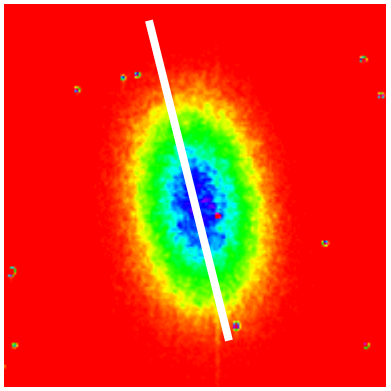

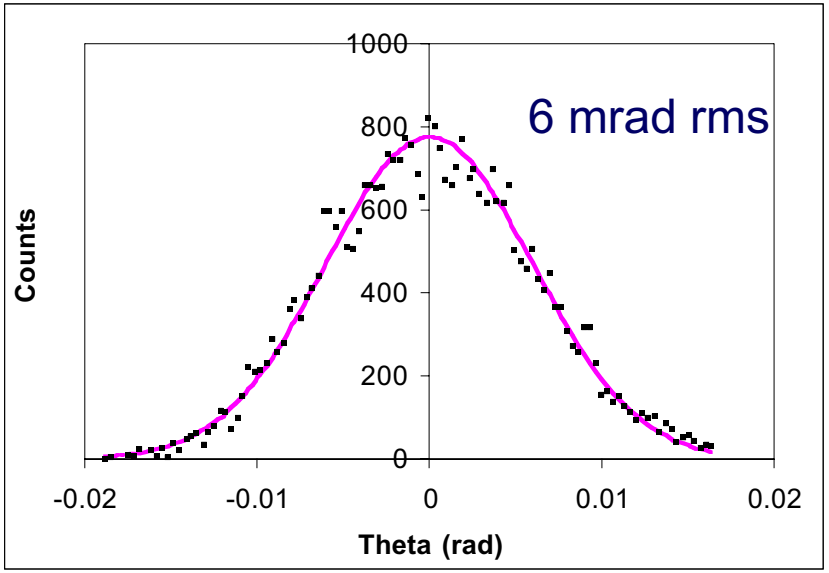

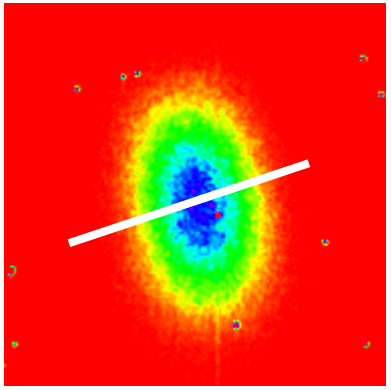

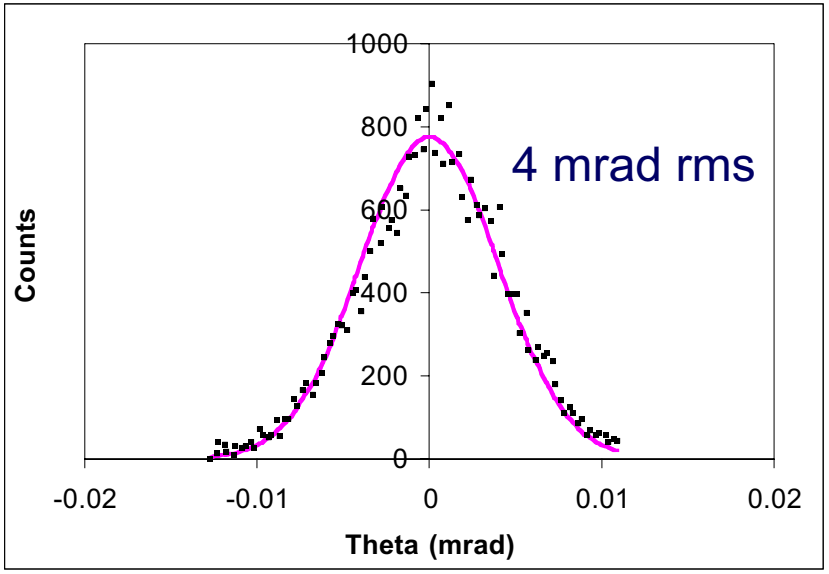

1.56 x 10^7 keV/shot on x-ray CCD

X-Ray Dose per Shot

Physics & Advanced Technologies

Transmission through the Laser Optic

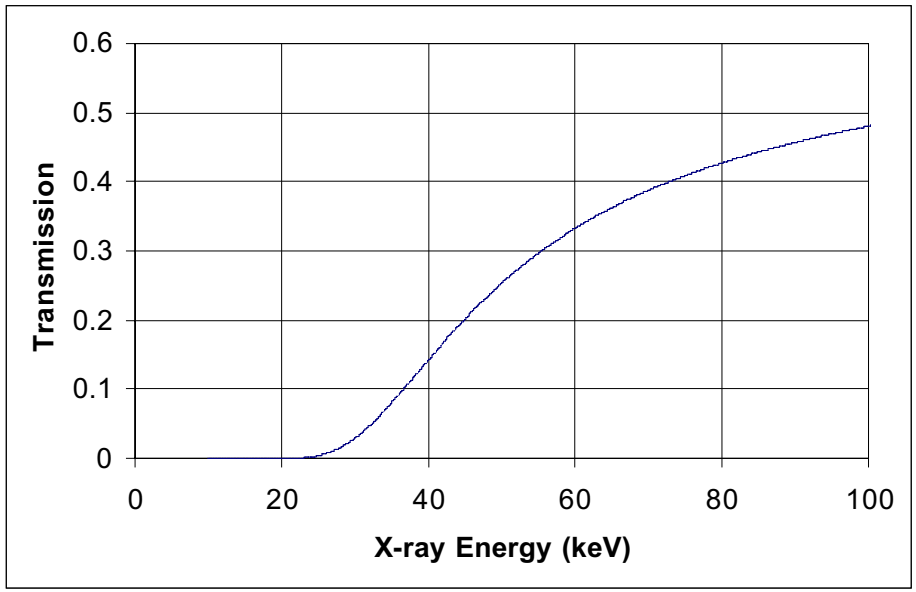

X

Integrated X-ray Spectrum

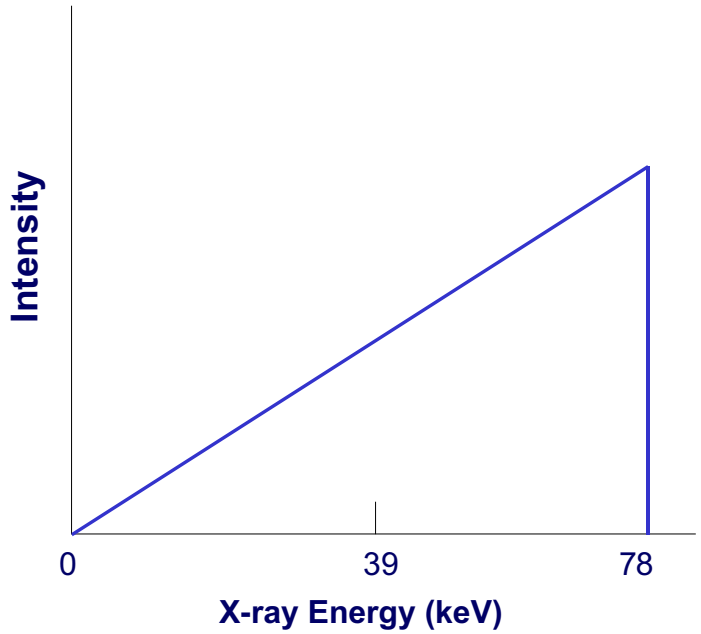

→ 30% Integrated Energy Transmission

At the interaction:

- 5.2 x 10^7 keV in shot
- Average photon energy = 39 keV
- 1.3 x 10^6 photons in the shot

X-Ray for Current Parameters

Physics & Advanced Technologies

Measured Electron Beam

- ❑ Charge = 0.27 nC
- ❑ Energy = 60 MeV
- ❑ σ_E = 0.2 %
- ❑ ε_n = 9 πmm-mrad

Laser Parameters

- ❑ 180 mJ
- ❑ M^2 = 1.4
- ❑ λ = 800 nm
- ❑ σ_t = 55 fs

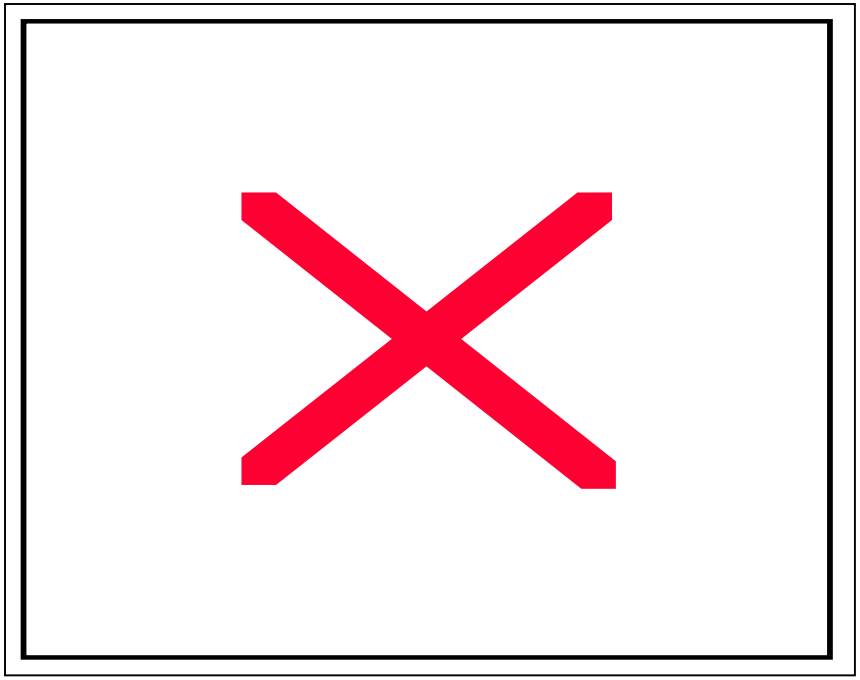

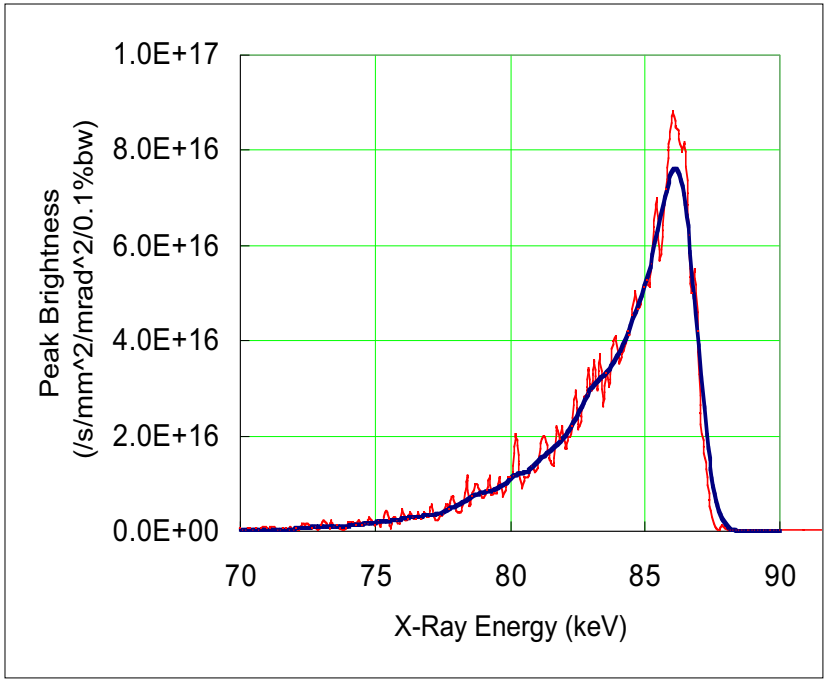

Integrated Dose: 2 X10^6 photons/pulse

Brightness: 10^{17} ph./s/mm^2/mrad^2/0.1%bw

Shorter X-Ray Pulses: Velocity Compression

- Velocity compression potentially avoids emittance and energy spread degradation observed in magnetic compression schemes

- Beam is injected ahead of peak accelerating phase, and compresses as it slips back in phase

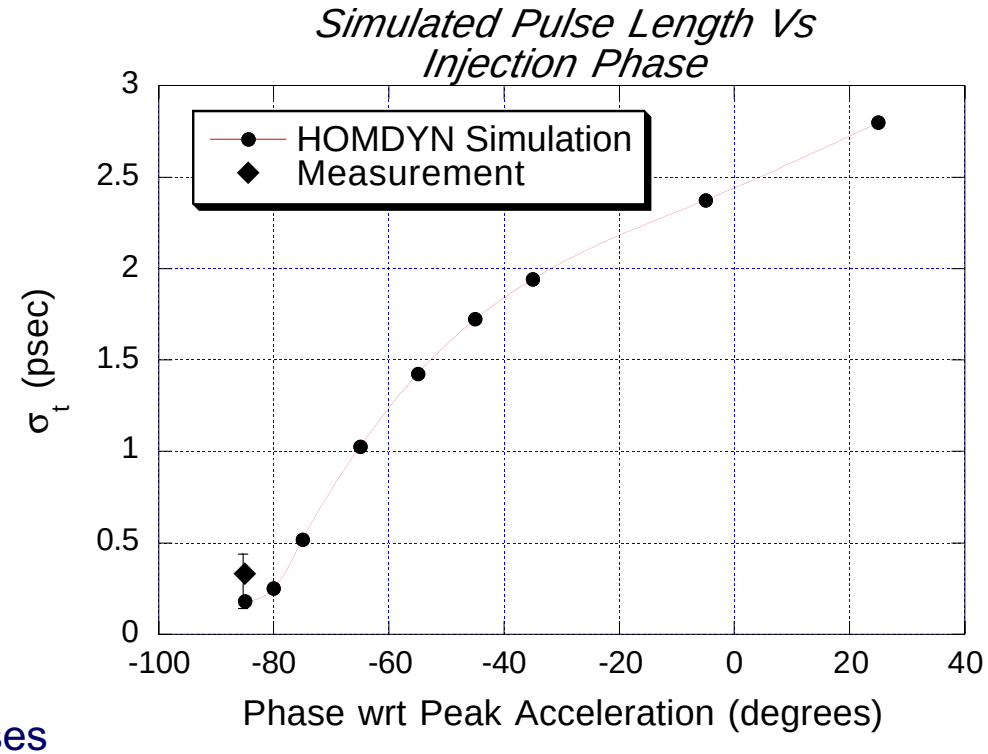

Beam run off-crest 'chirps' and compresses

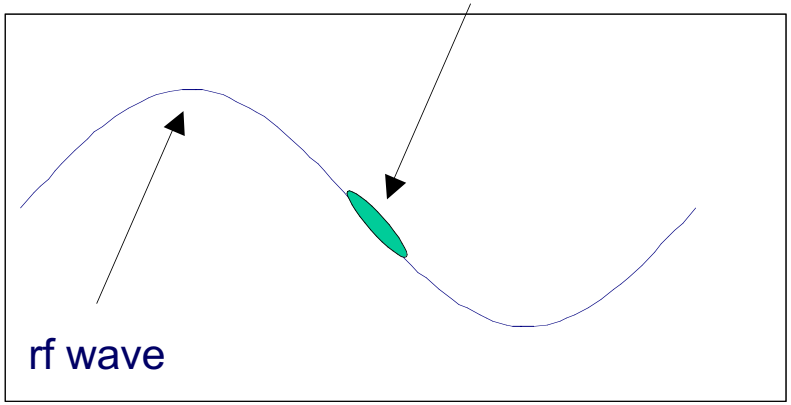

Velocity Compression Measurements: < 300 fs

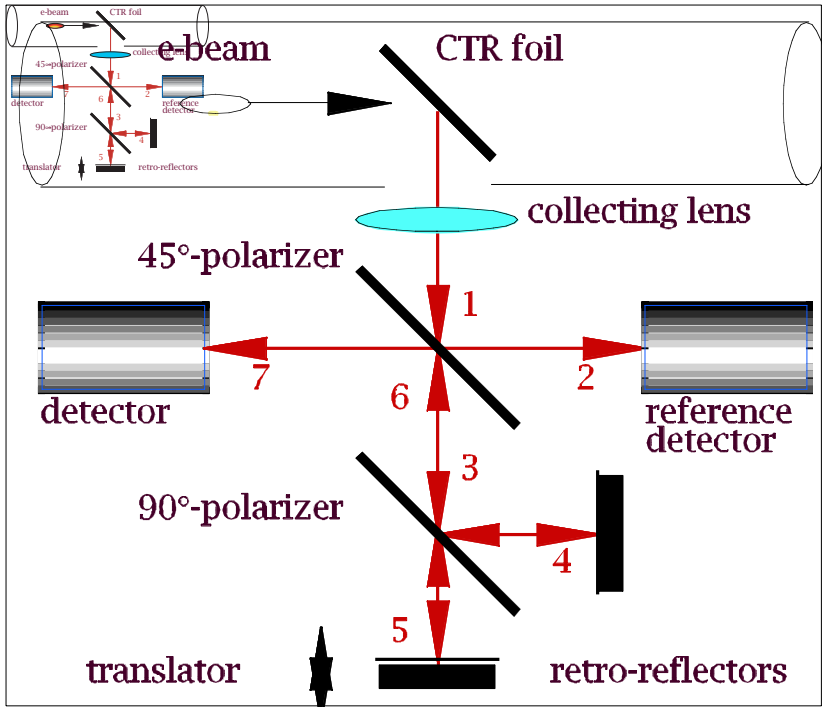

Coherent Transition Radiation (CTR) Diagnostic

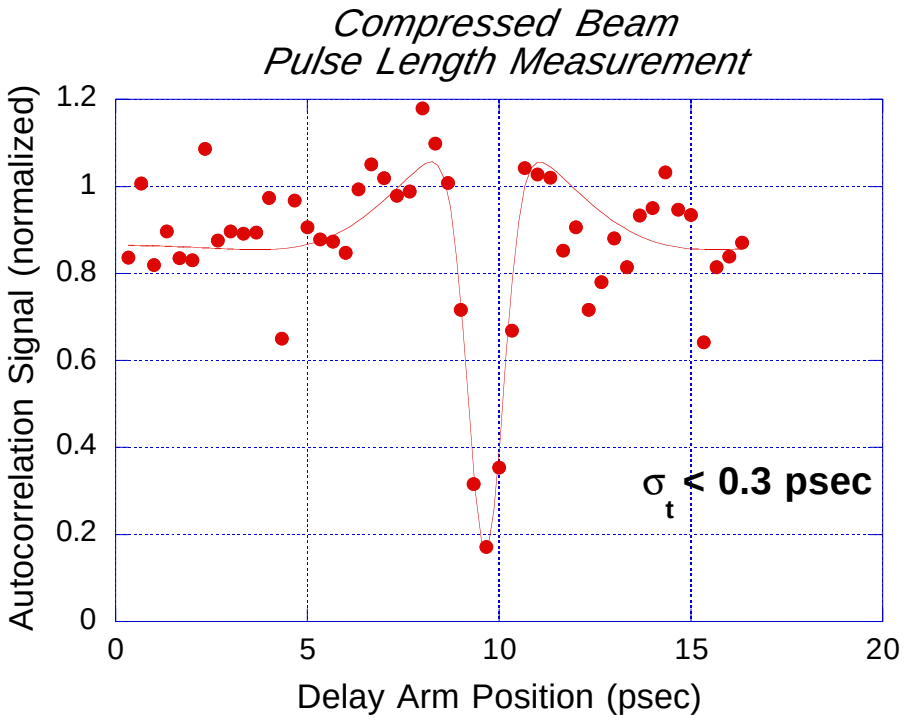

Measurement is *filtered* autocorrelation of bunch profile, due to loss of longer wavelengths; result is 'wings' in data.

Radiography & Tunability

0.005” Tantalum foil; K-edge @ 67.46 keV

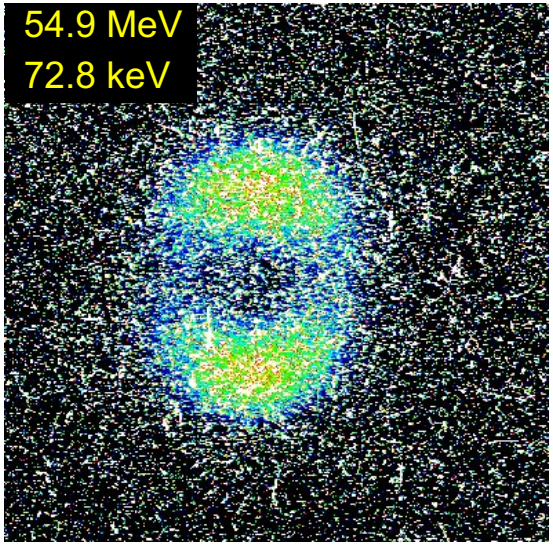

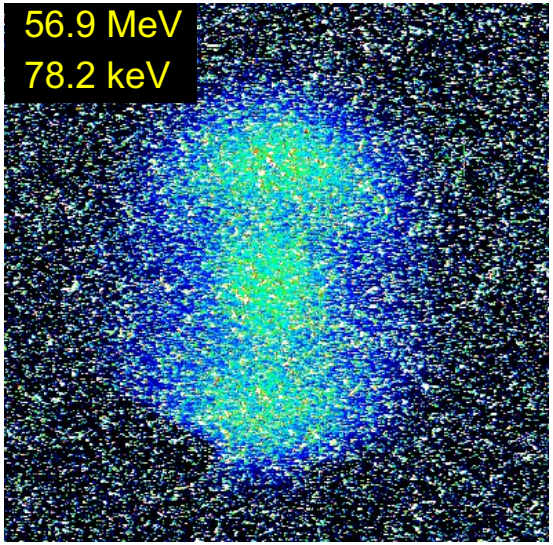

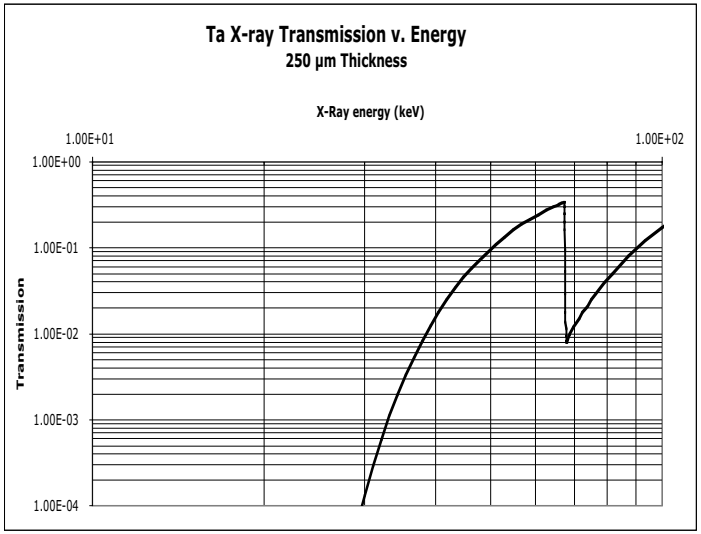

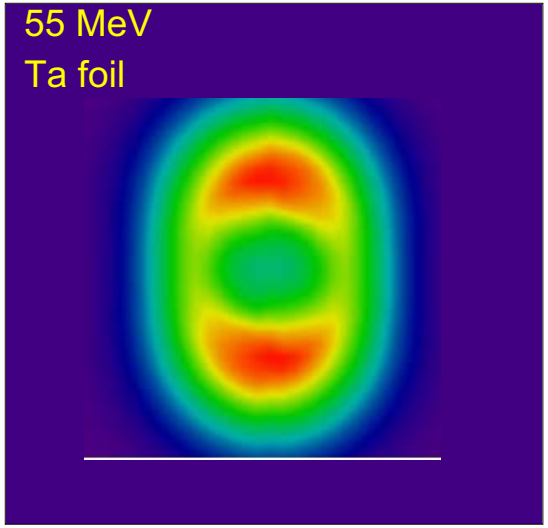

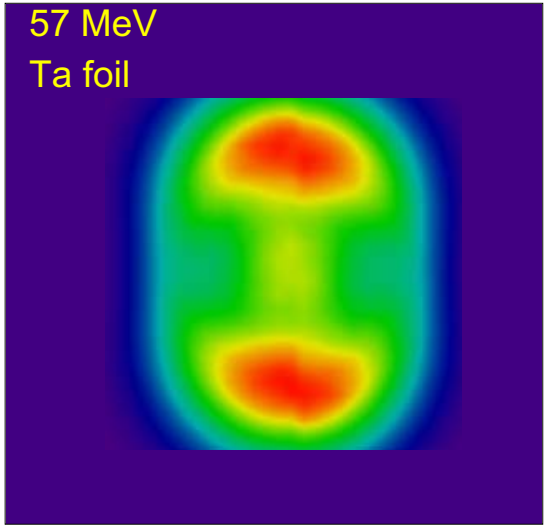

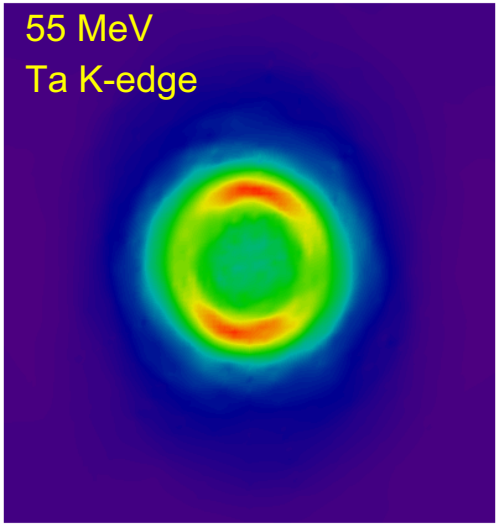

PLEIADES Applications

Absorption

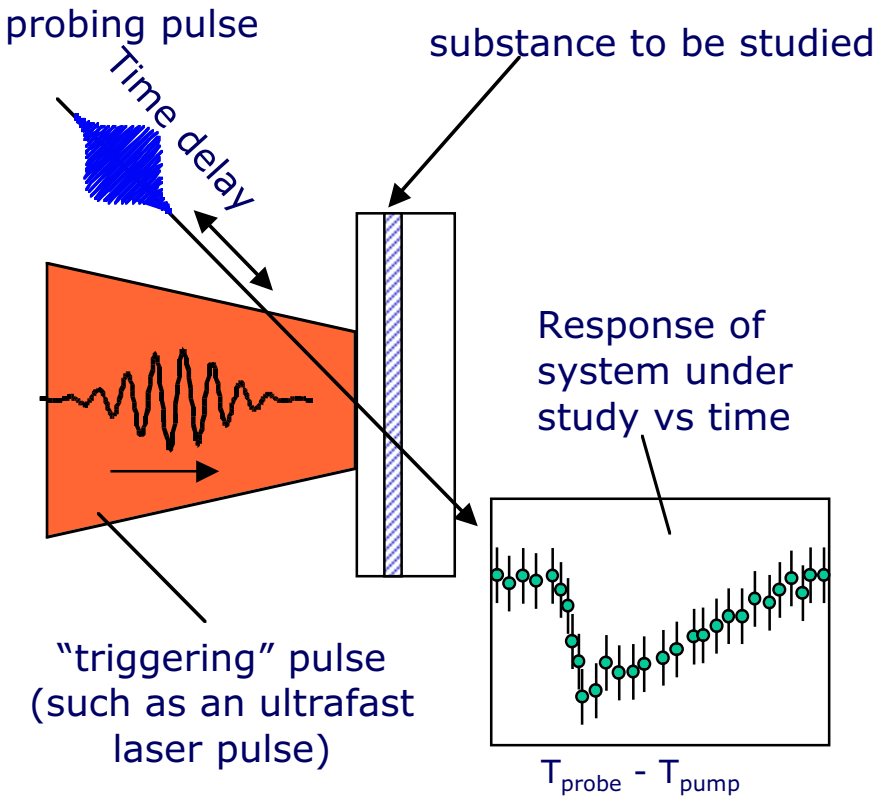

Diffraction

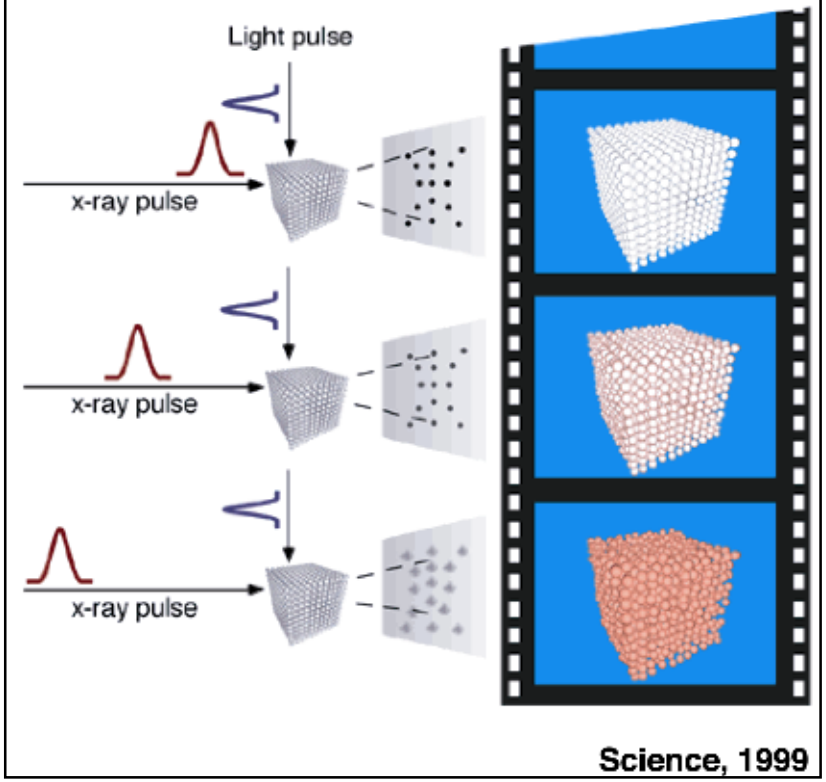

By varying the delay, the temporal dynamics of a physical, chemical or biological event can be mapped out

PLEIADES Applications

Physics & Advanced Technologies

Melt/Refreeze Experiment In Pb or Ta

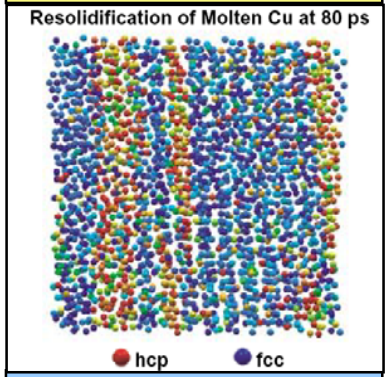

- Phase change kinetics
- Metastable amorphous
- Formation of grains

Volume collapse in Pr

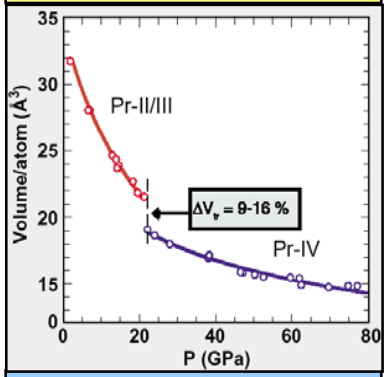

Role of f-electron in phase transition

Bismuth Phase Diagram

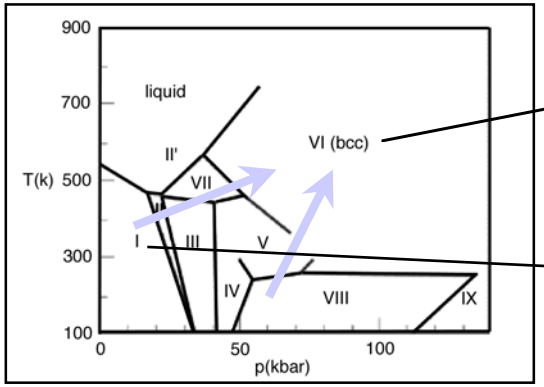

bcc

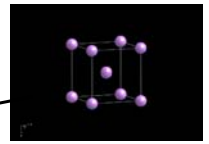

Rhombo-hedral

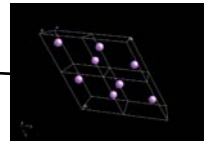

Resolidification of Molten Ta

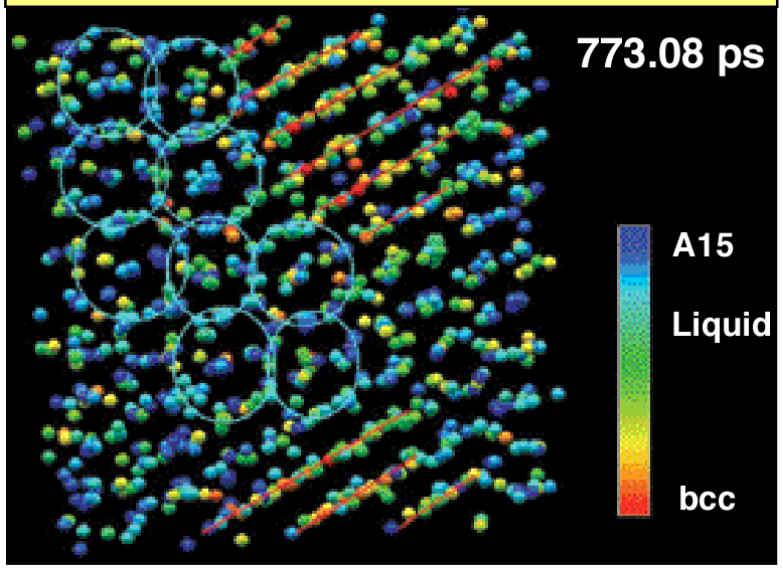

Initial

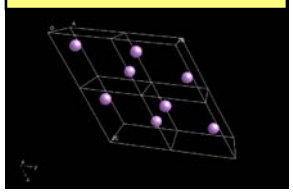

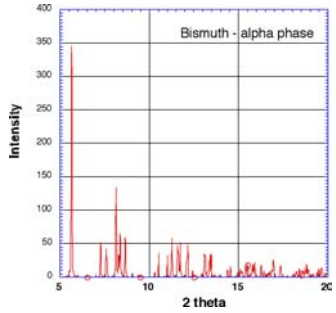

Shocked

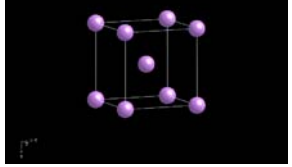

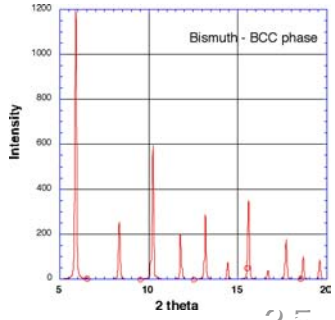

Dynamical Bragg Diffraction Experiment

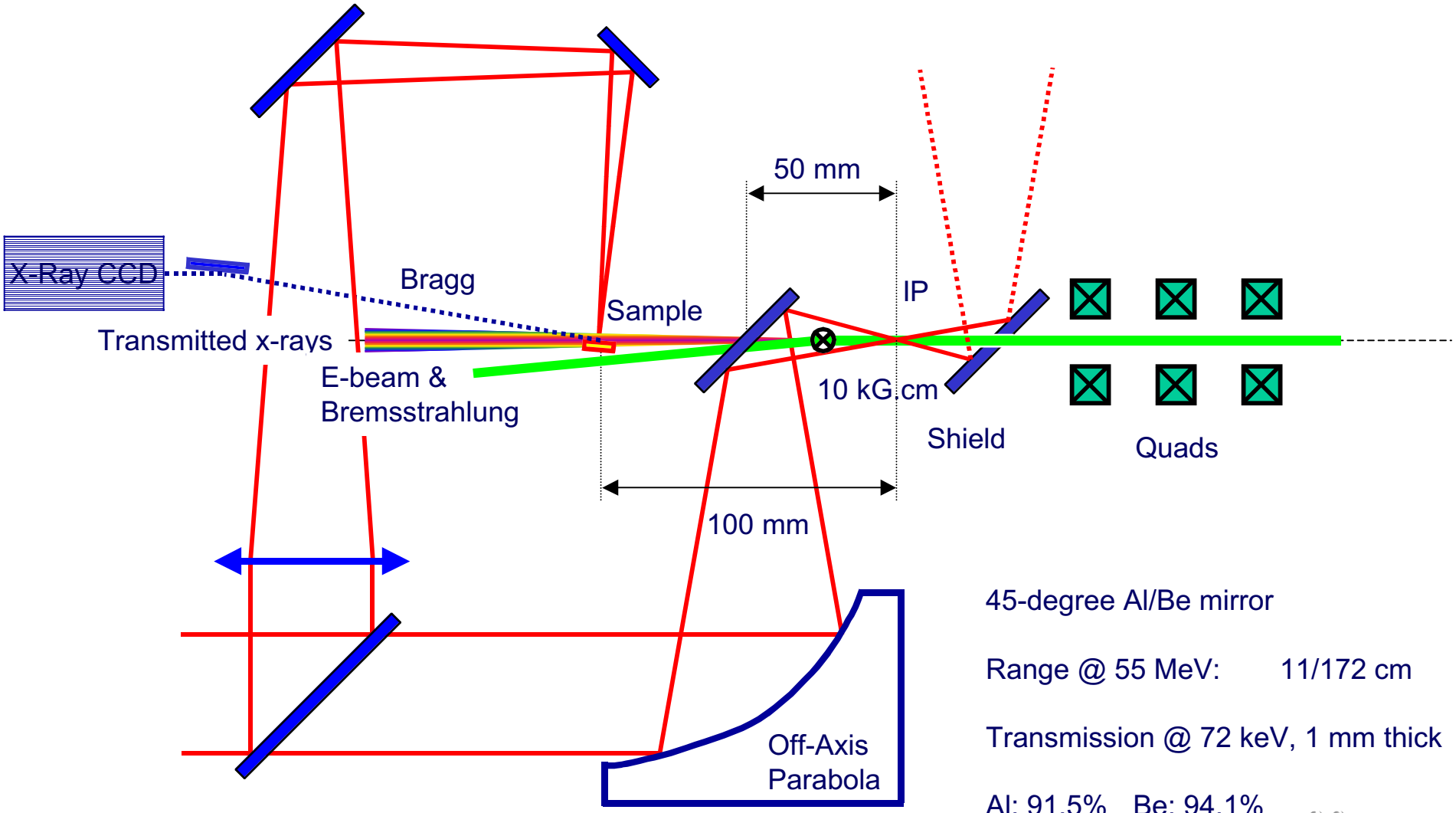

45-degree Al/Be mirror

Range @ 55 MeV: 11/172 cm

Transmission @ 72 keV, 1 mm thick

Al: 91.5% Be: 94.1%

Linear Compton Scattering

Physics & Advanced Technologies

$< 10^{17}$ W/cm^2

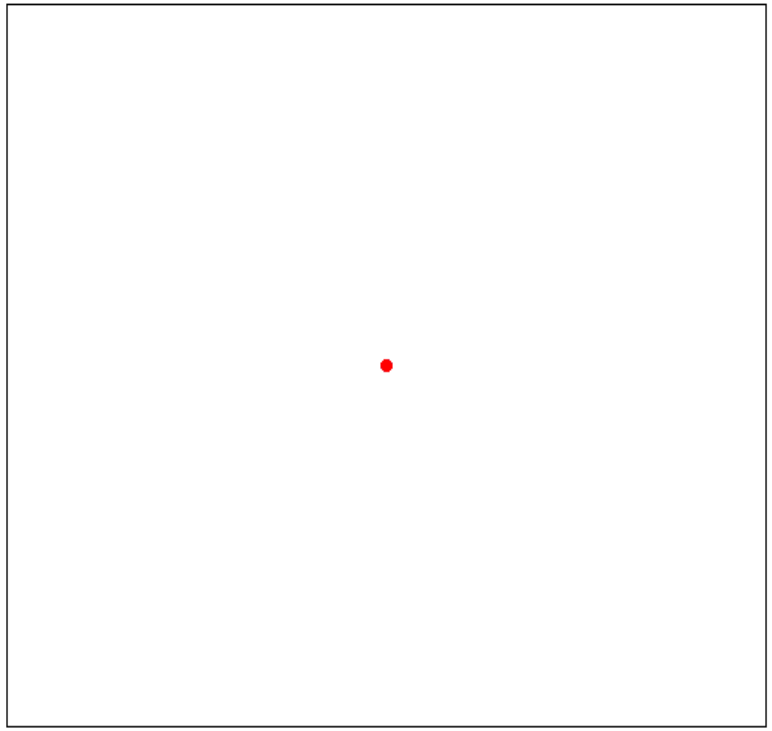

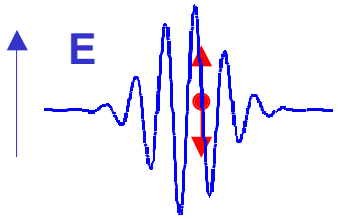

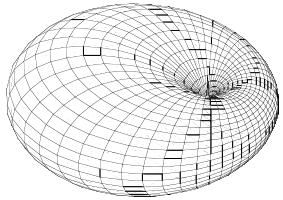

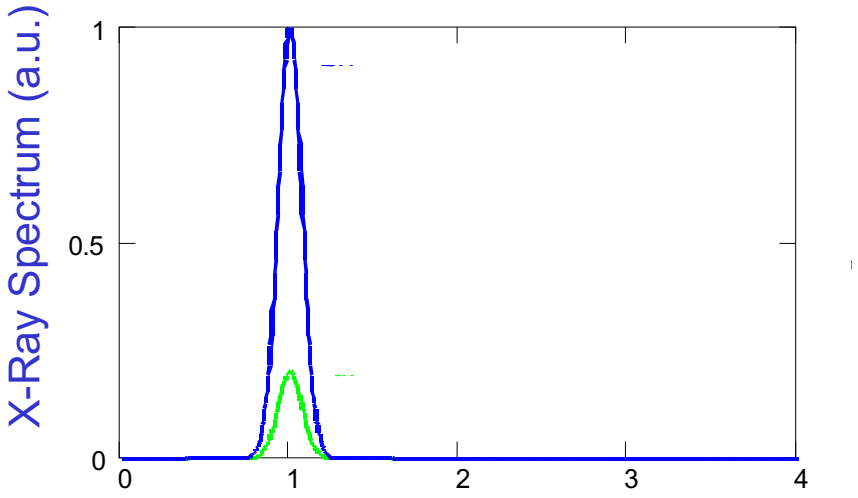

Nonlinear (Multiphoton) Compton Scattering

Physics & Advanced Technologies

Analogy: Strong Wiggler Field

X-Ray Harmonic Production

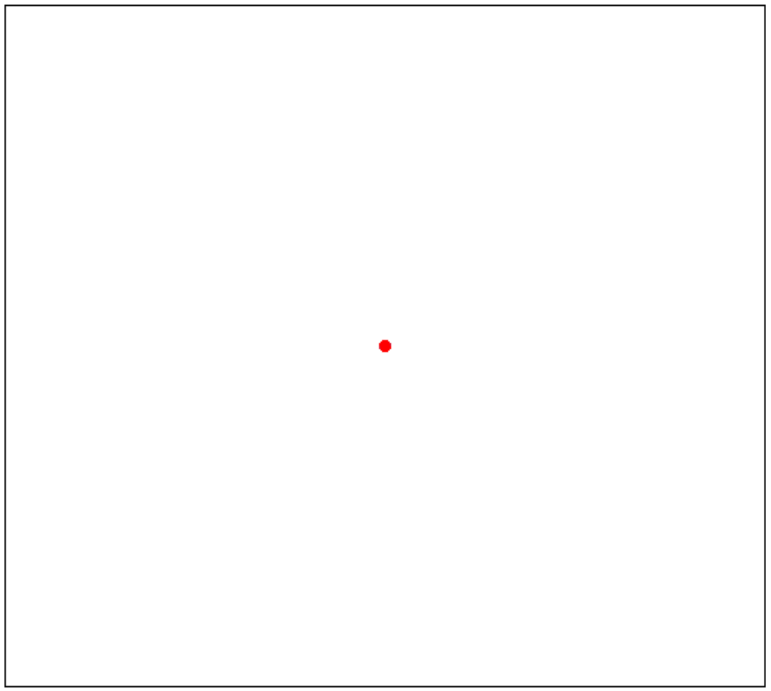

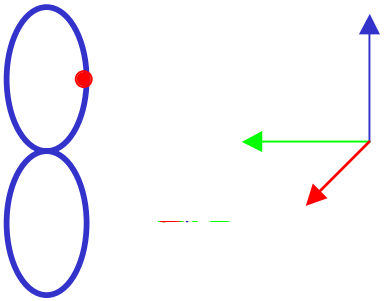

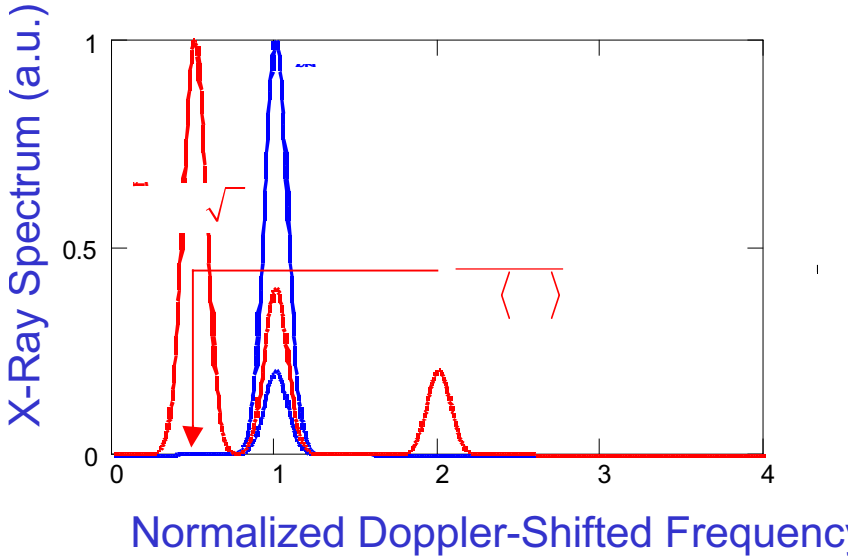

Spectral Control

Approach:

1) Circular Polarization, to Eliminate High Harmonics

2) Temporal Pulse Shaping, to Eliminate "Transient" Lines
(Heritage *et al*, low-power)

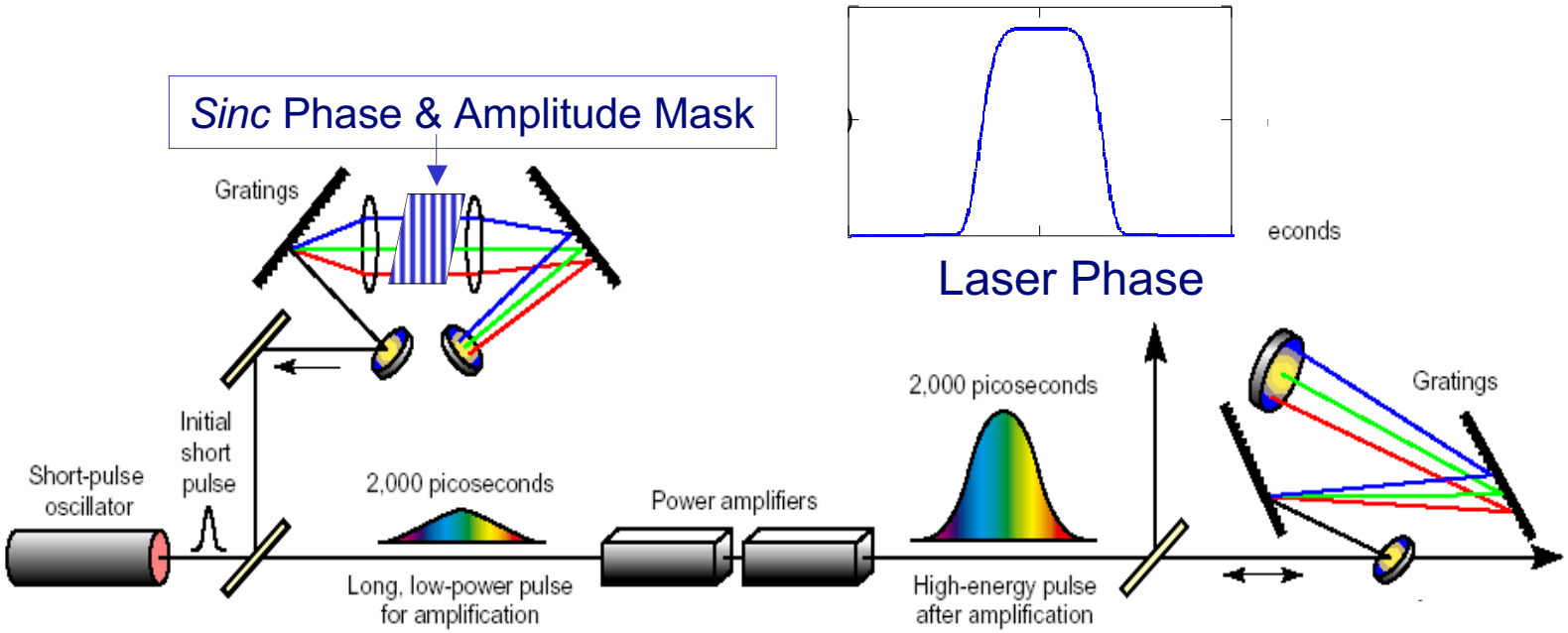

Higher Brightness: NL Compton Scattering

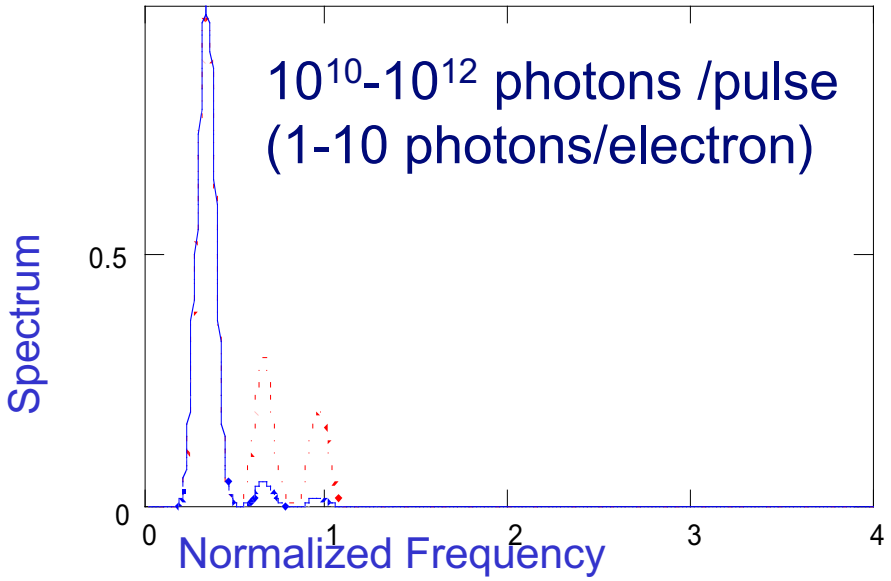

Decreases: Much Smaller Spot Size

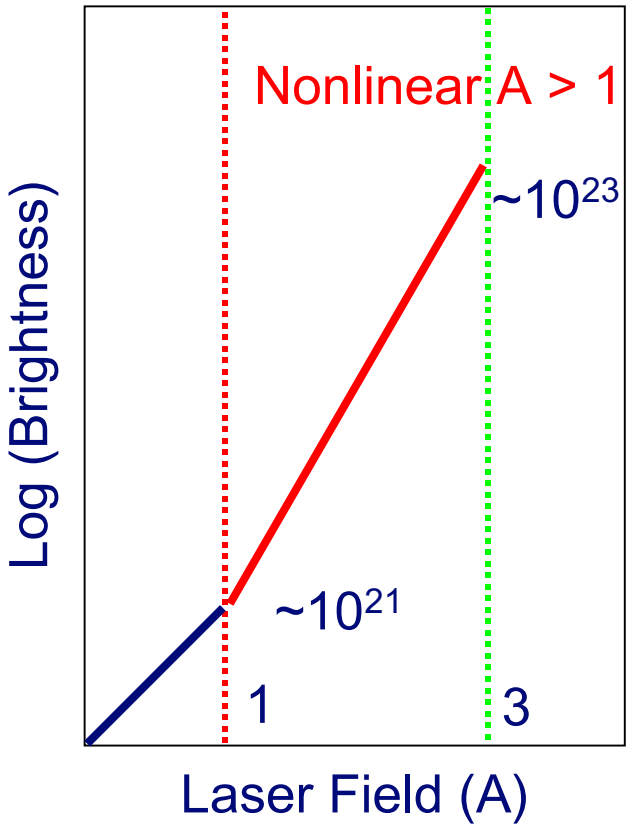

>10^{23} photons /mm^2/mrad^2/s/0.1%bw

Conclusions

- Linear Compton scattering sources can produce ps x-ray pulses, with > 10^6 photons/pulse
- Linear 3D theory agrees very well with experimental data
- The source is compact, tunable, and can reach photon energies > 100 keV
- X-Ray pulse durations < 100 fs can be reached at full dose using velocity compression
- Nonlinear Compton scattering provides a path to a compact, high-energy, tunable x-ray source with extremely high peak brightness

Interaction of Ultra-Intense Laser Pulses with Relativistic Ions

Ciprian Chiril_[1]

Charles Joachain[2]

Niels Kylstra[1,2]

Robert Potvliege[1]

[1]University of Durham, United Kingdom

[2]Université Libre de Bruxelles, Belgium

OUTLINE

1. The Relativistic Ion Beam-Intense Laser Facility at G.S.I.

2. Relativistic Doppler Effect. Lorentz boosts

3. Non-Dipole and Coulomb Effects in Laser-Atom Interactions

4. Photoemission by Relativistic Ions

5. Conclusions

GSI facility. Relativistic ion beam

GSI (Darmstadt, Germany):

- _ = 1053.7 nm
- peak intensity up to 10^{21} W/cm^2 and above
- ions with nuclear charge $2 \le Z \le 92$
- relativistic factor for the ion beam $\gamma \le 30$

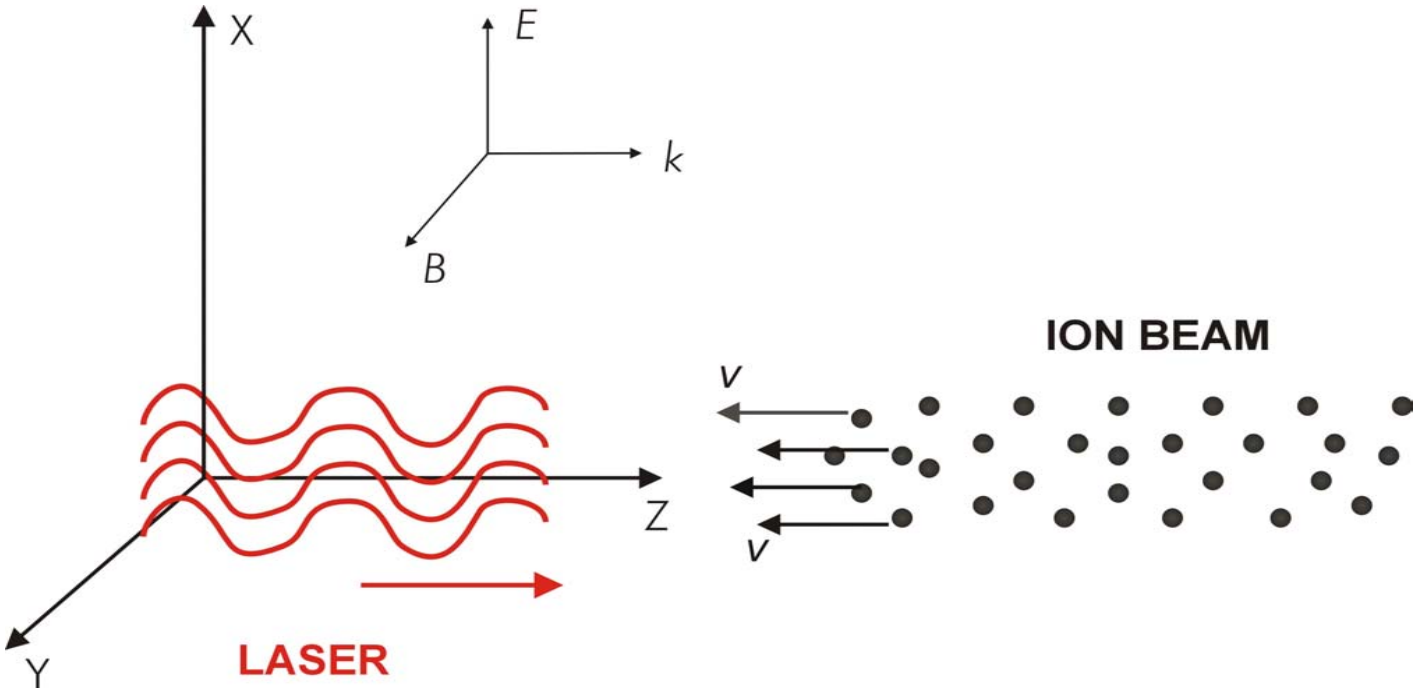

Ion beam setup

Relativistic Doppler Effect

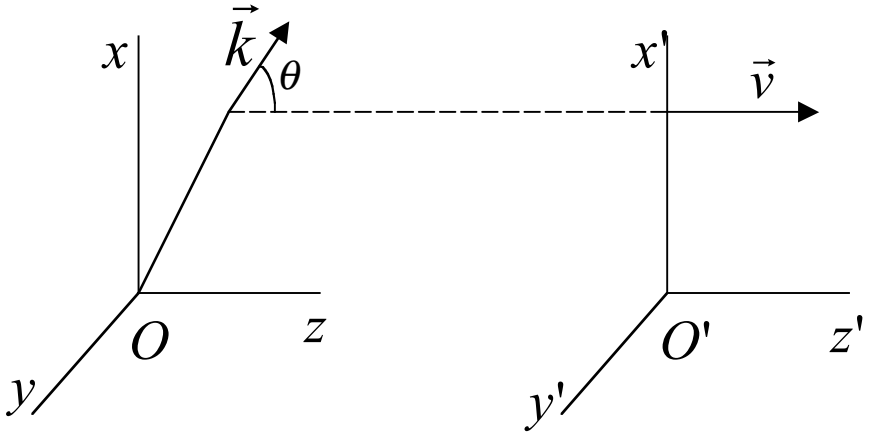

$\vec{k}$: wave vector in lab. frame $Oxyz$, with k = _/c

$\vec{v}$: velocity of moving frame $Ox'y'z'$

$$\cos\theta = \vec{k}\cdot\vec{v}/(kv)$$

- Let _ be the angular frequency in the lab. frame, and _' that in the moving frame. Then

$$\omega' = \omega\gamma(1-\frac{v}{c}\cos\theta)\ ,\quad \gamma = (1+\frac{v^2}{c^2})^{-1/2}$$

- When we have that _ = π, and with k along OZ, we have

$$\omega' = \omega\gamma(1+\frac{v}{c})$$

Lorentz boost

For our setup :

$$\gamma_{GSI} \cong 15 \rightarrow \beta \approx 1$$
$$\theta = \pi$$

The laser field in the reference frame of the ion:

$$\omega_{ION\ FRAME} = 2\gamma\omega_{LASER}$$
$$E_{ION\ FRAME} = 2\gamma E_{LASER}$$
$$B_{ION\ FRAME} = 2\gamma B_{LASER}$$

The ponderomotive energy $U_p = \frac{E^2}{4\omega^2}$ is a Lorentz invariant.

The period of the laser field decreases, while the peak of intensity of the laser increases in the ion reference frame.

The recollision picture. Dipole approximation

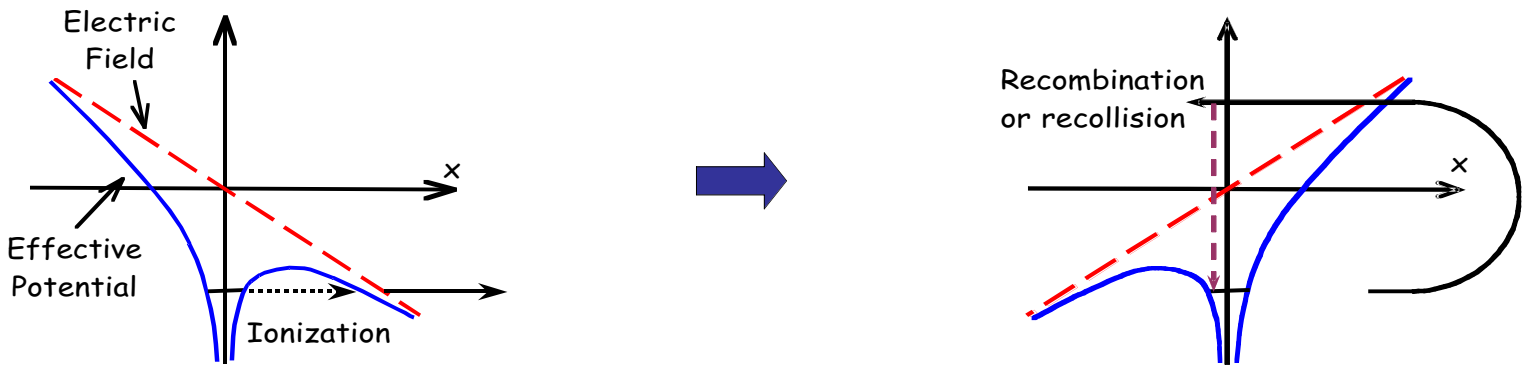

✓ What happens if we include the magnetic field component of the pulse?

We expect a deflection of the electronic wave packet before recombining with the ionic core. The efficiency of the process can be greatly reduced !

Muller and van Linden van den Heuvel; Corkum; Kulander and Shafer,.....

Non-Dipole Effects in Laser-Atom Interactions

- Non-dipole, non-relativistic time-dependant Schrödinger equation (TDSE) for one-electron atom (ion) in a laser pulse linearly polarized along $\hat{x}$ and propagating along $\hat{z}$:

$$i\frac{\partial}{\partial t}\Psi(\vec{r},t)=\left\{\frac{1}{2}[\vec{p}+\vec{A}(\eta)]^2+V(r)\right\}\Psi(\vec{r},t)$$

with $\vec{A}(\eta)=\hat{x}\,\vec{A}(\eta)$, $\eta=\omega(t-z/c)$ and $V(r)$ is the potential binding of the electron.

- To lowest order in $\frac{1}{c}$, $\vec{A}(\eta)=\vec{A}(\omega t)+\frac{z}{c}\vec{E}(\omega t)$ and the TDSE becomes

$$i\frac{\partial}{\partial t}\Psi(\vec{r},t)=\left\{\frac{1}{2}[\vec{p}+\vec{A}(\omega t)]^2+\frac{z}{c}\vec{p}\cdot\vec{E}(\omega t)+\frac{z}{c}\vec{A}(\omega t)\cdot\vec{E}(\omega t)+V(r)\right\}\Psi(\vec{r},t)$$

$$\Psi^L(\vec{r},t)=\exp[i\vec{A}(\omega t)\cdot\vec{r}]\Psi(\vec{r},t)$$

- Defining $\frac{1}{c}$ we can also write the TDSE, to lowest order in $\frac{1}{c}$, in the form

$$i\frac{\partial}{\partial t}\Psi^L(\vec{r},t)=\left\{\frac{p^2}{2}+\left[\vec{r}+\frac{z}{c}\vec{p}\right]\cdot\vec{E}(\omega t)+V(r)\right\}\Psi(\vec{r},t)$$

The non dipole non relativistic SFA for HHG

✓The non dipole approach : expand the vector potential to lowest order in $1/c$!

$$\vec{A}(\eta) = \vec{A}(\omega t) + \frac{z}{c}\vec{E}(\omega t) + ...$$

✓Retain lowest order terms in the non-relativistic Hamiltonian:

$$H = \left(\frac{1}{2}\left[\vec{p} + \vec{A}(\omega t)\right]^2 + V(r)\right) \quad + \frac{z}{c}\vec{p}\cdot\vec{E}(\omega t) \quad + \frac{z}{c}\vec{A}(\omega t)\cdot\vec{E}(\omega t)$$

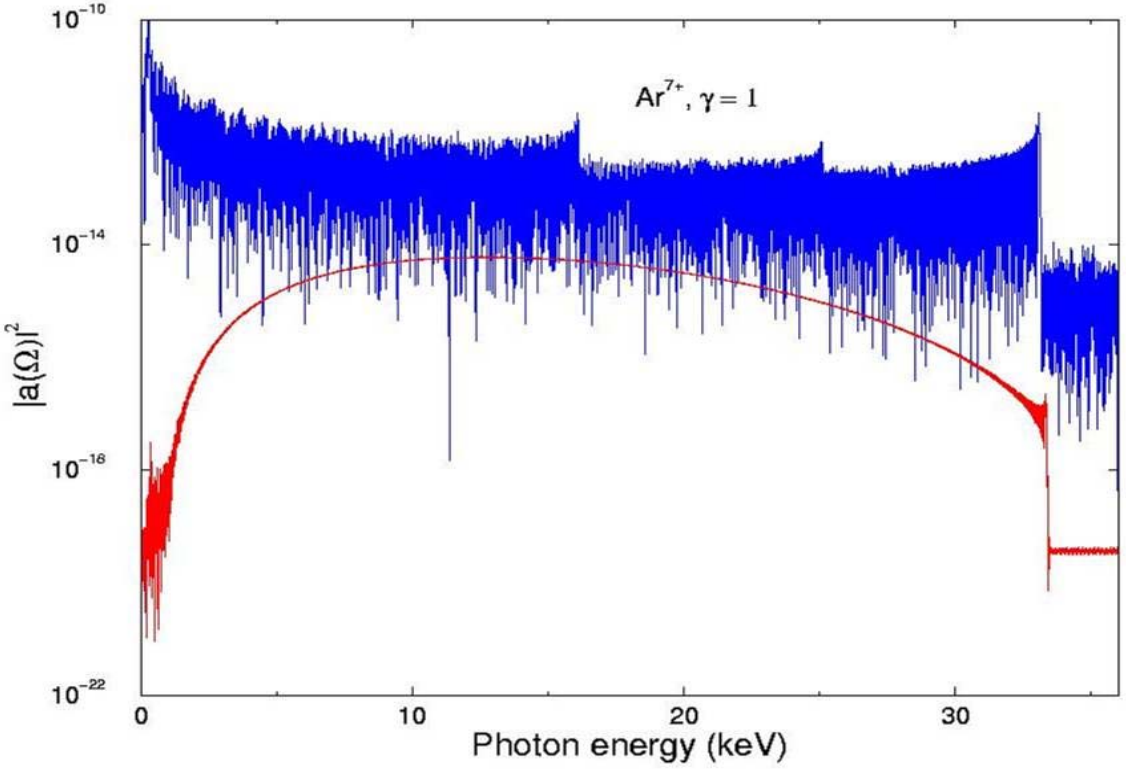

HHG spectra for Ar^{7+} ion:

z_{eff} = 3.247

I = 1 x 10^{17} W/cm^2

_ = 1053.7 nm

Dipole - blue curve

Non dipole - red curve

Obs.

The Fourier transform is :

$$a(\Omega) = \frac{1}{T}\int_0^T dt\, e^{-i\Omega t}\, \ddot{d}(t)$$

Correcting for the Coulomb potential (I)
Ionization amplitude

The non dipole SFA model can be extended in order to take better into account the Coulomb interaction between the electron and the core.

✓ Correction for the ionization amplitude :

$$\left\langle \Psi_p \left| H_{\text{int}} \right| \Phi_0 \right\rangle \rightarrow \frac{4I_p}{\left|E(t_d)\right|} \left\langle \Psi_p \left| \frac{1}{r} H_{\text{int}} \right| \Phi_0 \right\rangle ,$$

as proposed by Krainov, based on a WKB approximation for the slow electron tunneling out.

Where :

- Ψ_p is the final state approximated usually by a Volkov function ;
- H_{int} is the interaction hamiltonian ;
- Φ_0 is the initial (ground) state of the electron ;
- $E(t_d)$ is the electric field at the moment of detachment
- I_p is the binding energy of the electron

Correcting for the Coulomb potential (II)
Recombination amplitude

✓ Correction of the recombination amplitude will have to take into account the effects due to the fast electron colliding with the ionic core: the final state is represented by the wave function for field-free scattering by a Coulomb potential, rather than by a plane wave (as in the usual SFA).

This modification amounts to making the "impulse approximation"[1]

$$\left\langle \Phi_0 \left| \vec{r} \right| \Psi_p \right\rangle \rightarrow \left\langle \Phi_0 \left| \vec{r} \right| \Psi_p^{(C)} \right\rangle .$$

• For the intensities considered here, depletion is negligible.

[1]Milos_vi_ and Ehlotzky

The Coulomb-corrected SFA vs. full time-dependent results

Harmonic generation spectra for an He^+ ion in a 2-cycle Ti:sapphire laser pulse

λ = 800 nm , I = 1 x 10^{16} W/cm^2

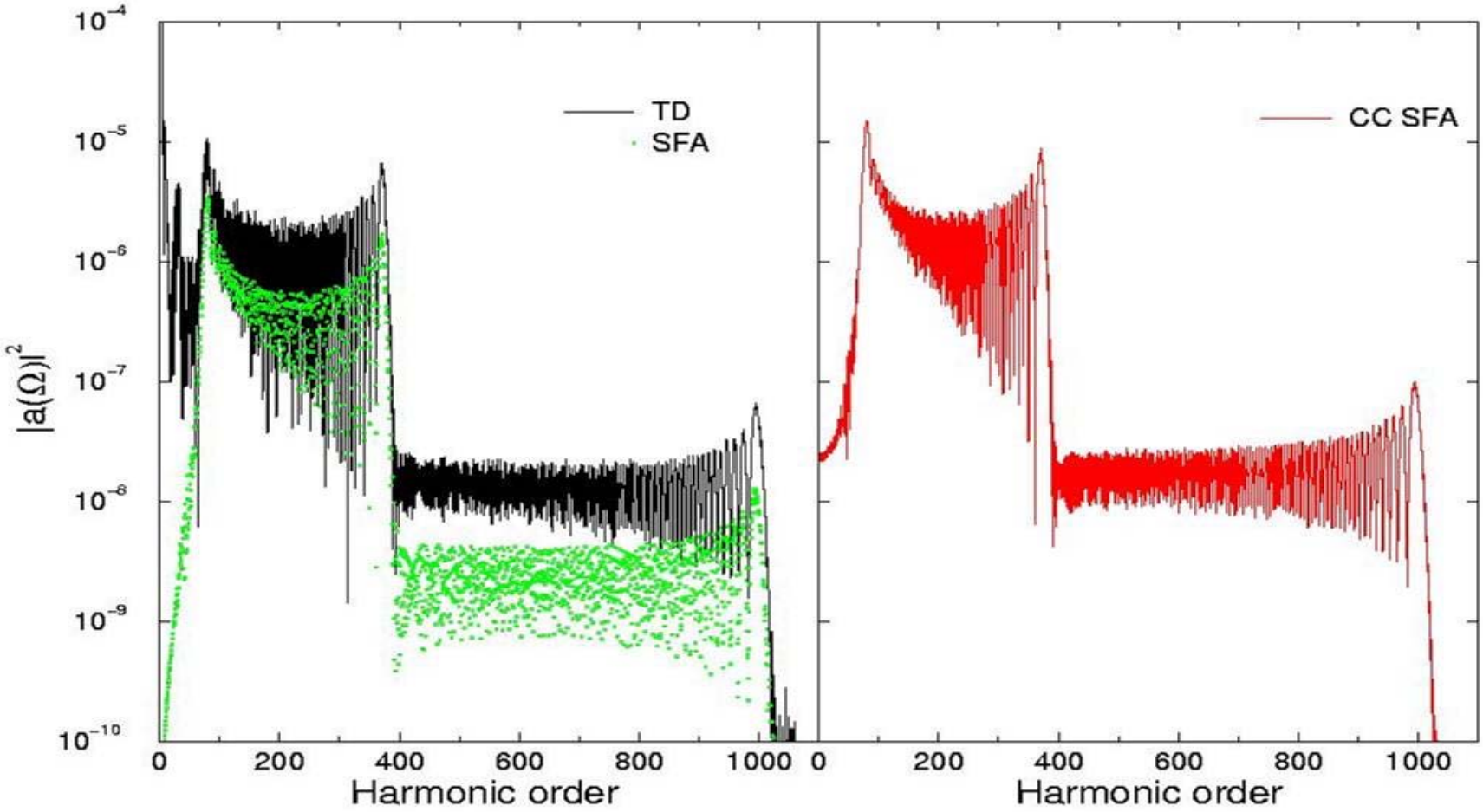

The effect of the Coulomb correction on the SFA harmonic generation spectra for a multicharged ion

HG spectra in dipole approximation for an Ar^{7+} ion in a stationary field

λ = 1053.7 nm , I = 1 x 10^{17} W/cm^2

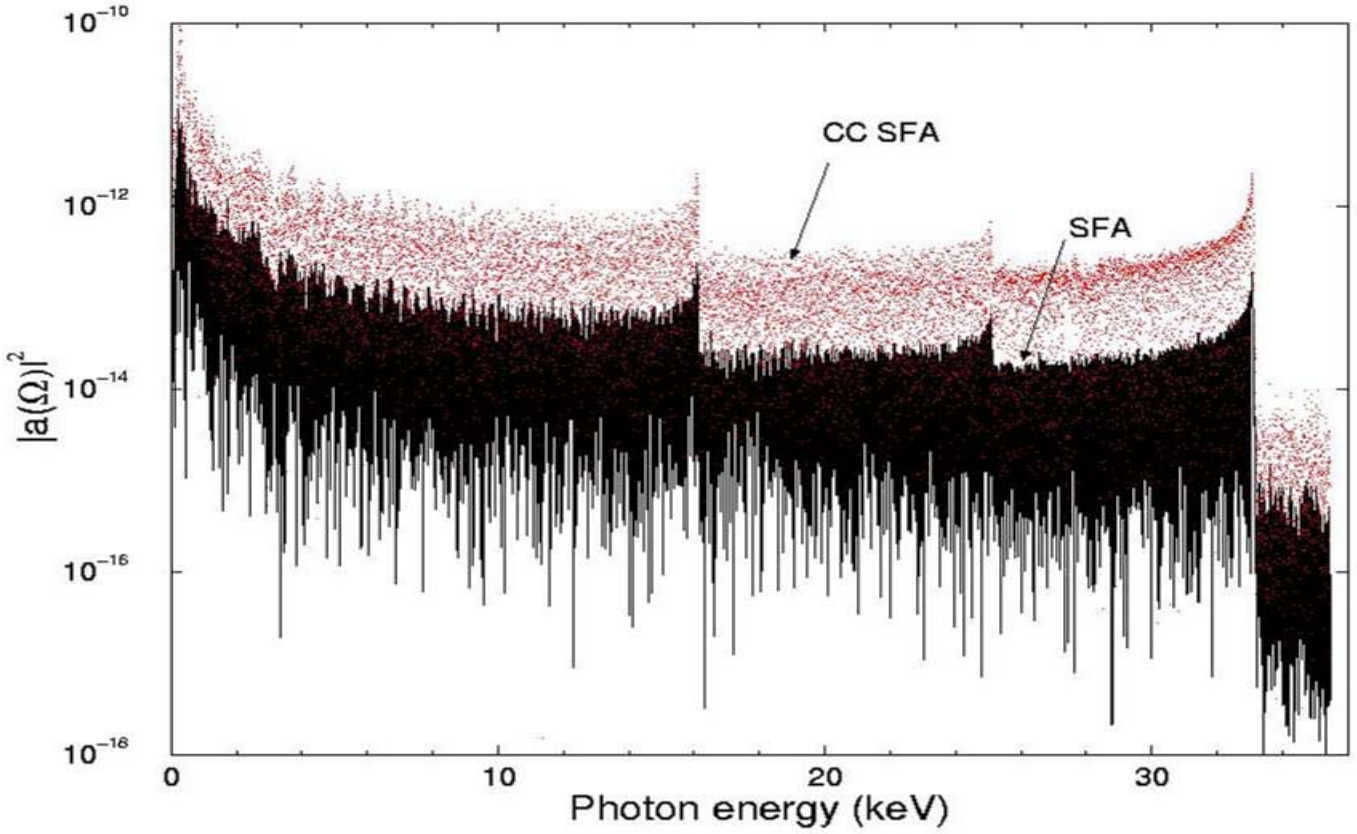

Ar^{7+} without dipole approximation

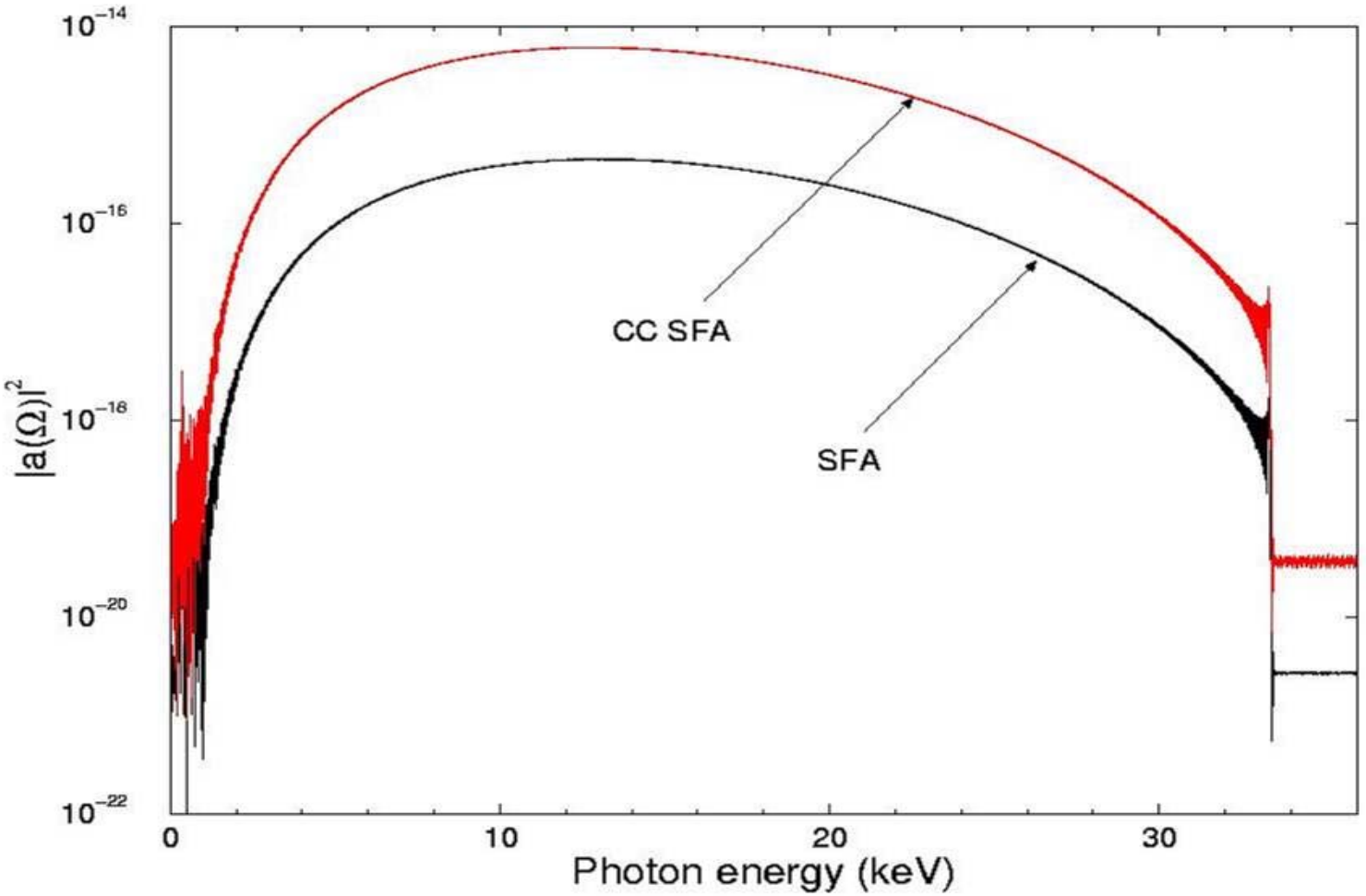

Ar^{7+} vs. Ne^{9+}

Consider a laser field with _ = 1054 nm and I_{lab} = 1x10^{17} W/cm^2.

Ion	Lorentz factor	Keldysh parameter	Ionization loss per cycle
Ar^{7+}	1	0.08	2.2 %
Ne^{9+}	15	0.26	1.0 %

- The intensity is below saturation for both ions ;

- The ions are both in the tunneling regime (small Keldysh parameter), so the SFA model is still applicable ;

- At the intensity considered, the motion of the electron is not yet relativistic, and can be described to a good approximation with our non dipole SFA ;

- Ne^{9+} was chosen for the purpose of comparison because at γ =15 this ion ionizes in the field at about the same rate as Ar^{7+} at rest.

Relativistic HHG results: still ions vs. fast ions (I)

Comparison between Ar^{7+} and Ne^{9+} in a stationary field, with _ = 1053.7 nm and I = 1 x 10^{17} W/cm^2. One can see the effect of the Lorentz boost for Ne^{9+}.

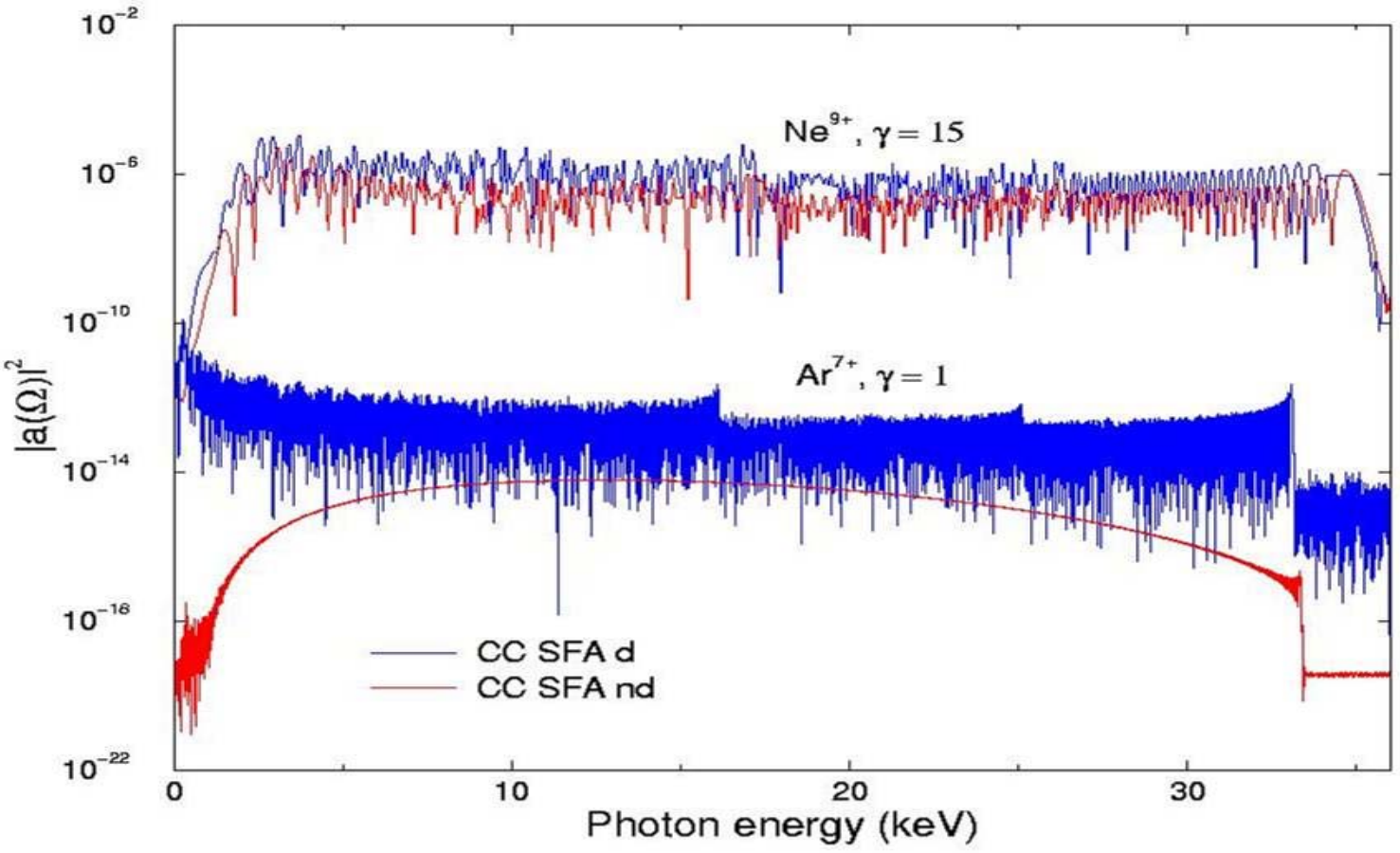

Relativistic HHG results: still ions vs. fast ions (II)
Dipole moment comparison

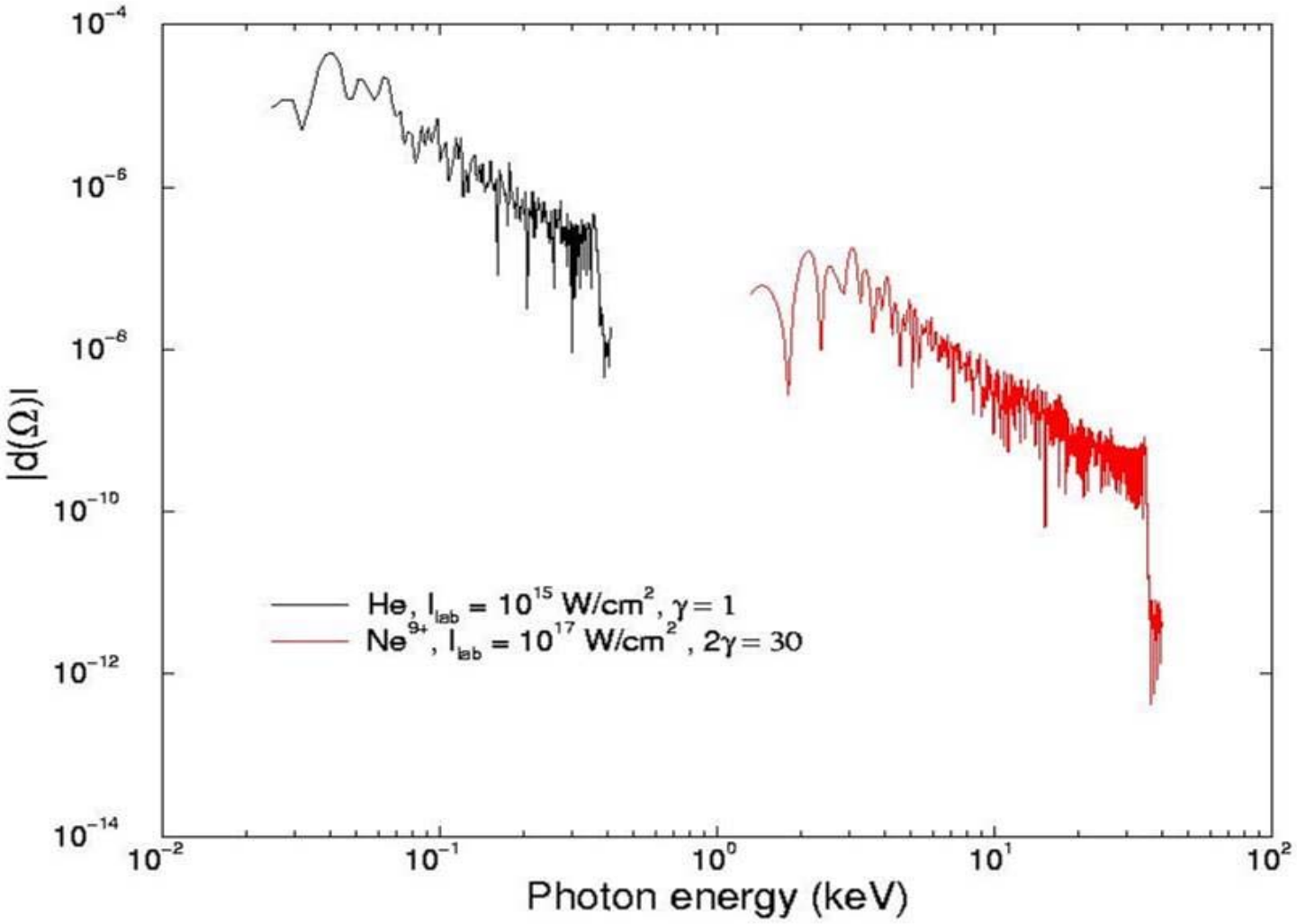

He is modelled as a 1-active electron atom, with z_{eff} = 1.4

Why are the non dipole effects smaller in Ne^{9+} ?

The ionization step[1] occurs at an effective rate proportional to:

$$w(v_{\|}) = \exp\left[-\frac{2}{3}\frac{(2I_p + v_{\|}^2)^{3/2}}{|E(t_d)|}\right]$$

I_p : ionization potential of the ion

$E(t_d)$: electric field at the time of detachment

$V_{||}$: velocity of the electron in the laser direction of propagation at the time of detachment (such as the drift at recollision, due to the magnetic field, would be zero)

λ_{lab} = 1054 nm, I_{lab} = 1x10^{17} W/cm^2 and v_0 = 2 a.u.

	w ($v_{||}$ = 0)	w ($v_{||}$ = v_0)
Ar^{7+}, γ = 1	1.4 x 10^{-6}	3.1 x 10^{-10}
Ne^{9+}, γ = 15	1.9 x 10^{-6}	8.6 x 10^{-7}

[1]M.W.Walser et al., PRL 85 (2000) 5082
[1]C.C.Chirila et al., PRA 66 (2002) 063411

What is happening for larger intensities or Lorentz factors ?

Non dipole vs. dipole effect
$w(v_{||}=v_0)/w(v_{||}=0)$

$w(v_{||}=0) = 1x10^{-6}$

$\lambda_{lab} = 1053.7$ nm

V_0 : velocity such that the electron returns to the nucleus with the maximum kinetic energy $E_c = 3.2\ U_p$

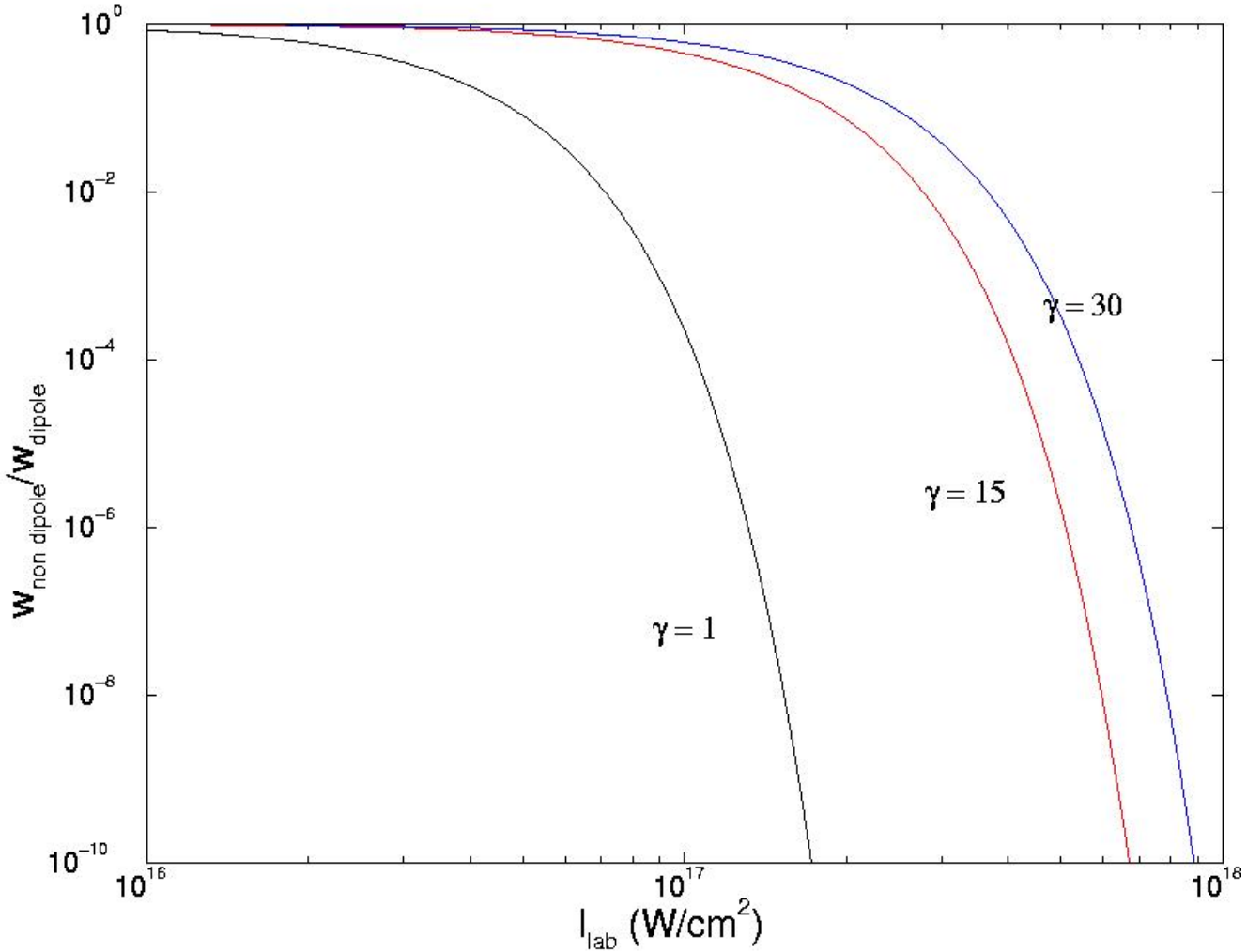

Summary and Conclusions

A new accelerator complex will be built over the next years at GSI-Darmstadt, capable of accelerating multicharged ions to Lorentz factors up to about 30. It will be possible to make the relativistic ions interact with ultraintense laser pulses.

At high intensities, three-step recollision processes, such as high-order harmonic generation and high-order ATI, are normally severely suppressed by the magnetic field component of the laser field.

Owing to the boosts in relative frequency and intensity that can be achieved by directing the laser against the ion beams, there is a range of intensities, Lorentz factors and ion charges for which suppression is not severe even for ponderomotive energies largely exceeding 10 keV.

Interaction of Ultra-short VUV Pulses with Solids- results from the TTF FEL Phase I

Jacek Krzywinski

Polish Academy of Sciences

and Deutsches Elektronen-Synchrotron

DESY

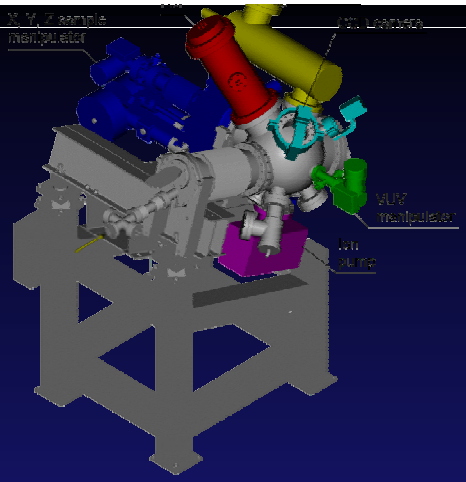

FELIS

Free Electron Laser - Interaction with Solids

A. Andrejczuk [1,4], [+]D. Chwostova, F.Felten [9], U. Hahn [2], S. Jacobi [8], M. Jurek [1], [+]L.Juha, A.Kauch[3], [+]J . Krasa, J.Krzywinski [1,2], J.B. Pelka [1], H. Reniewicz[4], E. Saldin[2], E.A.Schneidmiller [2], E.A. W. Sobala [5], R. Sobierajski [2,6], B. Steeg[2], [+] V. Vorlicek ,M.V. Yurkov[7] and TTF FEL team

[1]Institute of Physics, Polish Academy of Sciences, Poland, ,[+] Institute of Physics, Czech Academy of Sciences, Czech Republic, [2]HASYLAB at DESY, Germany, [3]Warsaw University, Poland, [4]University of Białystok, Poland, [5]Institute of Nuclear Physics, Cracow, Poland, [6]Warsaw University of Technology, Poland, [7]Join Institute for Nuclear Research, Russia, [8]GKSS Research Center,Germany, [9]Harburg-Hamburg Technical University

Outline:

- Motivation
- Experimental
- Damage and surface modification
- Plasma results
- Conlusions

Motivation

- Nowbody was there yet !
  - Strong XUV femtosecond pulses
- Damage of optics for short-wave sources
- Damage of samples
- Nanotechnology
- First plasma physics data

Experiment

- Layout
- Photon beam parameters
- Samples

Layout of the experiment

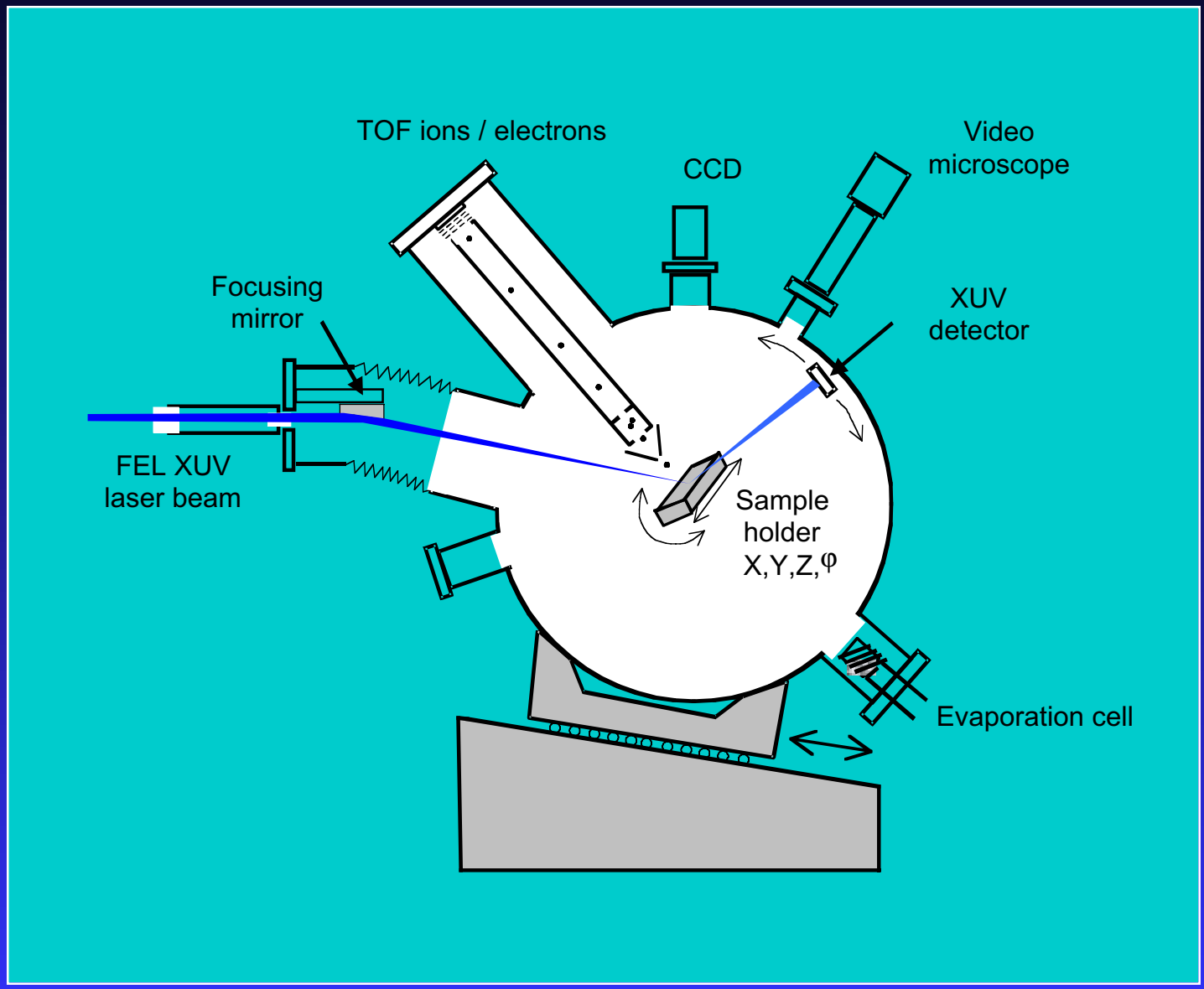

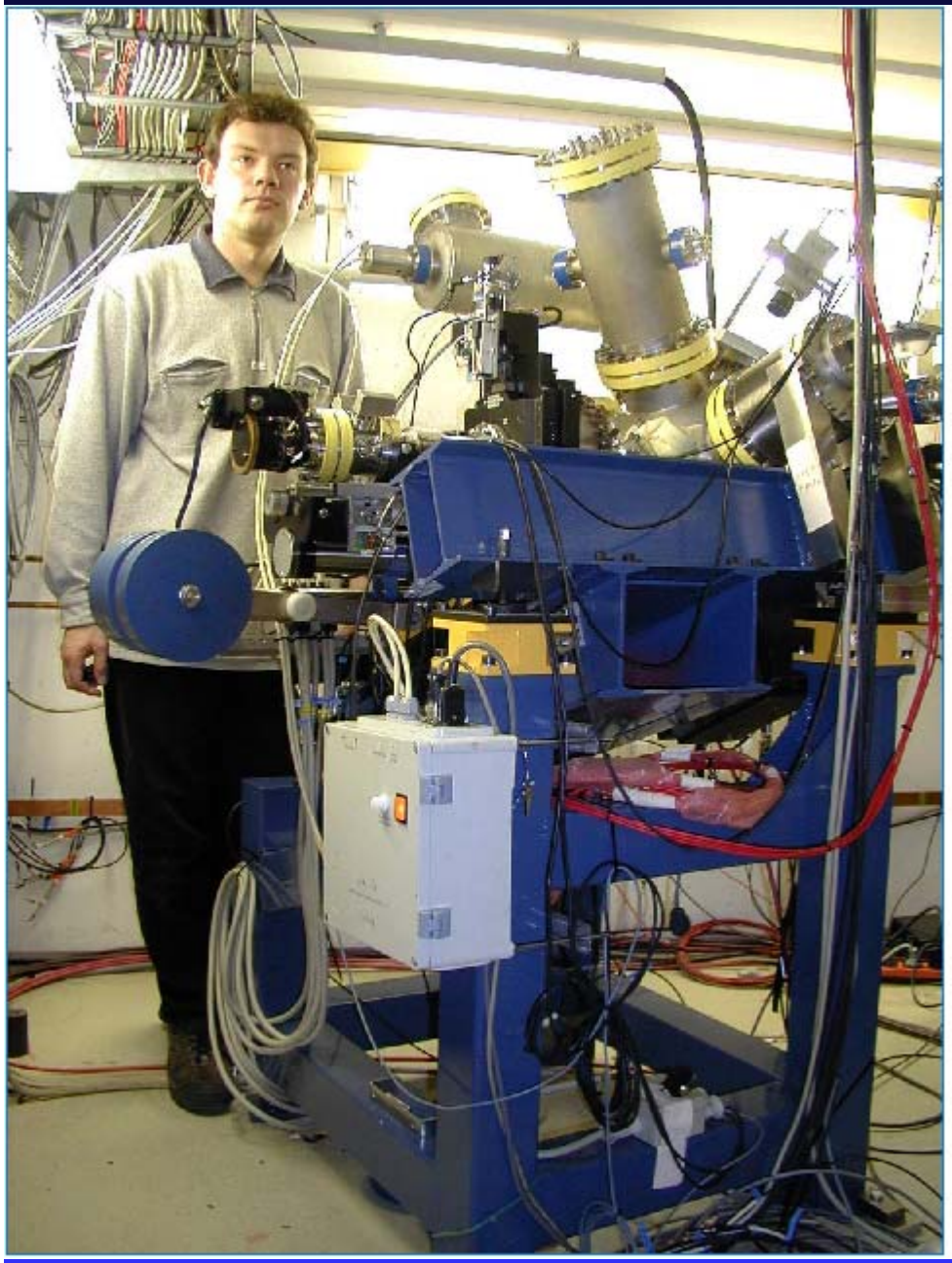

Photon Beam Parameters

Wavelength	80-98 nm
Pulse length	50 fs
Pulse energy	1-10 uJ
Min. Spot size	10 um
Max. Intensity	$\sim 10^{14}$ W/cm^2

TOF Spectrometer

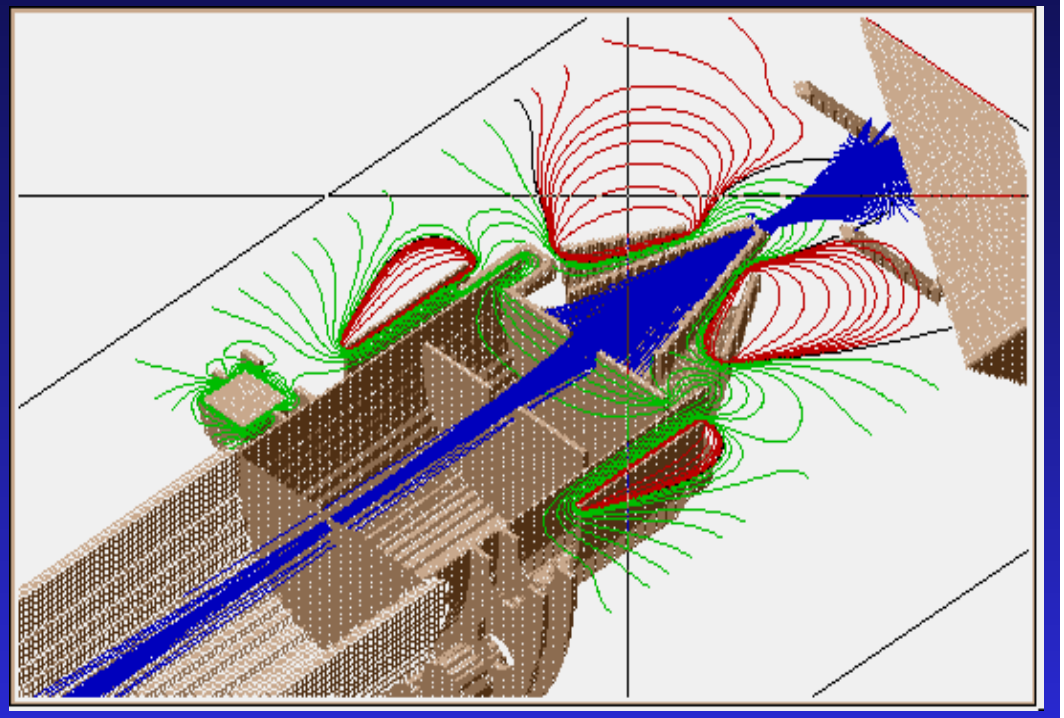

Samples

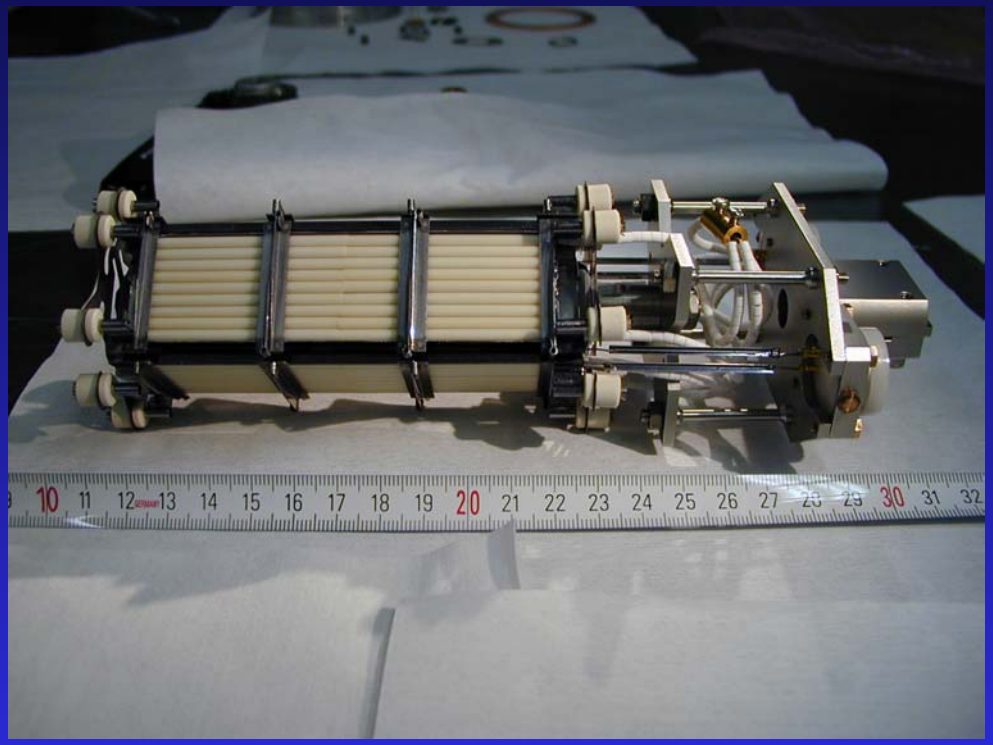

Metals:

Au, Al, Cu

Semiconductors

Si, Graphite

Insulators

Al_2O_3 SiO_2 YAG

MgF_2 BaF_2

Organic compounds

PMMA, PTFE

Morphology of irradiated surface as a function of radiation intensity

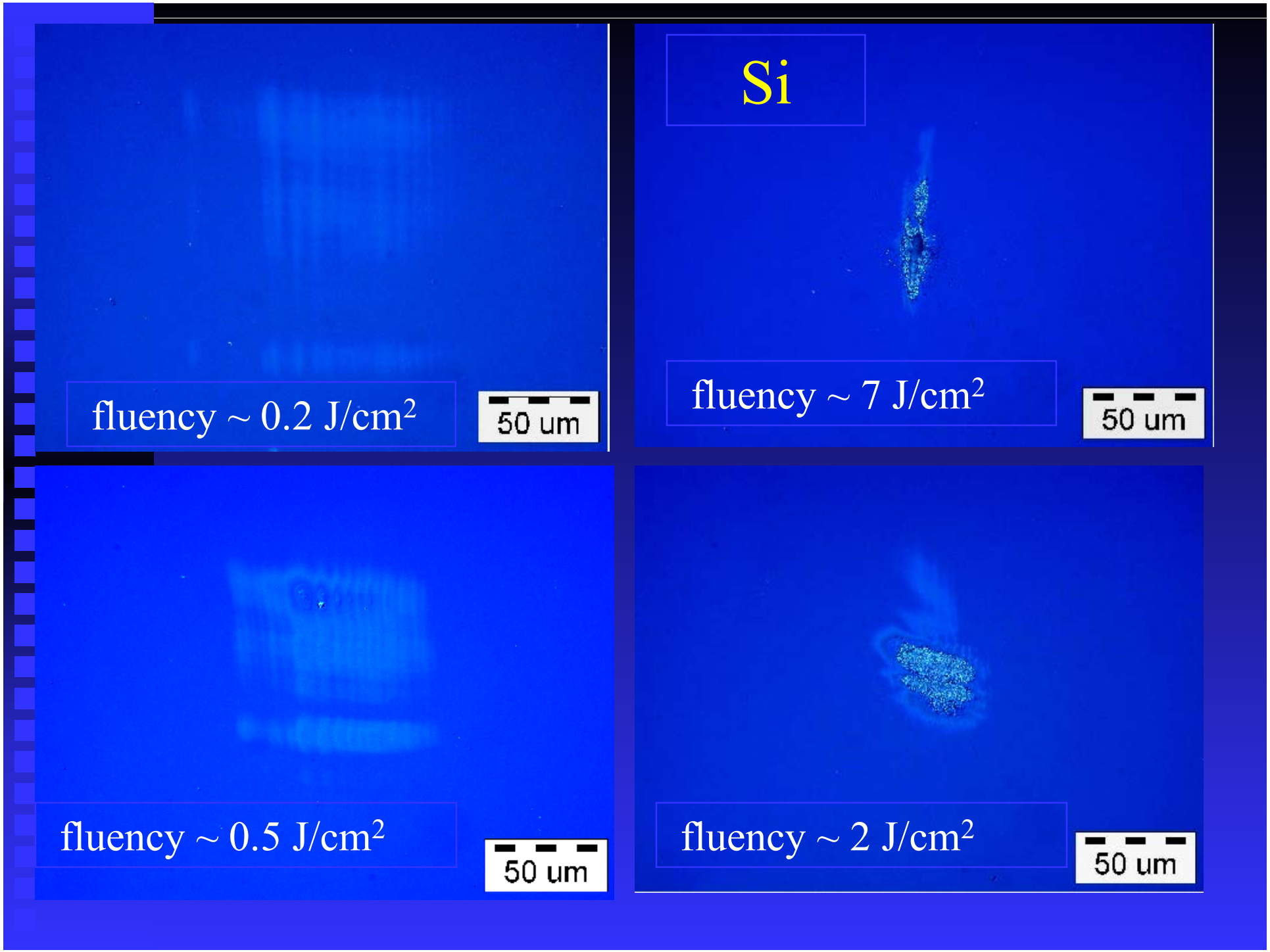
Si
fluency ~ 0.2 J/cm2
50 um
fluency ~ 7 J/cm2
50 um
fluency ~ 0.5 J/cm2
50 um
fluency ~ 2 J/cm2
50 um

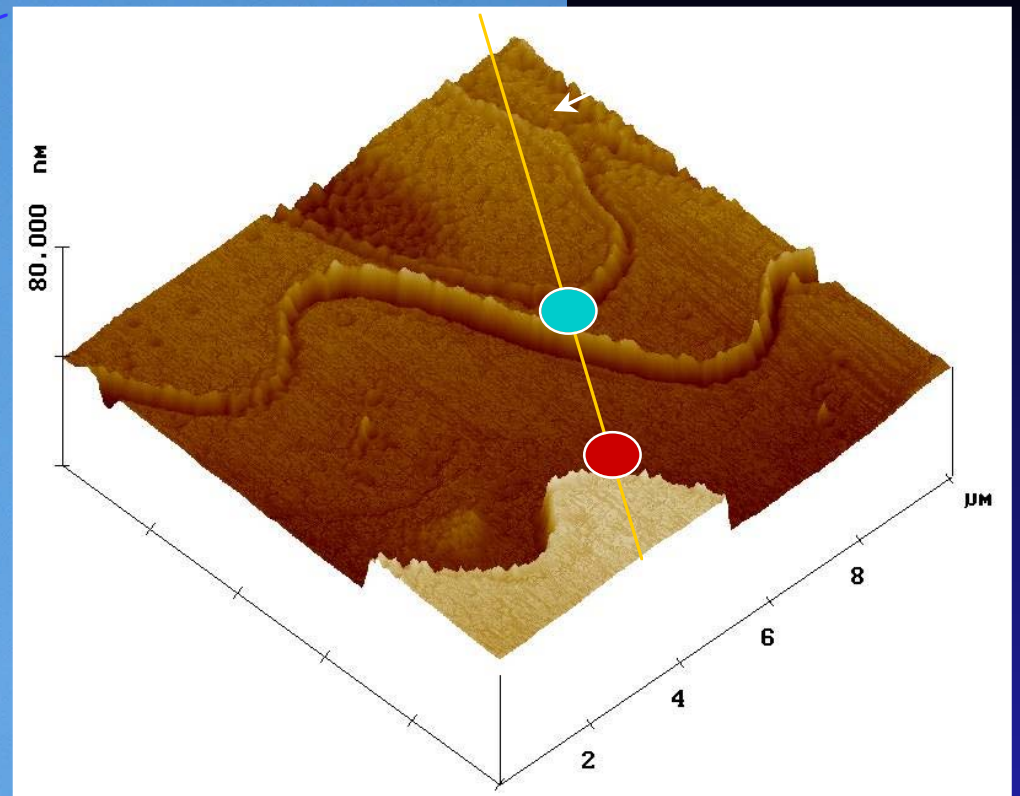

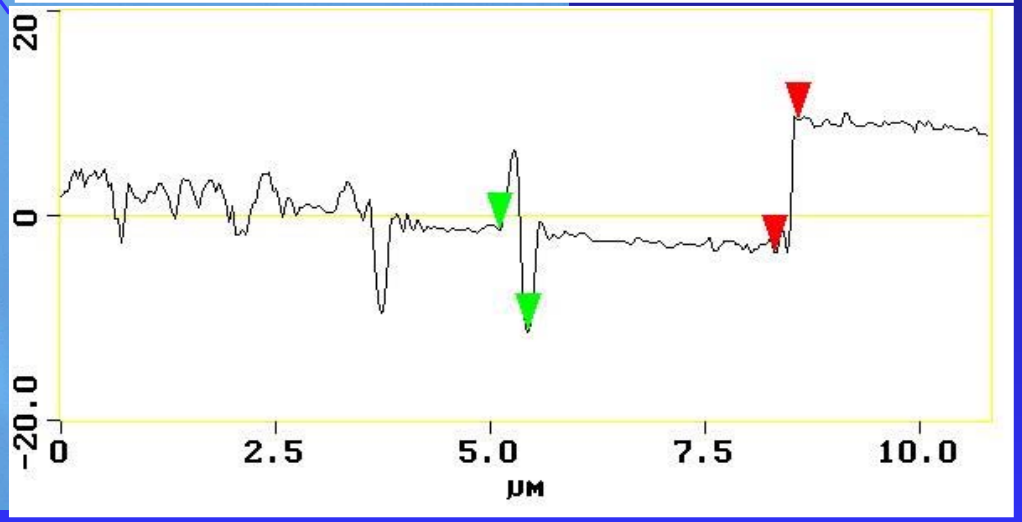

C film on Si substrate

fluency ~ 0.2 J/cm^2

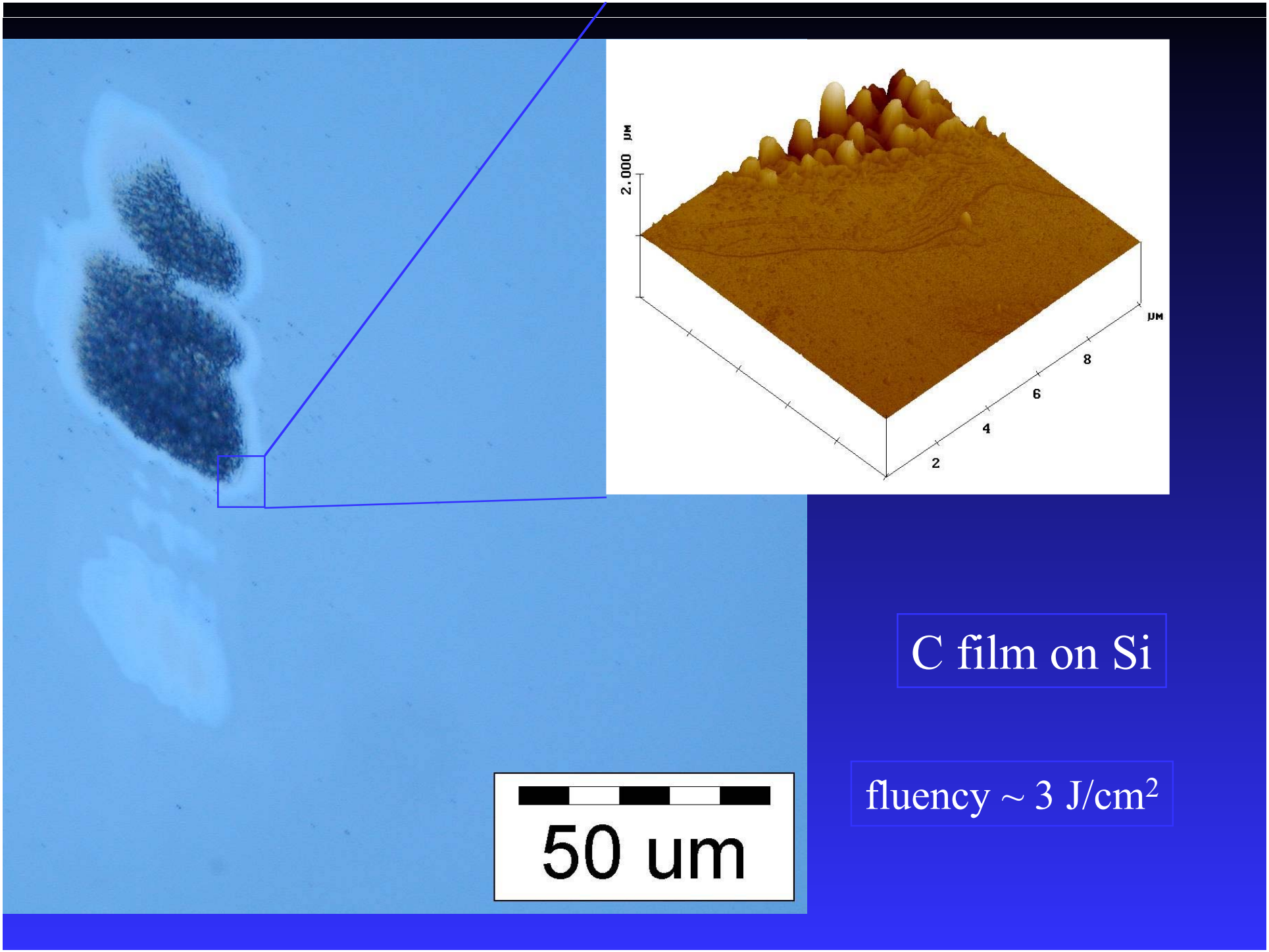
2.000 µm
µm
2
4
6
8
50 um
C film on Si
fluency ~ 3 J/cm2

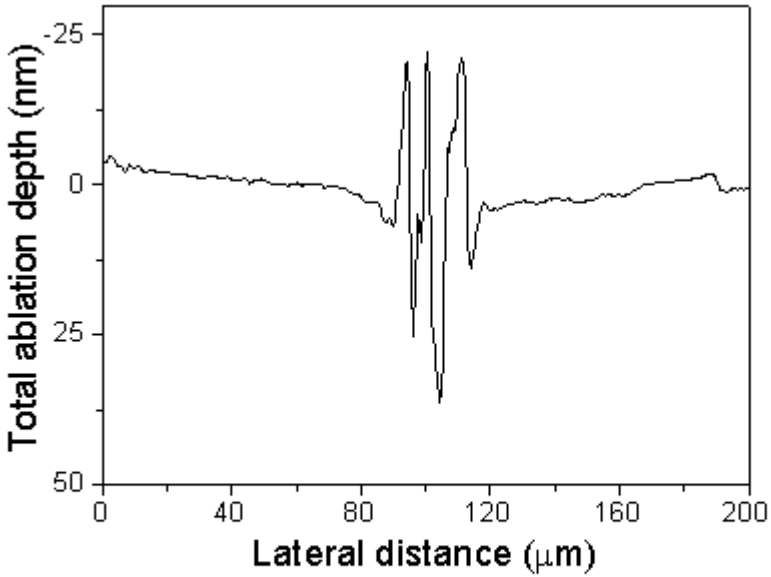
Total ablation depth (nm)
-25
0
25
50
0
40
80
120
160
200
Lateral distance (μm)

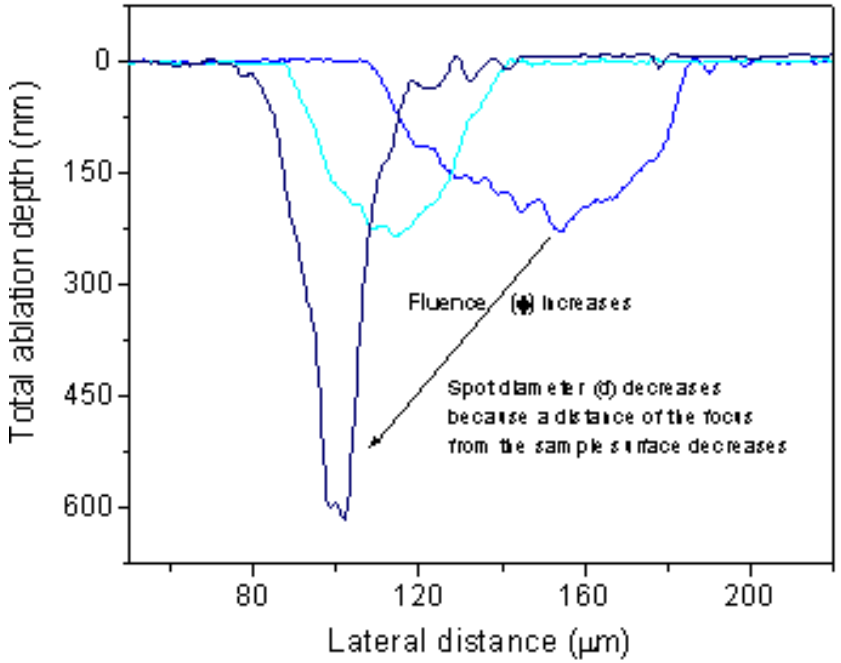
Total ablation depth (nm)
0
150
300
450
600
80
120
160
200
Lateral distance (μm)
Fluence (Φ) increases
Spot diameter (d) decreases
because a distance of the focus
from the sample surface decreases

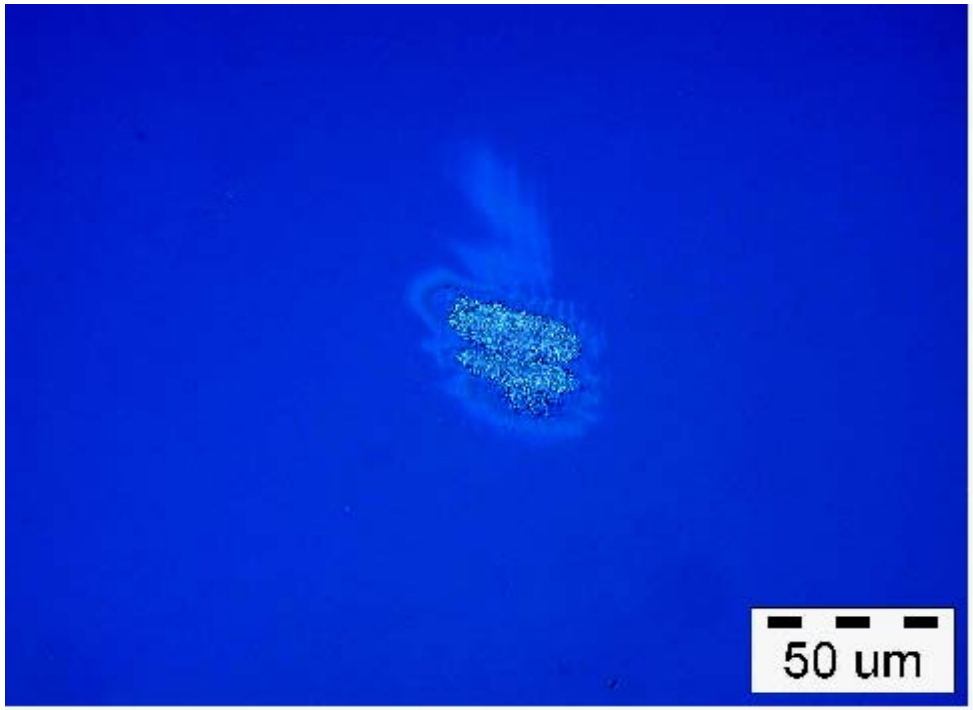
50 um

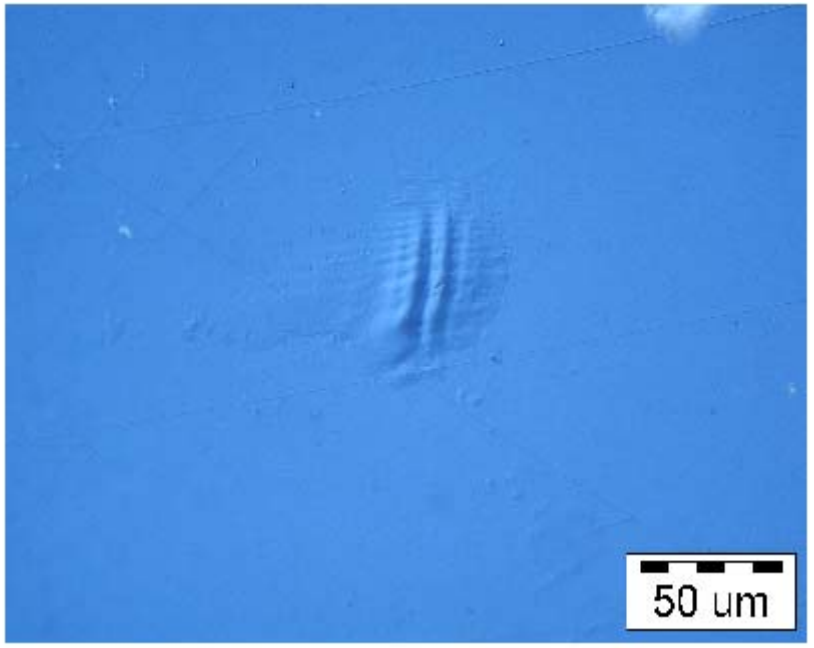
50 um

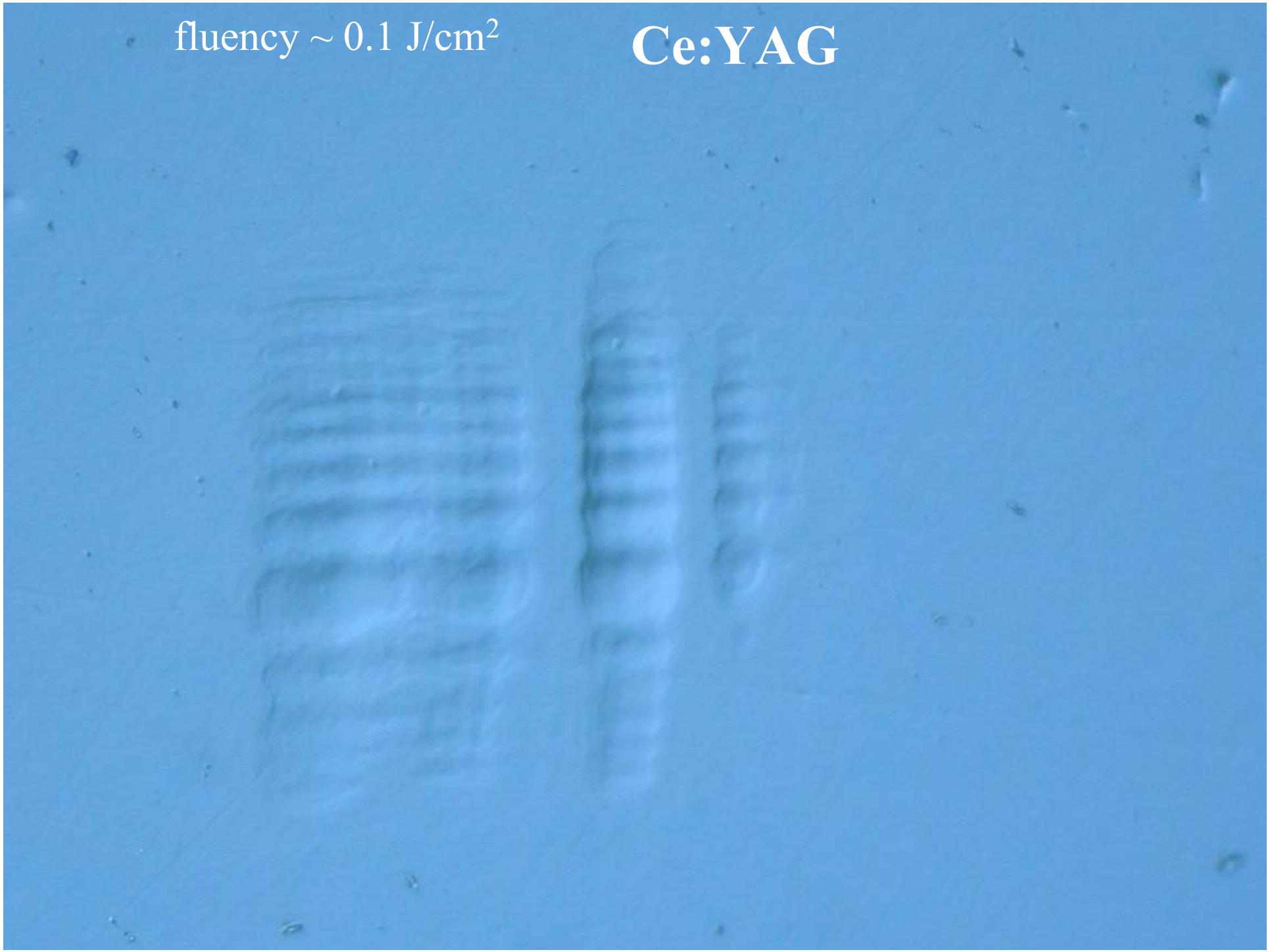
fluency ~ 0.1 J/cm²
Ce:YAG

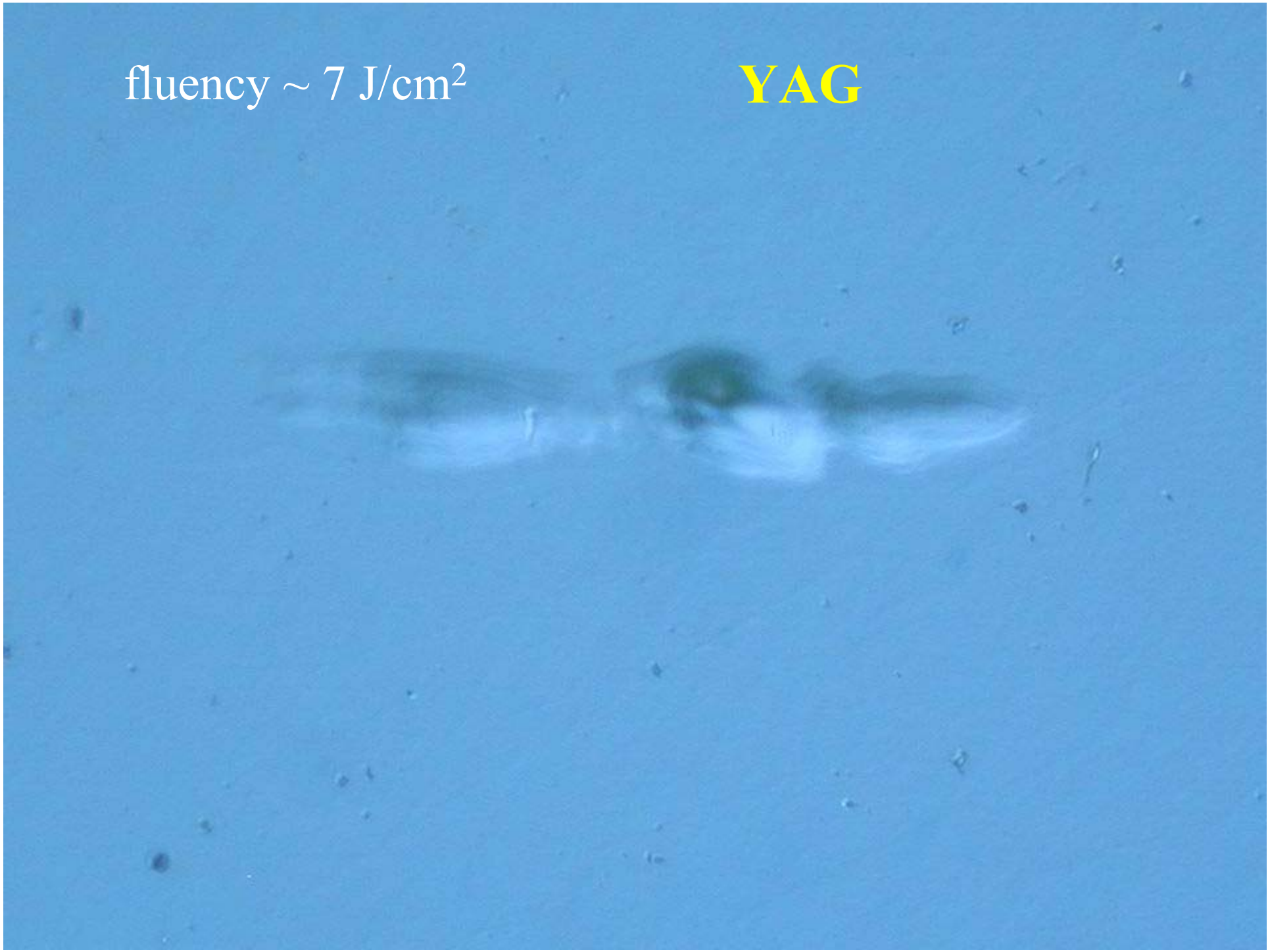
fluency ~ 7 J/cm2
YAG

Printing interference pattern into ionic crystal surface

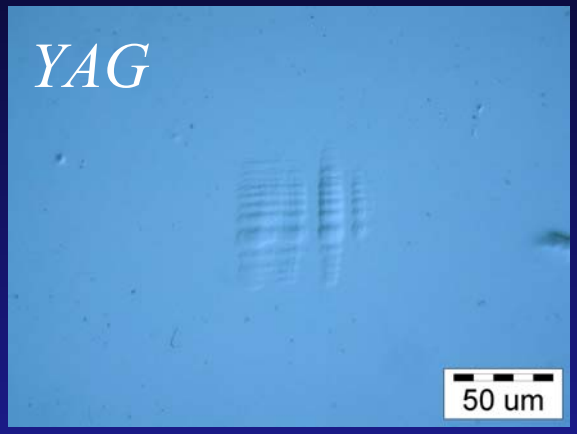

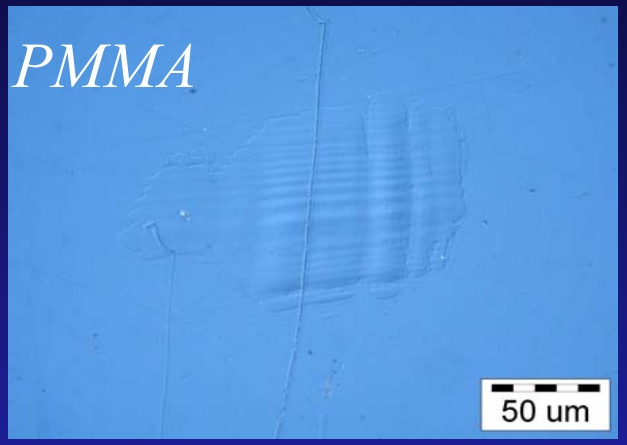

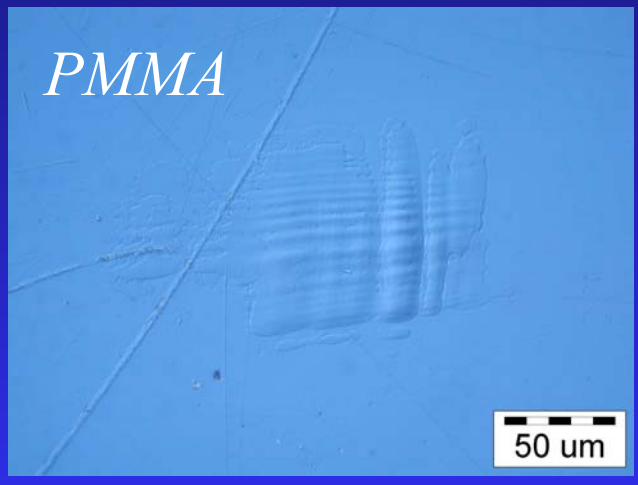

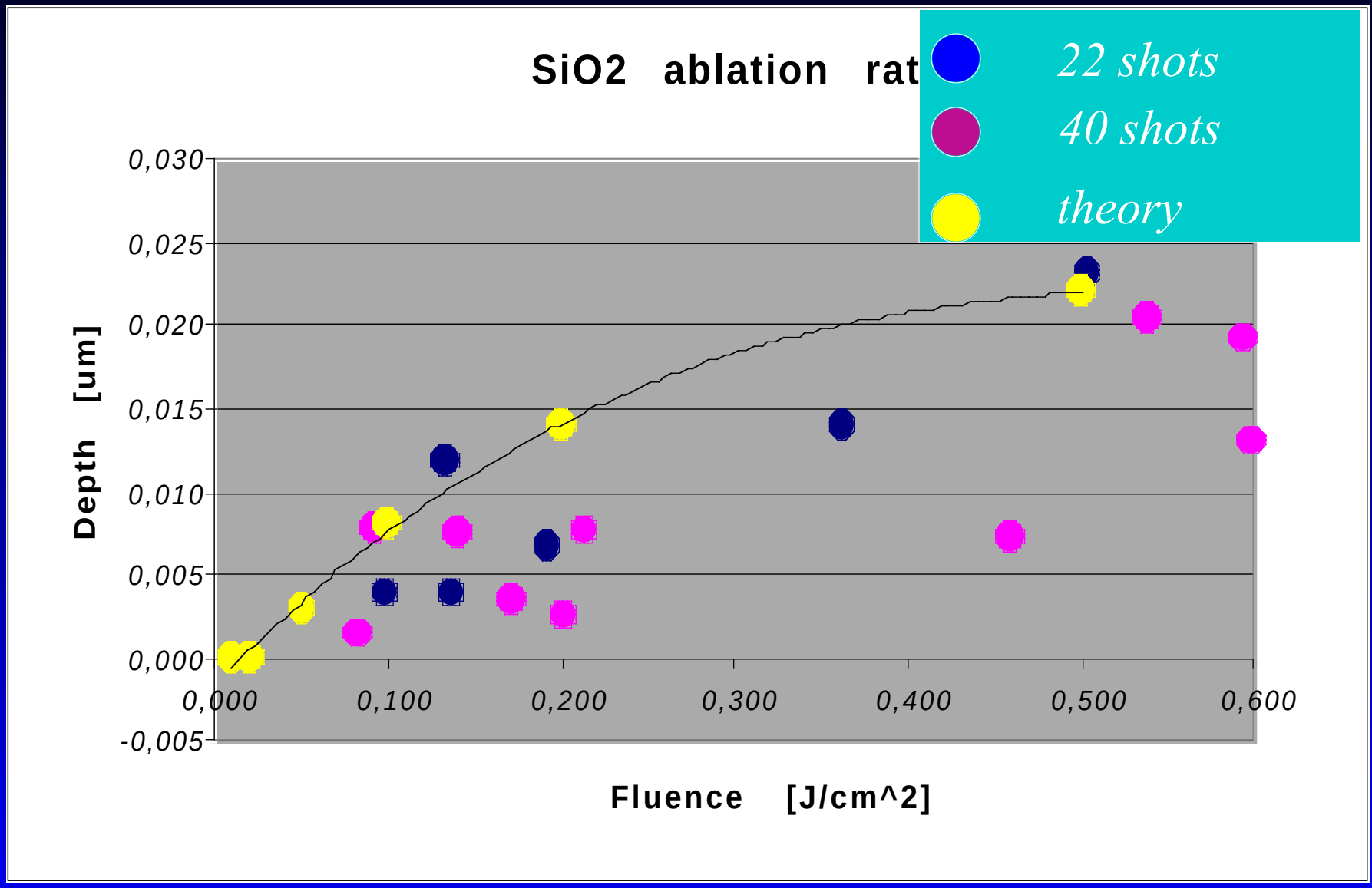

Spallation depth were calculated with a help of theABLATOR hydrodynamical code

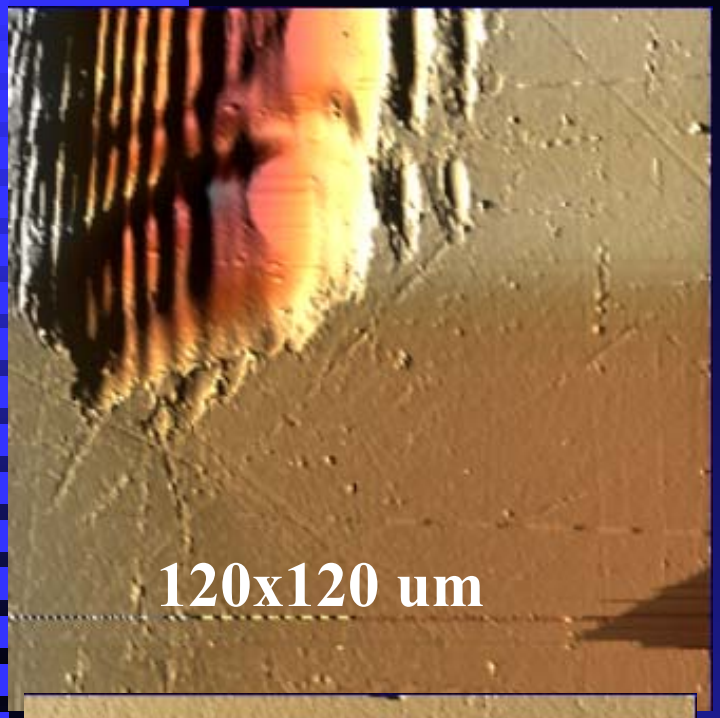

PMMA

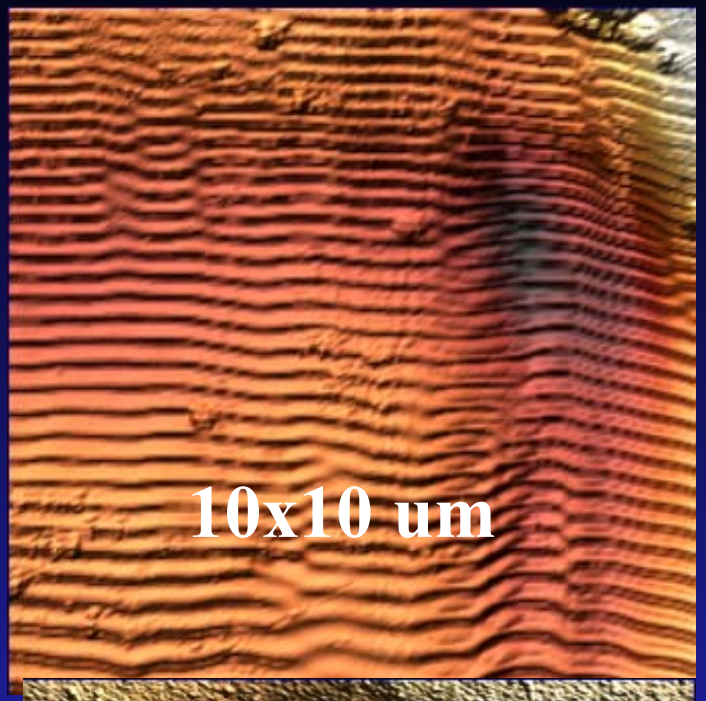

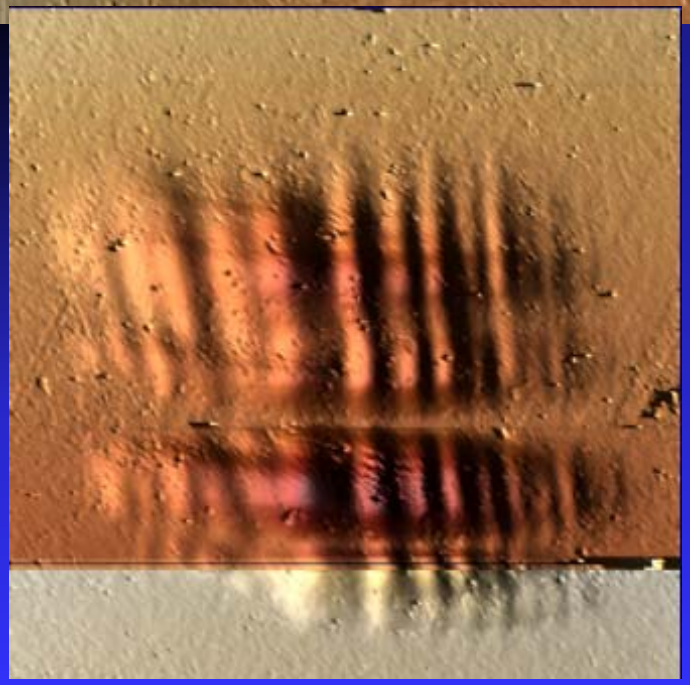

SiO_2

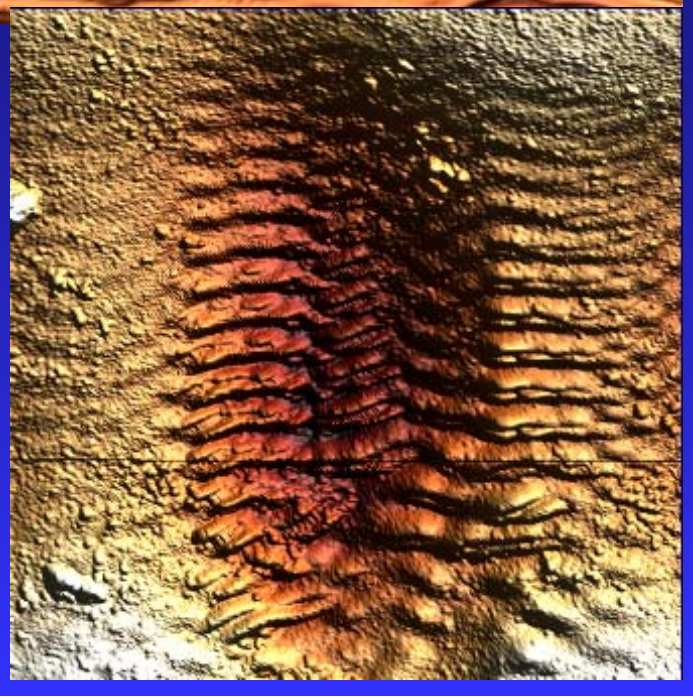

ionic crystals and organic compounds exhibit sharp ablation threshold with only a modest modification of crater's surrounding material

LIPSS - Laser Induced Periodic Surface Structures

period ~ 78 nm

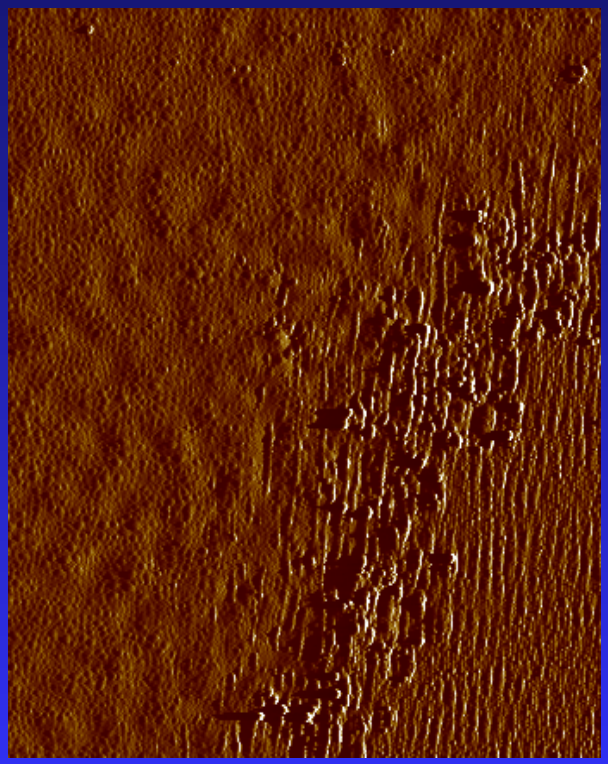

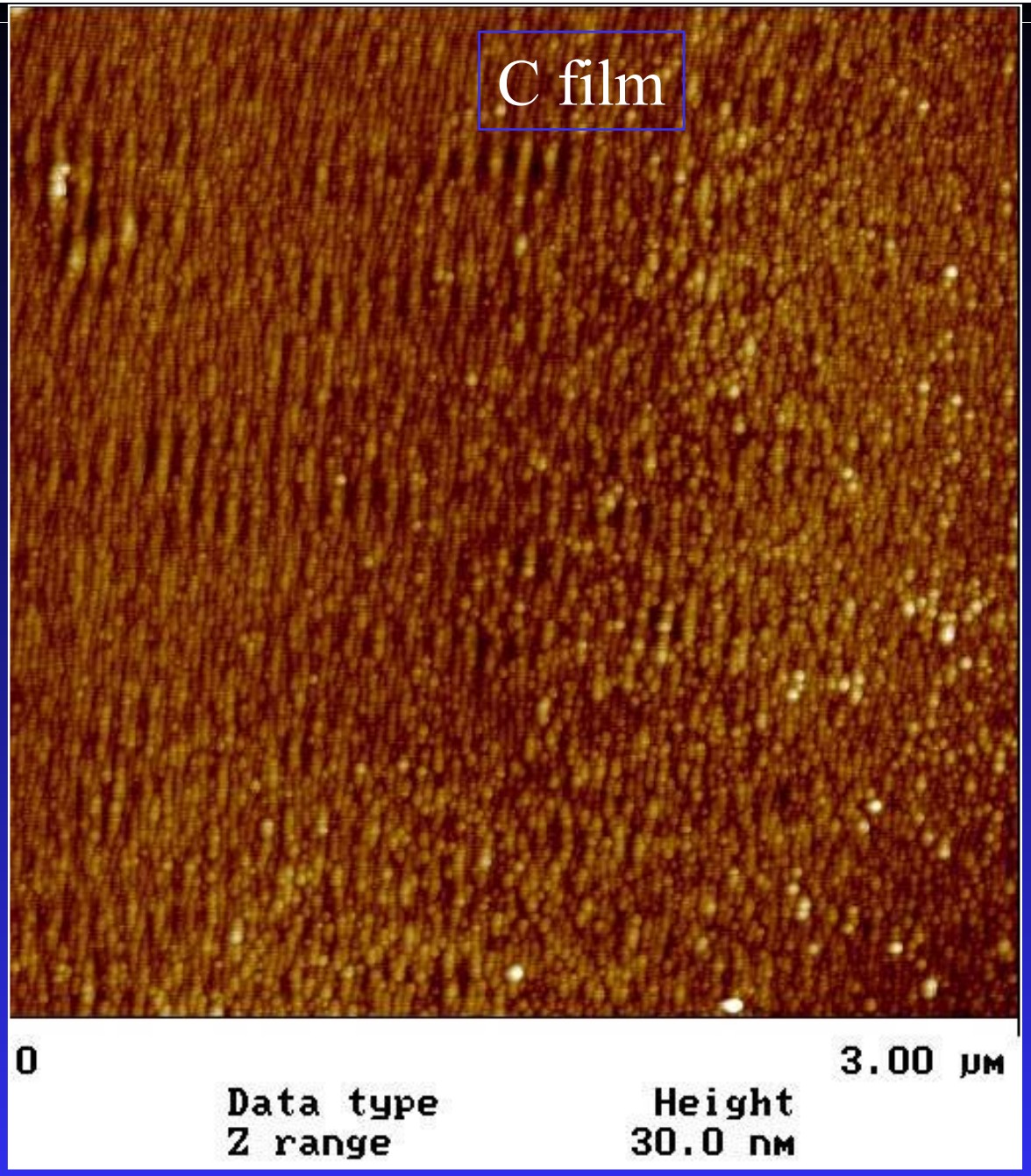

Summary:

- damage thresholds and material removal rates are consistent with hydrodynamical models
- Short XUV pulses are suitable for nano - processing of ionic crystals and organic compounds

Plasma formation

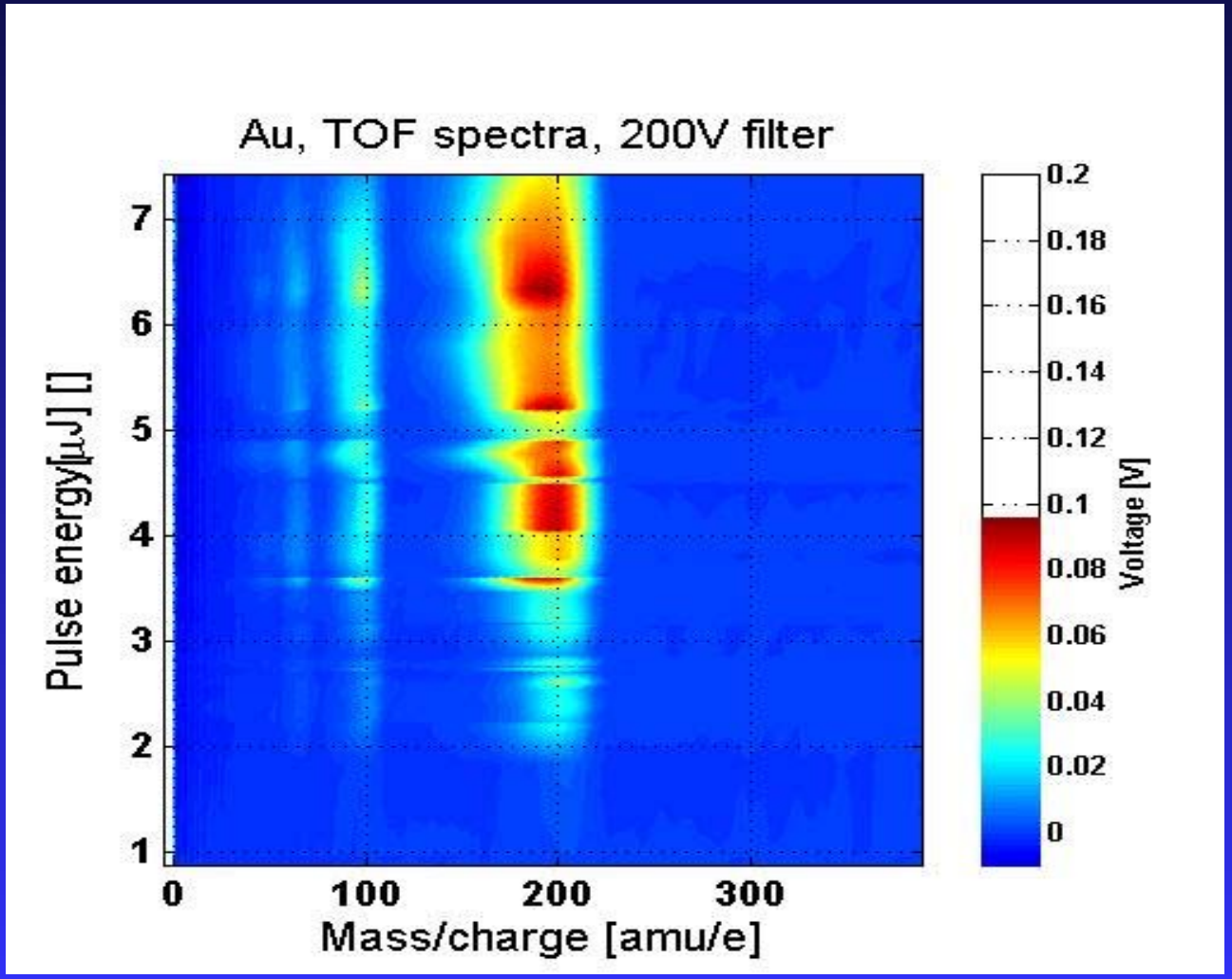

fluency ~ 10 J/cm^2

I~2·10^{14} W/cm^2

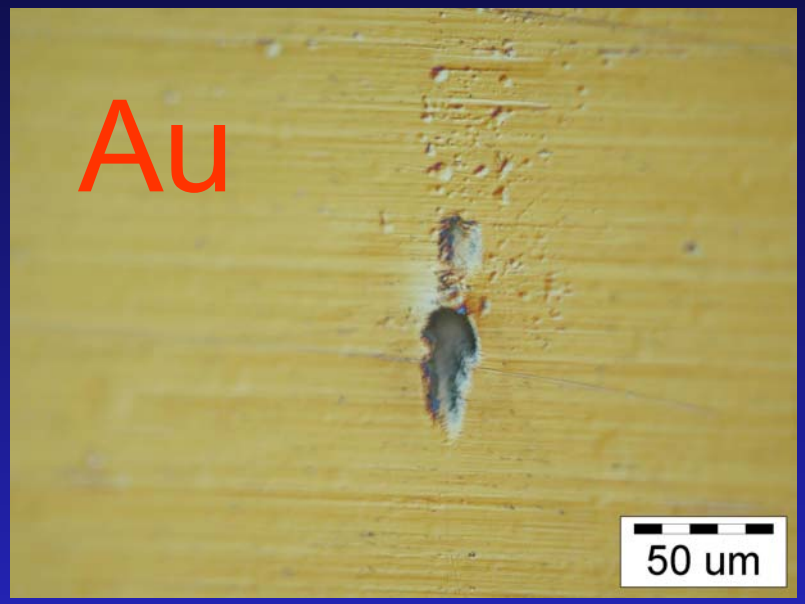

Au

High pass filter
200 V

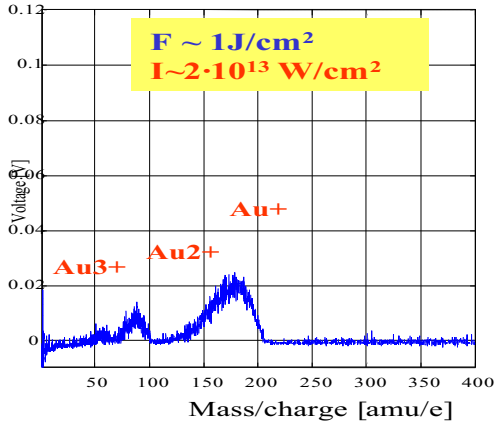

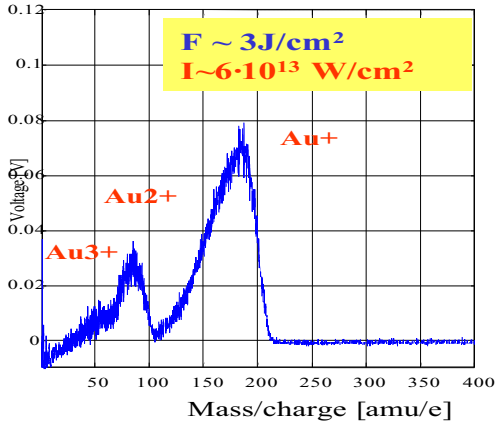

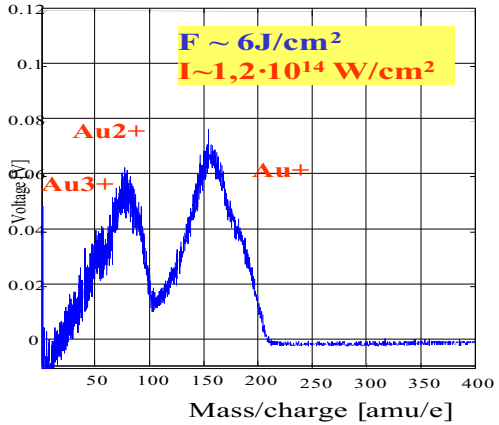

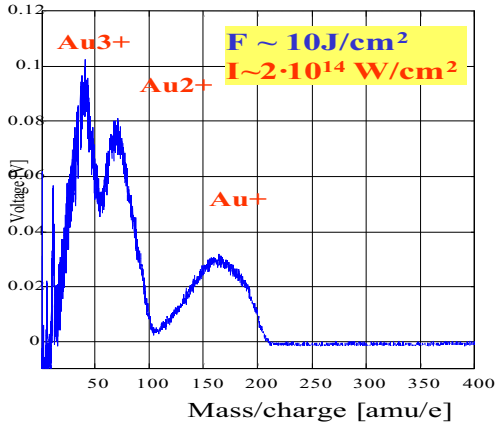

Measurements of ion energy distribution

F ~ 1 J/cm^2

I~2·10^{13} W/cm^2

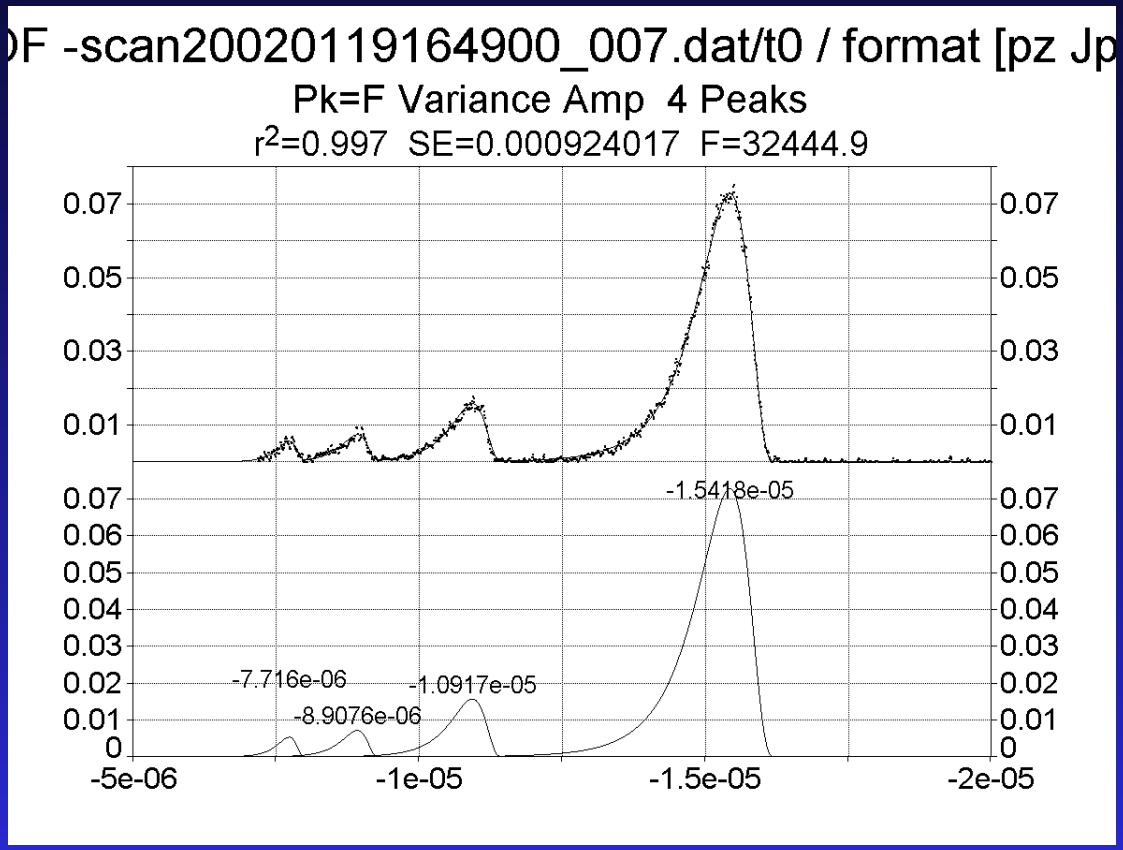

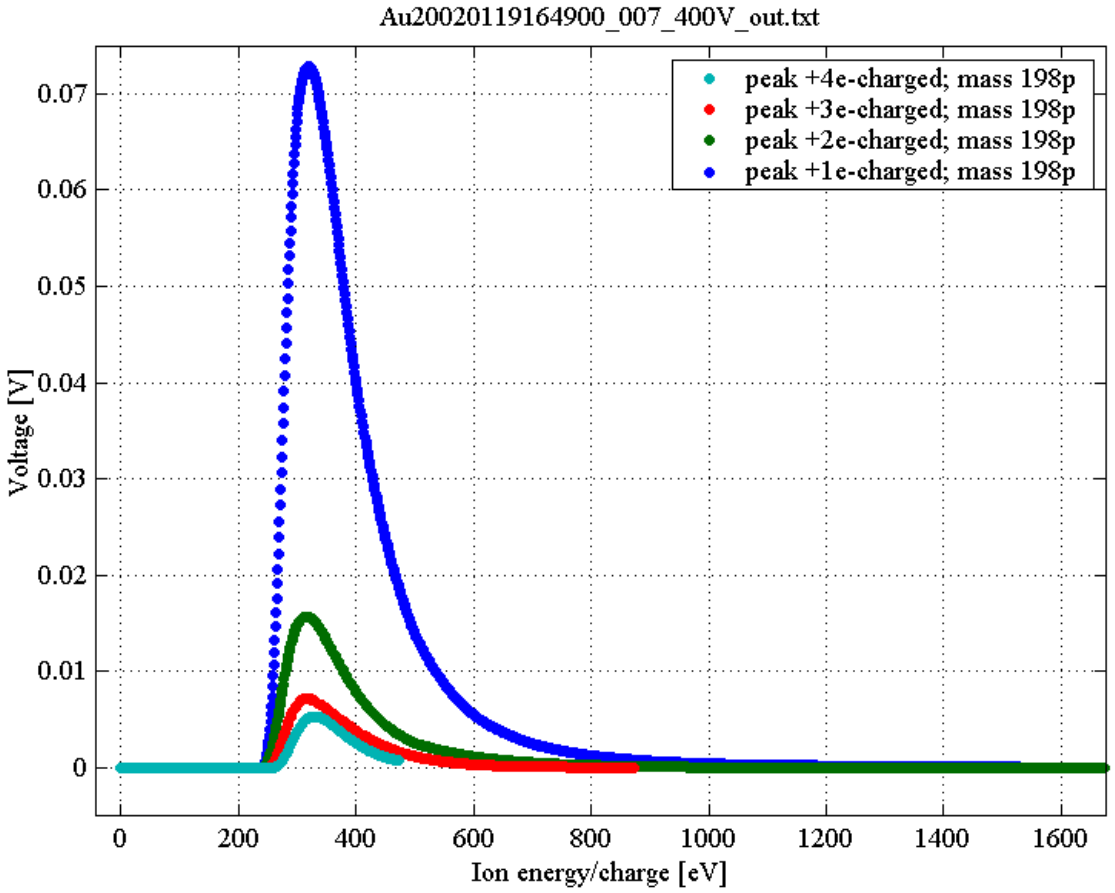
Au20020119164900_007_400V_out.txt
peak +4e-charged; mass 198p
peak +3e-charged; mass 198p
peak +2e-charged; mass 198p
peak +1e-charged; mass 198p
Voltage [V]
0.07
0.06
0.05
0.04
0.03
0.02
0.01
0
0
200
400
600
800
1000
1200
1400
1600
Ion energy/charge [eV]

Energy distribution scaling with a charge

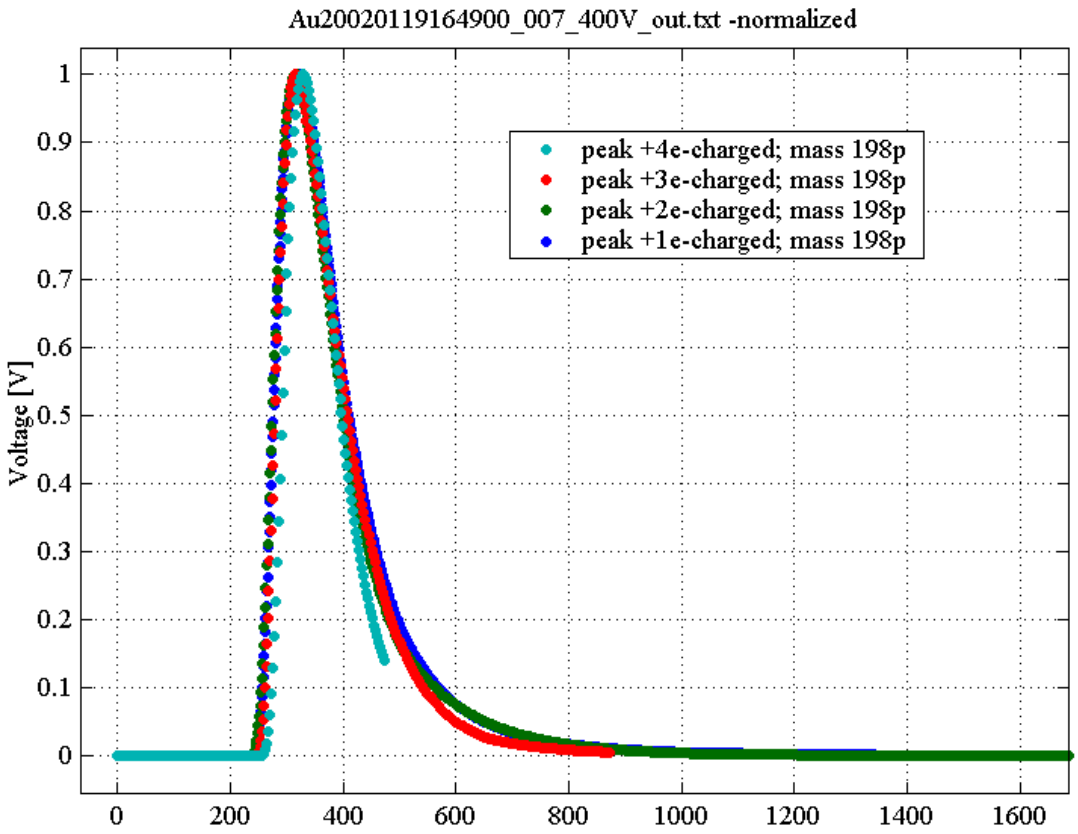

energy /charge [eV]

Energy distributions can be scaled with ion charge

What Does It Mean?

- Ions are emitted by electric field

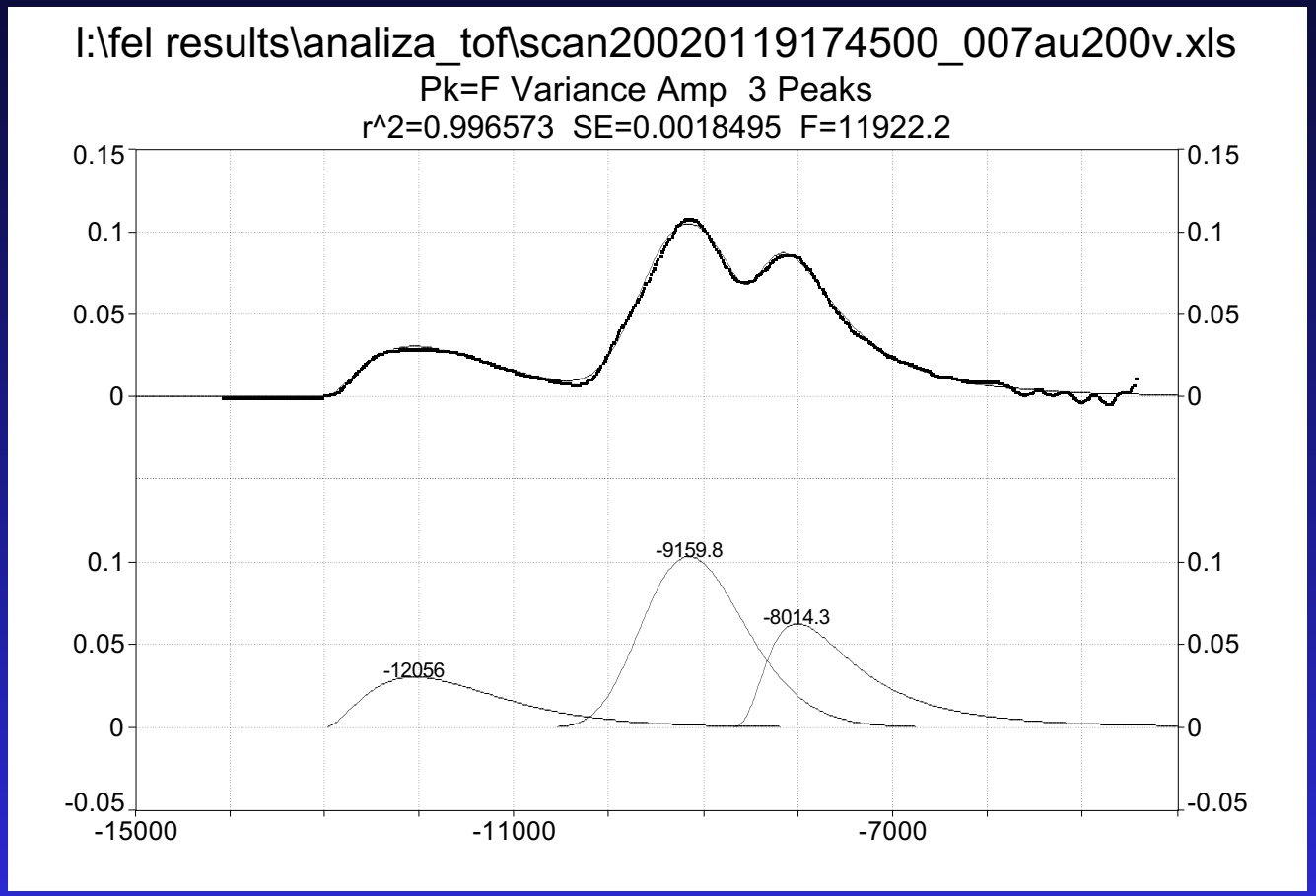
I:\fel results\analiza_tof\scan20020119174500_007au200v.xls
Pk=F Variance Amp 3 Peaks
r^2=0.996573 SE=0.0018495 F=11922.2
0.15
0.1
0.05
0
-0.05
-9159.8
-8014.3
-12056
-15000
-11000
-7000

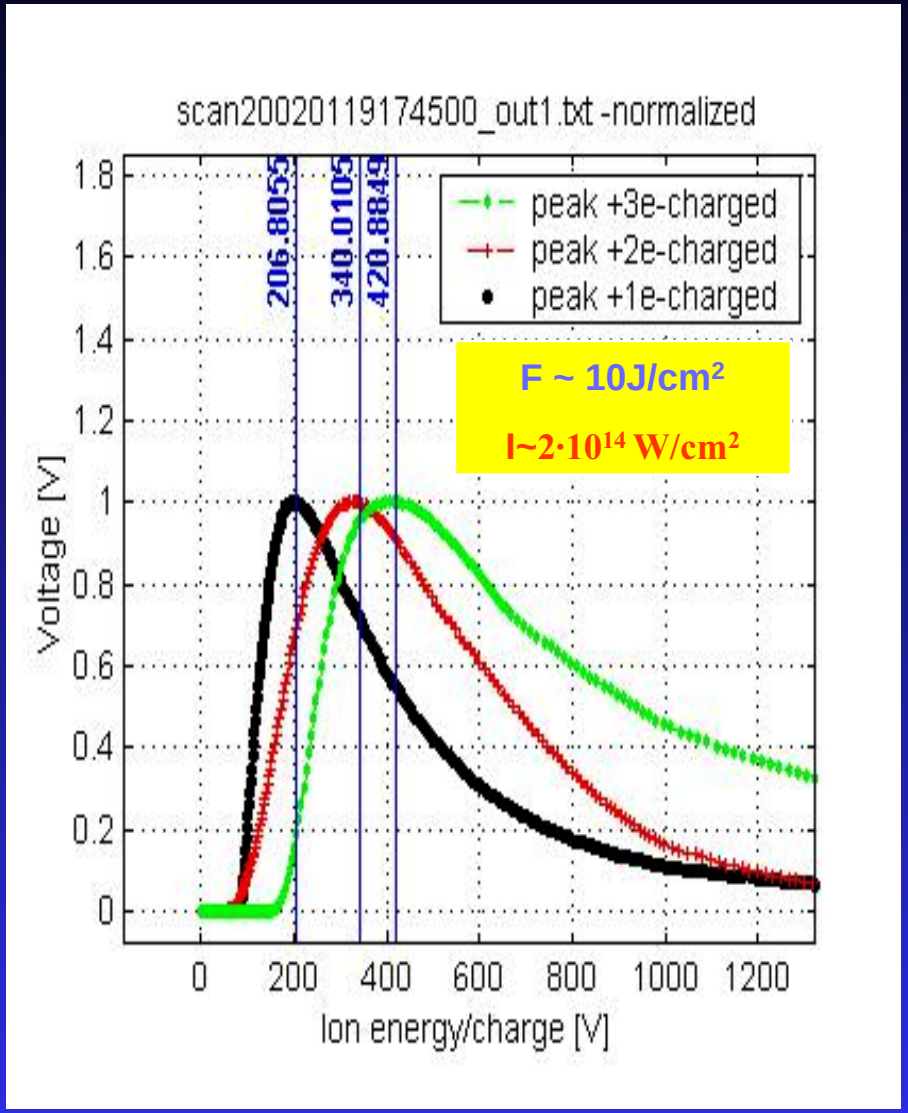
scan20020119174500_out1.txt -normalized
206.8055
340.0105
420.8849
peak +3e-charged
peak +2e-charged
peak +1e-charged
F ~ 10J/cm²
I~2·10¹⁴ W/cm²
Voltage [V]
Ion energy/charge [V]
0
0.2
0.4
0.6
0.8
1
1.2
1.4
1.6
1.8
0
200
400
600
800
1000
1200

Si
F ~ 10J/cm2
I~2·10^14 W/cm2
50 um

F ~ 10J/cm^2

I~2·10^{14} W/cm^2

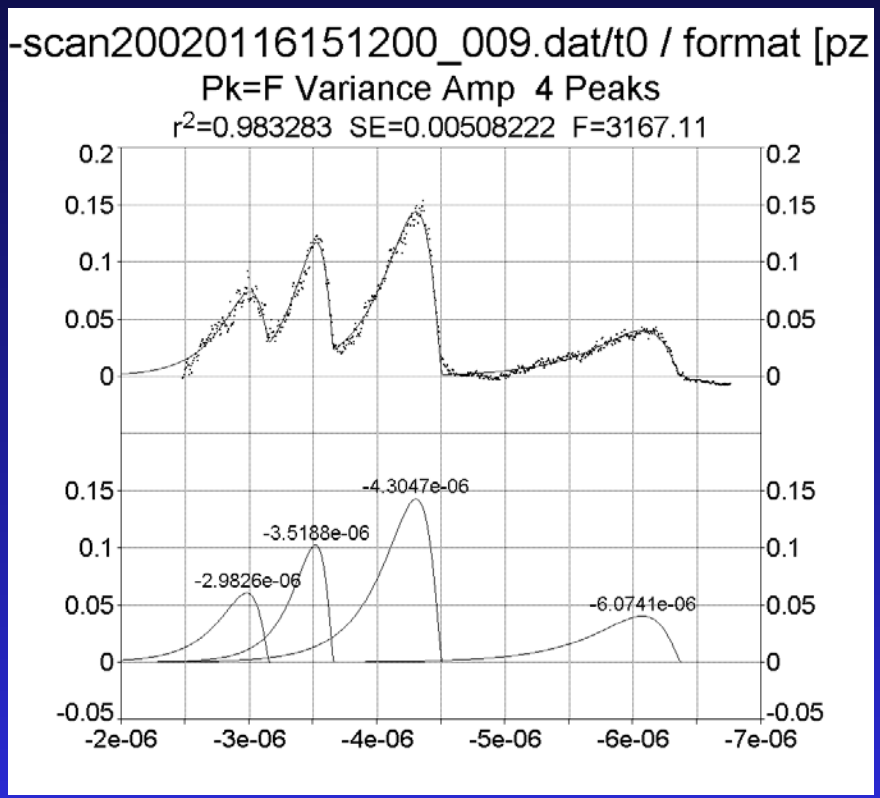

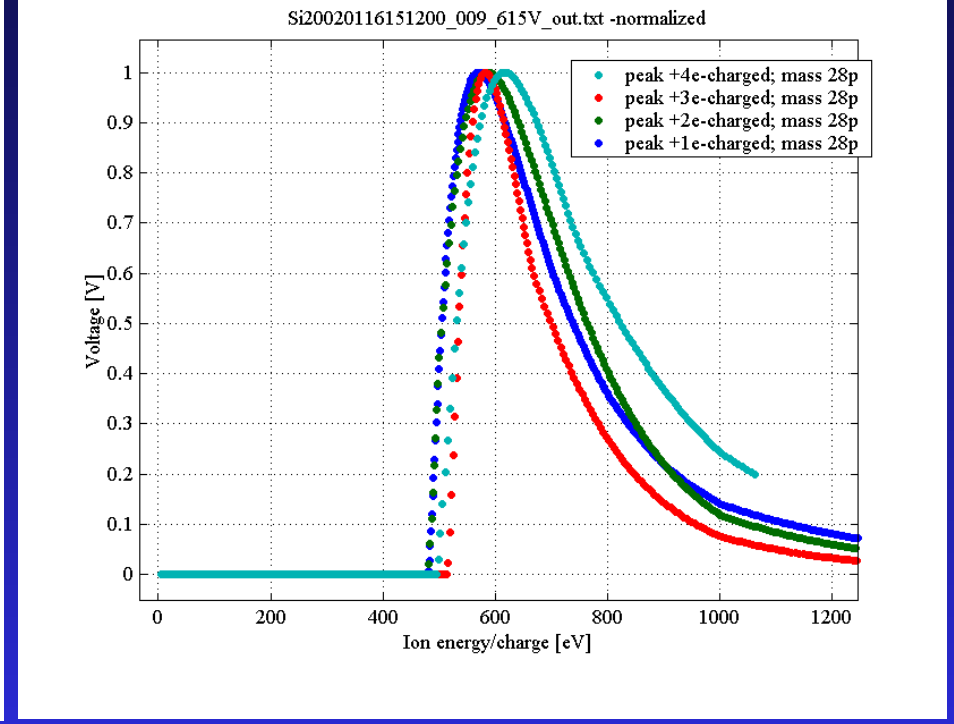

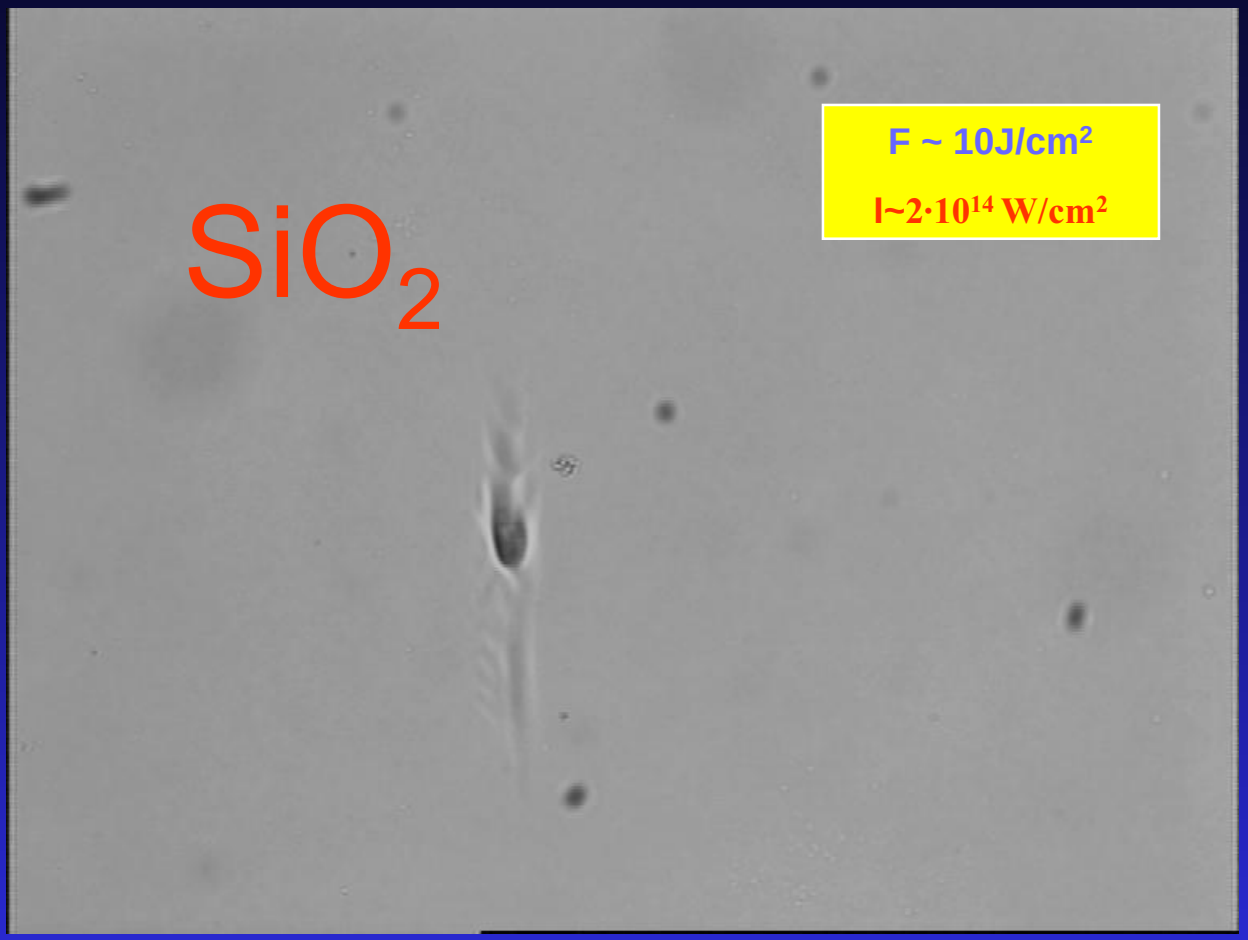
SiO_2
F ~ 10J/cm²
I~2·10¹⁴ W/cm²

SiO_2

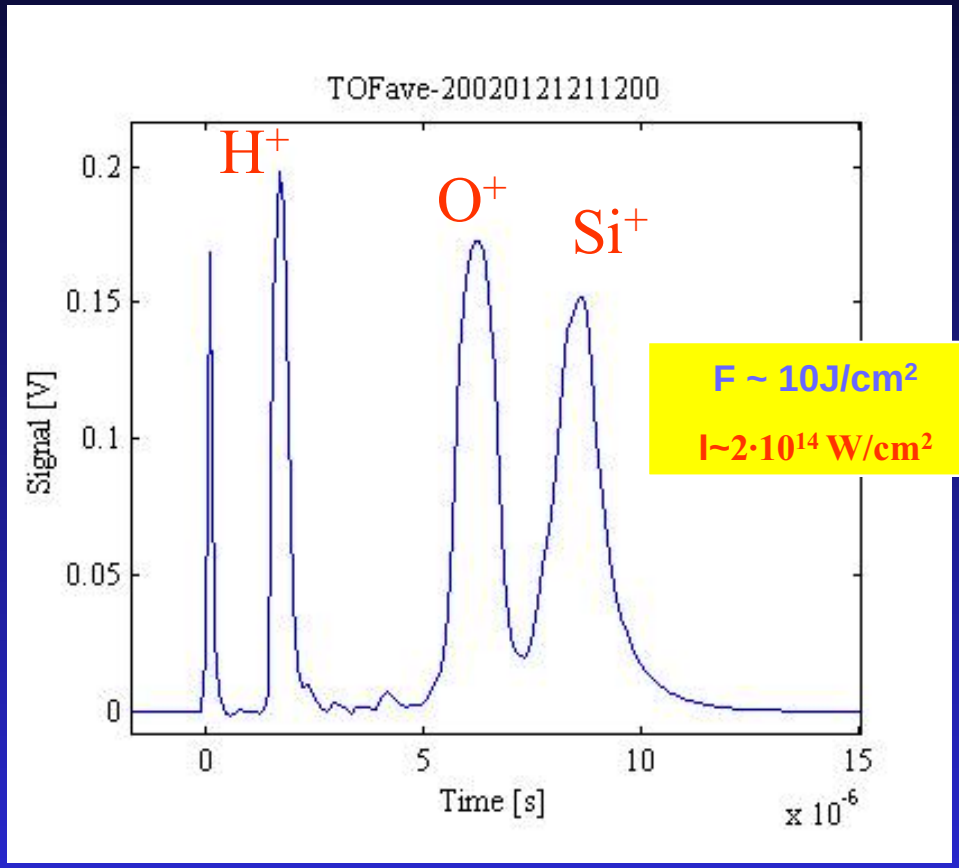
TOFave-20020121211200
H+
O+
Si+
0.2
0.15
0.1
0.05
0
Signal [V]
0
5
10
15
Time [s]
x 10-6
F ~ 10J/cm2
I~2·1014 W/cm2

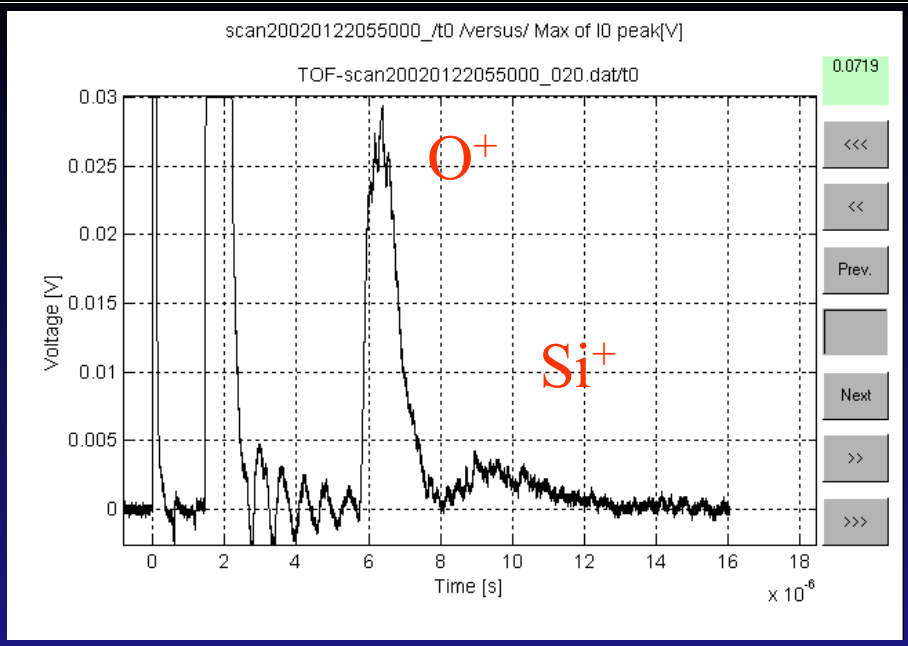

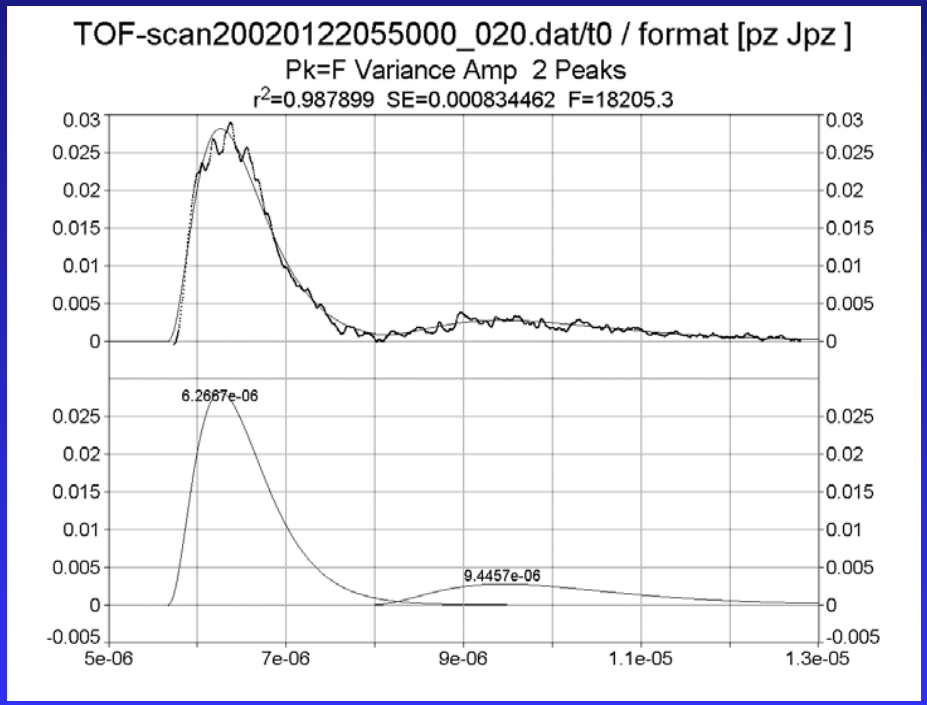

F ~ 1 J/cm²

I~2·10¹³ W/cm²

Energy distribution of Si^+ *and* O^+ *ions*

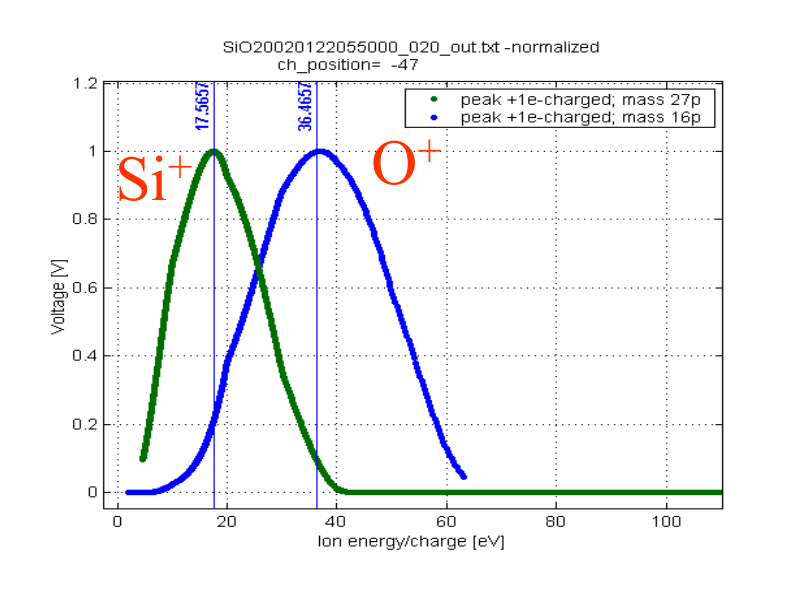

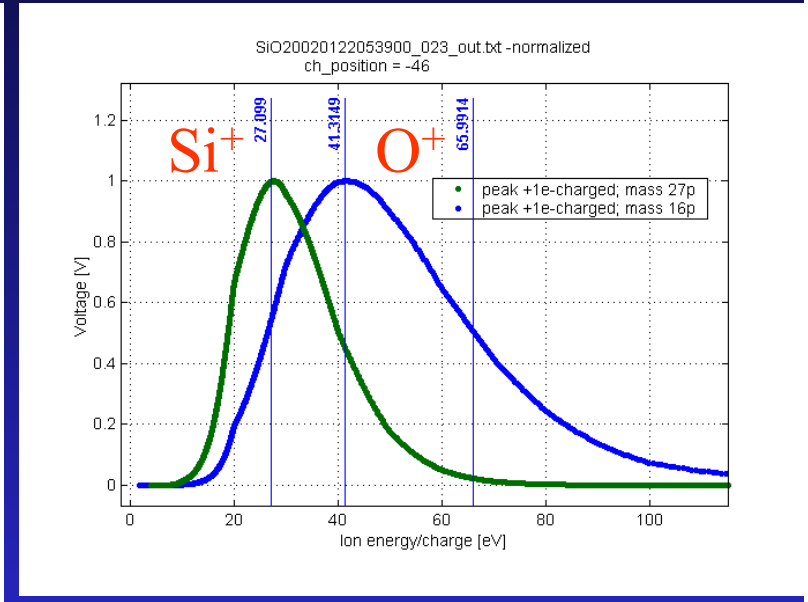

F ~ 1 J/cm^2

I~2·10^{13} W/cm^2

F ~ 10J/cm^2

I~2·10^{14} W/cm^2

Cluster experiments at the VUV-FEL

- Observation of multiphoton processes
- Cluster dynamics after irradiation
- Coulomb explosion at short wavelength

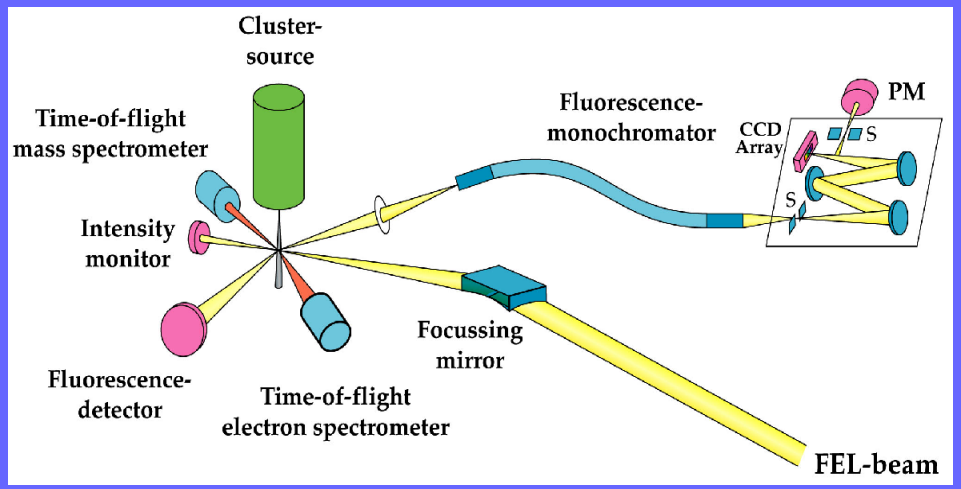

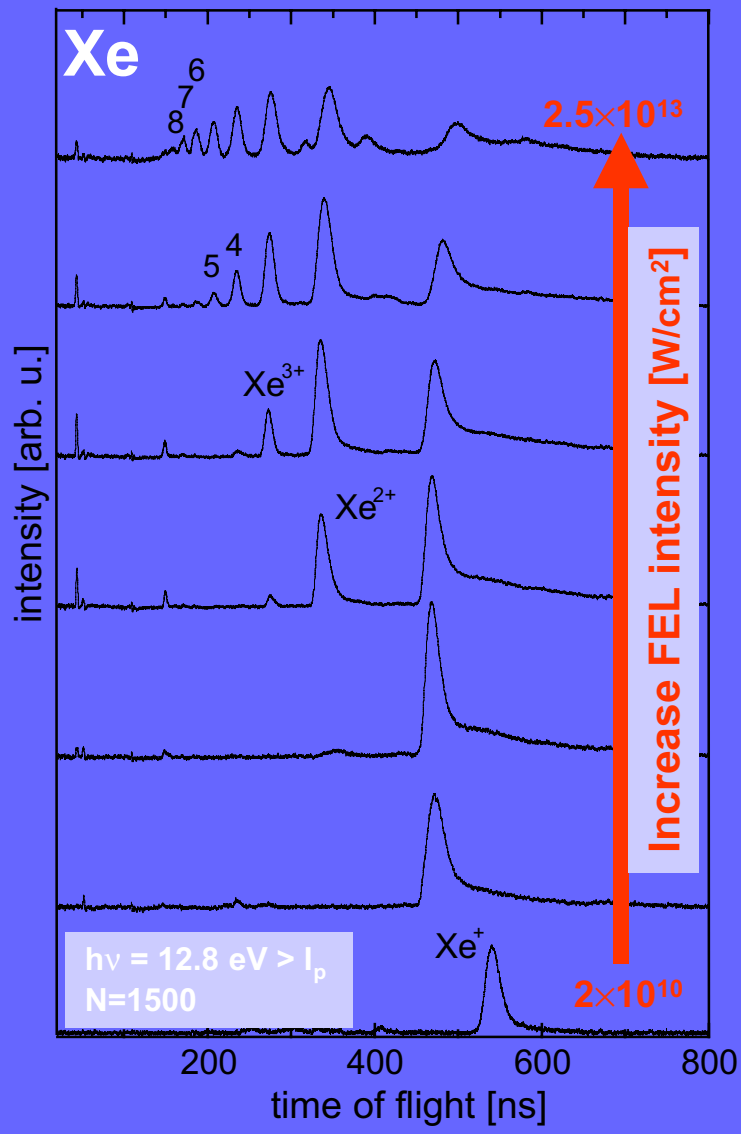

Thomas-Fermi Model

Marian Rusek

Institute of Physics, Polish
Academy of Sciences

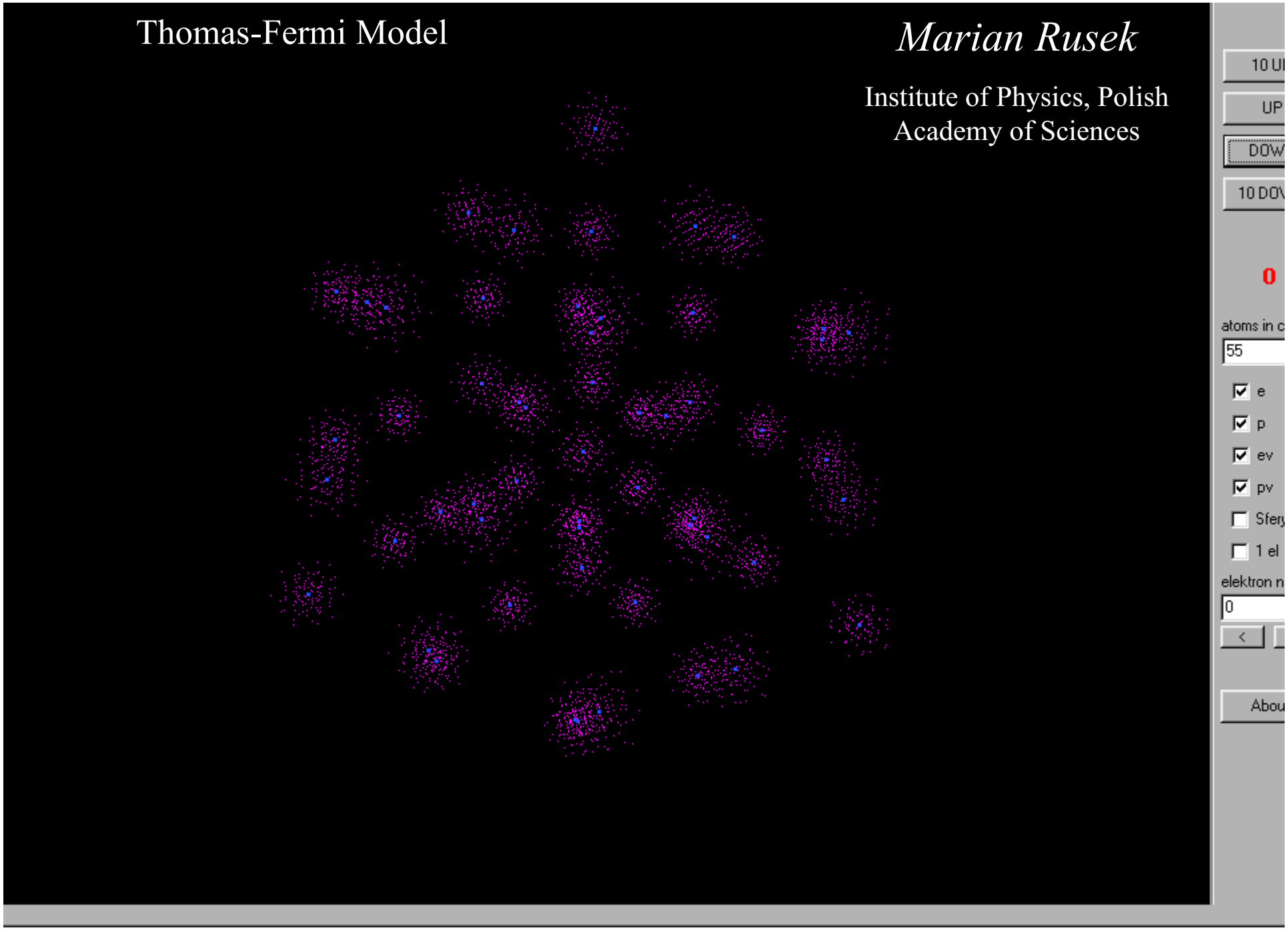

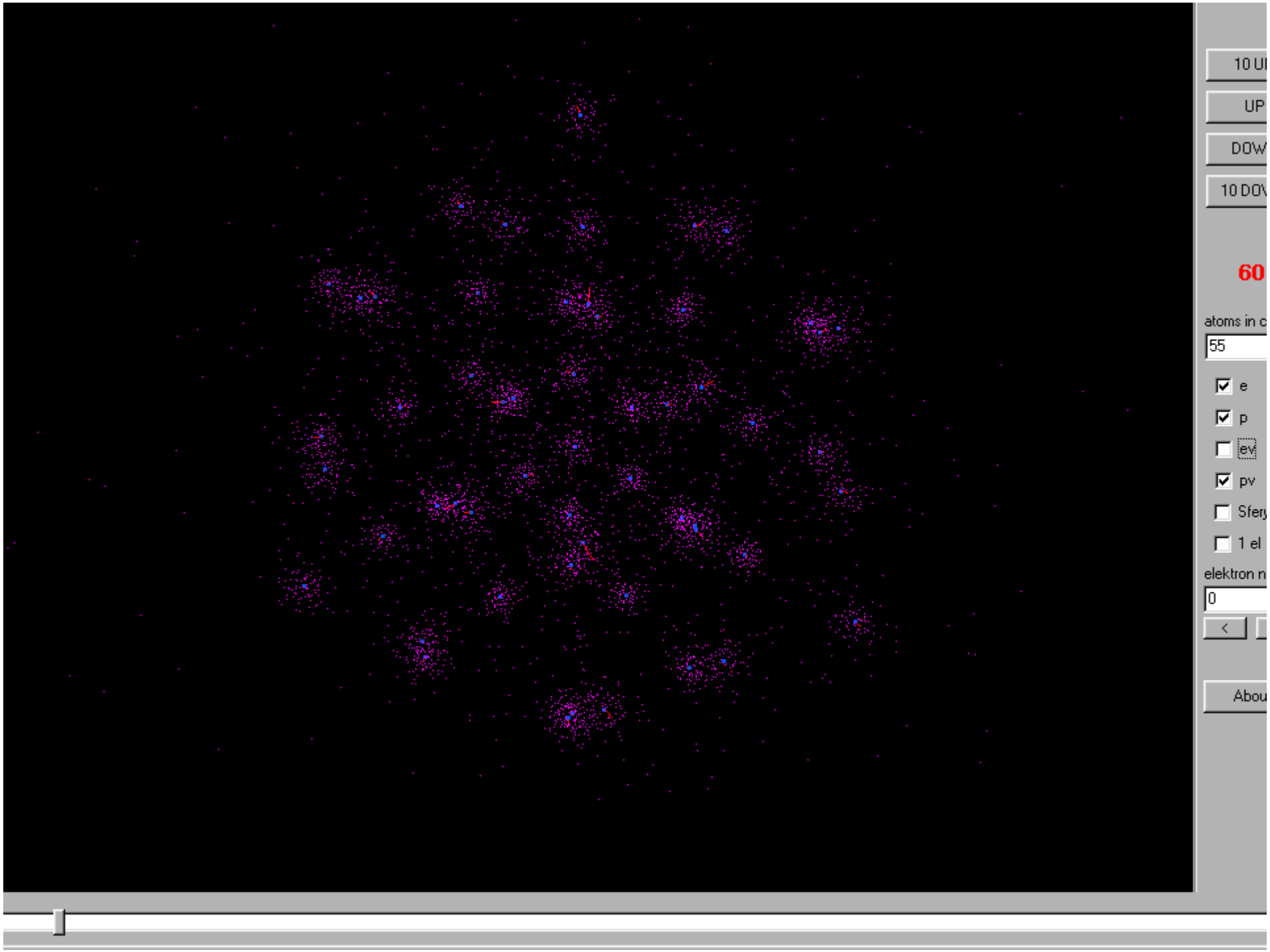
10 UI
UP
DOW
10 DOV
60
atoms in c
55
e
p
ev
pv
Sfery
1 el
elektron n
0
<
Abou

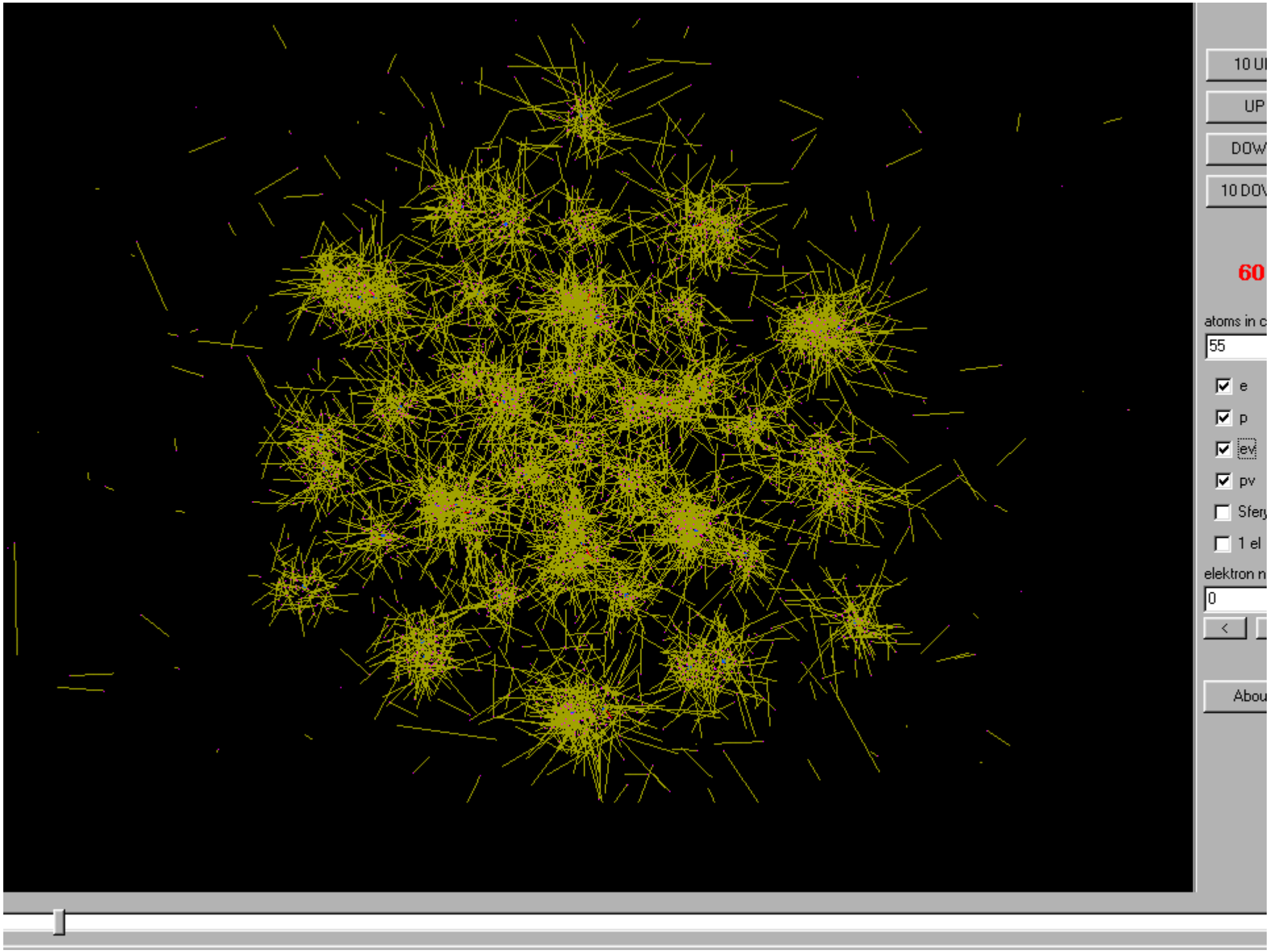
10 UI
UP
DOW
10 DOV
60
atoms in c
55
e
p
ev
pv
Sfery
1 el
elektron n
0
<
Abou

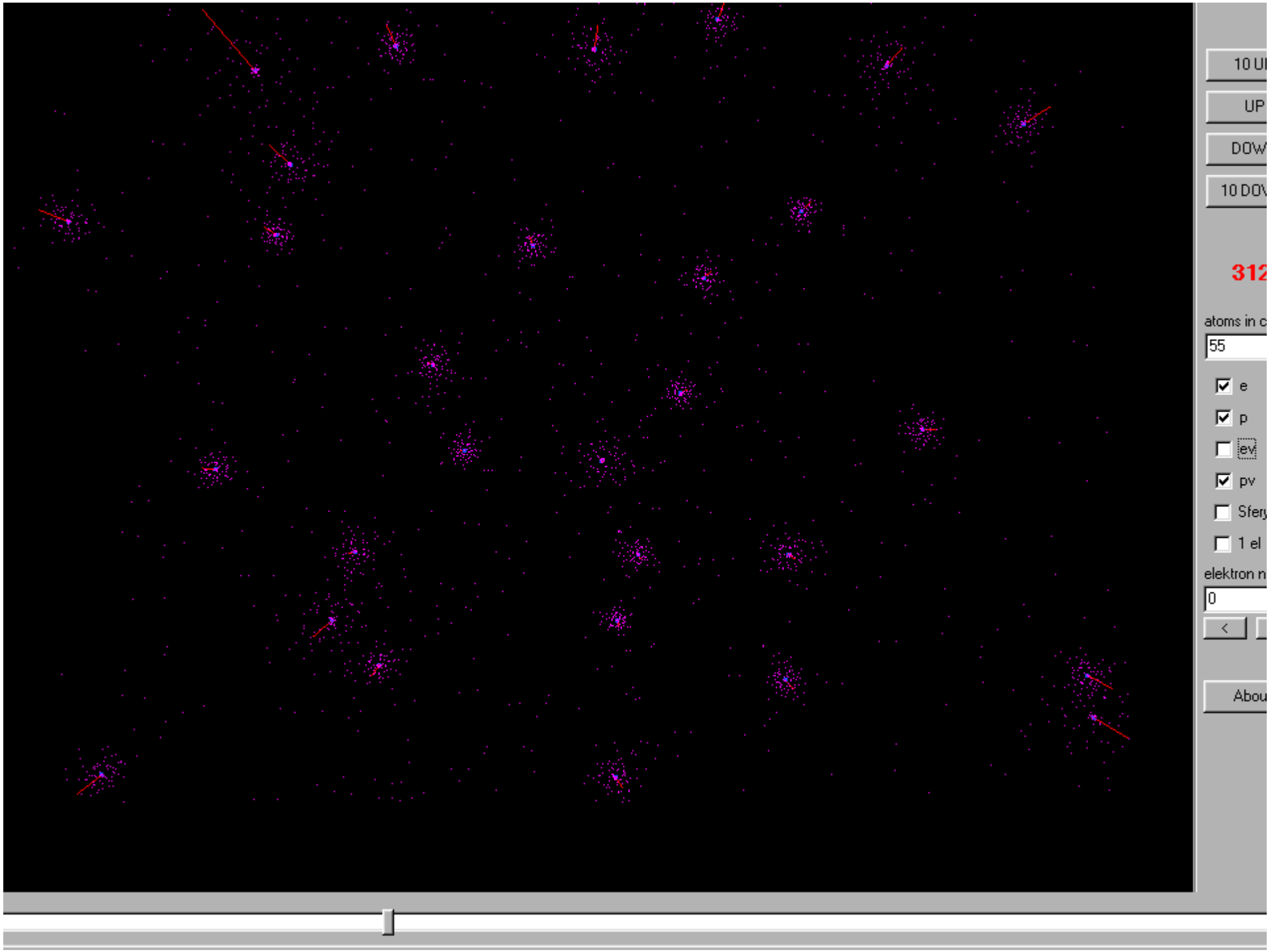
10 UI
UP
DOW
10 DOV
312
atoms in c
55
e
p
ev
pv
Sfery
1 el
elektron n
0
<
Abou

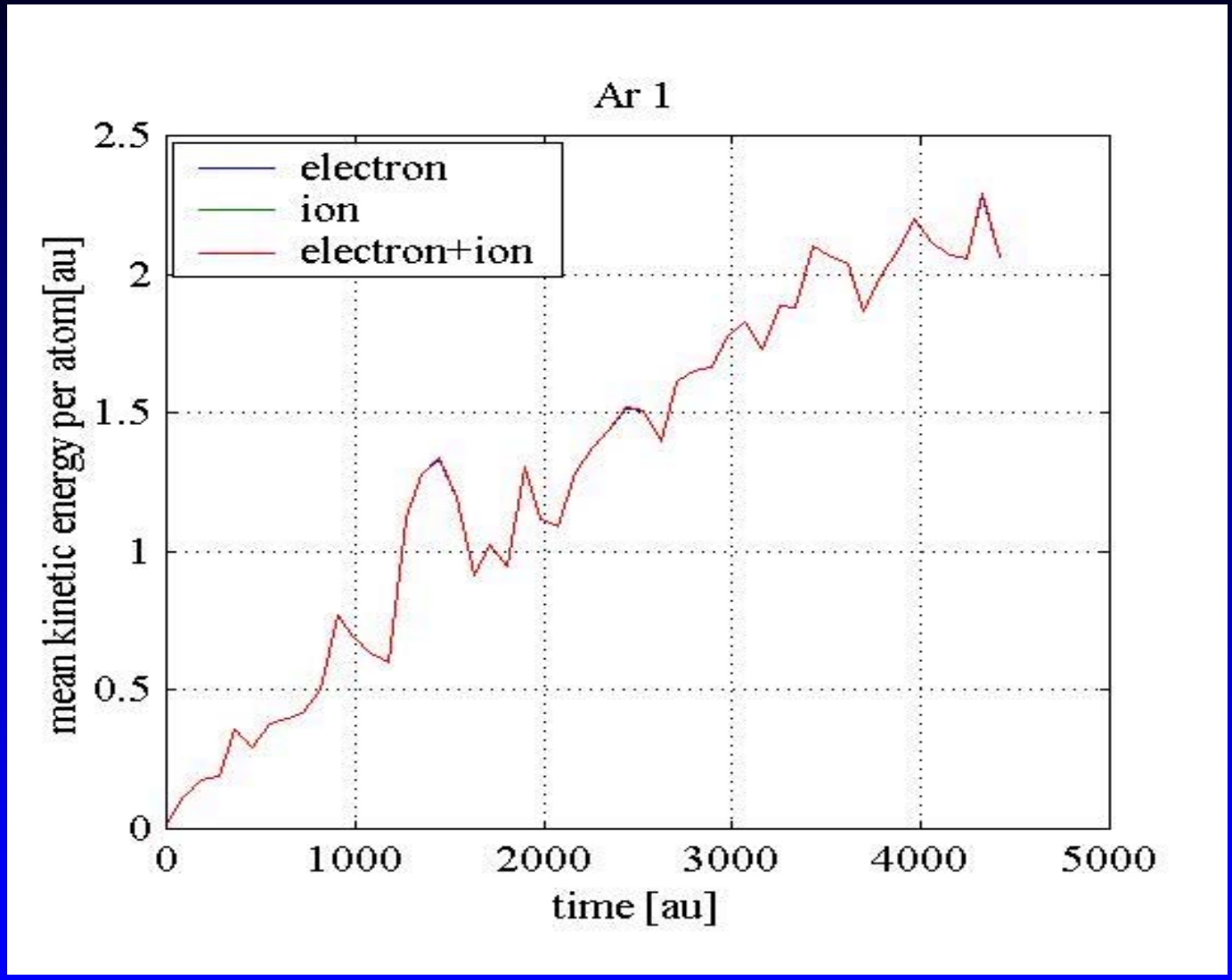
Ar 1
electron
ion
electron+ion
mean kinetic energy per atom[au]
time [au]
0
0.5
1
1.5
2
2.5
0
1000
2000
3000
4000
5000

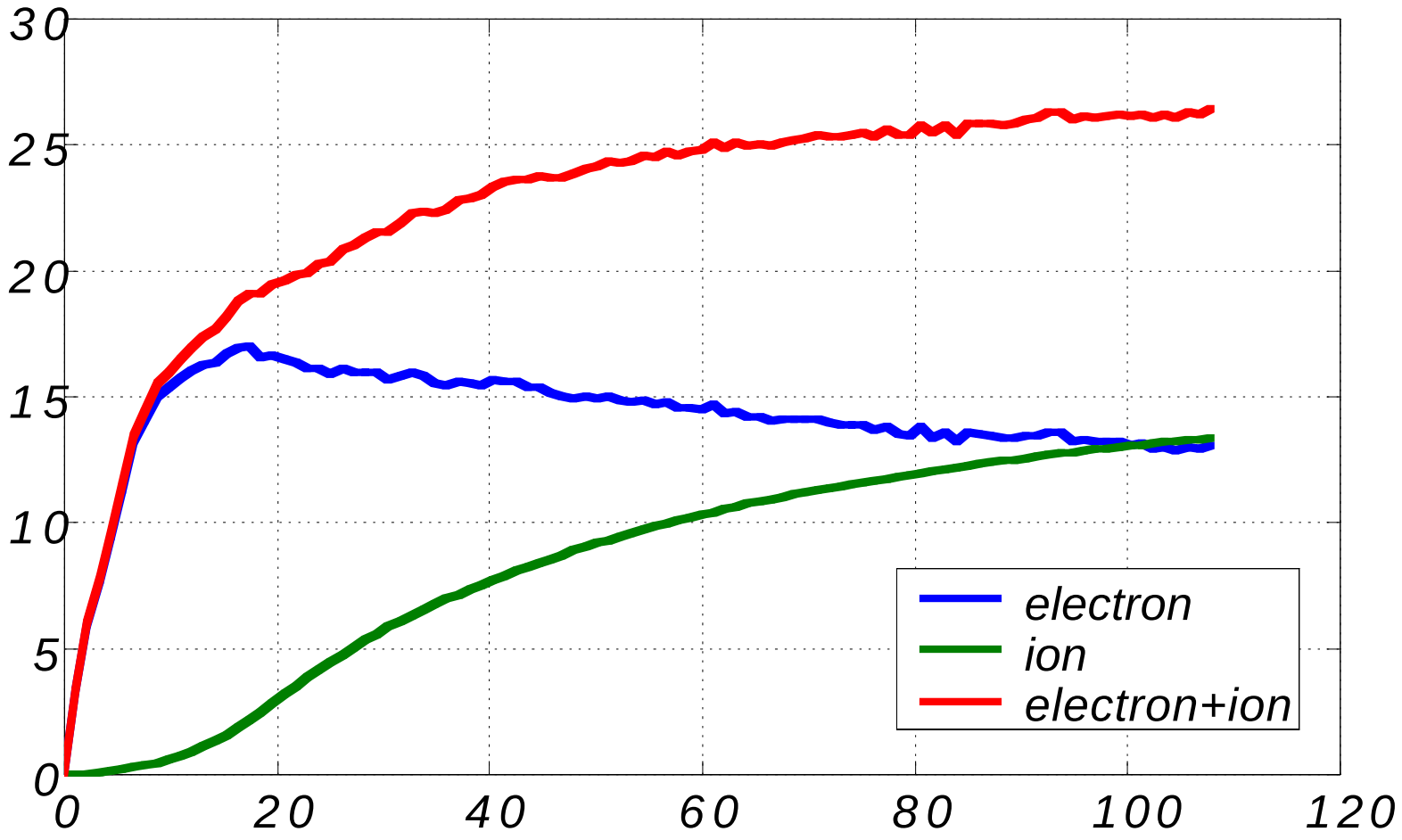
30
25
20
15
10
5
0
0
20
40
60
80
100
120
electron
ion
electron+ion

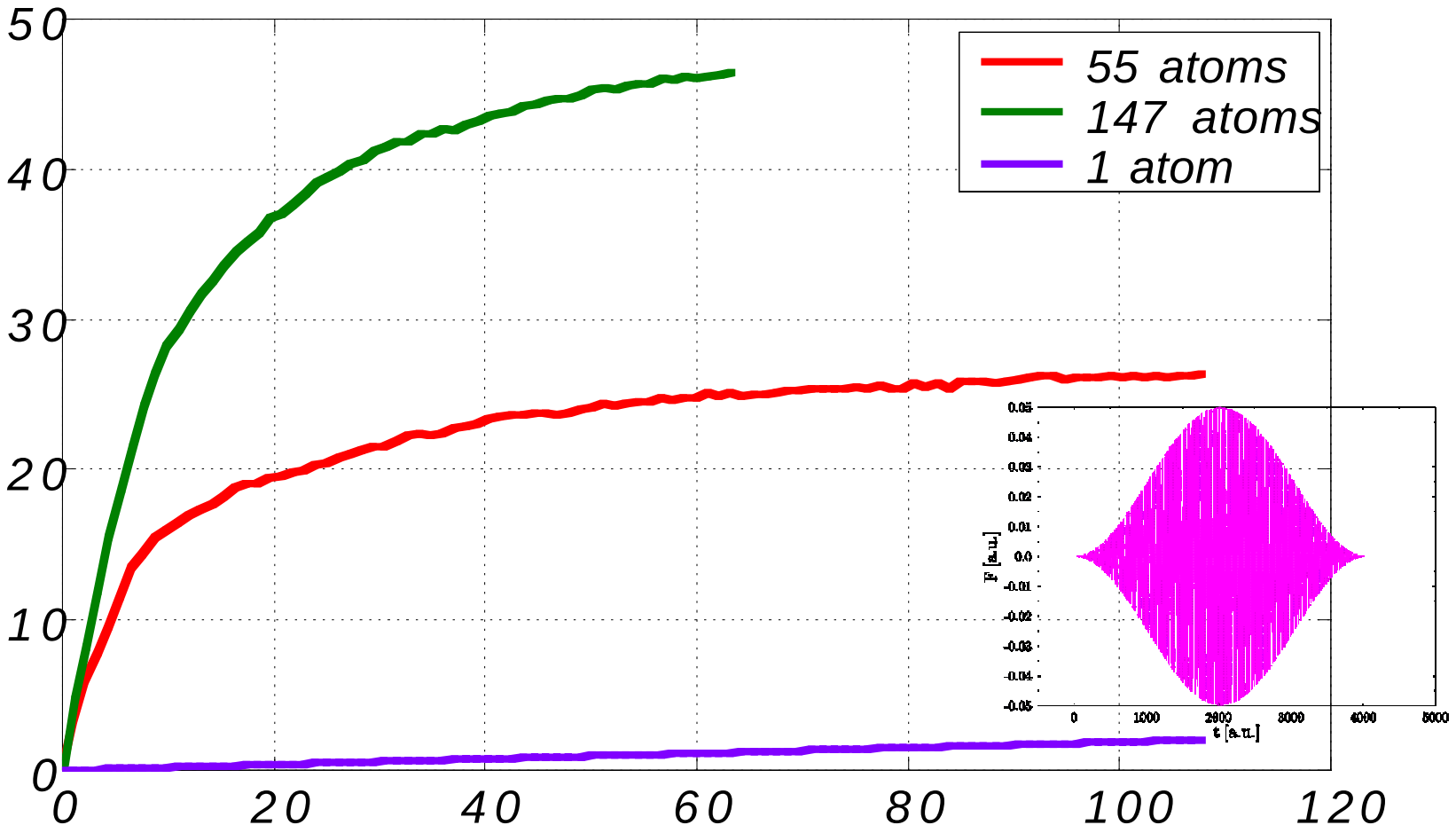
55 atoms
147 atoms
1 atom
0
10
20
30
40
50
0
20
40
60
80
100
120
F [a.u.]
t [a.u.]

Summary of plasma results:

Metals and semiconductors

- High energy ions (up to several keV) are observed
- Energy distribution can be scaled with charge. This suggests field emission mechanism
- At fluencies 10 J/cm^2 higher charge states (2+, 3+) dominate distribution

Insulators

- Low energy ions (up to 100 eV) are observed
- Only single charged ions are emitted

Conclusions:

- Short XUV pulses are suitable for nano - processing of ionic crystals and organic compounds and, at low fluences, also of semiconductors
- There is clear difference between insulators and conducting materials with respect to plasma formation and ablation processes

The Physics of X-Ray Material Interactions

Richard London
Lawrence Livermore National Laboratory

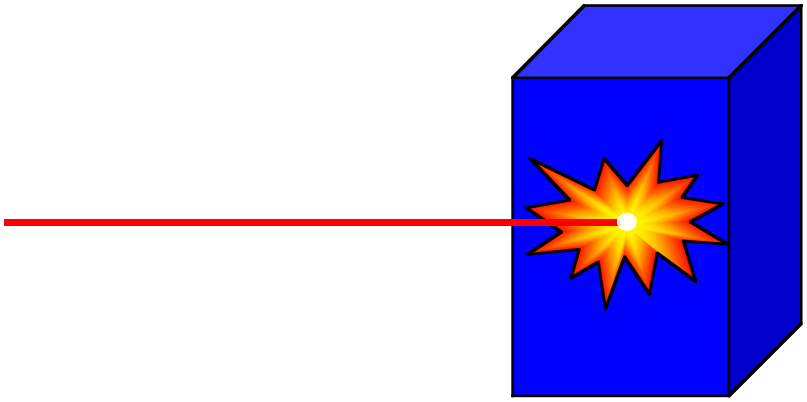

rlondon@llnl.gov

International Conference on
Ultrashort High-Energy Radiation and Matter
Varenna, October 7-10, 2003

This work was performed under the auspices of the U.S. Department of Energy by University of California Lawrence Livermore National Laboratory under contract No. W-7405-Eng-48

Acknowledgements

Collaborators

Richard Bionta

Henry Chapman

Janos Hajdu

Stefan Hau-Riege

Abraham Szoke

RomanTatchyn

Alan Wootton

Beata Ziaja

Funding

LLNL Laboratory Directed Research and Development (LDRD) Program

X-Ray Free Electron Lasers will open a new regime of x-ray material interaction

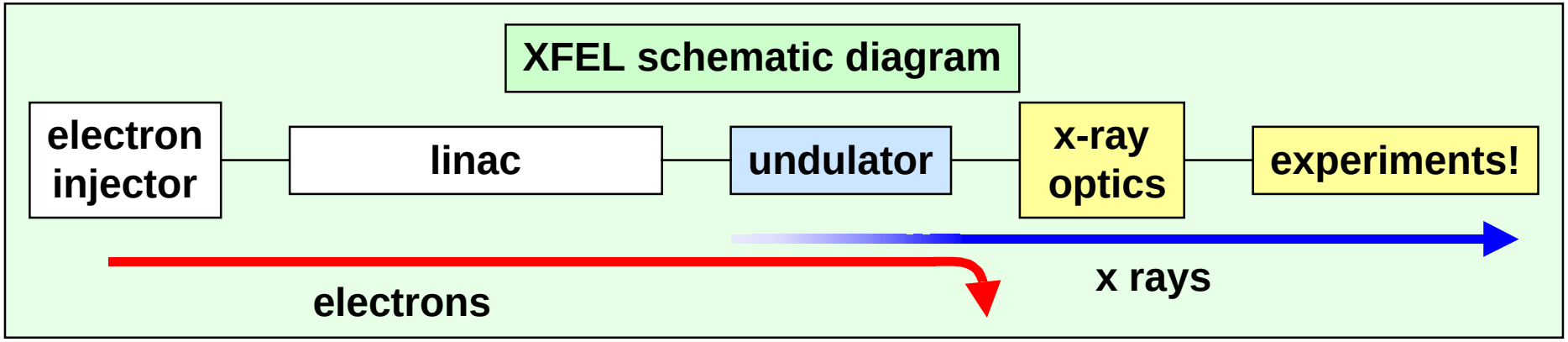

Facility	date
Stanford LCLS	2008
Hamburg XFEL	2011

x-ray parameters	
Photon energy	1-30 keV
# photons/pulse	10^{12} - 10^{13}
Output fluence	10-100 J/cm^2
Pulse length	10-250 fs
Spectral bandwidth	10^{-3}
Repetition rate	100 Hz
Spatial coherence	(high)

X-ray matter interaction spans a wide range of applications and energy density

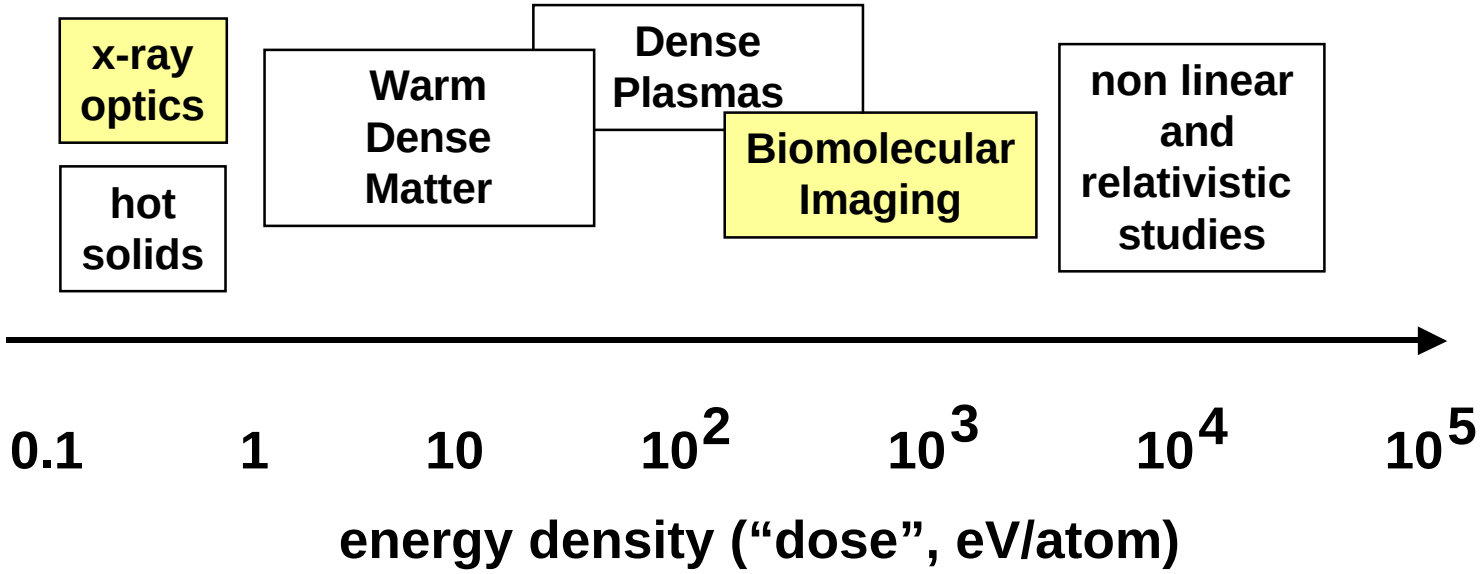

The dose increases with atomic number and decreases with photon energy

Gaussian beam model: $F = F_o(1+L\lambda/w_o^2)^{-2}$

Cold absorption model for dose: $D = F\,\sigma_a$

Dose at 15 m from end of undulator

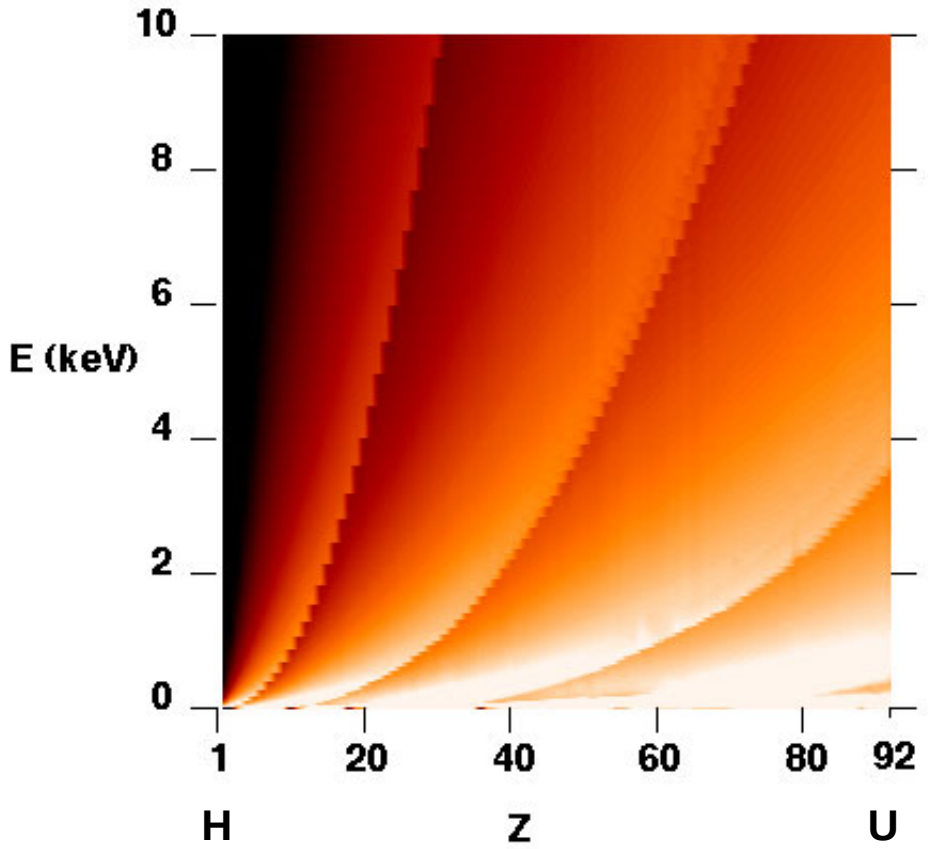

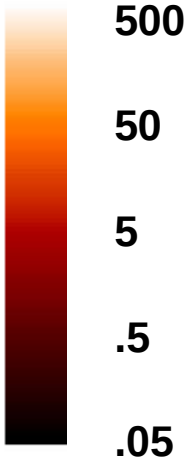

Dose (eV/atom)

500

50

5

.5

.05

F = fluence
D = dose
L = distance
λ = wavelength
w_o = beam waist
σ_a = abs. xsect/atom

Fundamental x-ray and electron processes

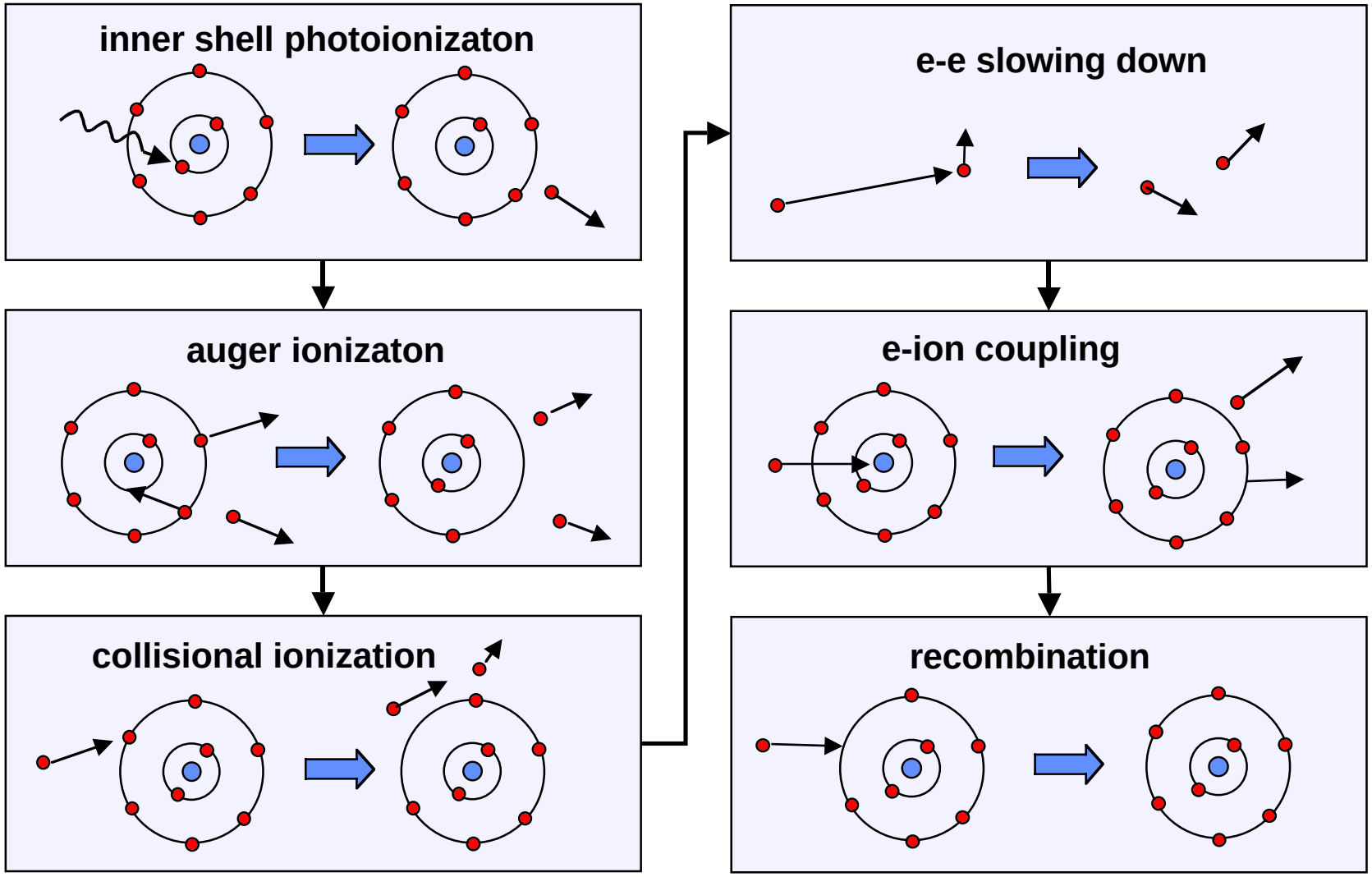

Energy-time picture of x-ray material interaction

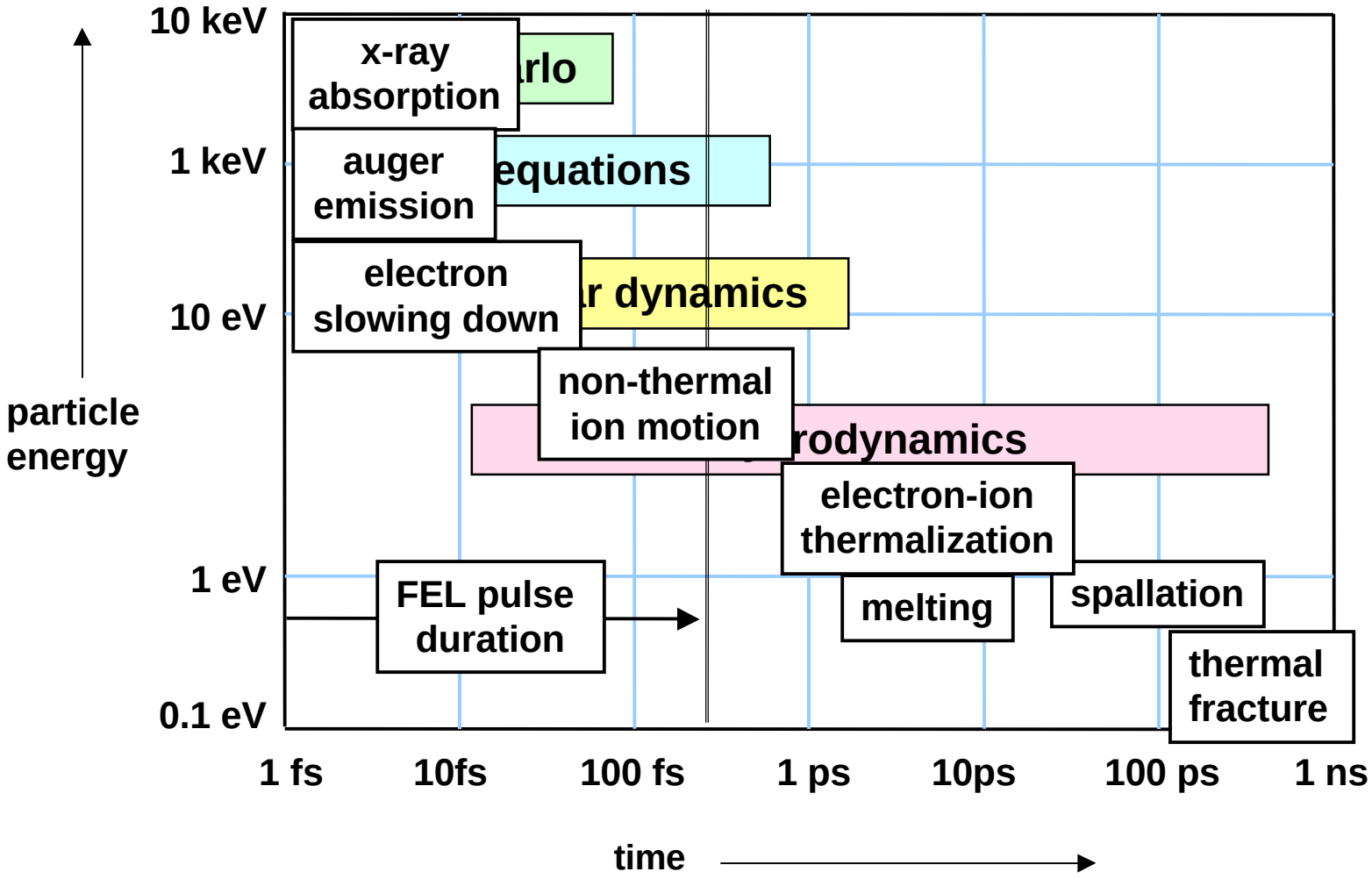

Energy-time picture of x-ray material interaction

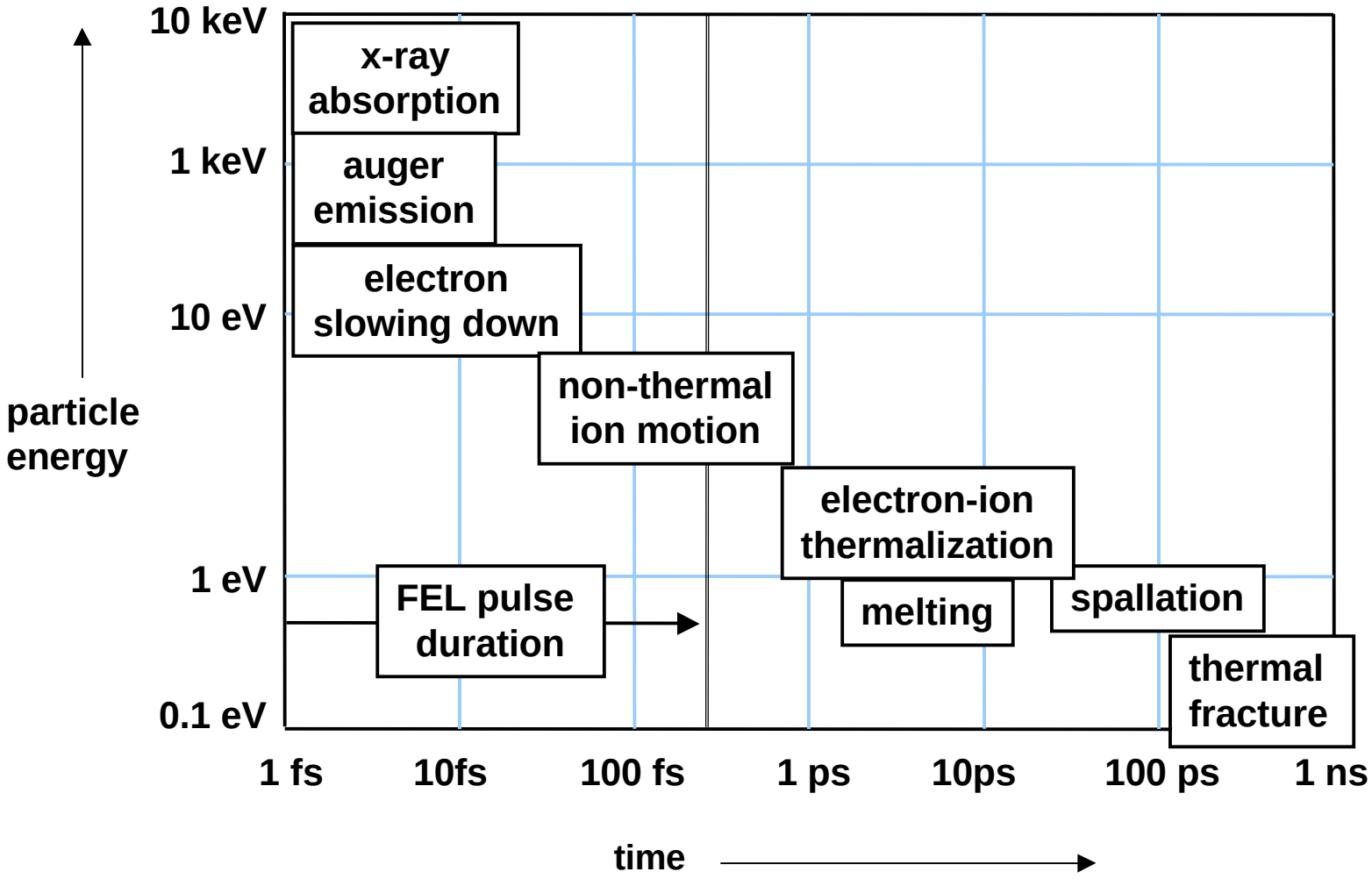

Methods and computer programs for simulating x-ray interaction with solids

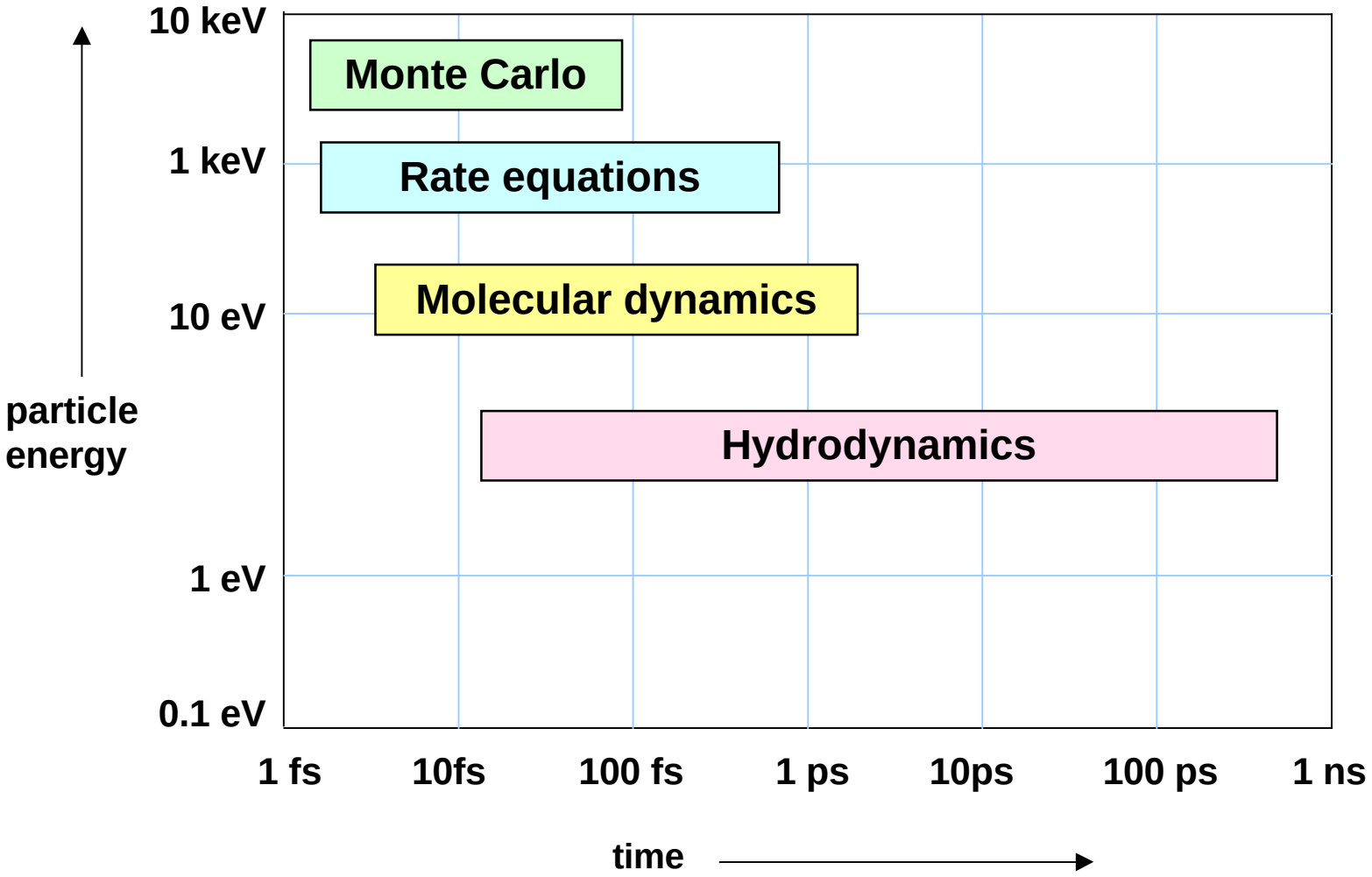

w. B. Ziaja, J. Hajdu, and A. Szoke

Monte Carlo calculations of photo-electron cascade

Time dependent evolution after absorption of a 10 keV photon in a thick diamond sample

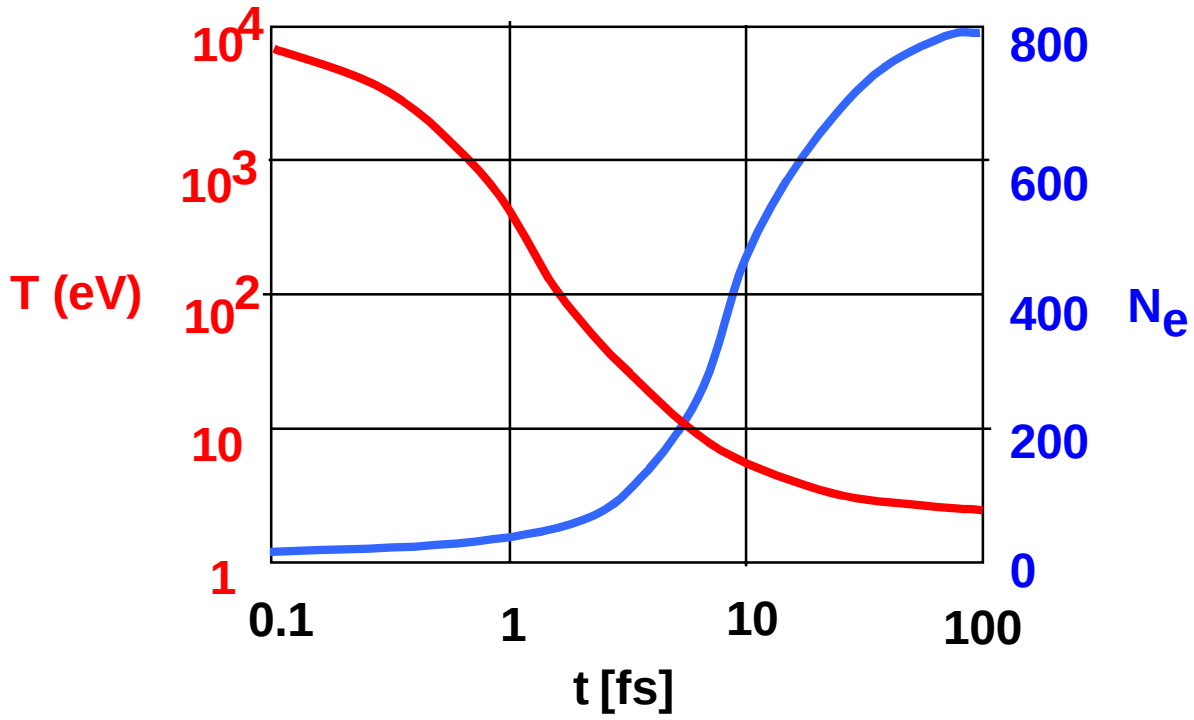

- Essential to include effect of both electron and holes
- cascade timescale ~ 10 fs.
- ~ 800 secondary electrons are generated per photo-electron.
- cascade spreads to ~ 0.2 μm diameter cloud.

X ray interaction must be considered when designing optical components

w. R. Bionta, R. Tatchyn, A.Wootton

Grazing incidence mirrors

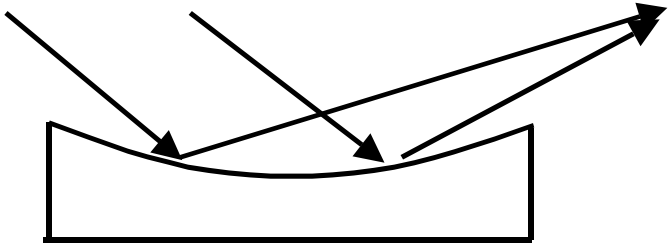

Fresnel lenses

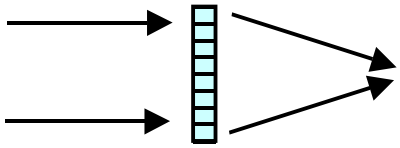

Diffraction crystals

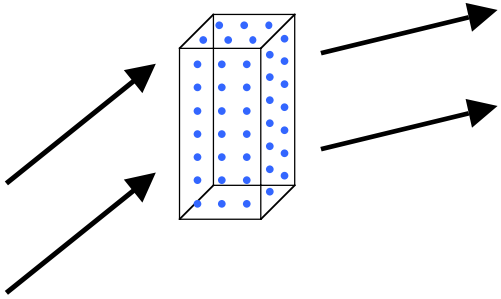

X-rays may alter the performance of an optical component during or after the x-ray pulse

The dose can be reduced by using grazing incidence optics

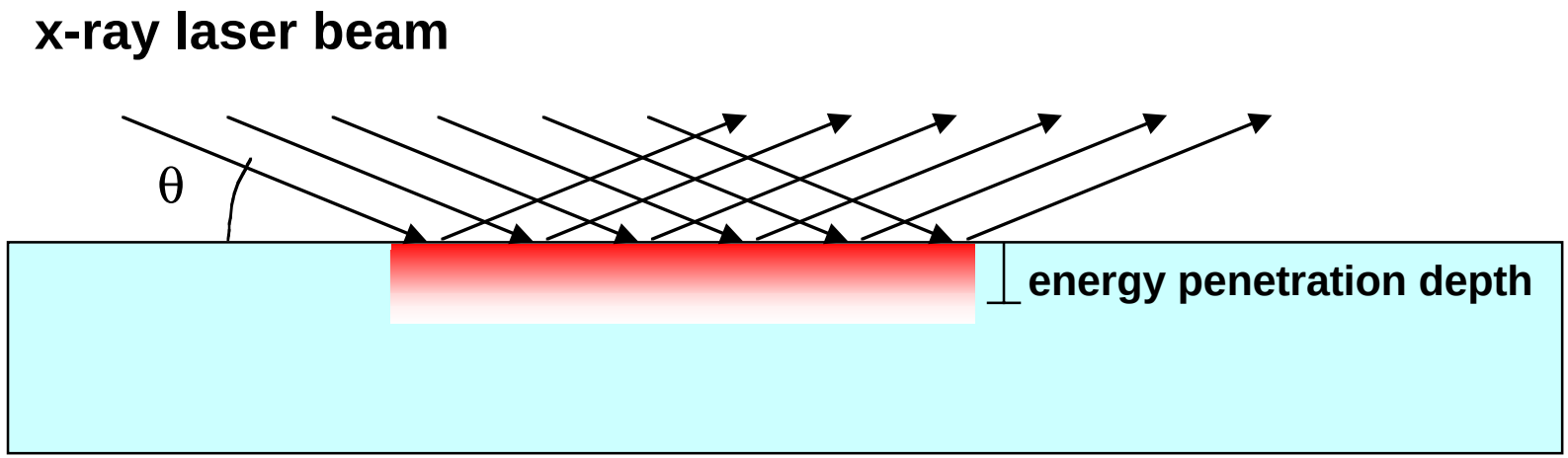

Calculated doses for grazing incidence optics

E_x = 1 keV, distance = 80 m

Analytic formula for surface dose

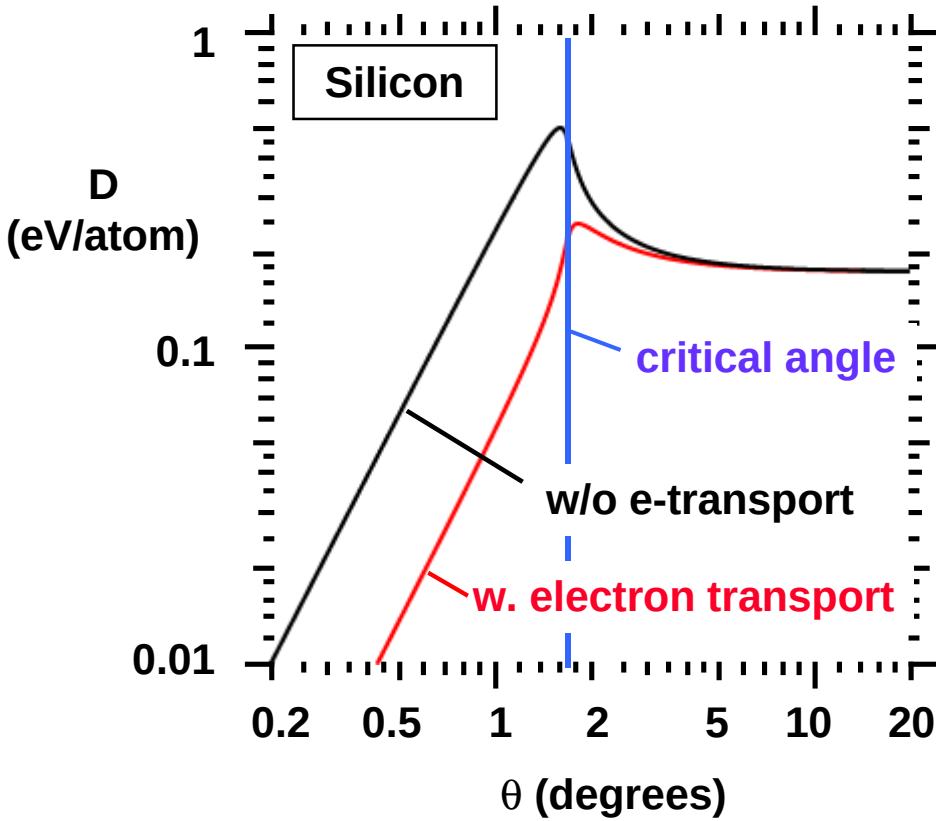

Monte Carlo calculations
θ=1 degree

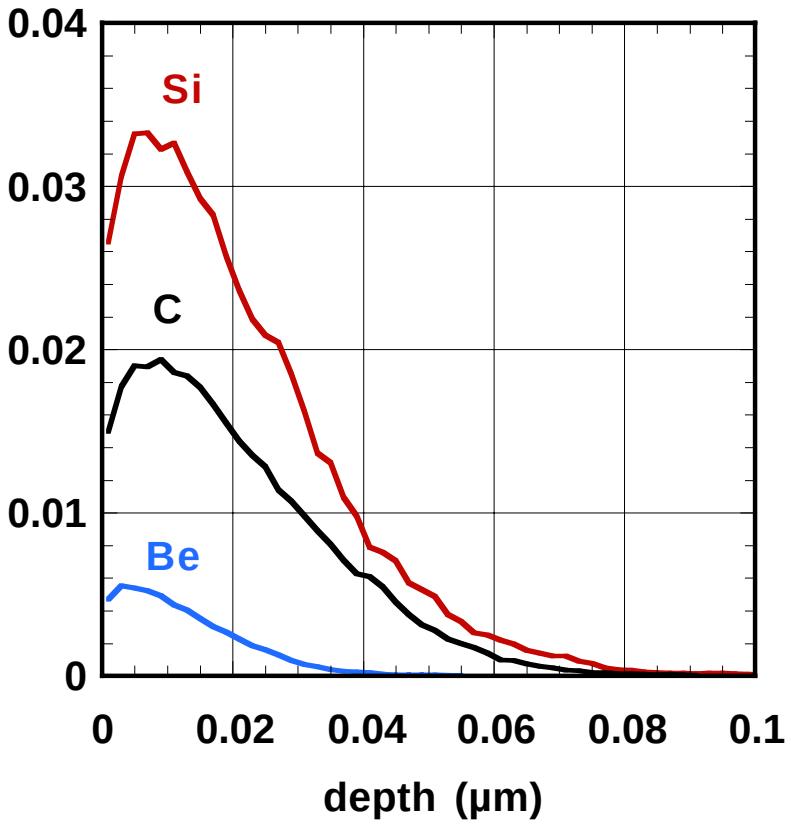

Hydrodynamic simulations illustrate thermal and pressure effects

Silicon
F = 1 J/cm²
E_x = 2 keV
D = 1.25 eV / atom

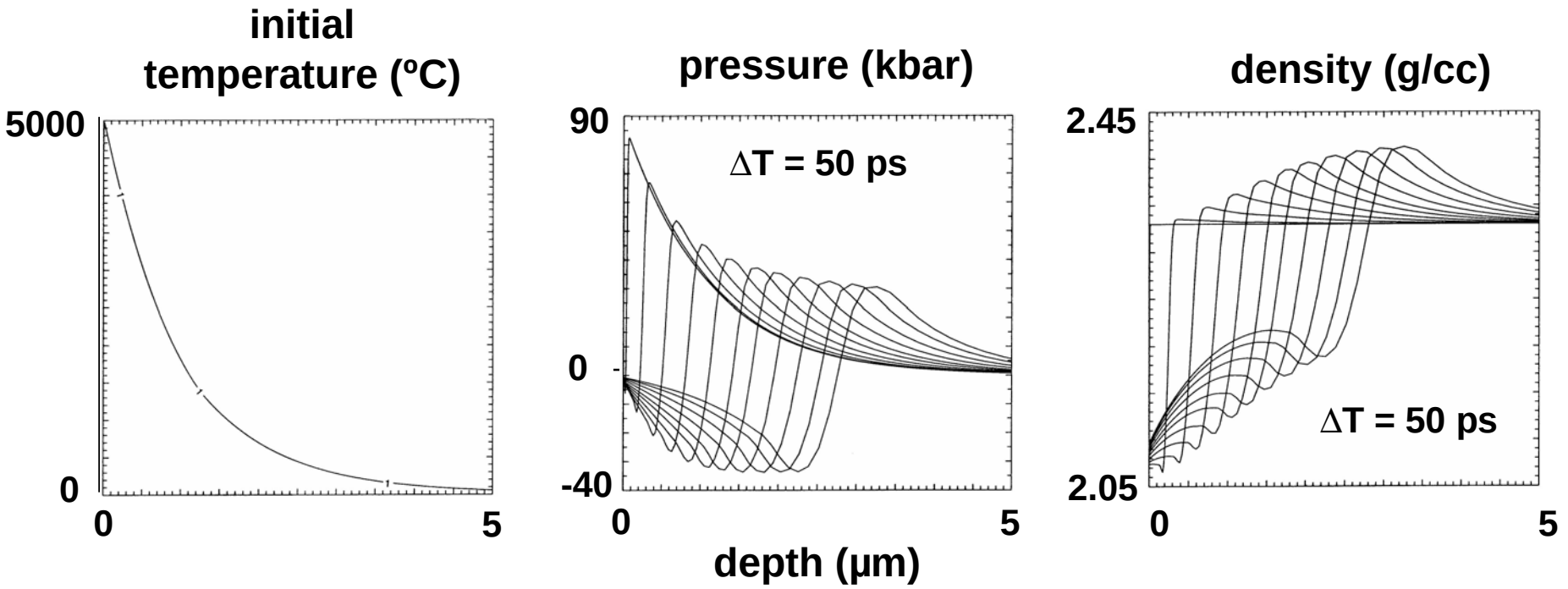

- **This exposure will lead to surface melting and late-time 2-D liquid movement.**
- **Higher fluences lead to surface ablation.**

Melting damage threshold

Analysis of optical laser-matter experiments and theoretical analysis of x-ray processes suggests that melting will be the threshold process for permanent damage

Candidate optics materials and projected melting thresholds

Material / Quantity	Be	C	Al	Si	B_4C
T_{melt} (K)	1560	3800	930	1690	2620
D_{melt} (eV/atom)	0.43	0.9	0.30	0.87	0.62

Recommendation: keep fluence well below melt threshold

Will the reflectivity of an x-ray crystal be reduced by ion motion before melt fluence is reached?

- Reflected intensity is function of Debye-Waller "M-factor"

$$I = I_0 \exp(-M), \text{ where } M = 2\pi^2 \frac{\langle \Delta r_i^2 \rangle}{d^2} \text{ at Bragg angle.}$$

For thermal motions: $\langle \Delta r_i^2 \rangle \propto \frac{T_i}{\Theta_D^2}$

- Example: Si (220).

  $2d$ = 3.84 Å, Θ_D = 550 K,

  T_i = 1500 K (just below melt):

  I = 75% I_0

- Since the thermal e-ion coupling timescale is ~ 1-10 ps, T_i should be lower during x-ray pulse (~100 fs).

- However, non-thermal e-ion coupling as observed in optical laser-matter experiments, may increase ion motion.

Summary of x-ray optics damage study

- Melting is an important threshold damage mechanism.
- To avoid damage, use a combination of
  - low-Z materials
  - grazing incidence
  - placement at a large distance from the XFEL
- Ion motion during the pulse may degrade performance of diffraction crystals at lower-than-melting dose.
- Future work
  - damage to multi-layer mirrors
  - ion motion during the pulse
  - multiple pulse effects (material fatigue)
  - experiments with intermediate sources (SPPS, TTF, etc)

XFELs are ideal for studying Warm Dense Matter

R. Lee

Aluminum phase diagram

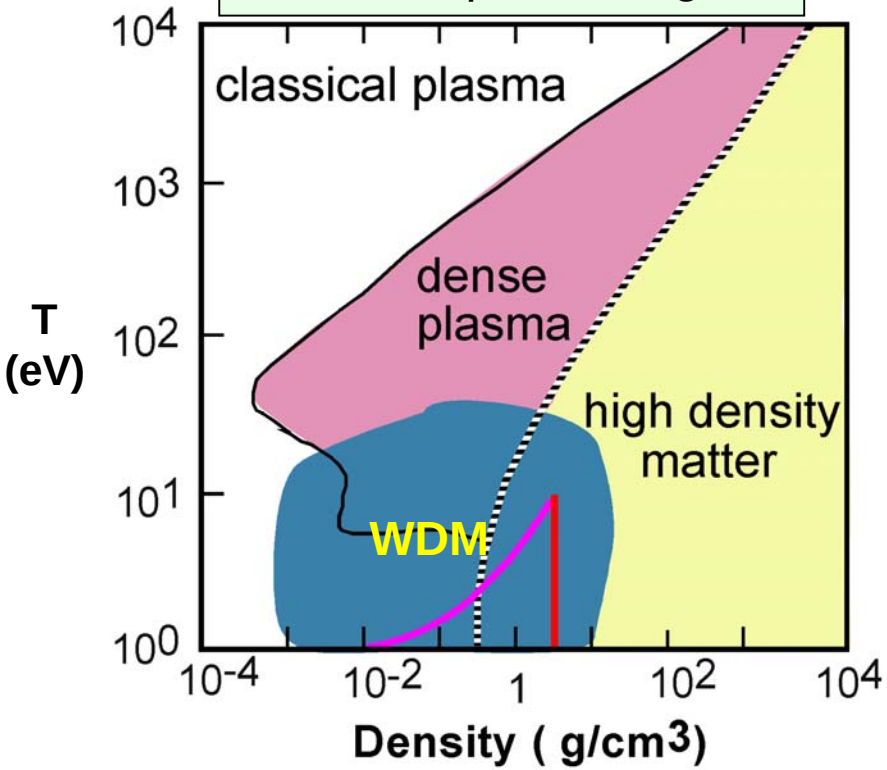

Uncertainly in Aluminum Equation-of-State (%)

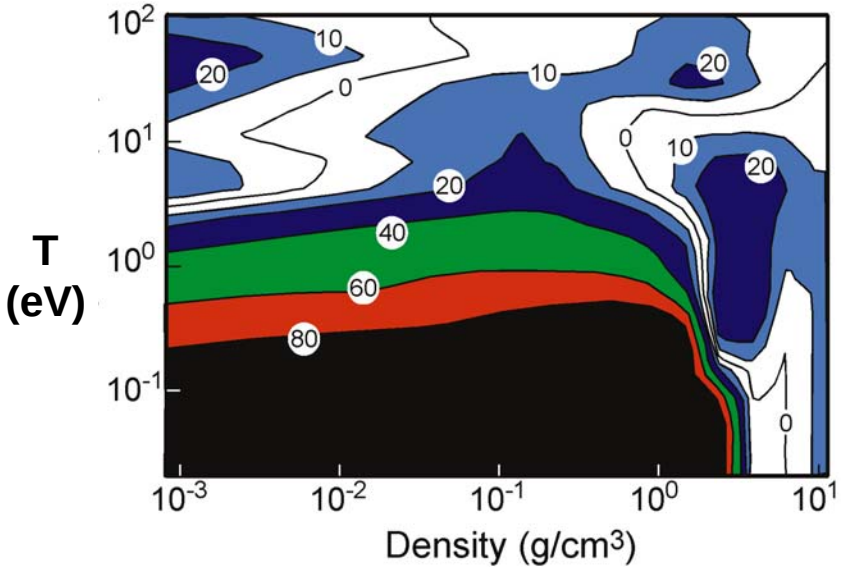

- WDM occurs in:
  - Cores of large planets
  - Inertial Confinement Fusion
  - Any system that starts solid and ends as a plasma

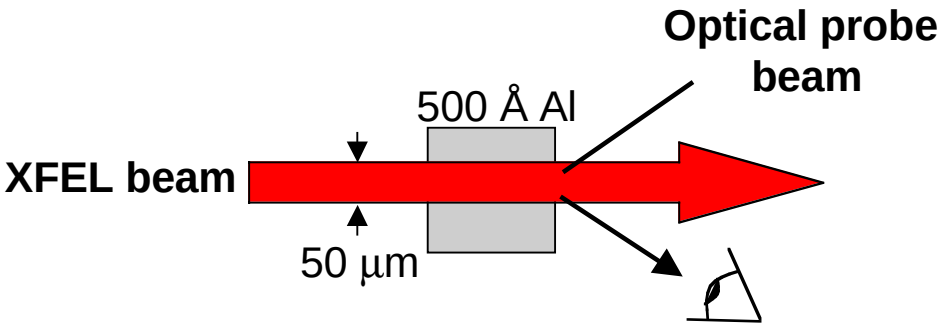

see talk of Meyer-ter-Vehn for more complete discussion

Dynamics of x-ray irradiated biological molecules

w. S. Hau-Riege and A.Szoke

- A method of imaging single molecules would be extremely valuable in structural biology.
- X-ray damage presents the major problem.
- With a very short XFEL pulse, we can capture a "snapshot" before the molecule is damaged.
- See talk by J. Hajdu for a more complete discussion!

Neutze, Wouts, Van der Spoel, Weckert, and Hajdu (Nature, 2000)

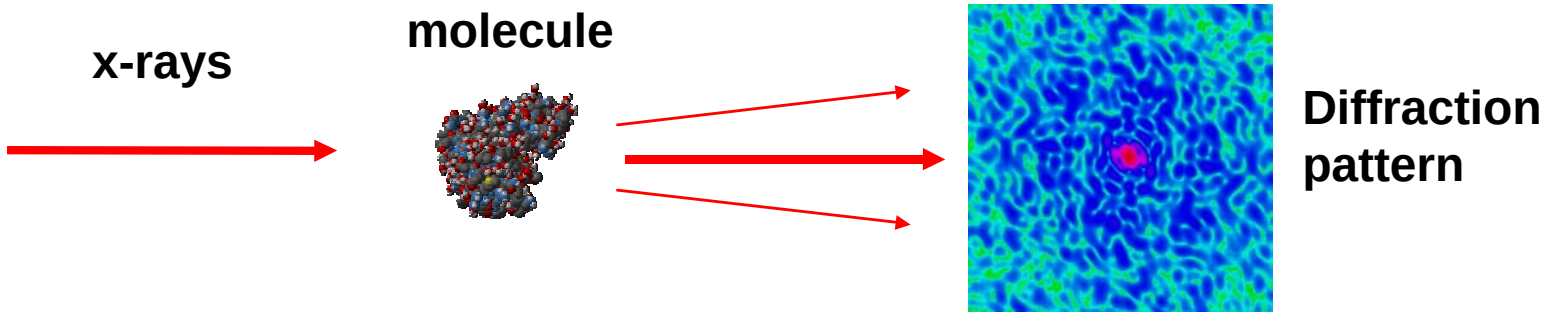

Several important questions remain

- **What x-ray fluence is required versus resolution and sample size? (Huldt, Szoke and Hajdu 2003)**
- **How many views are needed for 3D structure?**
- **Development XFEL optics**
  - **focusing**
  - **pulse compression**
  - **detector**
- **How short must the pulses be?**

We have developed a hydrodynamic model of sample damage to address pulse length question.

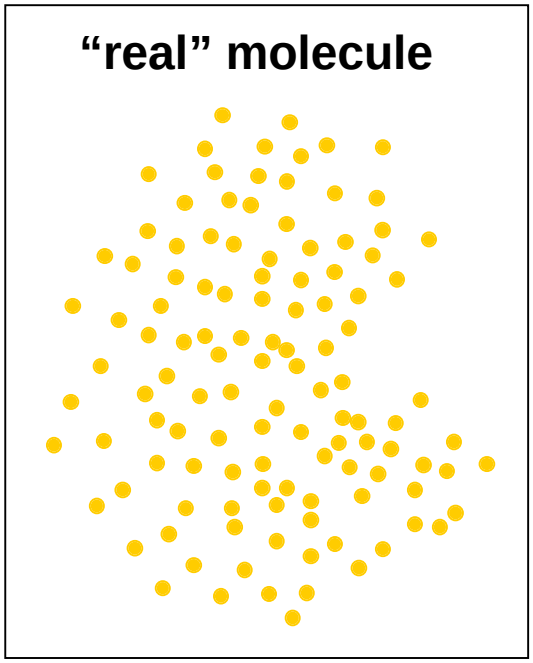

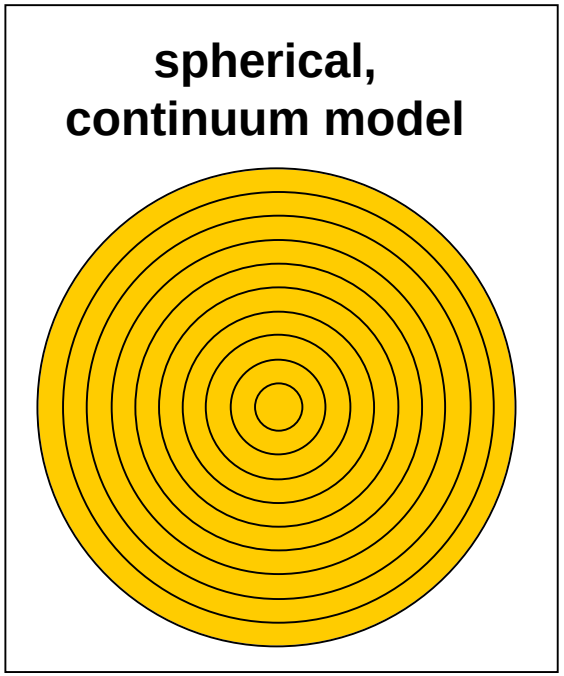

- **The hydro model does not treat early-time atomic motions as accurately as molecular dynamics (Neutze et al 2000, Jurek et al, 2003)**
- **However, it enables the inclusion of more physics, is much faster, and can treat larger molecules.**

First consider case of pure Coulomb explosion

- X-ray photo-ionization ejects electrons from the sample
- Explosive motion is caused by repulsion of the ions.

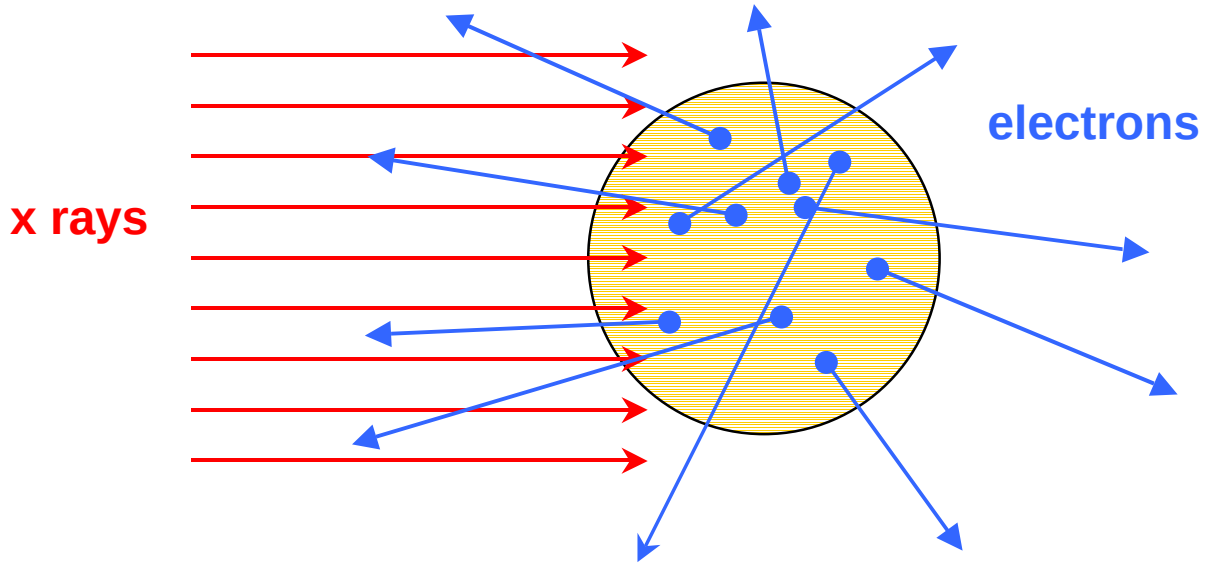

We have found an analytic solution to pure Coulomb model

Assume instantaneous ionization at t = 0.

$$t = \left(\frac{2\pi}{3} d\right)^{1/2} \frac{R^3}{Q} \frac{1}{r_o} \int_{r_o}^{r} \frac{x^{1/2} dr}{(x - r_o)^{1/2}}$$

Q=charge
R=molecule radius
d = density

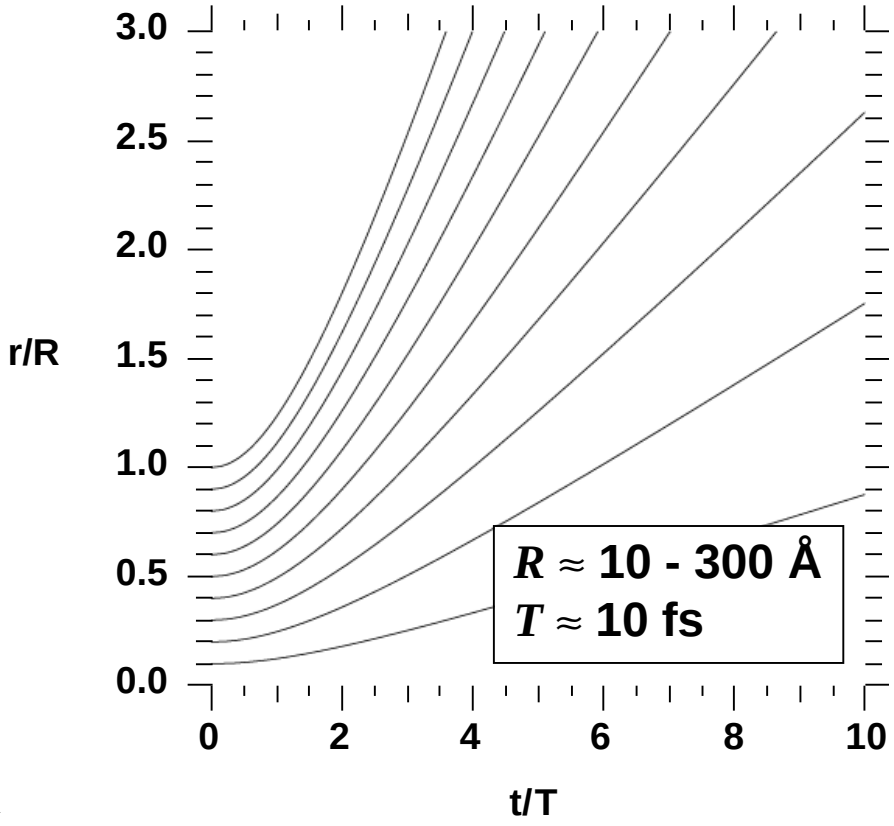

- Motion is self-similar
- Analytic solution is useful for scaling and to check numerical calculations.

Now consider a more complete numerical model

- Finite duration x-ray pulse.
- Time dependent photo and Auger ionization.
- Trapped electrons:

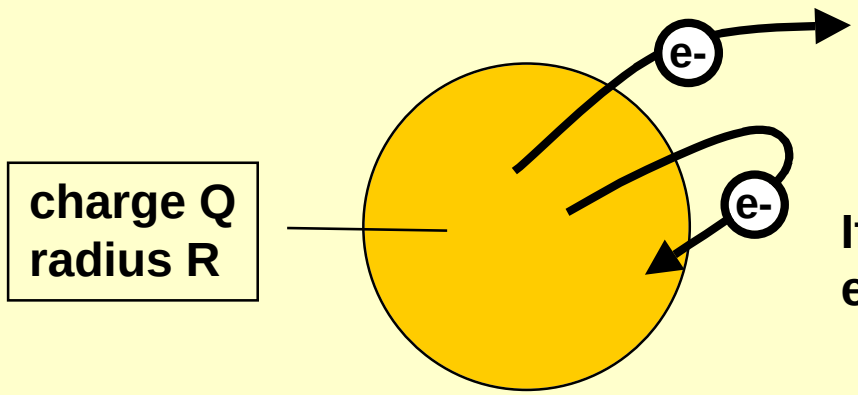

electron escapes if

$$E > \frac{3eQ}{2R}$$

If energy is smaller, electron is trapped

- Determine spatial distribution of trapped electrons by a balance between pressure and electrostatic forces
- Calculate secondary collisional ionization using time and space dependent rate equations

Numerical results for “standard model”

- **photon energy = 12 keV**
- **pulse length = 20 fs, flat-top profile.**
- **Fluence = 3×10^{12} photons/(100 nm^2)**
- **R = 60 Å**

The trapped electrons shield the core of the molecule, forming 2-layer configuration

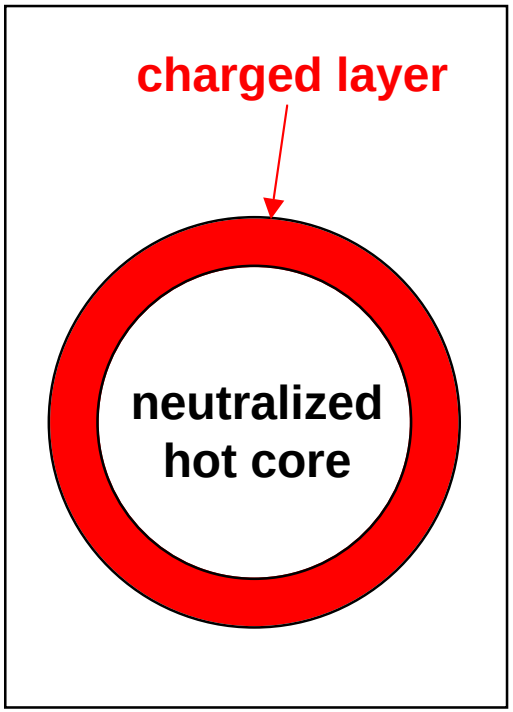

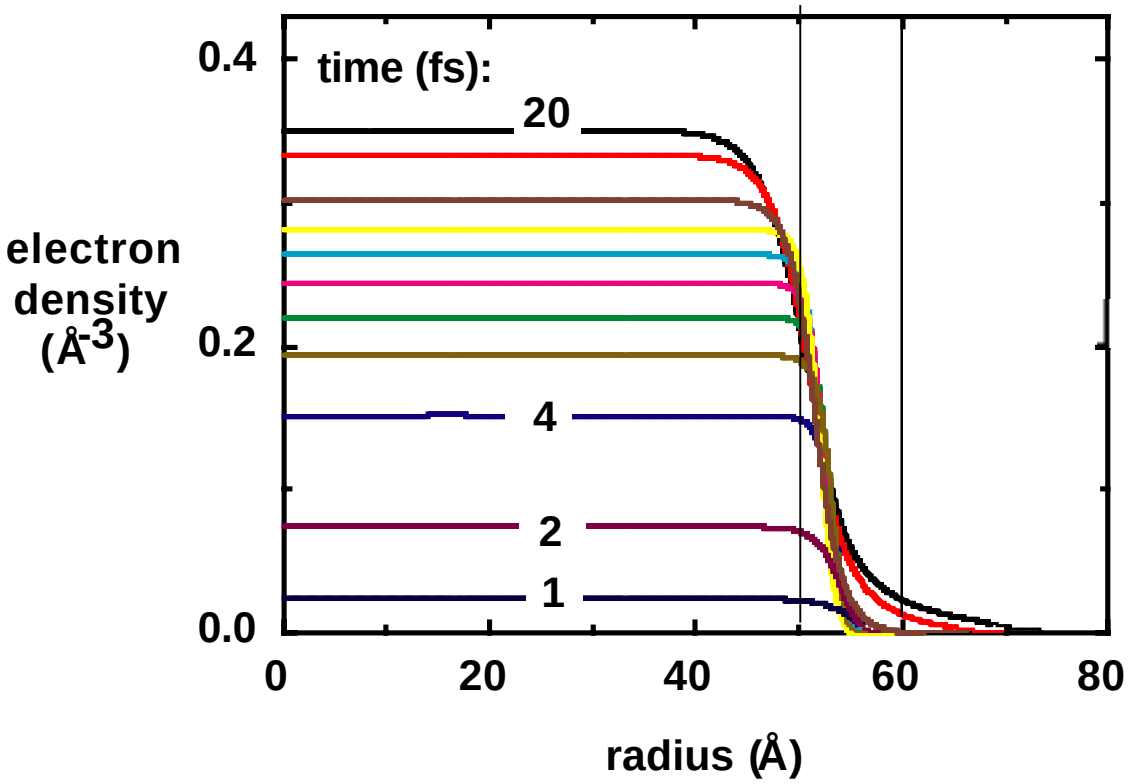

similar to Debye shielding, but on a molecular scale

Complete model shows faster expansion of outer region, but slower expansion of inner core.

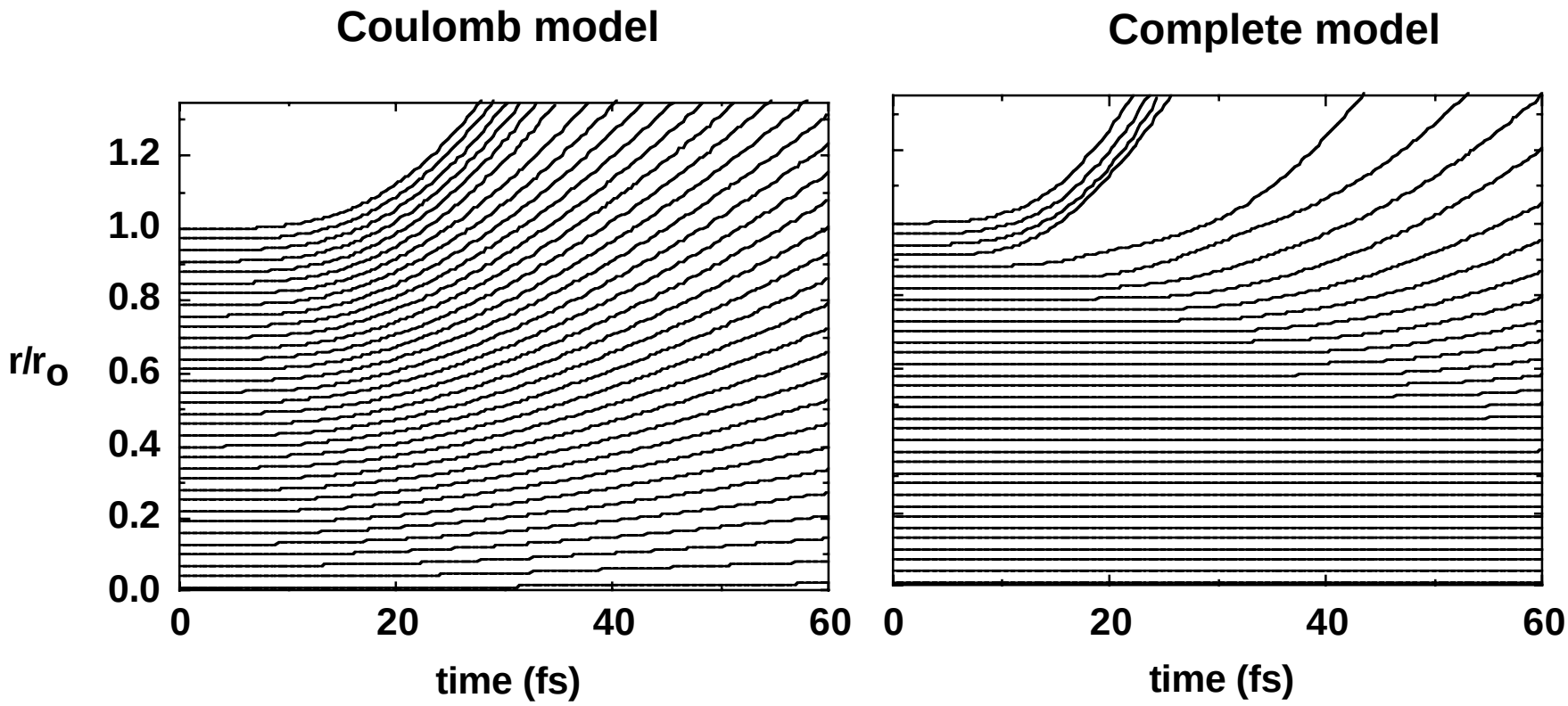

Complete model shows rapid ionization

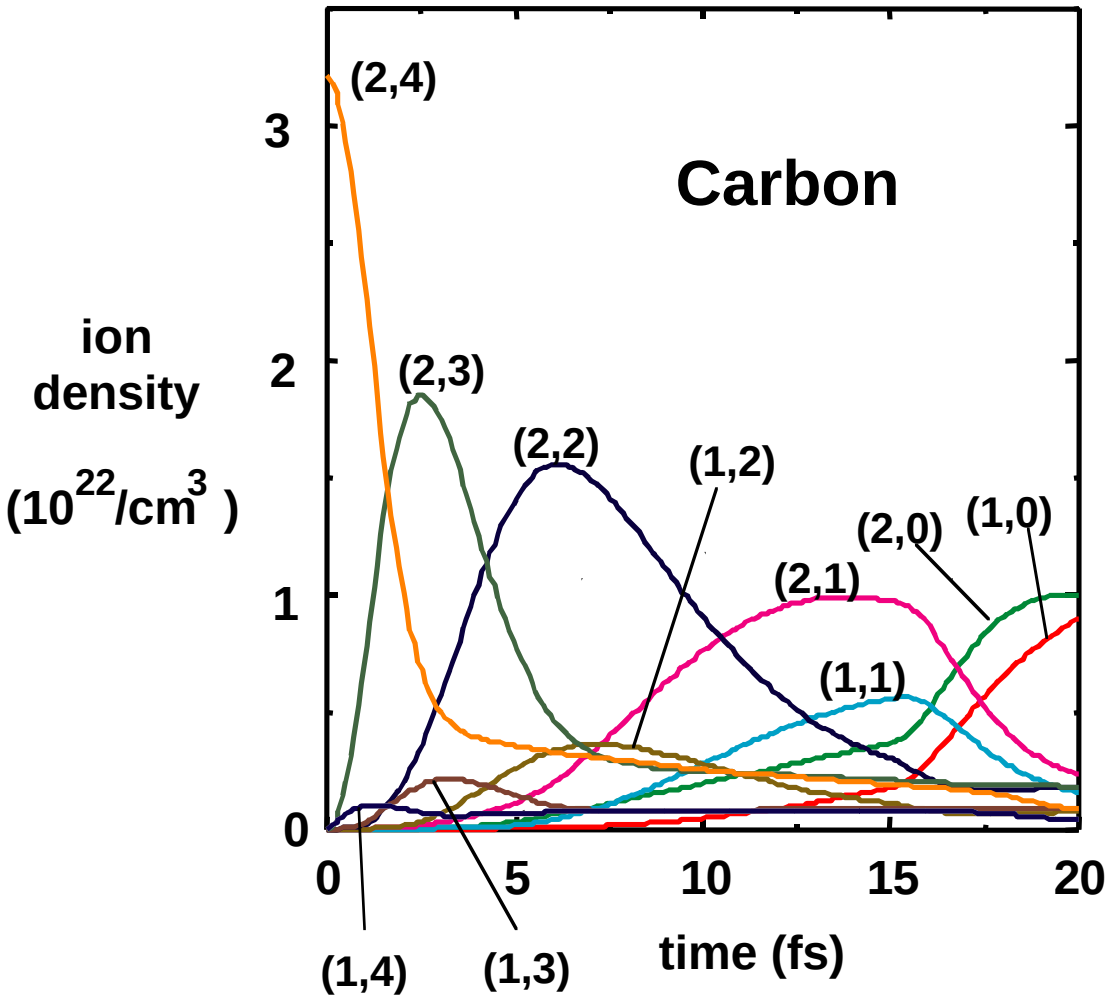

(k,l) =(# K-shell, # L-shell) electrons

- photo-ionization initiates a cascade.
- collisional ionization very quickly dominates.
- By 10 fs, carbon is stripped of 3 electrons.

We have used hydro model to perform a large parameter study vs. molecule size and x-ray flux

- **Results**
  - **atomic motion**
  - **ionization**

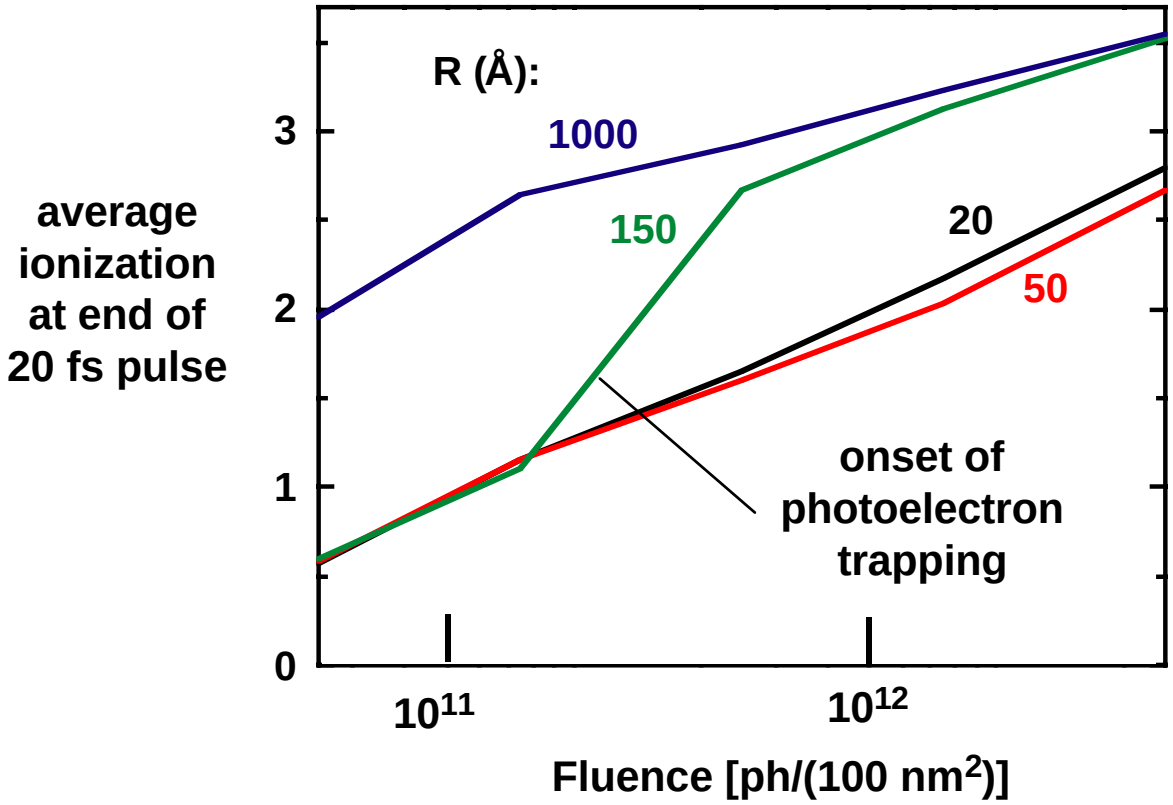

A molecule tamper might extend the allowable pulse length

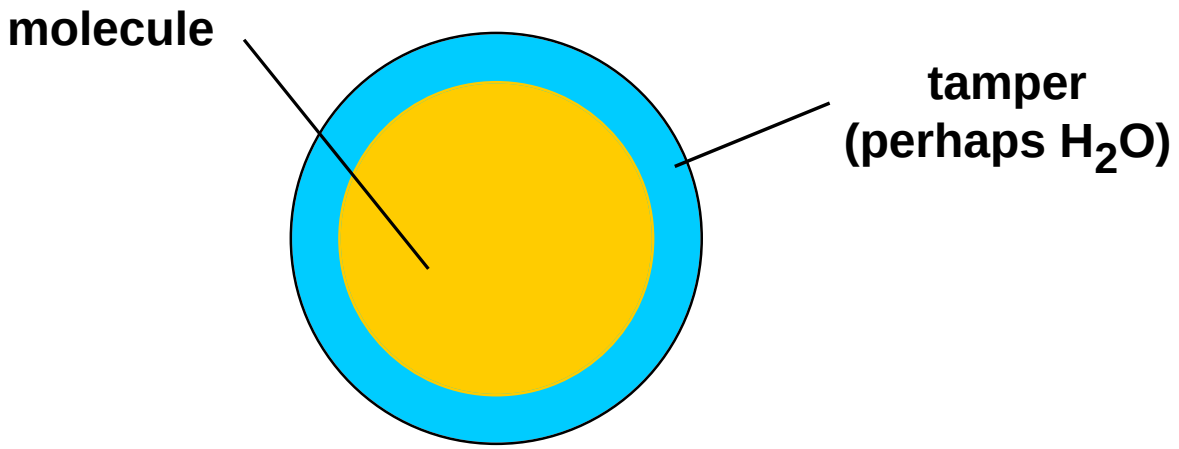

- Tamper holds back motion of the inner molecule ("inertial confinement") and provides extra electrons that neutralize the molecule.

- Tamper will also generate noise in the image, that must be overcome.

- Movie of explosion with and without tamper!!

Movie

Without Tamper

t= 0.0fs

Fluence = $3x10^{12}$
Radius = 20 Å
Tamper = 10 Å, H_2O
Pulse length = 20 fs

Tracer atoms

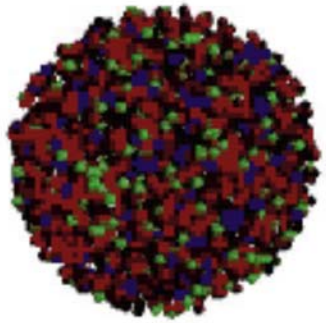

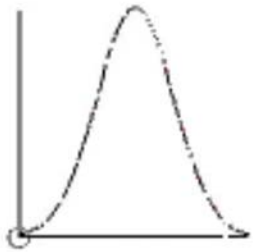

Results on x-ray interaction with biomolecules

- **Electron trapping and collisional ionization are very important.**
- **To limit the ionization to less than 15% we need pulses < 4 fs.**
- **It may be possible to extract atomic positions from diffraction images even if the atoms are partially ionized.**
  - **Since the atomic motion occurs on a ~10 fs timescale this would allow longer pulses.**

Overview of ultra-high intensity interactions

- **Non-linear effects**

  R. Freeman, Bucksbaum, Huber, Adams, Kornberg, et al.

  - Creation of double core holes by rapid photoionization
  - Parametric and harmonic processes
  - Multi-photon atomic transitions

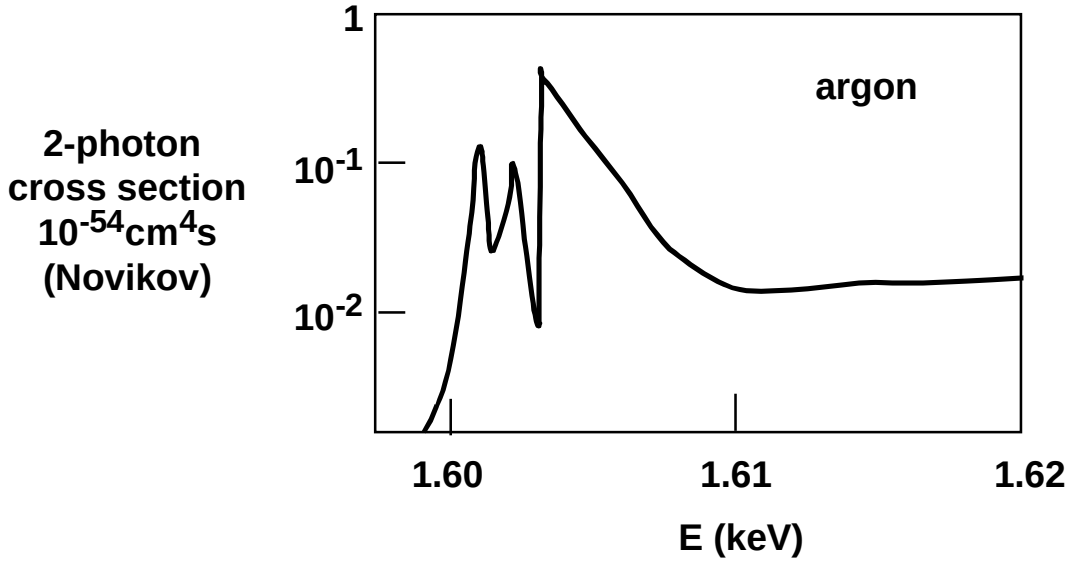

- **Relativistic effects** occur at $I\lambda^2 > 10^{26}$ (W/cm^2) Å^2
  - This requires 1000 times better focusing than currently possible.
  - It is probably best to pursue this with visible lasers for now !!

Experiments are being planned for intermediate facilities before XFELs are completed

- **Existing laser-produced soft x-ray lasers**
- **Short-pulse-photon-source (SPPS) at Stanford**
- **Compton scattering sources**
- **Tesla Test Facility (TTF) at Hamburg (soft x-ray free electron laser)**

We plan an experiment to study coulomb explosions with a soft XFEL

w. H. Chapman et al

Explosion of spherical particles will be measured by x-ray Mie scattering

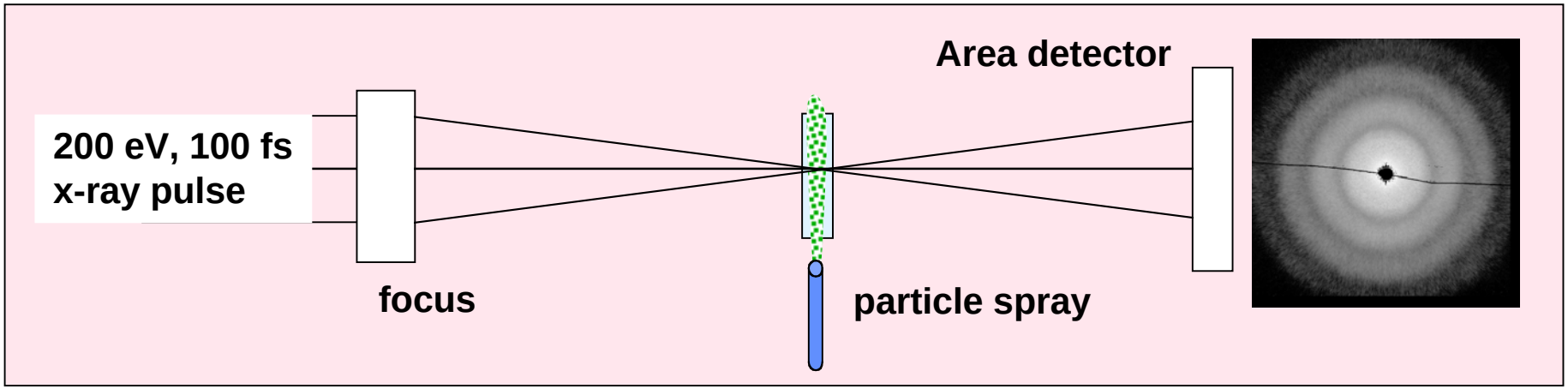

- We expect to be able to measure a 20% change in particle radius.
- We can also split and delay the x-ray pulse to generate flash images at various times.
- Experiment to be done in 2005 at TTF-2 at DESY.

Conclusions on X-Ray Material Interactions

- **The advent of XFELs will open an exciting new field of ultra-short, high intensity, x-ray material interaction.**
- **Several theoretical and simulation methods must be applied.**
- **Design of XFEL optics require a careful choice of composition, placement, and configuration to avoid damage.**
- **Single molecule imaging may revolutionize structural biology. X-ray pulses must be very short (sub-10 fs).**
- **Experiments on intermediate facilities will provide a glimpse of the future with XFELs.**

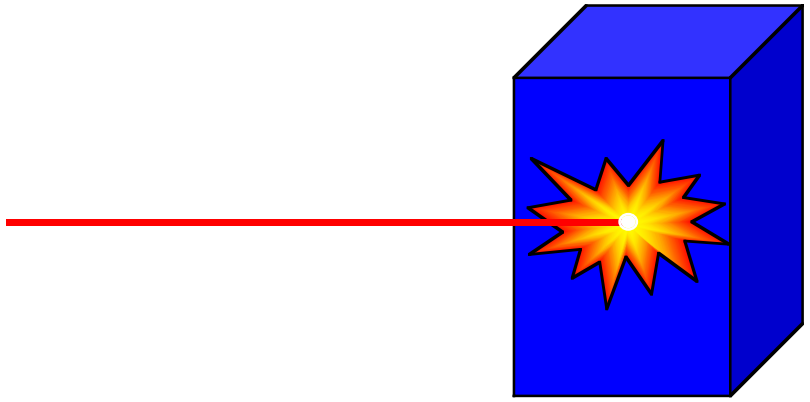

X-ray imaging applications of 3rd generation synchrotron sources in material science

Lucia Mancini

Sincrotrone Trieste - Italy

Outline

- X-ray imaging at a 3rd generation SR facility
- The applied imaging techniques
- Experimental results
- Conclusions and perspectives

X-ray imaging at a 3rd generation SR facility

- high energy photons and high flux
  - **heavy** and/or **bulky samples** in transmission geometry
  - **tunability** in a large energy range
  - **short** exposure times
- small angular source size and big source-to-sample distance
  - use of **natural coherence properties** of the beam

The **SYRMEP beamline**:

- Source size (h x v) **1100 m x 100 m**
- Source-to-sample distance: **D 24 m**
- Beam size at sample (h x v) **150 mm x 6 mm**
- Energy range: **8 ÷ 35 keV**, Bandwidth: **$\Delta E/E$ 2x10^{-3}**

SR X-ray imaging studies in material science

***In-situ* and *ex-situ* experiments in a large range of materials:**

- growth processes
- mechanical and thermal treatments
- phase transitions ….

The aim

to investigate the relationship between microstructural and physical properties

The applied imaging techniques

X-Ray Diffraction Topography (XRT)

- Based on **Bragg diffraction, defect** analysis in **single-crystals:**
  - images of singularities through **local inhomogeneities in reflectivity**
  - observation of long-range strain-field around defects ($\Delta d/d < 10^{-7}$)
  - **complementary** to TEM: poorer spatial resolution (few μm), larger observed volume ($\sim$ 0.1-1 cm x few cm^2), higher strain sensitivity.

$2\, d_h \sin \theta_B = \lambda$

Absorption and Phase Sensitive (PS) Radiography

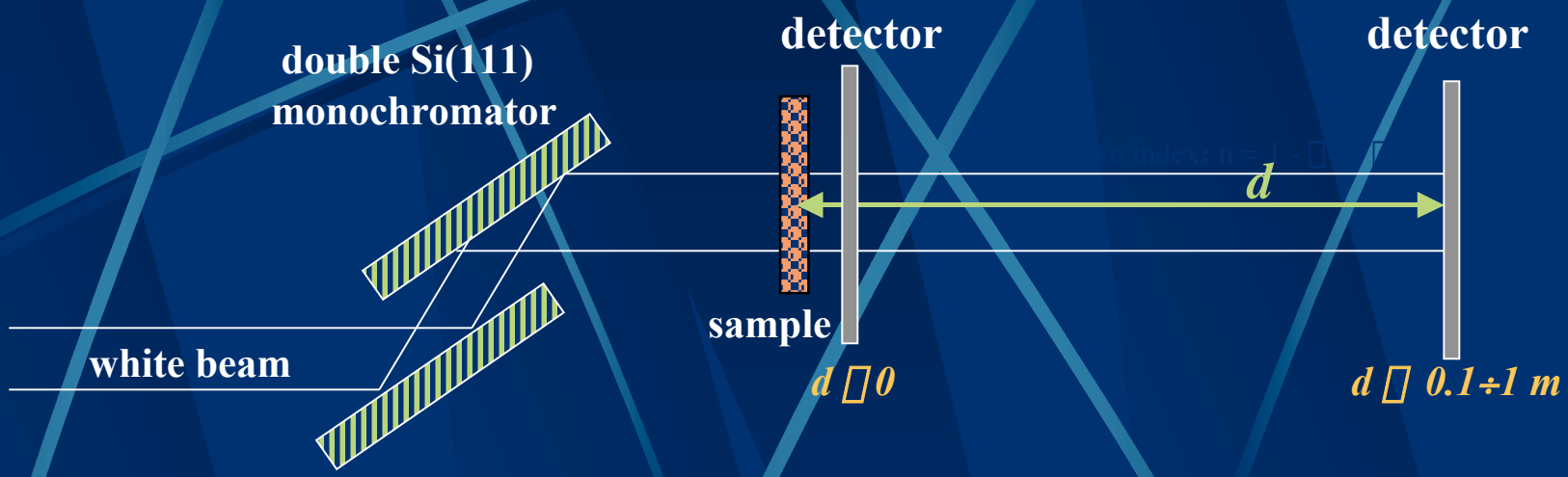

$(\Delta I/I)_{abs} = e^{c\,\mu\mu} - 1$

$\mu\mu = 2\pi\, c\, \mu\mu / \lambda$

$\mathbf{n} = 1 - \delta - i\beta$: refraction index

$\mu = 4\pi\, \mu\mu / \lambda$: linear absorption coeff.

c : object size // to beam direction

r « ***a*** ⇒ *edge detection regime*

r ≈ ***a*** ⇒ *holographic regime*

r » ***a*** ⇒ *Fraunhofer diffraction*

a : object size ⊥ to beam direction

$\boldsymbol{r} = (\lambda d)^{1/2}$: first Fresnel zone radius

Phase vs. amplitude effects with hard X-rays

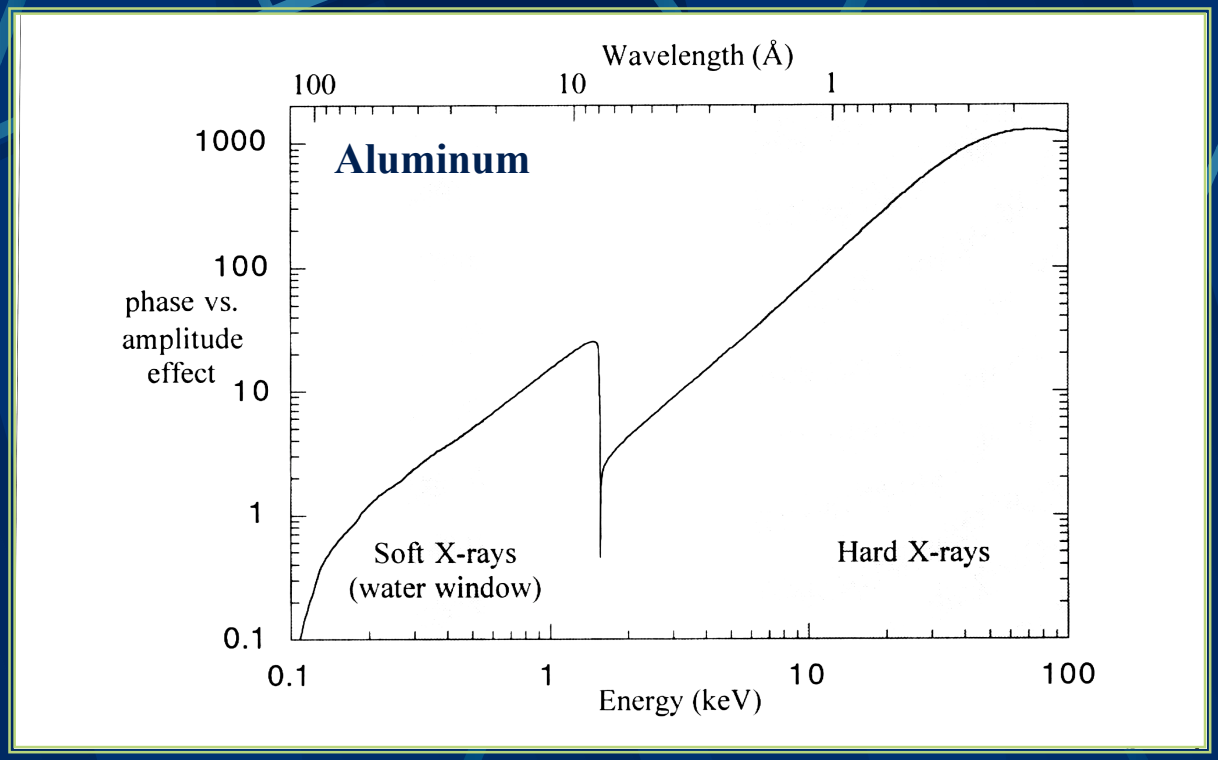

- Analysis of **materials**
  - **with weak absorption** with respect to hard X-rays
  - **producing significant variations of** X-rays **optical path**

Absorption and PS Computed □-Tomography (□□CT)

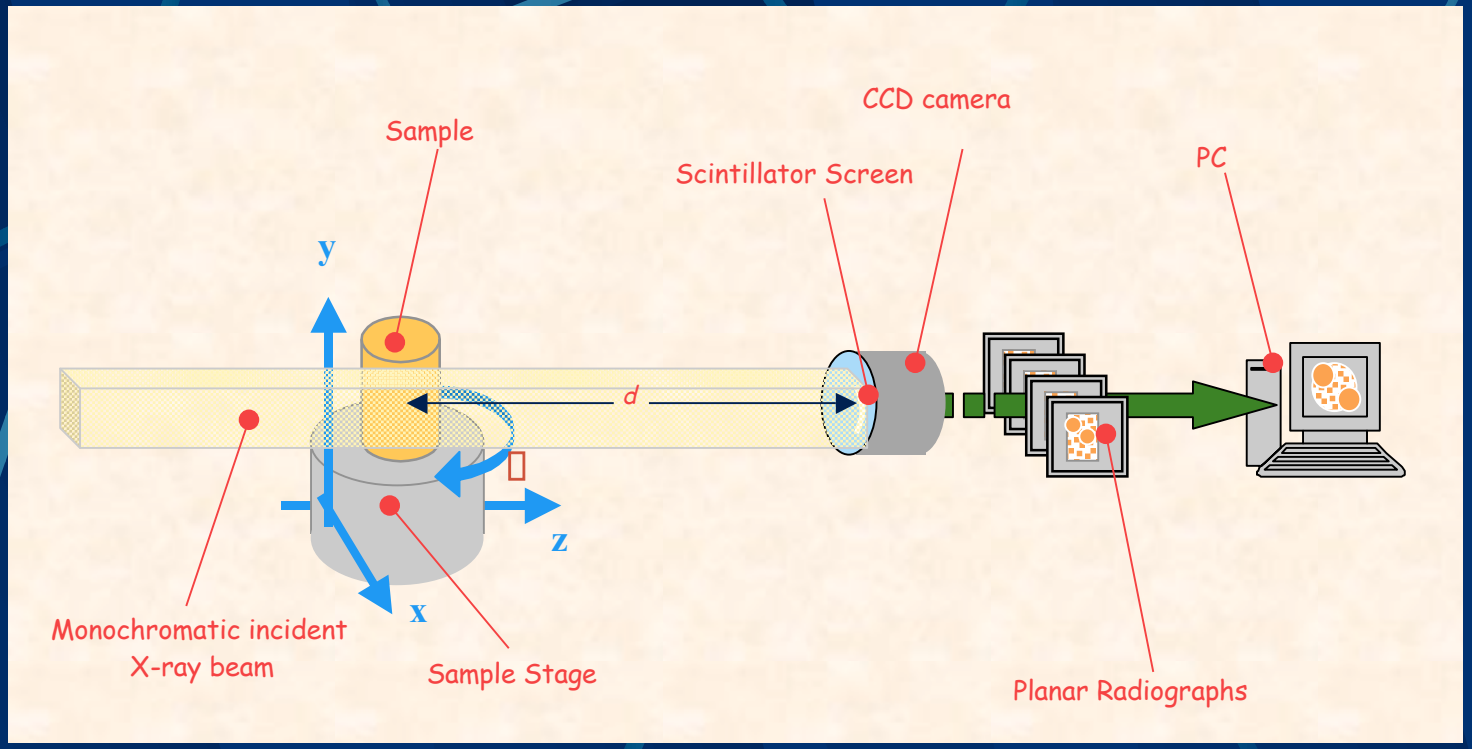

CCD camera: 2048x2048 pixels^2, pixel size: 14 μm, FOV: 28x28 mm^2

- **Precious** for investigation of **internal features** **without** sample **sectioning**:
  - in many cases the **sectioning procedure** modifies the structures under analysis
  - the sample can be after **studied by other** experimental **techniques**,
  - or submitted to several **treatments** (mechanical, thermal, etc...)

Vertical source size estimation from PSR of a nylon wire

Sample: Nylon wire (120 μm Ø)

E = 10 keV

Refraction index: = 2.55×10^{-6}, = 2.72×10^{-9}

d = 1 m

D = 24 m

Detector: 1 m resolution film

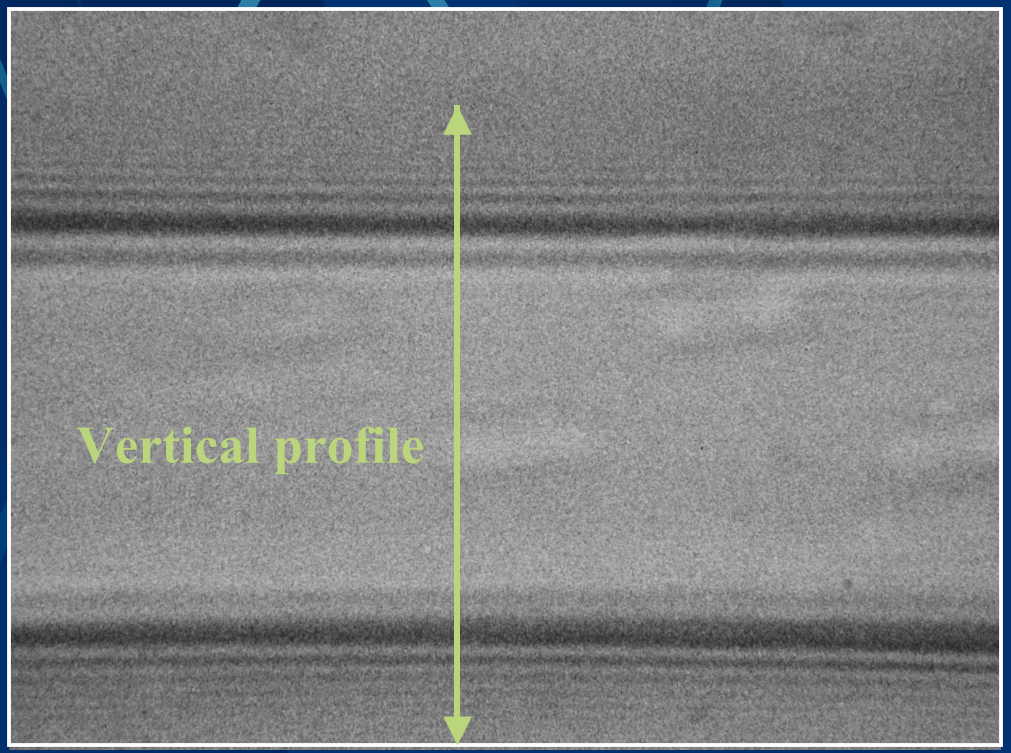

L. Mancini, F. Montanari, G. Tromba

Experimental and simulated profiles for different □ values

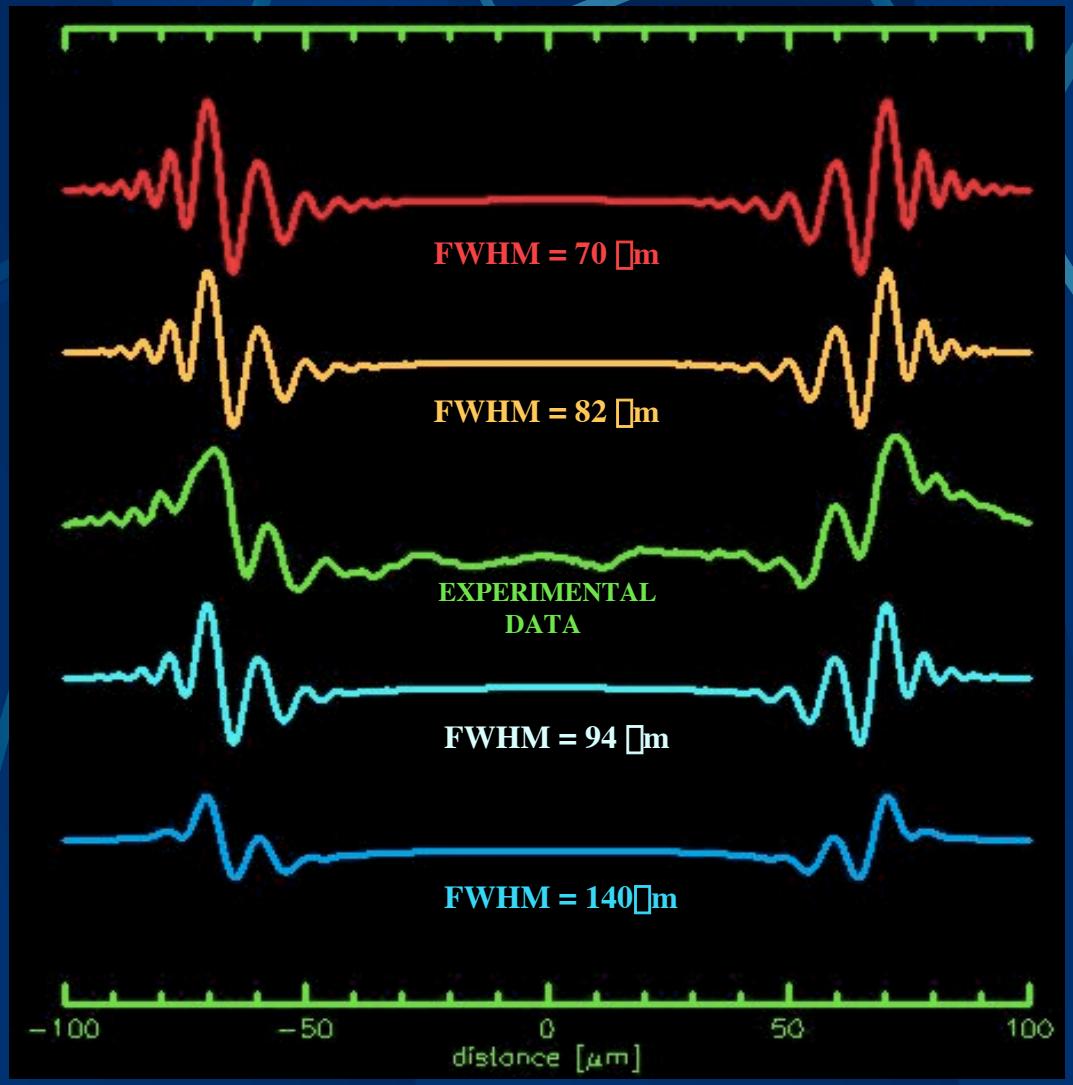

Nylon wire (120 □m Ø)
E = 10 keV
d = 1 m

□ < □ 100 □m

Results

- Possibility to work at **big sample-to-detector distances: $d > 1$ m**
- **Spatial resolution $\Delta = \lambda d / D < 1$ μm up to $d = 0.3$ m**
  4 μm at $d = 1$ m
- **High transverse coherence of the beam: $L_c = \lambda D/(2\pi) \approx 10$ μm**

Experimental Results

Fraunhofer ISC Institut Silicatforschung

elettra

Archeological glasses

H. Roemich, S. Gerlach*, E. López[1] F. Zanini, L. Mancini, L. Rigon, G. Tromba*

- Glasses develop corrosion layers during exposure to different environmental conditions. This process changes the surface morphology and its chemical composition.
- Corrosion layers may reach a thickness of up to several hundred μm. In extreme cases the fragment as such is endangered. These pieces are extremely fragile and require special conservation treatments.
- The effectiveness of polymers used for glass consolidation depends on the penetration of organic material in porous inorganic substrate. The detection of polymers in corroded layers: a special problem in conservation research.
- Recognized methods of analysis are destructive, requiring embedding in a polymer to prepare cross sections (SEM) or sputtering (depth profiles). Need for a non-destructive technique.
- EC project SMT-CT98-2261: a desktop X-ray μ-CT scanner was used, providing promising results for heavily corroded samples. It failed for polymer detection.

**ISC, Bronnbach-Branch, Germany, [1]Polytechnical University of Valencia, Spain*

Fraunhofer Institut Silicatforschung

elettra

Original glass covered by a thick corrosion layer

Middle Ages, excavated near Ulm (Germany)

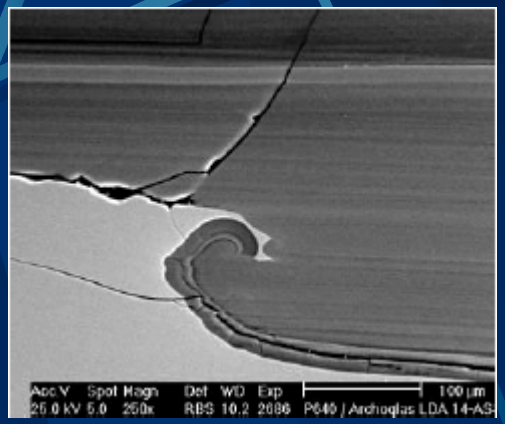

SEM cross section

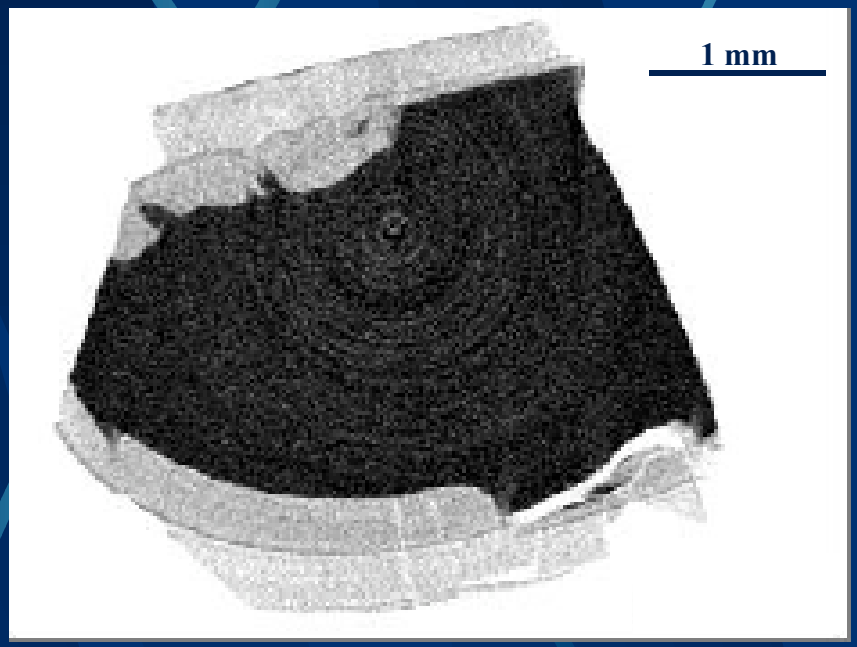

Laboratory □□CT

Corrosion layers *(from 100 up to 400 □m thick)*: visualized with SEM and laboratory □□CT.

Laminated structure with single laminae (< 1□m thick): visible with SEM, but not with laboratory □□CT.

Volume rendering and Stack of the whole studied sample region

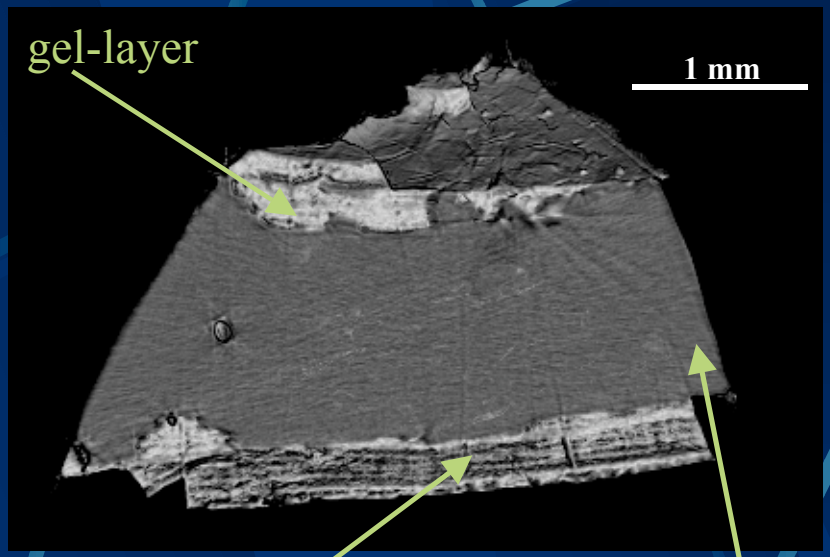

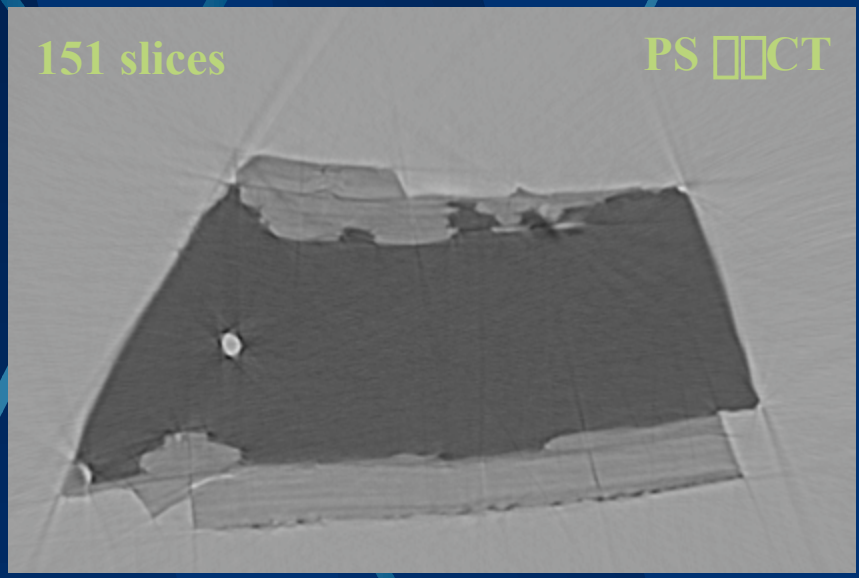

E = 25 keV, ***d*** **= 66 cm**

PS CT:

- low contrast between silica-rich gel-layer and corrosion crust
- laminated corrosion structure visible in both layers
- the corrosion layer not homogeneous in thickness

Sample: LDA14

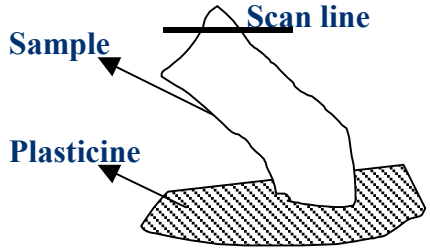

S. Gerlach et al., in press on the Elettra Highlights 2003.

Fraunhofer Institut Silicatforschung

elettra

Original waterlogged glass, completely corroded

Fragment provided by the Museum of London

Stack of 130 slices

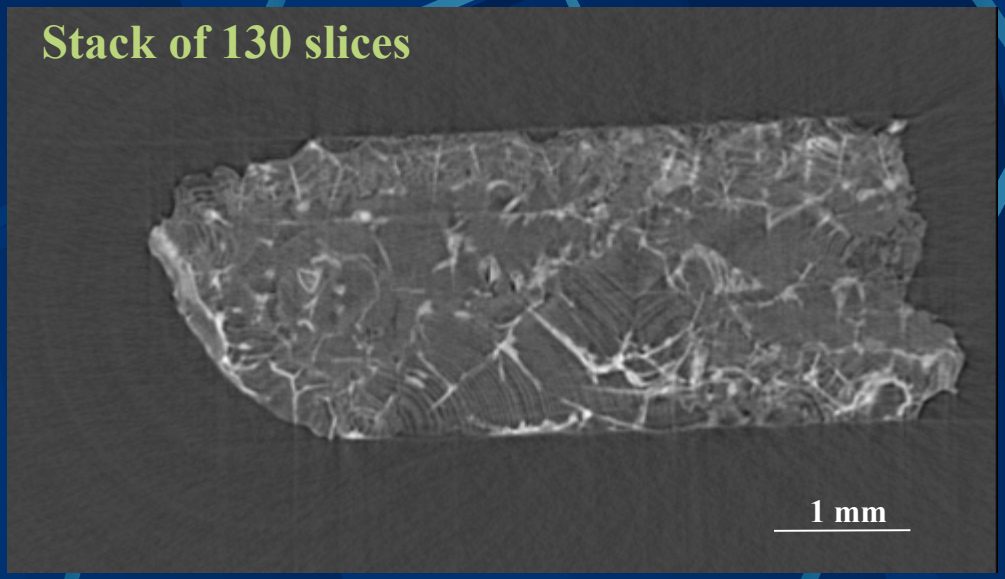

E = 25 keV **d = 66 cm**

Slice 207

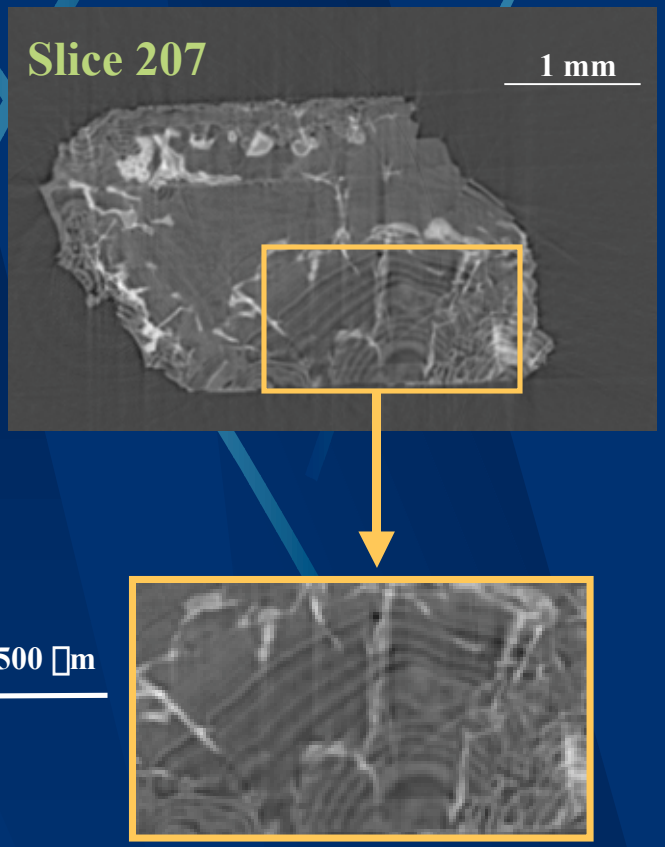

It is possible to visualize:

- the gel-layer channels
- the lamellar structure inside the corroded glass

Fraunhofer ISC Institut Silicatforschung

elettra

Original waterlogged glass, completely corroded

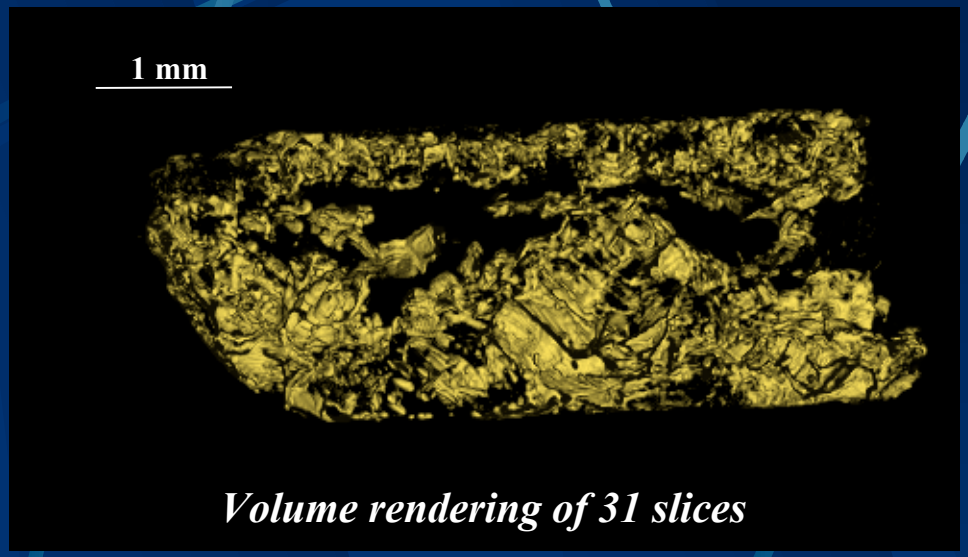

Volume rendering of 31 slices

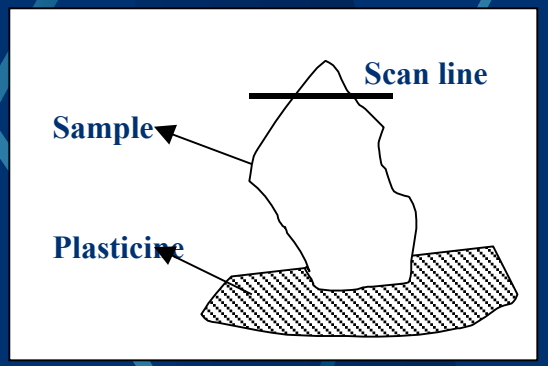

E = 25 keV, *d* = 66 cm

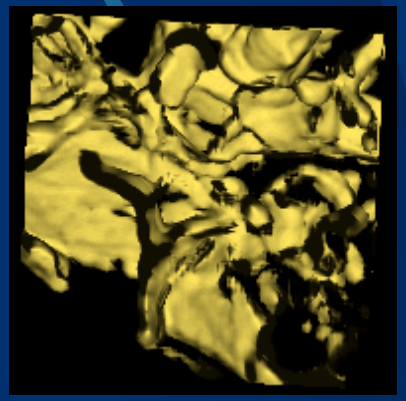

Cine rendering of channels (9.0 x 9.0 x 0.2) mm³

Fraunhofer Institut Silicatforschung

elettra

Model glass covered by a thick polymeric layer

Bulk polymers (acrylates) are used as consolidant materials

E = 25 keV
***d* = 66 cm**
Acquisition time: 3h

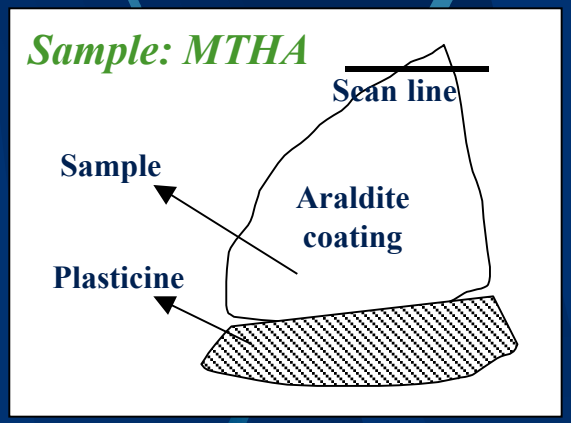

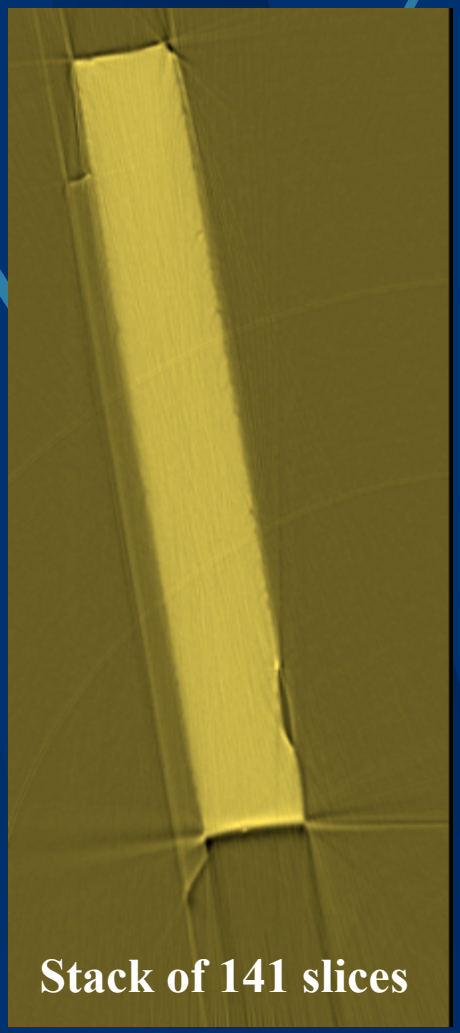

The 200 μm thick layer of Araldite is well visible.
Since there is no corrosion on the model glass, nothing more is detected.

Fraunhofer ISC Institut Silicatforschung

elettra

Concluding remarks

- The potential of PS □□CT for study of corrosion and polymeric layers thicker than 20 □m was demonstrated on original and model glasses.

- The protection of cultural heritage as an extremely promising new application field for PS □-CT. This could allow to visualize the 3D structure and to detect conservation materials non-destructively on glass fragments in their original state.

- Variations of the glass composition and simulation of well-defined corrosion layers can be used to obtain a variety of test samples. The development of conservation materials may gain new input, if a new non-destructive method is available to detect the effectiveness of treatments on these samples.

Engineering science: polymeric foams

Polyurethane (PU) foams:

- novel systems for energy absorption required in many applications such as packaging, helmets and other protective goods in the human, industrial and transport fields.

- Aim: to develop foam systems to improve the specific energy absorption of the traditional PS foams and to modify absorption path according to different load conditions. A non destructive technique important to follow the system behavior during loading.

PU foam structure

L. Sorrentino, L. Iannace*, L. Mancini, F. Montanari, F. Zanini, G. Tromba*

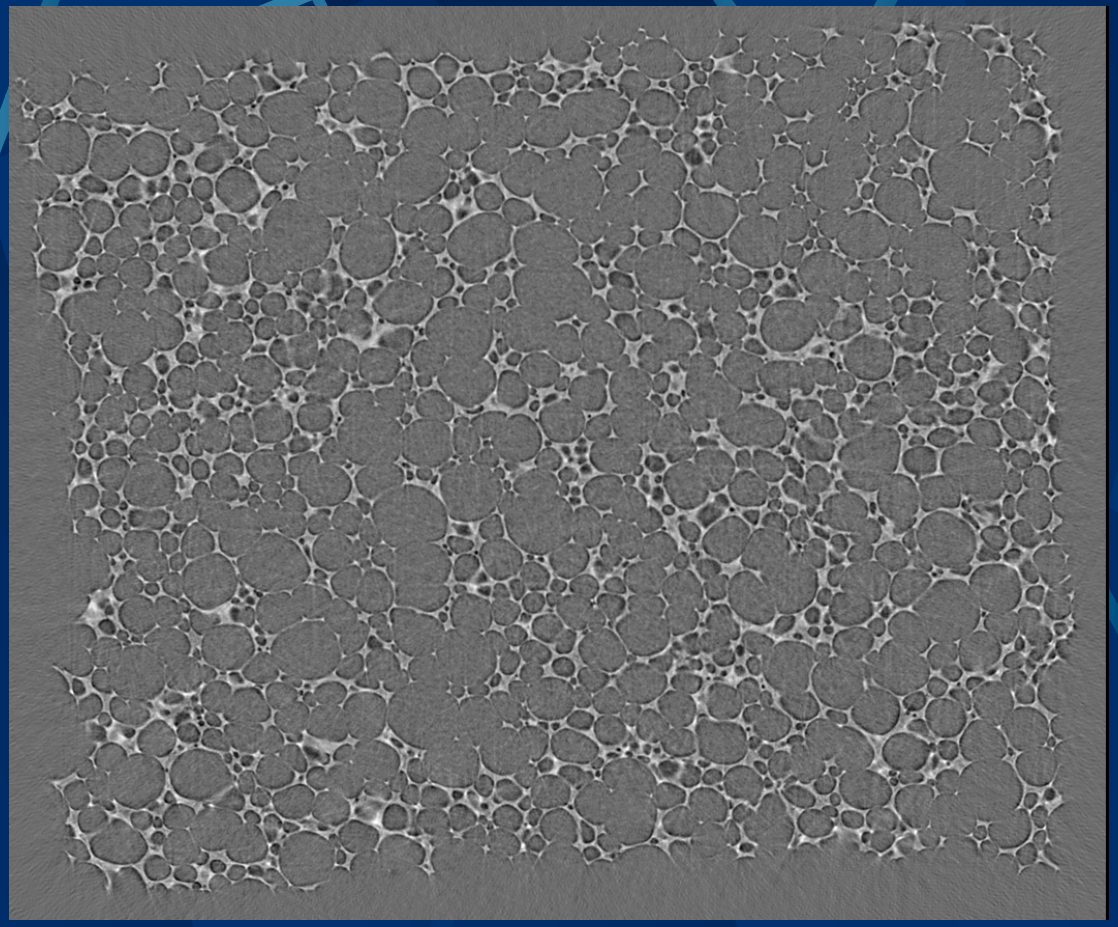

1 mm

Reconstructed stack of 100 slices

E = 12 keV

***d* = 32.5 cm**

**DIMP- Università di Napoli (Italy)*

Volume rendering and animation

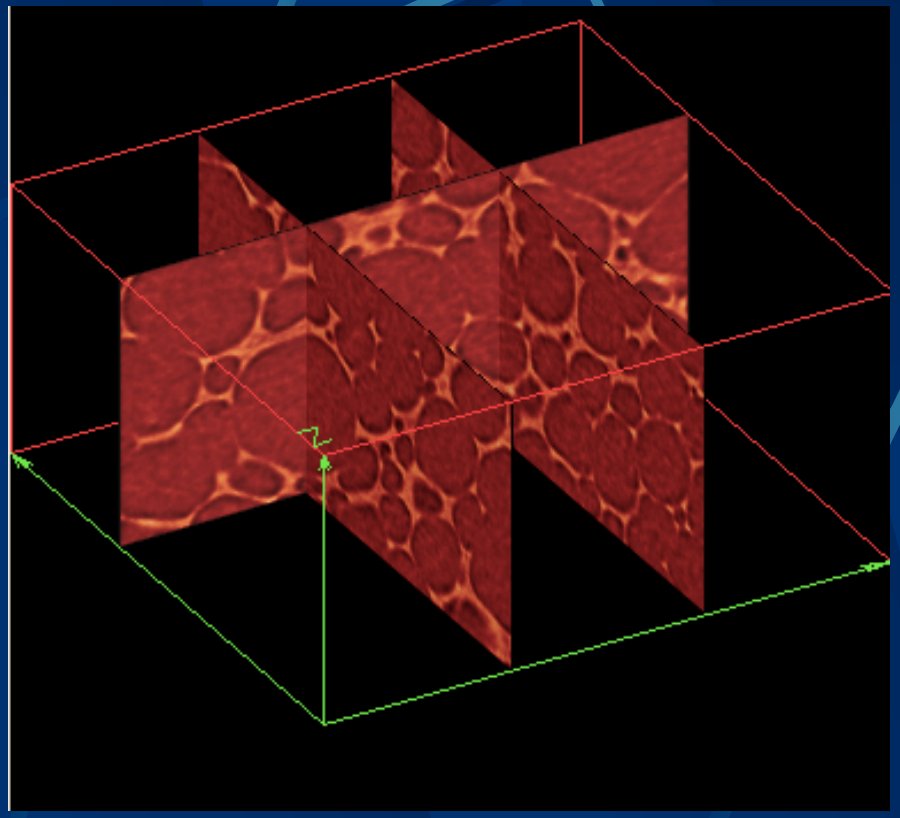

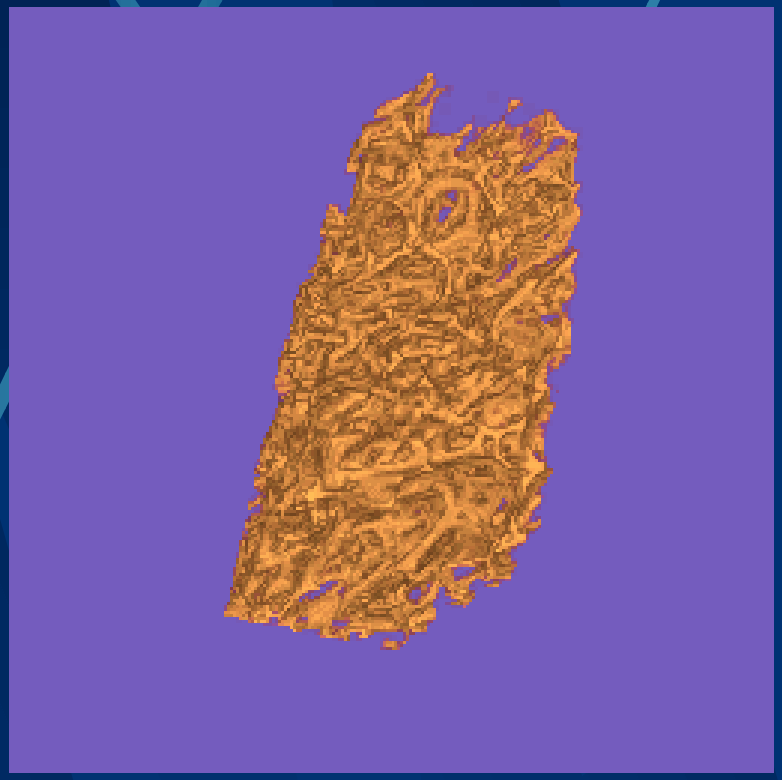

Virtual cut of the sample

(3.2 x 3.0 x 1.4) mm^3

PU foam under compression

Strain direction ⊥ to the image plane

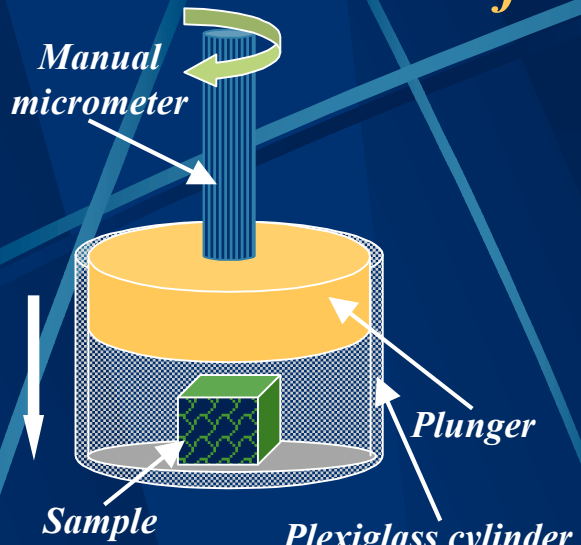

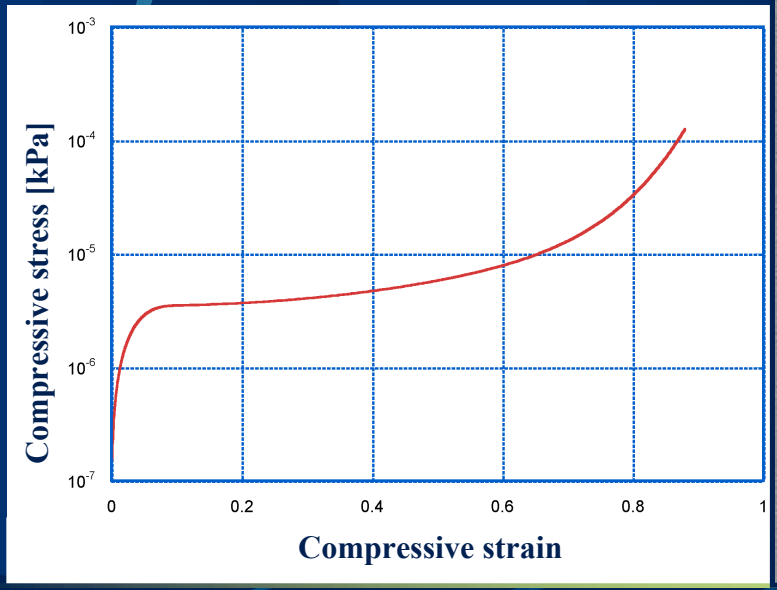

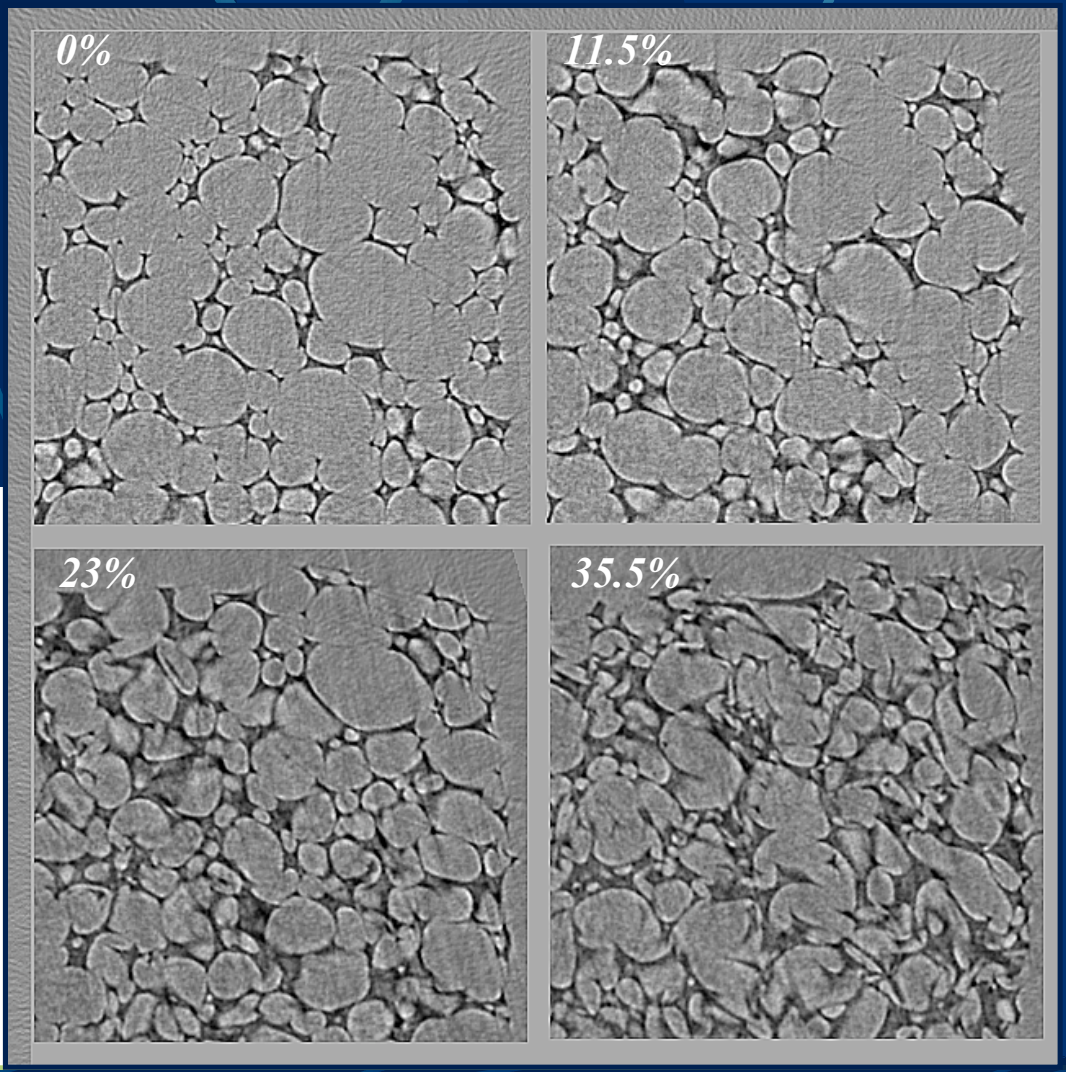

PU volume rendering as a function of strain

Strain direction ⊥ to the image plane

Strain 0%

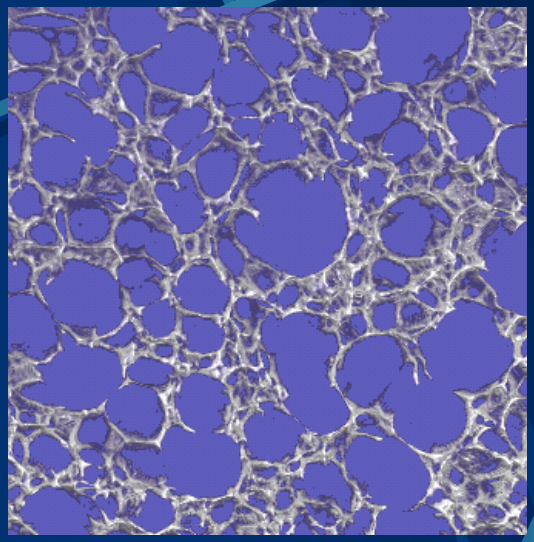

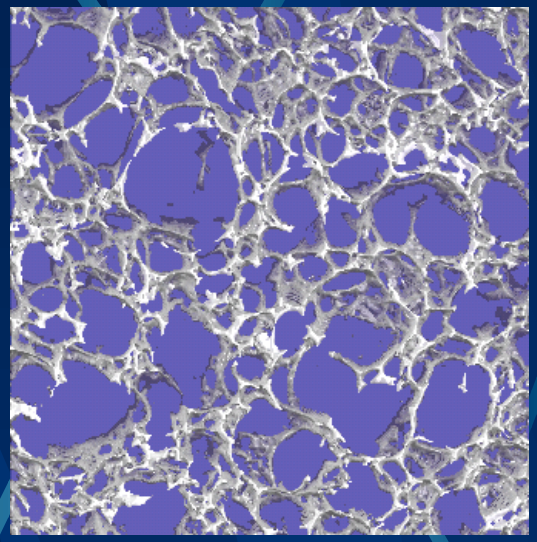

Strain 11.5%

Strain 23%

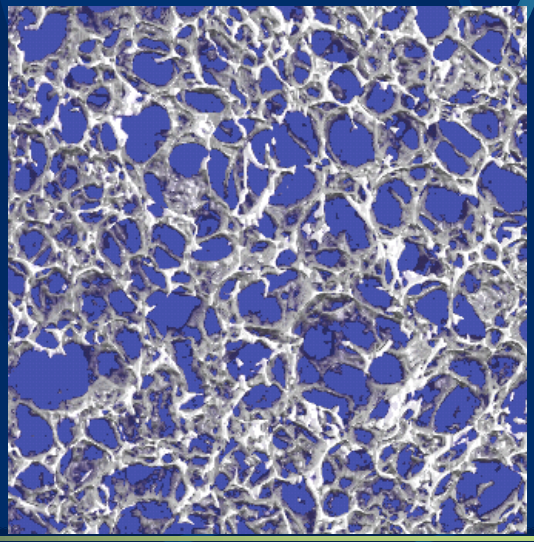

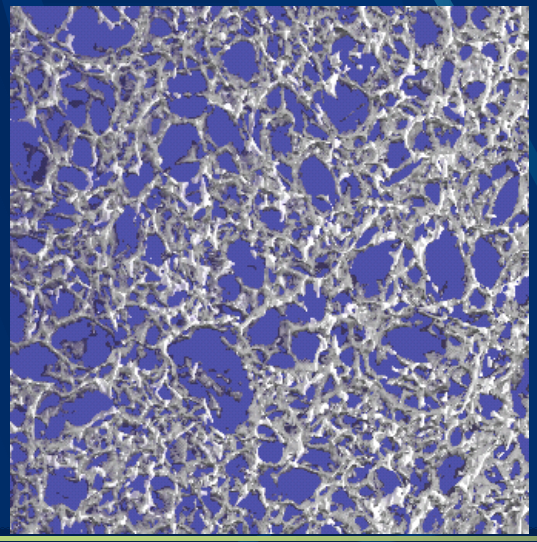

Strain 35.5%

E = 12 keV
***d* = 32.5 cm**

Images dimension:

(4.7 x 4.8 x 0.25) mm^3

PU volume rendering as a function of strain

Strain direction // to the image plane

Strain 0%

Strain 11.5%

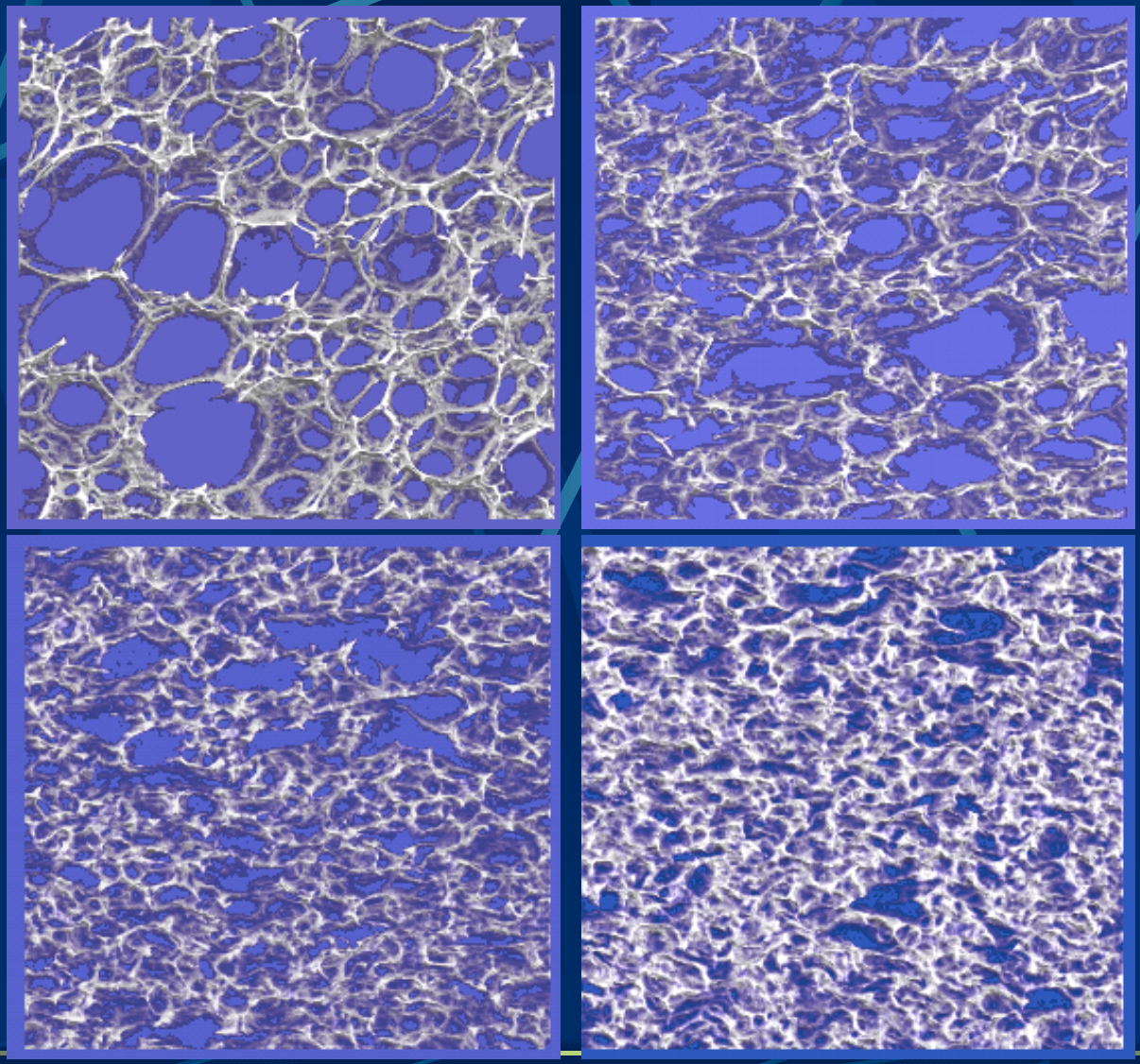

Images dimension:

(3.6 x 3.6 x 0.6) mm^3

Strain 23%

Strain 35.5%

E = 12 keV

***d* = 32.5 cm**

Strain direction

Concluding remarks

- The elastic properties of PU foams determined by composition, density and foam architecture.

- Numeric algorithms based on cells analysis under development. They will be applied to 3D reconstruction images obtained under different loading conditions to evaluate and simulate the elastic behavior of the structure.

FACOLTA' DI AGRARIA
UNIVERSITÀ DI FOGGIA

elettra

Industrial research: food products

P. M. Falcone*, M. A. Del Nobile*, F. Zanini, L. Mancini, G. Tromba, F. Montanari

- High moisture bakery products as starched based foams. To optimize the production process: use of mathematical models able to relate the porous structure to its mechanical properties need to determine experimentally the 3D structure of the product.

- PS X-ray -CT could be also used to investigate the relationships between roasted coffee beans microstructure and storage-related mass transport phenomena (mainly oxygen adsorption and CO_2 release).

- Few experimental methods available. Microscopy: a powerful tool for the investigation of structural changes in foods during and after processing. Not all histological methods for sample preparation suited for food sampling. Artifacts due to sample preparation quite common.

****Istituto Produzioni e Preparazioni Alimentari - Facoltà di Agraria - Università di Foggia - Italy***

FACOLTA' DI AGRARIA
UNIVERSITÀ DI FOGGIA

elettra

Optimization of d for the study of the bread structure

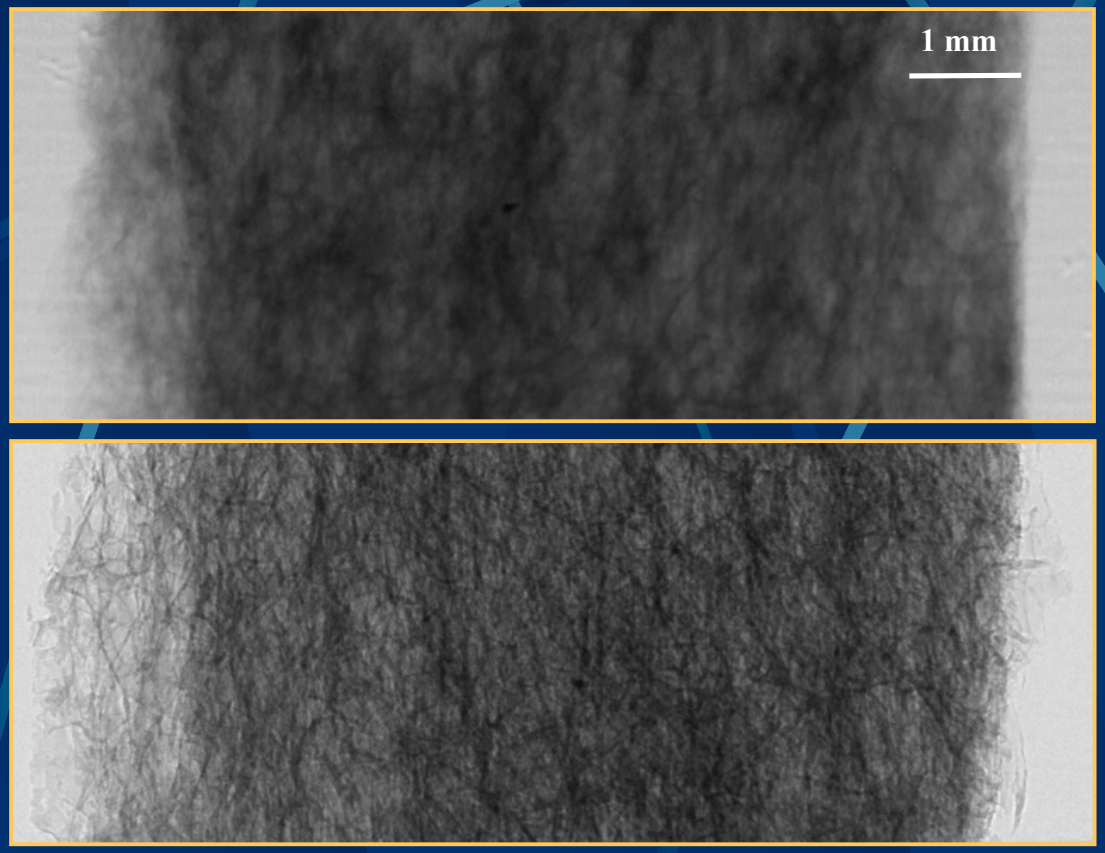

Absorption radiograph

***d* = 1.5 cm**

E = 12 keV

PSR

***d* = 20 cm**

Whitworth et al. (2000) used an X-ray CT scanner to image the internal structure of doughs after moulding non-invasively, but poor absorption contrast was a severe limitation in this study.

P. M. Falcone* et al., submitted to Journal of Food Science.

FACOLTA' DI AGRARIA
UNIVERSITÀ DI FOGGIA

elettra

Bread micro-structure

E = 12 keV
***d* = 20 cm**

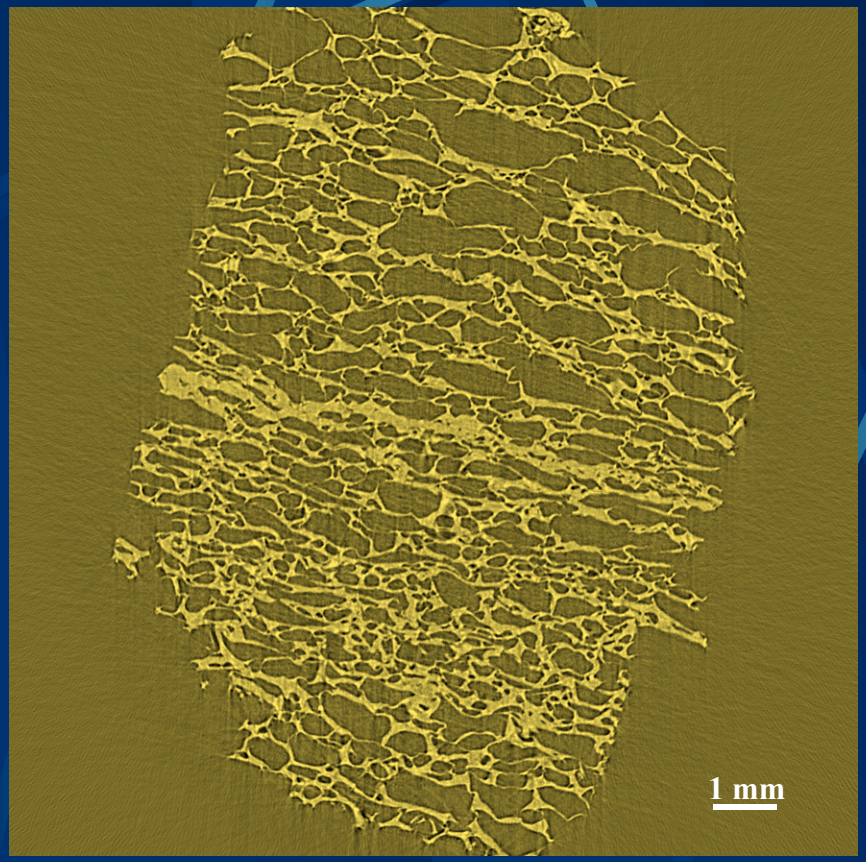

Reconstructed slice

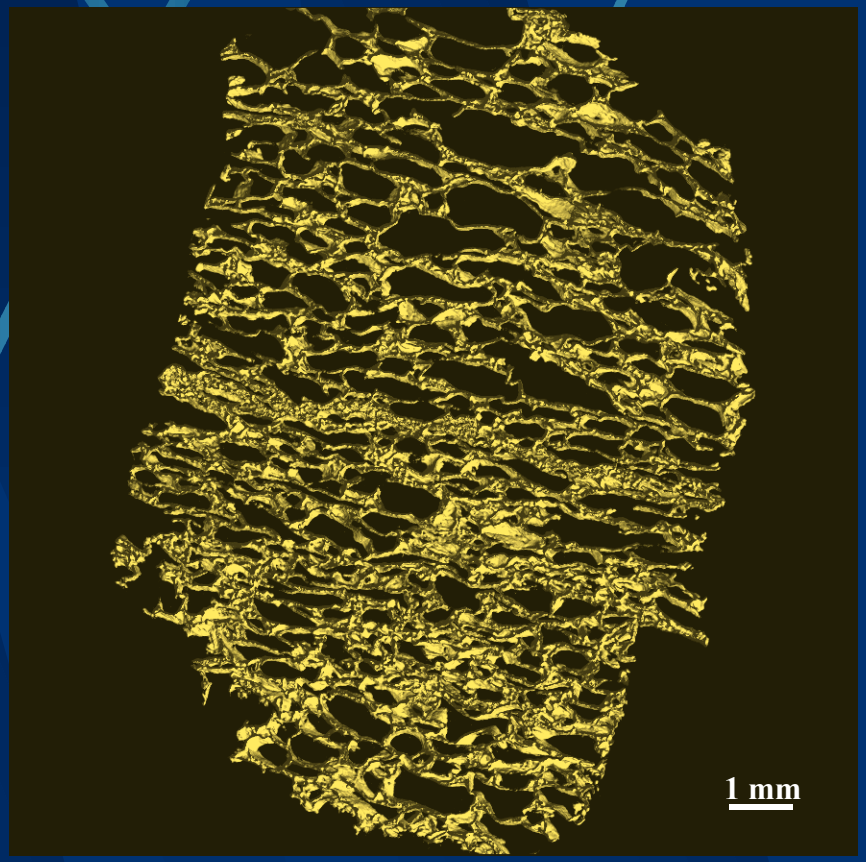

Volume rendering of 18 slices

FACOLTA' DI AGRARIA
UNIVERSITÀ DI FOGGIA

PS □-CT of a roasted coffee bean

elettra

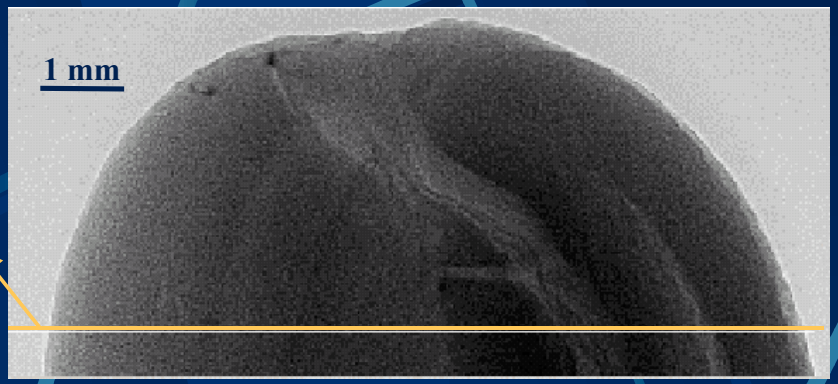

E = 12 keV *d* = 20 cm

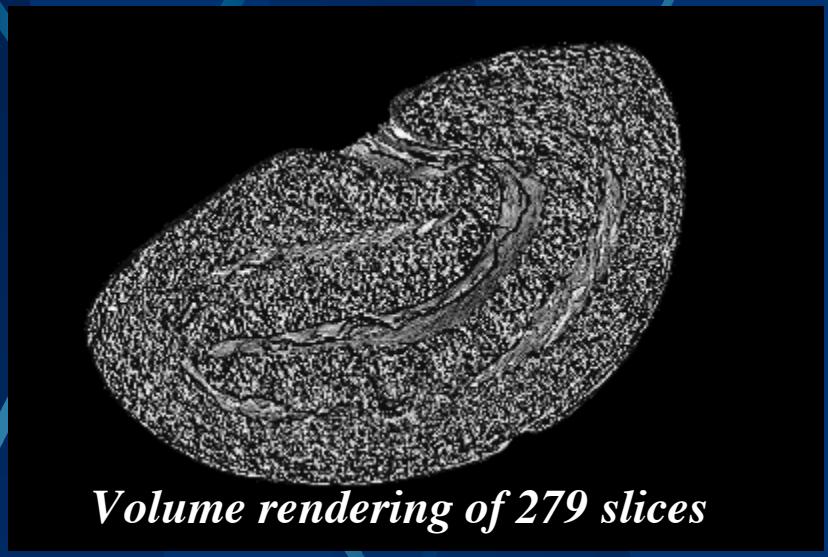

Volume rendering of 279 slices

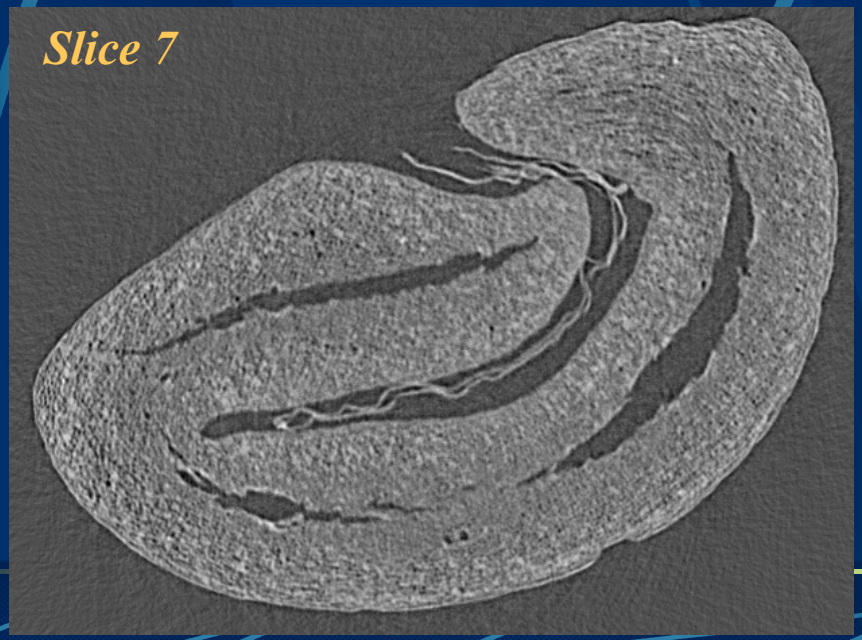

FACOLTA' DI AGRARIA
UNIVERSITÀ DI FOGGIA

elettra

Concluding remarks

- Cell structure aspect considered an important classification criterion of bread quality in both food industries and research laboratories (*Baruch and Atkins, 1989*). Bread sensorial quality related to crumb mechanical properties (*Aguilera and Stanley, 1999*).

- A quantitative analysis of bread microstructure under study to identify the cause-effect relationship among structural characteristics and mechanical properties.

- The analysis of roasted coffee bean microstructure could greatly enhance the understanding of basic mechanisms of the deterioration kinetics during storage. Experimental results showed that it is crucial to increase the available spatial resolution.

Conclusions and perspectives

- Many new topics can be studied by X-ray imaging:
  - dental implants, micro-structural defects in single crystals, *in-situ* phase transitions in shape-memory alloys, archeological wood and paper, ...
- High resolution imaging and detection of phase effects limited by X-ray flux and vertical source size:
  - **wider bandpass monochromators** (i.e. multilayer)
  - **beam focusing** and **image magnification** by **Fresnel zone plates/ lenses** and **bent crystals**
- **Phase retrieval experiments:**
  - for a **quantitative density mapping** in weakly absorbing samples
- **Combined Bragg and Fresnel imaging**

Acknowledgements

- ***F. Arfelli, A. Bergamaschi, E. Castelli, D. Dreossi, R. Longo, A. Olivo, S. Pani, L. Rigon, A. Zanetti***

  Dipartimento di Fisica - Università di Trieste and *INFN – Sezione di Trieste*

- ***F. Montanari***

  Université Joseph Fourier – Grenoble and *Istituto Colonnetti/CNR - Torino*

- ***C. Fava, A. Gambitta, L. Gregoratti, R. Menk, A. Pillon, G. Tromba, F. Zanini***

  Sincrotrone Trieste

Investigation of defects in quasicrystals

A new class of solids, discovered in 1984 (Shechtman et al.), exhibiting:

- **long-range orientational order** and ***quasiperiodic* translational order**
- orientational **symmetries forbidden for crystals** **(5-fold symmetry)**
- despite non-periodicity **sharp diffraction patterns**

Intriguing **physical properties**

- hardness and fragility at room T
- *plastic* transition at T ≈ 80% T_{melt}
- weak electric and thermal conductivity
- hydrogen storage (alloy Ti-Zr-Ni)
- surface properties: bad wetting and low friction coefficient, high resistance to corrosion and oxidation, hardness, …

Many **open questions**

- growth process
- role of defects to stabilize the structure
- why these spectacular physical properties?
- **.....**

Monochromatic-beam topograph and phase radiograph of the same region of an as-grown $Al_{68.6}Pd_{24.7}Mn_{6.7}$ IQC

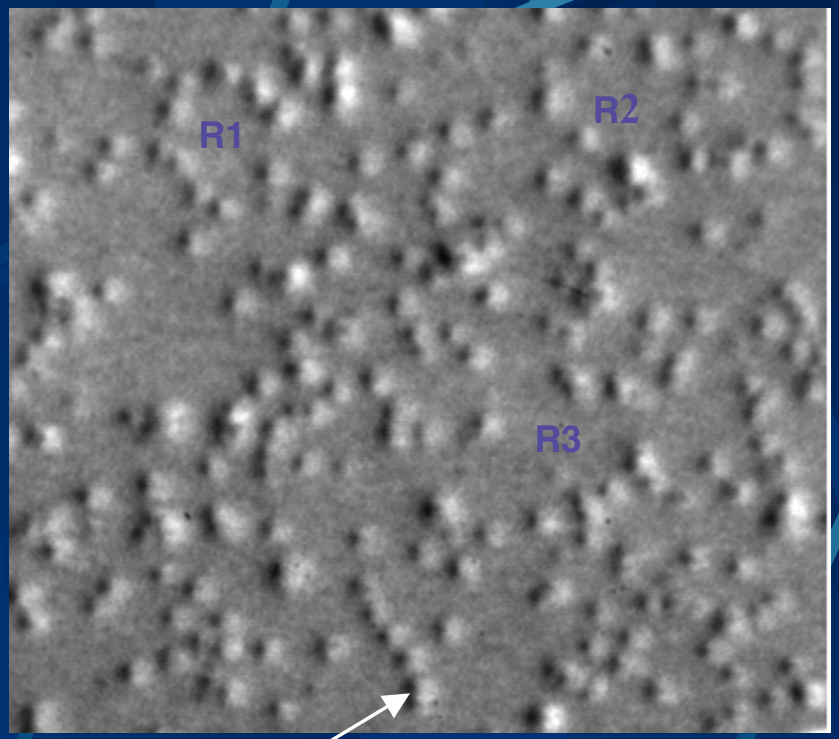

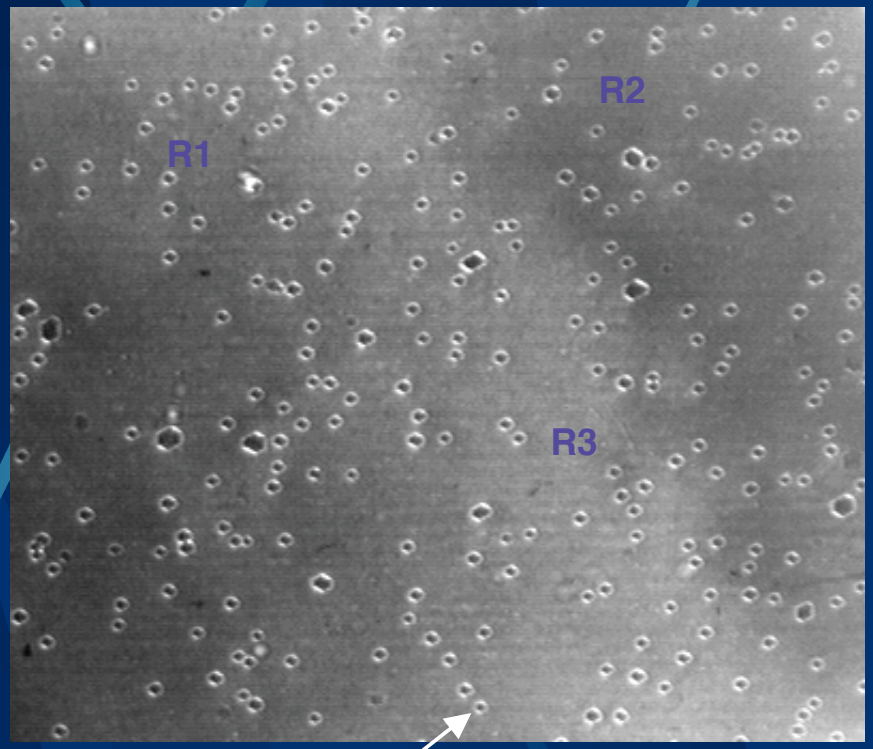

500 μm

d = 20 cm

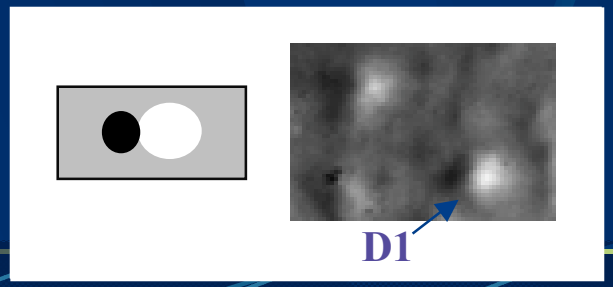

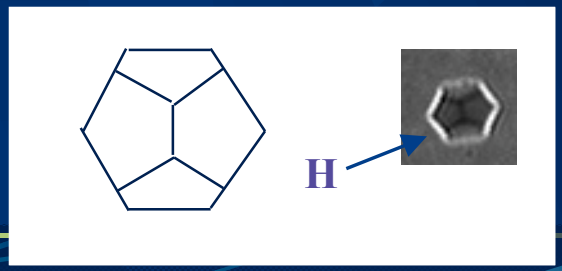

PSR of as-grown Al-Pd-Mn grains

2-fold axis parallel to the beam

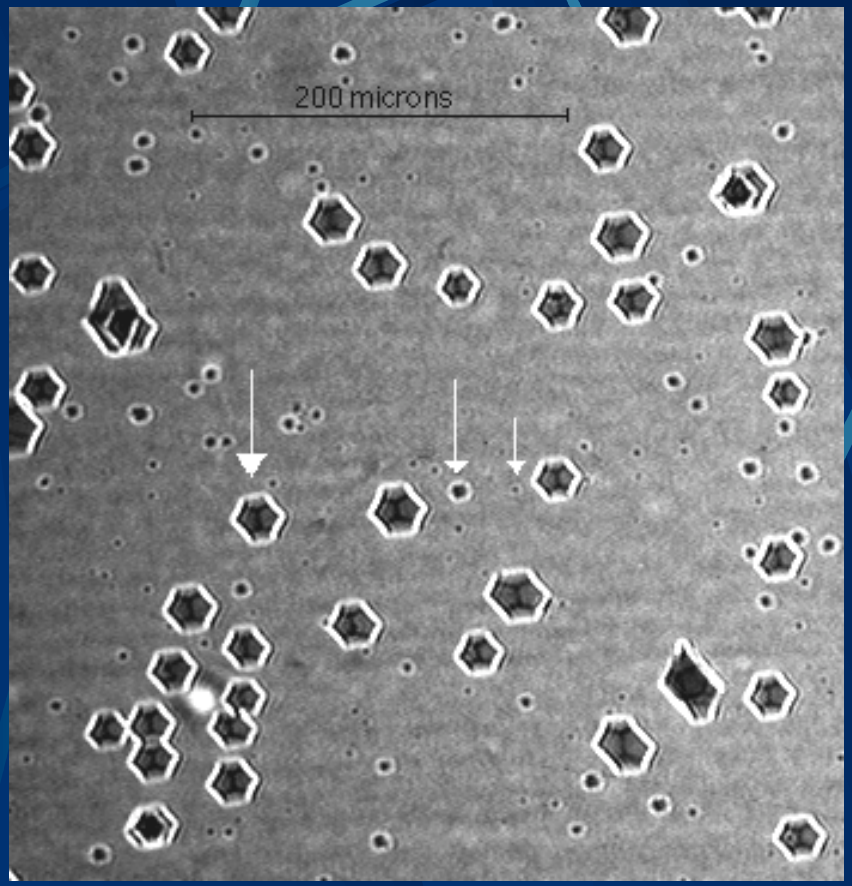

d = 50 cm

 = 0.35 Å

5-fold axis parallel to the beam

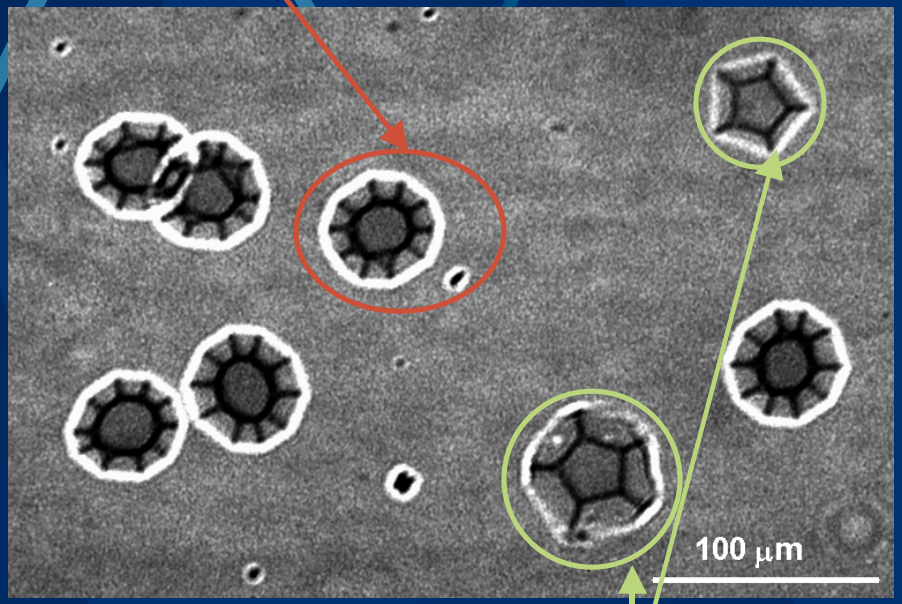

PSR of an Al-Pd-Mn grain after a 96h *annealing* at 750° C

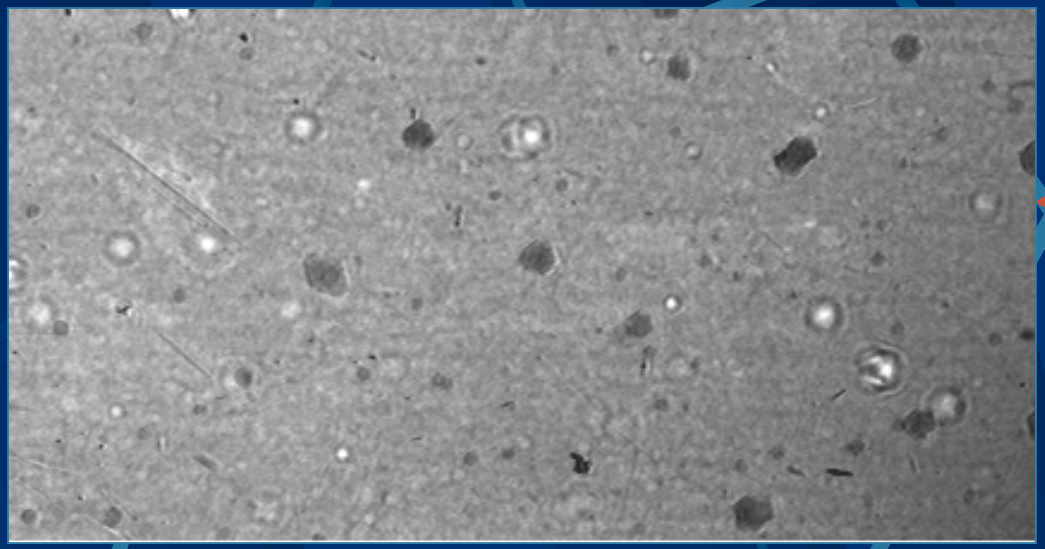

Absorption radiograph

d = 2 cm

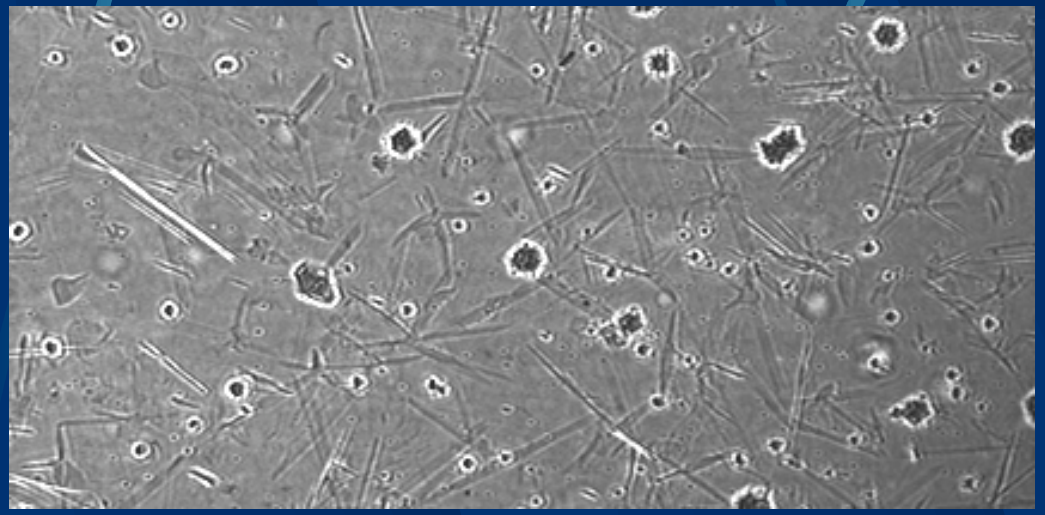

400 μm

d = 50 cm

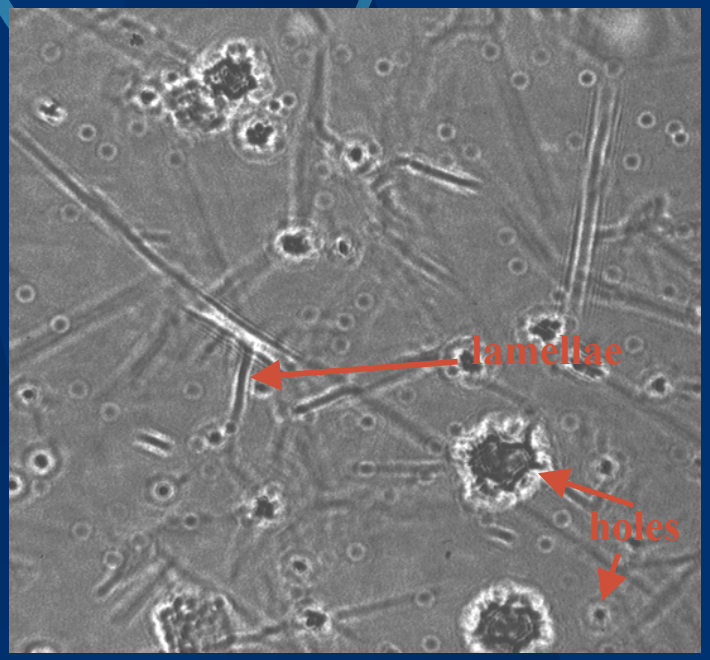

200 μm

Manipulating Intense XUV Coherent light

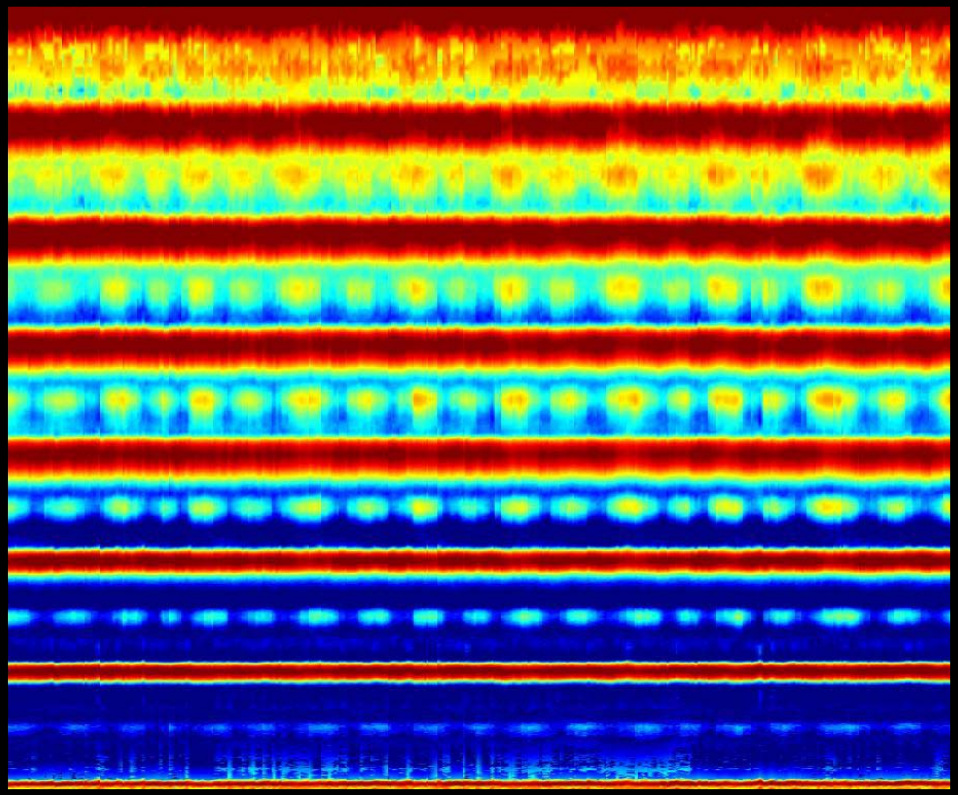

Hamed Merdji

International Conference on
Ultrashort High-energy Radiation and Matter
October 7-10 20003 Varenna (Italy)

SPAM

Atto Network

Optimized HHG: High Power in the XUV

Pulse duration 10fs, highly coherent, up to kHz

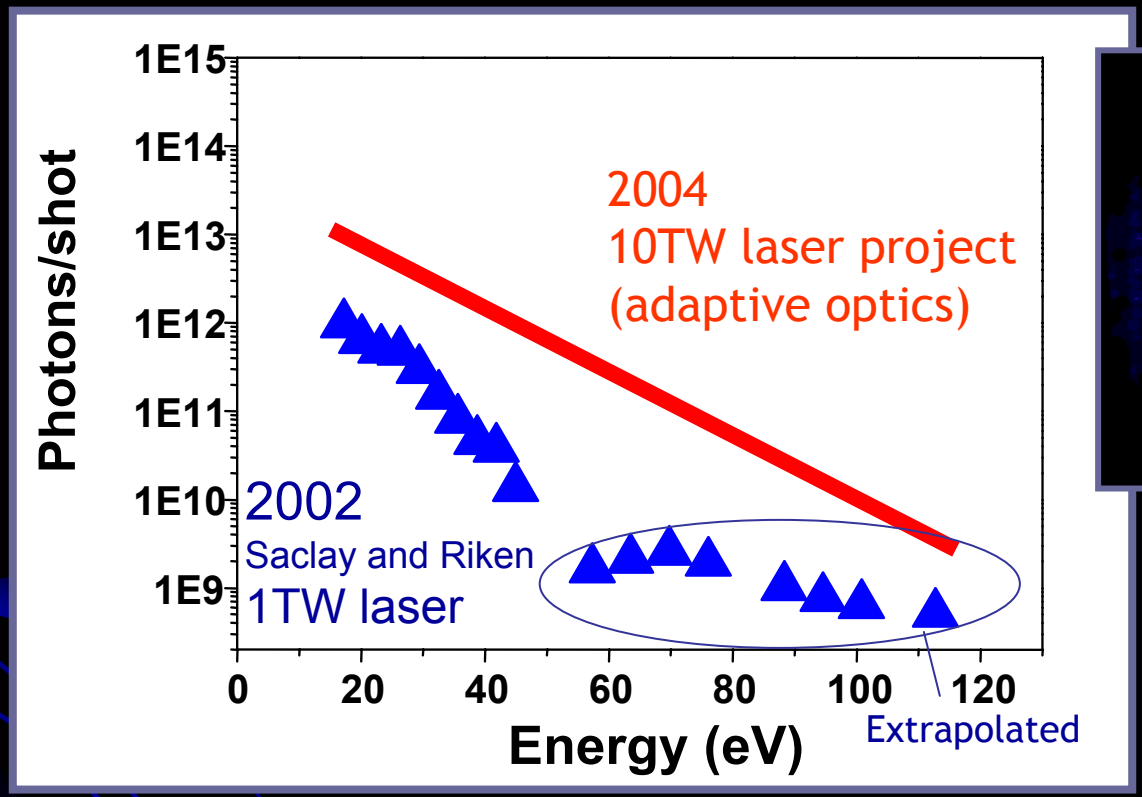

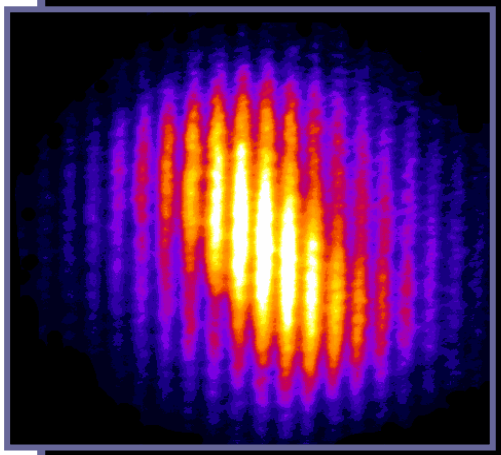

HHG

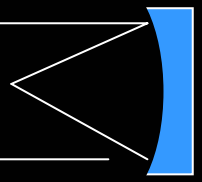

Ø5 µm
20% optical transmission
(already demonstrated)

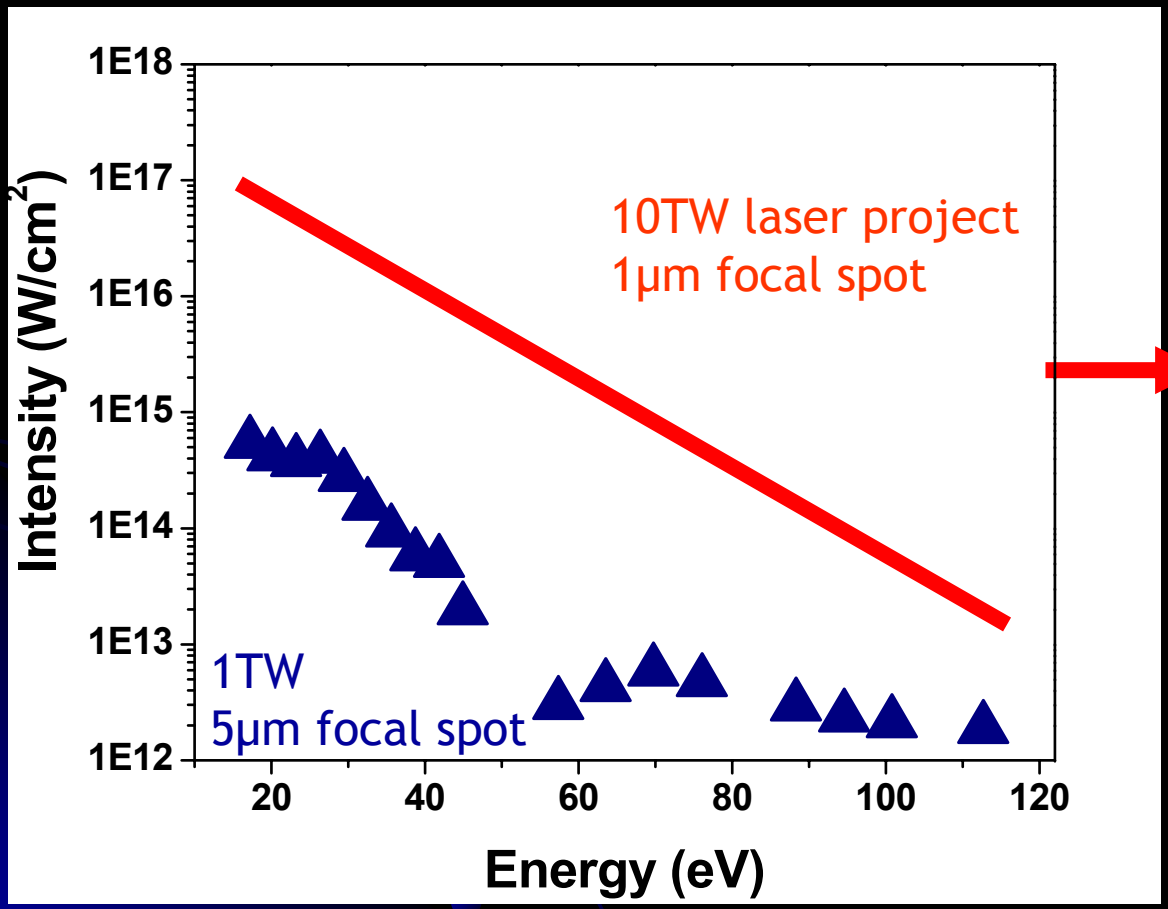

Background for
FEL experiments

Direct relation between spectral and time domains

Control of the spectral properties => Interferometry and Spectroscopy
Control of the pulse duration => Attosecond pulses

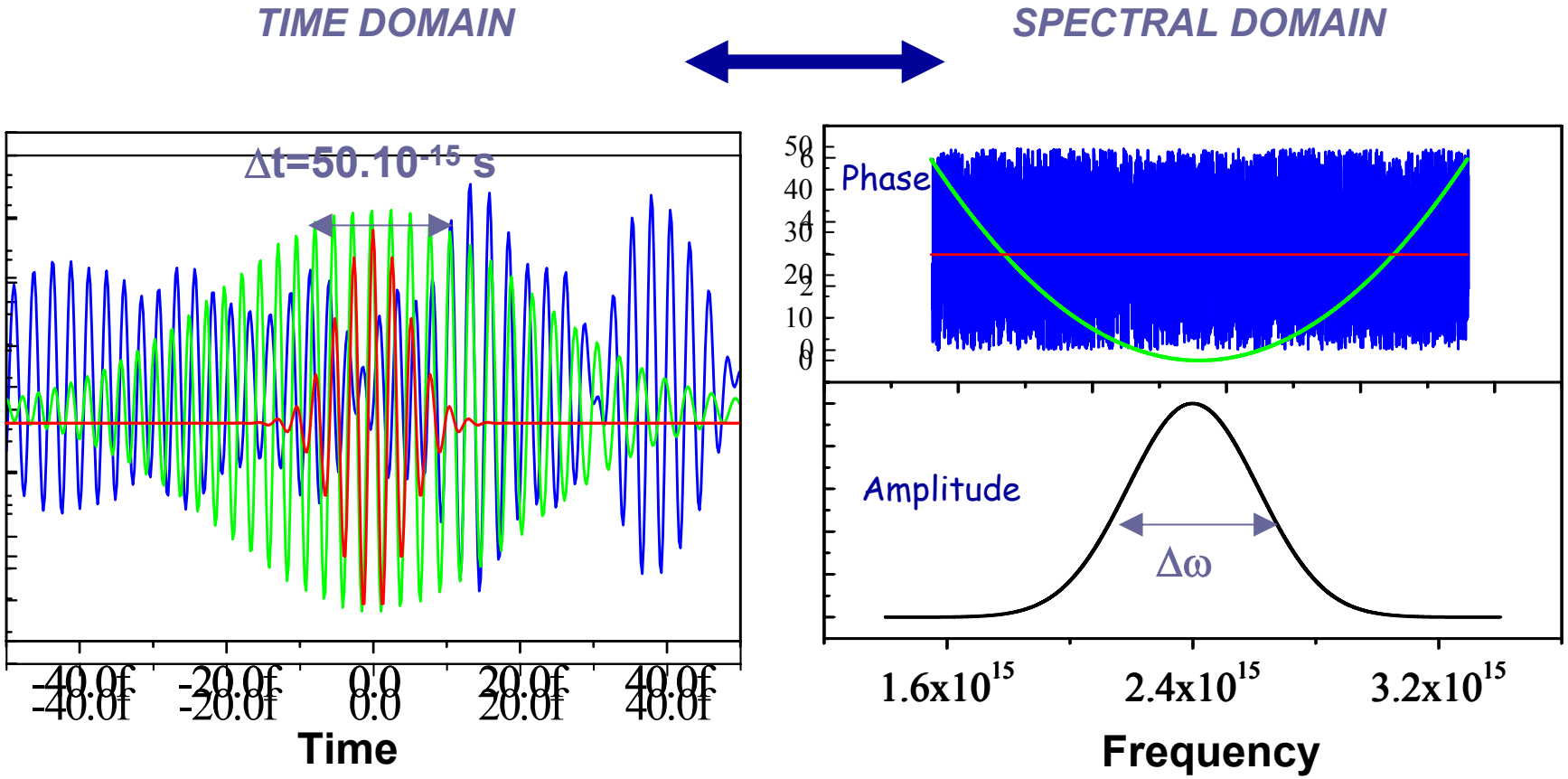

Mode-locked vs. non-mode-locked light

Mode-locked pulse train:
$\exp(i\varphi_m) = 1$

Non-mode-locked pulse train:
Random phase for each mode

$$\tilde{E}(\omega) = \sum_{m=-\infty}^{\infty} F(\omega)\exp(i\varphi_m)\exp(-im\omega T/2\pi)$$

Set of PHASE LOCKED
TIME-DELAYED pulses?

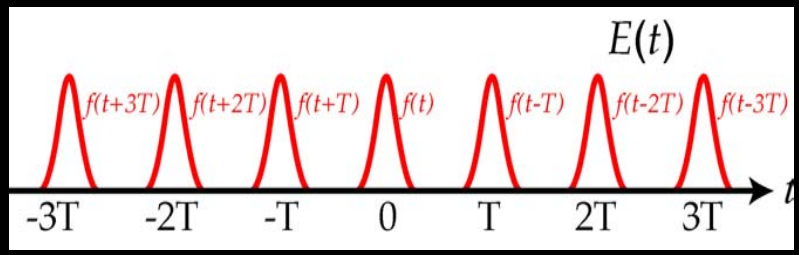

Spectral domain:
=> Interferometry, spectroscopy

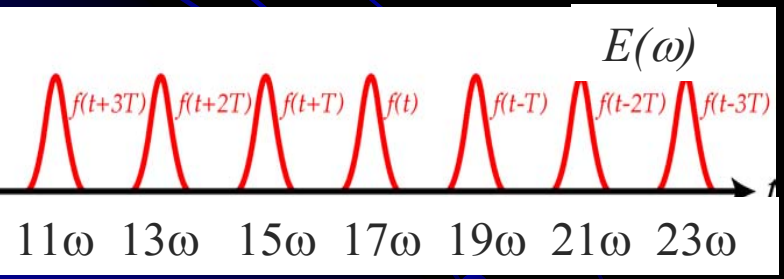

Set of PHASE LOCKED
SPECTRAL components

Time domain:
=>Attosecond pulse generation

Manipulating coherent XUV beams

in the time domain

Temporal Young experiment

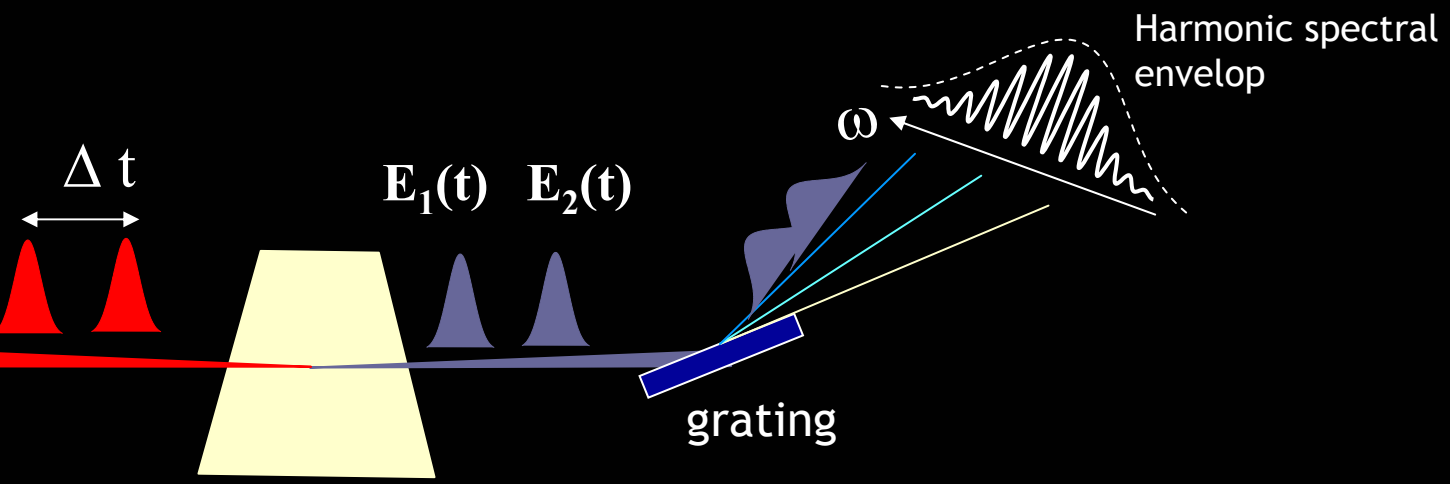

$$\Delta\lambda = \frac{\lambda^2}{c\,\Delta t}$$

XUV spectral interferences

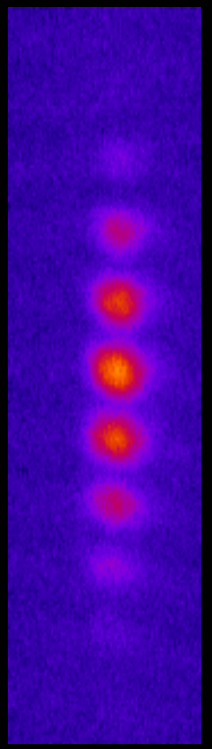

Salières et al., PRL 83, 5483 (1999) Hergott et al., JOSAB 20, 171 (2003)

Over-dense plasma diagnostics: Ultrafast XUV interferometry

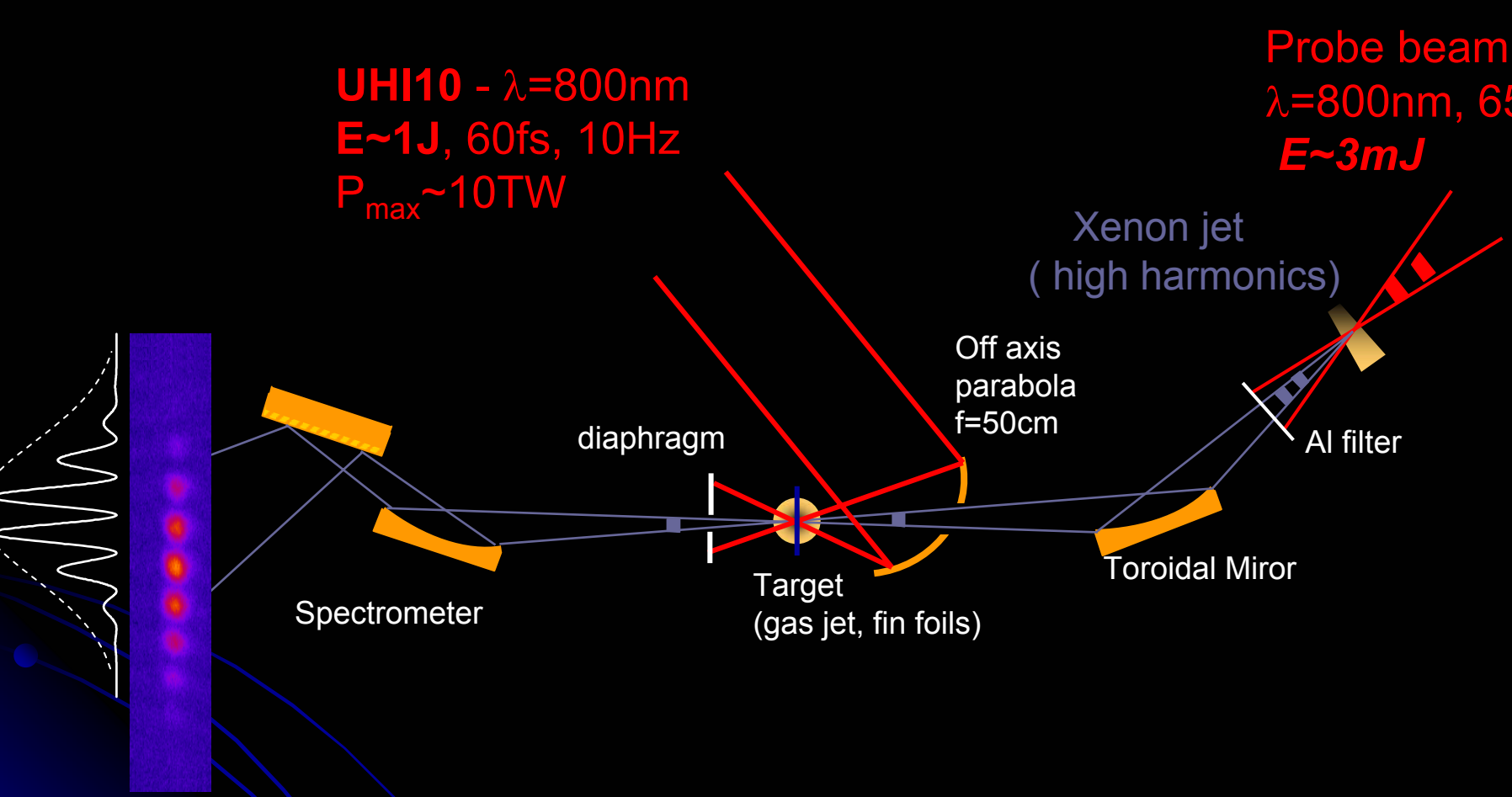

Delay between IR and XUV adjustable with jitter free delay

Ultra fast electron density evolution is followed

He plasma (OFI)

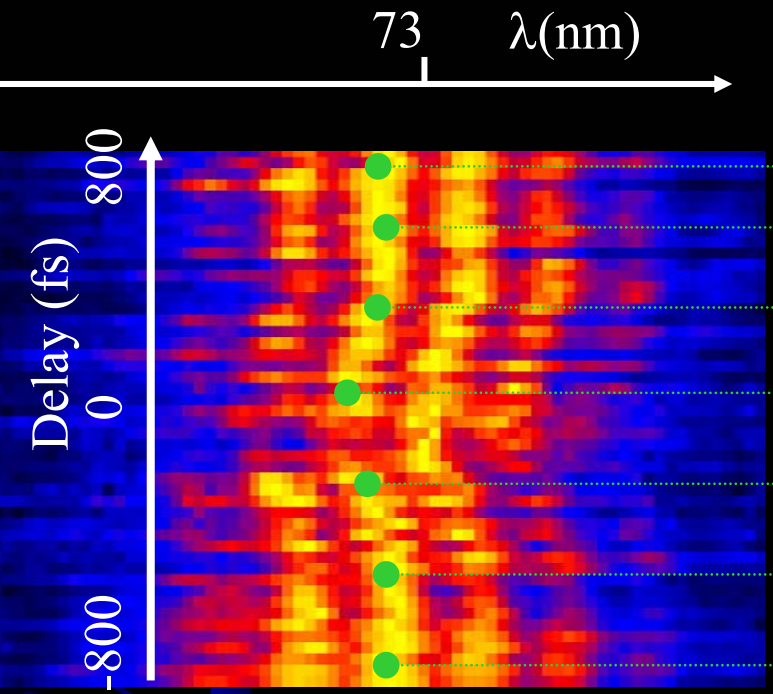

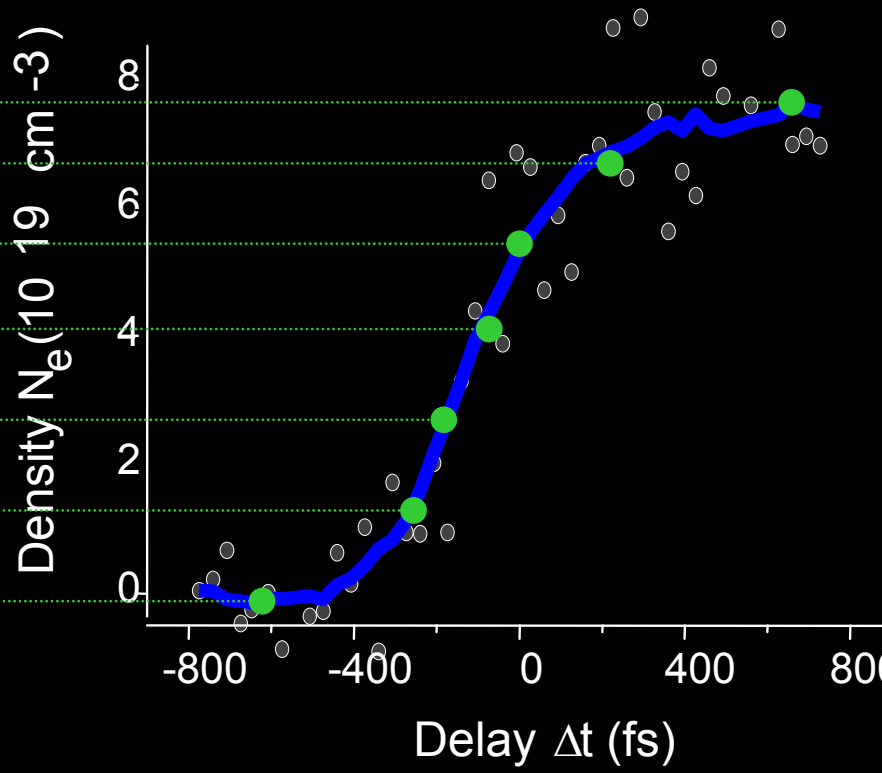

50fs time resolution

Plasma induced transparency reveals the ionisation dynamics

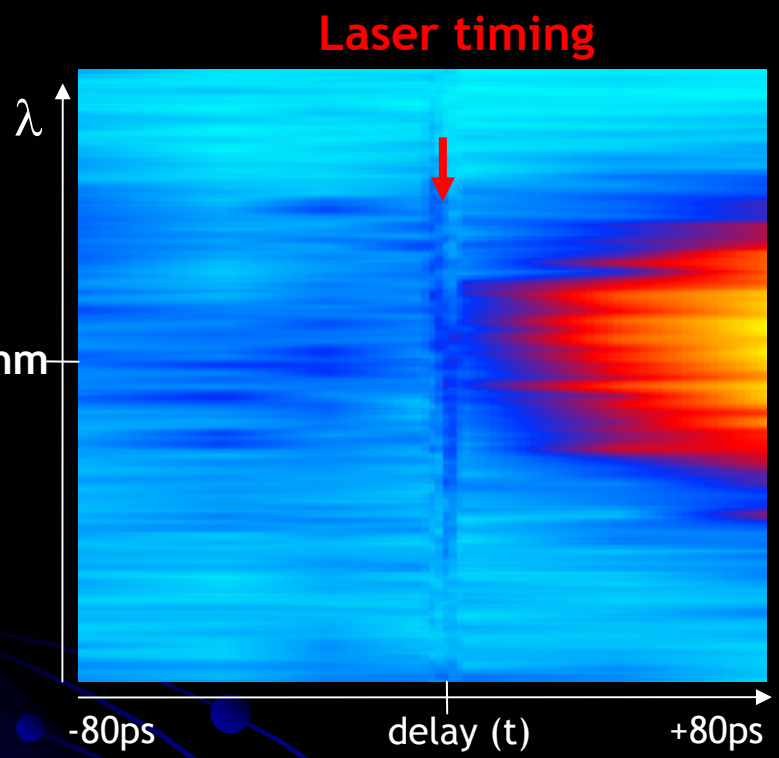

Exploded aluminium foil

Experimental conditions

- Al **1000Å**
- I~10^{18}W/cm^2
- H_{11} : λ~72nm

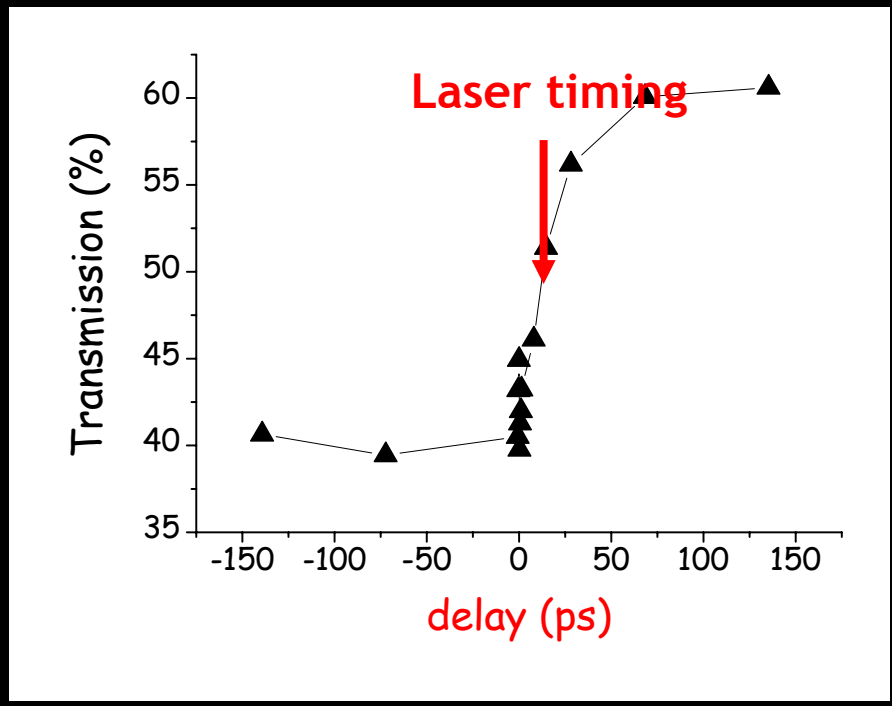

Around 0 delay ⇒ ultrafast transient transmission
reproducible and reversible process but not yet explained

We have show that we can generate 2 phase locked XUV beams

Due to constructive interferences
the spectral brightness is increased by a factor 4

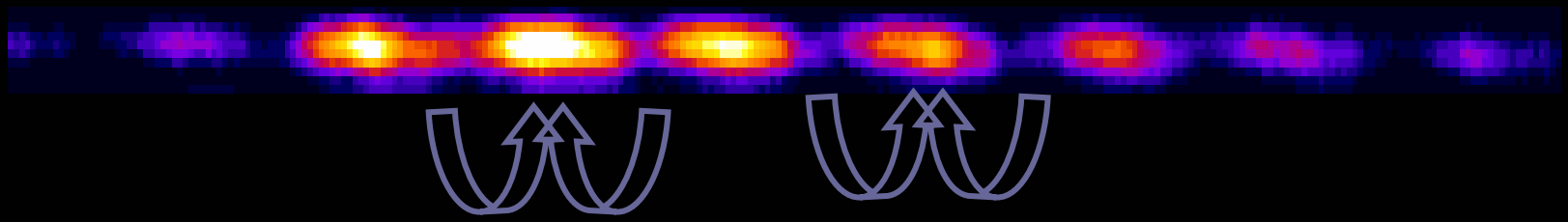

S IT POSSIBLE TO INCREASE MORE THE SPECTRAL BRIGTHNESS
USING MANY COHERENT BEAMS ??

4 phase locked XUV pulses : Attosecond phase sensitivity

• 2 pulses

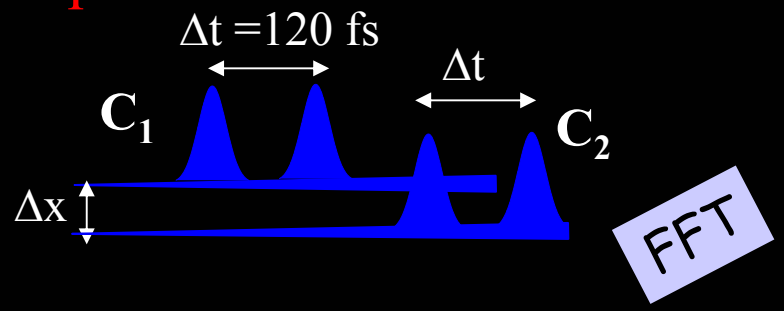

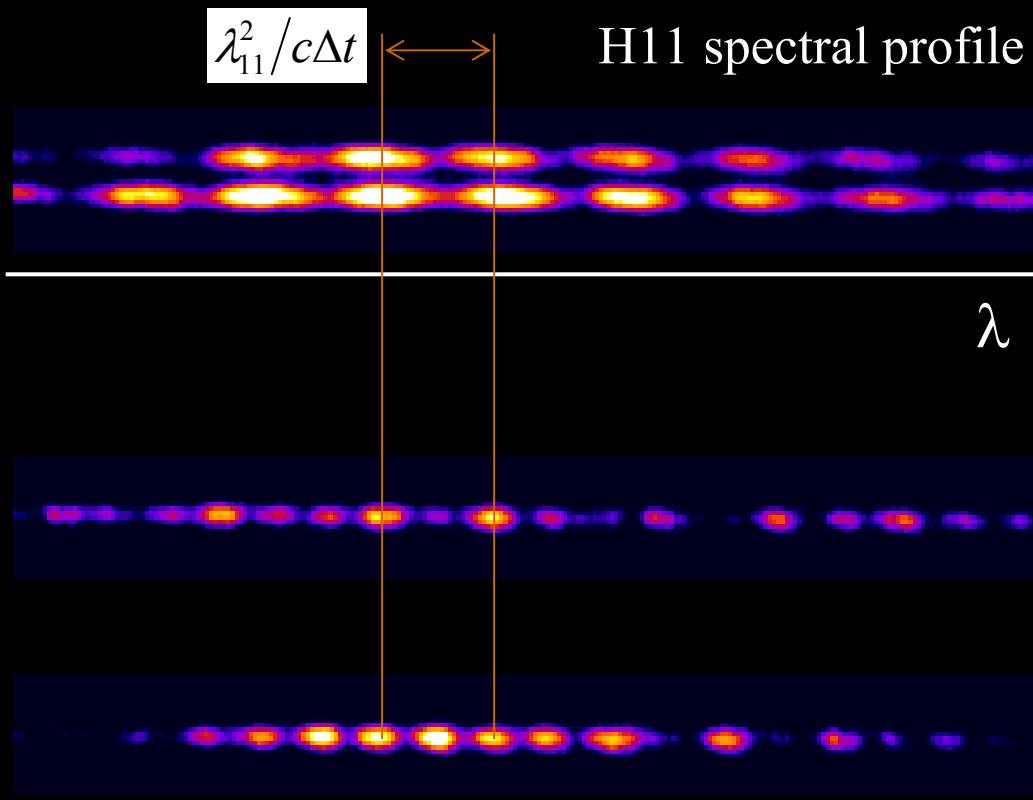

• 4 pulses

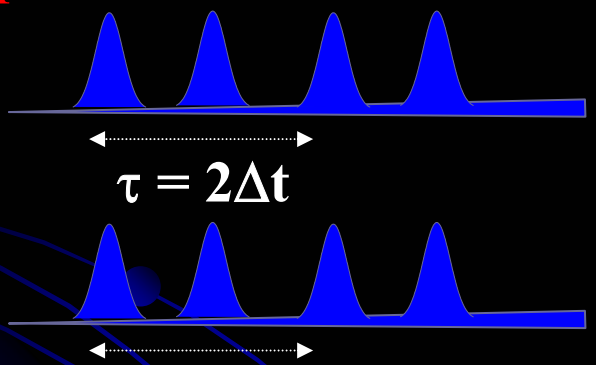

Sensitivity to extremely small phase-shift (few nm)

⇒ Time resolved diagnostic : optical breakdown, laser ablation

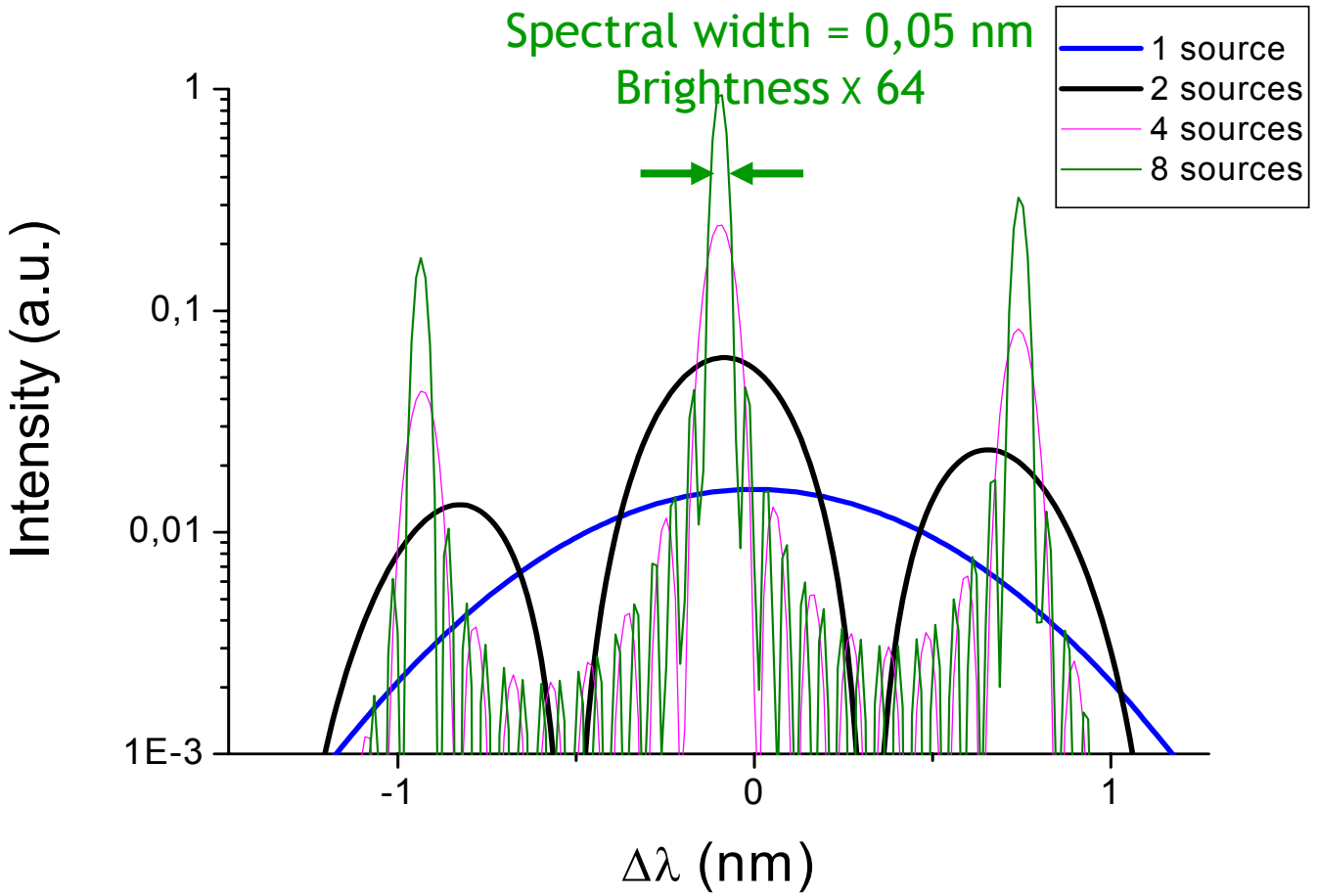

Narrow bandwidth and high brightness
=> Spectroscopy

Manipulating coherent XUV beams

in the spectral domain

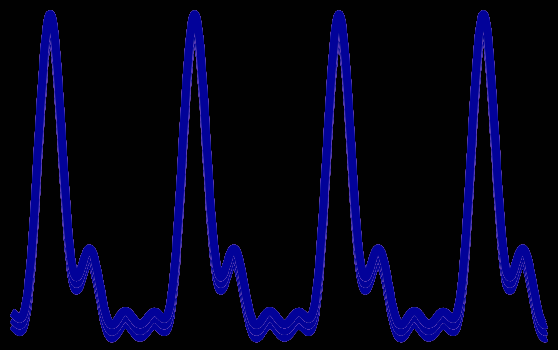

N “phase locked” spectral component

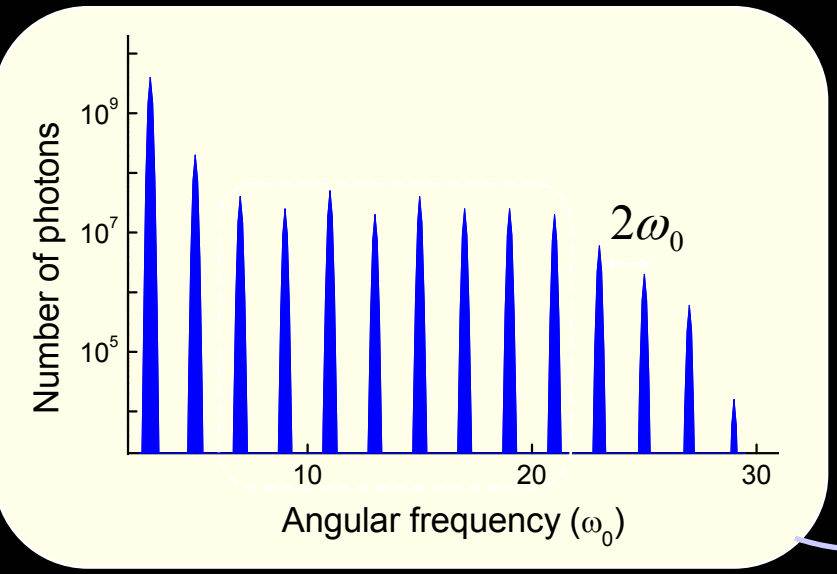

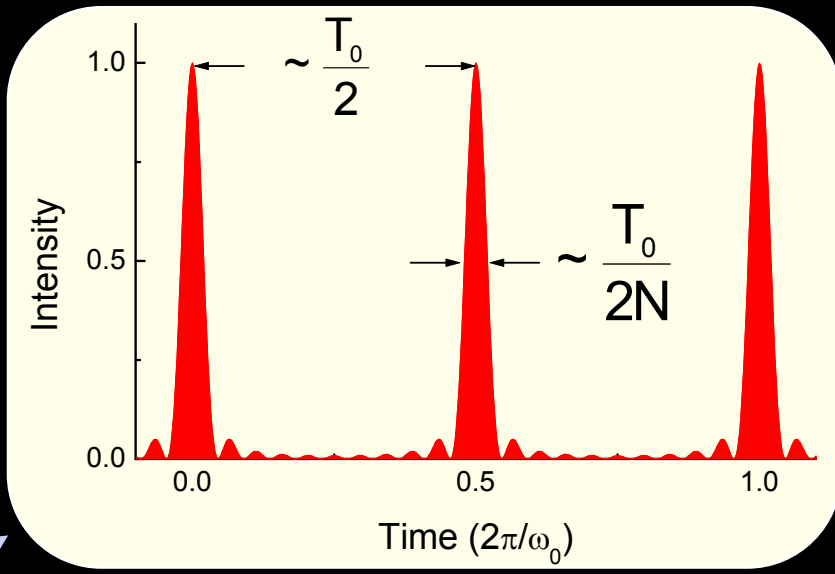

If N harmonics in phase:

$$I(t) \propto \left| \sum_q e^{-iq\omega_0 t} \right| = \frac{\sin^2(N\omega_0 t)}{\sin^2(\omega_0 t)}$$

N=11 => $\frac{T_0}{2N} \sim 120 \text{ as } (= 0.12 \text{ fs})$

Temporal characterization can be achieved through measurement of the harmonic spectral phases

ATTO-pulses measurement : two-color photoionization

Atom submitted to harmonic radiation +IR field

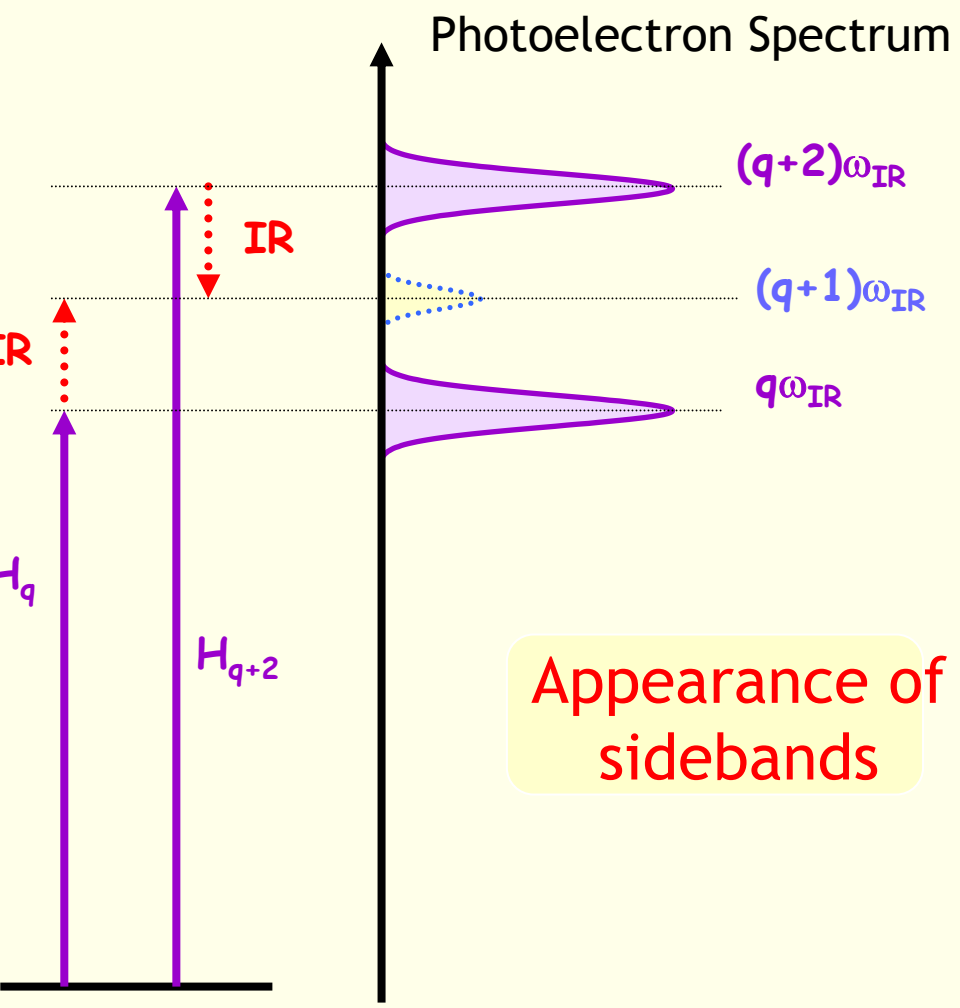

Appearance of sidebands

Sideband amplitude:

$$S_q = S_{q0}\cos(2\varphi_{IR} + \varphi_q - \varphi_{q+2} + \Delta\varphi^{at})$$

$\Delta\varphi^{at}$ can be calculated

φ_{IR} can be set by delaying the IR field: $\varphi_{IR} = \omega_{IR}\tau$

Oscillations of S_q at $2\omega_{IR}$

The sideband oscillations phase give the phase difference between 2 consecutive harmonics

Photoelectron spectra

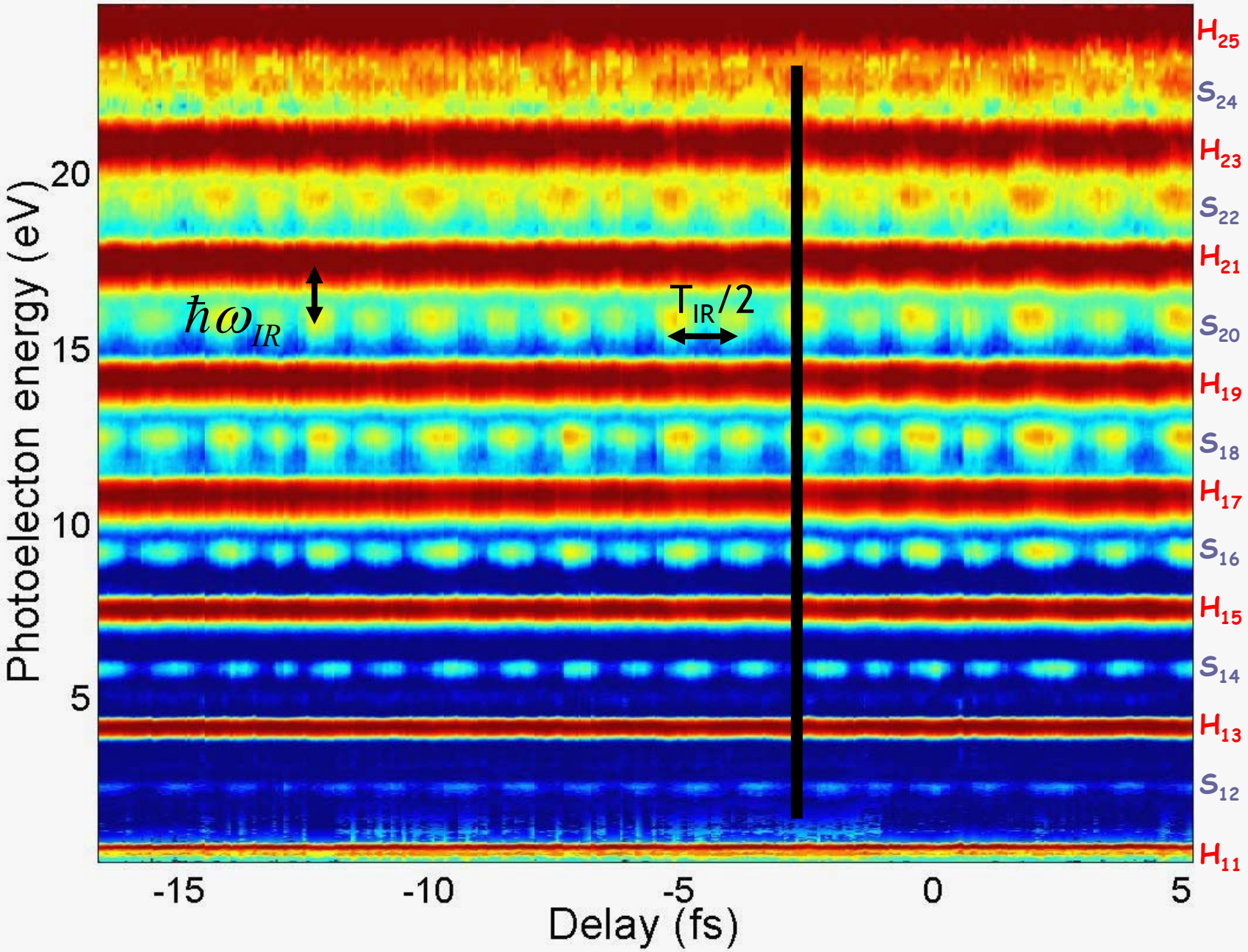

DIRECT RECONSTRUCTION of the ATTO PULSES

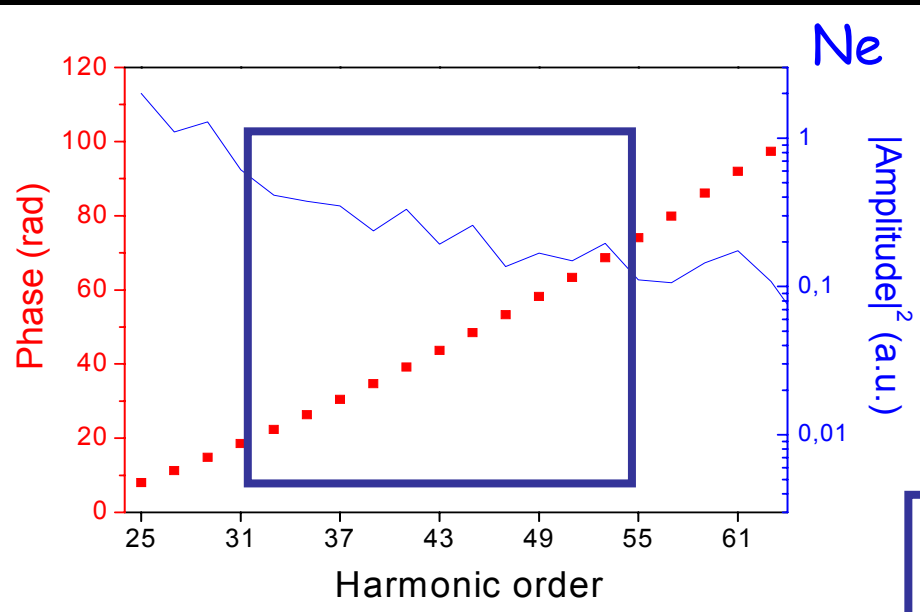

$$E(t) = \sum_{q_{min}}^{q_{max}} A_q \, e^{-i\,q\omega t + i\varphi_q}$$

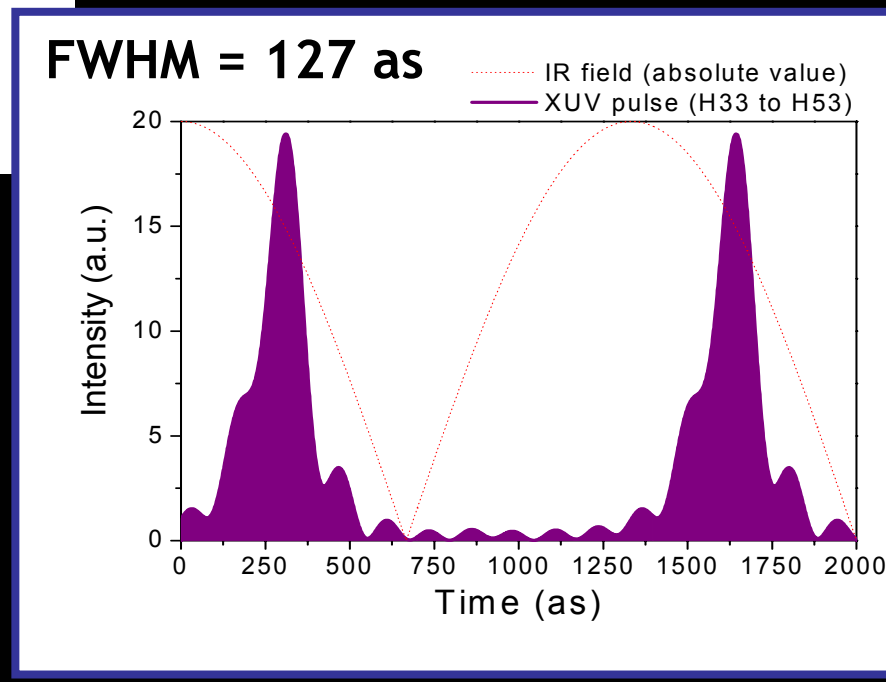

We select 11 harmonics

Fourier limit : $T_L/2N$ = 121 as

Chirp of the attosecond pulses

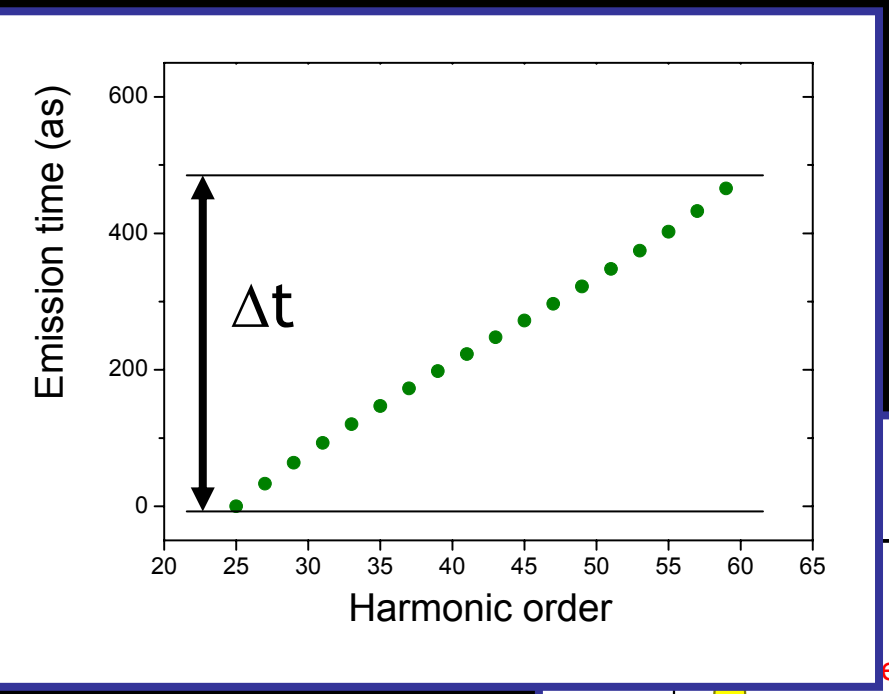

We select 20 harmonics

Fourier limit : $T_L/2N$ = 67 as

=> CHIRP

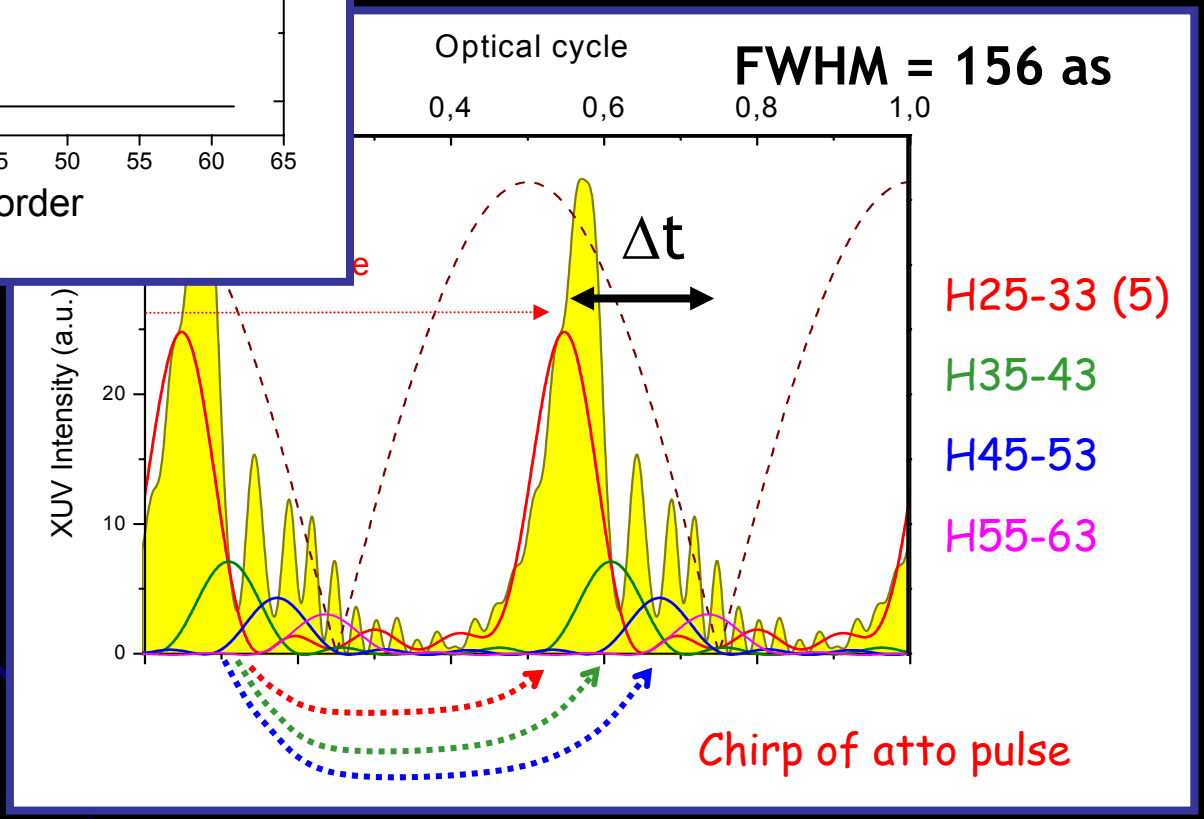

Phase compensation in dispersive medium => 70 as

Fourier limit : $T_L/2N$ = 67 as

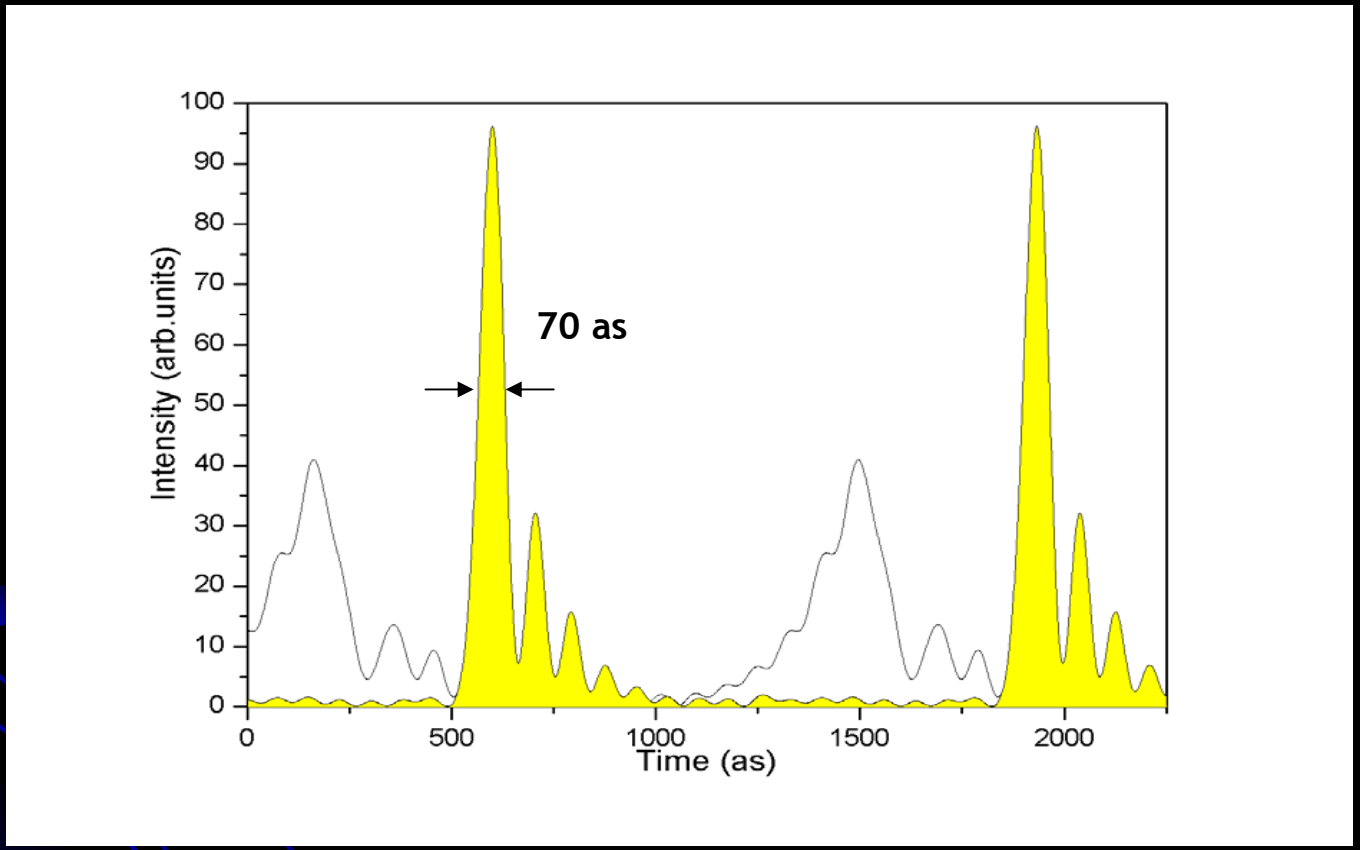

Conclusions

High Order Harmonic Generation :
Manipulating intense XUV coherent ligth:

- XUV interferometry
  Plasma diagnostics, Nanoscale manufacturing
- High resolution XUV spectroscopy
  Atomic and Molecular Physics
- Attosecond pulses generation
  127 as demonstrated! =>70as : easy
  Pushing the frontier of the control of ultra-short EM fields
  Next … applications

HHG applications in progress in many labs in femtochemistry, surface/solid state physics, life sciences

Background for FEL experiments

P. Agostini, P. Breger, A. de Bohan, J.F. Hergott, M. Kovačev, Y. Mairesse,P. Monchicourt, P. Salières, P. Monot, T. Auguste.

SPAM, CEA-Saclay, France

Plasma experiment

Atto experiment

L.J. Frasinski

University of Reading, J. J. Thomson Physical Lab., Reading, United Kingdom

L.C. Dinu, H.G. Muller

FOM Institute for Atomic and Molecular Physics, Amsterdam, The Netherlands

on support of European RTN ATTO and LIMANS III (SLIC)

Positions available at CEA/Saclay (20km from Paris)

- phd student:
  M. Curie Fellowship/1 to 12 months (1200€/month)

- Post Doc
  (2 years) (2300 €/month)

merdji@dreCAM.cea.fr

Dense Plasma Physics with DESY XFEL and TTF2

J. Meyer-ter-Vehn,

A. Krenz, Ke Lan, P. Pyrka,
K. Eidmann, E. Fill, Th. Schlegel

Max- Planck-Institut für Quantenoptik, Garching

TESLA XFEL at DESY/Hamburg (planned)

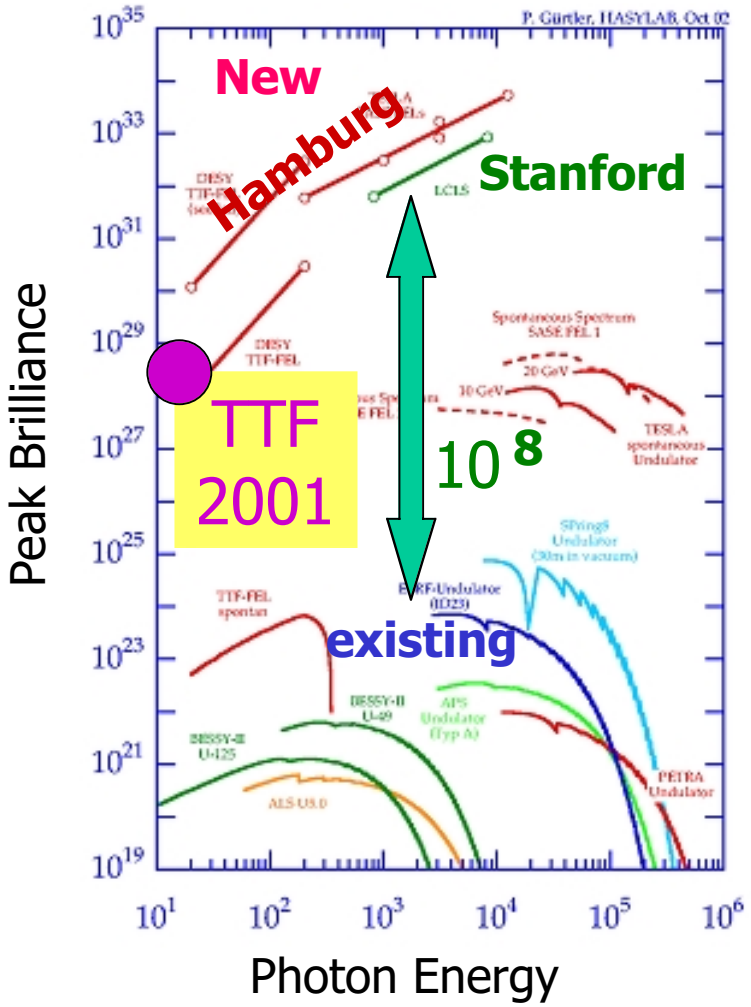

hν=15 eV	TTF1	2001
hν=20-200 eV	TTF2	2004/5
hν=12.4 keV	XFEL	2011

100 fs pulse (simulation)

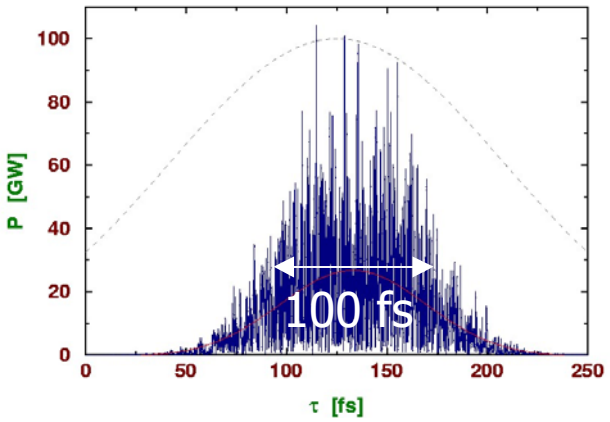

XFEL pulses expected to be focussed to 1μm focus and up to 10^{18} W/cm^2

	2004	2011
wavelength/energy	20 - 200 eV	1 Å / 12.4 keV
photons/pulse	10^{14}	2×10^{12}
pulse duration	100 fs	100 fs
pulse energy	1 mJ	4 mJ
pulse power	10 GW	37 GW

focus diameter	1-100 μm
intensity	10^{14}-10^{18} W/cm^2

XFEL Heating with 3 keV XFEL photons

Specific energy deposited:

e(J/g) = κ(cm^2/g) **I**(W/cm^2) τ(s)

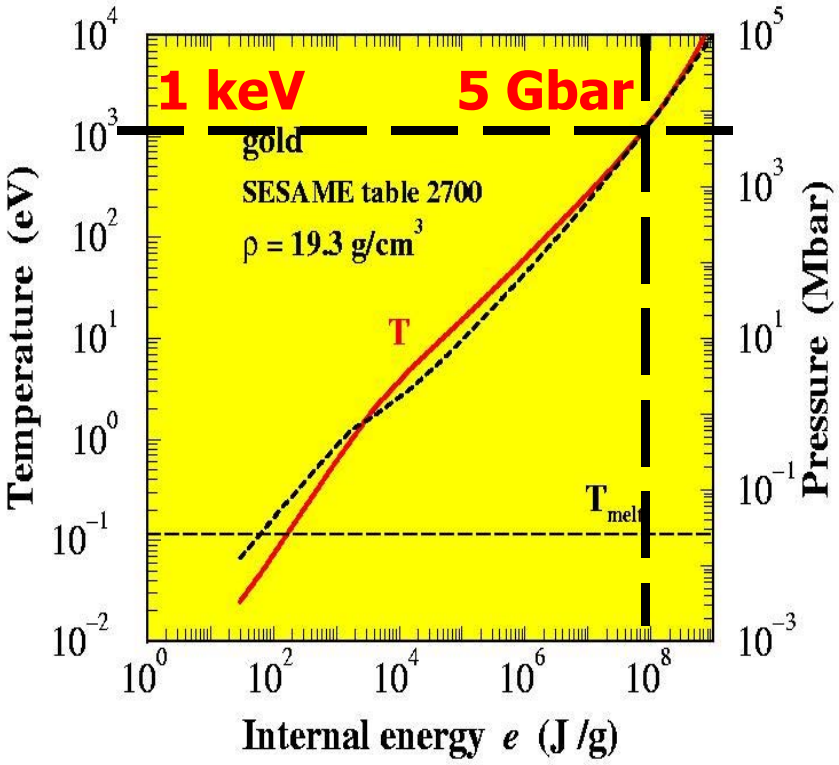

I = 10^{14} -10^{18} W/cm^2

τ = 100 fs

3.1 keV photons

κ= 10^3 cm^2/g
gold opacity

e = 10^4 -10^8 J/g

XFEL Heating of Au foil (2D simulation): Expansion sets in on ps timescale

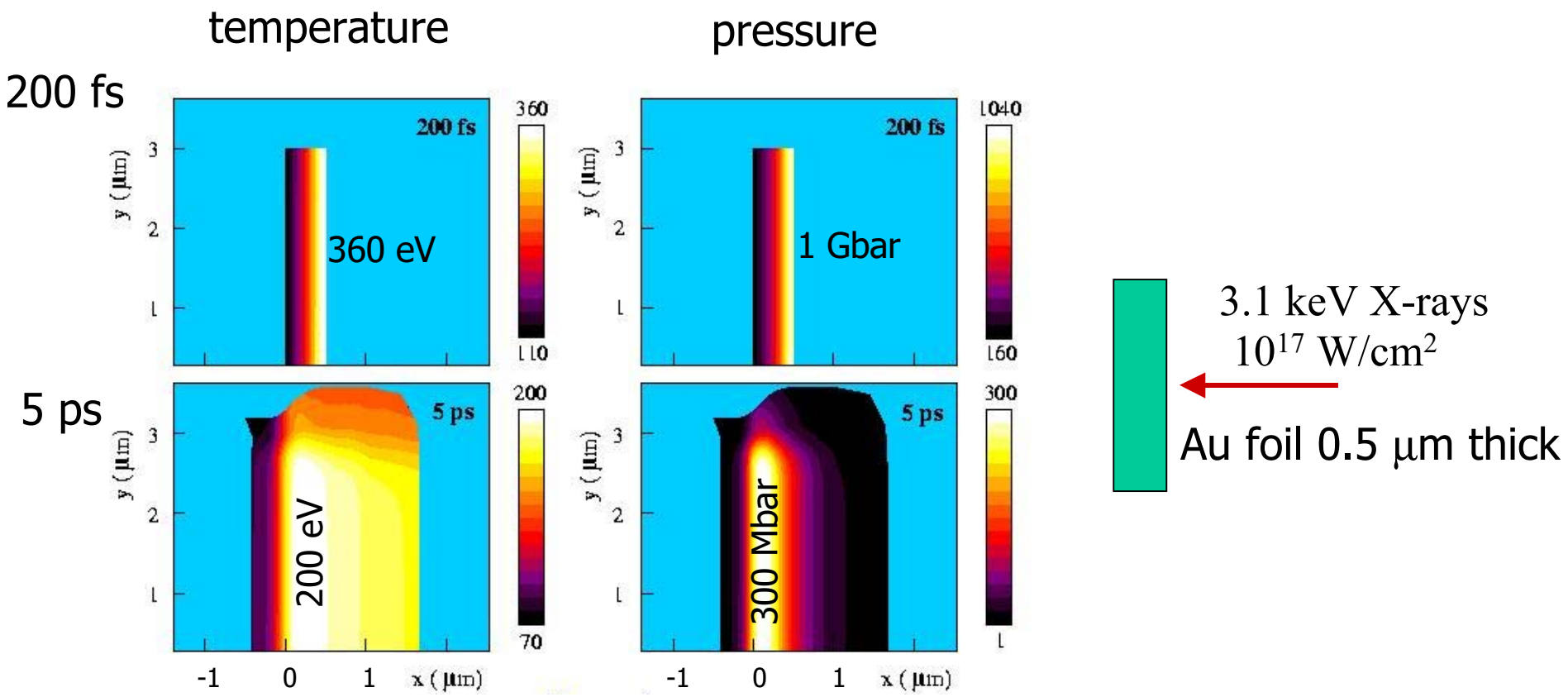

Hydrodynamic Response of Heated foil 200 fs - 5 ps

Al Layer , 10^{18} W/cm^2, 1 keV XFEL photons

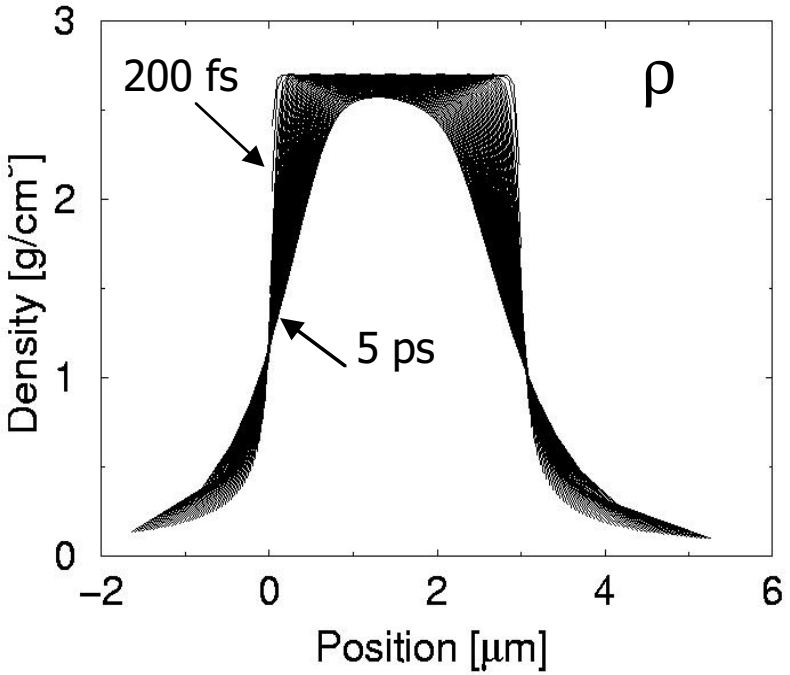

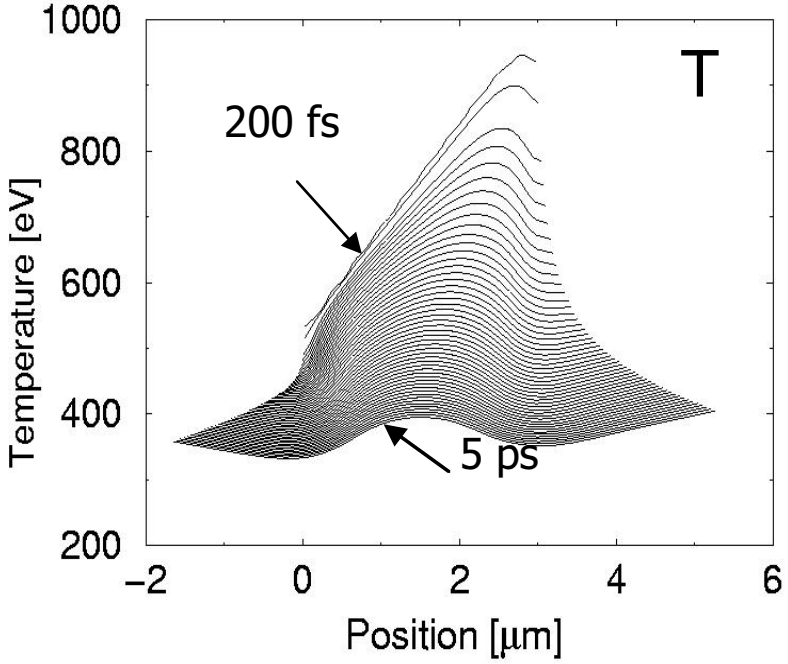

Compton scattering as plasma diagnostics

(from R. Lee et al., 2001)

Compton shift

$\Delta \lambda = \lambda_c (1 - \cos \theta)$

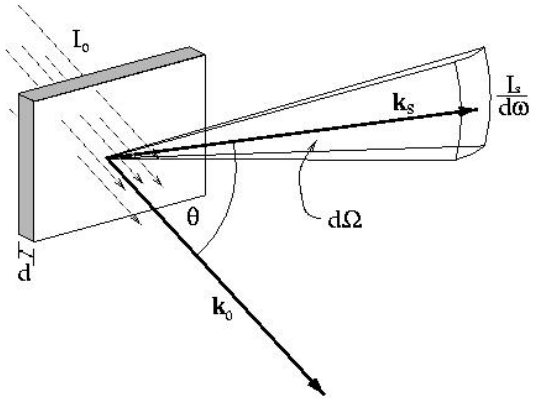

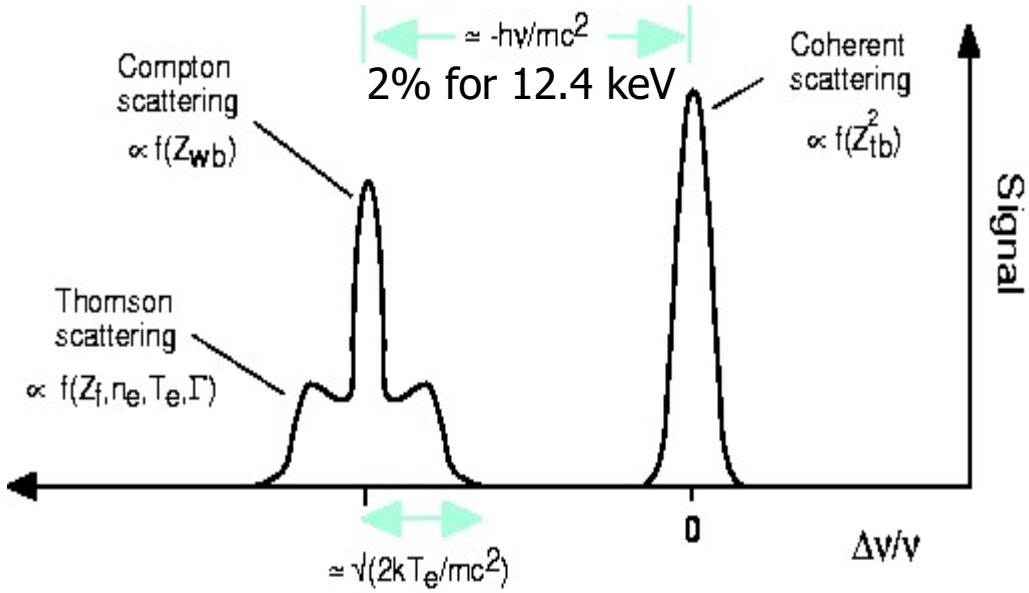

1% for T_e=25 eV

Calculated Compton spectra for Lithium

Patricia Pyrka, diploma thesis, MPQ/TU Munich 2002

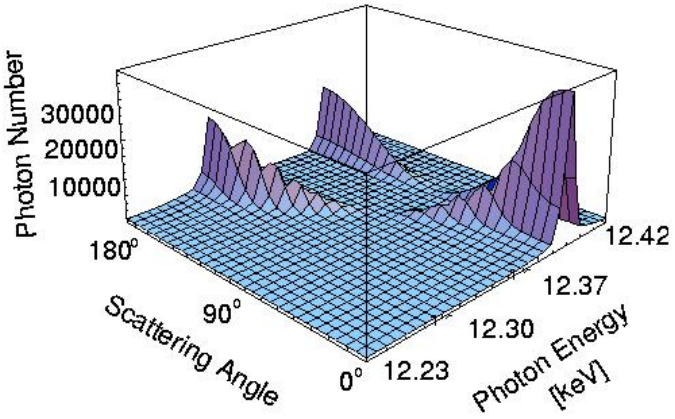

10^{13} photons of 12.4 keV scatterered on T_e=10 eV lithium

Li ionisation energies

Compton shift ($\theta = \pi$)

95 eV →

5.3 eV	free electron
74.8 eV	weakly bound
120.9 eV	strongly bound

10 -100 eV photons show maximum absorption in solid-density plasma

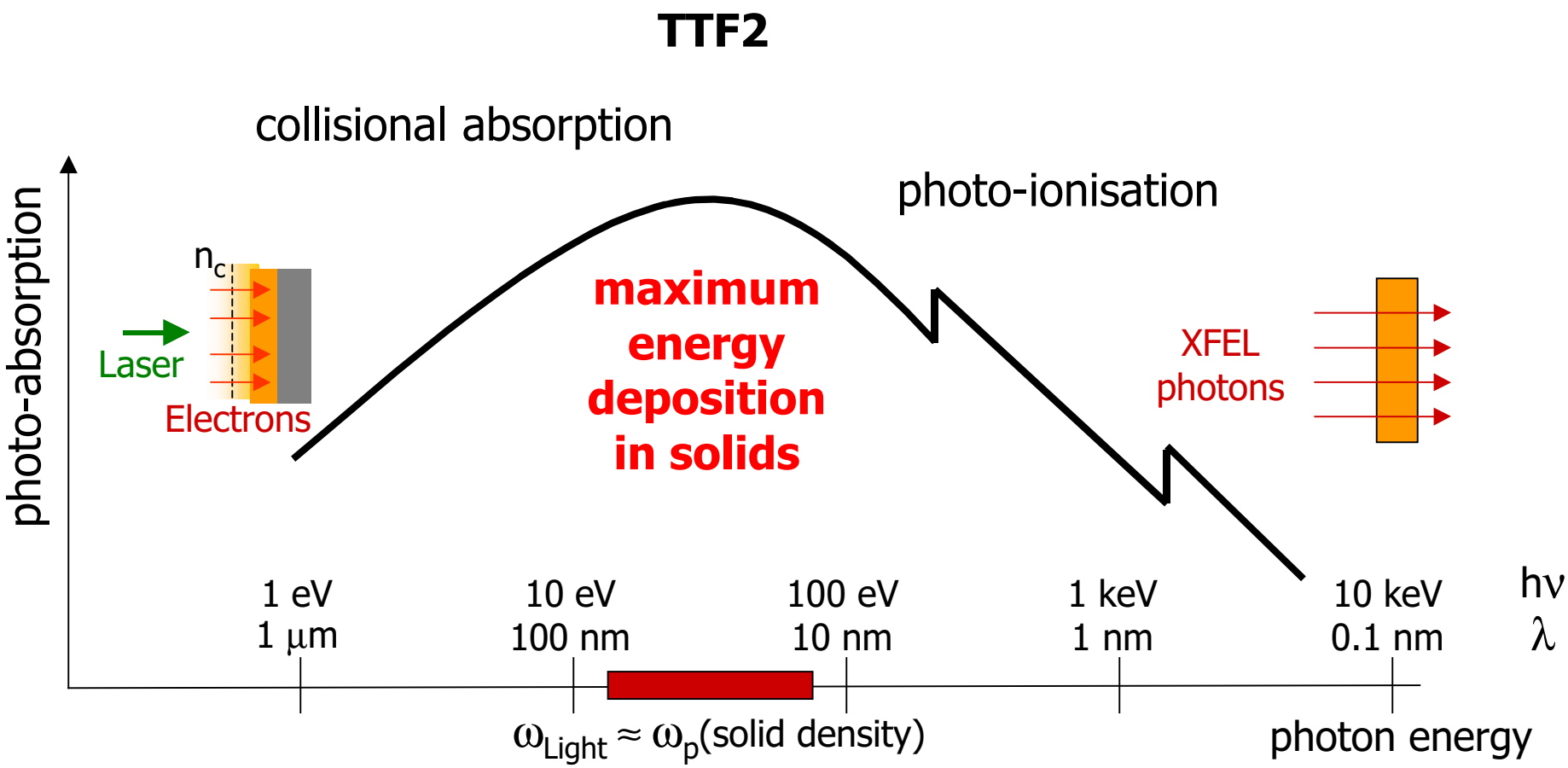

Light propagation in plasma

plane wave

$$\mathbf{E}_L = \mathbf{E}_0 \exp\{i\mathbf{kr} - i\omega t\}$$

Maxwell equation

$$(k^2 - \omega^2/c^2)\,\mathbf{E}_L = (4\pi i\omega/c^2)\,\mathbf{j}$$

electron current

$$\mathbf{j} = -en\mathbf{u}$$

$$-i\omega\,\mathbf{u} = -(e/m)\,\mathbf{E}_L - \nu_e \mathbf{u}$$

$d\mathbf{u}/dt$ collisions

plasma frequency

$$\omega_p^2 = 4\pi e^2 n/m$$

dispersion relation

$$\omega^2 = \omega_p^2/(1 + i\nu_e/\omega) + k^2 c^2$$

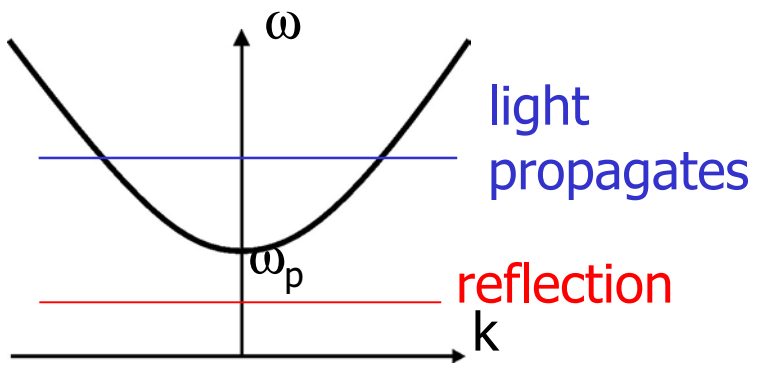

Collosional absorption

wave vector (from dispersion relation)

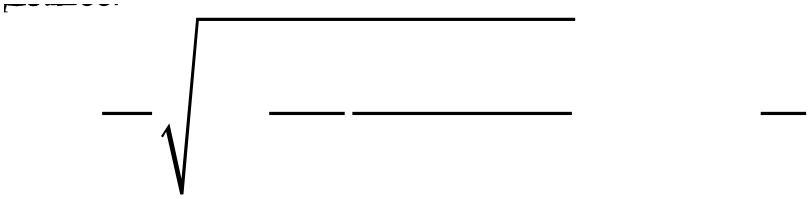

light intensity

$$I \sim |E|^2 \sim \exp(-\kappa x)$$

absorption coefficient ($\nu_e << \omega$)

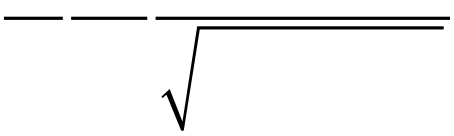

Electron collision frequency

Spitzer ($T >> T_{Fermi}$):

Collision frequency in warm dense matter poorly known.
Here recent fit and comparison with absorption data from solid aluminum heated by few 100 fs optical laser pulses:

Eidmann et al., PRE62, 1202 (2000)

coll.freq.model

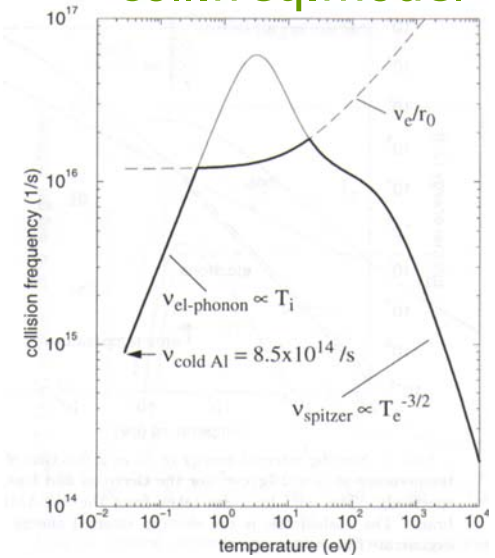

Exp. Al light absorption

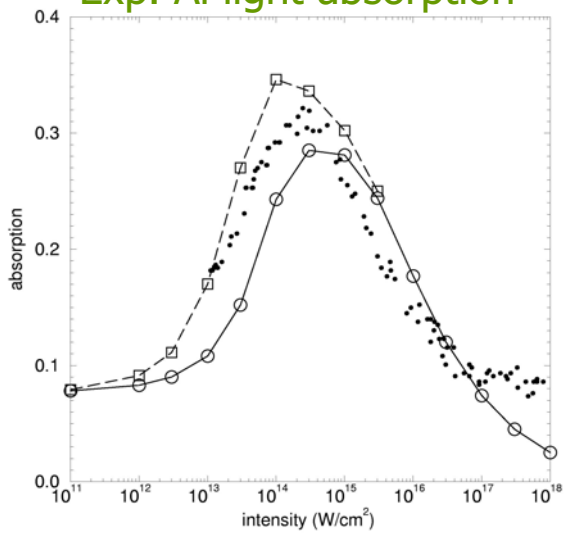

Uniform solid-density layers of 500 eV, e.g. for opacity measurements

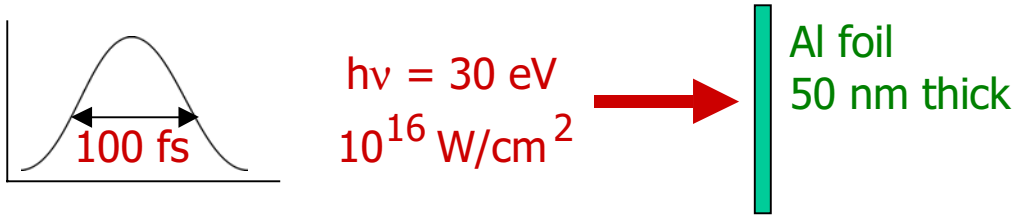

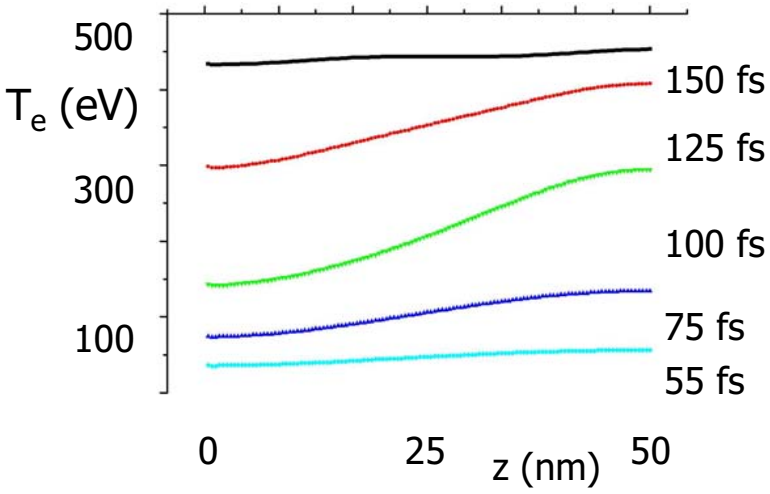

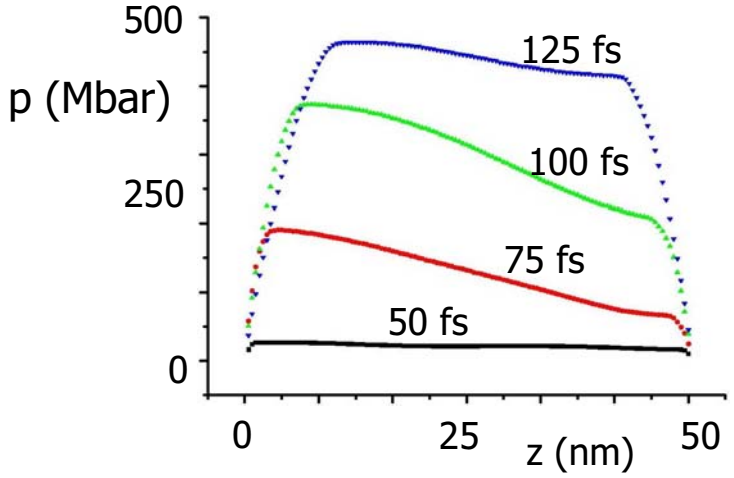

Foils as Ultra-Fast Switches

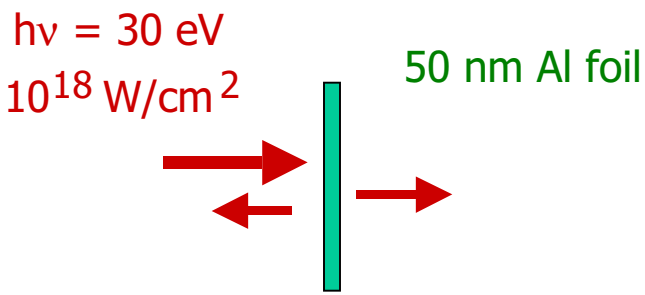

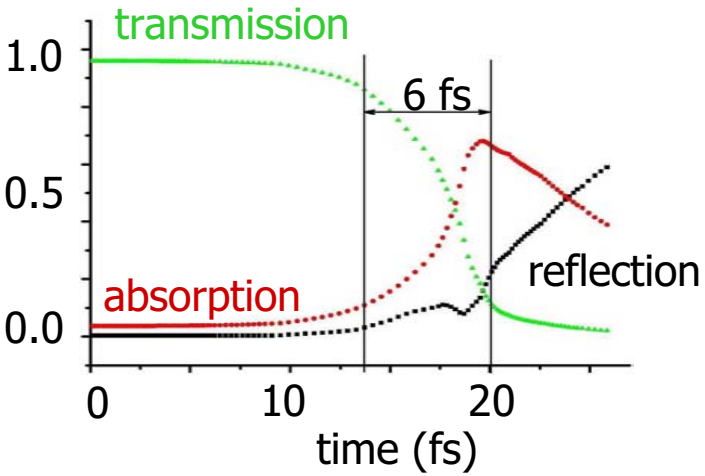

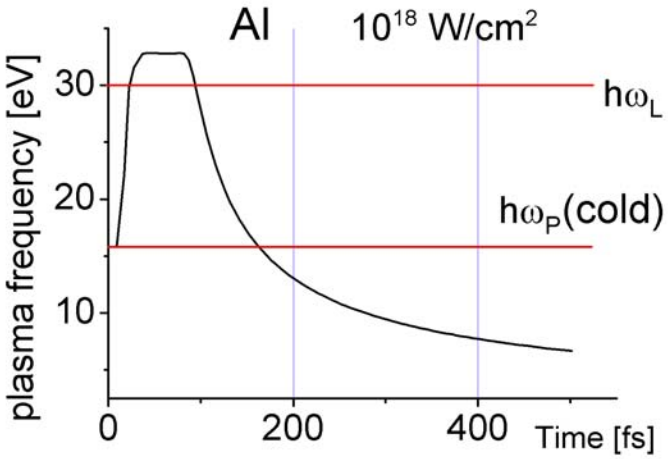

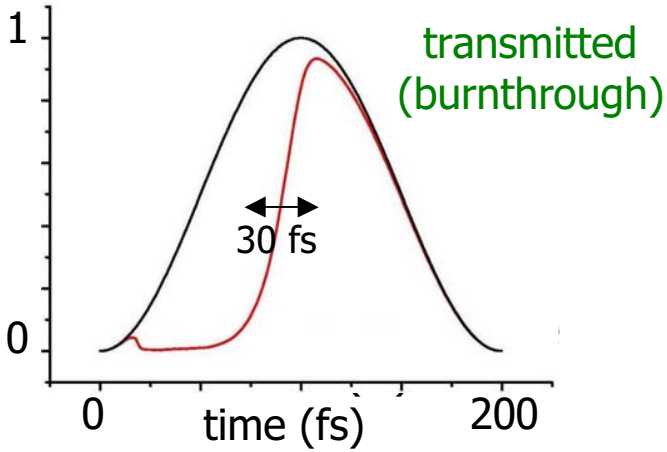

Hydrodynamic Response of Heated foil 200 fs - 5 ps

Al EOS
p,ρ diagram

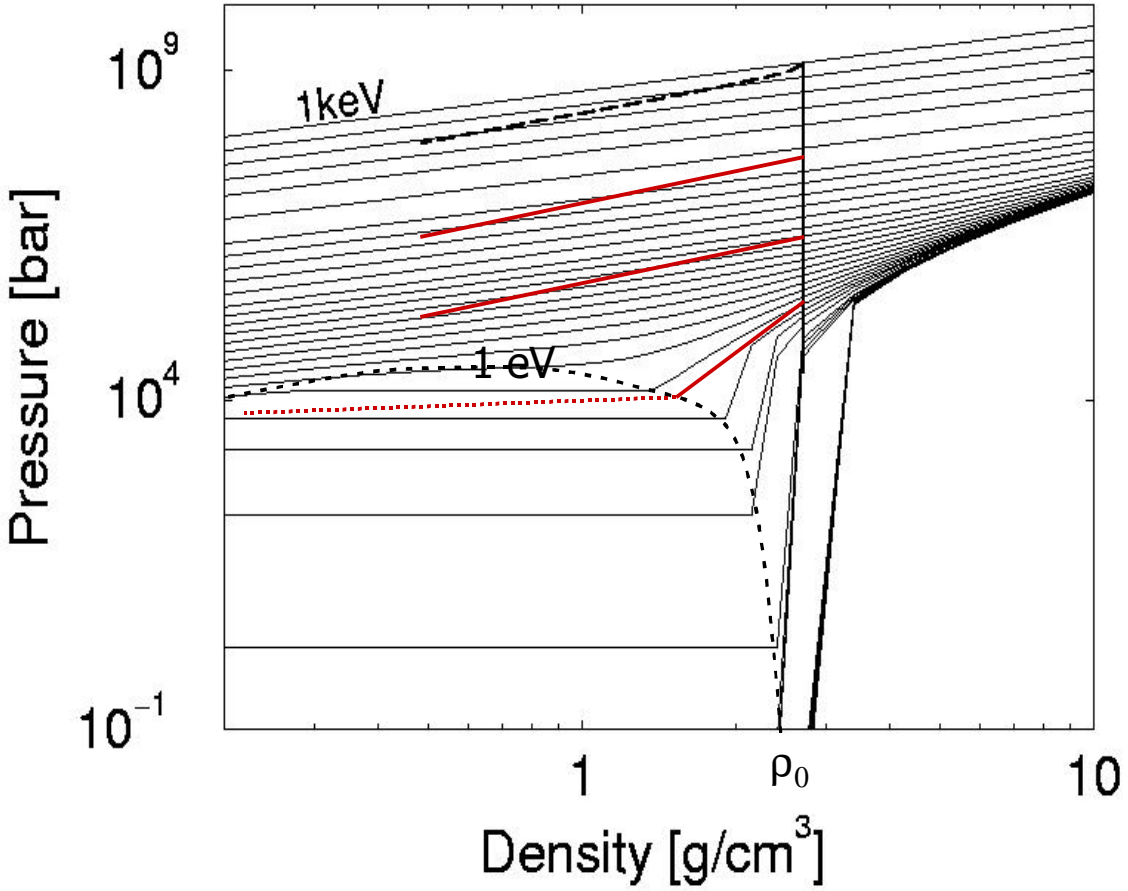

Phase trajectory of heated foil and different expansion isentropes

Phase Diagrams at T=1 – 10 eV are full of unexplored structure

Ogata, Kitamura, Ichimaru,
Elementary Processes in Dense Plasma,
Addison-Wesley, 1995.

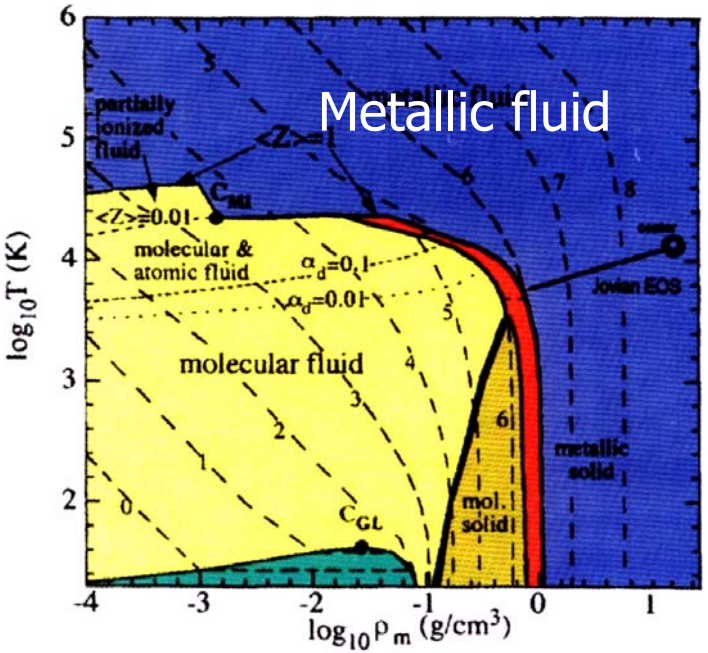

H

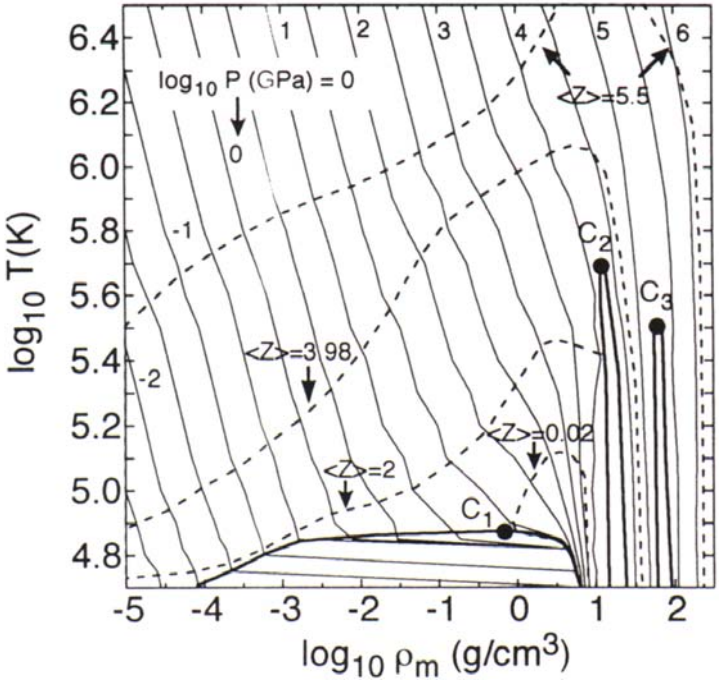

C

Phase-Transitions may trigger Amazing Hydro-Phenomena

K. Sokolowski-Tinten, J. Bialkowski, A. Cavalleri, D. von der Linde, A. Oparin, J. Meyer-ter-Vehn, A. Anisimov, PRL 81, 224 (1998)

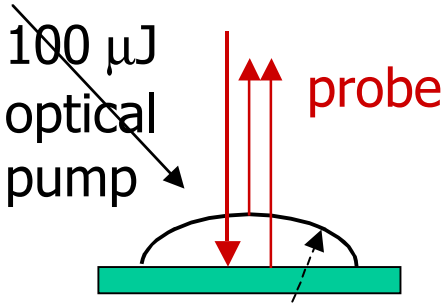

Thin layer (like soap bubble) of two-phase material, moves at velocity $c_o \ln \rho_0/\rho_1$, causes Newton rings.

Newton rings

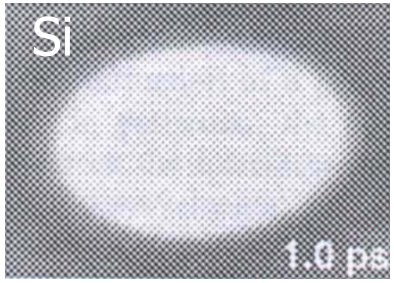

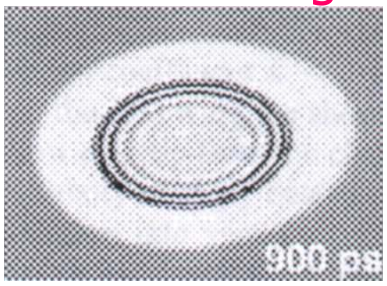

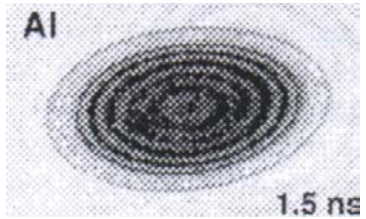

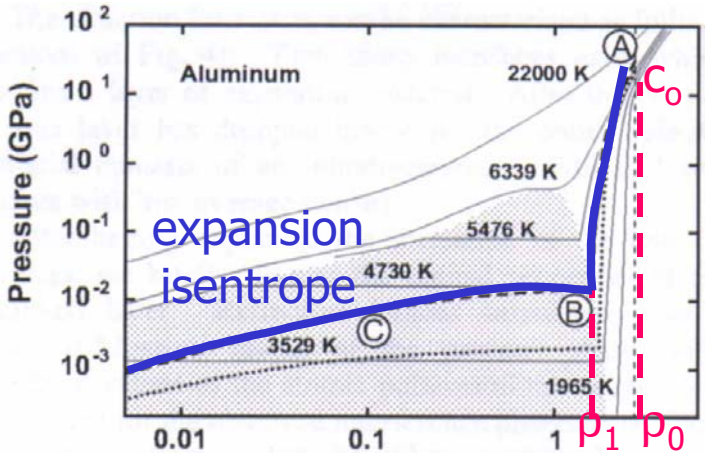

in XFEL experiment:

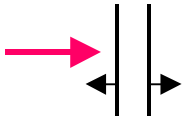

Thermalization time

for solid density, Te ≈ 100 eV

free electron system: 1 - 10 fs

electron-ion system: 100 fs - 1 ps

$$\tau_{ei} = 3.5\_10^{8}\ \mathrm{s}\ \ A T_e^{3/2} /(Z^2 n_e \ln \Lambda)$$

10^{19} cm^{-3} He gas pumped by 10^{14} W/cm^2 beam of 25 eV photons

Ke Lan, E. Fill, J. Meyer-ter-Vehn, to appear in EuroPhysics Letters (2003)

- He I laser at $\lambda = 58.4$ nm

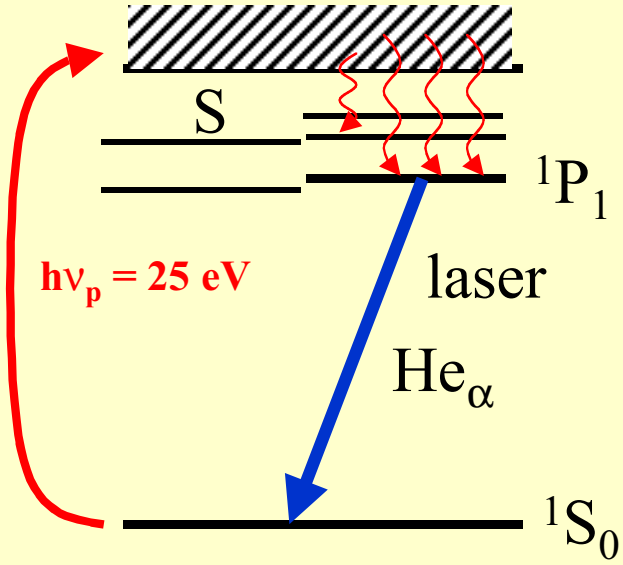

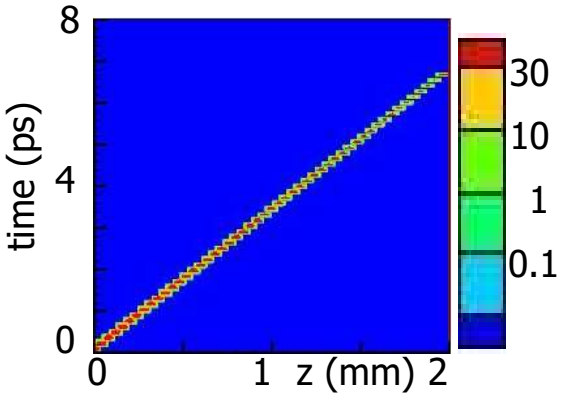

pump (TW/cm²)

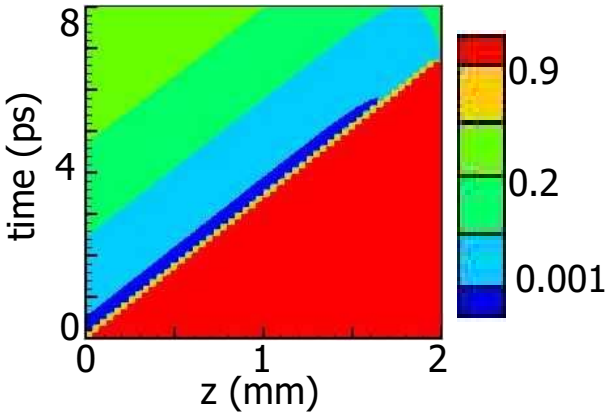

ground state population

Li (He-a) laser may generate 10-50 fs pulses at 20 nm

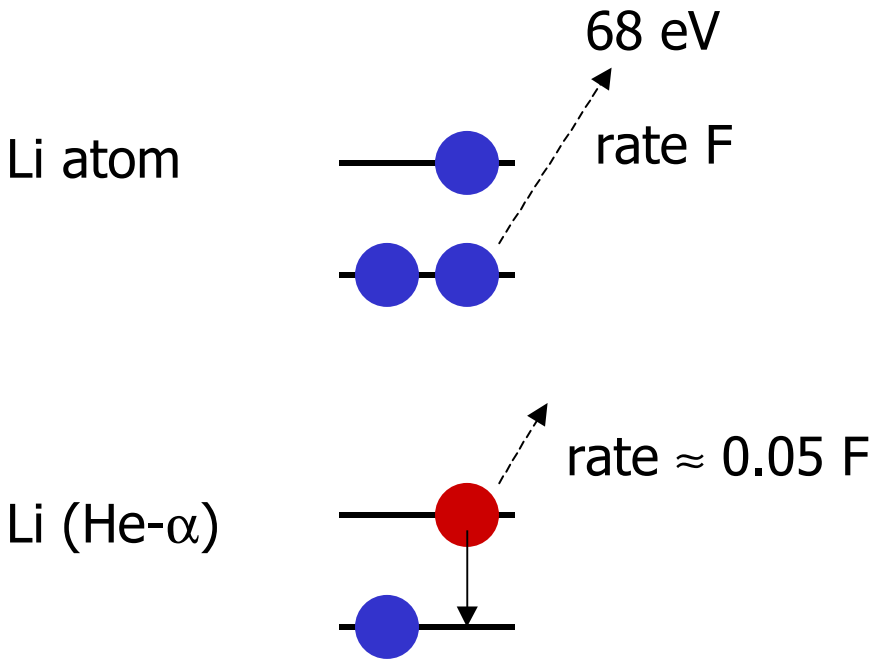

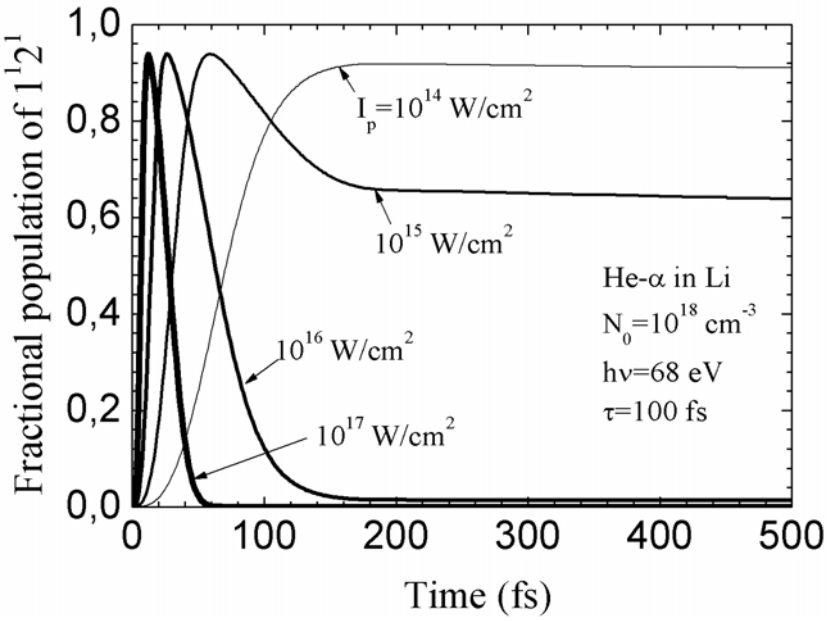

Conclusions

- TESLA XFEL pulses deposit specific energy up to e ≈ 10^9 J/g in solids producing uniform volumes of **solid-density pasma** with temperatures in the range of **T = 1 eV - 1 keV.** This opens a new era for dense plasma experiments.

- At photon energies 20 - 200 eV (TTF2 starting 2004), the XFEL pulses are close to the plasma frequency of hot solids and maximum absorption cross-sections. Hitting the resonance, foils act as ultra-fast switches.

- During the 100 fs interaction time, plasma non-equilibrium states are created with high densities of K-shell vacancies. This will allow to demonstrate **Ly-α and He-α laser** schemes in light elements (He, Li) experimentally for the first time.

Developments in Laser-Plasma Sources & Optics for X-Ray Microscopy & Microprobing

Alan Michette

S_awka Pfauntsch

Keith Powell

Thomas Graf

David Losinski

Chris McFaul

Rana Al-Mana

Kirk Atkinson

(also at GRAY CANCER INSTITUTE)

Varenna, October2003

Developments in Laser-Plasma Sources & Optics for X-Ray Microscopy & Microprobing

Overview

X-Ray Sources: Laser generated plasmas
Beam profiling

X-Ray Optics: Limited to a few 100 eV (a few nm)
to a few keV (a few tenths of a nm)

Developments in Laser-Plasma Sources & Optics for X-Ray Microscopy & Microprobing

The King s Laser Generated Plasma Source

Laser system		EKSPLA Nd:YAG
Wavelength		1064, 532, 355 nm
Beam size		~8 mm diameter
Divergence		~0.31, 0.16, 0.11 mrad (diffn. ltd.)
Pulse length		~850 ps
Pulse energy		~200, 80, 70 mJ
Energy variability		$\pm$2.5, 3, 3.5%
Repetition rate		Up to 50 Hz
Lens focal length		60 mm
Diffraction limited	Focal spot	~20, 10, 6.5 m
	Irradiance	~0.8, 1.3, 2.6$\times 10^{14}$ W cm^{-2}

Developments in Laser-Plasma Sources & Optics for X-Ray Microscopy & Microprobing

The King s Laser Generated Plasma Source

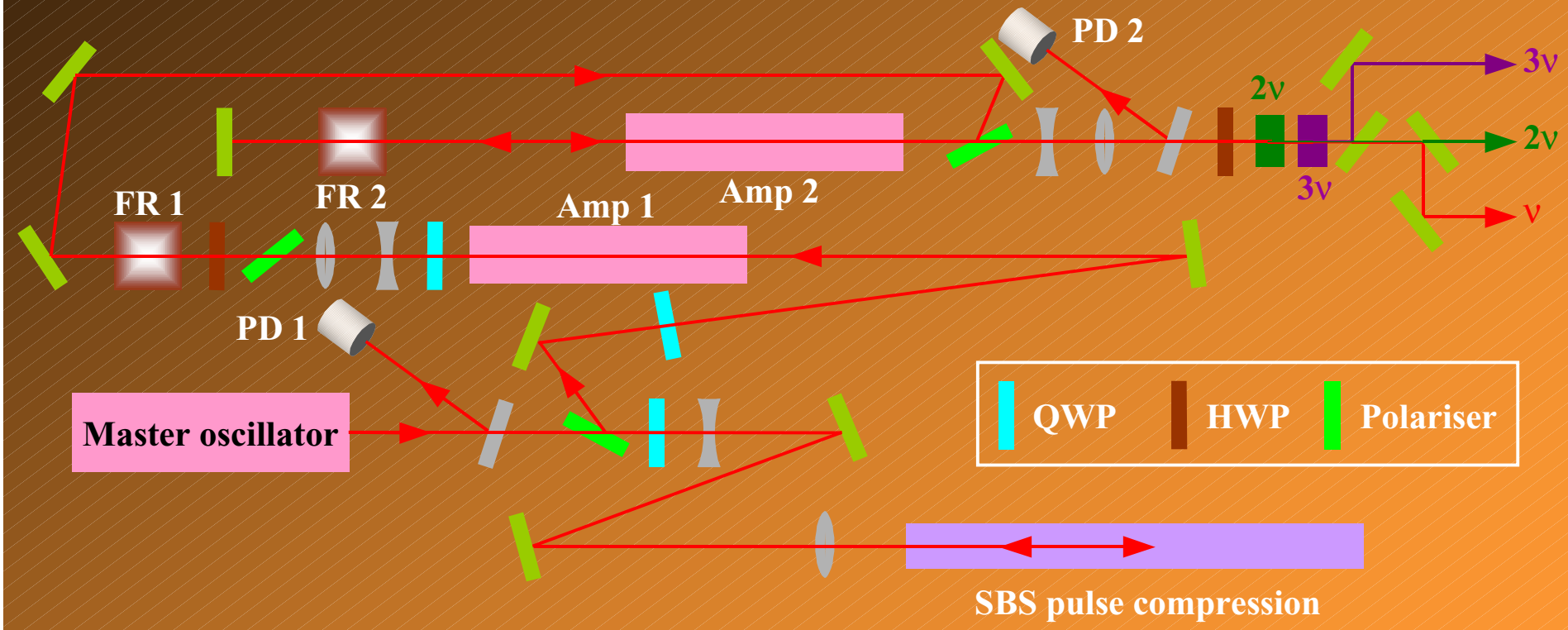

Centre for X-RAY SCIENCE

KING'S College LONDON
University of London

Developments in Laser-Plasma Sources & Optics for X-Ray Microscopy & Microprobing

The King s Laser Generated Plasma Source

Varenna, October2003

Developments in Laser-Plasma Sources & Optics for X-Ray Microscopy & Microprobing

The King s Laser Generated Plasma Source

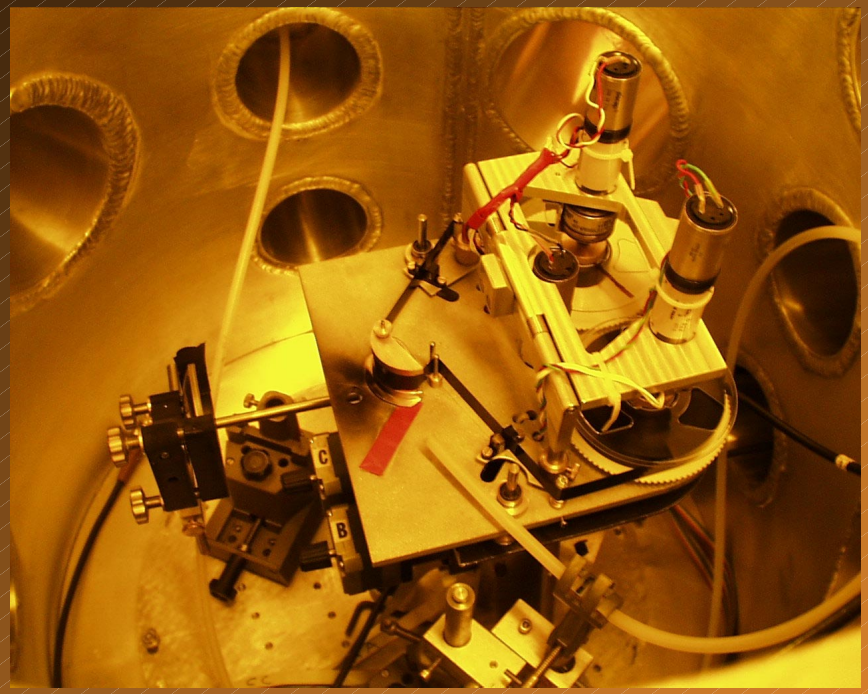

Tape targets:

- **Less debris than bulk material; can easily blow what there is away;**
- **Easy to arrange for a fresh surface for each pulse;**
- **A 12mm wide, 100m long tape will last for ~24hrs at 50Hz.**

Developments in Laser-Plasma Sources & Optics for X-Ray Microscopy & Microprobing

The King s Laser Generated Plasma Source

Source Size

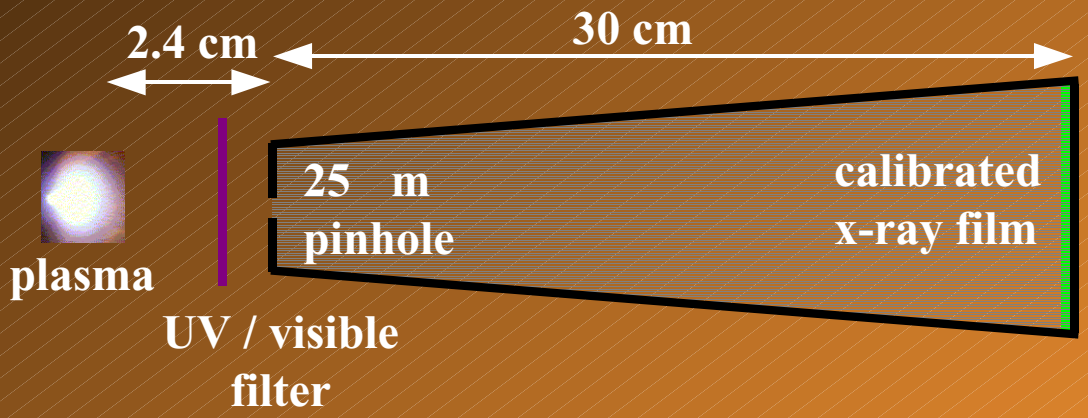

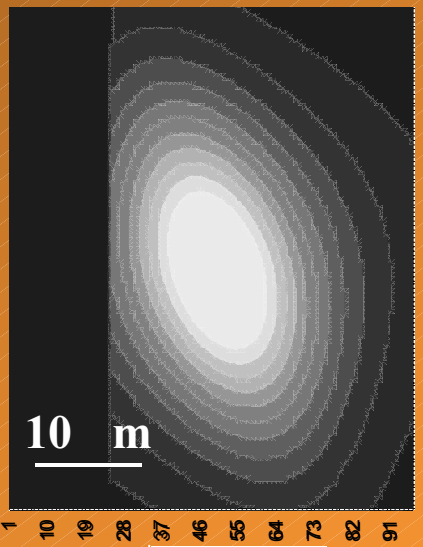

$$f(x) \propto \left[1 + \left\{ \frac{2(x - x_0)\sqrt{2^{1/M} - 1}}{w} \right\}^2 \right]^{-M}$$

(Pearson VII distribution)

Developments in Laser-Plasma Sources & Optics for X-Ray Microscopy & Microprobing

The King s Laser Generated Plasma Source

Laser system		EKSPLA Nd:YAG
Wavelength		1064, 532, 355 nm
Beam size		~8 mm diameter
Divergence		~0.31, 0.16, 0.11 mrad (diffn. ltd.)
Pulse length		~850 ps
Pulse energy		~200, 80, 70 mJ
Energy variability		$\pm$2.5, 3, 3.5%
Repetition rate		Up to 50 Hz
Lens focal length		89 mm
Diffraction limited	Focal spot	~29, 15, 10 m
	Irradiance	~0.4, 0.6, 1.2$\times 10^{14}$ W cm^{-2}
	Source size	not measured, ~20, 16 m

Developments in Laser-Plasma Sources & Optics for X-Ray Microscopy & Microprobing

Laser Generated Plasma Sources

Source Size Through Focus

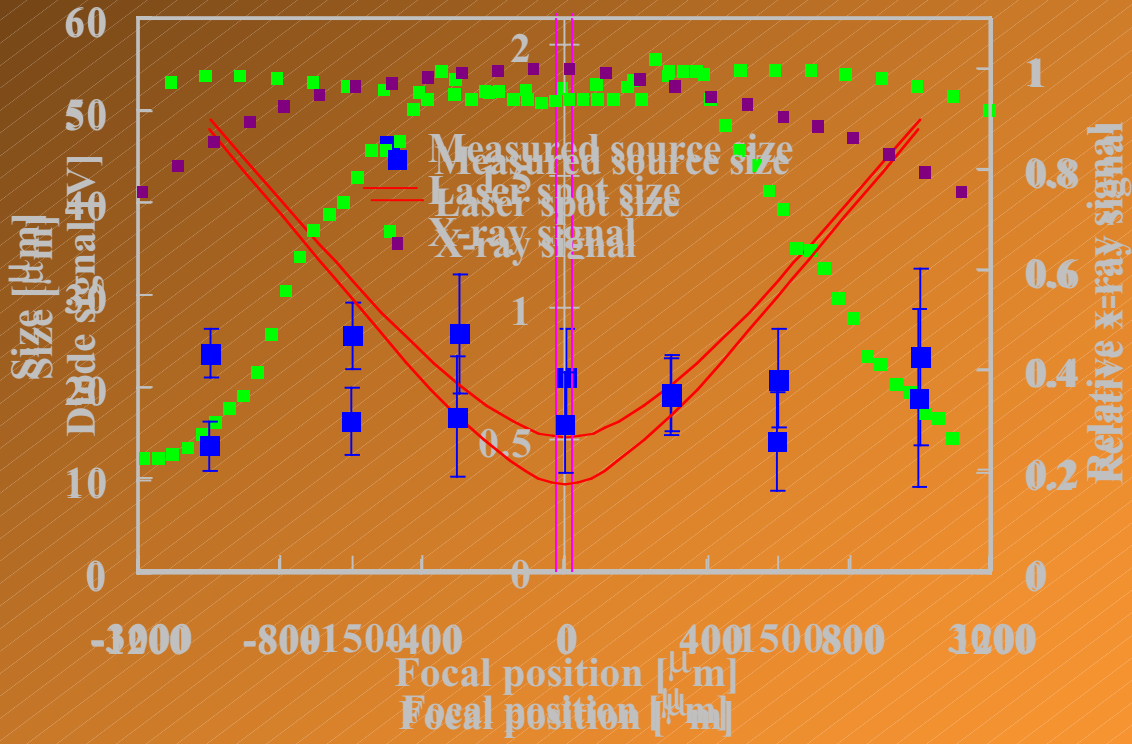

Varenna, October2003

Developments in Laser-Plasma Sources & Optics for X-Ray Microscopy & Microprobing

Laser Generated Plasma Sources

Source Size Through Focus

UV, 89mm lens

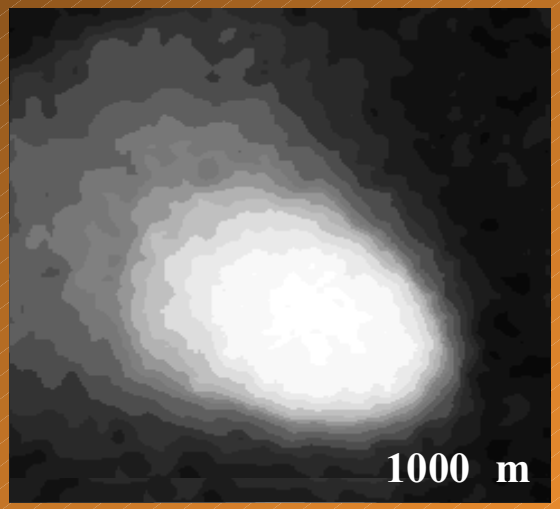

Developments in Laser-Plasma Sources & Optics for X-Ray Microscopy & Microprobing

Laser Generated Plasma Sources

Source Size Through Focus

UV, 89mm lens

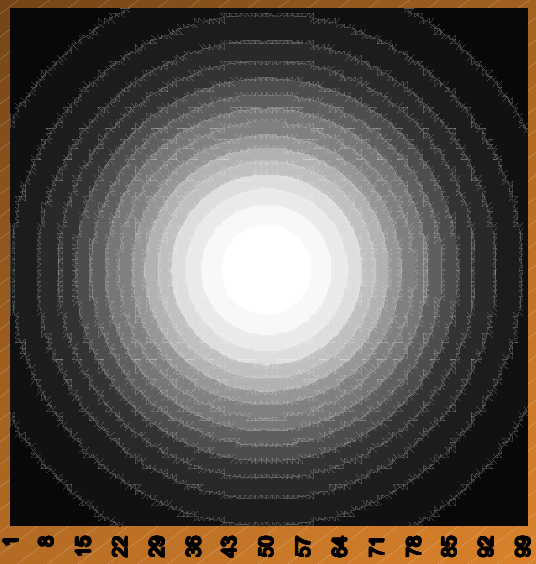

focal spot

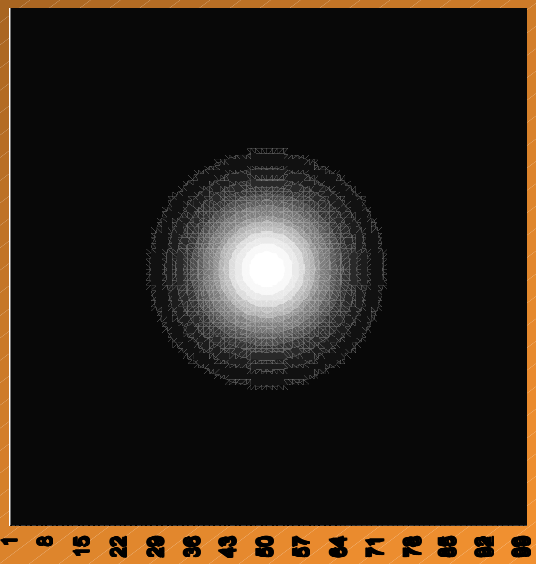

source

Developments in Laser-Plasma Sources & Optics for X-Ray Microscopy & Microprobing

Spectra Through Focus

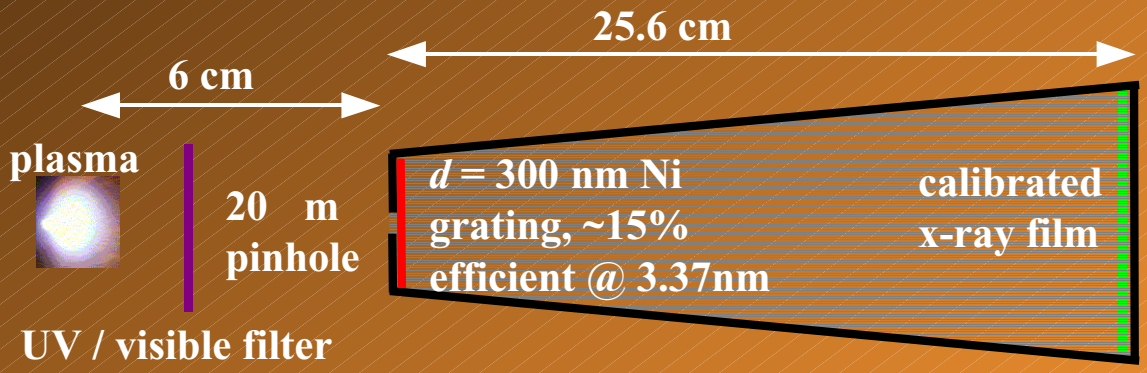

Target Mylar* Mainly line spectrum

*Video tape (reversed)
— BASF Vision is the best!

Helium filtering

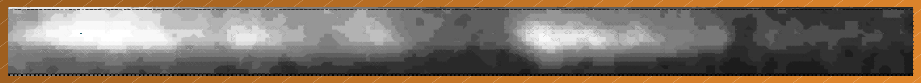

Focus
300 μm
600 μm
1 mm

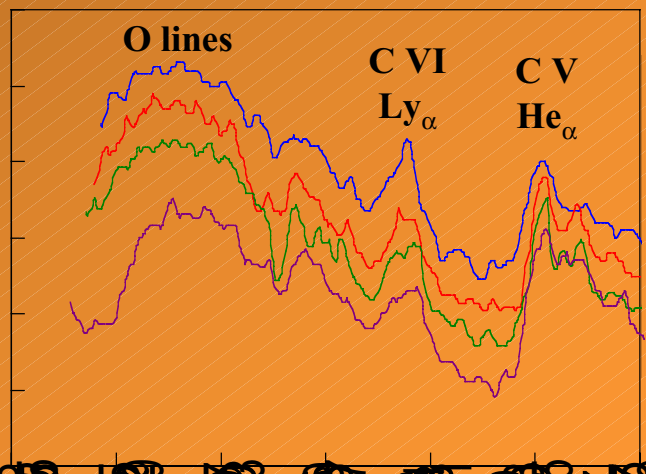

Wavelength [nm]

Varenna, October2003

Developments in Laser-Plasma Sources & Optics for X-Ray Microscopy & Microprobing

Spectra Through Focus

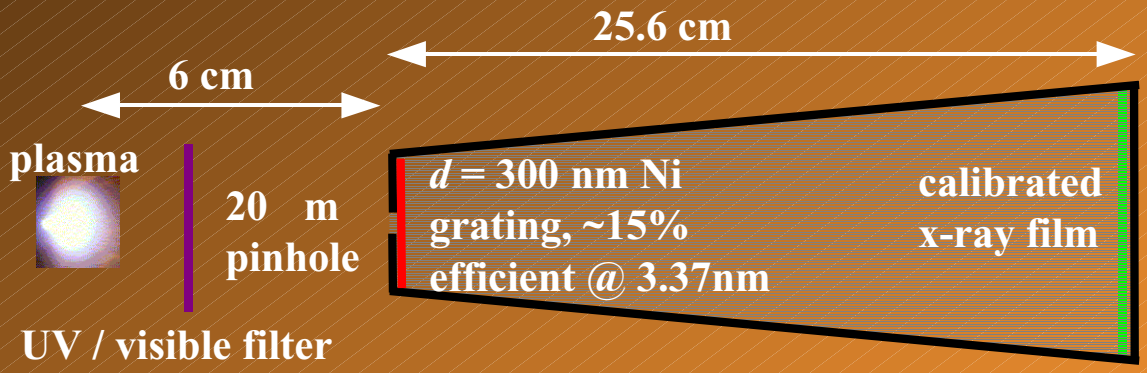

Target Mylar* Mainly line spectrum

*Video tape (reversed)
— BASF Vision is the best!

Nitrogen filtering

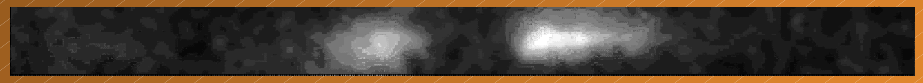

Line widths compatible with grating geometrical resolution for a 20 m source.

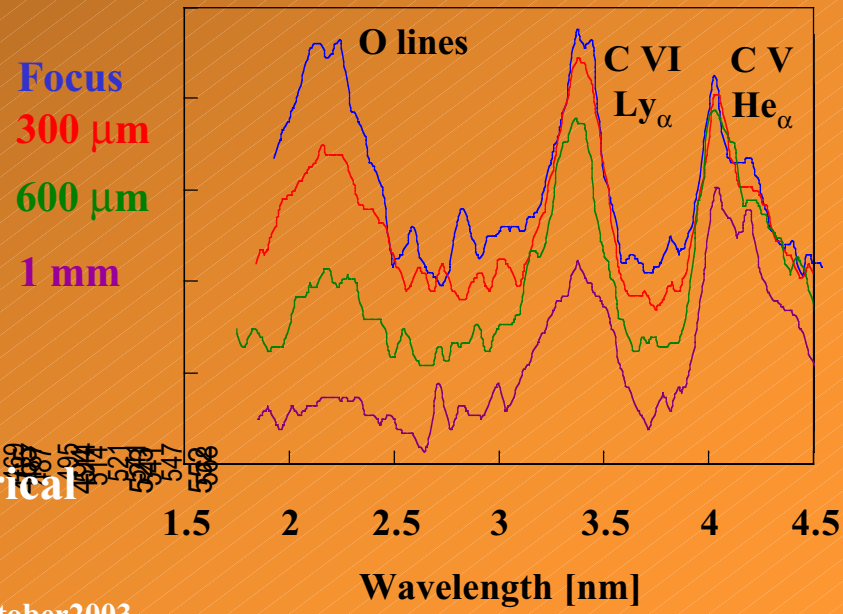

Developments in Laser-Plasma Sources & Optics for X-Ray Microscopy & Microprobing

Beam Profiling

One way of controlling the emission through focus is to use a computer-generated phase mask.

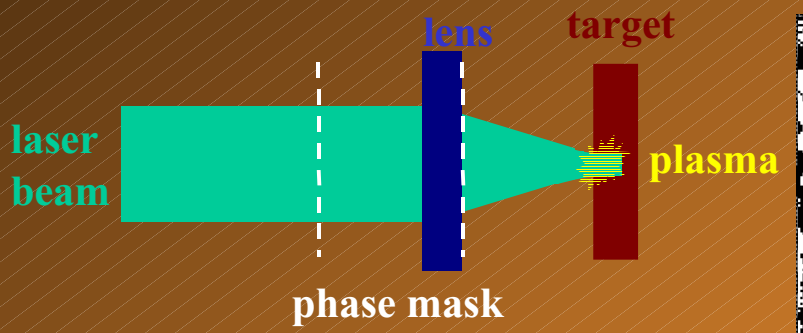

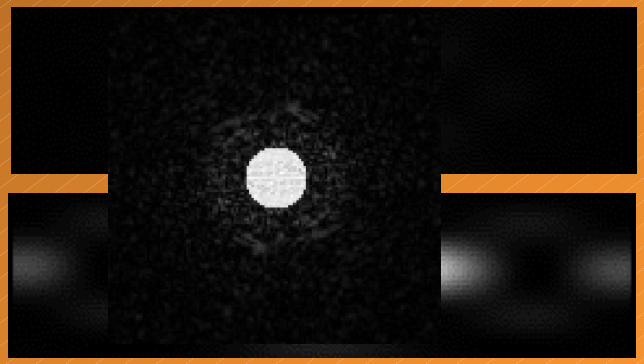

This binary mask shows a top hat for the focal depth of an 0.5NA lens with, leading to less interdiffraction-limited focal spot size. This could reduce any sensitivity to focal position.

Suitable masks can be made by the sol-gel process.

Developments in Laser-Plasma Sources & Optics for X-Ray Microscopy & Microprobing

X-Ray Optics for High Resolution Probes

What s wrong with current optics?

i.e. <1 m

Grazing incidence	Aberrations
Multilayer mirrors	Wavelength selective Insufficient resolution
Supermirrors	Hard to make Insufficient resolution?
Compound refractive lenses	Insufficient resolution
Zone plates	Inefficient Wavelength dependent focal length Low aperture

Developments in Laser-Plasma Sources & Optics for X-Ray Microscopy & Microprobing

Zone plates: state of the art

Manufacture	**e-beam lithography**
Substrate	**Si_xN_y**
N	**a few hundred to a few thousand**
D	**~100 –300 m**
d	**~25 –100 nm**
f_1	**a few mm at $\lambda = 3.37$ nm**
Efficiency	
Amplitude	**~7% achieved**
Phase	**~15% achieved**

Silicon support
Silicon nitride
Chromium etch stop layer
Tungsten (e.g.)
Photoresist

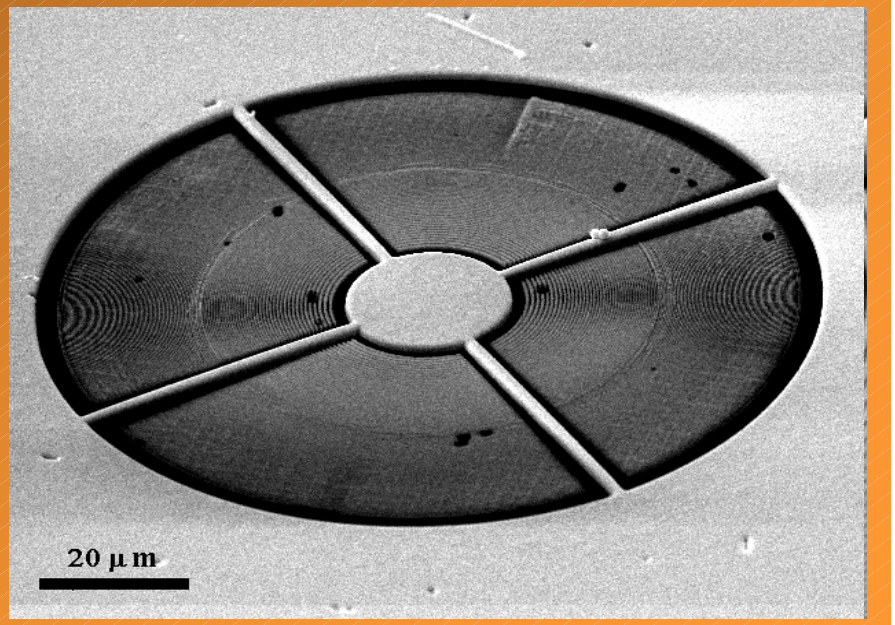

A 100 m / 95 nm, 700 nm tungsten zone plate,with a 2 m electroplated gold central stop. Designed for use at 4.5 keV on the x-ray microprobe at the Gray Cancer Institute.

Developments in Laser-Plasma Sources & Optics for X-Ray Microscopy & Microprobing

X-Ray Optics for High Resolution Probes

What s wrong with current optics?

Grazing incidence	Aberrations
Multilayer mirrors	Wavelength selective Insufficient resolution
Supermirrors	Hard to make Insufficient resolution?
Compound refractive lenses	Insufficient resolution
Zone plates	Inefficient Wavelength dependent focal length Low aperture
Capilleries Microchannel plates	Insufficient resolution

Developments in Laser-Plasma Sources & Optics for X-Ray Microscopy & Microprobing

Capillary Optics & Derivatives

Monocapillary & polycapillary optics & microchannel plate arrays have also been used for x-ray optics.

Grazing incidence reflections along ~10^6 small diameter channels.

Large apertures & bandpasses with transmission efficiencies of several tens of percent.

Current manufacturing methods limit channel diameters to ~ 0.5 m, arrays to a few millimetres square & focal spots to ~10 m.

Performances limited by channel tilting, curvature errors, waviness, diffraction & uncontrolled substrate bending.

Developments in Laser-Plasma Sources & Optics for X-Ray Microscopy & Microprobing

Capillary Optics & Derivatives

Performance also limited by:

Non-circular symmetry (in some cases),

leading to poor PSFs, e.g.,
cruxiform for square-packed
microchannel plate arrays.

Defects

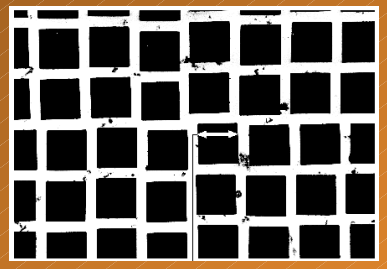

& (especially for microchannel plates) because they are primarily made for other purposes.

Developments in Laser-Plasma Sources & Optics for X-Ray Microscopy & Microprobing

Microstructured Optical Arrays

Could improve performances of capillary-type optics by manufacturing arrays designed for specific purposes.

Advances in micro- & nano-fabrication allow such micro - structured optical arrays (MOAs) to be designed & made.

These offer the possibility of much better performances through greater flexibility in the choice of channel geometry.

MOAs can also have built-in adaptivity & controllable focal length & can therefore act as **zoom lenses.**

Developments in Laser-Plasma Sources & Optics for X-Ray Microscopy & Microprobing

Microstructured Optical Arrays

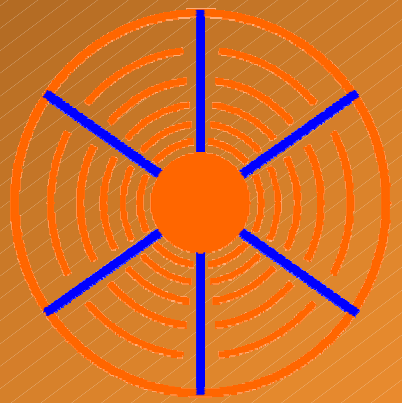

Channel widths increase outwards, to allow for the larger incidence angle.

Supporting spokes coated with bimorph material bend the MOA ⇒ focusing & controllable focal length.

By flexing (parts of) spokes independently the MOA can be made adaptive ⇒ aberrations corrected.

Similar bimorphs have been used in other applications, e.g., micro-cantilevers.

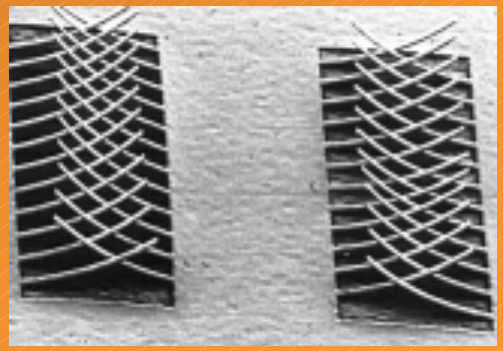

Courtesy Ejaz Huq, Rutherford Appleton Laboratory

Developments in Laser-Plasma Sources & Optics for X-Ray Microscopy & Microprobing

Microstructured Optical Arrays

The Abbe sine condition requires two reflections from the same wall of each channel, implying thick channels.

⇒ Manufacturing difficulties & hard to bend.

Solution: make the MOA in two parts, aligned using micromachined locators.

Components flexed independently.

More bending flexibility by using series of independent bimorph strips.

In practice, many more strips would be used.

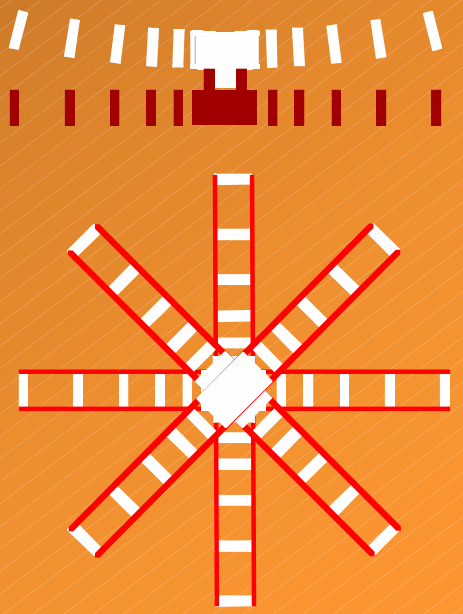

Developments in Laser-Plasma Sources & Optics for X-Ray Microscopy & Microprobing

Microstructured Optical Arrays

A 1D prototype has been made & is awaiting testing.

[illegible]

factor *G*.

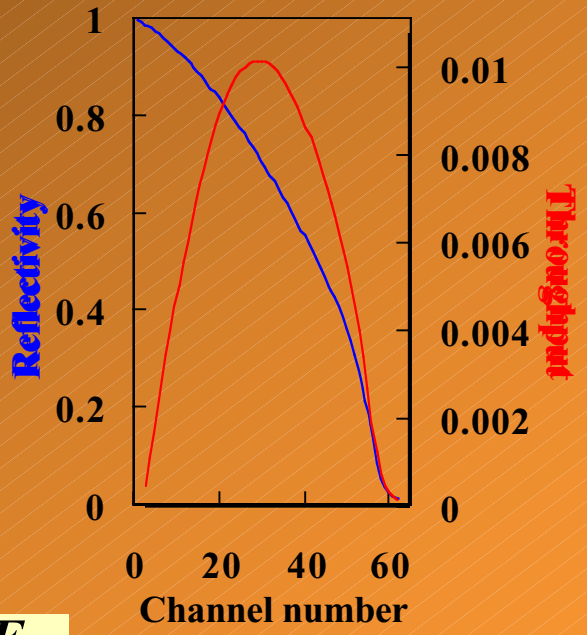

	R	*G*	*F* [m]
Prototype	75%	6.3	0.70
80% open area	75%	10	0.70
Varying channels	78%	17	0.67

Developments in Laser-Plasma Sources & Optics for X-Ray Microscopy & Microprobing

Conclusions

Laser generated plasmas are strong x-ray emitters.

Performances could be improved by:

beam profiling and

better x-ray optics.

They could then be competitive with synchrotrons for a range of applications including:

radiation biology and

x-ray microscopy.

Picosecond time-resolved X-ray diffraction from laser-shocked semiconductors

Kazutaka G. NAKAMURA

Materials and Structures Laboratory
Tokyo Institute of Technology

AgendaÅ

1.Motivation

2. Generation of pulsed hard X-rays

3. Picosecond time-resolved X-ray diffraction of 300-ps laser irradiated semiconductors: Si(111) & Ge(111)

Ultrashort high-energy radiation and matter, Villa Monastero, Varenna, Oct. 10, 2003

Motivation

Elucidate structural dynamics of phase transition and chemical reaction of solid

- Transition time (Dt) ?
- Pathway of structural changes (A-A1-A2-B) ?
- Transition structure (*) ?

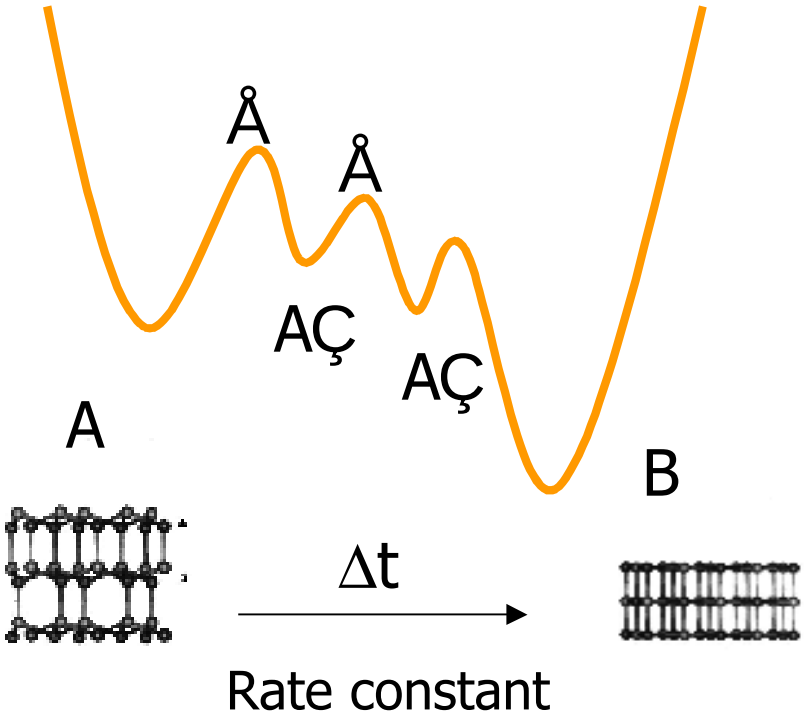

LEXS:Laser-driven electron X-ray sources

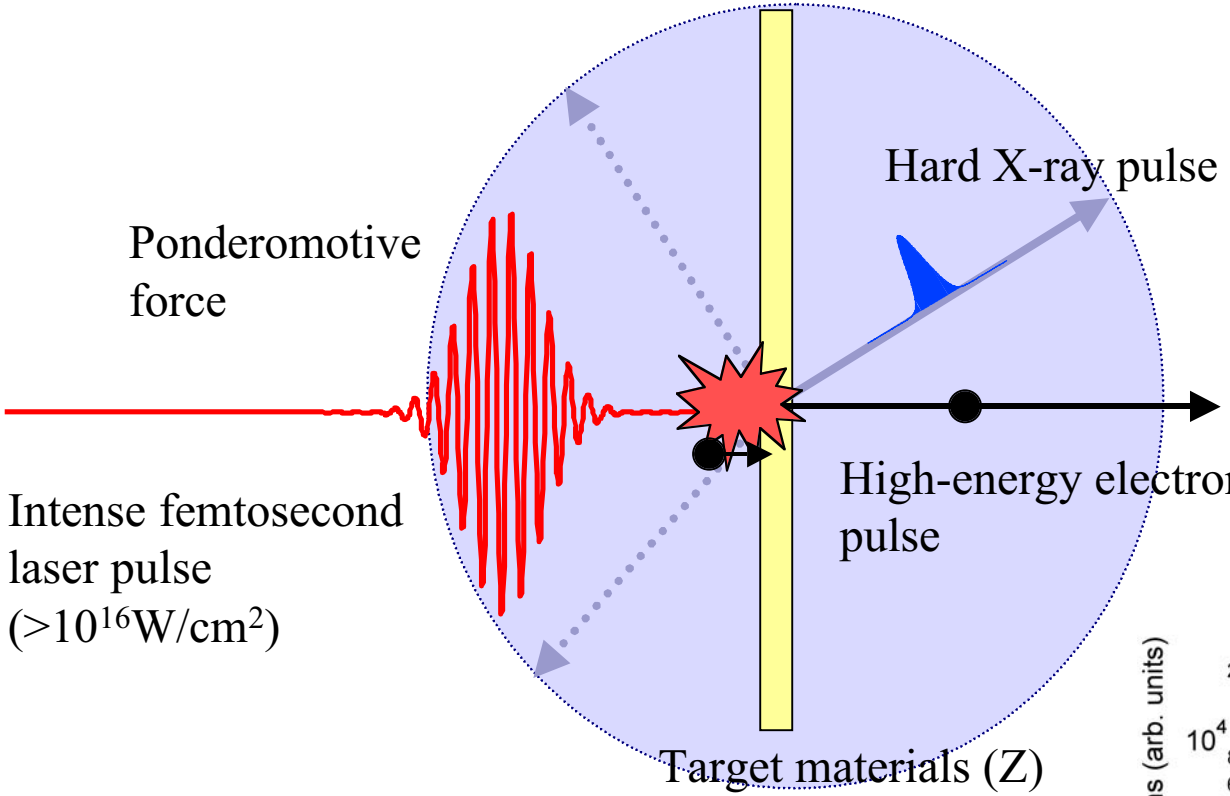

Cu film target (30 μm)
I=2.7x10^{18}W/cm^2

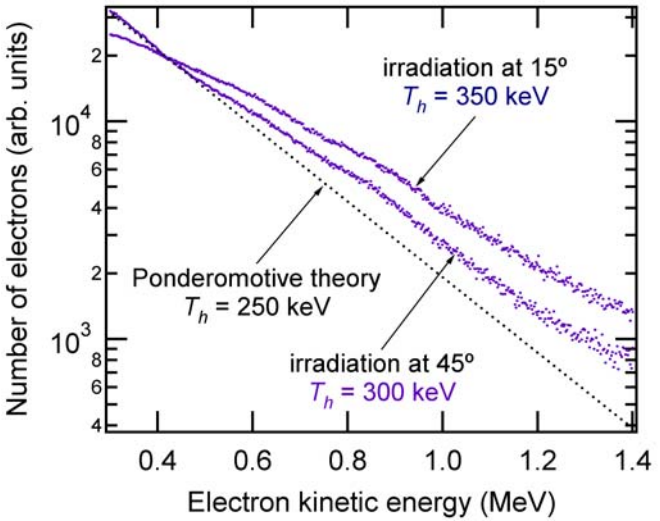

$$U_p = \frac{1}{2} m_e \langle v_{osc}{}^2 \rangle = \frac{eE_0{}^2}{4m_e\omega^2} = \frac{2\pi e^2 I}{m_e c\omega^2}$$
$$= 9.3\times10^{14} I(\mathrm{W/cm^2})\lambda(\mu\mathrm{m})^2$$

TW laser system in Tokyo Tech

Ti:sapphire Å780 nm) , pulse duration: 50 fs
laser energy Å200 mJ, pre-pulse: 10^{-6}

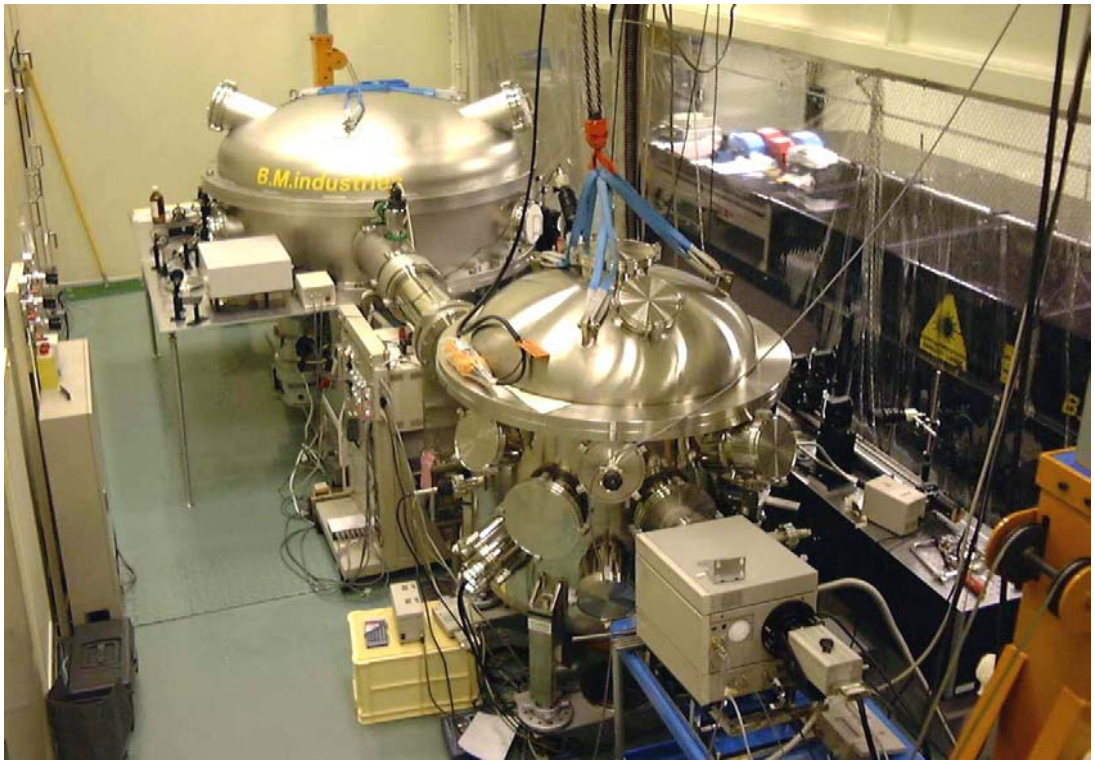

X-ray emission (I =10^{16} - 10^{17} W/cm^2)

- **Energy spectra**

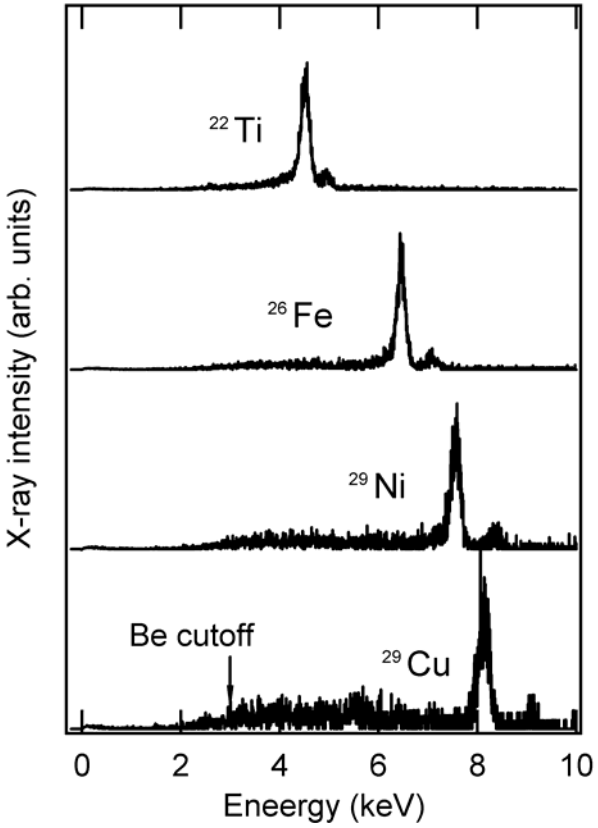

Characteristic X-rays obtained by X-ray CCD camera at power density of 3Å10^{16} W/cm^2.

- **Temporal profiles**

Cu:Kα 6.5x10^{10}photons/4πsr/pulse

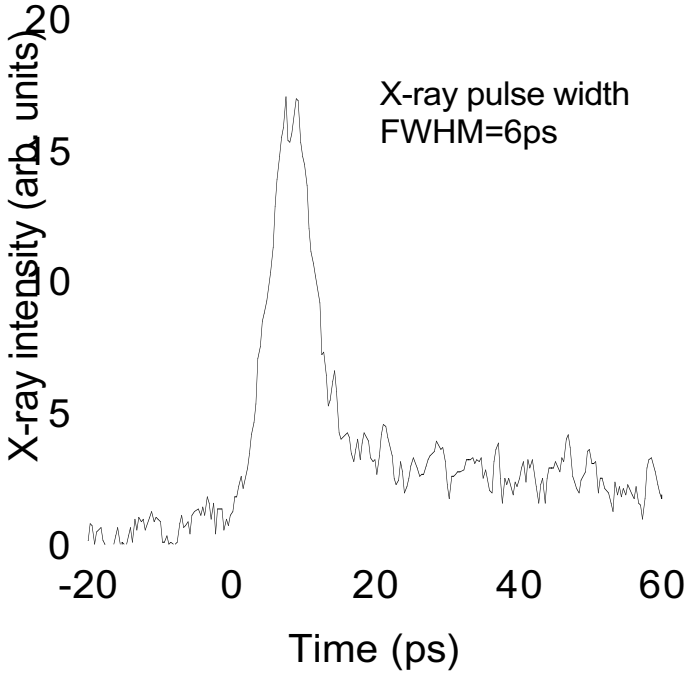

The temporal profiles obtained by the X-ray streak camera. The energy extends from 1 to 10 keV are accumulated. *I* ~ 10^{17} W/cm^2

M. Yoshida *et al.* APL 73 (1998) 2393; Y. Fujimoto *et al.* JJAP 38 (1999) 6754

Time-resolved X-ray diffraction from laser-irradiated Si(111)

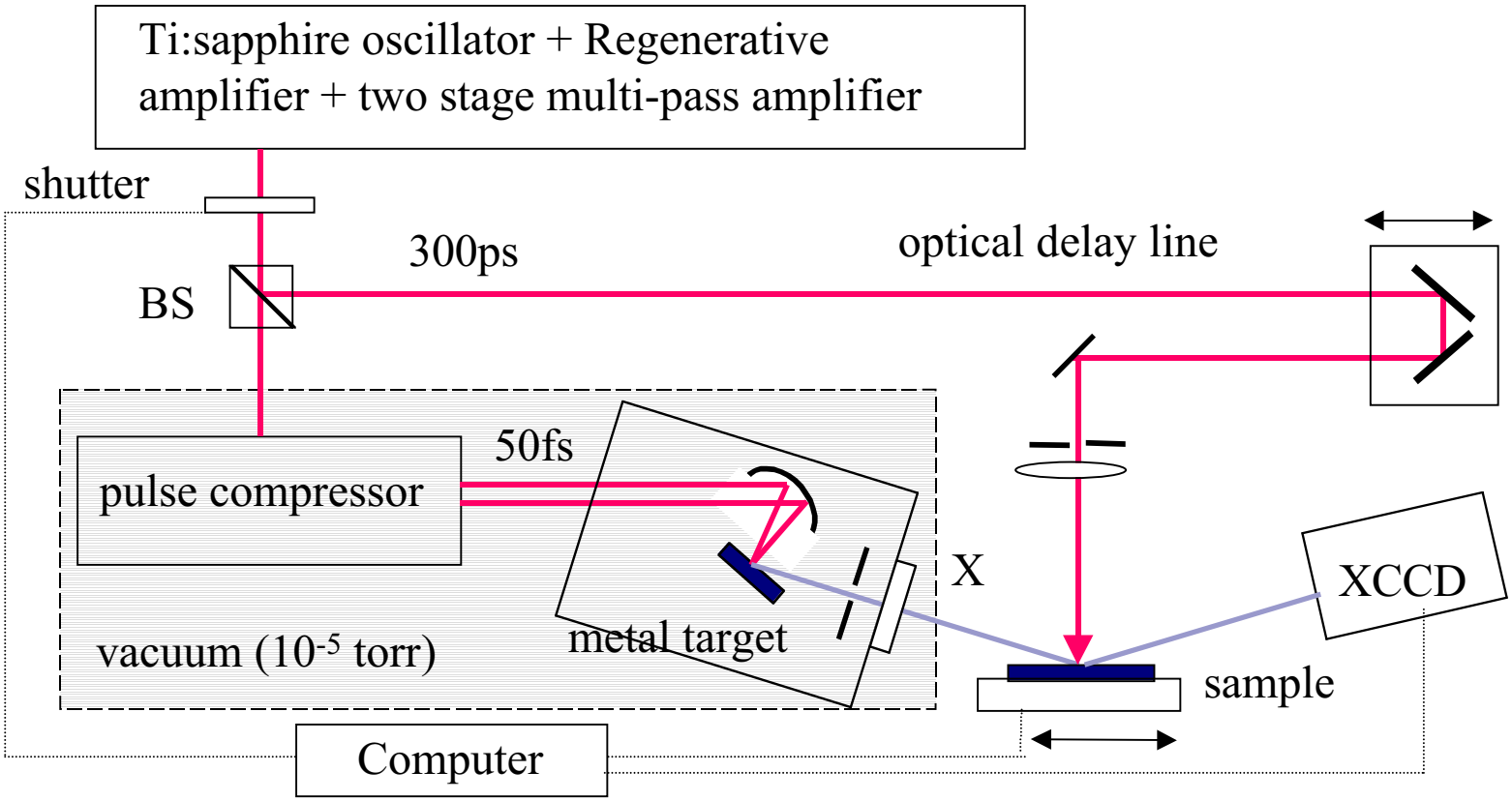

X-ray diffraction: single shot experiment

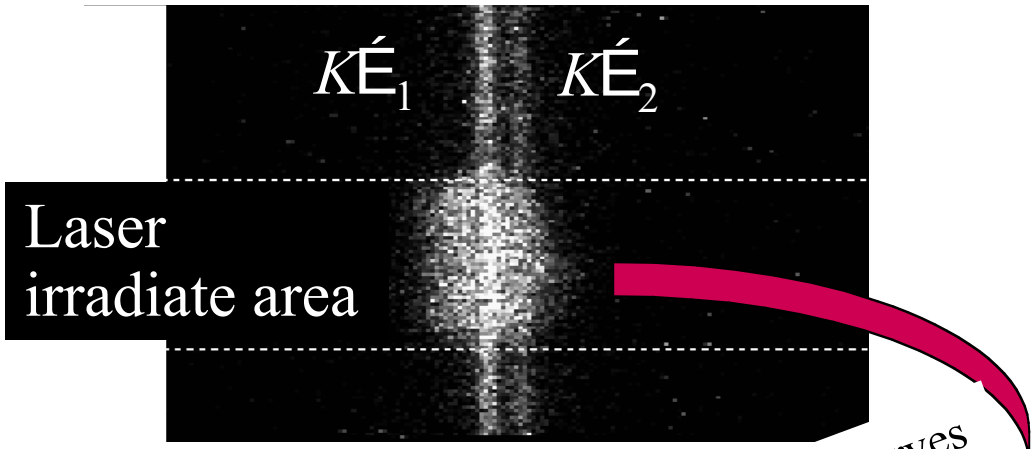

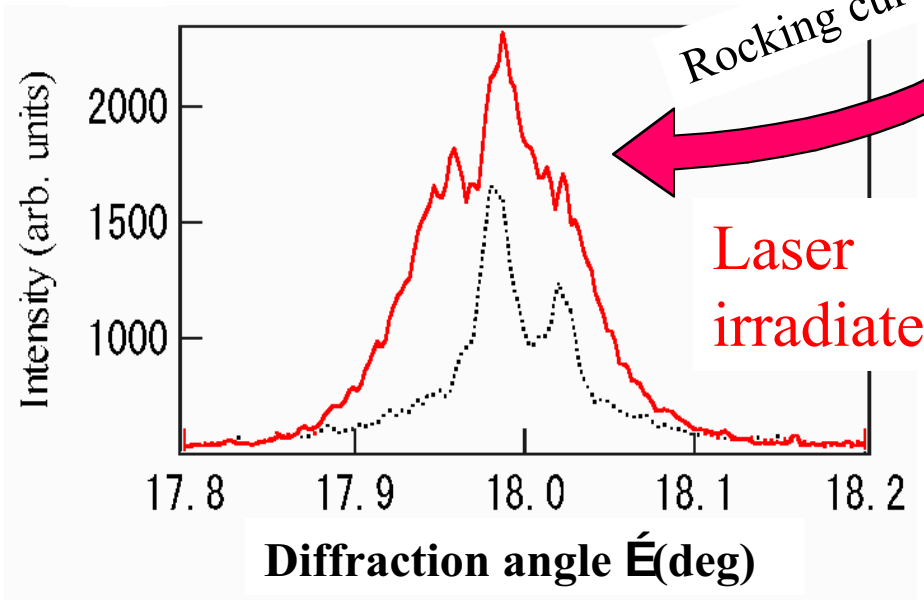

Bragg condition

2d SinÉÅÅ

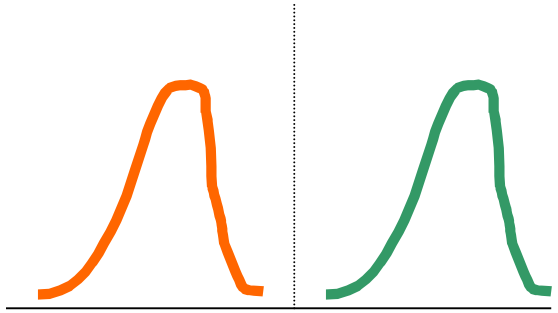

Ålow É HighÅ

Lattice Expansion

Lattice Compression

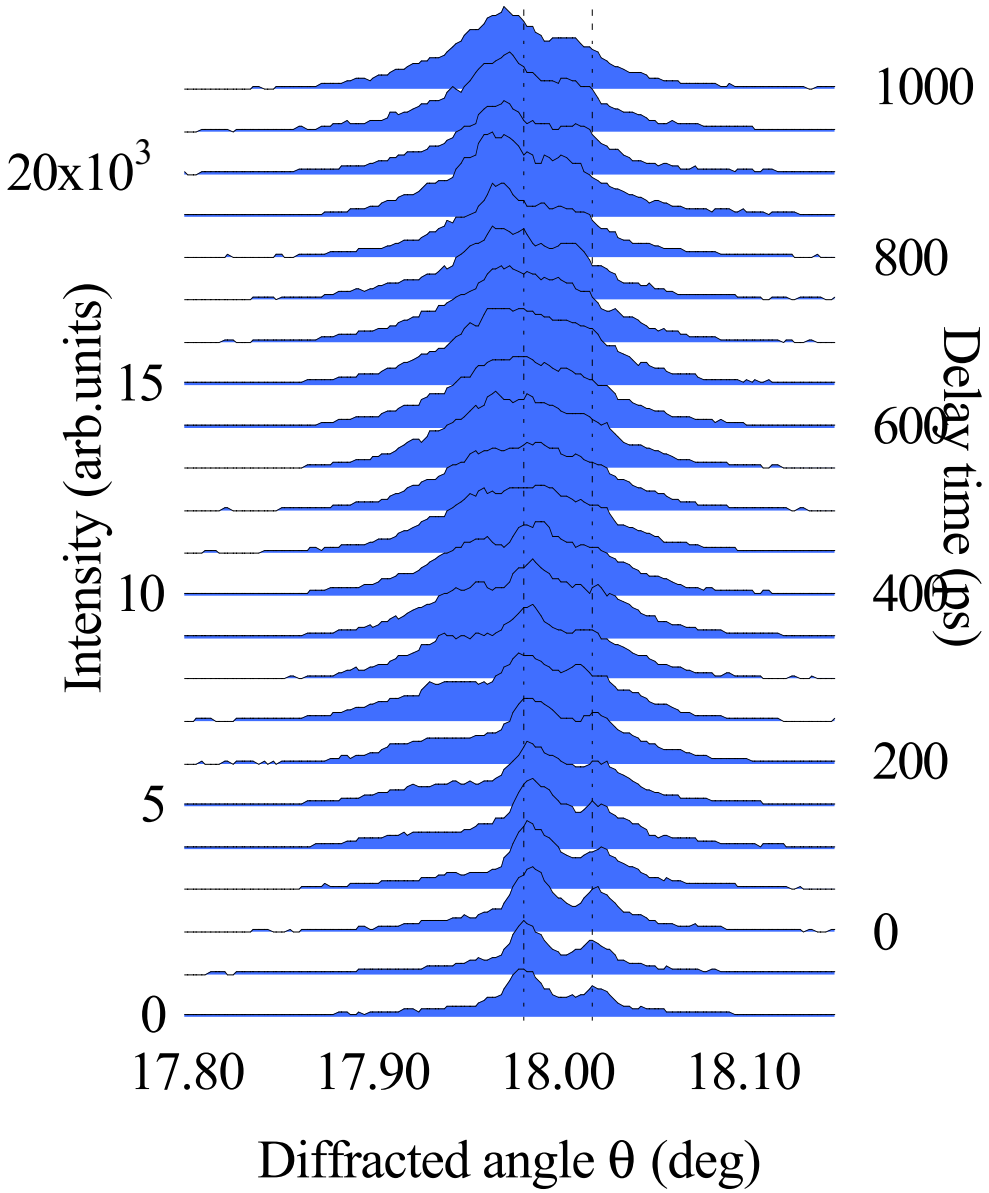

Single shotÅexperiment

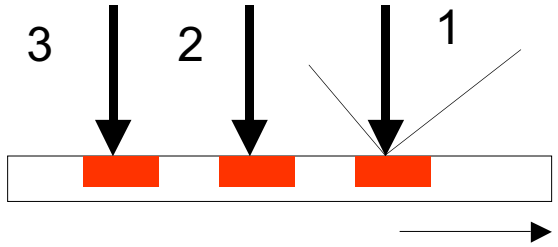

Picosecond time-resolved X-ray diffraction from Si(111) crystal under 300 ps laser irradiation at 1J/cm^2. Time step is 50 ps and accumulation of 600 data.

A. Yazaki et al. JJAP 41 (2002)1614;
H. Kishimura *et al.* J. Chem. Phys. (in press)

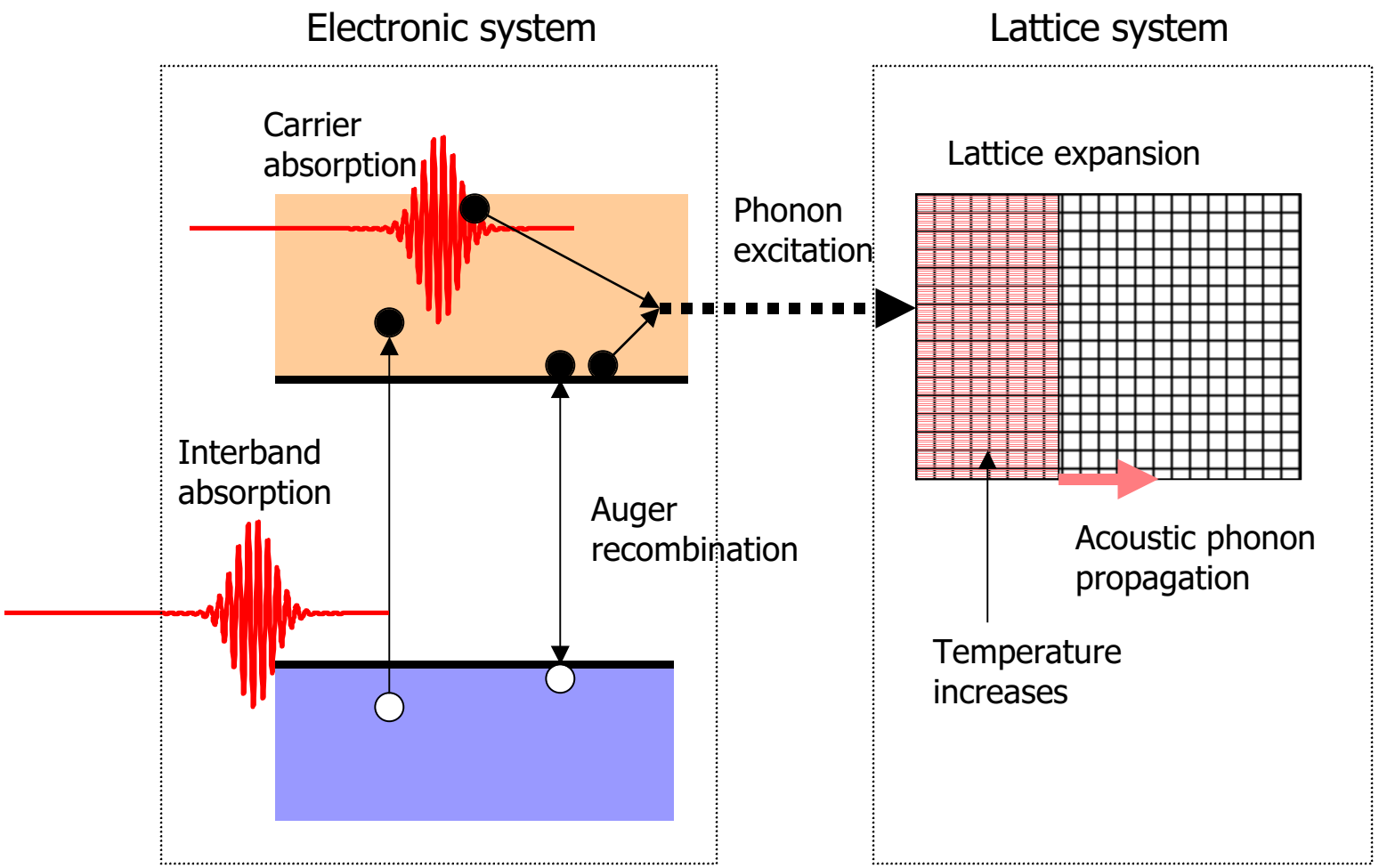

Rate equations: N(x,t), T(x,t)

Diffusion equations: T(x,t)

Hydro-dynamic equations: u(x,t)

Model of laser heating and phonon generation

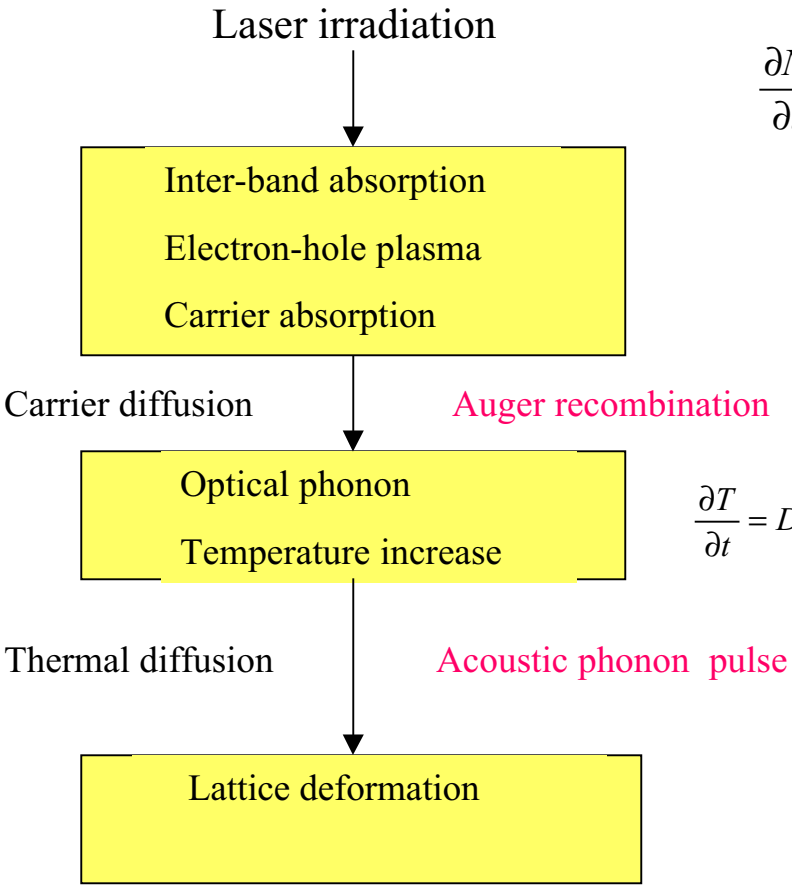

$$\frac{\partial N}{\partial t}+\frac{N}{\tau_R}=D\frac{\partial^2 N}{\partial x^2}+\frac{\alpha(1-R)}{E}I(x,t)+\frac{\beta(1-R)^2}{2E}I(x,t)^2$$

$$\frac{\partial}{\partial t}I(x,t)=-\left[\alpha+\Theta N+\beta I(x,t)\right]I(x,t)$$

Rate eq., diffusion eq.

$$\tau_R=\frac{1}{\gamma N^2}$$

$$\frac{\partial T}{\partial t}=D_T\frac{\partial^2 T}{\partial x^2}+\frac{E_g N}{C_v\tau_R}+\left(\frac{E-E_g}{C_v}\right)\left[\left(\frac{\alpha(1-R)}{E}+\Theta N\right)+\frac{\beta(1-R)^2}{2E}I(x,t)\right]I(x,t)$$

Hydro-dynamics

$$\rho\frac{\partial^2 u}{\partial t^2}=\rho v^2\frac{\partial^2 u}{\partial z^2}+B\frac{\partial E_g}{\partial P}\frac{\partial N}{\partial z}+3B\beta\frac{\partial T}{\partial z}$$

Carrier density and temperature at surface: 300ps pulse 3GW/cm^2

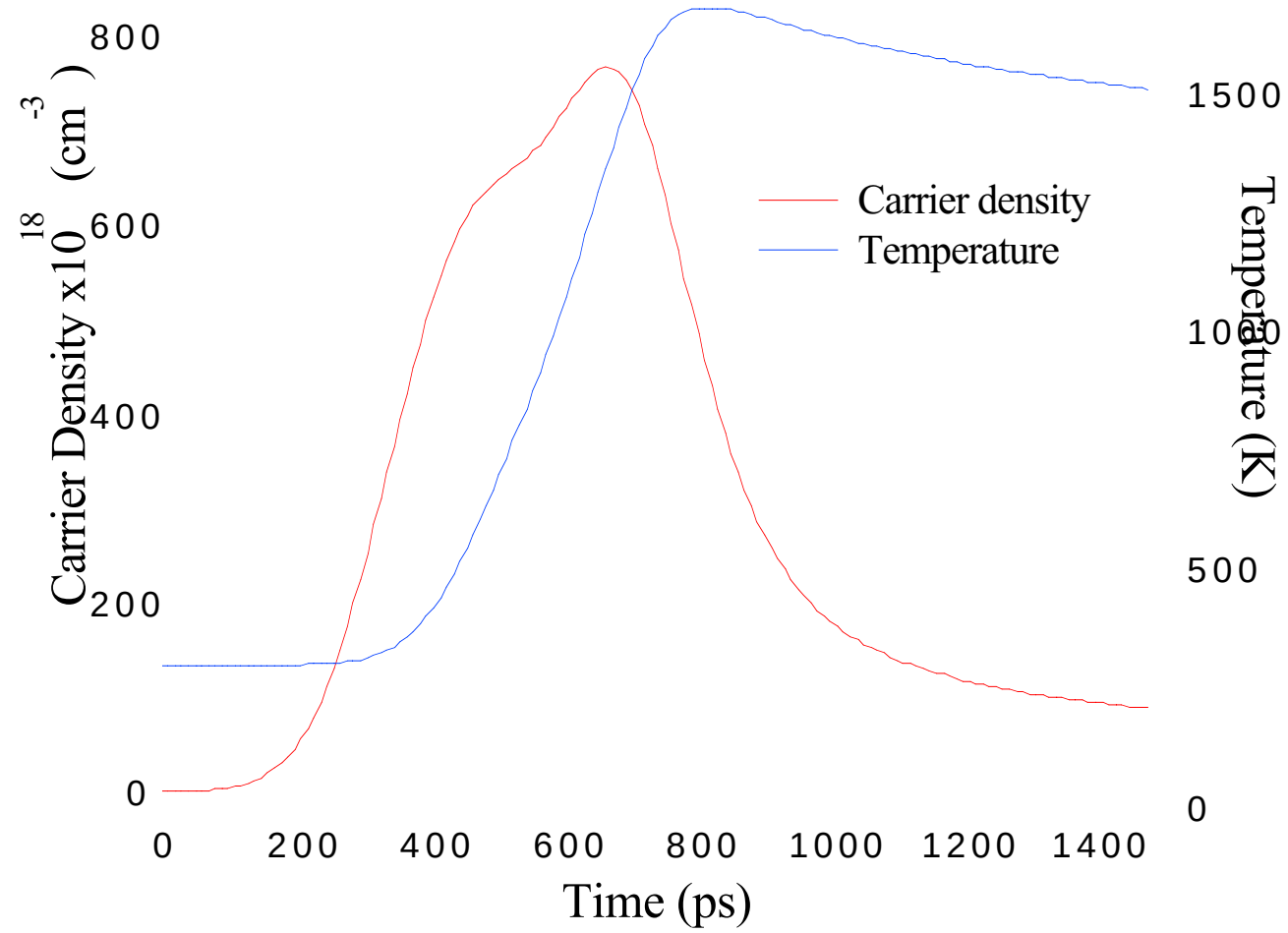

Strain profile, Acoustic phonon pulse propagation, 300ps 3GW/cm^2

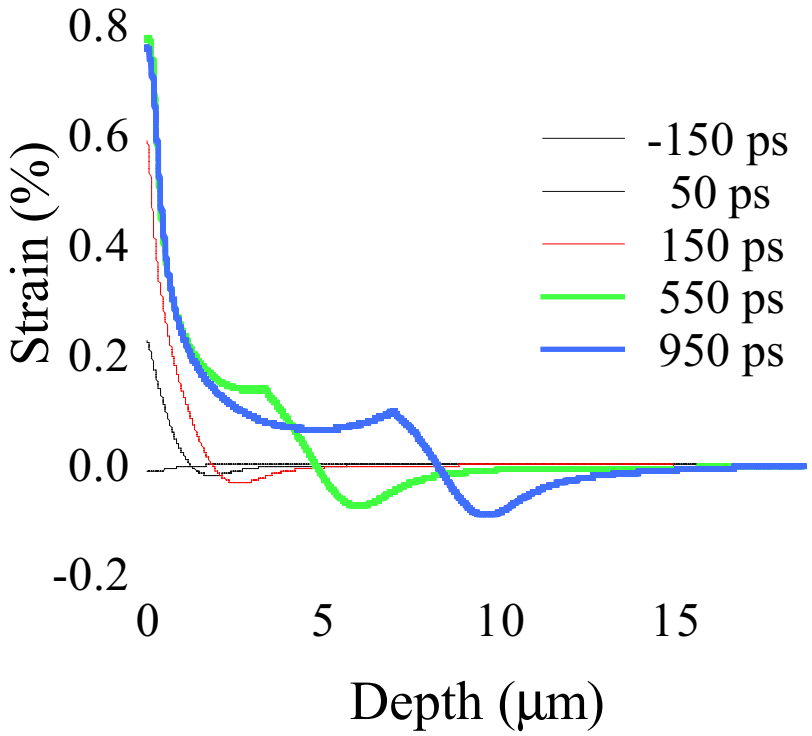

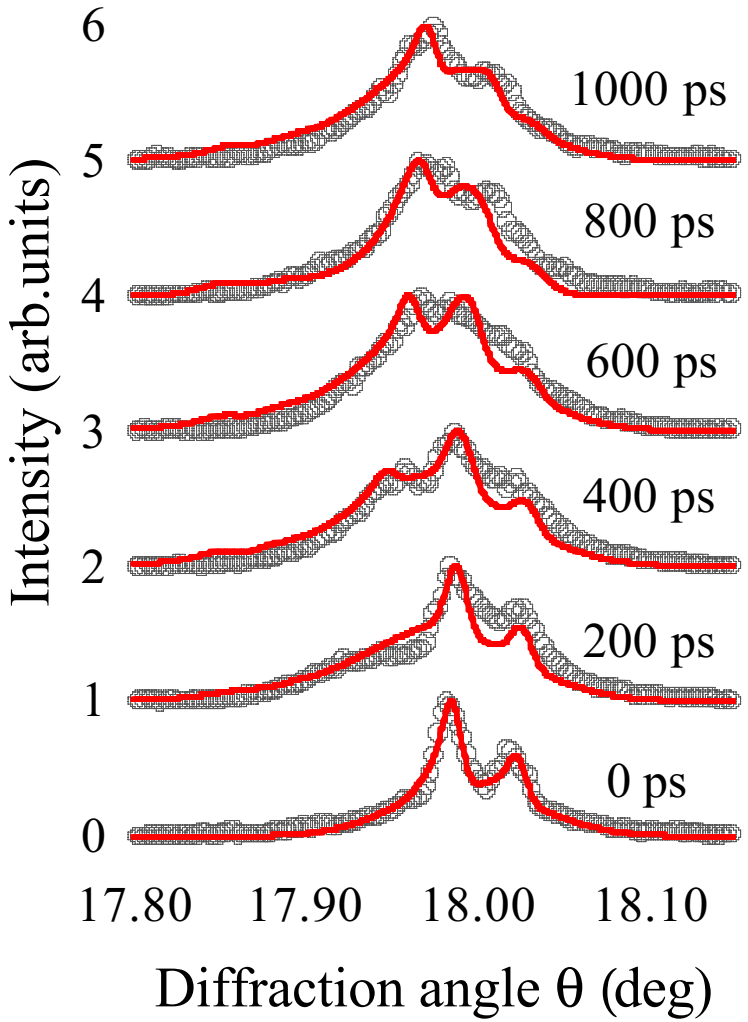

H. Kishimura *et al.* J. Chem. Phys. (in press).

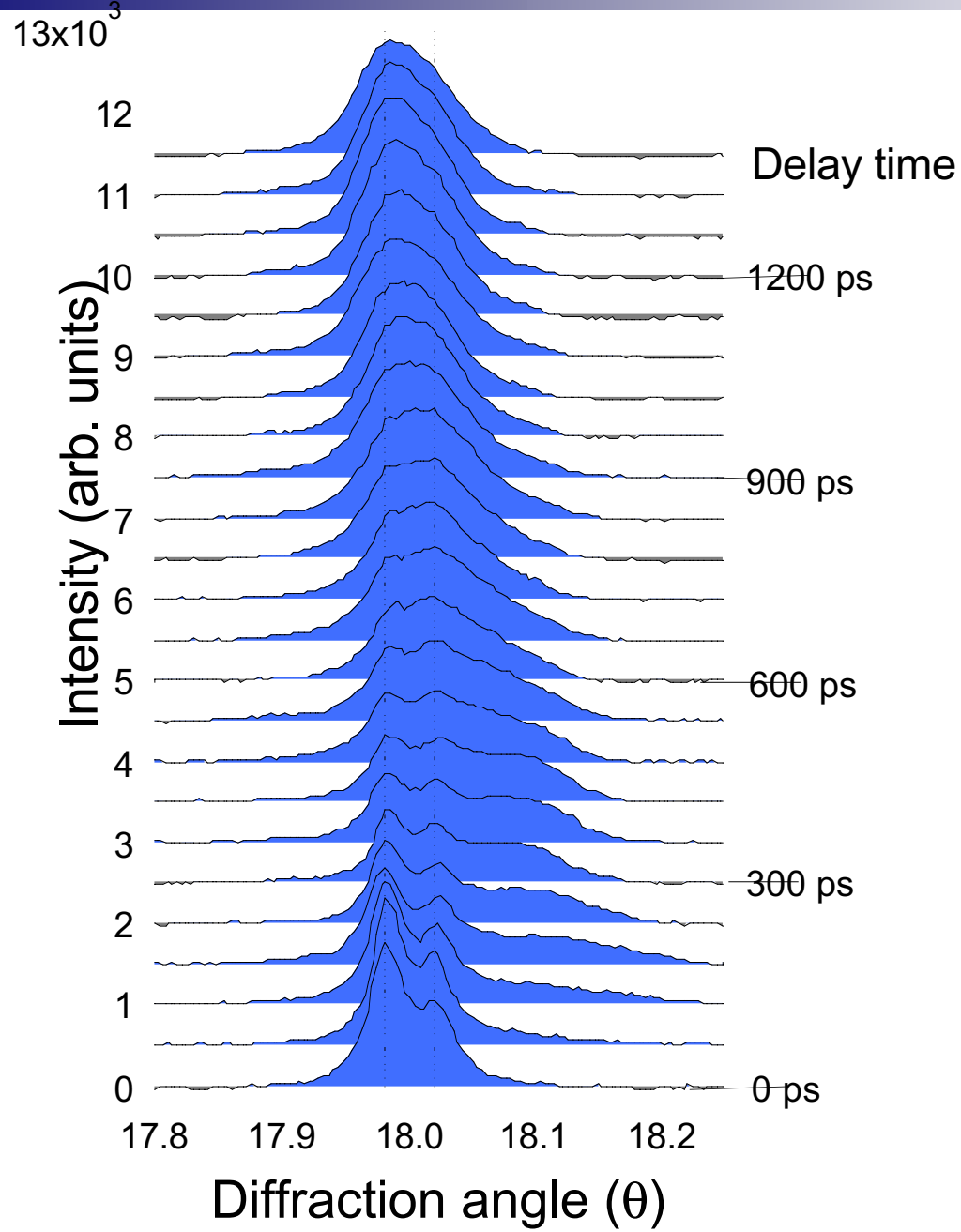

Mutiple shot experiment

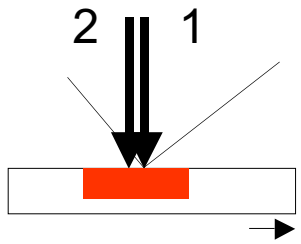

Picosecond time-resolved X-ray diffraction from Si(111) crystal under 300 ps laser irradiation at 1.4J/cm^2. Time step is 60 ps and accumulation of 600 data.

Average 200 shots irradiated.

Laser shock compression

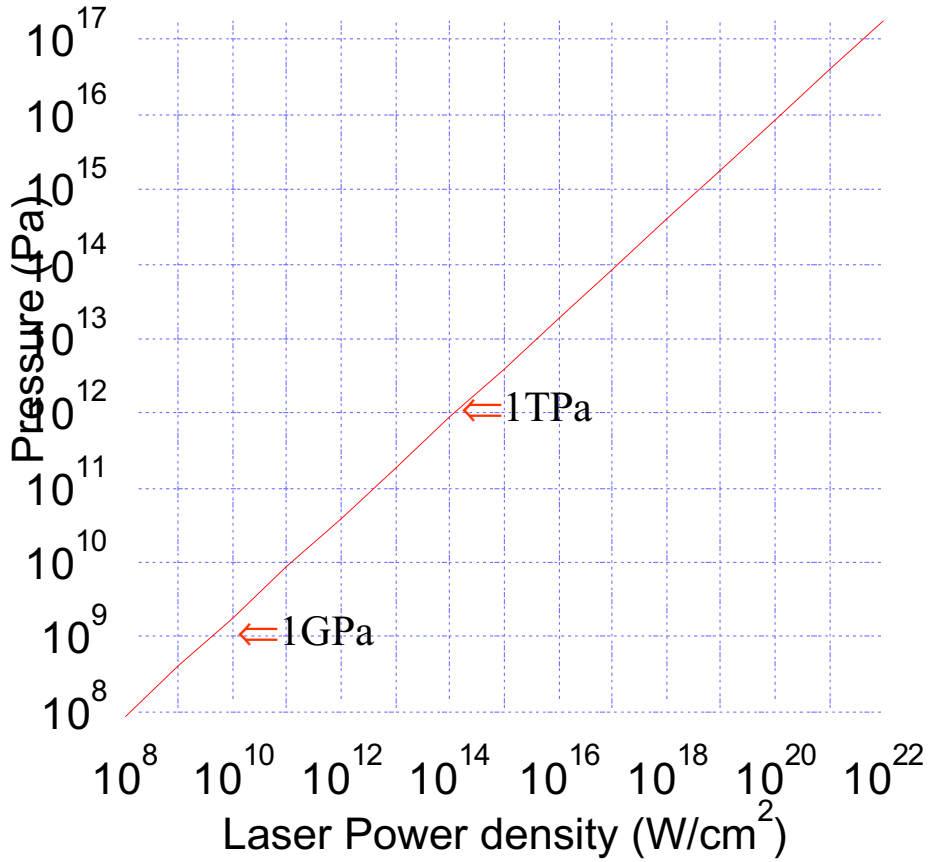

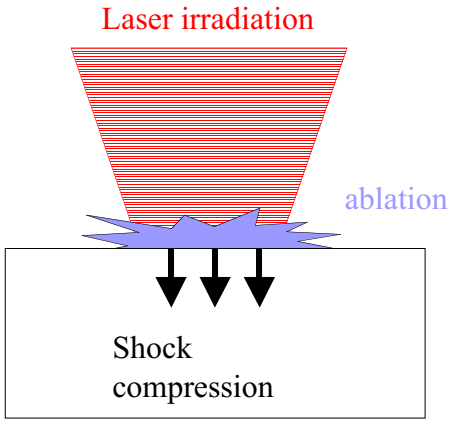

$P \approx 0.86\ I^{2/3}\ \lambda^{-2/3}$

P[TPa], I[10^{14}W/cm^2],λ[μm]

Benuzzi et al., Phys. Rev. E 54 (1996) 2162

Shock wave propagation

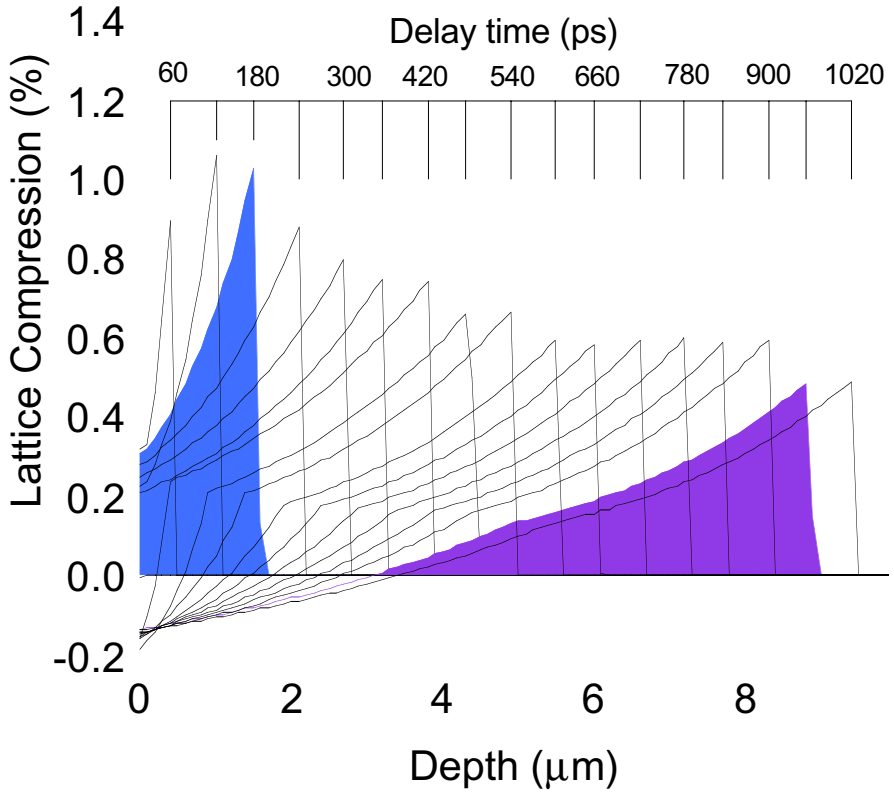

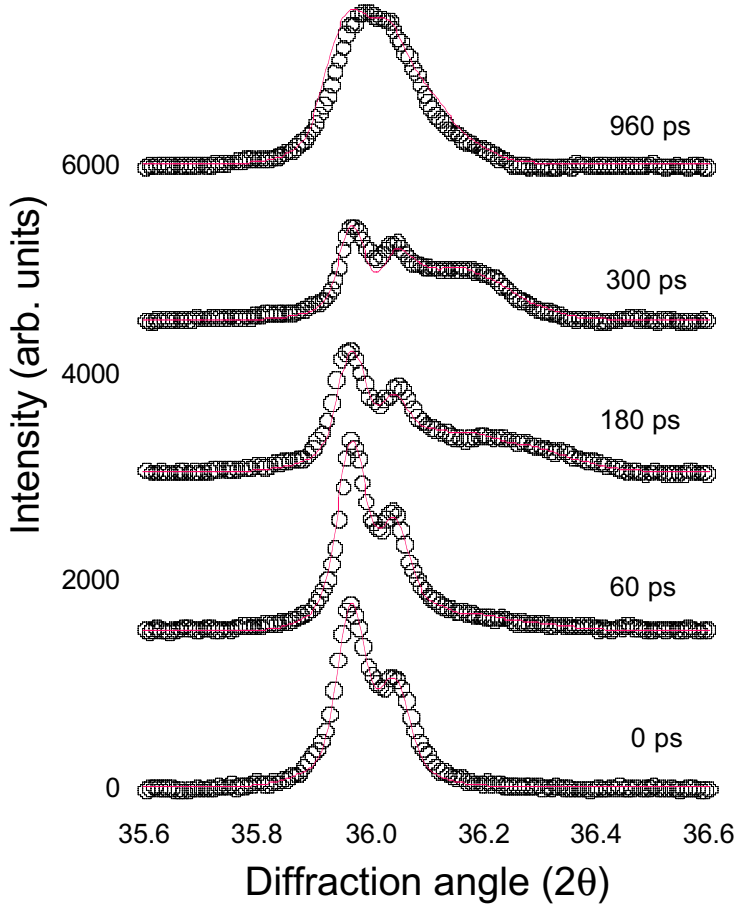

Peak pressure: 2.18 GPa, shock velocity 9.4 km/s

Time-resolved X-ray diffraction from laser irradiated Ge(111)

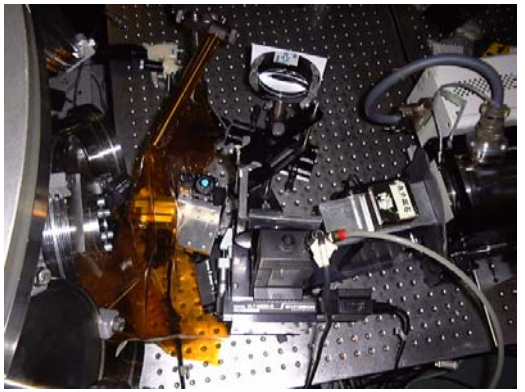

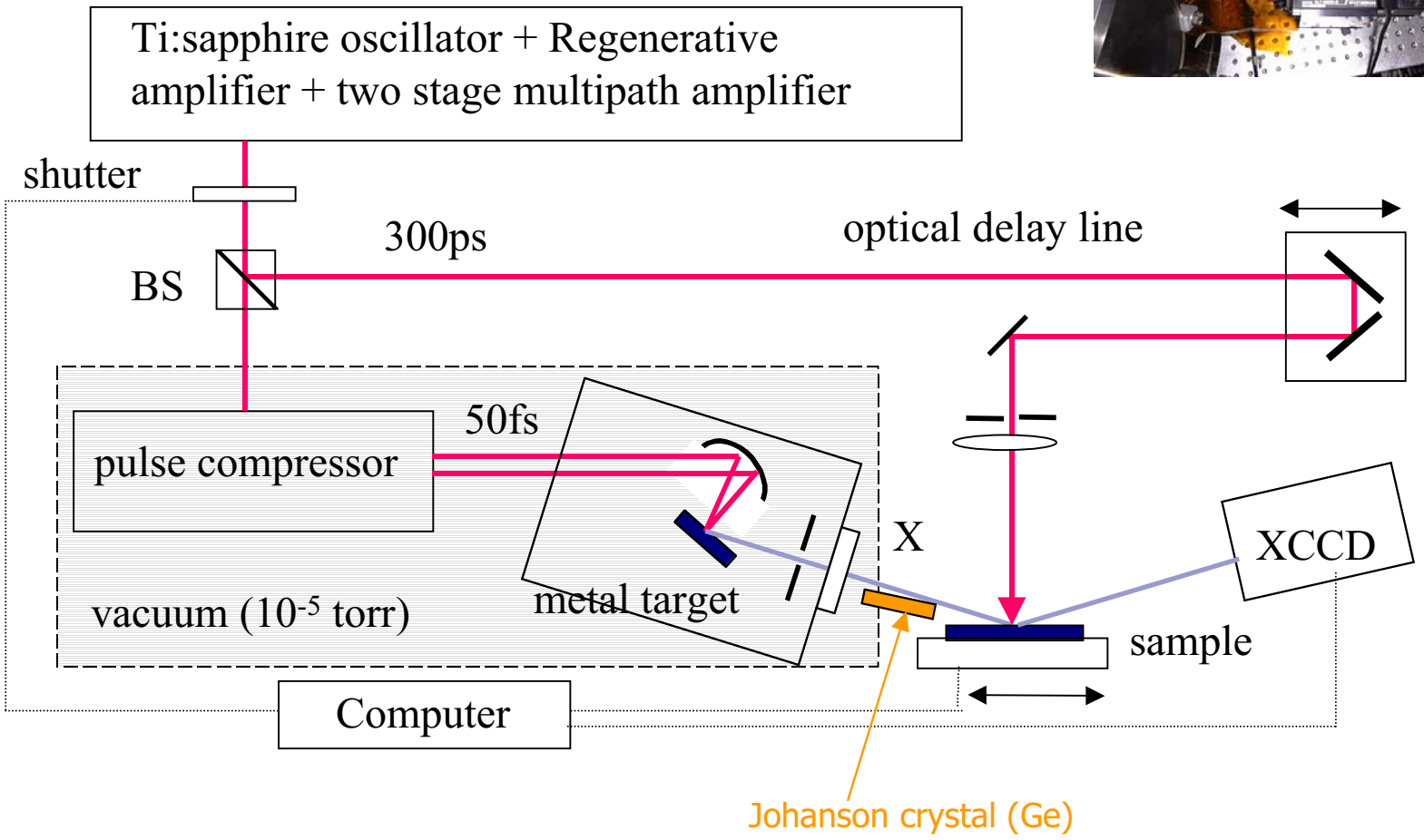

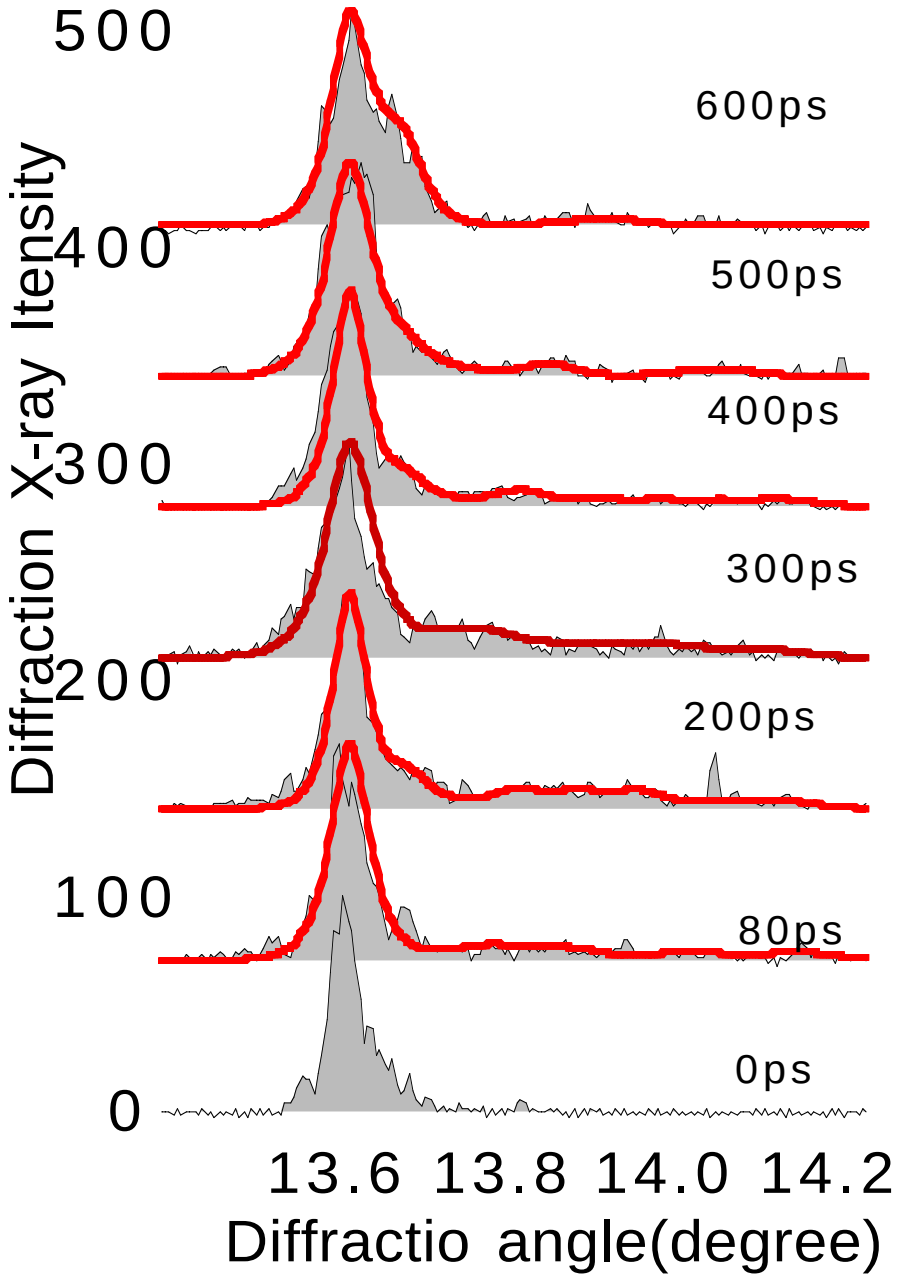

300-ps laser irradiated Ge(111)

wavelength:780nm,

power density:1.2GW/cm^2,

spot size:1.9Å1.5mm^2

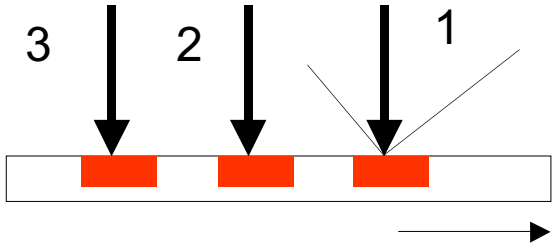

•Strain profile

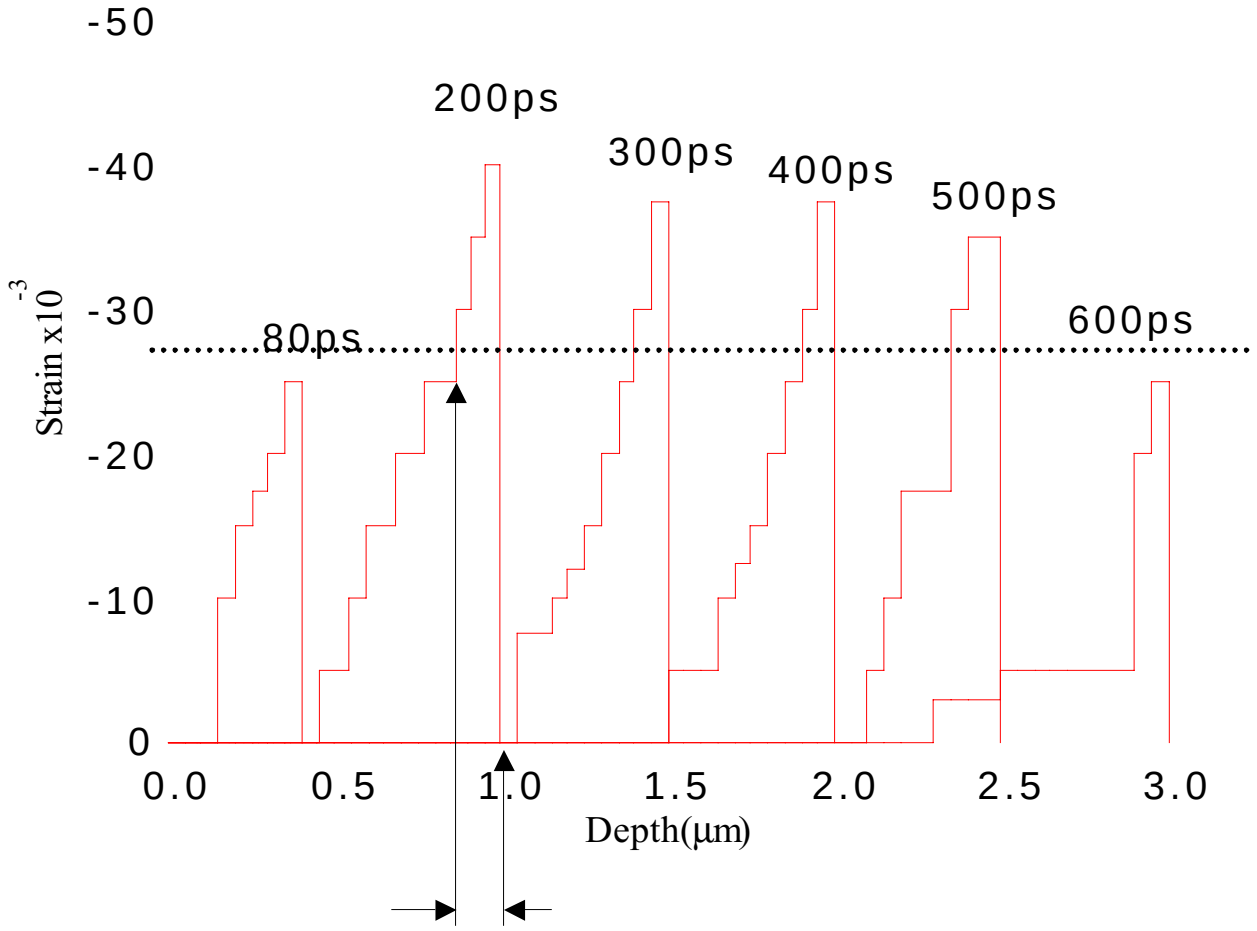

HEL:2.7% at 4.7GPa

Shock velocity:5 km/s

Maximum lattice compression: $d/d_0=0.96$

0.125μm corresponds to duration of 25ps

Hugoniot plot of GeÅ<111> orientation

Materials and Structures Laboratory
Tokyo Institute of Technology

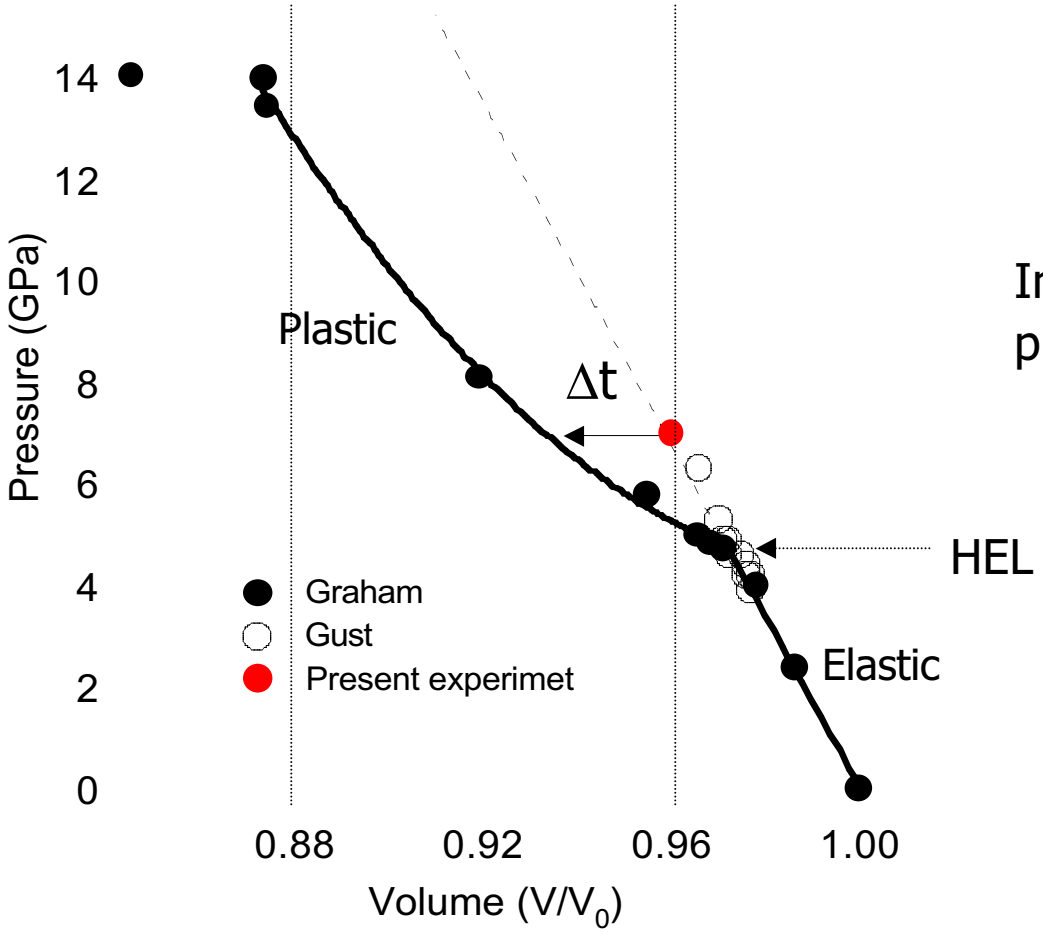

Incubation time (Δt) for plastic deformation > 25 ps

Summary

Dynamic lattice motion by shock wave propagation in Si(111) and (Ge(111)) is directly observed by picosecond time-resolved X-ray diffraction.

Material response to compression:

Plastic deformation in Ge can not occur during 25 ps in Ge at 7GPa

Acknowledgements:

Collaborators:Å@K. Kondo, Y. Hironaka, Y. Okano, H. Hishimura, H. Kawano
Funds:Å@Å@Å@ÅJST, MEXT

Laser-Produced-Plasma for EUV Light Source for Lithography

Katsunobu Nishihara
Institute of Laser Engineering, Osaka University

Outline of talk
- **requirement of light source and design window**
- **laser intensity scaling of conversion efficiency**
  - **experiments (Sn) and modeling**
  - **opacity and satellite line effect (Xe)**
- **further improvement of conversion efficiency (Sn, SnO2)**

In collaboration with
(theory) : T. Nishikawa, A. Sasaki, T. Kawamura, A. Sunahara, H. Furukawa, – M. Murakami, R. More, K. Fujima, F. Koike, T. Kagawa, V. Zhakhovskii, T. Kato and H. Tanuma,
(experiments) : H. Nishimura, M. Nakai, K. Shigemori, Y. Shimada, S. Uchida, S. Fujioka,– K. Hashimoto,T. Hibino, R. Matsui, T. Okuno, F. L. Sohnatzadeh, Y. Tao, M. Yamaura, K. Nagai, T. Norimatsu, M. Nakatsuka, H. Fujita, Y. Fujimoto, K. Tsubakimoto, H. Yoshida, N. Miyanaga and Y. Izawa

Light source for lithography for next generation ULSI

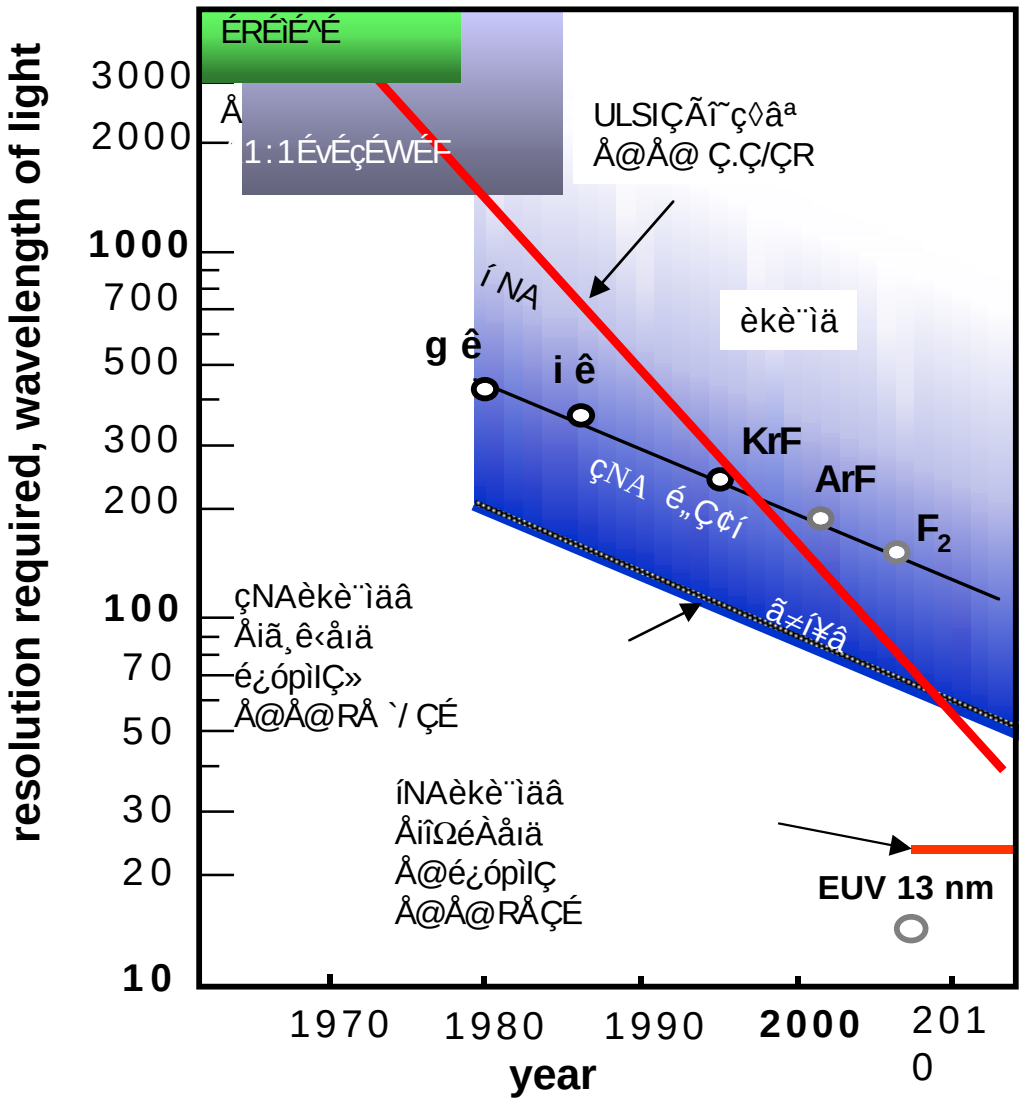

A new-five-year-long project for LPP EUV light source development has been started as the Leading Project promoted by MEXT.

The project aims at understanding physics of EUV light source for lithography, and providing database and guideline for practical use in collaboration with METI project (EUVA).

EUVL system

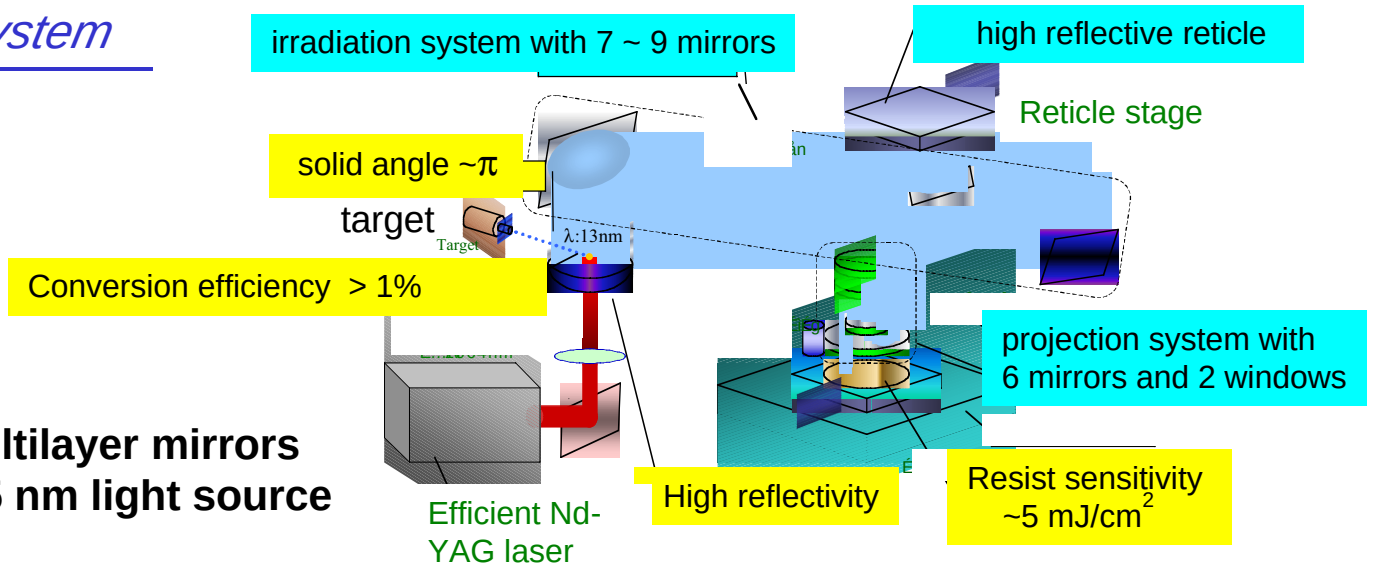

The project includes high performance laser development (5kW, 5kHz), plasma experiments, theory and simulation, and target fabrication.

Requirements of the light source and possible design windows

wavelength: 13.5 nm @2%BW / EUV power: > 115 W (after intermediate focus)
repetition: 10 kHz / etendue: 1 mm²str / conversion efficiency: > 1 %

EUV power at source / repetition :	300 W / 10 kHz
EUV energy per shot :	30 mJ / shot
source plasma size ($S = \pi Ç^{ç} = 1$ mm^{ç}str) :	_ ≈ 600 μm
EUV intensity ($I_{EUV} = E_{EUV} / (S \tau_{EUV})$) :	10^{9} Å 10^{10} W/cm^2
(pulse duration : τ_{EUV} = 1Å10 ns)	
laser intensity ($I_L = I_{EUV} / \eta_{EUV}$) :	10^{11} Å 10^{12} W/cm^2
(conversion efficiency : η_{EUV} = 0.01)	
ion density (Xe : $n_{5p\text{-}4d}$, Sn : $n_{4f\text{-}4d}$) :	10^{18} Å 10^{20} cm^{-3}

(photon number per unit time and area Å

$E_{EUV} / (h\nu\ \tau_{EUV}\ S) = 4 / _{OD=1}\ n_{4f\text{-}4d\ or\ 5p\text{-}4d}\ A_{Eien}$

Åopacity : $/_{OD=1}$ = 10μm, oscillator strength : $g_{n'}/g_n\ f_{n'n} = 1$,
abundance of $n_{4f\text{-}4d\ or\ 5p\text{-}4d}$ = 0.1)

An ideally "uniform" EUV radiator was produced by GEKKO-XII laser, to obtain laser intensity dependence of the conversion efficiency without lateral energy loss and geometrical effects.

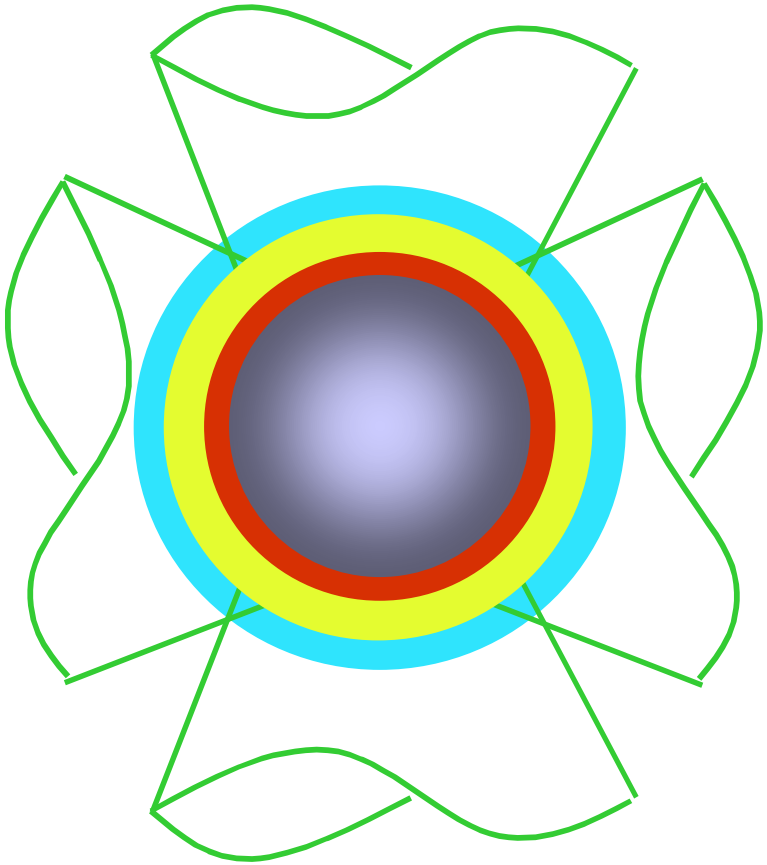

spherically uniform plasmas

Laser :

GEKKOXII, 12 beams

wavelength: ω (1.056 μm), 2ω (0.527 μm)

intensity: 5Å10^{10} ~ 1Å10^{12} W/cm^2

pulse width: 1.2 ns (FWHM, Gaussian)

Target :

Sn or SnO_2 coated on glass micro-balloon

300~2000 μmϕ (mostly 700 Ém–)

Diagnostics:

transmission grating (TDI) + CCD

grazing incident spectrometers (GIS)

x-ray backlight:

Laser intensity dependence of spectra shows that short wavelength (1-3nm) emission appears at high intensity (10^{12}W/cm^2), while long wavelength (>10nm) emission dominates at low intensity (10^{11}W/cm^2).

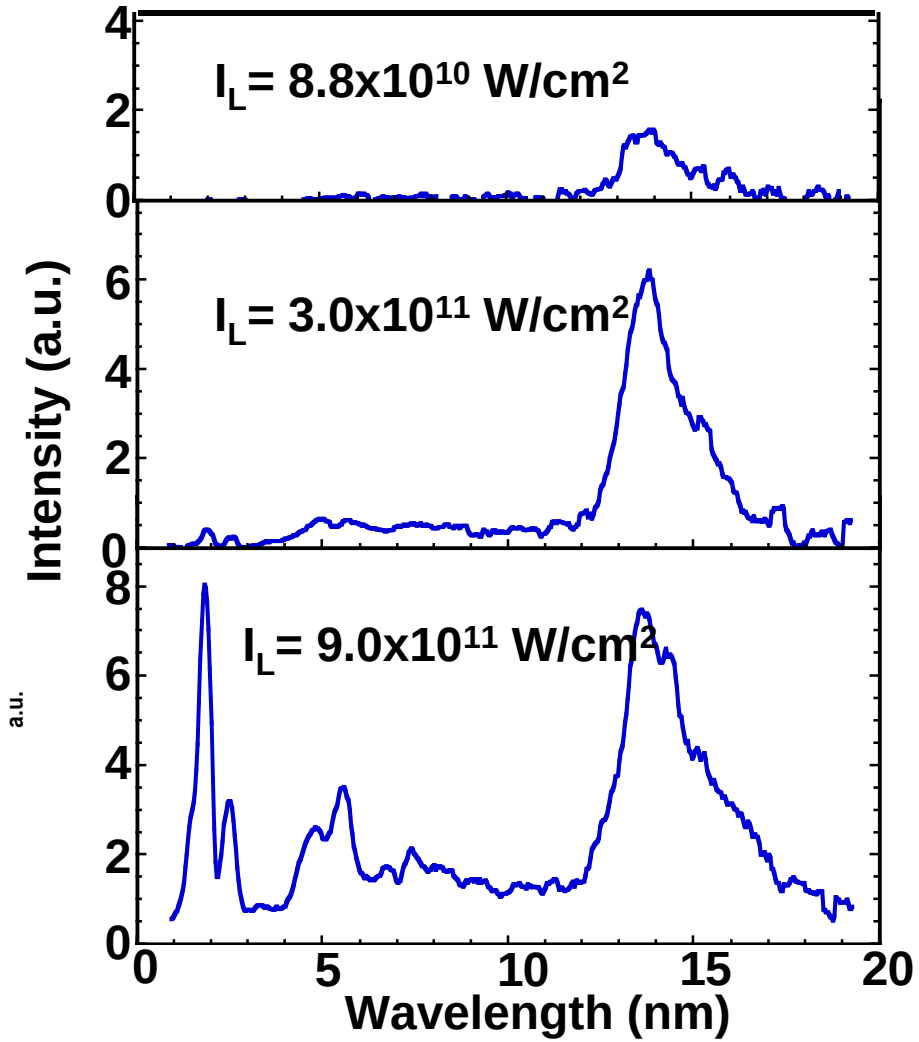

target Sn, laser ω
transmission grating + CCD

ÅEmission with wavelength of 13-15 nm is mainly due to 4d-4f transition.

ÅM-shell emission causes short wavelength emission < 3nm (1 - 0.5 keV), while N-shell emission does longer wavelength emission > 4nm (< 0.5 keV).

KN-YS030806-1

Spectral intensity normalized by laser intensity shows that conversion efficiency has its maximum around 1- 2 x 10 ^{11} W/cm^2.

Intensity dependence of EUV spectrum from spherical tin-oxide targets illuminated by 1.05-μm wavelength laser light.

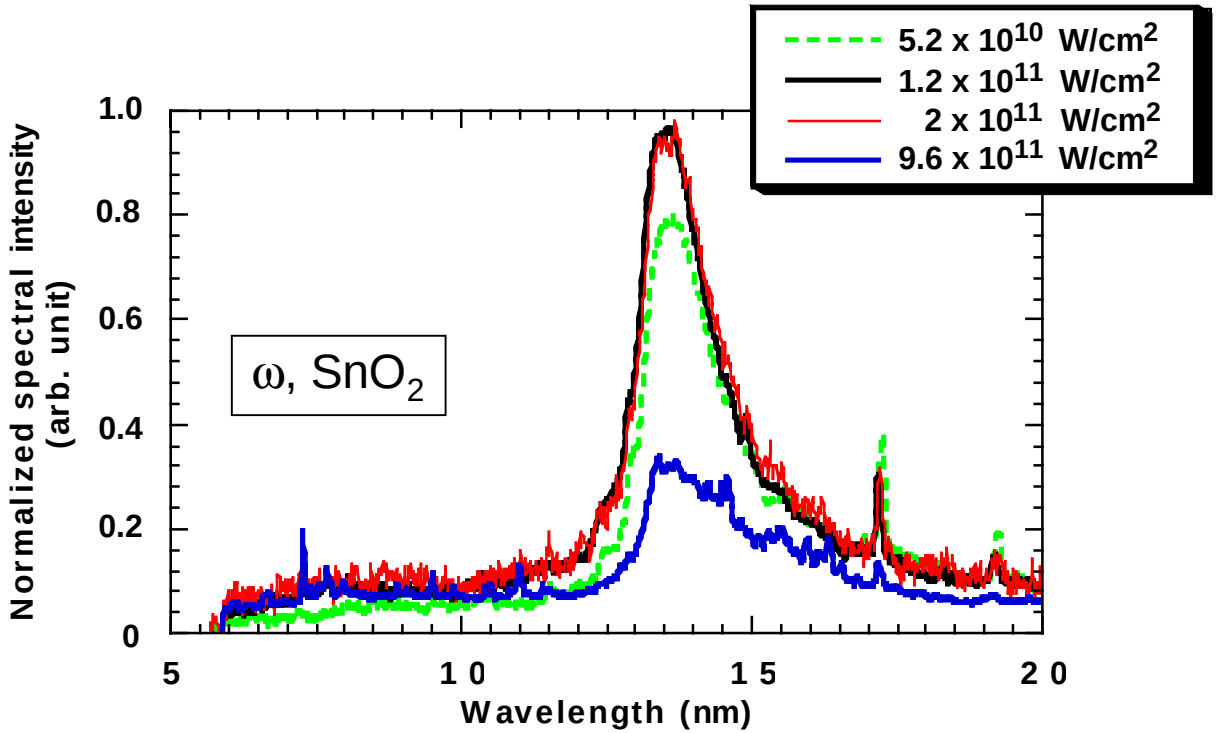

Detailed spectral features are observed by using grazing incident spectrometers (GIS) coupled with a back illumination CCD camera and an x-ray streak camera.

Transmission grating data also shows high conversion efficiency near 1-2x10^{11} W/cm^2 and relatively weak laser wavelength dependence.

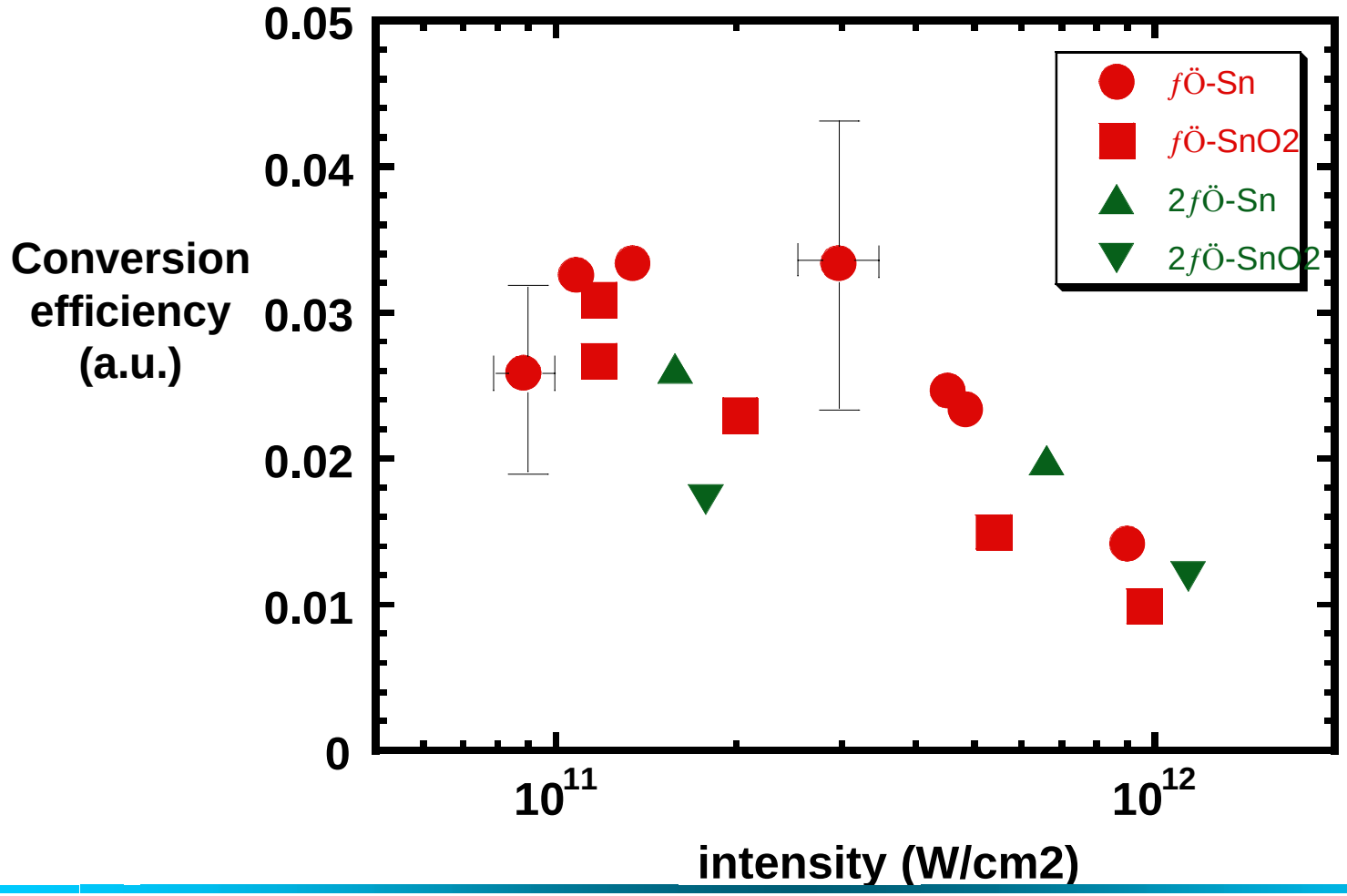

Features of Laser Produced High-Z Plasma

High density : high density / low temperature / LTE / b-f absorption region

Corona region : high temperature / low density / CRE / M-, N- band emission / isothermal expansion

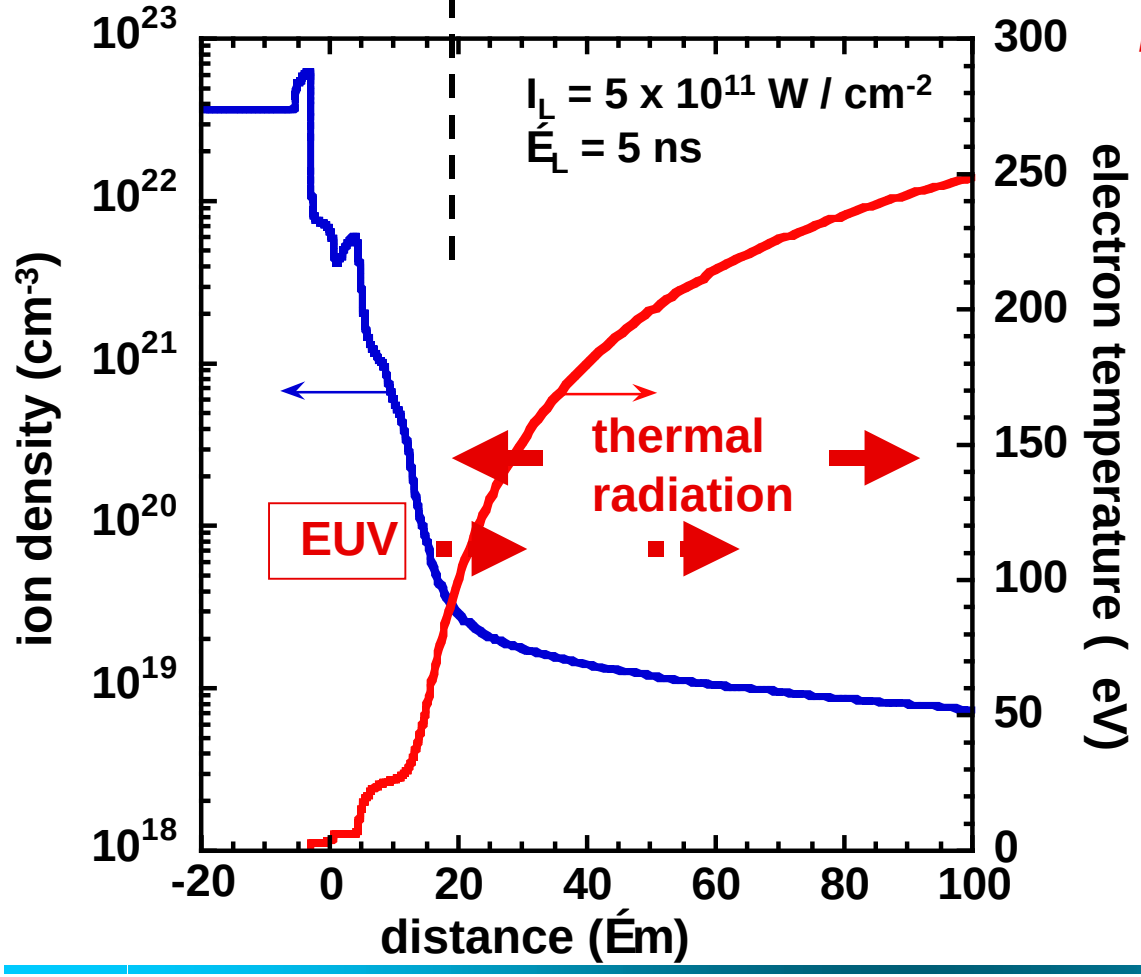

High density region was observed by side-on x-ray back light method .

I_L = 1.2 x 10^{12} W / cm^{-2}

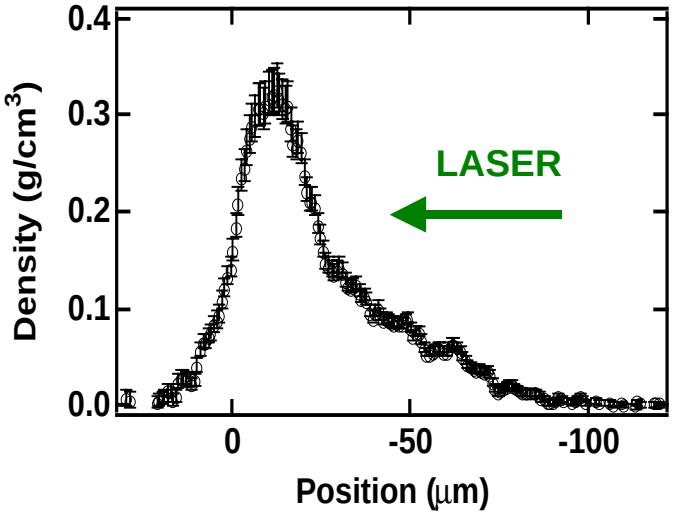

Modeling of EUV-LPP (power balance)

Consider following energy losses

- kinetic energy loss due to expansion, E_k

Å ionization loss, E_i

Å radiation loss, E_R ,

and assume a sum of the losses equals to laser flux.

$$I_L = E_k + E_i + E_R$$

Assume isothermal expansion in corona

$$E_k = 3\, Z^*(n_i, T_e)\, n_i\, T_e\, c_s ,$$
$$E_i = E_i(n_i, T_e, Z^*(n_i, T_e))\, n_i\, c_s ,$$
$$E_R = P_R(n_i, T_e)\, c_s\, \tau_L / \alpha ,$$

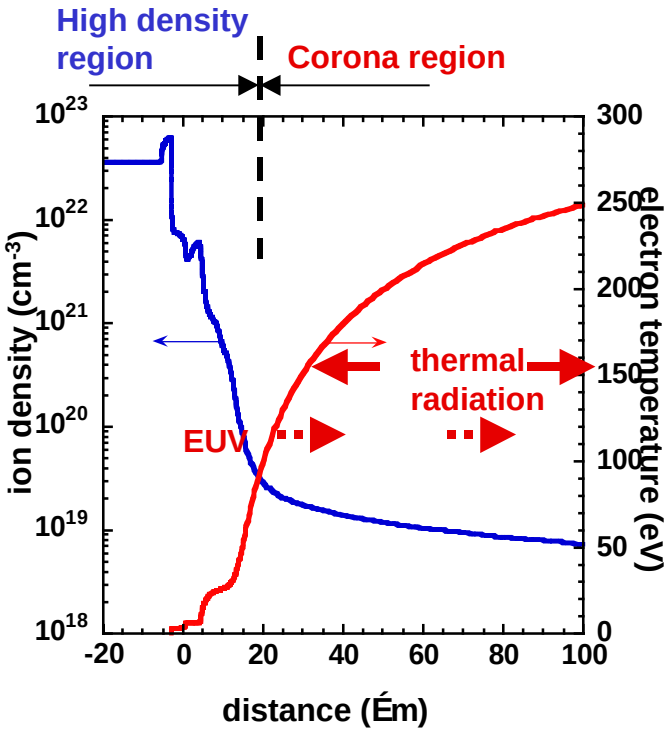

where Z^* : ionization state, n_i : ion density,
T_e : electron temperature, c_s : sound speed
τ_l : laser pulse duration, α (≈ 1.5) : $P_R \propto n_i^{\alpha}$,

KN030806-2

Dependence of the losses on laser intensity indicates that radiation loss is dominate (50%),ionization loss is large at low intensity and kinetic loss becomes large at high intensity, but still small.

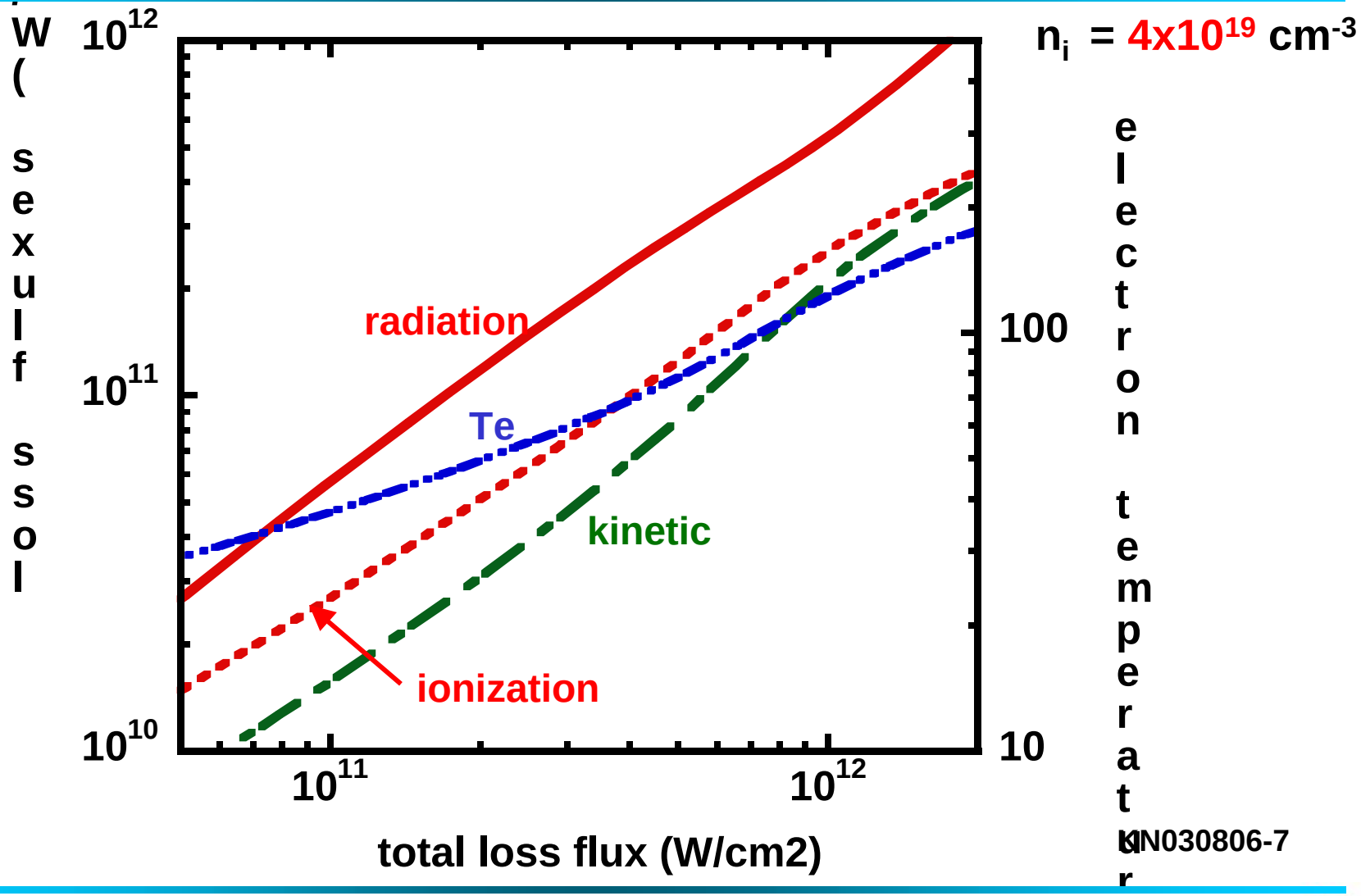

Model indicates that radiation spectra may drastically change with laser intensity, which agrees well with the experiments.

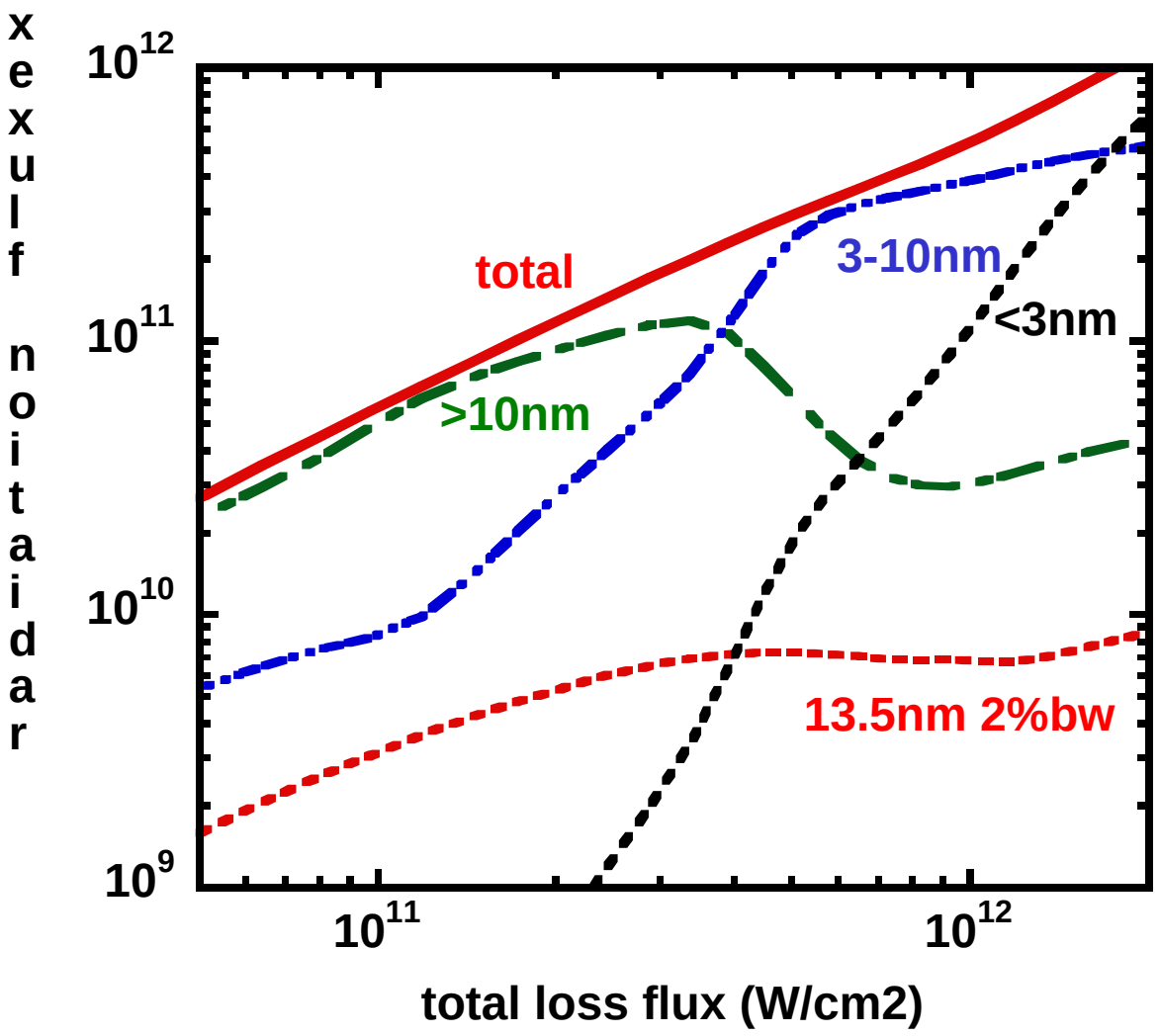

$n_i = 4x10^{19}$ cm^{-3}

13.5 nm with 2% bandwidth

assumptions

- 10% of 12.4-14.5 nm emission from the corona calculated from AAM with (*n,l*) splitting
- Planck radiation from the high-density region with radiation temperature estimated from the total radiation from the corona.

KN030806-9

Both opacity and satellite lines play important roles in LPP. (Xe plasma with 4d-4f, 4p-4d and 4d-5p satellite lines)

Plasma parameters

T_e=25eV

n_e=10^{21}/cm^3

r=10μm

with satellites

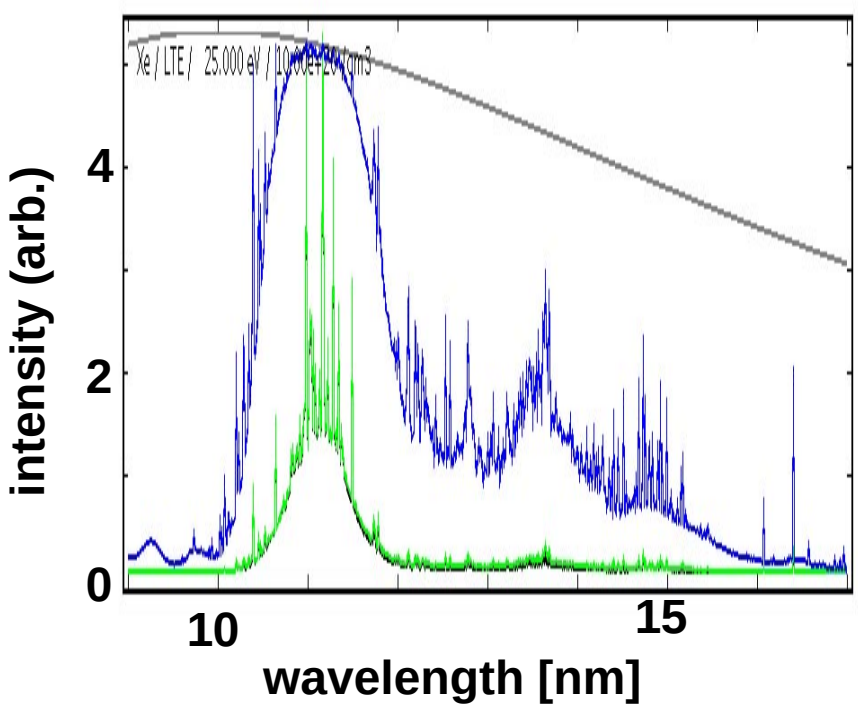

no satellites

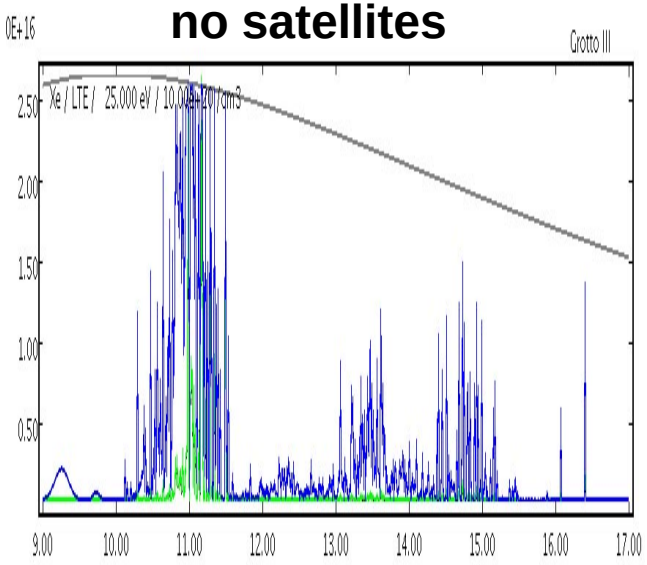

Theoretical conversion efficiency agrees fairly well with the experiments.
At low intensity, emission from the corona is dominate,
while that from the high density region becomes large at high intensity.

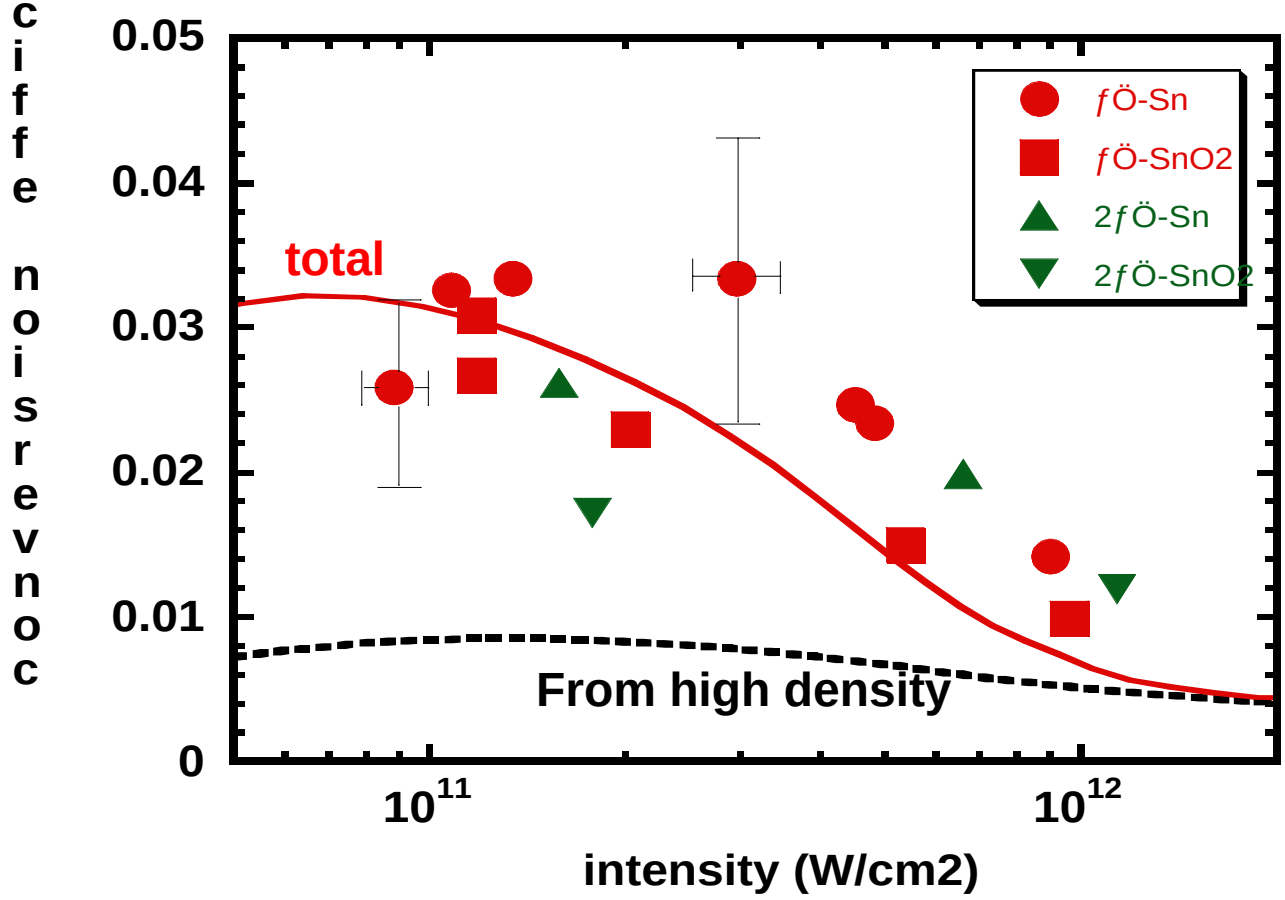

With decrease in density, spectrum becomes narrower but emission at 13.5 nm does not largely change. (planar target)

low density SnO_2 (23% of solid density)

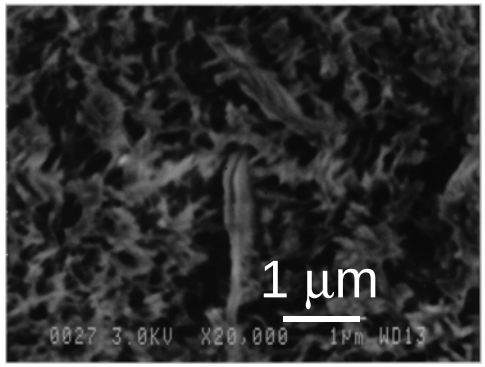

pinhole image (@13.5 nm 2%BW)

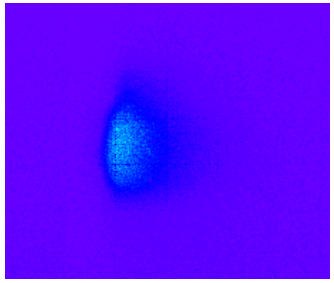

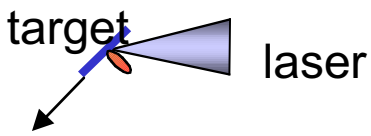

to EUV pinhole camera

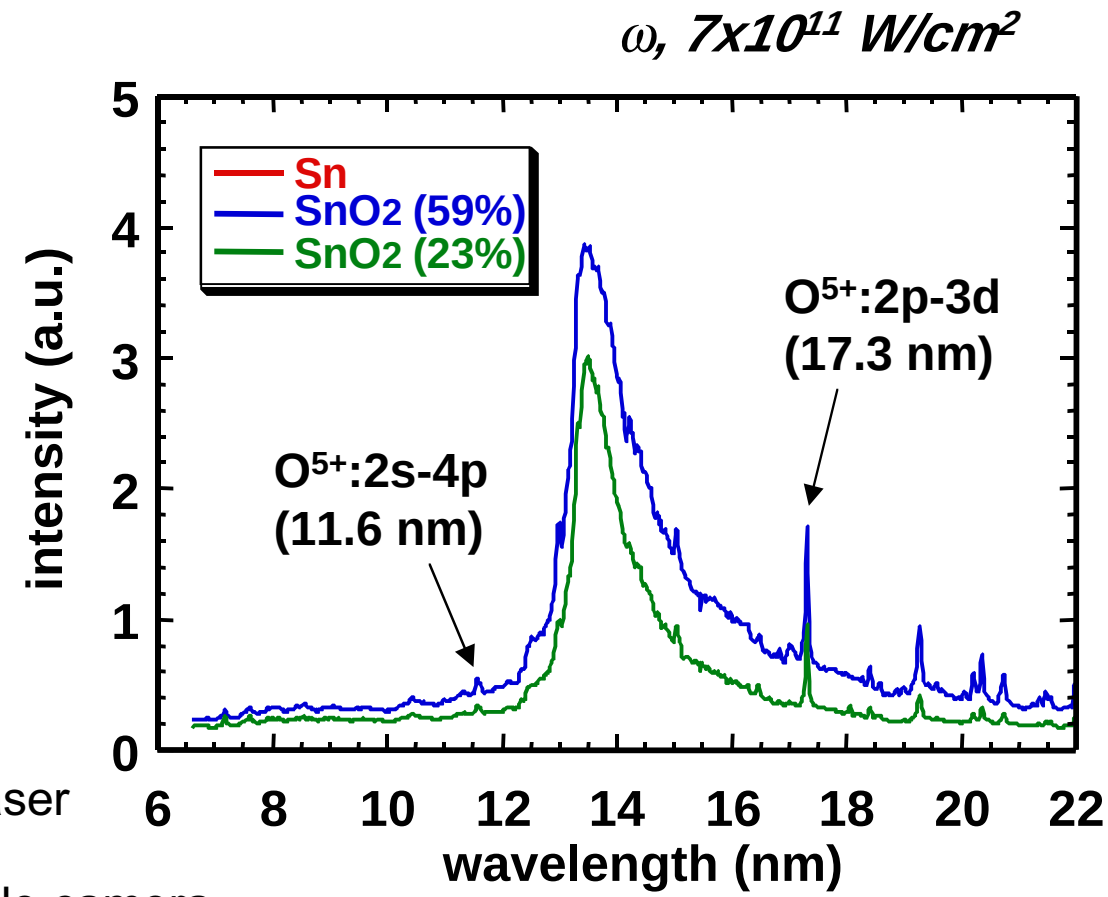

At low intensity of .5 – 1 x10^{11} W/cm^2, 2ω laser irradiation results in higher conversion efficiency, and SnO_2 is higher Sn (?).

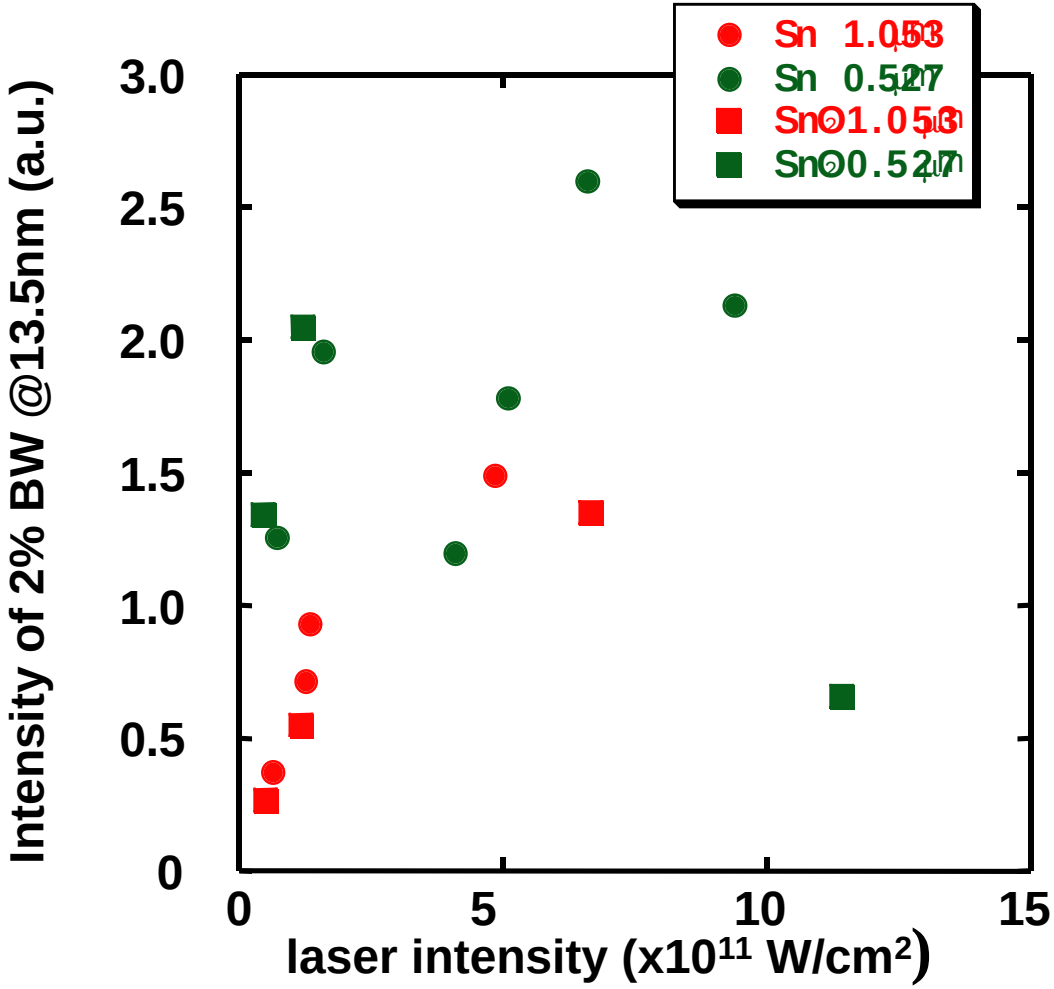

Conclusions

- The conversion efficiency of a few % to 13.5 nm EUV light of 2 % bandwidth has been attained at 1 - 2x10^{11} W/cm^2.
- Considering power balance, we present a scaling low of the conversion efficiency, which agrees fairly well the experiments.
- We show that13.5 nm EUV light is emitted in both the high-temperature corona and the high-density region, depending on the laser intensity.
- We also show that the Planckian intensity can be achieved for the lines due to the effects opacity and satellite lines in the high-density region.
- $2\omega_o$ laser irradiation on SnO_2 target leads to further improvement of the conversion efficiency at intensity of .5-1x10^{11} W/cm^2, although further study is required.

KN030930-1

Those results indicate that the source parameters for practical use can be achieved.

The SPARC/X Projects

Luigi Palumbo

Univ. Roma "La Sapienza" & INFN-LNF

on behalf of the SPARC collaboration:

a R&D Program toward an Italian 4th Generation Light Source

INTERNATIONAL CONFERENCE ON
"ULTRASHORT HIGH-ENERGY RADIATION AND MATTER"
Villa Monastero, Varenna, October 7 -10, 2003

The origins: 2000 National Research Plan

a) Feb 2001: Call for proposals- 7.5 M€ for R&D

SPARC (CNR-ENEA-INFN-INFM-Trieste-U.Roma2)

b) Dec 2001: Call for proposals- 67 M€ for a X-ray FEL source

SPARX (CNR-ENEA-INFN-Univ.Roma2)
FERMI (INFM-Sincrotrone Trieste)

SPARC project

(funded): R&D program toward high brightness e^- beam for SASE-FEL's

SPARX proposal

Conceptual study of a X-ray FEL-SASE source at 10 nm and 1.5 nm

S ource

P ulsed

self**A** mplified

R adiation

C oherent

Self-Amplified Pulsed Coherent Radiation Source

INFN Istituto Nazionale di Fisica Nucleare
Laboratori Nazionali di Frascati

INTERNATIONAL CONFERENCE ON
"ULTRASHORT HIGH-ENERGY RADIATION AND MATTER"
Villa Monastero, Varenna, October 7 -10, 2003

SPARC

SPARC Project Goals

- Ultra-brilliant photoinjector at 150 MeV , I=100 A, (INFN)
- Undulator for SASE FEL at 520 > 150 nm (green-UV),(ENEA)
- Optics for X-rays manipulation (CNR)
- Generation of incoherent low intensity X-ray (INFM)

A 3D model view of the SPARC Photo-Injector and FEL Undulator

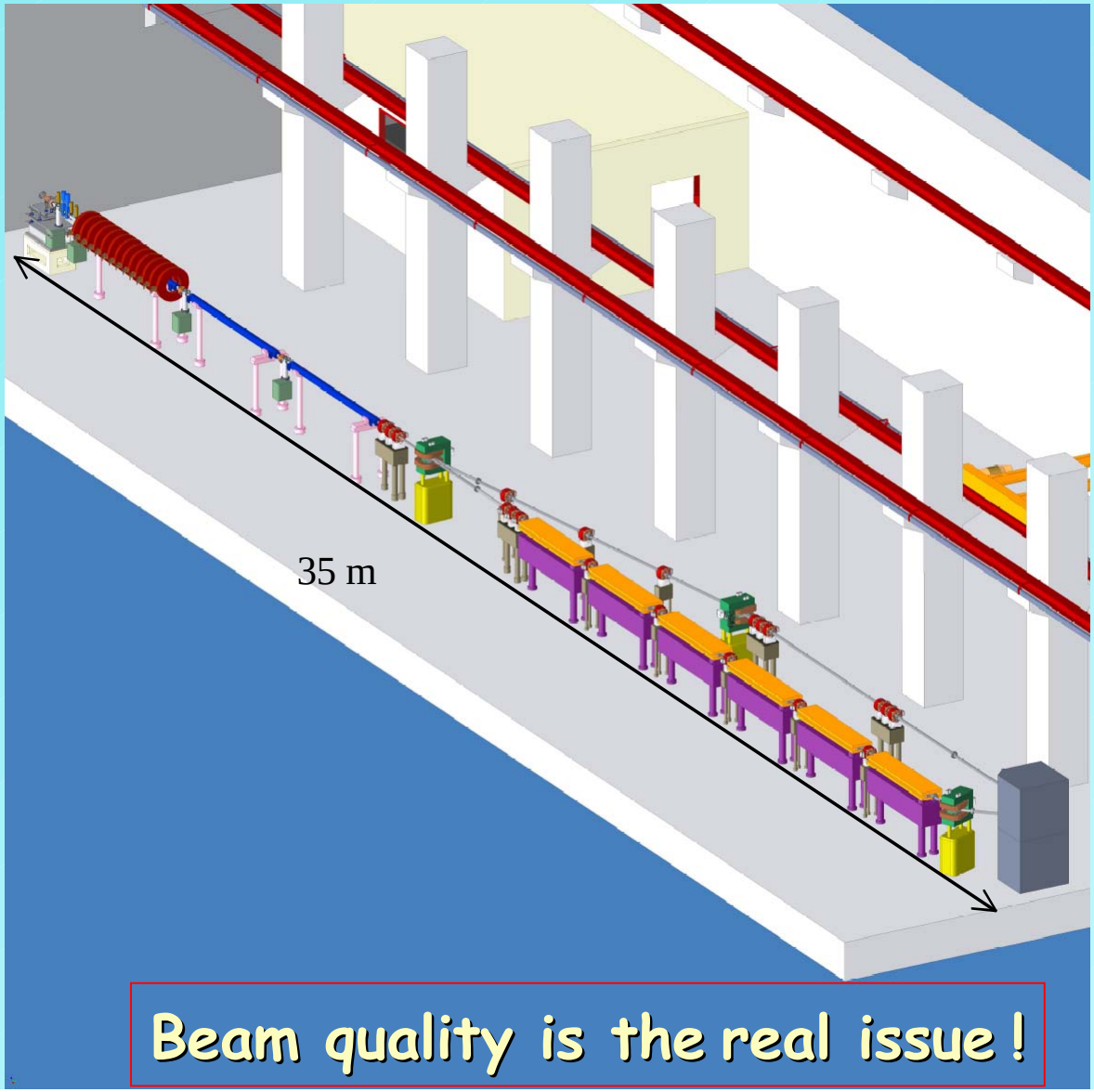

Beam quality is the real issue !

INFN Istituto Nazionale di Fisica Nucleare Laboratori Nazionali di Frascati

SPARC

SPARC SASE-FEL Experiment Updated Parameter List

ELECTRON BEAM	
Electron Beam Energy (MeV)	155
Bunch charge (nC)	1.1
Repetition rate (Hz)	1-10
Cathode peak field (MV/m)	120
Peak solenoid field @ 0.19 m (T)	0.273
Photocathode spot size (mm, hard edge radius)	1.13
Central RF launch phase (RF deg)	33
Laser pulse duration, flat top (ps)	10
Laser pulse rise time (ps) 10%? 90%	1
Bunch energy @ gun exit (MeV)	5.6
Bunch peak current @ linac exit (A)	100
Rms normalized transverse emittance @ linac exit (?m); with thermal emitt. (0.3)	< 2
Rms slice norm. emittance (300 ?m slice)	< 1
Rms longitudinal emittance (deg.keV)	1000
Rms total correlated energy spread (%)	0.2
Rms incorrelated energy spread (%)	0.06
Rms beam spot size @ linac exit (mm)	0.4
Rms bunch length @ linac exit (mm)	1

UNDULATOR	
Undulator period (cm)	2.8
Undulator parameter k	2.143
Undulator gap (mm)	9.25
# Undulator sections	6
# Undulator periods per section	78
Drift length between undulator sections (cm)	36.5
Additional quadrupole gradient (T/m)	5.438
Additional quadrupole length (cm)	8.4
FEL radiation wavelength (fundamental, nm)	499.6
Average beta function (m)	1.516
Expected saturation length (m)	< 12

SASE-FEL Experiments

	UCLA-LANL (Los Alamos) (1998)	LEUTL (Argonne) (2000)	TTF_I (DESY) (2001)	VISA (Brookhaven) (2001)
LINAC [GHz]	3 N.C.	3 N.C.	1.3 S.C.	3 N.C.
E [MeV]	18	217	233+/-5	71
I [A] (injector)	167		50	85
I [A] (undulator)	167	150	400+/-200	85
$\Delta\gamma/\gamma$ [%]	0.25	0.1	0.13	
ε_n [mm mrad] (injector)	7 (@ 2 nC)		4+/-1 (@ 1 nC)	1.5 (@ 0.2 nC)
ε_n [mm mrad] (undulator)	7	5	8+/-2	
Compression	1		8	1
ε_n [mm mrad] (slice)	5		6+/-3	0.8
K Undulator	1.04	3.1	1.17	1.21
λ[nm]	12000	530	98.1	830
Saturation	NO	YES	YES	YES

X-Ray FEL's are based on SASE (no mirrors !) need Ultra-High Brightness e- Beams

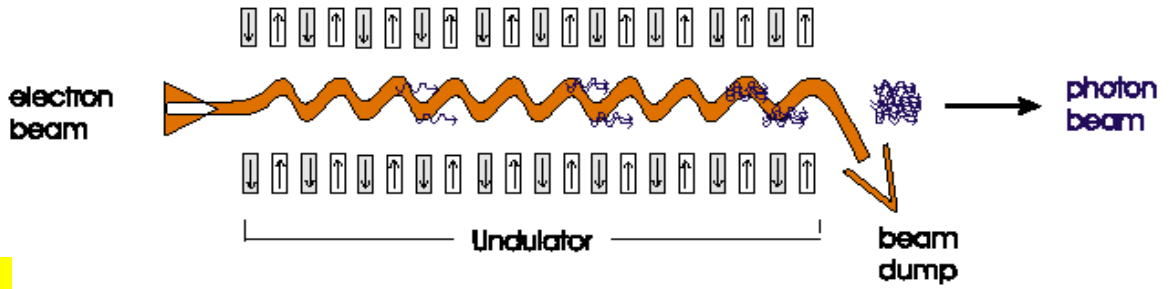

Resonance Condition

$$\lambda_r = \frac{\lambda_u}{2\gamma^2}\left(1+\frac{K^2}{2}\right)$$

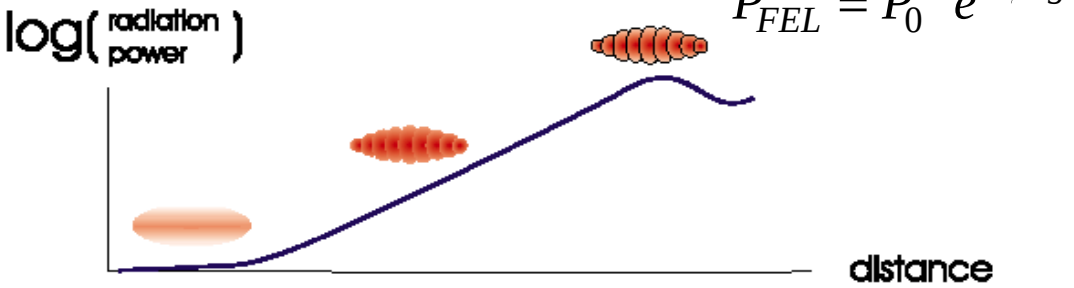

$$P_{FEL} = P_0 \; e^{2z/L_g}$$

- Self-Amplified-Spontaneous-Emission amplifies the spontaneous radiation exponentially in a single pass
- Interaction of a *bright electron beam* with *noise* in an undulator magnet results in a density modulation of the electron bunch at the optical wavelength: *SASE instability* leads to *COHERENT EMISSION*

Conditions for SASE

γ = norm. energy ε_n = r.m.s. normalized emittance
I = peak current $\frac{\delta\gamma}{\gamma}$ = energy spread
K = undulator parameter $\propto \lambda_u B_u$

A) Photon and Electron Beams must overlap in phase space

$$\varepsilon_n \le \frac{\gamma\lambda_r}{4\pi}$$

B) Cold Electron Beam (no damping of instability growth)

$$\frac{\Delta\gamma}{\gamma} \le \rho;\quad \rho = \frac{\lambda_u}{4\pi\sqrt{3}L_g} \cong \begin{cases} 10^{-3} @\ 1\ nm \\ 5\cdot 10^{-4} @\ 1\ \text{Å} \end{cases}$$

R. Saldin et al. in *Conceptual Design of a 500 GeV e+e- Linear Collider with Integrated X-ray Laser Facility*, DESY-1997-048

$$\lambda_r^{MIN} \propto \frac{\varepsilon_n}{K}\left(\frac{\delta\gamma}{\gamma}\right)\sqrt{\frac{\left(1+K^2/2\right)}{I\gamma}} \propto \left(\frac{\delta\gamma}{\gamma}\right)\sqrt{\frac{\left(1+K^2/2\right)}{\gamma B_n K^2}}$$

$$L_g \propto \frac{\varepsilon_n\gamma^{3/2}}{K\sqrt{I\left(1+K^2/2\right)}} \propto \frac{\gamma^{3/2}}{K\sqrt{B_n\left(1+K^2/2\right)}}$$

Brightness is what really matters !

INFN Istituto Nazionale di Fisica Nucleare Laboratori Nazionali di Frascati

SPARC

Photo-Injector Beam dynamics R&D challenges for future X-ray sources

$$B_n = \frac{2I}{\varepsilon_n^2} \approx 10^{15}\,\frac{A}{m^2}$$

$$\left(\frac{\delta\gamma}{\gamma}\right) \le \rho \begin{cases} 10^{-3} & @ \quad 1\,\mathrm{nm} \\ 5\cdot 10^{-4} & @ \quad 0.1\,\mathrm{nm} \end{cases}$$

Three Major Tasks to accomplish:

1. Minimize all mechanisms leading to degradation of the rms normalized transverse emittance en
2. Peak current enhancement by a factor 20-100
3. Damp the beam energy spread below the threshold $\Delta\gamma/\gamma < \rho$

Innovative Concepts / Components in SPARC to reach max. brightness

- **Use of Shaped Laser Pulses** (minimize space charge non-linearities)
- **Implementation of new optimized lay-out for an integrated photo-injector** (proper phase tuning of emittance oscillations for max. brightness)
- **Produce RF bunch compression with Emittance Preservation** (increasing peak current at no expense of transverse emittance)

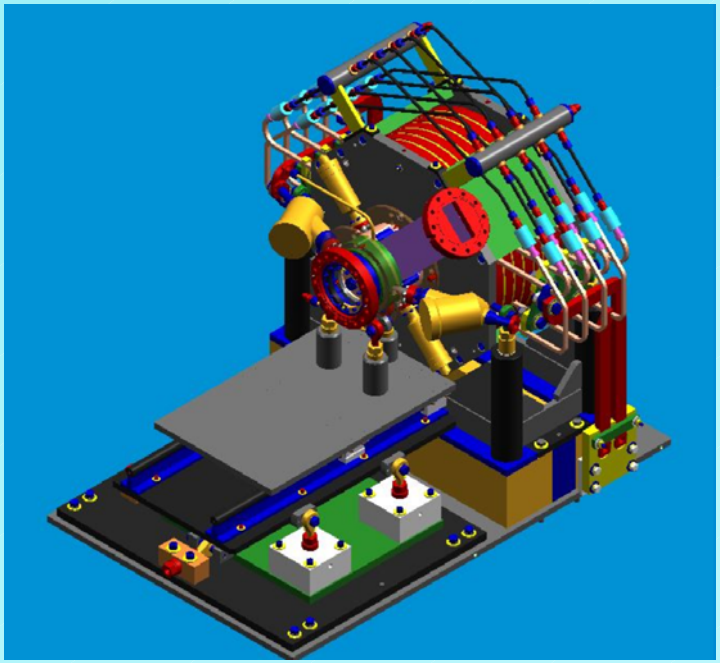

INFN Istituto Nazionale di Fisica Nucleare
Laboratori Nazionali di Frascati

INTERNATIONAL CONFERENCE ON
"ULTRASHORT HIGH-ENERGY RADIATION AND MATTER"
Villa Monastero, Varenna, October 7 -10, 2003

SPARC

Achieving Record Emittances @ Sumitomo SHI + FESTA

Emittance measurements for gaussian and square laser pulse shapes

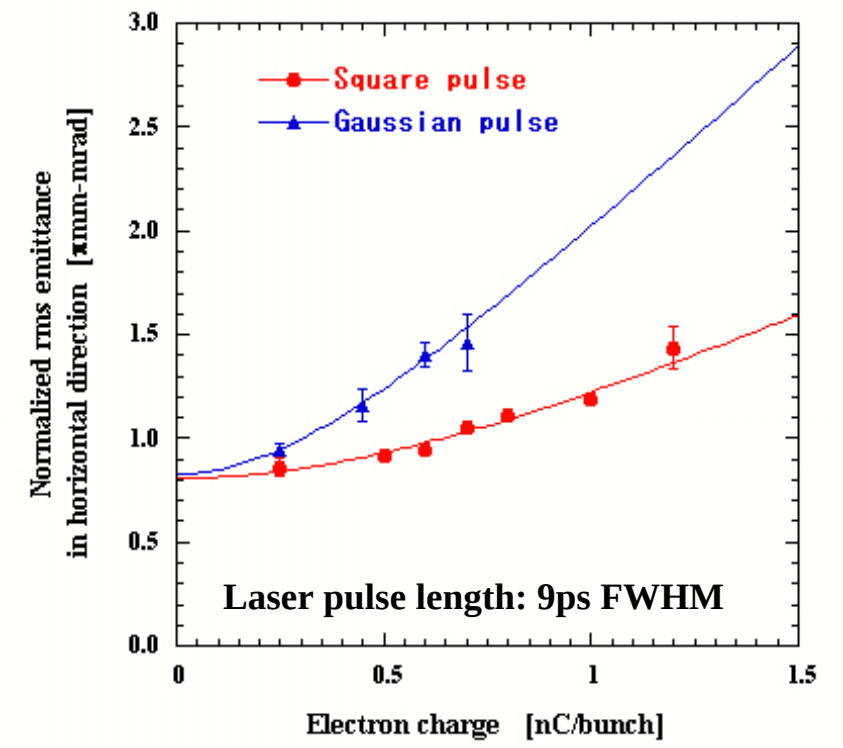

Courtesy of F. Sakai

Laser Pulse Shaping Techniques

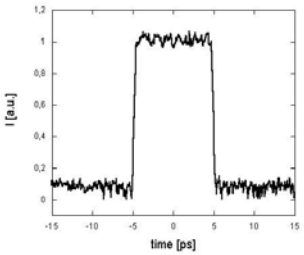

Figure 4.12: Optimum pulse shape as predicted by a GA algorithm on the fundamental.

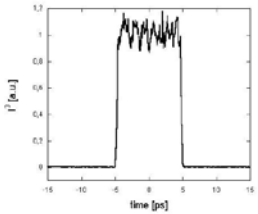

Figure 4.13: Optimum pulse shape as predicted by a GA algorithm on the third harmonic.

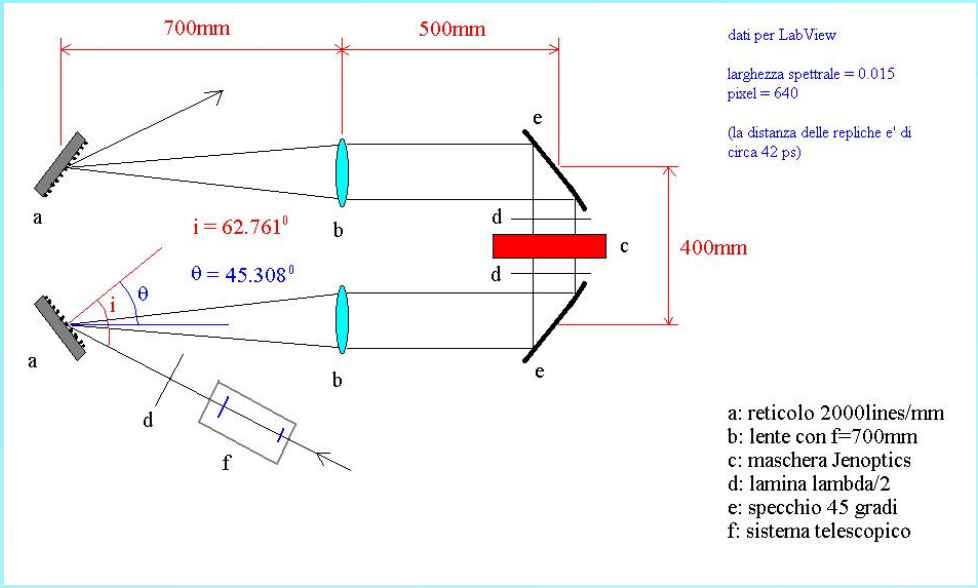

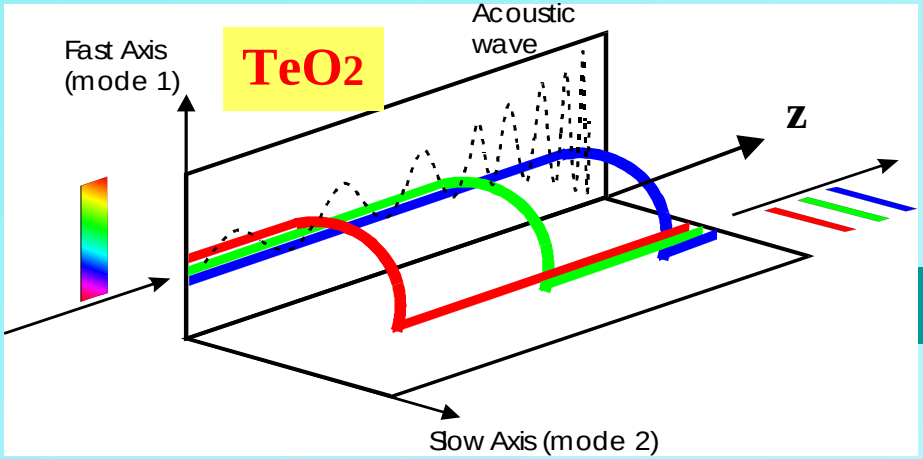

Liquid Crystal Phase Mask

DAZZLER

Collinear Acousto-Optic modulator (AOM)

Beam envelope and emittance

Q=1.1 nC, pulse length (FWHM) = 10 psec, rise time=1 psec

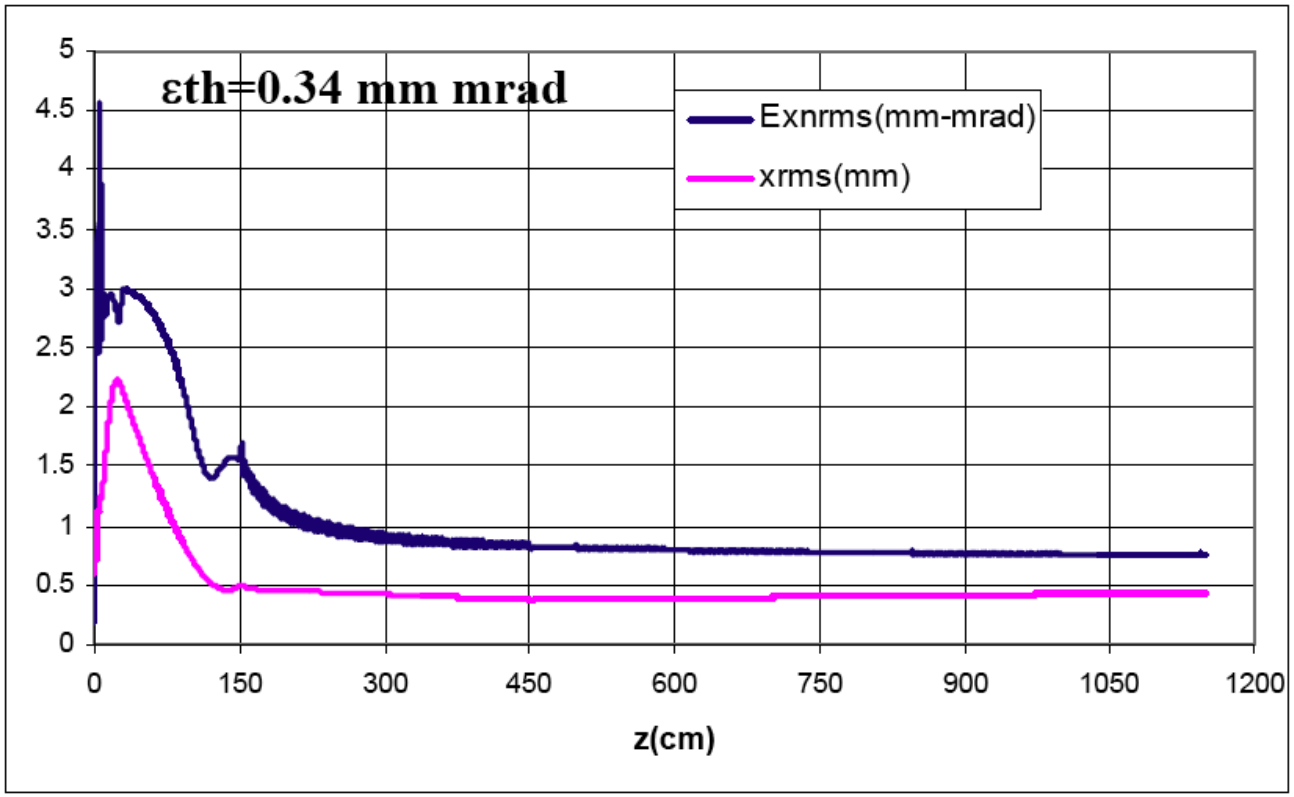

ϕgun=33°, rcathode=1.13 mm, Bgun=2.73 Kgauss,B(TW1)=750 gauss

Slice analysis through the bunch

Q=1.1 nC, pulse length (FWHM) = 10 psec, rise time=1 psec

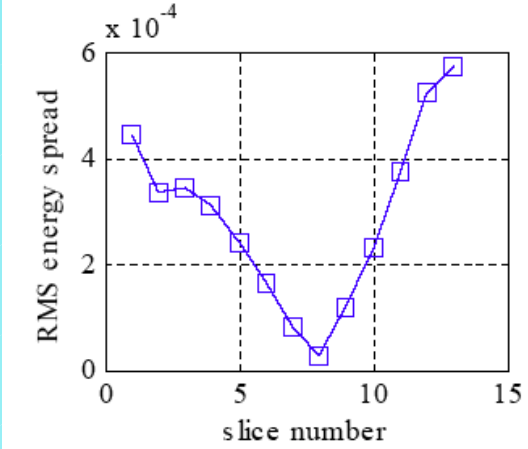

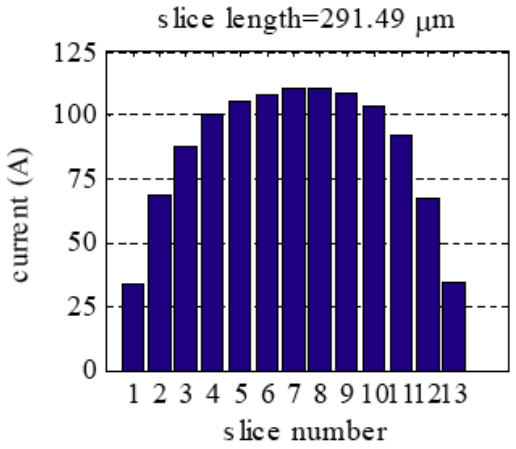

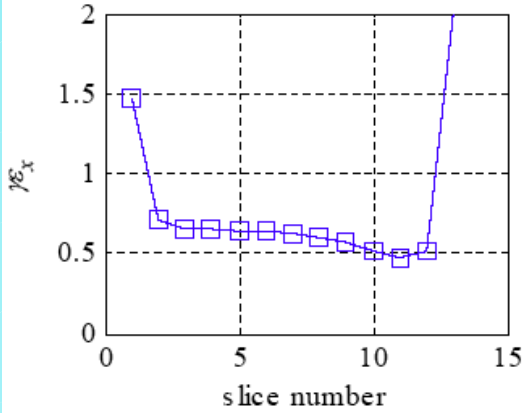

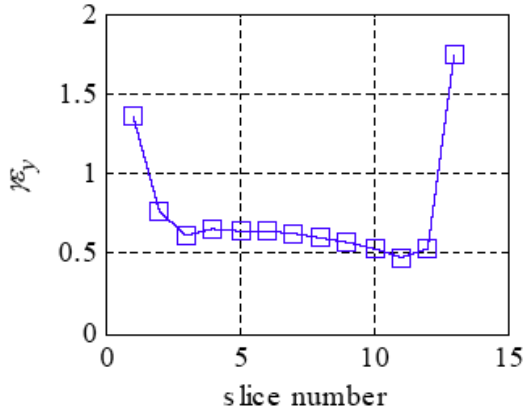

Max. slice current=110 A

Current ≥ 100 A in 54% beam

Projected emittance= 0.75 mm mrad

GENESIS simulation of the SPARC SASE-FEL

Radiation power growth along the undulator @ 530 nm

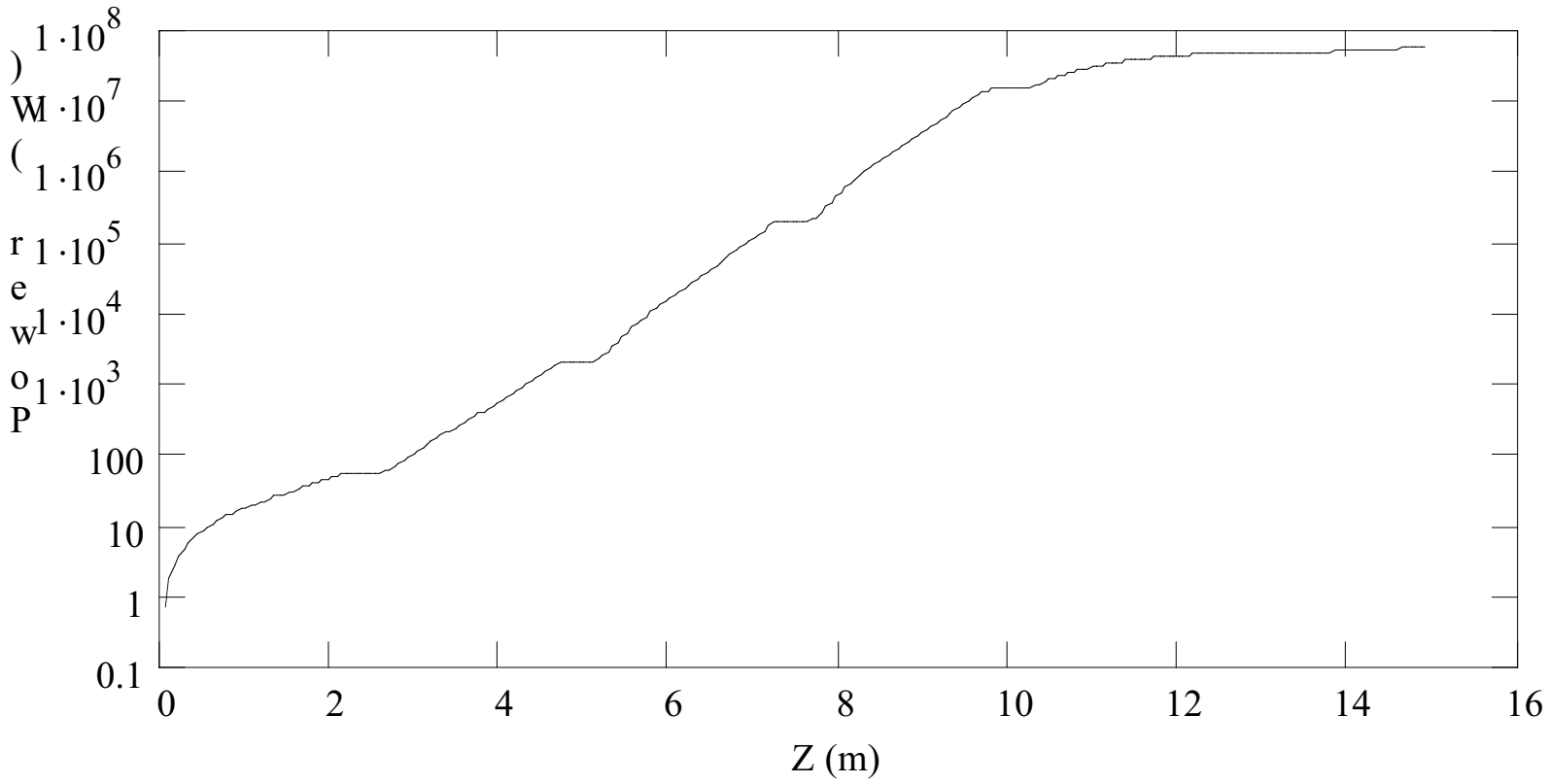

RF Deflector: principle of operation

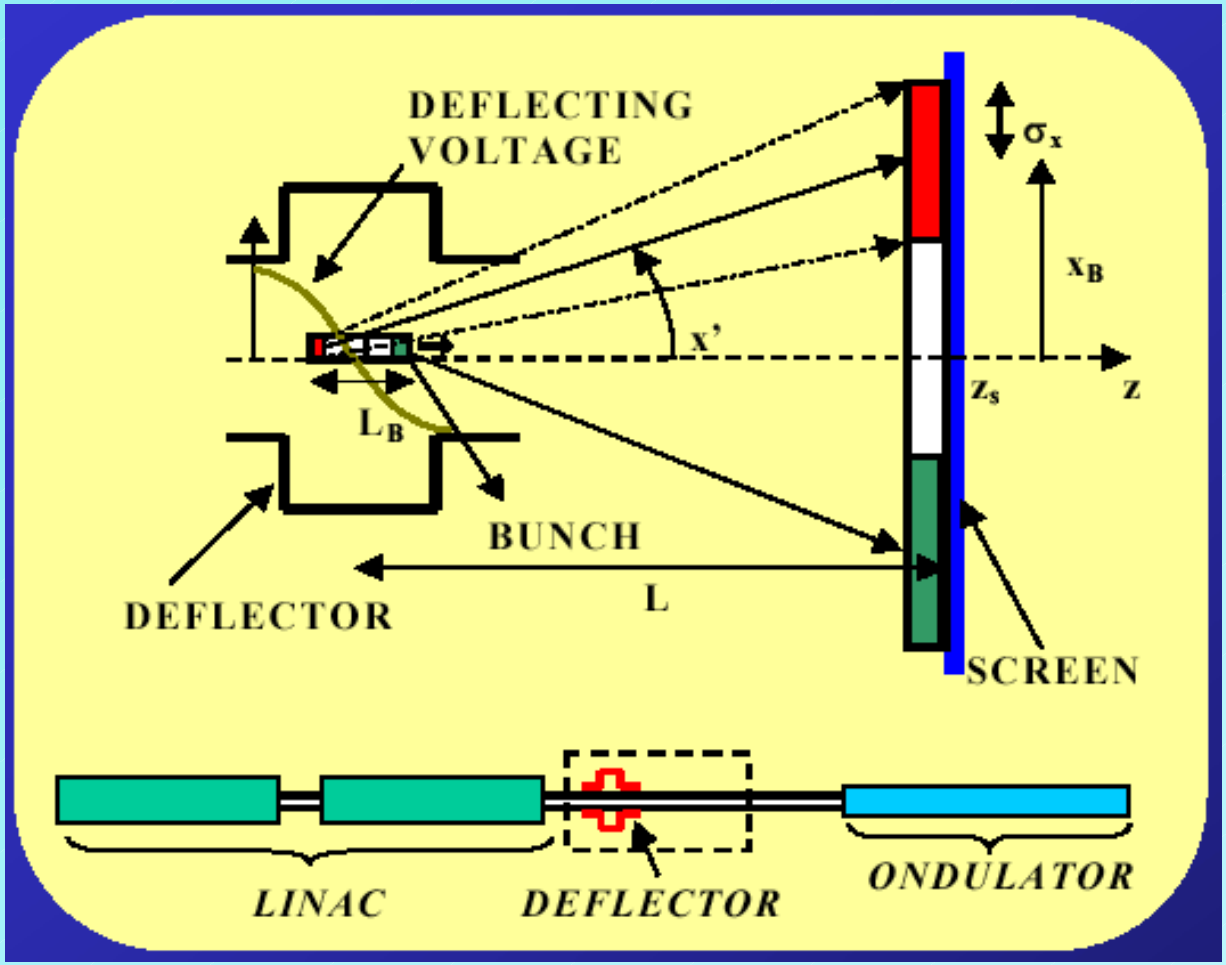

SPARC measurement layout for high energy beam characterization

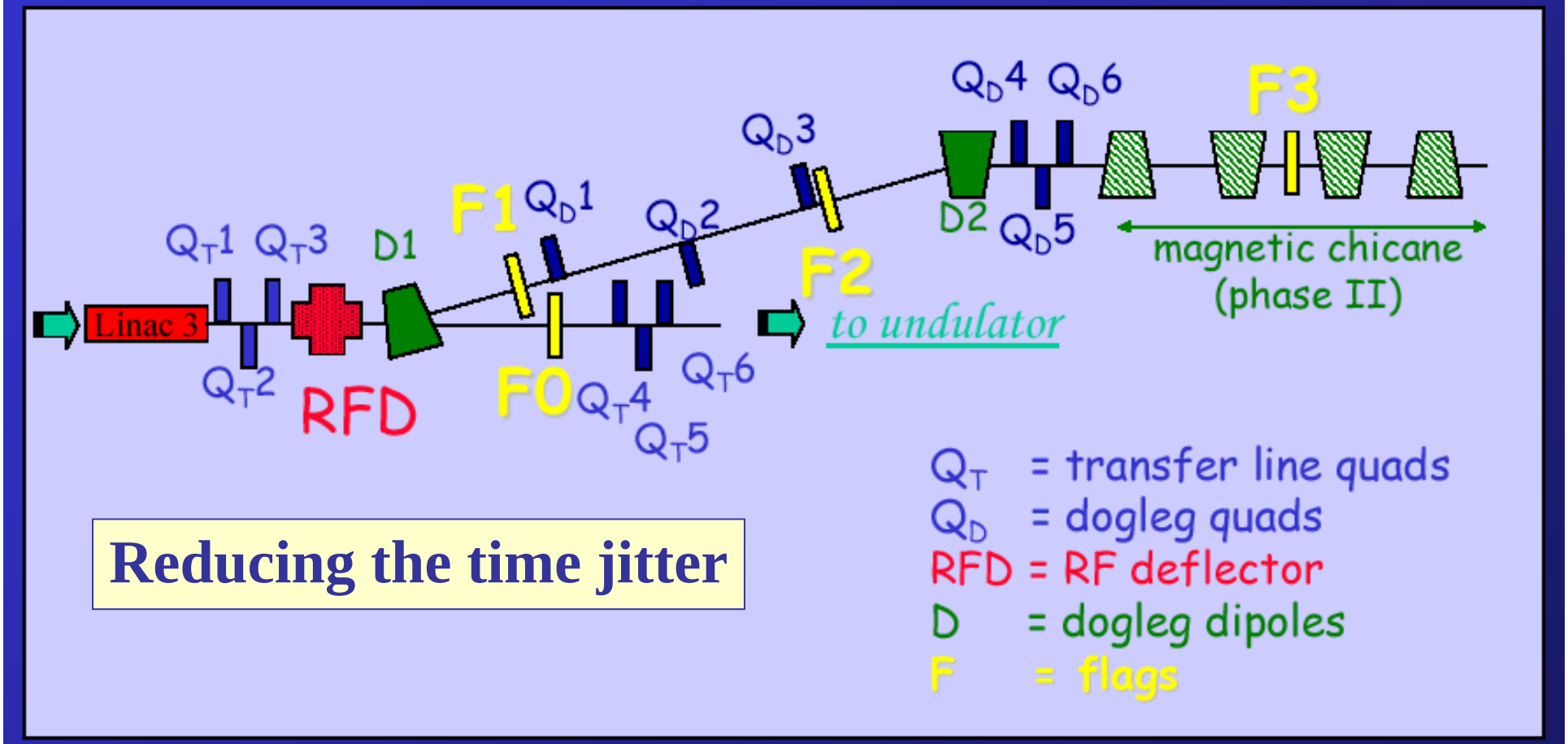

Reducing the time jitter

Slice selection @ SPARC using a slit and RF Deflector, with and without clipping

Bunch transverse distribution* at the screen location F0

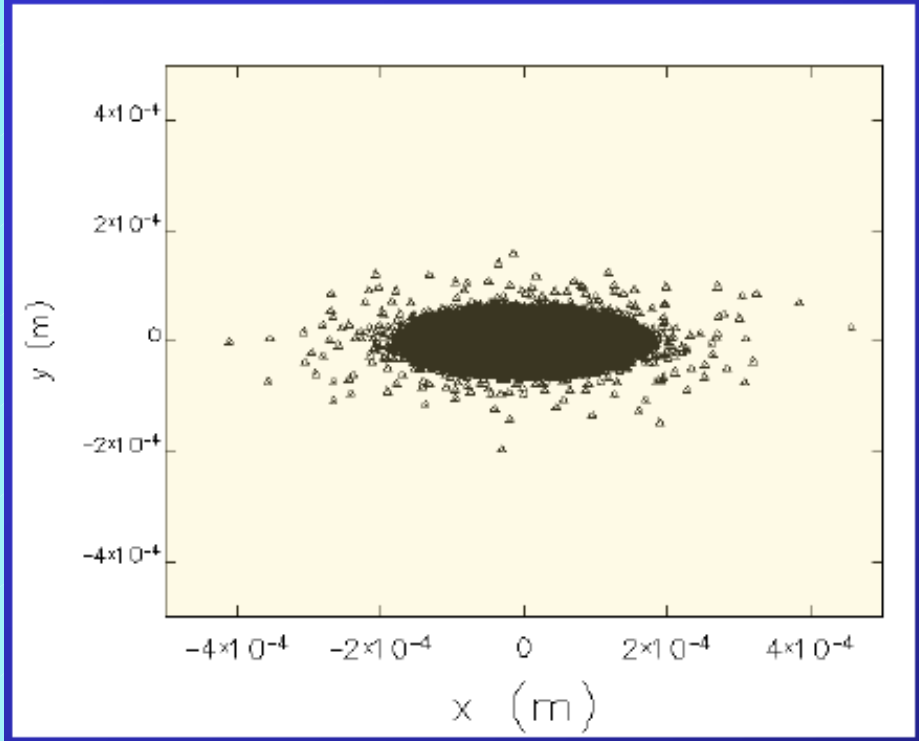

RFD OFF

Coupling of time-transverse coordinate with 1:1 c.c.

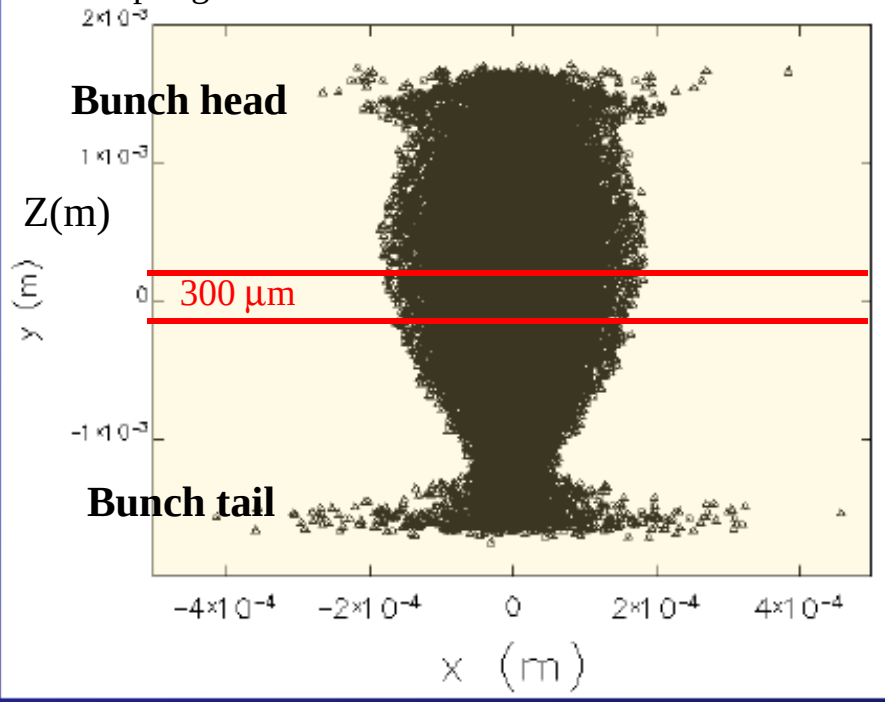

RFD ON ($V_{\perp}$ = 1 MV)

4a) Prototype measurements (Oct. 2003)

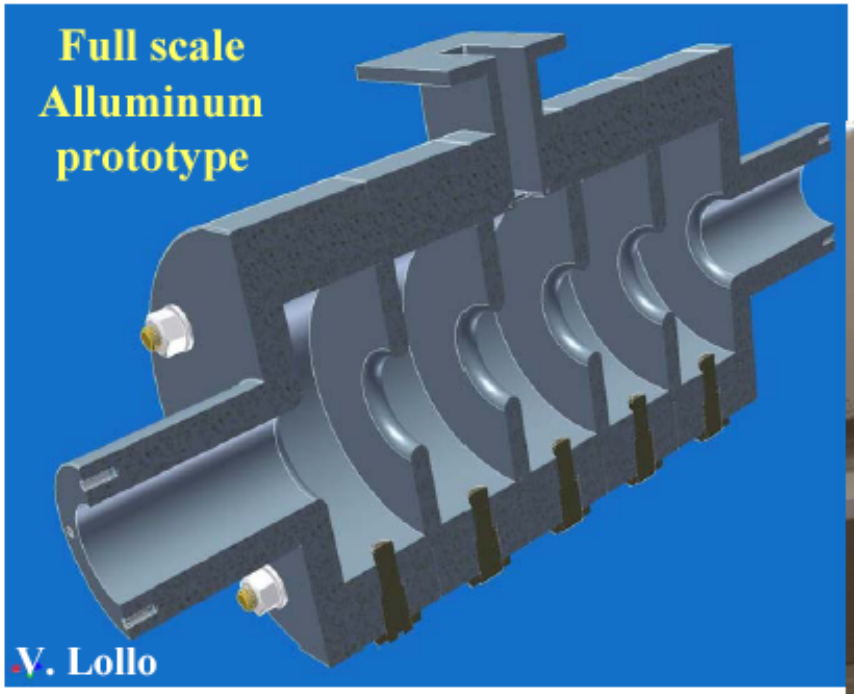

Bead-pull measurement set up
(Univ. of Rome "La Sapienza" Dip. Energetica)

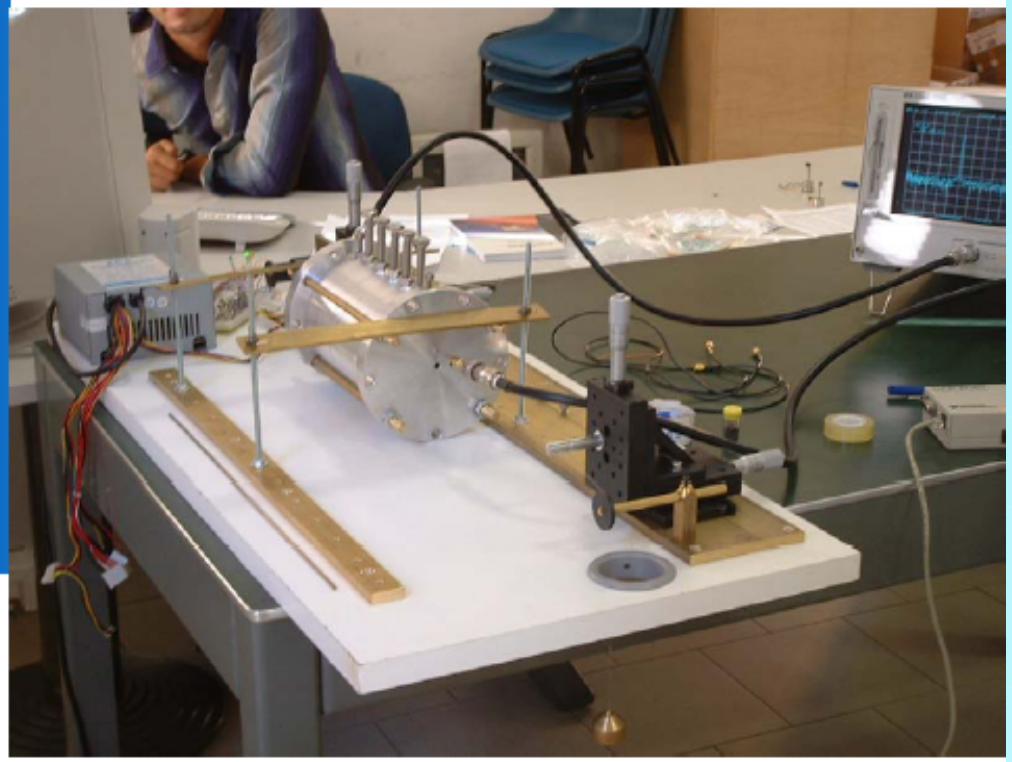

4b) Brazing tests @ LNF (Oct. 2003): to invetsigate the effect of the brazing procedure on the resonant frequency of the cells

4c) Final device on Cu_{OFHC} (Jan. 2004) machined outside and brazed @ LNF

A 3D Model View of the buildings

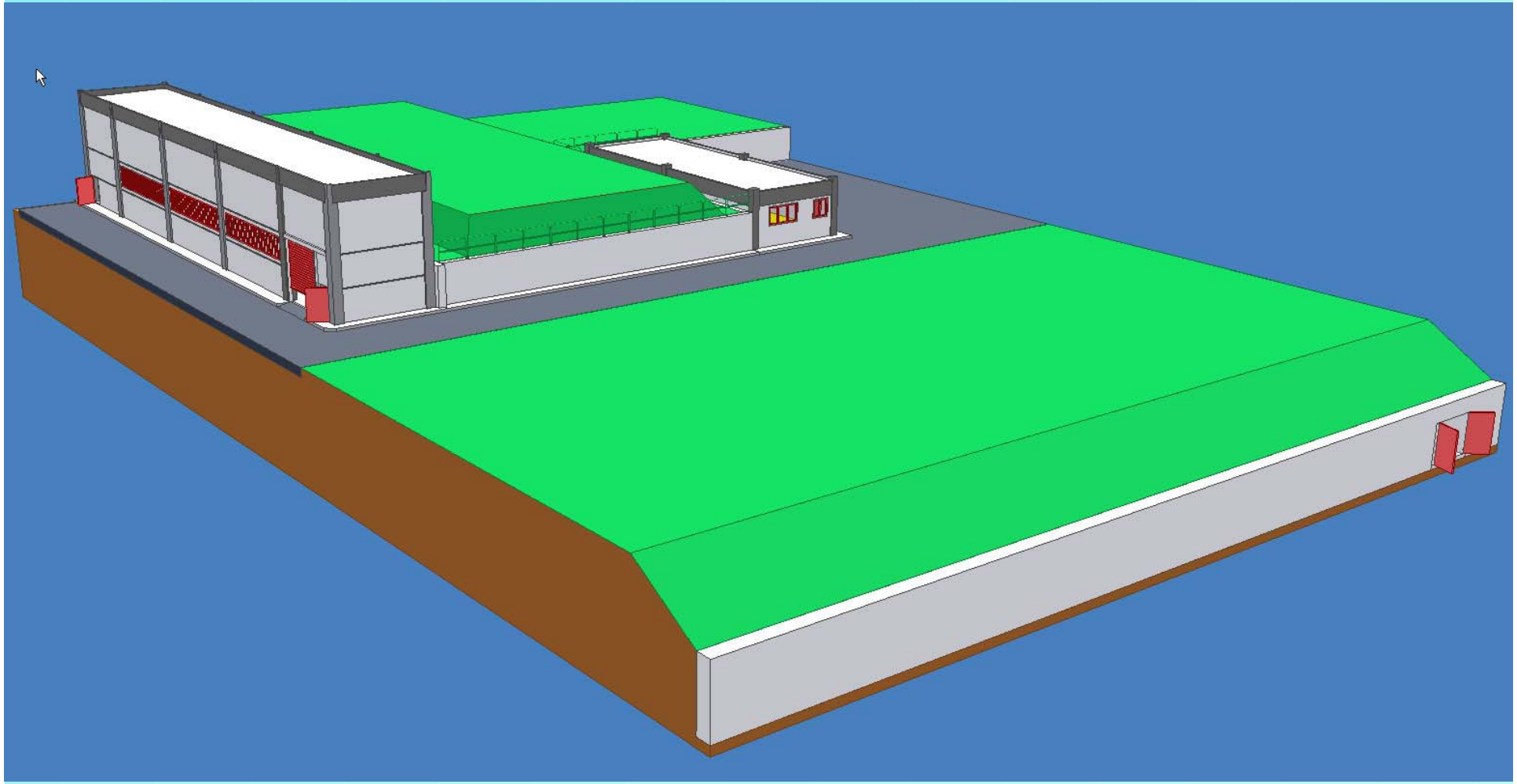

A 3D Model View of the buildings

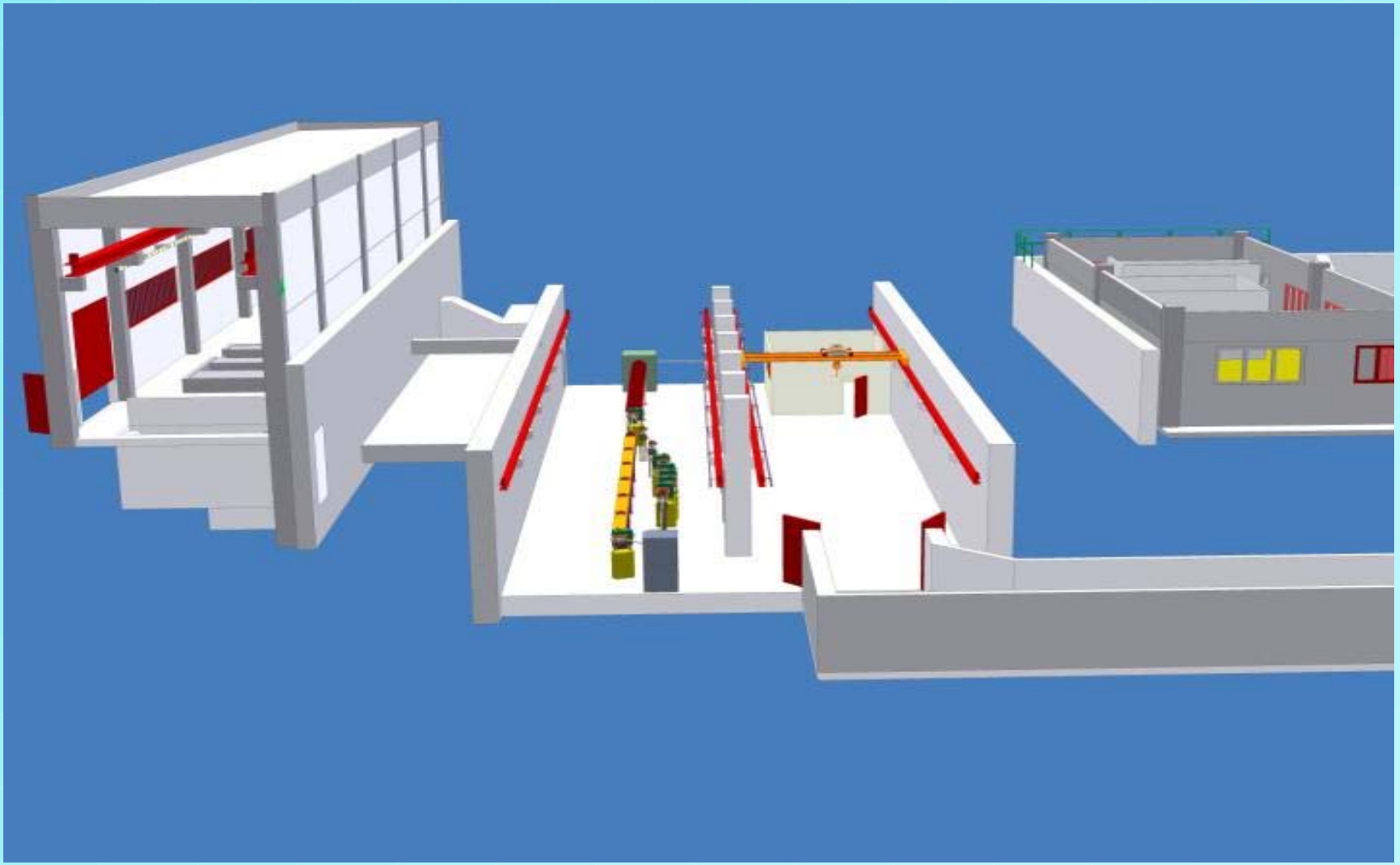

INFN Istituto Nazionale di Fisica Nucleare
Laboratori Nazionali di Frascati

INTERNATIONAL CONFERENCE ON
"ULTRASHORT HIGH-ENERGY RADIATION AND MATTER"
Villa Monastero, Varenna, October 7 -10, 2003

SPARC

Start April 30, 2003

SPARC-Phase 2: Beam Compression - the road map toward ultra-short bunches

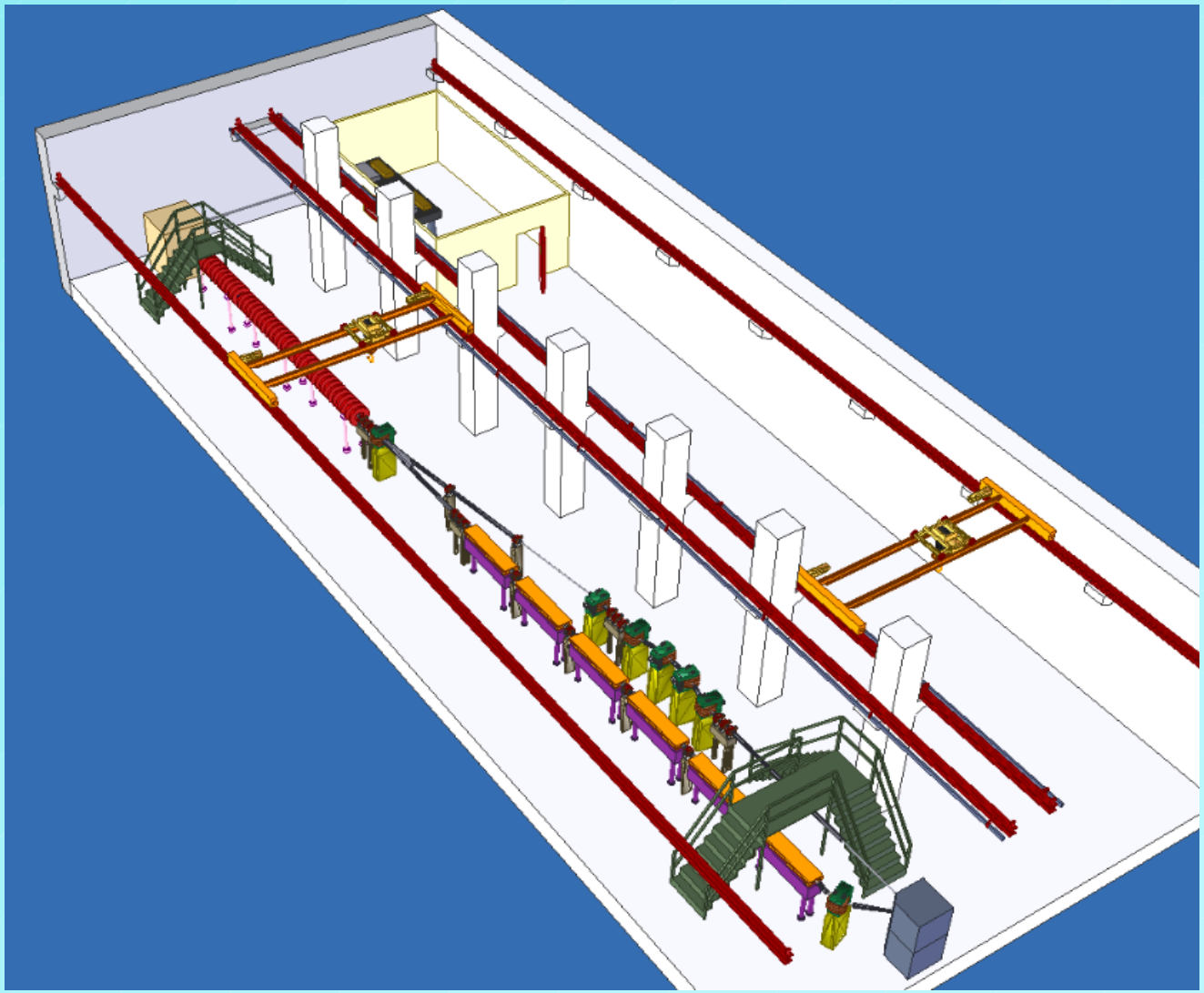

INFN Istituto Nazionale di Fisica Nucleare
Laboratori Nazionali di Frascati

SPARC

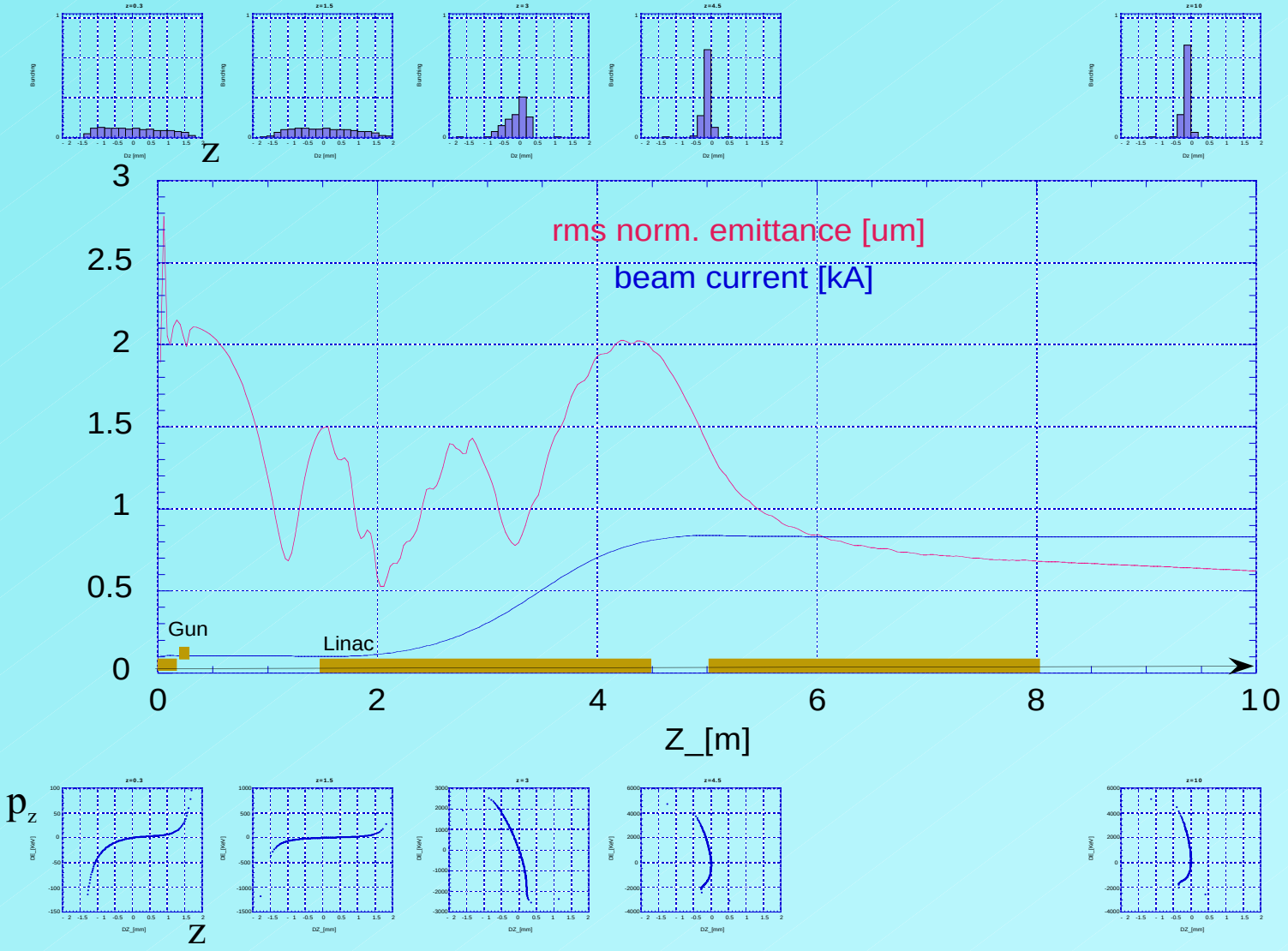
z
rms norm. emittance [um]
beam current [kA]
Gun
Linac
Z_[m]
p_z
z

Compact Sources of Monochromatic X-rays based on Relativistic Thomson back-scattering

$\lambda_X \cong \lambda_{las} / 4\gamma^2((1-\cos\Psi)/2)$ $\lambda_{las} = 0.8\ \mu m$ $\gamma = 80$ (40 MeV)

$\lambda_X = 0.32$ Å, 37 keV

$$N_X \propto \Sigma_T f \frac{N_{e^-} N_{h\nu}}{\sigma_{coll}^2}$$

$$\Sigma_T = 7 \cdot 10^{-29} \quad m^2$$

$$N_X = 2 \cdot 10^{9/11}$$

$$\left(f = 10 Hz, N_{e^-} = 10^{10}, N_{h\nu} = 10^{18}, \sigma_{coll} = 50,5 \mu m \right)$$

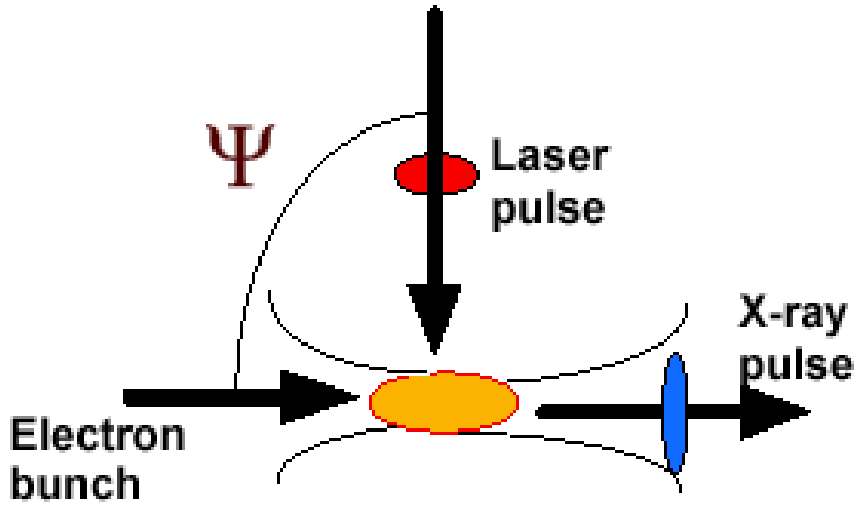

Fig. 2 Thomson scattering geometry

INFN Istituto Nazionale di Fisica Nucleare
Laboratori Nazionali di Frascati

SPARC

Two additional beam lines at SPARC: plasma acceleration and monochromatic X-ray beams

100 fs synchr. Ti:Sa multi-TW Laser System

1 J, 10 ps gaus

2 nC, 10 ps*

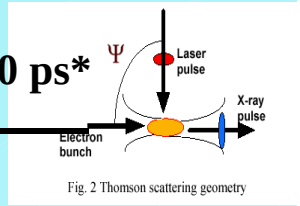

Fig. 2 Thomson scattering geometry

Compr. 1 J, 100 fs gaus

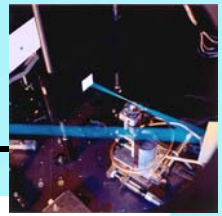

20 mJ, 10 ps flat top

500 μJ

20 pC, 20 fs$

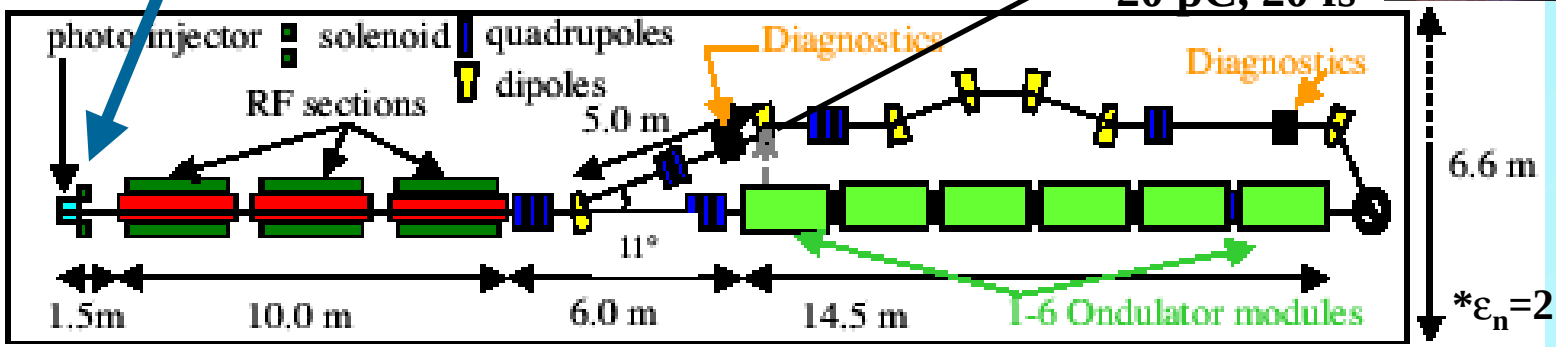

1 nC, 10 ps, ε_n=1 μm

*ε_n=2 μm, σ_x =50 μm

$$\varepsilon_n$=0.2 μm, σ_x =10 μm

CONCLUSIONS (SPARC)

- SPARC is aimed at delivering within 3 years a top brightness electron beam (Phase 1)
- Velocity Bunching will ultimately allow to reach unprecedented quality beams in a compact system (200 MeV)
- SPARC has the chance to become an advanced facility in the international scenario to conduct frontier beam physics

  (*High Gradient Acceleration and Advanced X-ray Beams*)

S ource

P ulsed

selfA mplified

R adiation

X

Self-Amplified Pulsed X Radiation Source

INTERNATIONAL CONFERENCE ON
"ULTRASHORT HIGH-ENERGY RADIATION AND MATTER"
Villa Monastero, Varenna, October 7 -10, 2003

INFN Istituto Nazionale di Fisica Nucleare
Laboratori Nazionali di Frascati

SPARC

Which technology for a 2.5 GeV Linac with long term evolution toward 1 Å ?

- **2.5 GeV is consistent with $\lambda = 1.5$ nm**

• λ [nm]	1.5	$\Rightarrow$	**1 Å**
• **I [kA]**	2.5	$\Rightarrow$	3-5
• ε_n [μm]	2.0	$\Rightarrow$	$\cong 1$
• $\Delta\gamma/\gamma$ [%]	≤ 0.1	$\Rightarrow$	$\cong 0.07$
• **T [GeV]**	2.5	$\Rightarrow$	$\cong 10$

Examined different solutions:

S-band Room-Temperature

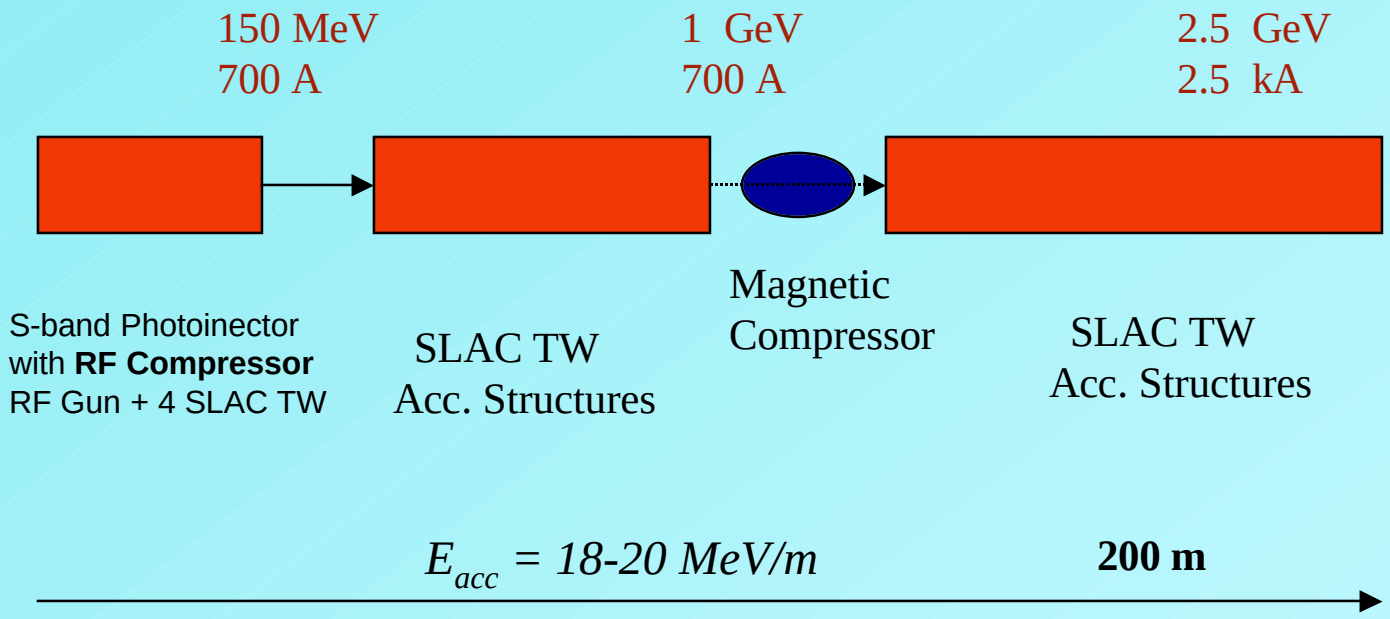

Linac schemes with RF compressor

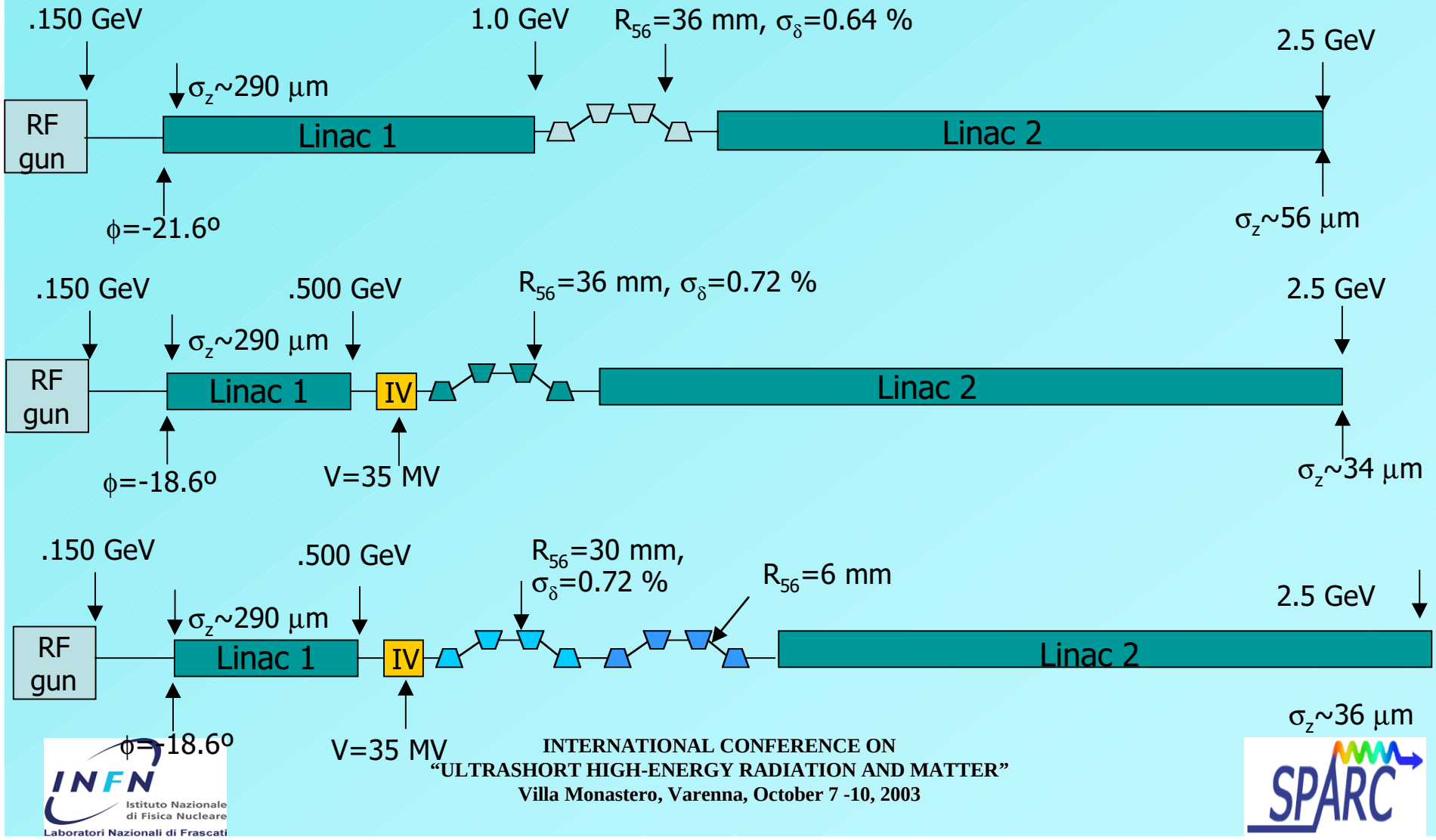

Purely magnetic compression for SPARX

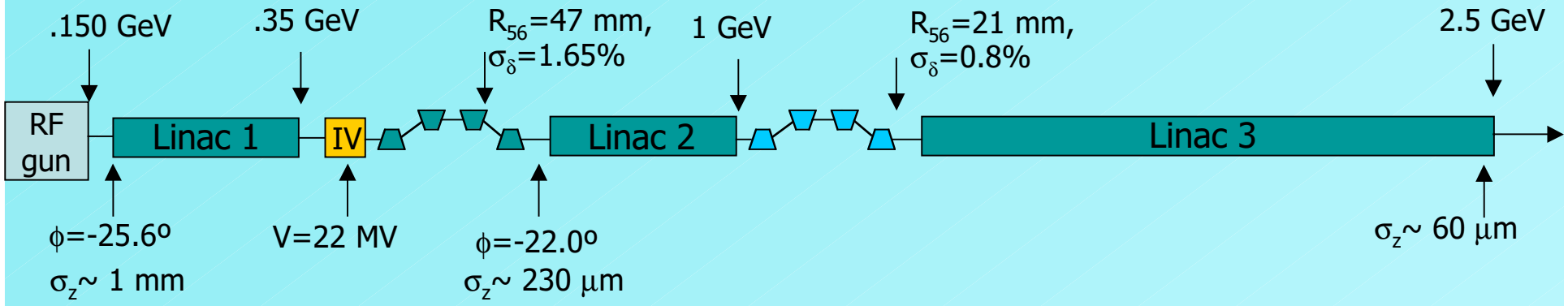

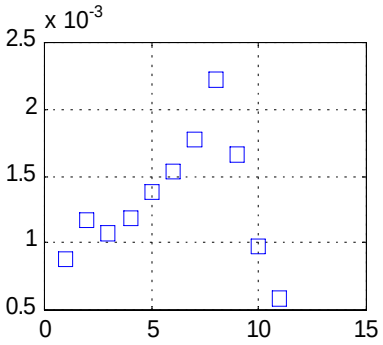

1 ps jitter optimization

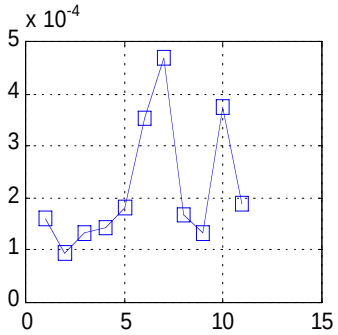

3D simulation with GENESIS @ 1.5 nm

Tab. 3: Undulators characteristics

	Undulator 1 @1.5 nm	Undulator 2 @13.5 nm
Type	Halbach	Halbach
Period	3 cm	5 cm
K	1.67	4.88
Gap	12.67 mm	12.16 mm
ResidualField	1.25 T	1.25 T

Tab. 4: FEL-SASE expected performances

Wavelength (?)	1.5 nm	13.5 nm
Saturation length	24.5 m	14.5 m
Peak Power	10^{10} W	4 10^{10} W
Peak Power 3° harm.	2 10^{8} W	5 10^{9} W
Peak Power 5° harm.	3 10^{7} W	2 10^{8} W
Brilliance	1.8 10^{31}	2 10^{32}
Brilliance 3° harm.	10^{29}	10^{31}
Brilliance 5° harm.	9 10^{28}	3 10^{29}

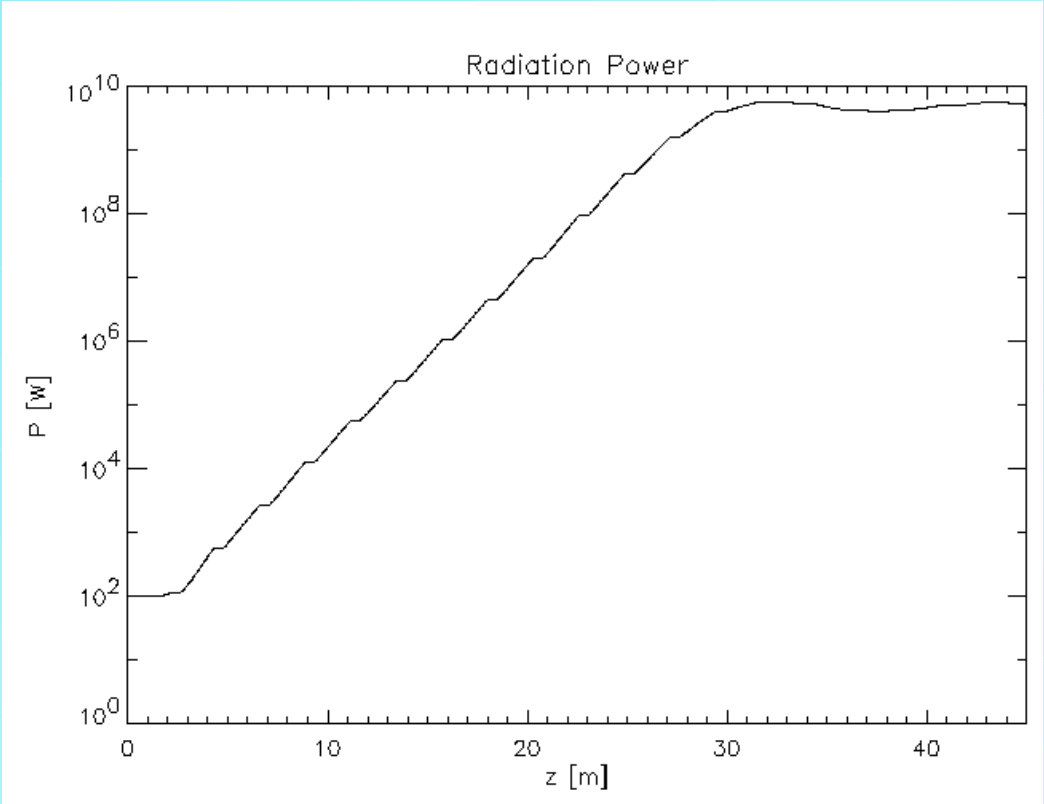

rms spot size 50 μm
rms divergence 5 μrad

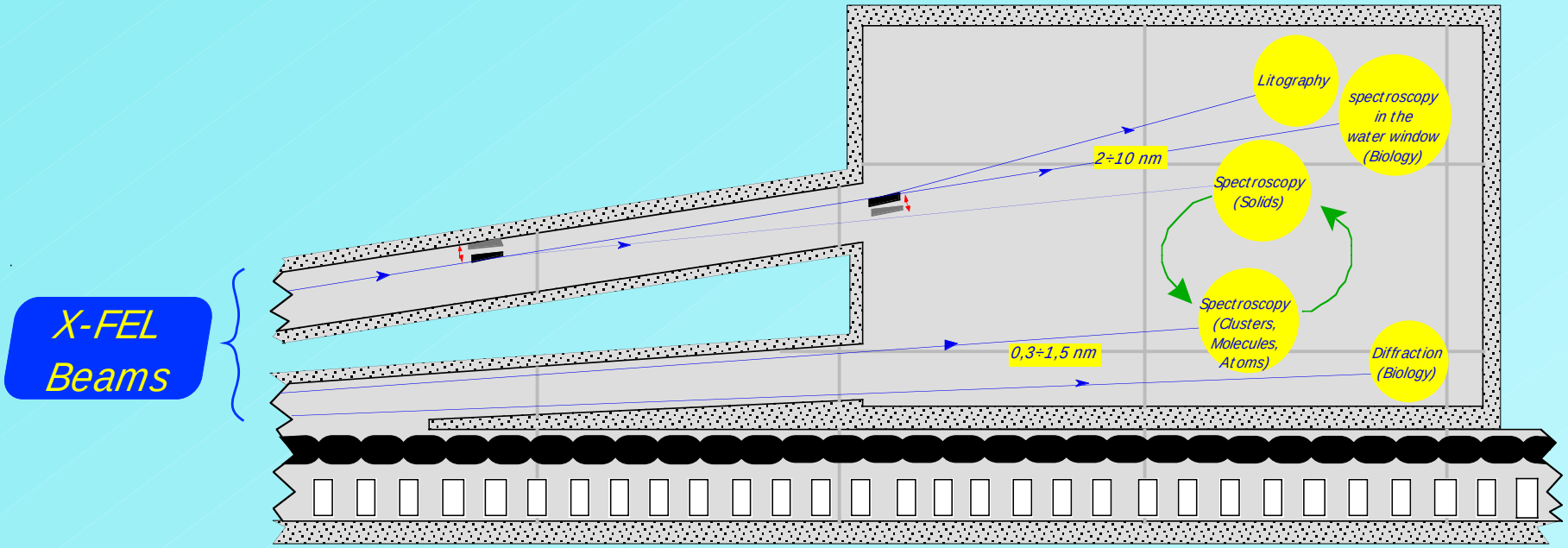
X-FEL
Beams
Litography
spectroscopy
in the
water window
(Biology)
2÷10 nm
Spectroscopy
(Solids)
Spectroscopy
(Clusters,
Molecules,
Atoms)
0,3÷1,5 nm
Diffraction
(Biology)

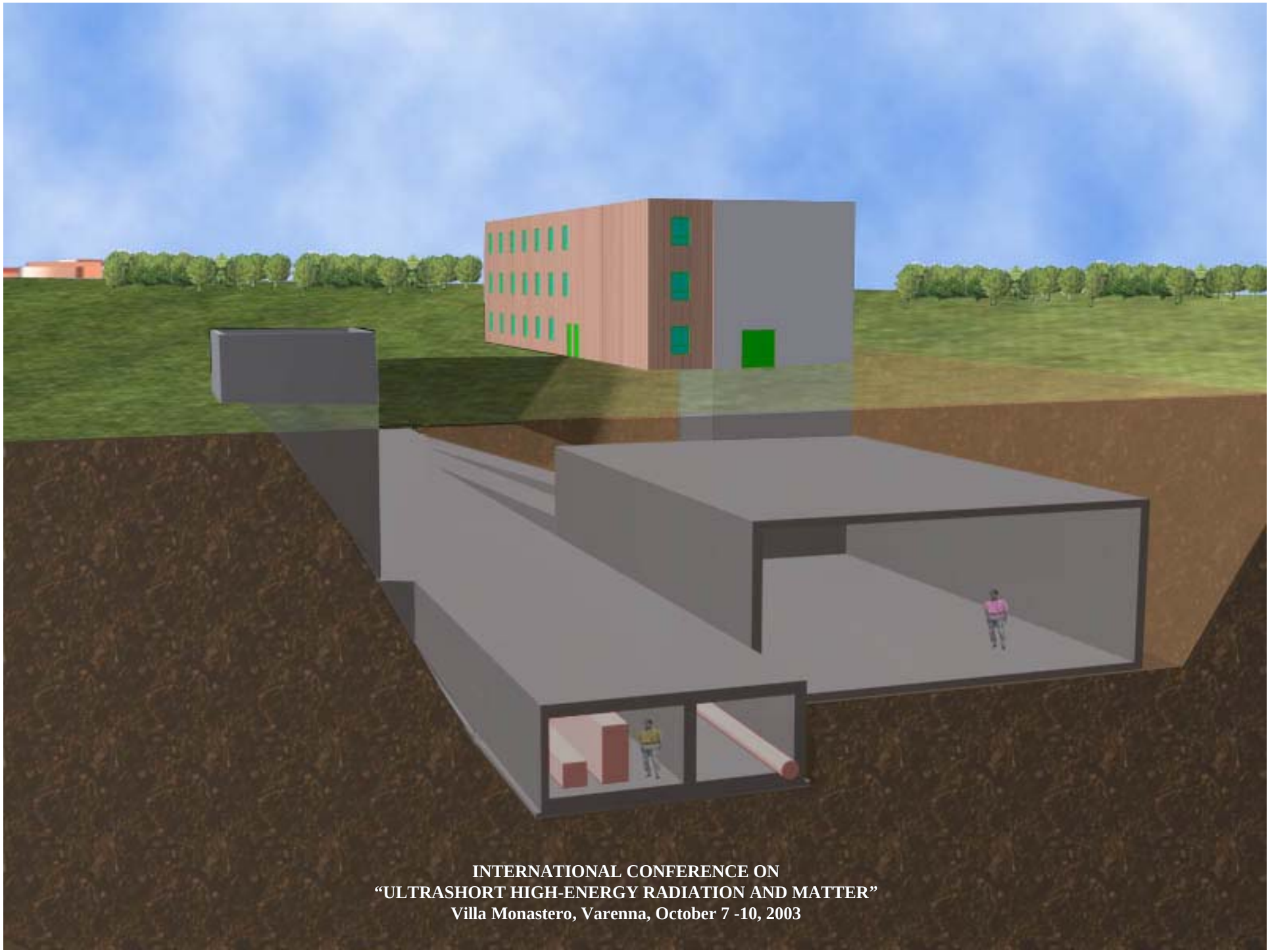

INTERNATIONAL CONFERENCE ON
"ULTRASHORT HIGH-ENERGY RADIATION AND MATTER"
Villa Monastero, Varenna, October 7 -10, 2003

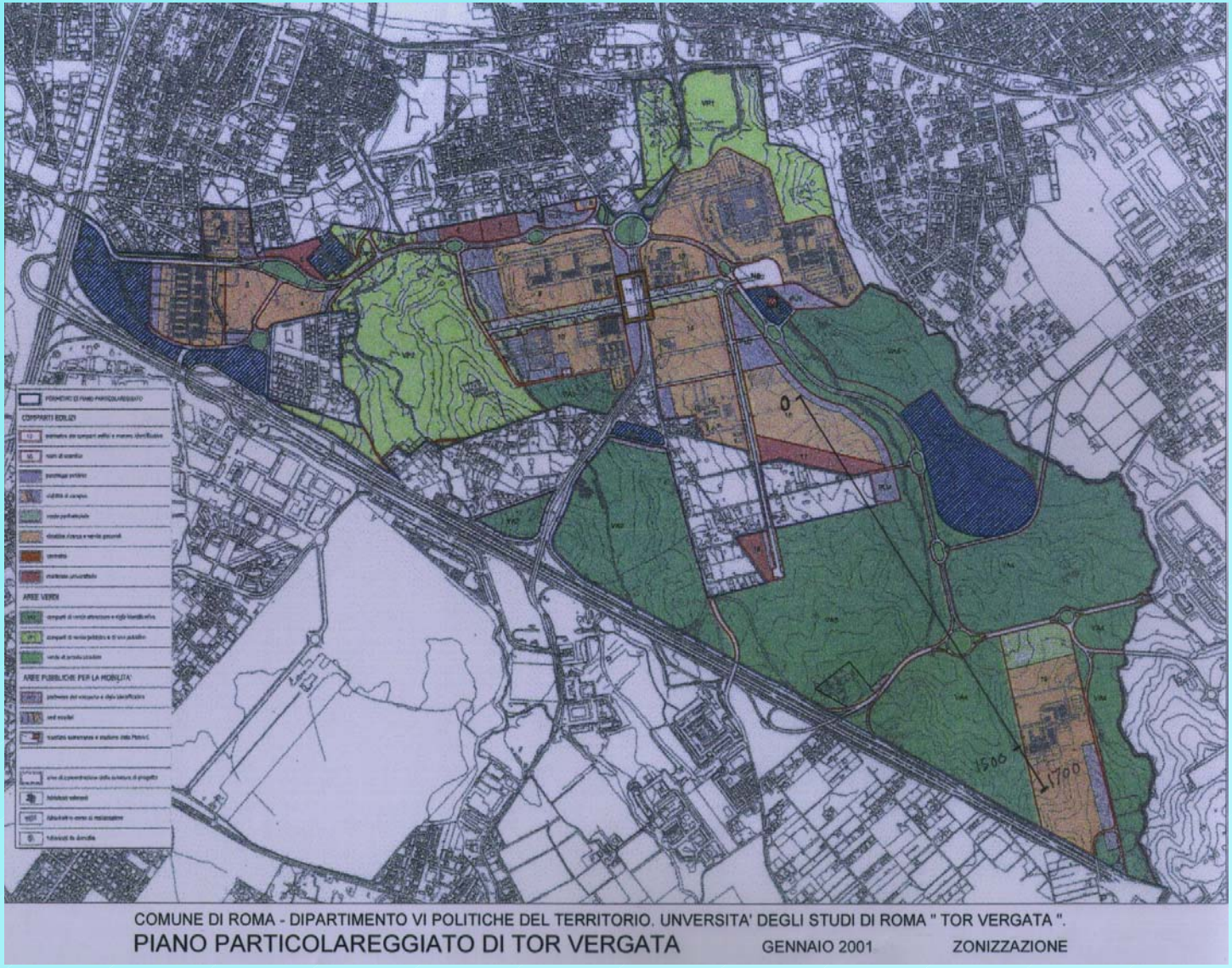

INFN Istituto Nazionale di Fisica Nucleare
Laboratori Nazionali di Frascati

INTERNATIONAL CONFERENCE ON
"ULTRASHORT HIGH-ENERGY RADIATION AND MATTER"
Villa Monastero, Varenna, October 7 -10, 2003

SPARC

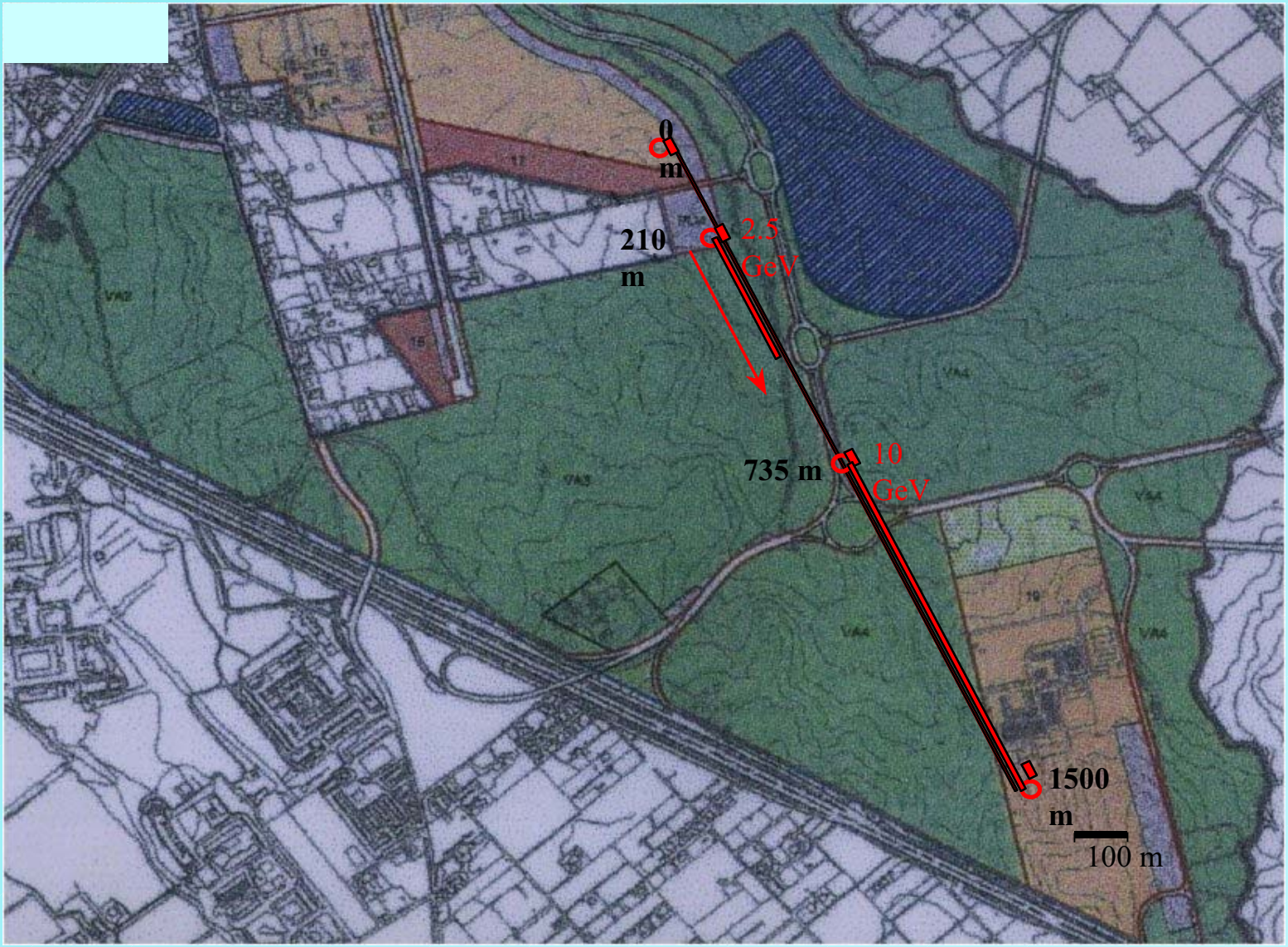

INFN Istituto Nazionale di Fisica Nucleare
Laboratori Nazionali di Frascati

INTERNATIONAL CONFERENCE ON
"ULTRASHORT HIGH-ENERGY RADIATION AND MATTER"
Villa Monastero, Varenna, October 7 -10, 2003

SPARC

Cost of a 1.5 nm source

Costs (in M€)	77
Linac (2.5 GeV)	32
Undulators	10
Radiation beam lines	10
Contingency	13
Infrastructures	12

Construction time: 6 years

Conclusions SPARX

- The budget is consistent with the goal of 1.5 nm
- We have an innovative solution for the Linac lay-out which appears to relax the criticality of beam compression
- The facility can be built inside the "Torvergata" Campus

Layout and photon beam diagnostics for the VUV-FEL user facility at DESY

Elke Plönjes for the VUV FEL collaboration

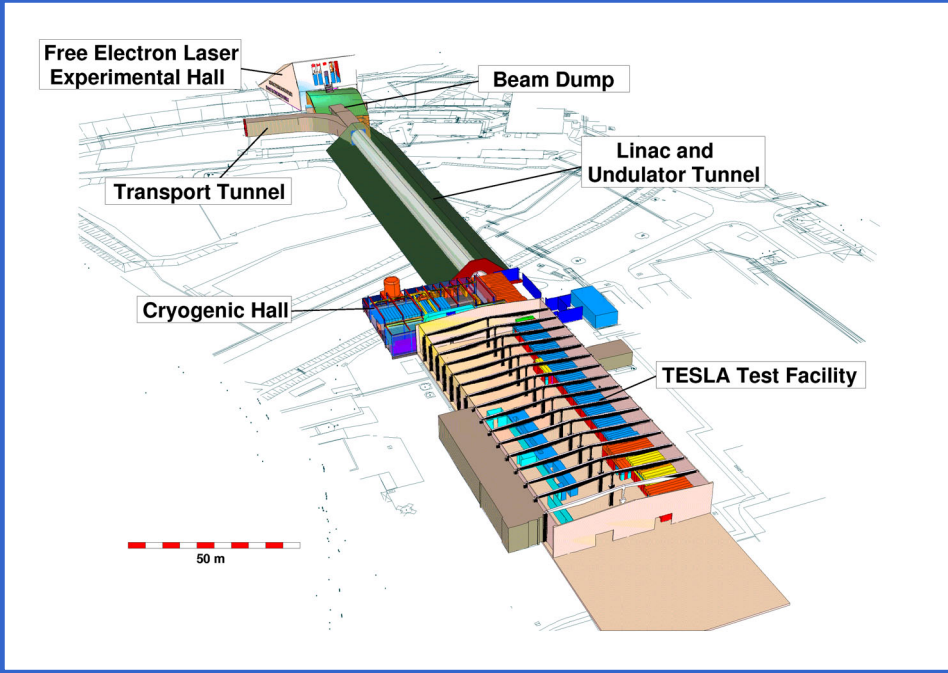

Introduction

SASE FEL at the TESLA TEST Facility at DESY

- 2000 First self amplified spontaneous emission (SASE) around 108 nm
- 2001 SASE FEL gain up to saturation was reached between 80 – 120 nm
- End 2001 – 2002 First set of user experiments on the interaction with cluster beams and surfaces
- Currently the linear accelerator is being upgraded to 1 GeV which will provide radiation wavelengths down to 6 nm

VUV FEL at DESY

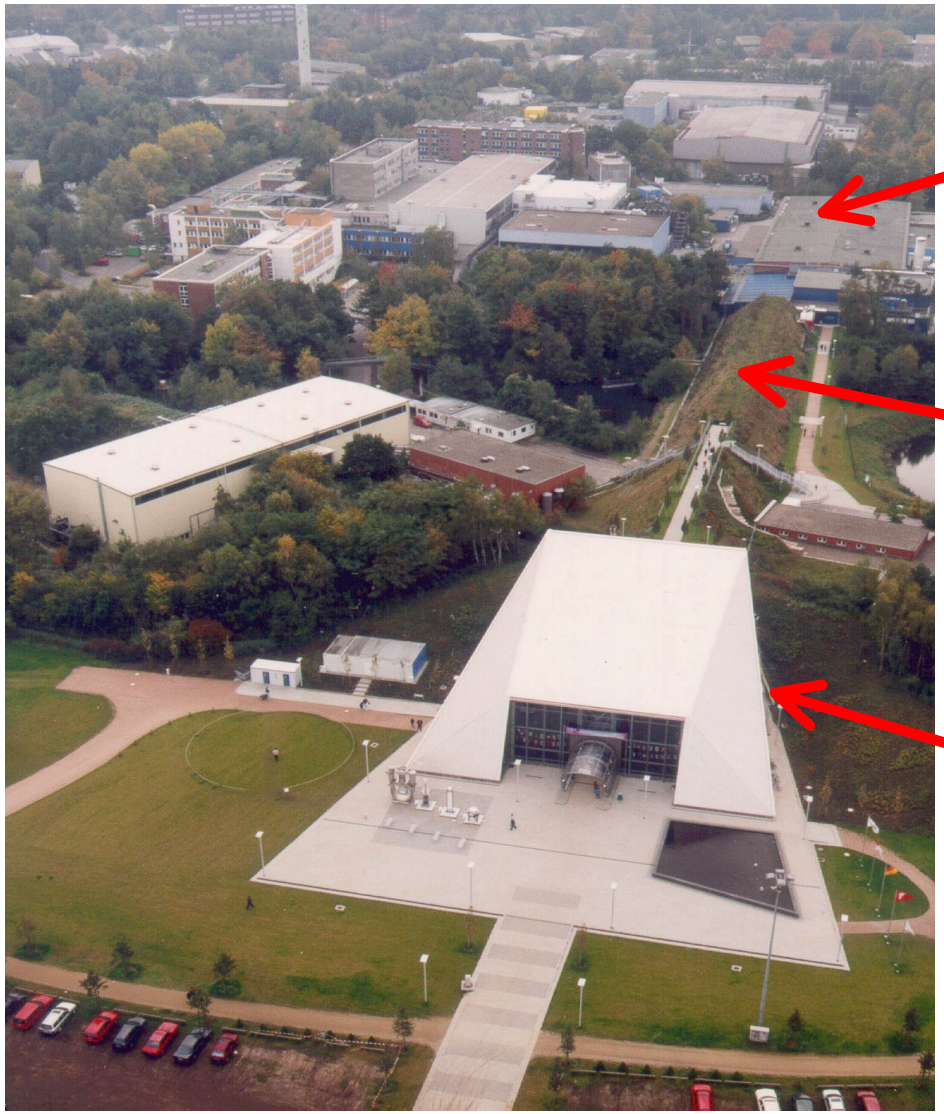

Phase1

- 80-120 nm
- 30-100 µJ
- 1 GW_{peak}
- 30-100 fs

Linac and FEL
extension for Phase2

Experimental hall
(User Facility, starting 2004)

- 6 - ~100 nm
- 0.03 – 1 mJ
- 30 - 400 fs

Areas of Proposed Research

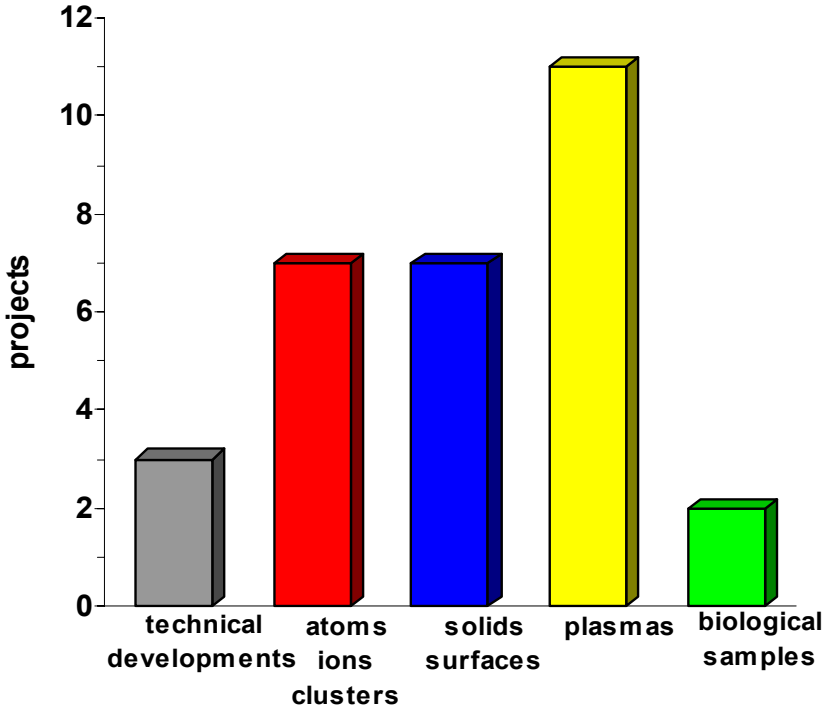

- 30 proposals submitted
- about 200 scientists from 60 institutes in 11 countries involved
- total beamtime requested: 98 weeks for the first year (49 weeks with two experiments in parallel)

Basic requirements for the FEL user facility for successful experiments

- **Control of wavelength, pulse timing, intensity etc.**

- **FEL beam transport**
  - **a nice focal spot of some µm**
  - stable beam direction of a few µrad, keep on reference orbit
  - stable, reproducible optical systems for deflection, focusing, beam splitting without degrading coherence and pulse duration

- **FEL beam diagnostics: Online, single pulse**
  - Pulse energy and spectral distribution
  - Intensity distribution, coherence
  - Temporal structure and exact timing

Layout of experimental hall

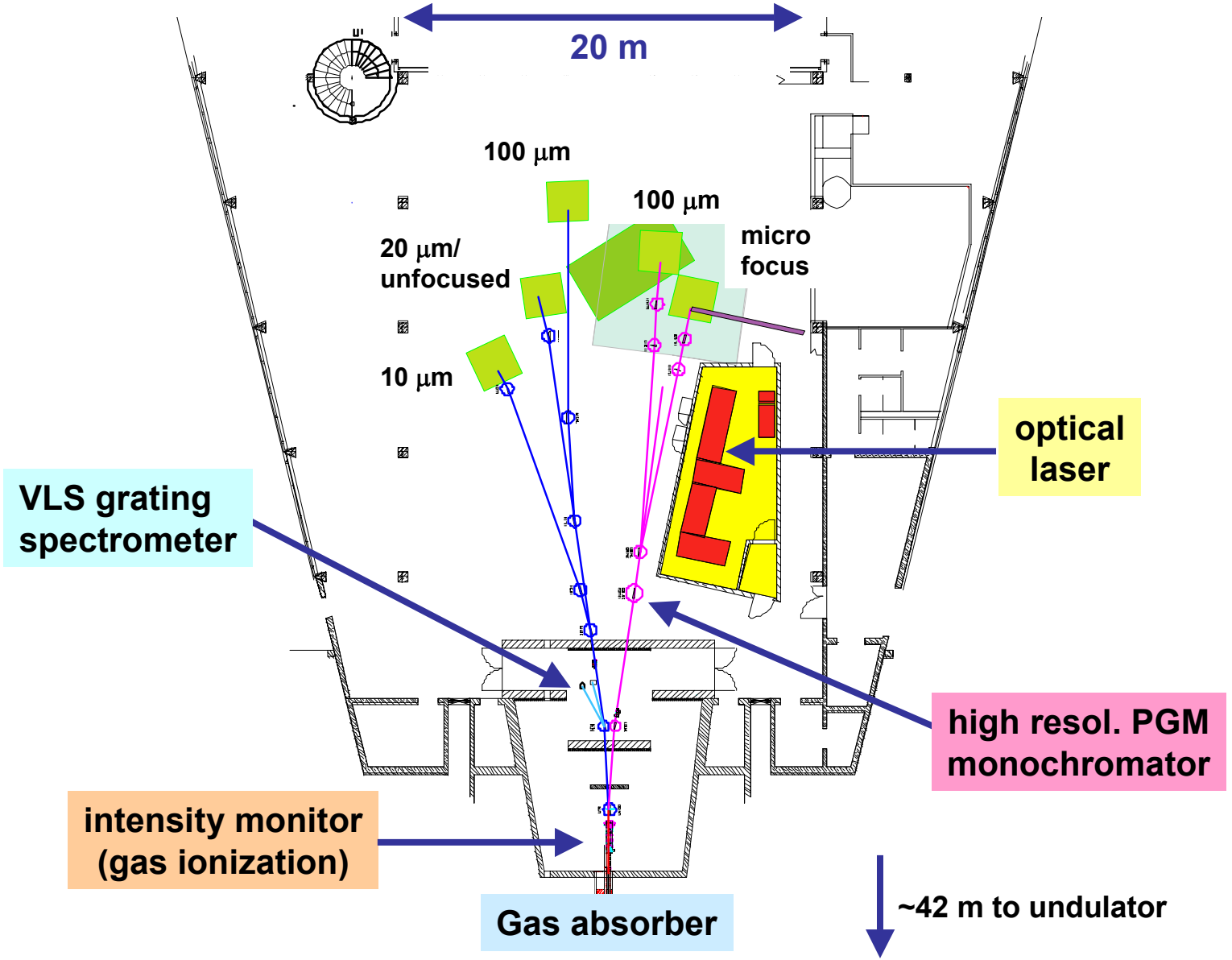

TTF1 results: FEL saturation at 95 nm

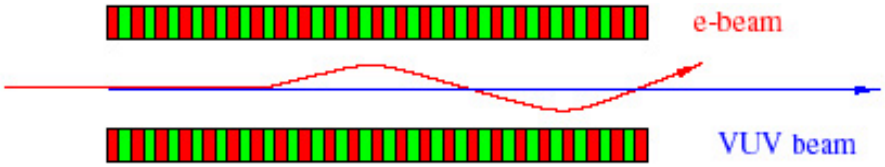

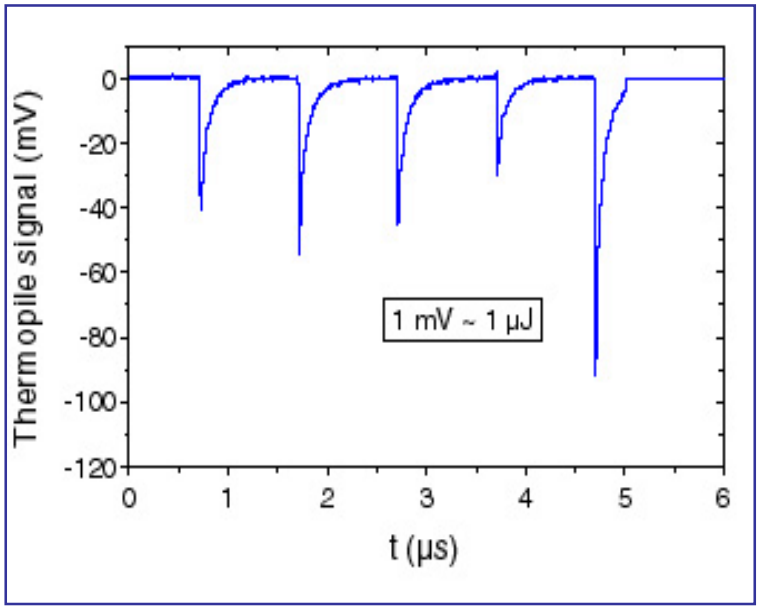

FEL pulse energy

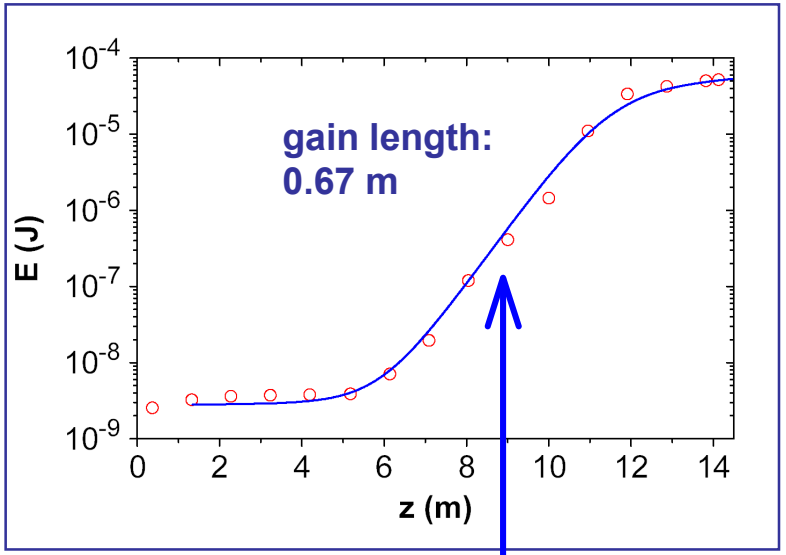

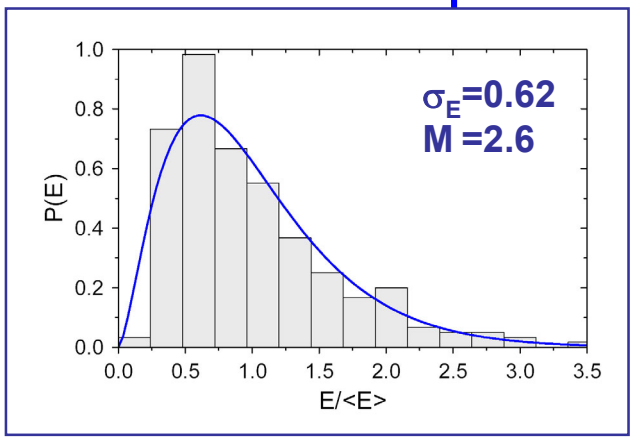

Intensity distribution at z = 9 m

Gas ionisation detector

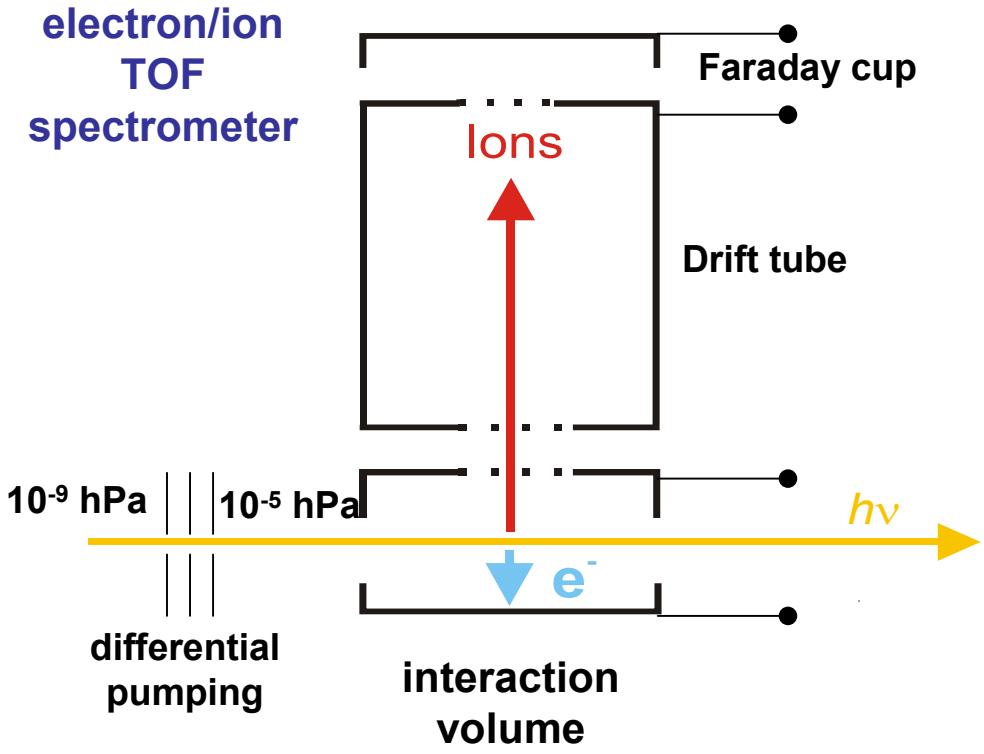

Online monitor of single-pulse FEL intensity

+ transparent
+ wide dynamic range (spont. to sat.)
+ independent of beam position
+ can measure beam position
+ no saturation effects
+ 6 nm < λ < 93 nm
+ absolute calibration (~10%)

- **successfully tested at TTF1**
- **needs some more work:**
  - **saturation limit**
  - **beam position**
  - **photon energy**

Collaboration with PTB, Berlin, and Ioffe Institute, St. Petersburg

Single photoionisation:

$$N = N_{ph} \times n \times s \times l$$

N	= number of electrons or ions
N_{ph}	= number of photons
n	= target density
s	= photoionisation cross section
l	= length of interaction volume

Controlled attenuation of FEL radiation using a gas aborber

- **Controlled attenuation of FEL beam for 6-120 nm**
- **Attenuation of 10^{-6} (depends on gas)**
- **Preserves beam attributes (coherence, statistics, spectrum, etc.) - not possible by changing LINAC settings**

calc. transmission of gas absorber

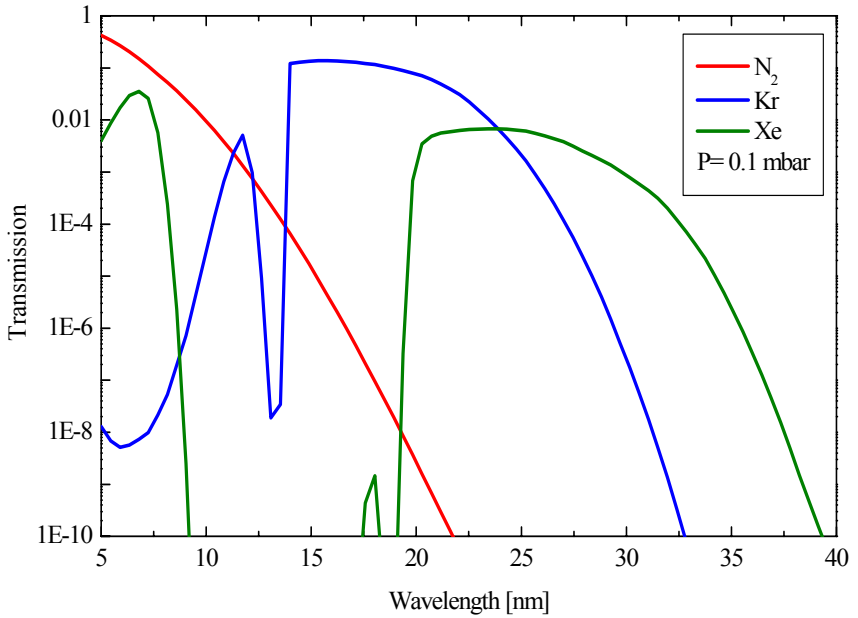

gas absorber cell (length: 15 m, Ø: 35 mm)

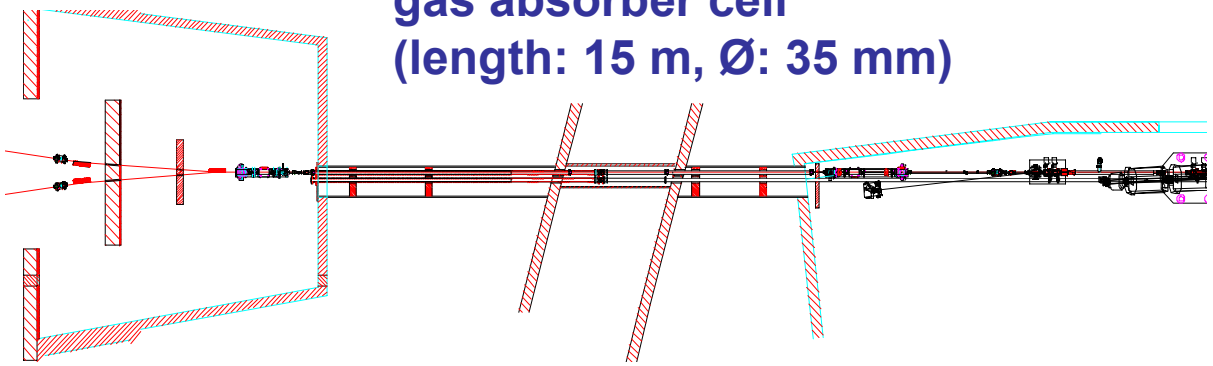

FEL hall PETRA tunnel LINAC tunnel

TTF1 results: Spectra of single FEL pulses

short pulse
(~100 fs)

long pulse
(~200 fs)

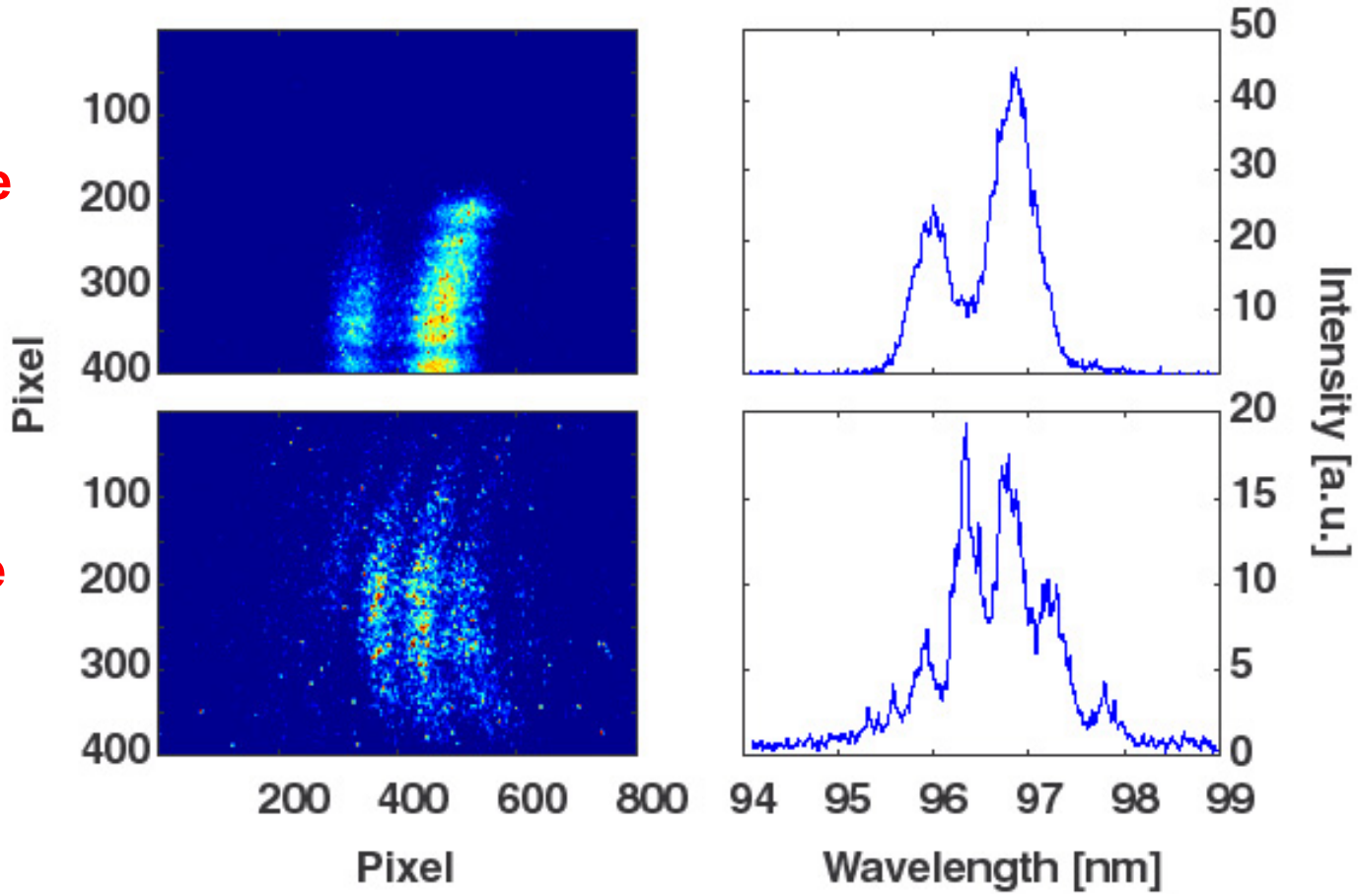

Radiation pulse length τ_{rad}:

$\tau_{rad} \cong 2\pi^{1/2}/(\Delta\omega)_{FWHM}$

Experimental pulse spectra of Phase 1

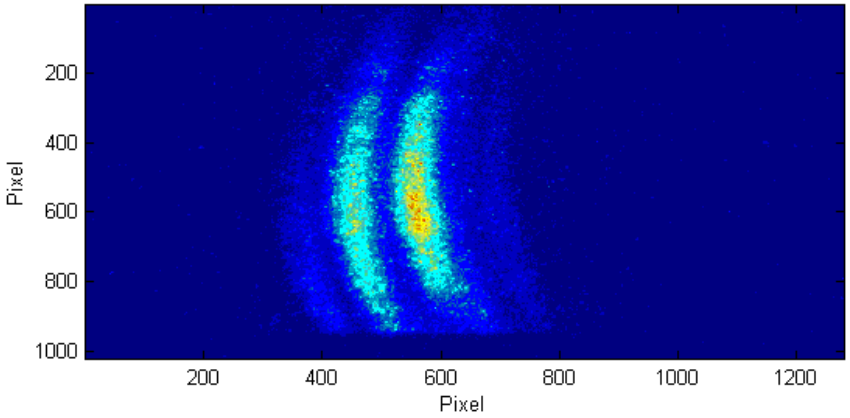

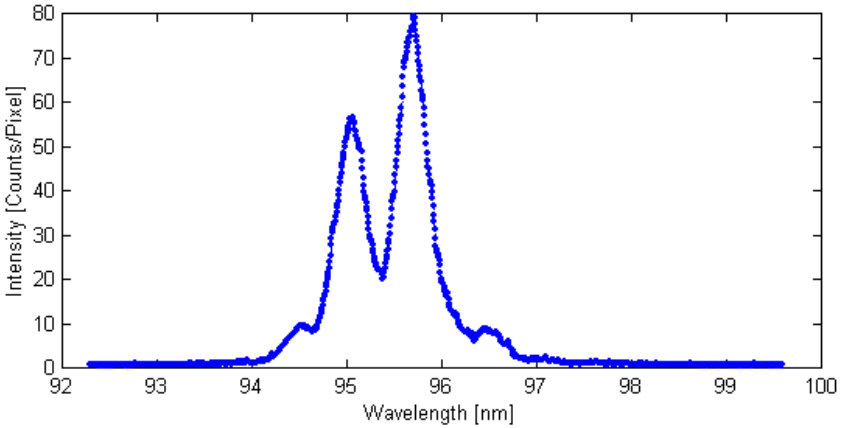

1 m normal incidence monochromator + intensified CCD

each pulse is different → **need online diagnostics with single shot resolution**

Online spectrometer for single pulses

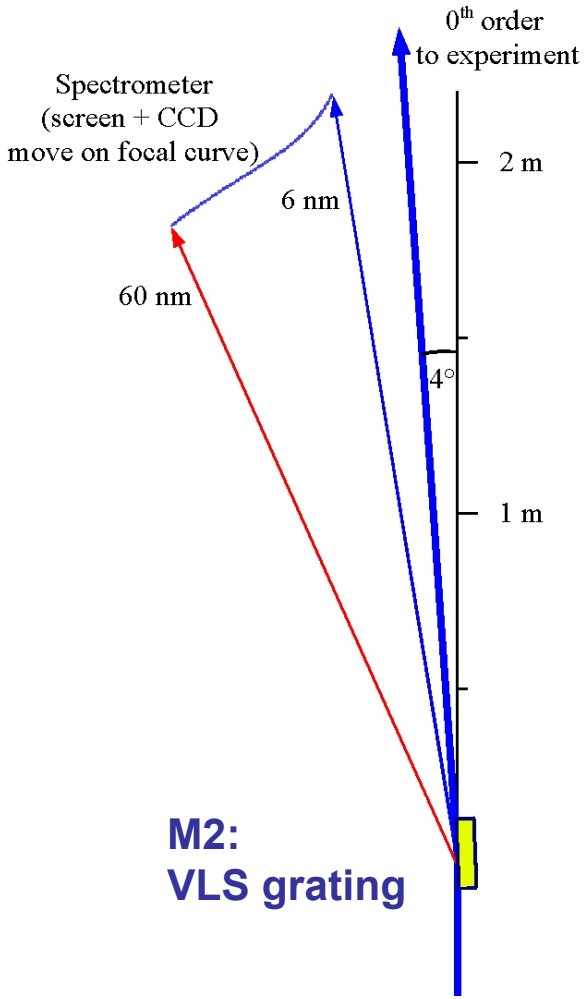

resolving power 1200 lines/mm

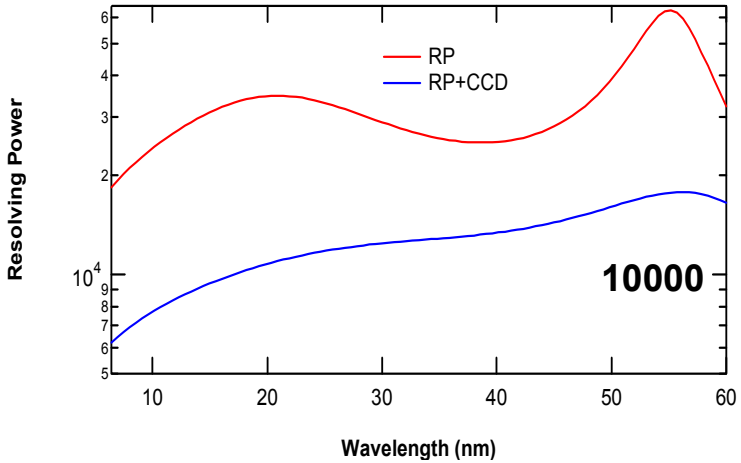

collaboration with:
R. Reininger (SAS),
F. Quinn (CLRC) et al.

grating efficiency

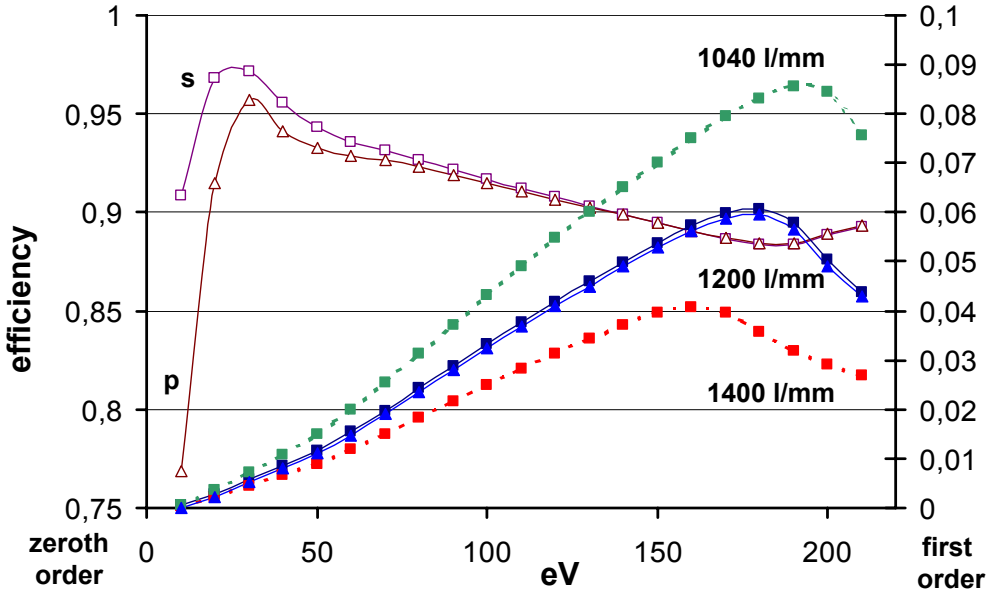

High resolution monochromator beamline

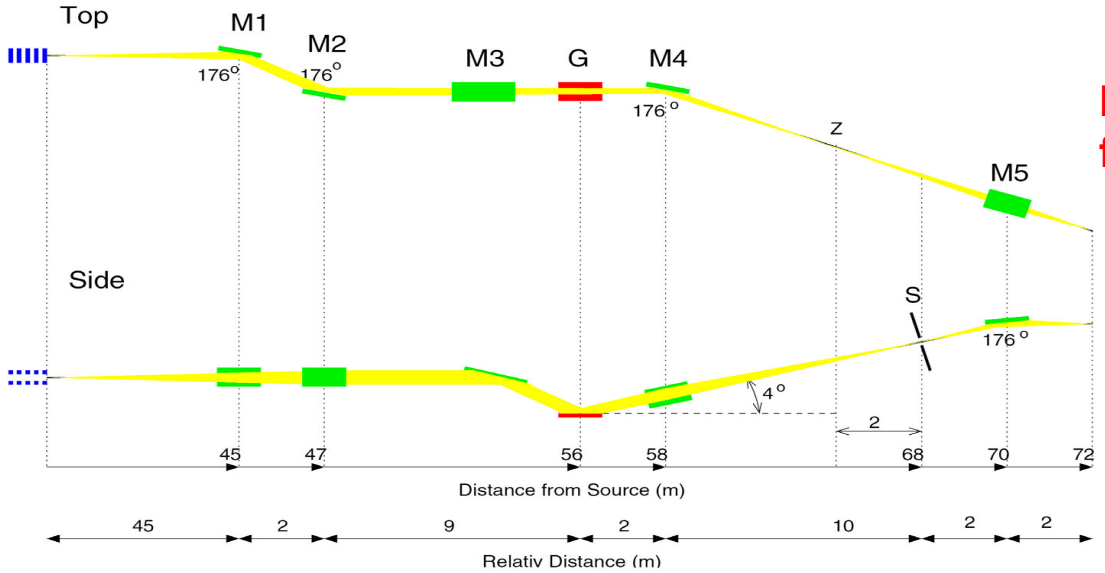

M. Martins et al., funded by BMBF

resolving power 1200 lines/mm

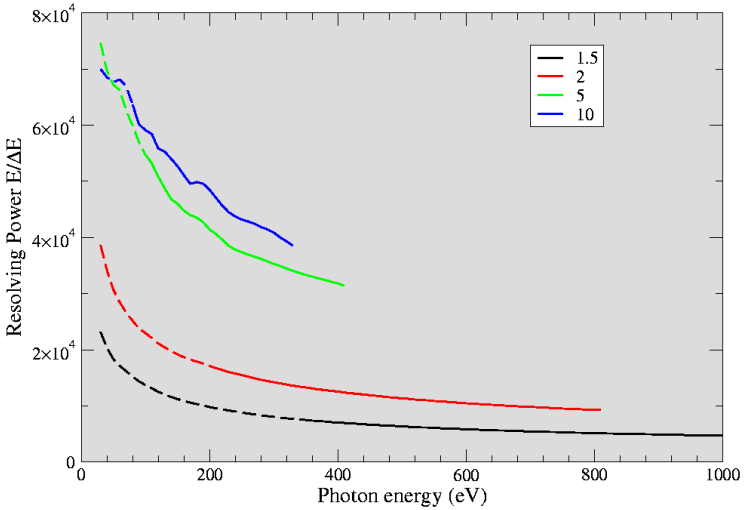

transmission 300 lines/mm

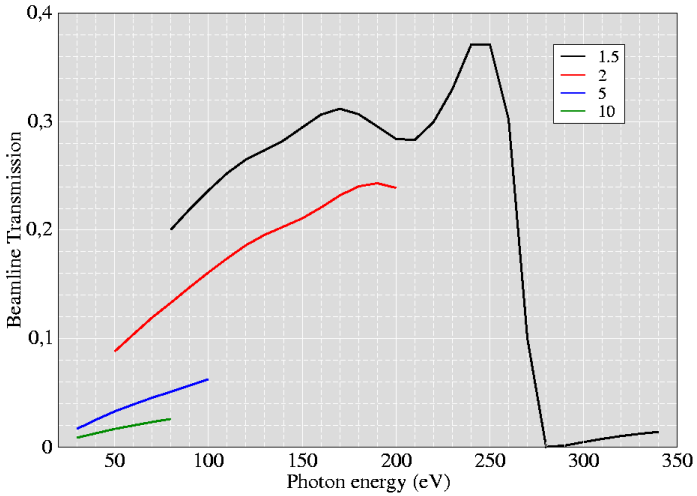

Two-undulator seeding

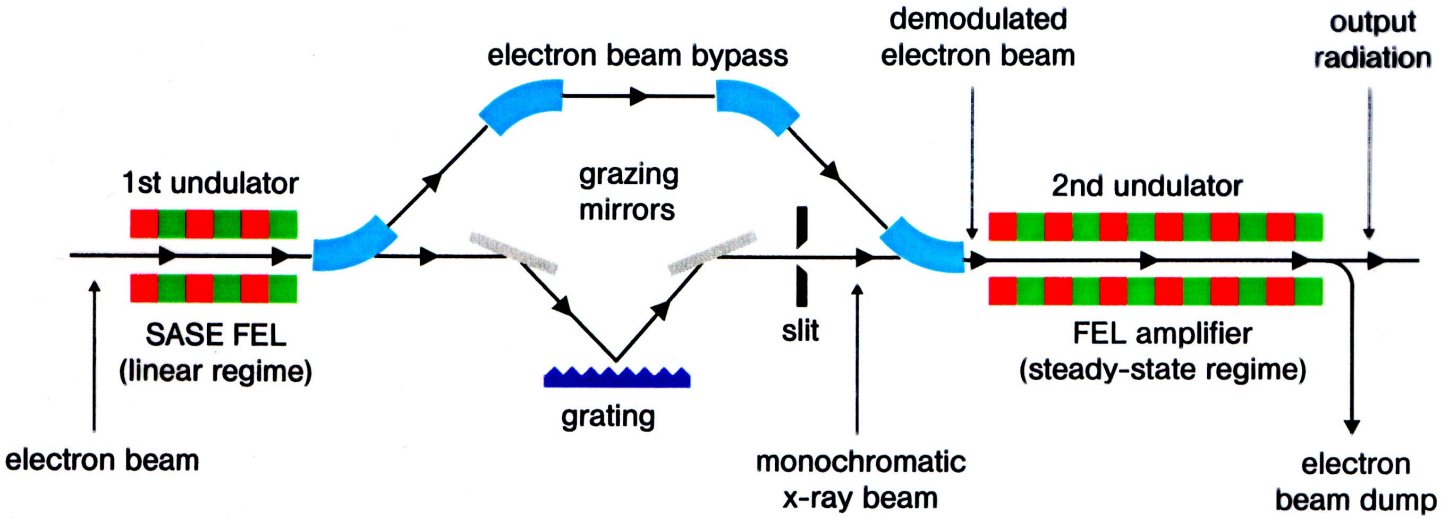

Spectrum before - after seeding

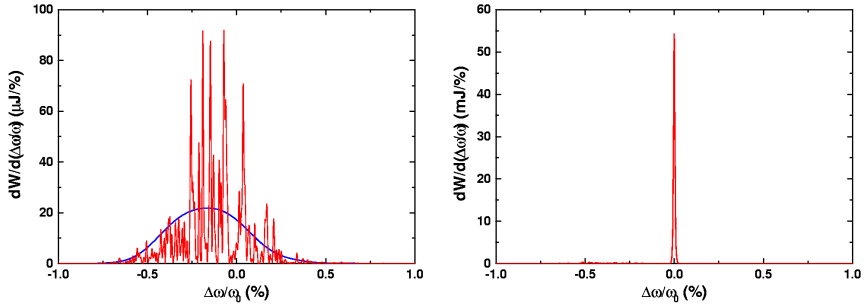

funded by the Hermann von Helmholtz-Gemeinschaft of German Research Centers (HGF), in collaboration with GKSS, Geesthacht, and ISA, Arhus

TTF1 results: Transverse coherence

Diffraction pattern at 95nm observed on a Ce:YAG crystal 3m behind the slits (near zone)

parallel slits
each 2mm long
200µm wide
separation 1mm

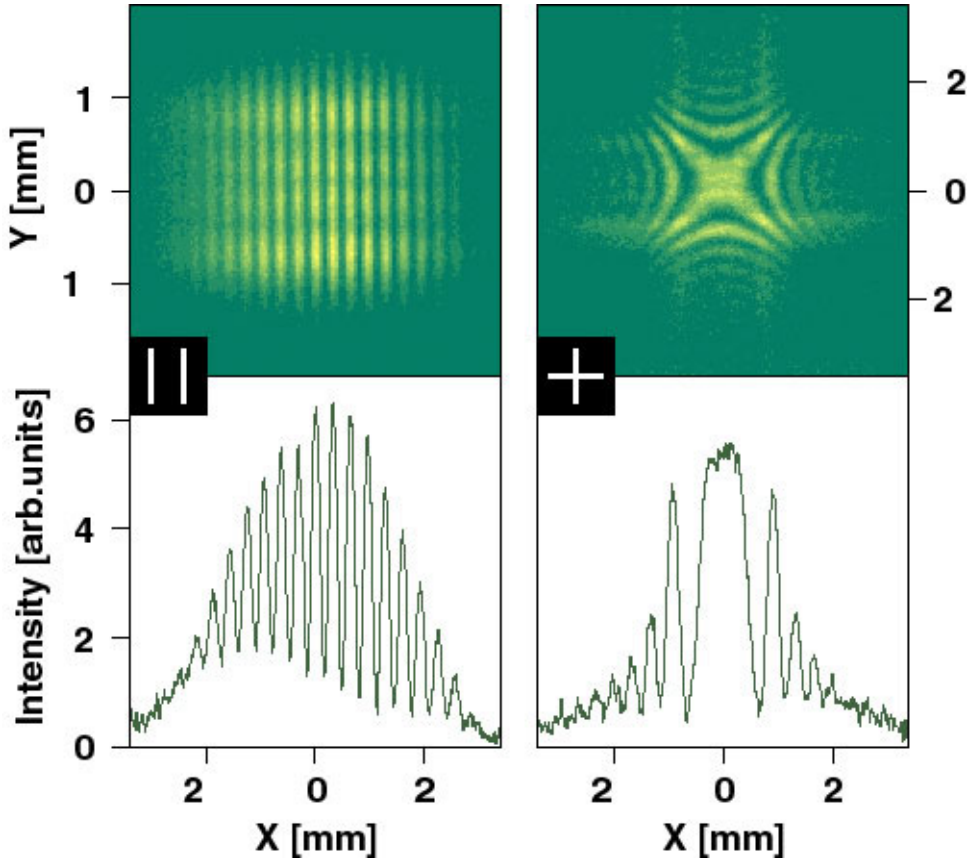

crossed slits
100µm wide
4mm long

TTF1 results: Coherence

Diffraction from a 5 mm aperture

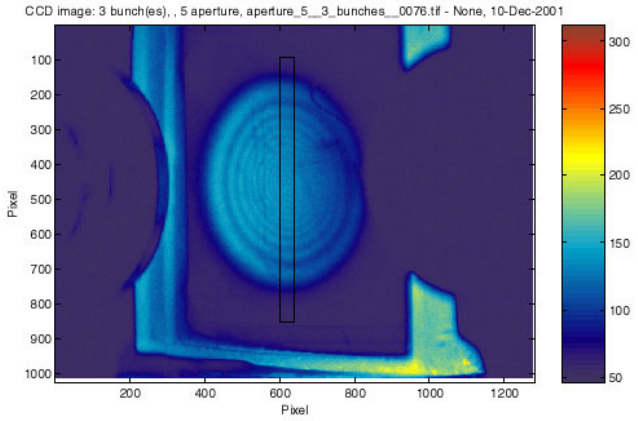

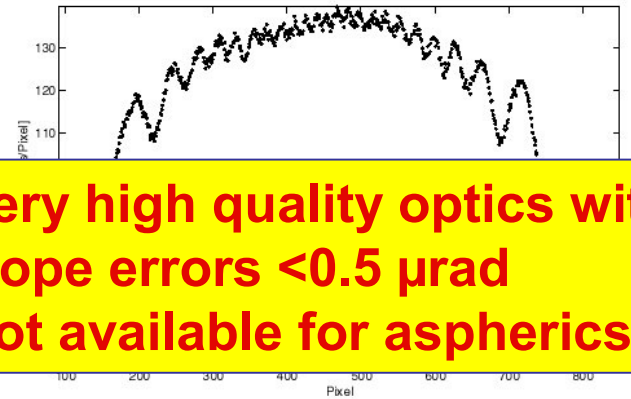

Very high quality optics with slope errors <0.5 µrad
Not available for aspherics!

Damage of C coatings

R. Sobierajski et al., IFPAN, DESY, GKSS

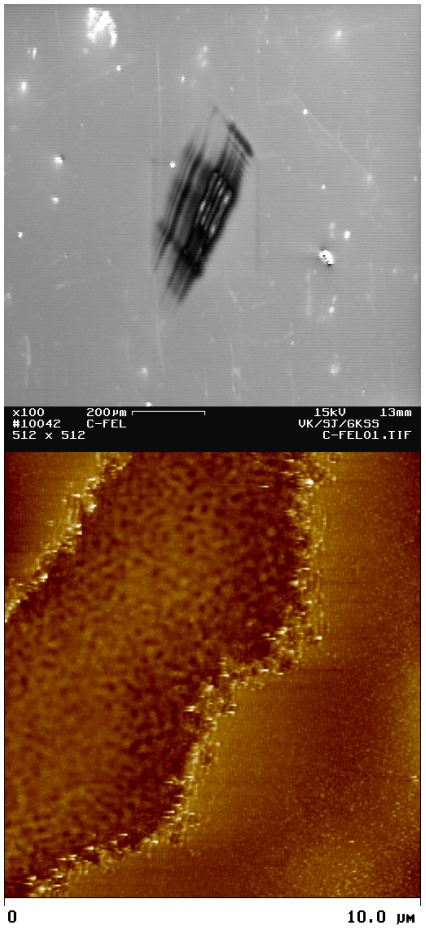

SEM

AFM

Pump-probe facility
with sub-picosecond time resolution
combining a high-power optical laser and a VUV FEL

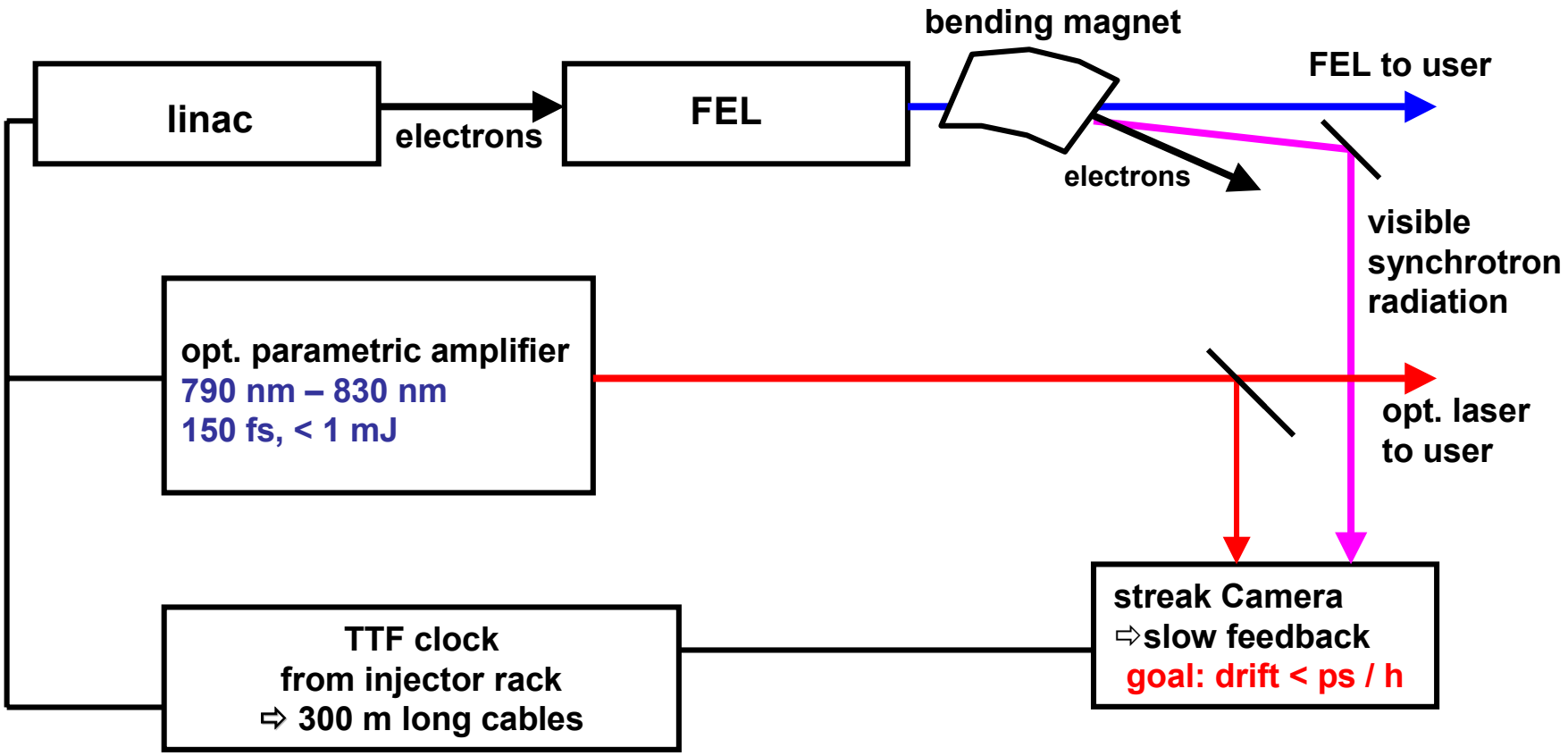

Goal:
Synchronization with FEL ⇨ 200 fs

- HASYLAB/DESY (Coordinator)
- Research Centre Jülich / BESSY
- Max-Born-Institute, Berlin
- Dublin City University
- CNRS / LURE
- Lund Laser Centre / MAX-Lab

Funded by the 5th Framework Programme of the European Commission

Measurement of exact timing

- Photocathode laser and pump-probe laser independently synchronised with the RF master oscillator of the accelerator
- Accuracy of the electronic synchronisation probably limited to ~100 fs ?
- Phase jitter of the accelerator RF causes up to 0.1% energy jitter o the electron bunches

timing jitter of ~1ps
due to energy dependent path lengths through the bunch compressors

Single-shot cross correlator
Proposal by M. Drescher

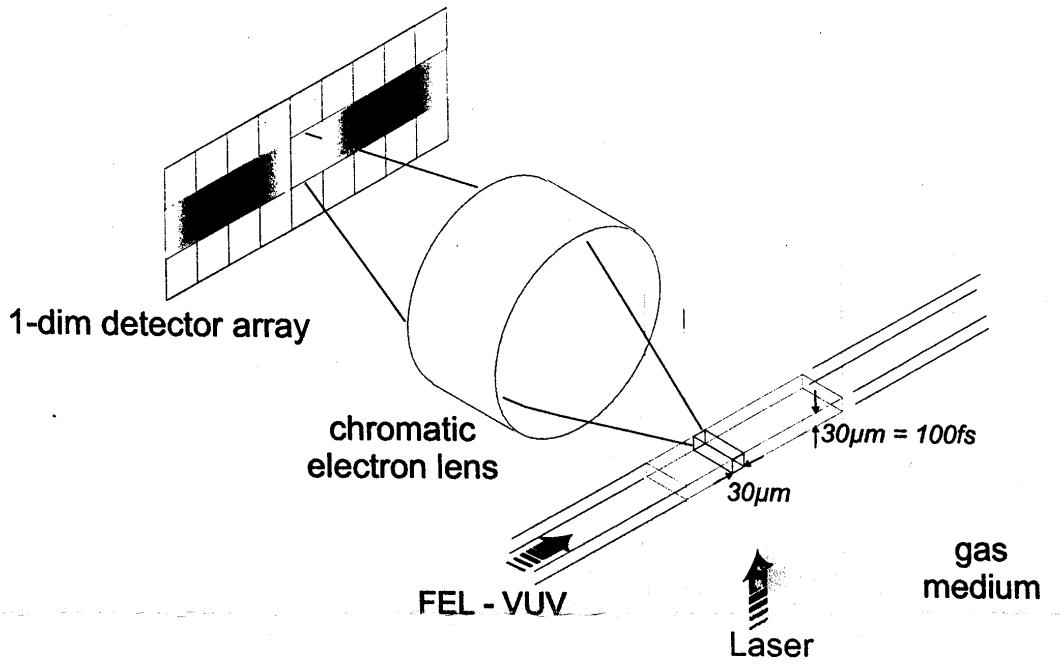

Conclusions

- **SASE FELs work as expected**

  Basic techniques for FEL beam distribution and diagnostics are available

- **First experiments demonstrate the enormous power of the FEL beam and the scientific potential**

  it is important to get started with user experiments in order to trigger

  - **machine and source development**
  - **experimental and diagnostics developments**
  - **new scientific applications**

  ⇒ VUV FEL User Facility at DESY , end of 2004

University of
L'Aquila

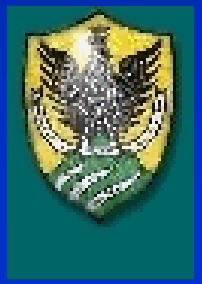

Tabletop soft x-ray laser systems: characterization and applications

Department of Physics
Laser X laboratory

A. Ritucci

Varenna 2003

Research group and cooperations

G.Tomassetti, A.Ritucci, A.Reale, L.Palladino, L.Reale
Phys. Dept. Univ. of L'Aquila, gc LNGS of INFN, INFM, Italy

F.Flora, L.Mezi,
ENEA Dip. Innov., Div. Fisica Applicata, C R E Frascati, Italy

S.V.Kukhlevsky,
Department of Experimental Physics, University of Pécs, Hungary

A.Faenov, T.Pikuz
MISDC of VNIIFTRI, Mendeleevo, Russia

J.Kaiser
Institute of Phys. Eng., Brno Univ. of Technology, Czech Republic

Outline

Generalities

- Soft x-ray lasers: general scheme of operation
- Laser pumped plasma schemes and capillary discharges

Capillary discharge laser (in L'Aquila)

- Demonstration of lasing at 46.9nm
- Laser beam characterization and optimization
- Applications

SXLs as powerful soft x-ray sources

Lasers at λ<50nm by single pass amplification in high density (10^{18}-10^{20}cm^{-3}) and temperature plasmas (50-500eV)

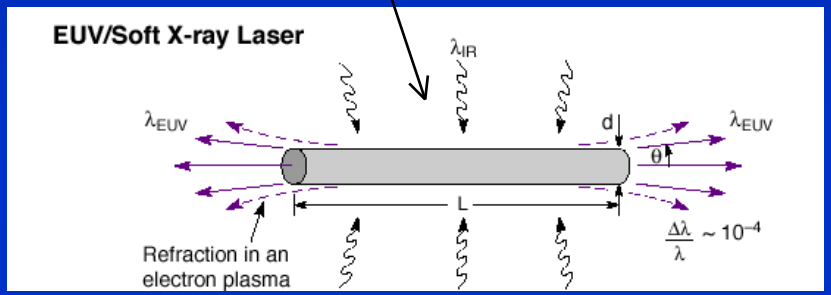

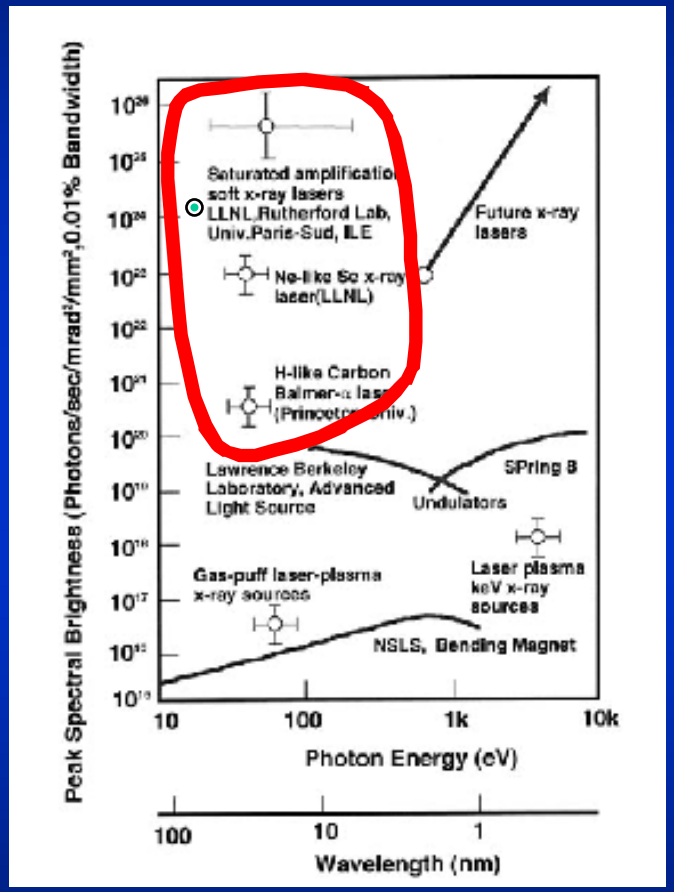

What to improve:

- **Efficiency of pumping schemes**
- **Compactness of experimental devices**
- **Repetition rate**

Varenna 2003

Pumping by Collitional Excitation

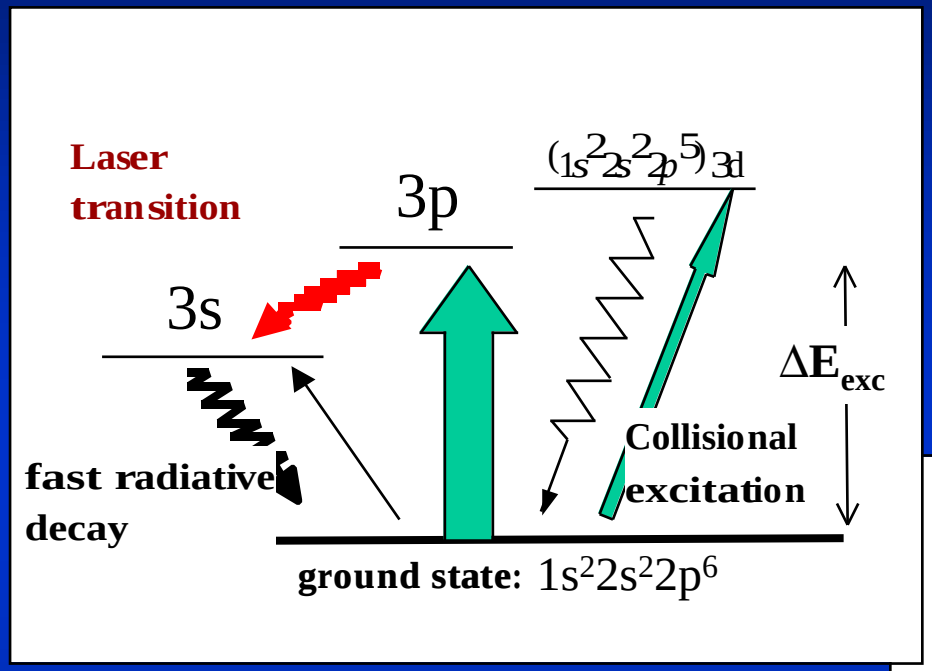

Lasing transitions ground state

3p-3s of Ne-like ions $(2p^6)$

4d-4p of Ni-like ions $(3d^{10})$

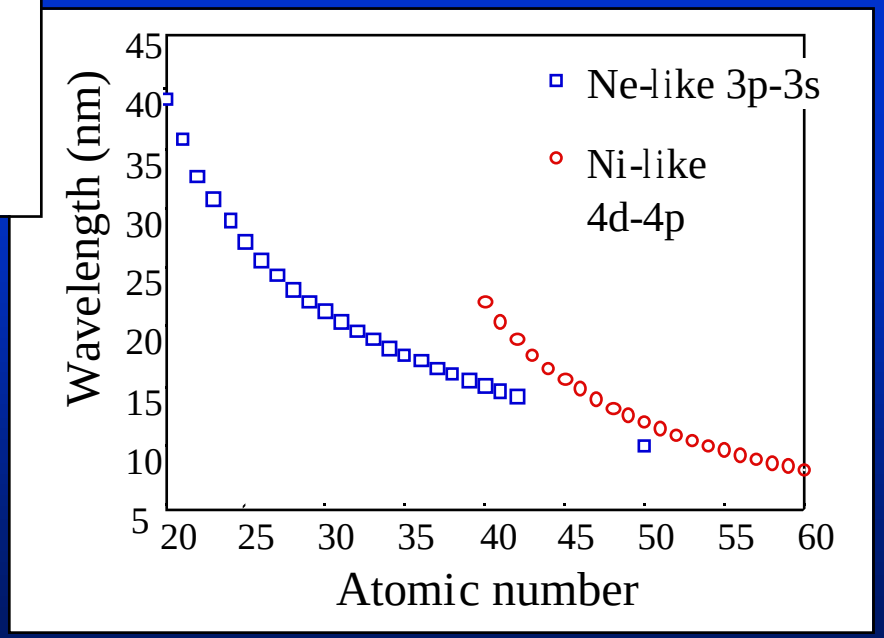

Varenna 2003

Laser pumping techniques

QSS regime:

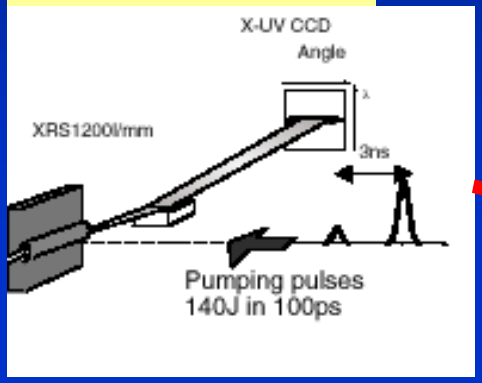

Scaling of the pumping energy

TCE regime:

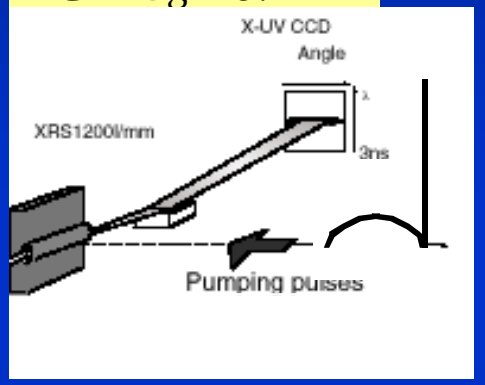

Single pulse $E_1 \approx$ **100–1000 J**, $\Delta T_1 \approx$ **1ns**

Repetition rate: 1shot/20min
output energy: few mJ

Prepulse $E_1 \approx$ **1–5 J**, $\Delta T_1 \approx$ **1ns** +
Main pulse $E_2 \approx$ **1–10 J**, $\Delta T_2 \approx$ **1 ps**

Repetition rate: 1shot/2min
output energy: 10 µJ

Scaling of the ouput x-ray energy

Capillary discharges

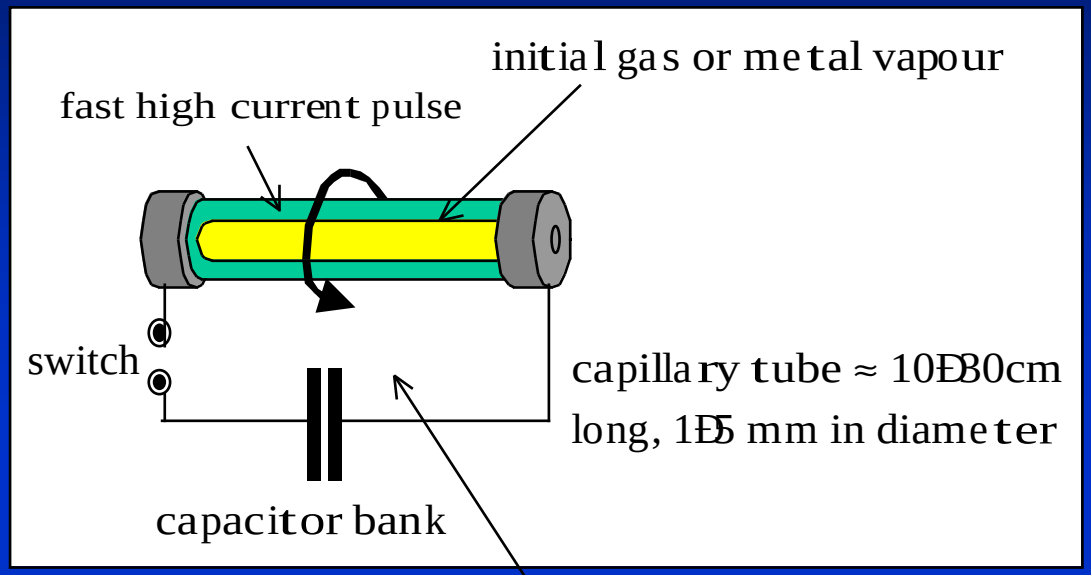

Z-pinch compression

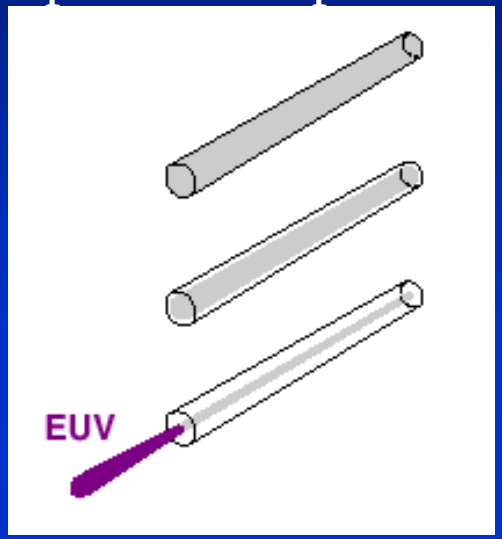

The z-pinch compression heats the plasma column to the desired temperature :

$$N_e \cdot T_e \approx \frac{\mu_0 I^2}{8\pi^2 r^2}$$

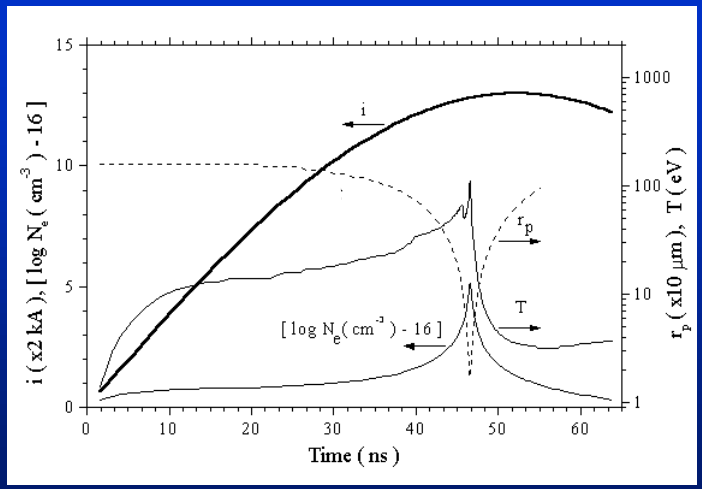

Varenna 2003

Capillary discharges

Positive elements

¥Possibility of generating plasma columns up to few tens of centimeters with ratio length/diameter>1000: **high quality soft x-ray laser beams**

¥Compact experimental devices

¥Pulse repetition rate of few Hz

Negative

¥Scaling to shorter wavelegth?

Rocca et al., Phys. Rev. Lett. 73 (1994) 2192

Benware, Phys. Rev. Lett. 81 (1998), 5804.

Our experimental device

200kV - 100J PULSE DRIVER

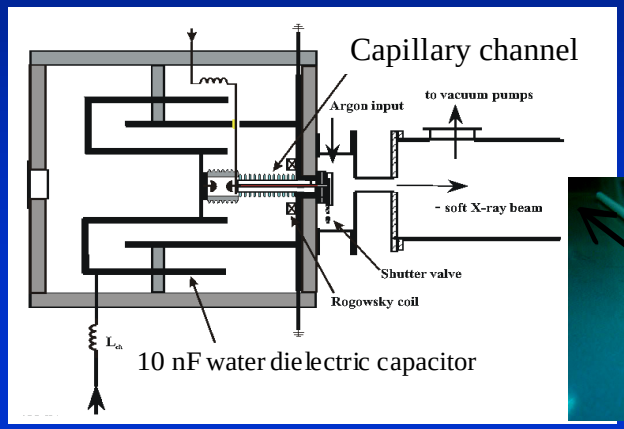

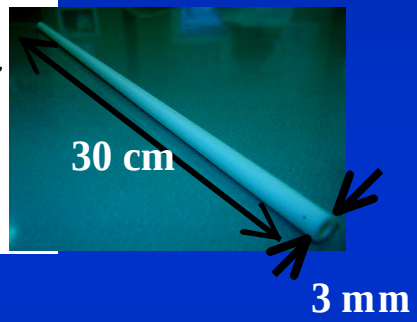

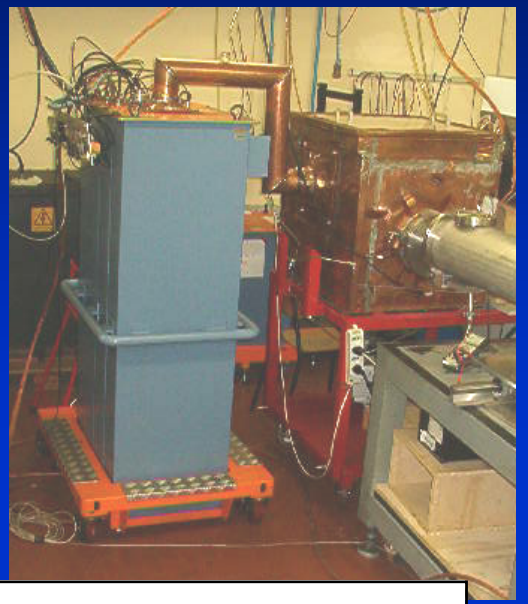

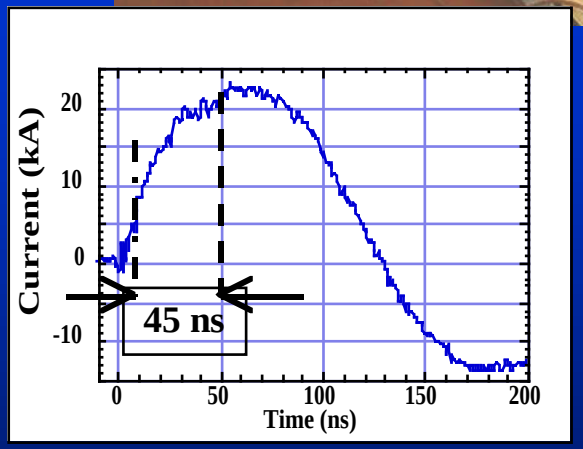

Alumina capillary channel:
D ≈ 3mm
L ≈ 10-45cm

10-20A preionization current +
a main discharge current pulse: 15-40kA
with half-cycle duration: 140-180ns

Varenna 2003

Identification of the 46.9nm laser line of Ne-like Ar

*** Tomassetti et al., Eur. J. D, 19, 73 (2002)**

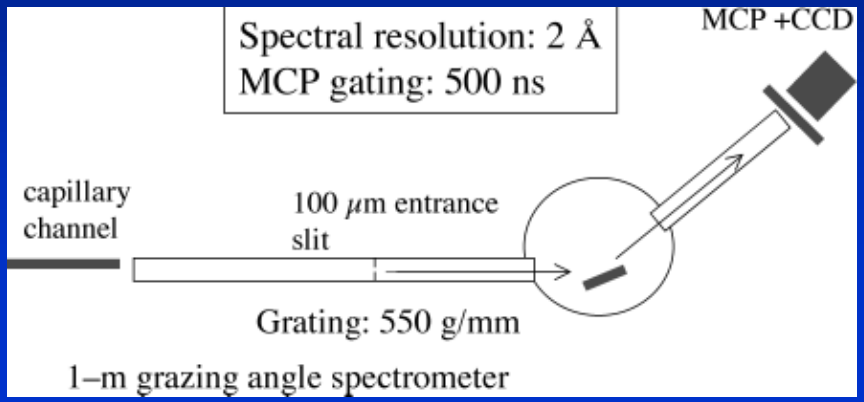

Initial Ar pressure: **0.25-0.5Torr**
Current = **17-30kA**
Preionization current **20A**
λ = **46.9nm**

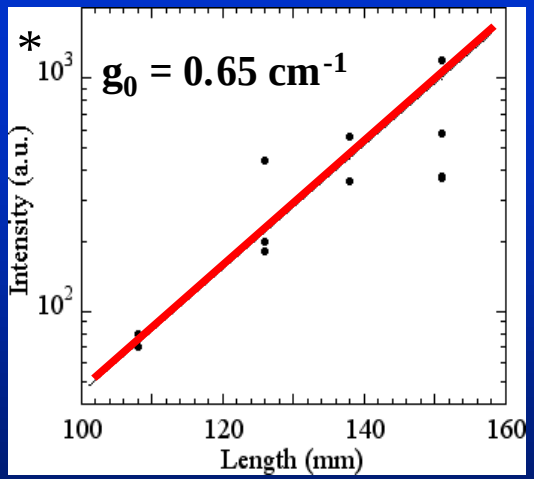

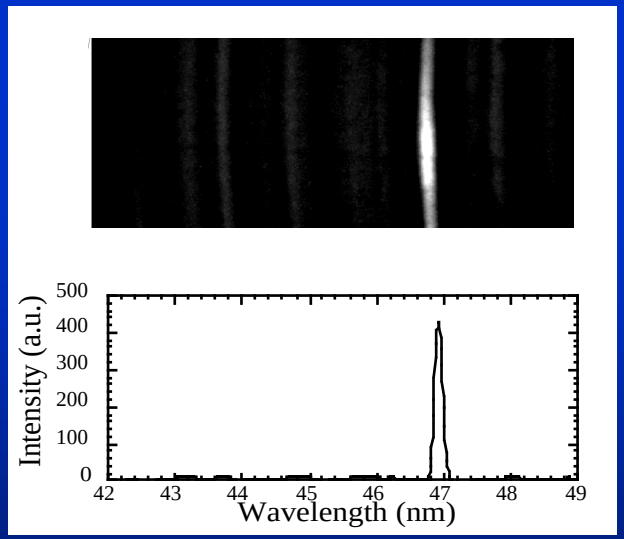

Varenna 2003

Pulse characteristics

*** Ritucci et al., Contrib. to Plasma Phys. 43, 88 (2003)**

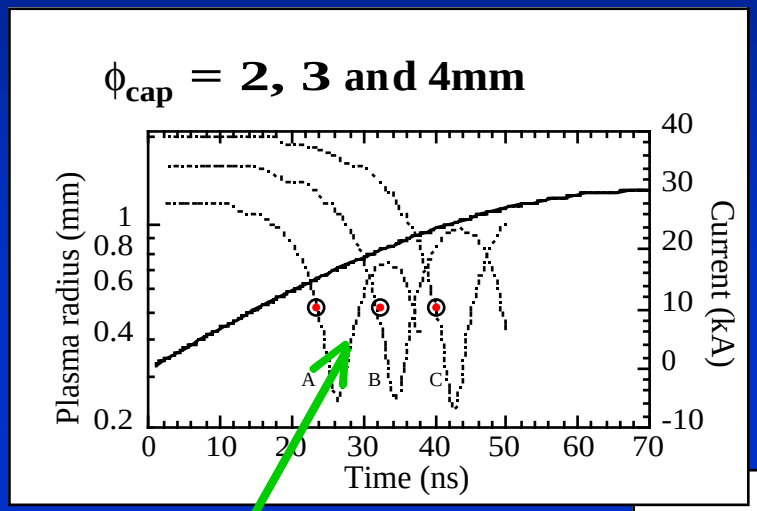

P = 0.45 Torr
Lcap = 16 cm
Current rise time ≈ 50 ns

Gain duration ≈ $t_{laser} \cdot (g\text{-}L)^{1/2} \sim$ 3ns

Lasing times during plasma compression

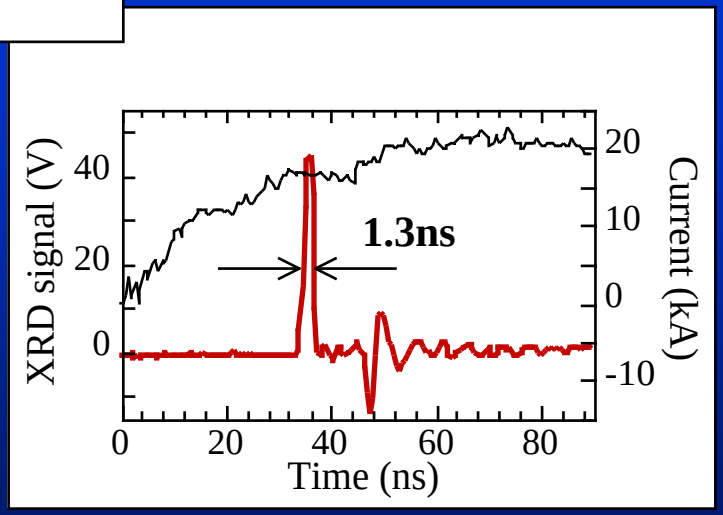

Varenna 2003

Saturated laser output

* Tomassetti et al., submitted for publication

Saturated operation:

Output intensity

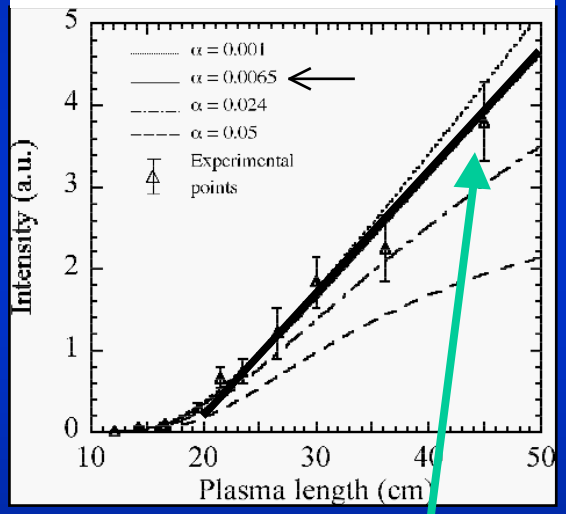

$I_{out} \longrightarrow 20 \times I_s$

$E_{out} \longrightarrow 300\mu J$

$P_{out} \longrightarrow 0.6MW$

Pulse stability

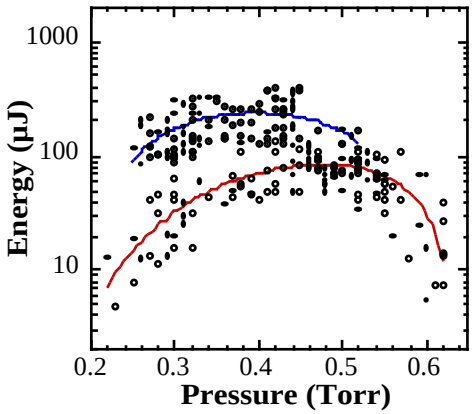

Repetition rate ~ 0.2Hz

Pulse duration

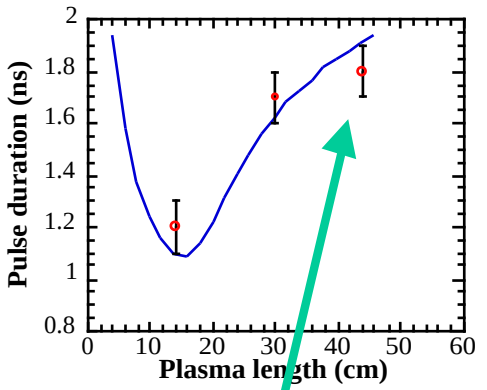

$t_{laser} \longrightarrow 1.7ns$

Varenna 2003

Soft x-ray laser coherence

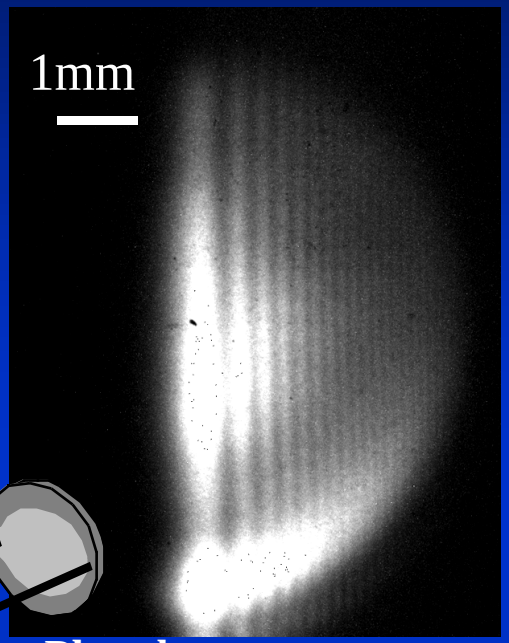

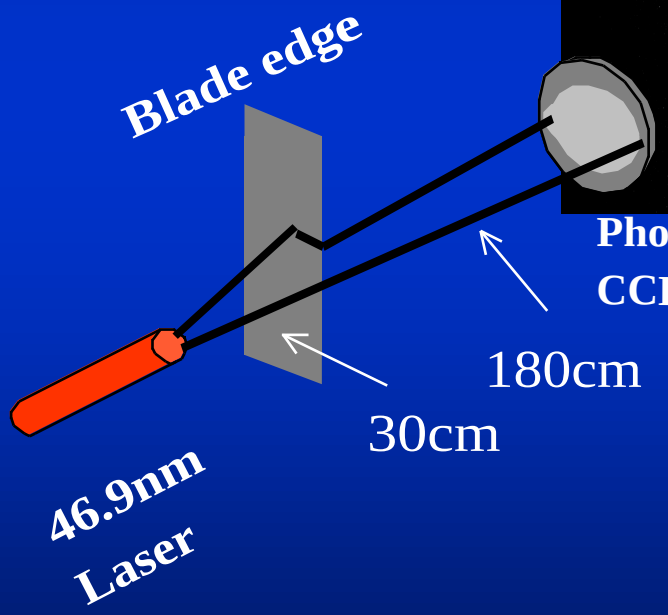

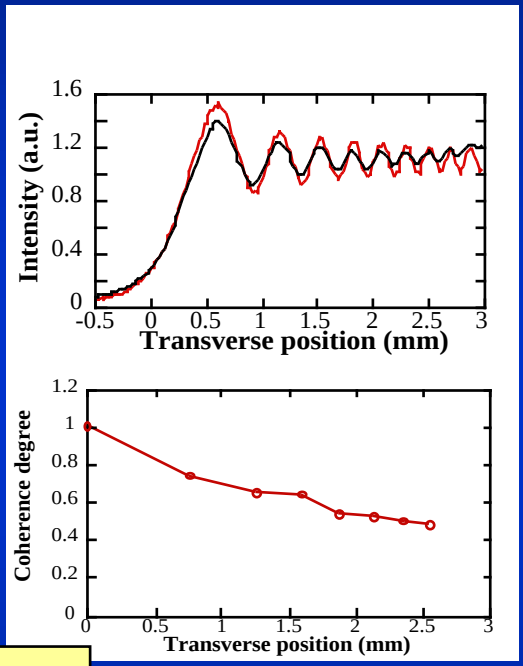

L_{Plasma} = 45cm
P= 0.4Torr
$L_{coherence}$ ≈ 3mm at 2m from capillary output

Varenna 2003

Laser beam intensity distribution

L≈ 45cm,
I = 20kA
HCD ≈ 150ns

Near field

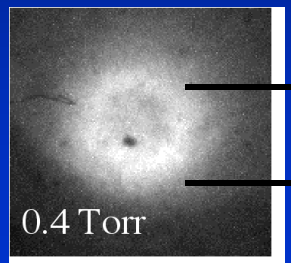

550µm

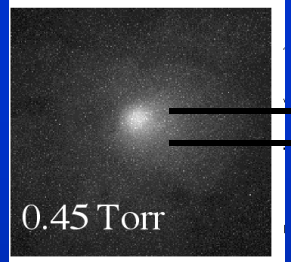

200µm

far field

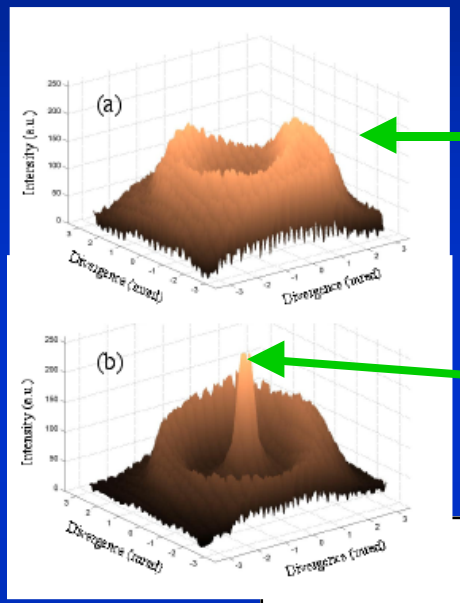

4.5mrad

0.6mrad

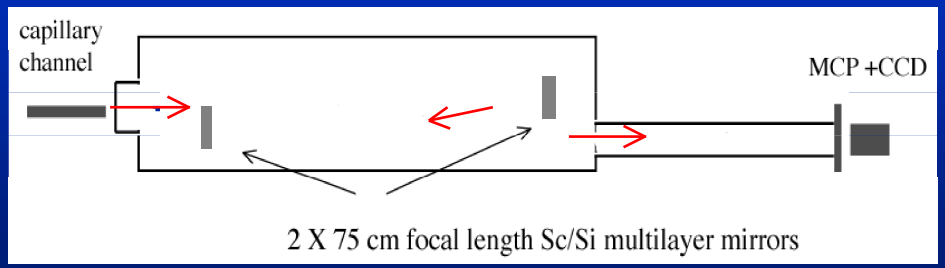

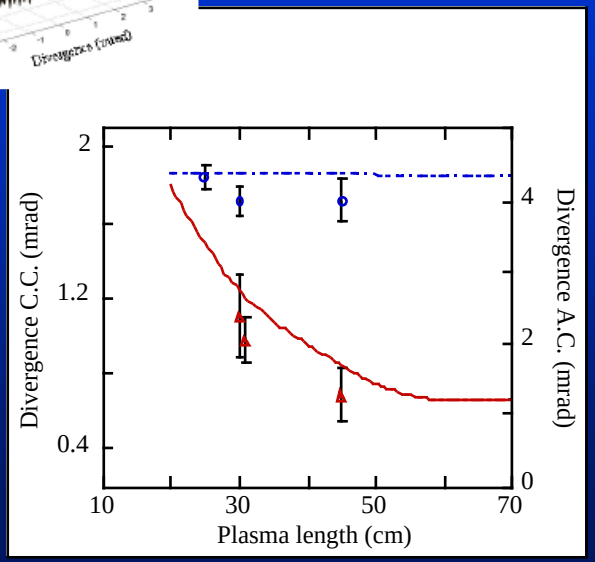

Varenna 2003

Laser amplification in a discharge plasma waveguide

*** Ritucci et al., Europhys. Lett., 63, 694 (2003)**

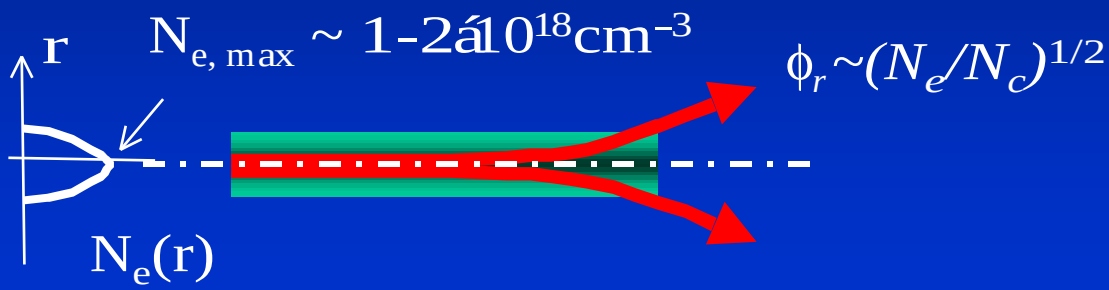

Refraction guided rays

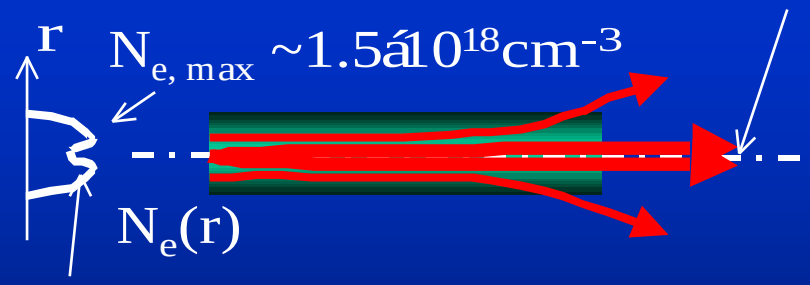

Depression: ΔN_e ~3á10^{17}cm^{-3}

Near field

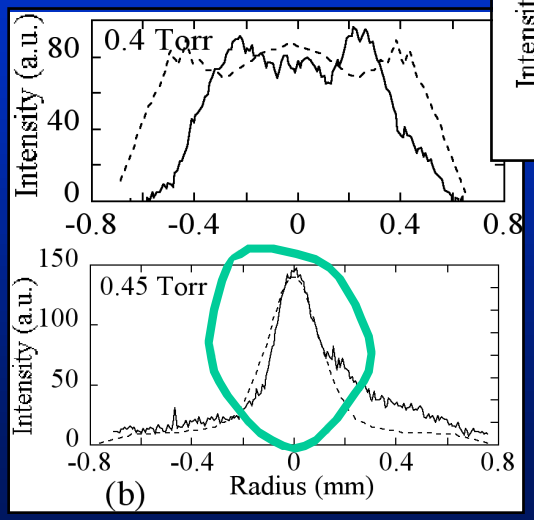

Far field

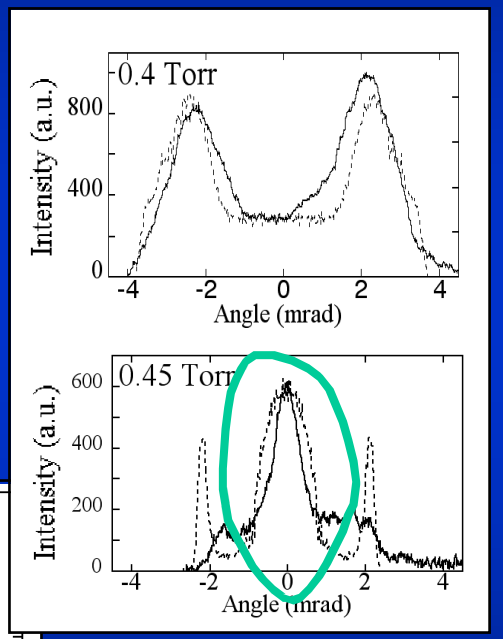

waveguiding

Varenna 2003

Application:
Color Center excitation on Lithium Fluoride films

ionizing radiation (electrons, x–rays, etc...)

Color Center (CCs) can be formed by XUV irradiation using bright source emission (CCs are very stable at room temperature)

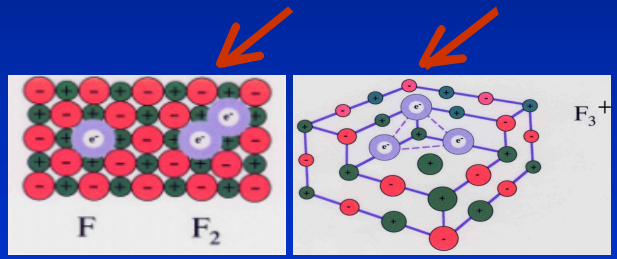

Fluorescence emission excited by blue ligth pumping

Blue ligth pumping :~ 450 nm

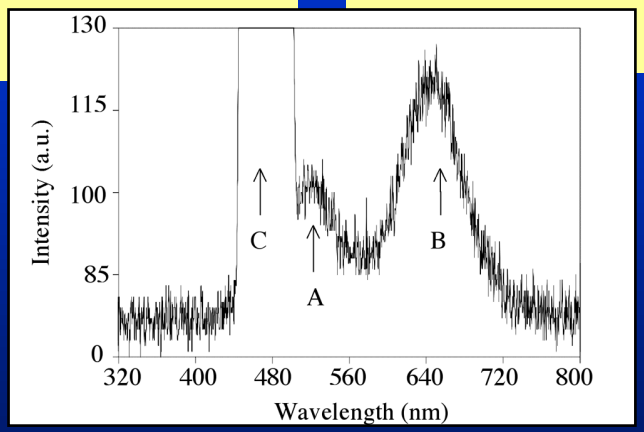

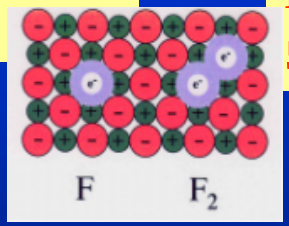

Ligth emission: 541, 678nm

Varenna 2003

*** R.M. Montereali et al., Appl. Phys. Lett., 78, 4082 (2001)**

High-spatial resolution imaging on LiF films

◊ **Minimum energy fluence required: 0.1mJ/cm^2;**

◊ **Dinamic range ≈ 1000; in the range 1mJ/cm^2- 1J/cm^2 the F center density is proportional to ~ K (D)$^{1/2}$;**

◊ **Efficiency of CCs production strongly increases with the dose rate.**

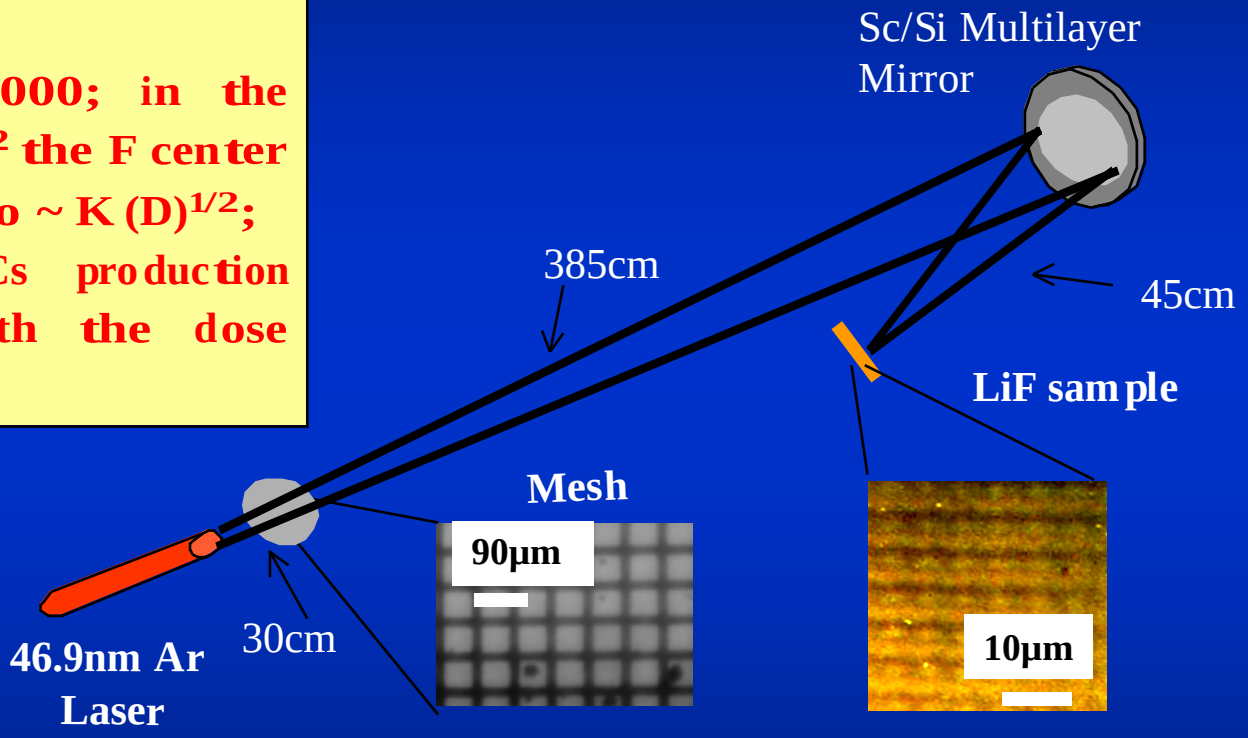

Printed pattern are observed by optical microscope in fluorescence mode;

The resolution is determined by the readout process (< 1 micron).

Varenna 2003

Laser beam imaging

*** Tomassetti et al., Europhys. Lett., 63, 681 (2003)**

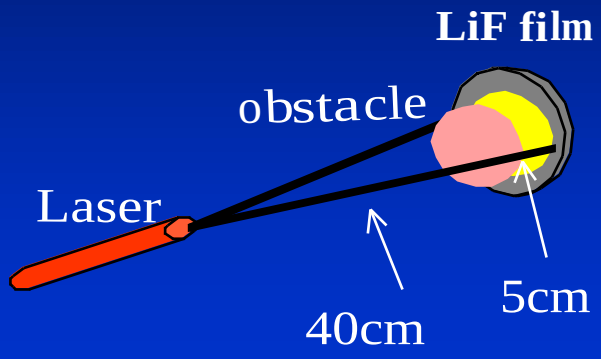

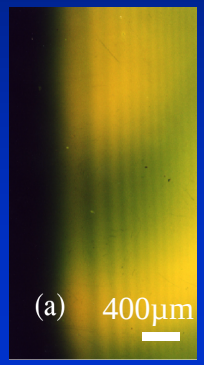

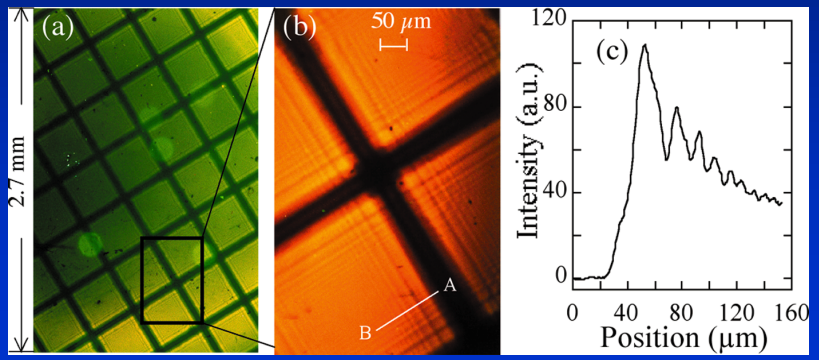

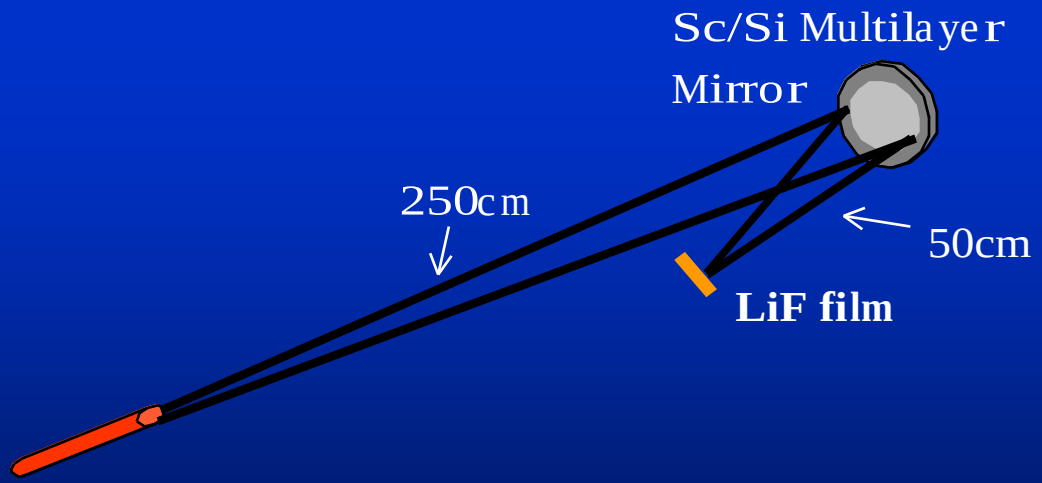

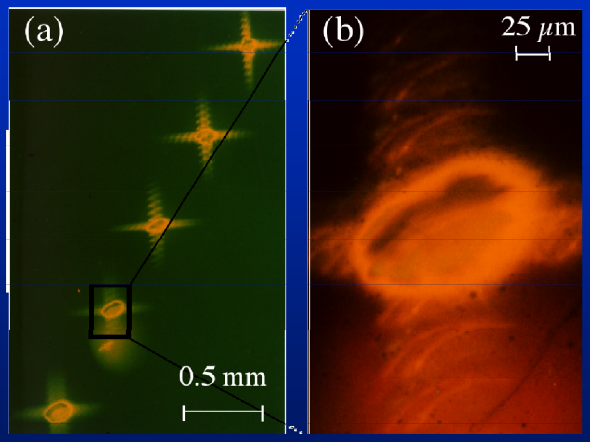

Varenna 2003

Soft x-ray laser focusing

f_L= 40cm Sc/Si mirror

46nm laser beam

Gold film thickness ≈30nm

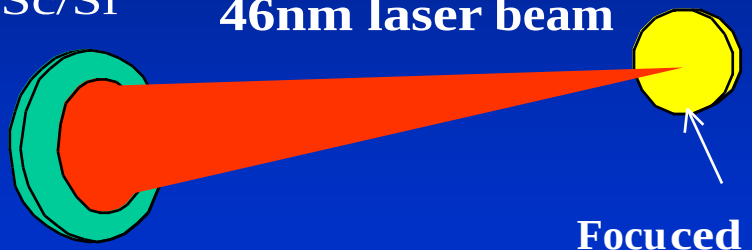

Focuced diameter: 30μm

Laser intensity 10^{10}W/cm^2

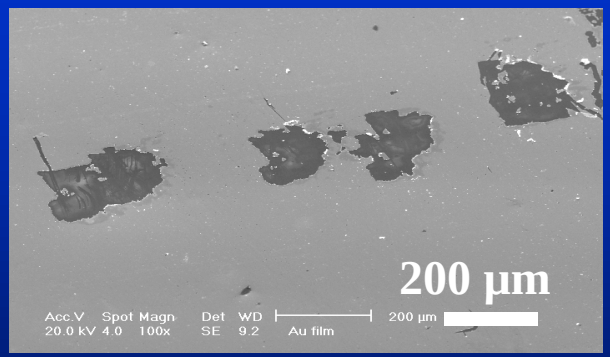

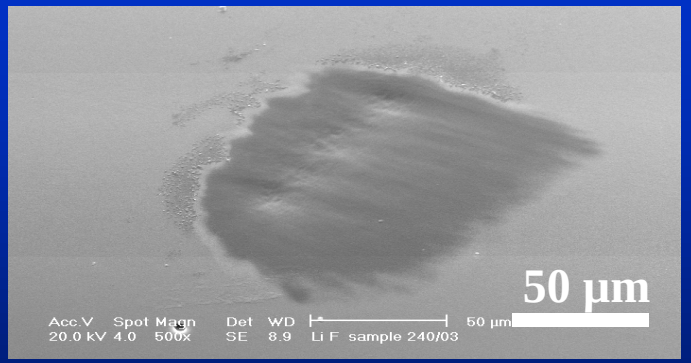

Perspectives

- Development of applications ($B_p \approx 10^{24}$ ph/s mm^2 mrad^2 in 0.01 % bw)
  - Surface science (this radiation is easily absorbed by surfaces on thickness of few nanometers): UV photoemission spectroscopy, UV photoemission spectroscopy, etcÉ;
  - Interferometry of high-density plasmas, soft x-ray holography;

- Use of capillary discharges for lasing at shorter wavelengths (use of Nitrogen, Kripton, etcÉ) ?

TECHNISCHE UNIVERSITÄT DARMSTADT

GSI

X-Ray and particle diagnostics for warm dense matter research

Markus Roth

International Conference on

ULTRASHORT HIGH-ENERGY RADIATION AND MATTER

Villa Monastero, Varenna, Italy

October 7 -10, 2003

PHELIX

TECHNISCHE UNIVERSITÄT DARMSTADT

Why warm dense matter?

GSI

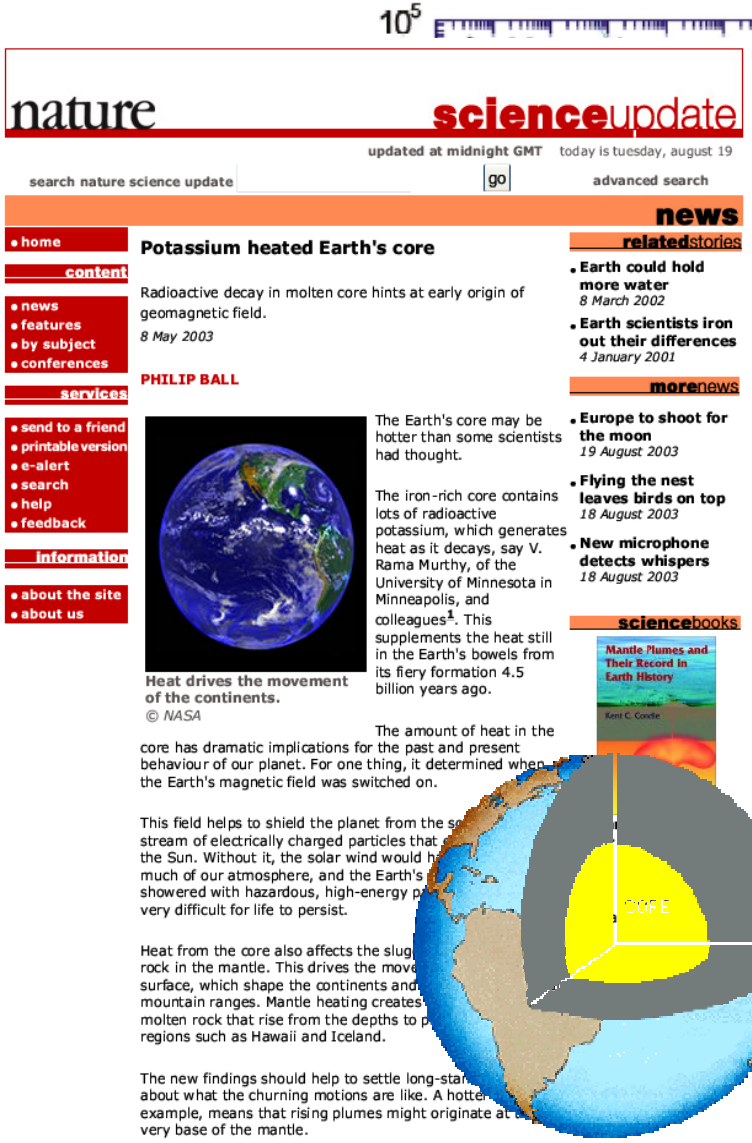

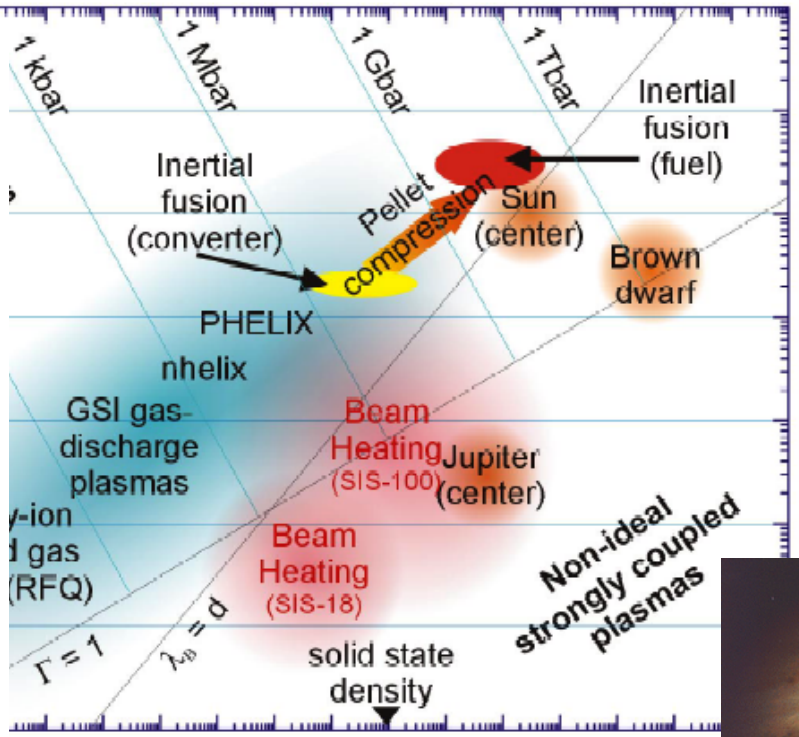

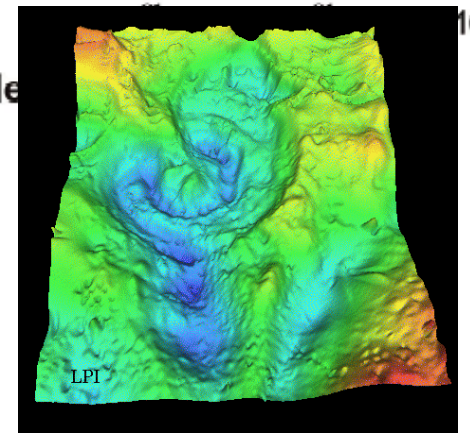

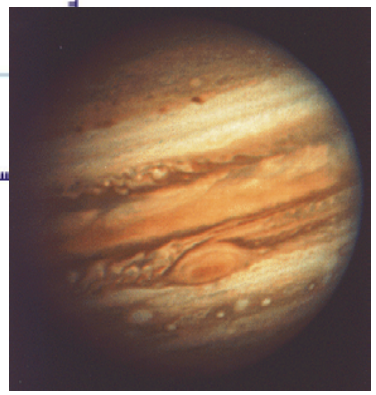

PHELIX

TECHNISCHE UNIVERSITÄT DARMSTADT

Why heavy ions?

GSI

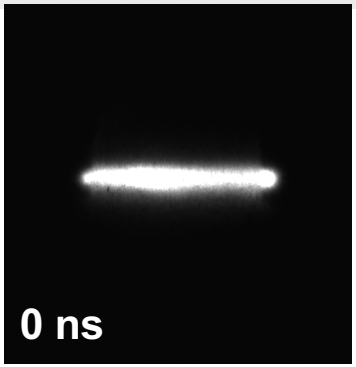

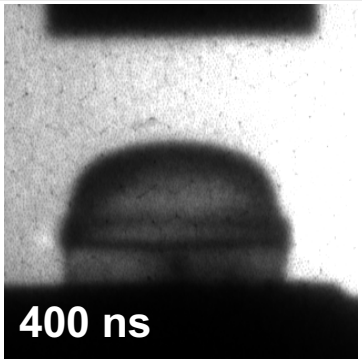

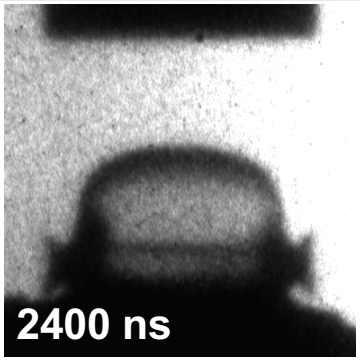

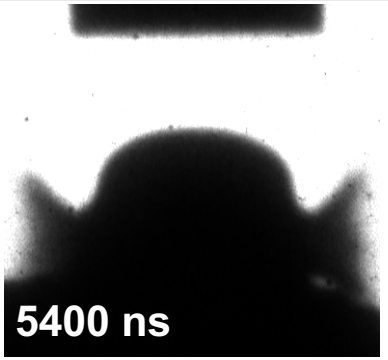

experiment: optical shadowgraphy

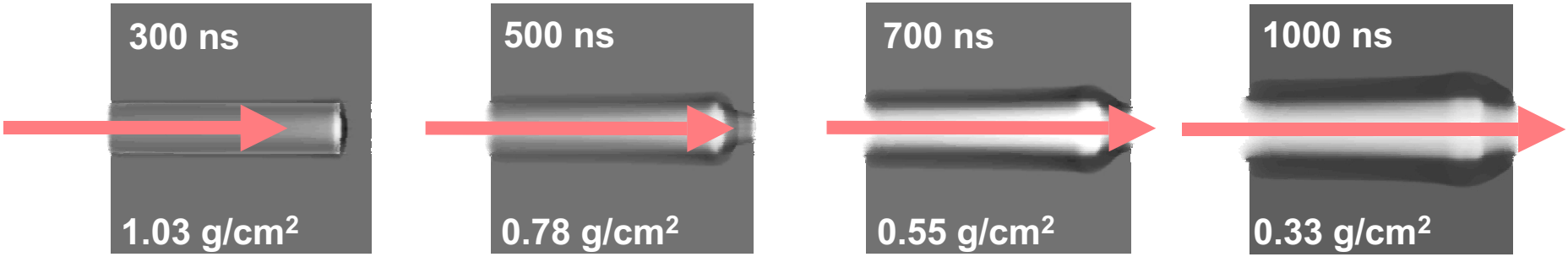

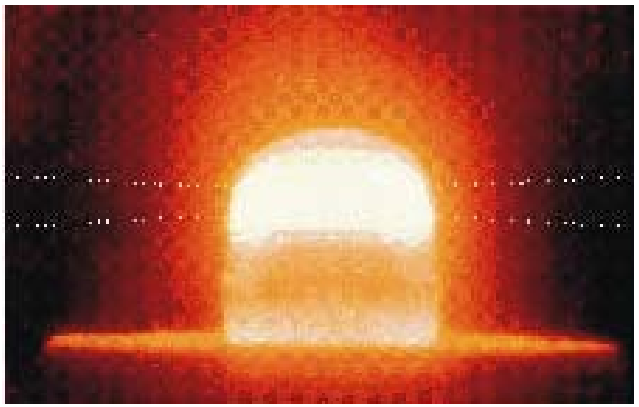

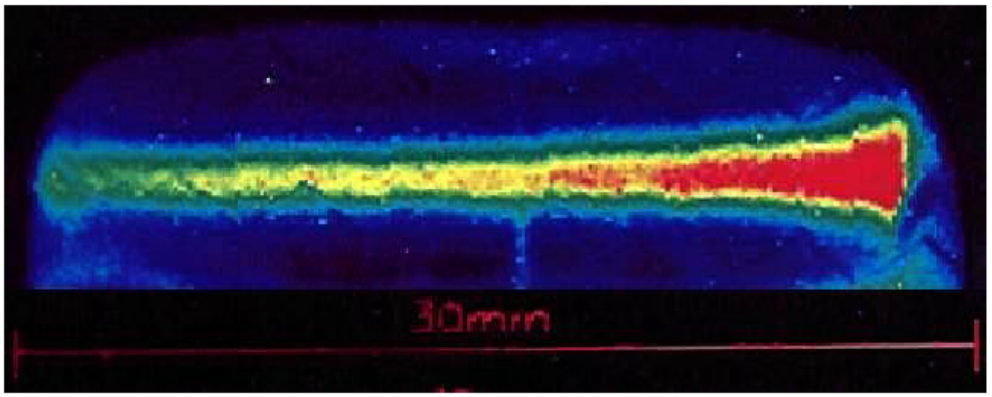

Time Resolved Energy Loss Spectrometry

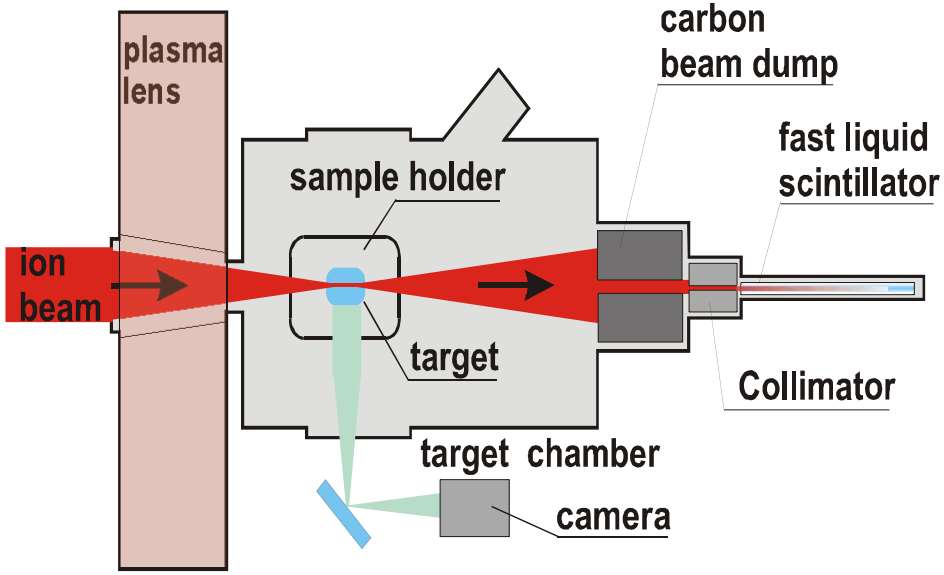

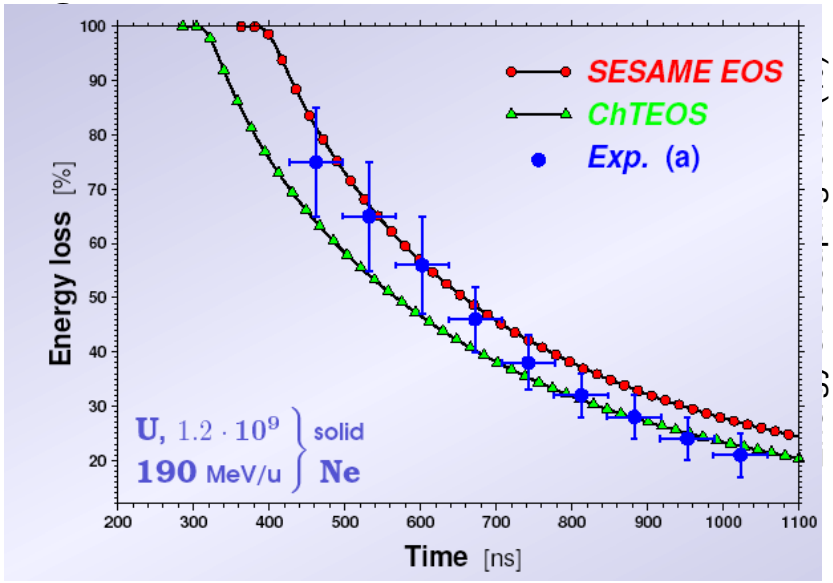

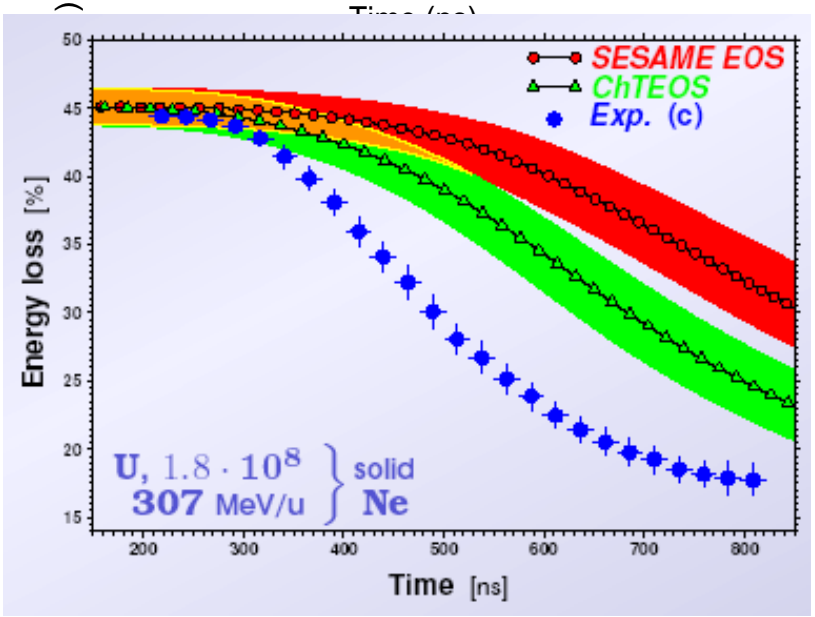

Transmitted beam ions can give important information on the state of matter in the target

D. Varentsov et al., Nucl. Instr. Meth. 2000 in print

TECHNISCHE UNIVERSITÄT DARMSTADT

Why heavy ions?

GSI

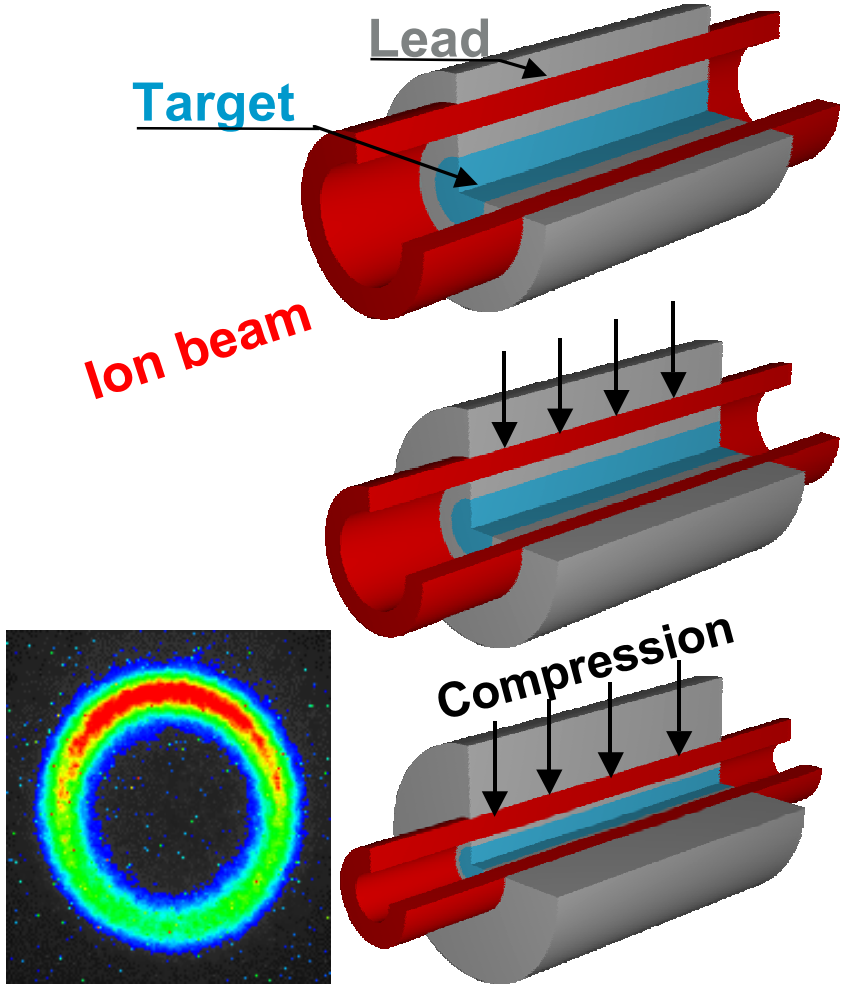

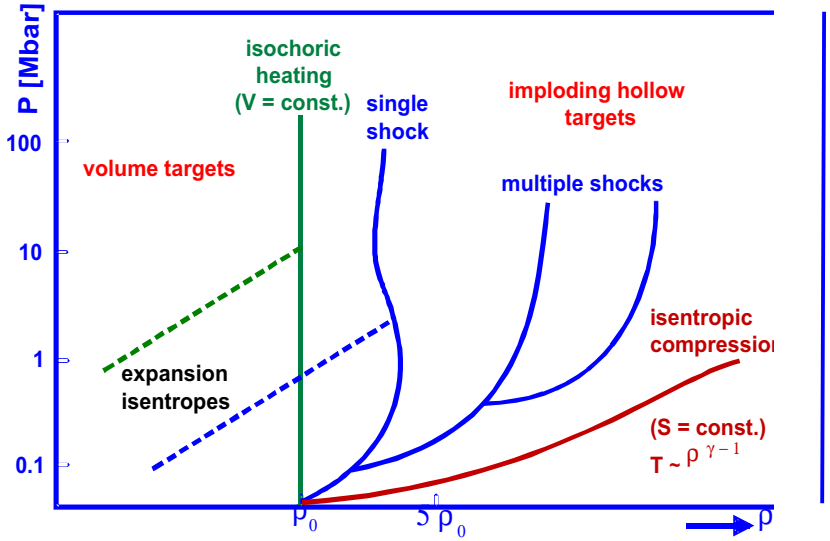

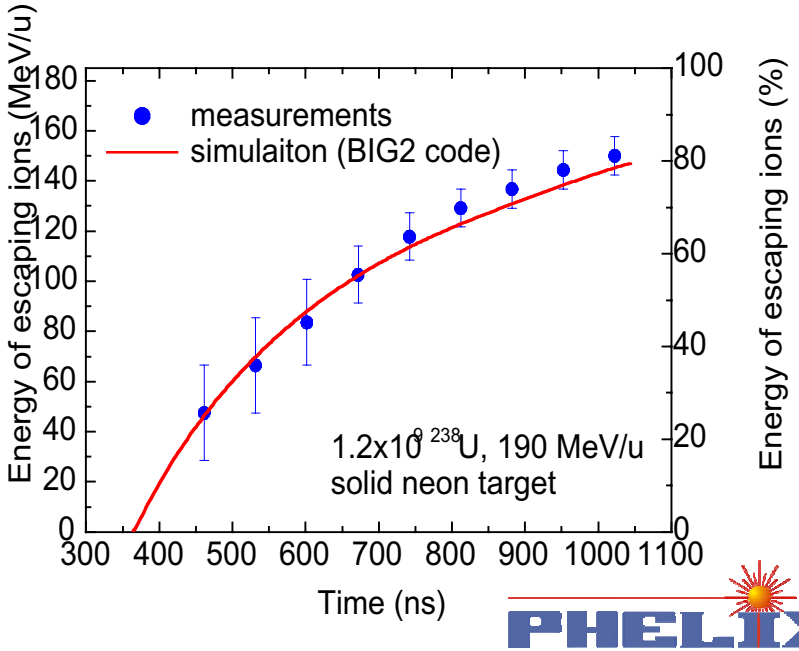

PHELIX

TECHNISCHE UNIVERSITÄT DARMSTADT

Warm dense matter research will take benefit of the upcoming SIS-200

GSI

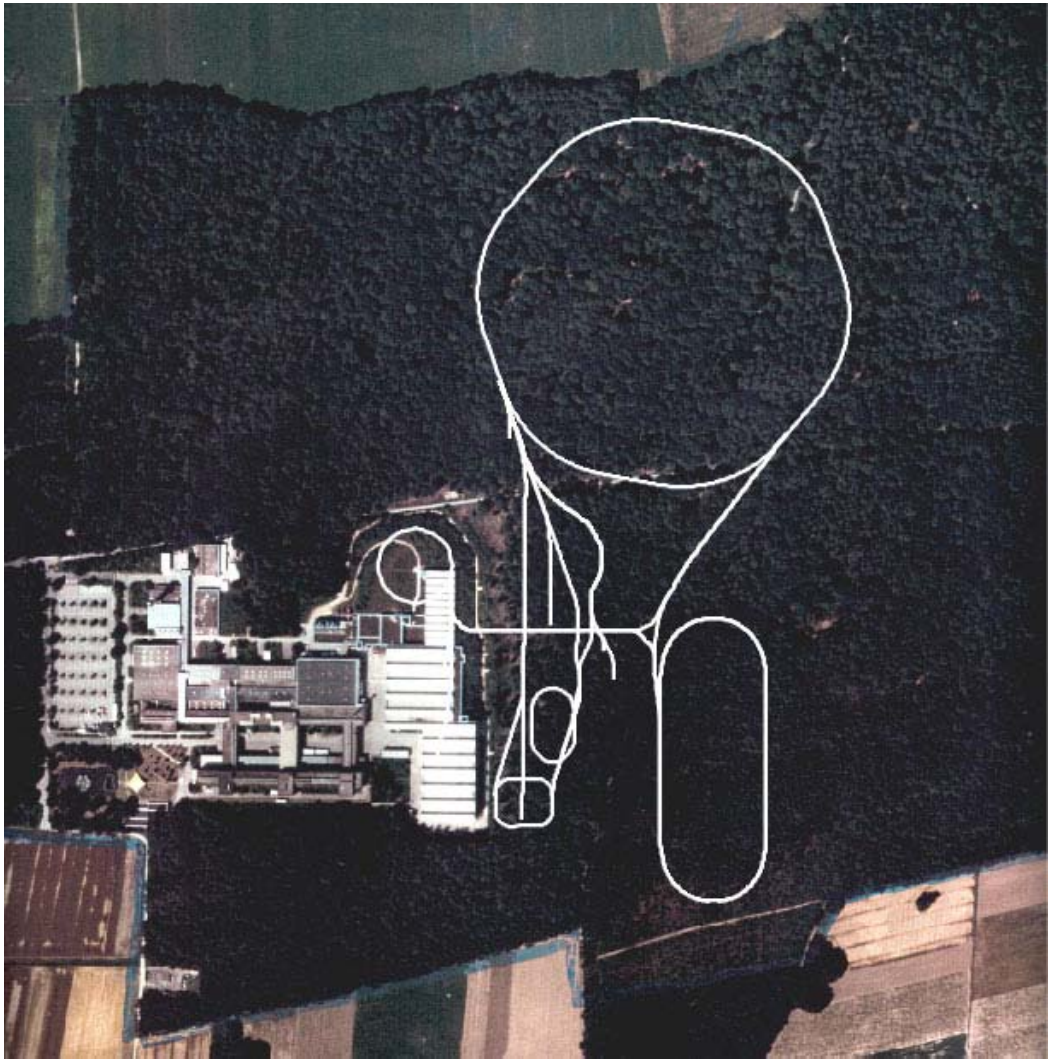

PHELIX

TECHNISCHE UNIVERSITÄT DARMSTADT

Intense Laser and Ion Beams

GSI

LLNL
General Atomics
CEA / LULI
Max-Born Institut
TU-Darmstadt

PHELIX

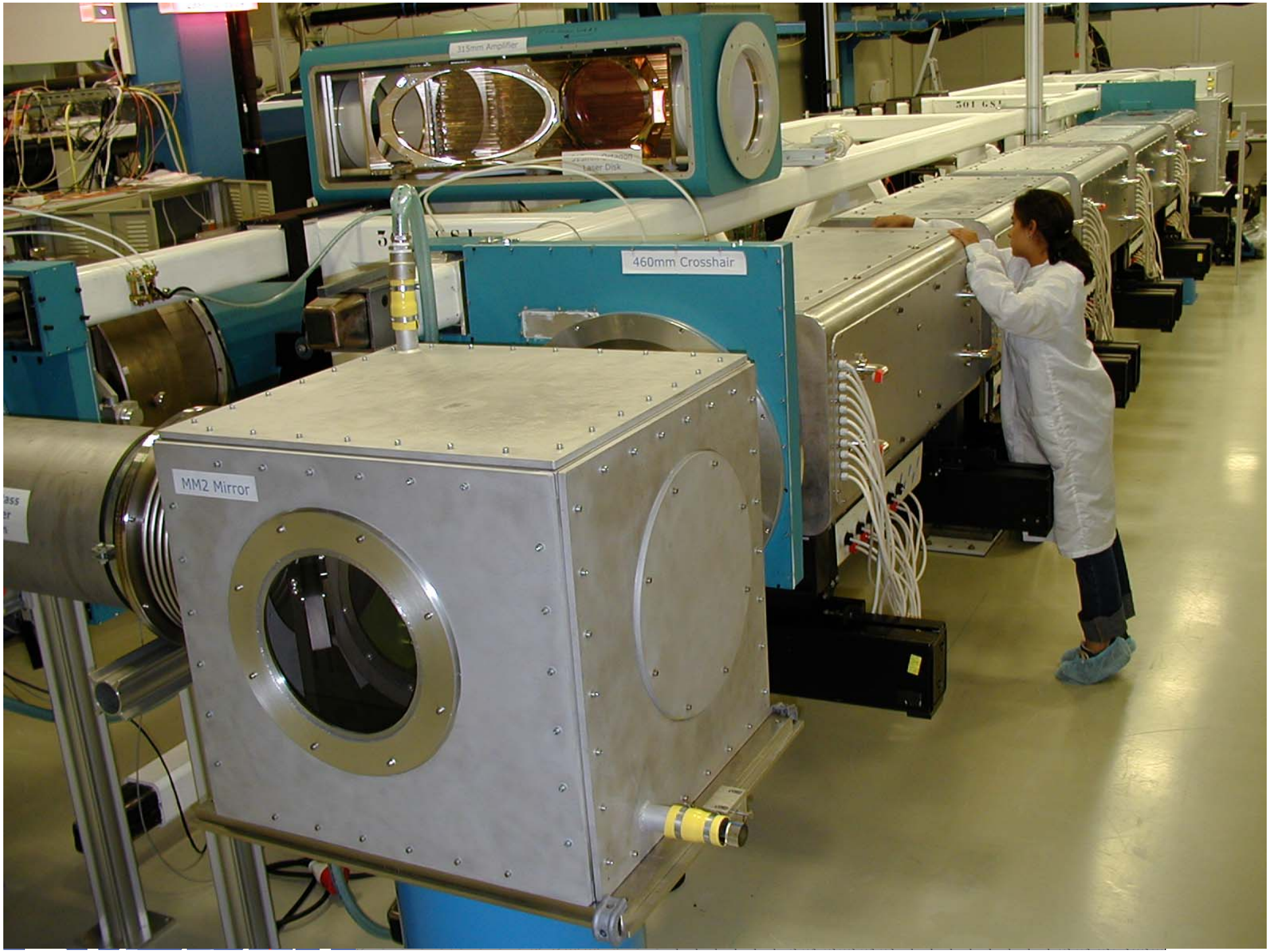
315mm Amplifier
460mm Crosshair
MM2 Mirror

TECHNISCHE UNIVERSITÄT DARMSTADT

Femtosecond Frontend

GSI

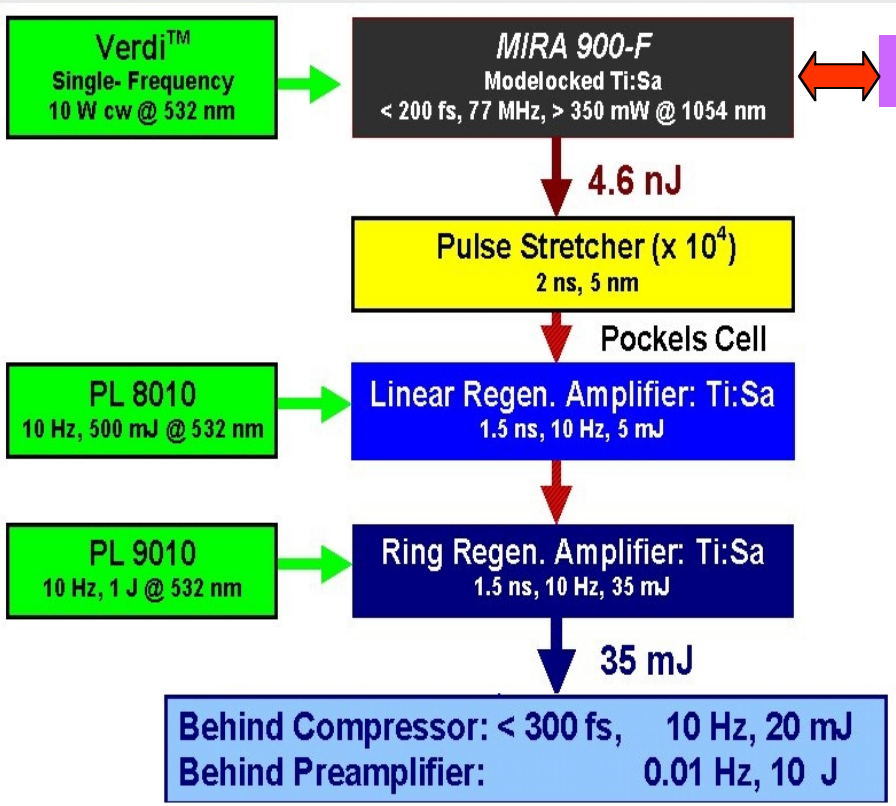

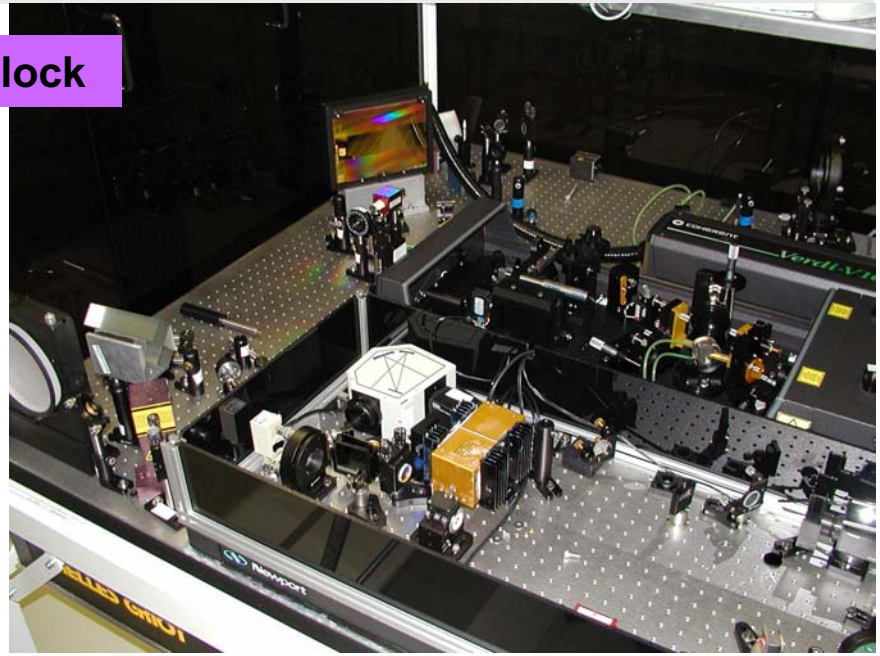

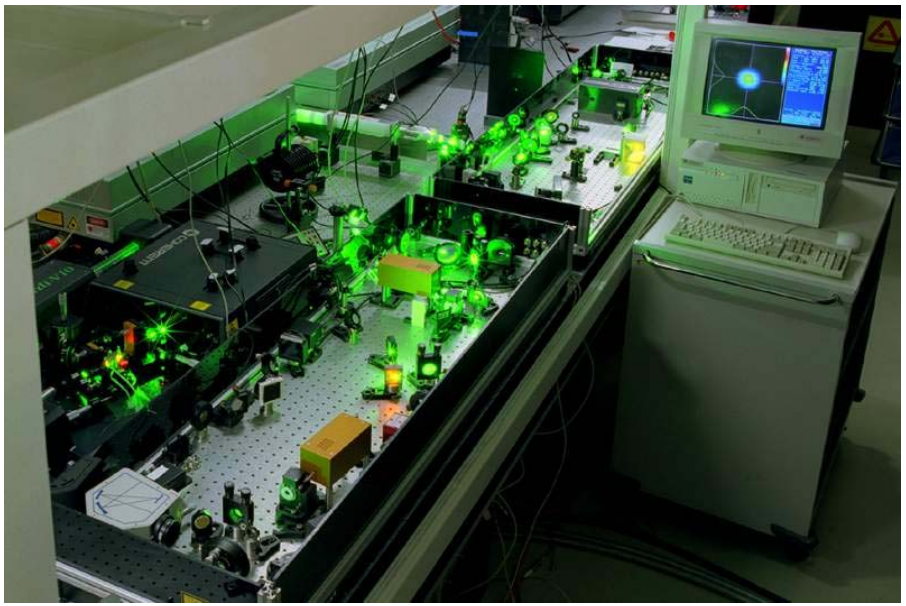

✓

- > 40 mJ output out of regenerative amplifier
- synchonization operating
- mode quality and stability up to specification

PHELIX

PHELIX has the capability to generate arbitrarily shaped pulses

X-ray pulses to diagnose plasmas

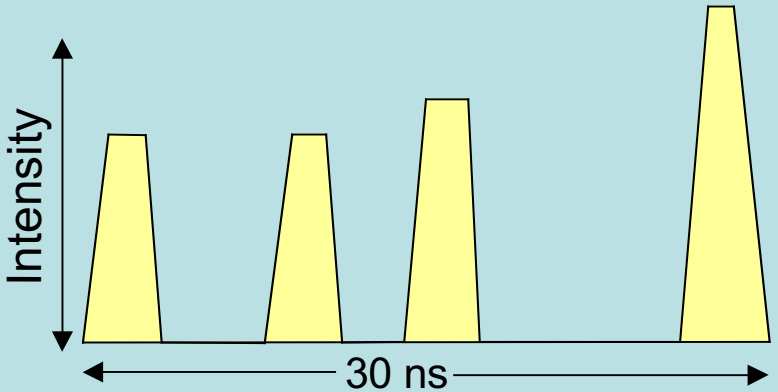

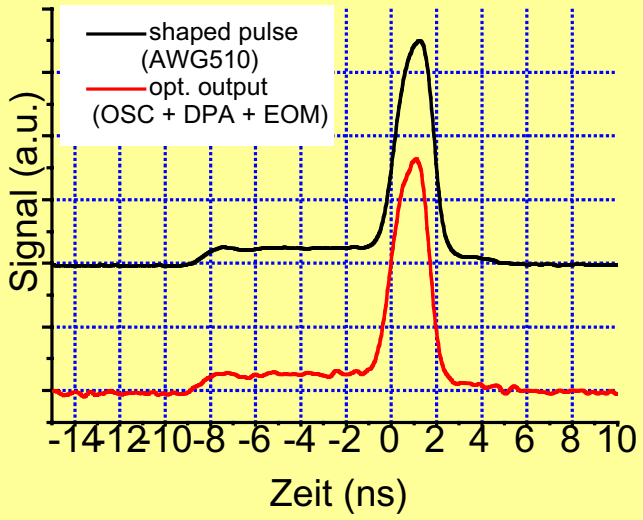

PHELIX serves as a diagnostic tool for dense plasmas

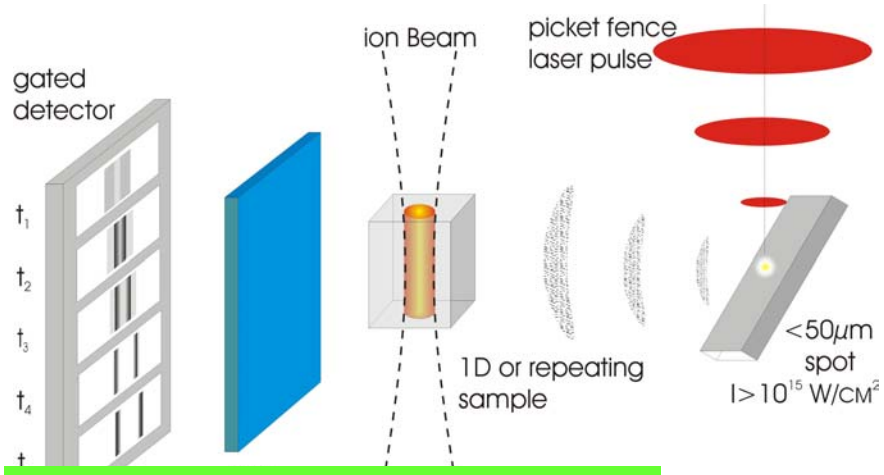

"Single point projection"
multiple, nanosecond pulses to look for the temp
of the target

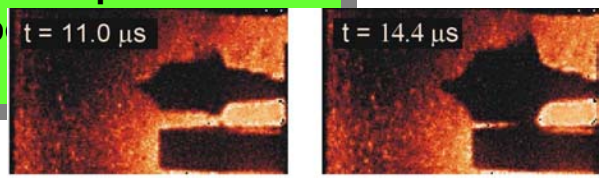

"Multiple point projection"
multiple, nanosecond pulses for tomography of the target

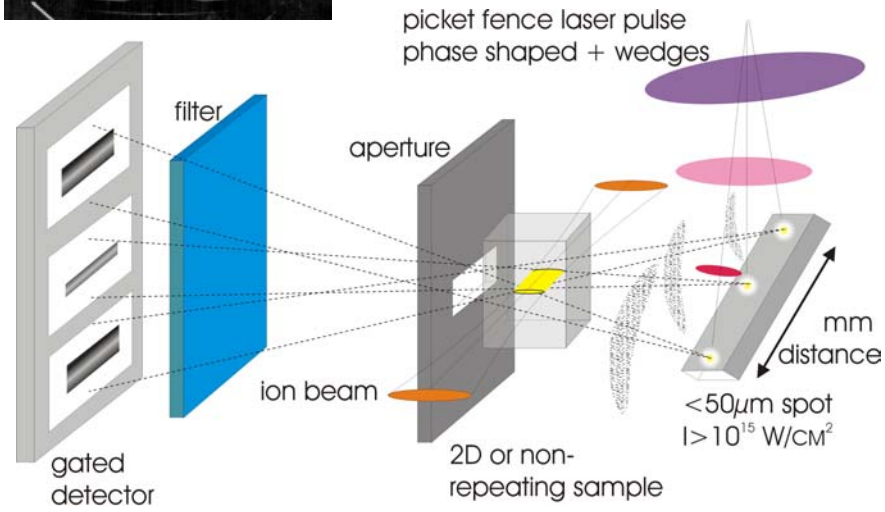

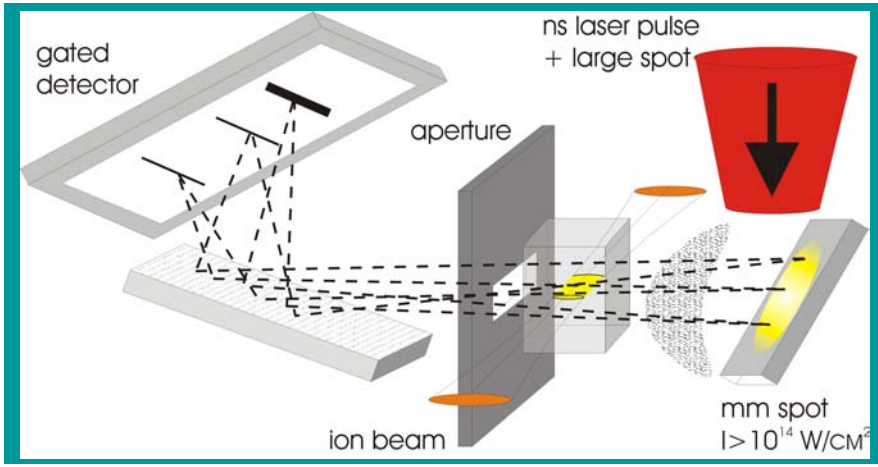

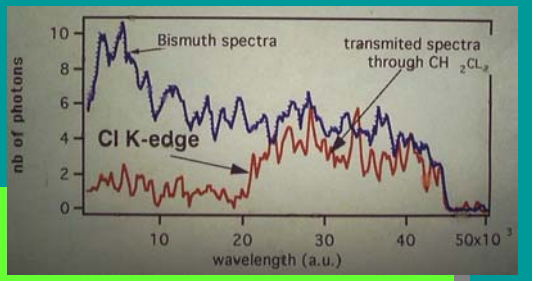

"Large area projection"
and absorption spectroscopy to measure the opacity of the target

X-ray Spectroscopy with high spectral and spatial resolution

Nhelix produced
Mg-Plasma

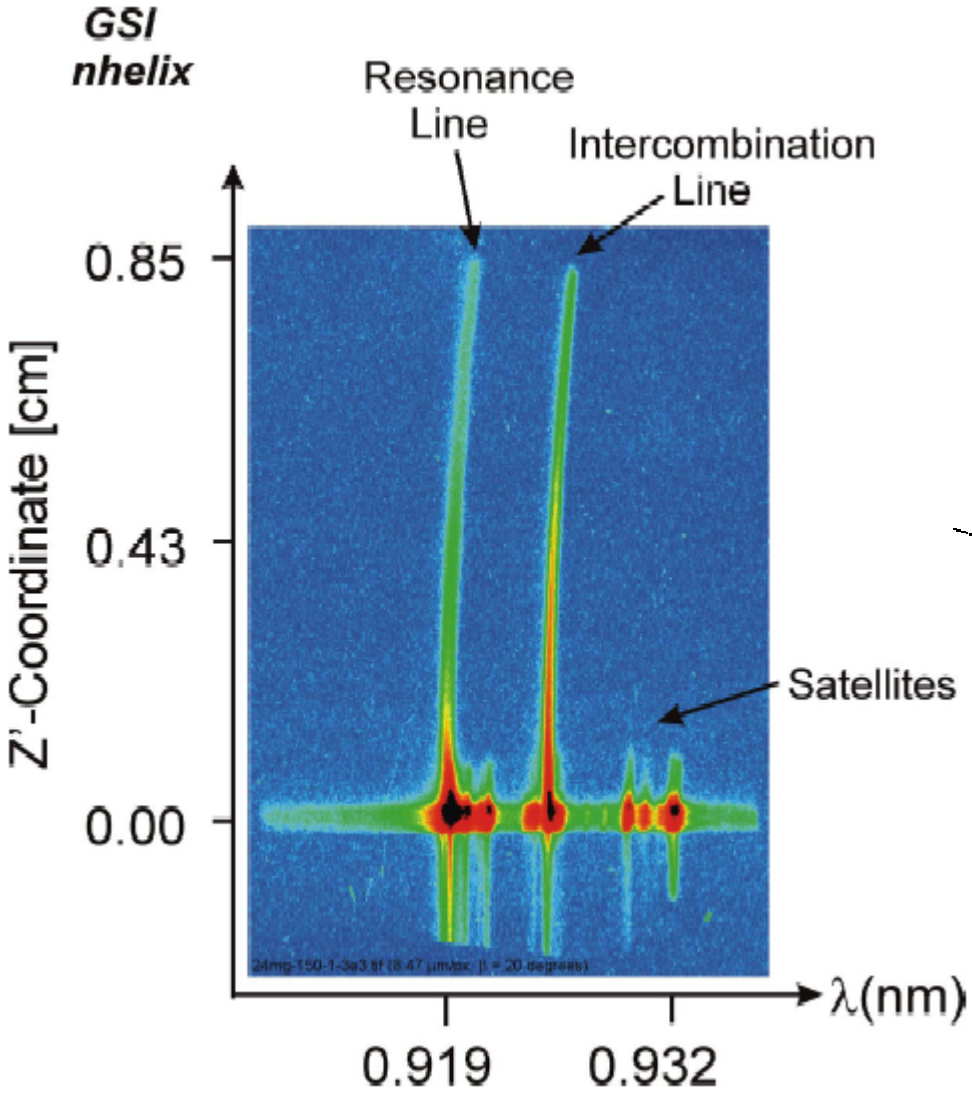

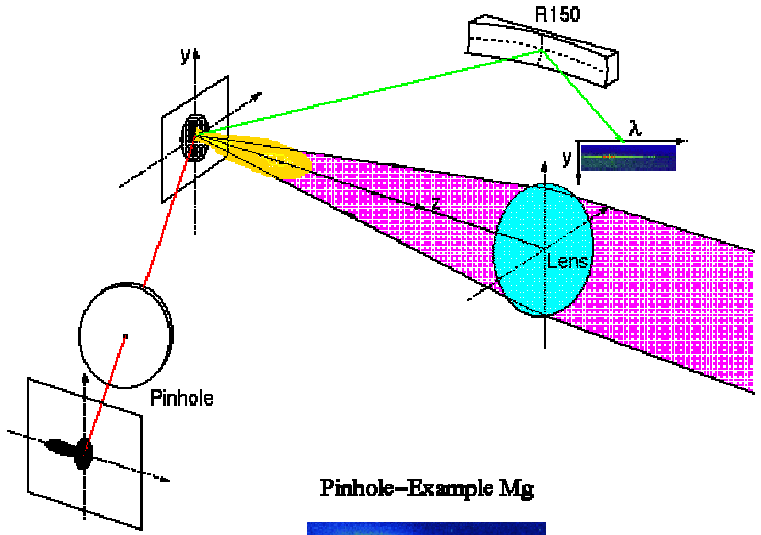

Pinhole–Example Mg

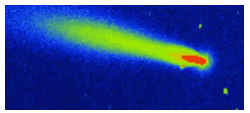

TECHNISCHE UNIVERSITÄT DARMSTADT

PHELIX can also be used to drive an X-ray laser

GSI

X-ray laser can be used for interferometry of dense plasma

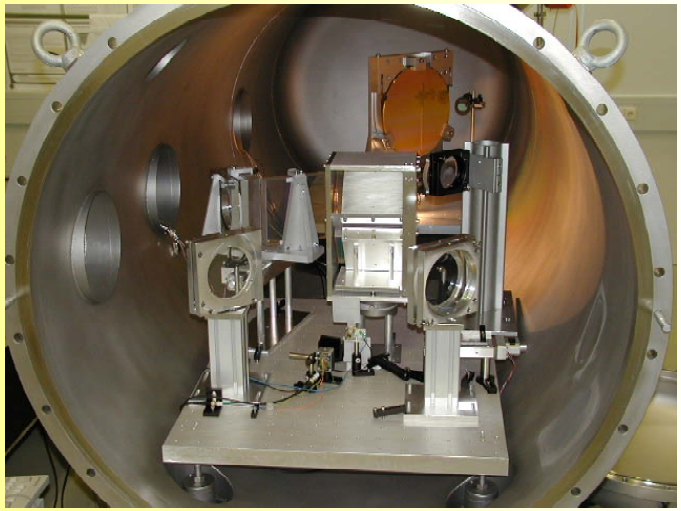

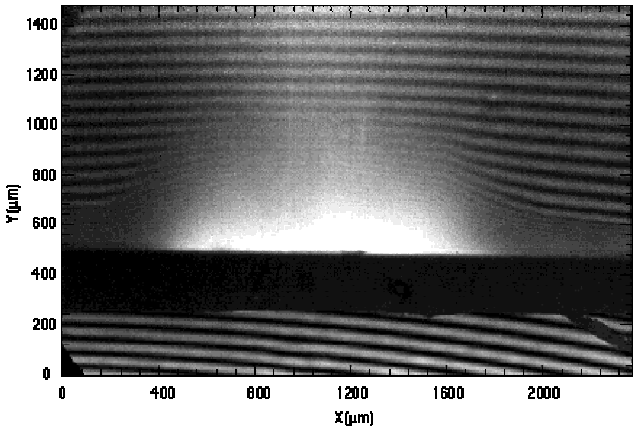

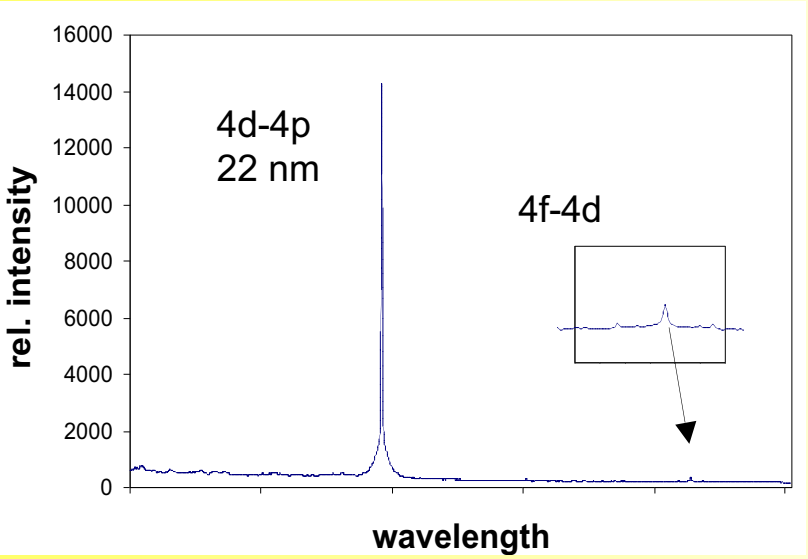

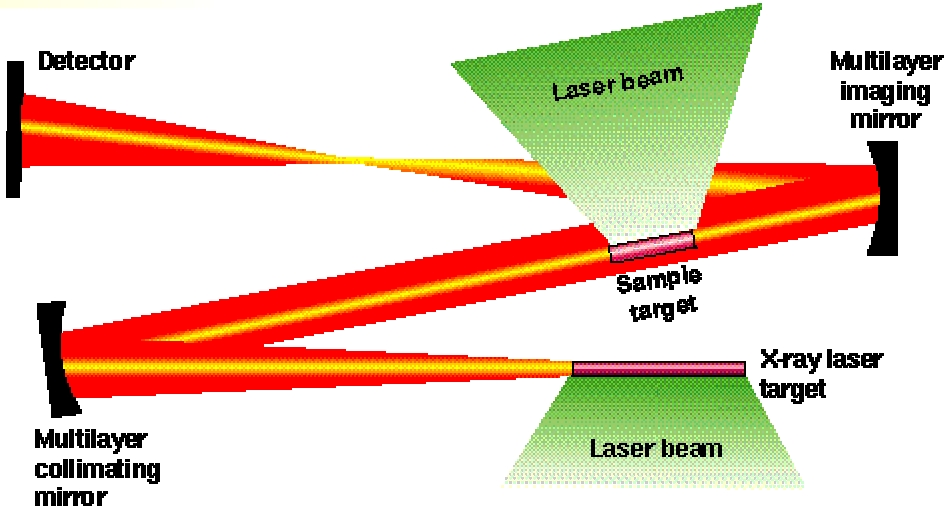

First successful experiments using the PHELIX preamplifier @ 5 J and 350 fs

PHELIX

Laser Driven Ion Beams

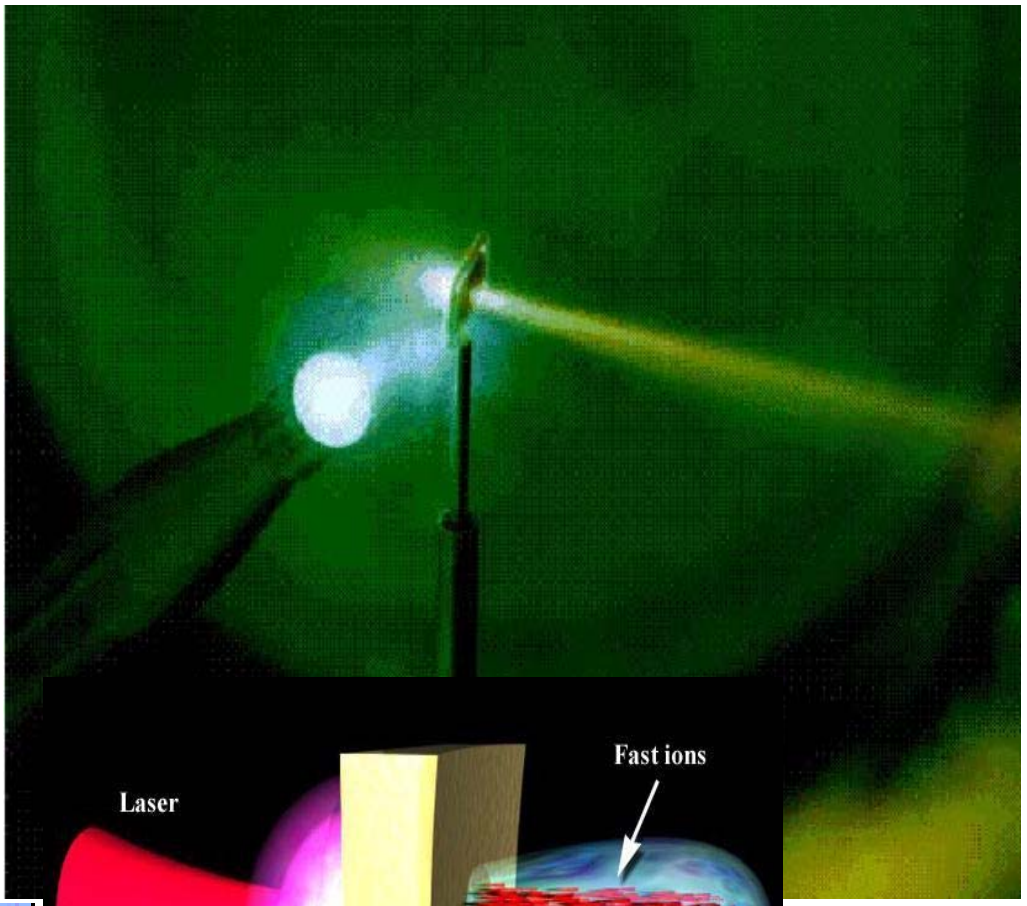

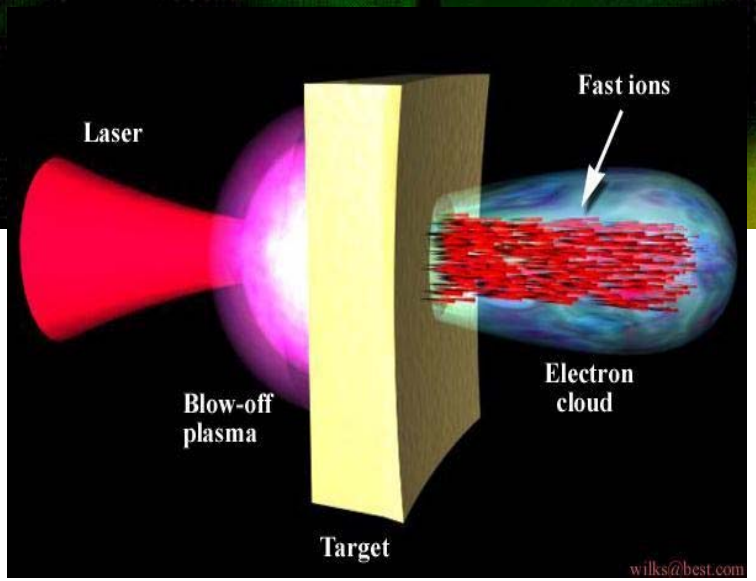

Number of accelerated protons:
10^{13} (LLNL- Petawatt)

Pulse duration:
several Picoseconds

Maximum energy:
60 MeV (LLNL Petawatt)

Divergence:
<10° for high energy part

always normal to the rear surface

origin of protons: surface contaminants

TECHNISCHE UNIVERSITÄT DARMSTADT

GSI

Laser accelerated ions as a new diagnostic tool: Short pulse proton radiography

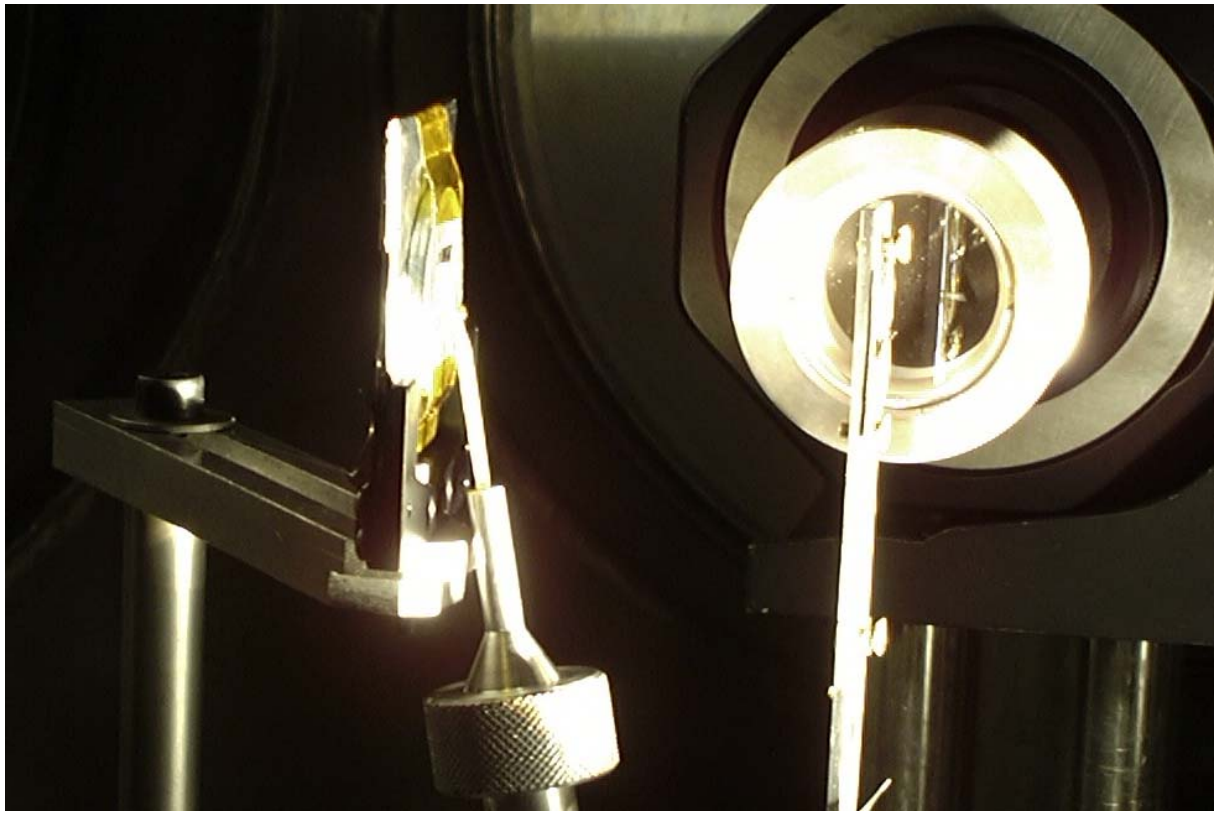

PHELIX

Recent Experiments at the 100 TW Laser at LULI have demonstrated proton radiography

Target Setup

Cu-wires 250µm
Steel Hohlraum
300 µm wall thickness
Ti - layers 100µm
Epoxy-ring 1.5mm
Glass semi - spheres
900 µm dia., 20 µm wall

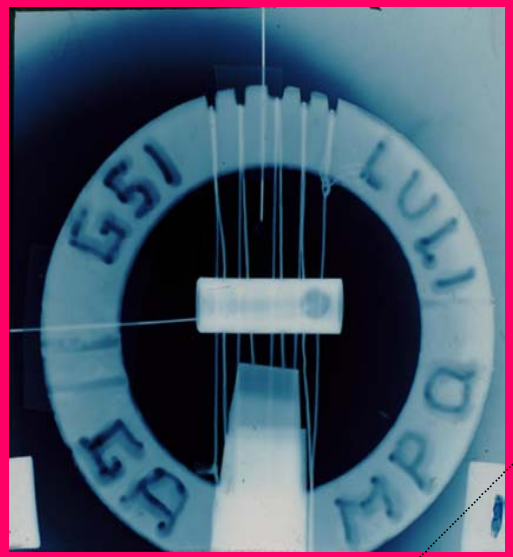

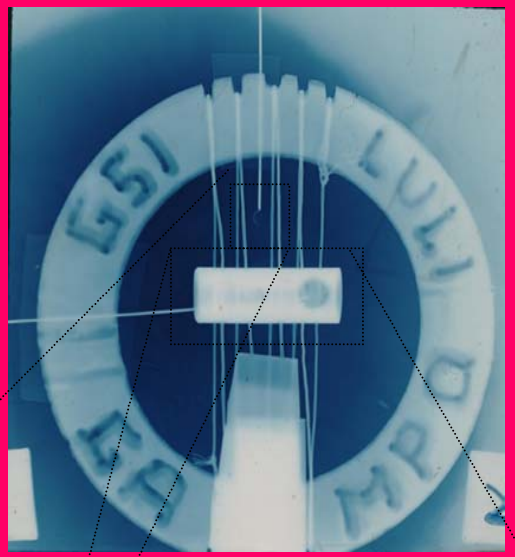

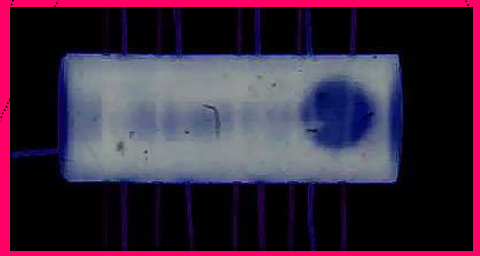

Radiographic image: resolution ≈ 25µm
determined by the resolution of the RCF

TECHNISCHE UNIVERSITÄT DARMSTADT

First experiments using NIF-capsules show excellent agreement with simulations

GSI

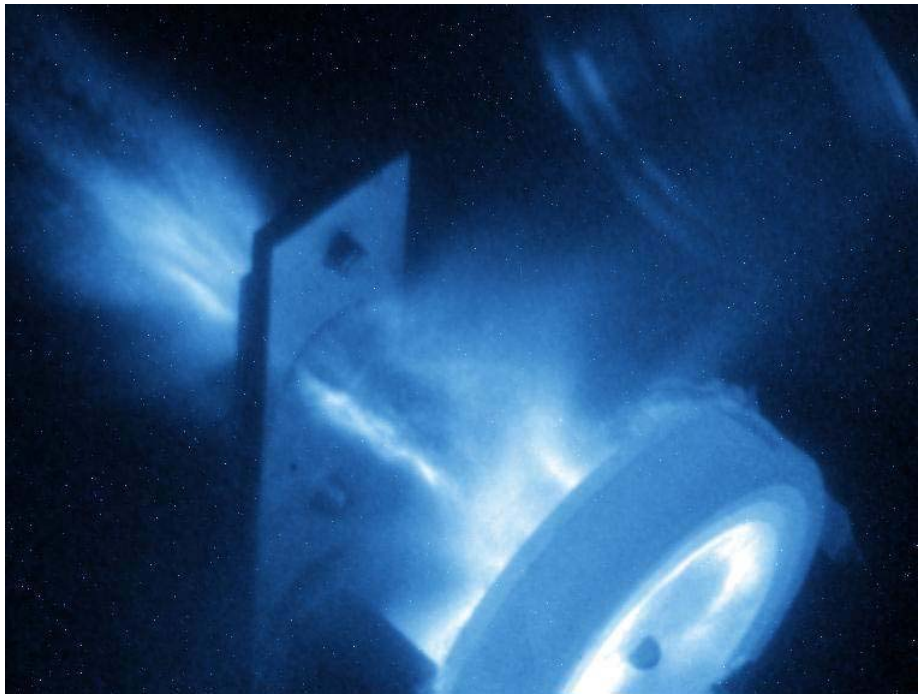

Simulation

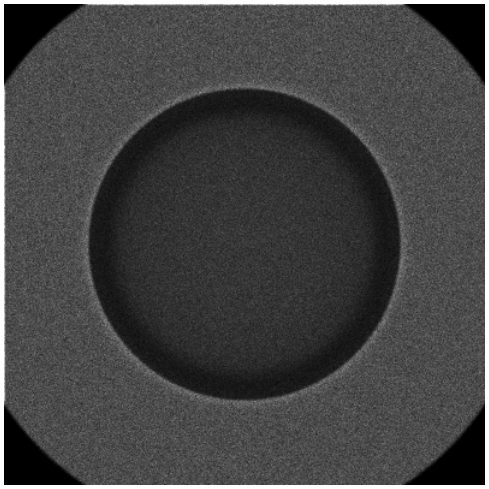

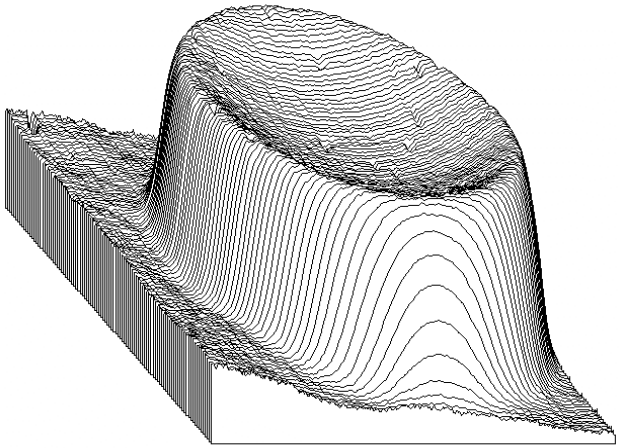

Experiment: 20J/350 fs laser accelerated proton image of empty NIF-shell

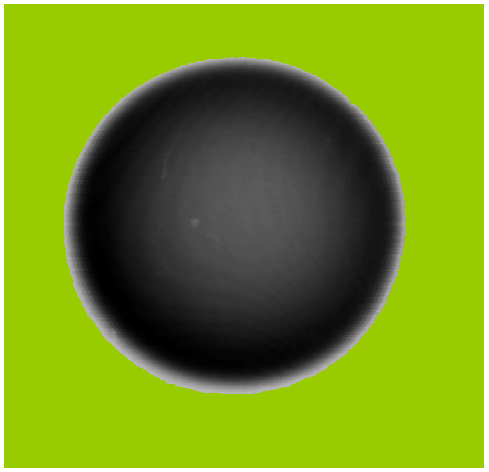

PHELIX

Proton Radiography is able to detect thin layers of low-Z material behind high-Z shielding

100 µm Tantalum
50 µm layers CH

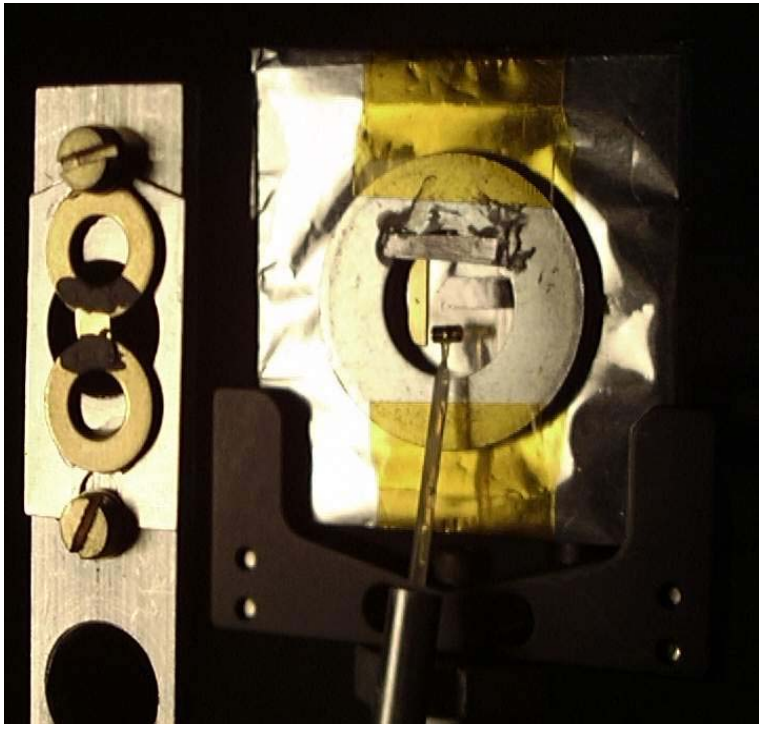

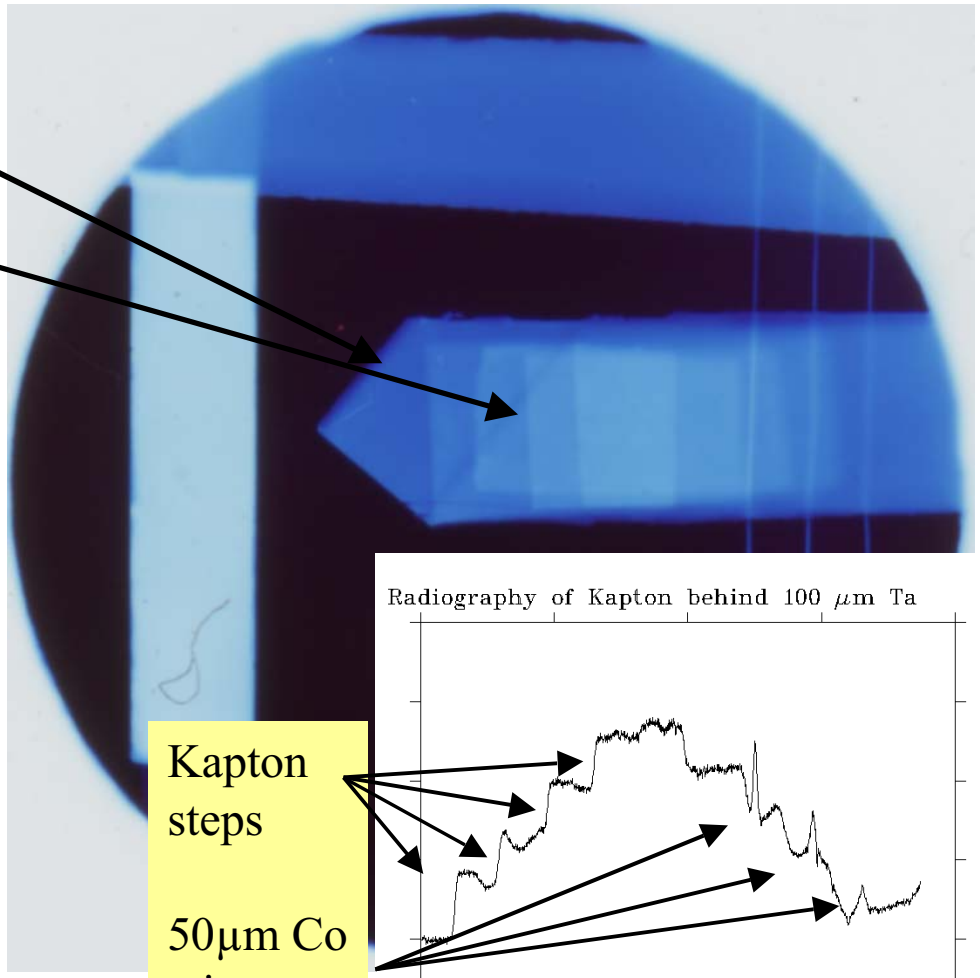

Kapton steps

50µm Co wires

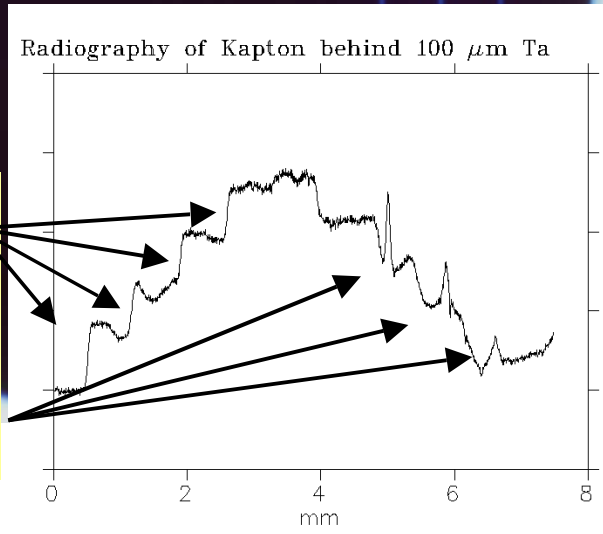

Target rear surface imprint in ion beam

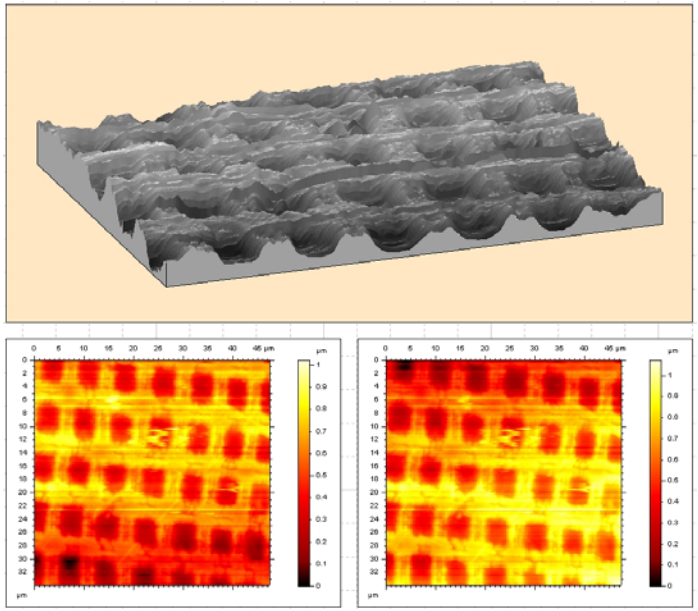

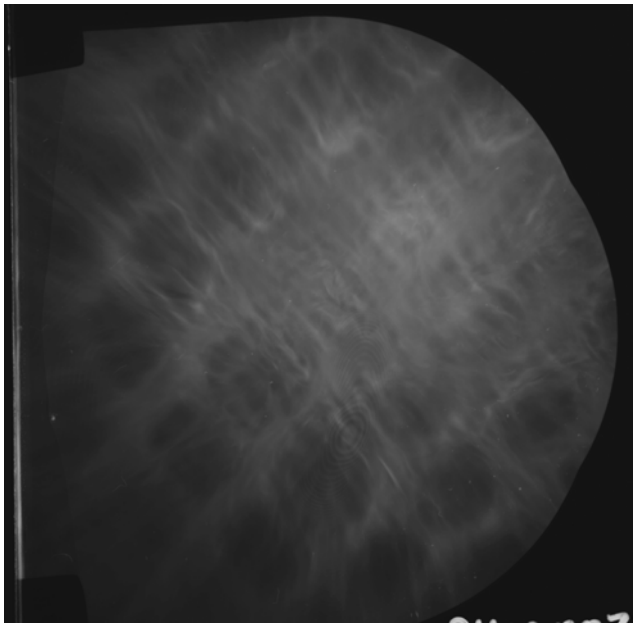

LANL Trident-Laser shot E_{laser} = 26 J, I = 7 x 10^{18}W/cm^2

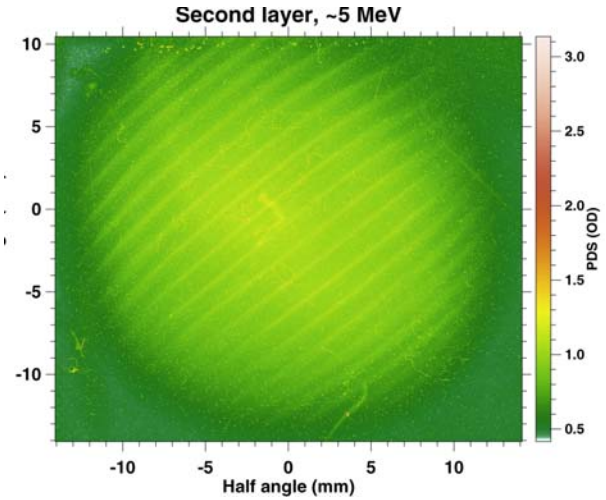

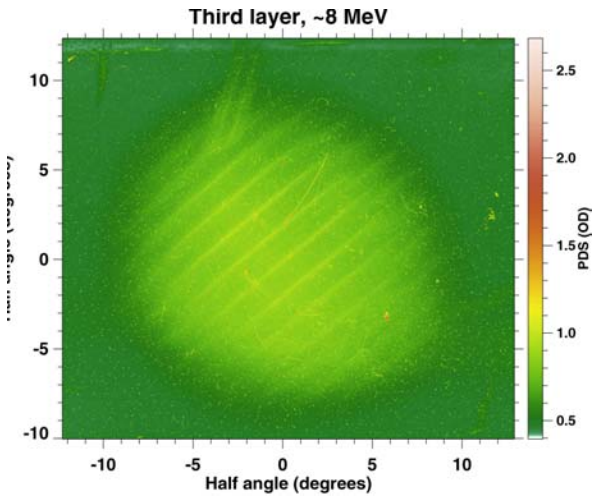

TECHNISCHE UNIVERSITÄT DARMSTADT

A wire hit by a short pulse laser

GSI

Target: 50 µm wire

Time of proton exposure (relative to experiment ± 10 ps)

-10 ps **0 ps** **+10 ps** **+20 ps** **+30 ps** **Laser**

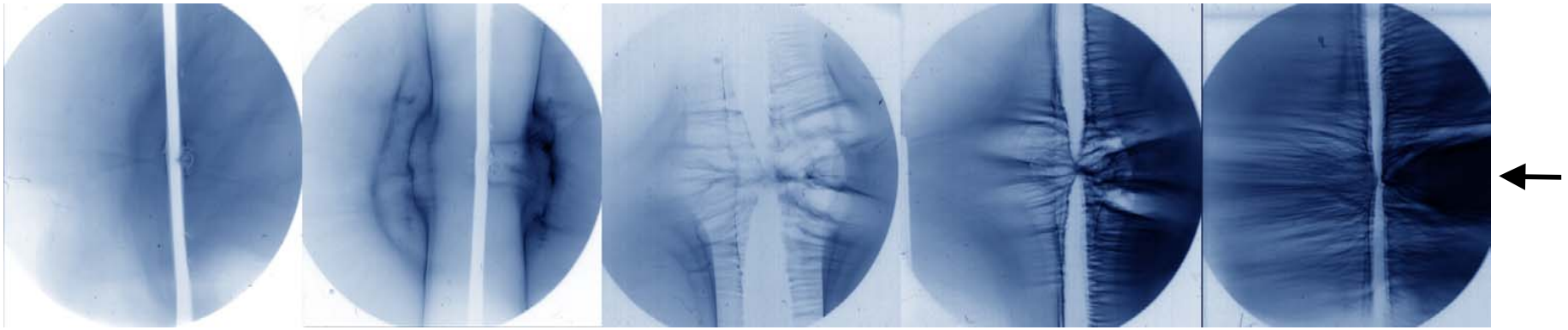

Charge- and Discharge time of the target appox. 30 ps
Small structures: Onset of instabilities?

5 mm

400 µm

M. Borghesi et al.

Queen's University Belfast

PHELIX

Thank you !

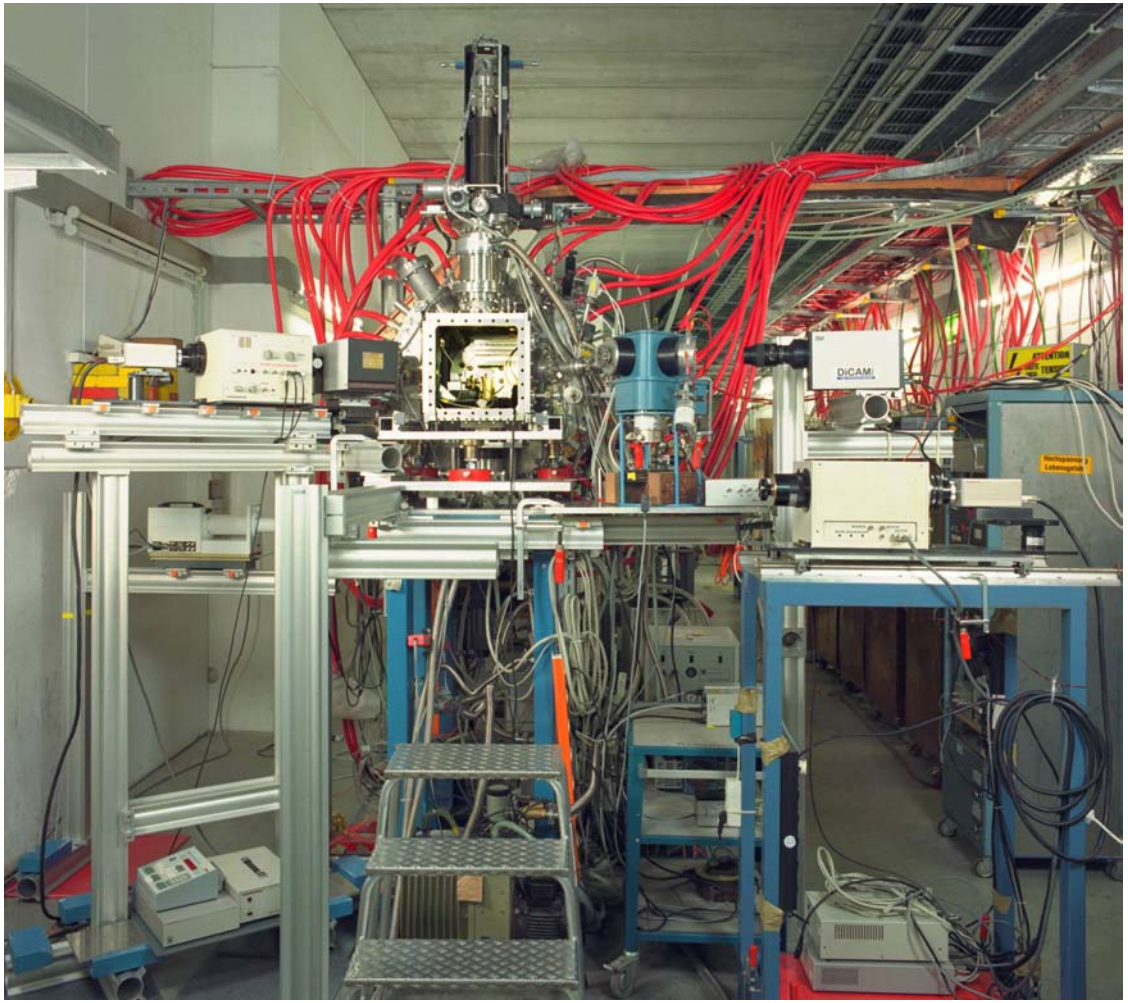

V. Arsov
M. Basko
B. Becker-de Mos
A. Blazevic
R. Bock
E. Brambrink
C. Constantin
E. Dewald
M. Geißel
U. Geißler
S. Hakuli
D.H.H. Hoffmann
J. Jacoby
A. Kozyreva
U. Neuner
C. Niemann
V. Orsic
D. Penache
P. Pirzadeh
F. Rosmej
O. Rosmej
M. Rytter
G. Schaumann
T. Schlegel
N. Tahir
A. Tauschwitz
S. Udrea
D. Varentsov
H. Wahl
K. Weyrich
J. Wieser
M. Youssef

Collaborations:

Univ. Frankfurt
Univ. Rostock
Univ. Greifswald
Univ. Neapel
MPQ Garching
LULI, Palaiseau
General Atomics
LBNL, Berkeley
LLNL, Livermore
TITech, Tokio
ITEP, Moskau
ICP, Chernogol.
VNIEEV, Sarov
UNR, Reno

Ultrafast X-rays: production with laser-produced plasma and applications

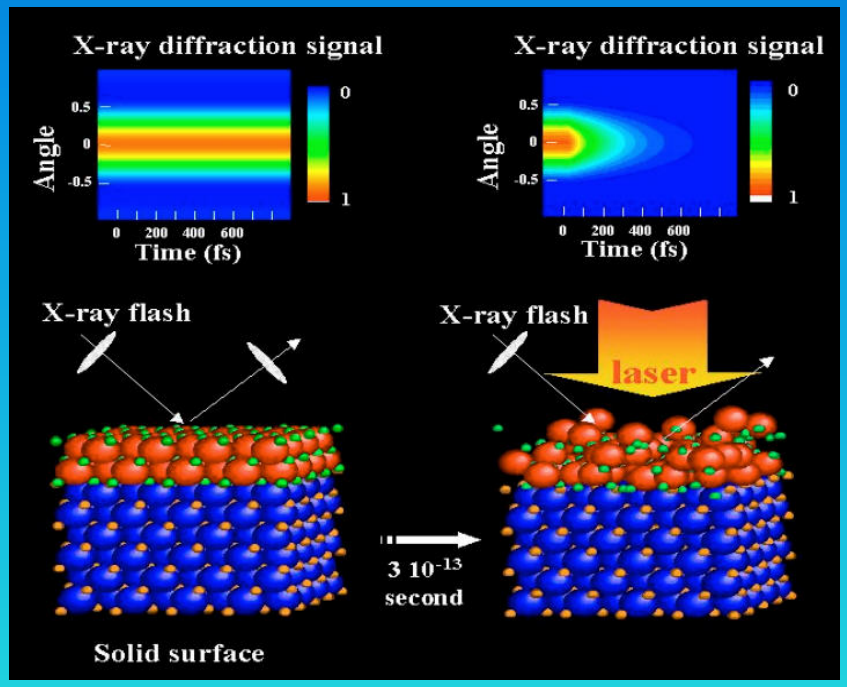

Antoine ROUSSE

LOA - Laboratoire d 'Optique Appliquée

antoine.rousse@ensta.fr

Ultrafast X-rays with laser-plasmas

1) Why ?

2) The existing source

3) pionneering application experiments

4) The next source

X-rays have opened the Ultra-Small World

the New Source will open the
Ultra-Small and Ultra-Fast Worlds

1 Å **100 femtosecond**

$1 Å = 10^{-10} m$ **$1 fs = 10^{-15} s$**

Realm of the femtosecond

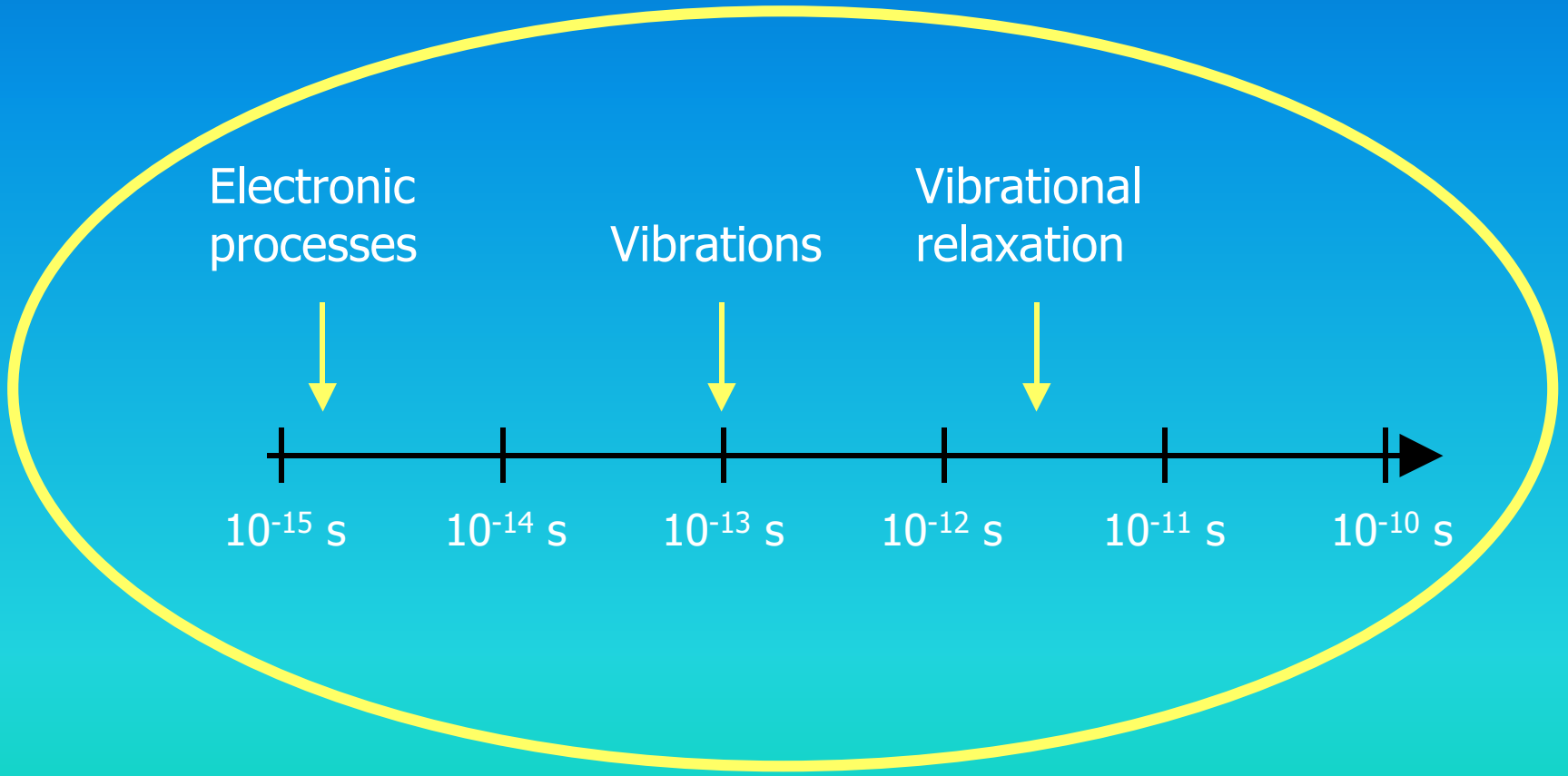

Realm of the femtosecond

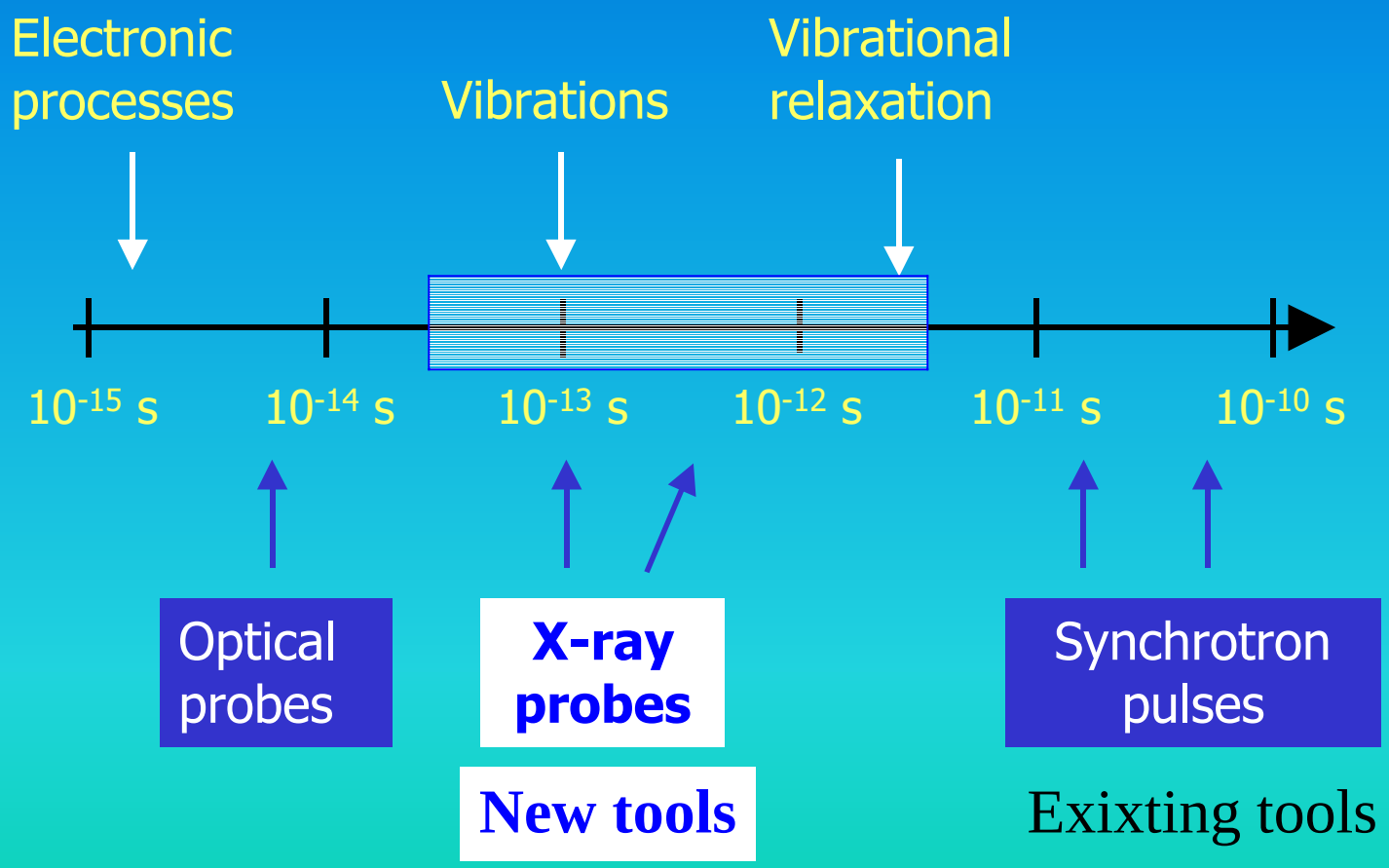

fs excitation

-

x-ray probe

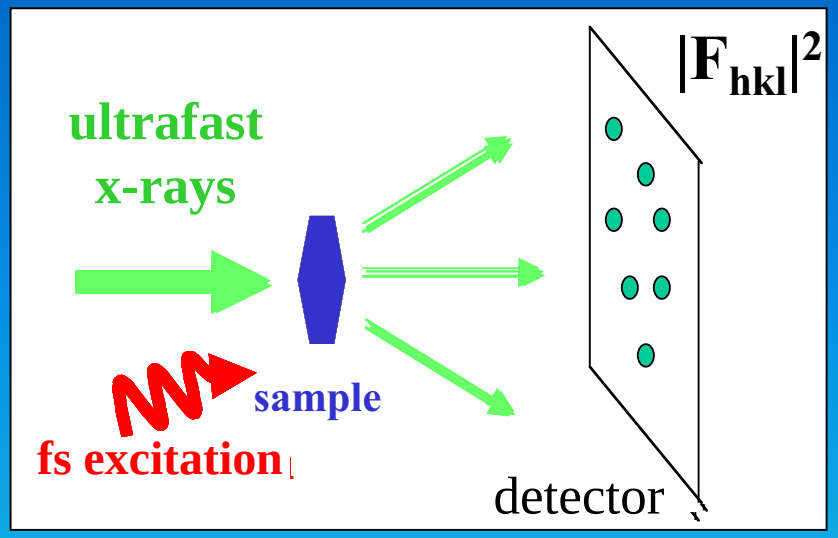

fs x-ray excitation

-

x-ray or visible probe

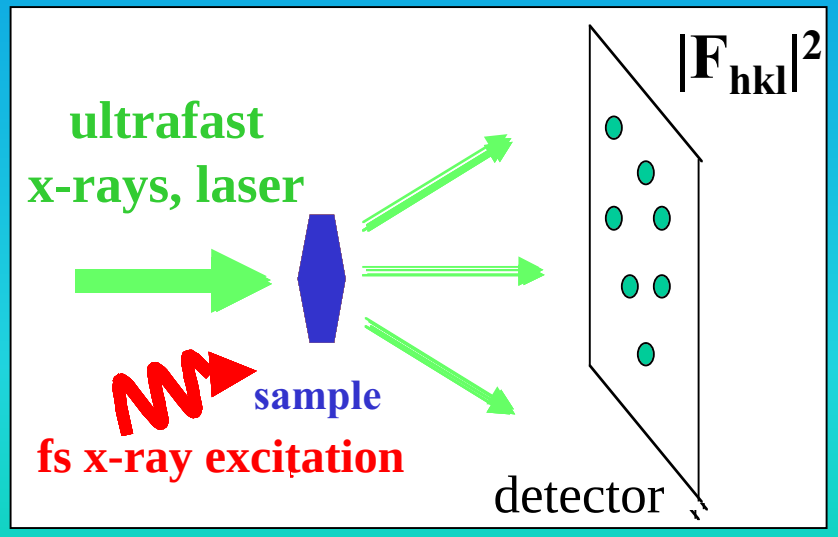

L.O.A

ENSTA

POLYTECHNIQUE

CNRS

Multidisciplinary applications

Warm dense matter

Femto-chemistry

Femto-biology

Femto-magnetism

Phase transition

Atomic & molecular physics

Nano-scale dynamics

R.W. Lee (LLNL)

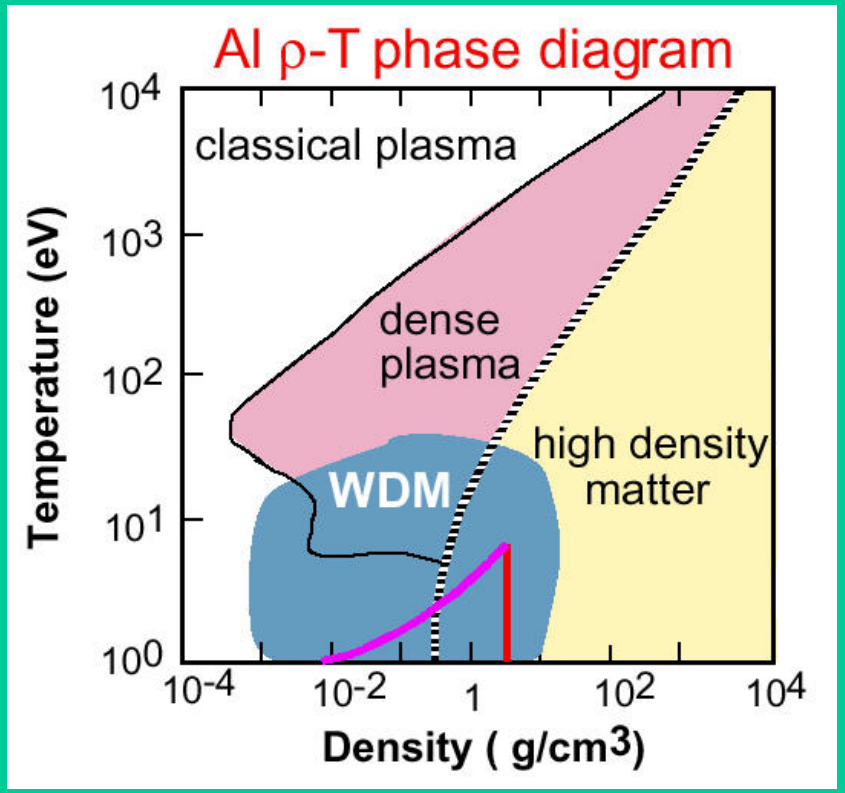

Heat the matter rapidly and uniformly to create isochore (_ is constant) and release isentrope (entropy is constant).

Multidisciplinary applications

Warm dense matter

Femto-chemistry

Femto-biology

Femto-magnetism

Phase transition

Atomic & molecular physics

Nano-scale dynamics

LCLS report (the first experiments)

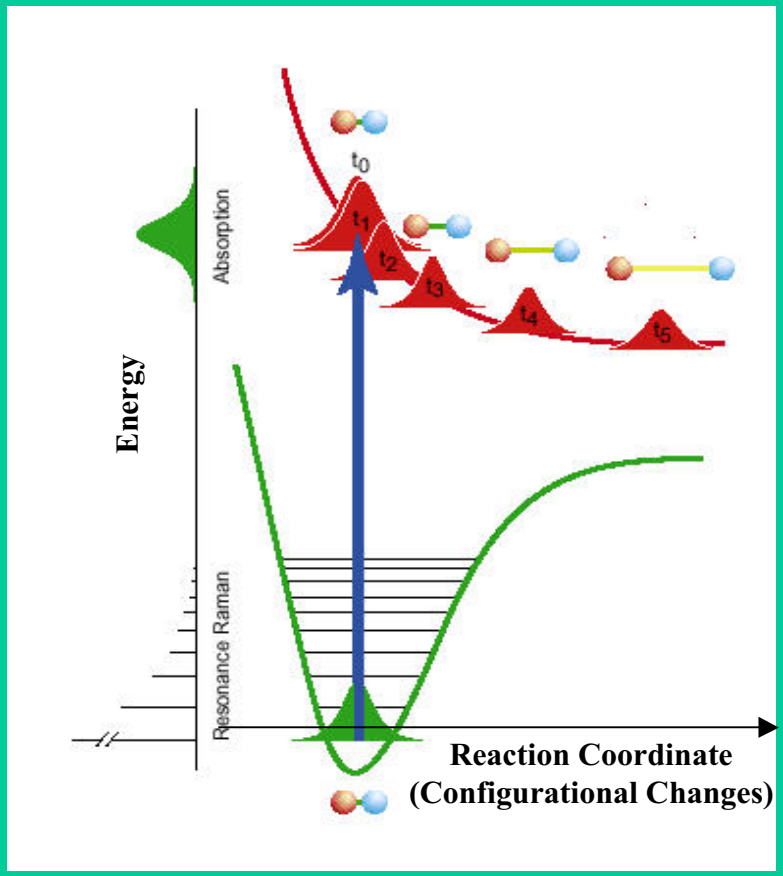

Track in-situ the reaction dynamics (bond breaking, bond formation,…)

Multidisciplinary applications

Warm dense matter

Femto-chemistry

Femto-biology

Femto-magnetism

Phase transition

Atomic & molecular physics

Nano-scale dynamics

ESRF

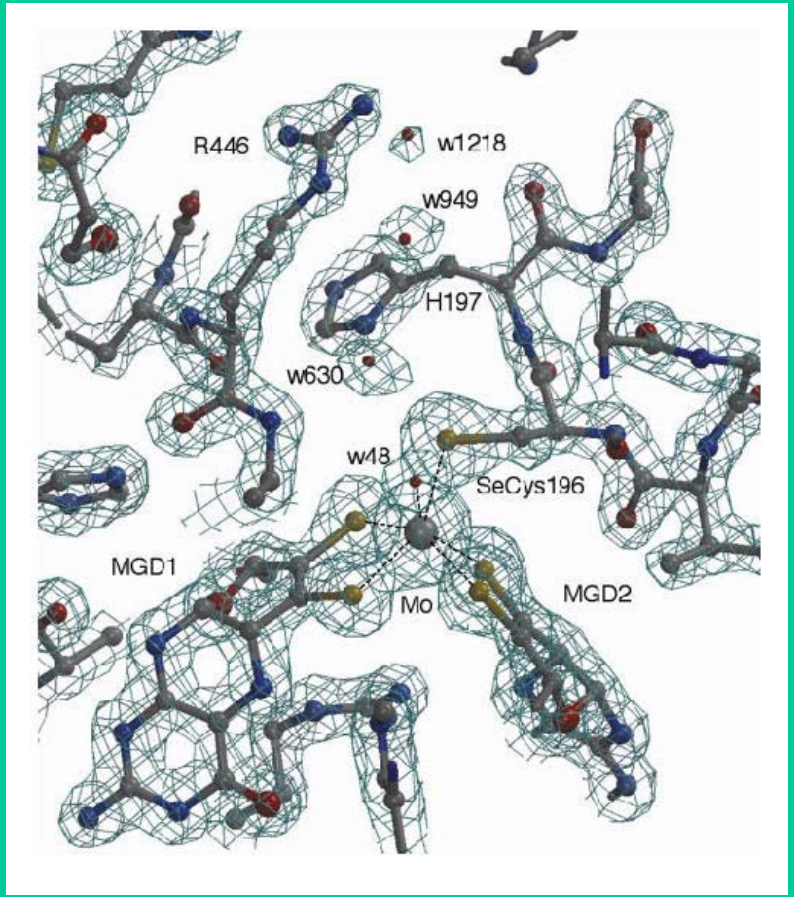

Mapping out the transient states (structure of proteins = biological function)

Multidisciplinary applications

Warm dense matter

Femto-chemistry

Femto-biology

Femto-magnetism

Phase transition

Atomic & molecular physics

Nano-scale dynamics

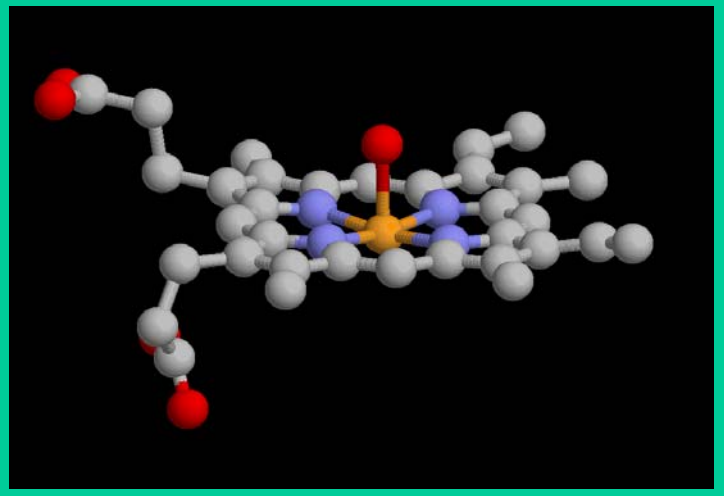

spin transition

Molecular magnet

Ferromagnetic to paramagnetic phase switch

spin transition dynamics

spin-lattice coupling

Multidisciplinary applications

Warm dense matter

Femto-chemistry

Femto-biology

Femto-magnetism

Phase transition

Atomic & molecular physics

Nano-scale dynamics

Tesla report XFEL'2000

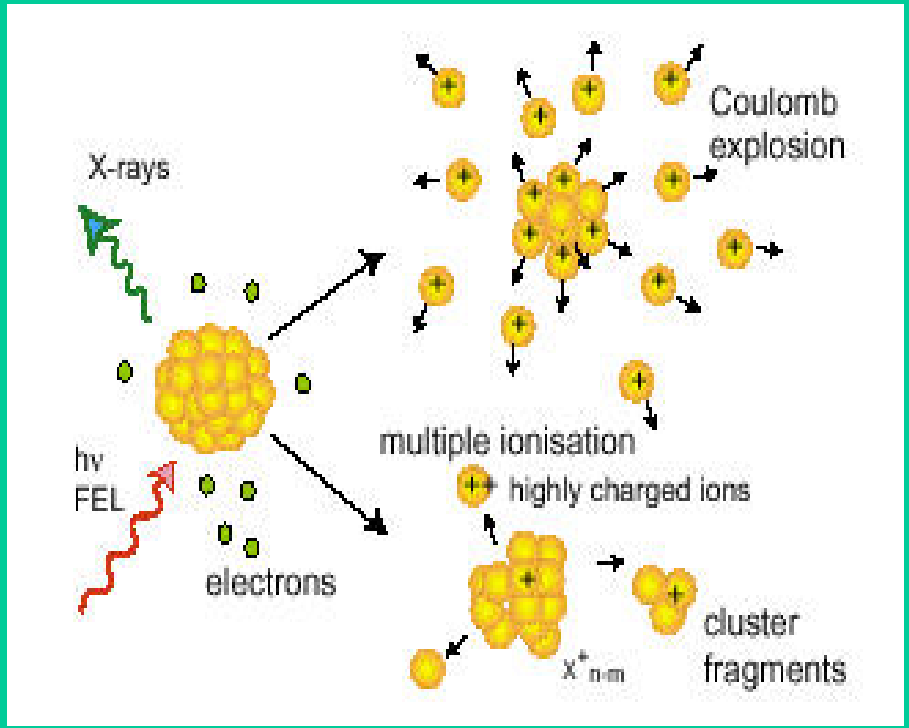

Multiphoton ionization, hallow atoms,
Coulomb explosion, fragmentation …

Multidisciplinary applications

Warm dense matter

Femto-chemistry

Femto-biology

Femto-magnetism

Phase transition

Atomic & molecular physics

Nano-scale dynamics

LCLS the first experiments report

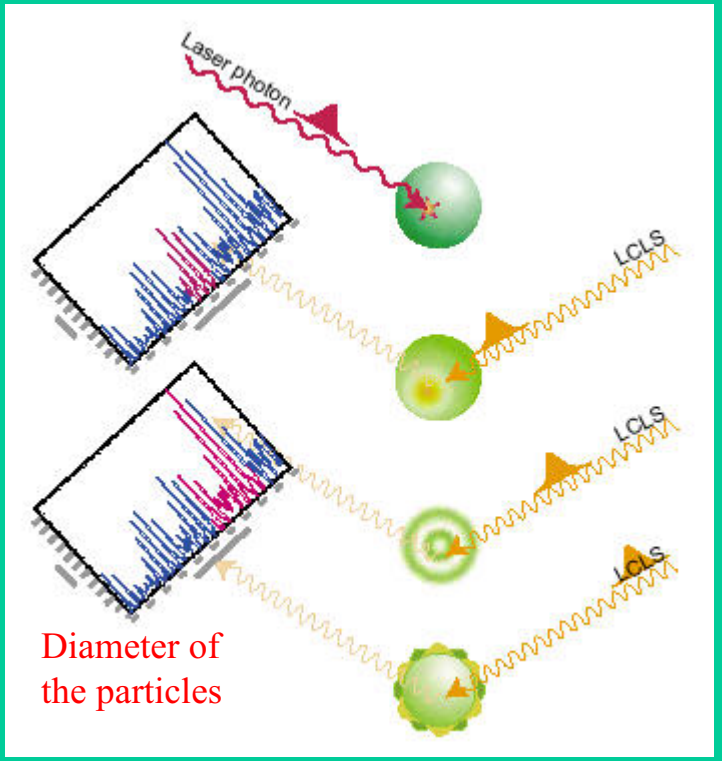

Nanoparticle vibrational and surface modes, nanoscale melting, nucleation,...

Multidisciplinary applications

TESLA report

Warm dense matter

Femto-chemistry

Femto-biology

Femto-magnetism

Phase transition

Atomic & molecular physics

Nano-scale dynamics

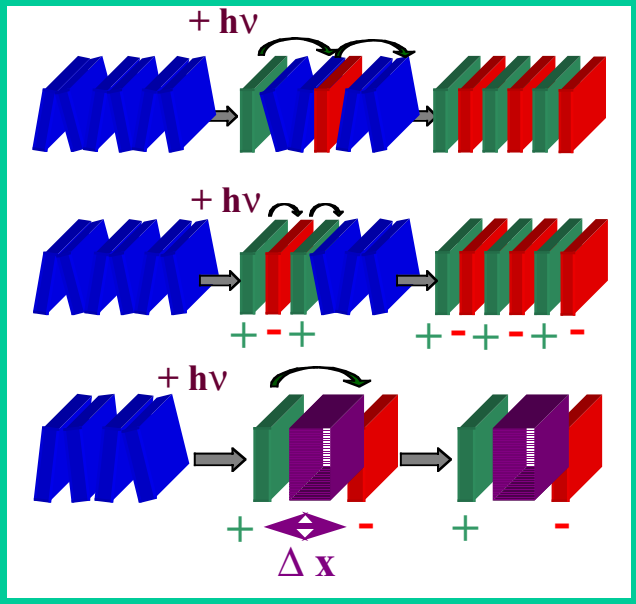

Isolator ↔ Conductor

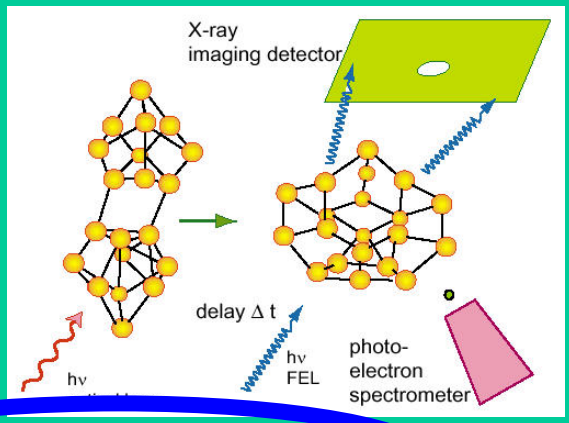

Solid-solid, solid liquid intermolecular electron transfert, …

Ultrafast X-rays with laser-plasmas

1) Why ?

2) The existing source

3) pionneering application experiments

4) The next source

Battle to become the Next Generation X-ray Source

SCIENCE 298 (15 November 2002)

"For the first time in decades, researchers are looking past synchrotrons storage rings for their x-ray future"

Ultrafast X-ray sience

Femtosecond X-ray tube

key word: 100 fs, several keV, 10 Hz

laser-plasma x-ray source

Nature **390** 490 (1997)	LOA
Nature **398** 310 (1999)	UCSD
Nature **410** 65 (2001)	LOA
PRL **87** 225701 (2001)	Essen
PRL **87** 237401 (2001)	UCSD
Nature ... (march 2003)	Essen

developped in 1994-1996
(LOA / LULI, Palaiseau, France)

solid-state physics applications

It works already !

M. Murnane *et al* Phys. Rev. Lett. (92)
A. Rousse *et al*, Phys. Rev. E 50 (3) 2200 (94)
S. Bastiani *et al*, Phys. Rev. E 56 (6) 7179 (97)

How it works ?

femtosecond x-ray tube = laser-produced plasma x-ray source

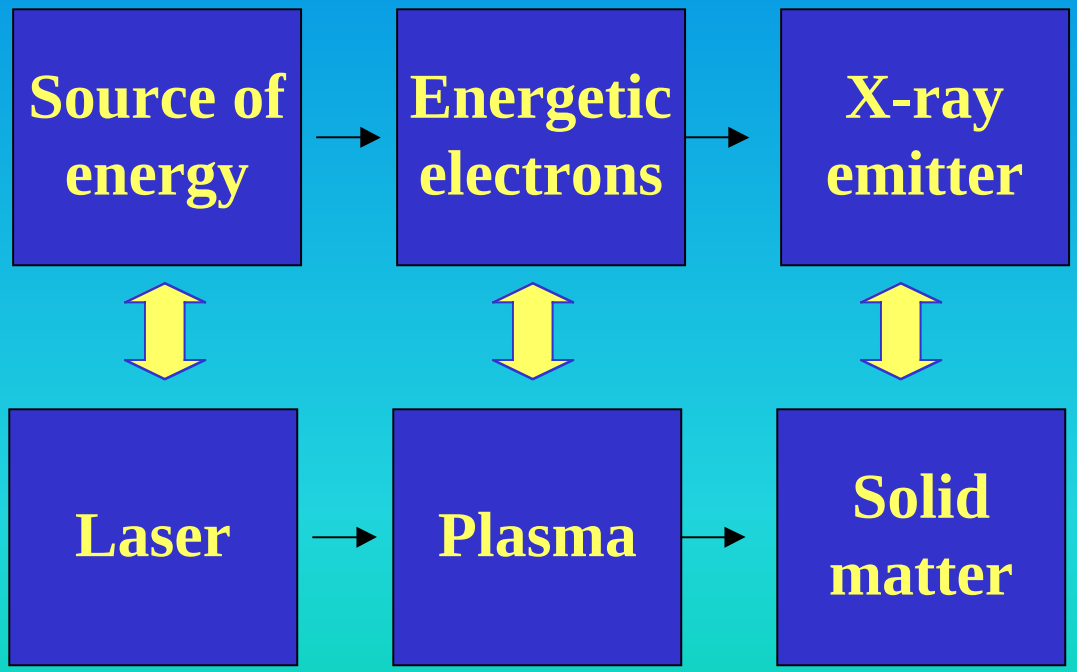

Does it work ?

Feasability Applications

Yes, but ...

Laser-produced plasma K_α source

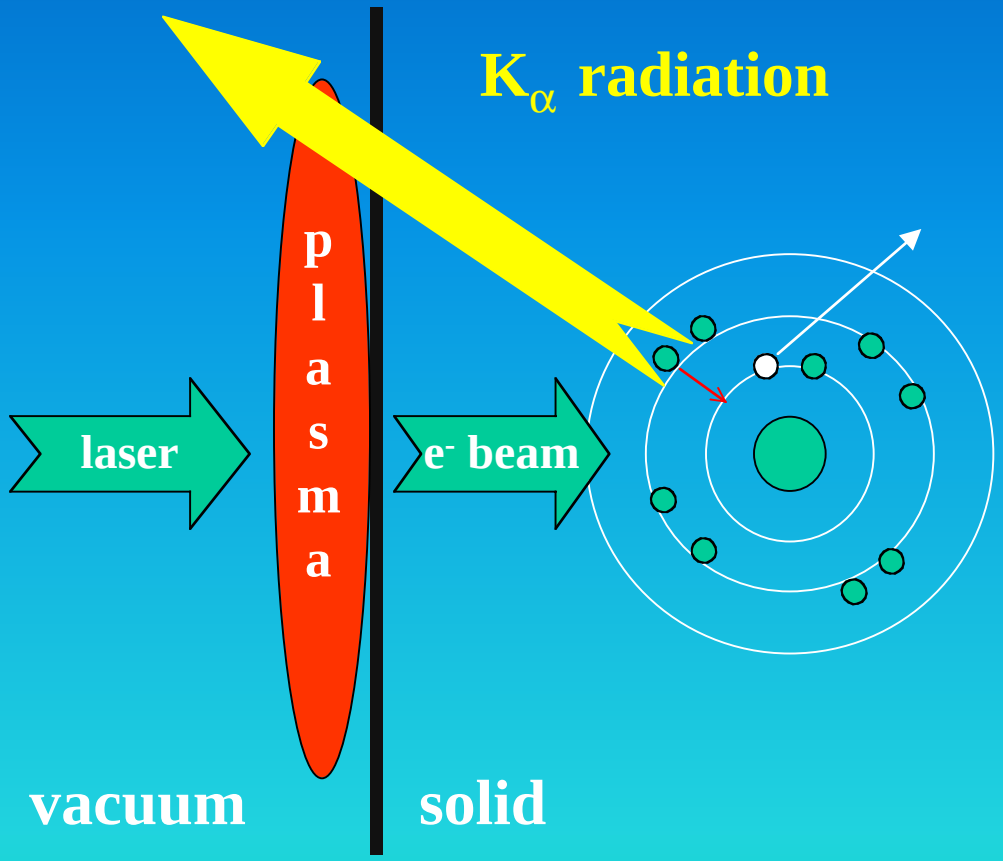

M. Murnane *et al* Phys. Rev. Lett. (92)
A. Rousse *et al*, Phys. Rev. E 50 (3) 2200 (94)
S. Bastiani *et al*, Phys. Rev. E 56 (6) 7179 (97)

How many photons ? (100 fs, several keV, 10 Hz)

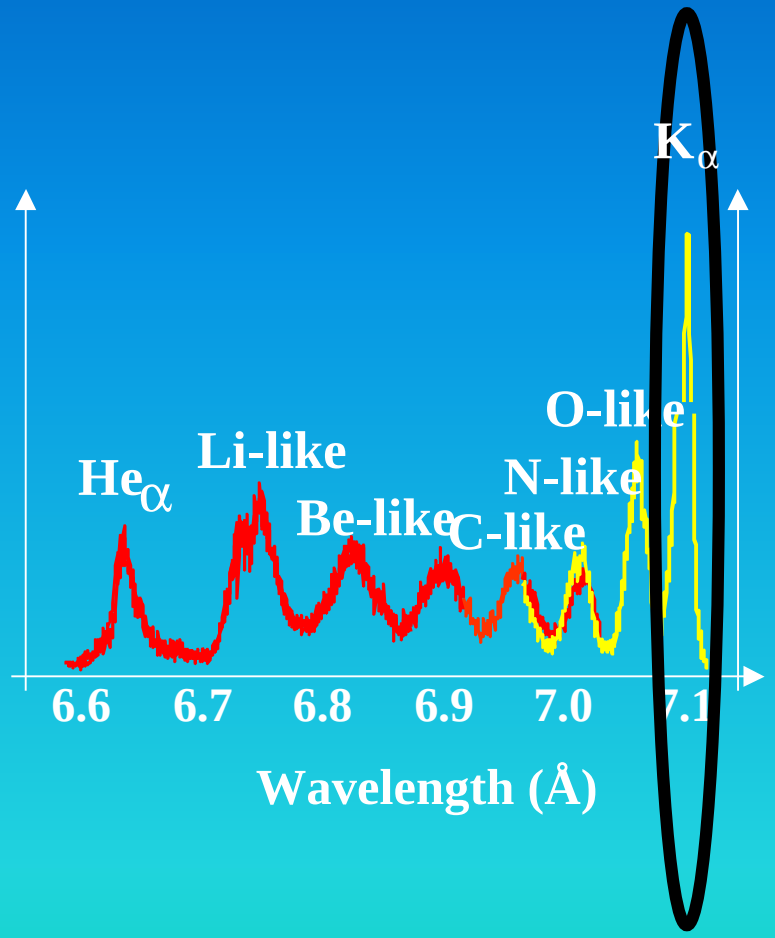

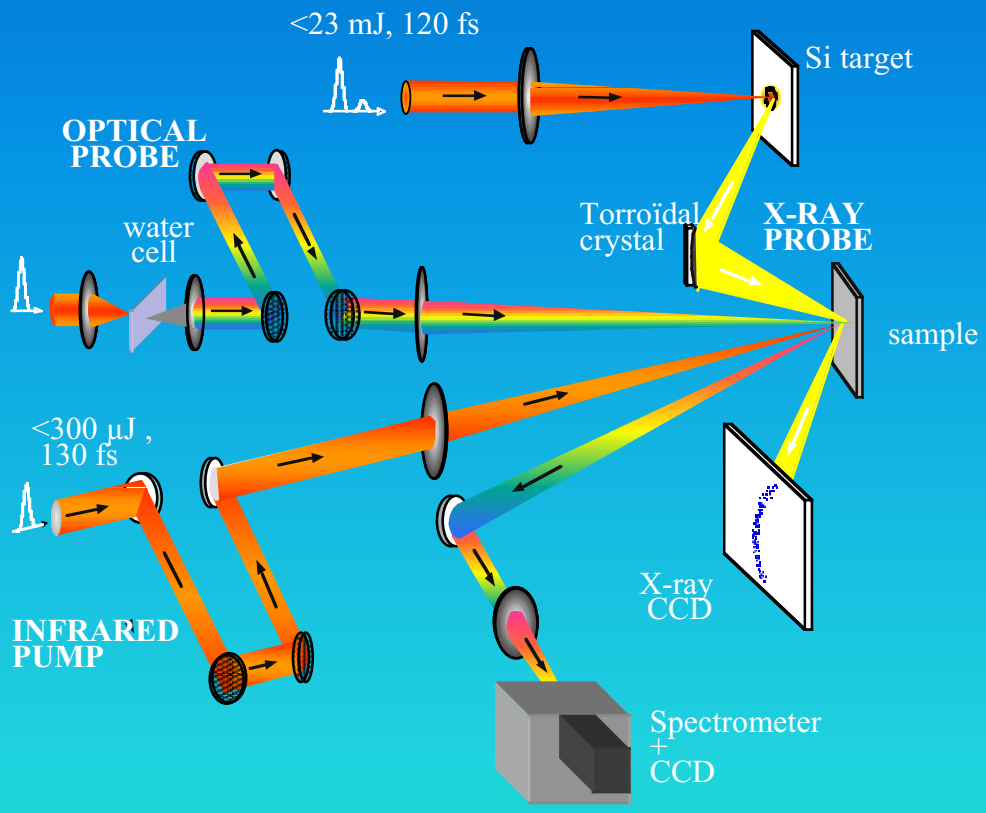

onto the sample
10^5 ph/s/shot/2° 10 Hz

LOA

Bottlenecks of ultrafast X-ray experiments

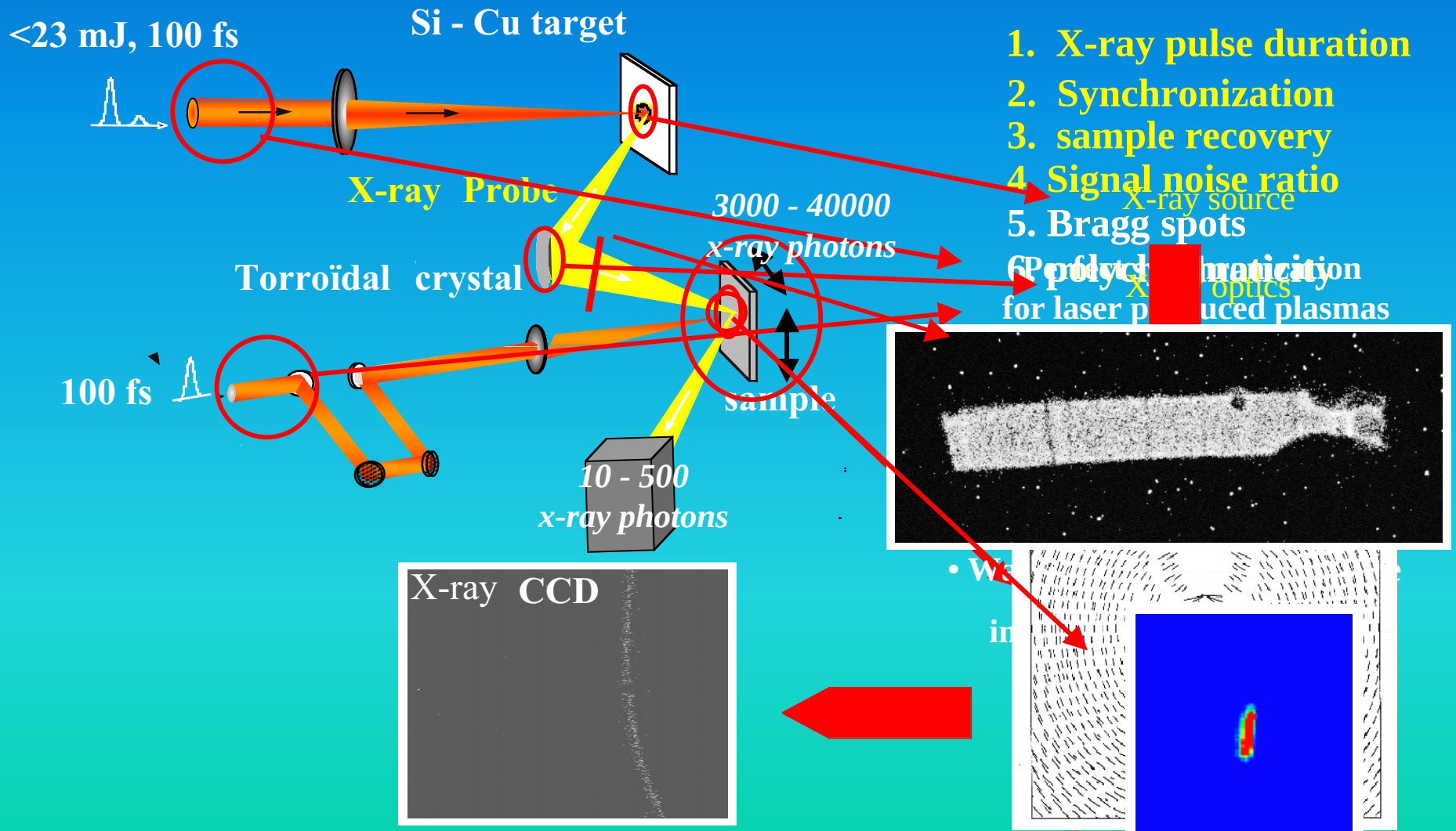

How can we increase the x-ray flux onto the sample, while keeping the pulse duration short (100 fs) ?

10^5 --> 10^9 photons

1) Increase the repetition rate

10 Hz --> 1 kHz: x 100

2) design new (expensive) x-ray optics

collect more & recollimate x 100

3) Change the process of x-ray production

Ultrafast X-rays with laser-plasmas

1) Why ?

2) The existing source

3) pionneering application experiments

4) The next source

Femtosecond x-ray diffraction: Demonstration

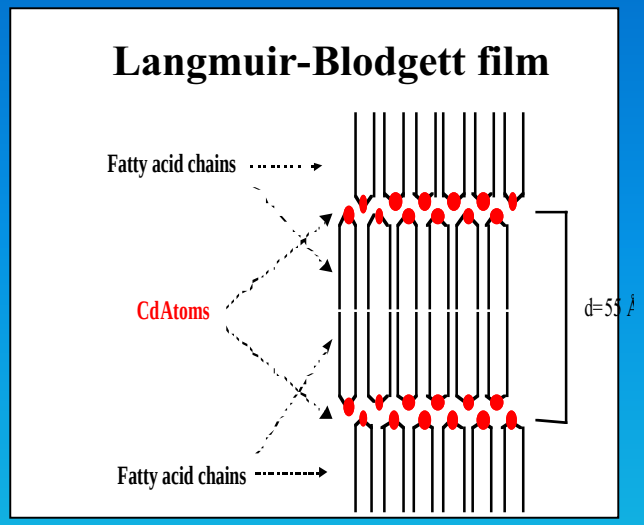

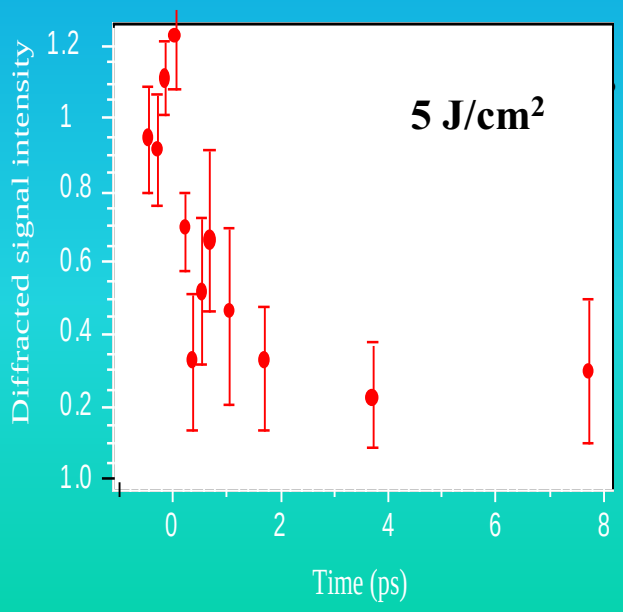

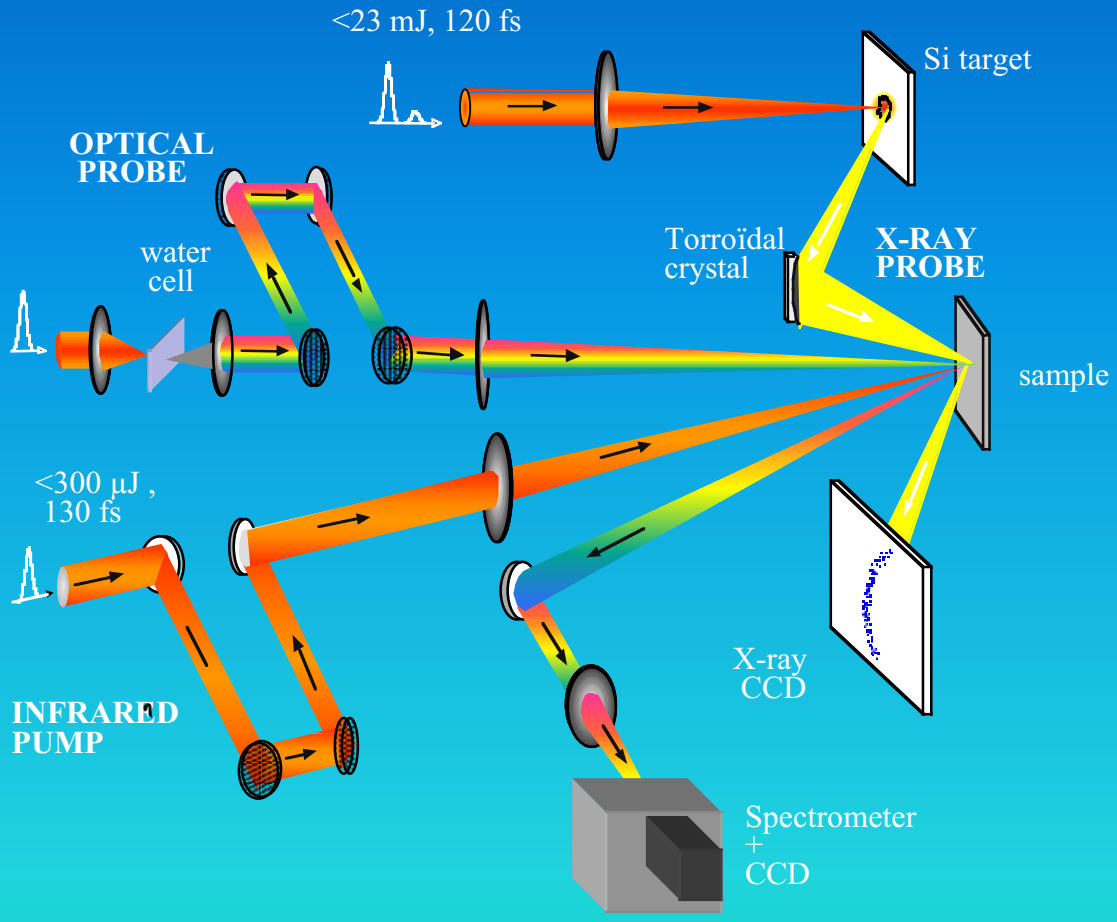

C. Rischel, A. Rousse, I. Uschmann, *et al*

Nature 390, 490 (1997)

Femtosecond x-ray diffraction: Applications

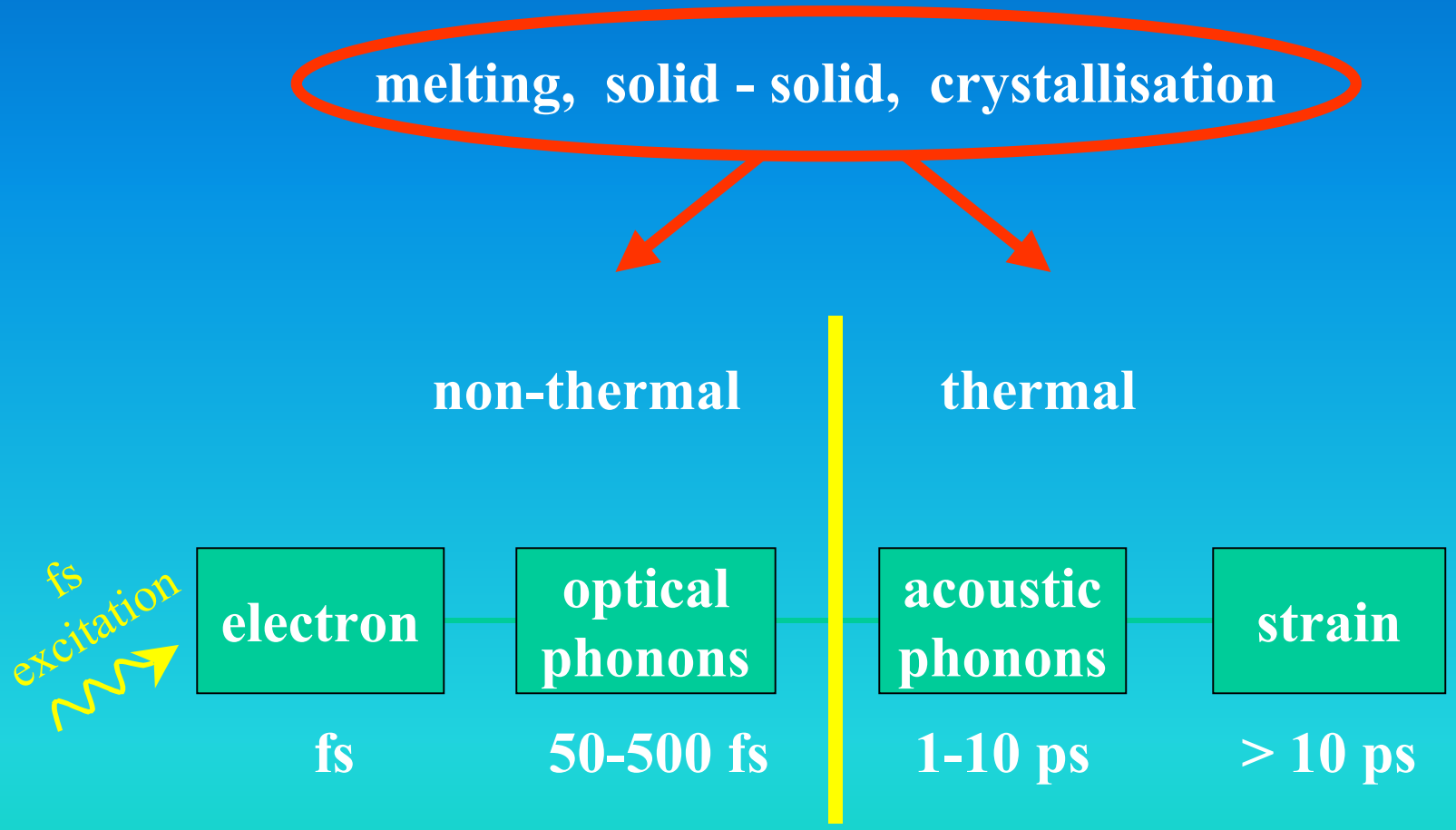

L.O.A

ENSTA

POLYTECHNIQUE

CNRS

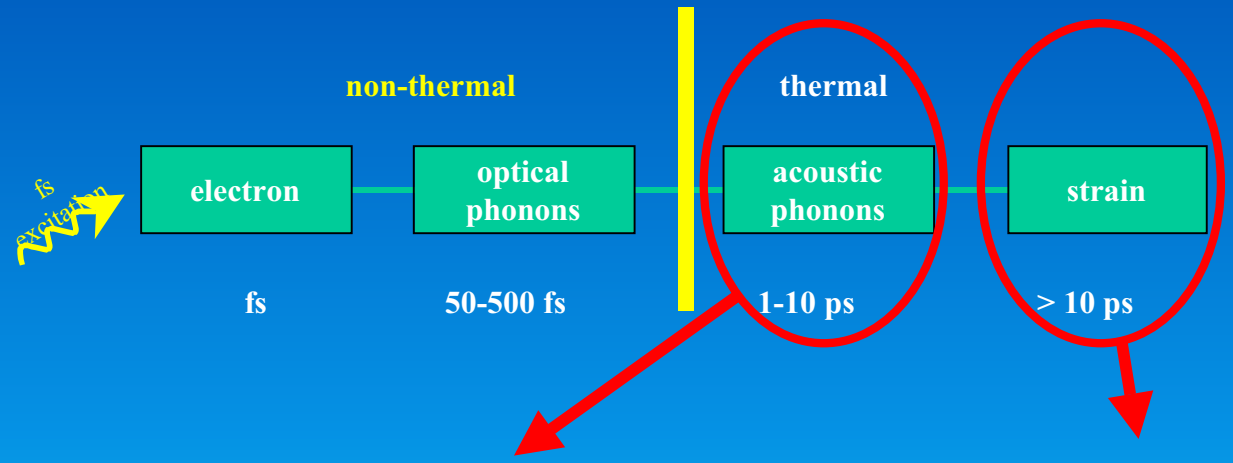

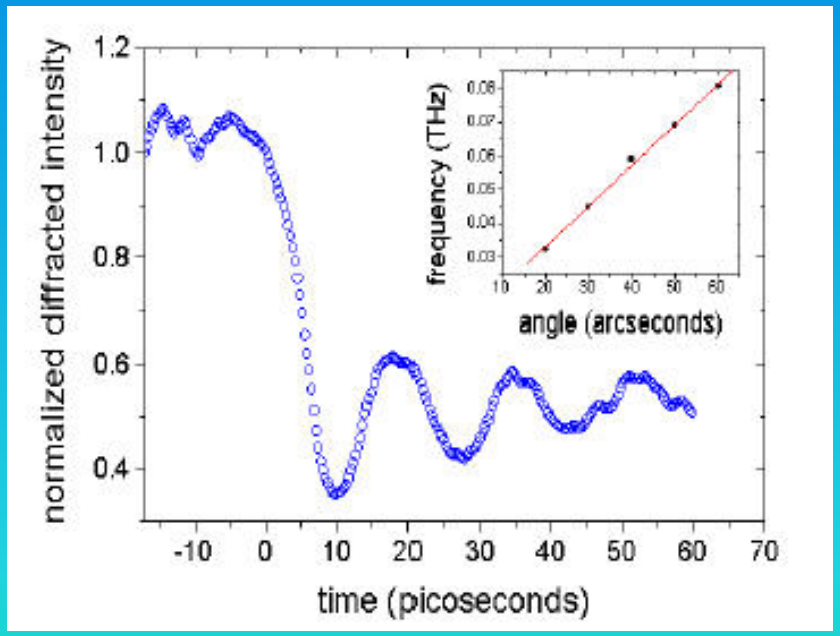

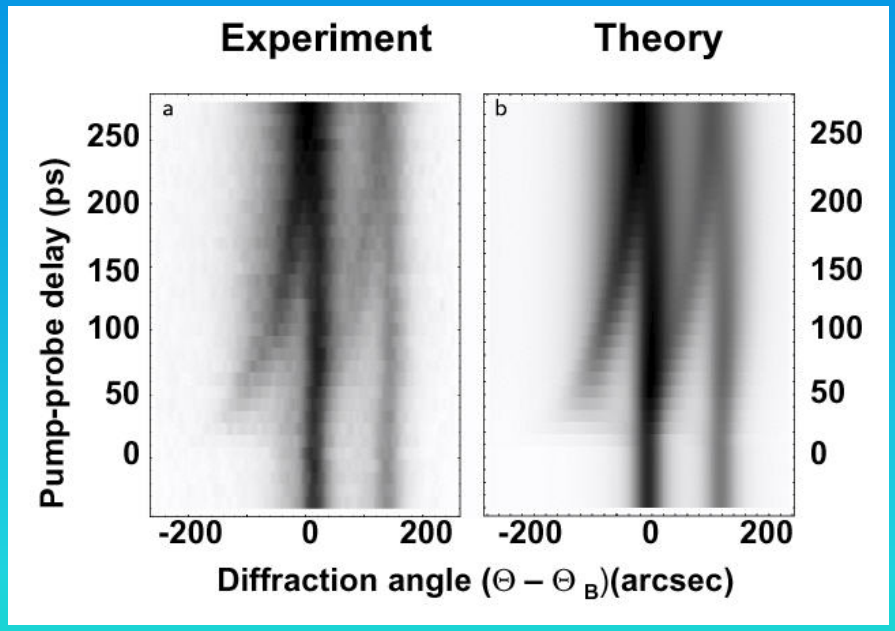

Lindenberg et al, PRL'2000

Rose-Petruck et al, Nature'1999

Ultrafast Solid-Liquid phase transition

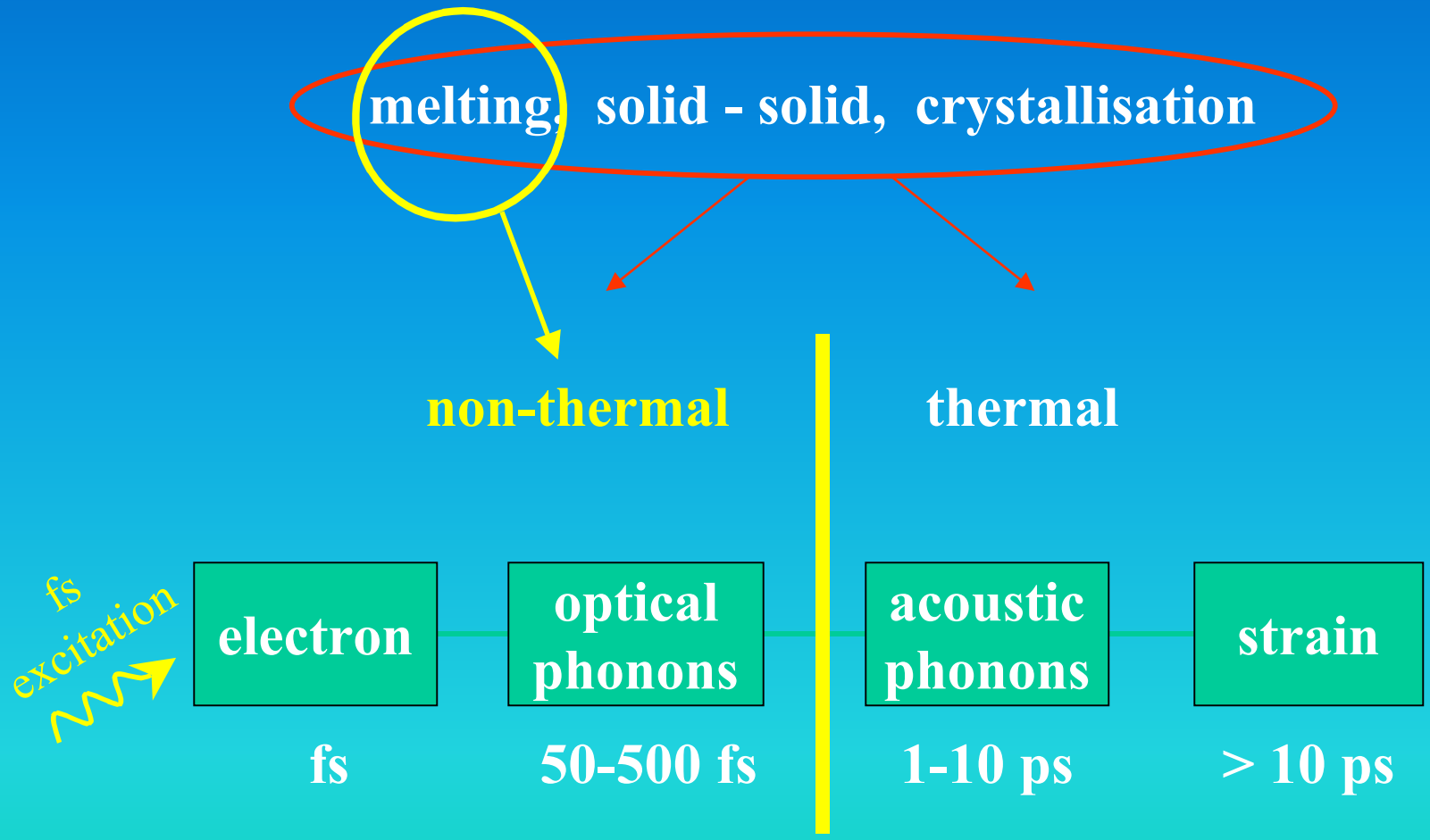

Ultrafast Solid-Liquid phase transition

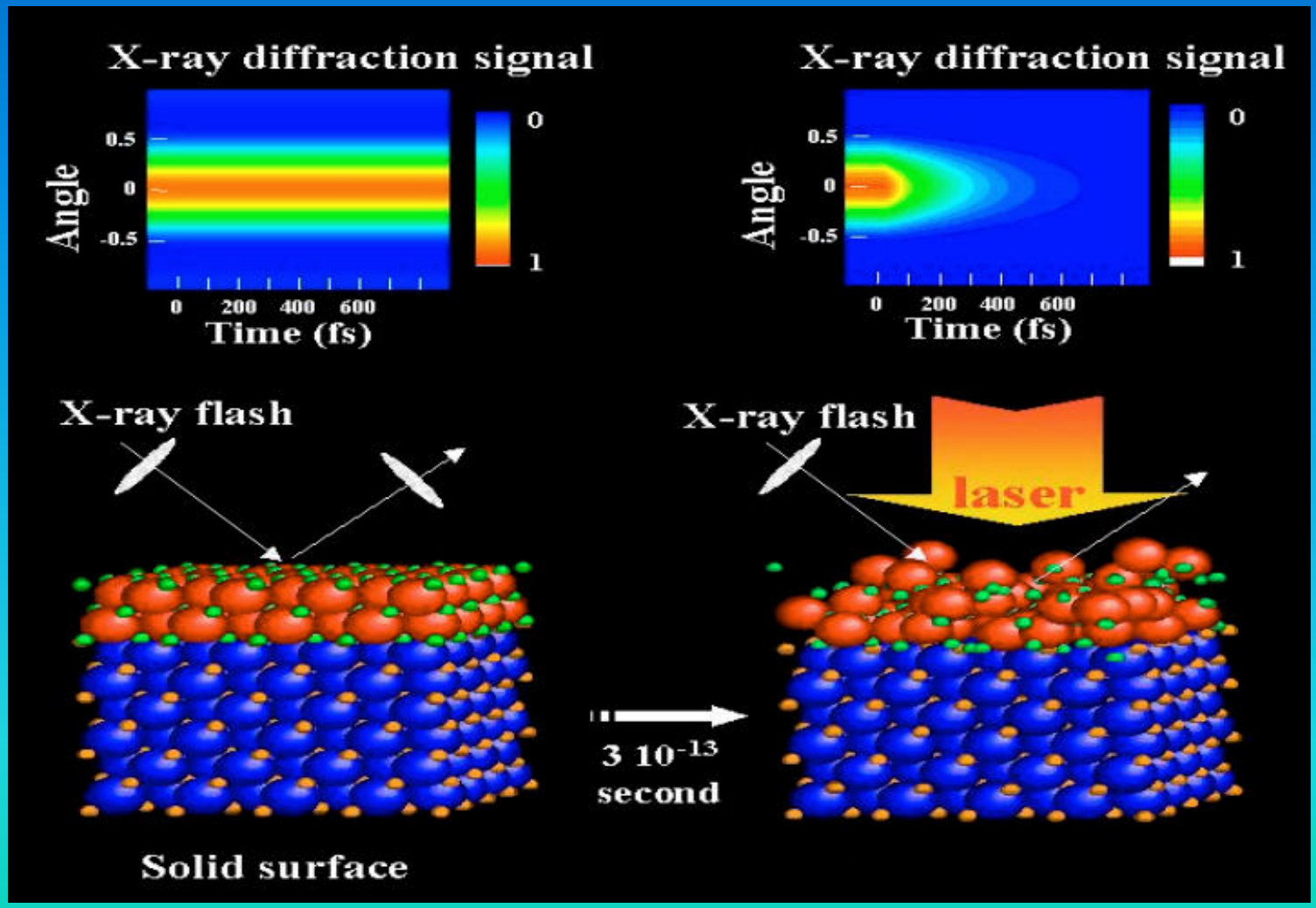

A. Rousse et al, Nature 2001 (LOA)

Non-thermal melting of semiconductors

10 % of the electrons
to the conduction band

↓

Band collapses to zero

↓

Destabilisation of the lattice

↓

Atomic desordering

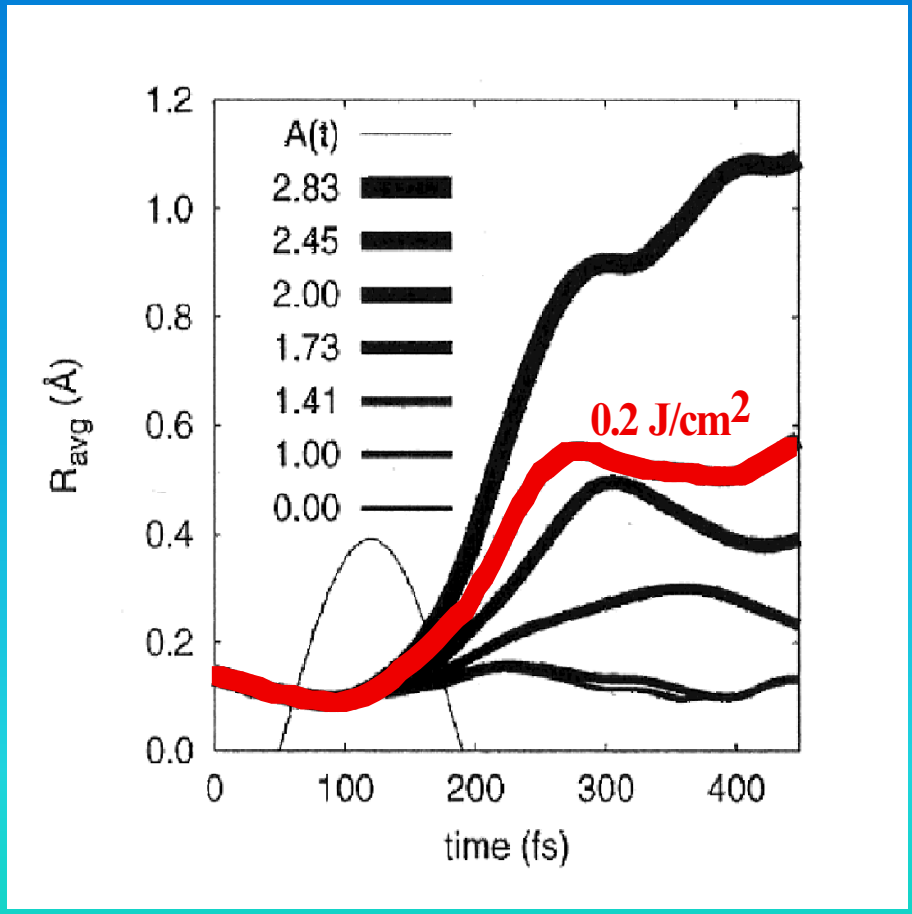

The X-ray probe signal drops by 18% in 350±100 fs : --> non-thermal atomic melting on 600 Å

L.O.A

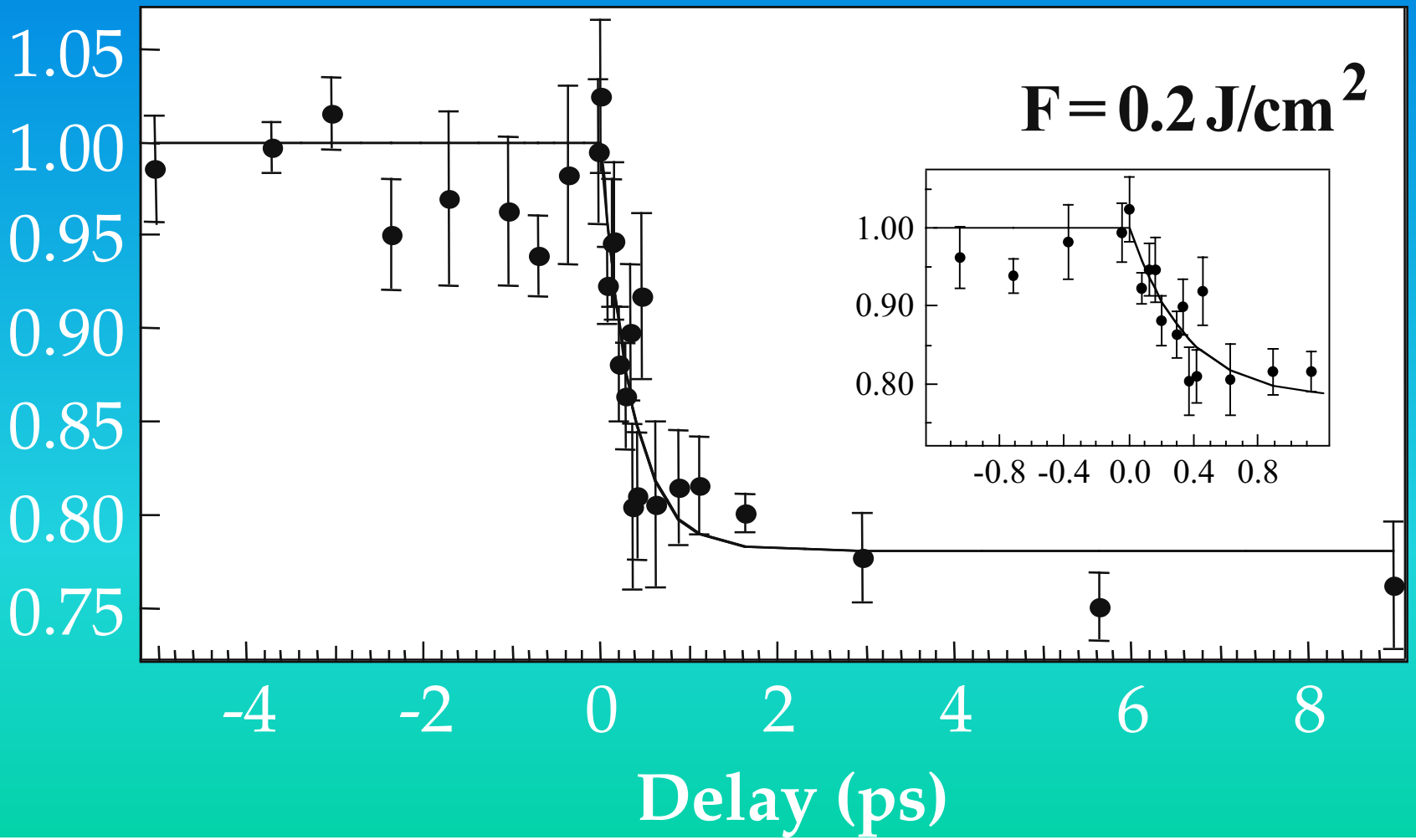

Non-thermal Melting of InSb:
- duration
- thickness

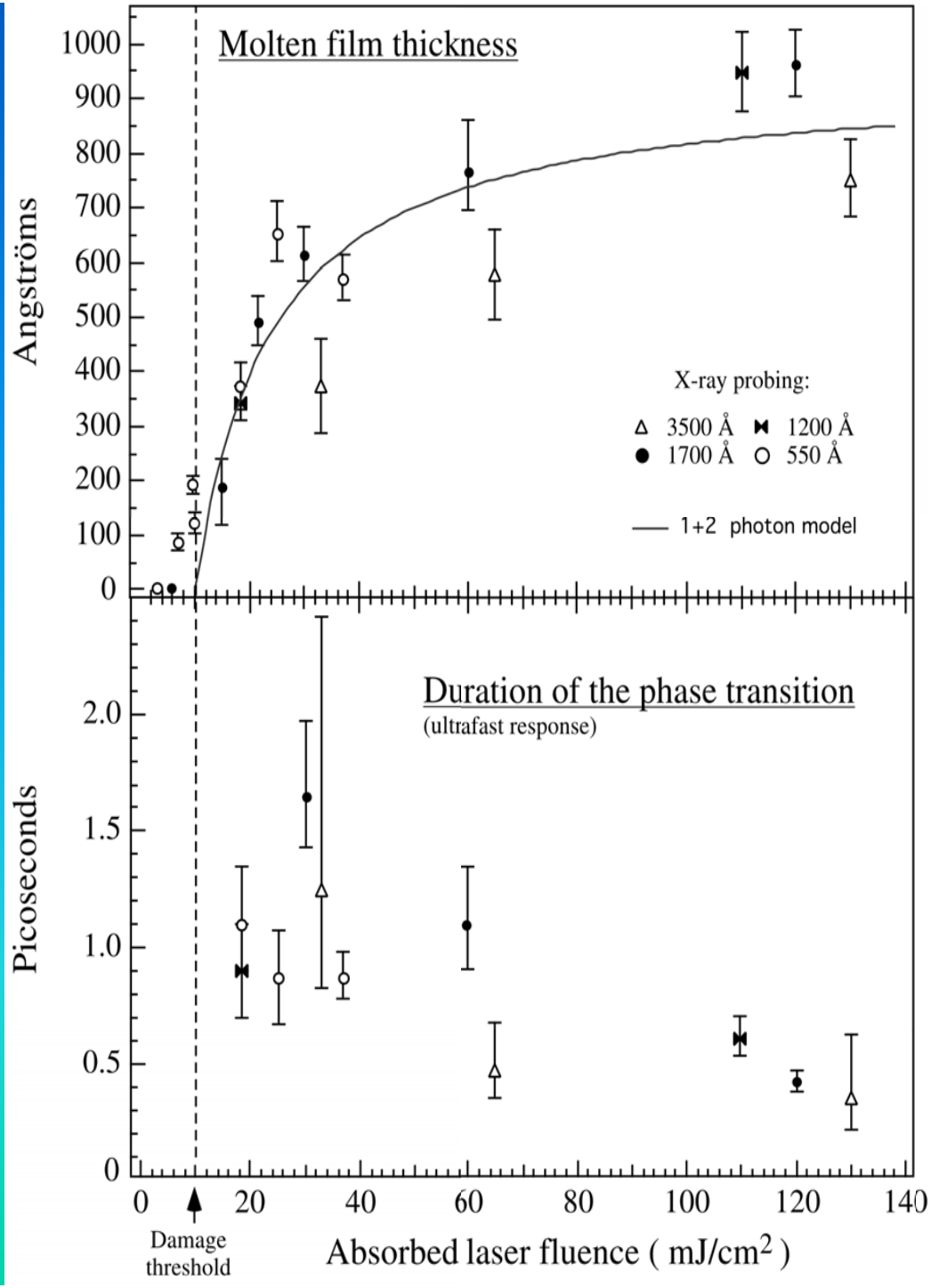

Optical phonons

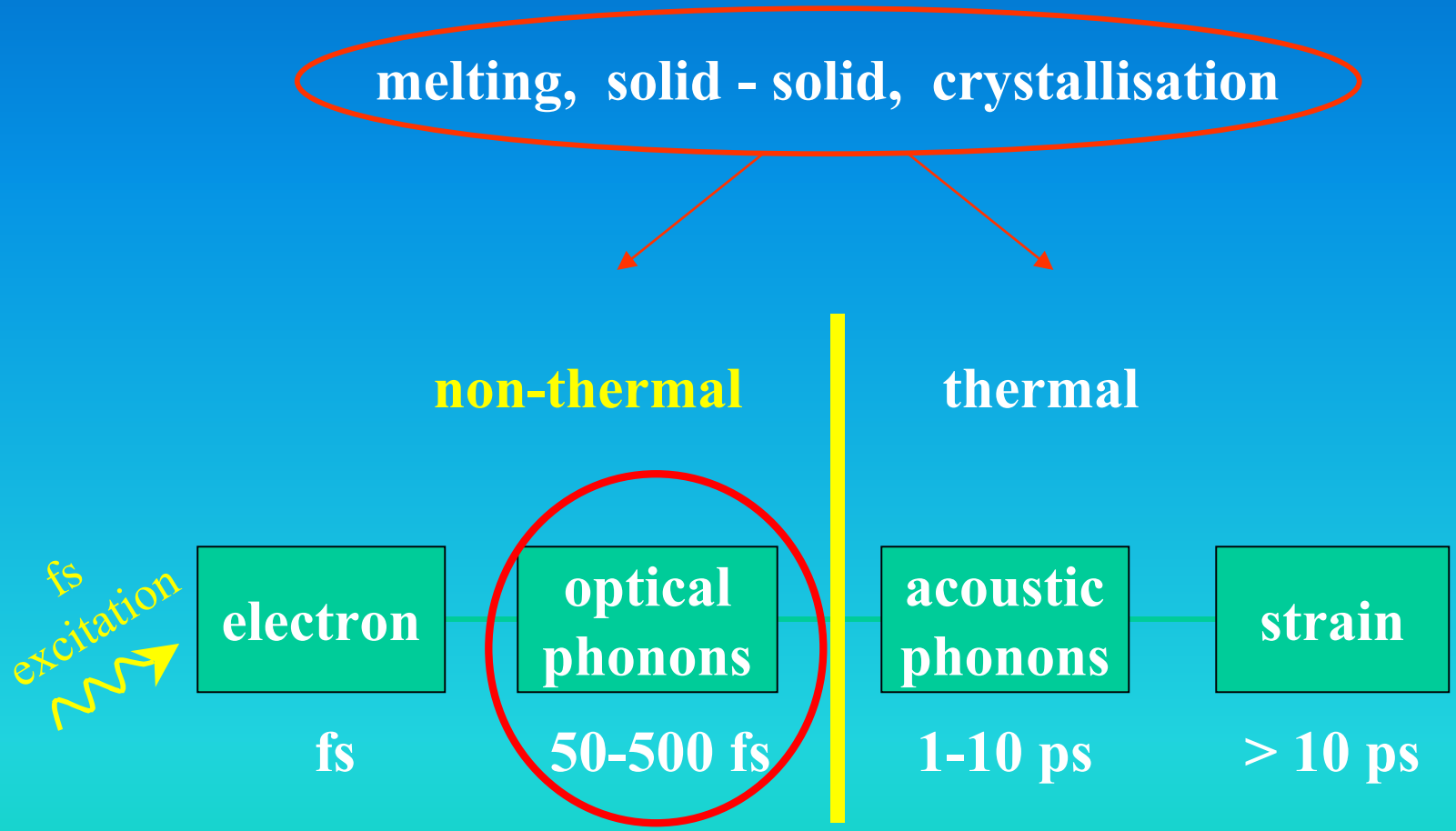

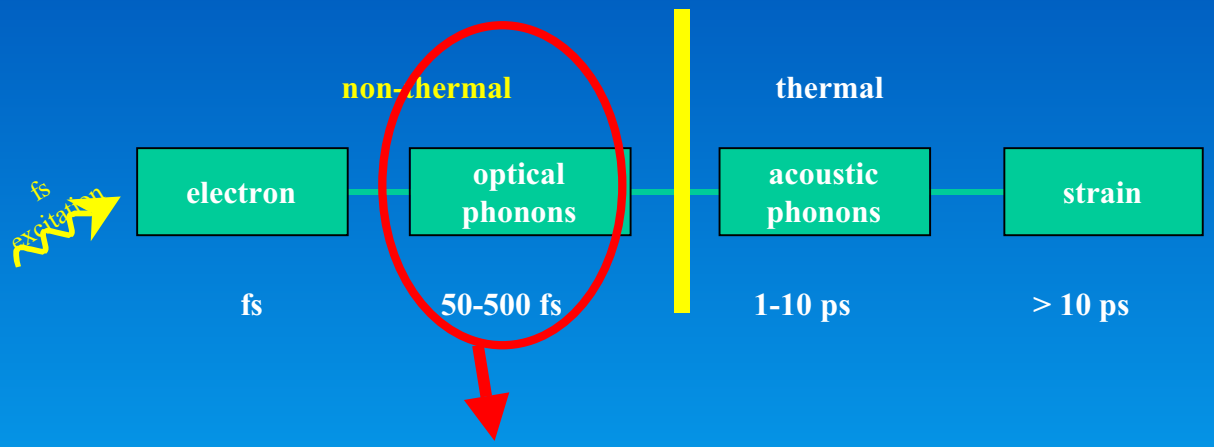

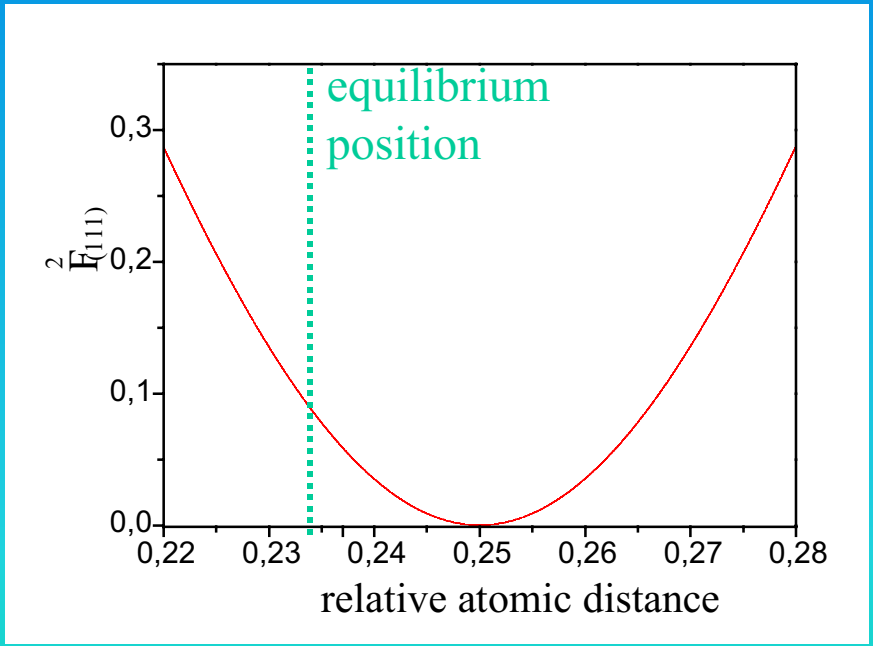

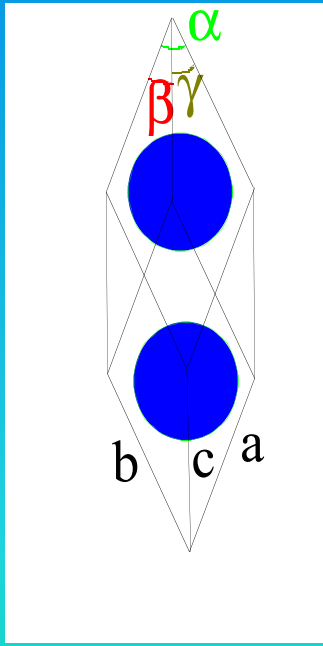

Essen, Sokowloski et al Nature Mars 2003
LOA, Boschetto et al, submitted

Simulation of time-dependent rocking curve from the *(1 1 1)*-plane in presence of coherent optical phonon of amplitude 0.013 Å in 12.5 nm Bismuth film

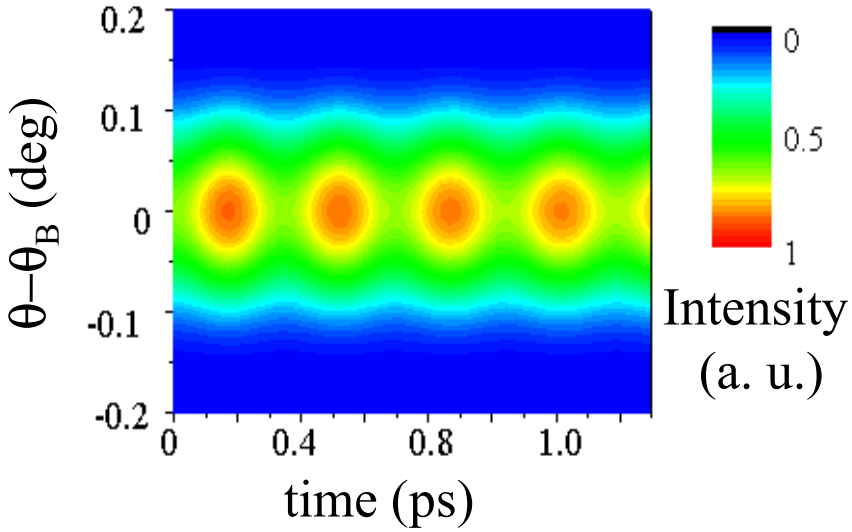

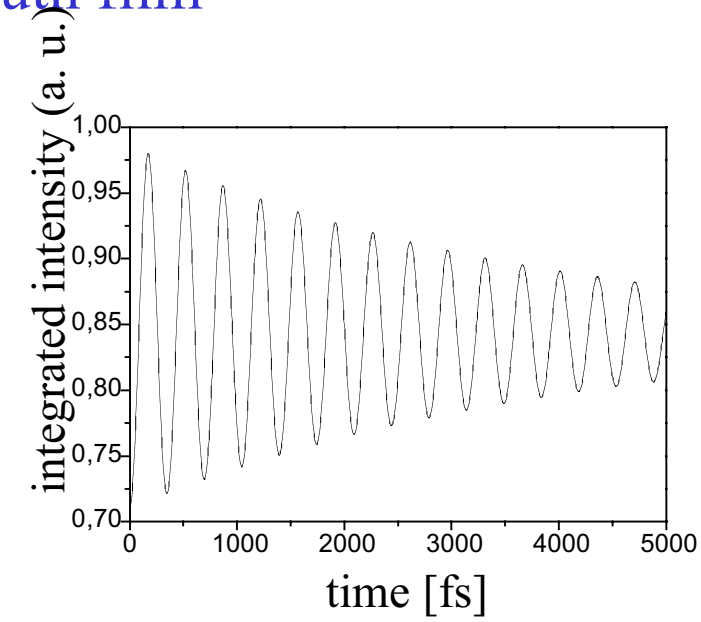

The change in integrated intensity is about 15 %

Coherent atomic displacement in Bi single crystal

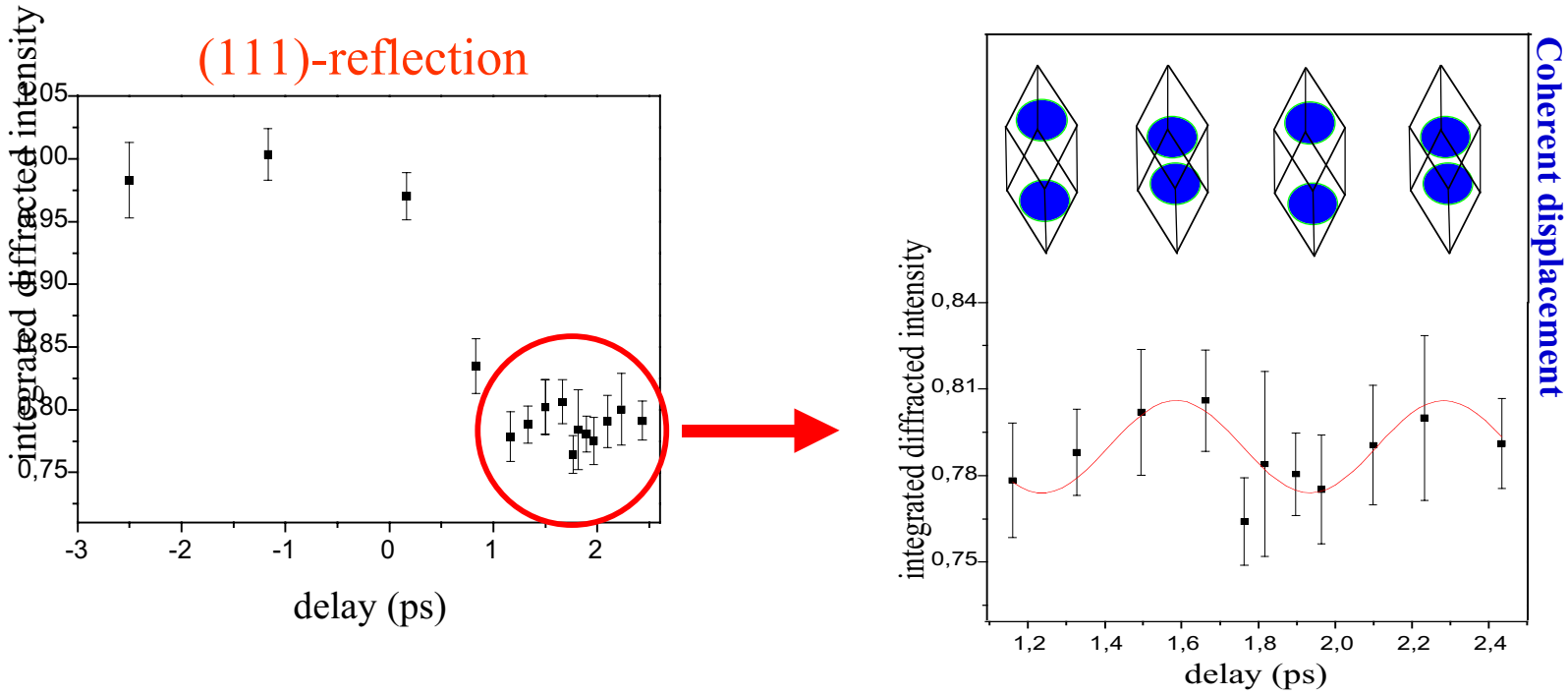

LOA, D. Boschetto et al, submitted

Goal: femtosecond crystallography

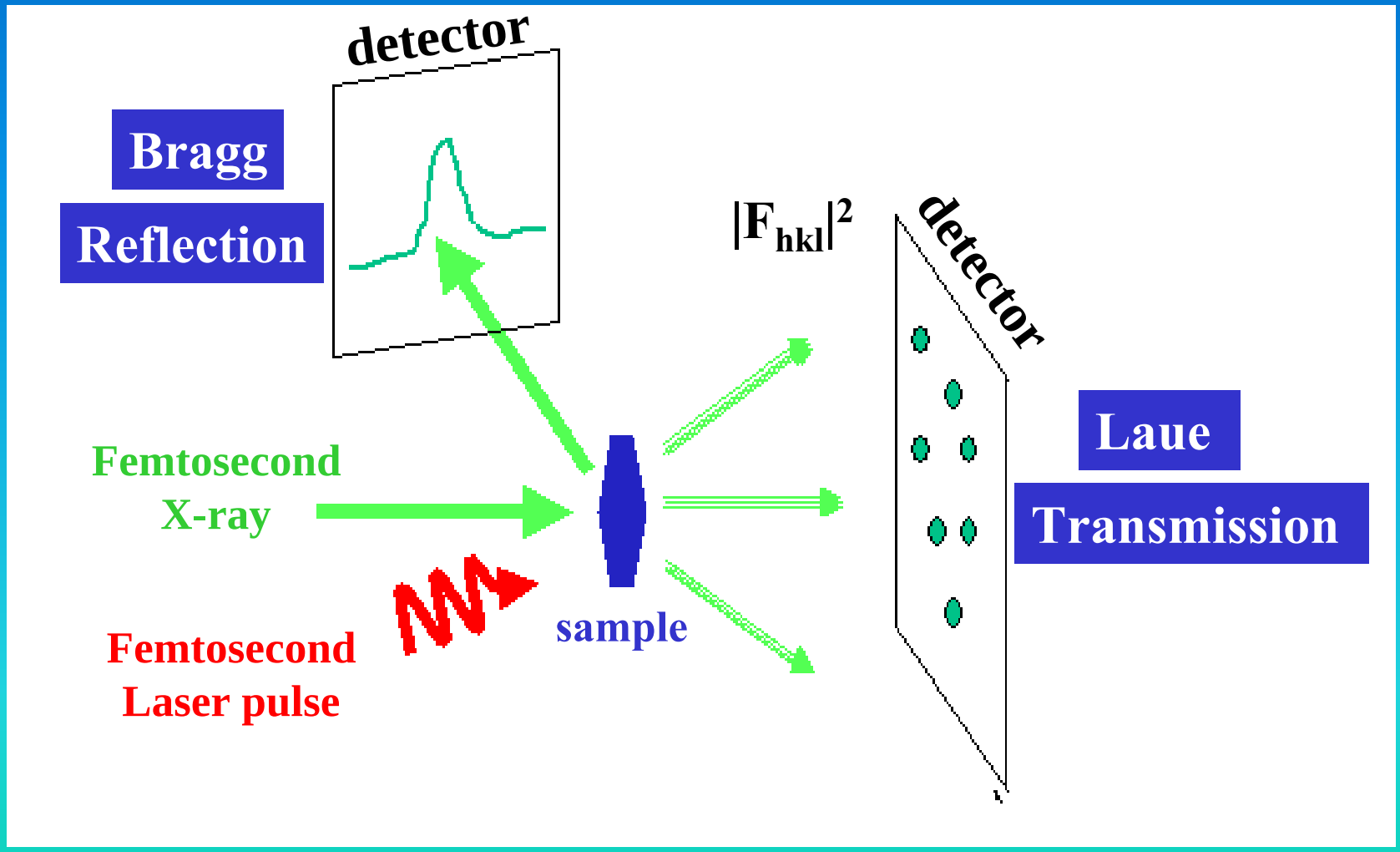

L.O.A

ENSTA

POLYTECHNIQUE

1) Transmission geometry

Standard Laue Technique:
Polychromatic and Collimated Beam

Pseudo-Laue Technique:
Monochromatic and divergent beam

2) The phase problem

Structure factor $|F_{hkl}|^2$

$$F_{hkl} = \sum f_j \, e^{[2\pi i \, (hxj + kyj + lzj)]}$$

xj,yj,zj = coordinates of the atom f_j = atomic scattering factor

j^{th} atom of the unit cell

Pseudo-Laue Technique: Monochromatic and divergent beam

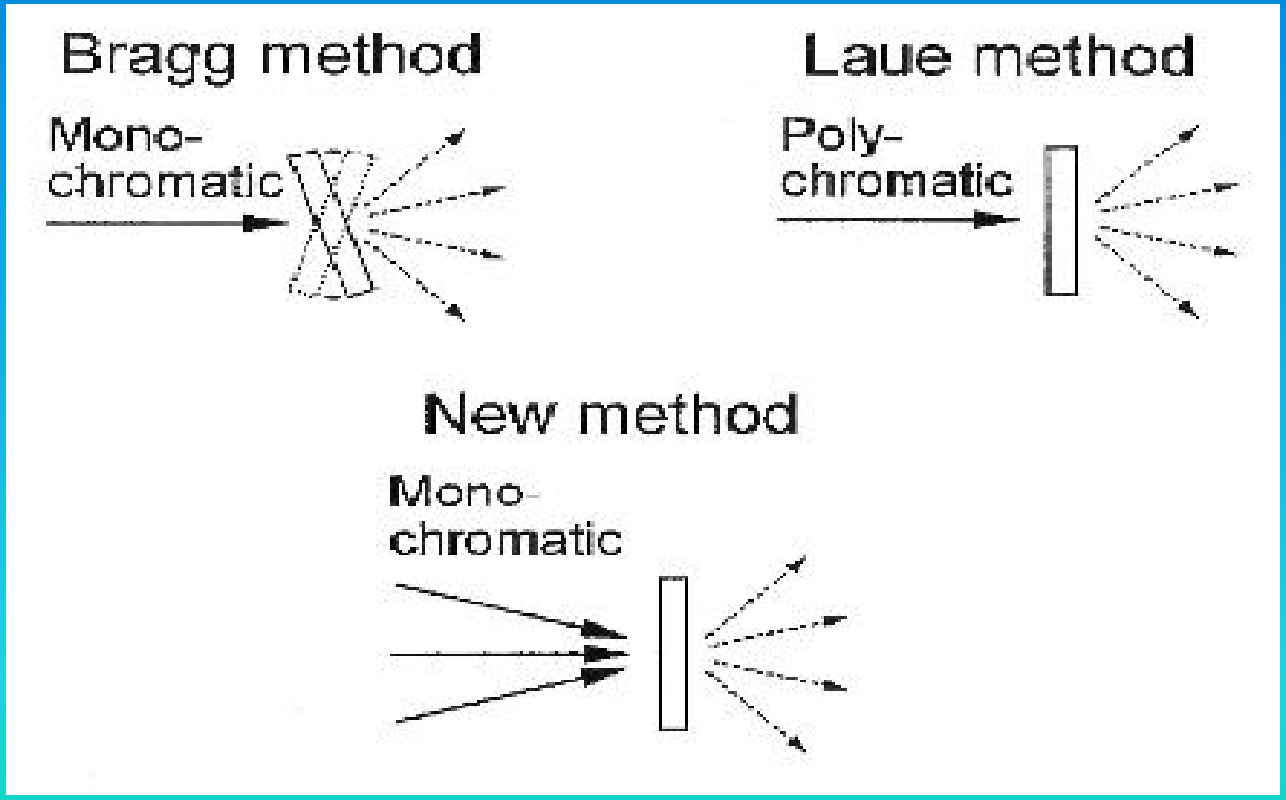

Experimental set-up for testing the divergent geometry in transmission configuration with standard X-ray tube

performed at Institut fuer Optik und Quantenelektronik, Jena, Germany

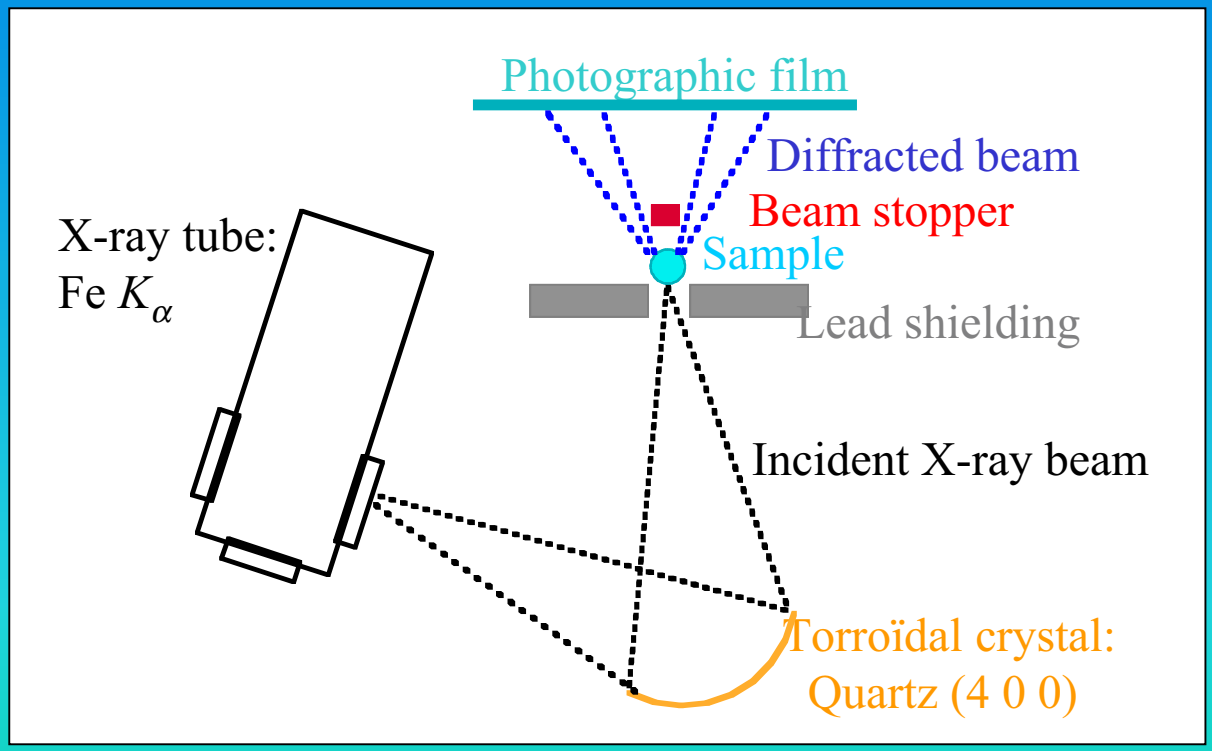

LOA

ENSTA

POLYTECHNIQUE

CNRS

Protein crystal
Lysosyme

Exposition time: 12 h

Incident photon/sec:

$1.5 * 10^6$

Plasma X-ray source:
X-ray photons / sec:
$4 * 10^4$

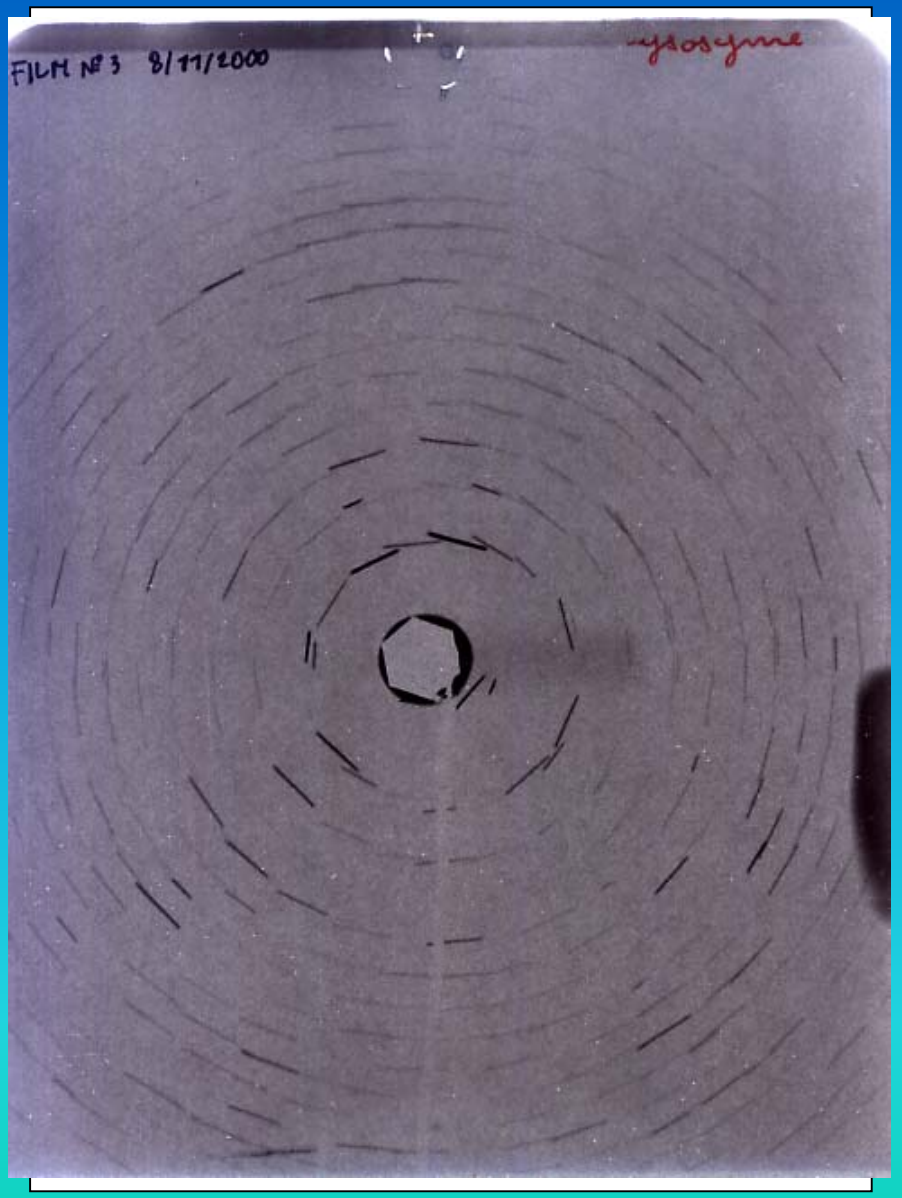

L O A

ENSTA

POLYTECHNIQUE

CNRS

Experimental set-up for testing the divergent geometry in transmission configuration with the plasma X-ray source

performed at Laboratoire d'Optique Appliquée, Palaiseau, France

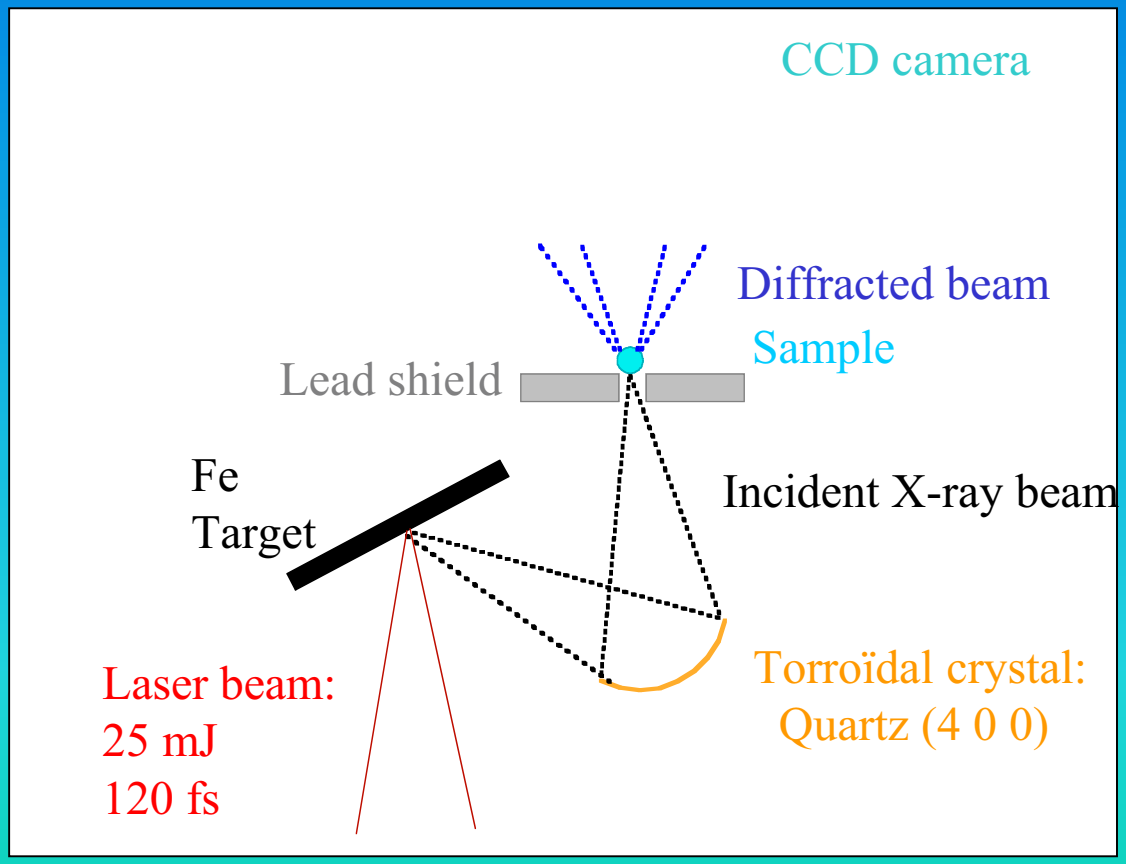

L O A

ENSTA

POLYTECHNIQUE

CNRS

Protein crystal
Lysosyme

Exposition time: 2 h

X-ray photons / pulse: 4000

repetition rate: 10 Hz

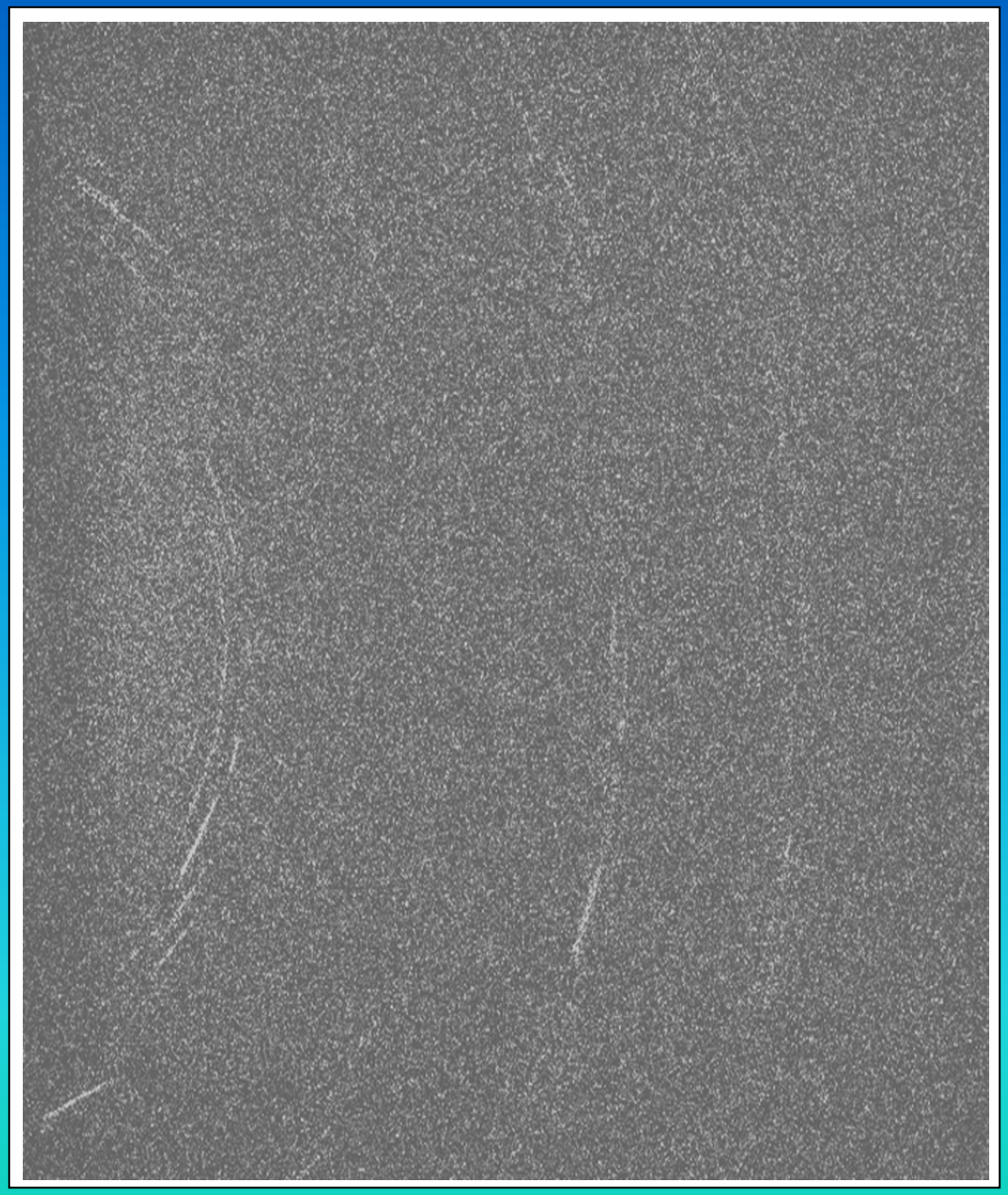

L O A

ENSTA

POLYTECHNIQUE

CNRS

Ultrafast X-rays with laser-plasmas

1) Why ?

2) The existing source

3) pionneering application experiments

4) The next source

Synchrotron (20 ps) + ultrafast detector (1 ps)

ESRF, ...

Synchrotron + slicing (300 fs)

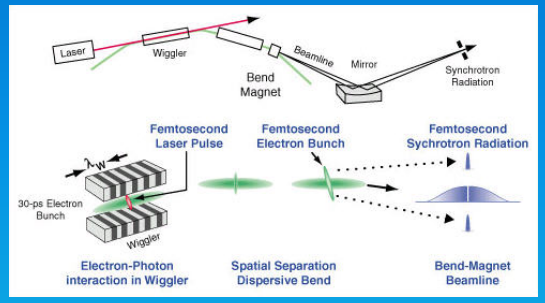

ALS, SLS, Soleil,Bessy ...

LINAC + undulator (100 fs)

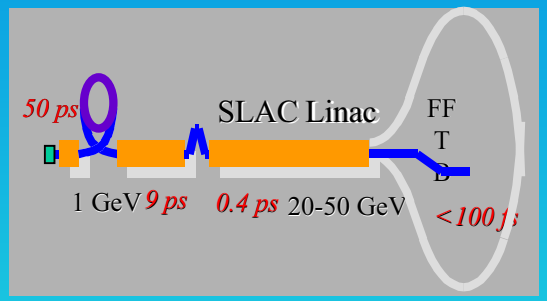

Stanford

X-FEL (100 fs)

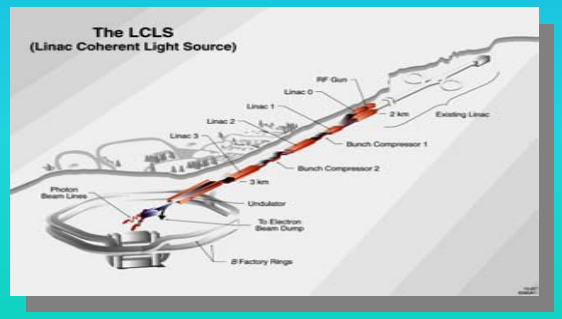

Stanford, Hamburg, ...

Thomson scattering (100 fs)

?

LLNL

New laser-plasma x-ray source

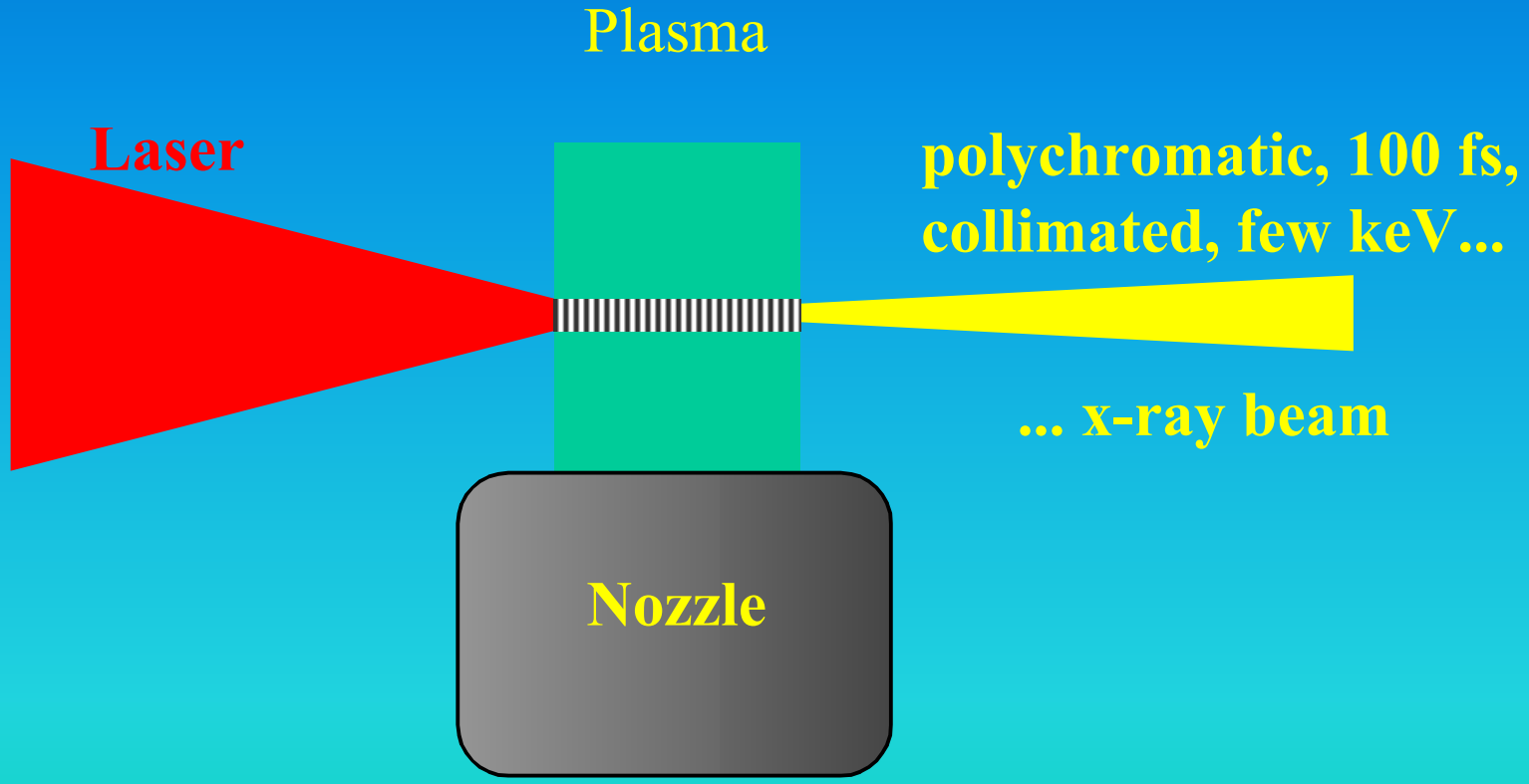

New laser-plasma x-ray source (1)

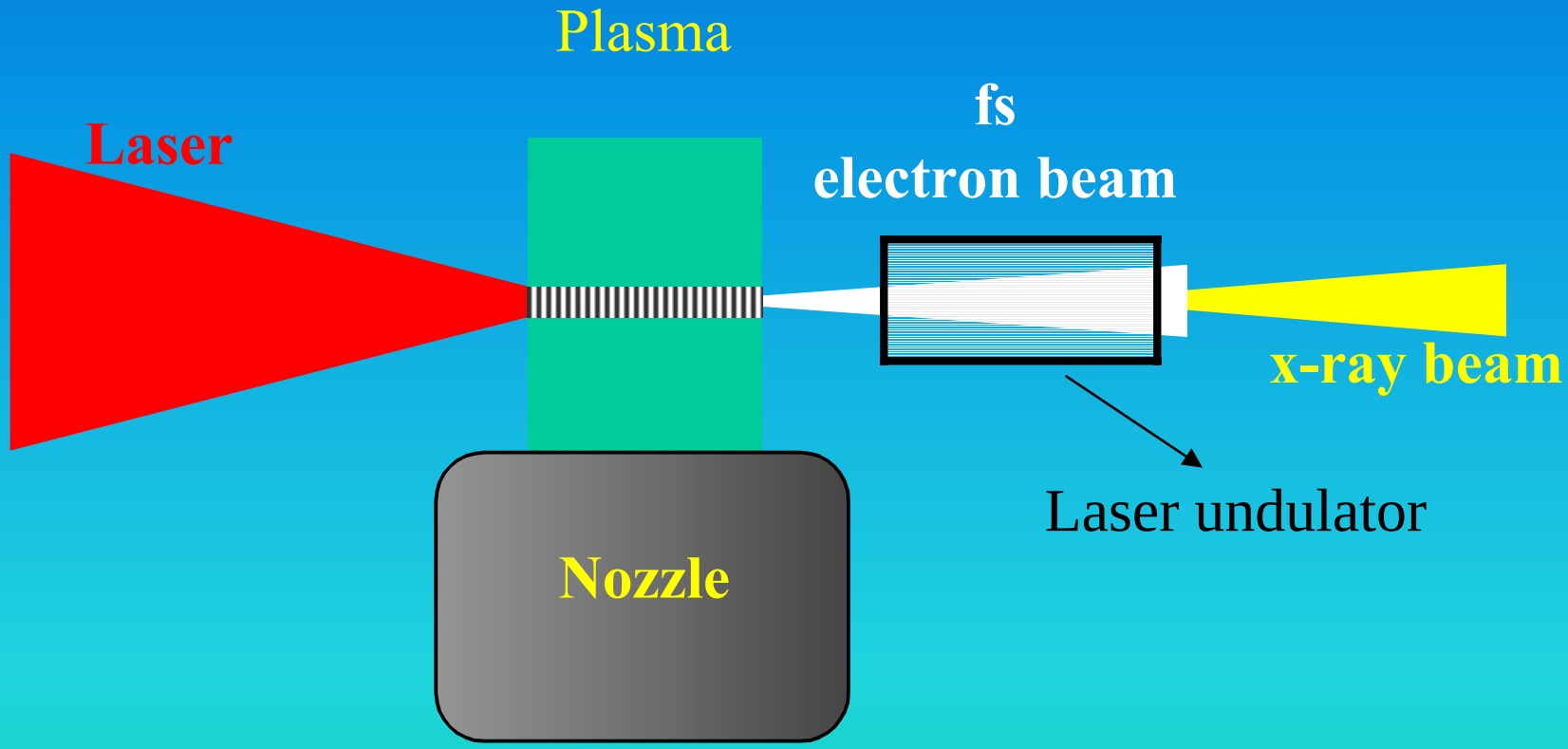

Wakefield: electron beam up to 200 MeV

Total Charge : 5 nC

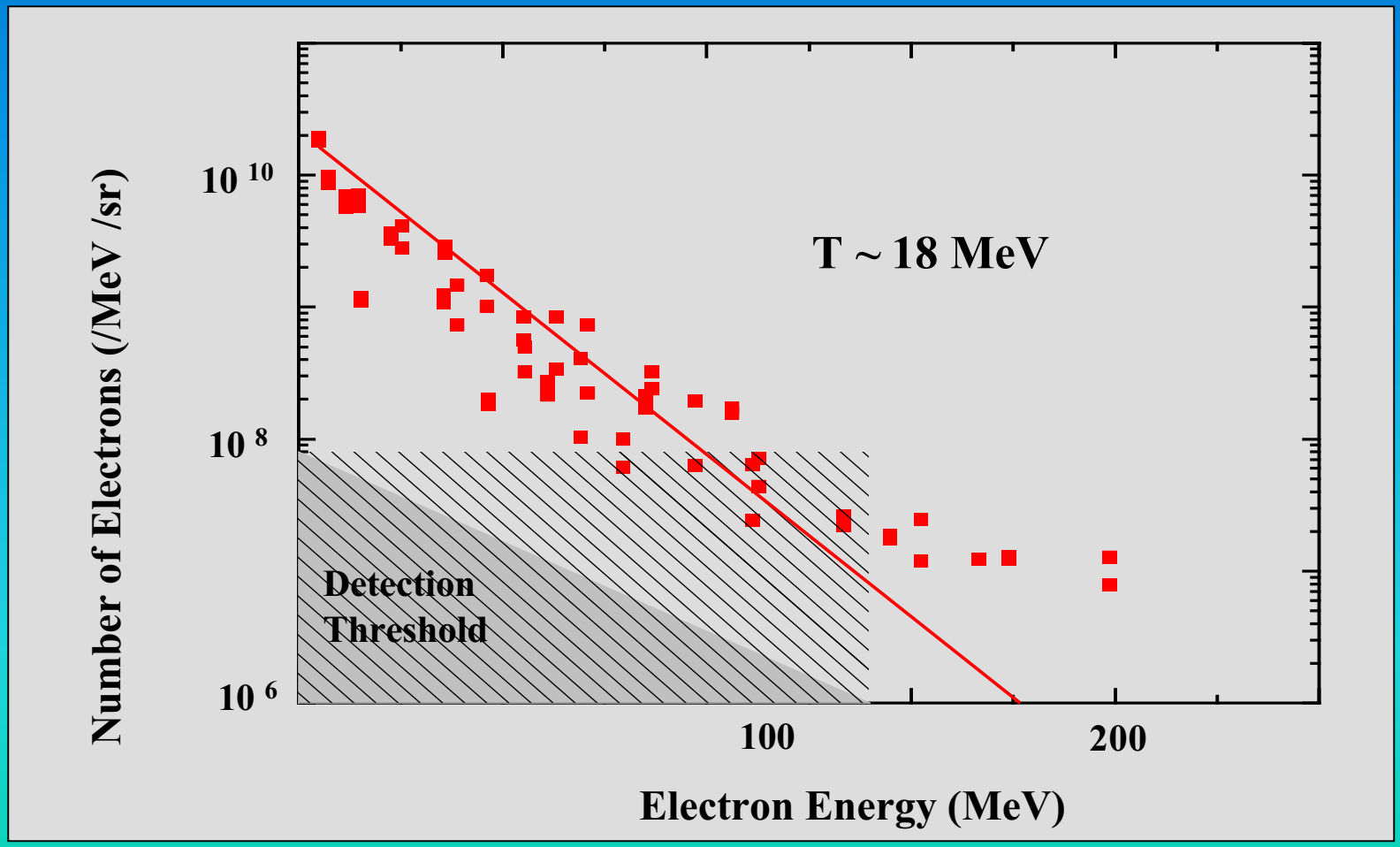

Laser-based synchrotron X-ray radiation
[*non-linear thomson scattering*]

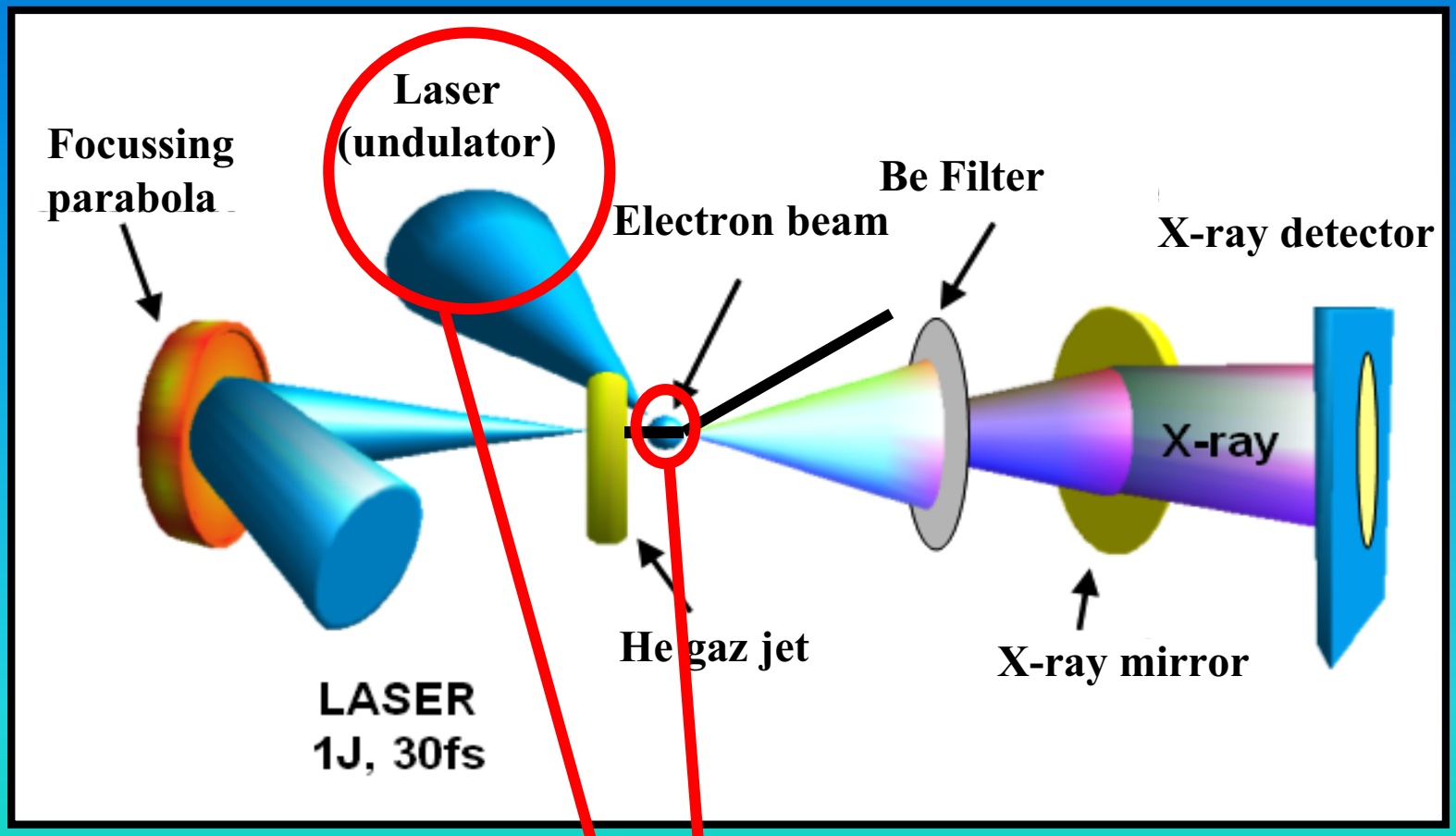

Accelerated electrons & laser undulator outside the plasma

Laser-based synchrotron X-ray radiation
[*non-linear thomson scattering*]

Electron Laser beam :
30 fs, 500 mJ, 10 µm

Thomson Laser beam :
30 fs, 50 mJ, 10 µm

Electron spectrum → **X-ray spectrum**

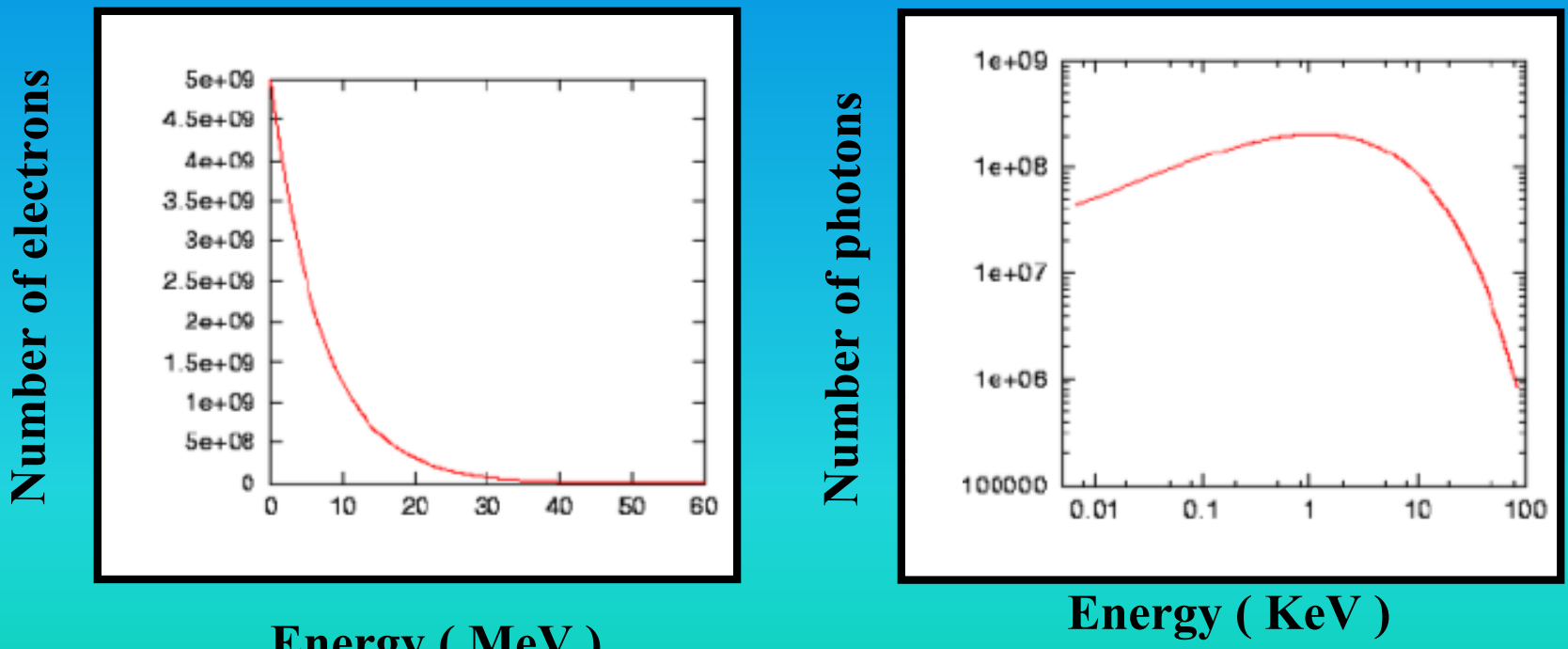

New laser-plasma x-ray source (2)

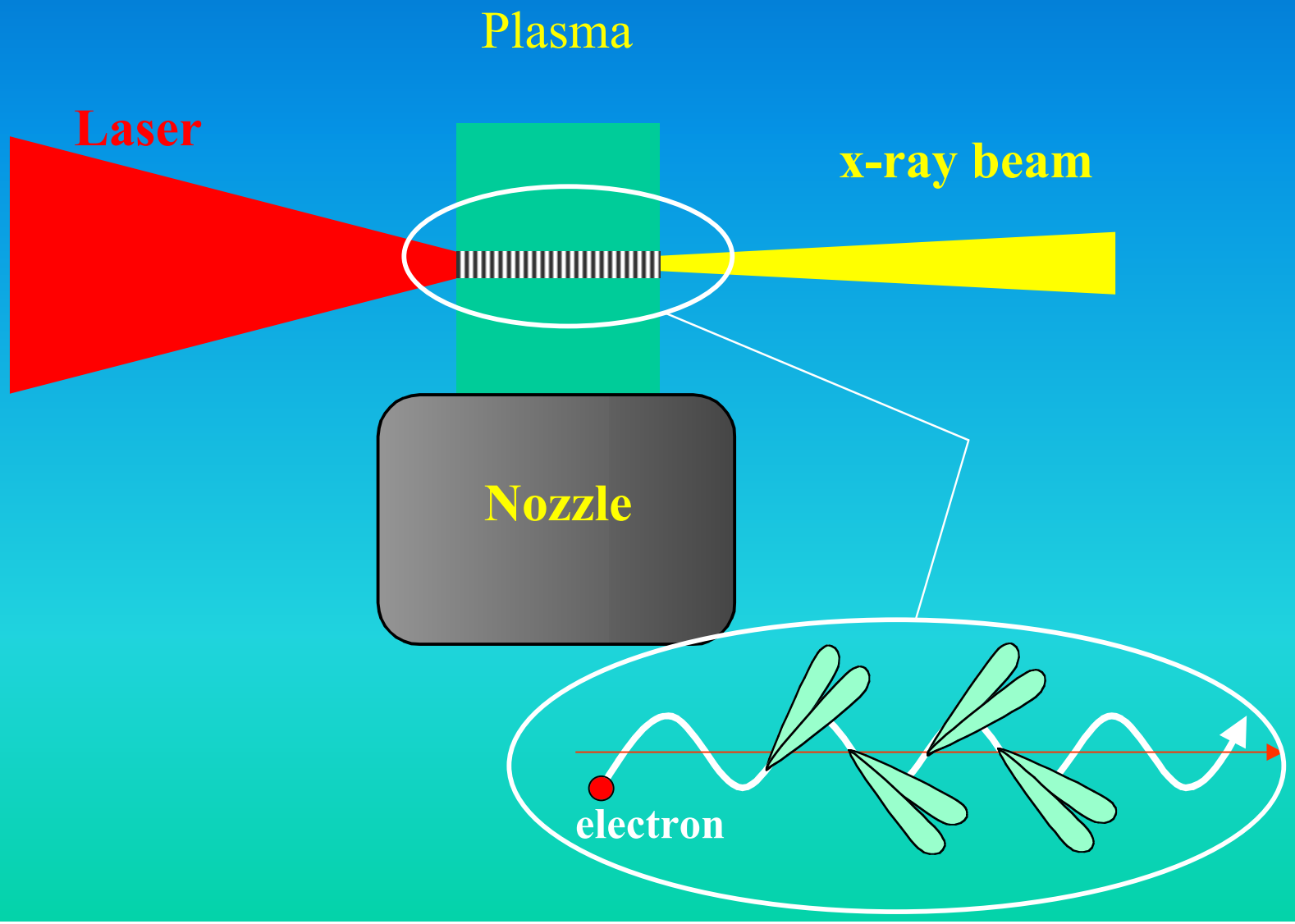

Laser-based technology: synchrotron-like radiation

[*non-linear thomson scattering*]

Conventional Synchrotron

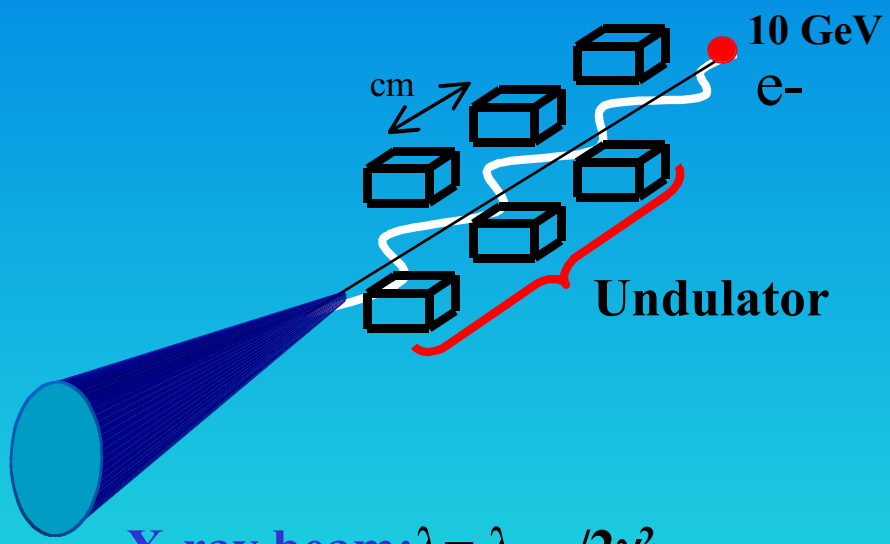

X-ray beam: $\lambda = \lambda_{und}/2\gamma^2$

Laser-based Synchrotron

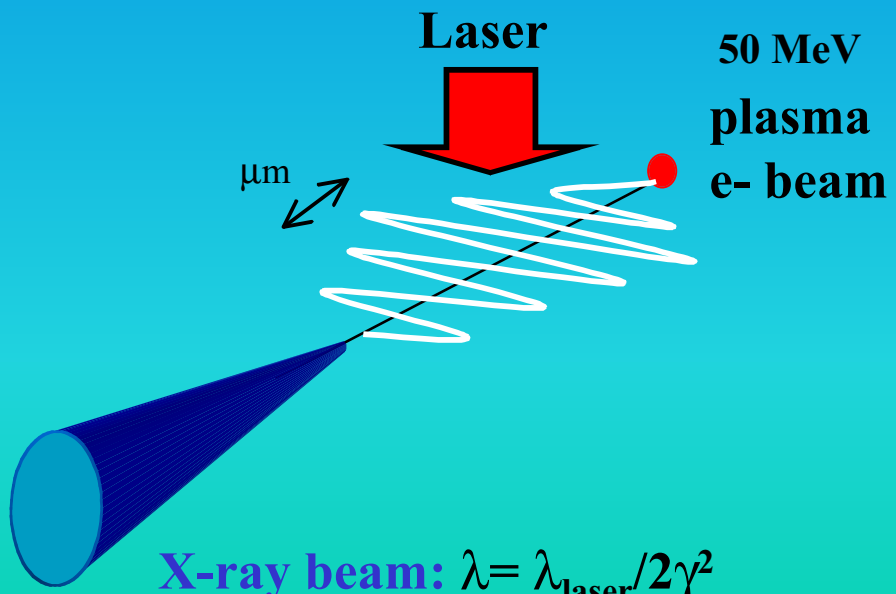

X-ray beam: $\lambda = \lambda_{laser}/2\gamma^2$

Basic formulas of the Larmor radiation

$$\vec{E}(\vec{x},t) = e\left[\frac{\vec{n}-\vec{\beta}}{\gamma^2(1-\vec{\beta}.\vec{n})^3 R^2}\right]_{RET} + \frac{e}{c}\left[\frac{\vec{n}\times\left\{(\vec{n}-\vec{\beta})\times\dot{\vec{\beta}}\right\}}{(1-\vec{\beta}.\vec{n})^3 R}\right]_{RET} \quad \text{and} \quad \vec{B}(x,t) = \left[\vec{n}\leftarrow\vec{E}\right]_{ret}$$

$$Power = \frac{2e^4}{3m^2c^3}\gamma^2\left\{(\vec{E}+\vec{\beta}\mid\vec{B})^2-(\vec{\beta}.\vec{E})\right\}$$

$\vec{\beta} = \vec{v}/c$

$\vec{n}$ = direction of observation

The characteristics of the radiation are fully determined by the trajectory and the position of the observer.

LOA

ENSTA POLYTECHNIQUE CNRS

main parameter

$$a_0 = 0.85\sqrt{\lambda^2(\mu m) I / 10^{18}}$$ for linear polarization

At LOA : $a_{0\,max} = 6$

LOA

ENSTA

POLYTECHNIQUE

CNRS

Electronic trajectories

Circular polarization

Linear polarization

$a_0 = 5$

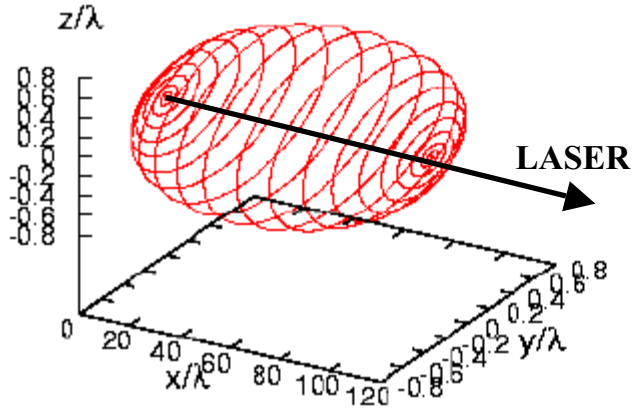

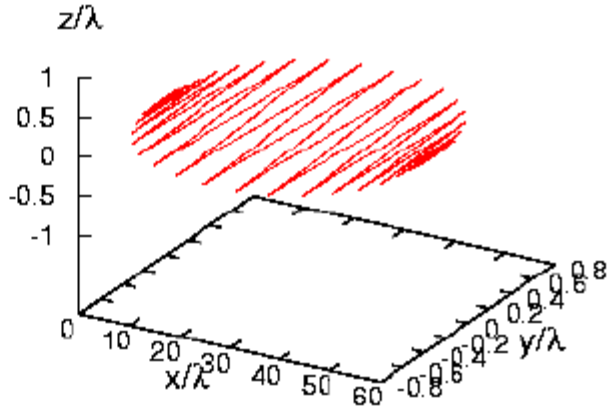

Evolution with a_0

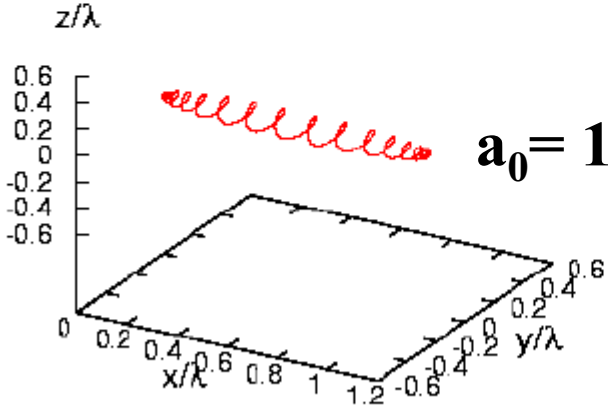

$a_0 = 1$

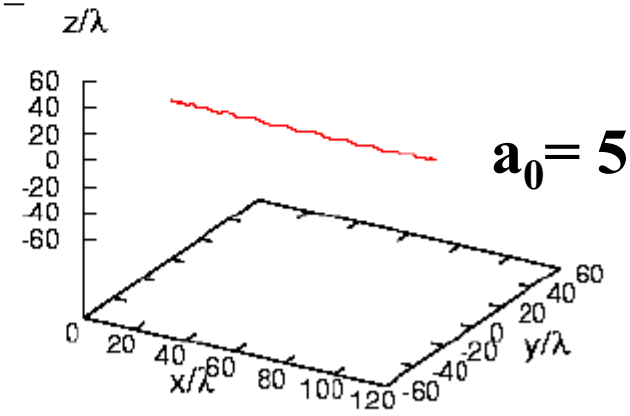

$a_0 = 5$

Laser-based synchrotron X-ray radiation
[*non-linear thomson scattering*]

Spatial distribution

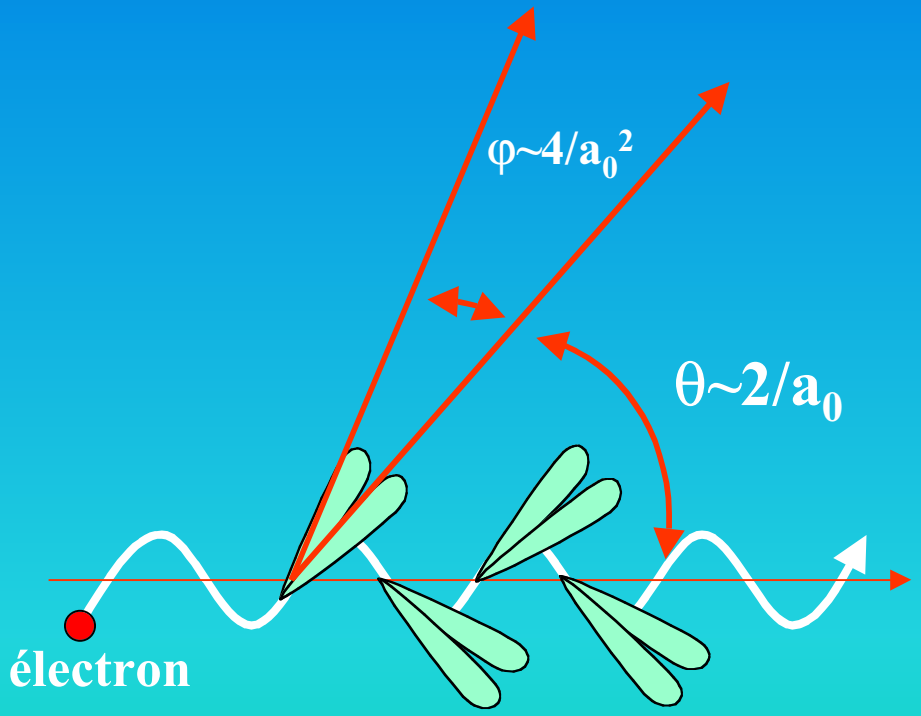

$$[\vec{S}.\vec{n}]_{ret} = \frac{e^2}{(4\pi)^2\epsilon_0 c}\frac{1}{R^2}\frac{(\vec{n}\wedge((\vec{n}-\vec{\beta})\wedge\dot{\vec{\beta}})^2}{(1-\vec{\beta}.\vec{n})^6}\Big|_{ret}$$

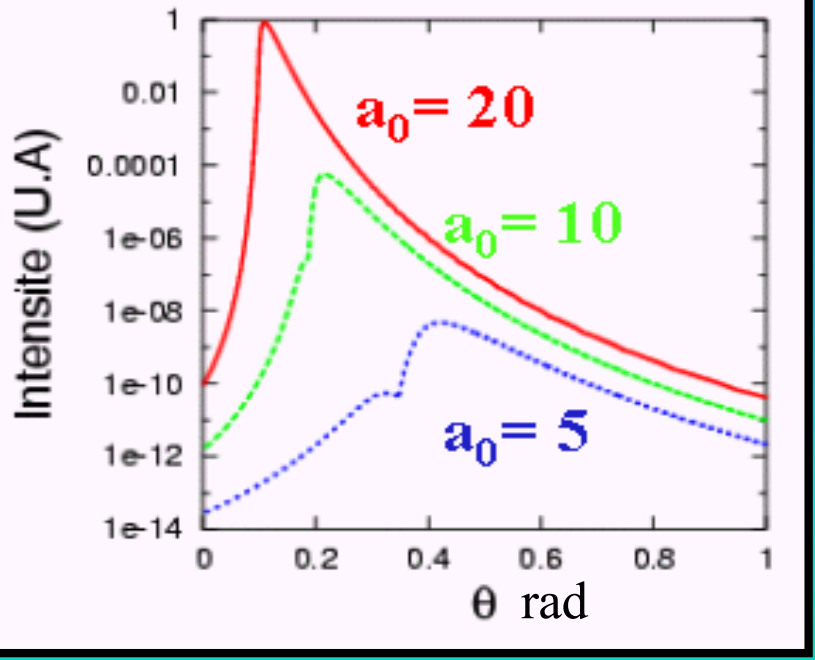

Laser-based synchrotron X-ray radiation
[*non-linear thomson scattering*]

Linear polarization

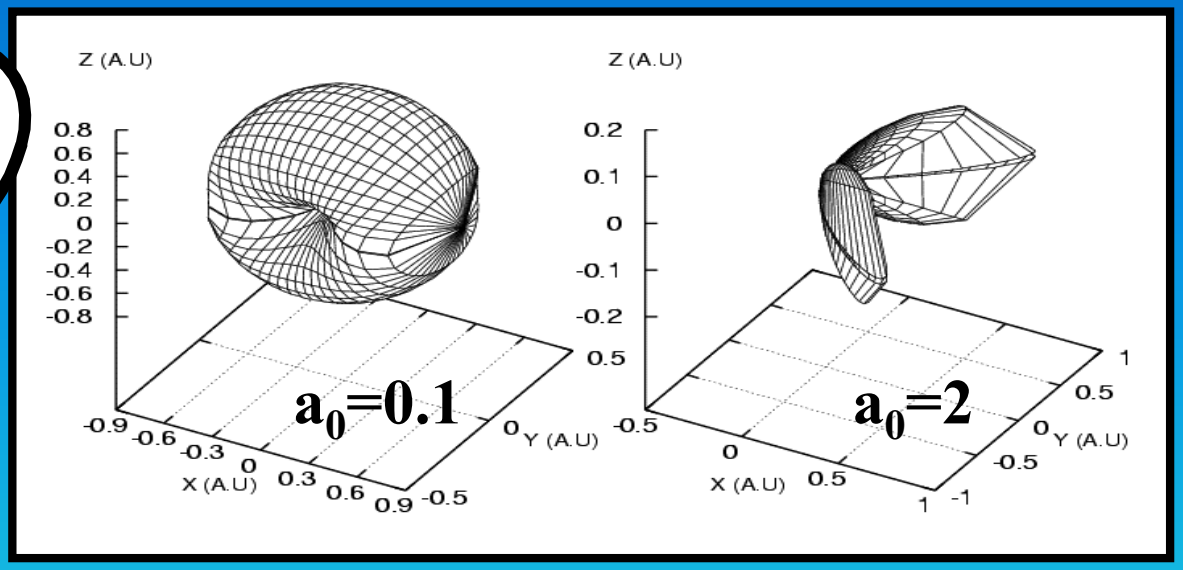

circular polarization

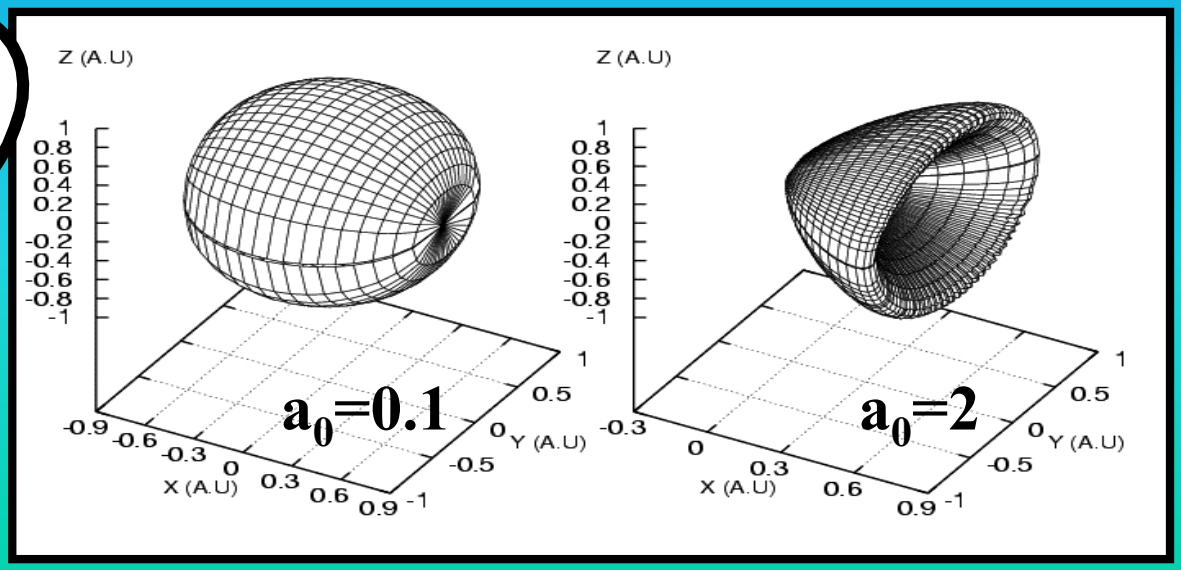

Laser-based synchrotron X-ray radiation
[*non-linear thomson scattering*]

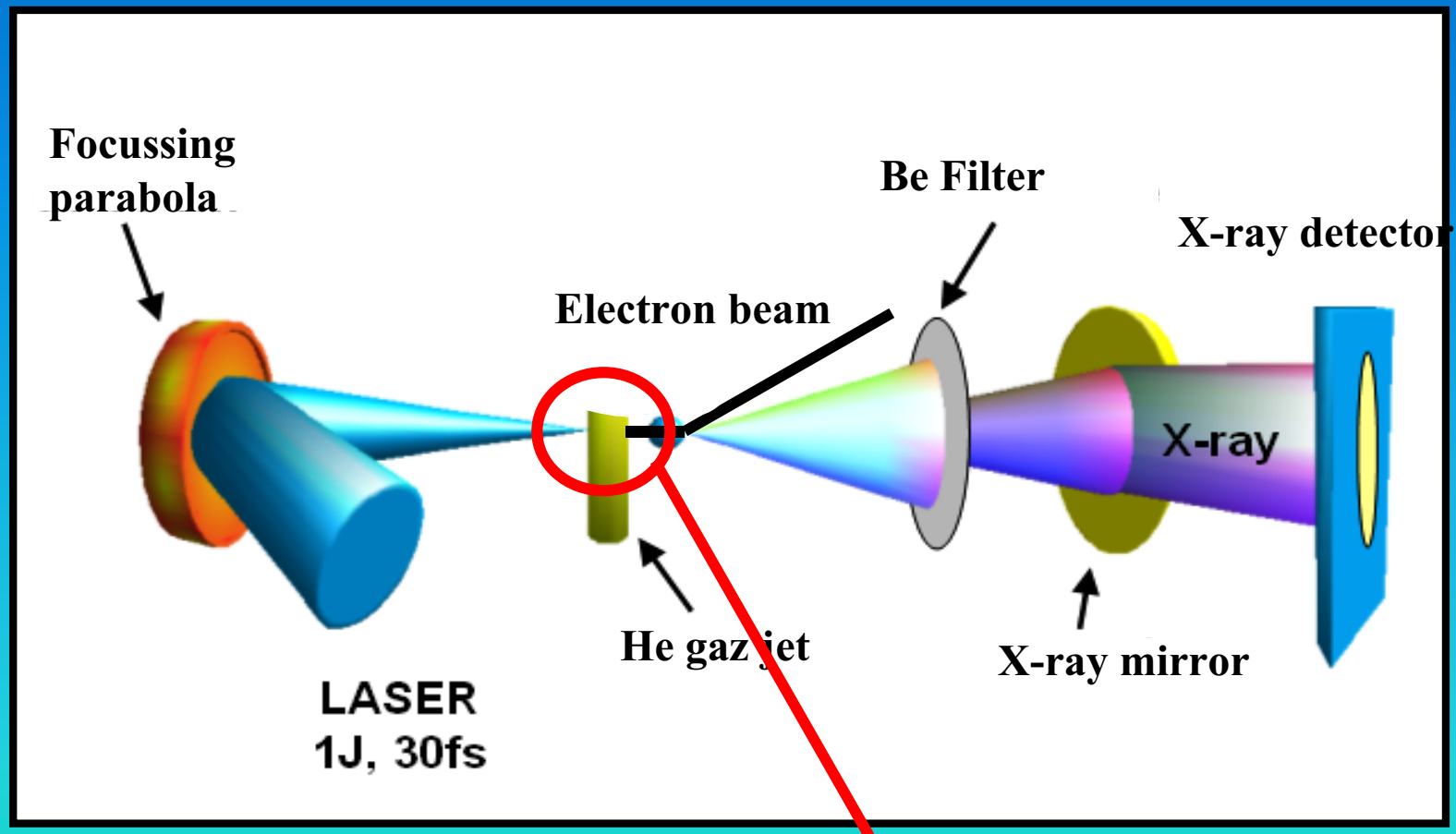

Accelerated electrons & laser undulator inside the plasma

Laser-based synchrotron X-ray radiation
[*non-linear thomson scattering*]

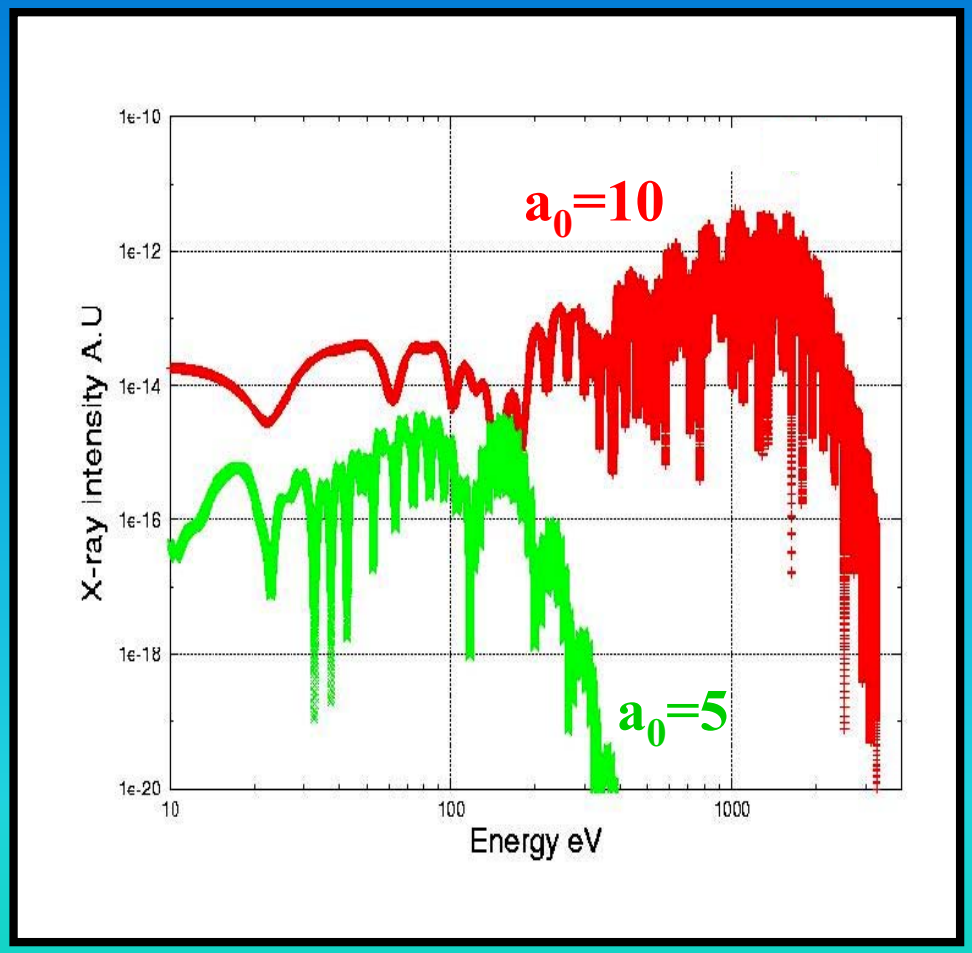

- Peaked spectrum

- The peak shift to high energy with a_0

- The x-ray intensity increases with a_0

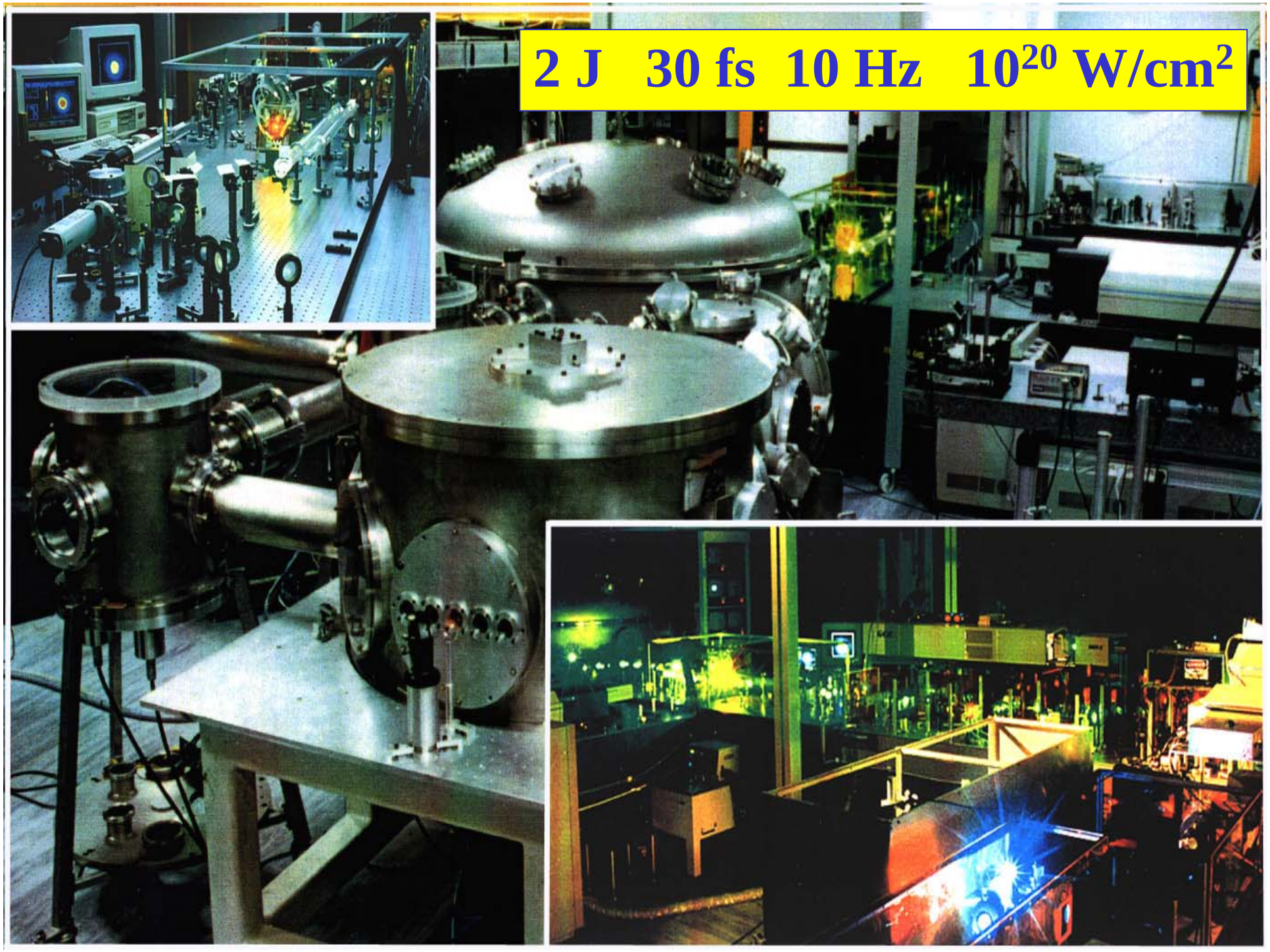
2 J 30 fs 10 Hz 10^{20} W/cm^2

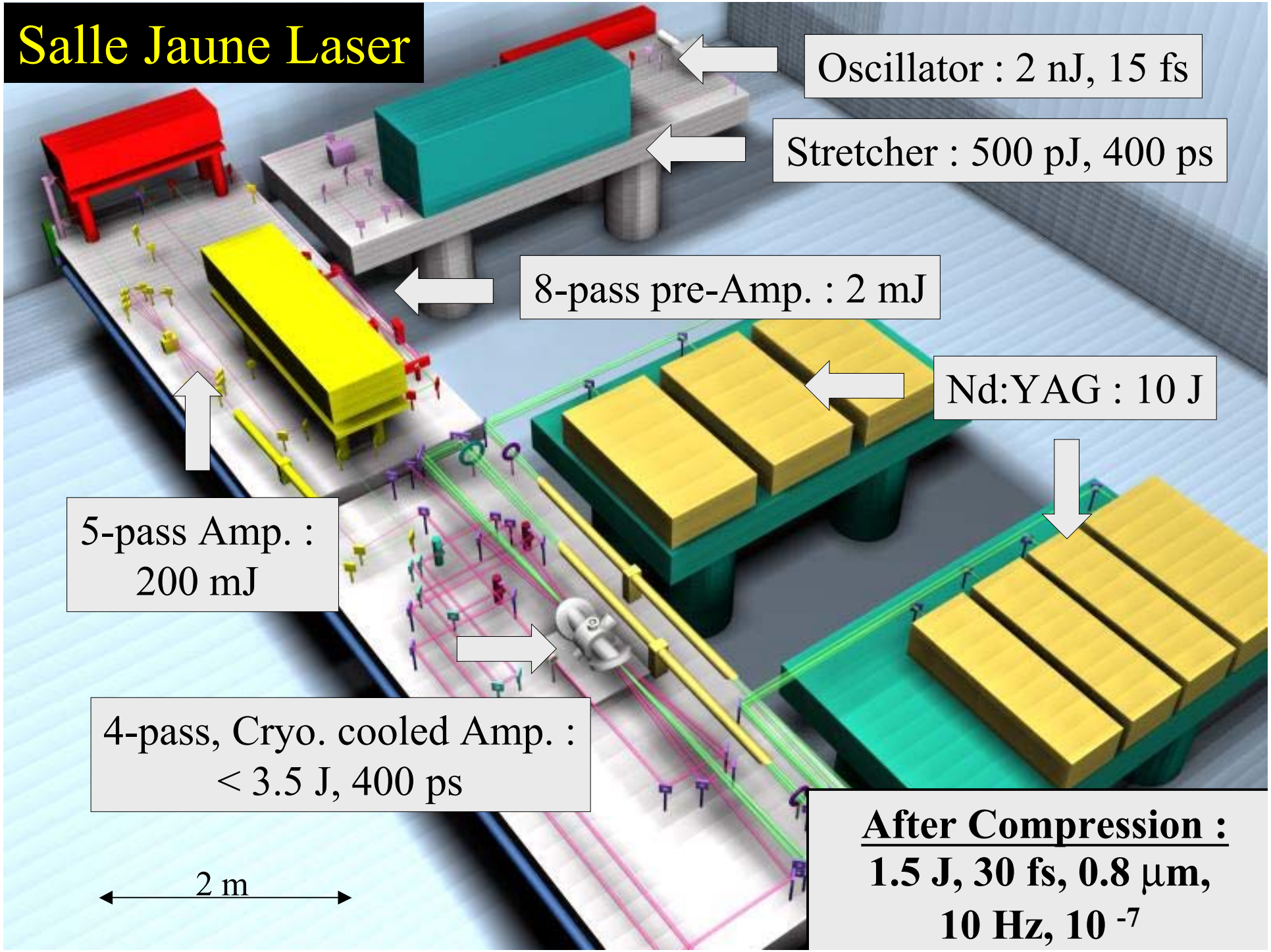
Salle Jaune Laser
Oscillator : 2 nJ, 15 fs
Stretcher : 500 pJ, 400 ps
8-pass pre-Amp. : 2 mJ
Nd:YAG : 10 J
5-pass Amp. :
200 mJ
4-pass, Cryo. cooled Amp. :
< 3.5 J, 400 ps
2 m
After Compression :
1.5 J, 30 fs, 0.8 µm,
10 Hz, 10 -7

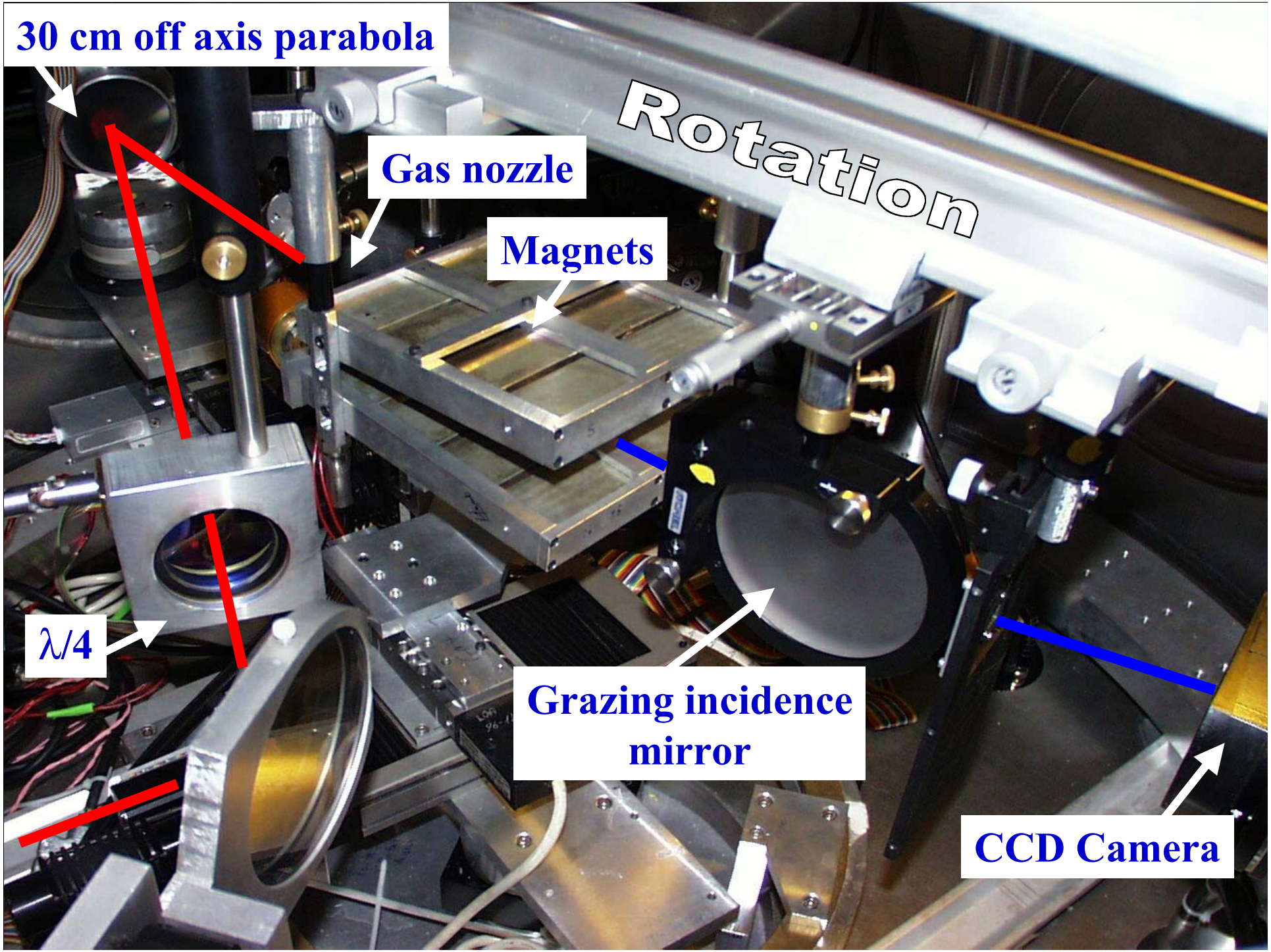
30 cm off axis parabola
Gas nozzle
Magnets
Rotation
λ/4
Grazing incidence mirror
CCD Camera

X-ray energy spectra are in good agreement with theory

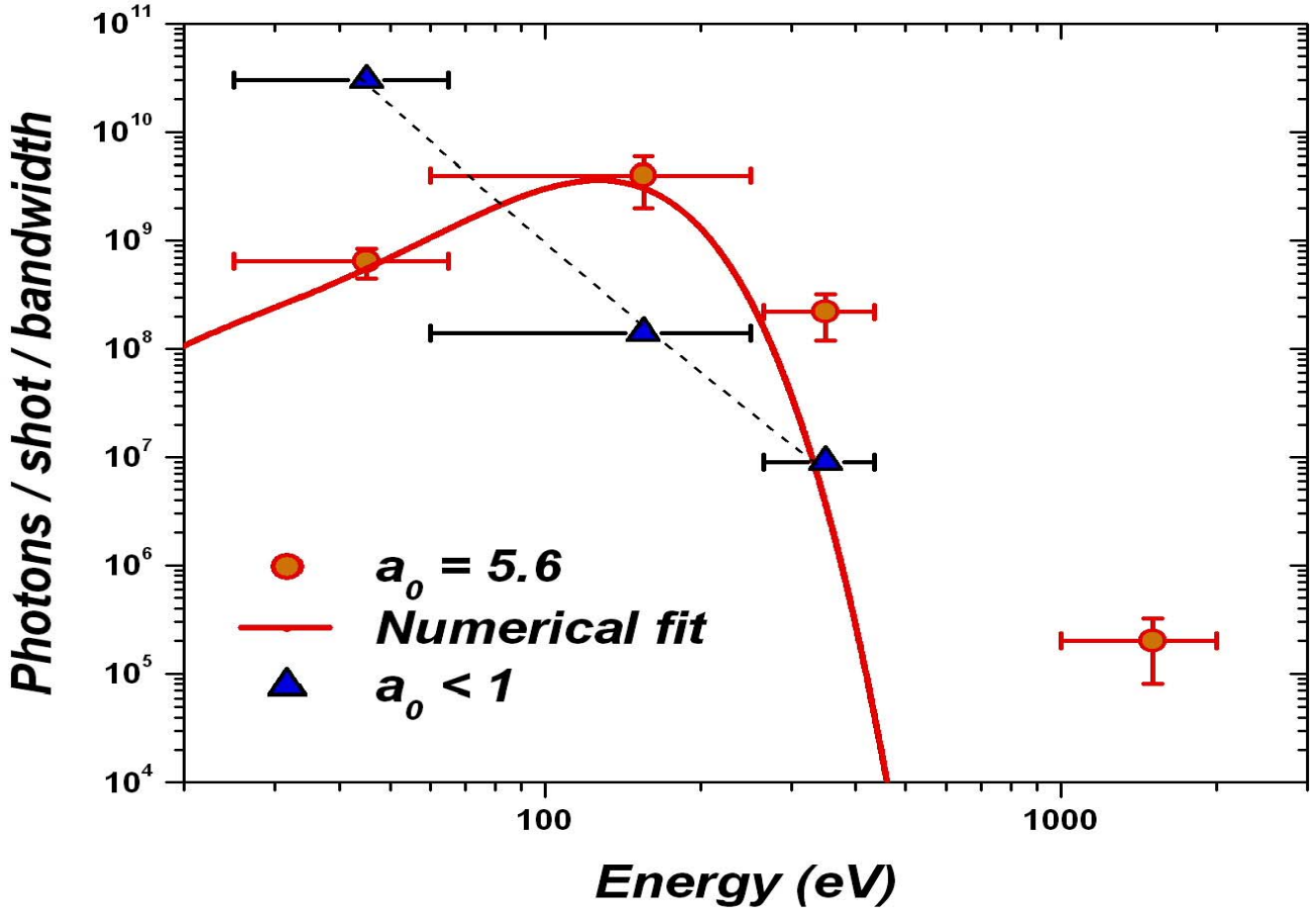

Laser-based synchrotron X-ray radiation
[*non-linear thomson scattering*]

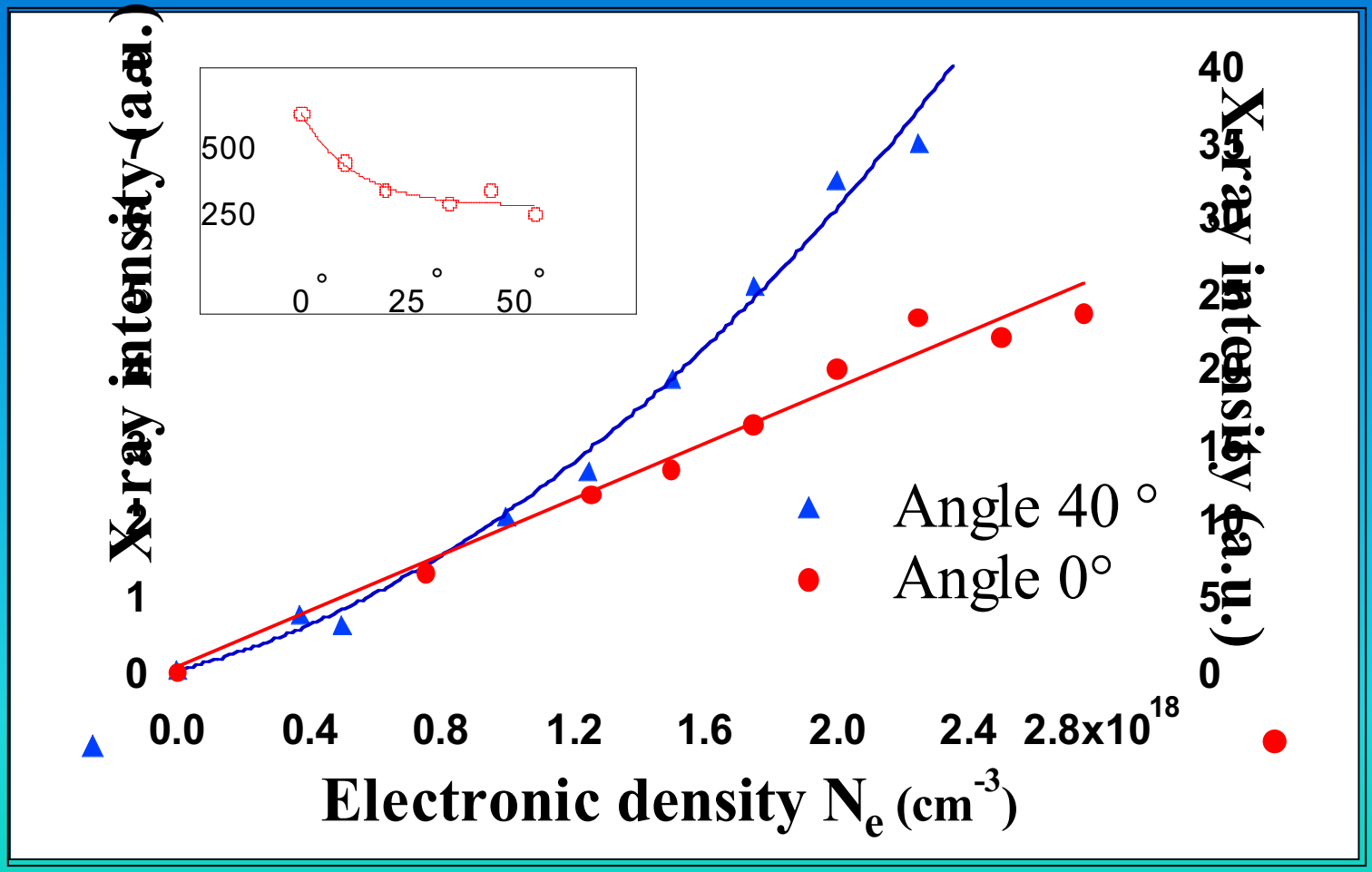

Angular distribution : theory/experiment

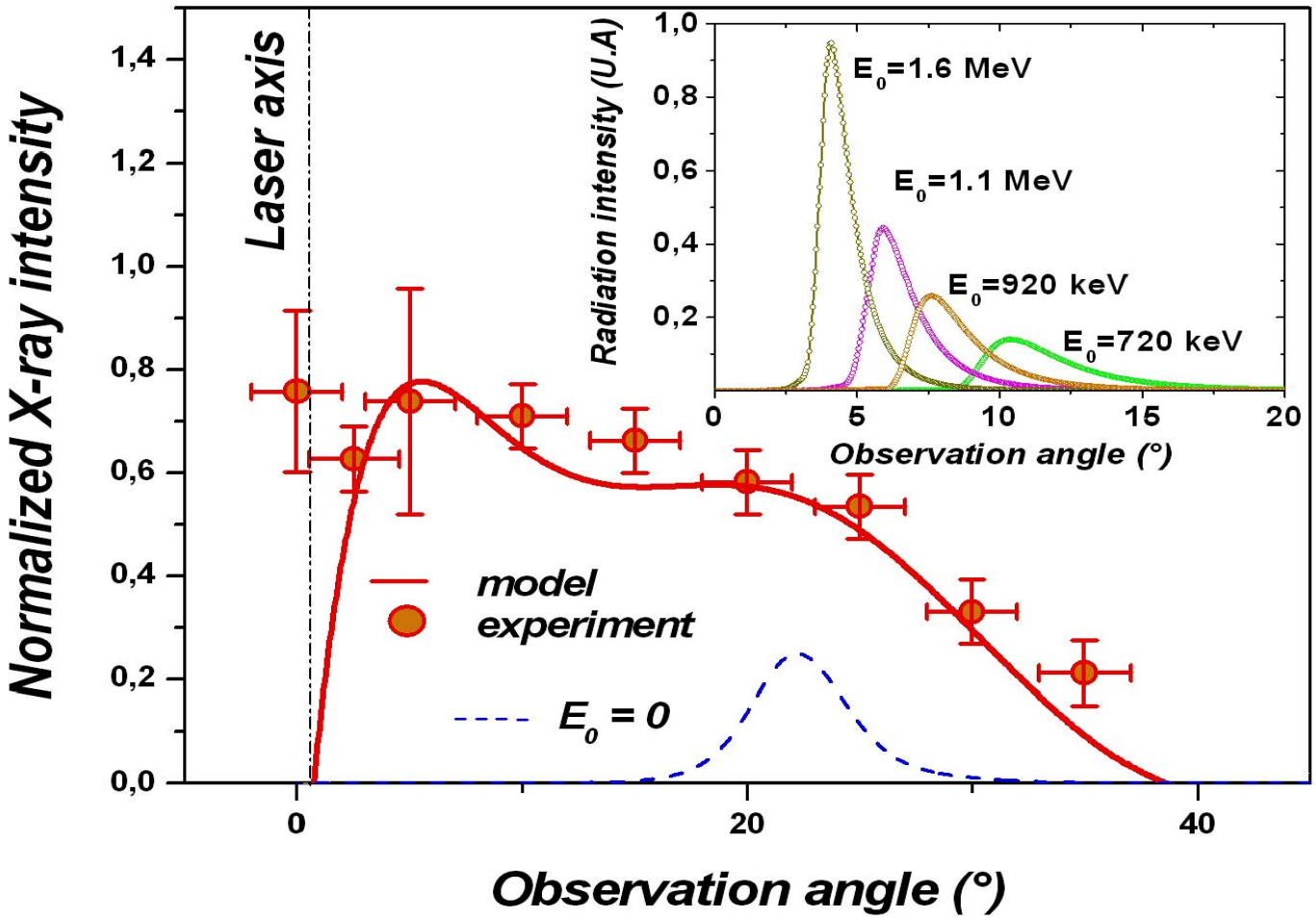

LOA

ENSTA

POLYTECHNIQUE

CNRS

New laser-plasma x-ray source (2)

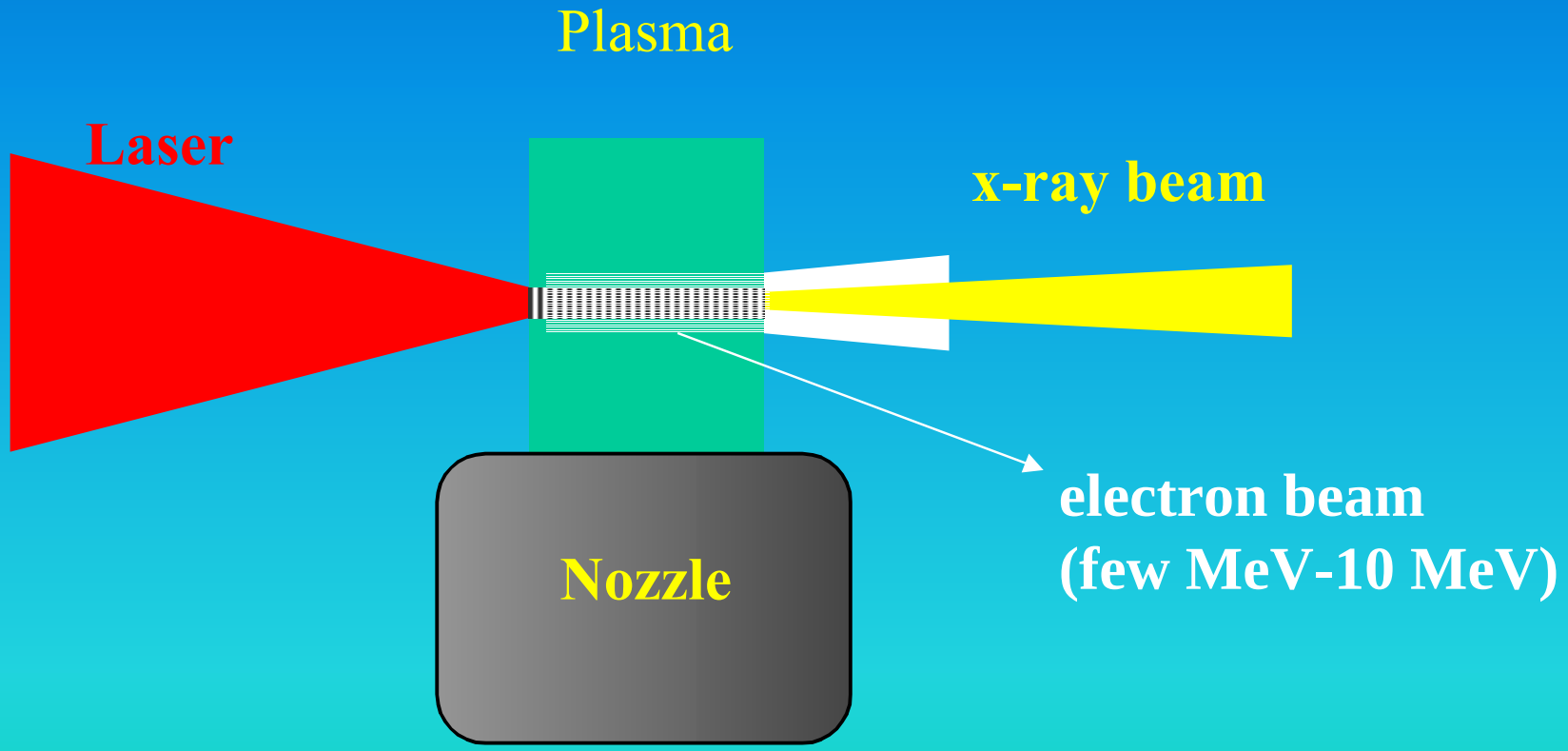

Angular distribution : theory/experiment

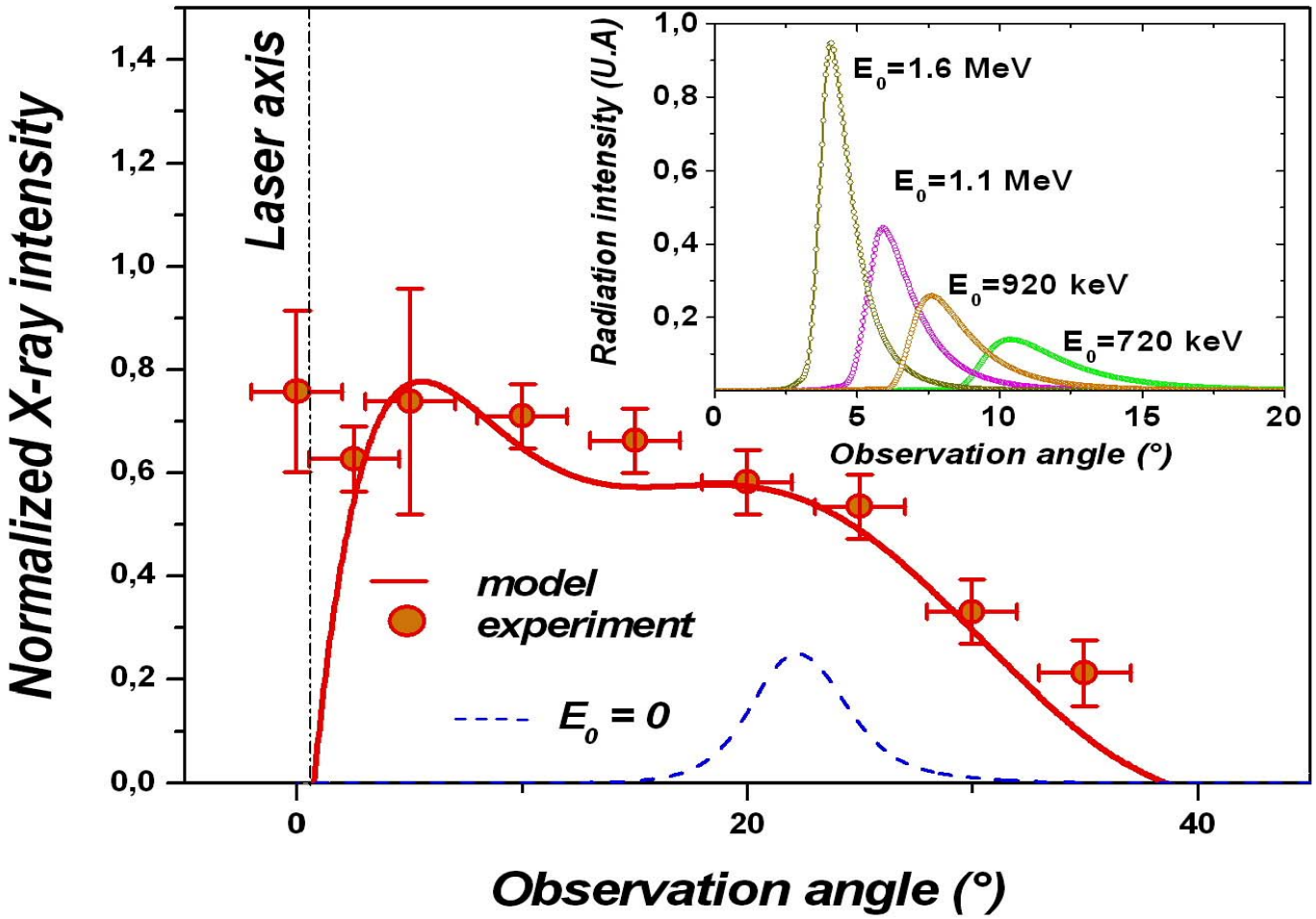

LOA

ENSTA

POLYTECHNIQUE

CNRS

Laser-based synchrotron X-ray radiation
[*non-linear thomson scattering*]

λ	150 eV	2 keV
average brightness ph/s/mrad^2/mm^2/0.1%BW	**$8\ 10^4$**	**$1.5\ 10^4$**
average flux (10 Hz) ph/s/0.1%BW	**$6\ 10^7$**	**$2\ 10^3$**

scale as: wavelength $\propto a_0$, collimation $\propto 2/a_0$

In the near future

(with the LOA parameters)

Laser-plasma keV ultrafast x-ray beam

30 fs

polychromatic: 1 keV to 8 keV

collimation: 2° - 3°

10^5 photons/shot/0.1%BW

10 Hz

Laue & absorption x-ray experiments in the 100 fs timescale

Conclusion

. Flux of the present laser-plasma x-ray source: x 10^4

. on sample 10^9 photons/sec @ few keV monochromatic

. extend the number of application experiments

. useful for developping x-ray diagnostics of future large scale instruments

. New polychromatic & keV fs x-ray source

. start fs absorption x-ray experiments

. start fs « Laue » diffraction experiments

Summer School " *Ultrafast X-ray Science* "
wwwy.ensta.fr/ufx

Fs x-ray diffraction

Ch. Rischel (Copenhagen)
I. Uschmann (Jena)
S. Fourmaux (LOA)
D. Boschetto (LOA)

High energy electron source

V. malka (LOA)

K_α x-ray source

P. Audebert (LULI)
JP Geindre (LULI)
JC Gauthier (LULI)

New x-ray sources
(Larmor)

Kim Ta Phuoc (LOA)

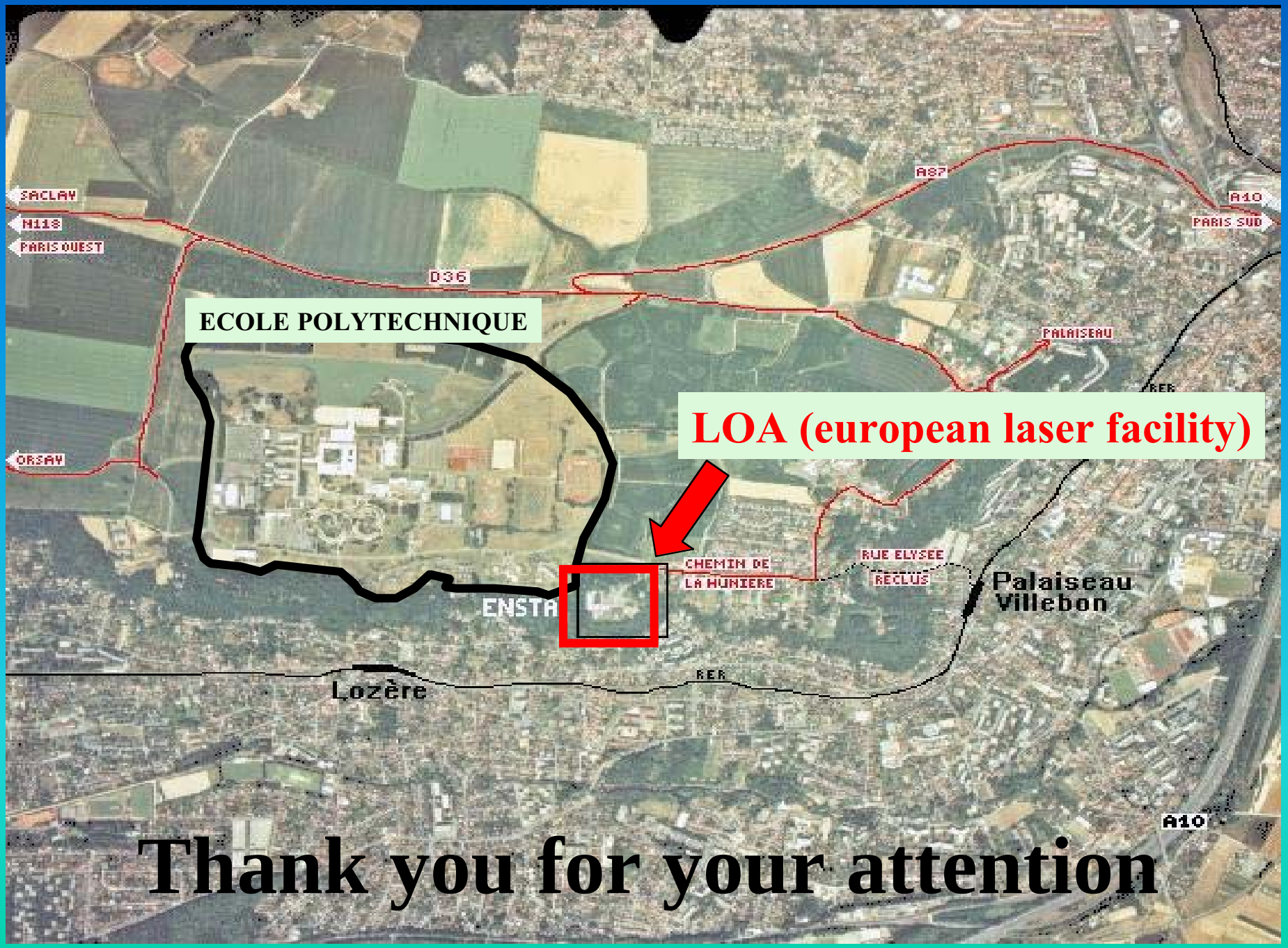

Thank you for your attention

Efficient hard X-ray source using femtosecond plasma at solid and liquid targets

ANDREI SAVELEV

Lomonosov Moscow State University

Ludwig Maximilians Universität München

LMU

MPQ

Hot electron diagnostics using X-rays and Cerenkov radiation

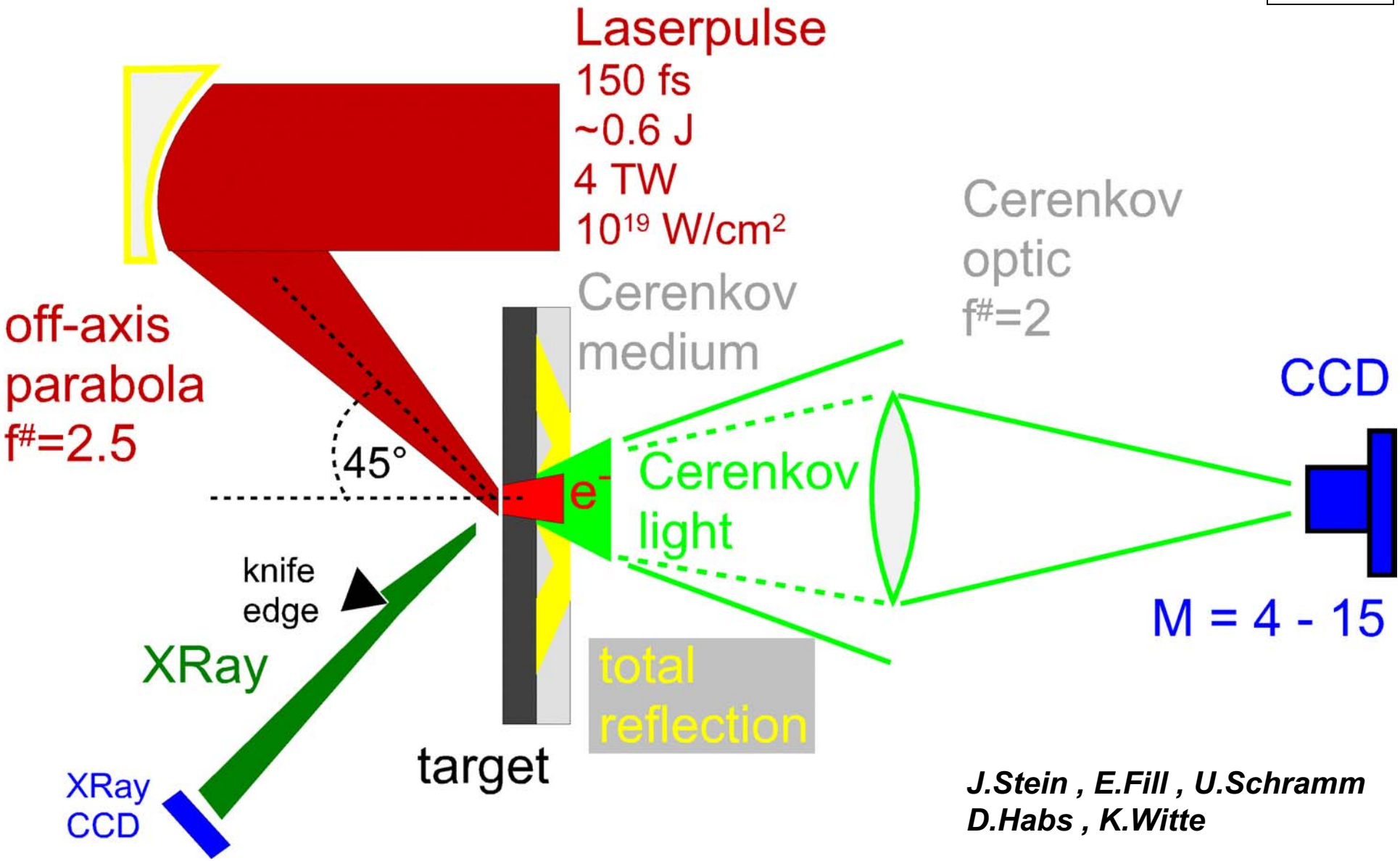

J.Stein , E.Fill , U.Schramm
D.Habs , K.Witte

X-rays demonstrate effect of self-fields

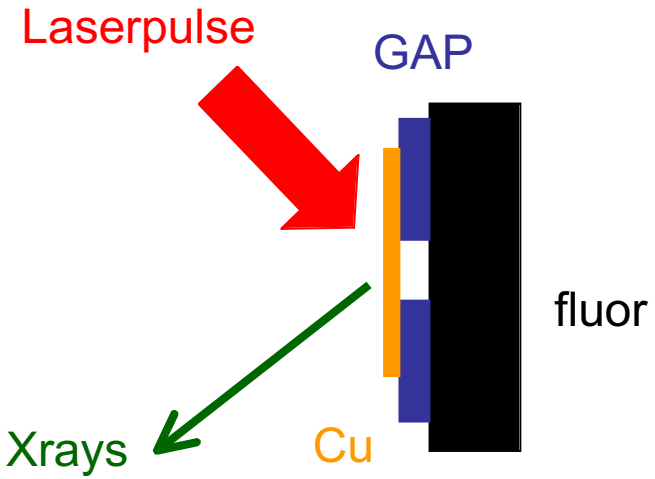

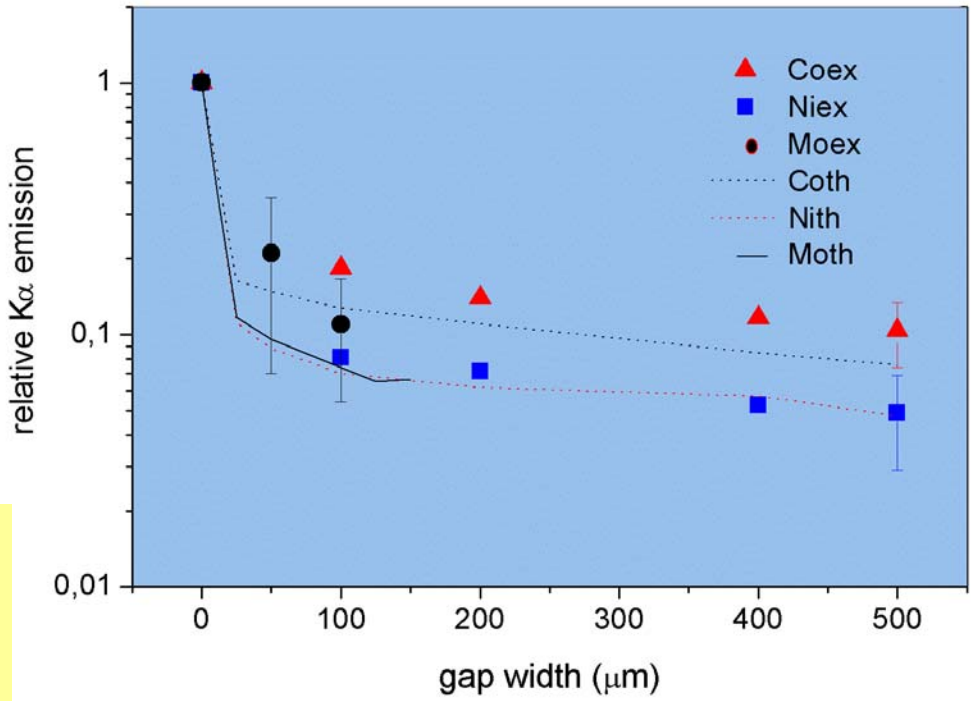

- Self-fields prevent electrons from propagating across vacuum-GAPs
- Emission of X-ray „fluors“ (Co, Ni, Mo) is significantly reduced
- Co is photopumped by Cu Kα
- Good agreement between experiment and theory

Cerenkov Medium

Polypropylene

$n \approx 1{,}48$

ϑ_{max} limited by f#2-Optic

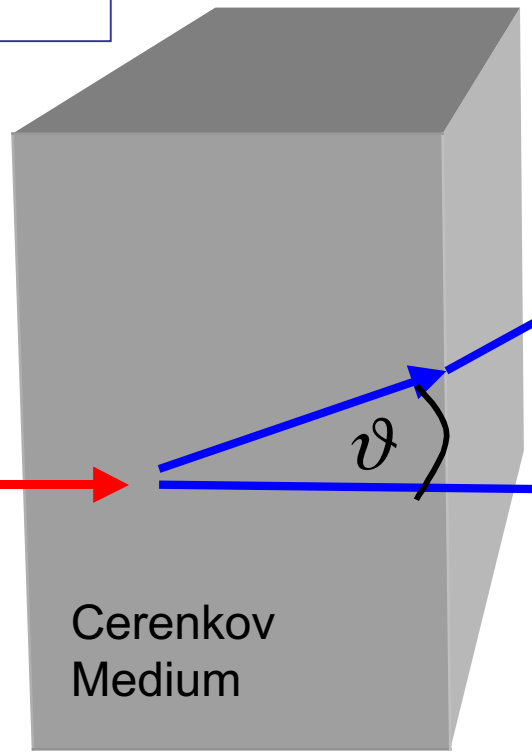

relativistic electrons

e^-

ϑ

$$\beta = \frac{v}{c}$$

$$\beta_{max} = \frac{1}{n \cdot \cos \vartheta_{max}} = 0.8$$

$$\beta_{min} = \frac{1}{n} = 0.67$$

$$\cos \vartheta = \frac{1}{n \cdot \beta}$$

thickness
10 - 100 µm

100 µm Al

10^{19} W/cm_

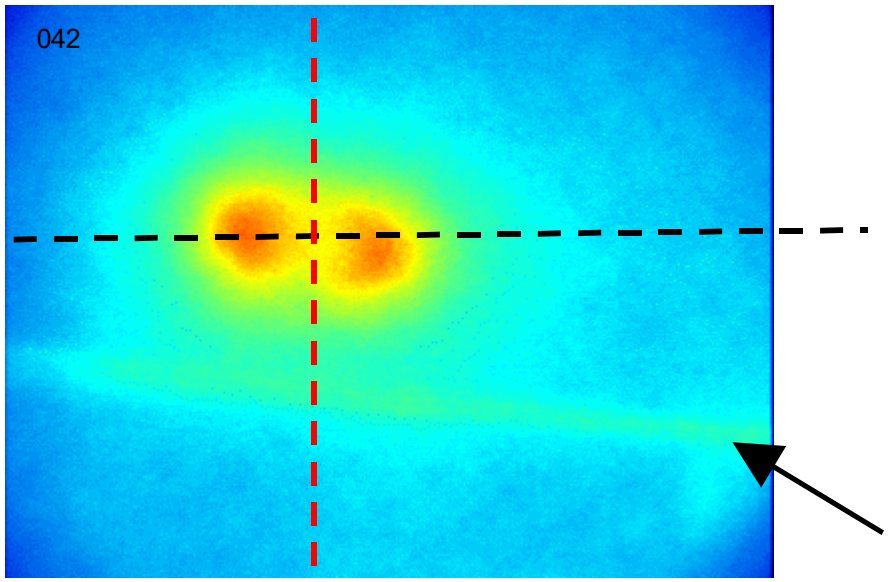

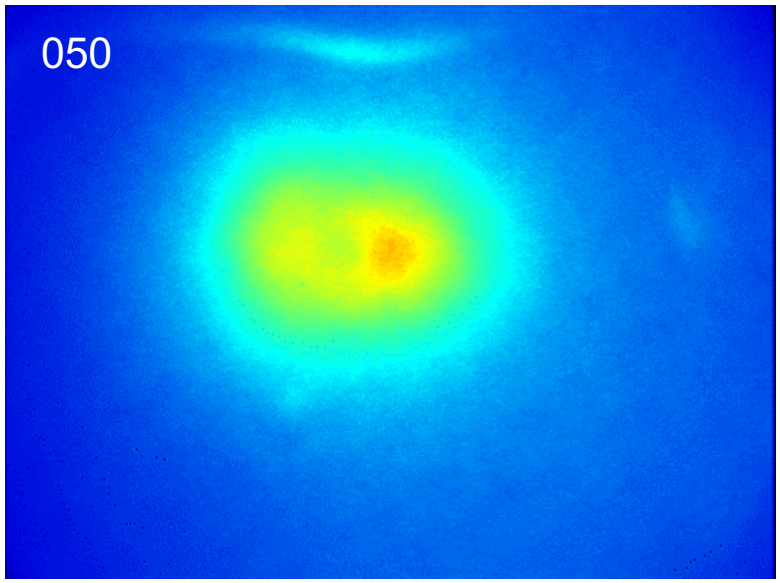

$0.5\ 10^{19}$ W/cm_

?!

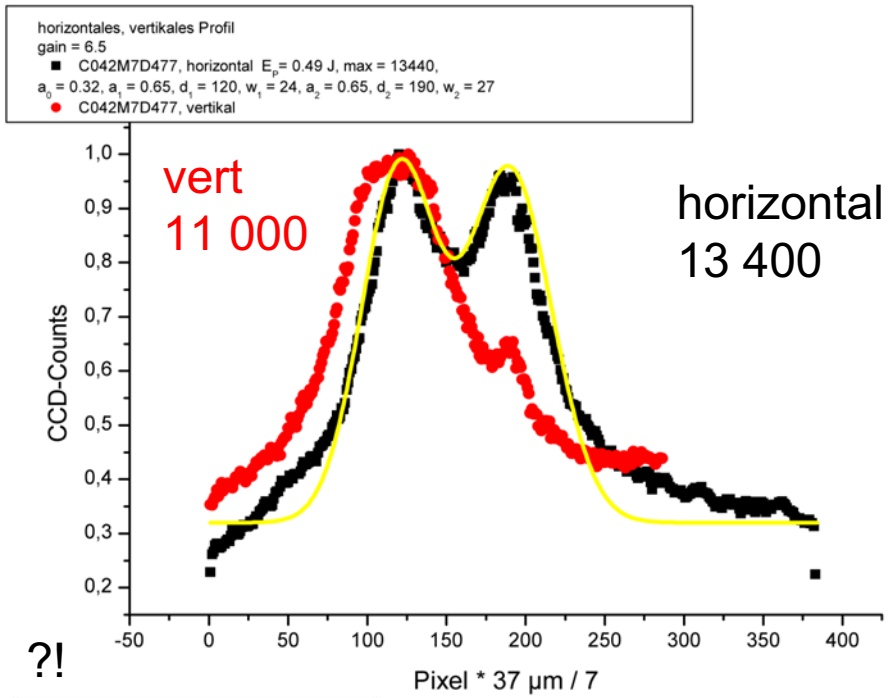

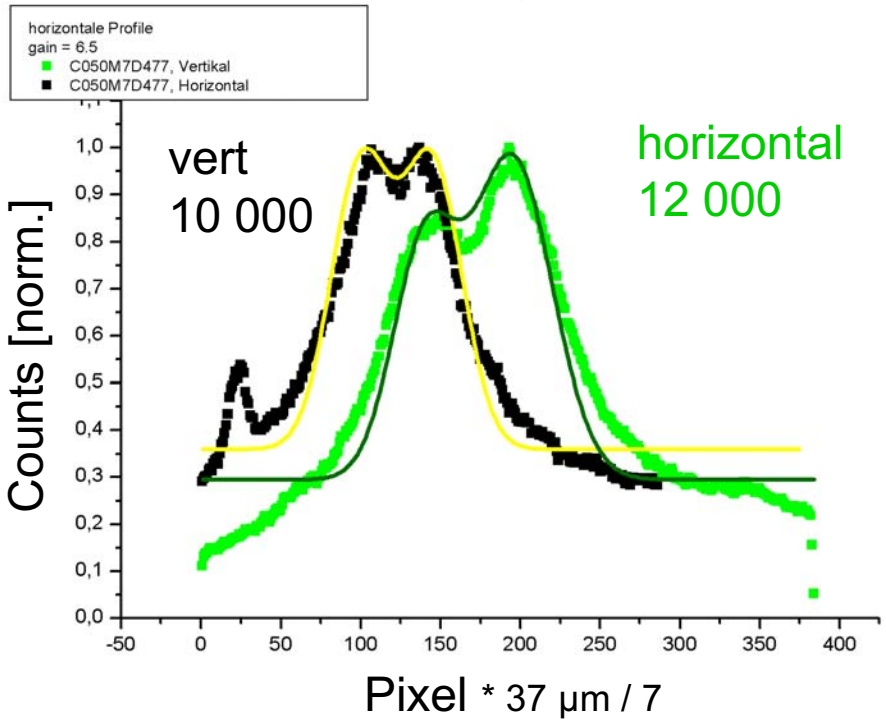

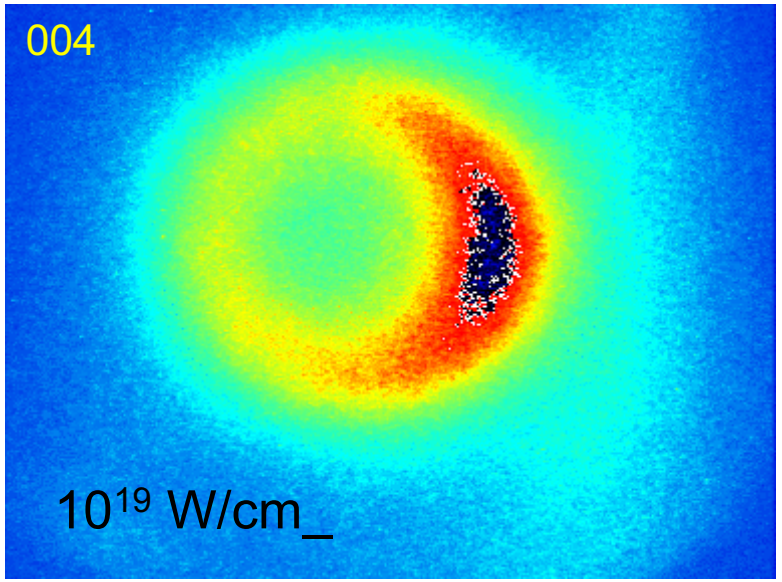

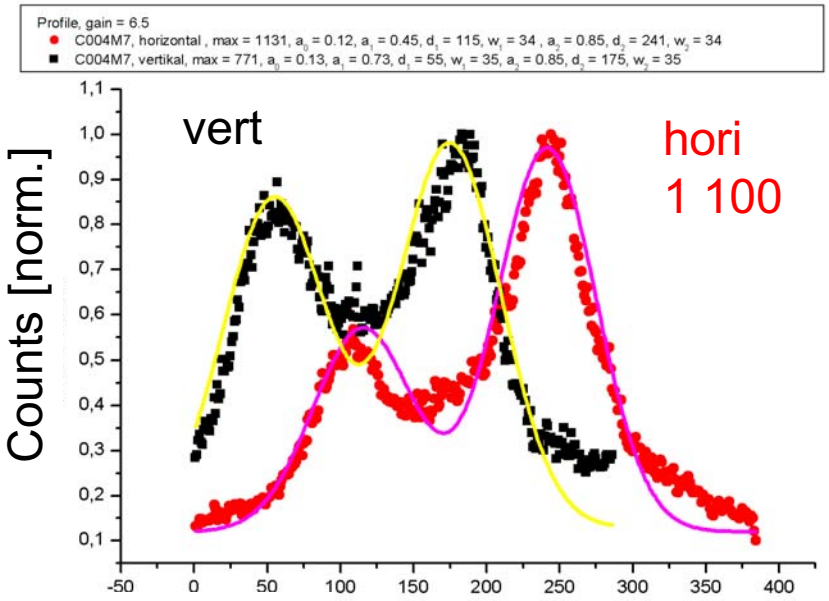

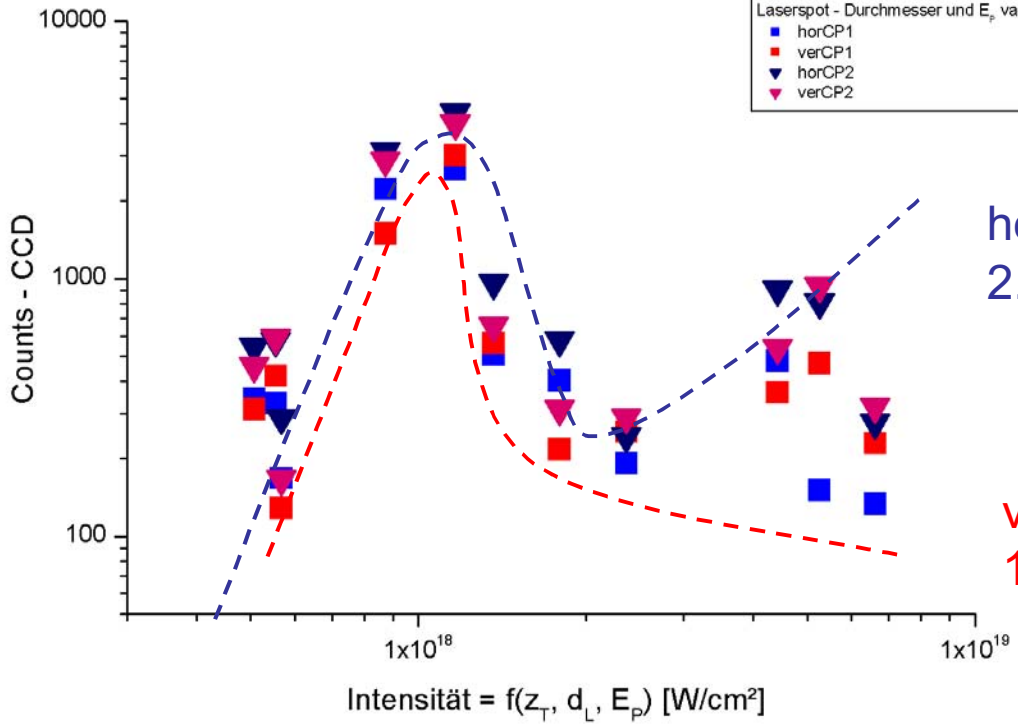

100 µm Cu, 50 µm GAP
60 µm PP, M = 7

horizontal
2. Peak-Counts

vertical
1. + 2. Peak-Counts

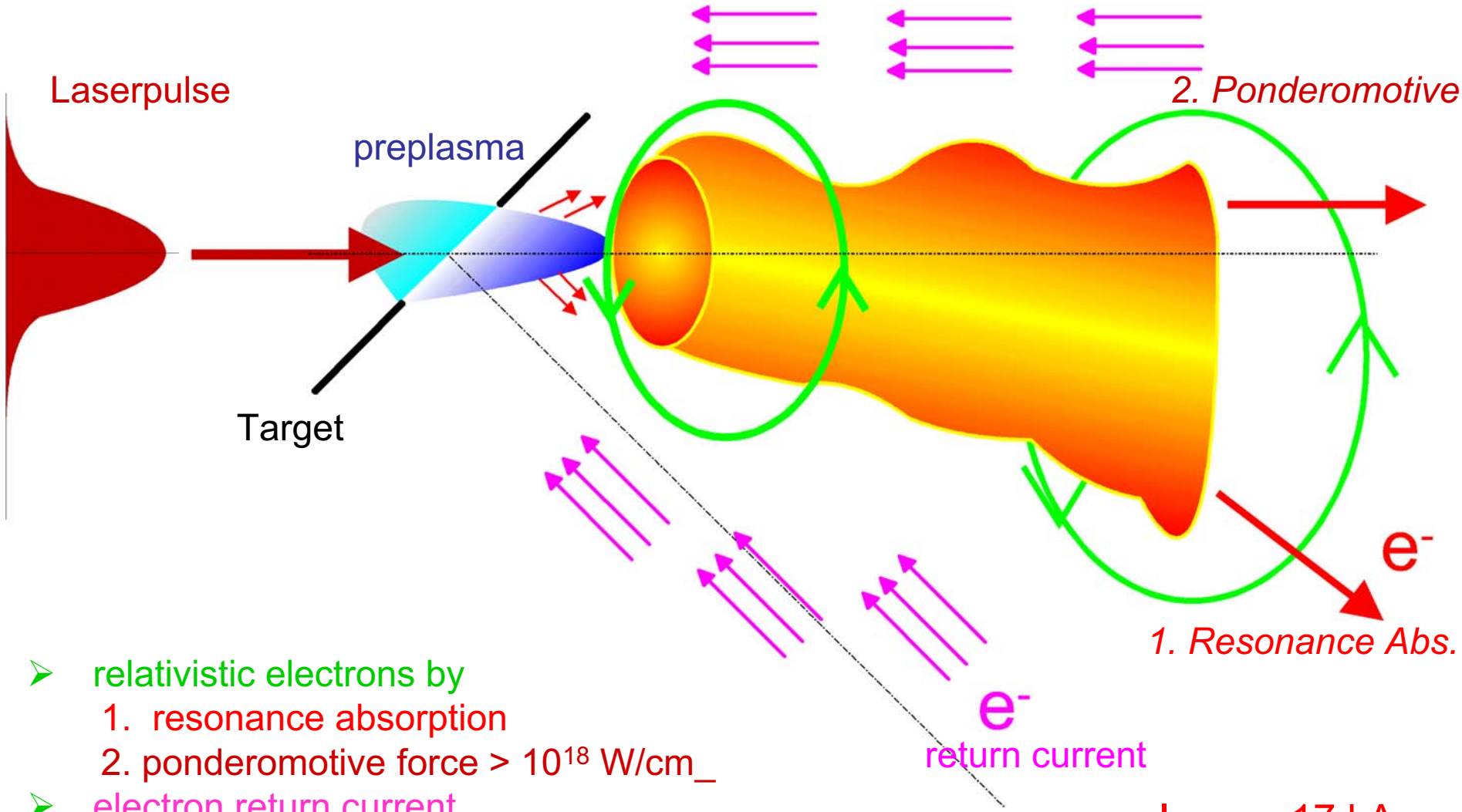

- relativistic electrons by
  1. resonance absorption
  2. ponderomotive force > 10^{18} W/cm_
- electron return current
- unstable dynamics
- filamentation of the electron current
- „stiffening“ by ions
- coalescence of the electron filaments

$$\omega_P \sim n_e^{\frac{1}{2}}$$

I_{Alfven} ~ 17 kA
$n_e > 10^{22}$ cm^{-3}
$N_e > 10^{11}$
j > 10^{12} A/cm_
I > MA >> I_{Alfven}
B > 1.000 Tesla

Electron Energy – Distribution

100 µm Al

by Bethe-Bloch calculation

$$\frac{dN_{in}}{N_0 dT} = \frac{1}{T_{eff}} \cdot e^{-\frac{T}{T_{eff}}}$$

Resonance Absorption

$$T_{eff} = 100keV \cdot \left(I_{17} \cdot \lambda_L^2\right)^{1/3}$$

$I_L = 10^{17}$ W/cm_

T_{eff} = 90 keV

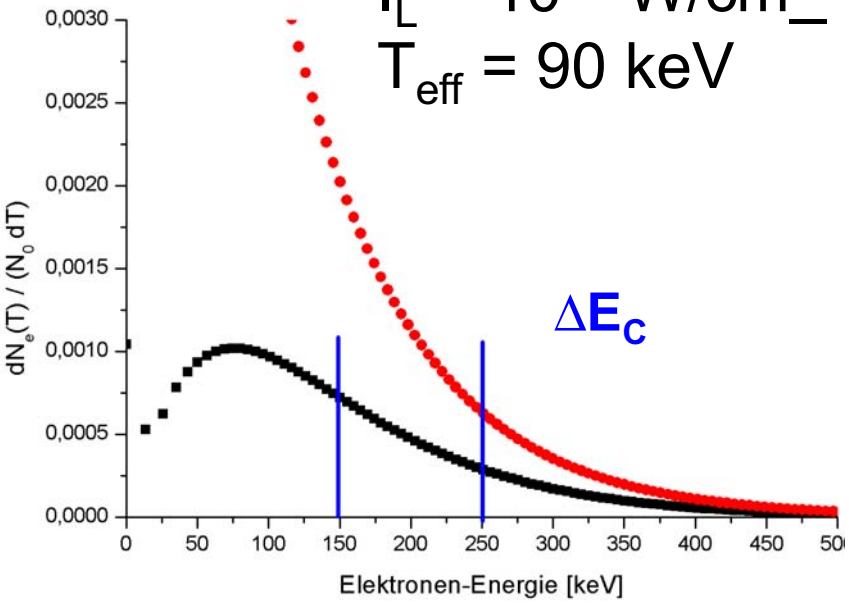

E_{kin} [keV]

$I_L = 10^{19}$ W/cm_

T_{eff} = 400 keV

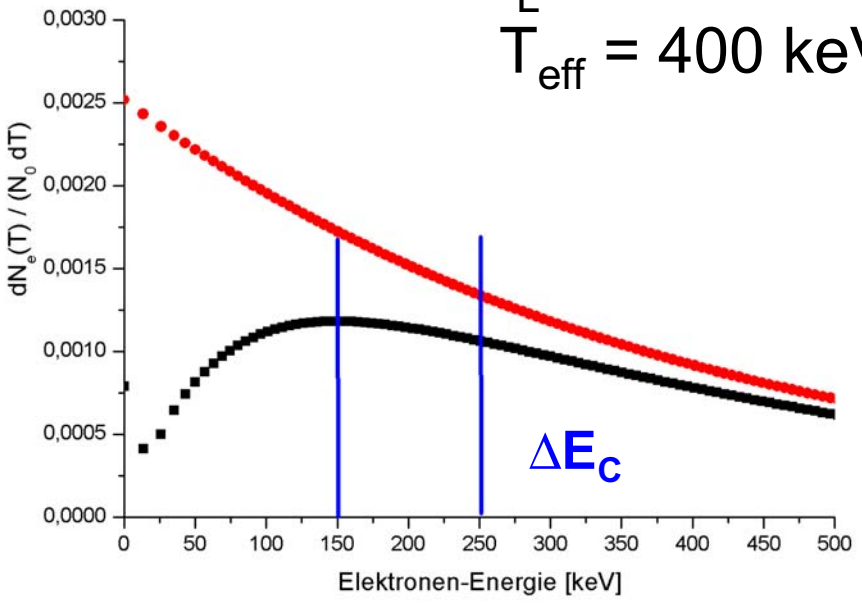

E_{kin} [keV]

Cerenkov – Detection

1. assumption

$$\int_{\Delta E_C} \frac{dN_{out}}{dE} dE$$

$$\eta_{L,R} \approx \eta_{L,P}$$

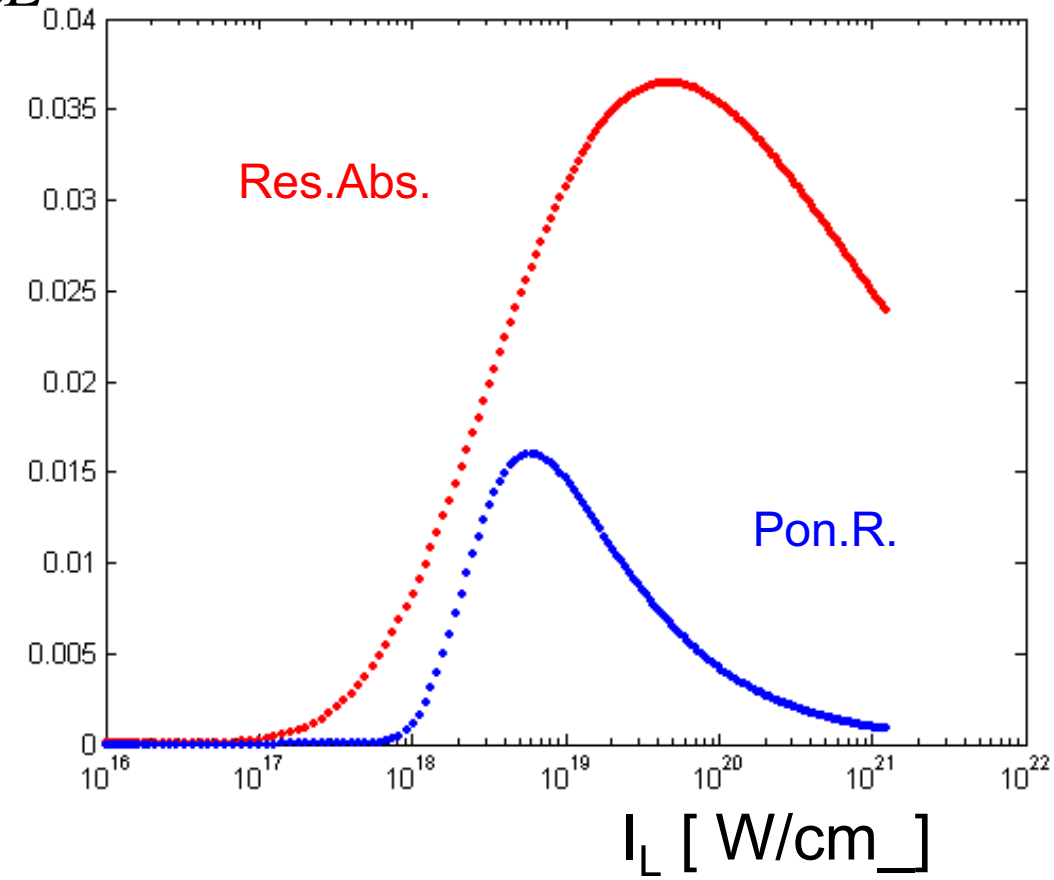

$$\eta_{L,R} \cdot E_L = N_{e,R} \cdot T_{eff,\mathrm{Re}s}$$

$$\eta_{L,P} \cdot E_L = N_{e,P} \cdot T_{eff,Pon}$$

$$N_{e,R} + N_{e,P} = 1$$

Electron acceleration
by Ponderomotive Force

$$T_{eff} = 511keV \cdot \left[\left(1 + \frac{I_{17} \cdot \lambda_L^2}{13.7} \right)^{1/2} - 1 \right]$$

Filamentation

H. Ruhl
3D-PIC-Simulations
with overdense plasma

filaments ~ 1 µm

Weibel
Instabilities

Laserpulse
150 fs
< 1 J

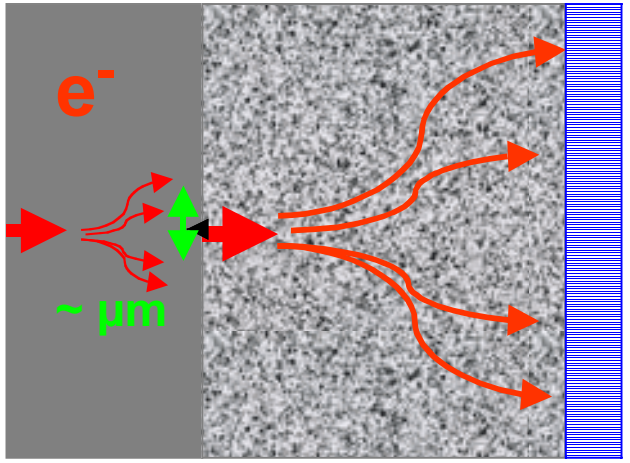

~ 5 µm

$\lambda_C \sim 500nm$

~ 100 µm
Metal
Target

Aerogel 100 µm
0,05 g/cm_

Cerenkov
Medium
60 µm

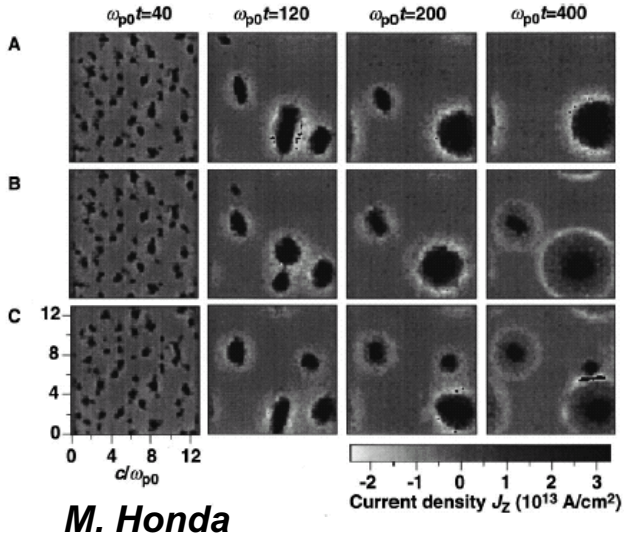

M. Honda
J. Meyer-ter-Vehn
A. Pukhov
2D-PIC-Simulations
relativistic currents in plasma

plasma
frequency

$$\omega_P \propto n_e^{\frac{1}{2}}$$

electron
density

scale
length

$$l_S \approx \frac{c}{\omega_P}$$

Cerenkov - Spectral Distribution

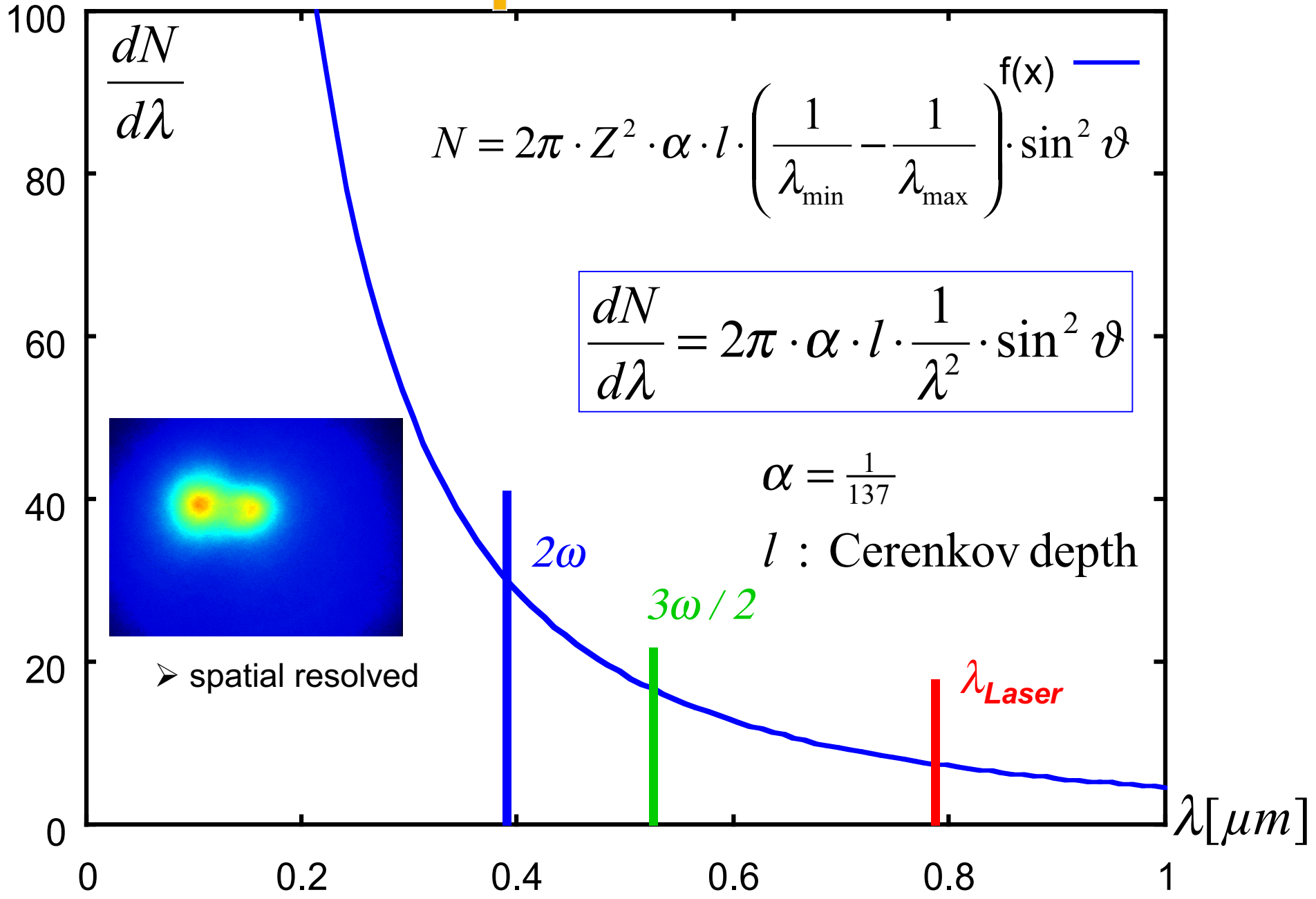

Time Resolved Measurement of the Cerenkov Light

Fast Ignition Confinement Fusion

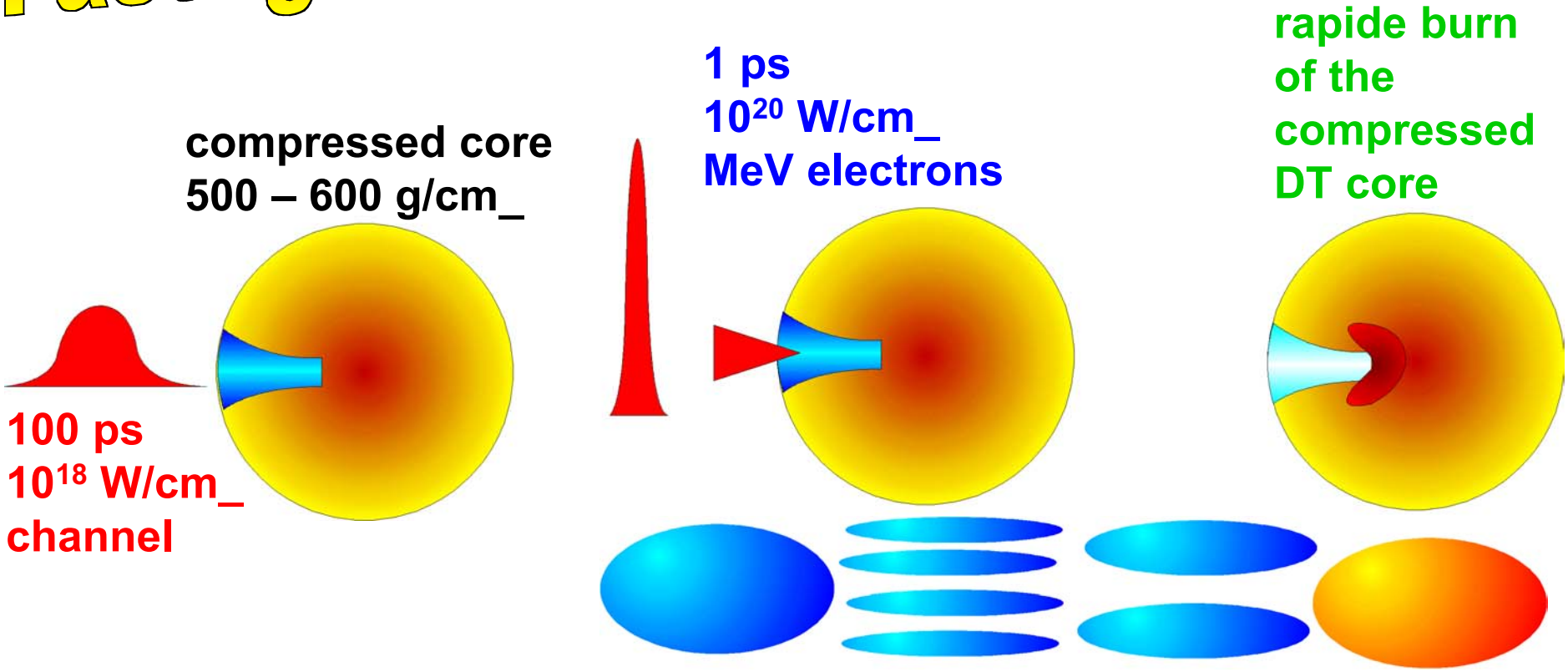

A. Pukhov
J. Meyer-ter-Vehn

Short-wavelength free-electron lasers

Facilities and experiments

thomas.tschentscher@desy.de

International workshop *Ultrashort High-Energy Radiation and Matter*

Varenna, October 07-10, 2003

Hamburger Synchrotronstrahlungslabor

Deutsches Elektronen-Synchrotron
member of the Helmholtz-Society

Reminder on X-ray FELs

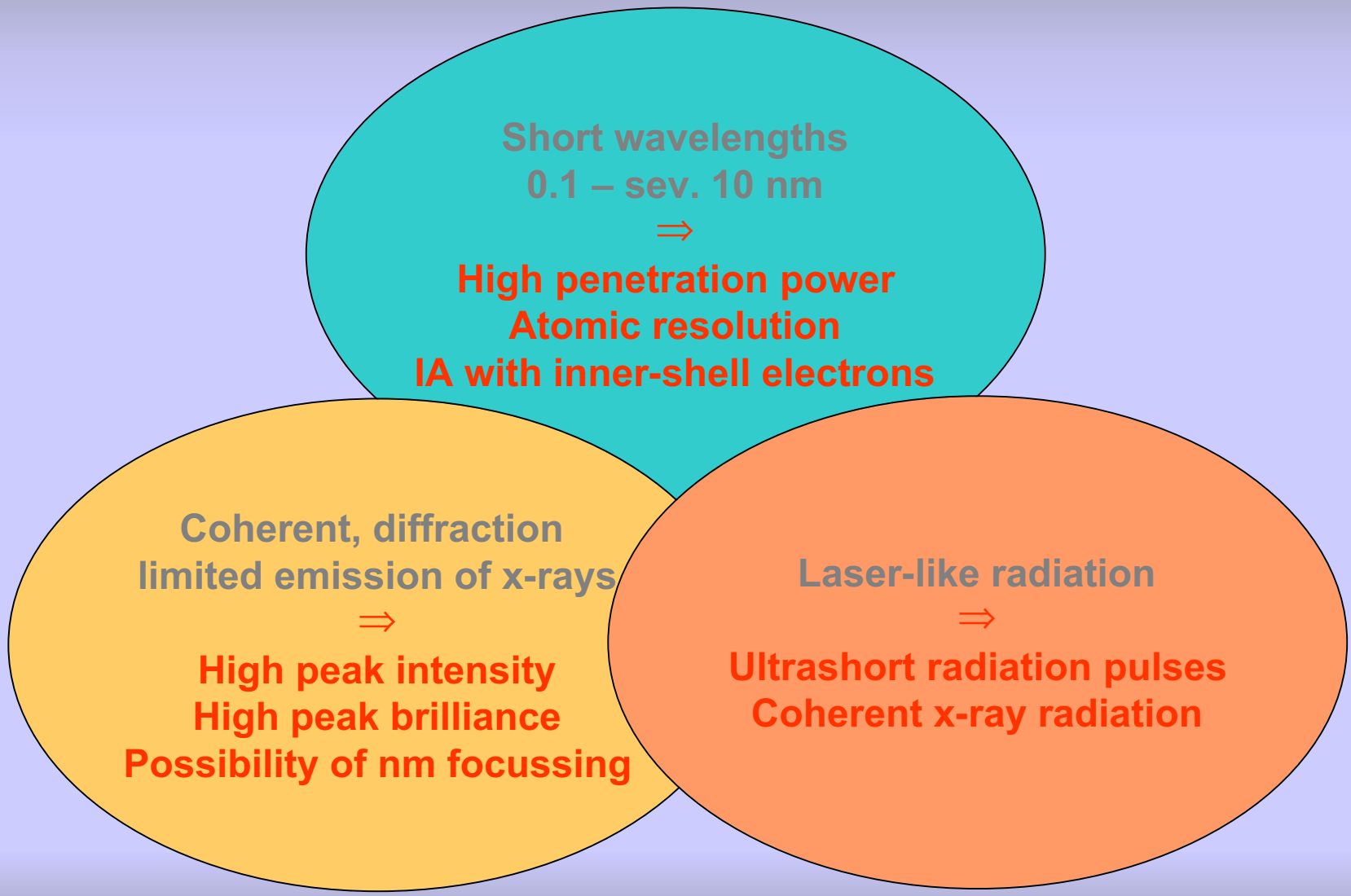

Outline

- **Scientific applications using FEL radiation**
- **Review of parameters**
- **Roadmap towards short-wavelength FELs**

Scientific applications using FEL radiation

- **Short wavelength ↔ High photon energy : X-rays**
- **High intensity/number of photons per pulse**
- **Ultrashort duration**
- **Spatial & temporal coherence**

Peak Brightness

PB

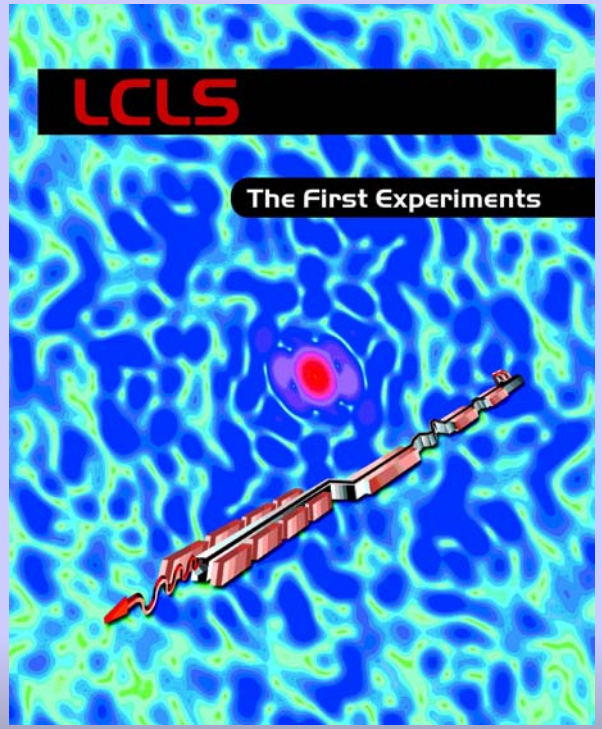

- Atoms, molecules, cluster
- Plasma physics
- Hard-condensed matter
- Surface & interface studies
- Materials science
- Chemistry
- Life sciences
- Nonlinear phenomena & quantum optics
- FEL physics

http://slac.stanford.edu/lcls
http://xfel.desy.de

Life sciences
Structure determination of single particles

State-of-the-art

- Synchrotron radiation experiments
- Structure determination of large macromolecules
- Standard tool in structural molecular biology

X-ray diffraction from crystals

- Atomic resolution (~2Å) to obtain function
- Need of crystallization (& good crystal quality)

Wouldn‘t it be wonderful.....

... to be able to investigate single molecules

... to investigate entire organisms

... to look time-resolved at ultrafast processes

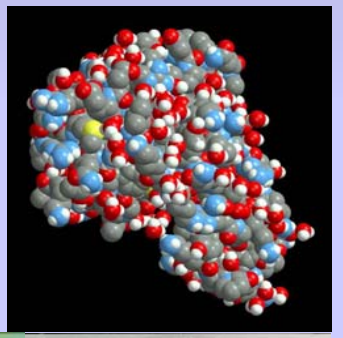

Lysozyme

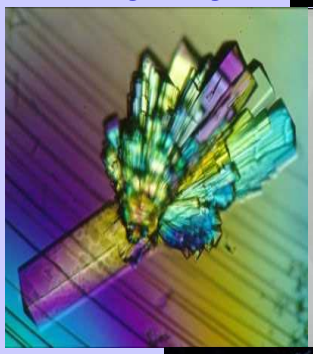

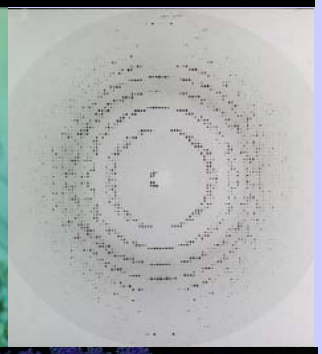

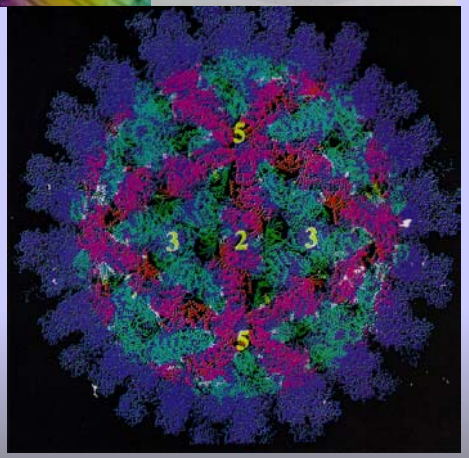

Blue-tongue virus
(core particle)

Life sciences
Single particle diffraction

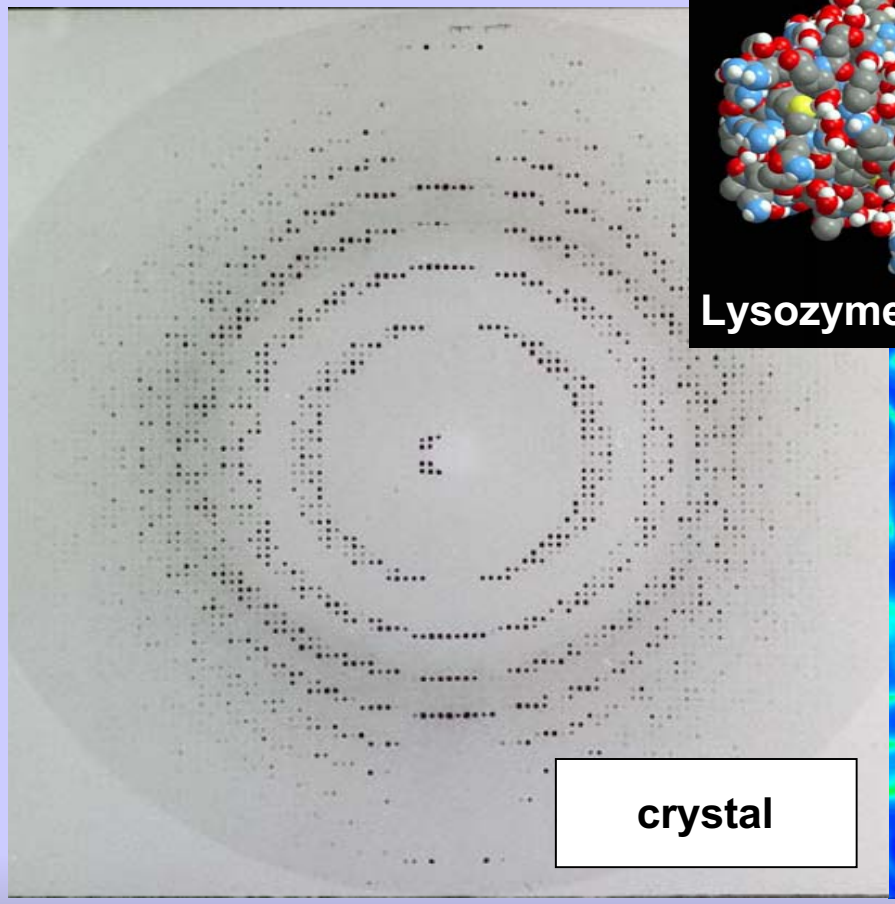

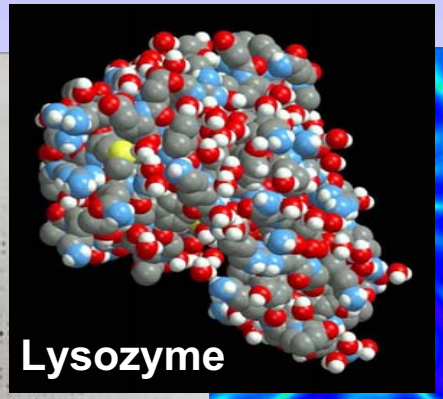

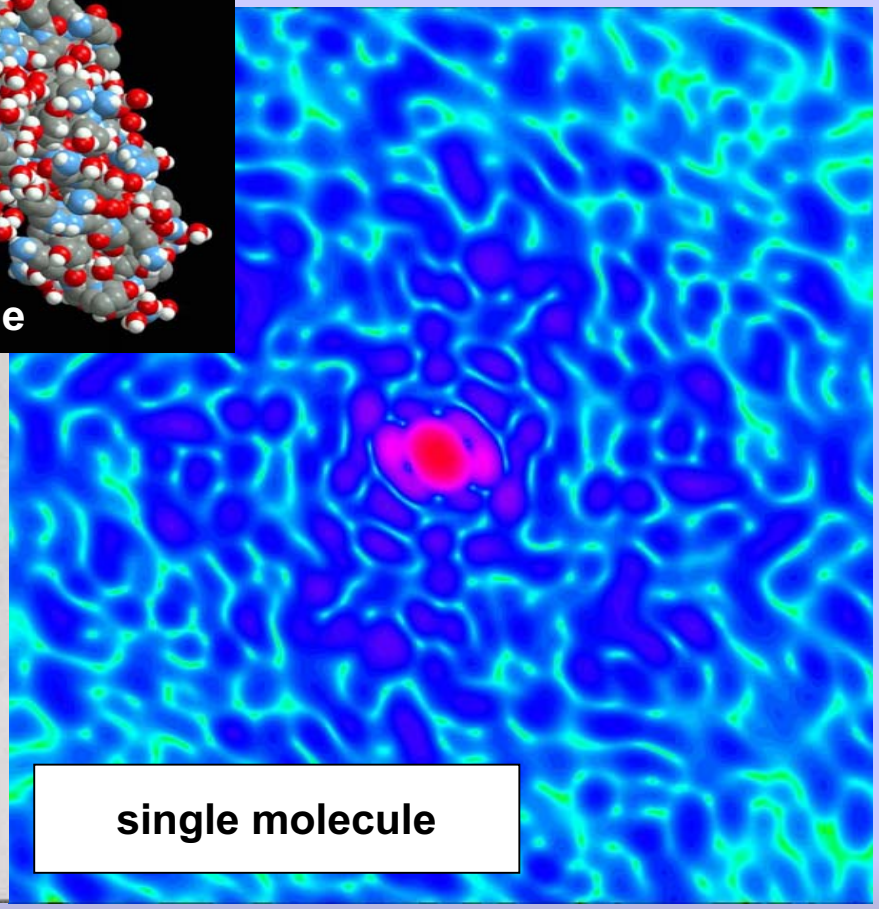

crystal

single molecule

Life sciences
Technique & molecular transform

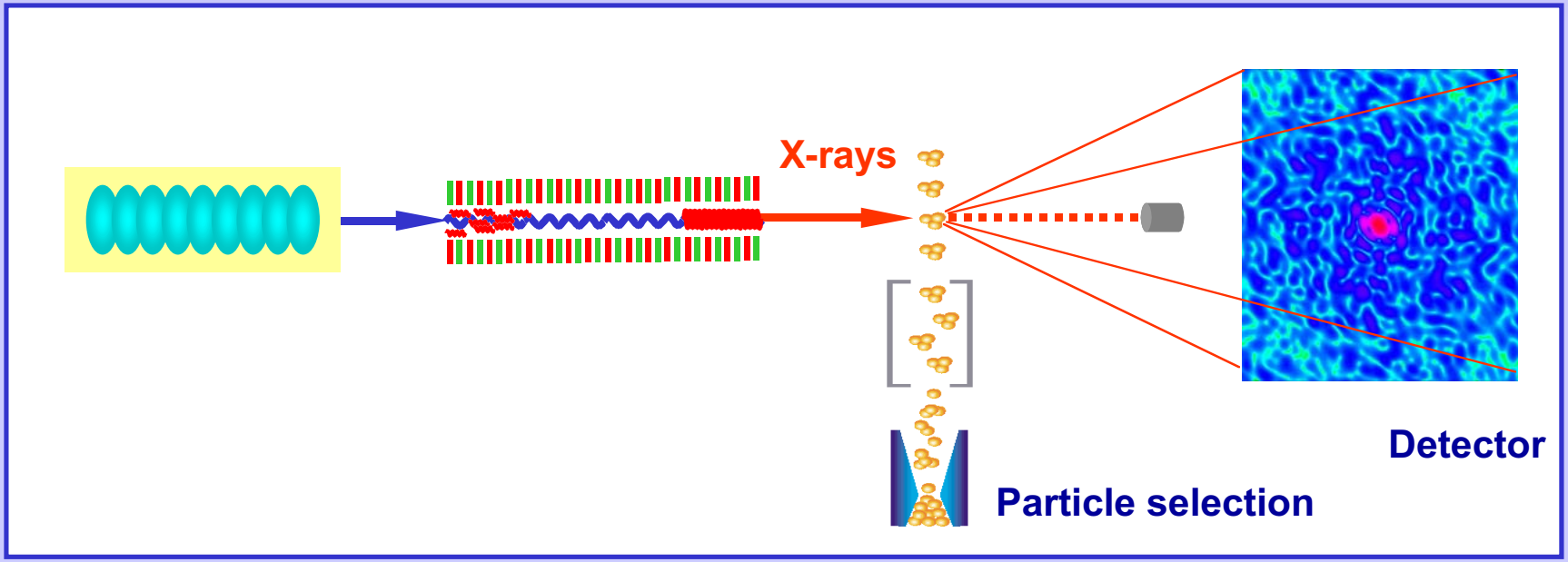

The scattering leads is a continuous scattering pattern, the

molecular transform $|F(\underline{k})|^2 = |FT\ \{\rho(\underline{x})\}|^2$,

that contain, like the Bragg diffraction pattern, the information about the three-dimensional electron density distribution. Measurement of several cuts and reconstruction allows then to determine the full 3D structure.

Femtochemistry
Initiation and probing of reactions

Ultrafast X-ray scattering

- Direct information about atomic positions (in contrast to optical spectroscopy)
- Several techniques to investigate crystals, disordered solids, or liquids

Electron transfer
Excitations
Vibrations
Bond breakage
Bond formation
Rotations
Melting

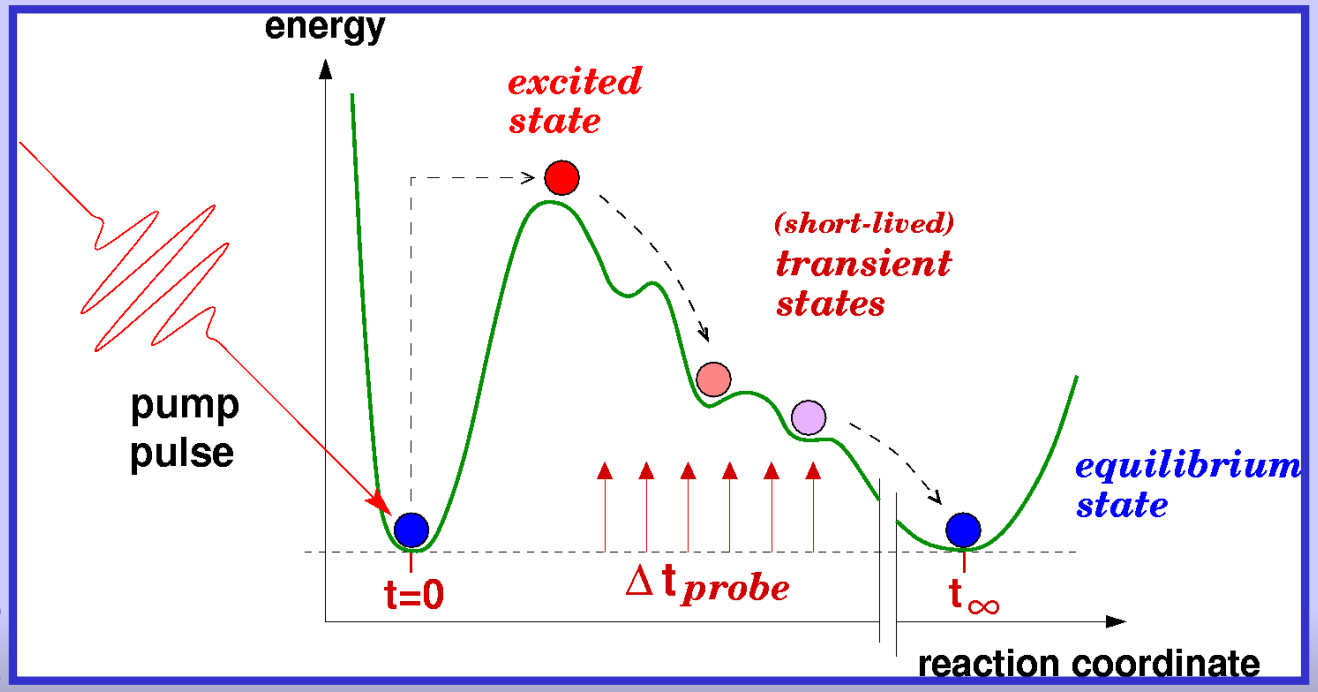

principle of pump-probe experiments

Condensed-matter physics
Dynamic properties

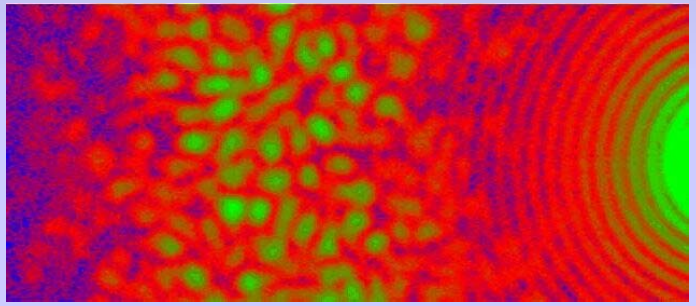

Disordered/Soft matter

- Coherent scattering to observe dynamics
- Surface/interface reconstruction
- Friction

Ultrafast phase transitions

- Magnetic switching
- Structural changes ↔ electronic properties

Electronic transitions

- Excitation and relaxation of electron states
- Changes of band structure

Phenomena

- Solidification
- Melting
- Nucleation, growth, ...

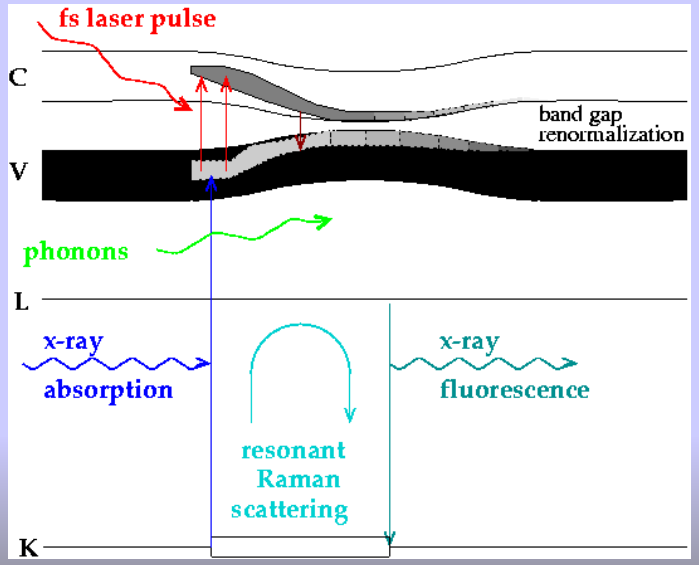

XFEL Technical Design Report (2001)

Condensed-matter physics
Beyond thermal equilibration

- Energy deposition by intense laser irradiation
- Different dynamics of e-h ($T_{e\text{-}h}$) and lattice (T_L)
- Equilibration phenomena

Non-thermal melting

Coherent optical phonons

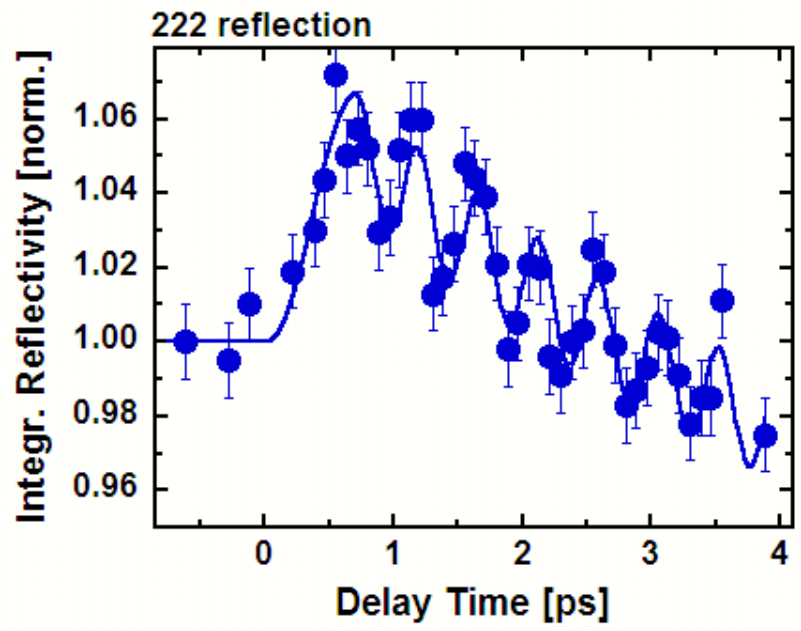

K. Sokolowski-Tinten et al., Nature 422, 287(2003)

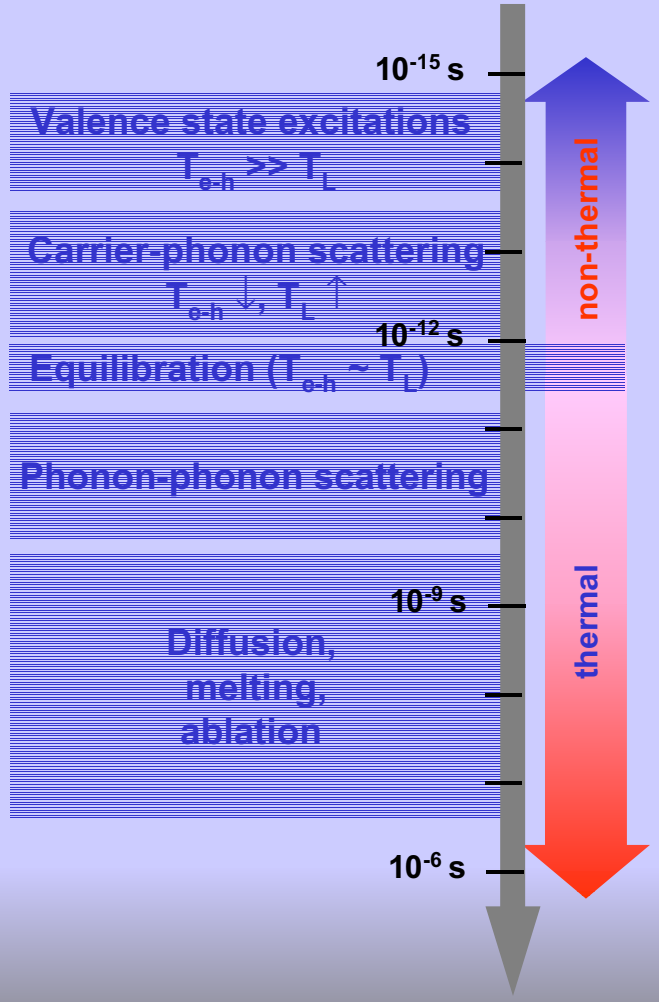

Plasma physics

Interaction with matter
- Opacity measurements
- Pumping laser transitions

Isochoric heating of plasmas
- Solid density plasmas
- T_e up to few 100 eV
- Plasma phase transitions

Diagnostics of plasmas
- Thomson scattering
- Plasma dynamics
- Time-resolved pump-probe

Study of ablation processes
- Bulk ablation
- Microscopic processes

Talks by Fill, Eidmann, London, Krzywinski, Meyer-ter-Vehn,
Poster by Redmer et al.

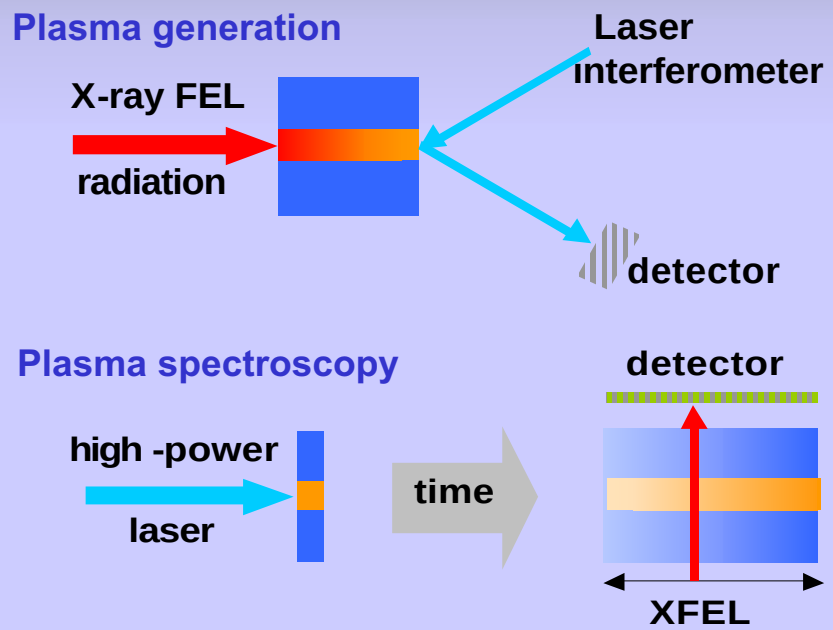

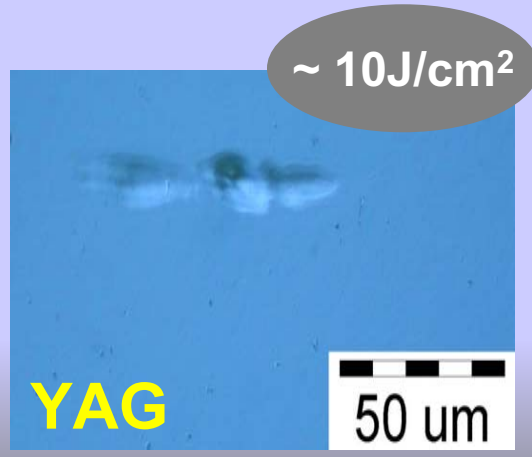

Data obtained in TTF experiments at ~12 eV
Courtesy:
J. Krzywinski

X-ray source requirements

PB !

Life sciences — **Intensity, Focus, Ultrashort**

- Structure and function or virus particles, membranes proteins and assemblies, or entire cells
- Time-dependent processes, e.g. first steps of protein folding

Femtochemistry — Intensity, **Ultrashort**

- Atomic understanding of chemical reactions at real-time
- Solid-state and liquid chemistry

Condensed-matter physics — Intensity, **Ultrashort, Coherence**

- Atomic understanding of chemical reactions
- Solids, liquids

Plasma physics — **Intensity, Focus, Ultrashort**

- Create plasmas using X-rays
- Plasma diagnostics

Minority phases, forbidden reflections, diffuse scattering — **high average flux**

Multiphoton processes, Non-linear processes, ...

High repetition rate FELs

Superconducting machines allow to accelerate trains of electron bunches

- choice of filling pattern and beam distribution to various FELs
- sub-Hz to few 10 kHz repetition rates

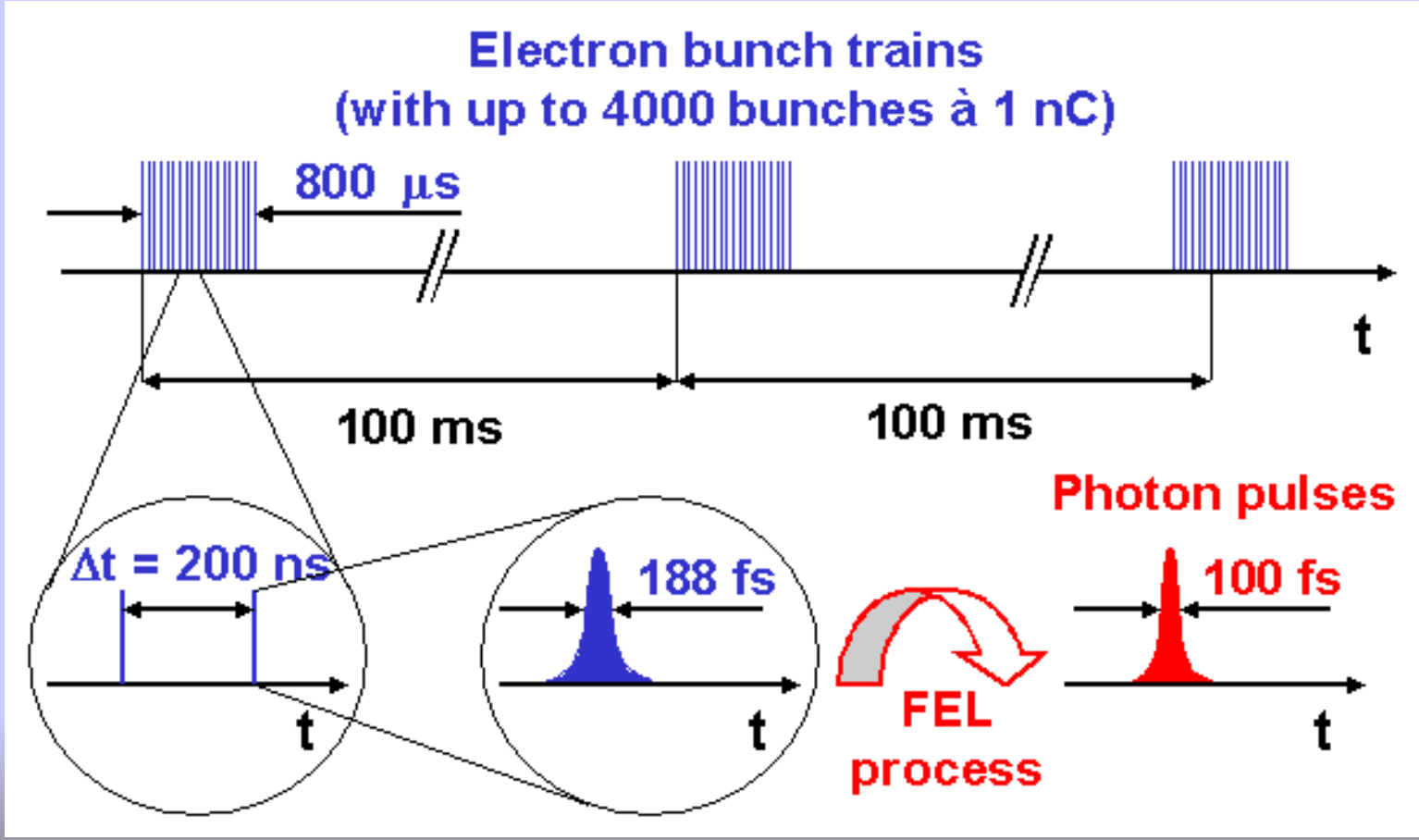

XFEL Technical Design Report (2002)

Outline

- Scientific applications using FEL radiation
- **Review of parameters**
- Roadmap towards short-wavelength FELs

FEL beam parameters

		XFEL		VUV-FEL	
	units	0.1 nm	1.0 nm	6 nm	40 nm
peak brilliance	ohts/s mm^2 mrad^2 0.1%	5.4×10^{33}	4.0×10^{32}	2.4×10^{30}	2.4×10^{29}
ave. brilliance	ohts/s mm^2 mrad^2 0.1%	1.6×10^{25}	2.0×10^{24}	3.5×10^{20}	5.0×10^{20}
photons/pulse	#	1.2×10^{12}	2.0×10^{13}	1.8×10^{13}	6.6×10^{12}
peak power	GW	24	100	2.8	0.8
power density*	W/cm^2	2.4×10^{18}	1.0×10^{19}	2.0×10^{17}	8.0×10^{16}
source size	µm	110	65	140	350
divergence	µrad	0.8	3	24	40
bandwidth	%	0.08	0.4	0.36	0.4
pulse duration	fs	100	100	200	55

* focusing assumes 100% efficiency, 1 µm^2 focal spotsize

From: XFEL Technical Design Report (DESY, Hamburg, 2002)
SASE FEL at the TESLA Facility, Phase 2 (DESY, Hamburg, 2002)

Radiated power

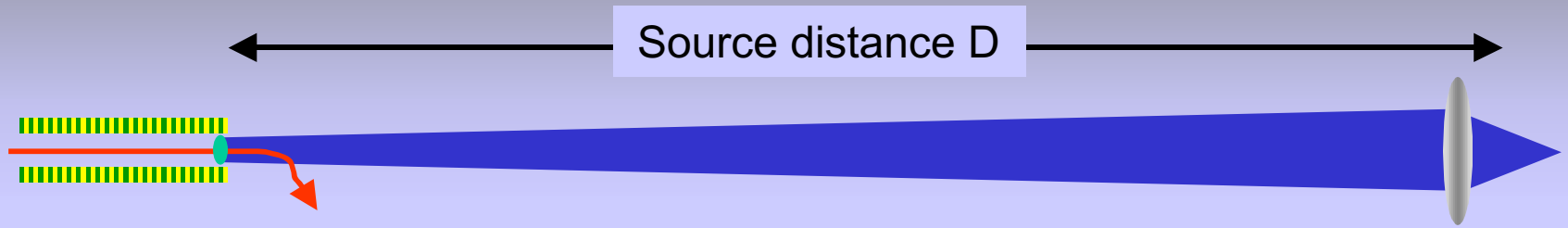

Source	λ [nm]	**Pulse energy** [mJ]	**D** [m]	**A_1** [mm]	**PD_{A1}** [W/cm^2]	**$PD_{A2=1\mu m}$** [W/cm^2]
XFEL	0,1 1,0	2,4 10	800 400	0,64 1,2	7×10^{12} 9×10^{12}	3×10^{18} 1×10^{19}
VUV-FEL	6,0 40,0	0,6 0,03	75 75	1,8 3	1×10^{11} 1×10^{10}	2×10^{17} 8×10^{16}
3rd SR	0,1	0,02	40	1	2×10^{7}	2×10^{13}
SPPS	0,15	0,00001	100	2	$2,5\times10^{6}$	1×10^{13}

* focusing assumes 100% efficiency, 1 μm^2 focal spot

Single particle imaging

Intense X-ray pulses lead to damage

- Photoelectric effect (90%)
  - ⇒ **Auger effect, shake-up processes, secondary electron cascades**
- Elastic scattering (7%)
- Inelastic scattering (3%)

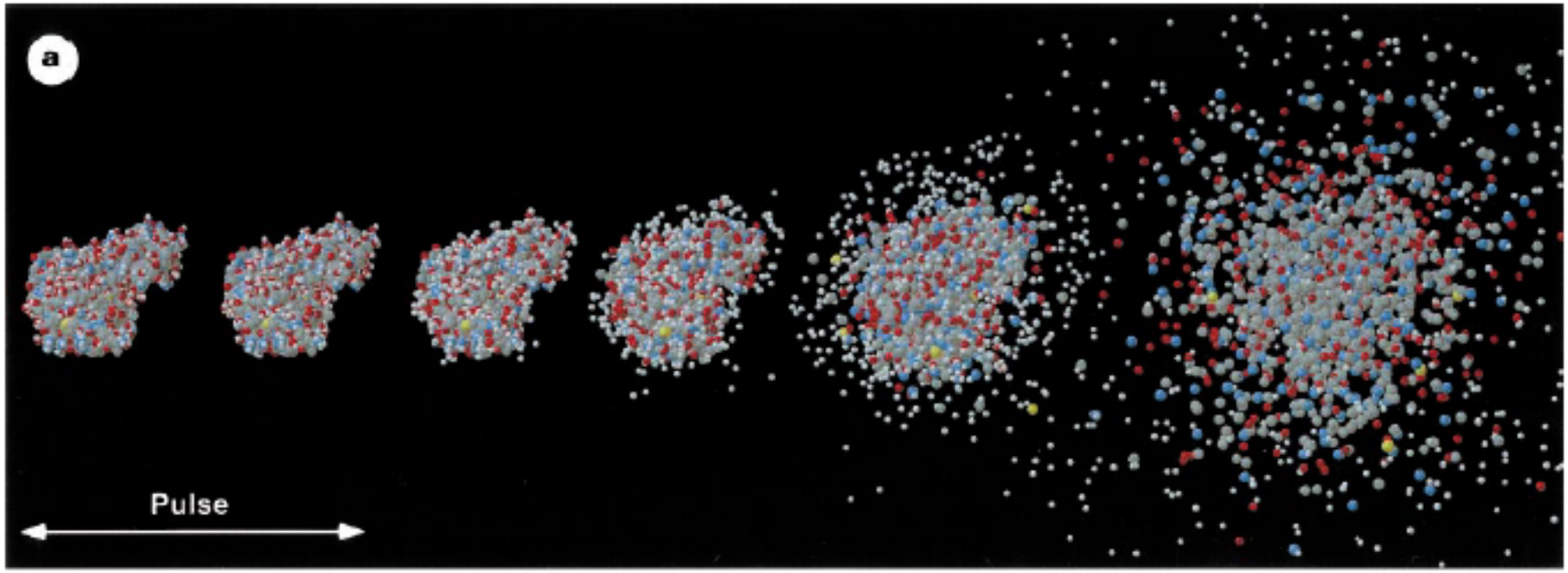

R. Neutze et al., Nature 406, 752(2000)

Cluster experiments at the VUV-FEL

- Observation of multiphoton processes
- Cluster dynamics after irradiation
- Coulomb explosion at short wavelength

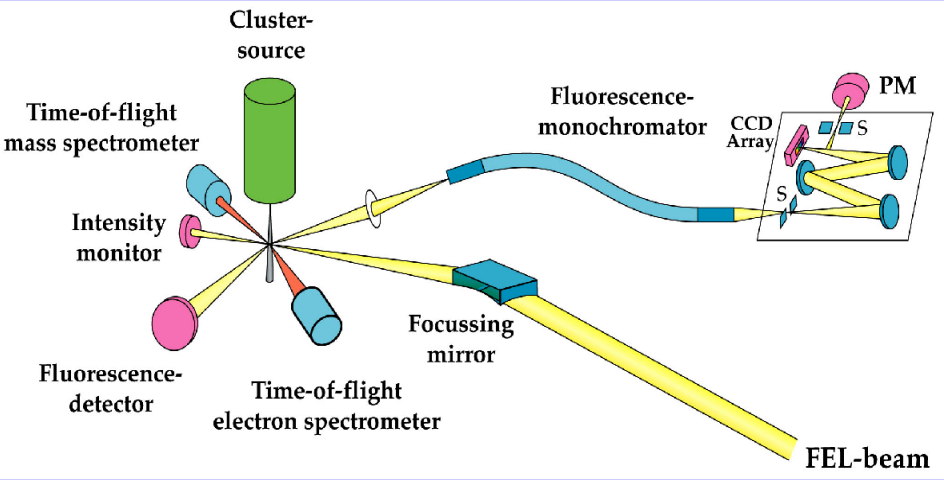

H. Wabnitz et al., Nature 420, 482 (2002)

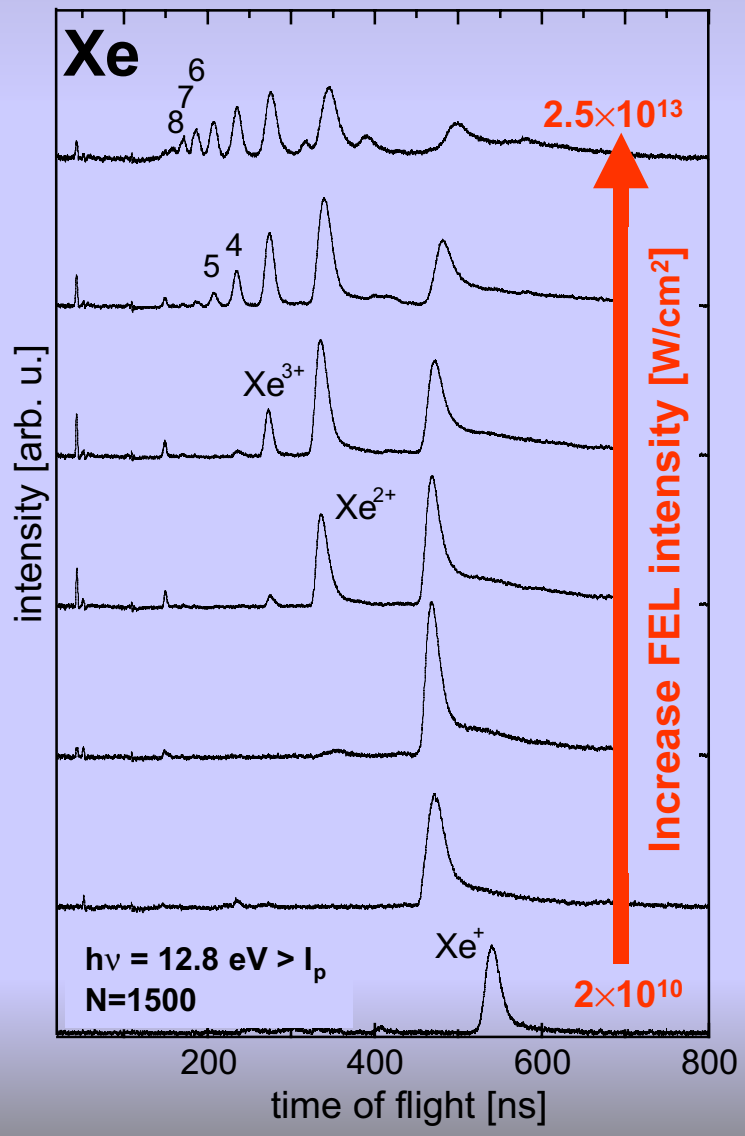

Average power load on optics

Mirror optics

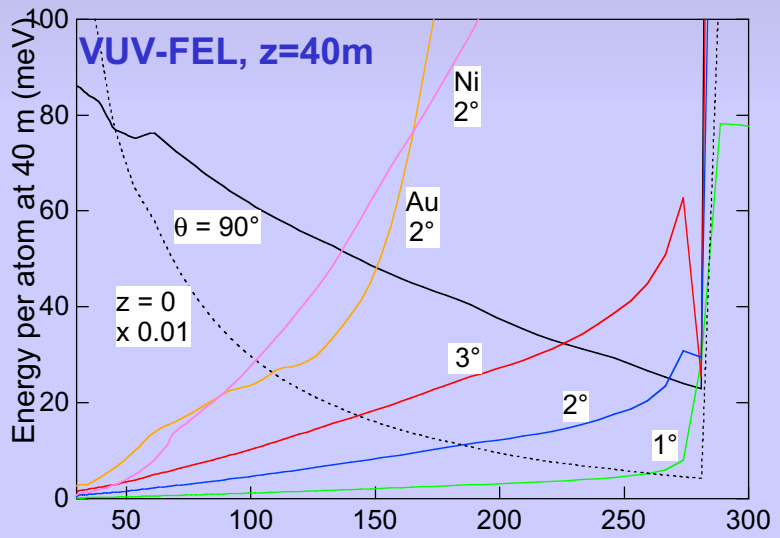

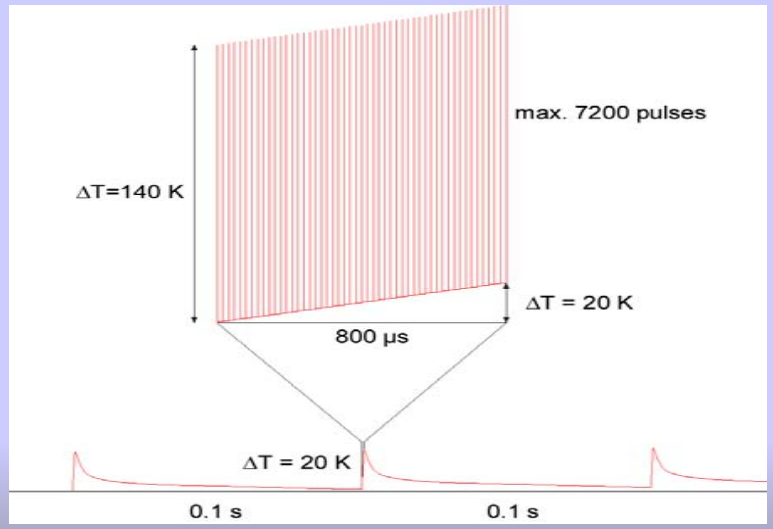

Crystal optics

XFEL diamond

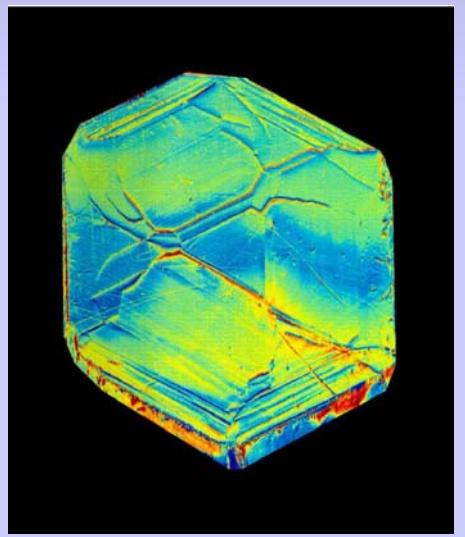

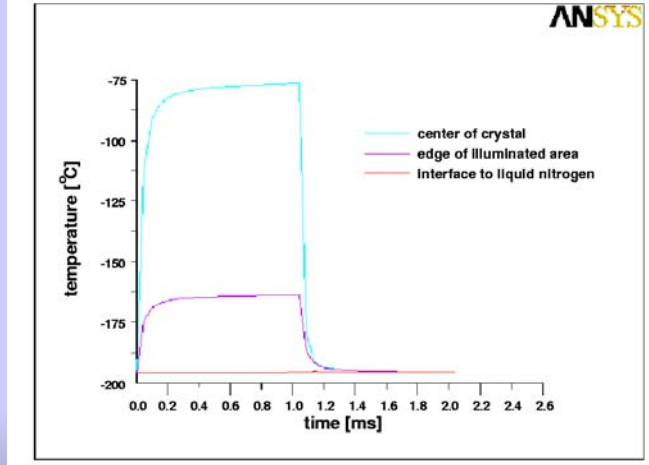

But how does the interaction occur at times smaller thermalisation ?

Outline

- Scientific applications using FEL radiation
- Review of parameters
- **Roadmap towards short-wavelength FELs**

Status of short-wavelength projects

Name	Location	Wavelength	S.o.O.	Status
DUV-FEL	**BNL**	**? - 266 nm**	**2003**	**operating**
VUV-FEL	**DESY**	**6 - 100 nm**	**2004**	**building**
SCSS	**Harima**	**3.6 - 40 nm** later upgrade	**2006**	**funding started**
LCLS	**SLAC**	**0.15 - 1.5 nm**	**2008**	**building**
XFEL	**DESY**	**0.1 - 6 nm**	**2011**	**funding phase** (multi-national)
4GLS	**Daresbury**	**2 - >1000 nm**	**2011**	**funding for detailed proposal**
FERMI	**ELETTRA**	**2 – 100 nm**	**?**	**proposed**
SPARX	**Frascati**	**1,5&13,5 nm**	**A + 6y**	**proposed**
MIT-XRL	**MIT**	**2 – 100 nm** later upgrade	**A + 6y**	**proposed**

Roadmap towards 0,1 nm

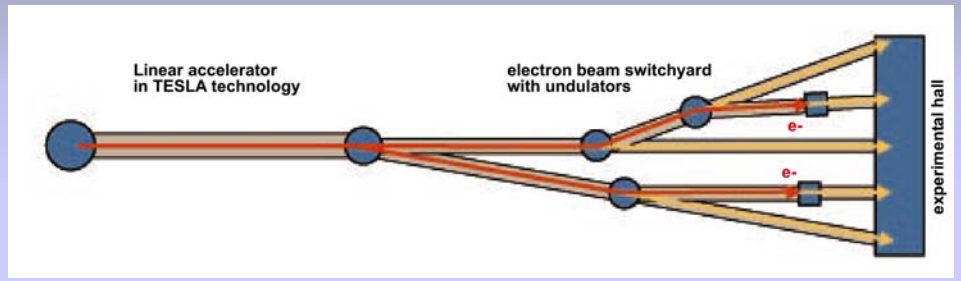

2011 European
XFEL (Hamburg)

2008 LCLS (Stanford)

2003-06 SPPS

Laser sources
HHG, Plasma, ..

2004 VUV-FEL
@ TTF
(Hamburg)

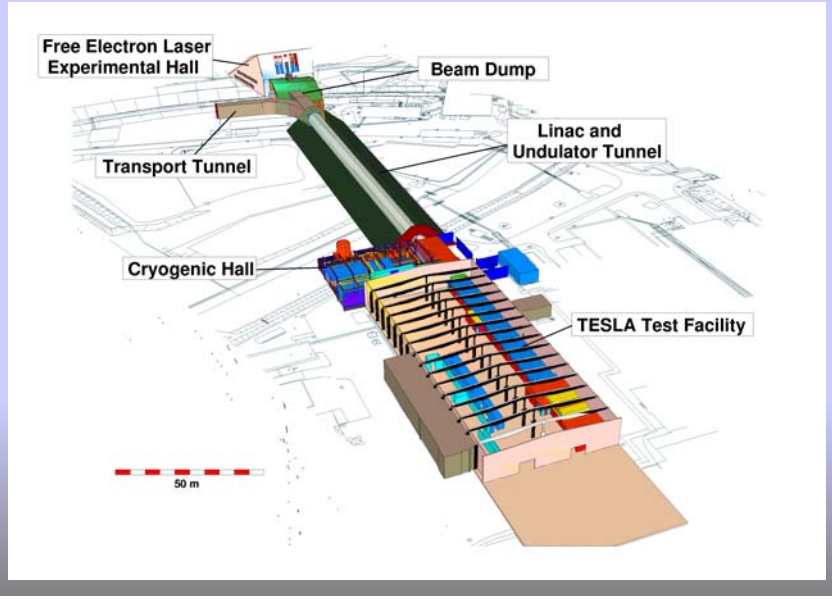

2000-02 TTF-1 (Hamburg)

2000-01 LEUTL (Argonne)

1980 initial paper

VUV-FEL at the TESLA Test Facility

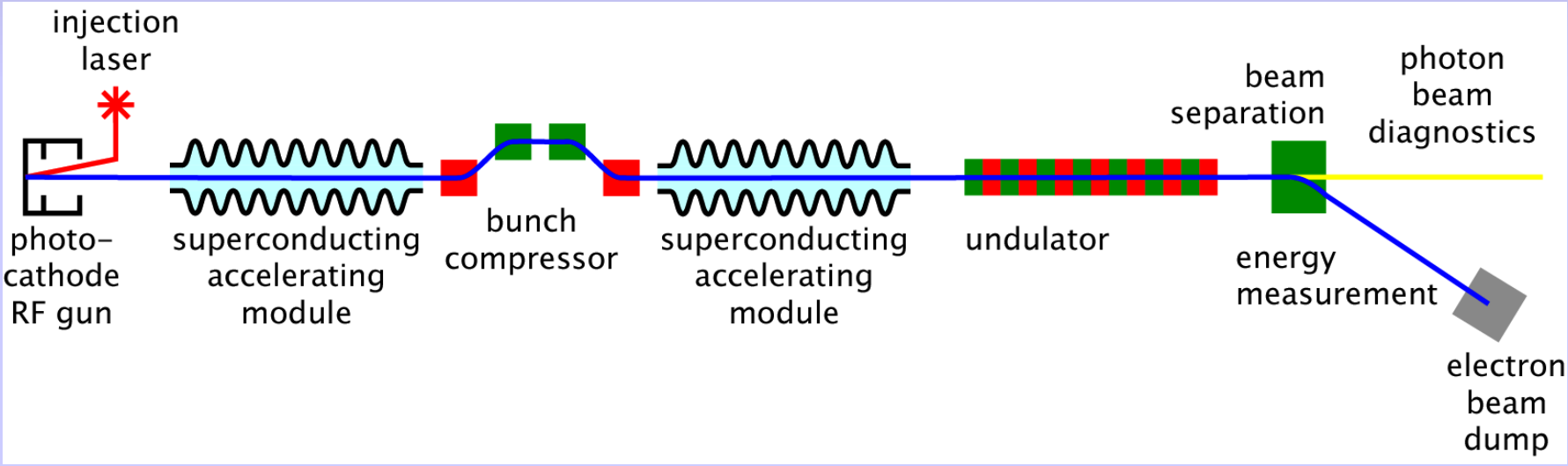

Phase I: The ‚photon' goal of TTF was to demonstrate the SASE principle at short wavelength and for initial experiments.

Phase II: User experiments and FEL science

Talks by Krzywinski, Plönjes

User experiments at the VUV-FEL

First round of proposals in 2002

- User operation starting 2005
- FEL / user operation shared
- Start at ~ 40nm/30eV
- Unfocused/Focal spot 20µm
- High resolution monochromator

- Strong oversuscription
- Wide range of scientific areas
- Open facility
- Future calls for proposals will follow

Talk by E. Plönjes

Atoms, molecules and clusters

Condensed-matter

Plasma physics

- Interaction with solid matter
- Ablation
- Heating of solid-density matter
- Plasma phase transitions
- New plasma diagnostics

Life sciences

- Coulomb explosion of clusters & biomolecules

Technical developments

- Diagnostics
- Pump-probe experiments

Linac Coherent Light Source

The LCLS
(Linac Coherent Light Source)

first hard x-ray FEL radiation source
0.15 – 1.5 nm wavelength range

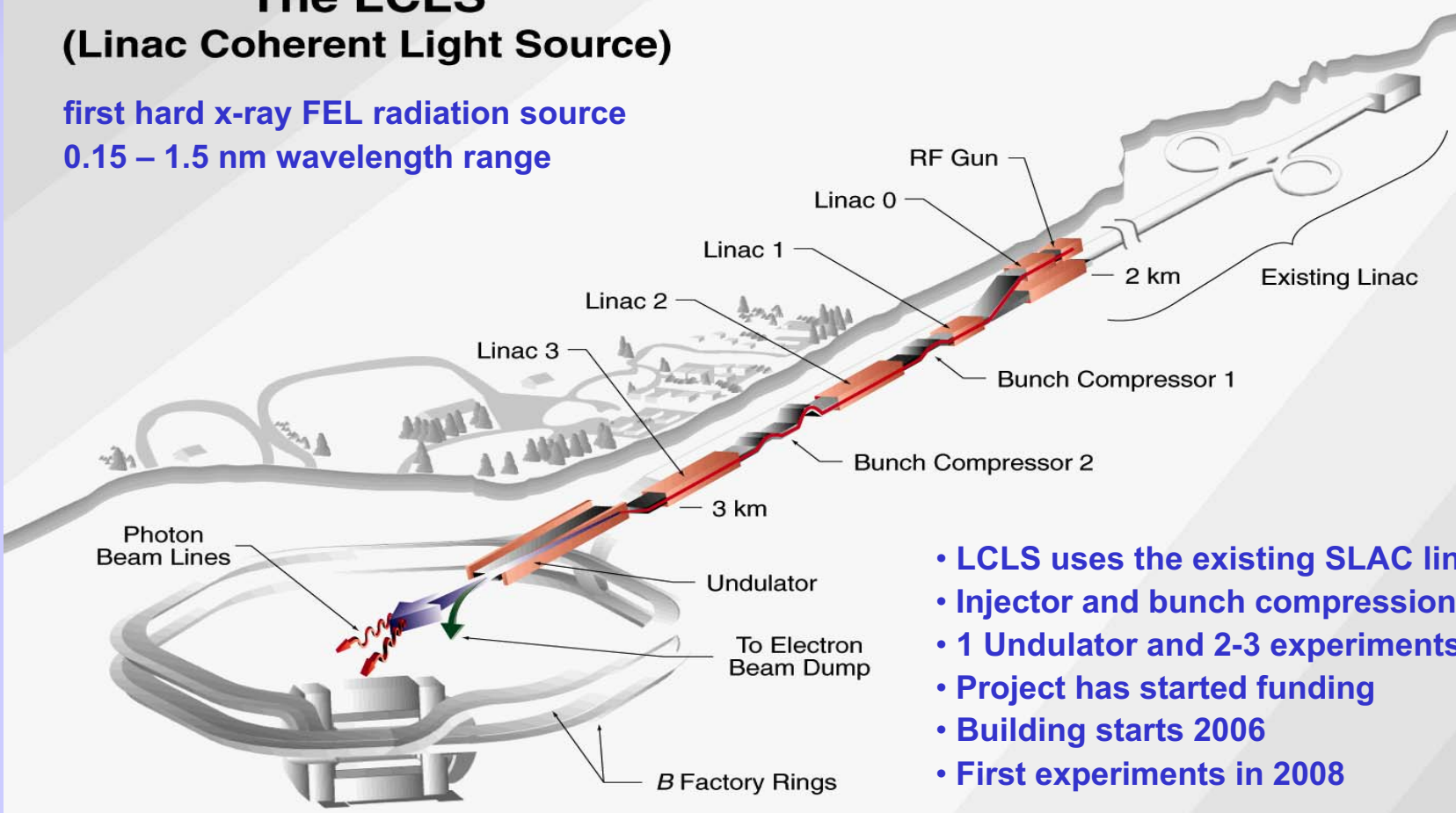

- **LCLS uses the existing SLAC linac**
- **Injector and bunch compression**
- **1 Undulator and 2-3 experiments**
- **Project has started funding**
- **Building starts 2006**
- **First experiments in 2008**

- **Possibility for later upgrade**

10-97
8360A1

The European XFEL laboratory

- **Original proposal (March 2001) was to use part of the TESLA linear accelerator.**
- **Based on a decision by the German Government both projects it is now planned to build an XFEL with its own linear accelerator.**
- **Germany proposes a site and will cover 50% of the building cost.**
- **Site and technical parameters are currently reconsidered.**
- **Formation of European working groups**

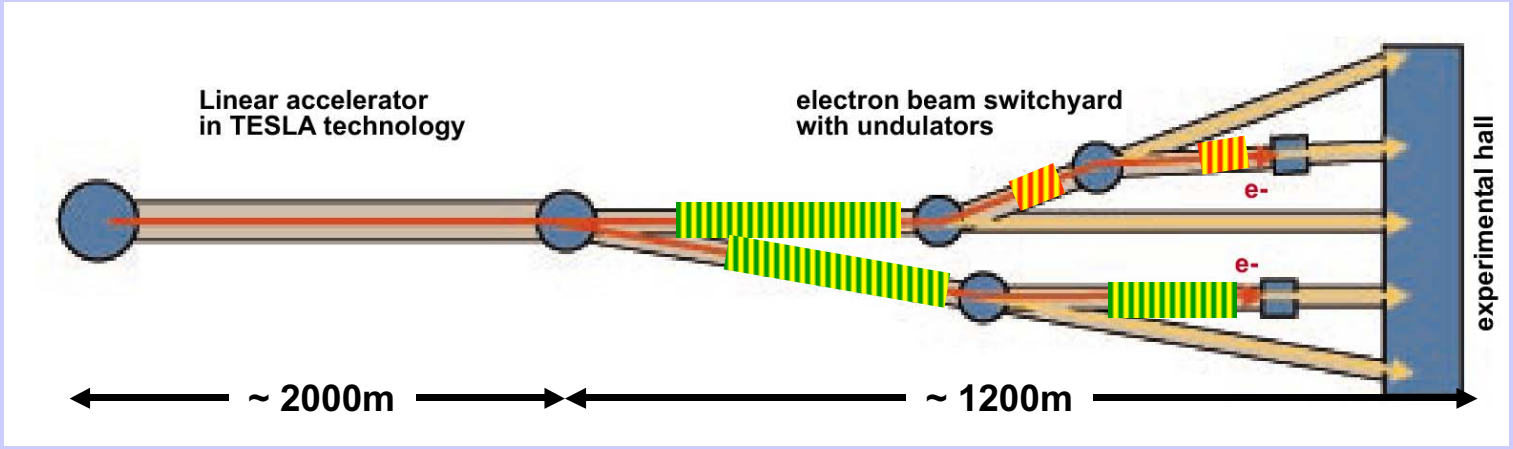

3 FEL and 2 beamlines for spontaneous synchrotron radiation with 10 independent experimental stations

Challenges for 0,1nm FEL experiments

Accelerator issues

- Emittance
- Coherent synchrotron radiation
- Stability

Pump-probe experiments

- Synchronization
- Arrival jitter
- 1-color, 2-color, FEL beam split&delay

X-ray optics

- Stability
- Radiation damage

Diagnostics tools

- Pulse duration measurement
- Coherence quantification

Experimental techniques

Use present and up-coming shortpulse X-ray facilities to tackle these fields

SPPS
Plasma sources
HHG
VUV-FEL

Sub-Picosecond Pulse Source

The SPPS collaboration

Stanford Linear Accelerator Center SLAC
Deutsches Elektronen-Synchrotron DESY
Universities of Uppsala & Lund & Chalmers
University of Copenhagen
Advanced Photon Source
University of California Berkeley
University of Michigan - FOCUS
University of Chicago - BioCARS
Brookhaven National Laboratory

Aim of the SPPS experiments:

Develop and test experimental techniques for ultrafast x-ray science using accelerator sources.

- Measurement of the pulse duration
- Determination and optimization of jitter between independent sources
- Scientific exploratory experiments

Sub-Picosecond Pulse Source

Sub-ps pulse generation

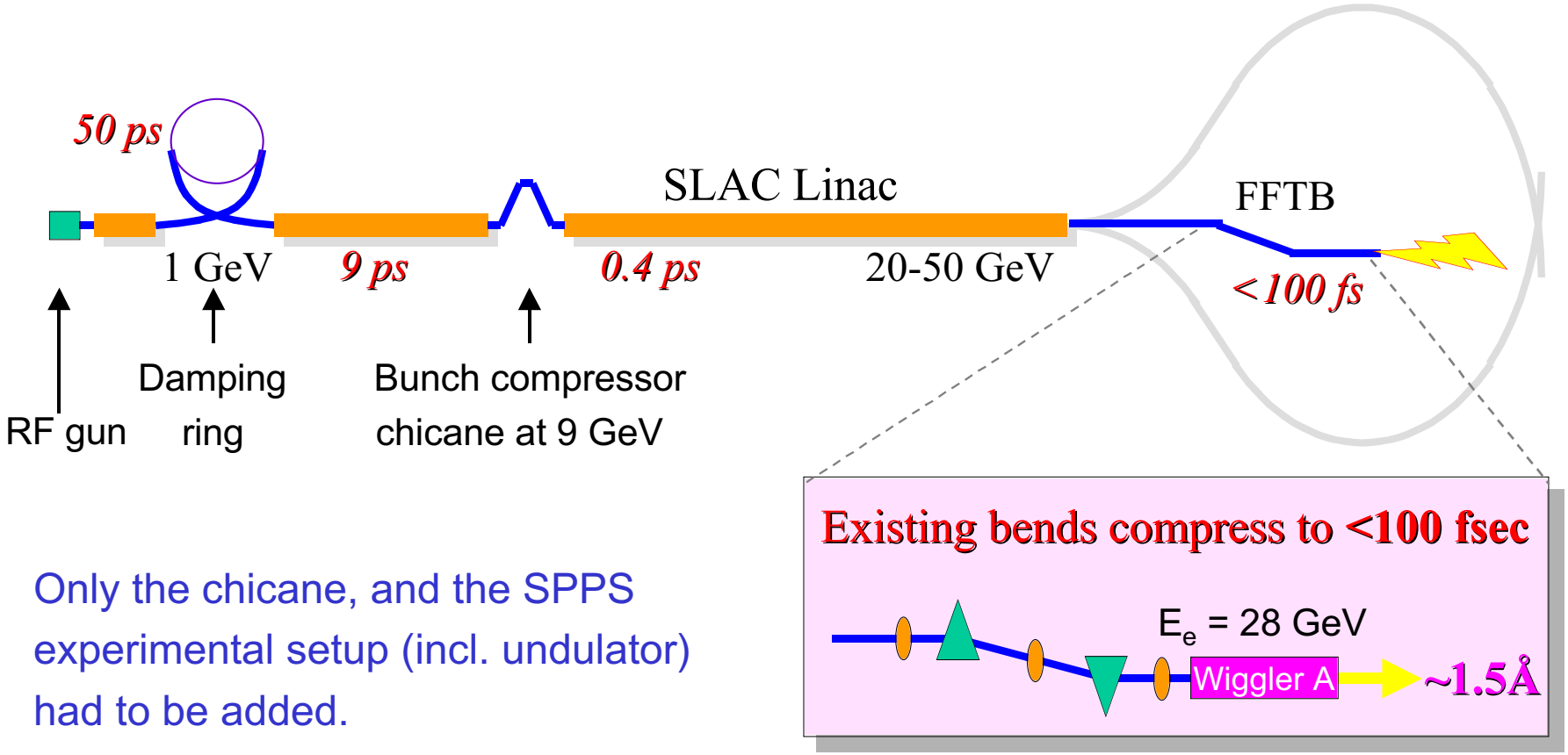

Only the chicane, and the SPPS experimental setup (incl. undulator) had to be added.

Operation: May 2003 – 2006

Sub-Picosecond Pulse Source

X-ray beam performance

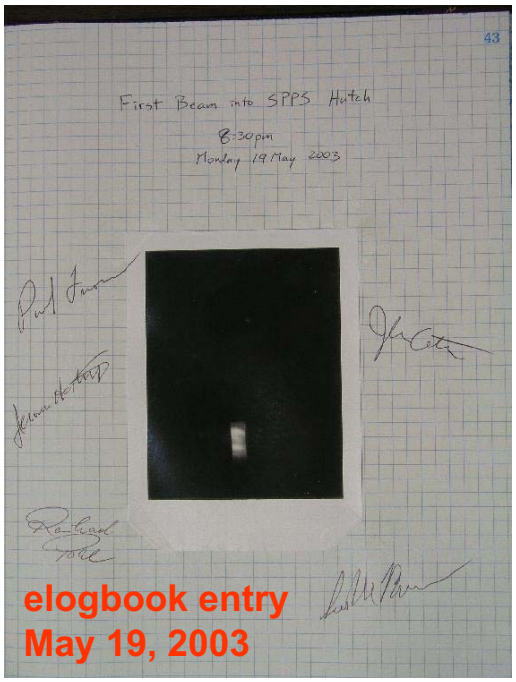

elogbook entry
May 19, 2003

- X-ray beam had been adjusted for the 1st run to an energy of 9.3 keV (1.4 Å)
- integral flux ~7.3×10^7 photons/pulse
- unfocused spot size 2 x 2 mm^2
- bandwidth 1-2 %
- intensity fluctuations 10-20%

Diffraction tests (all static)

photo-active Xtals & powders, organic Xtals, water, ice

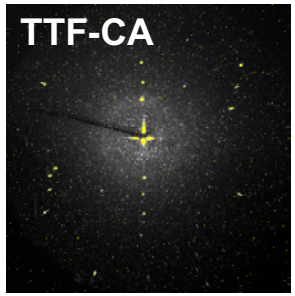

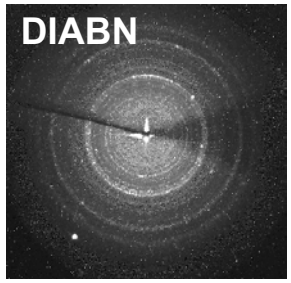

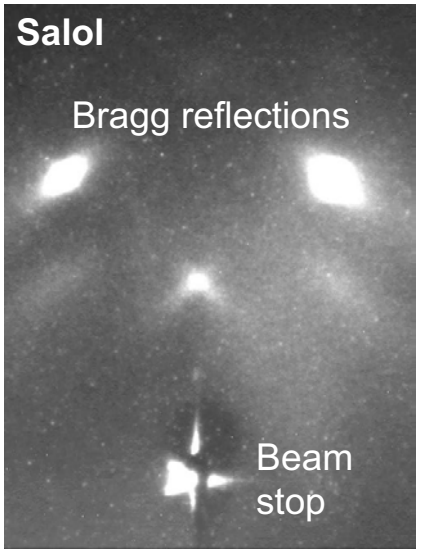

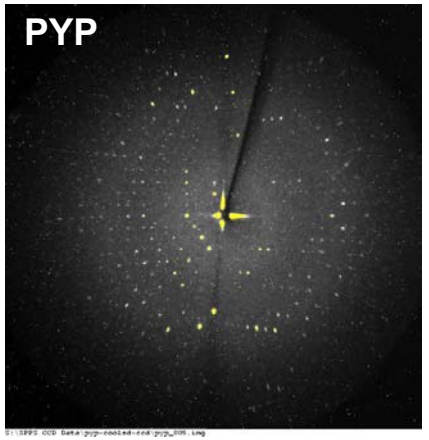

Sub-Picosecond Pulse Source

Single shot X-ray diffraction

Intensity fluctuations

- 90 exposures @ 10 Hz,
- gated CCD, 62 ms
- $\Delta\Phi$=0, Max. of rocking curve

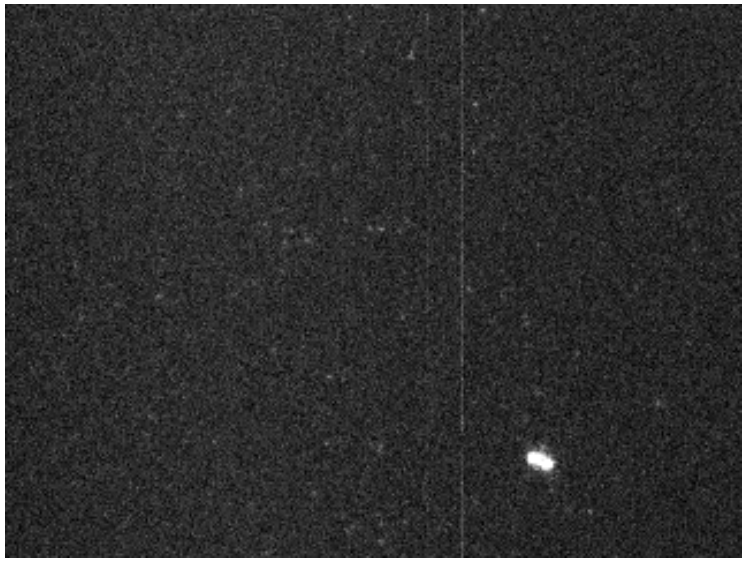

Probing the rocking curve

- 18 steps: $\Delta\Phi$=-1.0° to $\Delta\Phi$=+0.4°
- Single exposures
- gated CCD, 62 ms

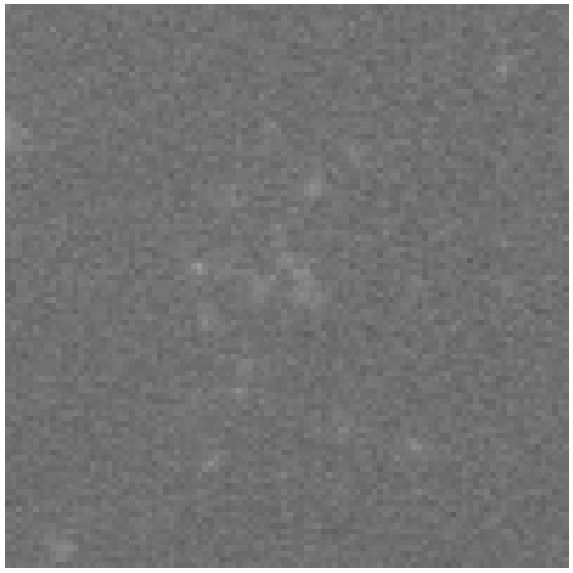

SLAC

DESY

Summary

- **Science case for FEL is wide spread and very ambitious.**
- **FEL will deliver high intense radiation, ultrashort pulse duration for the short-wavelength regime down to 0,1nm.**
- **The detailed understanding of the interaction process of the intense radiation with matter at ultrashort time scales is missing.**
- **Experiments using the regime 6-100nm will become possible in the near future at the VUV-FEL at DESY**
- **Other acelerator-based and laser-based shortpulse sources will be used to develop, verify, and establish techniques and applications**
- **There is a clear path towards 0,1nm FEL experiments in 2008/2011**

Acknowledgements

Th. Möller and collaborators
J. Krzywinski and collaborators
TESLA collaboration
SPPS collaboration
All authors contributing to the various design reports for the XFEL

The end

Soft X-Ray Laser-Plasma Sources and Applications

I.C.E. Turcu
Central Laser Facility
Rutherford Appleton Laboratory, UK

Ultrashort High Energy Radiation and Matter

10th of October, 2003, Varenna, Italy

CONTENTS

- LPP Source Spectrum and Brightness
- High power LPP X- ray (1nm) and EUV (13nm) sources for Lithography
- Radiobiology and DNA damage and repair studies (1.2 keV/1nm)
- Microscopy (3.37nm/368eV)
- X-ray fluorescent imaging: elemental mapping (0.9 keV/1.4nm)
- Conclusions
- Acknowledgements

LPP Source Spectral Brightness estimates in Red (300W/300Hz/800ps JMAR laser driver)

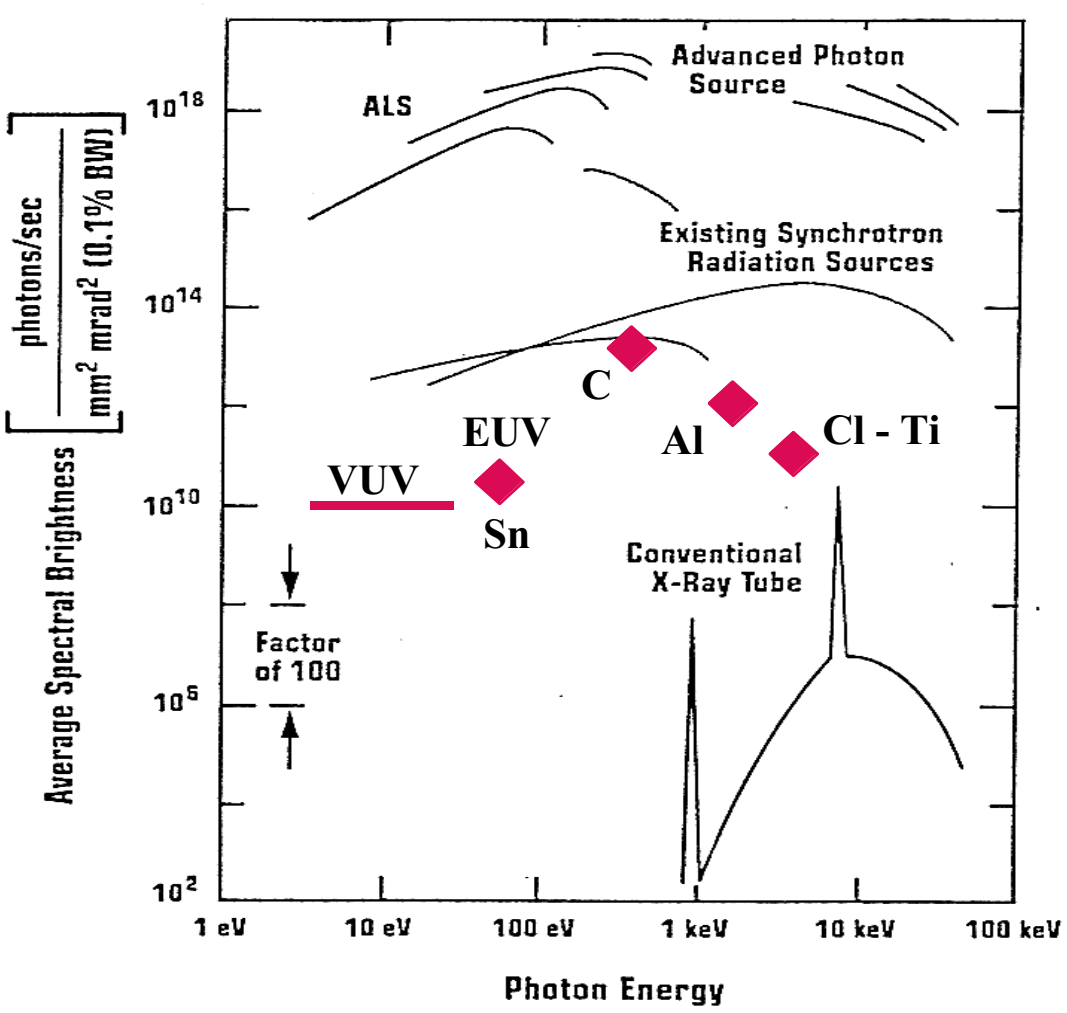

VUV Beamline on Psec LPP (Gray Lab, RAL)

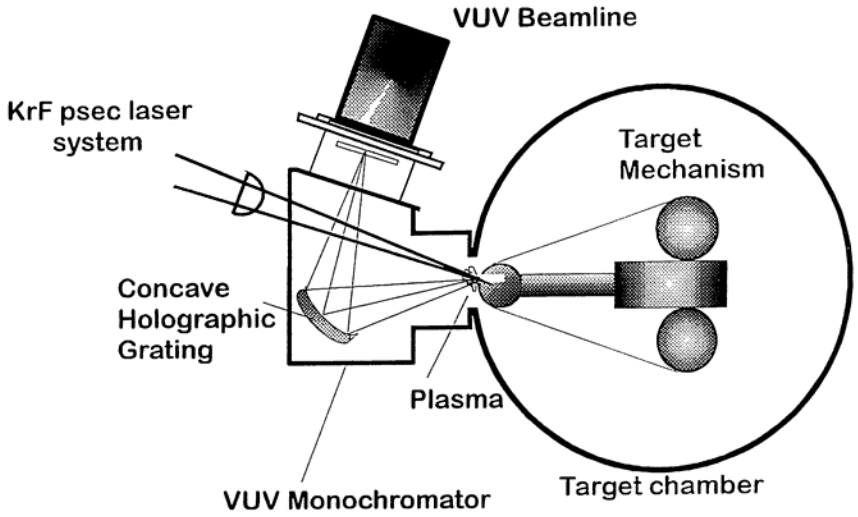

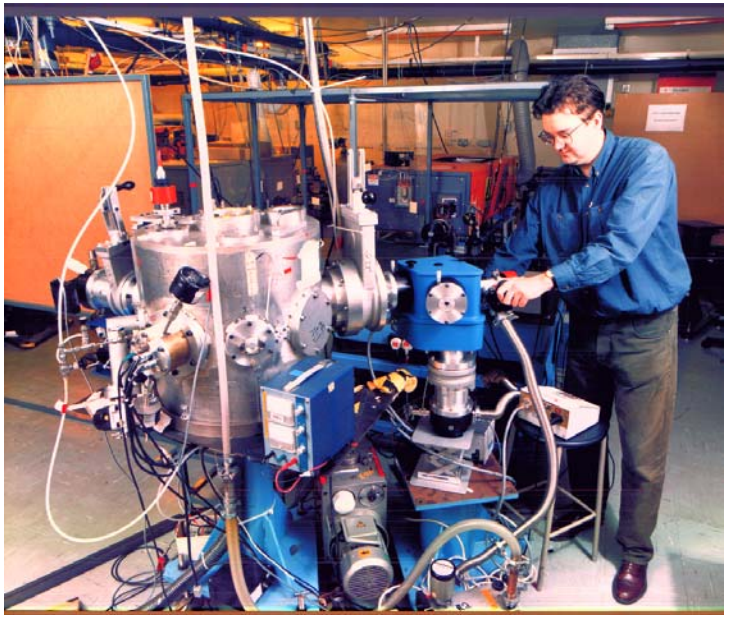

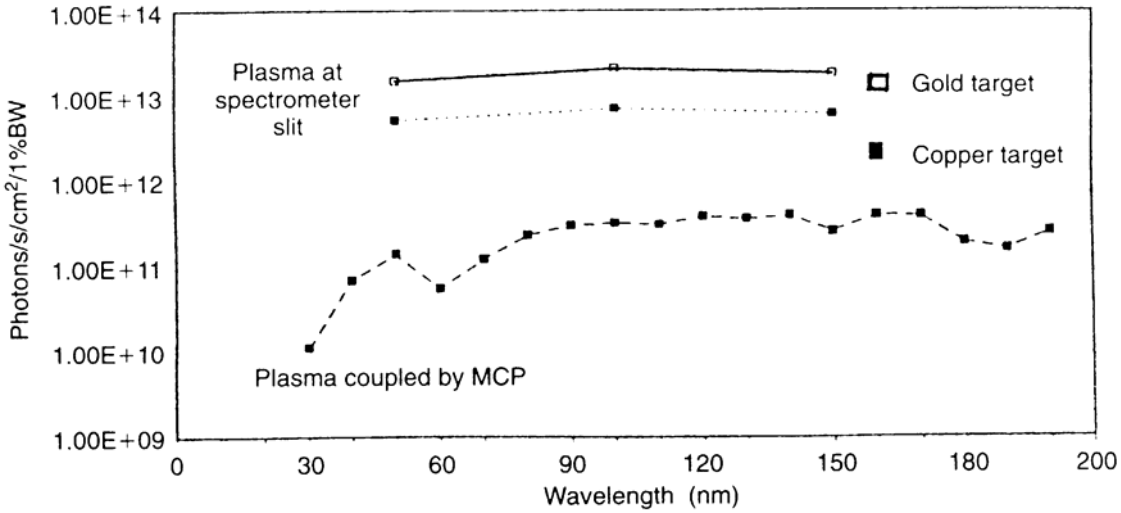

VUV Beamline exit slit is 5mm x 0.25mm

VUV detectors used: electrometer, PIN diode, photographic Q-plate

Water-Window (280-530 eV) Soft X-ray Emission from Laser-Plasmas (RAL, KCL, Essex U , Osaka U)

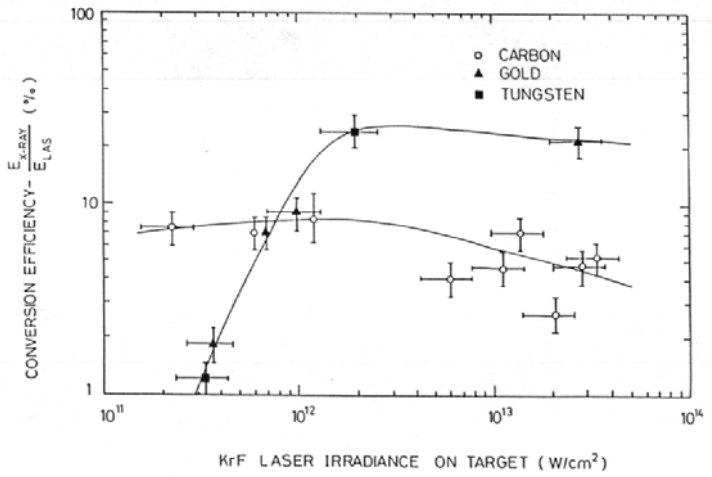

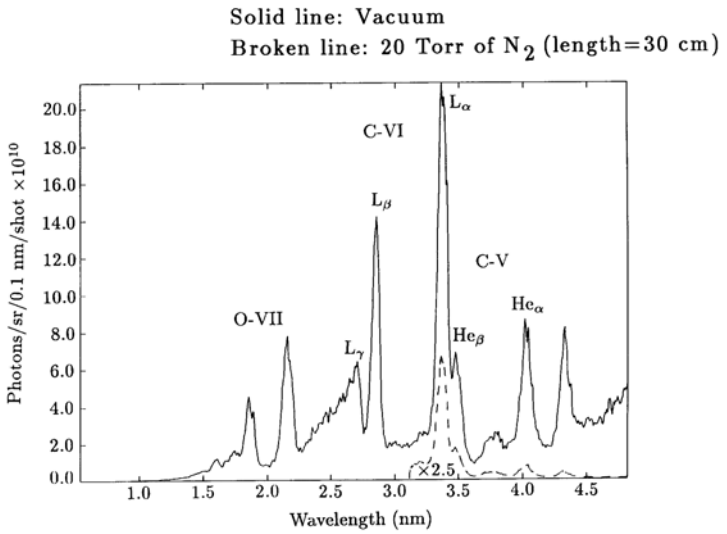

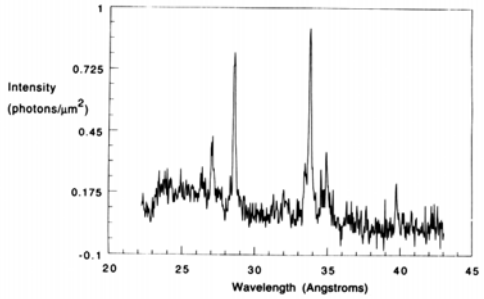

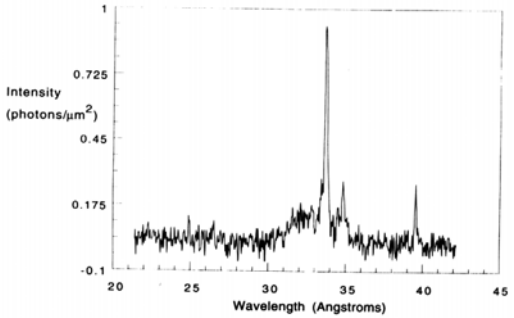

X-ray lateral coherence length is 20μm at 30cm from plasma source

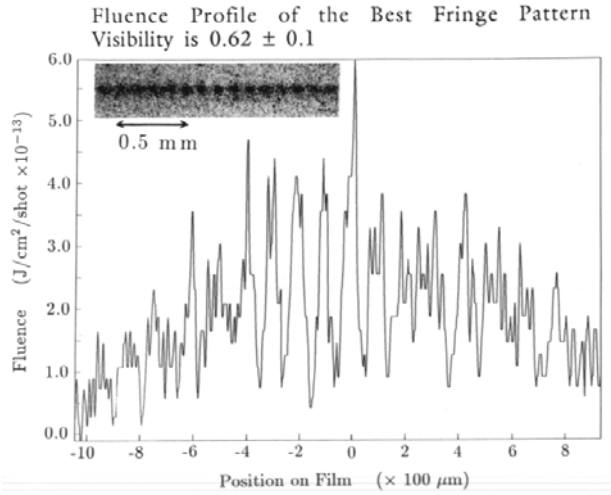

KeV X-Ray Emission from 4ps KrF Laser-Plasmas (RAL, Essex U)

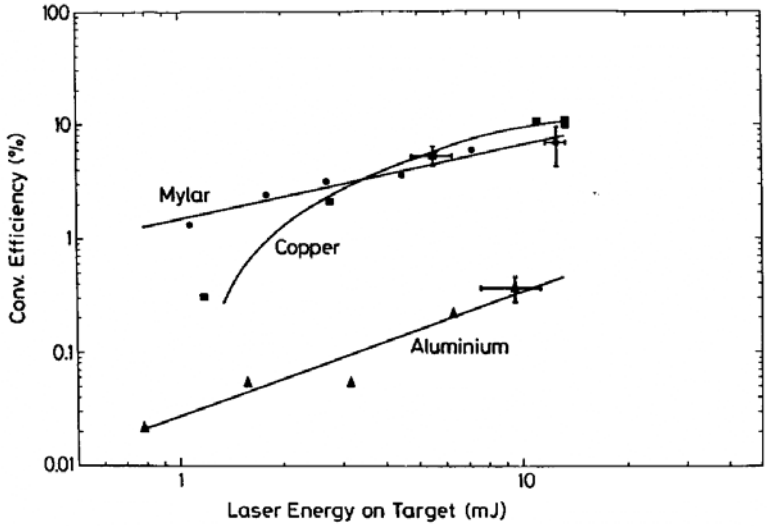

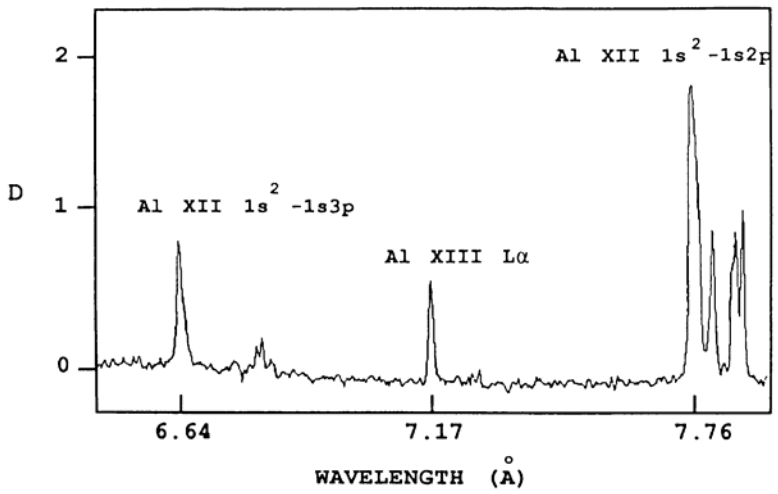

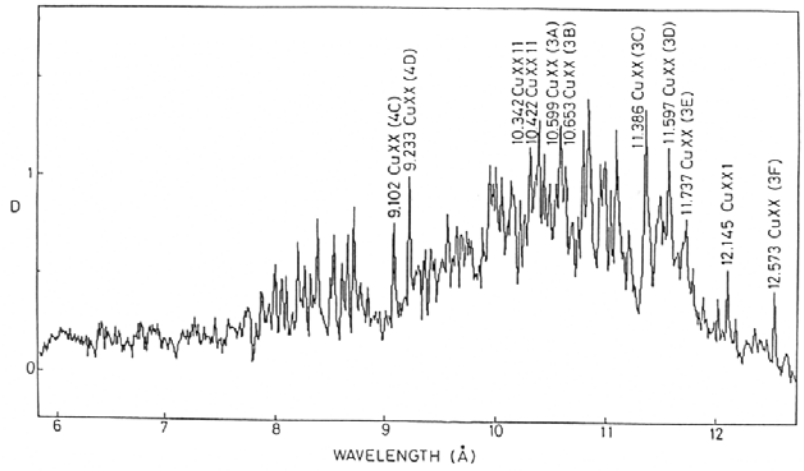

Laser-Produced-Plasma Source Spectrum: Potential Applications

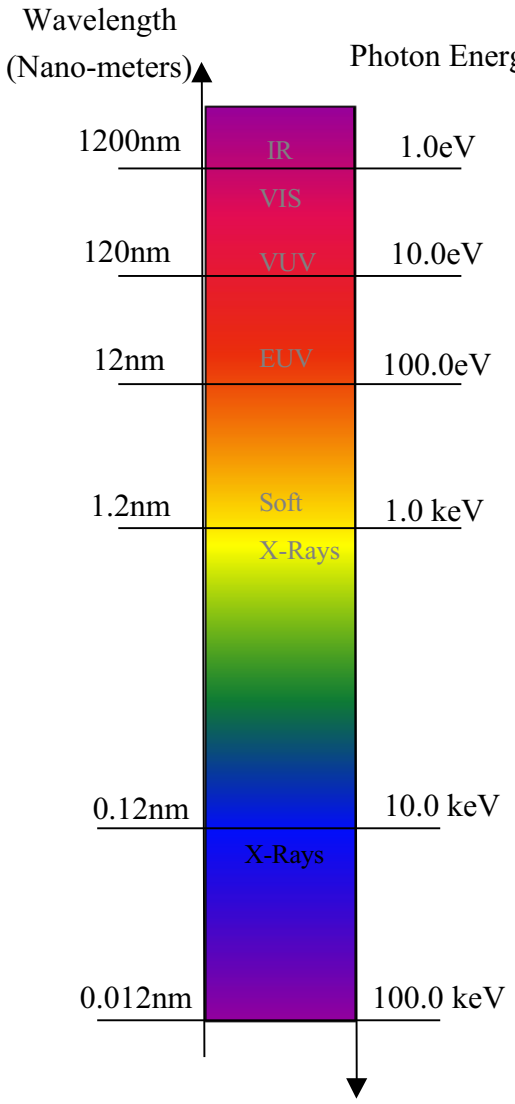

IR / VIS / UV (PS / FS LASER ITSELF): ABLATION, MICROMACHINING

VACUUM ULTRAVIOLET: PHOTOBIOLOGY/CHEMISTRY

EXTREME ULTRAVIOLET :
EUVL (PROJECTION, 90eV) 4-256 GBIT MEMORY
SPECTROSCOPY (CONTINUUM)

SOFT X-RAYS : CPL (PROXIMITY, 1.2keV) 4-256 GBIT MEMORY IC
DEEP LITHOGRAPHY FOR THz COMMUNICATIONS, MEMS
MICROSCOPY OF BIOLOGICAL CELLS (367 eV)
XRF AND XPS (1keV) ELEMENTAL SURFACE MAPPING SEMICON
RADIOBIOLOGY OF DNA REPAIR - BIOMEDICAL

HARD X-RAYS WITH FEMTOSECOND LASER:
MOLECULAR STRUCTURE BY XRD (9keV) - BIO-MEDICAL
MAMMOGRAPHY & ANGIOGRAPHY: (20-50 keV) -MEDICAL
ROCK TOMOGRAPHY - OIL INDUSTRY

X-Ray Lithography Source (JMAR)

JMAR Collimated Plasma Lithography (CPL)

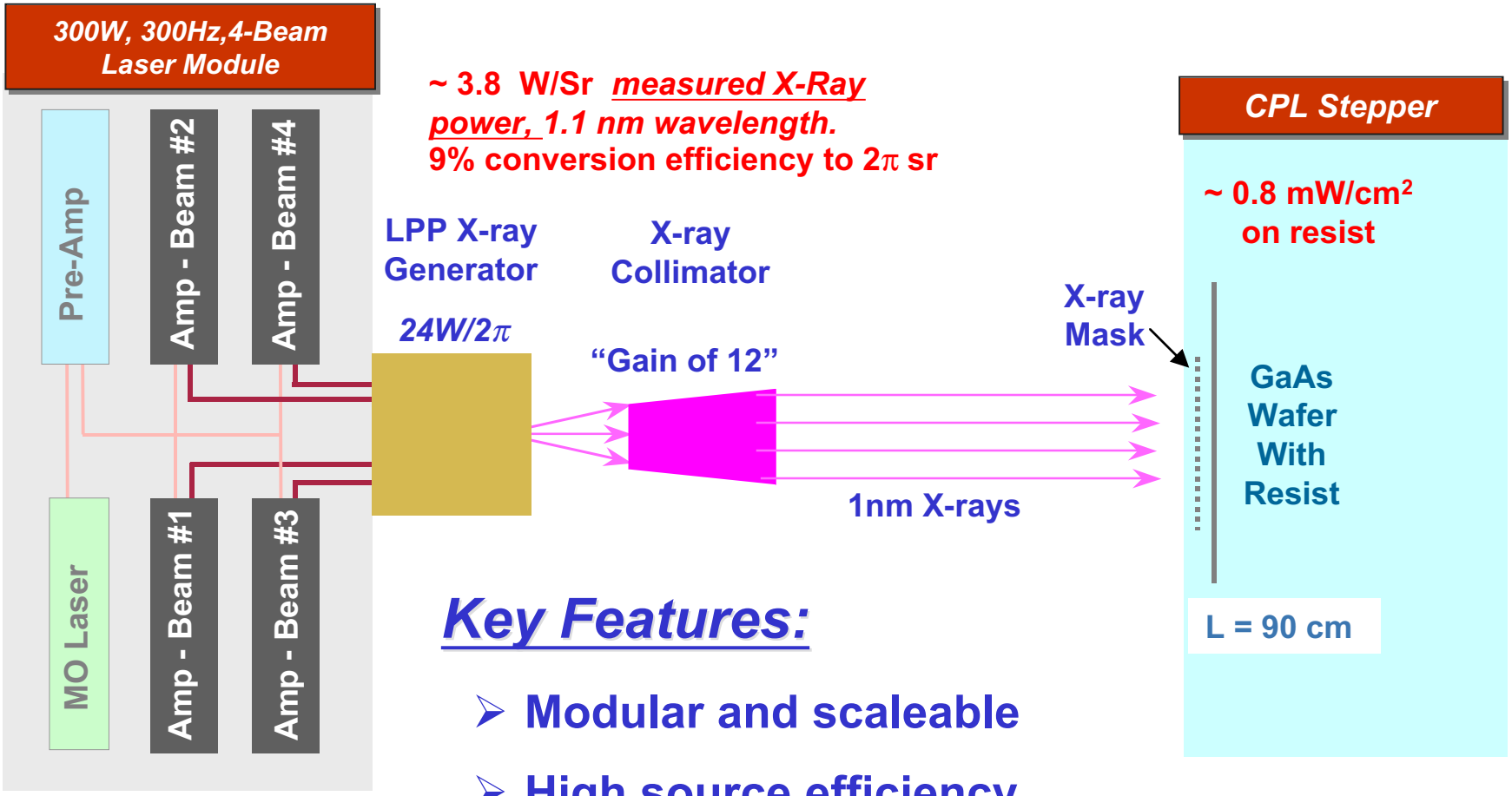

Key Features:

- Modular and scaleable
- High source efficiency
- Collimator gain

Table-Top 24 W X-Ray Source (JMAR)

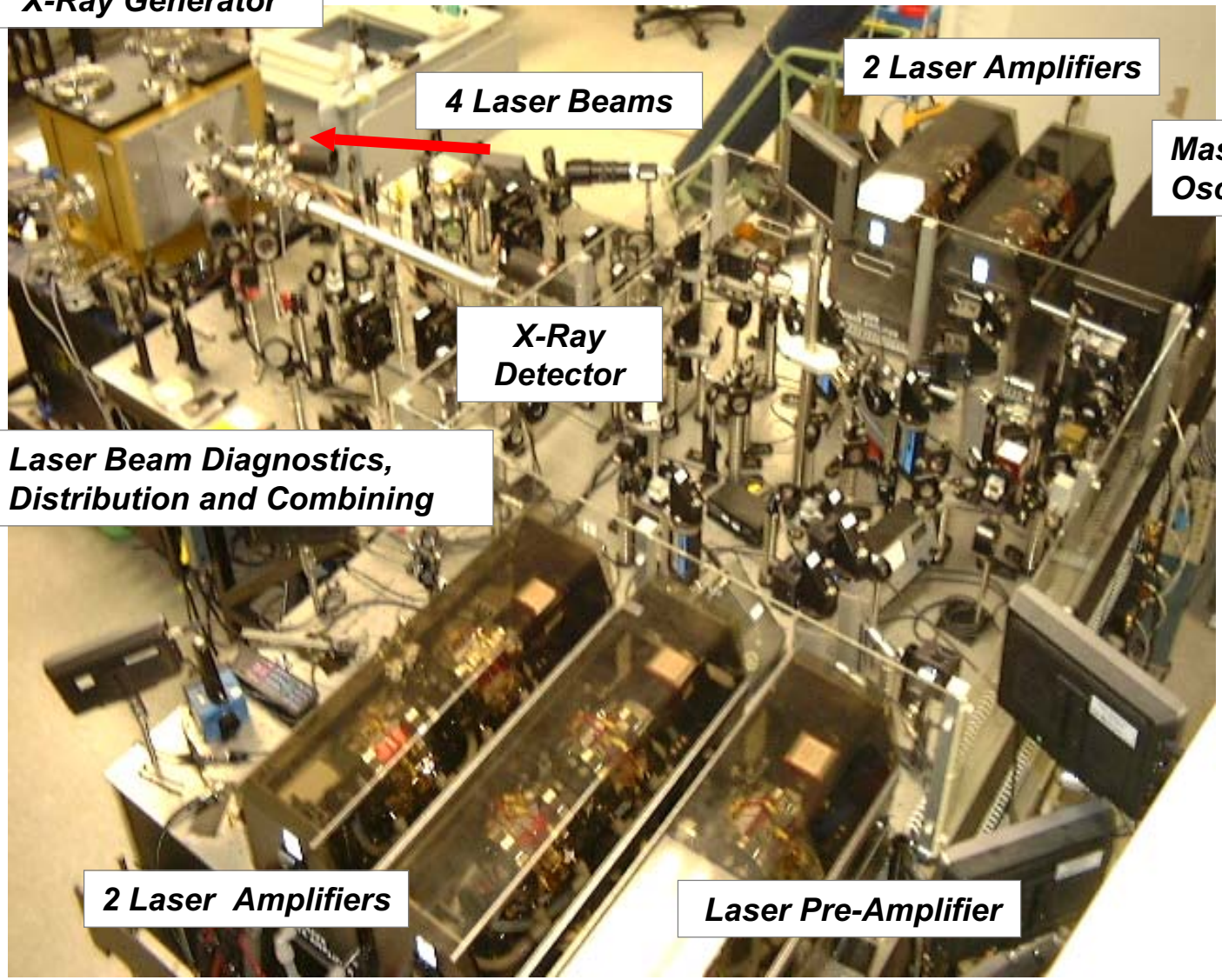

Dimensions:

Laser Table:
8 x 4 ft^2

Laser Amplifier
1.5 x 1 x 1 ft^3

X-ray Generator
1.5 x 1.5 x 1.5 ft^3

CPL LPP Generator Concept (JMAR)

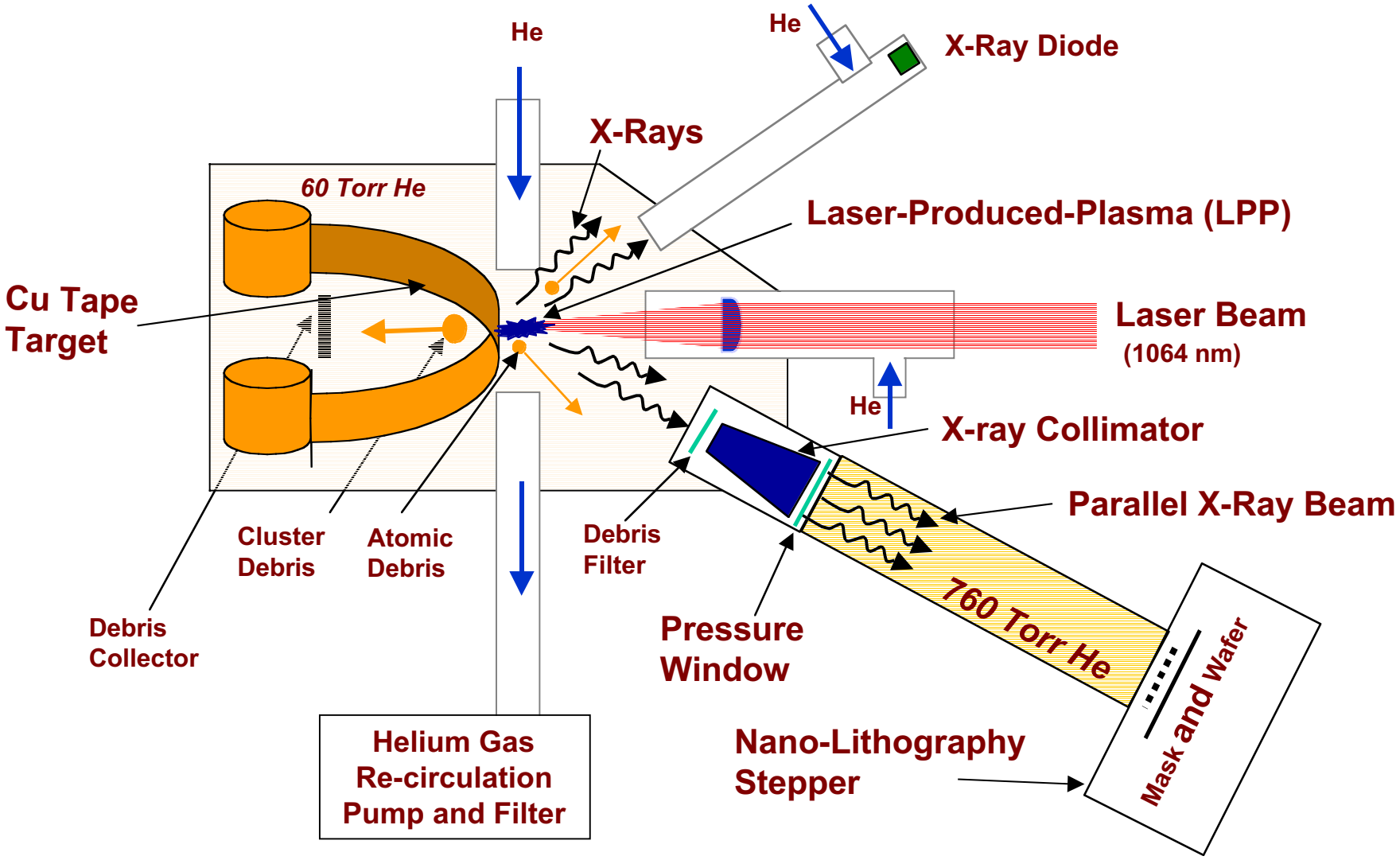

Scaling of X-ray Conversion Efficiency (JMAR)

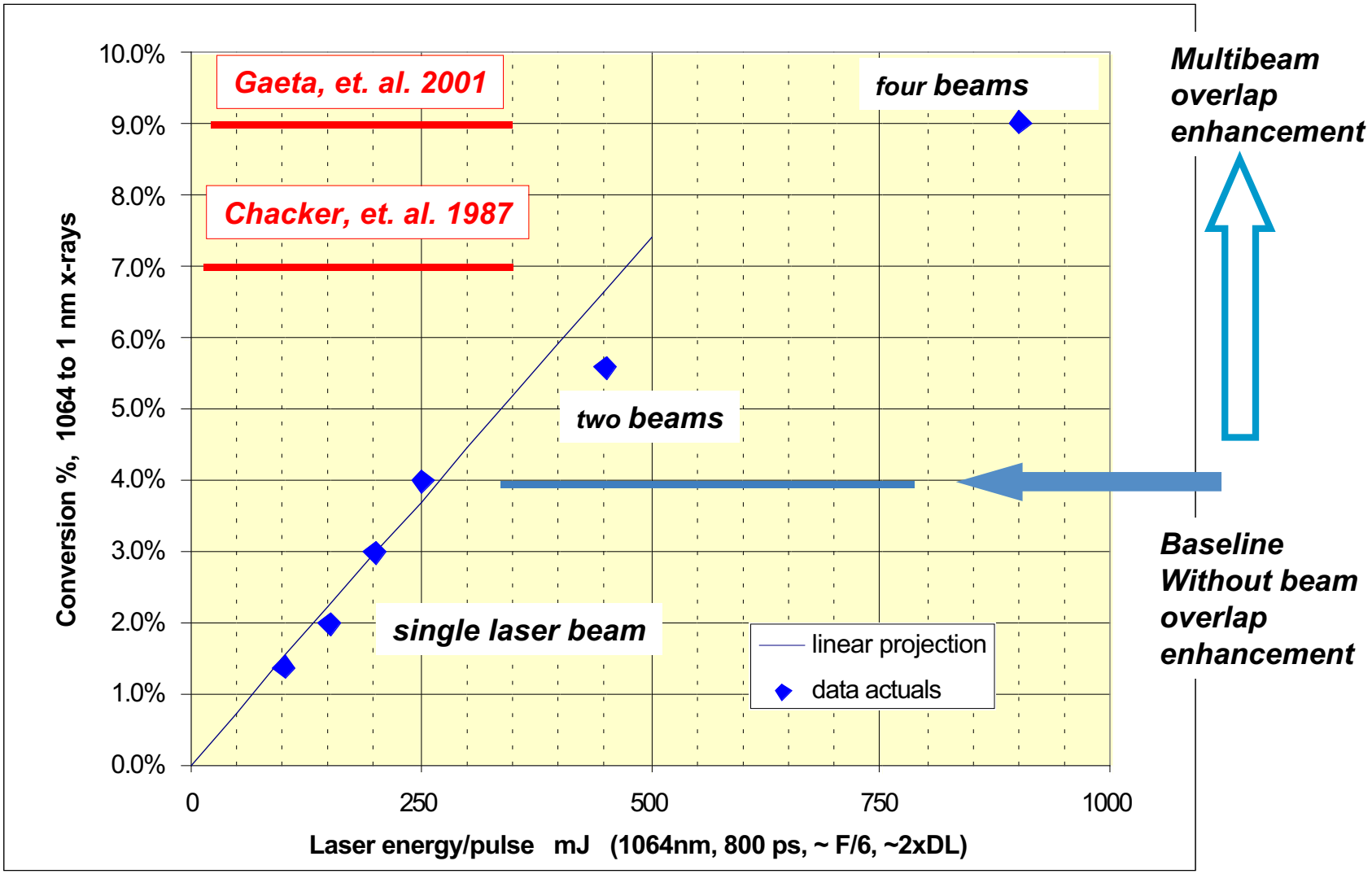

X-ray Optical Systems (XOS) Collimators (JMAR)

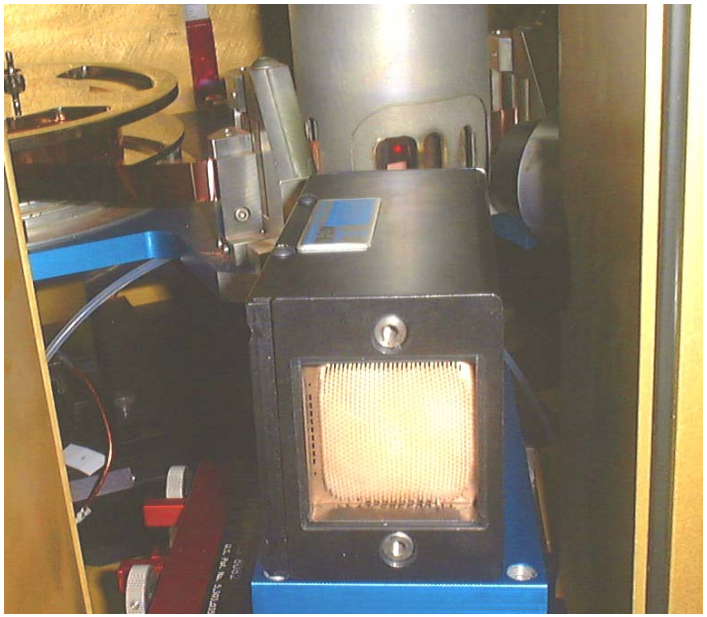

20x20 collimator in POC x-ray chamber

New development

- *Improve uniformity - goal +/- 2%*
- *Increase field size - 30x30, or more*

Performance, 22x22 optic

• Gain (at 90 cm)	12.9 +/- 0.8
• Global Divergence	~ 0.5 +/- 0.5 mrad
• Local Divergence	4.0 +/- 0.4 mrad
• Uniformity	~ ± 5%
• Field size	22 x 22 mm^2

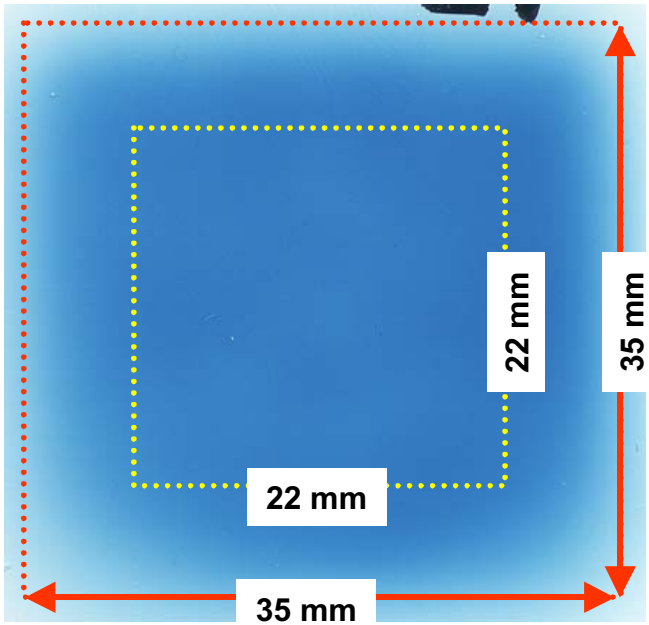

X-RAY OPTICAL SYSTEMS INC.

Beta CPL Source with Stepper Beamline (JMAR)

Duplicate Stepper Beamline with Static Exposure Cell

Laser-Produced-Plasma Generator

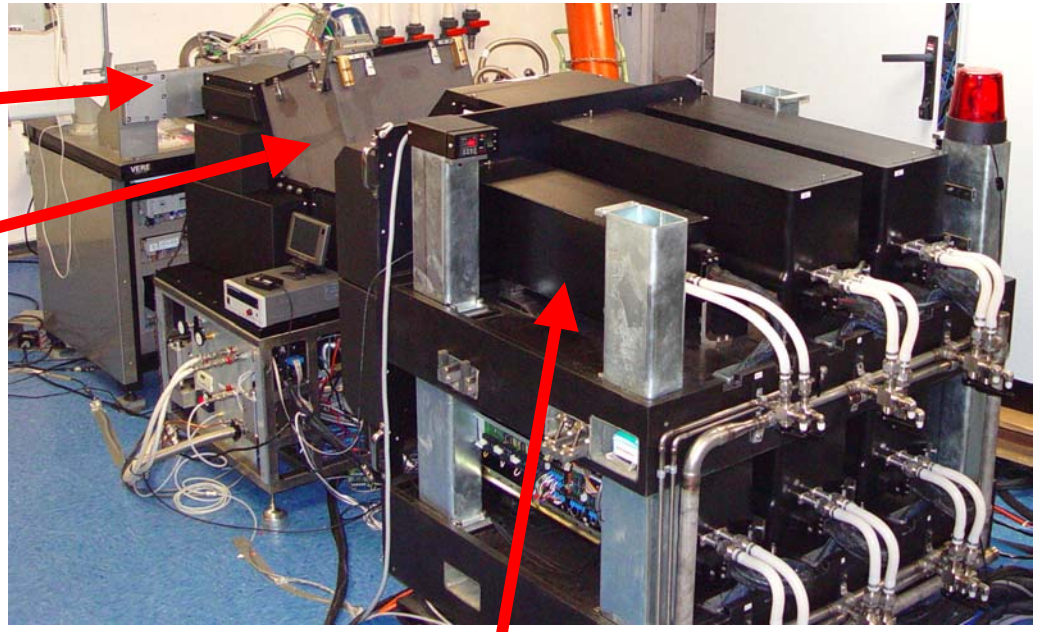

Beta 4-Beam Laser Module

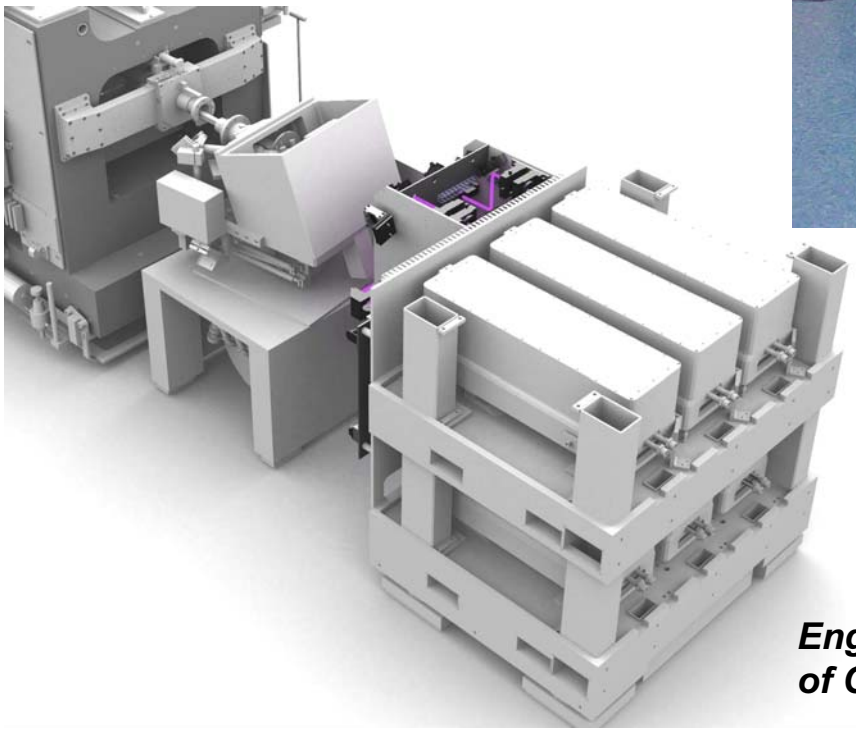

Engineering CAD Rendering of CPL Tool

CPL System (Source + Stepper) Integration (JMAR)

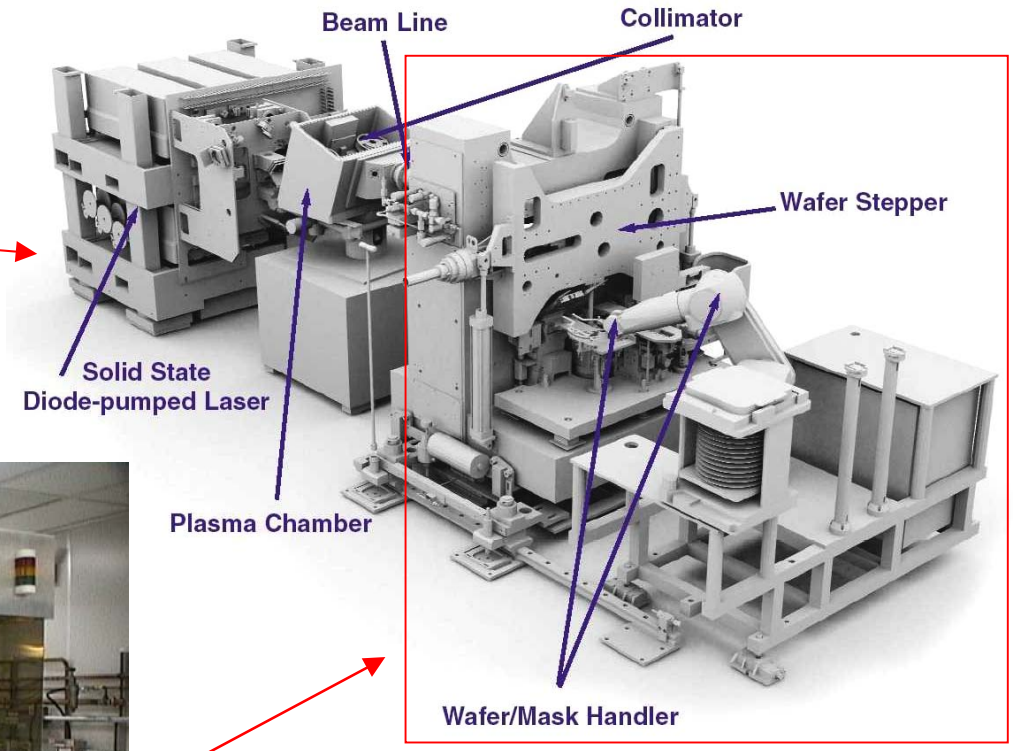

CPL Intra-field Exposure Feature Versatility (JMAR)

Resist Images

130 nm contact holes

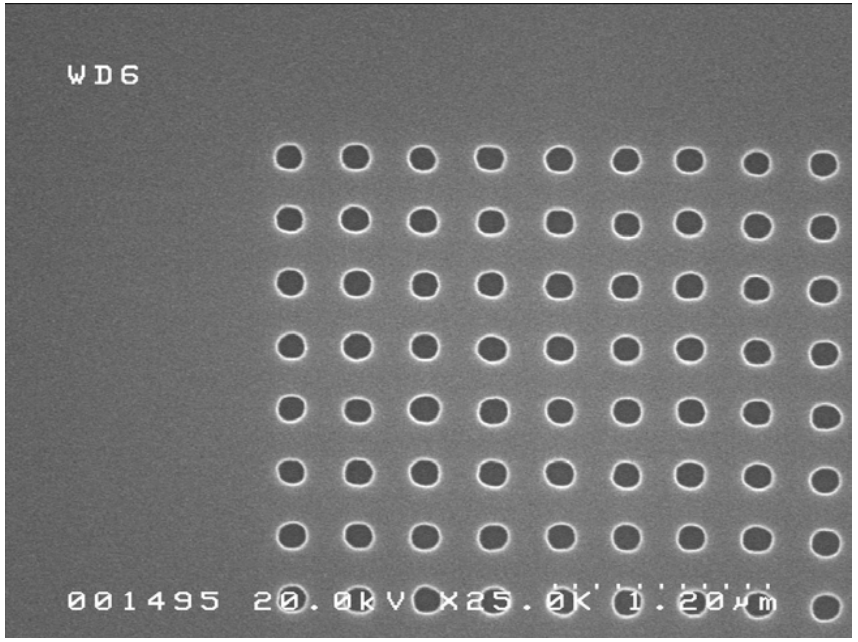

100 nm lines

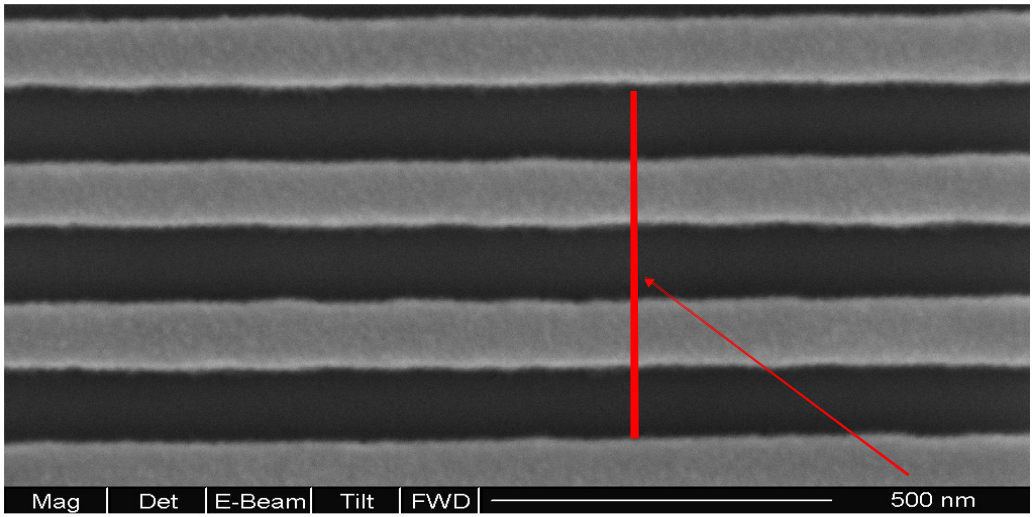

100nm line/space

110 nm posts and contact holes

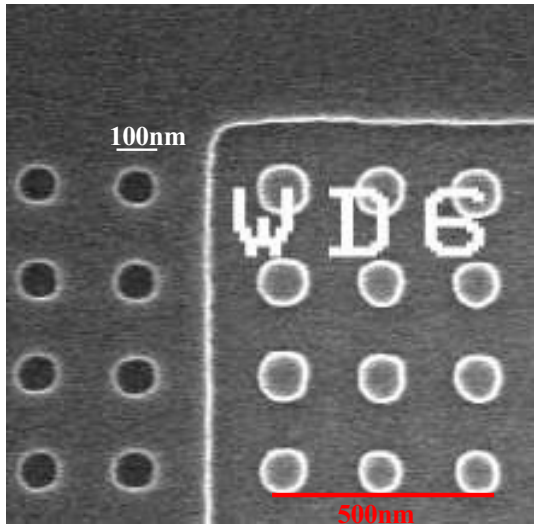

CPL of Sub - 100 nm Contact Holes (JMAR)

Resist Images

100 nm contact holes

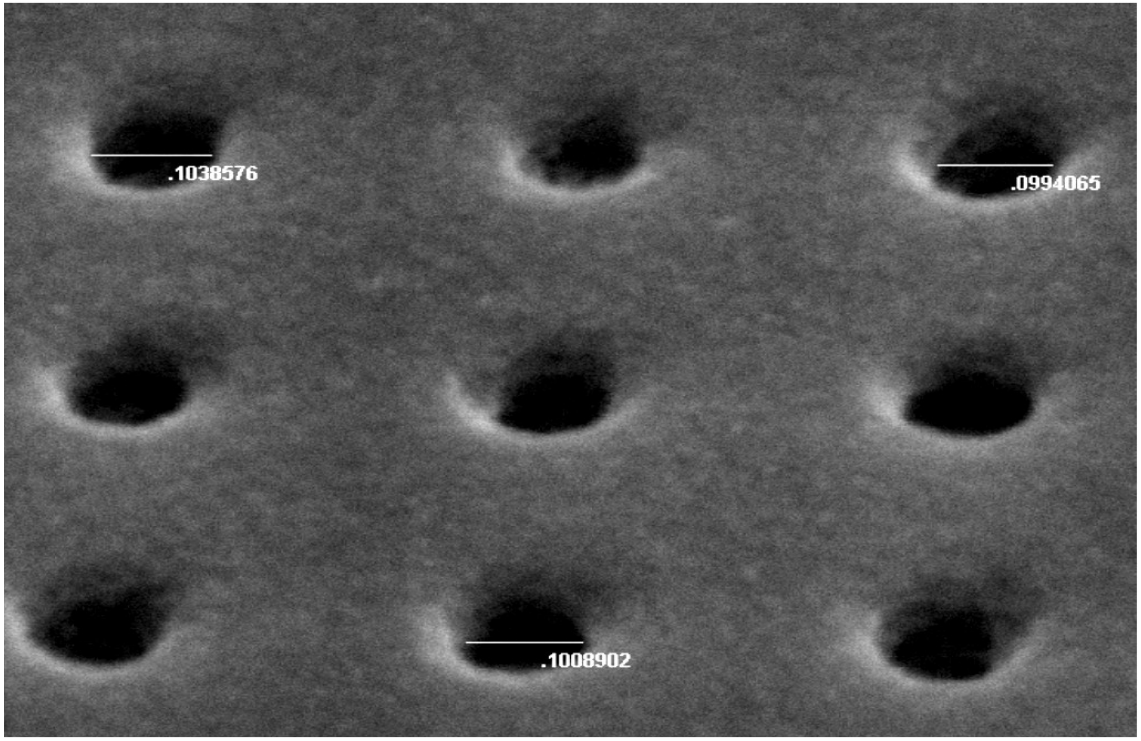

60 nm contact holes

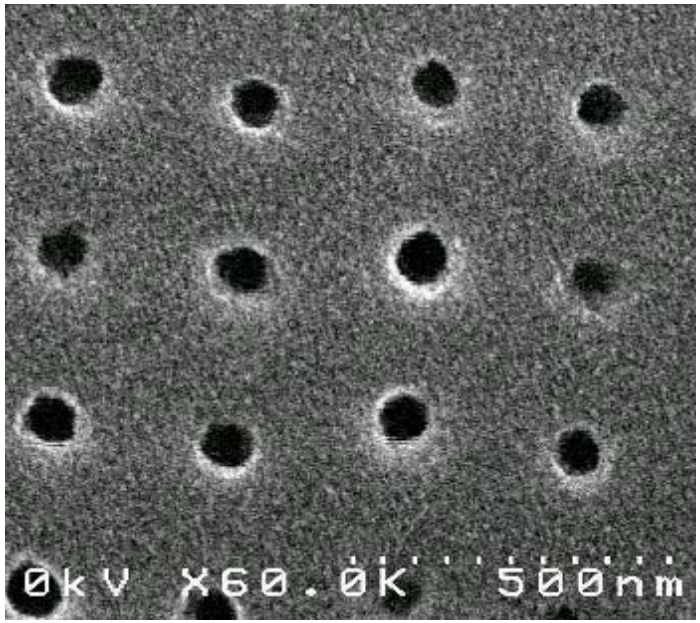

2.5 THz Microwave Detector Cavity and Waveguide Fabrication by 1nm X-ray LIGA (RAL)

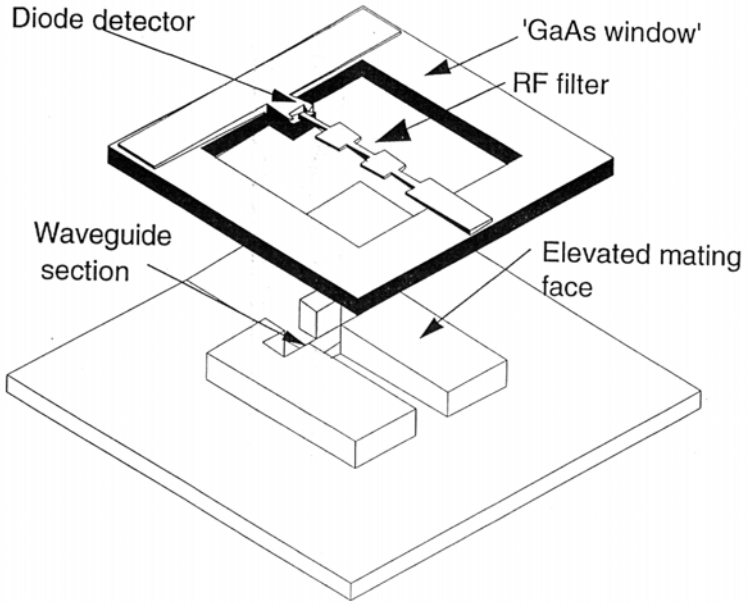

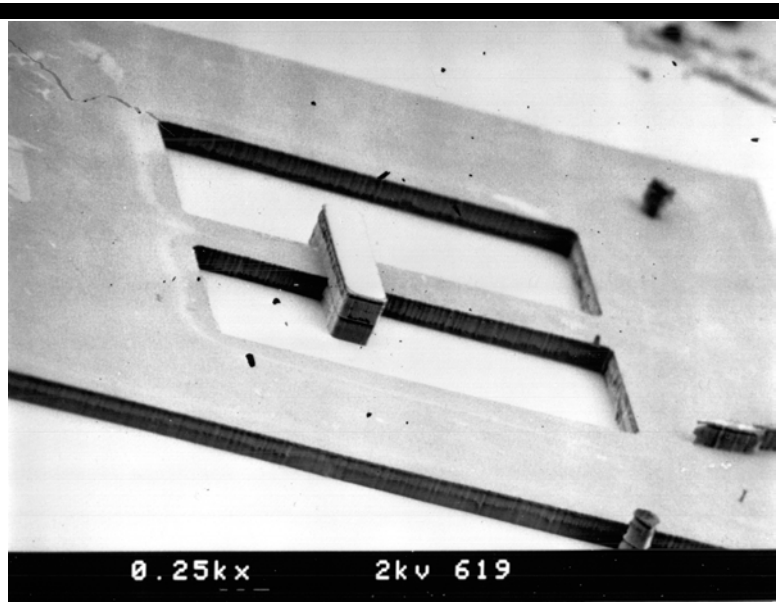

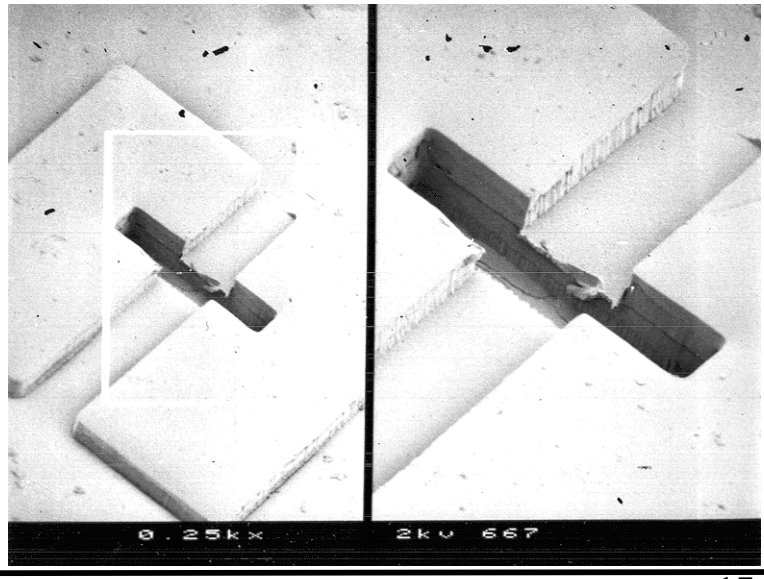

The microwave cavity is 48 μm deep and the waveguide channel is 24 μm deep. Four successive exposure - development steps. Each exposure step is 12 μm deep

The technique is fast and could be used for MEMS prototyping.

LPP EUV Source Concept For High Wafer Throughput (JMAR)

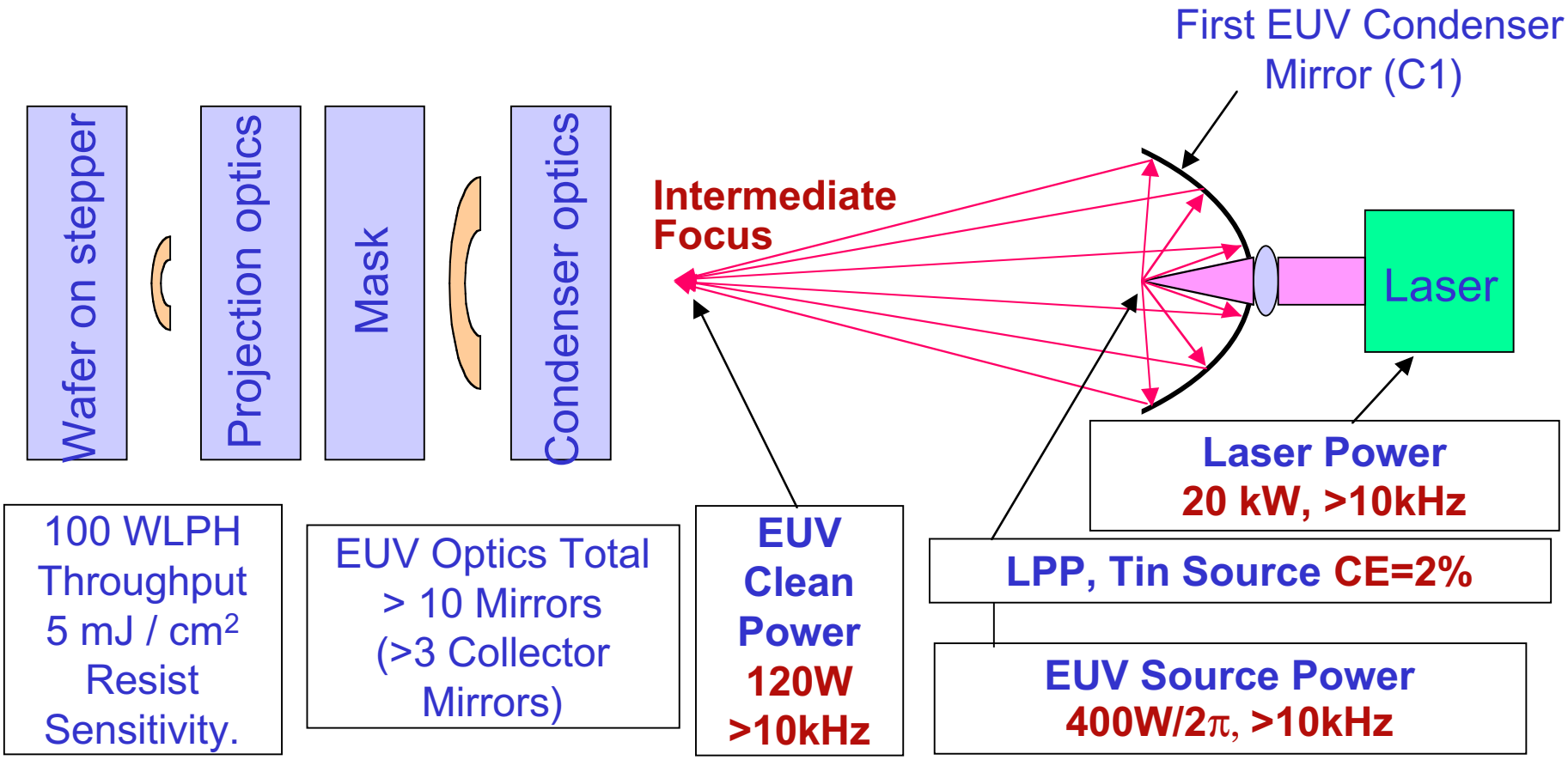

Development of High Conversion Efficiency EUV Sources (UCF/JMAR)

UCF has developed (proprietary) Tin containing sources possessing high EUV conversion efficiency

(patents pending)

Sn material droplet target

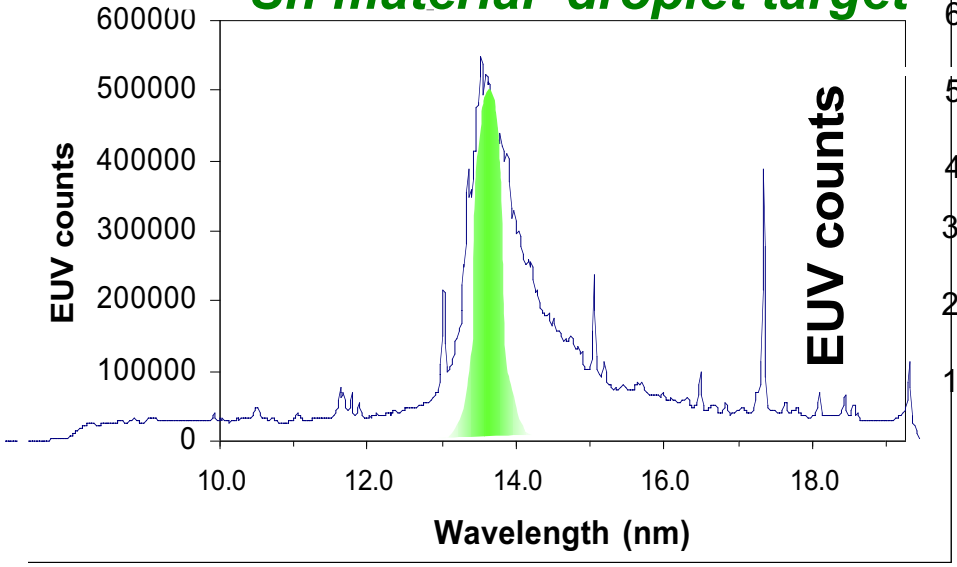

Water droplet target

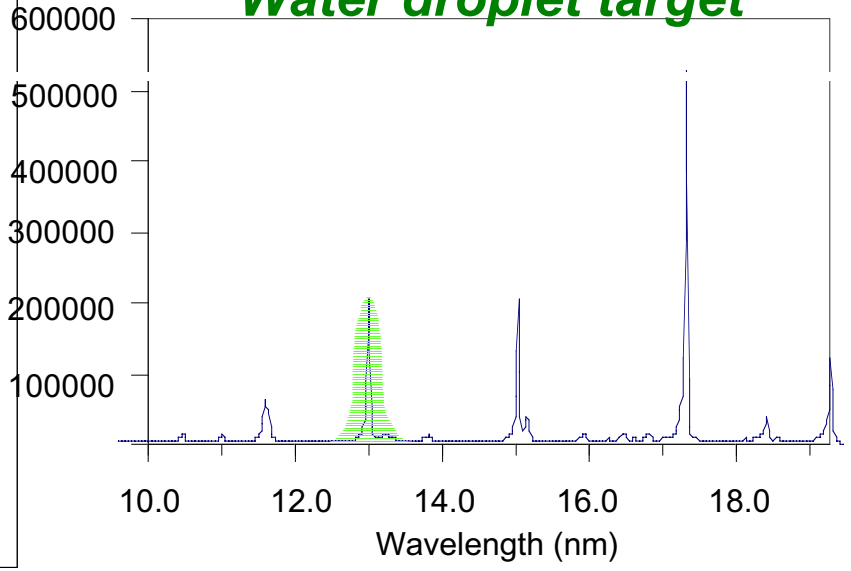

Conversion efficiency ~ 2% at 13.6 nm into 2% BW and 2π - based on measured CE for water of 0.315% in 2% BW and 2π

250 mJ, 10 ns, 1064 nm, 100 Hz laser. Spectra recorded for 150 shots

Nd:YAG Laser (sample) for EUVL LPP Source (JMAR)

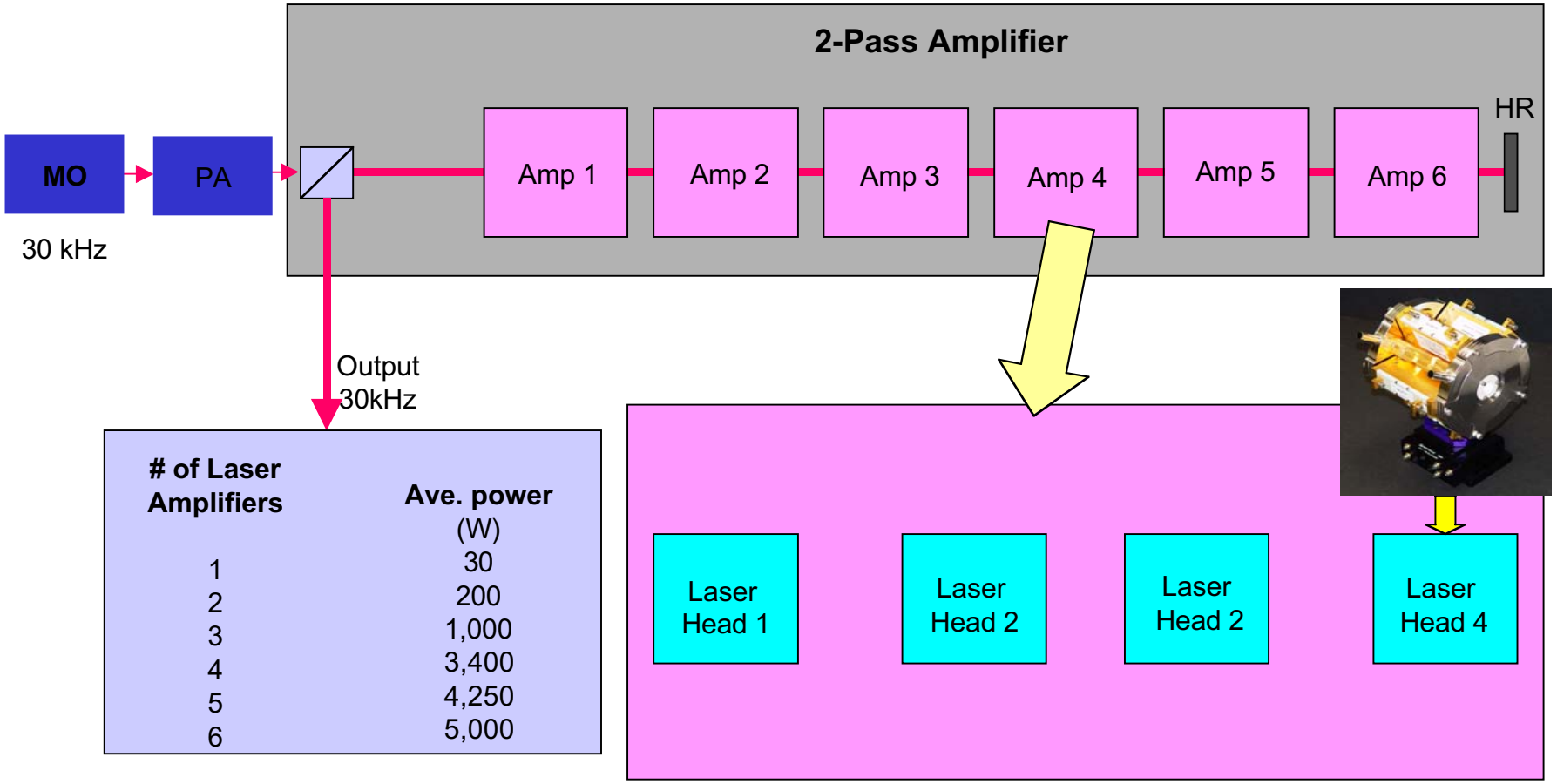

Radiobiology with Soft X-Rays (1.2keV) (MRC, RAL)

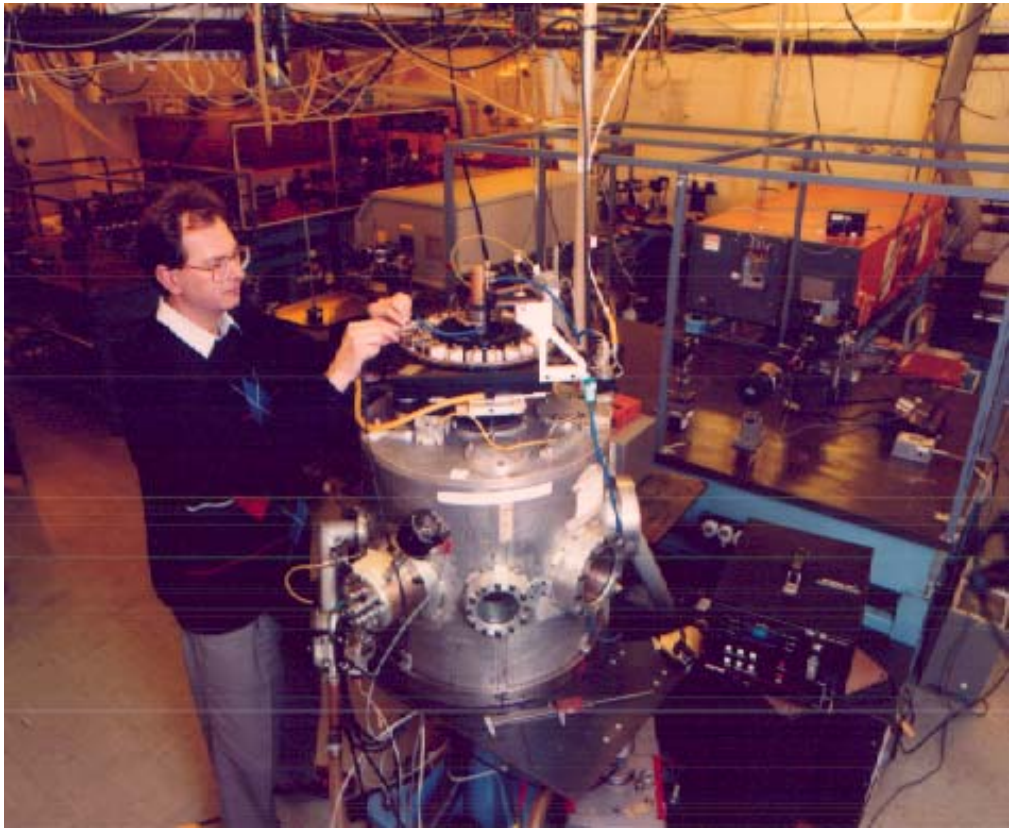

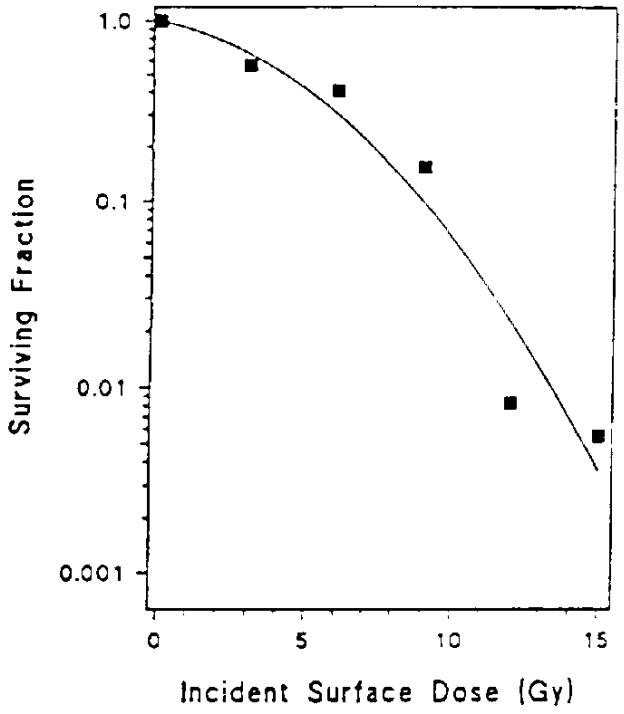

Cell survival of monolayers of V79 cell when exposed to 1.2keV soft X-ray pulses. X-ray pulse duration 5ps.

Biolochemistry with Soft X-Rays (1.2keV) (B'ham U, RAL)

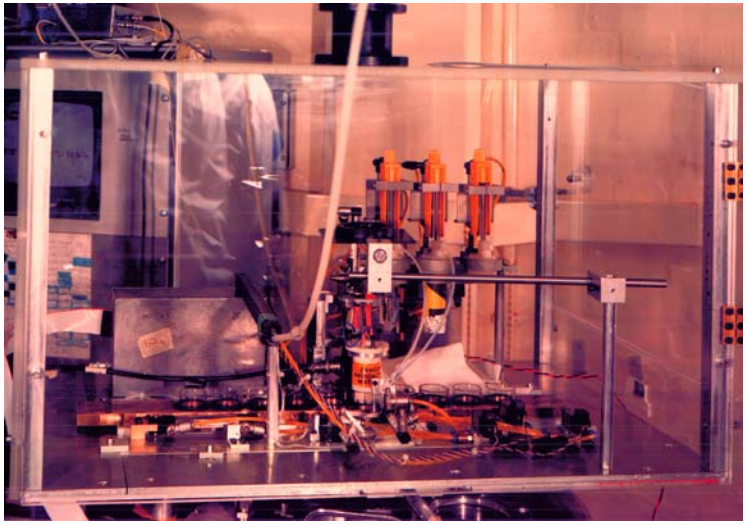

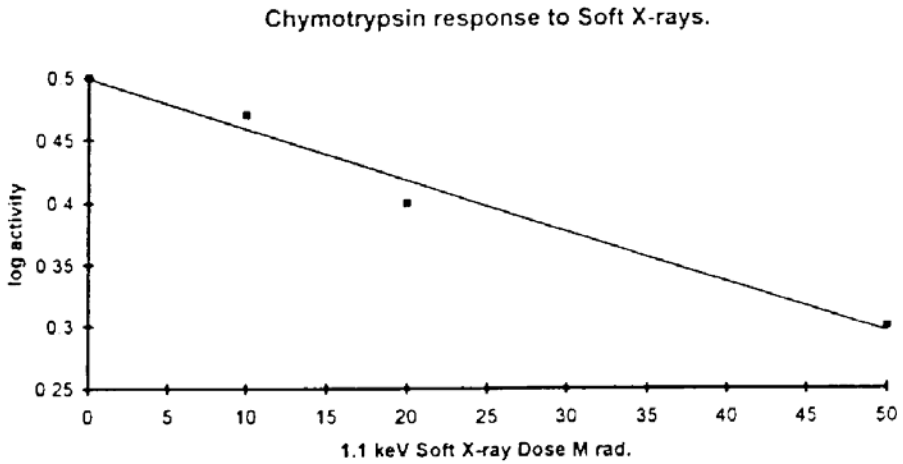

Above: DNA exposure robot on top of X-ray chamber

Bellow: Fast transient repair response of DNA

Top right: Mega-Rad exposures for protein identification

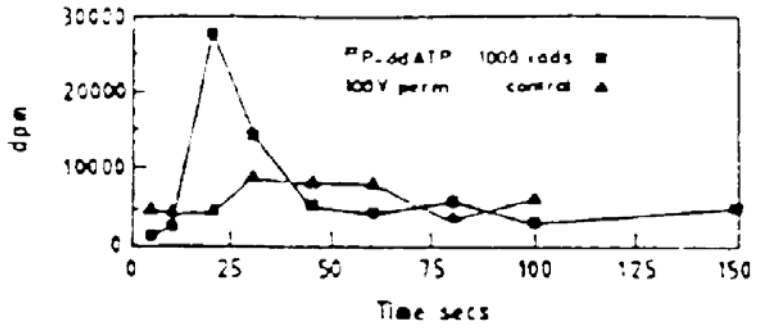

(a)

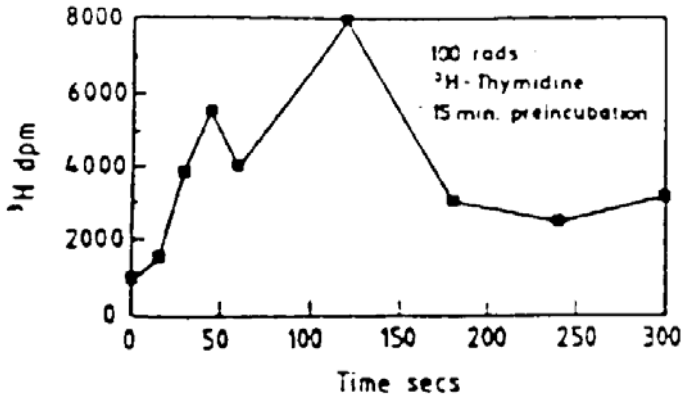

(b)

Soft X-Ray (367eV) Scanning Transmission Microscopy (KCL, RAL)

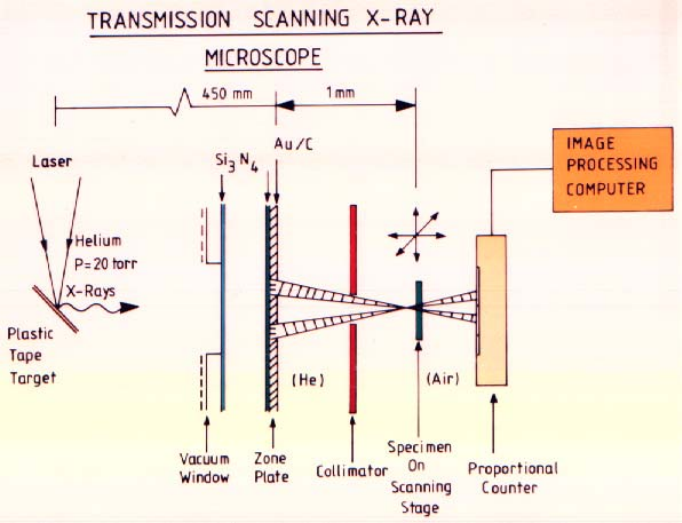

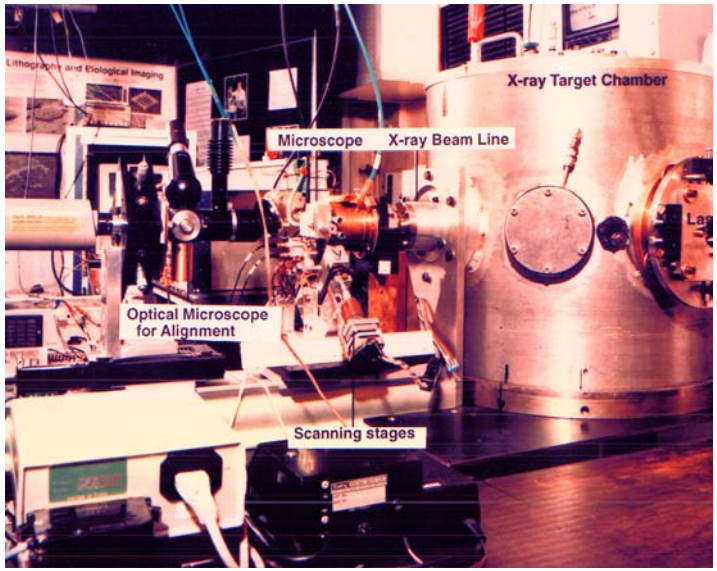

Images have resolution limited by EM noise.

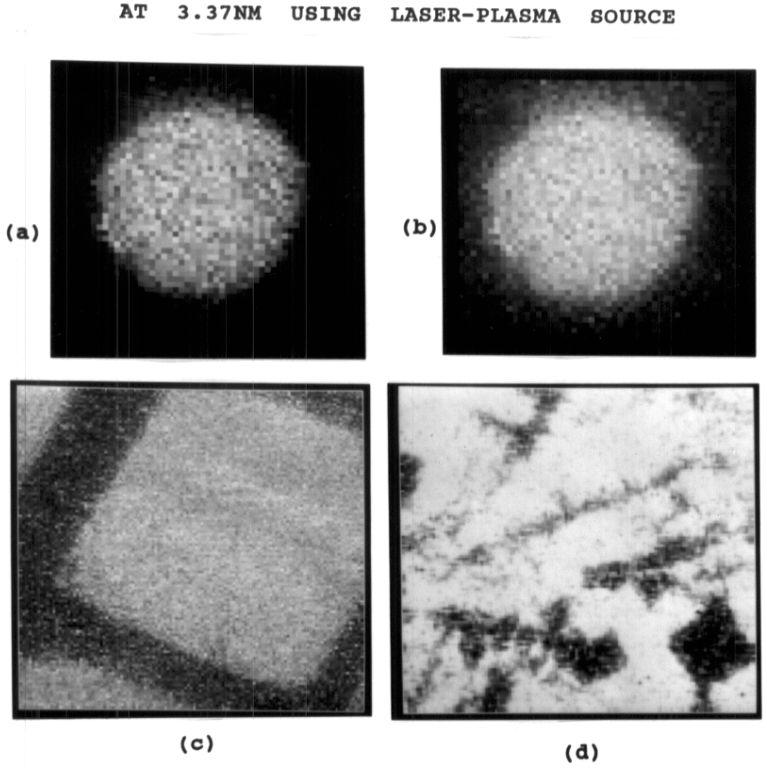

THE LASER-PLASMA SOURCE EMISSION IS MONOCHROMATIZED BY FILTERING THE X-RAYS, IN THE MICROSCOPE, WITH NITROGEN GAS MIXED IN ATMOSPHERIC PRESSURE HELIUM GAS (1:10 BY VOLUME).
THE STXM FOCUSSES THE X-RAYS WITH A GOLD REPLICA ZONE PLATE OF 70MICRONS DIAMETER AND 65NM OUTER ZONE WIDTH.
THE IMAGES ARE OBTAINED AT 20 PIXELS / SECOND, EACH PIXEL BEING EXPOSED WITH ONE LASER SHOT.

(a) 64X64 PIXEL IMMAGE OF A 6MICRON PINHOLE OBTAINED WITH 160NM /PIXEL. THE EDGE RESOLUTION IS 650NM DUE TO ELECTRICAL NOISE.
(b) SAME AS (a), BUT NO NITROGEN FILTER IN MICROSCOPE.
(c) 128X128 PIXEL IMAGE OF GOLD GRID : 550NM/PIXEL.
(d) 128X128 PIXEL IMAGE OF SILICA GEL : 1.25MICRON/PIXEL.

Fast Elemental Mapping with mm Spatial Resolution by Soft X-Ray Fluorescence (Leicester U, RAL)

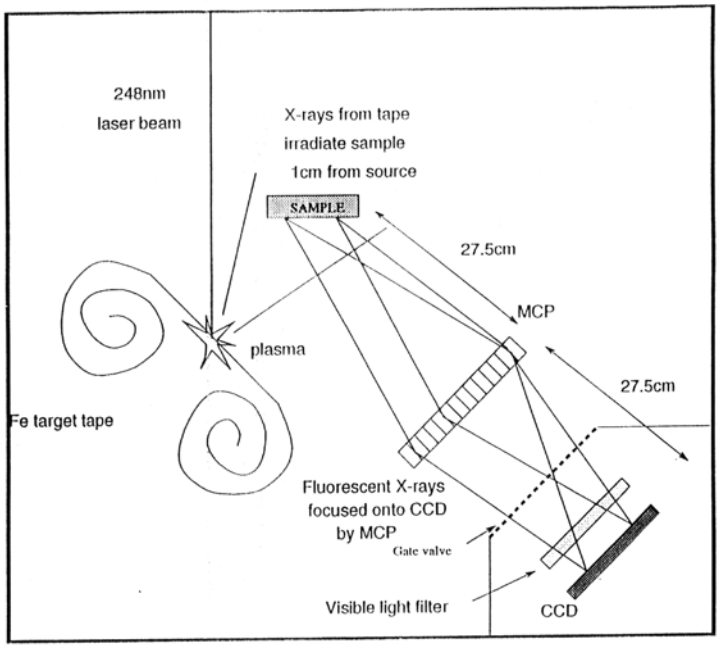

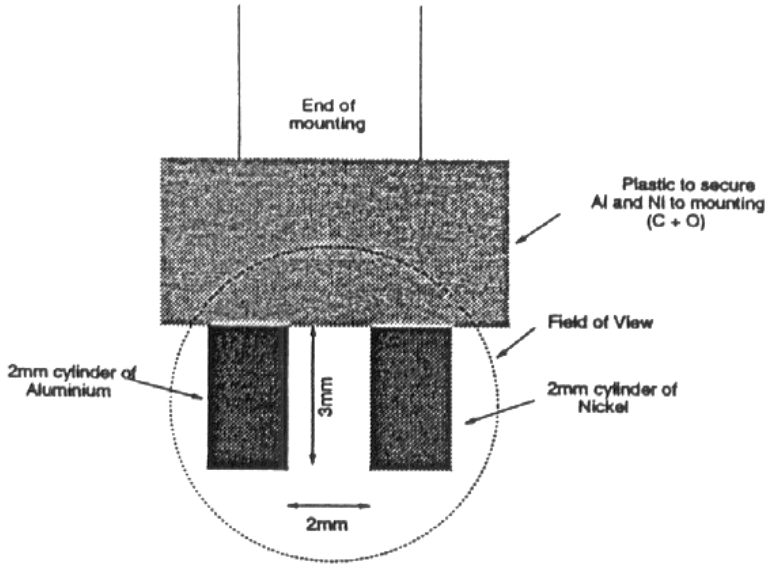

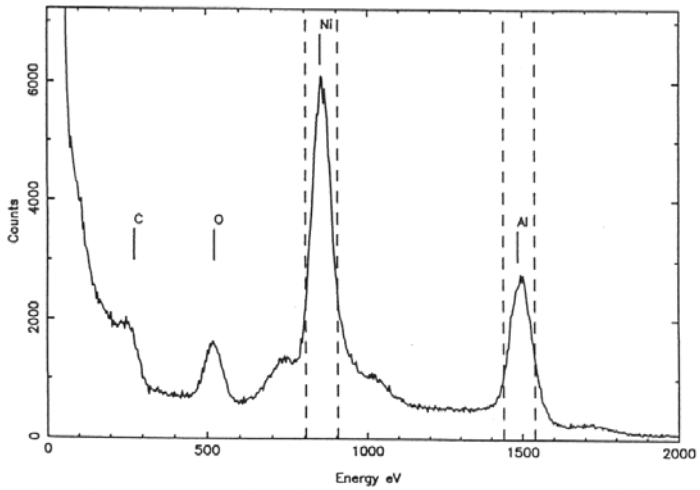

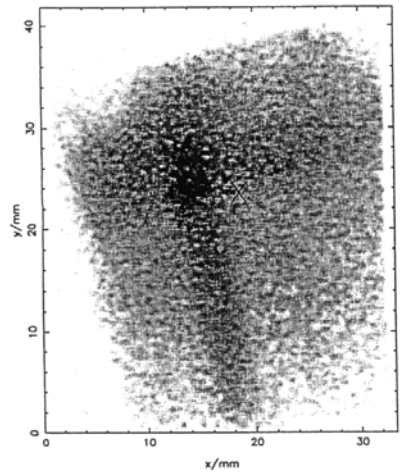

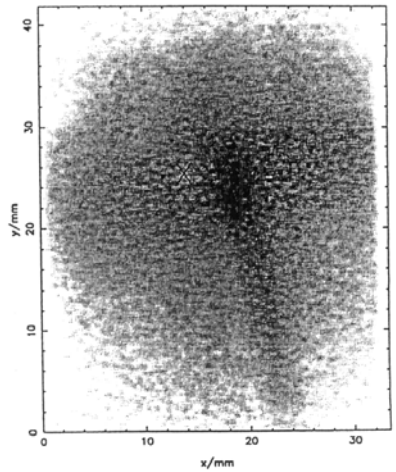

Summary

- ***24 Watt of 1nm x-rays generated from 300 Watt, 300 Hz DPSS laser . Beamline with x-ray collimator. X-ray stepper.***
- ***X-ray lithography of sub-100nm structures. LIGA with soft x-rays for THz microwave communication.***
- ***EUV LPP source concept for high throughput projection lithography.***
- ***Soft X-ray radiobiology and biochemistry.***
- ***Soft X-ray "water-window" microscopy.***
- ***Soft X-ray fluorescence for elemental mapping of surfaces.***

Acknowledgements

- **In US: colleagues from JMAR, LLNL, XOS, LBL, NIST, ETEC, IBM.**
- **in Europe : colleagues from RAL, Edinburgh U, Glasgow U, Queens U. Belfast, Dublin City U., Leicester U, Birmingham U, Leica Lithography Systems, King's College London, Gray Laboratory, MRC Harwell, U. of Milano, ENEA-Frascatti.**
- **In Japan: colleagues form Osaka U.**

Bibliography

1. "X-Rays From Laser-Plasmas: Generation and Applications", I.C.E. Turcu and J.B. Dance, John Wiley and Sons, 1999.
2. Brent Boerger, et al "Advances in CPL, Collimated Plasma Source & Full Field Exposure for Sub-100nm Lithography" , in "Emerging Lithographic Technologies VII", RL Engelstad Ed., Proc. SPIE 5037, in print in 2003.
3. CJ Gaeta, et al. "High-power collimated laser-plasma source for proximity x-ray nano-lithography", J. Vac. Sci. Technol. B 21, 280-7 (2003).

Toward the single-cycle regime in the generation of high-order harmonics and multiphoton ionization

Paolo Villoresi

ULTRASHORT HIGH-ENERGY RADIATION AND MATTER, VILLA MONASTERO, VARENNA, ITALY, ***October 7, 2003 - Invited Paper***

Toward the single-cycle regime in the generation of high-order harmonics and multiphoton ionization

M. Pascolini, L. Poletto, P. Villoresi, G. Tondello
INFM – LUXOR Laboratory for Ultraviolet and X-Ray Optical Research
DEI - Università di Padova (Italy)

M. Nisoli, E. Priori, G. Sansone, S. Stagira, C. Vozzi, S. De Silvestri
CUSBO - Centre for Ultrafast Science and Biomedical Optics
Politecnico di Milano (Italy)

INFM – ULTRAS National Laboratory for Ultrafast and Ultraintense Optical Science

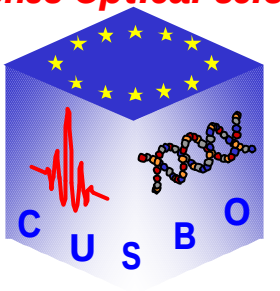

G.G. Paulus, F. Grasbon, H. Walther
Max-Plank-Institute for Quantum Optics
Garching (Germany)

ULTRASHORT HIGH-ENERGY RADIATION AND MATTER, VILLA MONASTERO, VARENNA, ITALY, ***October 7, 2003 - Invited Paper***

Outline

- Generation of high-peak power few-optical-cycle light pulses
  - Hollow fiber compression technique
- Role of the absolute phase on high-order harmonic generation
  - Experimental evidence
  - Physical interpretation
- Role of the absolute phase on photoelectron emission and changes on spectrum with few-cycle pulses

What *near-single-cycle* means?

- Evolutions of laser science has lead to pulses whose duration is comparable to their period
- Thin light disk, thickness ct » 1-2 μm
- Pulse energy about tenths of mJ
- Intensity at focus up to a few 10^{15} W/cm^2
- Optical ionization induced for a few half-cycles

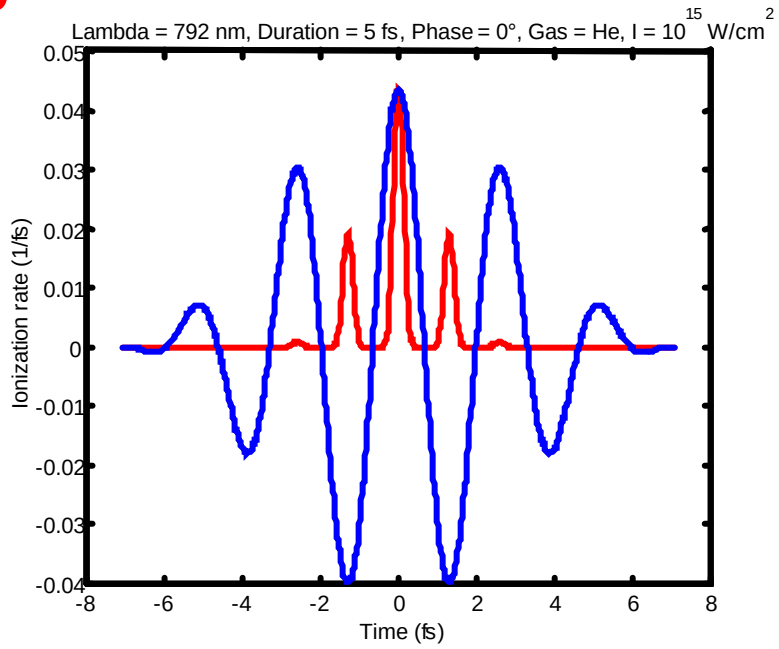

A thin *light-sheet*

- Harsh task keeping intensity front under control
- 5 fs pulse is like a glass window 3 mm thick and with diameter of 20 m

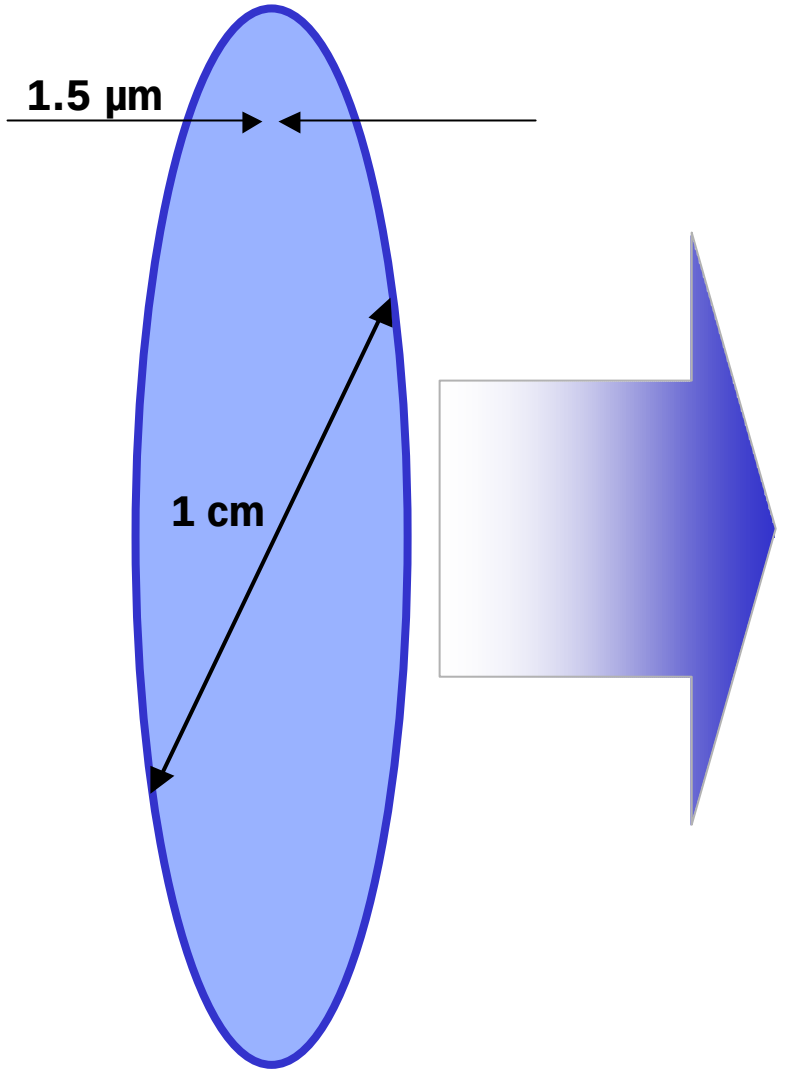

Same envelope but..

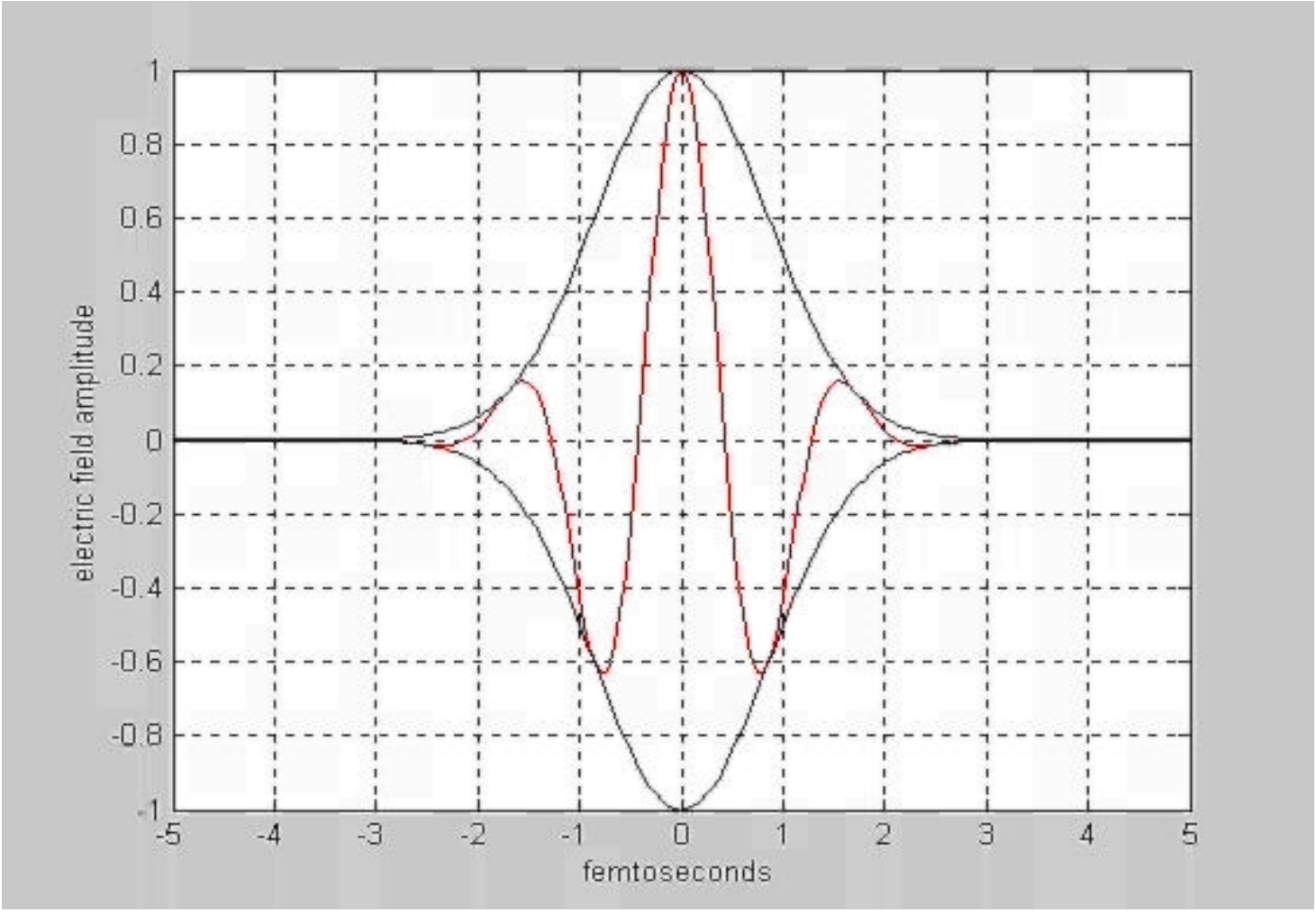

$$E(t) = E_0(t) \cos (\omega t + \phi)$$

Why is the *absolute phase* important ?

- **Time variation of the electric field in few-optical-cycle pulses depends on the *absolute phase***

- **All the physics of intense laser - matter interactions depends on pulse electric field**

  $\Rightarrow$ *absolute phase* is important for many different fields in laser physics

  - **strong-field photoionization**
  - **generation of coherent soft-x-ray radiation**
  - **generation of single attosecond pulses**
  - **coherent control of chemical reactions**

The non-adiabatic regime

- Scenario of nonlinear processes where there is a

  ***cycle-to-cycle intensity change*.**

- The matter response show up a single-particle nature, eventually evidencing the quantum interference between different paths yielding to the same transition, changing each cycle

  new physical problems to be addressed both from experimental and theoretical point of view

- The high-order harmonics are interesting sources of coherent XUV radiation

  ⇒tabletop size apparatus

  ⇒very short temporal duration

  ⇒with sub-10 fs pump source only few optical cycles are involved in the HHs generation: attosecond processes in the time domain

Influence of Absolute Phase on High-order harmonic generation

Sub-TW Sub-10-fs Laser Pulses

So far the only proven way to produce powerful pulses in the 5-fs regime relies on the hollow-fiber technique

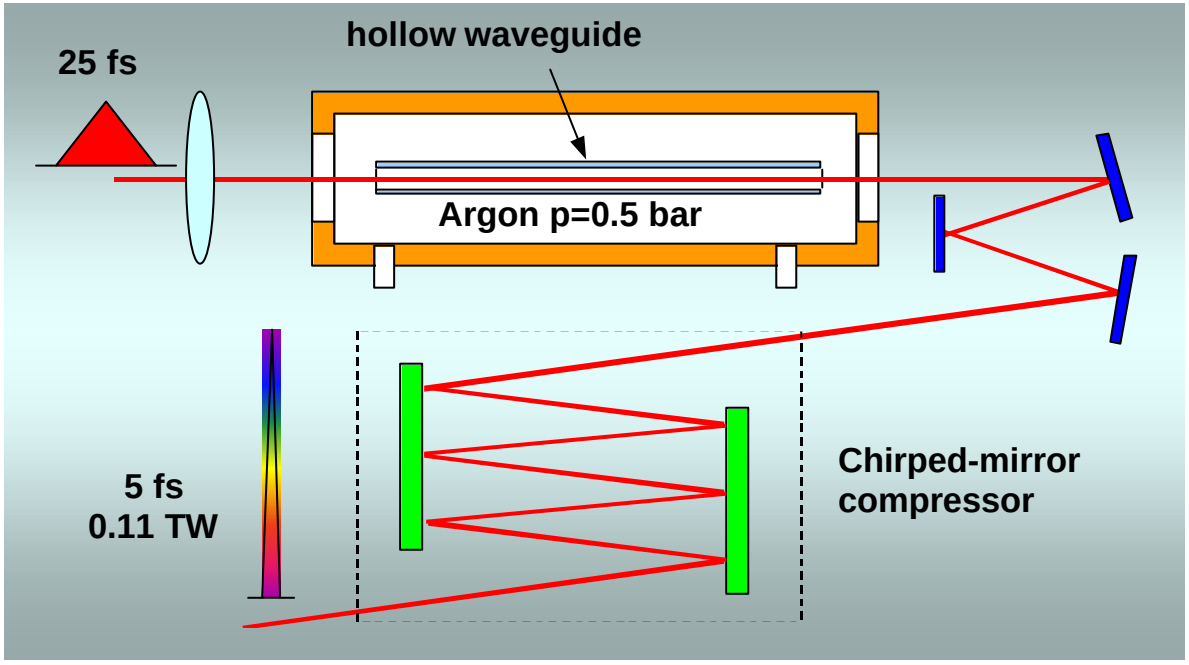

⇒ **Guiding medium with a large diameter mode and a fast nonlinear medium with high damage threshold**

⇒ **Ultrabroad-band dispersion control by chirped-mirrors**

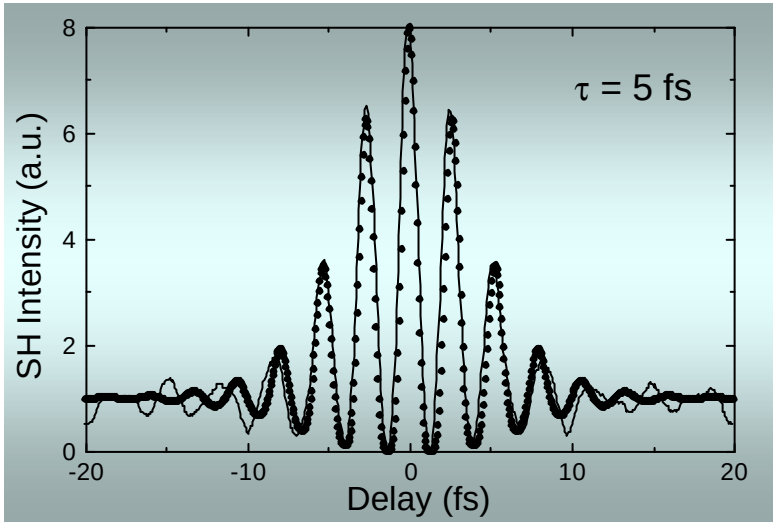

M. Nisoli *et al.*, Appl. Phys. Lett. **68**, 2793 (1996)
M. Nisoli *et al.*, Opt. Lett. **22**, 522 (1997)

HHs brightness per single order Ne 6.5 fs 0.14 mJ

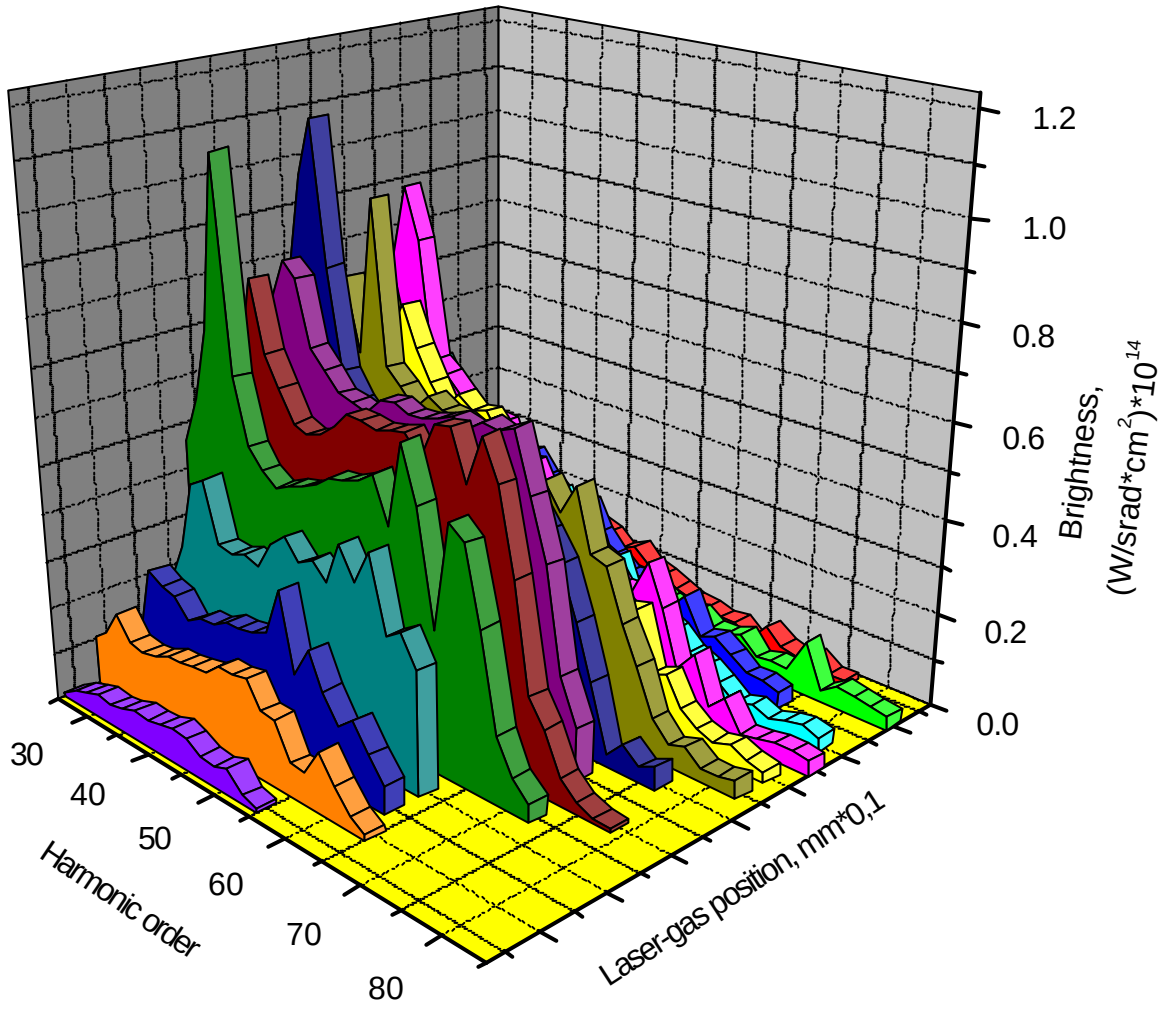

M. Nisoli *et al.*, Physical Review Letters **88** 033902 (2002)

Single-shot acquisition

- gas jet synchronized with driving pulses
- 10 Hz repetition rate
- 300-ms valve opening time
- 85-ms CCD integration time

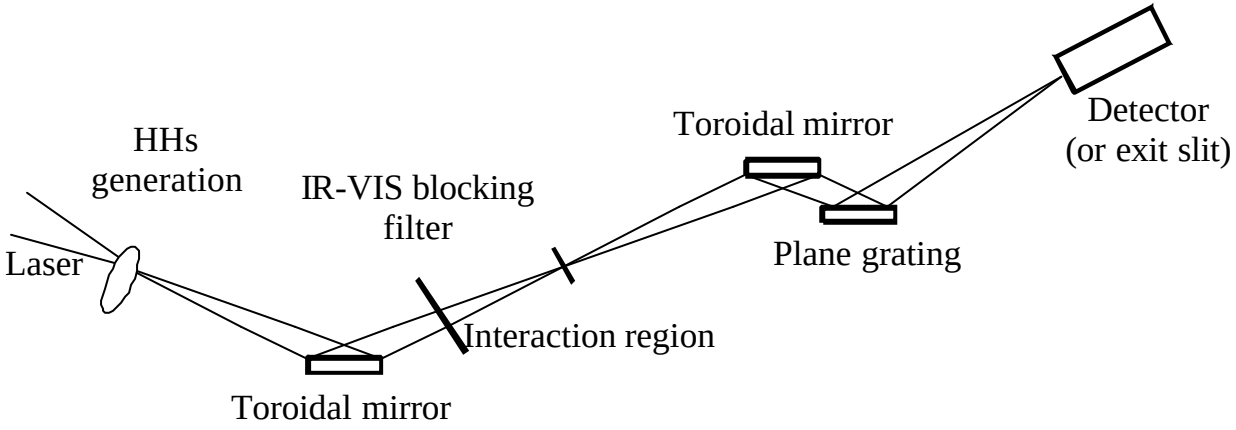

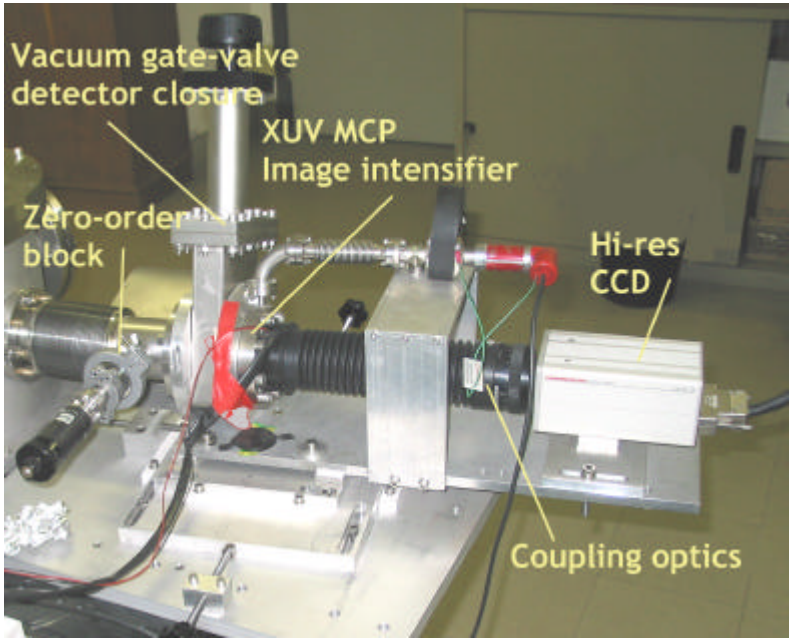

L. Poletto, G. Tondello and P. Villoresi, to appear in Appl. Opt.,

Ultrafast XUV beamline

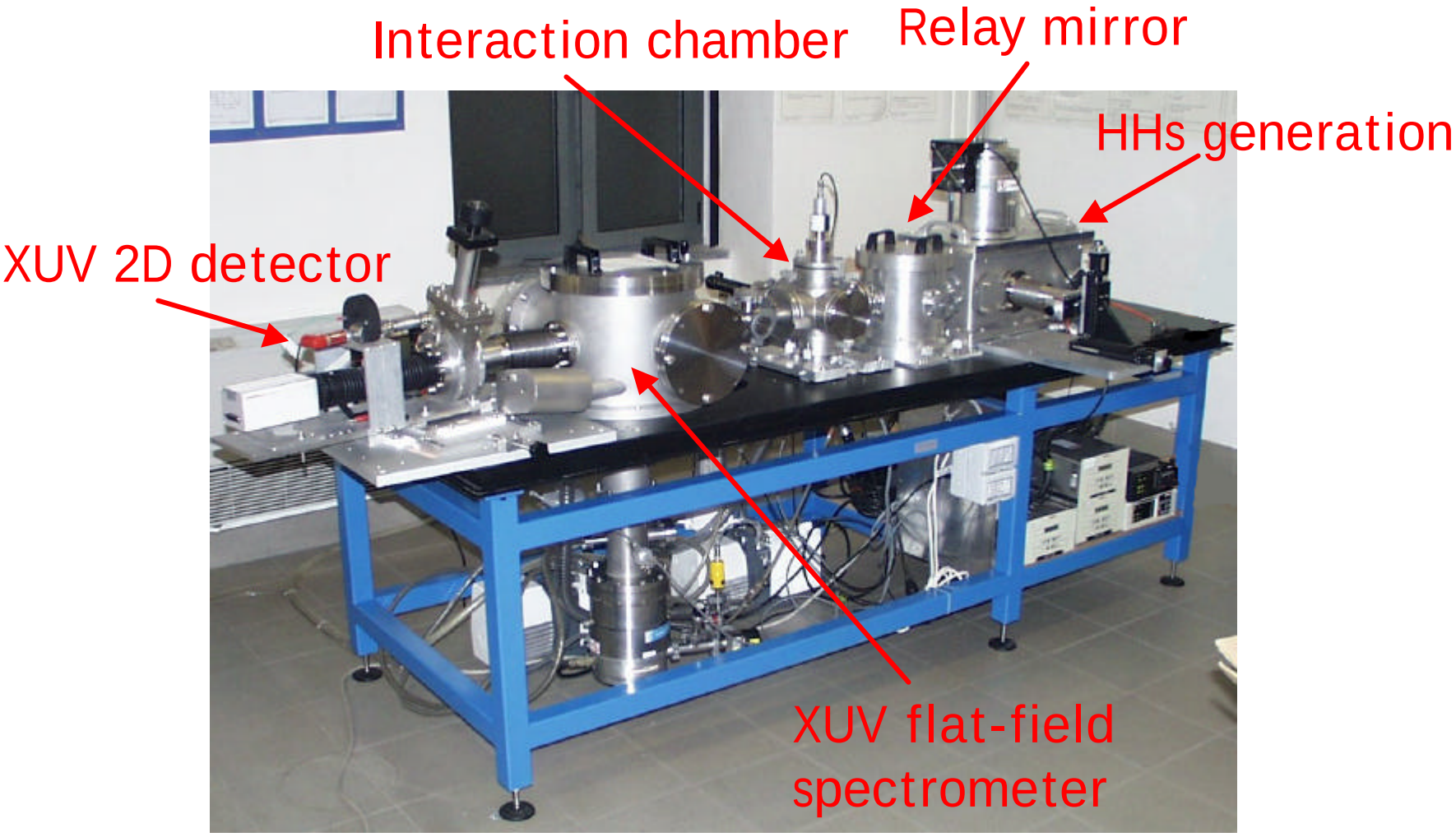

L. Poletto, M. Pascolini, G. Tondello and P. Villoresi, sub. to Rev. Sci. Instrum., 2003

Single-shot harmonic spectra

- **Neon; pulse duration: 6 fs**

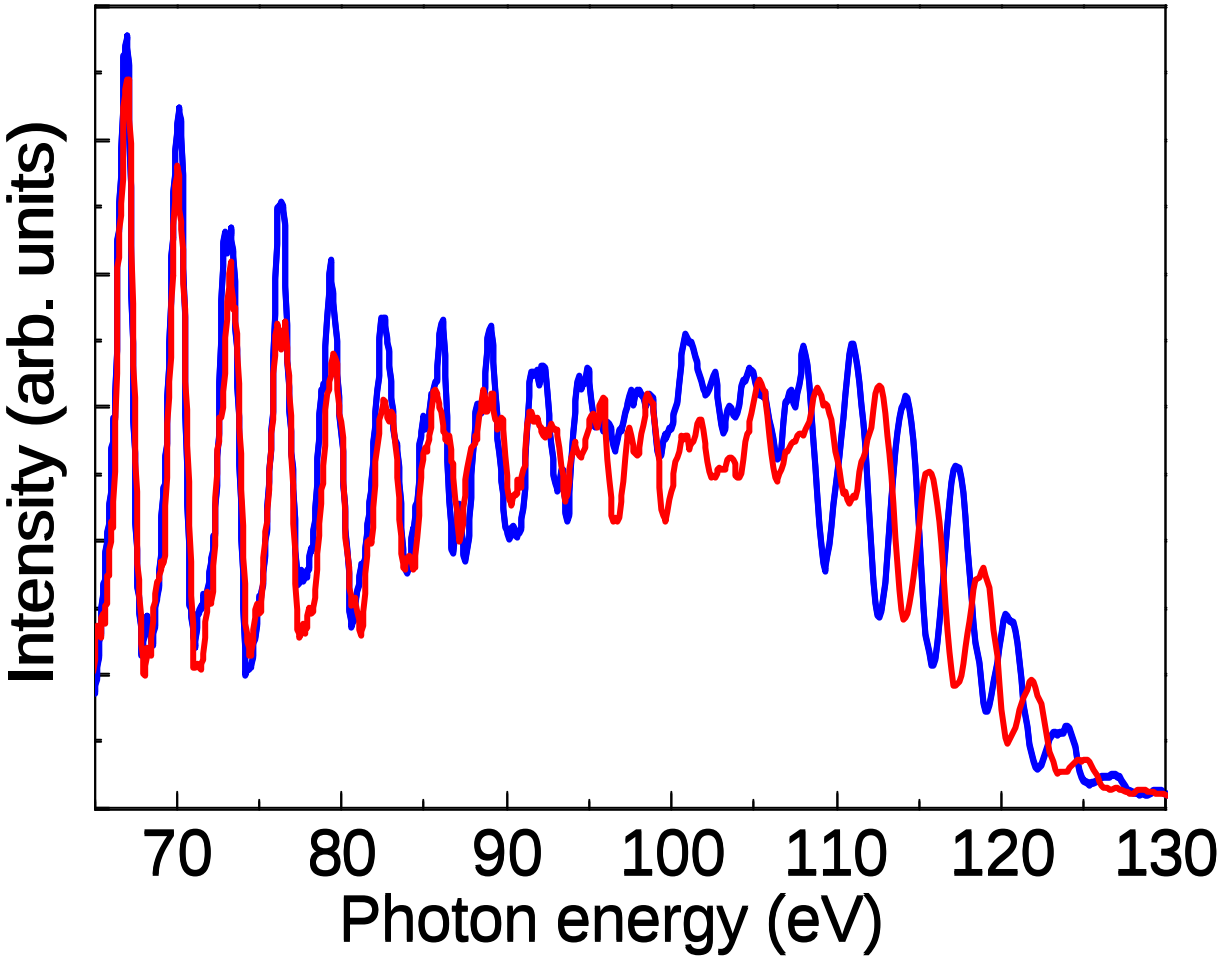

- ➔ **Plateau: no shift**
- ➔ **Upper plateau: irregular peaks**
- ➔ **Cutoff: spectral shift of harmonic peaks**

Single-shot harmonic spectra

- **Neon; pulse duration: 6 fs**

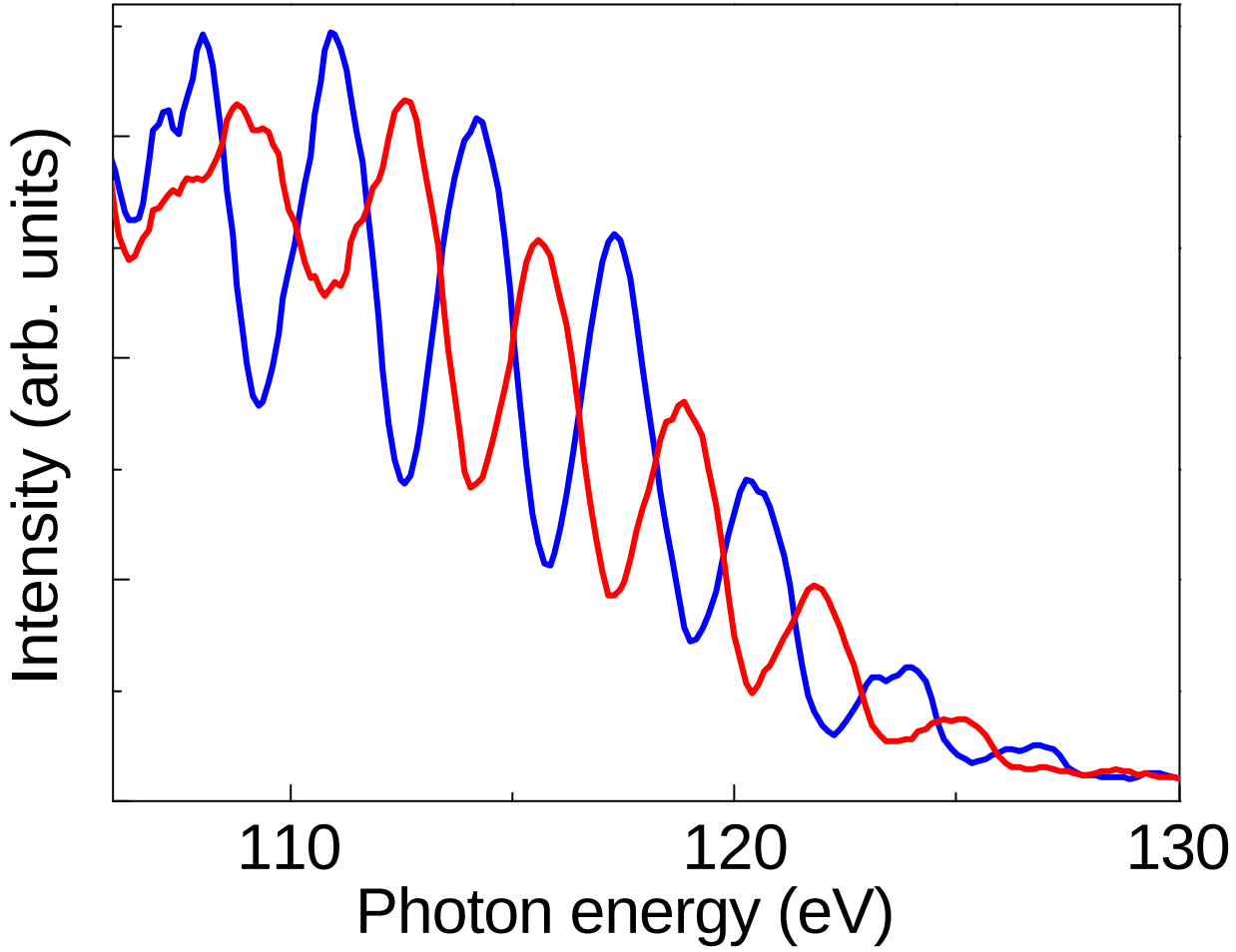

➔ **Cutoff: spectral shift of harmonic peaks**

Nonadiabatic 3-D model

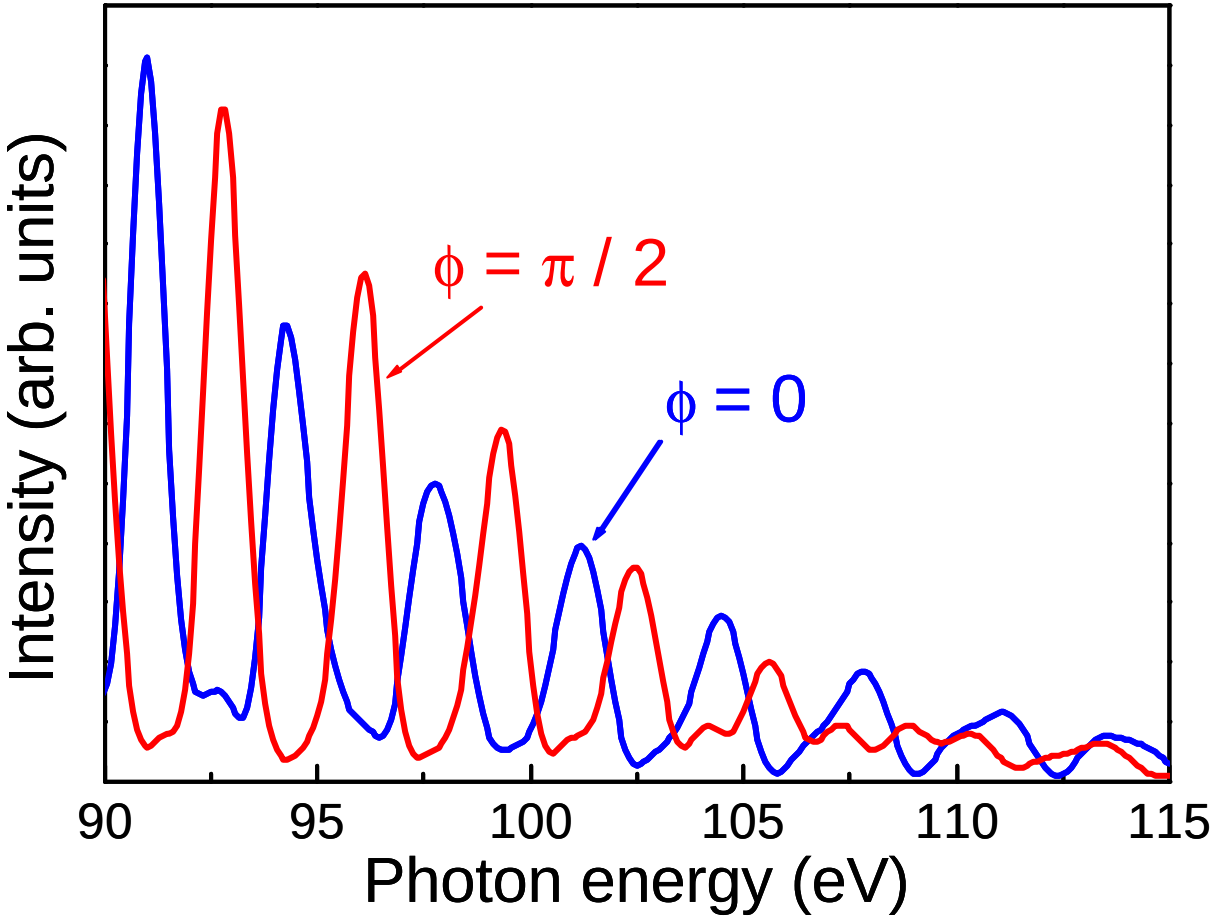

$E(t)=A(t)\cos(\omega_0 t+\phi)$

- **gas: neon, 50 torr**
- **pulse duration: 6 fs**
- **pulse peak intensity: $5.6\acute{}10^{14}$ W/cm²**

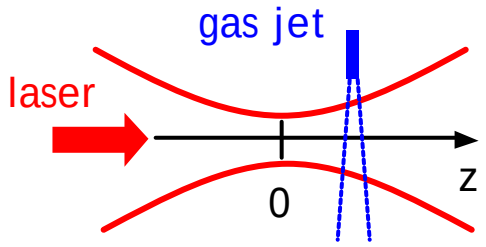

P. Villoresi *et al.*, Physical Review Letters, **85** 2494 (2000)
E. Priori *et al.*, Phys. Rev. A **61** 63801 (2000)

Effects of small intensity fluctuations

3-D modeling

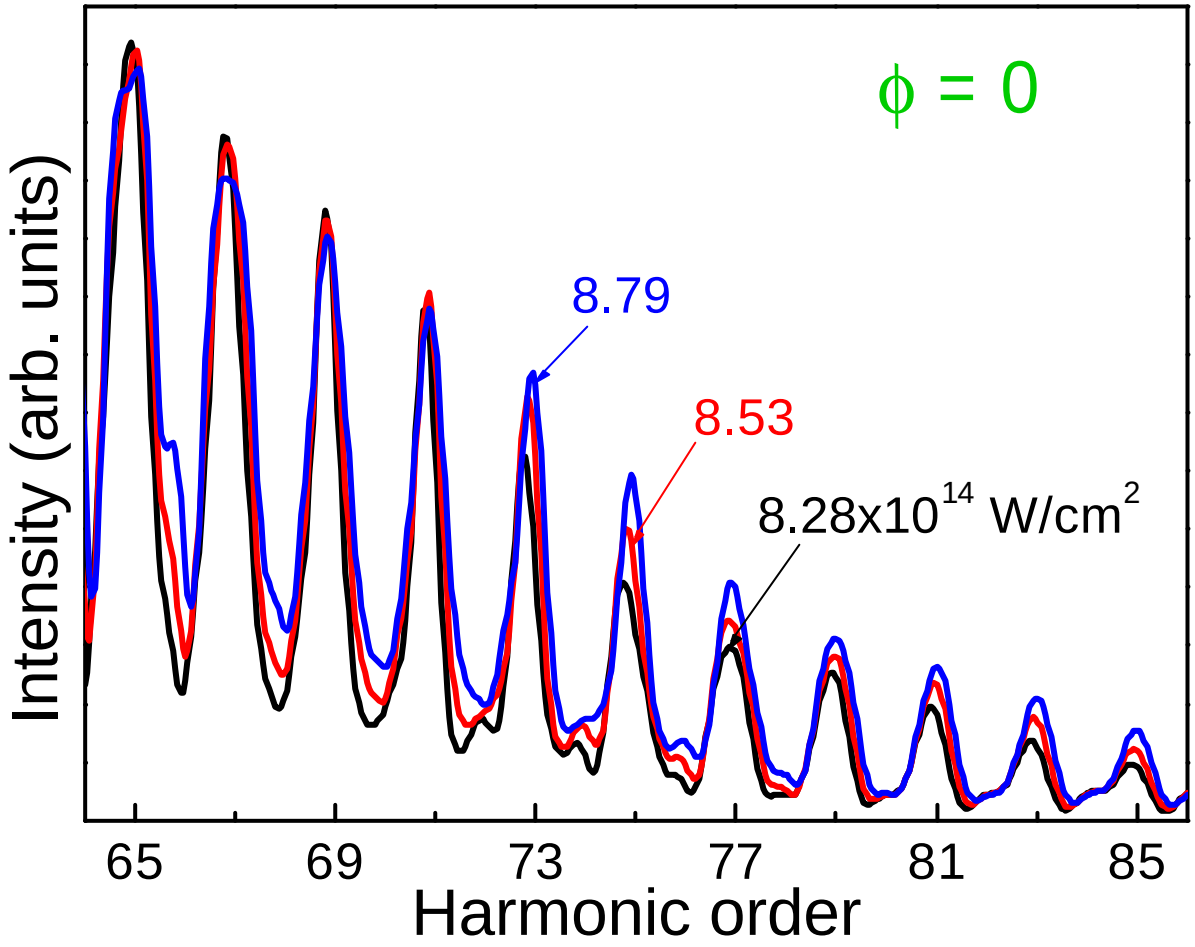

➔ **negligible frequency shift of the harmonic peaks at fixed absolute phase**

Effects of chirp: 3-D modeling

- **Gas pressure: 0.5 torr Þ negligible plasma-induced SPM in the gas jet**

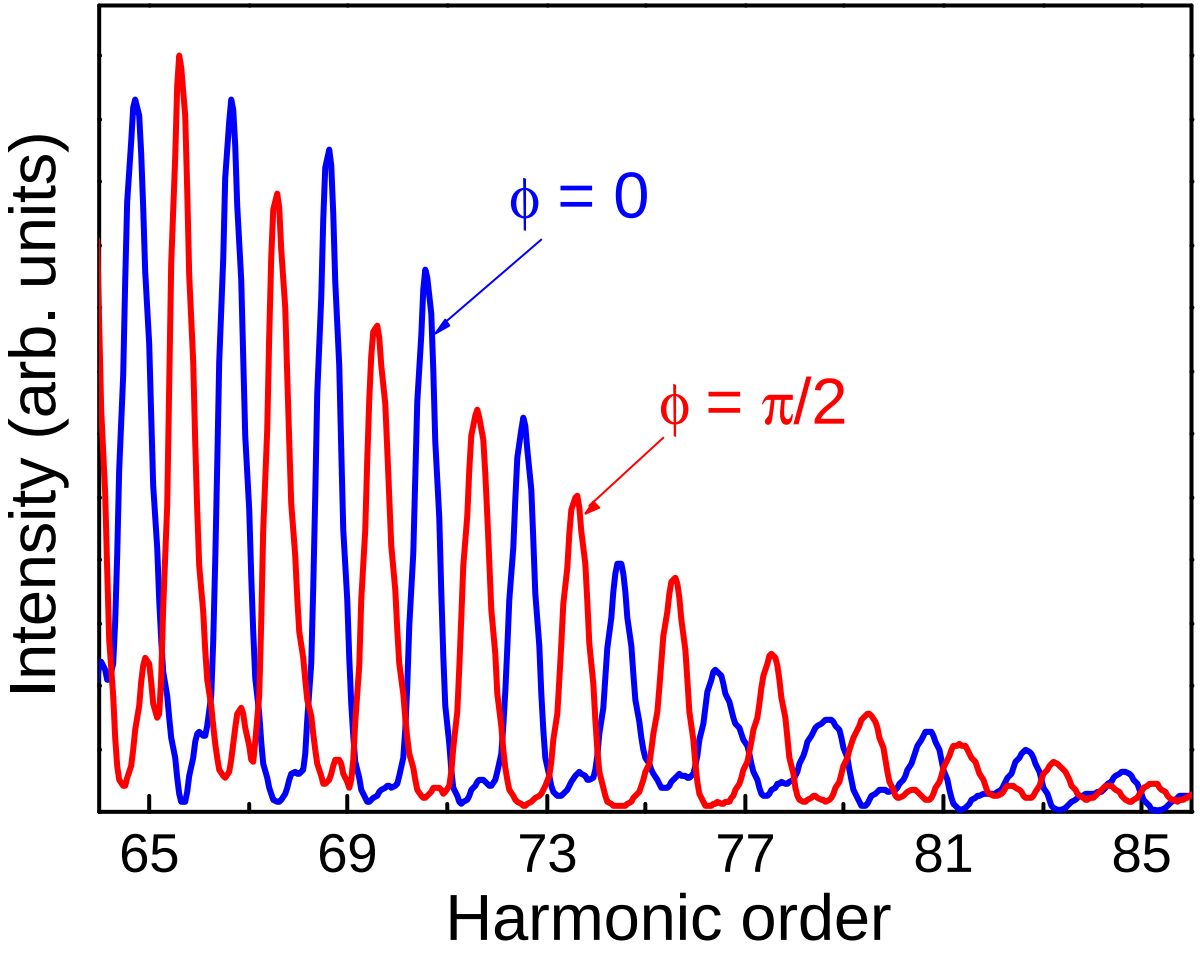

➔ **harmonic shift not induced by chirp**

Nonadiabatic single-atom response

- **Strong-field approximation**

  ➔ **Nonlinear dipole moment**

$$x(t) = i \int_{-\infty}^{t} dt \left(\frac{p}{e + it/2} \right)^{3/2} d^*[p_{st}(t,t) - A(t)]\, d[p_{st}(t,t) - A(t-t)]\, E(t-t)\, \exp[-i S_{st}(p,t,t)]$$

***d*: dipole matrix element for bound-free transitions**

p: canonical momentum

A: vector potential

S: quasiclassical action

$$S(p,t,t) = \int_{t-t}^{t} dt' \left(I_p + \frac{[p - A(t')]^2}{2} \right)$$

M. Lewenstein *et al.*, Phys. Rev. A **49**, 2117 (1994)

Nonadiabatic single-atom response

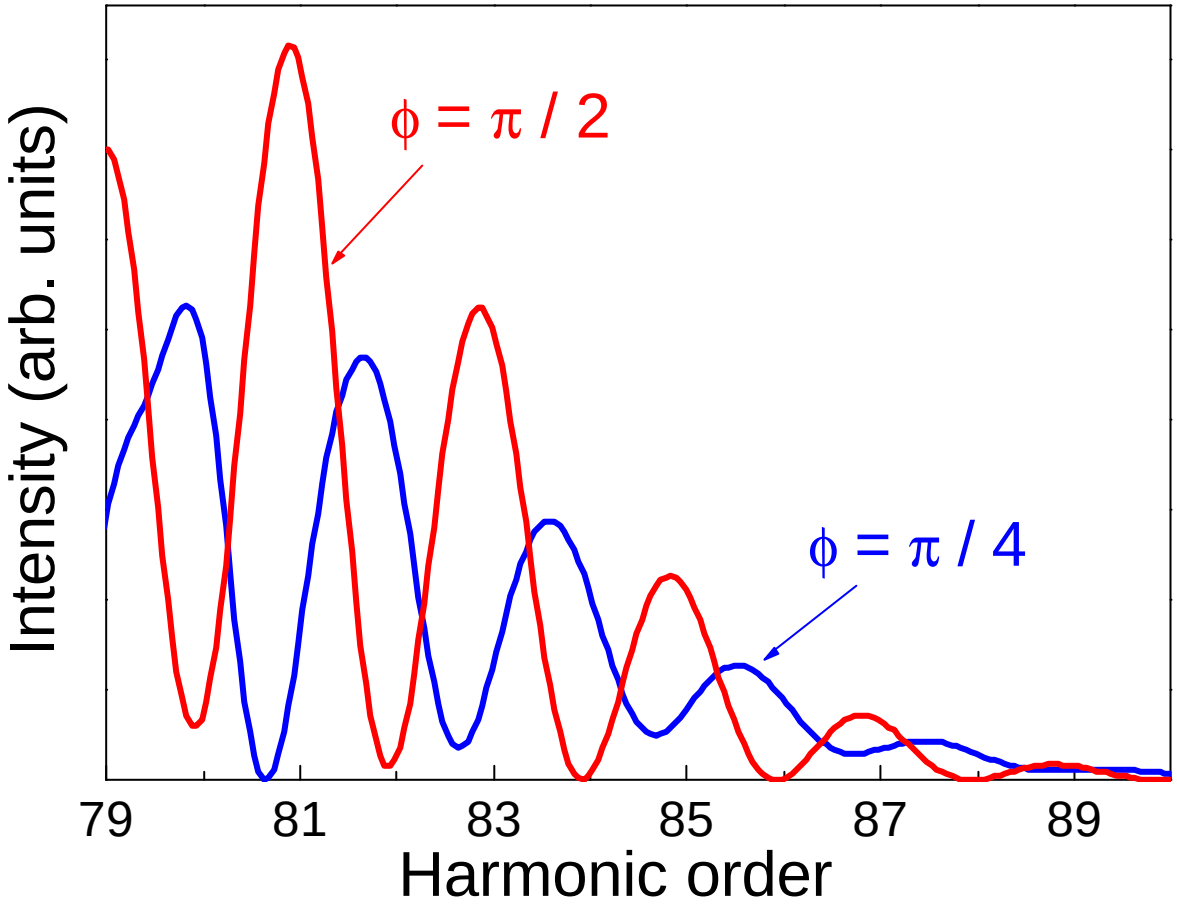

➔ ***harmonic* shift** Þ **single atom effect**

Saddle points of Feynman's path integral

evaluate

$$x(t) = i \int_{-\infty}^{t} dt \left(\frac{p}{e + it/2} \right)^{3/2} d^*[p_{st}(t,t) - A(t)]\, d[p_{st}(t,t) - A(t-t)]\, E(t-t)\, \exp[-i S_{st}(p,t,t)]$$

with saddle points

$$x(w) = \int_{-\infty}^{\infty} x(t) \exp(-iwt)\, dt$$

$$x(w) = \sum_s C_s(p_s, t_s, t_s) \exp[-iS(p_s, t_s, t_s) + iwt_s]$$

- **Coherent superposition of contributions from a few quantum paths**
- **Sum over the relevant saddle points with $0<\mathrm{Re}(t)<T_0$**

Two quantum paths give the most relevant contribution

- Short quantum path
- Long quantum path

Quantum path selection

- **Phase matching provides a powerful method to identify contributions of individual quantum paths**

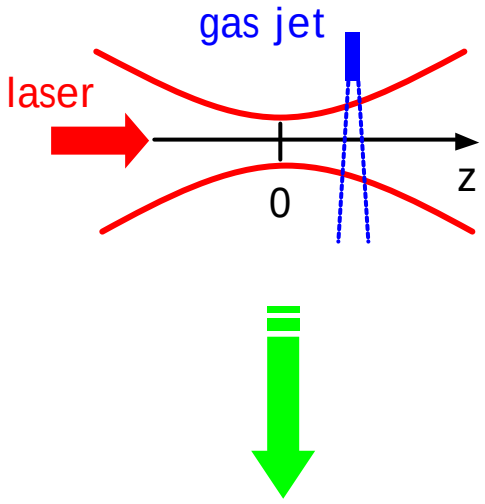

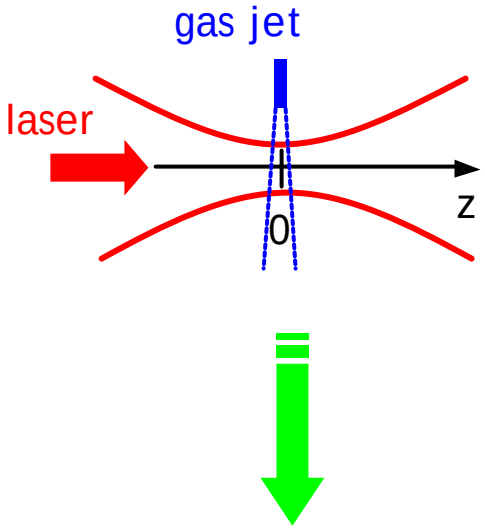

Short quantum path selection

Long quantum path contribution increases

P. Salières *et al.*, Science **292**, 902 (2001)

Saddle point approximation

- **Calculated harmonic spectrum**

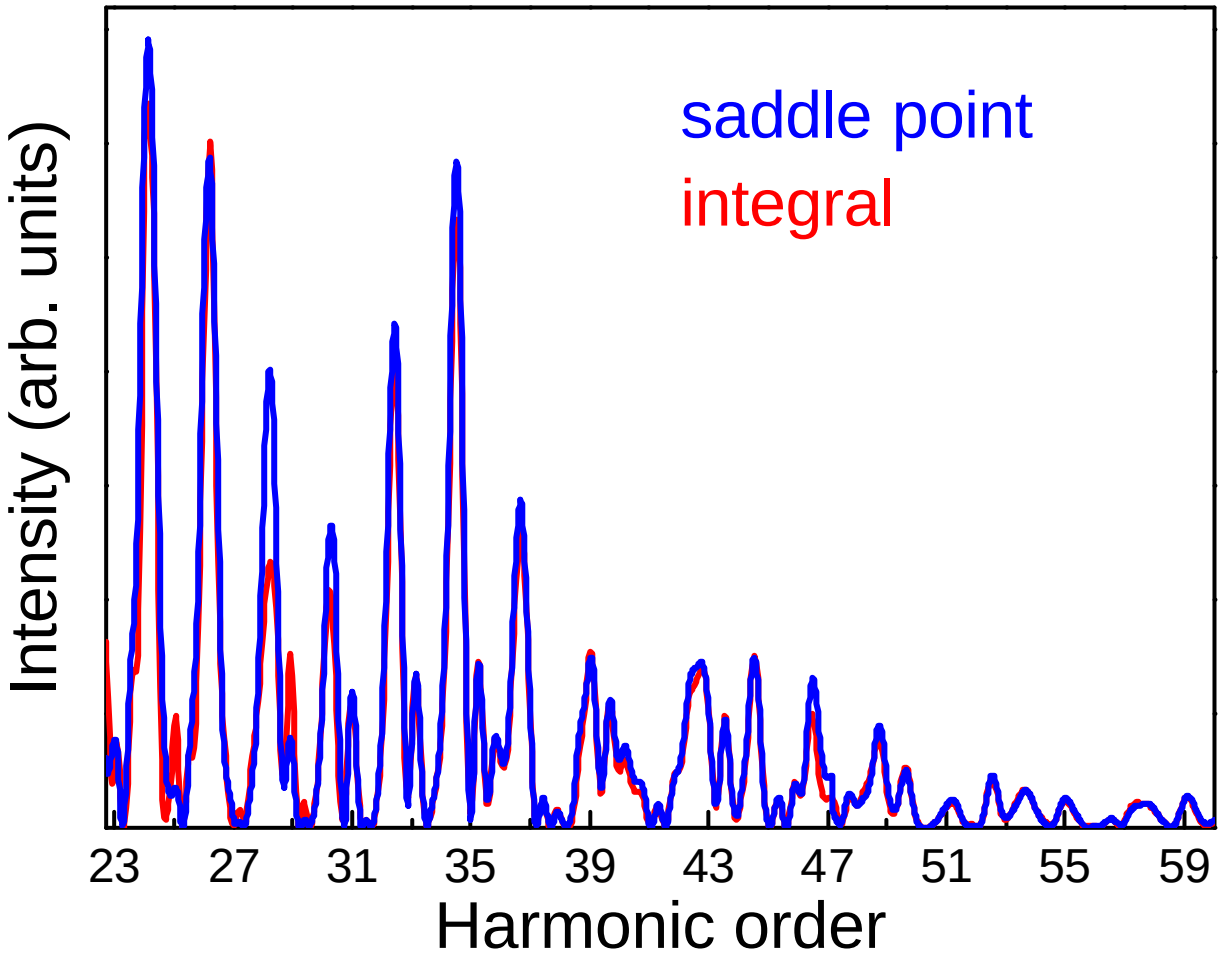

➔ **excellent agreement between the two methods**

Short quantum paths

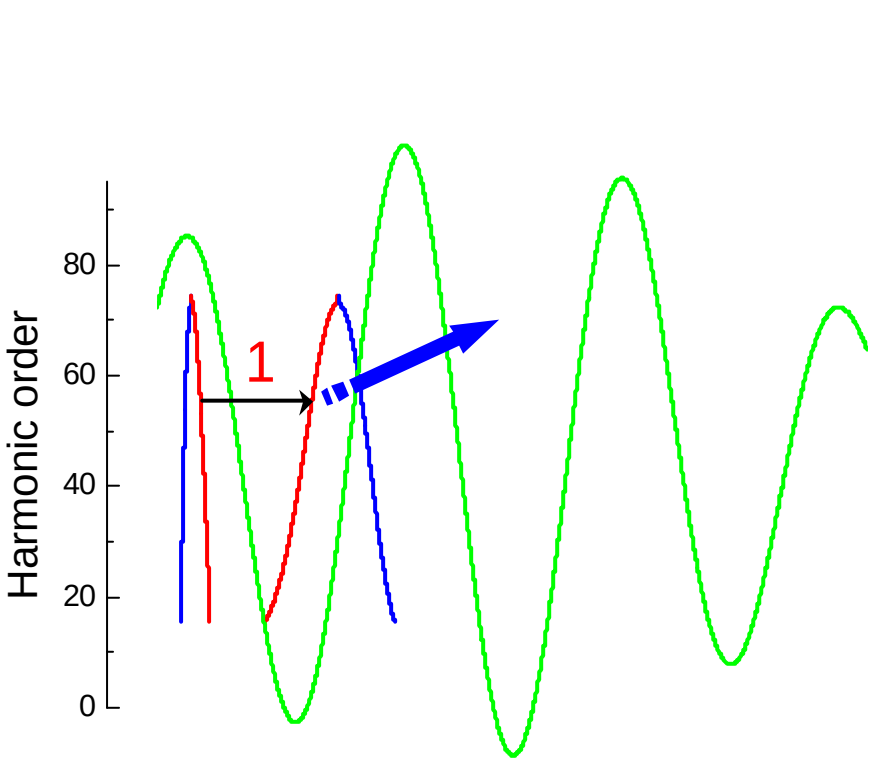

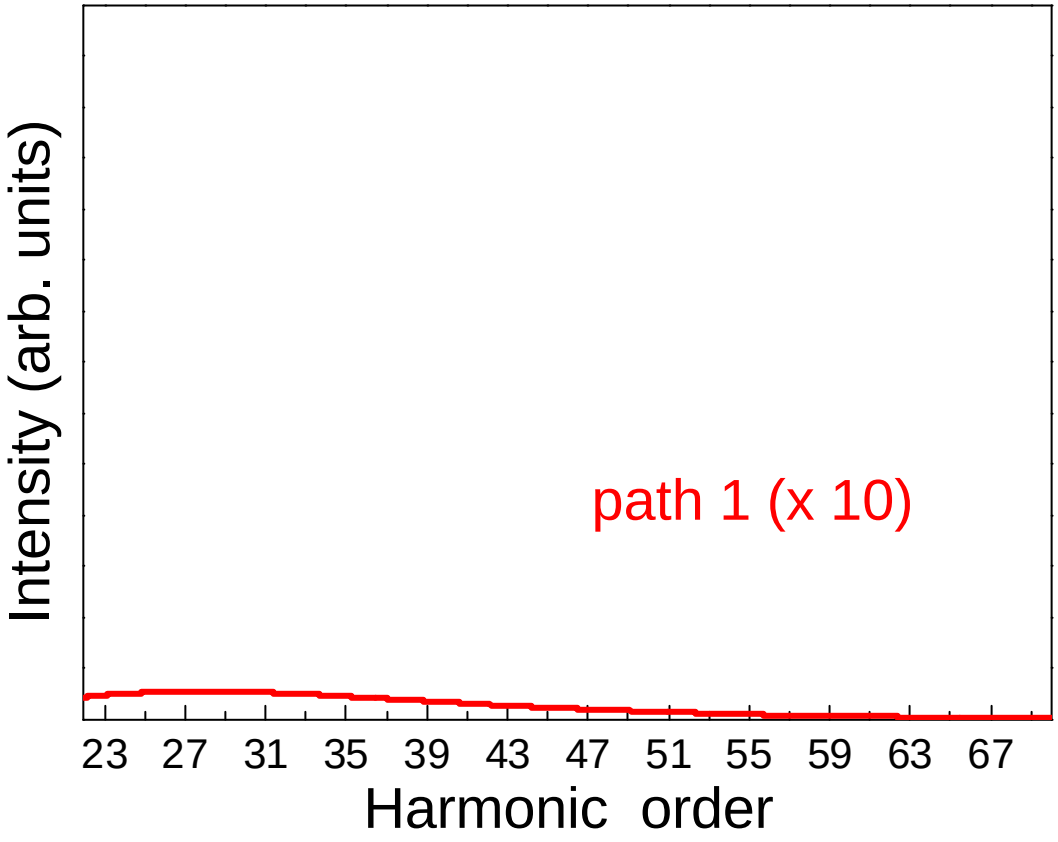

Short quantum paths

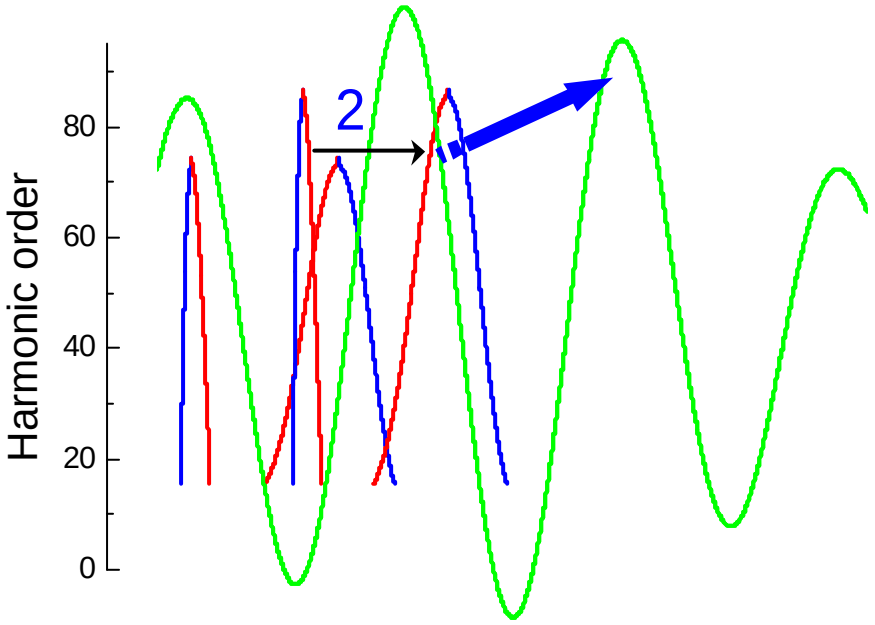

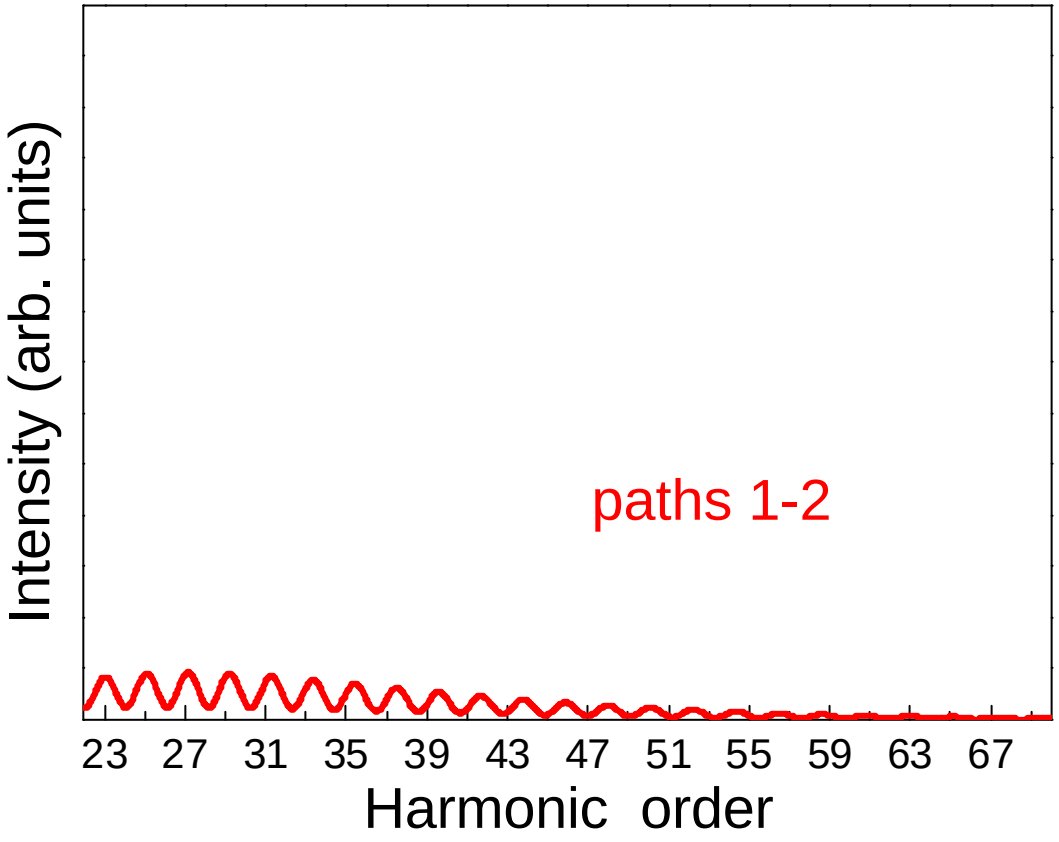

Short quantum paths

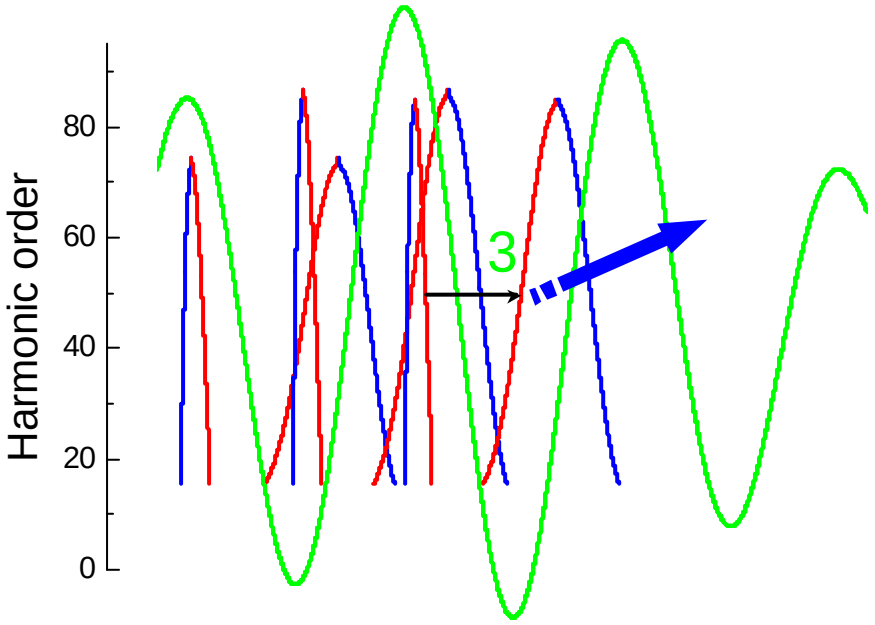

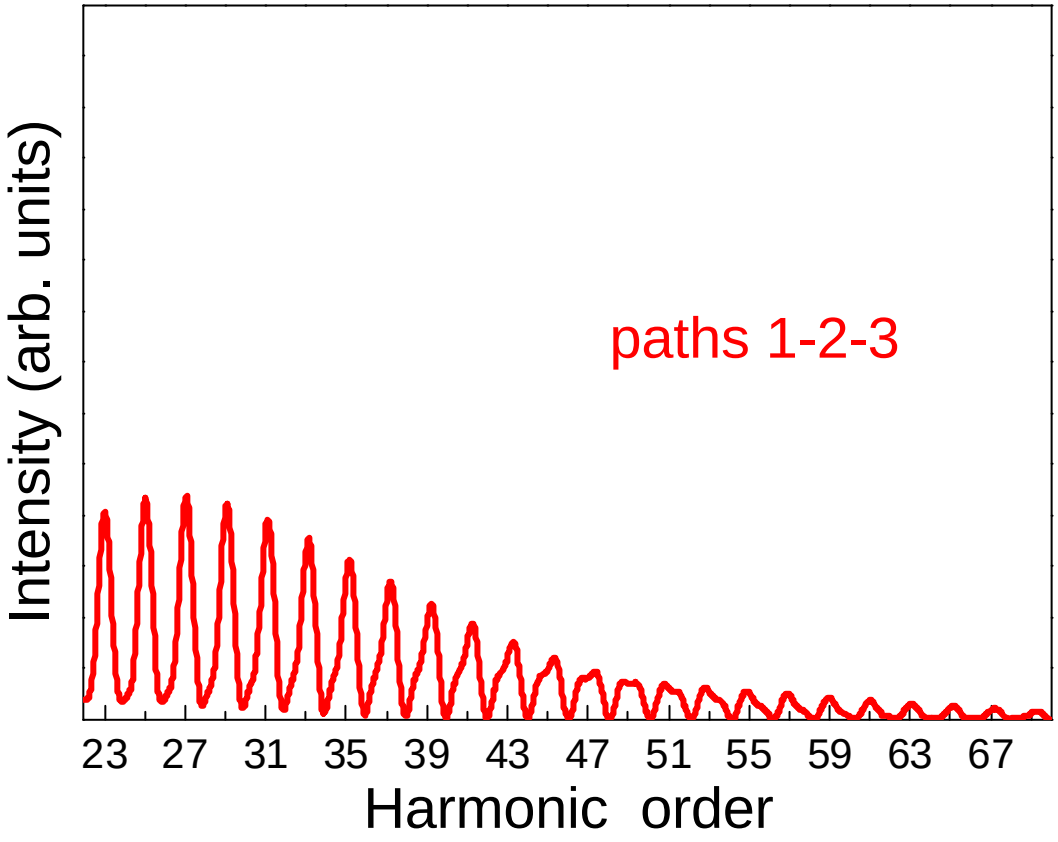

Short quantum paths

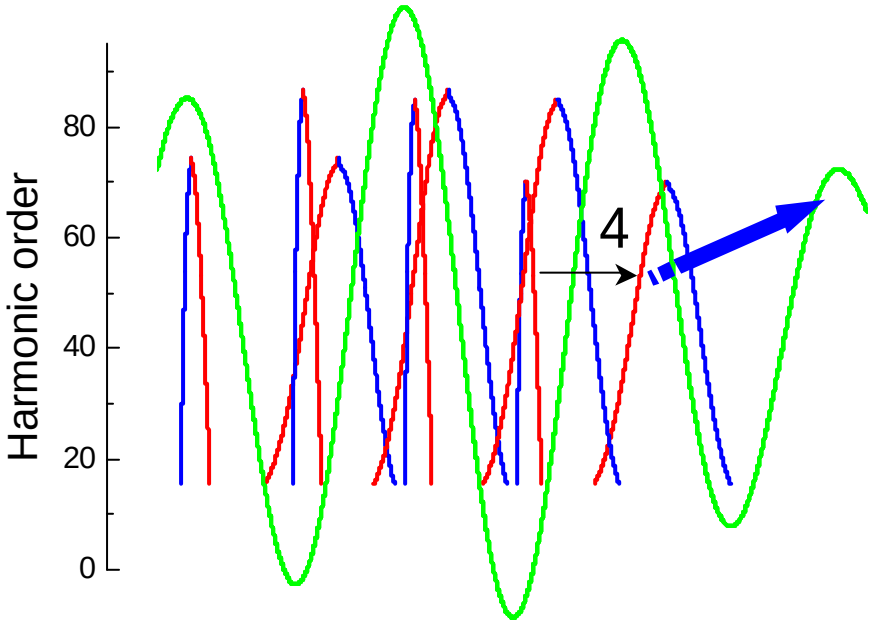

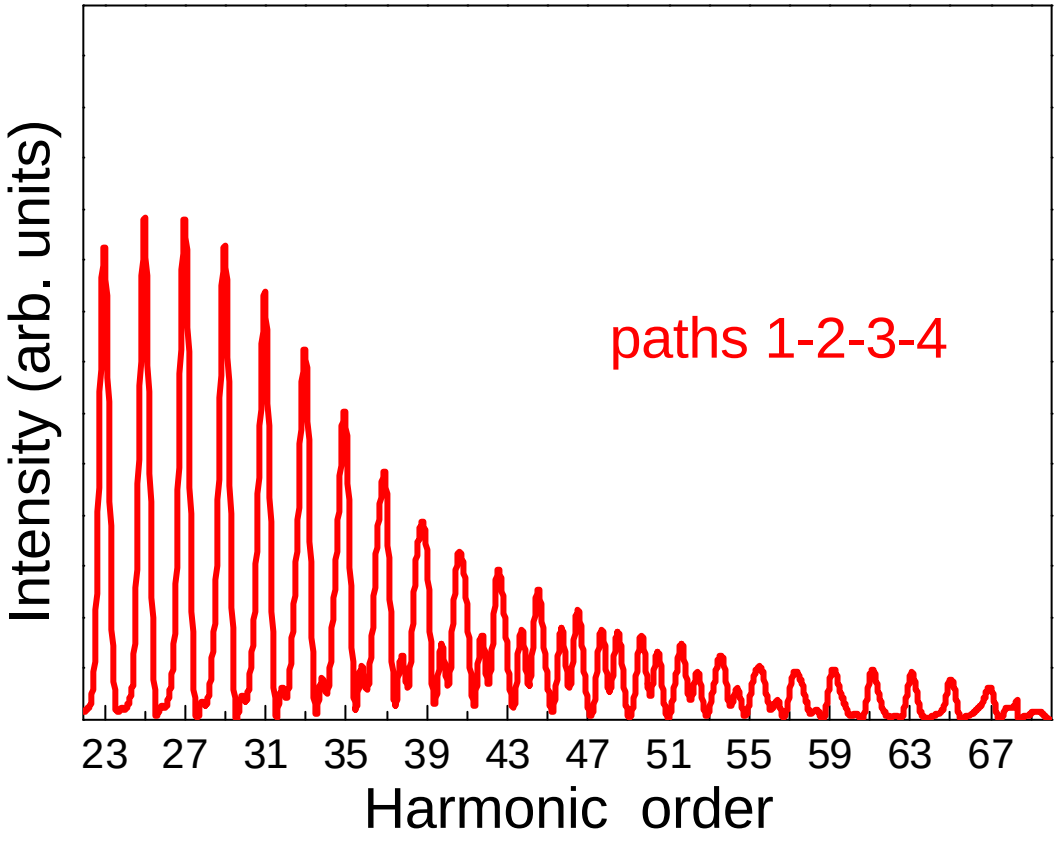

Short quantum paths

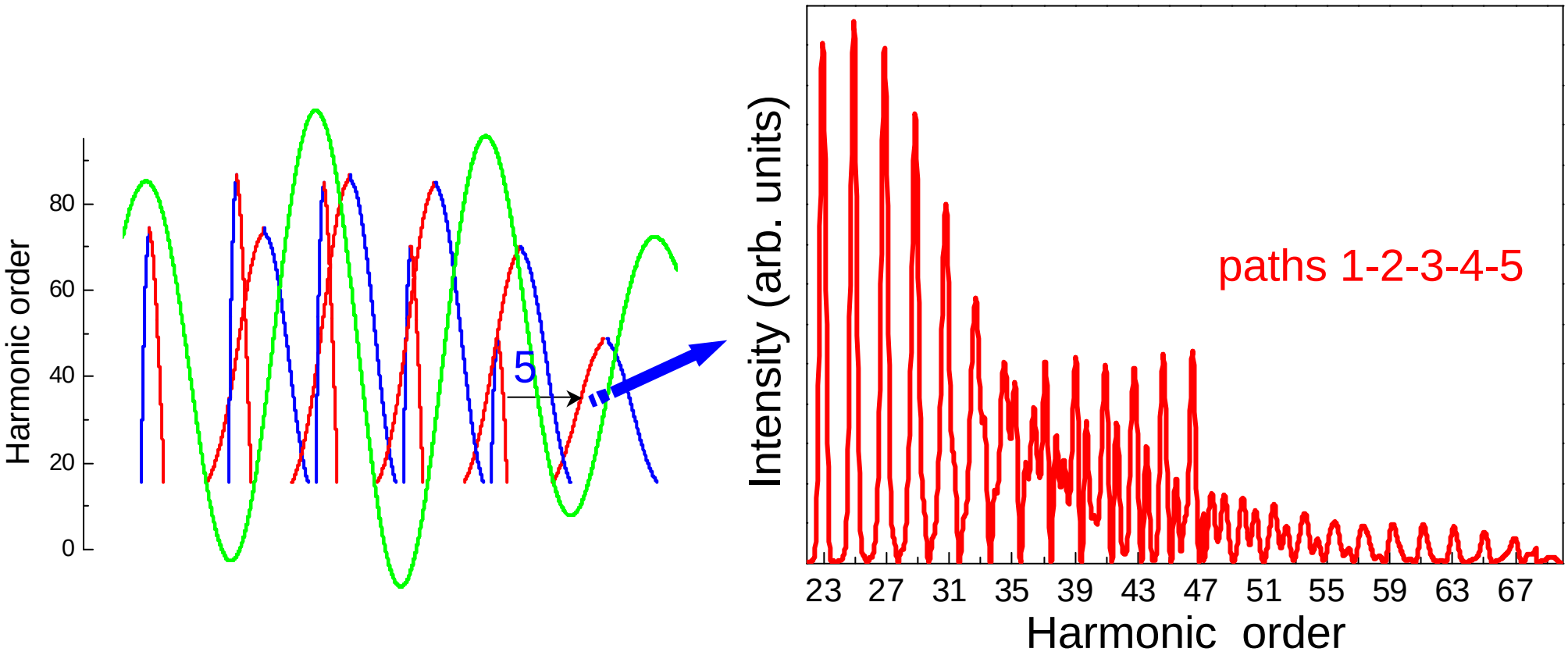

Role of the absolute phase

- **Saddle-point approximation**

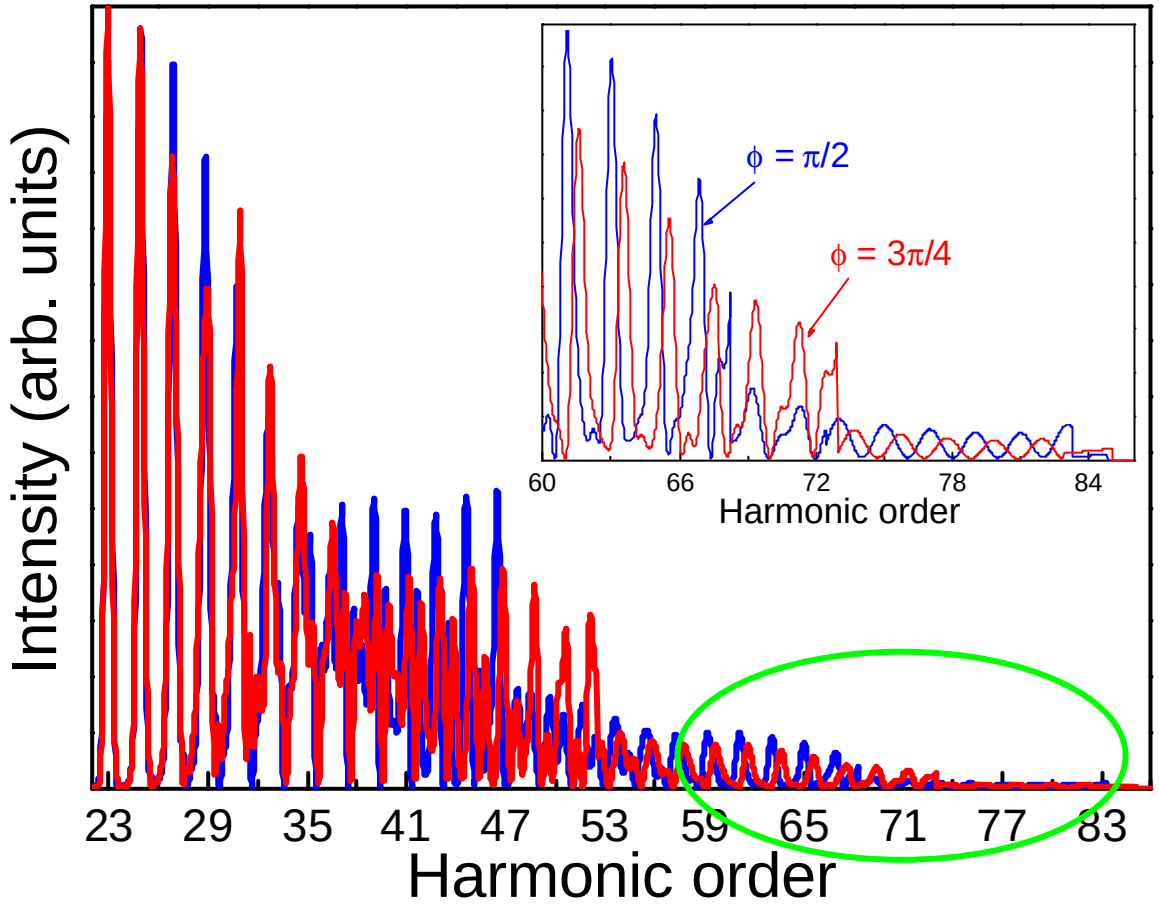

➔ **Plateau: no shift**

➔ **Upper plateau: irregular peaks**

➔ **Cutoff: spectral shift of harmonic peaks**

Physical picture

- ***Harmonic peaks*** ➔ **constructive interference of periodically emitted XUV spectra**

  ➔ **Cutoff: one or two recombination events**

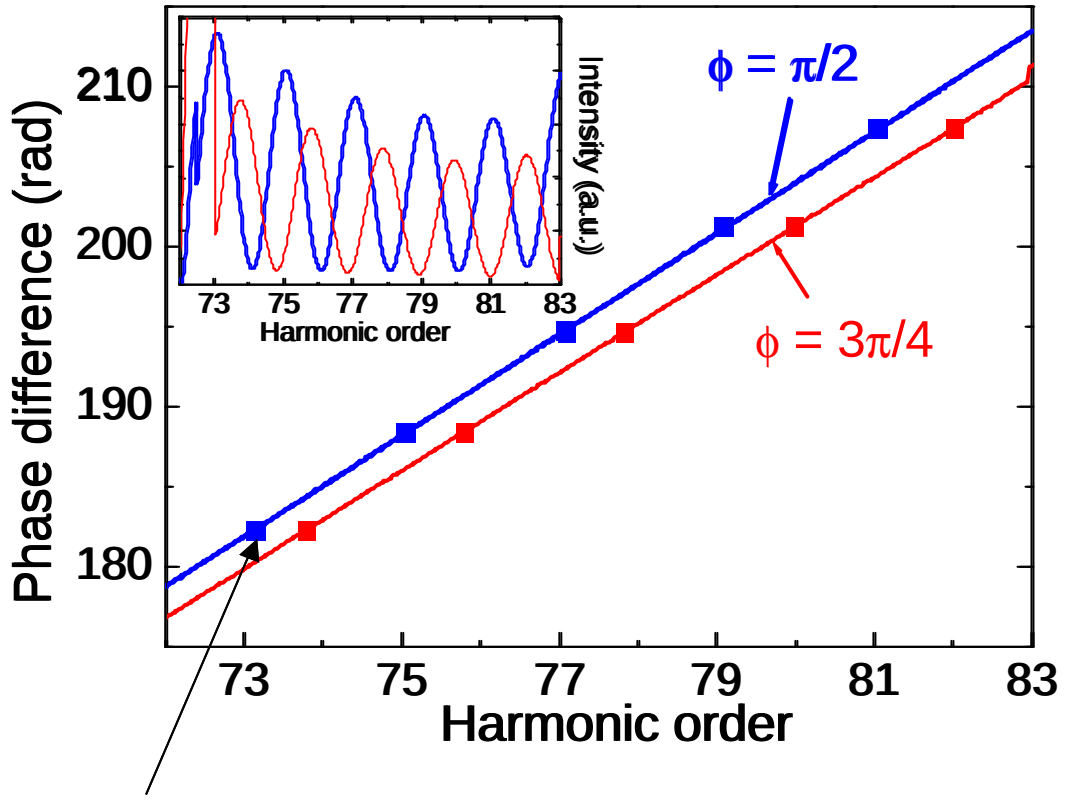

constructive interference $\Delta\Theta = 2m\pi$

M. Nisoli *et al.* to appear in Physical Review Letters, 2003

HHG conclusions

- HHs are brilliant and ultrafast
- Coherent process driven by the laser electric field (for present intensities)
- The single shot acquisition reveals the absolute phase signature
- Cutoff shifts are explained by interference of emission processes

Influence of Absolute Phase on Photoelectron Emission

Electron Emission with Multi-cycle Pulses

$\varphi = \pi/2$

$$E = E_0 \cos(w t + j)$$

$\varphi = 0$

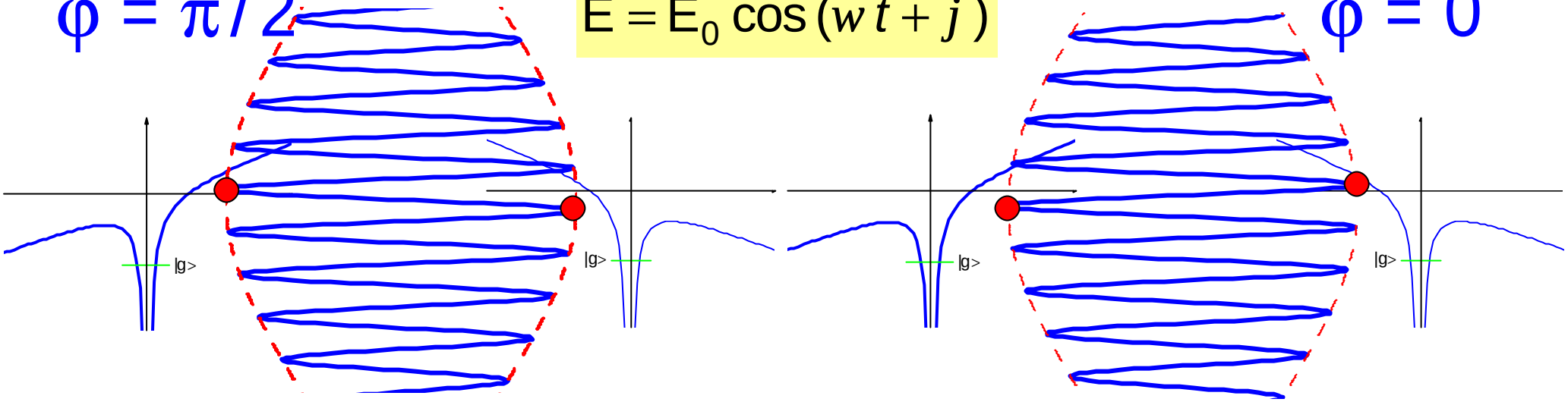

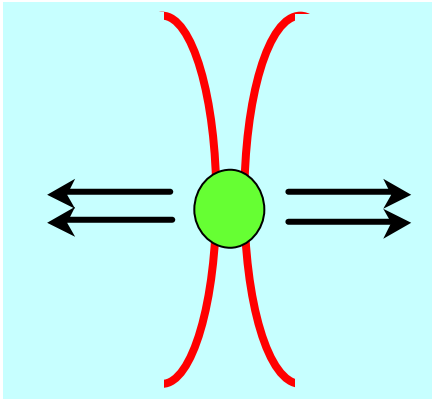

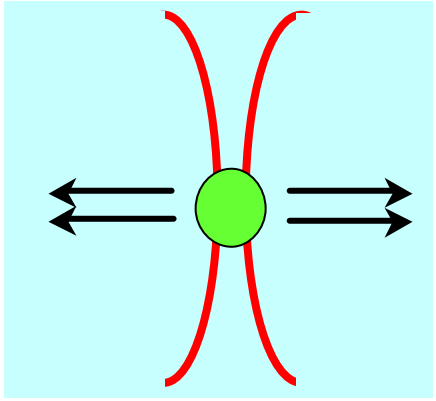

- **Inversion symmetry of electron angular distribution**

  ➔ **No absolute phase effects !!**

Breaking inversion symmetry with a few-cycle pulse

$\varphi = \pi/2$

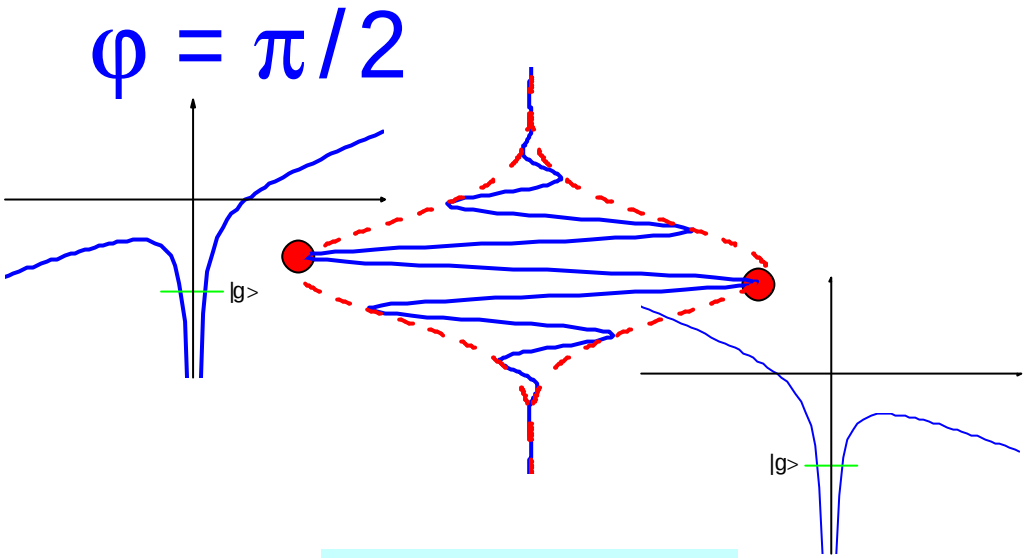

$\varphi = 0$

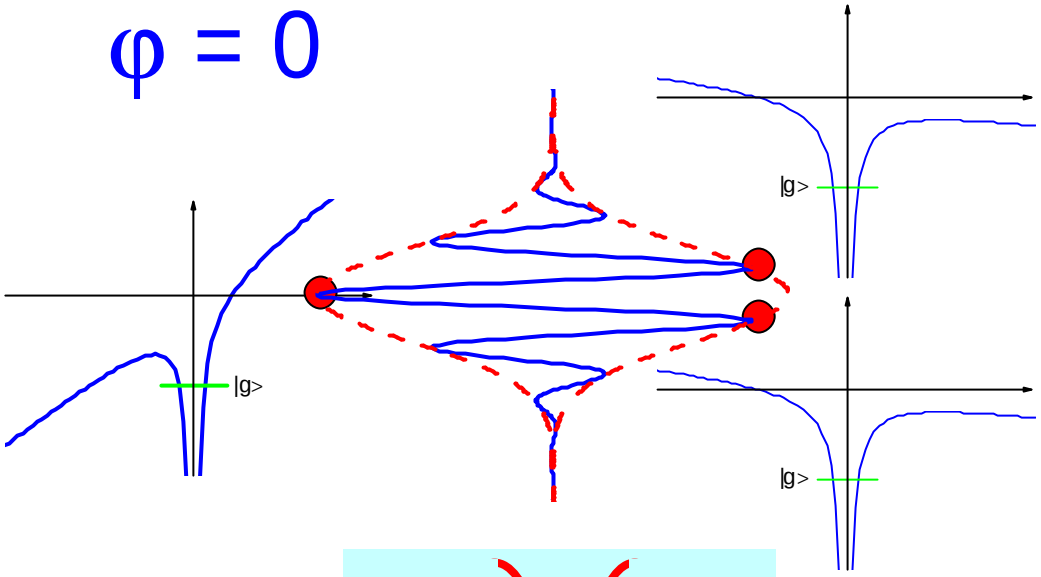

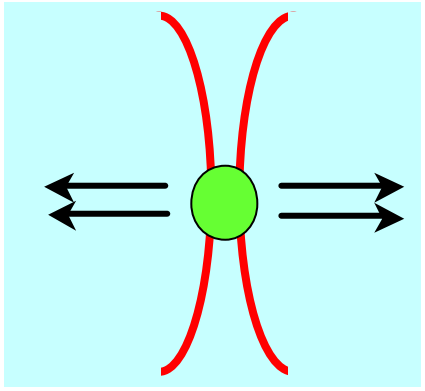

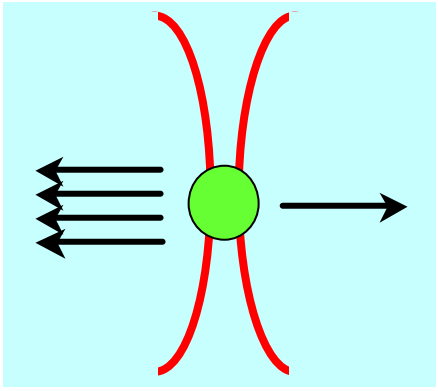

- The angular distribution of photoelectrons loses its inversion symmetry as soon as the absolute phase starts playing a role
- The lack of inversion symmetry translates into an anticorrelation of the number of electron flying in opposite directions

A circulary-polarized ultraintense few-optical-cycle light pulse emits asymmetrically

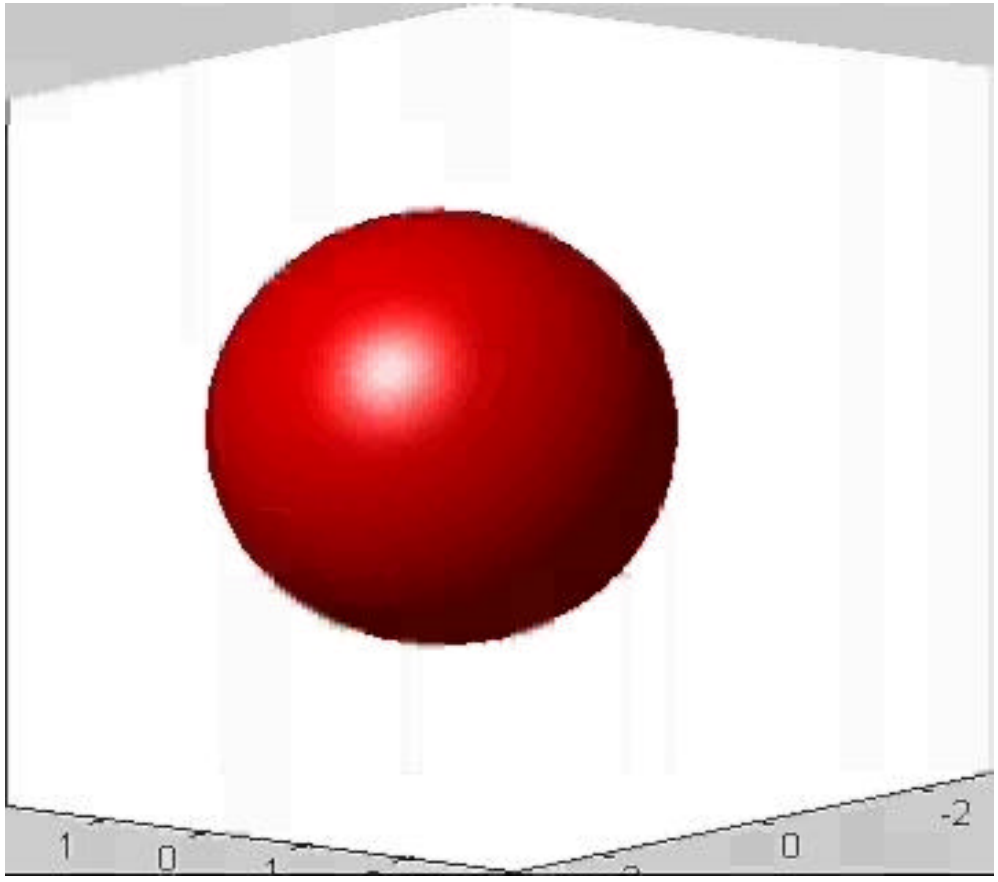

Basic Idea of the Experiment

- **Stereo ATI experiment**

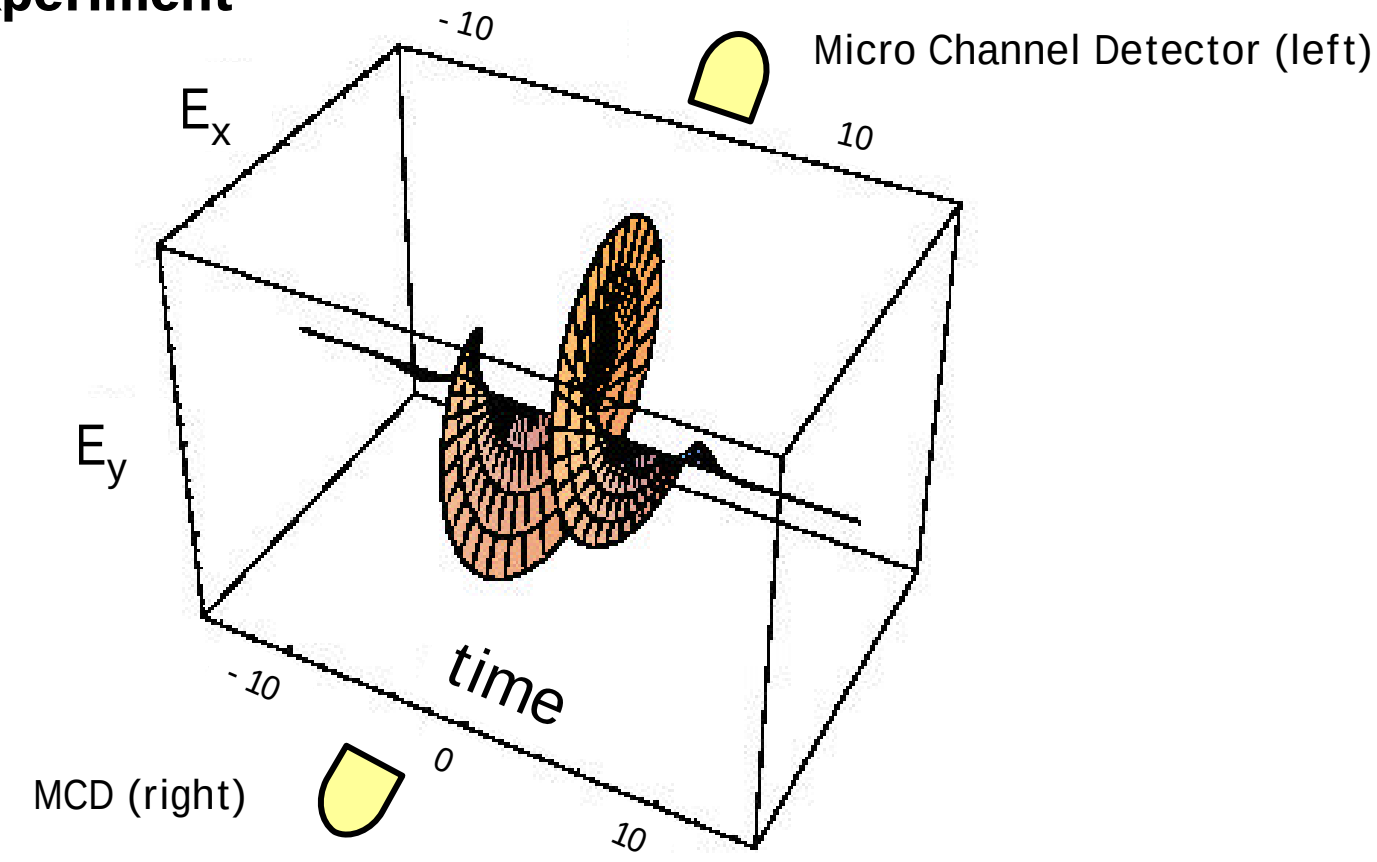

- **Use of circularly polarized light:**

  ⇒ electric field amplitude varies smoothly with time:
  ionization not modulated by rapidly changing electric field

  ⇒ preventing electron rescattering off the parent ion:
  direction of photoelectron uniquely determined by the absolute phase

Correlation technique

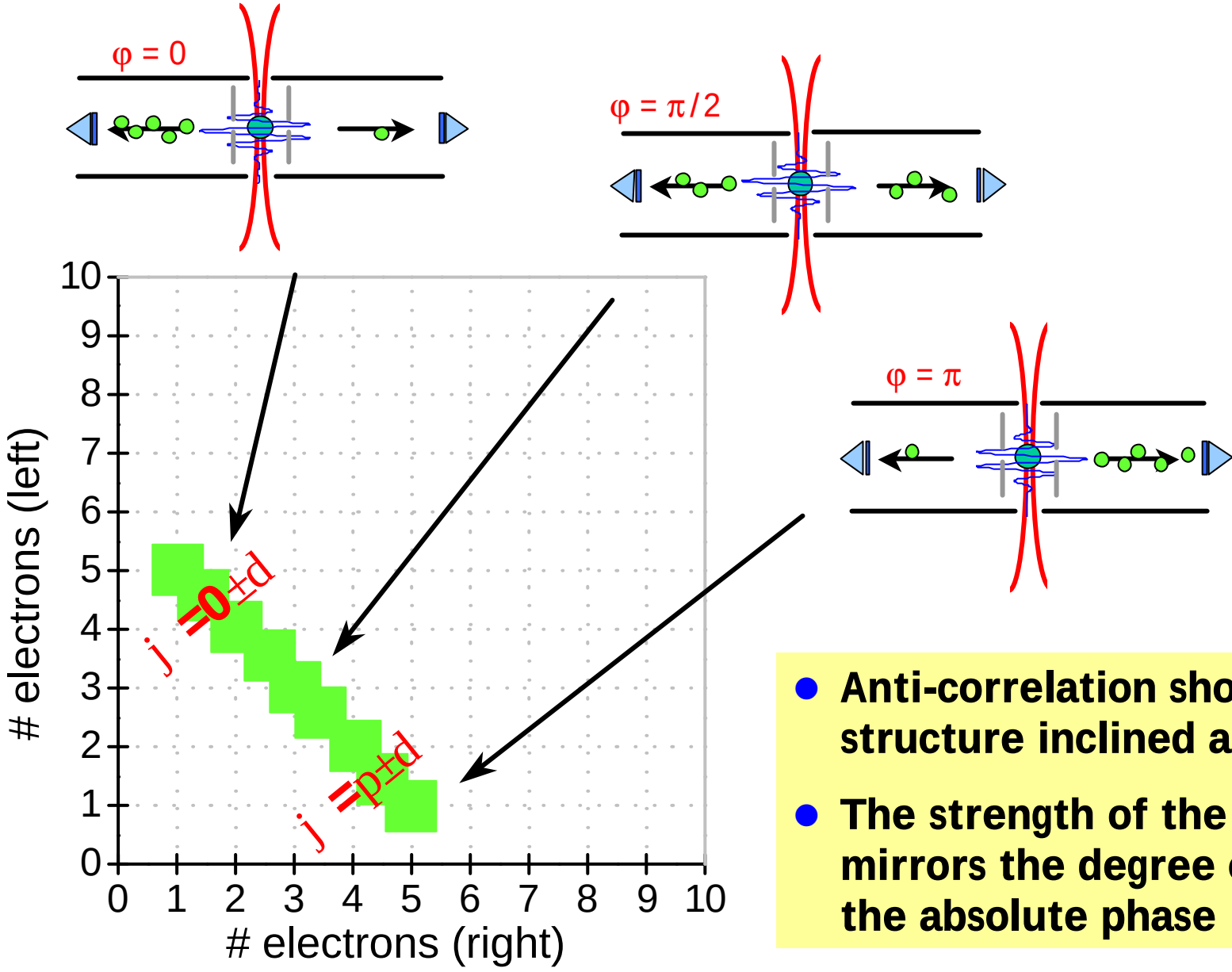

- **Anti-correlation shows up as a structure inclined at - 45°**
- **The strength of the anticorrelation mirrors the degree of influence of the absolute phase**

Strength and Significance of Anticorrelation

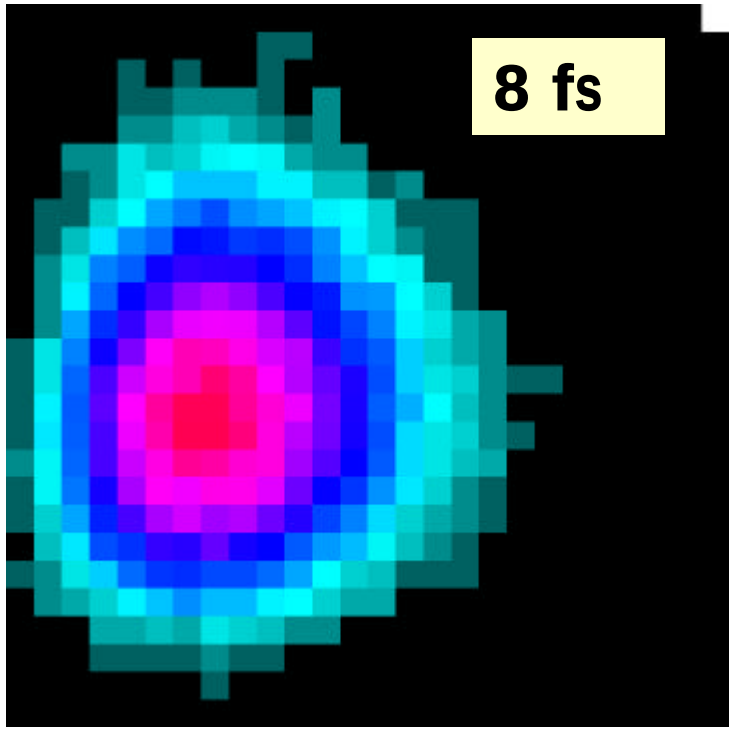

$t > 0$

significance > 6 standard deviations

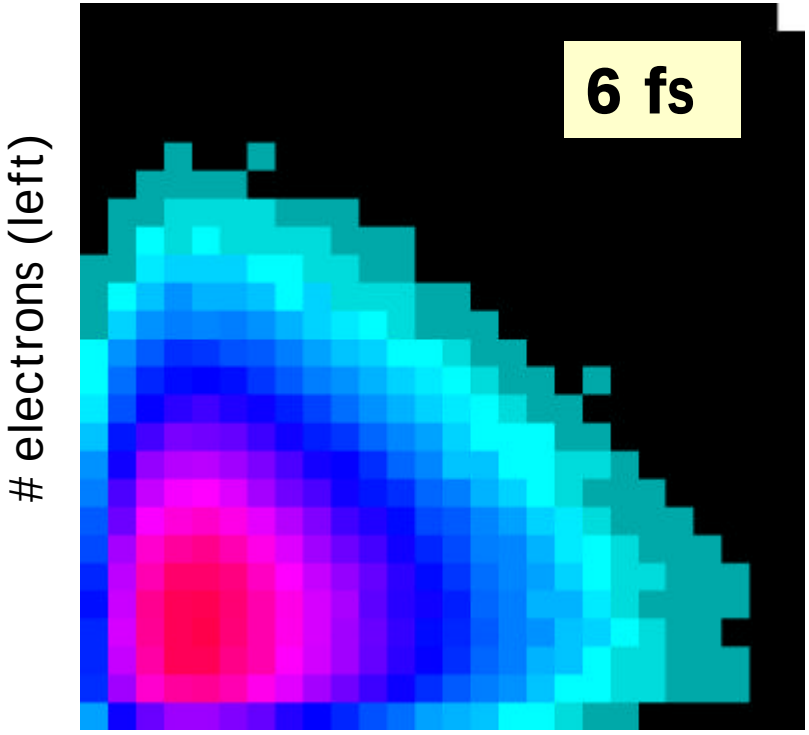

$t \approx$ **- 0.05**

clear significance: > 2 standard deviations of the null hypothesis of no correlation

G.G. Paulus, F. Grasbon, H. Walther, P. Villoresi, M. Nisoli, S. Stagira, E. Priori, S. De Silvestri, **Nature 414**, 182 (2001)

Xe 8 fs – spectrum vs. intensity

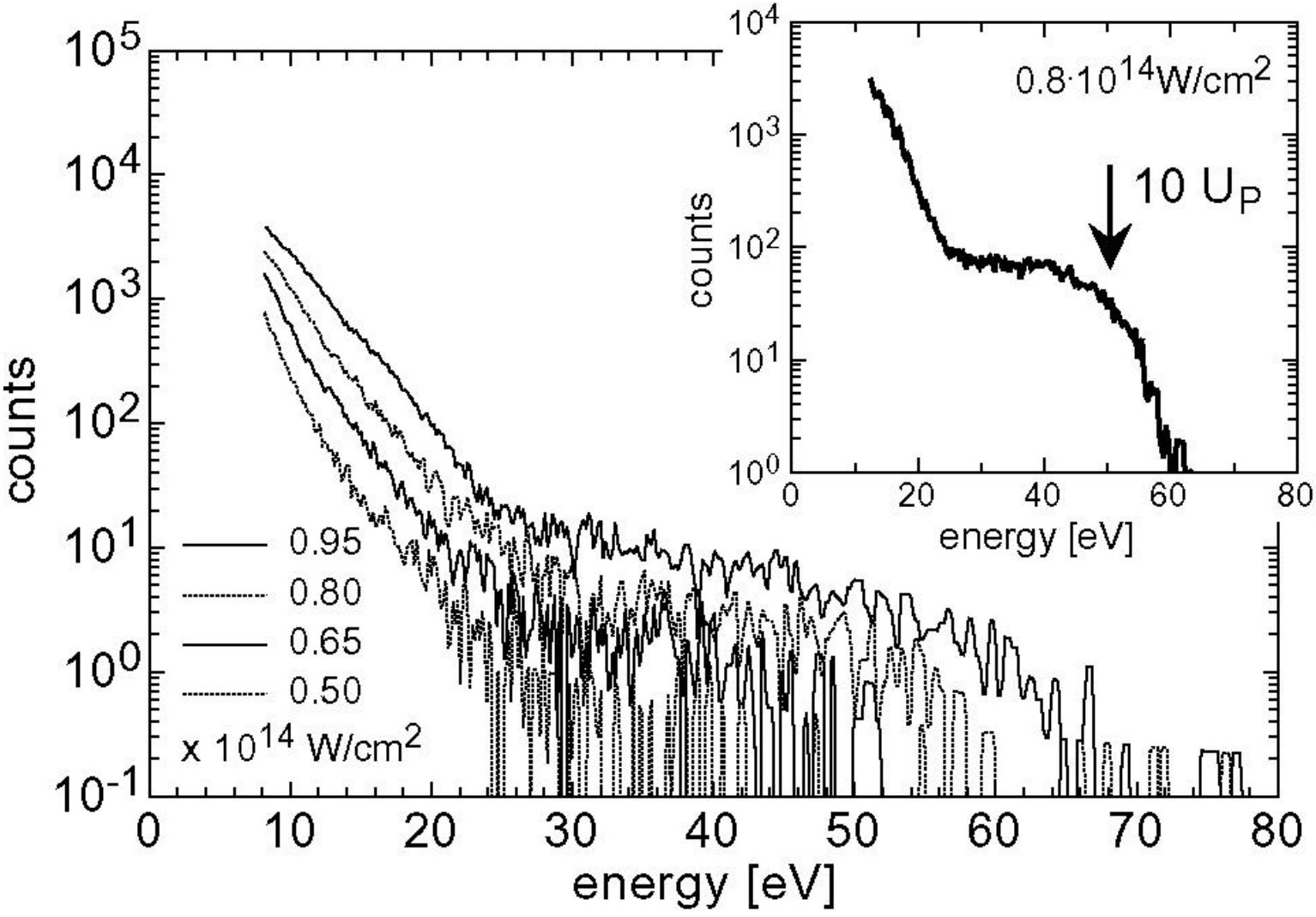

F. Grasbon *et al.* to appear in Physical Review Letters, 2003

ATI conclusions

- Novel features of photoelectron spectra in the few-optical-cycle regime
- First experimental demonstration of the influence of the absolute phase of a few-cycle light pulse on intense-field photoionization
- Using the stereo-ATI scheme it is not necessary to stabilize the absolute phase in order to investigate its effects

endline/startline

- Few-femtosecond dynamics differs from framework of plasma formation and thermal motion
- Individual processes not repetitive may be observed/exploited
- New schemes for the interaction and the measure were introduced, more needed
- New perspectives foreseen

..keep in mind that

CUSBO is an European facility

Provides access to investigators involved in Ultrafast Physics

Director: sandro.desilvestri@fisi.polimi.it

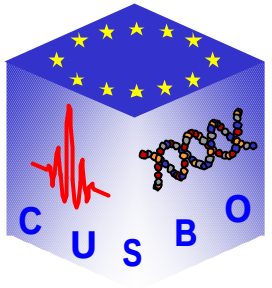

ULTRAS INFM
NATIONAL LABORATORY FOR ULTRAFAST AND ULTRAINTENSE OPTICAL SCIENCE

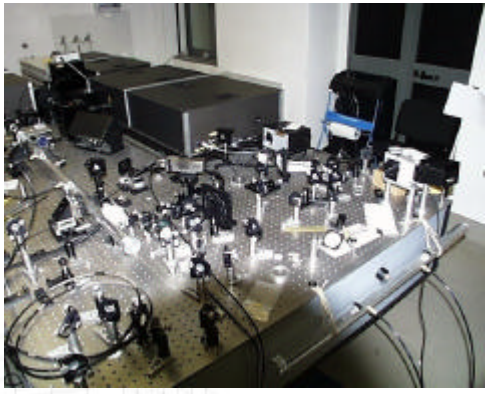

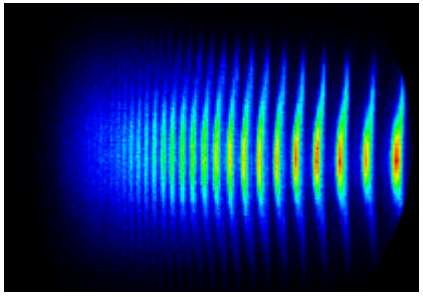

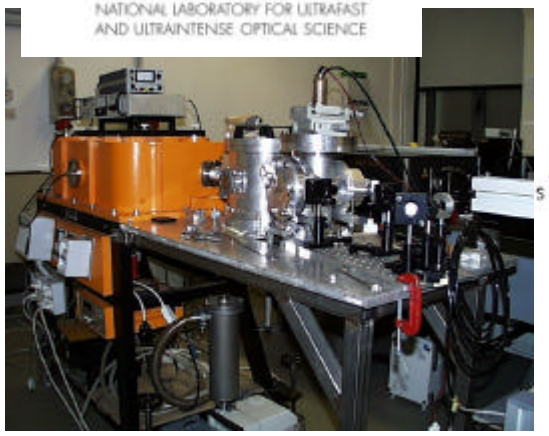

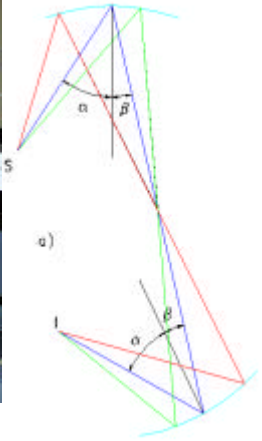

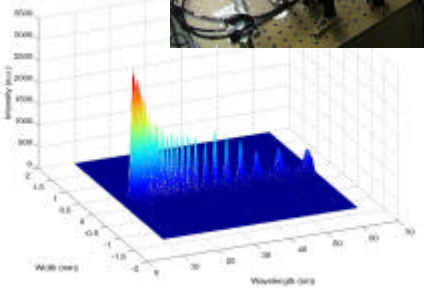

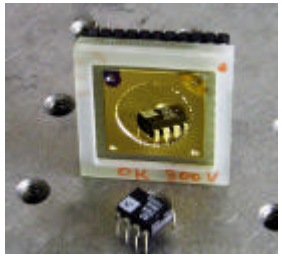

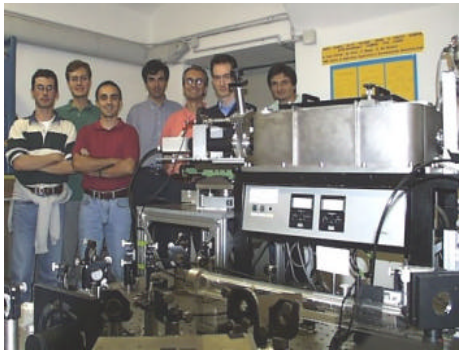

Gamma ray beam production and probing

Matthew Zepf
Queen's University, Belfast

K. Krushelnick et al.
Imperial College, London, UK

P. Norreys et al.
Imperial College, London, UK

E. Clark, R. Edwards et al.
AWE, Aldermaston, UK

Overview

- Motivation
- Hot electron production
  - Solid targets vs gas targets
- Test experiment:Probing of high areal density materials
- Conclusion

Motivation
Why use laser produced gamma rays?

- X-ray and gamma ray beams are well established probes
- High intensity ($>10^{18}$ Wcm^{-2}) lasers are a copious source of X-rays
  - High coupling efficiency to MeV electrons (up to 50%)
- fs and ps lasers can produce ps bursts of gamma rays
  - Temporally resolved radiography with ps resolution
  - Gating allows noise reduction and dose reduction
- The electron source is ~ laser spot size
  - High resolution point projection is possible.
- Flexible geometry
  - 3D radiographic movies (through multiple views)

γ-ray production

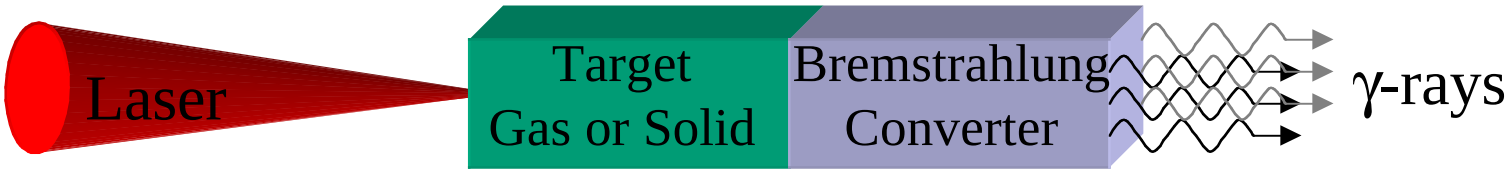

- Laser energy is converted to MeV electrons
  - Gas or solid target
- Electrons are converted to Bremsstrahlung in High Z converter.
  ⇒ γ-ray beam

γ-ray beam quality

- Small source size
  - Requires small laser focal spot.
    - <10μm common in high power laser systems
  - Low divergence of electron beam
    - γ-ray source size is determined by e-beam spread in converter.
- Highly directed γ-ray beam.
  - Bremstrahlung cone angle Θ~1/γ

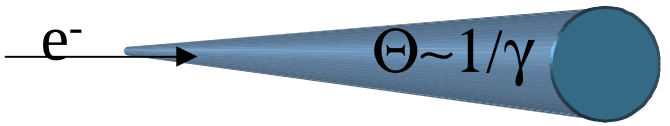

    - About 3° for γ=20 ⇒ high electron temperature required.
    - highly directional electron beam required to achieve min. cone angle.
- Pulse duration
  - Effectively set by the electron bunch length ~ laser pulse duration

High yield

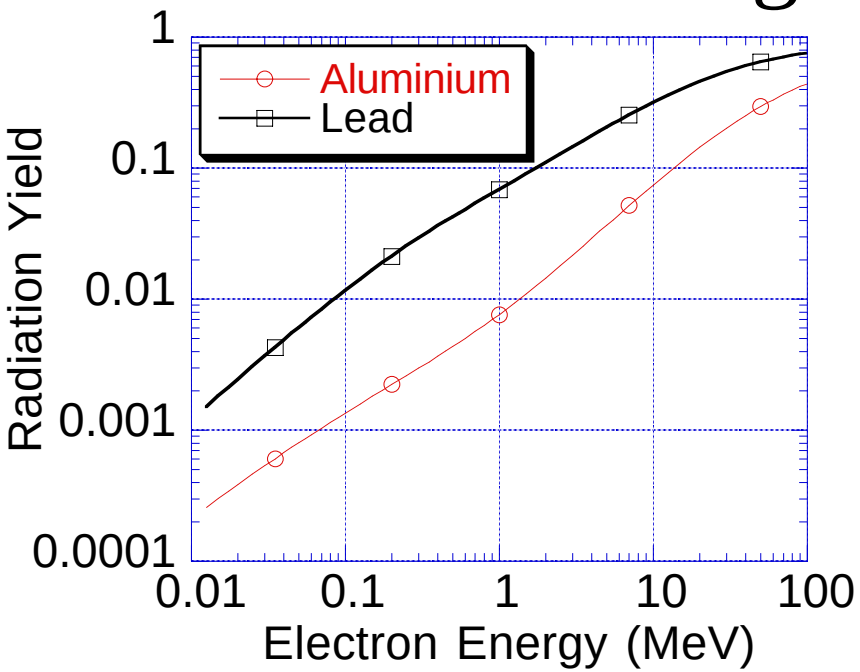

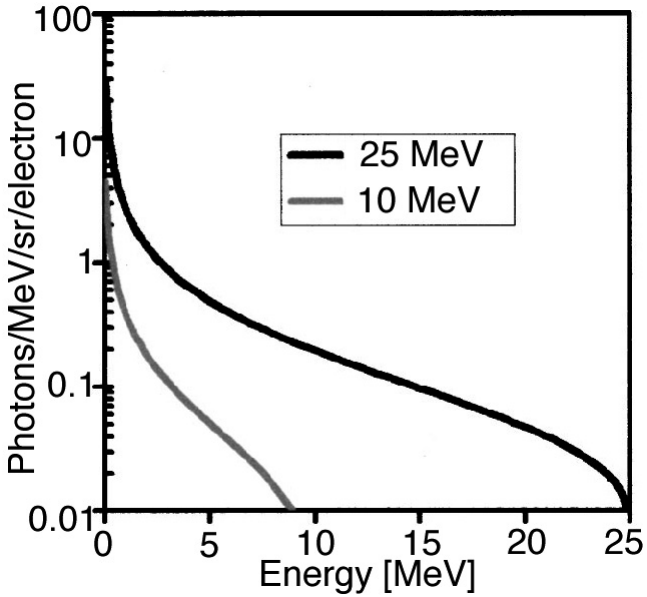

- High conversion efficiency to MeV electrons required.
  - >10% conversion into hot electrons
- High Z converters give maximum radiative yield
- High beam energy maximises radiative yield

Solid target geometry

- High coupling efficiency to hot electrons (~50%)
- Thick target acts as converter (1-3mm of Pb,Au,Ta…)
- Destruction of target-> repetition rate?
- Debris
- Collective, non-radiative stopping effects at high energies

Solid targets
Acceleration mechanisms

- vxB heating
- Vacuum/resonance absorbtion (for short scalelengths)
  - MeV electron temperatures can be achieved for $I>10^{19}Wcm^{-2}$,
- Electron temperature is ~ electron quiver energy
  - Quiver (ponderomotive) energy scaling:
    - $kT_{HOT}=(\gamma_{osc}-1)mc^2 =511[(1+I_{10\wedge 18}/1.37)^{1/2}-1]keV$
- For long scalelengths, electron acceleration in the underdense plasma contributes significantly

Solid targets
typical electron spectrum

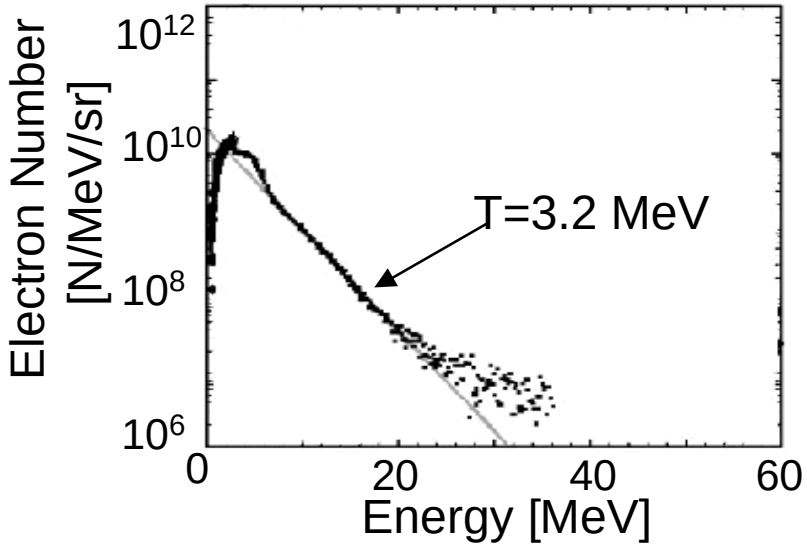

- Electron spectra obtained with a 100TW laser focused onto a plane Al target.

Solid targets
electron angular distribution

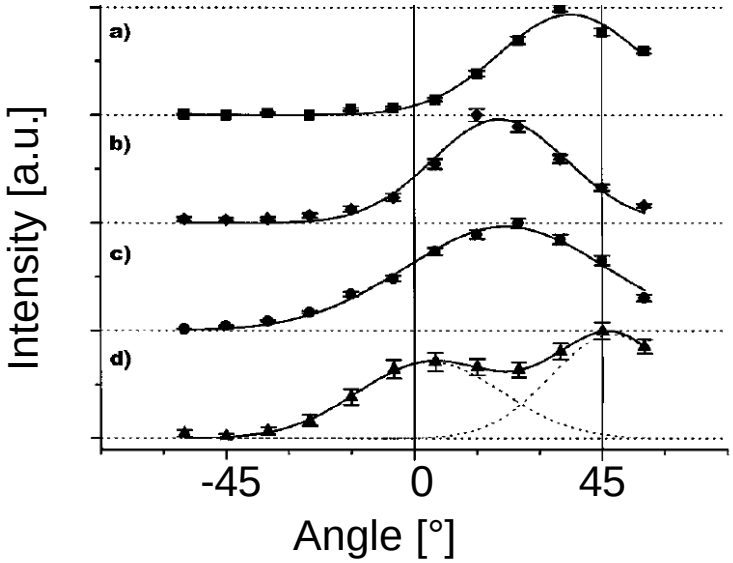

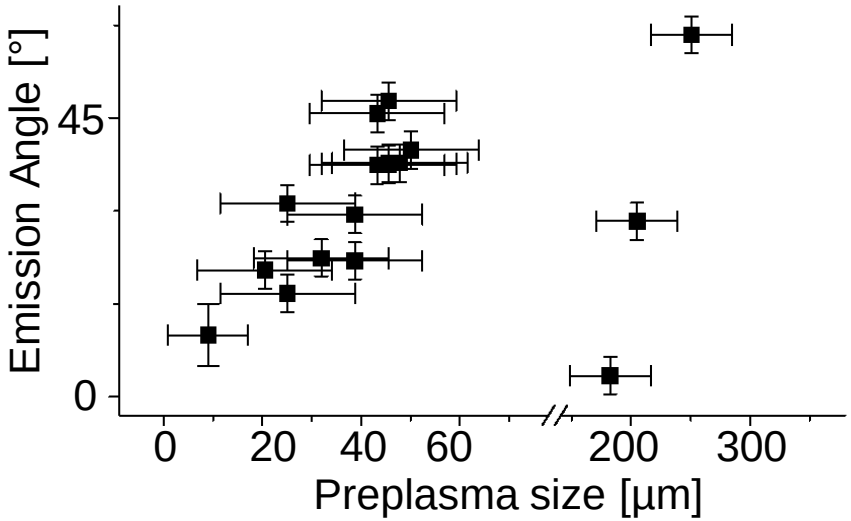

- Emission cone angle is fairly broad (>40°) for Eγ>10MeV
- Emission direction depends on preplasma length
  - Competition between e-beam from underdense plasma and critical surface
  - Direction becomes random for long scalelengths
  - Measurements taken at 45° incidence p-polarisation.

Gas jet geometry

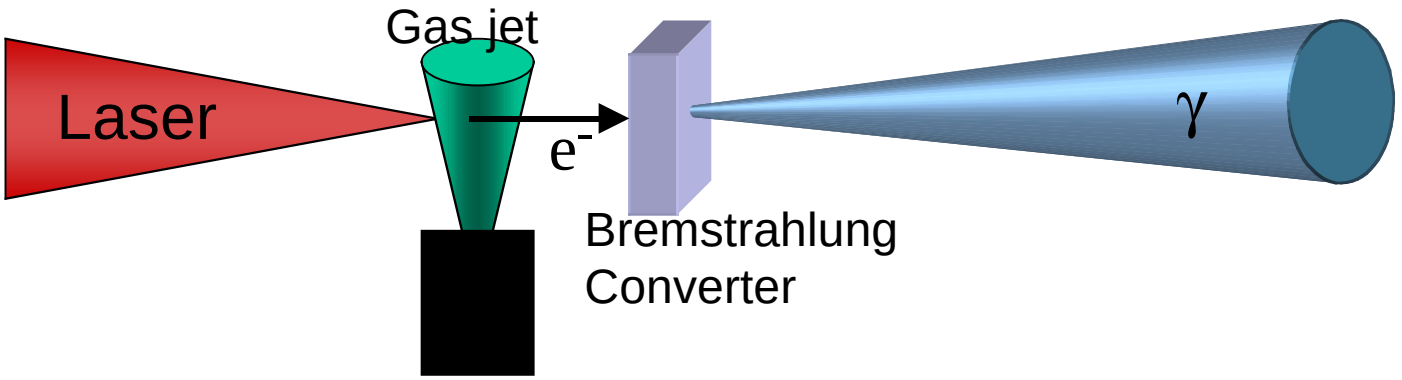

- Gas jets are suited to high repetition rates
- No issue with debris
- Higher electron temperature

- Lower conversion efficiency (1-10%)

Acceleration Mechanisms

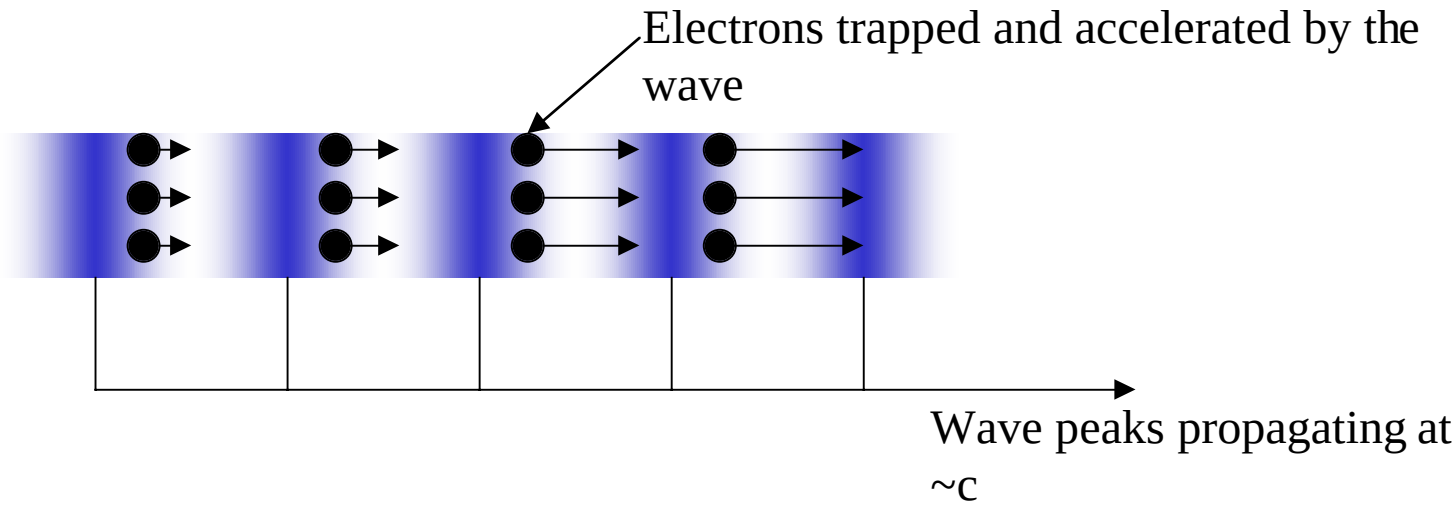

- Electron acceleration in gases rely on the generation of an electron plasma wave propagating at ~c
  - Electrons trapped by the wave will be accelerated to ~c
  - Typical approaches:
    - Laser wake field (LWF) (very short pulses)
    - Self modulated laser wakefield (ps pulses)
  - Other mechanisms also contribute (direct laser acceleration)

Typical electron spectra

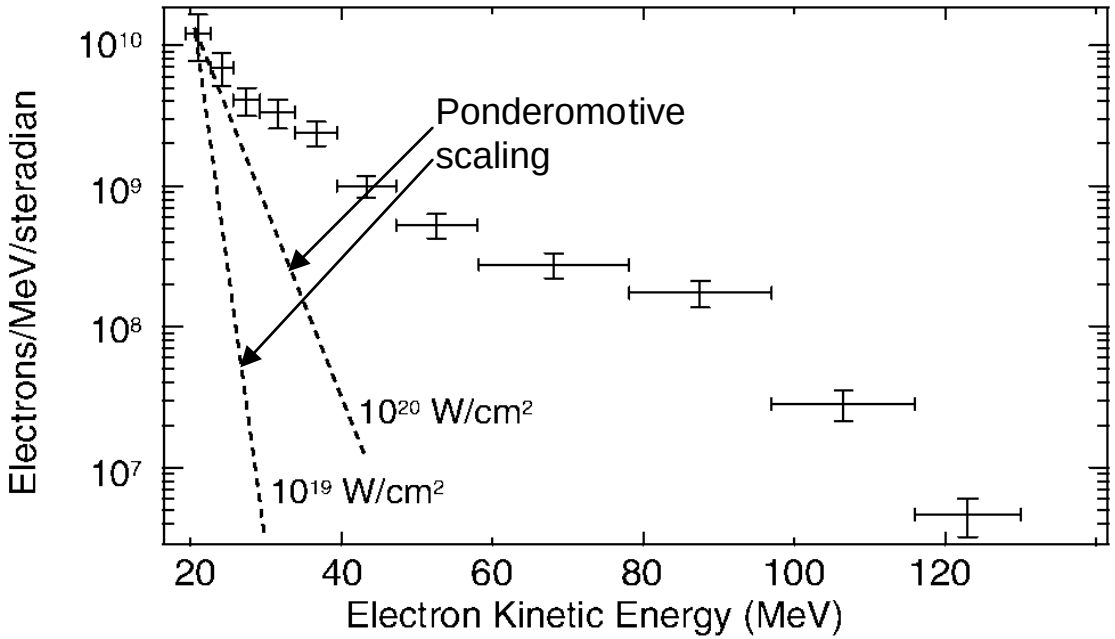

- Spectrum of from a self modulated LWFA experiment
  - Spectrum from 100TW laser focused into a gas jet. I~5 10^{19}Wcm^{-2}
  - Substantially higher temperature than ponderomotive in solid target case.
  - Conversion efficiency measured ~2%>10 MeV
    (PIC simulations suggest ~1%>10MeV and 10% total conversion

Gas Targets
Angular distribution

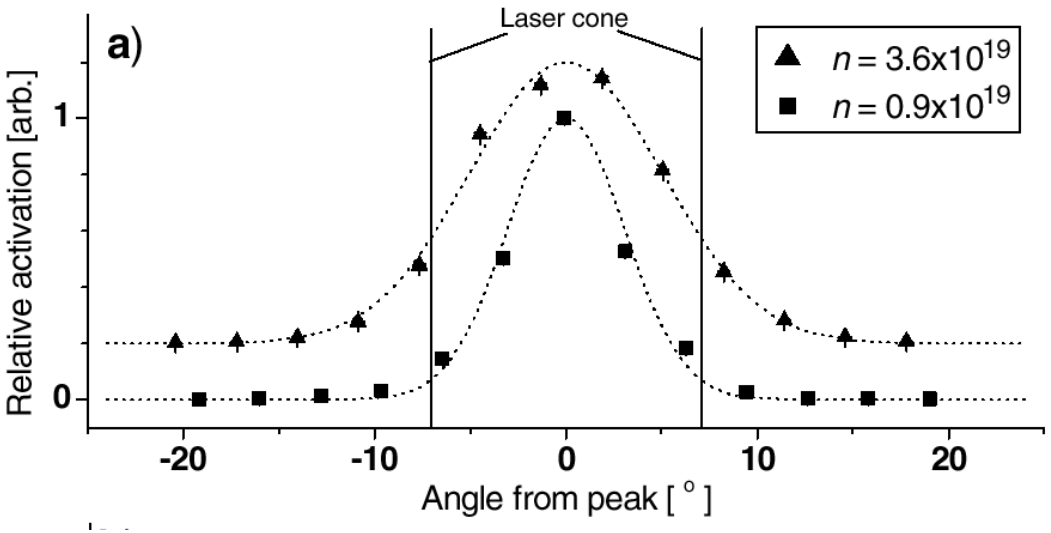

- Electron angular distribution measured via nuclear activation
  - Angular distribution depends on
    - Target density, laser parameters, electron energy
  - Less than 10° can be easily achieved
  - Less than 5° has been achieved for electrons >35MeV in the forced LWF regime (30fs, 1J pulses) [V.Malka et al, Science, 298,p1596 (2002)]

Direct source comparison - Setup

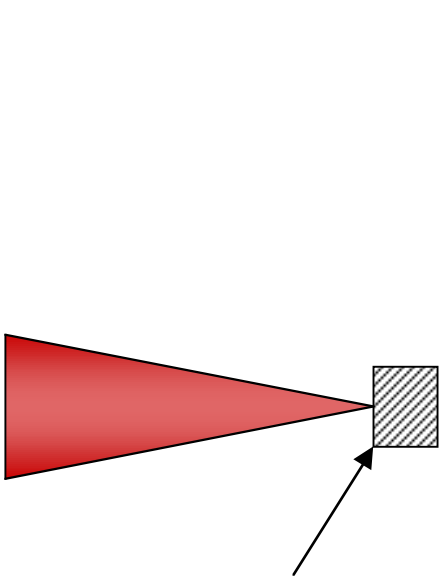

Solid (45°P-pol
or gas target

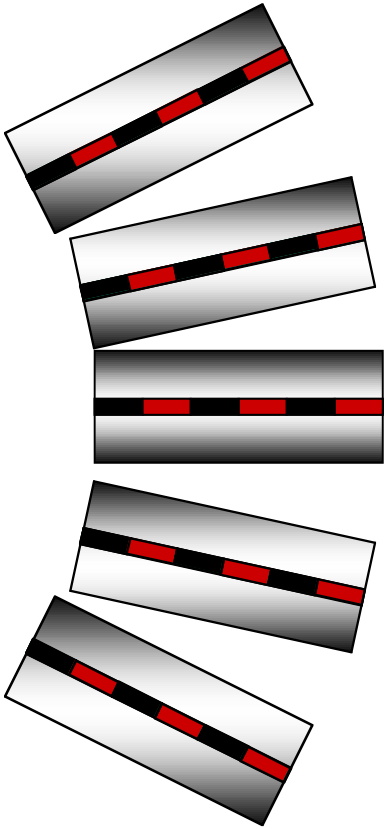

16 Tungsten collimators,
4 LiF detectors separated by
4mm Tungsten slugs

- LiF thermoluminescent dosimeters were used to measure the dose for both solid and gas target setups
  - Vulcan laser: 80 J, 800fs pulse, I_{max}~5 10^{19} Wcm^{-2}

Source comparison

45° p-pol onto 1.75 mm Ta target.

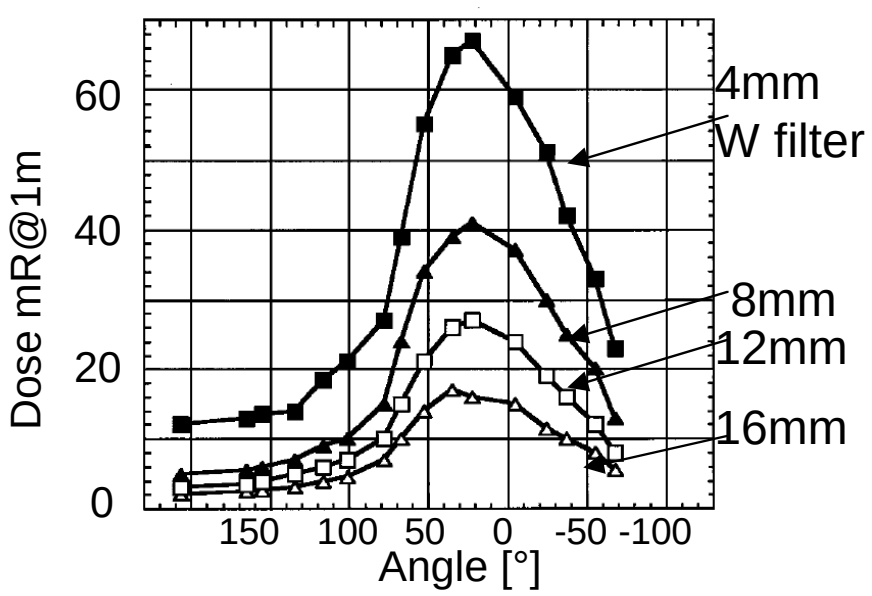

Gas target with 1.75 mm Ta converter behind jet

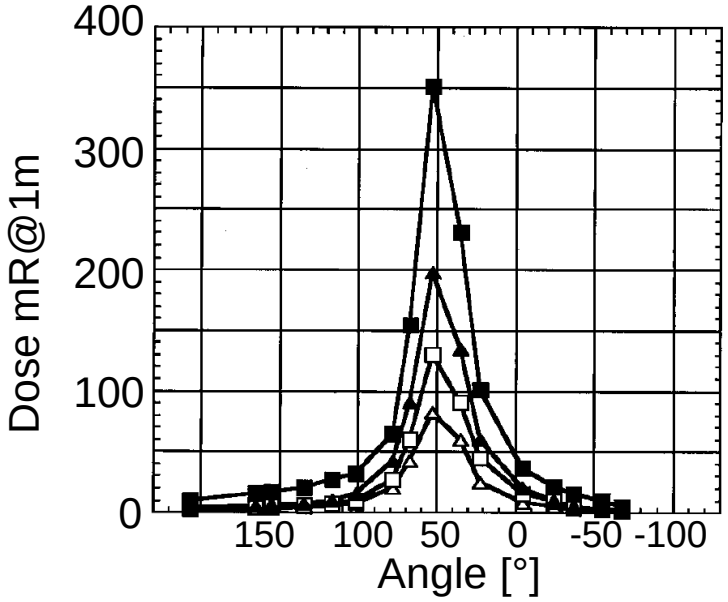

Gas targets deliver a substantially higher peak dose than the solid targets
Total integrated dose for both shots is estimated to be comparable.

Source comparison

- Solid targets
  - High conversion (50%)
  - Multi-MeV electrons
  - Gamma cone angle 10s of degrees
  - Debris issue
- Gas targets
  - Resonable conversion (few %)
  - Tens of MeV electrons
  - Gamma cone angle <10 degrees
  - No debris
  - Higher peak dose

→ Gas targets provide a more favourable source

Radiography of high areal densities

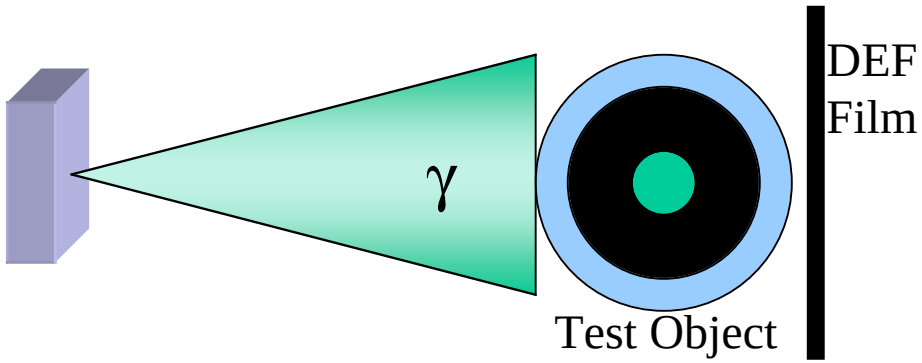

- Test application: Radiograph an object with a peak areal density of >120 g/cm^2
  - Can we obtain single shot images?
  - Can we obtain high resolution?
- Simples possible setup

Radiography of high areal densities

- Point projection radiography
  - Extremely large areal densities can be radiographed.
    - The low density lead ball is clearly resolved in the surrounding tungsten.
  - Single exposure (ps temporal res)
  - High resolution (0.3 mm, limited by geometry)
  - No scatter reduction was employed
    - Substantially better S/N with optimised setup.

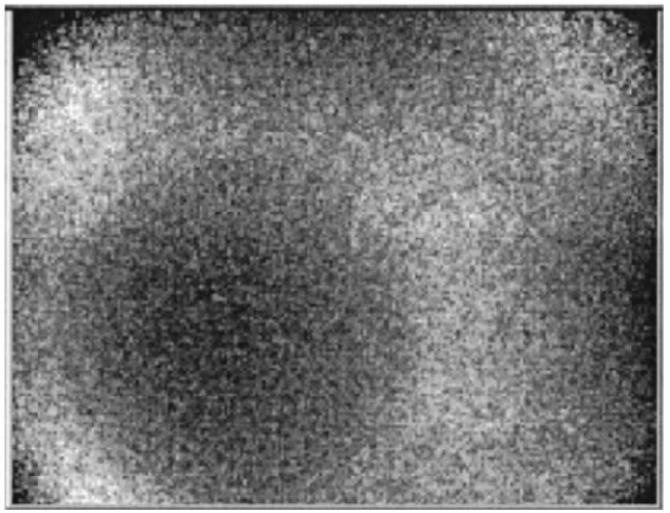

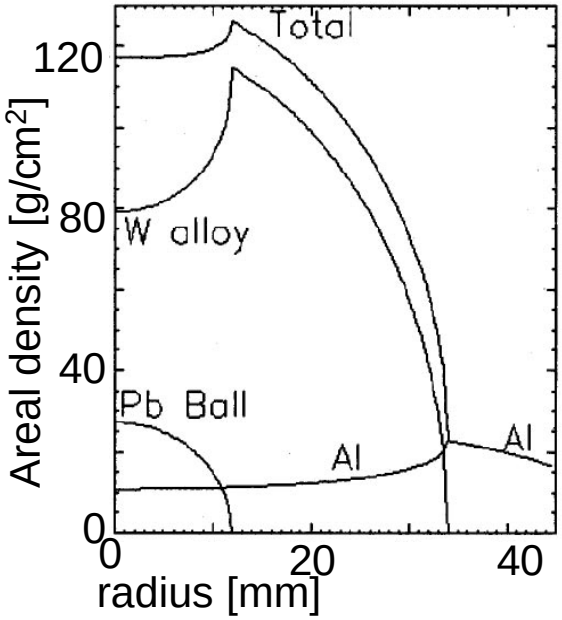

Comparison of pulsed γ ray radiography sources

	Conventional pulsed power source	Laser based source
• Pulse duration	20-30 ns	~1-10ps
• Source size	5mm	<0.1mm
• Single shot	Yes	Yes
• Flexible geometry	No	Yes

→ Lasers produced pulsed γ-ray provide an excellent radiography source.

Summary

- Laser produced gamma rays sources have highly desirable properties.
  - Short pulse
  - Single shot exposures possible
  - Small source size
- Large areal densities have been radiographed in a single shot
  - Ultrafast 3D imaging is possible
- Combination of gas target laser accelerators with bremstrahlung converters have the most attractive source properties.
- Current laser based sources provide better source parameters than pulse power sources.

POSTER PRESENTATIONS

Carbon single layers for total reflectance and their combination in Carbon / Carbon multilayers

R.Dietsch*, St.Braun**, Th.Holz*, D.Weißbach**, Th.Böttger**
* AXO DRESDEN GmbH, Siegfried-Rädel-Strasse 31, D-01809 Heidenau, Germany / www.axo-dresden.de
** Fraunhofer Institut Material and Beam Technology (IWS), Winterbergstrasse 28, D-01277 Dresden, Germany / www.iws.fhg.de

For the deposition of C- single and multilayers with low or high sp^3 / sp^2 bond ratios in the C- films i.e. low and high material densities, established PVD techniques like magnetron and ion beam sputtering, vacuum ARC deposition are mainly used. Because of the wide variability of film growth conditions, the high flexibility of the Pulsed Laser Deposition (PLD) process, the layer-by-layer process control and the UHV-clean deposition conditions PLD becomes more and more an interesting alternative for the deposition of C- single and C/C- multilayers. The high quality of pulsed laser deposited C- single and C/C- multilayers is demonstrated by investigations of the performance in the soft and hard X-ray regime, and of the thermal and long term stability.

C- single layers

hard X-ray regime

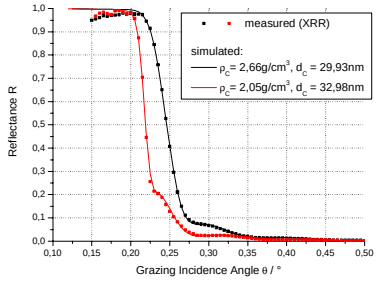

Measured reflectance at λ = 1.54 Å (Cu-Kα) of C- single layers prepared by LA-PLD. The simulations indicate material densities of about ρ_C = 2.66 g/cm³ and ρ_C = 2.05 g/cm³.

soft X-ray regime

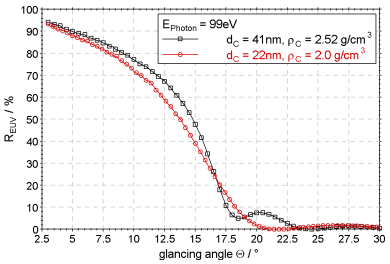

Measured reflectance in the soft X-ray range at E_p= 99 eV. For a C-layer with d=41nm and ρ_C= 2.52 g/cm³ experimental results of R= 94.0 % at Θ = 3° and 87.4 % at Θ = 6° are close to the theoretical values. The measurements were done with the new Fh-IWS soft X-ray-reflectometer (see also: Proc. SPIE Vol. 5038 (2003) pp. 12 - 21).

C/C- multilayers

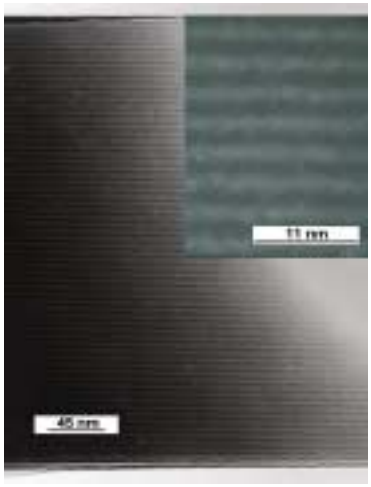

TEM cross section image (R.Scholz / MPI Halle) of a C / C- layer stack (PL 307) d= 3.78 nm; N= 100; Δρ= 0.2 g/cm³ (Overview and at higher magn.)

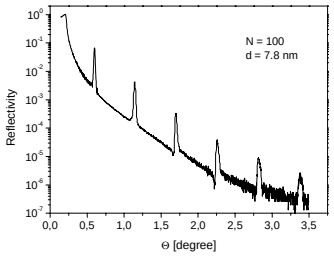

C/C-multilayers

X-ray reflectometry results R (Cu Kα) for a 100 period layer stack (PL 369)
d = 7.8 nm
R= 6.5%
ρ_1= 2.4 g/cm³
Δρ= 0.2 g/cm³
σ_R= 0.35 nm; Γ≈ 0.4

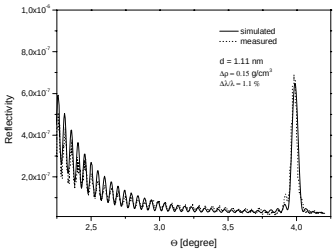

C/C-multilayers with low period thicknesses d

80 period C/C-multilayer
d= 1.11 nm
Δρ= 0.15 g/cm³
Δλ= 1.1%
σ_R= 0.44 nm; Γ≈ 0.5

Thermal and long term stability

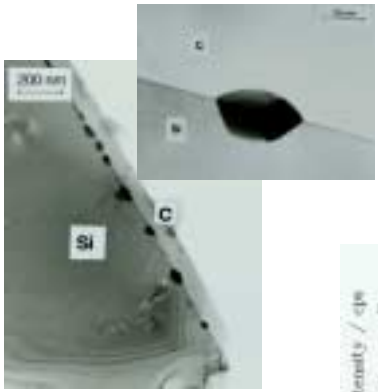

HREM micrograph of the remainder of a C/C-multilayer heated up to 800°C at lower and higher magnification (R.Scholz / MPI Halle)

Measured and simulated X-ray reflectance of a 30 period C/C –multilayer
d = 7.44nm
Γ~0.5
λ=0.154nm

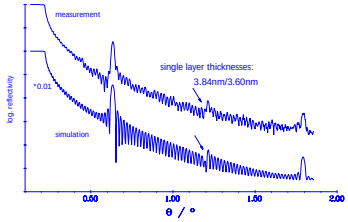

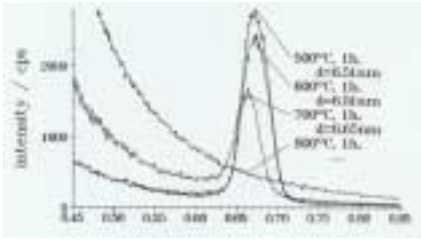

In-situ X-ray reflectometry during thermal treatment from 500°C...800°C (C/C-multilayer, d=6.51nm)

No remarkable modifications were observed in a C/C- multilayer for a period of 8 years.

Summary

An advanced large area PLD technology is used to deposit C-single layers and C/C-multilayers showing X-ray optical quality.
C-single layers of different material densities show high reflectance both in the hard and in the soft X-ray regime.
Thermal stability up to 600 °C was observed for a C/C- multilayer, at 800 °C a formation of SiC was found.
C-single und C/C-multilayers show interesting applications as high power X-ray optics and high resolution multilayers.

Influence of optical thickness and hot electrons on Rydberg spectra of Ne– and F–like copper ions

A. Faenov [1], A. I. Magunov [1], T. A. Pikuz [1], I. Yu. Skobelev [1], K. B. Fournier [2], V. S. Belyaev [3], V.I. Vinogradov [3], A. S Kyrilov [3], A. P. Matafonov [3], M. Francucci [4], S. Martellucci [4], G. Petrocelli[4], G. Ritucci [5], G. Tomassetti [5], A. Reale [5], L. Reale [5], F. Flora [6], S. Bollanti [6], P. Di Lazzaro[6], D. Murra[6], T. Auguste[7], S. Hulin[7], P. Monot[7], P. D'Oliveira[7]

[1]Multicharged Ions Spectra Data Center of VNIIFTRI, Mendelevo, Moscow region, 141570, Russia
[2]Lawrence Livermore National Laboratory, P.O. Box 808, L-41, Livermore, California 94550, USA
[3]Central Research Institute of Machine Building, Korolev, Moscow region, 141570, Russia
[4] INFM–Dipartimento di Scienze e Tecnologie Fisiche ed Energetiche, Università di Roma Tor Vergata, 00133 Roma, Italy
[5]Dipartimento di Fisica e INFM, INFN g.c. LNGS, Università dell'Aquila, 67010 L'Aquila, Italy
[6]ENEA, Dipartimento Innovazione, Settore Fisica Applicata, 00044 Frascati (Roma), Italy
[7]CEA, Centre D'Etudes de Saclay, DRECAM, SPAM, 91191 Gif–Sur–Evette, France

Abstract

High–n transitions in the spectra of Ne–like and F–like ions of Cu observed in a variety of laser–produced plasmas (LPPs). The spectra are recorded with a high spectral resolution λ/Δλ=3000–8000 using four different laser sources: a 15ns–pulse length Nd:Yag/Glass, a 1 ps–pulse length Nd:glass, a 60fs pulse length Ti:Sa and a 12ns pulse length XeCl lasers. These spectral observations are used to classify the transitions in the 2p–nd and 2s–np (n up to 14) Rydberg series of the Ne–like copper. The plasma X–ray emission is simulated with a steady – state collisional – radiative model that includes the effect of self – absorption on the line intensities, and the effect of hot electron populations on the ionization balance. These spectra provide a comprehensive set of data that can test the accuracy of atomic structure calculations, and to demonstrate the importance of opacity and hot electron effects on high–n transitions, especially in pico – and femtosecond laser produced plasmas.

Experimental description

Four laser installations have been used for measurements of X–ray spectra from copper plasmas.

The first set of experiments (so called type I) was carried out in the Tor Vergata University of Rome (Italy) where plasmas was produced using the fundamental output wavelength of a Nd:Yag/Glass laser, 1064nm, in a vacuum chamber, which has a pressure of 10^{-2}mbar.
The laser source was a Quantel Nd:Yag/Glass laser delivering pulses with a maximum energy of 20J and a temporal duration of 12 – 15ns. A 20cm focal length doublet lens focused the laser beam on the target at a 45° angle of incidence. The estimated beam diameter at the focal point was 300 µm. In our experiments the laser energy was varied between 1 – 8J and the resulting intensity on target for type I experiments is 10^{11} – 10^{12}W/cm^2.

The second set of experiments (type II) was carried out on the "Neodym" laser facility at the Central Research Institute of Machine Building near Moscow. The laser energy was up to 1.0J and the pulse duration in these experiments was kept to 1ps. The fundamental wavelength of the Nd:glass laser was used. The laser pulses were focused into a spot focal with diameter within the range of 10 to 900 µm, yielding the intensity within the range from 10^{14} to 10^{17}W/cm^2.

In such a setup there are two types of prepulses before the main pulse. The first prepulse arises from amplified spontaneous emission (ASE) in the regenerative amplifier. This prepulse occurs for about 8ns before the main pulse and has around 0.3mJ of energy, such that the intensity contrast, I_{main}/I_{pp} (the peak intensity to prepulse intensity ratio) is about 1.3×10^{7}. In the experiment the intensity of this prepulse has not been varied. The second prepulse arises from the many pass regime of amplification in the regenerative amplifier and the finite transmission of Pockel cells. This prepulse occurs about 13ns before the main pulse and had duration of 1ps.

In the type II experiments the intensity of this prepulse has been changed :
"low contrast" = the intensity contrast is about 7 x 10^4;
"high contrast" = the intensity contrast is about 3.8 x 10^7.

The third set of experiments (type III) was performed with the Saclay (France) 10TW Ti:Sapphire laser (UHI10), which was designed to generate 60fs pulses at a 10Hz repetition rate. The total energy in the pulse laser is about 800mJ. The 80mm diameter laser beam was focused with an *f*/2.35 off – axis parabolic mirror onto copper targets, which were placed at a 22.5° angle from the direction of the incident laser beam. The focal spot diameter in vacuum was about 30 μm, giving a laser intensity on the target in the 10^{18}W/cm^2 range.

The fourth set of experiments (type IV) was carried out at the ENEA "Hercules" laser facility in Frascati, Italy. This is a XeCl excimer laser with an active volume of 9 x 4 x 100cm^3 and an operating wavelength of 0.308 μm. The laser energy was 0.5 – 1J, the pulse duration was 12ns and the repetition rate was 0.5Hz. The laser radiation was focused onto solid targets by a lens. The spot diameter was 50 – 70 μm, giving a laser intensity on the target was about 10^{12}W/cm^2.

In the type I, II and IV experiments a stepped target was used; one part of the target contained copper, while the second part contained NaF, Mg or Al, which produced spectral lines used for reference wavelengths.
The height of the steps was 300 – 800 μm. Between laser shots, the target was moved in the plane perpendicular to the laser beam to obtain spectra of the material investigated and reference materials on the same spectrograph film.
The target step served to physically separate the two spectral images on the film..

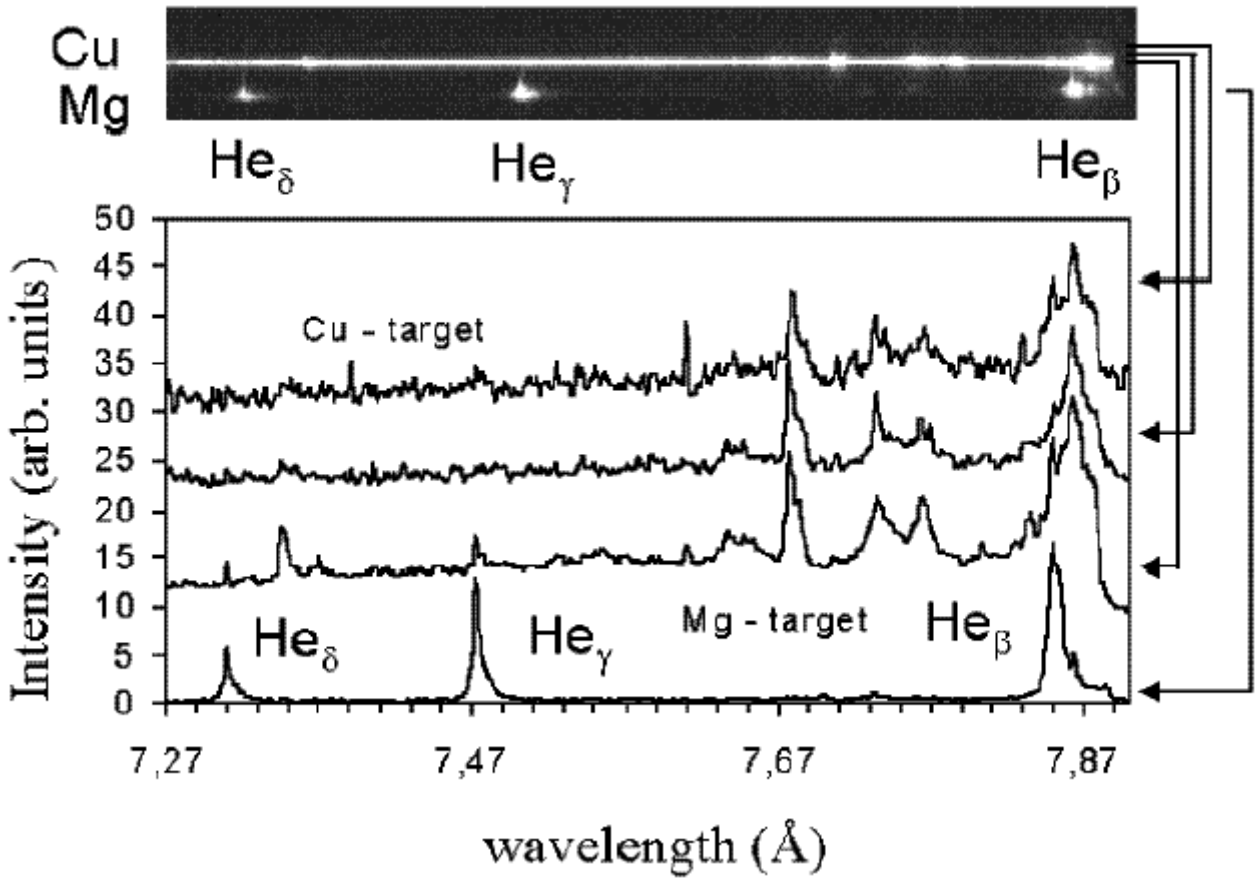

Space resolved images in the direction of plasma expansion of Mg K– shell and Cu L– shell X–ray line emission obtained at the XeCl laser installation (type IV). The step between Mg and Cu targets was 600 mm. Trace of $He_{â,ã,ä}$ lines of Mg are used as reference lines.

Experimental results

In Fig. 1 two picosecond (I = 10 ^{16}W/cm^2) LPP spectra produced with high (middle) and low (bottom) ratios of the main pulse to the prepulse peak intensities are shown. Also shown is a high intensity (I = 10 ^{12}W/cm^2) spectrum for the type I experiments. The 2p – nd and 2s – np Ne– like transitions are indicated with the standard notation.

In Fig. 2 is shown a comparison between two LPP spectra from the type II experiments in which the focusing lens has been moved from the best focus (middle) to a 1mm displacement (bottom). This results in a lower plasma temperature in the bottom trace, as is demonstrated by the diminished F– like Cu^{20+} ion features. The same reduction in signal from lines of the ions more highly charged than Ne– like Cu $^{19+}$ is also observed in the Type I spectrum.

Fig. 3 reports on data taken in the type I, II and III experiments for laser intensities of 7x10 ^{10}W/cm^2, 10 ^{16}W/cm^2 and 10 ^{18}W/cm^2, respectively. In the case of the 1ps experiment, the contrast between the main pulse and the prepulse was about 10 ^{7}. Enhancement of F– like Cu $^{20+}$ ion features in the type II and III spectra can be assumed as evidence of hot electron populations.

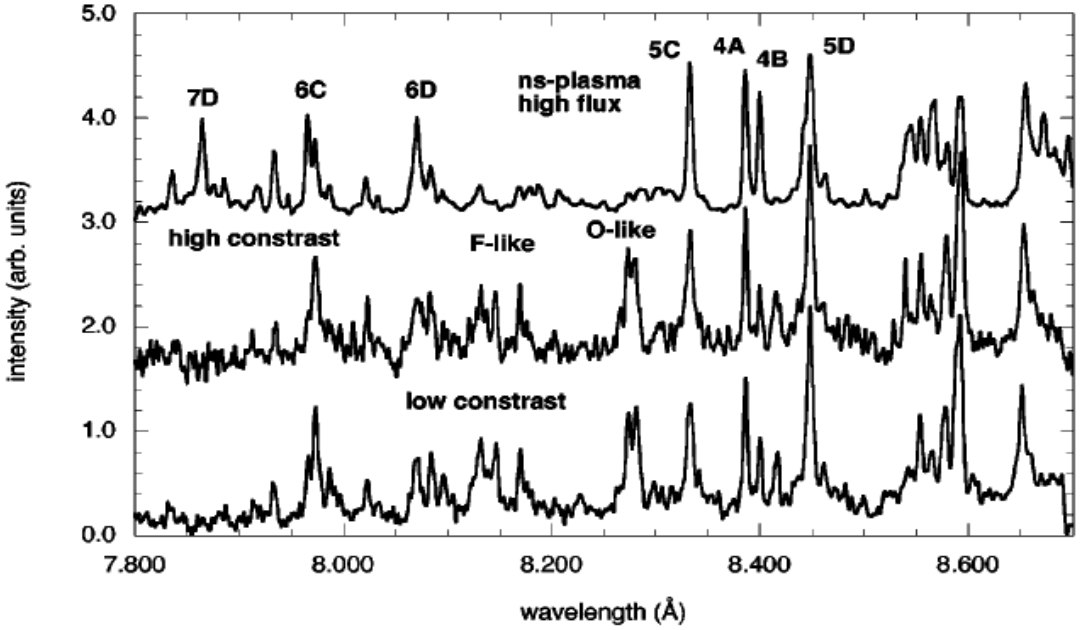

Fig. 1 Two ps – pulse LPP (laser produced plasma) spectra recorded with high and low contrast between the main laser pulse and the prepulse. Both spectra are for the laser at best focus. Also shown is a high intensity 15ns pulse LPP spectrum.

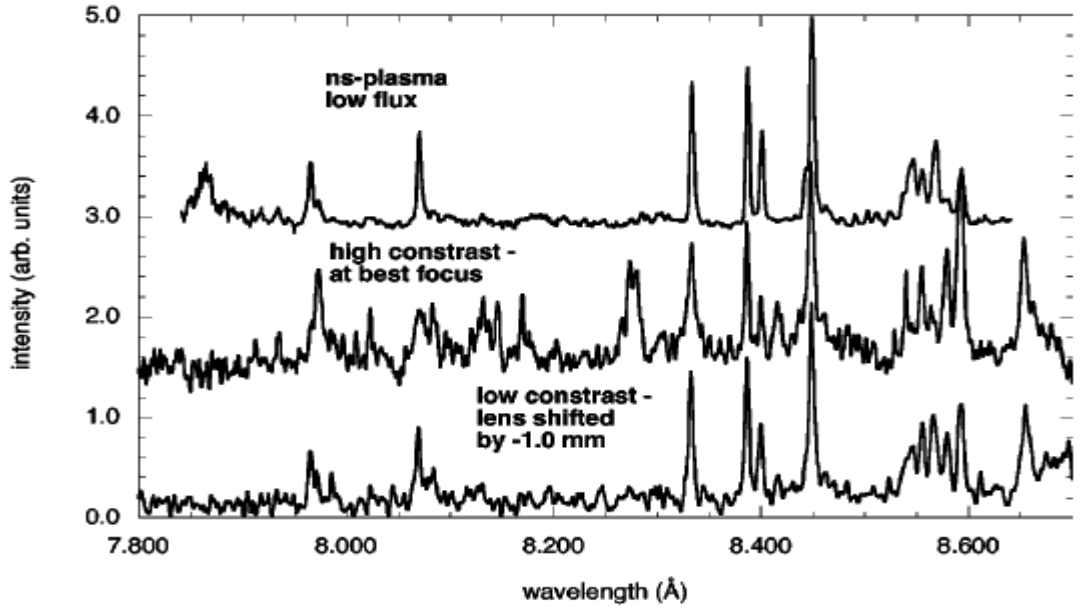

Fig. 2 Two ps – pulse LPP spectra, both with high contrast between the main pulse and the prepulse, and with the laser at the best focus and with the lens moved 1mm from best focus. Also shown is a low intensity 15ns pulse LPP spectrum.

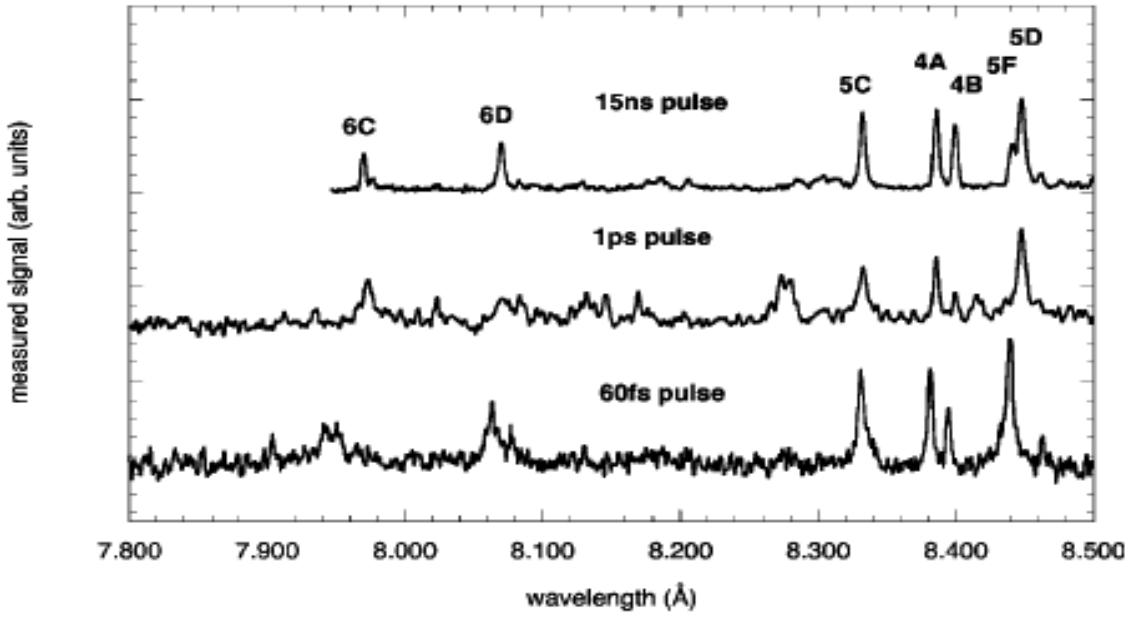

Fig. 3 Data taken in the type I, II and III experiments for laser intensities of 7 x 10^{10}, 10^{16} and 10^{18} W/cm^2. Enhancement of F–like Cu^{20+} ion features in the type II and III spectra is evidence of hot electron populations.

Simulation results

The steady Collisional Radiative (CR) model has been used to simulate the observed line intensities of high – n Rydberg lines in near – neon like ions (Mg– like to O– like). Effects of the hot electrons on the collisional excitation and ionization rates have been taken in to account in the description of the ion kinetics. Also opacity effects on the strength of the different transition lines have been considered.
The observed line intensities have been compared with theoretical spectra calculated using atomic data from HULLAC package. Energy levels, radiative transition rates and autoionization rates have been calculated using the RELAC atomic structure code.

Figure 4 shows T_e dependence in the CR spectra for highly charged copper ions. The average copper ion charge increases as T_e goes from 200eV to 500eV from **18.76** to **20.70**, thus going from a fraction of an electron in the M–shell to an average charge state that is dominated by O – like Cu^{21+}. This is reflected in Fig. 4 as the F– and O– like lines become more prominent with increasing temperature. By T_e = 400eV, the characteristic Ne– like lines are less prominent than features composed of multiple strong F– and O– like transitions.

Figure 5 shows the electron density dependence in the CR spectra for highly charged copper ions. As the electron density goes from $10^{20}cm^{-3}$ to $5x10^{21}cm^{-3}$, the average ion charge increases from **18.81** to **19.27** for fixed T_e= 250eV. As the density increases above $5x10^{21}cm^{-3}$, the model predicts that recombination is strongly enhanced and the average ion charge actually drops again, reaching **18.84** when $N_e = 5 \times 10^{22}cm^{-3}$. Above $N_e=5x10^{21}cm^{-3}$, the populations in the levels of the Ne– and F– like ions are near to local thermodynamic equilibrium with the levels of the ground configuration of the F– and O– like ions, respectively.

For high – density plasmas, it is essential to account for self – absorption radiation in order to calculate accurately the ratios of diagnostic lines. Fig. 6 shows the calculated dependence of the intensity lines on the optical depth, expressed in terms of the escape factors, by varying the assumed plasma diameter L. It appears from the reported calculations that an increase of the plasma diameter L and, by consequence, of the escape factor determines a reduction of the strength of the 5D line relative to the 4A, 4B and 5C lines, and a reduction of the strength of 6D relative to 6C.

The dependence of the synthetic spectrum (including Cu^{21+} to Cu^{17+}) on hot electron fraction for the optically thin case is shown in Fig. 7 and in Fig. 8 The simulation parameters assumed (T_{bulk} = 200eV, $N_e = 10^{21} – 10^{22} cm^{-3}$, T_{hot} = 5keV) are typical of the Nd:glass and Ti:Sapphire experiments. The results show a dramatic enhancement of the F– like emission relative to the Ne– like emission features as the hot electron fraction goes from **0** to **$5.0x10^{-5}$** of the bulk population.

Looking at the case of $N_e = 1.0 \times 10^{21} cm^{-3}$ (Fig. 7), the average charge of the ion distribution is shifted only slightly by the inclusion of small fractions (***f_{hot}* = 10^{-5}**) of hot electrons, i.e., **$\langle Z \rangle$ = 18.76, 18.77,** and **18.84** for ***f_{hot}* = 0, 10^{-6},** and **10^{-5}**, respectively. For ***f_{hot}*>10^{-5}** the **<Z>** increase is larger.

In Fig. 8 one observes that by increasing the density by an order of magnitude ($N_e = 10^{22} cm^{-3}$), the effect of the hot electrons is somewhat mitigated. This is seen particularly in the relative strengths of the **6D** and **á** transitions, and the **6C** and **ç** transitions. The increase in electron density raises the fraction of the O– like ions present by a factor of 2 for all values of f_{hot}, but the O– like lines are still too weak for T_{bulk} = 200eV and f_{hot} =$5x10^{-5}$ to be seen.

Figs. 9 and 10 show the same comparison as in Figs. 7 and 8, now with escape factors included in the calculation, in this case a plasma diameter of 30 has been assumed. This size is still large enough to cause appreciable self absorption of some of the Ne– like lines. According to these calculations, opacity effects perturb the **nC** and **nD** series in the Ne– like ion differently than the **nA**, **B**, **F** and **nG** series.

Fig. 11 compares data from a type II LPP with simulations that include both hot electrons and escape factors. For this case, the data are from high intensity ($I=10^{16}W/cm^2$), low contrast ($I_{main}/I_{pp} = 10^5$) shots. The simulations shown are for an optically thin plasma with $T_e = 400eV$ and $N_e = 10^{21}cm^{-3}$ (middle) and for a plasma with $T_e = 350eV$, $N_e = 10^{21}cm^{-3}$, $n_H = 50$ (escape factors included) and $f_{hot} = 10^{-5}$ (bottom). The two simulations give comparable reproductions of the data; the higher temperature, optically thin matches the strength of the F– like and the O– like lines better.

Fig. 12 shows data from a type II LPP shot with high contrast between the prepulse and the main pulse. The focusing lens has been shifted slightly from the position of best focus, so the intensity ($I = 3.3 \times 10^{15}W/cm^2$) and consequently the plasma bulk electron temperature is slightly lower than in Fig. 11. The data in this figure extend to shorter wavelengths than in Fig. 11, and very high – **n** members of the **nC** and **nD** series in Ne– like Cu^{19+} can be seen. The relative intensities of the F– and O– like lines to each other, and to the relatively weak Ne– like lines, do not demonstrate sensitivity to hot electron populations. The strength of the F– and O– like lines in this spectrum is strongly dependent on the inclusion of escape factors in the simulation.

Both the spectra in Figs. 11 and 12 do not give unambiguous evidence of hot electron populations. From the simulations only an upper limit of $1x10^{-5}$ on the hot electron fraction can be deduced.

Fig. 13 shows data from a type III plasma produced by a 60fs Ti:Sapphire laser pulse ($E_{pulse} = 800mJ$, $I = 10^{18}W/cm^2$). The synthetic spectra for the Ne–, F– and O– like lines from the CR model at $T_e = 200eV$, $N_e = 10^{22}cm^{-3}$ including a population of 5keV electrons ($f_{hot} = 5 \times 10^{-5}$) are also shown in Fig. 13. The relative intensities of the **5D**, **5C**, **4A** and **4B** transitions show good agreement with the observed lines. The relative strengths of these lines are unaffected by the presence of the hot electrons. The strength of the F– like features **á**, **ç** and **è** are in good agreement with each other and with the Ne– like features in the simulation. The good reproduction of the experimental results can only been obtained introducing an suprathermal electron fraction of $5x10^{-5}cm^{-3}$.

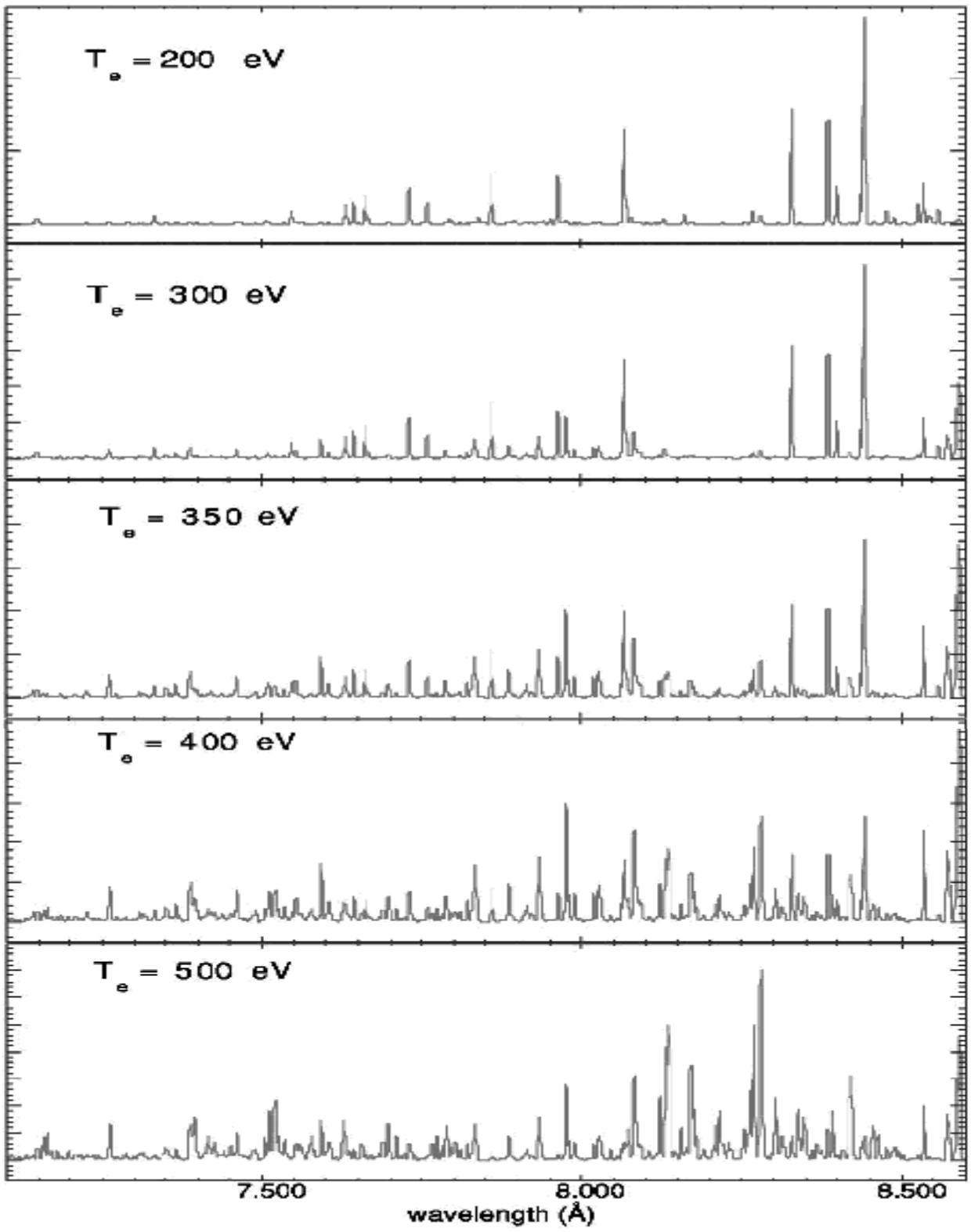

Fig. 4 Optically thin CR (collisional – radiative) spectra for Mg–, Na–, Ne–, F– and O– like Cu ions computed for $N_e = 10^{21} cm^{-3}$ and different electron temperatures. Each line feature has been given a Gaussian profile with a 3.0mÅ FWHM.

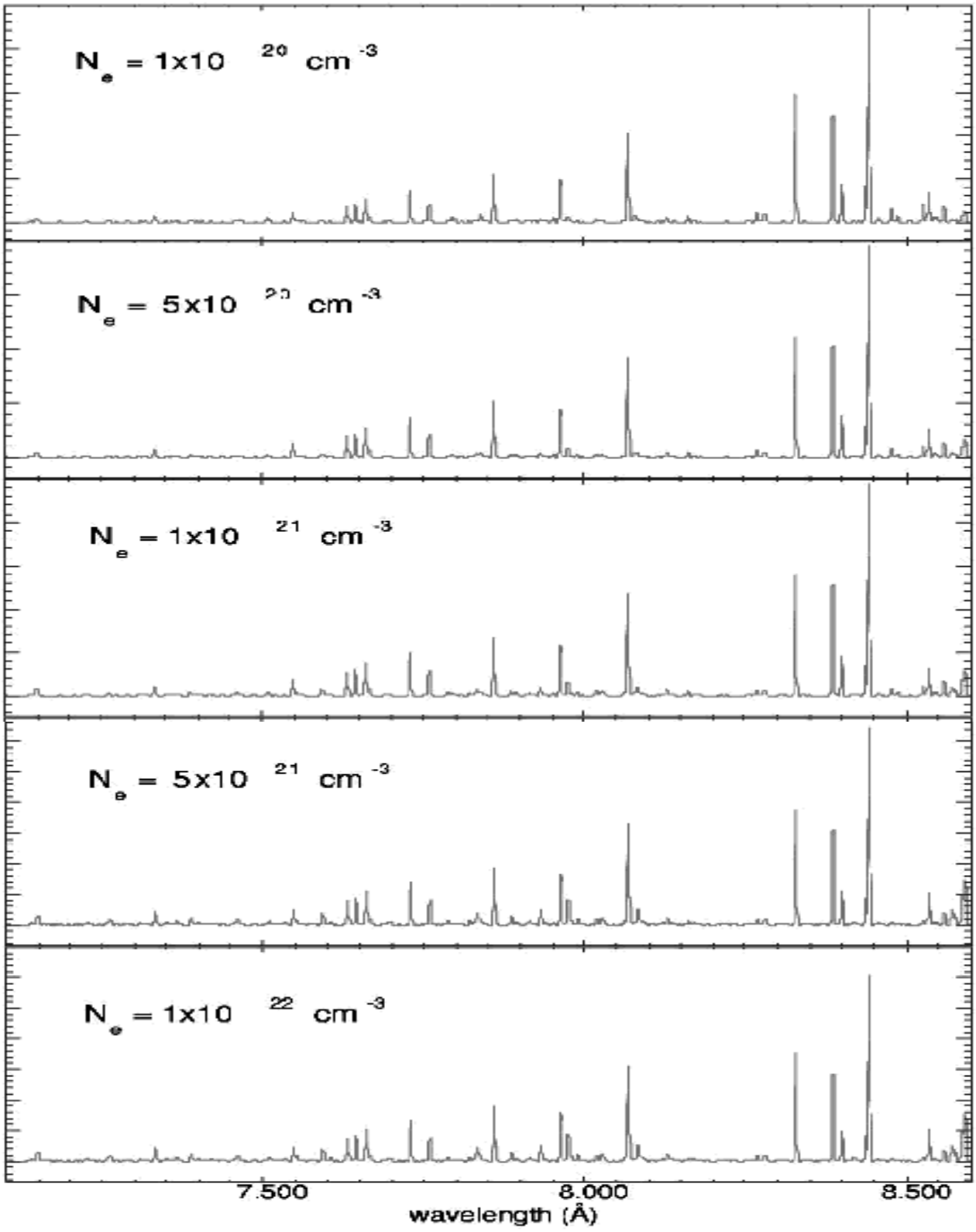

Fig. 5 Optically thin CR (collisional – radiative) spectra for Mg–, Na–, Ne–, F– and O– like Cu ions computed for T_e = 250eV and different electron densities. Each line feature has been given a Gaussian profile with a 3.0mÅ FWHM.

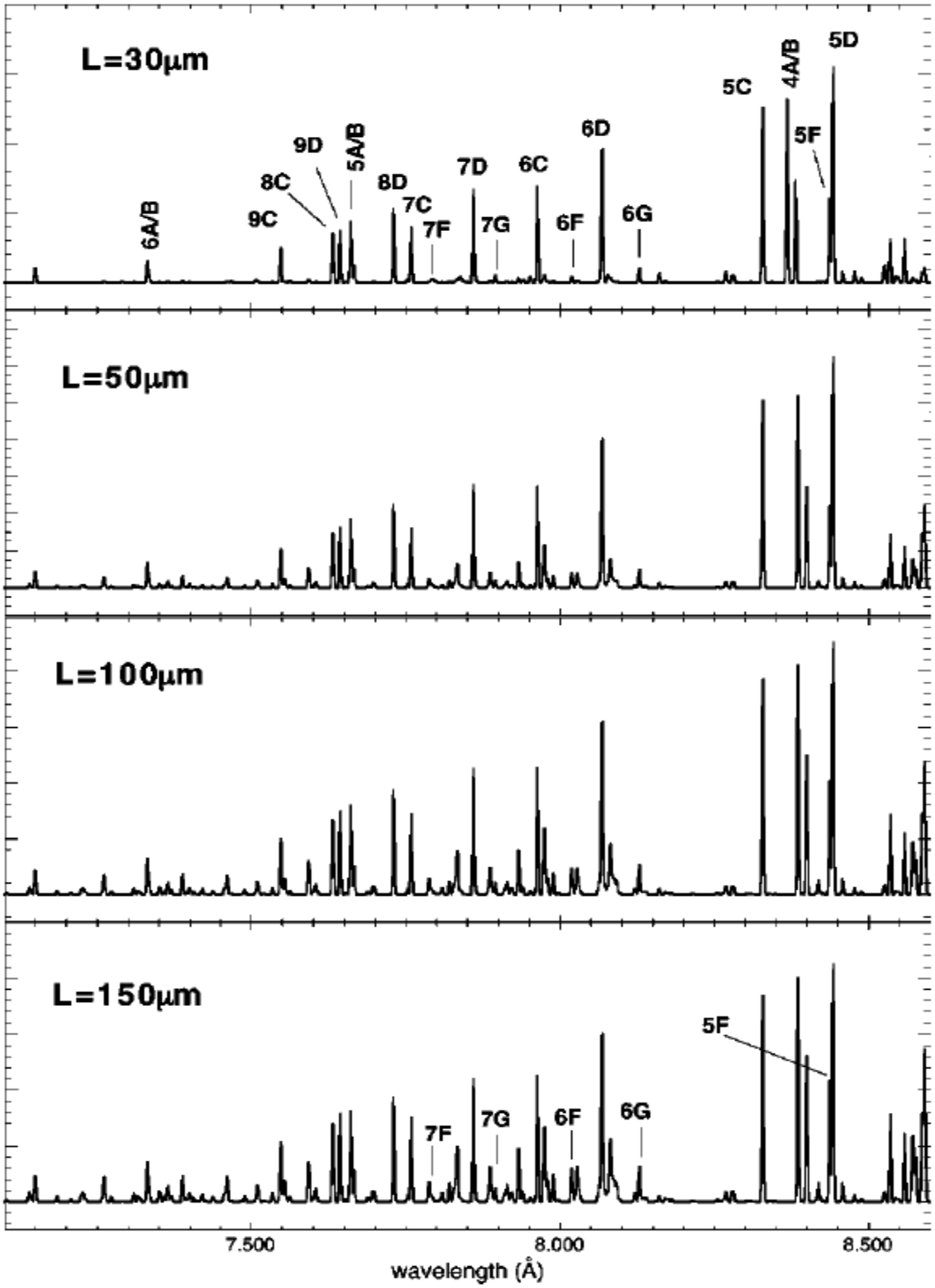

Fig. 6 CR spectra with escape fact ors for Mg–, Na–, Ne–, F– and O–like Cu ions computed for $T_e = 250$eV, $N_e = 10^{21}$cm^{-3} and different plasma diameters. The Ne–like Cu $^{19+}$ lines have been labeled in the upper panel, all line features have been given a Gaussian profile with a 3.0mÅ FWHM.

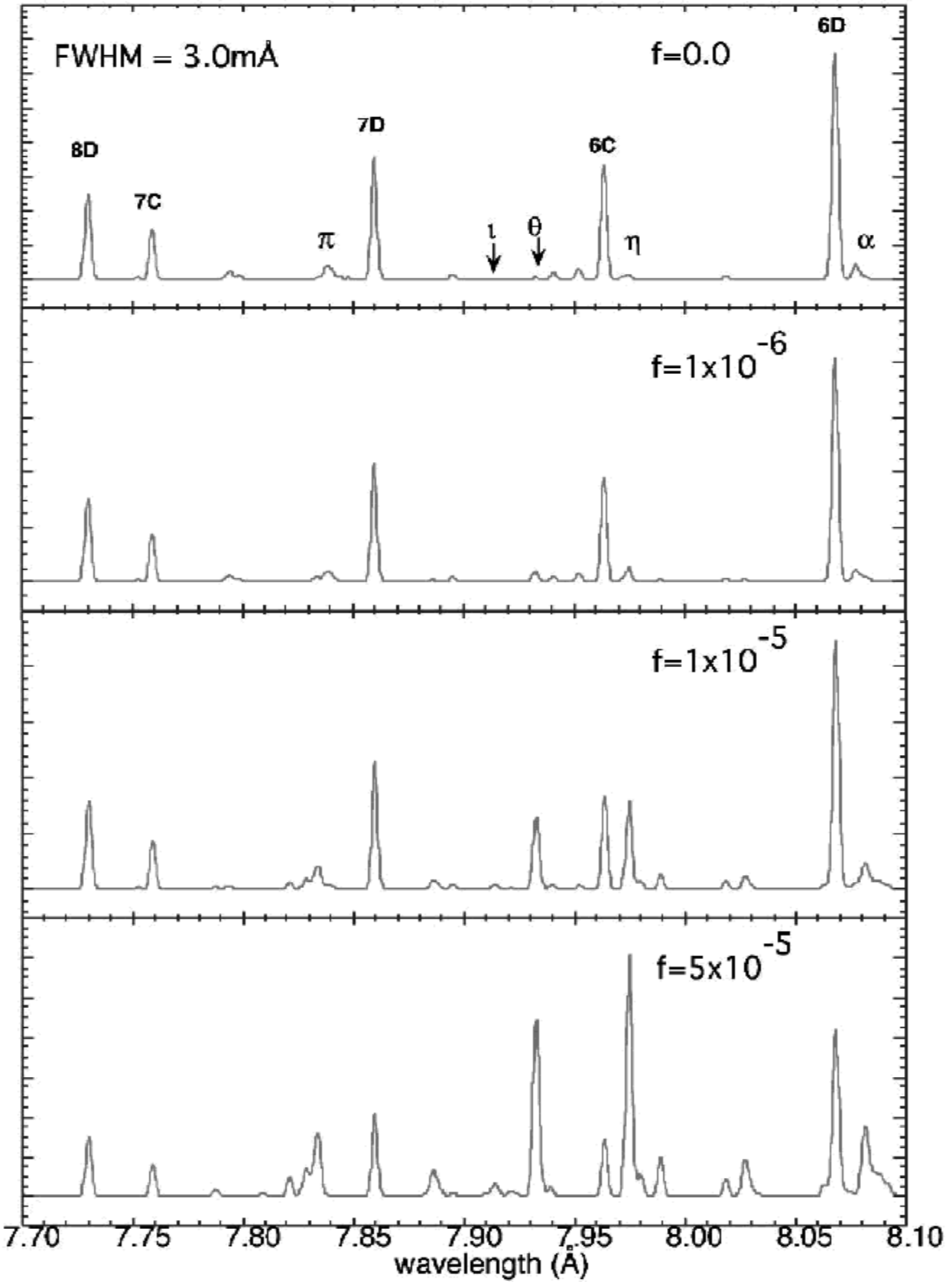

Fig. 7 CR models for O–like to Mg–like copper ions with T_{bulk}=200eV, N_e = 1.0 x 10 ^{21}cm^{-3} and increasing hot electron (T_{hot} = 5keV) fraction (from top to bottom), as labeled in the figure.

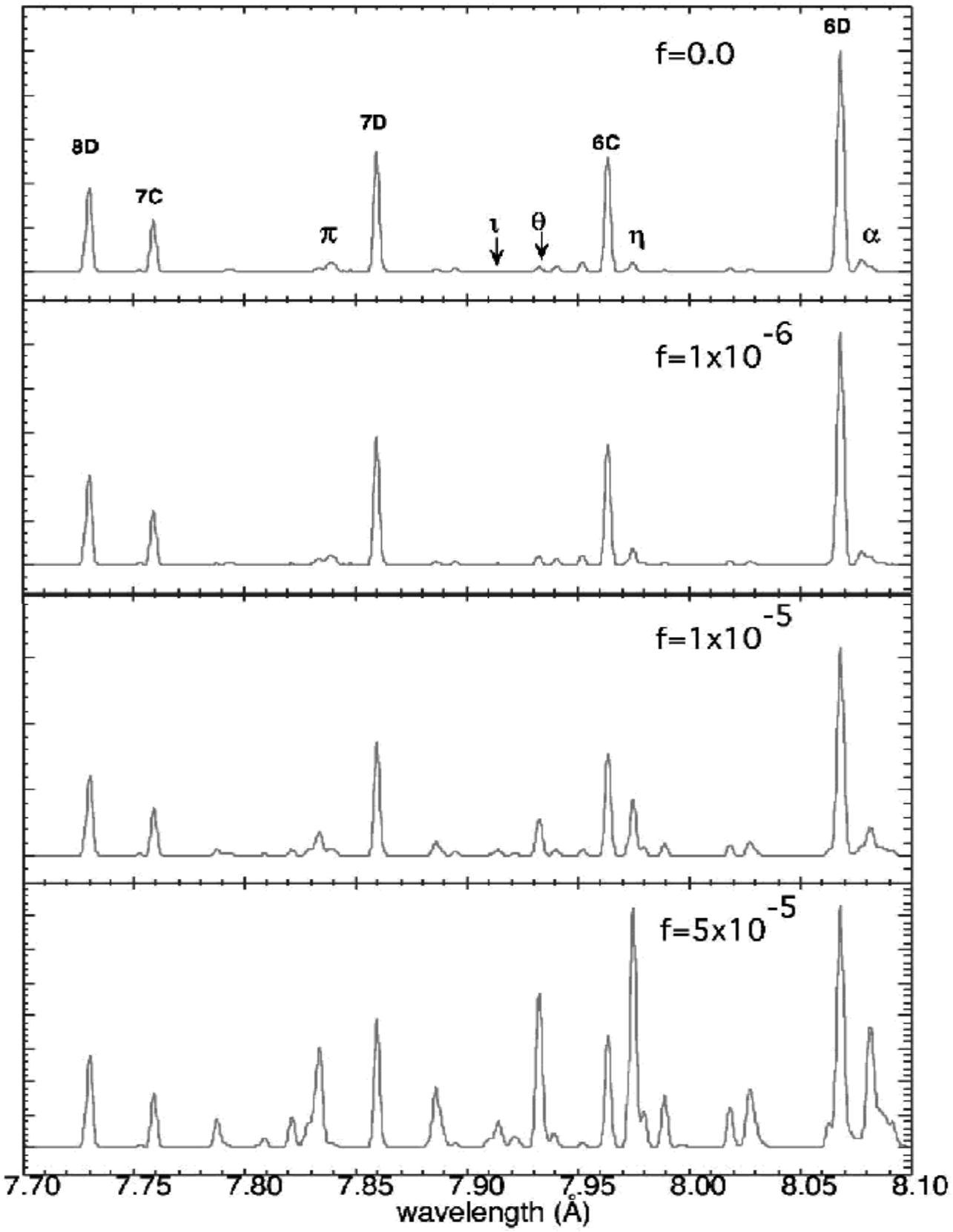

Fig. 8 CR models for O–like to Mg–like copper ions with T_{bulk}=200eV, N_e = 1.0 x 10 ^{22}cm^{-3} and increasing hot electron (T_{hot} = 5keV) fraction (from top to bottom), as labeled in the figure.

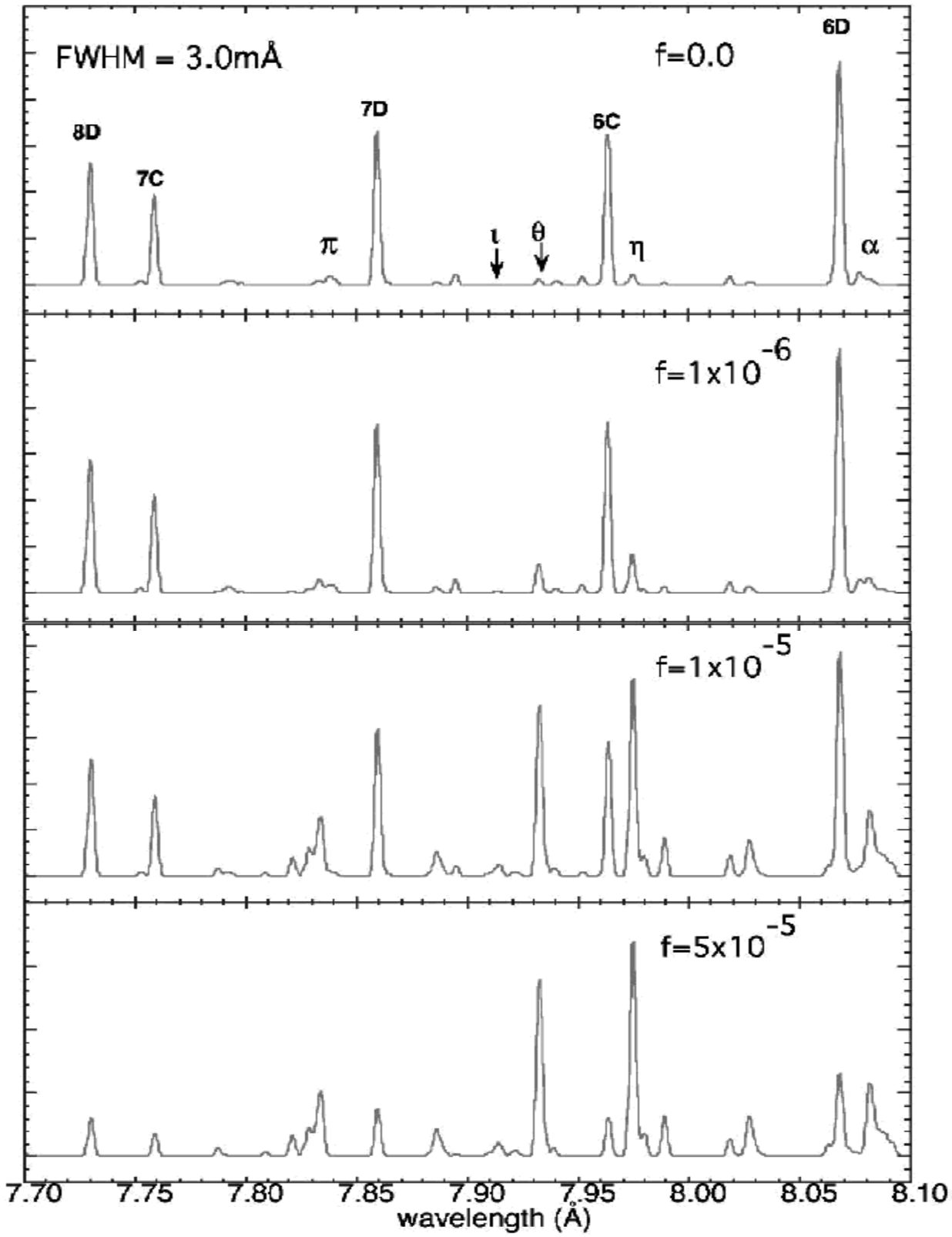

Fig. 9 CR models for O–like to Mg–like copper ions with T_{bulk}=200eV, N_e = 1.0 x 10^{21}cm^{-3}, computed with escape factors for all transitions (L = 30 ion, $T_{ion} = T_e$) and increasing hot electron (T_{hot}=5keV) fraction (from top to bottom), as labeled in the figure.

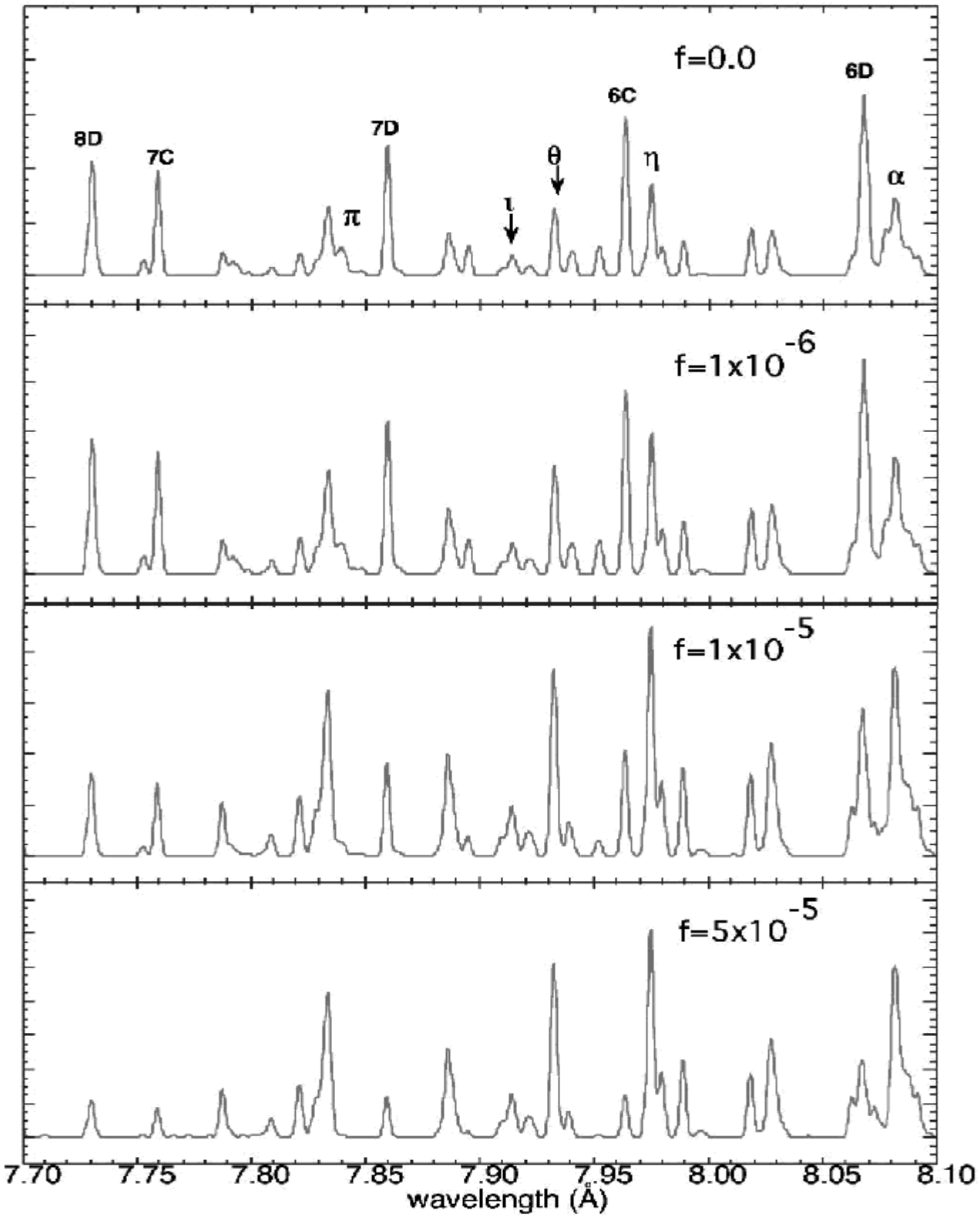

Fig. 10 CR models for O–like to Mg–like copper ions with T_{bulk}=200eV, N_e = 1.0 x 10^{22}cm^{-3}, computed with escape factors for all transitions (L = 30 mm, $T_{ion} = T_e$) and increasing hot electron (T_{hot}=5keV) fraction (from top to bottom), as labeled in the figure.

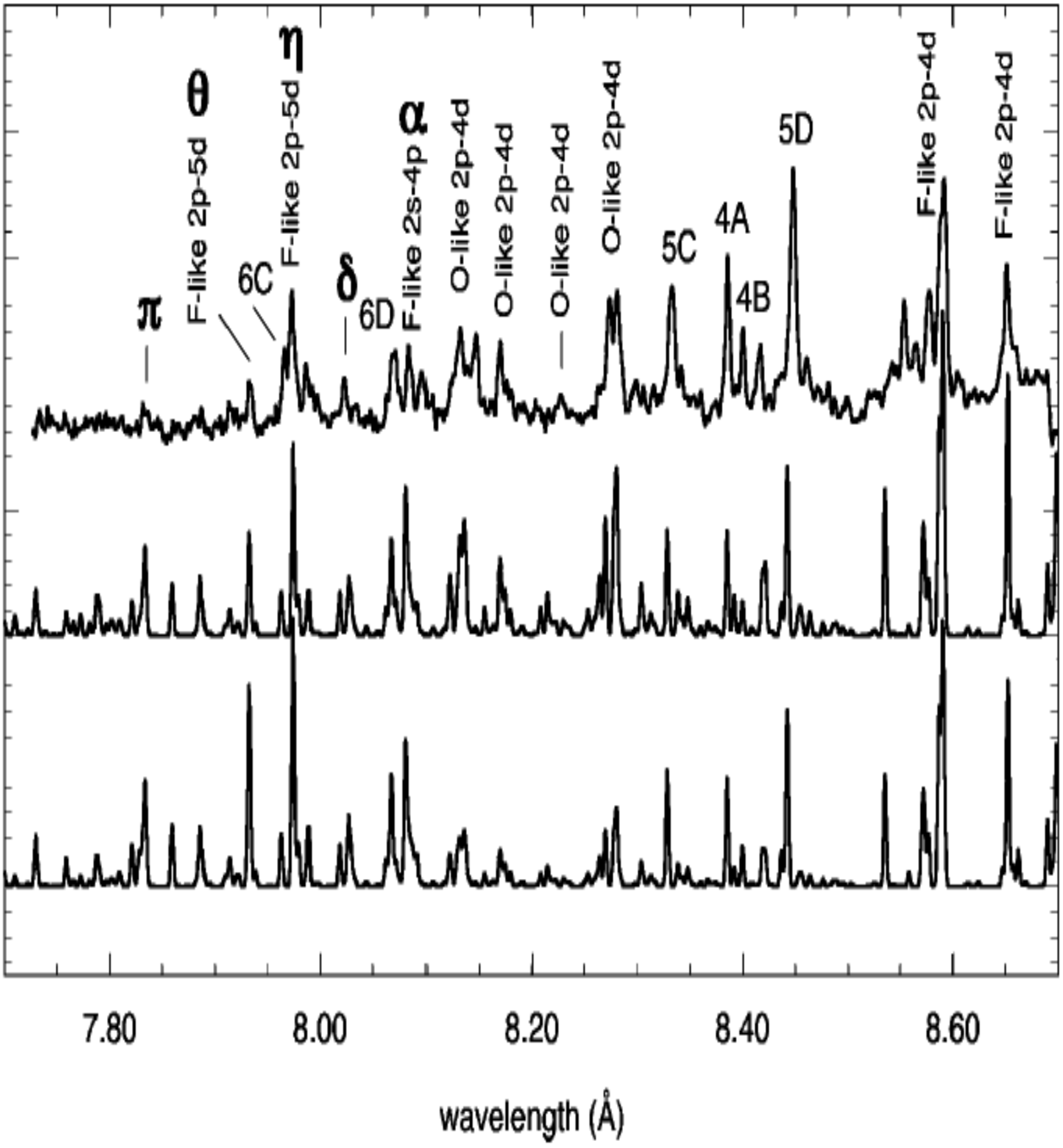

Fig. 11 High intensity (10^{16}W/cm^2) type II (ps pulse) LPP spectrum (top) with the laser at the best focus and low contrast between the main pulse and the prepulse ($I_{main}/I_{pp} = 10^5$). Also shown are two simulations with (middle) $T_e = 400$eV, $N_e = 10^{21}$cm^{-3} and $f_{hot} = 0$ and with (bottom) $T_e = 350$eV, $N_e = 10^{21}$cm^{-3}, $f_{hot} = 10^{-5}$ and instrument shape factors included (L = 50 mm).

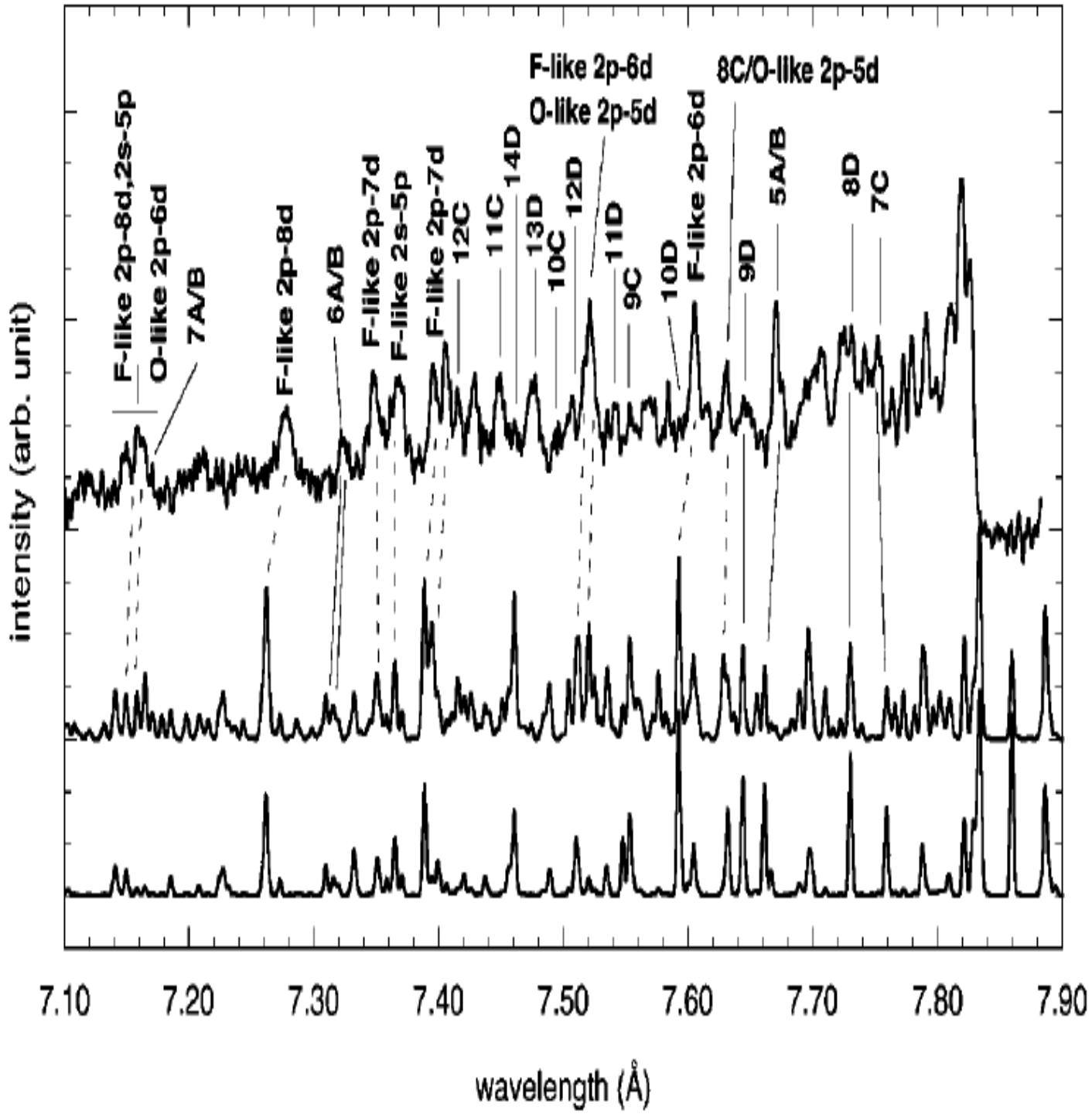

Fig. 12 High intensity (3.3 x 10 ^{15}W/cm^2) type II (ps pulse) LPP spectrum (top) with the focusing lens shifted 0.22mm from best focus and high contrast between the main pulse and the prepulse ($I_{main}/I_{pp}=10^7$). Also shown is a simulation with T_e = 300eV, $N_e=10^{22}$cm^{-3}, f_{hot} = 10^{-5} and with escape factors included (L = 30 μm, middle) and a spectrum calculated with T_e = 300eV, $N_e = 10^{21}$cm^{-3}, $f_{hot} = 10^{-5}$ and escape factors (L = 50 μm).

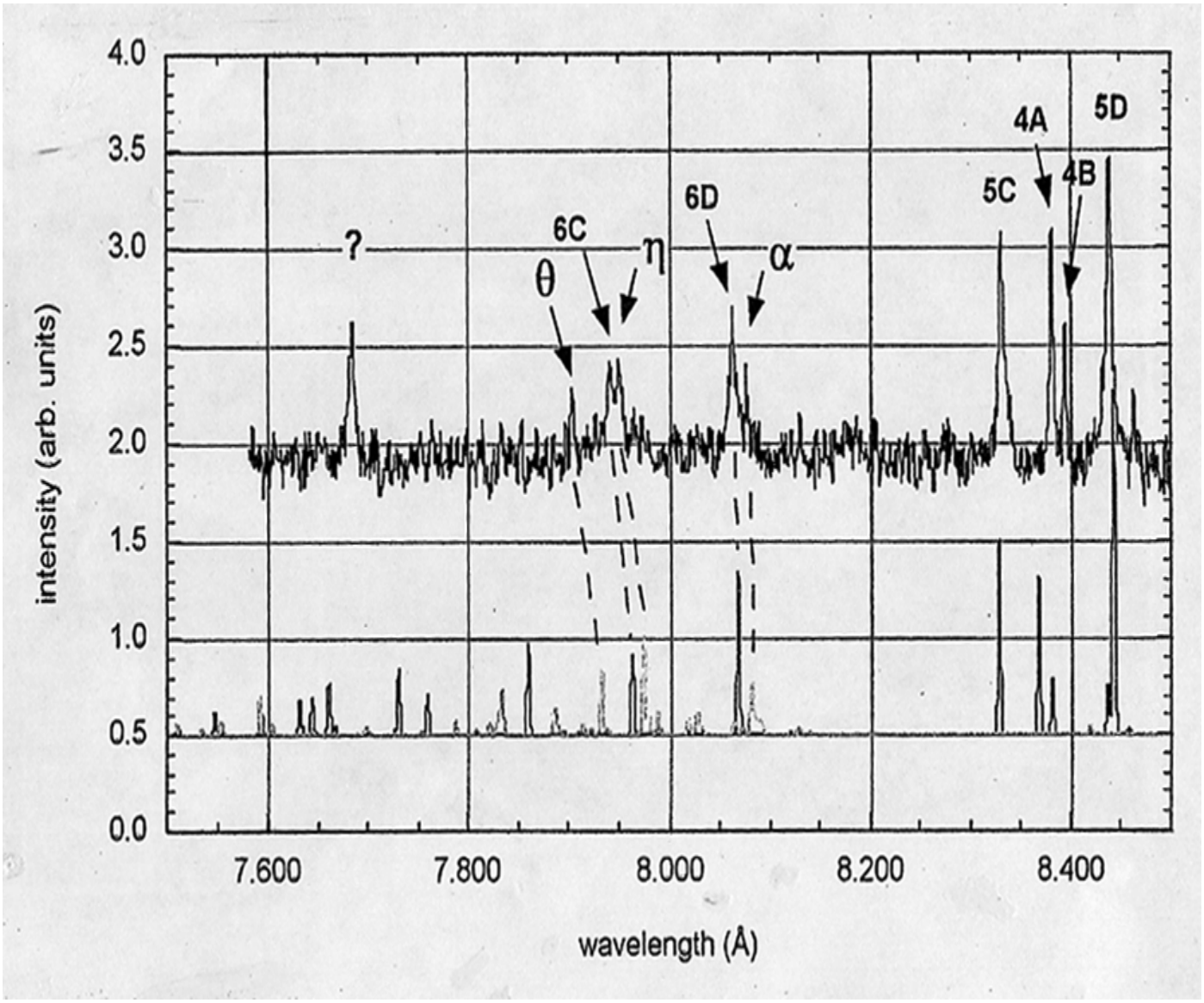

Fig. 13 Above: data from a type III LPP (60fs pulse, I = 10^{18}W/cm^2). Below: calculated CR spectra for Ne–, F– and O– like Cu ions. The synthetic trace is from an optically thin calculation with T_{bulk}=200eV, N_e = 10^{22}cm^{-3}, T_{hot} = 5keV and f_{hot} = 5 x 10^{-5}.

Conclusion

Spectra in the 7.10 to 8.60Å range from highly charged copper ions are observed from four different laser produced plasma (LPPs). The LPPs are formed by a 15ns Nd:Yag/Glass laser pulse (type I: E_{pulse} = 1 – 8J, 1064nm), a 1ps Nd:Glass laser pulse (type II: E_{pulse} = 1J, 1055nm), a 60fs Ti:Sapphire laser pulse (type III: E_{pulse} = 80mJ, 790nm) and a 12ns XeCl laser pulse (type IV: E_{pulse} = 300mJ, 308nm). The spectra of high – **n** (**n = 14**) transitions in highly charged copper ions (from Cu^{19+} to Cu^{21+}) are recorded with a high spectral resolution (= 3000 – 8000) spectrometer using a spherically bent mica crystal. Collisional radiative models are computed for the emission from each plasma. The sensitivity of the model spectra to opacity effects and to populations of superthermal electrons is studied. For the type I and type IV LPPs, opacity effects, treated with escape factors, are necessary to get the correct relative intensities of high – **n** (**n = 5, 6**) Ne– like Cu^{19+} emission features.

In the case of the type II LPPs, the contrast between the main pulse and the laser prepulse has been varied from low ($I_{main}/I_{pp} = 7 \times 10^{4}$) to high ($I_{main}/I_{pp} = 3.8 \times 10^{7}$). From the comparison of the experimental data with the theoretical models an upper limit of the superthermal electron fraction of 10^{-5} of the bulk population can be deduced.

For the type III 60fs LPPs, a population of hot electrons (T_{hot} = 5keV) which corresponds to a fraction $f_{hot} = 5 \times 10^{-5}$ of the bulk electron population (T_{bulk}=200eV) is required to reproduce the observed spectra.

International Conference on Ultrashort High - Energy Radiation and Matter, Oct. 7-10, 2003, Varrenna

X-ray spectral diagnostics for satellite lines of H-like Mg ions measured by high resolution spectrometer

T. Kato, N. Yamamoto* and F. B. Rosmej***,

National Institute for Fusion Science, Toki, Japan

*Rikkyou University, Tokyo, Japan

***GSI-Darmstadt, IPP, Darmstadt, Germany

Introduction

- In high temperature and high density plasmas, satellite lines emitted through doubly excited states are important for plasma diagnostics.
- We have made collisional-radiative model (CRM) including the doubly excited states for H-like and He-like ions.
- X-ray spectra of H-like Mg ions were measured from a laser produced plasma with a high resolution spectrometer by F. B. Rosmej.
- We identify satellite lines for 1s*nl* lines (n = 2 – 4) and analyzed the spectra using our CRM.
- We compare three kinds of atomic data for spectral analysis.
- We derive temperatures of 180, 200, 210 eV at the three points imaged by the spectrometer.

X-ray spectra from laser produced plasma of Mg target were measured with high resolution spectroscopy at GSI

Spectra were measured from three directions

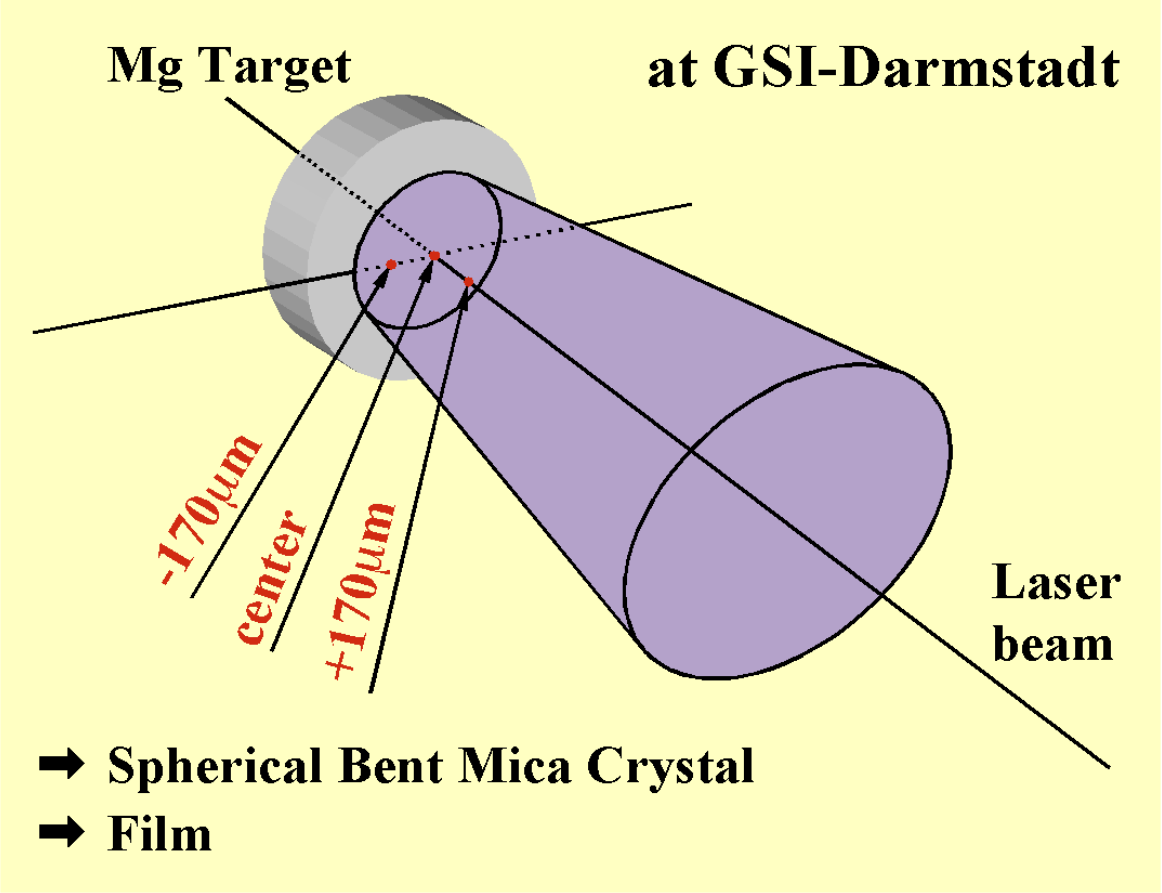

Nd-Glass Laser
(λ = 1.046μm)
Pulse width 15ns
Laser Power 17J
Focal spot 500 μm

Spectral resolution
($\lambda/\Delta\lambda \sim 5000$)
Spatial resolution
Å@ 14 μm

Three different points for measurement

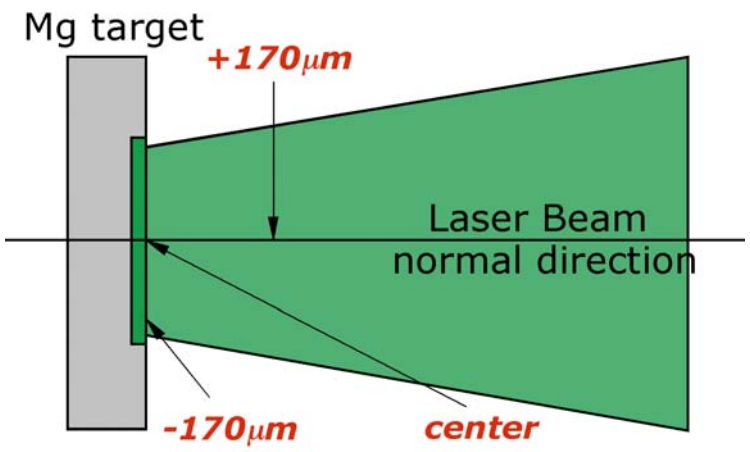

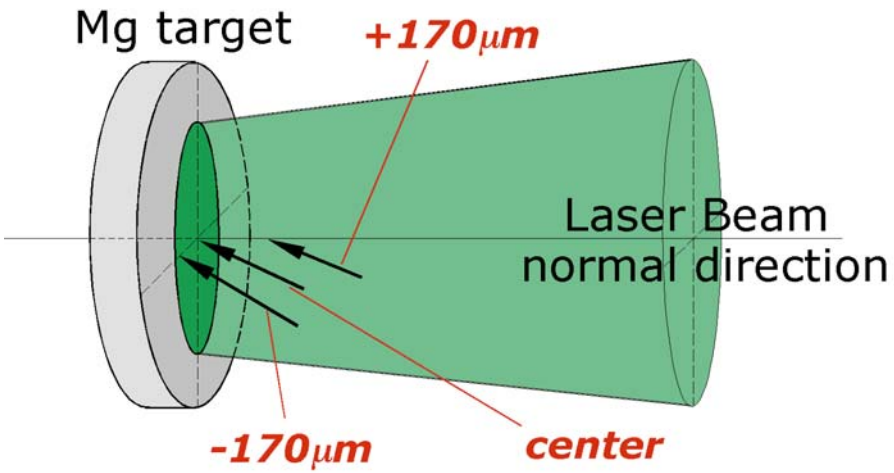

Spectrograph
(Sperical Bent MicaCrystal+Film)

We identified the satellite lines of H-like Mg ions

We used atomic data by MZ code to identify satellite lines.

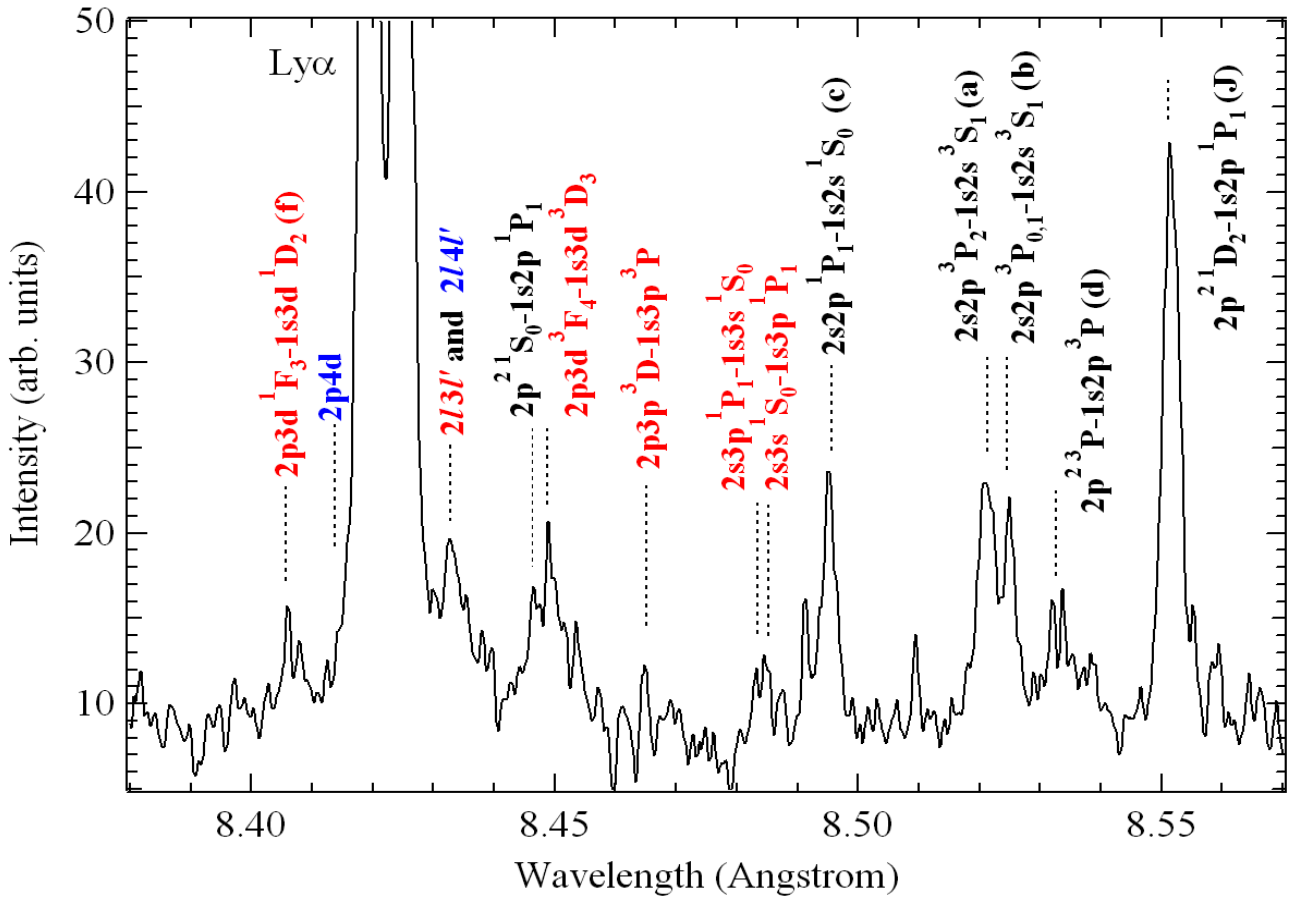

1s2*l* – 2*l*'2*l*''
1s3*l* – 2*l*'3*l*''
1s4*l* – 2*l*'4*l*''
satellite lines are identified

1s4d $^3D_3$ - 2p4d $^3F_4$ at 8.43 26 A is the strongest among 1s4*l* – 2*l*'4*l*'' *lines*

We constructed a Collisional Radiative Model (CRM) including doubly excited states

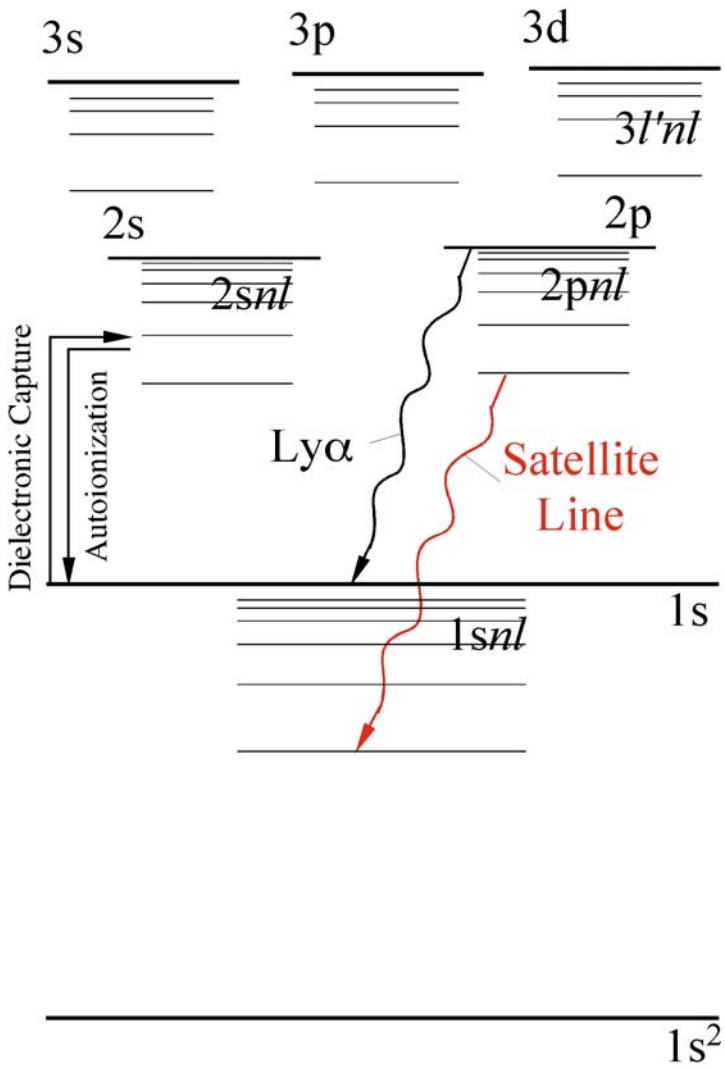

The levels included are

1s, 2s, 3s, 3p, 3d,
$1s^2$,
1snl (60 levels),
2snl, 2pnl (230 levels),
3snl, 3pnl, 3dnl (70 levels)
$n \leq 20$

We compare three kinds of atomic data
for our CRM including doubly excited states

1) **MZ**: **MZ method** by L. Vainshtein and U. Safronova,
2) **MBS**: **Relativistic Many Body perturbation Theory**
calculated by U. Safronova
3) **MBL**: **Relativistic Many Body perturbation Theory combined with complex rotation** calculated by E. Lindroth

We compare **three kinds of atomic data** for satellite lines

MZ(MZ method by Safronova), MBS(MBT by Safronova), MBL(MBT by Lindroth)

The difference are found for 2l4l' and 2l5l' transitions. The intensities by MZ are higher than MBT. Q_d = g Aa Ar / (ΣAa + ΣAr)

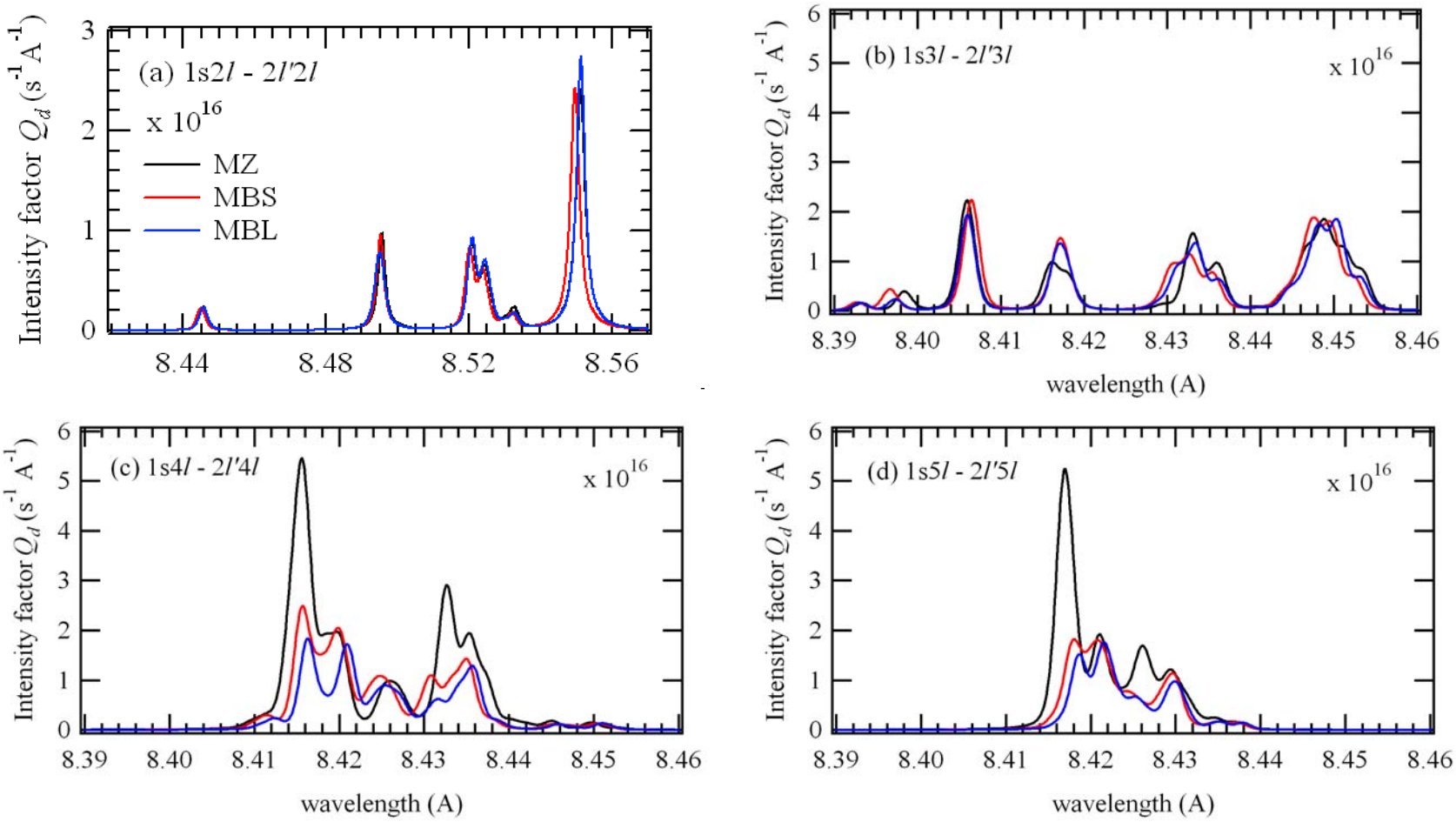

Comparison of three kinds of atomic data for satellite lines

Sum of satellite lines of 1s2*l* – 2*l*2*l*, 1s3*l* – 2*l*3*l*, 1s4*l* – 2*l*4*l*, and 1s5*l* – 2*l*5*l*.

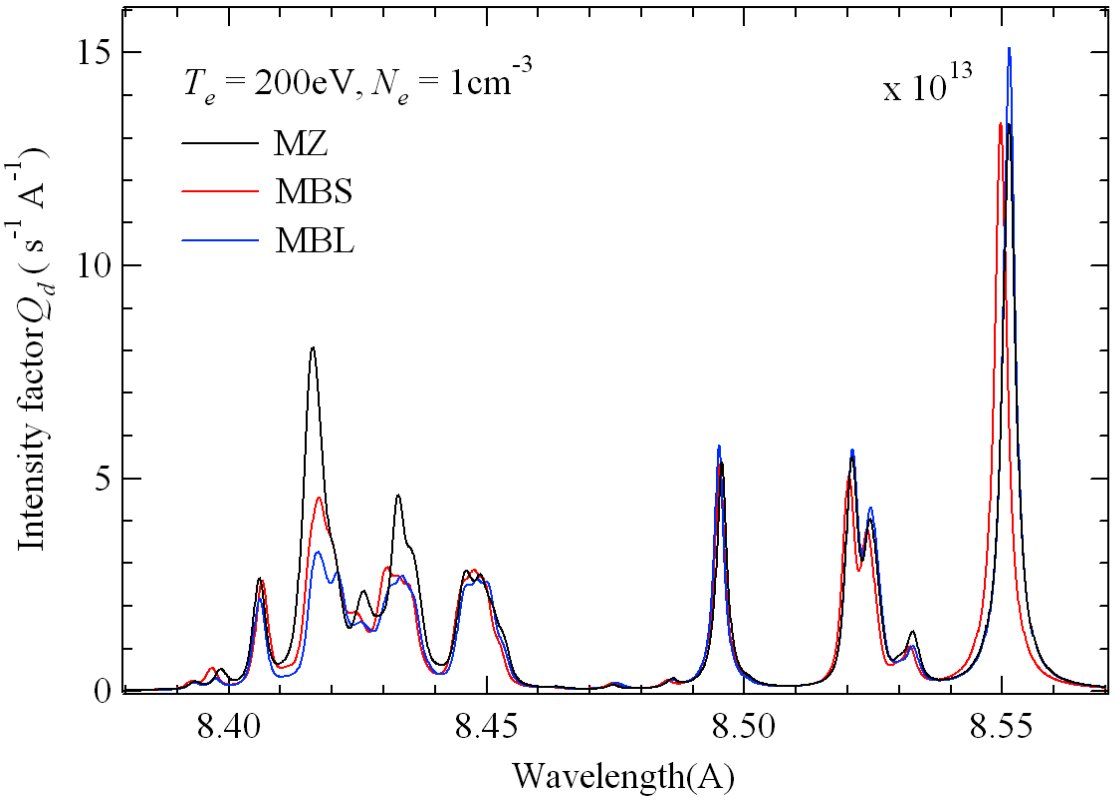

Average level model

1)When we have to take into account numerous excited states in CRM, we consider an average model for simplicity.

2)We did some calculations combining fine structure levels into average levels

$\langle A^a \rangle = \Sigma g_i A^a_{ij} / \Sigma g_i$ $\langle A \rangle = \Sigma g_i A_{ij} / \Sigma g_i$ g_i = statistical weight

3) Population density is calculated distributing according to the statistical weight to obtain the line intensities from fine structure levels.

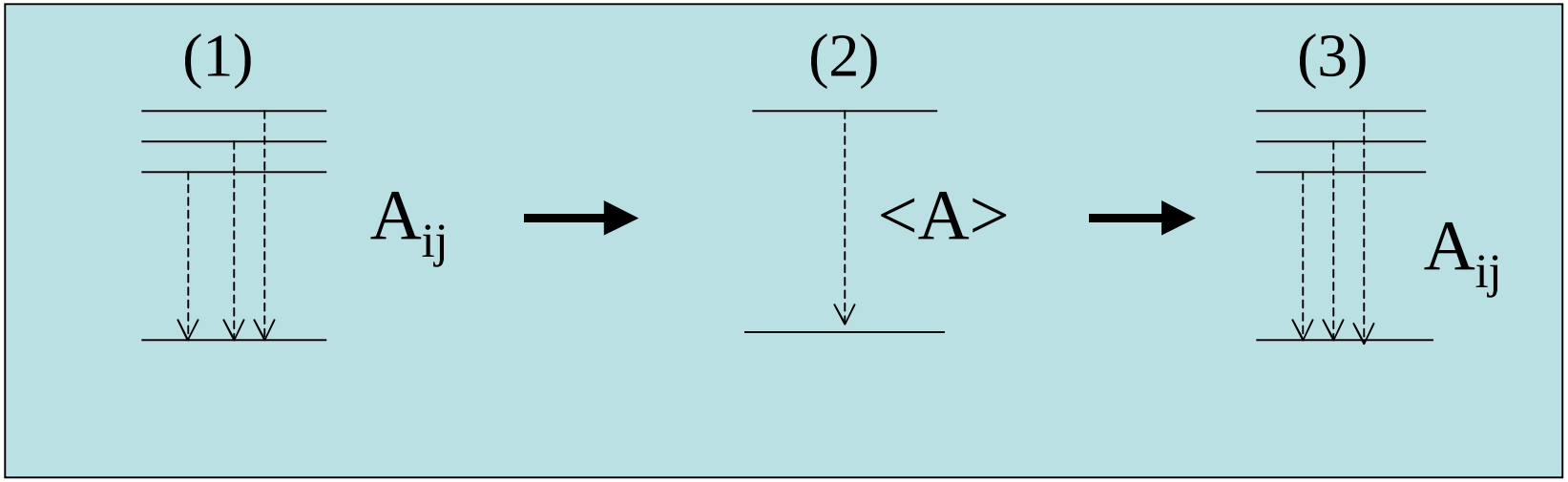

Average level model exaggerates intensities for certain lines

- Black lines (average level model)
- Red lines (detailed level model with fine structures)

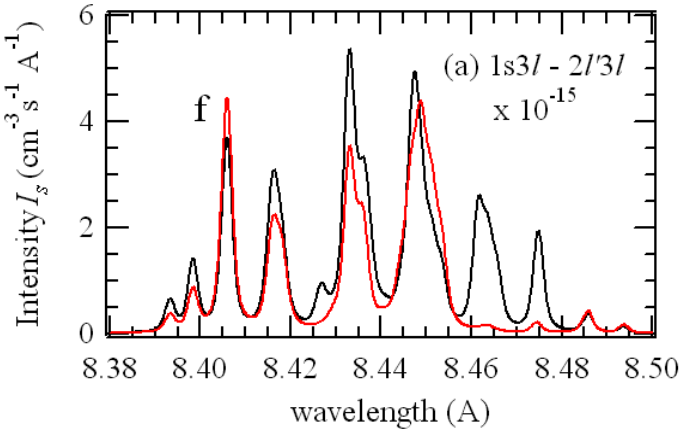

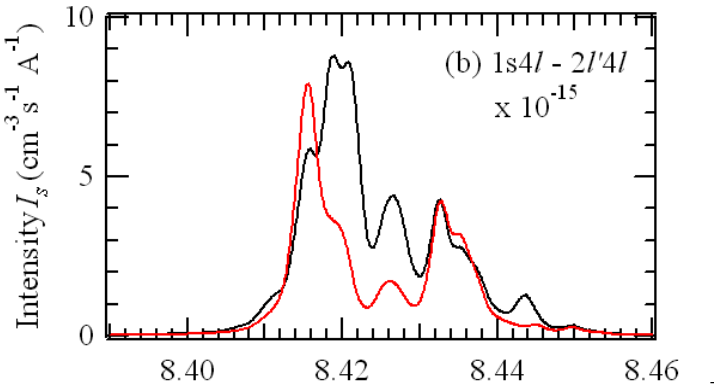

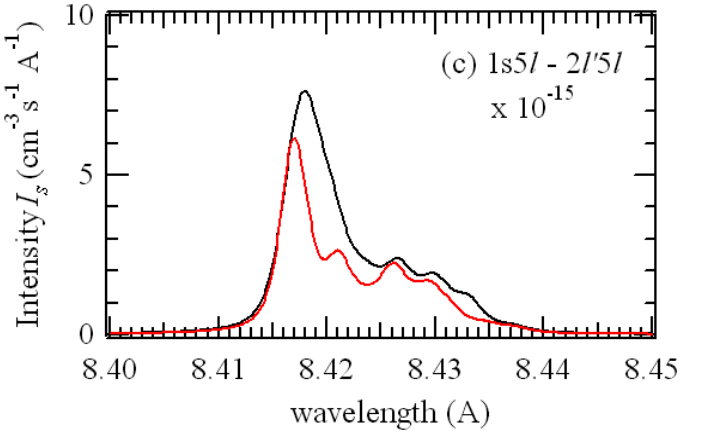

N_e and T_e dependence of satellite line intensity ratios

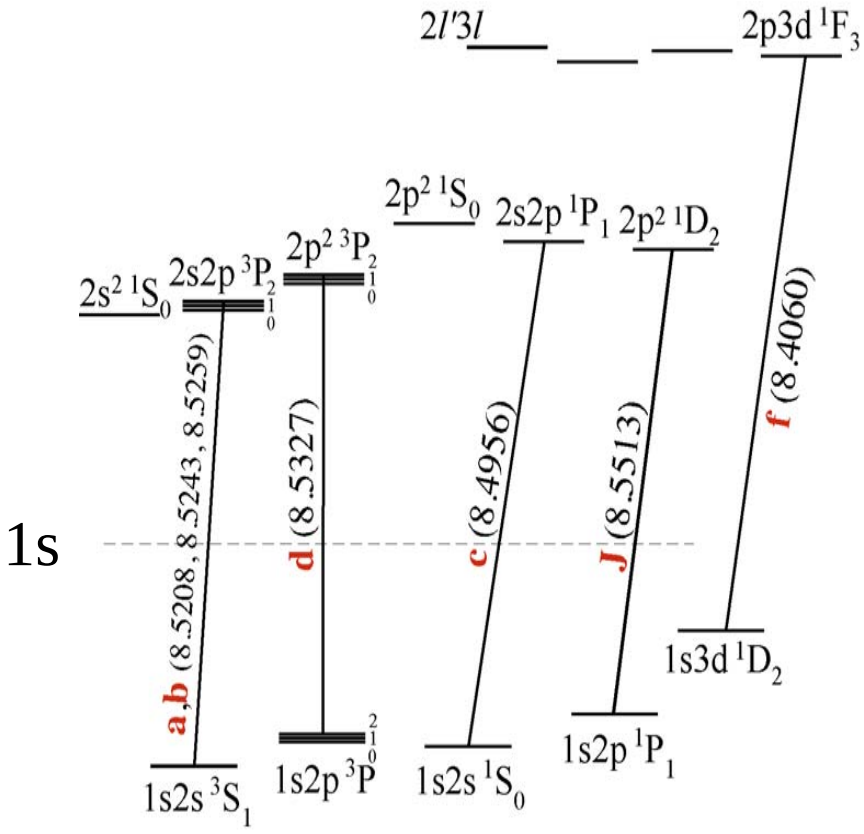

- At low density

l n(2s2p $^3P_2$) > n(2p^2 $^3P_2$)

- With increasing electron density ($N_e \geq 10^{19}cm^{-3}$) n(2p^2 $^3P_2$) is increased by excitation from 2s2p $^3P_{2Å}$ (d/J)
- Ratios of lines with different upper level n can be used for temperature diagnostics (f/J)

N_e dependence of satellite line intensity ratios

Density dependent line ratio:

- **d / J**: $I_d\,(1s2p\,^3P_2 - 2p^2\,^3P_2)$ / $I_J(1s2p\,^1P_1 - 2p^2\,^1D_2)$

has strong density dependence

- **f / J**: $I_f\,(1s3d\,^1D_2 - 2p3d\,^1F_3)$ / $I_J\,(1s2p\,^1P_1 - 2p^2\,^1D_2)$
- **a / J**: $I_a\,(1s2s\,^3S_1 - 2s2p\,^3P_2)$ / $I_J\,(1s2p\,^1P_1 - 2p^2\,^1D_2)$
- **c / J**: $I_c\,(1s2s\,^1S_0 - 2s2p\,^1P_1)$ / $I_J\,(1s2p\,^1P_1 - 2p^2\,^1D_2)$

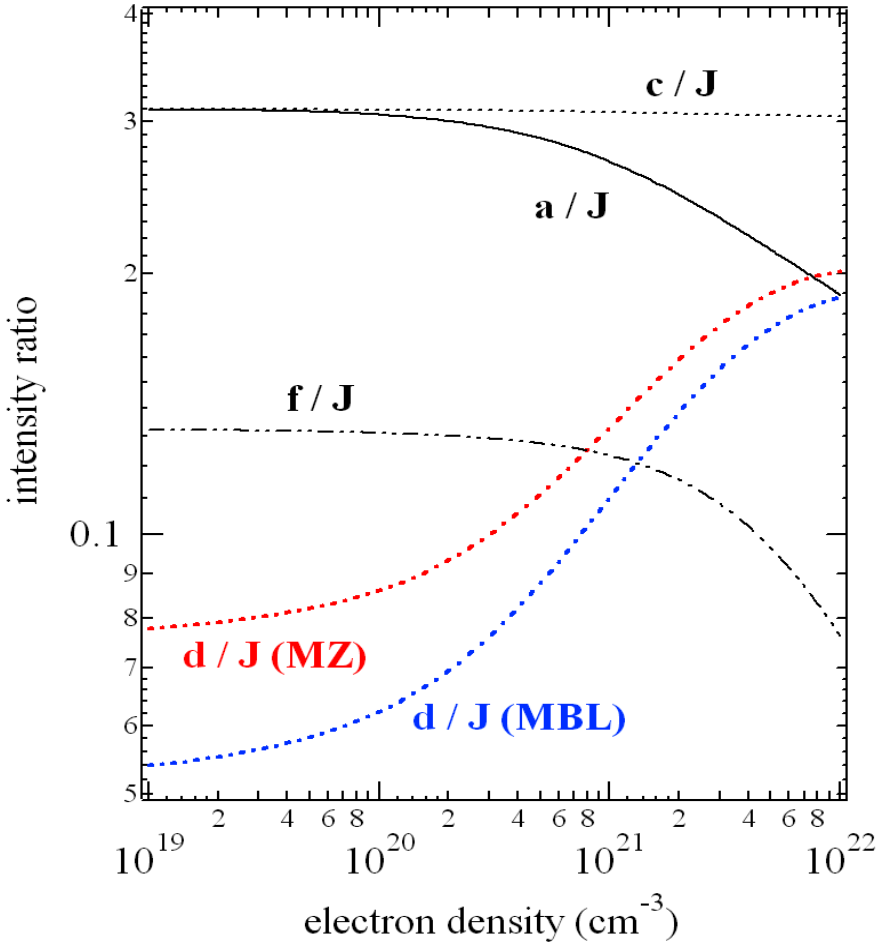

T_e dependence of satellite line intensity ratios

- **f / J**: $I_f\,(1s3d\ ^1D_2 - 2p3d\ ^1F_3)$ / $I_J\,(1s2p\ ^1P_1 - 2p^2\ ^1D_2)$

has strong temperature dependence

- **d / J**: $I_d\,(1s2p\ ^3P_2 - 2p^2\ ^3P_2)$ / $I_J\,(1s2p\ ^1P_1 - 2p^2\ ^1D_2)$
- **a / J**: $I_a\,(1s2s\ ^3S_1 - 2s2p\ ^3P_2)$ / $I_J\,(1s2p\ ^1P_1 - 2p^2\ ^1D_2)$
- **c / J**: $I_c\,(1s2s\ ^1S_0 - 2s2p\ ^1P_1)$ / $I_J\,(1s2p\ ^1P_1 - 2p^2\ ^1D_2)$

c / J has no T_e and N_e dependence.

c / J can be used to define the background level.

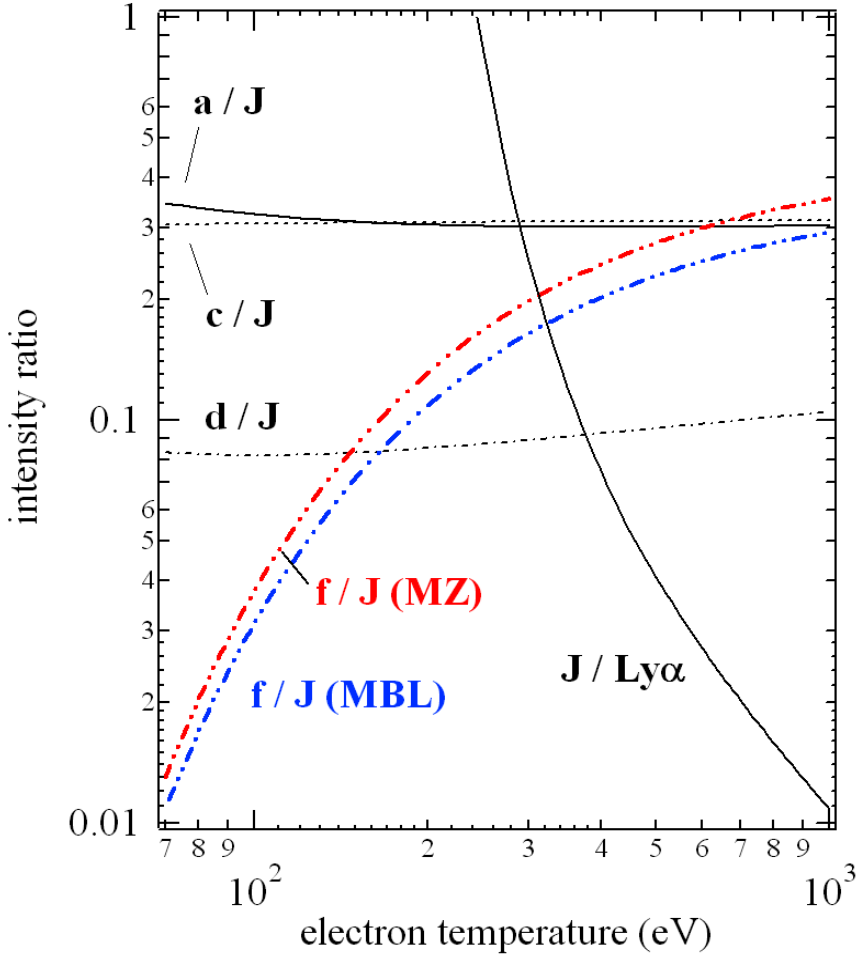

Spectral line profile

Voigt profile is used with doppler broadening, natural width and instrumental width.

Instrumental width w = 0.5mA is derived from the strongest satellite line J-line

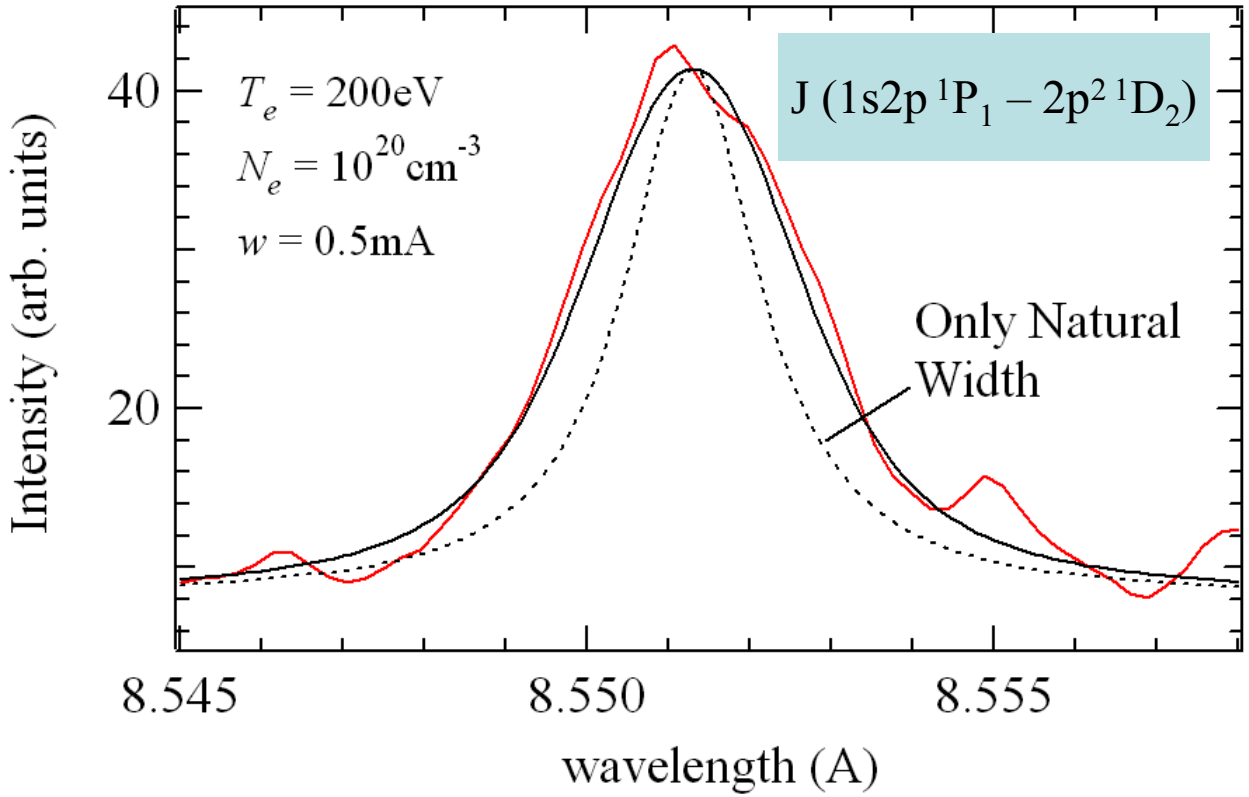

X-ray spectra from center of focal spot

Experiment (red line) and CR Model with atomic data by **MZ** code (black line:total, green line: satellite lines, blue line: Lyα lines)

T_e = 200eV and N_e = 5x10^{20}cm^{-3} are derived from spectral fit.

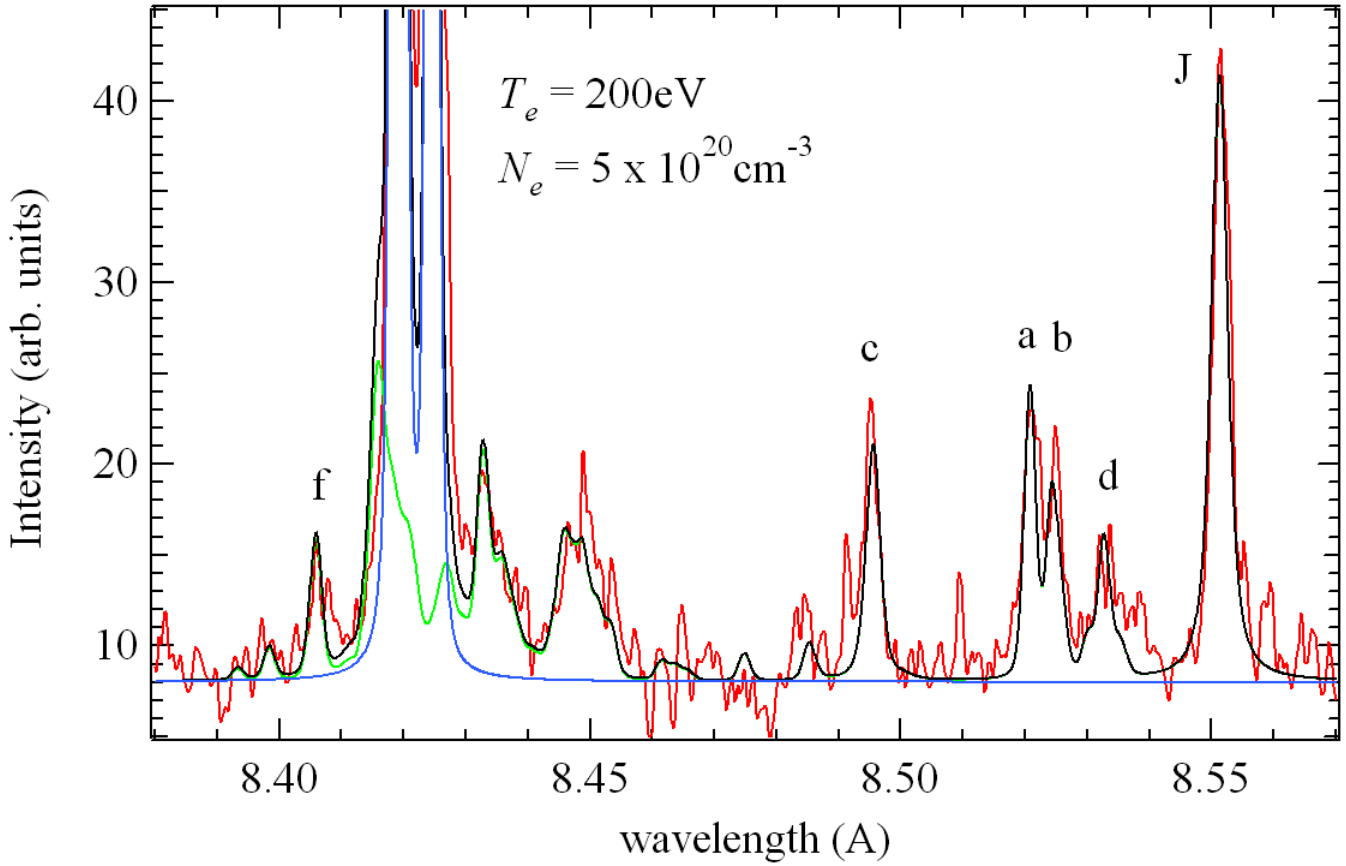

Overall good agreement except that theoretical intensity (2l5l' transitions) is too high near 8.415A at Lyα foot.

X-ray spectra from center of focal spot

Experiment (red line) and CR Model with atomic data by **MBL**
(black line:total, green line: satellite lines, blue line: Lyα lines)
T_e = 230eV and N_e = 8x10^{20}cm^{-3} are derived from spectral fit.

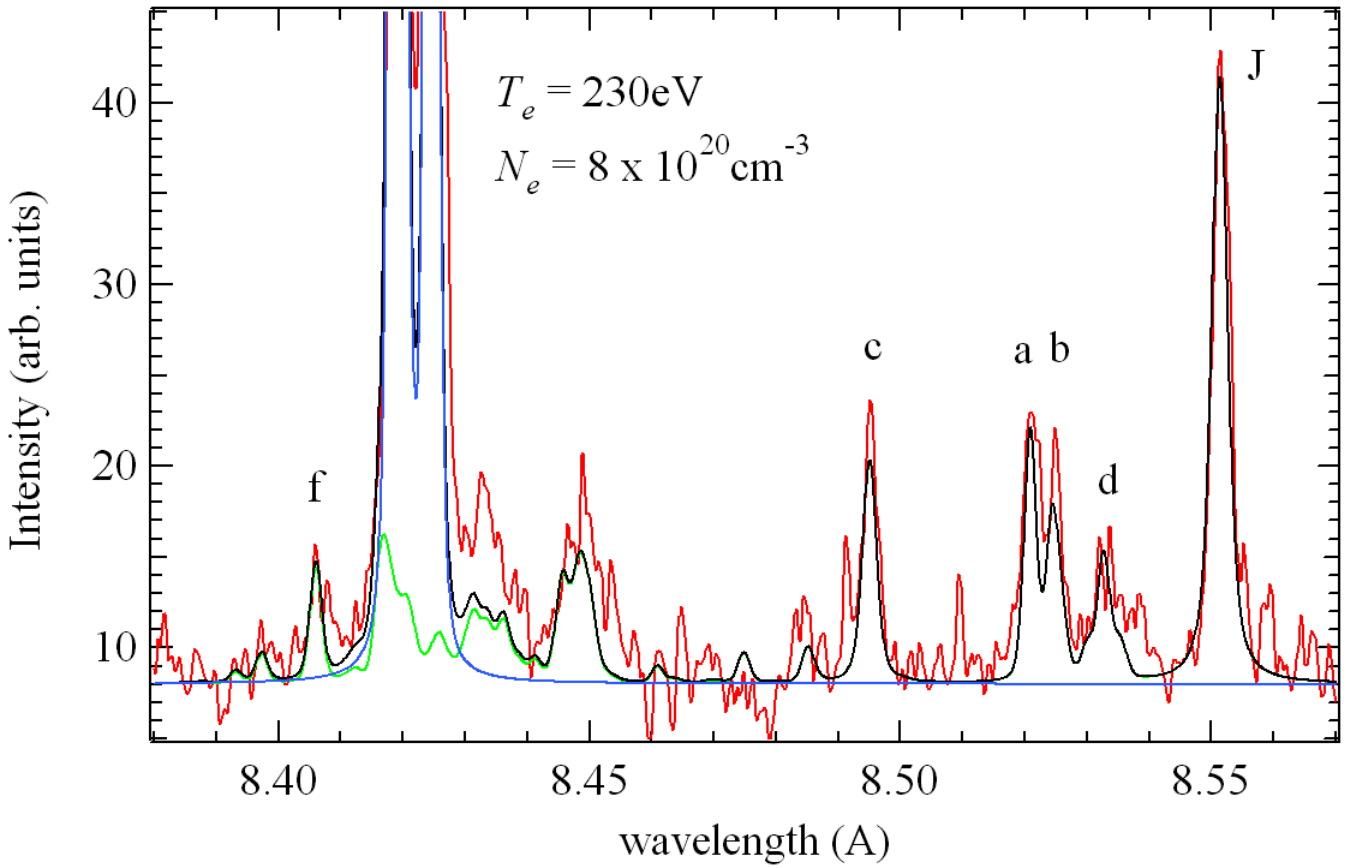

The wavelength range 8.43 - 8.44A (mainly 2l3l' and 2l4l' transitions) show disagreement with theoretical values by MBL

Theoretical satellite spectra by MZ showing the contribution from different components

(background level taken from experimental data)

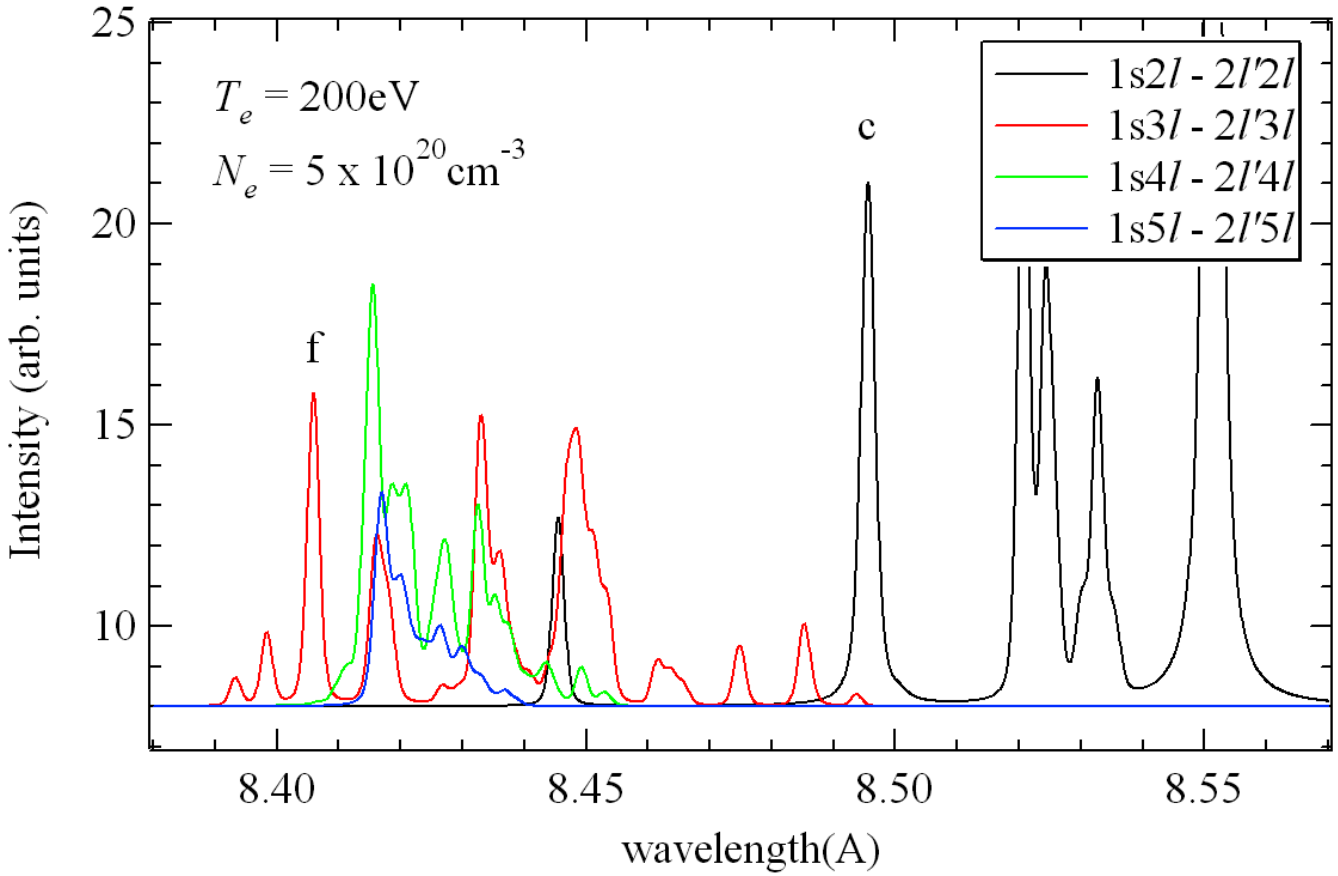

It is difficult to fit the X-ray spectra from +170μm because of statistics. Experiment (red line) and CR Model with atomic data by **MZ** code (black line)

+170μm

Derived electron temperature T_e = 300 eV from I_f/I_J gives too high intensities for Lyα.
T_e = 210 eV is derived considering both the intensity ratio and Lyα line intensities.

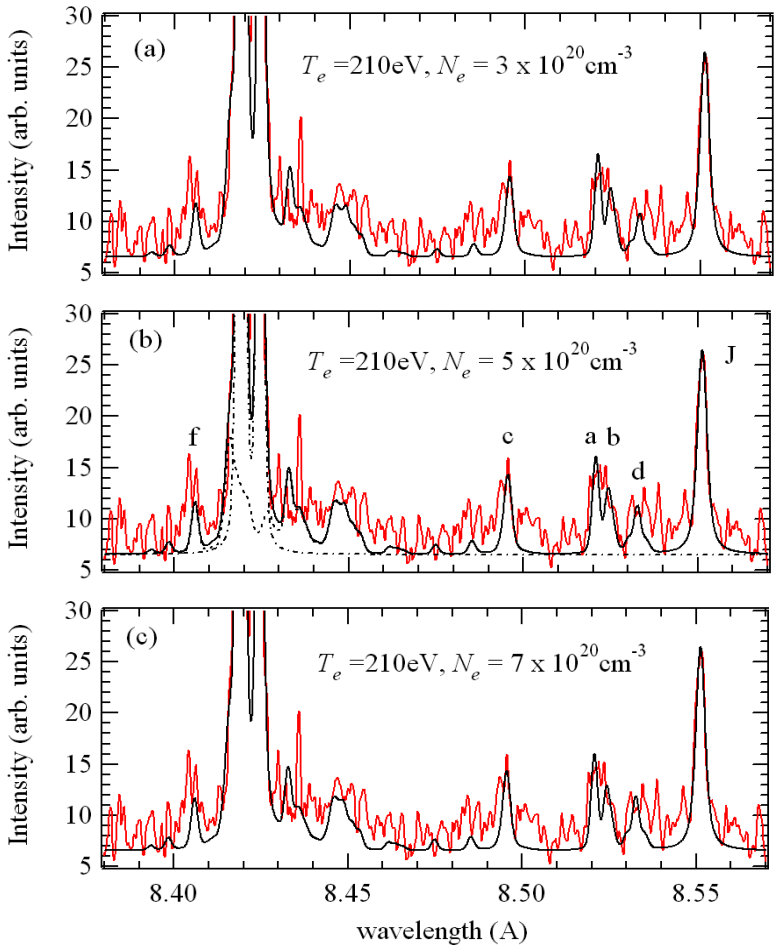

It is difficult to fit the X-ray spectra from –170μm because of statistics. Experiment (red line) and CR Model with atomic data by **MZ** code (black line)

– 170μm

Derived electron temperature T_e = 160 eV from I_f/I_J gives too low intensities for Lyα.
T_e = 180 eV is derived considering both the intensity ratio I_f/I_J and Lyα line intensities.

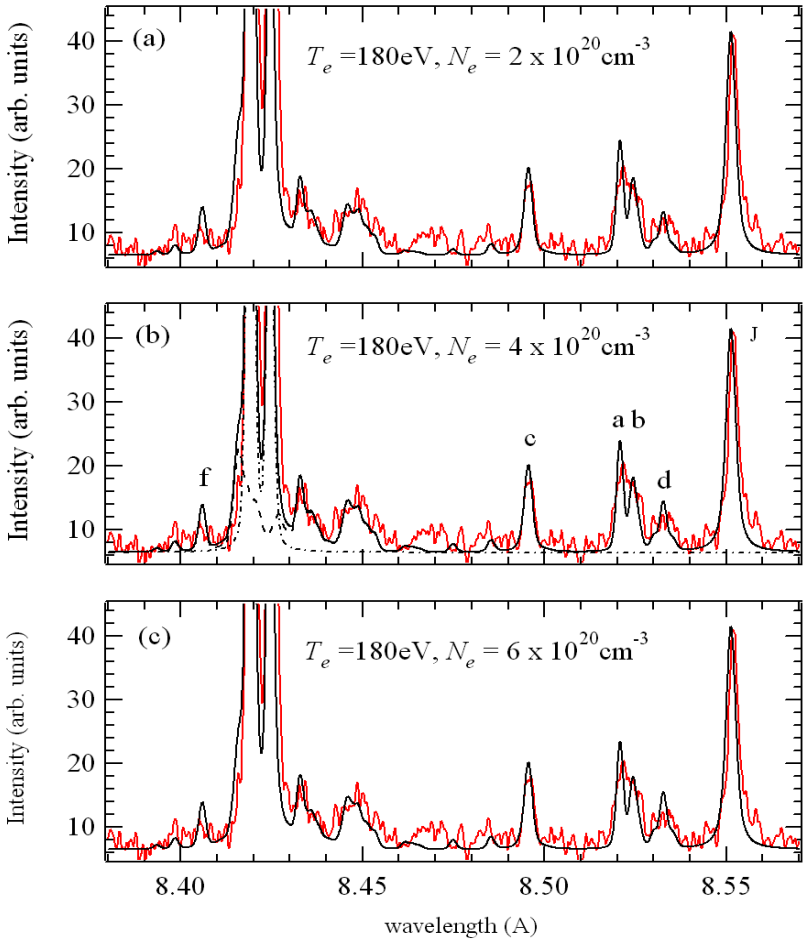

Summary and discussions

- We have constructed CRM including doubly excited states and analyzed X-ray spectra of H-like Mg ions measured at GSI.
- We identified satellite lines for 2l2l', 2l3l' and 3l4l' transitions.
- We study the density and temperature dependences of satellite line intensity ratios.
- We compared three kinds of atomic data for spectral analysis.

  We found a better spectral fit with MZ data than MBT in 8.43 - 8.44A (2l4l' lines). However MBT is better than MZ near 8.415A (2l5l' lines).
- The plasma parameters are derived with the satellite line intensity ratios.

  $T_e = 200 \pm 10$ eV, $N_e = 5 \pm 2 \times 10^{20}$ cm^{-3} for the center position

  $T_e = 210$ eV, $N_e = 5 \times 10^{20}$ cm^{-3} for +170μm

  $T_e = 180$ eV, $N_e = 4 \times 10^{20}$ cm^{-3} for -170μm
- The derived Temperatures from satellite line intensity ratio and Lyα intensity are different. This might be dynamic effect.

International conference on ultrashort high-energy radiation and matter
Villa Monastero, Varenna, Italy October 7-10,2003

Flatness study of X-UV beamsplitters for Michelson interferometry

Anne-Sophie MORLENS*, Philippe ZEITOUN, Laurent VANBOSTAL, Pascal MERCERE, Grégory FAIVRE, Sébastien HUBERT
Laboratoire d'interaction des rayonnements X avec la Matière, LOA-ENSTA, chemin de la HunièreF-91761 Palaiseau cedex, France

Philippe TROUSSEL, Christian REMOND, Rémy MARMORET
CEA-DAM/ DRIF/ DCRE/SDE, BP 12, 91680, Bruyères-le-Châtel, France
Frank DELMOTTE, Marie-Françoise RAVET, Marc ROUILLAY
Laboratoire Charles Fabry de l'Institut d'Optique - CNRS UMR 8501

X-UV Michelson interferometry

•**Why Interferometry?**
–To make 2D map of the electron density of the plasma
=> information on the beam phase
–To caracterise XRL laser

•**Why X-UV?**
To probe up to 10^{22} el/cm^3 at λ=13.9nm (Nc@3ω)

•**Why Michelson?**
–To have a large field (# Fresnel bimirror, D.Joyeux)
–To have a flexible system (# Mach Zender, Da Silva)

VUV Fourier-transform spectroscopy

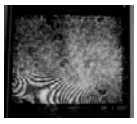

At LULI (Palaiseau,France) (2001)
•λ=13.9nm
• pulse duration=130ps
•Low magnification(5 x 5 mm²)

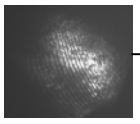

At LLNL (Livermore, USA) (2002)
•λ=14.7nm
• pulse duration=5ps
•Low magnification(0.5 x0. 5 mm²)

Measurements of the Transient Collisional X-ray Laser

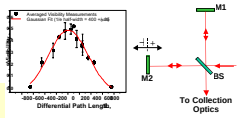

R.Smith et al., Opt. Lett., 2003

With plasma → For the future

Conception of beamsplitters for X-ray laser interferometry

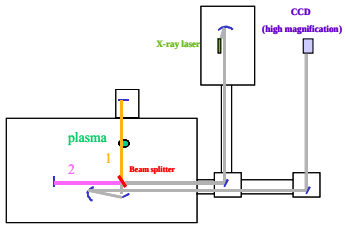

Required parameters for the B.S.:

• intensity(1)=intensity(2) in order to maximise the contrast
➢ B.S. symetric
•Reflection_Transmission maximum
➢T max @ 13,9nm=> very thin
➢R max @ 13,9nm => Mo/Si coating

Mo/Si multilayer structure optimized by **modeling**

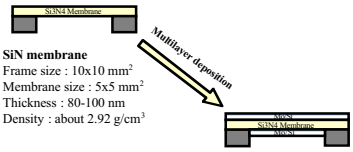

SiN membrane
Frame size : 10x10 mm²
Membrane size : 5x5 mm²
Thickness : 80-100 nm
Density : about 2.92 g/cm³

Performance of beamsplitters for X-ray laser interferometry

	Transmission and reflectivity	Homogeneity	Flatness
Method of measurement	Beamline SA23 of Super-Aco LURE, Orsay	Beamline SA23 of Super-Aco LURE, Orsay 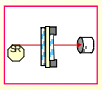	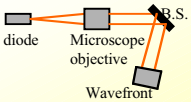
Results	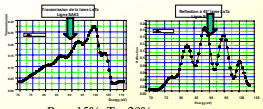 Rs = 15%, Ts=29% Agrees with the theorie	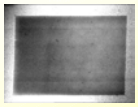 No homogeneity problem	***Shack Hartmann:*** Δz(RMS)=78+/-8 nm Δz(P-V)=485+/-30 nm The B.S. is deformed,this explains the fringes deformations observed during experiments

Influence of the holder

influence of the screw tightening

Far from tight	A little tighter	Still tighter	Very tight
Δ_z(RMS)=45+/-5 nm Δ_z(P-V)=275+/-30 nm	Δ_z(RMS)=60+/-5 nm Δ_z(P-V)=350+/-30 nm	Δ_z(RMS)=75+/-5 nm Δ_z(P-V)=450+/-30 nm	Δ_z(RMS)=90+/-5 nm Δ_z(P-V)=550+/-30 nm
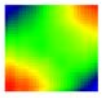	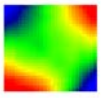	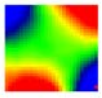	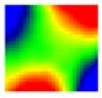

The tightening of the screw deformes the B.S. Solution: metal leg => a point of glue

influence of the screw position

Initial position	+1/4 of turn	+1/4 of turn	+1/4 of turn
Δ_z(RMS)=75 +/-5 nm Δ_z(P-V)=440 +/-30 nm	Δ_z(RMS)=30 +/-5 nm Δ_z(P-V)= 210 +/-30 nm	Δ_z(RMS)=50 +/-5 nm Δ_z(P-V)=350 +/-30 nm	Δ_z(RMS)= 31 +/-5 nm Δ_z(P-V)=220 +/-30 nm
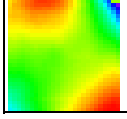	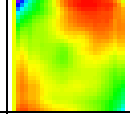	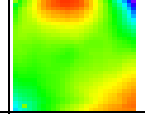	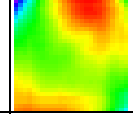

The position of the leg either amplifies or corrects the proper deformation of the B.S.

Influence of the coating stress

How to reduce the stress of the coating
(the initial stress of the nitride membrane is 1GPa):

•Change the coating method :
ion beam sputtering =>magnetron pulverisation……σ =-900MPa => σ =-750MPa

•Change the parameters of the coating:

1. Optimisation of the cyclic ratio of Mo : Γ=0,25 => Γ=0,5 ….σ =-750MPa => σ =-350MPa
2. Pressure of Ar…… Negligeable effect
3. Power of activation of the targets …… Negligeable effect
4. Period thickness and number of period…… σ =-350MPa => σ =-150MPa
5. The coating's speed and the number of scans……Negligeable effect
6. The heating…… Negligeable effect

B.S. with a coating stress of –150MPa and hold with a point of glue

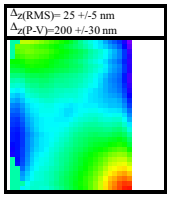

Conclusion

• We succeed to correct the deformation of the B.S. by changing the coating parameters and the B.S. holder:

Δz(RMS)= 90 nm => 25 nm

Δz(P-V)=550 nm => 200 nm

For a diameter of 3mm Δz(RMS)<4 nm (less than _ fringe à à 13.9nm)

• The transmission x reflectivity and the homogeneity are still good

Perspectives

• Change the λ
• Self supported B.S.
• Larger aperture

morlens@ensta.fr

Spectrally tunable X-ray imaging and backlighting schemes based on the spherically bent crystals

T. Pikuz[1], A. Faenov[1], I. Skobelev[1], A. Magunov[1], M. Sanchez del Rio[2], L. Alianelli[3] , G. Baldacchini[4], F. Flora[4], S. Bollanti[4], P. Di Lazzaro[4], D. Murra[4], G. Tomassetti[5], A. Ritucci[5], A. Reale[5], L. Reale[5], M. Francucci[6], S. Martelluci[6], G. Petrocelli[6]

[1]MISDC of VNIIFTRI Mendeleevo, Moscow region, 141570, Russia

[2] European Synchrotron Radiation Facility, BP 220, F-38043 Grenoble Cedex, France

[3]Institute Laue Langevin BP 156 38042 Grenoble and Istituto Nazionale di Fisica della Materia, Italy

[4]ENEA, UTS Tecnologie Fisiche Avanzate, C.R. Frascati, Via E. Fermi 45, 00044 Frascati, Rome, Italy

[5]INFM Dipartamento di Fisica dell'Aquila and LNGS-INFN, Assergi (L'Aquila), Italy

[6]INFM- Universita' di Roma Tor Vergata, Via del Politecnico, N. 1, 00173 Roma , Italy

Topics

- Introduction
- X-ray monochromatic projection imaging: experiment description and results
- X-ray monochromatic imaging of self emitting objects
- Conclusions

Traditional backlighting scheme

Bragg angle Θ ~ 90°

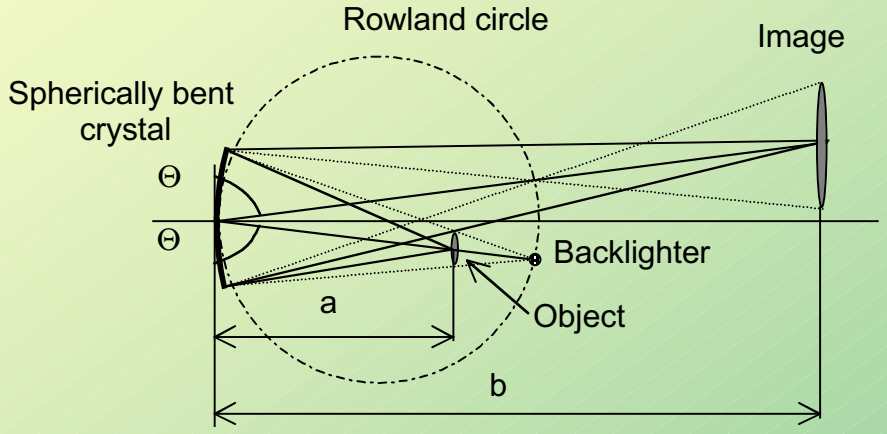

Shadow backlighting scheme (SMB)

Bragg angle Θ ~ 35 ° ÷ 70°

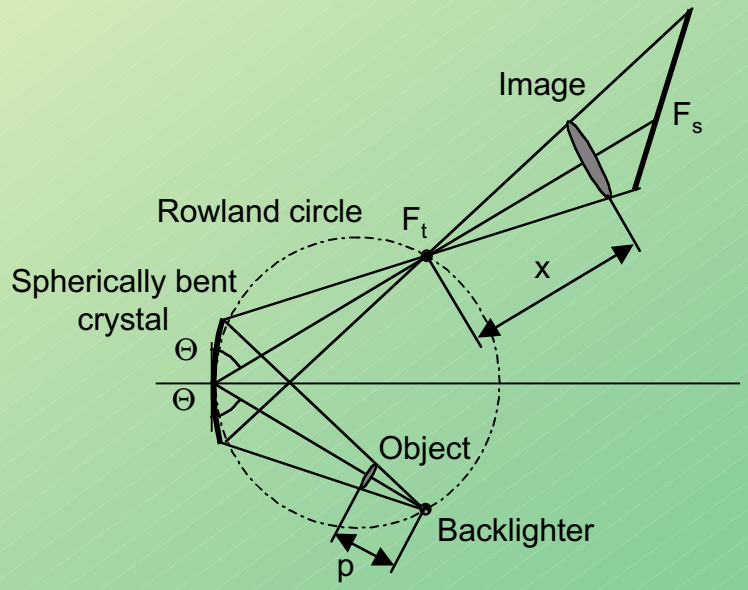

SMB: Θ = 39.4°

Laser: XeCl, λ = 0.308 μm, τ = 10 ns, E =1.3 J, f = 10 Hz Target: Ni-Cr

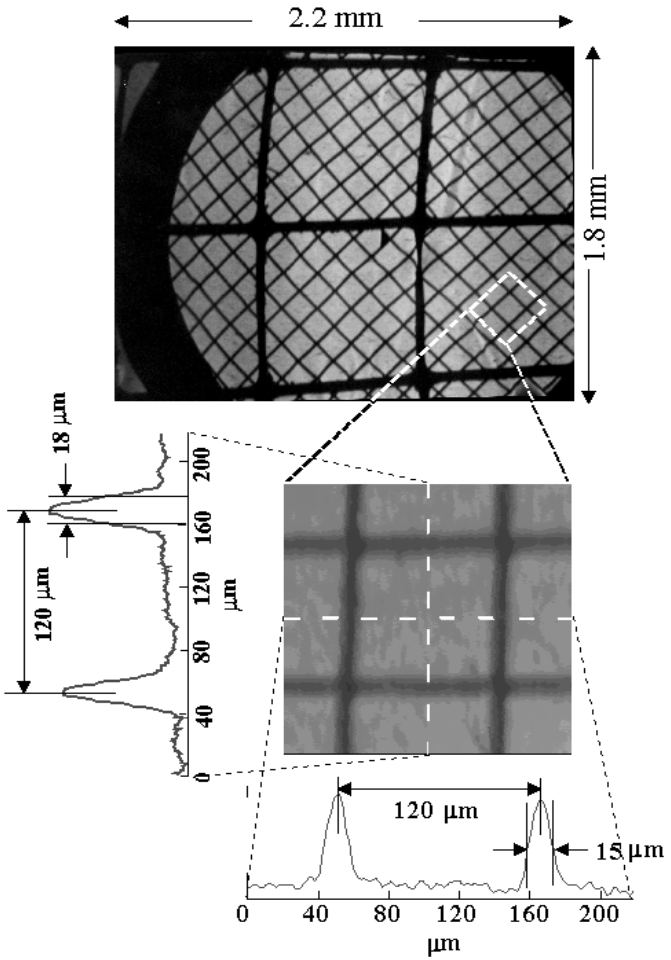

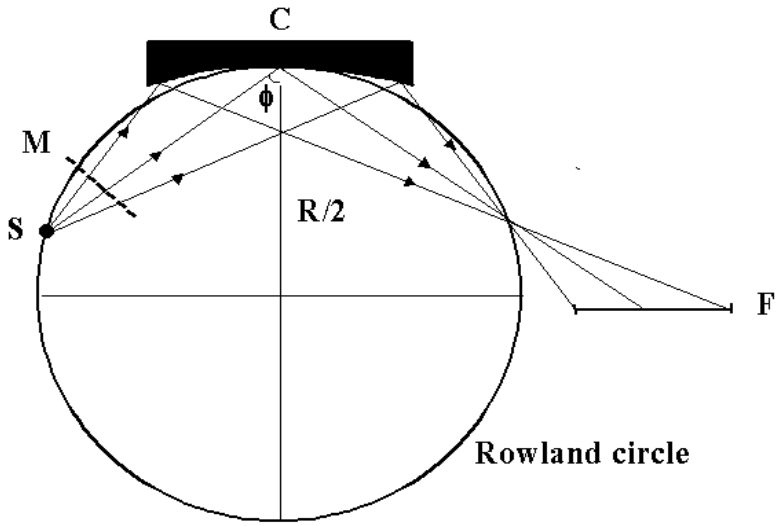

Magnification : K = 5
Mica Crystal, R = 80 mm
ϕ = 50.6°
θ = 39.4 °

CF = 98 mm
SM = 14 mm
SC = 50.8 mm

ENEA, Frascati, Italy
L'Aquila University, Italy

SMB: Θ = 53.7°

XeCl laser: pulse energy of 1.0 J, duration of 10. Target: Cu

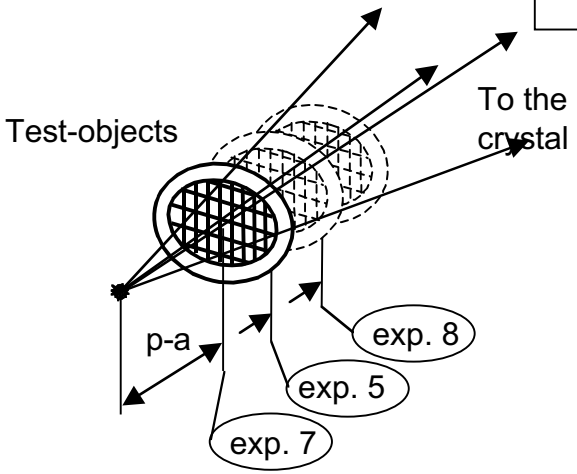

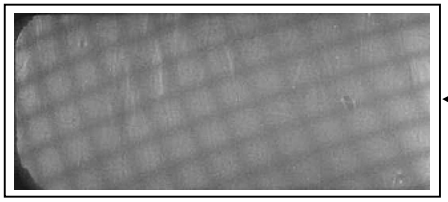

Grid: period 60 μm
wire thickness 10 μm

exp. 7 p-a = 5 mm M=38x

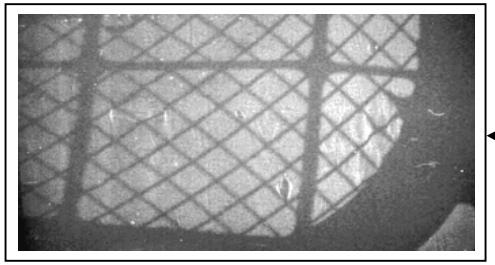

Small grid: period 120 μm
wire thickness 14 μm

exp. 5 p-a = 8 mm M=25x

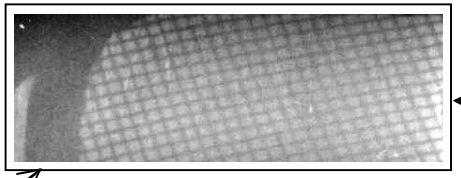

Grid: period 50 μm
wire thickness 10 μm

p-a = 11.5 mm M= 15x

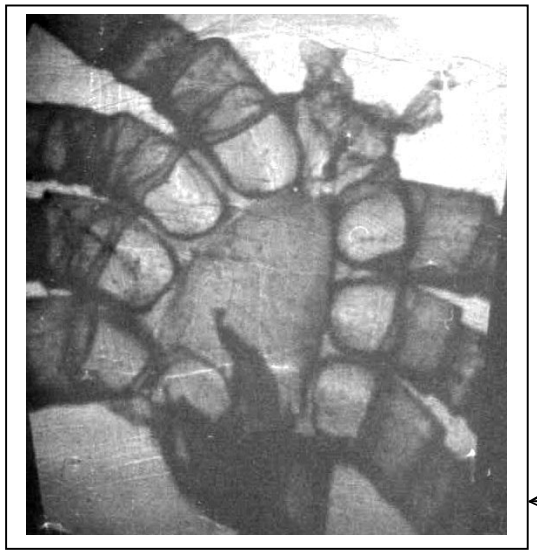

exp. 8

ENEA, Frascati, Italy
L'Aquila University, Italy

Monochromatic X-ray projection imaging with X-ray laser produced plasma source

Bragg angle Θ =80.5°

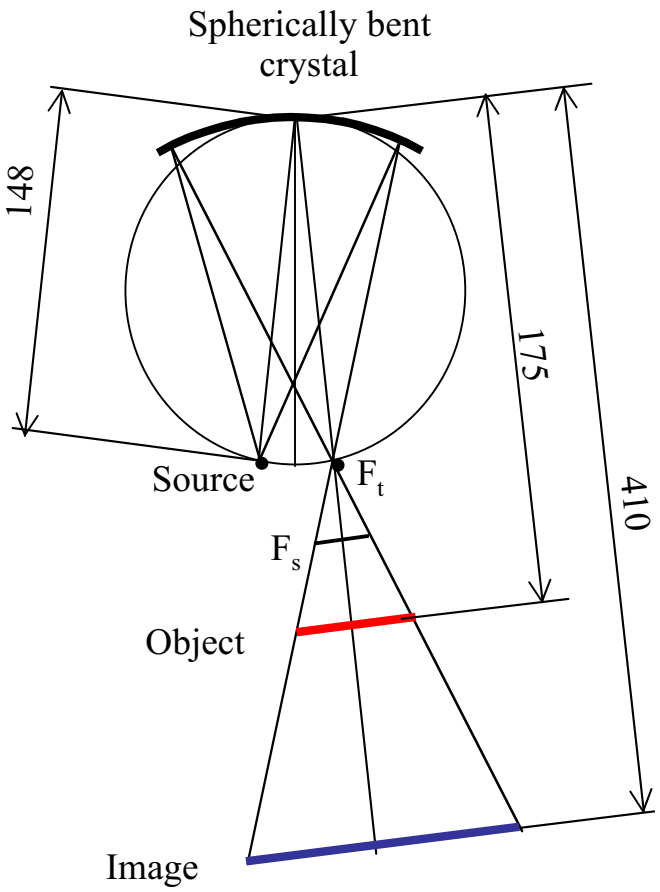

Object was placed after sagittal focus!

Mica, R = 150 mm; Target: Cu

Source size - ~ 15 μm

Big grid: period 800 μm, wires 50±5 μm

Small grids: period 60 μm, wires 14 μm

$\Delta\lambda/\lambda \approx 10^{-3}$

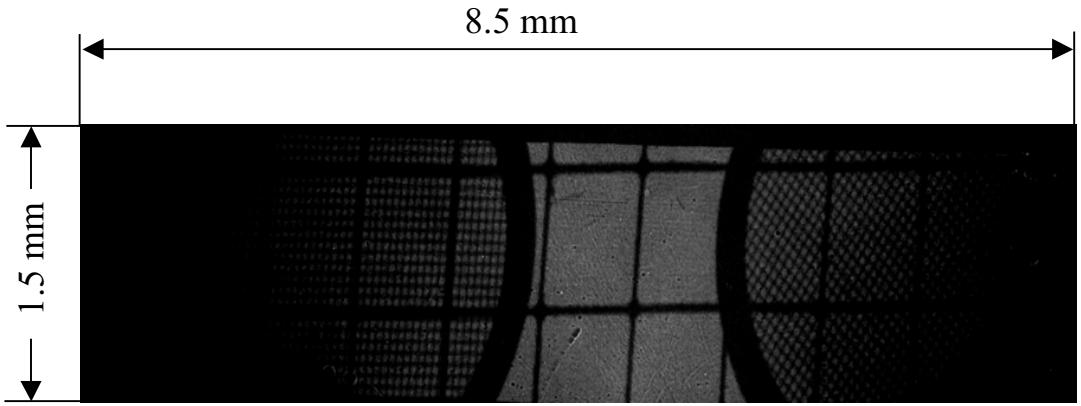

ENEA, Frascati, Italy
L'Aquila University, Italy

Transformed image

I II

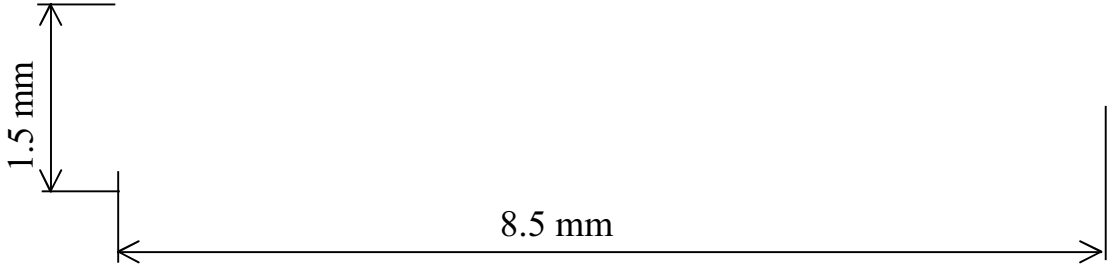

Magnification M ≈ 9.4x

I)

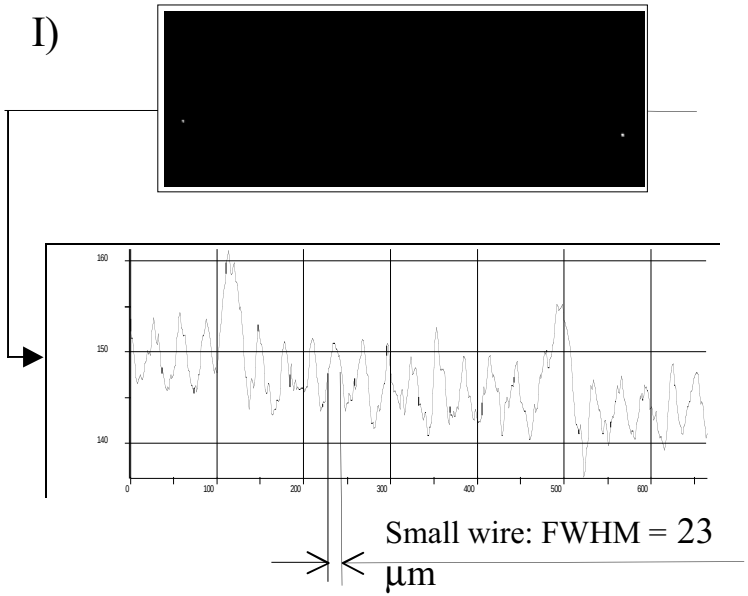

II)

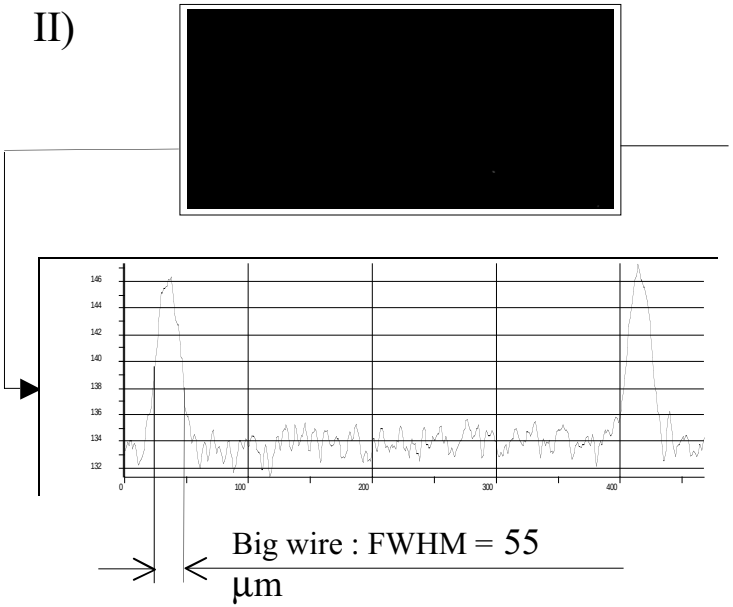

Monochromatic projection imaging with X-ray laser produced plasma source

Bragg angle Θ = 80.5°

Object was placed between crystal and tangential focus!

Mica, R = 150 mm Target: Cu

Source size - ~ 15 μm

Big grid: period 800 μm, wires 50±5 μm; small grids: period 60 μm, wires 14 μm

$\Delta\lambda/\lambda \approx 10^{-3}$

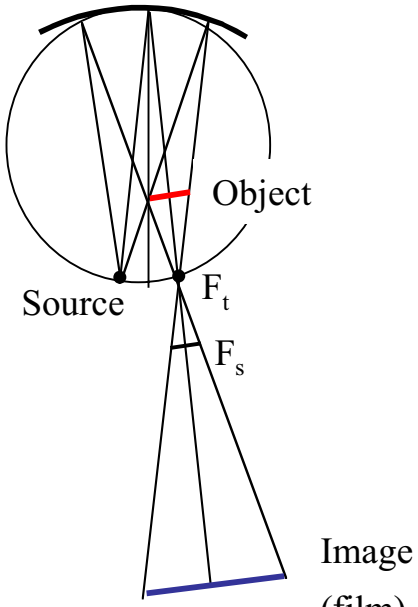

Transformed image Magnification M = 5.2x

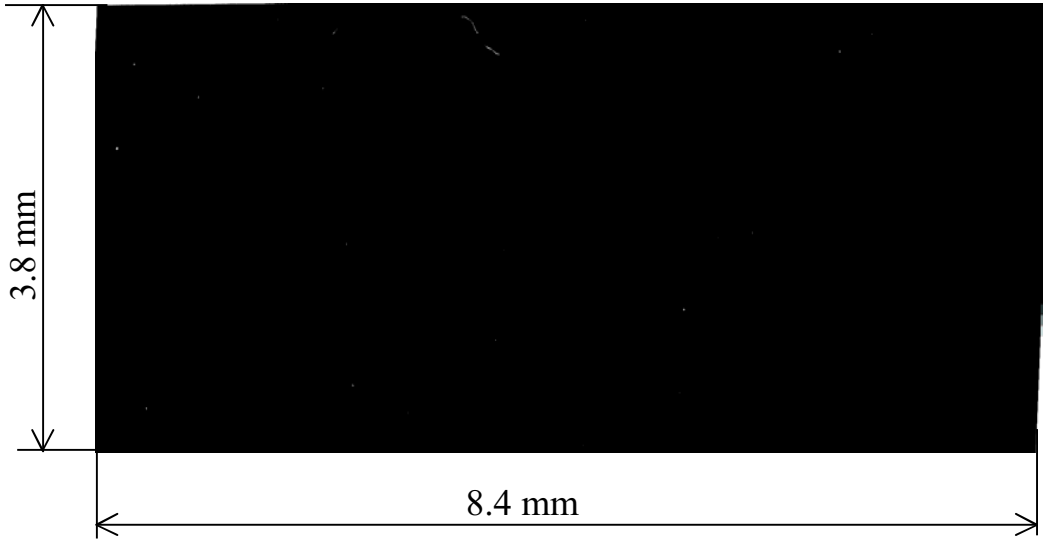

ENEA, Frascati, Italy
L'Aquila University, Italy

Monochromatic projection imaging with X-ray laser produced plasma source

Bragg angle $\Theta = 67.9°$

Object was placed between crystal and tangential focus

(Object and film oriented parallel to the crystal)

Mica, R = 150 mm Target: Cu

Source size - ~ 15 μm

Big grid: period 800 μm, wires 50±5 μm; small grids: period 60 μm, wires 14 μm

$\Delta\lambda/\lambda \approx 10^{-2}$

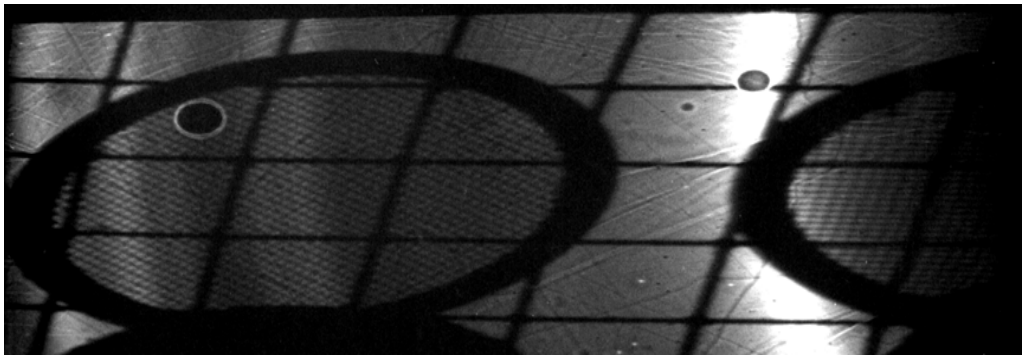

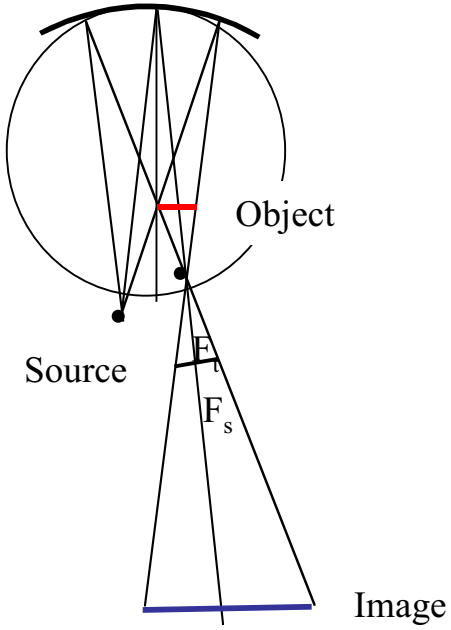

Transformed image Magnification M = 5.3x

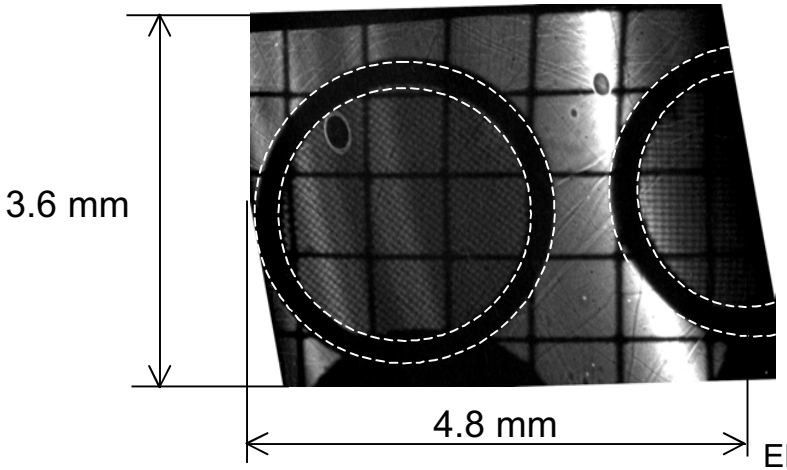

ENEA, Frascati, Italy
L'Aquila University, Italy

Ray-tracing simulation using **the SHADOW package**

Bragg angle Θ = 67.9°

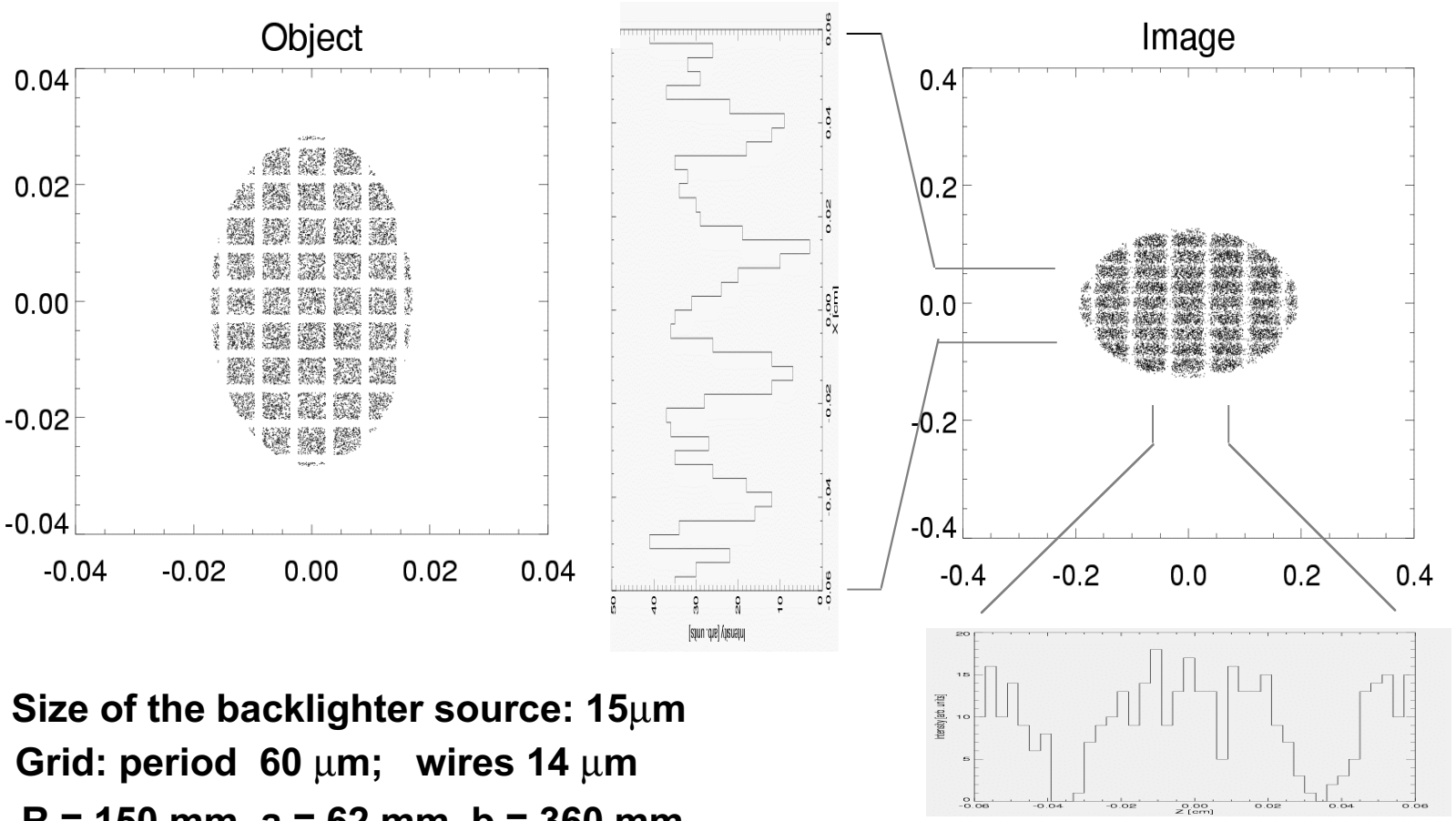

Size of the backlighter source: 15μm

Grid: period 60 μm; wires 14 μm

R = 150 mm, a = 62 mm, b = 360 mm

Magnification M = 5.3x

Focusing spectrometer with spatial resolution (FSSR)

FSSR-1D

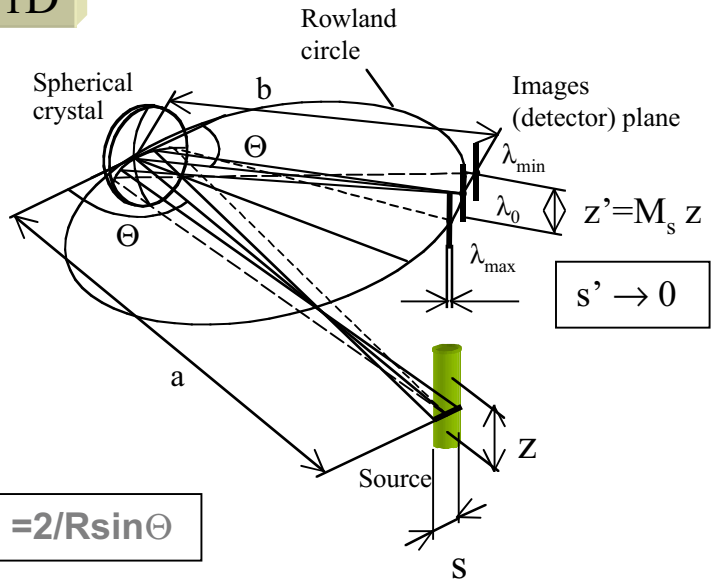

1/a + 1/b =2/RsinΘ

FSSR-2D

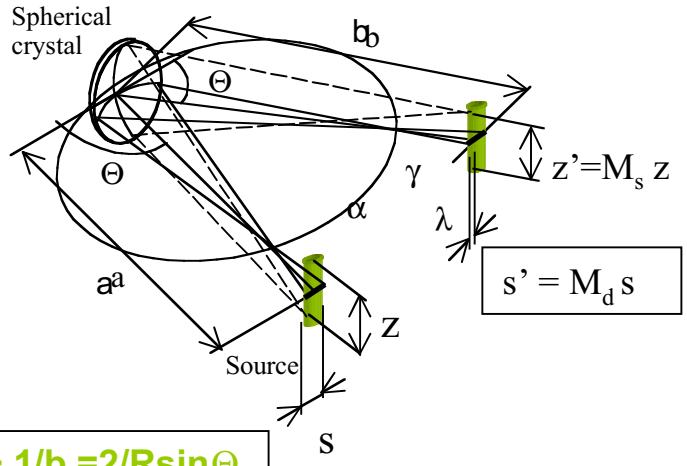

1/a + 1/b =2/RsinΘ

$$a = R\frac{\sin\Theta}{\cos 2\Theta}$$

$$b = R\sin\Theta$$

$$M_s = \cos 2\Theta$$

$$a = Rb / (2b\sin\Theta - R)$$

$$b = M_s\, a$$

$$M_d = \frac{R\left[a - \cos\Theta\left(2a\cos\Theta - R\right)\right]}{\left(R\cos\Theta - a\right)\left(2a - \cos\Theta - R\right)}$$

Observation of radiation properties of laser produced plasma under interaction with a solid obstacle

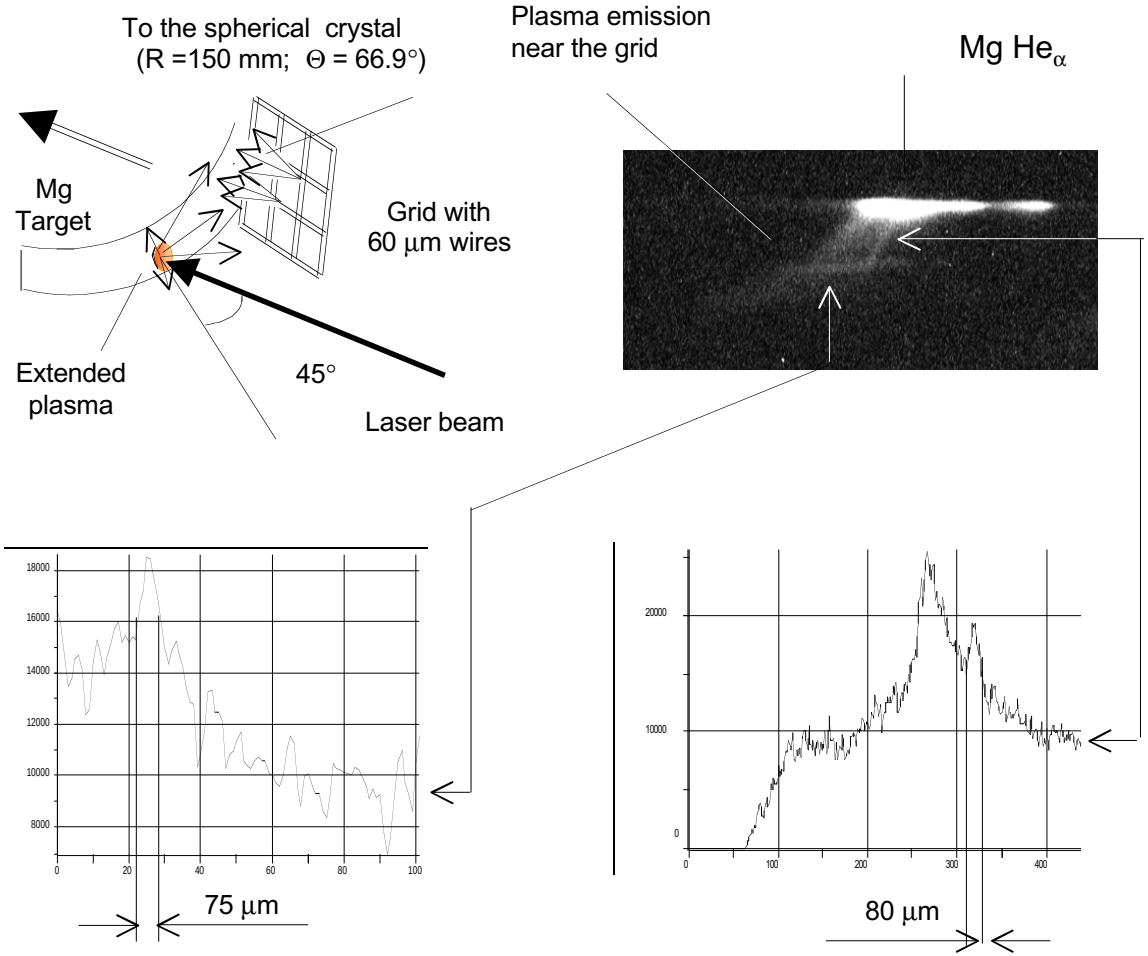

Ng:glass laser (λ = 1.06 μm, τ = 15 ns, E =5 J)

Tor Vergata University, Rome, Italy

Observation of radiation properties of laser produced plasma under interaction with solid screen

FSSR-2D

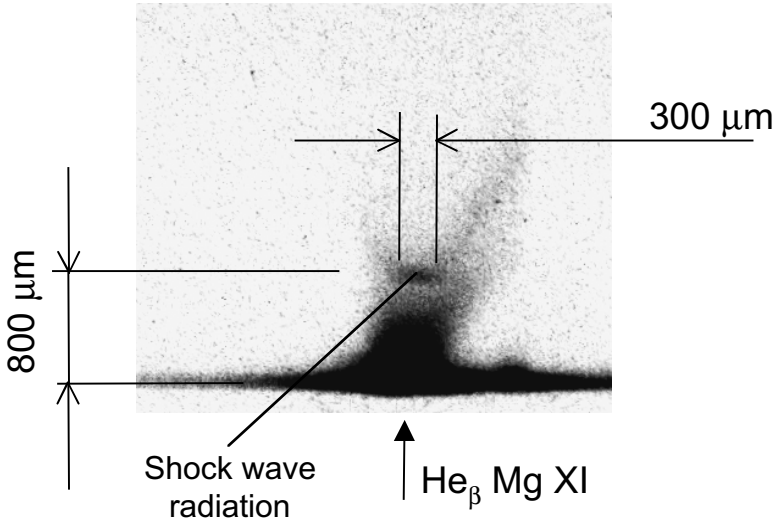

FSSR-1D

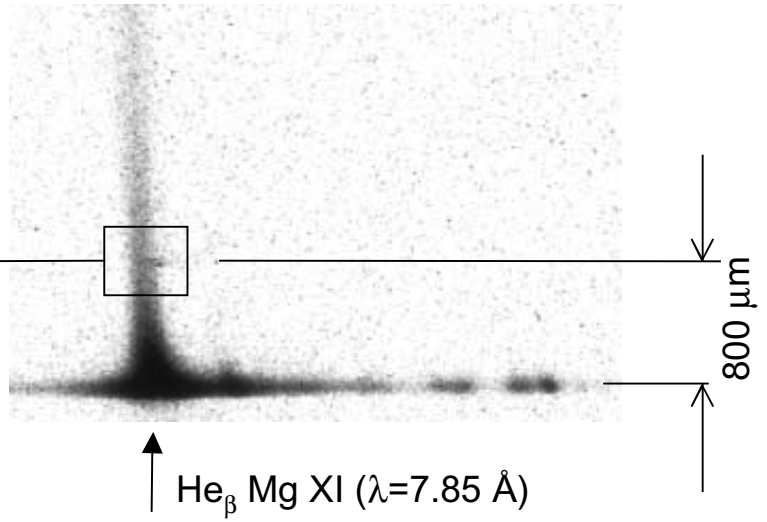

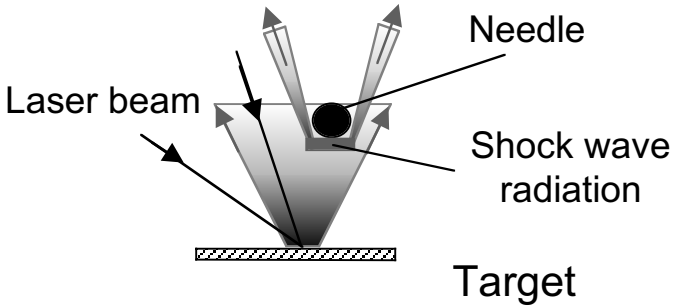

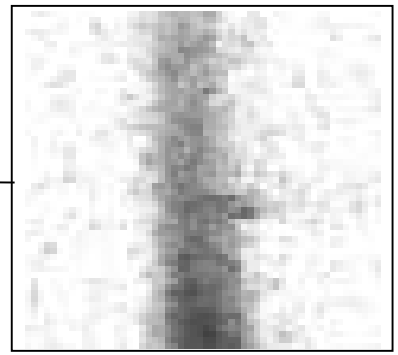

Ng:glass laser (λ = 1.06 μm, τ = 15 ns, E =5 J)

Tor Vergata University, Rome, Italy

Conclusions

New approaches of a spectrally tunable backlighting schemes with spherically bent crystal were considered:

- In a contrary to traditional backlighting scheme, in which investigated object should be placed between backlighter and crystal, for considered schemes the object is placed downstream of crystal before tangential or after sagittal focus and an image of the object is recorded at the distance from the object corresponded to the needed magnification;

- Magnification is defined by ratio of distances form sagittal focus to detector and from object to sagittal focus;

- Ray tracing modeling and experimental images of test meshes, obtained in the incidence angle of backlighter radiation 22° show the possibility to obtain spatial resolution comparable with the size of the backlighter;

- The spatial resolution around 10 μm in the field of view some mm^2 is achieved for spectral range around 9 A.

- It is demonstrated that at the angles of incident up to 22° a linear transformation of the obtained astigmatic images allows to reconstruct them with an accuracy (5 - 15)% .

It is demonstrated that spherically bent crystals could be used for X-ray imaging of a self emitting plasma structures with spatial resolution at least 50 μm in a field of view some square millimeters for angles of incident up to 22°.

X-ray microscopy of *Caenorhabditis elegans* nematode using a laser plasma pulsed x-ray source

G. Poletti[a], F. Orsini[a], J. Ullschmied[b], J. Skala[b], B. Kralikova[b], M. Pfeifer[b], C. Kadlec[b], T. Mocek[b], A. Pr g[b], F. Cotelli[c], C. Lora Lamia[c], D. Batani[d], A. Bernardinello[d], T. Desai[d], A. Zullini[e]

[a]Istituto di Fisiologia Generale e Chimica Biologica and INFM, Universit di Milano, Italy

[b]PALS Research Centre, Prague, Czech Republic

[c]Dipartimento di Biologia, Universit di Milano, Italy

[d]Dipartimento di Fisica and INFM, Universit di Milano-Bicocca, Italy

[e]Dipartimento di Biotecnologie e Bioscienze, Universit di Milano-Bicocca, Italy

Abstract

An experiment on Soft X-ray Contact Microscopy (SXCM) performed on *Caenorhabditis elegans* nematodes is discussed. This sample has been selected since it is a well studied case used as model in many biological contexts. The experiment has been performed using the iodine PALS laser source to generate pulsed soft X-rays from laser-plasma interaction, using Teflon, molybdenum and gold as targets. Typical intensities on the targets exceeded 10^{14} W/cm^2. The SXCM imprints have been recorded on Polymethilmetacrylate (PMMA) photo resists which have been chemically developed and analyzed with an Atomic Force Microscope (AFM) operating in constant force mode. The use of error signal AFM images together with topography AFM images, did allow an easier recognition of biological patterns, and the identification of observed structures with internal organs. Several organs were identified in the SXCM images, including cuticle annuli, alae, pharynx, and three different types of cell nuclei. These are the first SXCM images of multi-cellular complex organisms.

Introduction

An intense laser beam focused on a solid target produces a micro size hot dense plasma over a duration comparable to the laser pulse. Such plasmas can be used as a source for Soft X-ray Contact Microscopy (SXCM) of living biological specimens in their living environment.

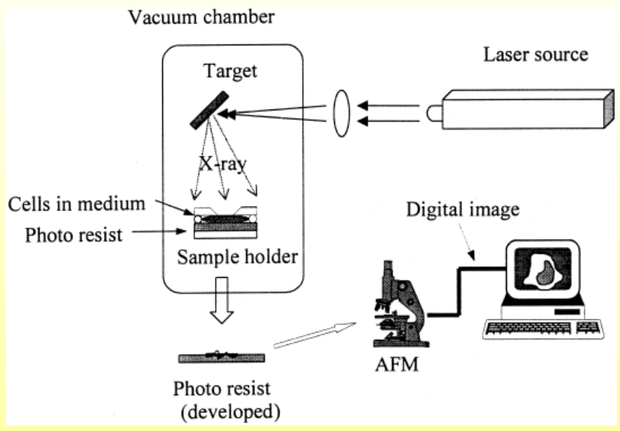

In the sample holder, a droplet of water containing the biological specimens is sandwiched between a silicon nitride window and a photo resist (PMMA). X-rays, in the water window spectral range, are incident on the silicon nitride window, transparent to X-radiation, and are absorbed by the sample. An image based on natural contrast, since biological structures absorb more than the surrounding water is produced. The chemical development of the photo resist gives rise to a profile of the sample that is analysed by means of AFM.

The goal of the present work was to explore the potentialities of SXCM to study multi-cellular organisms. To this aim, the well biologically characterized *Caenorhabditis elegans* nematode has been chosen.

It is the first time that small (semi-microscopic) but complex multi-cellular samples are studied by means of SXCM.

Experiments

Experiments were performed using the PALS Iodine laser system in Prague which emits 1.314 µm radiation in fundamental.

Laser pulse duration was ~ 400 ps.

The maximum optical energy in a single beam was 600 J and the beam diameter at the entrance of the plasma chamber was ~ 290 mm.

Laser radiation was focused on the target surface using a f = 600 mm focusing lens and the intensity was varied in the range ~ 10^{14} — $10^{?}$ W/cm^2.

The interaction chamber was evacuated to better than 10^{-4} mbars.

Three types of planar solid targets were used to produce X-rays: Teflon, molybdenum and gold.

Results

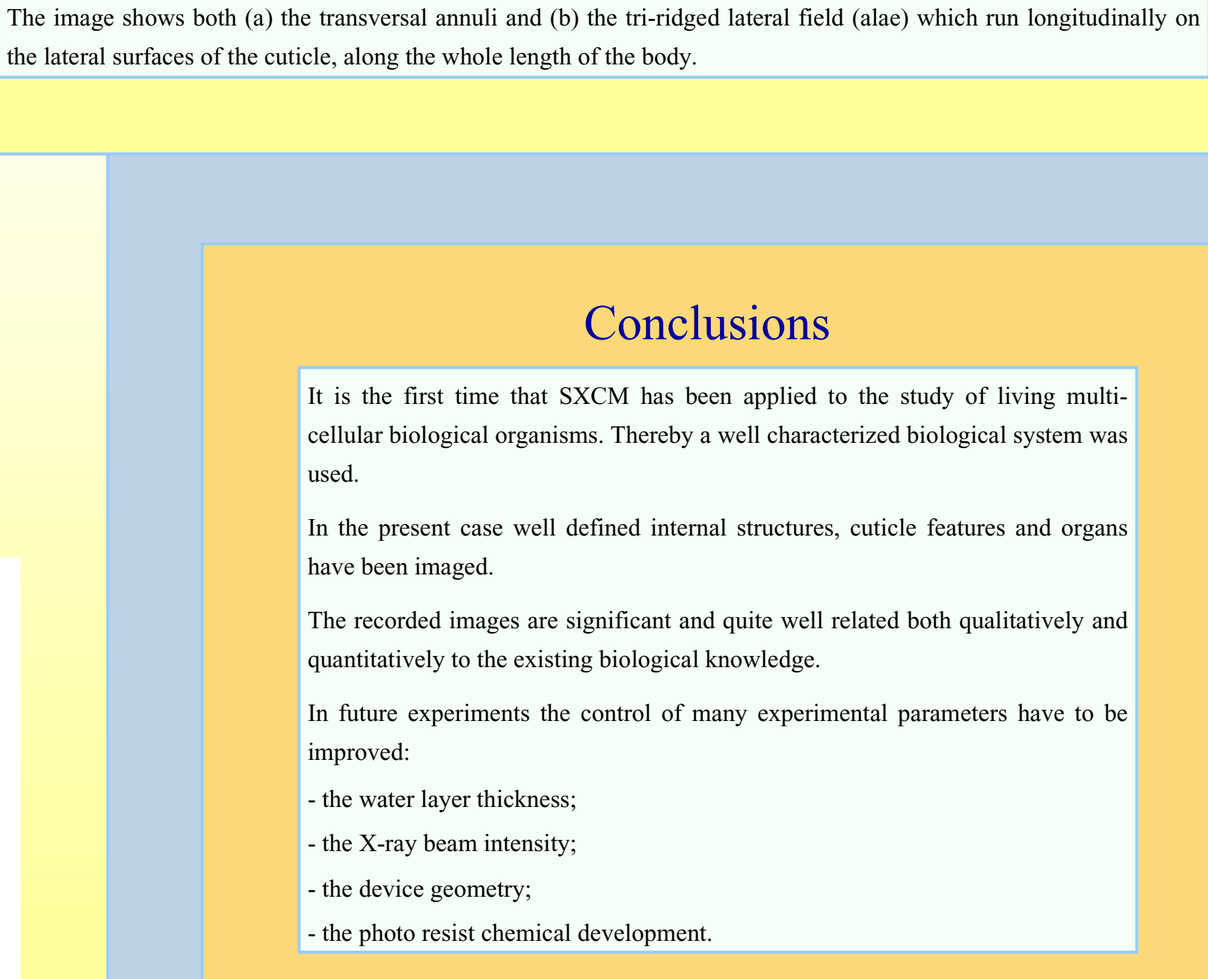

Reconstruction of a SXCM imprint on a PMMA photo resist of a *Caenorhabditis elegans* nematode obtained combining 72 error signal AFM images. Each single AFM image has a scan area of 20x20 µm^2 (see insert). The nematode length is 500 µm approximately.

The image shows both (a) the transversal annuli and (b) the tri-ridged lateral field (alae) which run longitudinally on the lateral surfaces of the cuticle, along the whole length of the body.

Results

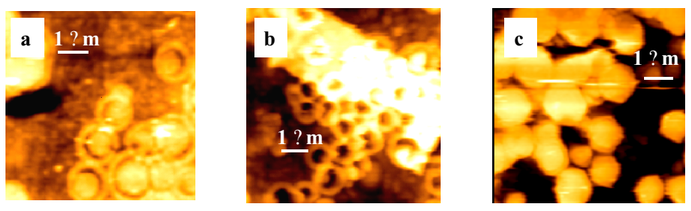

6x6 µm^2 topography AFM images of a SXCM imprint on a PMMA photo resist of a *Caenorhabditis elegans* nematode. Nuclei of three different cell types have been individuated:

(a) hypodermal and gut nuclei, round with a large, prominent nucleolus;

(b) neuronal nuclei, smaller, round and without prominent nucleoli;

(c) muscle nuclei, oblong and less regular.

a) The image shows two distinct oval structures in relief whose dimensions and position prove that the pharyngeal metacorpus and terminal bulb of the nematode pharynx have been imaged.

b) The image shows three small semicircular protrusions similar in shape to the six lips that symmetrically surround the buccal cavity of the nematode.

c) The image shows a well defined relief separating two areas having well different roughness.

d) The image shows regularly repeating bands giving rise to a structural periodicity ranging from 700 to 900 nm depending on bending of the body worm. Its interpretation is still in discussion.

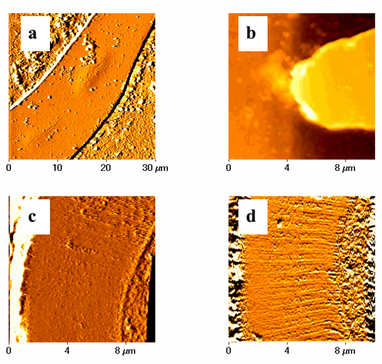

Conclusions

It is the first time that SXCM has been applied to the study of living multi-cellular biological organisms. Thereby a well characterized biological system was used.

In the present case well defined internal structures, cuticle features and organs have been imaged.

The recorded images are significant and quite well related both qualitatively and quantitatively to the existing biological knowledge.

In future experiments the control of many experimental parameters have to be improved:

- the water layer thickness;
- the X-ray beam intensity;
- the device geometry;
- the photo resist chemical development.

A 46.9nm tabletop soft x-ray laser: characterization and applications

University of L'Aquila

A. Ritucci[1], G. Tomassetti[1], A. Reale[1], L. Palladino[1], L. Reale[1], G. Baldacchini[2], F. Bonfigli[2], F. Flora[2], L. Mezi[2], R. M. Montereali[2], S.V. Kukhlevsky[3], J. Kaiser[4], A. Faenov[5], T. Pikuz[5]

[1] *Phys. Dept. Univ. of L'Aquila, gc LNGS of INFN, INFM, 67010 Coppito, L'Aquila, Italy*
[2] *Department of Experimental Physics, University of Pécs, Ifjúság ú. 6, Pécs, 7624, Hungary*
[3] *ENEA Dip. Innov., Div. Fisica Applicata, C R E Frascati C.P. 65, 00044, Italy*
[4] *Institute of Phys. Eng. Brno Univ. of Techn., Technická 2, 616 69 Brno, Czech Republic*
[5] *MISDC of VNIIFTRI, Mendeleevo, Moscow Region, 141570, Russia*

Abstract. Capillary discharges represent a powerful tool for soft x-ray laser development in tabletop devices. The technique is based on the Z-pinch compression of a gas medium initially filling a capillary channel, driven by high and fast current pulse. The effective use of such scheme for soft x-ray laser pumping, dates back to 1994 when the first experimental evidence of amplification was obtained in Ne-like Ar at 46.9nm by Rocca et al [1]. In spite of the effective results reported by the group of Rocca [2-3] on the 46.9nm laser, this laser is still susceptible of further improvements. The long duration of the laser gain into the slow moving discharge plasma column, and the surprisingly stable z-pinch compression should allow further increase of the plasma column length and a more efficient extraction of laser energy. In this report we present the recent results, which regard the improvements and the applications of a 46.9nm discharge laser realized at University of L'Aquila [4].

Experimental device

Laser chamber

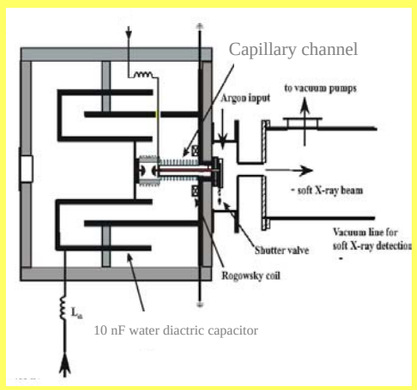

The active medium is created by discharging a water dielectric capacitor through a 3mm in diameter alumina capillary channel initially filled with Ar the pressure of 0.25–0.5Torr. The capacitor is initially charged to high voltage by a six stage Marx generator. A preionization current of 20A precedes the main discharge having value between 17 and 30kA.

Laser pulse

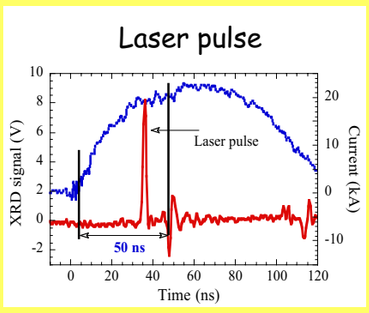

The strong laser emission at 46.9nm, which is strongly dominating on the spontaneous emission, is produced at about 30ns from the current on set.

Soft x-ray laser amplification into a discharge plasma waveguide

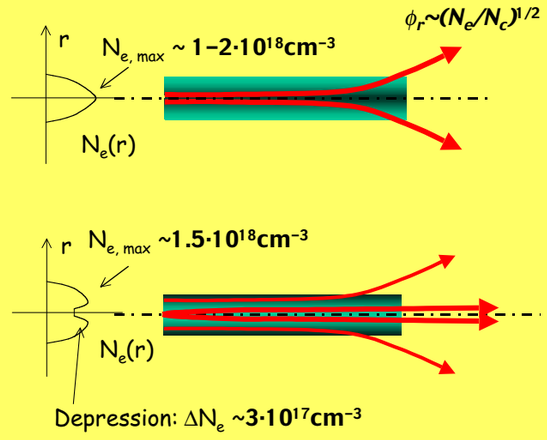

Far field

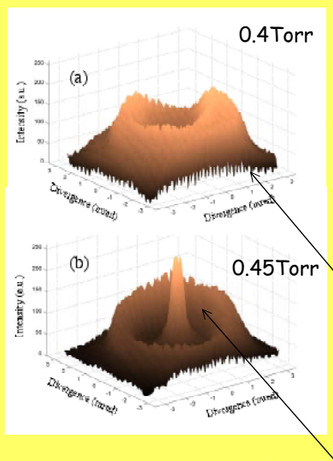

Near field

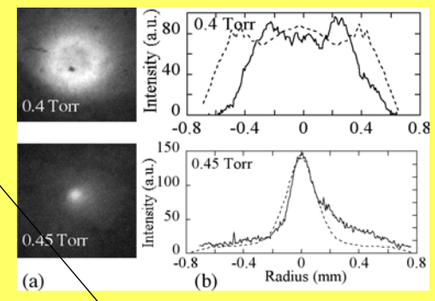

$B_p \approx 10^{24}$ ph/s mm² mrad² in 0.01 % bw

At the low pressures (typically lower than 0.45Torr), the intensity distribution with large (4–5mrad) annular profile is found. At higher pressures (P>0.45Torr) the laser beam undergoes to a dramatic reduction of its divergence. A high-intensity and low divergent axially peaked structure with a sub-milliradiant divergence emerges over the annular distribution. The plasma elongation improves the divergence of this component to 0.6mrad. Considering the plasma diameter of 200μm and the capillaries of the 45cm, the central component of the beam is about three times the diffraction limit. The presence of the low-divergent high-intensity component is peculiar of our excitation conditions [5], Theoretical analysis: different distributions of the electron density have been taken into account into a two-dimensional ray-tracing code. The gain was assumed to have a spatial distribution with parabolic profile, with an on-axis value of 0.7cm⁻¹. We find that, the highly collimated central-peak is produced by the refraction index plasma-waveguiding of the laser radiation provided by an electron density distribution with depression on-axis.

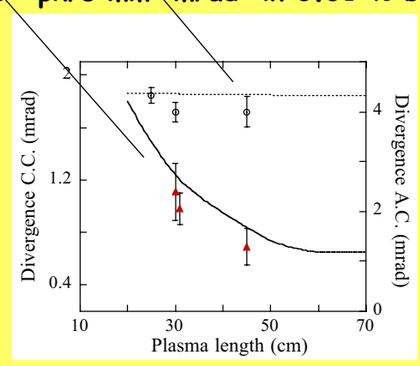

Beam saturation up to 45cm long plasma columns

Energy extraction

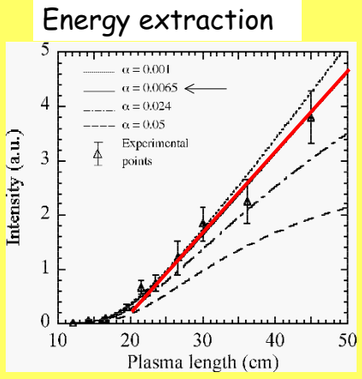

Pulse duration

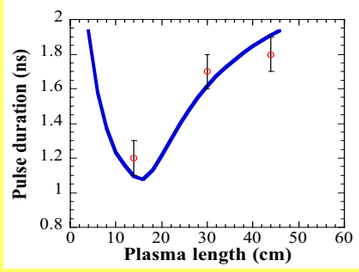

Coherence length at 2m from capilalry output

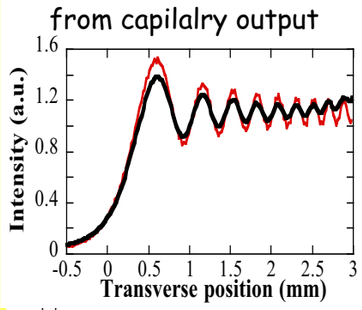

Laser pulse stability

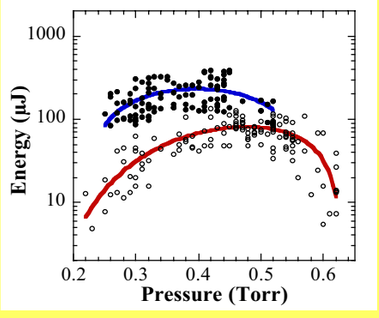

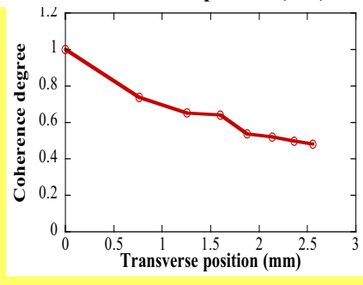

Surprisingly stable plasma columns with apect ration (L/D) exceeding 1000 have been generated up to the length of 45cm. The increase of the plasma length has leaded to the increase of the output pulse intensity up to $I_{out} \approx 8 \cdot 10^8$ W/cm², which is 20 times the saturation intensity ($I_{sat} \approx 4 \cdot 10^7$ W/cm²), and to the output energy of E_{out}=300μJ. The gain duration at FWHM, estimated of about 3ns, should allow further increase of the plasmacolumn length and the laser intensity. The rate of increase of the laser intensity is of a factor 2 each 10cm and should lead the achievement of millijoule level energy at 60cm. The stability of the laser emission is not affected by the increase of the plasma length. Laser pulses where produced at the pulse repetition rate of 0.2Hz.

Application: characterization of a high resolution x-ray sensitive detector based on Color Center excitation in LiF films

Formation of CCs

Color Center (CCs) can be formed by XUV irradiation using bright source emission (CCs are very stable at room temperature)

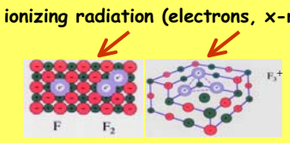

Fluorescence emission excited by blue ligth pumping

Blue ligth pumping :~ 450 nm

Ligth emission: 541, 678nm

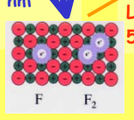

Fluorescence spectra of a CCs in LiF

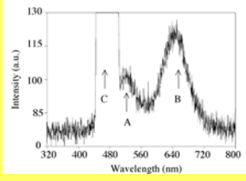

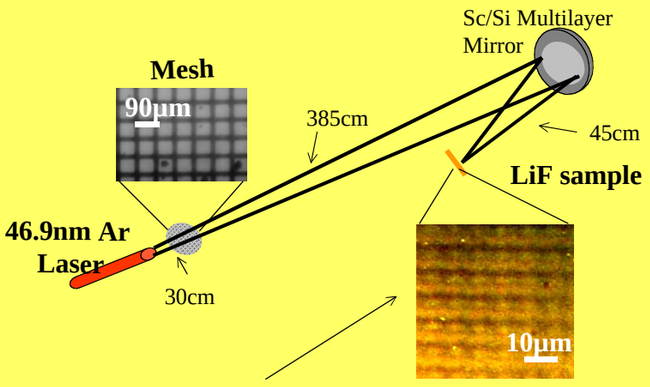

Irradiation requirements
- Minimum energy fluence required: 0.1 mJ/cm²;
- Dinamic range ≈ 1000; in the range 1 mJ/cm²–1 J/cm² the F center density is proportional to ~ K (D)$^{1/2}$;
- Efficiency of CCs production strongly increases with the dose rate.

Printed pattern are observed by optical microscope in fluorescence mode;
The resolution is determined by the readout process (< 1 micron).

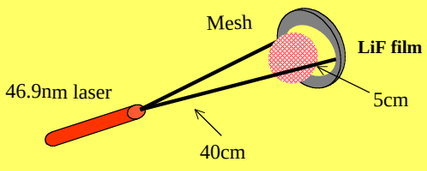

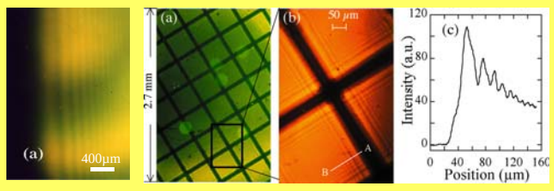

[1] J.J. Rocca, V. Shlyaptsev, F.G. Tomasel, O.D. Cortàzar, D. Hartshorn, and J.L.A. Chilla, Phys. Rev. Lett. **73** (1994) 2192.
[2] J.J. Rocca, Rev. Sci. Intrum., **70** (1999) 3799.
[3] B. R. Benware, C. D. Macchietto, C. H. Moreno, and J. J. Rocca, Phys. Rev. Lett. **81** (1998), 5804.
[4] G. Tomassetti, A. Ritucci, A. Reale, L. Palladino, L. Reale, S.V. Kukhlevsky, F. Flora, L. Mezi, J. Kaiser, A. Faenov and T. Pikuz, Eur. Phys. J. D **19** (2002) 73-77.
[5] A. Ritucci, G. Tomassetti, A. Reale, L. Palladino, L. Reale, F. Flora, L. Mezi, S.V. Kukhlevsky, A. Faenov, T. Pikuz, J. Kaiser, Europhys. Lett., **63**, 2003, 694.
[6] G. Tomassetti, A. Ritucci, A. Reale, L. Palladino, L. Reale, L. Arrizza, G. Baldacchini, F. Bonfigli, F. Flora, L. Mezi, R.M. Montereali, S.V. Kukhlevsky, A. Faenov, T. Pikuz, J. Kaiser, *Europhys. Lett.*, **63**, 681-686, 2003.

Simulations of the Phonon-Bragg Switch in GaAs

J.M.H.Sheppard[1], P.Sondhauss[2], R.Merlin[3], P.Bucksbaum[3], R.W.Lee[4], J.S.Wark[1]

[1]Department of Physics, Clarendon Laboratory, University of Oxford, Parks Road, Oxford, OX1 3PU, UK.
[2]MAX-lab, Lund University, Box 118, 22100 Lund , Sweden
[3]Department of Physics, The University of Michigan, Ann Arbor, MI 48109-1120, USA
[4]LLNL, P.O.Box 808 Livermore, CA 94551

1. Introduction

It has recently been suggested that X-rays can be switched on sub-picosecond time-scales by using laser generated coherent optical phonons: the so-called Phonon-Bragg switch[a].

Here we take the first step in investigating this proposal in detail by investigating perturbative solutions of the dynamical diffraction equations for diiffraction from the (004) planes of GaAs in the presence of a constant phonon field.

It has already been shown that such a phonon field can be switched on and off within half a phonon period by optical excitation and de-excitation of the crystal lattice[b]. Such switching generates two counter propagating phonons. Initially we will deal with a simplified case, involving only a single phonon.

The next pane shows the Laue condition for diffraction from the planes associated with $\mathbf{G_h}$ in the presence of a phonon with wavevector $\mathbf{q}$. The magnitude of $\mathbf{q}$ here is grossly exaggerated as the actual ratio of $\mathbf{G_h}$ to $\mathbf{q}$ in this case is ~ 10^4.

2. Modified Laue Condition

k - Incoming and outgoing X-ray wavevectors

G_h - Reciprocal lattice vector for planes with Miller indicies denoted by h

q - Phonon wavevector

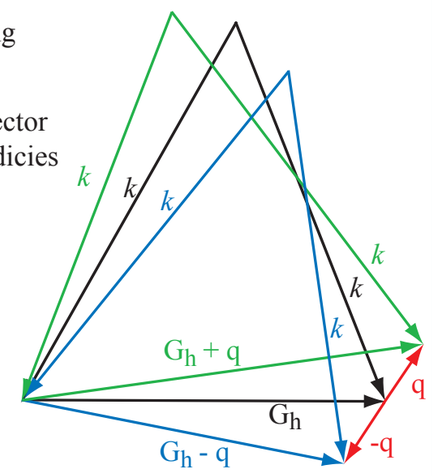

3. Single Phonon Solution

The generalised Takagi-Taupin equation[c] for $\mathbf{D'}_h$, the electric displacement, and given an electric susceptibility, χ'_h is given by

$$2i(\mathbf{k}_h.\nabla)\mathbf{D}'_h + k^2\frac{2i}{\omega}\frac{\partial \mathbf{D}'_h}{\partial t} + (k_h^2 - k^2)\mathbf{D}'_h = k_h^2\sum_l \chi'_{h-l}\mathbf{D}'_{l[h]}$$

where $\mathbf{D}'_h(\mathbf{r},t) \equiv \sum_{N=1}^{M}\mathbf{D}_{Nh}\exp(i.\mathbf{G}_h.\mathbf{u}_N)$ $\quad \chi'_h \equiv \sum_{N=1}^{M}\chi_{Nh}\exp[i\mathbf{G}_h.(\mathbf{r}_N+\mathbf{u}_N)]$

with the Nth atom in a unit cell displaced by

$$\mathbf{u}_N = \mathbf{p}_N\cos(\Omega t - \mathbf{q}.\mathbf{r}) \qquad N = 1,\ldots, M$$

Given a general phonon and a unit cell containing M atoms, for small $\mathbf{p}_N$,

$$\chi'_h = \chi_h + \delta\chi_h\cos(\Omega t - \mathbf{q}.\mathbf{r}) \qquad \mathbf{D}'_h = \mathbf{D}_h^{(p)} + \delta\mathbf{D}'_h$$

Substituting these expressions into the generalised Takagi-Taupin equation and with the ansatz

$$D_h(\mathbf{r},t) = D_h^{(p)} + d_h^+\exp[i(\Omega t - \mathbf{q}.\mathbf{r})] + d_h^-\exp[-i(\Omega t - \mathbf{q}.\mathbf{r})]$$

we obtain an algebraic expression for $d_h^{\pm}$ that depends on the phonon, X-ray and crystal parameters.

4. Integrated Intensity Profile

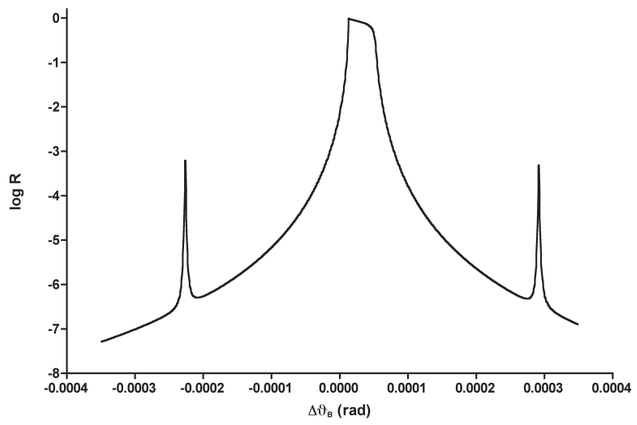

This graph shows $|D_h|$ for the (004) reflection of polarised X-rays at 1.54 Angstroms in GaAs with an 8.12 THz phonon of spatial frequency 1.8$\times10^7$ rad m^{-1} and a mean atomic displacement amplituide of 0.96 Angstroms. Here $\mathbf{q}$ is parallel to $\mathbf{G}_h$.

5. Bragg Switch Geometry

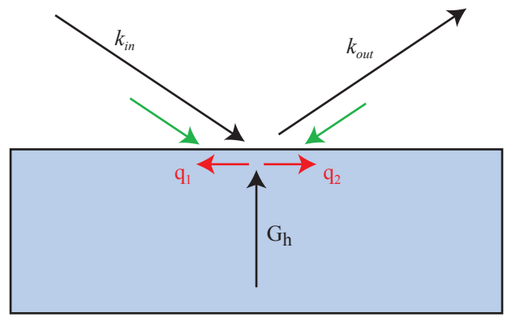

The green arrows correspond to the laser pulse used to excite the phonons by means of scattering of photons from one pulse to the other. The phonons can then be switched off by a similar pair of pulses delayed by half a phonon period using an optical delay line[b].

This gives a switch duration of ~100fs for 8.12THz phonons in GaAs. Smaller switch durations could be achieved in materials with higher phonon frequencies.

6. Two Phonon Solution

The optical excitation of the phonons in the proposed Bragg Switch geometry leads to two counter propagating phonons of the same frequency. This sets up a standing wave field in the crystal. As the equations for D_h are linear the resulting X-ray amplitude is a superposition of amplitudes from the two phonon modes.

$$D_h(\mathbf{r},t) = D_h^{(p)} + d_h^+\exp[i(\Omega t - \mathbf{q}.\mathbf{r})] + d_h^-\exp[-i(\Omega t - \mathbf{q}.\mathbf{r})] + \bar{d}_h^+\exp[i(\Omega t + \mathbf{q}.\mathbf{r})] + \bar{d}_h^-\exp[-i(\Omega t + \mathbf{q}.\mathbf{r})]$$

where the d_h are barred as they are not invariant under reversal of $\mathbf{q}$.

We can collect these terms to give amplitudes corresponding to three plane waves. One propagating in the normal diffraction direction and another two displaced by ± $\mathbf{q}$.

The far field intensity in each direction will be given by the separate squared moduli of these amplitudes.

7. Far Field Satellite Intensity

This figure shows a section of the rocking curve off to one side of the main peak for phonons in the Bragg switch geometry. The two separate peaks are due to the two counter propagating phonons. They are at slightly different angles due to their differing Doppler shifts.

There are another two peaks on the other side of the main peak corresponding to scattering from the two phonons in the opposite direction.

The peaks are modulated in time at twice the phonon frequency (Ω = 8.12 THz).

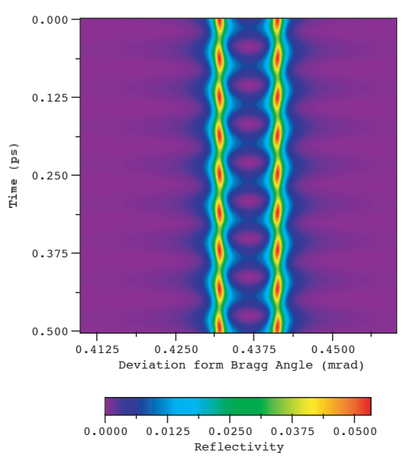

8. Effect of Phonon Amplitude

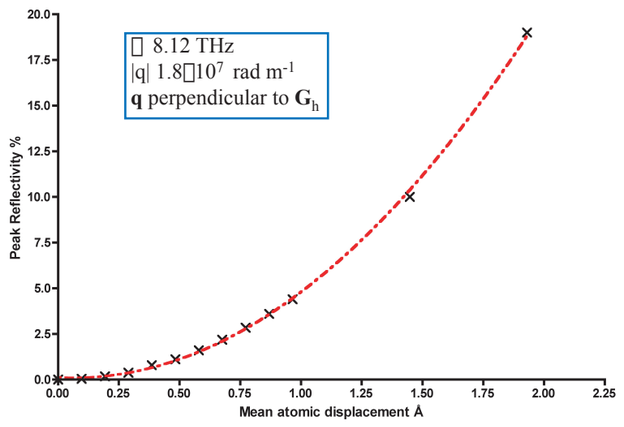

As is expected the peak reflectivity increases as the square of phonon amplitude. As can be seen, for reflectivities of more than a few percent very large amplitudes are required. Total reflectivity will obviously depend on the angular divergence of the incoming X-rays.

9. Effect of Phonon Wavevector

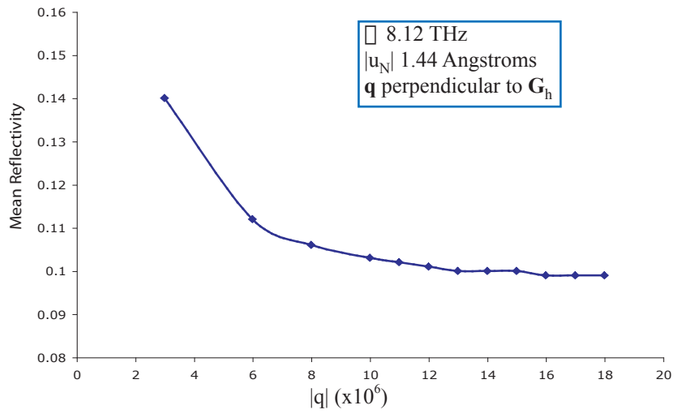

Reflectivity increases as $|\mathbf{q}|$ decreases due to the $\mathbf{q}$ dependence of $d_h^{\pm}$. This would seem to allow almost unlimited reflectivity in the satellites. However, the perturbative approach becomes less valid at small $\mathbf{q}$ as the satellites are less well separated from the main peak.

10. Double Crystal Monochromator

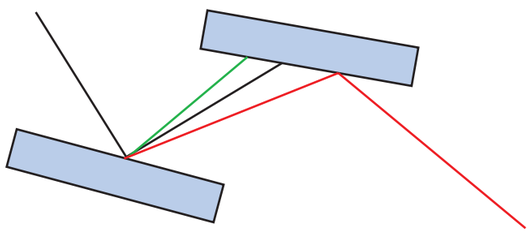

One possible way of separating the switched satellites from the main peak is to incorporate the Bragg Switch into a double crystal monochromator.

Here the first crystal acts as the switch. The second is misaligned with respect to the first so that only the red ray, corresponding to one set of satellites, lies within its Darwin width. This is easily accomplished as it has already been shown that the satellite peaks are several times narrower in angle than the main Bragg peak.

As the peak reflectivity of GaAs (004) is nearly 100% this configuration introduces little additional loss of X-ray energy.

11. Conclusion

We have shown that the Phonon-Bragg switch may be a viable method of switching X-rays on very short time scales.

With realistic phonon amplitudes, peak reflectivities of a few percent may be achieved in the geometry described. These reflectivities may be enhanced by utilising different materials or different lattice planes.

Preliminary simulations indicate that use of asymmetric reflection geometry will not serve to enhance satellite reflectivity and in general causes a slight decrease in reflected intensity.

Further work will employ fully time dependent simulations and also a time dependent phonon amplitude so that the actual switching process itself can be modelled. Numerical methods of solution will also be used to properly model satellite reflectivity at smaller values of |q|.

12. References

[a] P. H. Bucksbaum and R. Merlin, Sol. Stat. Comm. 111 (1999) 535-539

[b] M. Hase, K Mizoguchi, H. Harima, S. Nakashima, M. Tani, K. Sakai, M. Hangyo, Appl. Phys. Lett. 69 (1996) 2474.

[c] P. Sondhauss and J. S. Wark, Acta. Cryst. (2003) A59, 7-13.

Introduction to *New Light Source I* & the Simulation of a Thomson Scattering X-ray Source

Bing Xia

Dep. Engineering Physics, Tsinghua University, Beijing 100084, China P. R.

Collaborators

- Zheng Li, Kejun Kang, Wenhui Huang, Gang Huang, Xiaozhong He, Mingchao Shao, Chuanxiang Tang

  ——Dep. Engineering Physics, Tsinghua University, Beijing 100084, China P. R.

Thomson scattering x-ray source

- Ultrashort x-ray pulse through Thomson scattering
  - Ultrashort pulse
  - Low emittance
  - High peak brightness
  - Quasi monochromatic
  - Tunable parameters

X-ray Source Based on Thomson Scattering

- X-ray energy

$$E_x \approx \frac{2\gamma^2}{1+\gamma^2\theta_x^2}(1-\cos\alpha)E_L$$

- Differential cross-section

$$\frac{d\Sigma}{d\Omega} = \frac{r_0^2}{2}\frac{(1+\beta^2)(1+\cos^2\theta_x)-4\beta\cos\theta_x}{\gamma^2(1-\beta\cos\theta_x)^4}$$

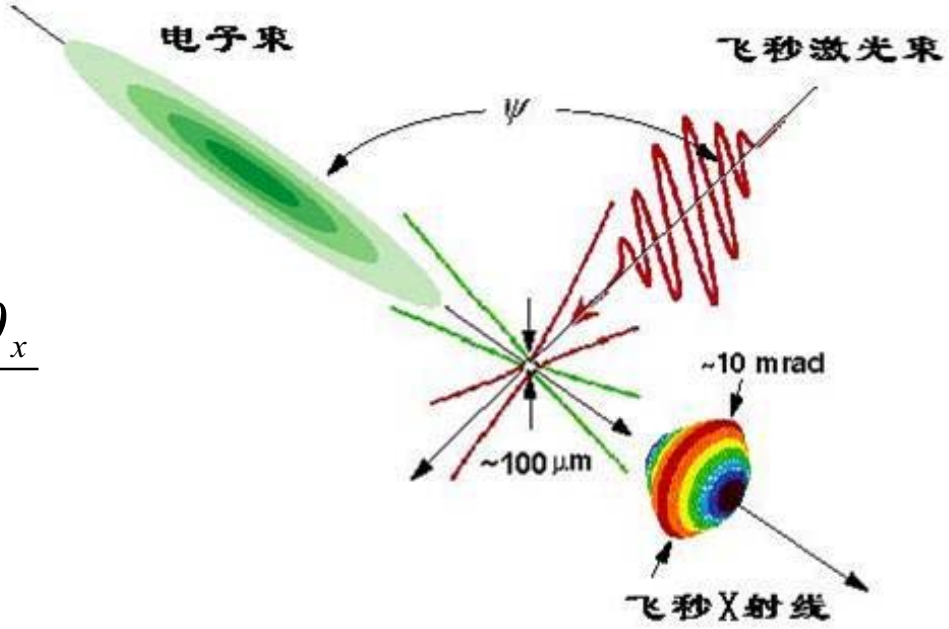

- X-ray yield

$$n_x = C_{off}\frac{n_e n_l}{\sqrt{2\pi}}\Sigma\frac{1}{\sqrt{(\sigma_{ey}^2+\sigma_{ly}^2)[(1-\cos\alpha)(\sigma_{ex}^2+\sigma_{lx}^2)+(1+\cos\alpha)(\sigma_{ez}^2+\sigma_{lz}^2)]}}$$ [1]

Energy and angular distribution

- It means that photons are emitted in a narrow cone and quasi-monochromatic [2]

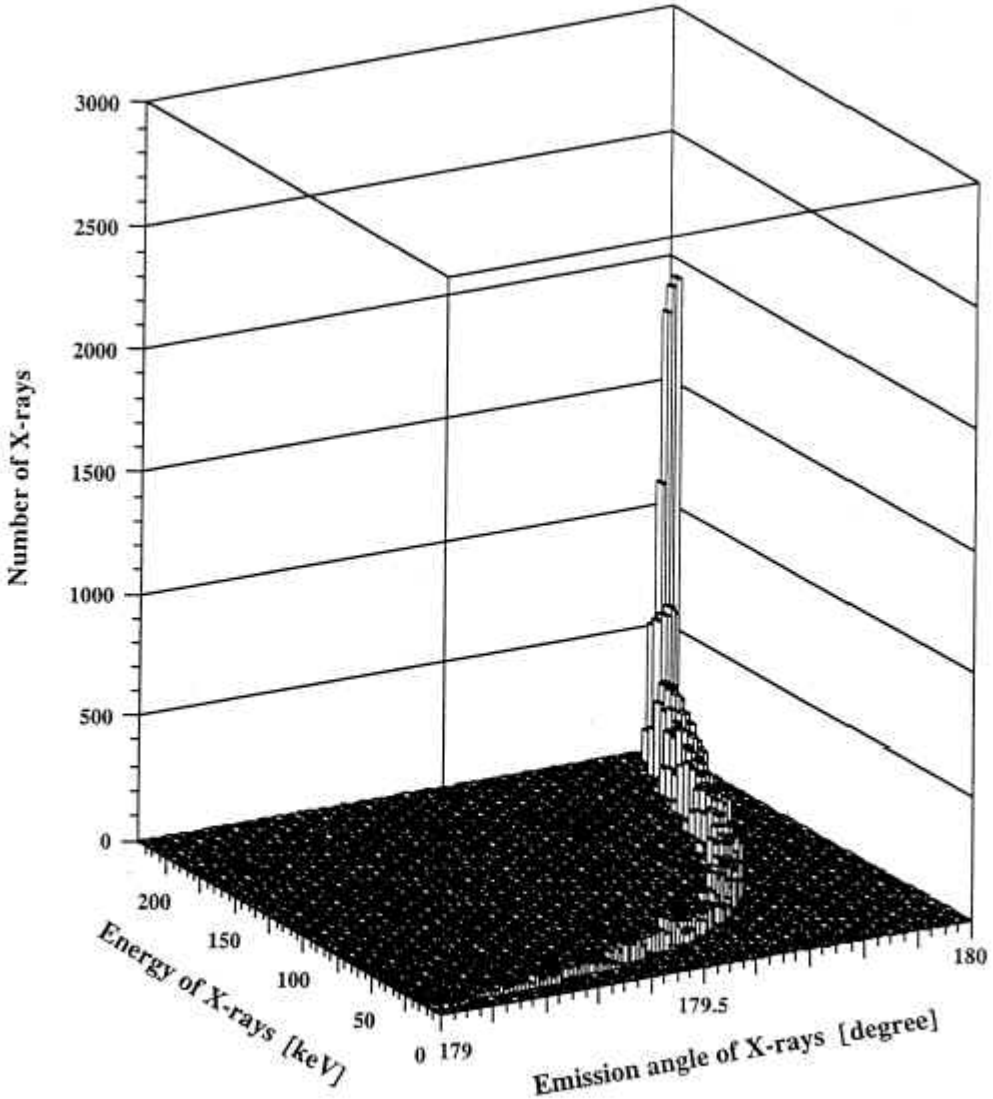

Fig. 10. Energy and angular distributions of the X-rays produced by the Thomson scattering under the linear interaction. The t
number of X-rays is 4.7×10^7.

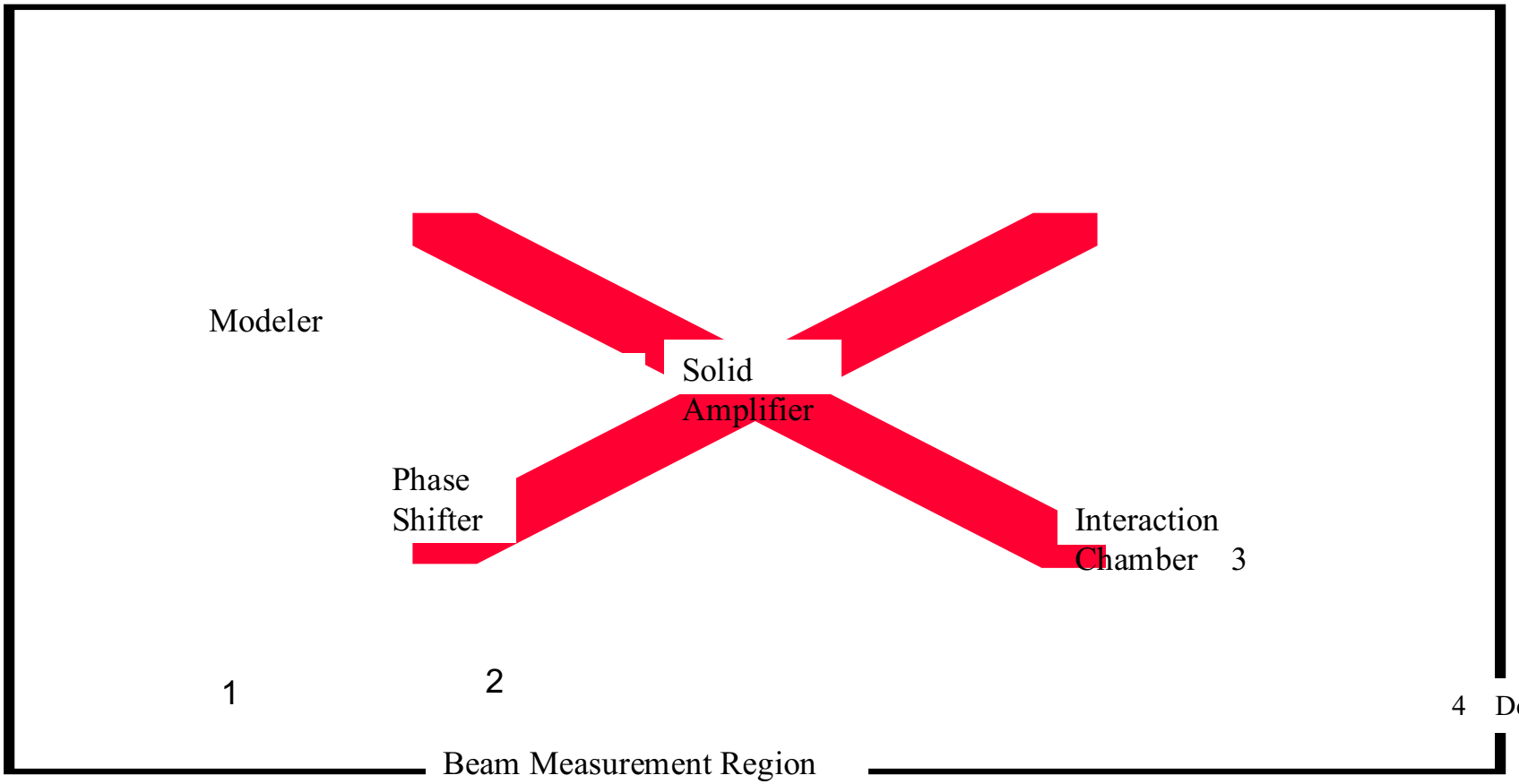

- *New Light Source I* is a proposed high-brightness x-ray facility based on Thomson scattering.
- Its key components are T^3 laser and LINAC with RF electron gun[3]

Arrangement of the real facility of *New Light Source I*

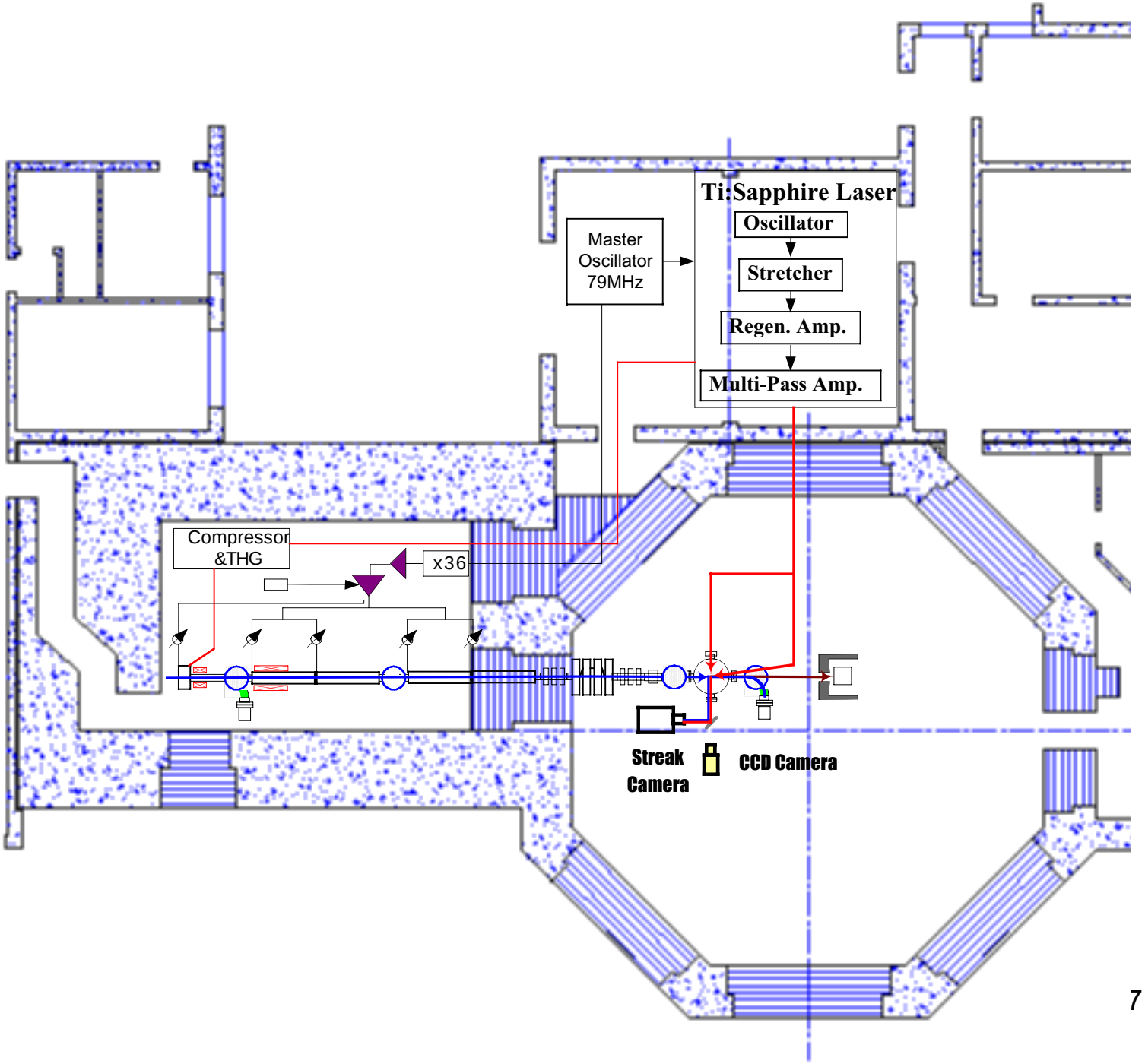

Parameters of Electrons and Laser

Wavelength(×)	0.8
Peak power(TW)	20
Pulse duration (fs)	30
Energy/pulse(J)	0.6
Spot size(×)	50
Power density(W/cm^2)	
____(Hz)	10

Energy (MeV)	60~100
Energy dispersion (rms)	<1%
Normalized transverse emittance (rms)π_m·rad	2
Bunch length (before compress)(ps)	10
Bunch length (after compress) (ps)	1
Bunch charge(nC)	1
Repetition rate(Hz)	<100

The left is parameters of laser and the right is that of electrons. All these are given according to the present technology level we can achieve.

Photocathode Microwave Electron Gun

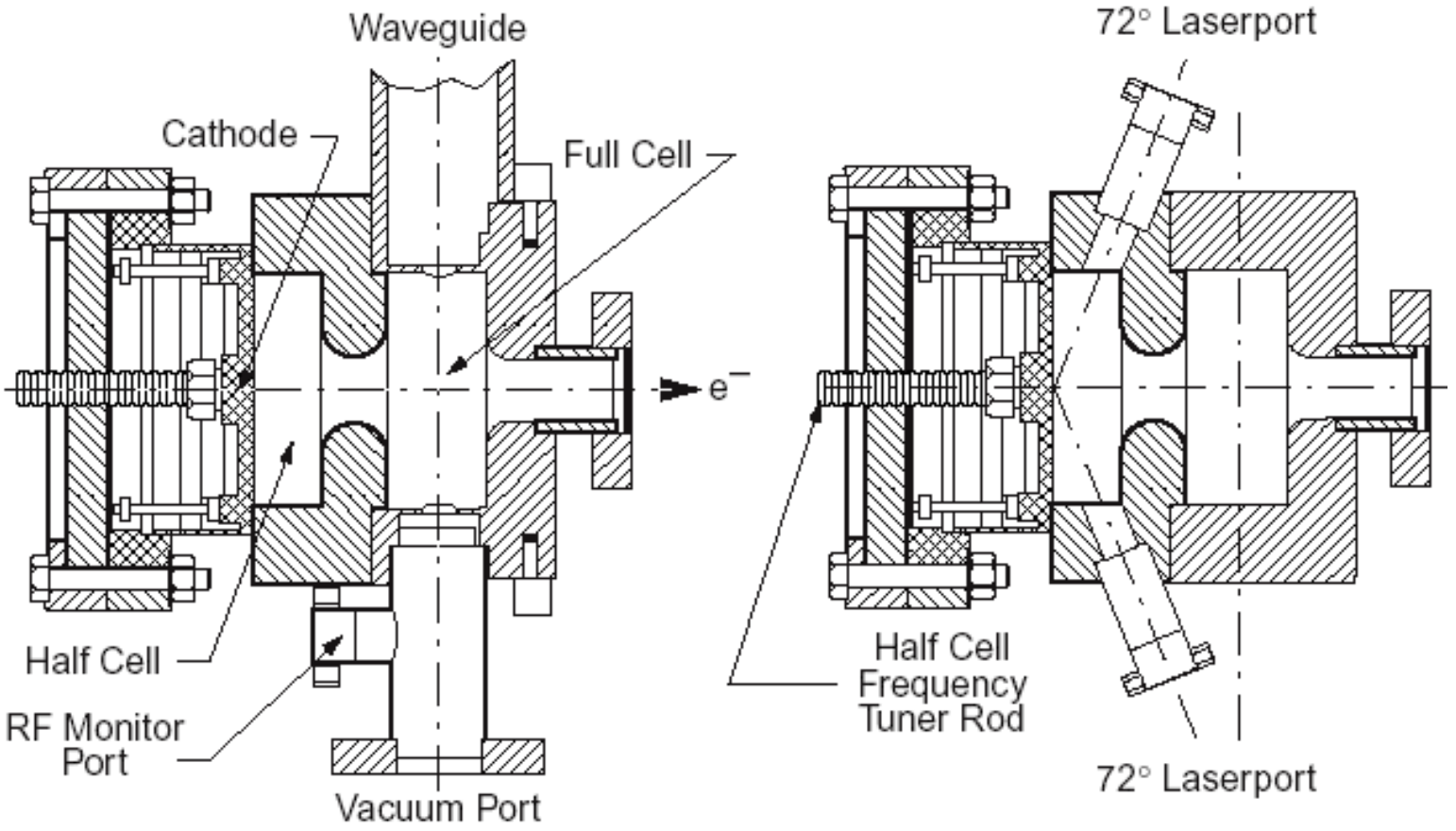

The gun cavity model is Brookhaven 1.6 Cell 2856MHz microwave cavity. The length is 15cm, and the minimum inner diameter is 2.5cm.

Bunch Compress

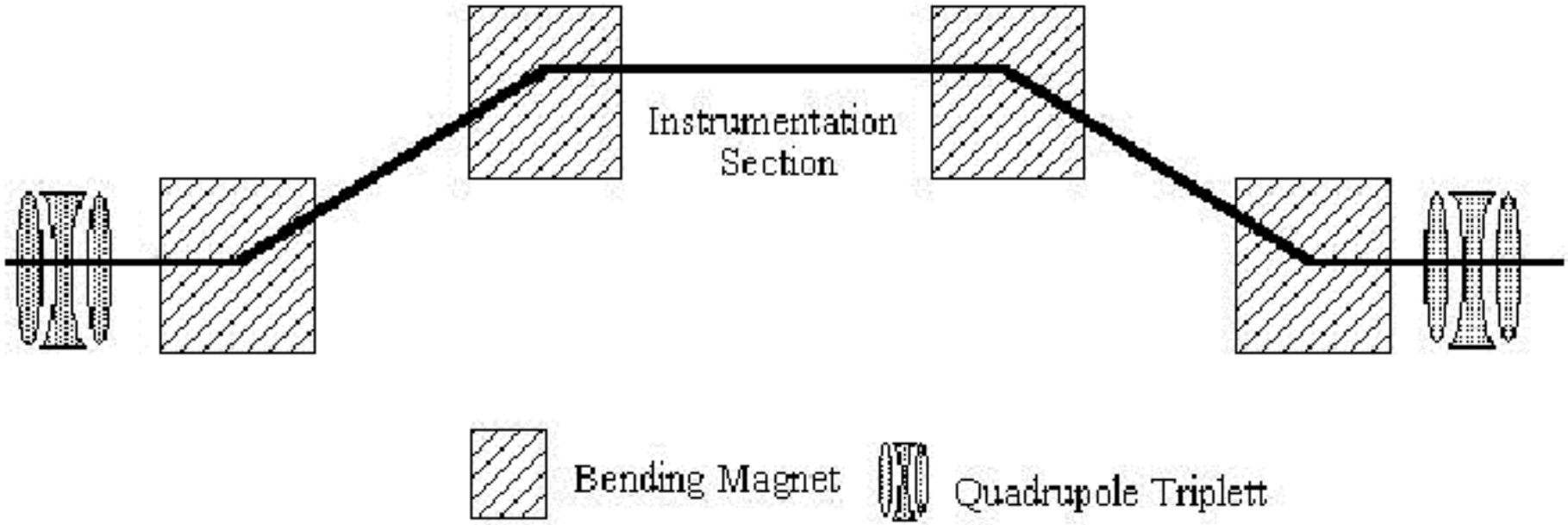

- Magnetic compress: composed by 4 dipole bending magnets and two quadrupole triplets (chicane)
- Factors to enlarge the emittance: space charge effects and coherent synchrotron radiation.

Type	Distribution	Number	Function
Position detector	Point 1_2_3	3	Beam position detection
Cross-section detector	Point 1_2_3	3	Monitoring beam position and shape, measuring emittance
Wall current detector	Point 1_2_3	3	Monitoring temporal distribution
Integral flux detector	Point 1_3	2	Beam average flux
Energy analysis station	Point 1_4	2	Energy and energy dispersion
OTR detector	Point 3	1	Measuring energy dispersion and emittance precisely
Streak camera	Point 3	1	Measuring bunch size precisely

Electron beam measurements. The point 1~4 are shown in the schematic figure.

Ray Tracing Model for Thomson source based on SHADOW[4]

Parameters of the electron beam and laser in our simulation.

Laser beam	Wavelength/ μm	0.8	Electron bunch	Energy/MeV	60
	Peak power/TW	20		Charge per pulse/nC	1.0
	Pulse length/fs	30		Pulse length/ps	1.0
	Spot radius/ μm	50		Normalized emittance (RMS) /mm mrad	3π
	Power Density/ $W\ cm^{-2}$	$8°10^{17}$		Transverse radius	50

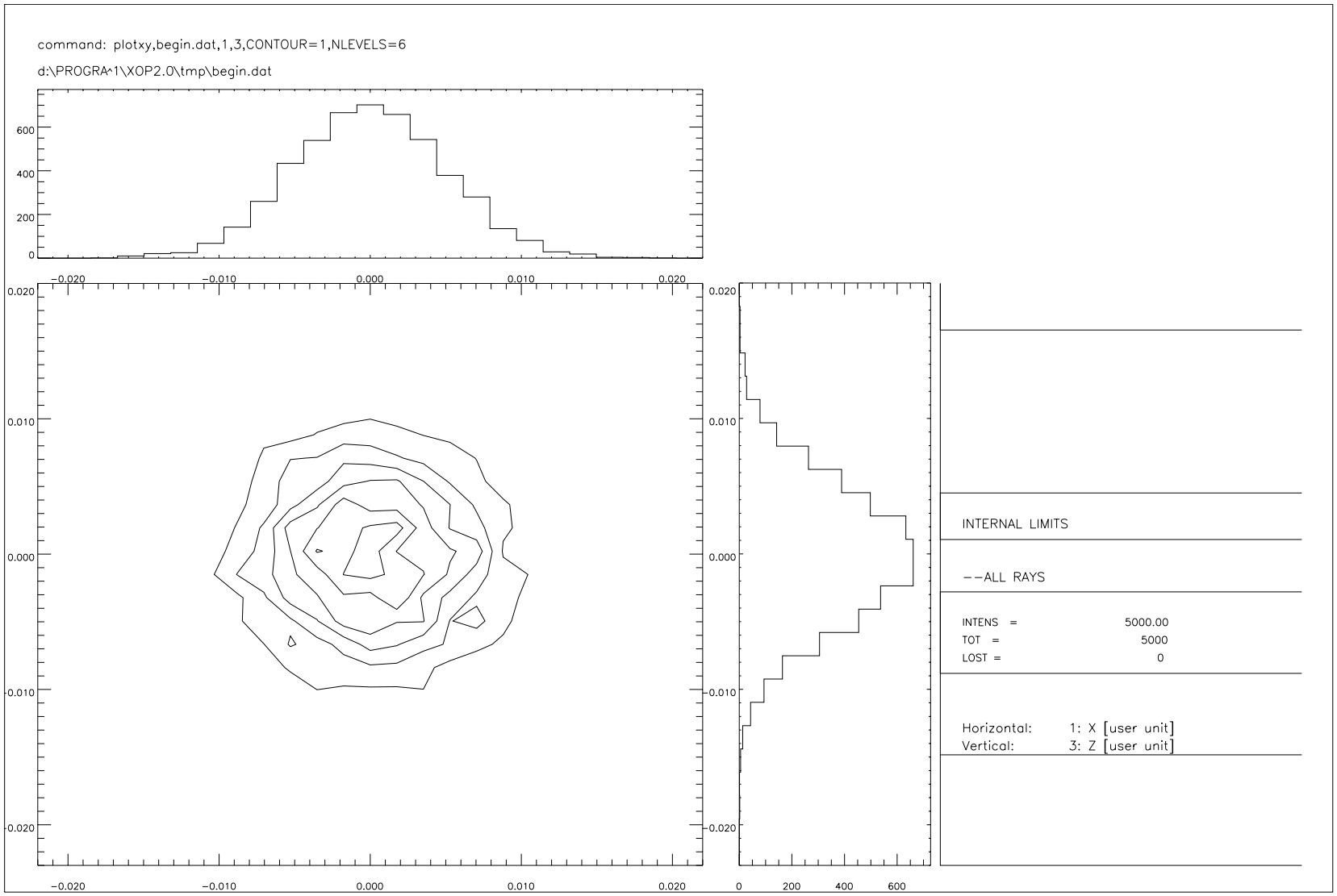

The Thomson dcattering source transverse spatial distribution. The contour represents intensity distributions. On the top and right are histograms

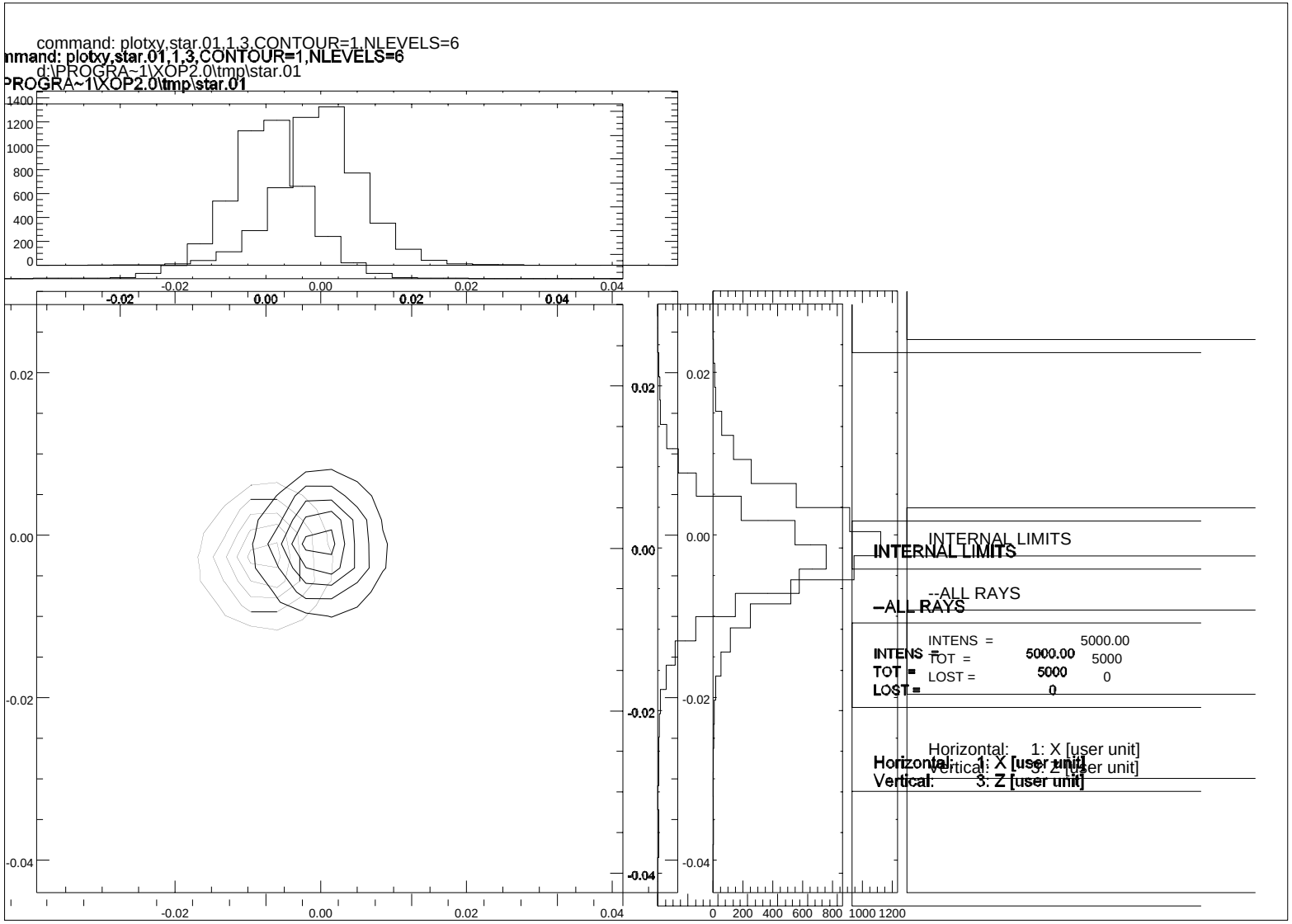

Image of the Thomson scattering source passed through a toroidal mirror at a grazing incident angle

Spectral Measurement of Thomson x-ray source by crystal diffraction

Problem: low aperture, cannot measure the broad spectrum

$$\frac{\lambda}{(\Delta\lambda)_{RC}} = \frac{tg\theta}{(\Delta\theta)_{RC}} \quad [5]$$

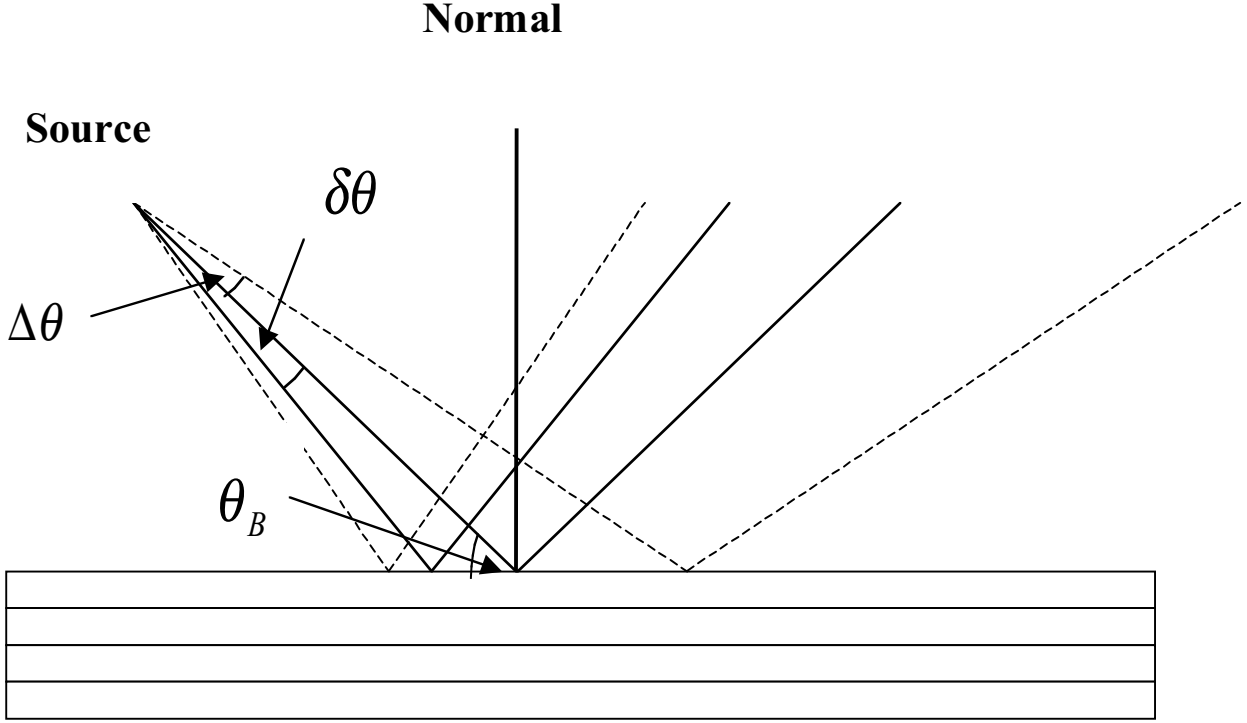

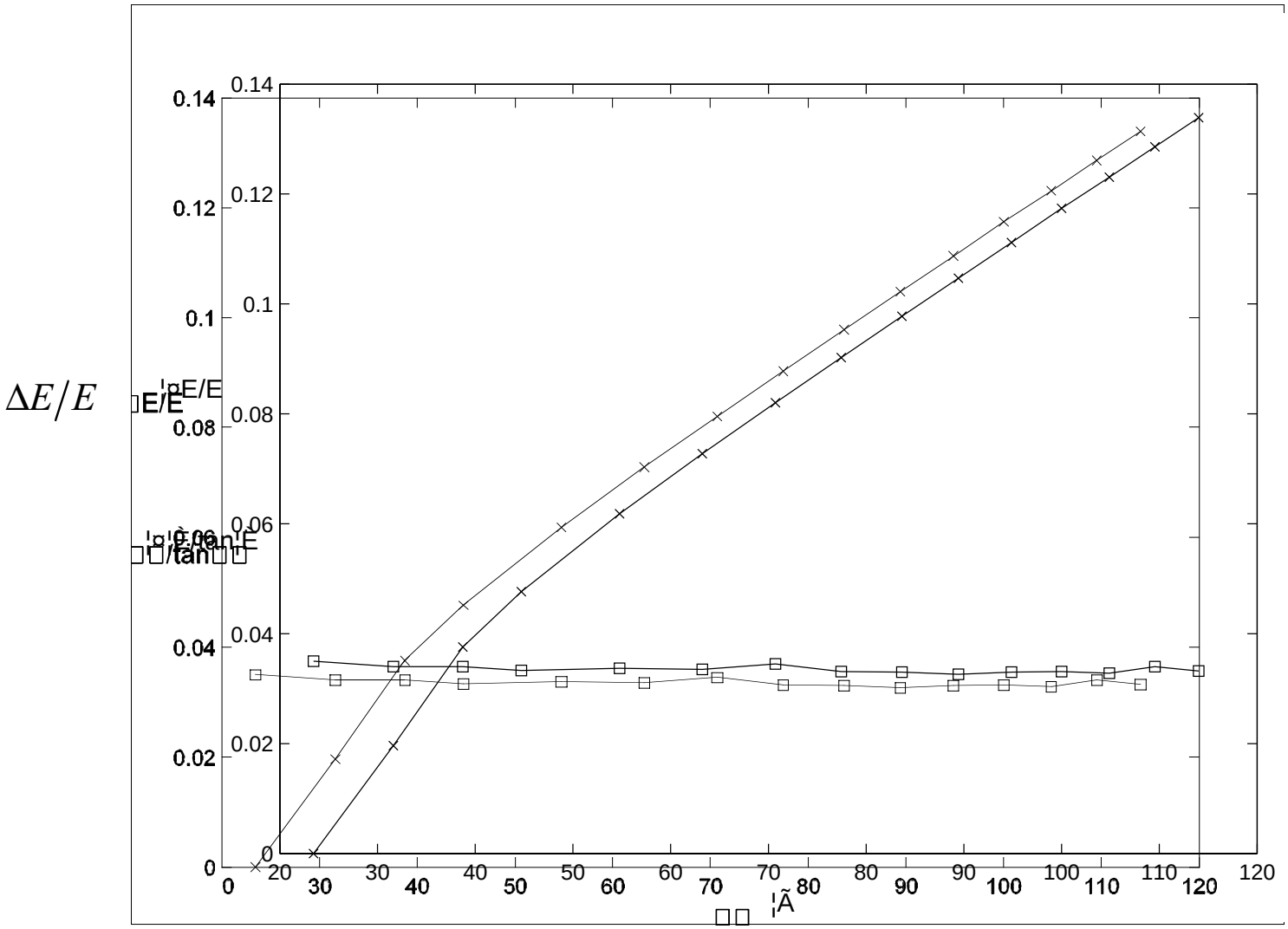

$\Delta E/E$ $\Delta\theta/\tan\theta$ γ

$\Delta E/E$ and $\Delta\theta/\tan\theta$ as a function of γ $\Delta\theta \approx 1/\gamma$ means the divergence of the incident beam. The reflection surface is Si 111, only if $\Delta E/E$ $\Delta\theta/\tan\theta$ can the whole spectrum be measured

- We have the joint probability density function

$$\frac{dn_x}{d\Omega dE_x} = f(\theta_x, E_x)$$

- Then d_ is separated into d_d_

$$dn'_x = d\theta d\phi \int_{E_x} f(\theta_x, E_x) dE_x$$

- Considering on the intersection of the incident plane and the image plane, the intensity distribution will be, according to Bragg equation

$$I(\theta) = \frac{dn_{xi}}{d\theta} = f\left(\theta_x, \frac{hc}{2d\sin(\theta_B + \theta_x)}\right) d\phi dE_x$$

- In numerical computation, one can suppose dE_x and d_ as a certain interval

- For simplicity, the probability density function $f(\theta_x, E_x)$ can be separated into the product of $g(\theta_x)h(E_x)$ in which $g(\theta_x)$ and $h(E_x)$ are the individual distributions of θ_x and E_x, respectively. This is based upon the assumption that the distribution onto θ_x and E_x are independent. By specific mathematical process, one can solve the energy spectrum of the scattered photons. A direct method is to regard the angular distribution as a weight and divest it from the measured spectrum recorded on the image plane.

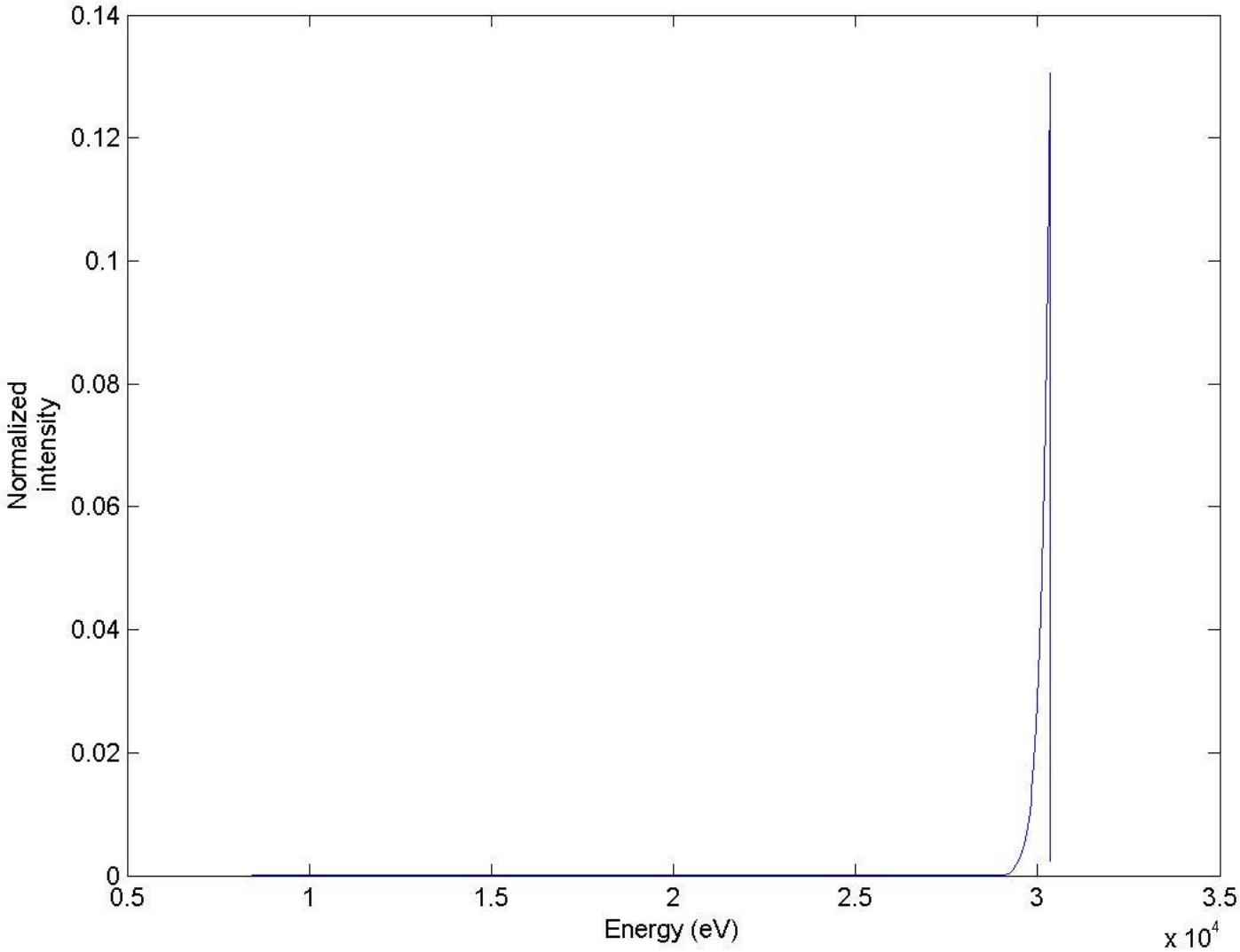

A resolved spectrum by ray tracing crystallography simulation, using the parameters listed above

REFERENCES

- [1] W.H. Huang, et. al. (will be pressed in *Intense Laser and Particle Beams (Chinese)*)
- [2] J. Yang et al., **Evaluation of femtosecond X-rays produced by Thomson scattering under linear and nonlinear interactions between a low-emittance electron beam and an intense polarized laser light,** Nuclear Instruments and Methods in Physics Research A, 428 (1999): 556~569.
- [3] W.H. Huang, et. al. **The Scheme and Parameters of *New Light Source I*.** Report of Dep. Engineering Physics of Tsinghua University.
- [4] Lai B. et al. **SHADOW: a synchrotron radiation ray tracing program.** Nucl. Instr. Meth. A, 1986, 246: 337-341.
- [5] G. Hölzer, et al. J. X-ray Sci. Tech. 7(1997),50-70.